NUCLEAR PHYSICS

JOURNAL DEVOTED TO THE EXPERIMENTAL AND THEORETICAL STUDY OF THE FUNDAMENTAL CONSTITUENTS OF MATTER AND THEIR INTERACTIONS

EDITOR: L. ROSENFELD - COPENHAGEN
ASSOCIATE EDITOR: O. NATHAN - COPENHAGEN

VOLUME XXI

NORTH-HOLLAND PUBLISHING COMPANY - AMSTERDAM

NUCLEAR PHYSICS

EDITORIAL BOARD

AUSTRALIA & NEW ZEALAND:	H. Messel (Sydney), M. L. Oliphant (Canberra)
AUSTRIA:	B. Karlik (Vienna), H. Thirring (Vienna)
BELGIUM:	M. de Hemptinne (Louvain), J. Verhaeghe (Ghent)
CANADA:	G. Volkoff (Vancouver)
DENMARK:	C. Møller (Copenhagen), S. Rozental (Copenhagen), G. E. Brown (Copenhagen)
FINLAND:	L. Simons (Helsinki)
FRANCE:	A. Berthelot (Saclay), S. Gorodetzky (Strasbourg)
GERMANY (DEM. REP.):	G. Hertz (Leipzig)
GERMANY (FED. REP.):	W. Gentner (Freiburg i. B.), J. H. D. Jensen (Heidelberg)
GREAT BRITAIN:	W. E. Burcham (Birmingham), T. H. R. Skyrme (Harwell)
HUNGARY:	L. Janossy (Budapest)
INDIA:	H. Bhabha (Bombay), R. Ramanna (Trombay)
IRISH REPUBLIC:	J. McConnell (Maynooth)
ISRAEL:	G. Racah (Jerusalem)
ITALY:	E. Amaldi (Rome)
JAPAN:	S. Kikuchi (Tokai), S. Tomonaga (Tokyo)
MEXICO:	M. Moshinsky (Mexico)
NETHERLANDS:	H. Brinkman (Groningen), S. R. de Groot (Leiden)
NORWAY:	E. Hylleraas (Oslo), A. Lundby (Oslo), H. Wergeland (Trondheim)
POLAND:	L. Infeld (Warsaw), J. Werle (Warsaw)
PORTUGAL:	*J. M. Araújo (Porto), J. R. de Almeida Santos (Coimbra)*
SOUTH AMERICA:	G. Beck (Saõ Paulo), J. Leite Lopes (Rio de Janeiro)
SPAIN:	J. M. Otero (Madrid), C. Sanchez del Rio (Madrid)
SWEDEN:	O. Klein (Stockholm), K. Siegbahn (Uppsala), I. Waller (Uppsala)
SWITZERLAND:	P. Huber (Basel), P. Scherrer (Zürich)
U.A.R. & ARAB COUNTRIES:	F. El Bedewi (Cairo), M. G. Nooh (Cairo)
U.S.A.:	H. H. Barschall (Madison, Wisconsin), S. Devons (New York), V. F. Weisskopf (Cambridge, Mass.)
U.S.S.R.:	M. A. Markov (Moscow), I. S. Shapiro (Moscow), D. V. Skobeltzyn (Moscow)
YUGOSLAVIA:	I. Supek (Zagreb)

NUCLEAR PHYSICS

JOURNAL DEVOTED TO THE EXPERIMENTAL AND THEORETICAL STUDY OF THE FUNDAMENTAL CONSTITUENTS OF MATTER AND THEIR INTERACTIONS

EDITOR: L. ROSENFELD - COPENHAGEN

VOLUME XXI

NOVEMBER 1960 — DECEMBER 1960

NORTH-HOLLAND PUBLISHING COMPANY-AMSTERDAM

PRINTED IN THE NETHERLANDS

2.B

Nuclear Physics **21** (1960) 1—14; © *North-Holland Publishing Co., Amsterdam*

Not to be reproduced by photoprint or microfilm without written permission from the publisher

THE ANGULAR DISTRIBUTIONS OF THE GAMMA RADIATION FROM THE $Li^7(p,\gamma)Be^8$ REACTION FROM E_p = 200 keV TO 1100 keV

B. MAINSBRIDGE

Research School of Physical Sciences, Australian National University, Canberra

Received 30 May 1960

Abstract: Angular distributions of the gamma radiation from the $Li^7(p,\gamma)Be^8$ reaction have been measured as a function of proton energy from E_p = 200 keV to 1100 keV with targets 5 to 20 keV thick. Separation of the gamma rays corresponding to transitions to the ground state and first excited state of Be^8 has shown the respective angular distributions to differ markedly in the neighbourhood of the 441 and 1030 keV resonances as a result of the interference between the resonant, even parity states and proton interactions of opposite parity.

The angular distributions of the resonant gamma rays are isotropic at E_p = 441 keV and are consistent with the resonance being p-wave ($J = 1^+$) with channel spins 1 and 2 in the ratio of 1/5; they do not lead to definite conclusions on the mechanism of the 1030 keV resonance but are not inconsistent with the resonance being p-wave ($J = 1^+$) with channel spins 1 and 2 in the ratio 1/5, the resonance radiation being isotropic but mixed with a d and s-wave contribution in the non-resonant background.

A $\cos^2\theta$ term in the angular distributions above E_p = 460 keV which rises steadily with proton energy, has been attributed to d-wave proton interaction in the background.

1. Introduction

The $Li^7(p,\gamma)Be^8$ reaction has been investigated over a number of years [1]) and it is convenient to summarise the information already known which is of interest in the proton energy range of E_p = 200 keV to 1100 keV.

Resonances in the reaction have been observed at proton energies of 441 and 1030 keV [2–4]). Gamma rays of energy $(17.2+\frac{7}{8}E_p)$ and $(14.3+\frac{7}{8}E_p)$ MeV have been observed corresponding to transitions to the ground state (0^+) and the 2.9 MeV level (2^+) of Be^8 respectively [5, 6]). For convenience, the gamma rays are referred to in the text by their energies at the 441 keV resonance, 17.6 MeV and 14.8 MeV respectively.

Above the 441 keV resonance the cross section is larger than can be explained in terms of the neighbouring resonances [2, 7]) and the weak 1030 keV resonance is superimposed on a steadily rising non-resonant background [3, 4]).

The 441 keV resonance is p-wave ($J = 1^+$) and the 17.6 MeV gamma ray is magnetic dipole (M1) [8]) while the 14.8 MeV gamma ray is a mixture M1+E2 [9]).

Anomalies in the elastic scattering of protons by Li^7 have been observed at the 441 keV and the 1030 keV resonances [10]) and the analysis of the elastic scattering data [11, 12]) assigns p-wave ($J = 1^+$) to both resonances with channel

spins 1 and 2 in the ratio of $\frac{1}{5}$. This predicts isotropy of the $Li^7(p, \gamma)Be^8$ radiation at both resonances.

Angular distributions of the two unresolved gamma rays have been reported at $E_p = 440$, 650 and 890 keV [13]) and between 880 and 1240 keV [3]). In addition, Devons and Hine [13]) have shown that there is interference in the neighbourhood of the 441 keV resonance by measuring the ratio of intensity of the radiation at 15° and 145°. At the 441 keV resonance, the radiation is isotropic to within 6 % while at the 1030 keV resonance it has been found to include a term in $\cos^2 \theta$, which disagrees with the predicted isotropy from the elastic scattering data. The contribution of the background radiation at this resonance is considerable and it is not known if the anisotropy is due to the background.

The separate angular distributions of the two gamma rays have been measured at the 441 keV resonance and have been found to be similar [6, 14, 15]), but measurements at $E_p = 1.15$ MeV with a target 250 keV thick suggest that the angular distributions of the two gamma rays differ in this energy region [6]).

The present experiment was designed to measure separately the angular distributions of the two gamma rays for proton energies between 200 keV and 1100 keV, with particular emphasis on the behaviour of the background radiation above the 441 keV resonance and the predicted isotropy of the radiation from the 1030 keV resonance.

2. Experimental

The target chamber (figure 1) was a brass cylinder of 7.6 cm diameter, 12.7 cm high with walls 0.32 cm thick, a perspex inspection window being included in the base.

The proton beam from the Canberra 1.2 MeV Cockcroft-Walton accelerator was analysed by a 90° deflecting magnet, and was defined at the entrance to the magnet by a 0.64 cm slit and at the exit by the jaws of the electronic voltage stabiliser set to a 0.64 cm gap. The emergent beam was focussed by strong focussing electrostatic lenses, deflected by a 45° analysing magnet through a 0.48 cm diameter aperture, (beam stop) on to the target. The aperture and the 0.48 cm diameter target spot defined the direction of the beam. The long path length of the protons defined the beam energy which was believed to be stable within 1 keV.

The machine was calibrated at the 340, 484, 672, 874 and 935 keV resonances in the $F^{19}(p, \alpha\gamma)$ reactions.

Targets 5 to 20 keV thick were deposited by evaporating natural lithium metal on to silver plated brass backings 0.038 cm thick. Each backing was masked so that four targets 0.48 cm in diameter and 0.95 cm apart were deposited as well as a 1.3 cm by 1.3 cm rectangle of lithium, which was used to measure the thickness of the deposit at the 441 keV resonance. The targets were transferred from the evaporator to the angular distribution chamber in an atmosphere

of dry argon. In the angular distribution chamber the target backing was screwed to a water-cooled holder which could be raised using a series of 0.95 cm spacers to position each target in the centre of rotation of the detector. Each target was changed after the measurement of one angular distribution.

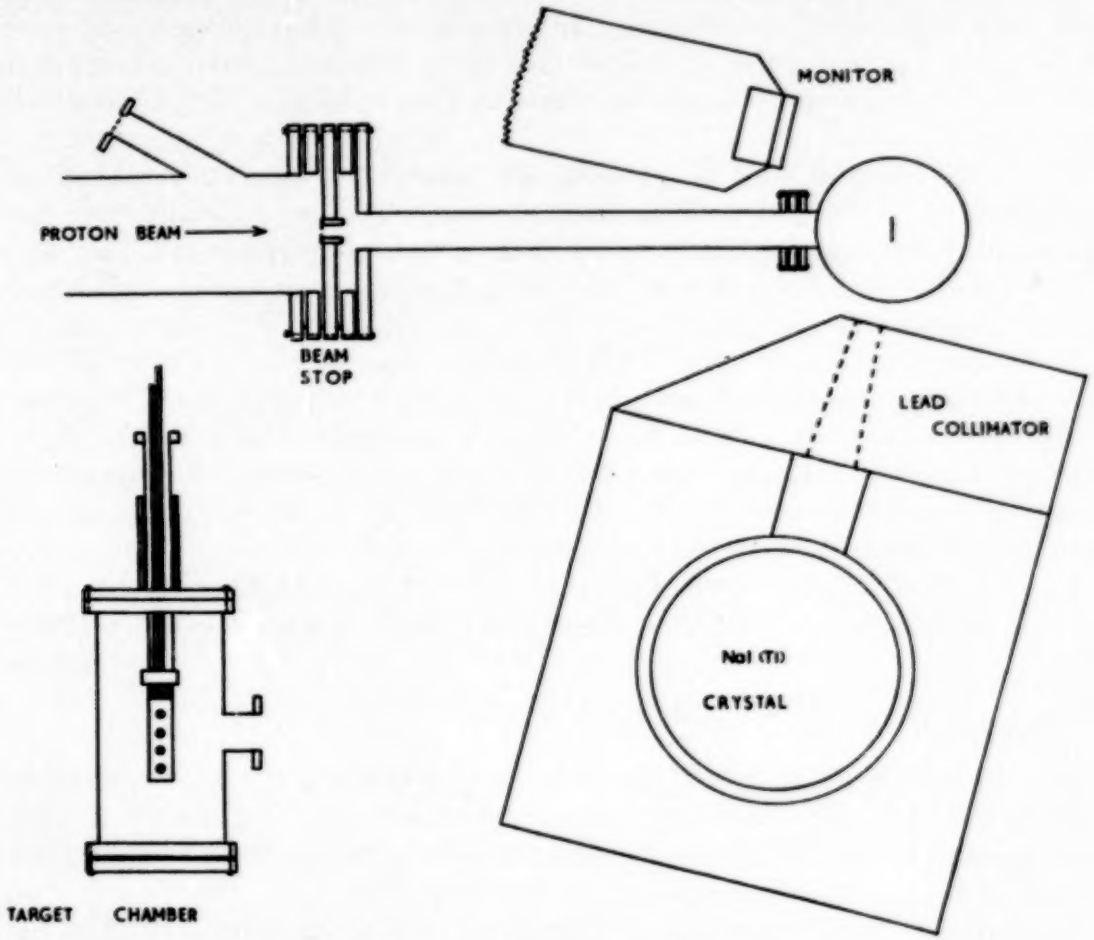

Fig. 1. Experimental arrangement.

Proton currents of 1 to 15 μA were used and measured with a beam current integrator. The additional focus provided by the electrostatic lenses limited the stop currents to 0 to 4 μA. Because of the large number of targets employed, no attempt was made to measure an excitation function accurately. The current integrator was used to measure each target thickness at the 441 keV resonance and to monitor the change of yield with running time. In 2 hours running time, at $E_p = 600$ keV and current of 10 μA, the gradual accumulation of carbon on the target increased the thickness by 5 keV, despite the use of liquid air traps, while after 3 to 4 hours, the yield began to fall rapidly. For these reasons, the running time was limited to 3 to 4 hours for each angular distribution.

2.1. DETECTORS

The gama rays were detected by a 12.7 cm diameter × 10.2 cm long sodium iodide crystal mounted, with the cylindrical axis vertical, in a 23 cm × 23cm × 15 cm steel block. The gamma radiation was collimated into the crystal centre by a conical hole through a lead block 7.6 cm thick. The collimator was tapered so that the detector observed through a solid angle of 0.074 steradians a 0.64 cm diameter spot at the target. The other five sides of the block were not shielded with lead. The distance between the target and the front face of the collimator was 5 cm.

A 12.7 cm Dumont 6364 photomultiplier, surrounded by a mu-metal shield was mounted on the large sodium iodide crystal. The pulse output from the photomultiplier was amplified by a Fairstein [16]) non-overload amplifier and fed to a Hutchinson-Scarrott type 100-channel pulse height analyser biased at 6 MeV gamma ray energy.

A 2.5 cm × 3.8 cm diameter NaI(Tl) crystal mounted on an EMI 6097B photomultiplier was set as a gamma ray monitor at 130° and 15 cm from the target. The output from the photomultiplier was amplified by a Higinbotham type non-overload amplifier and fed to a scaler set to count all events above 10.6 MeV gamma ray energy. The bias point was calculated by measuring the pulse height of the 1.33 MeV gamma ray from a Co^{60} source.

The large NaI(Tl) crystal stood with the steel housing and the collimator on a rotating table set so that the axis of rotation passed through the centre of the target.

2.2. BACKGROUND

Because of the sharp focus, the beam stop and the target were the only significant sources of background reactions. Gamma rays from the 6.1 and 7.1 MeV levels of O^{16} in the $F^{19}(p, \alpha\gamma)$ reactions were present but were eliminated by accepting the spectra above $E_\gamma = 8.5$ MeV.

The variation of the background with angle of observation was checked by raising the target from the beam path and allowing the beam to strike the back of the target chamber. It was found to be independent of the angle of observation beyond $E_\gamma = 8.5$ MeV and entirely due to cosmic rays.

Above a gamma ray energy of 8.5 MeV, the pulse height distribution of the cosmic ray background was found to be flat and the spectra were corrected for this contribution.

2.3. SCATTERING

The apparatus included a considerable amount of heavy scattering material but the energy spectra obtained from the large crystal suggested that most of the scattered gamma rays detected were of low energy and significant only below $E_\gamma = 8$ MeV. The discriminator of the monitor scaler was set to count

all events above 10.6 MeV gamma ray energy and measurements at the 441 keV resonance showed the ratio of monitor counts to current integrator counts was independent of the position of the crystal mounting.

2.4. GAIN STABILITY

Examination of the pulse height distributions of the lithium gamma rays showed that the gain of the 12.7 cm photomultiplier and the associated electronics was stable within 1 %. The gain of the monitor photomultiplier and amplifier was checked by placing a Co^{60} source close to the monitor and measuring the peak height of the 1.33 MeV gamma ray on the pulse height analyser set to the $\times 10$ scale. A gain shift of 2 % could be detected and the system was found to be stable within this limit.

3. Separation of the two Gamma Rays

Figures 2, 3, 4, 5 and 6 show typical spectra from the pulse height analysis of the radiation. Possible contributions from transitions to levels of Be^8 above 2.9 MeV are small [17, 18]) and have not been considered in this work.

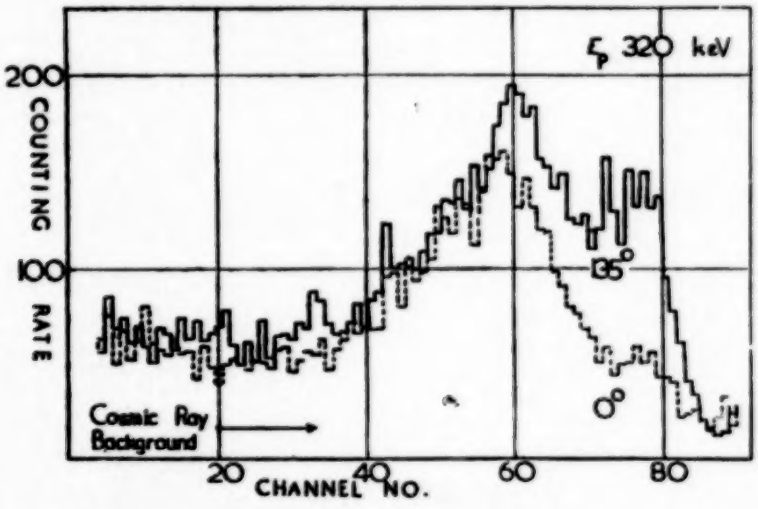

Fig. 2. Pulse height distributions of gamma rays from the $Li^7(p, \gamma)Be^8$ reaction observed at 0° and 135°. $E_p = 320$ keV, target 20 keV thick.

The relative yield of the gamma rays is clearly a function of proton energy and of the angle of observation, and a separation of the two components is necessary before attempting to measure the separate angular distributions.

The pulse height distribution of the 17.6 MeV or the 14.8 MeV gamma rays is not directly available from the spectra because of the overlap of the two components. A comparison of the pulse height distributions of 16.6 and 20.3 MeV gamma rays from proton capture in B^{11} and H^3 using the apparatus of fig. 1 showed the line shapes to be identical. It was assumed that the line shape

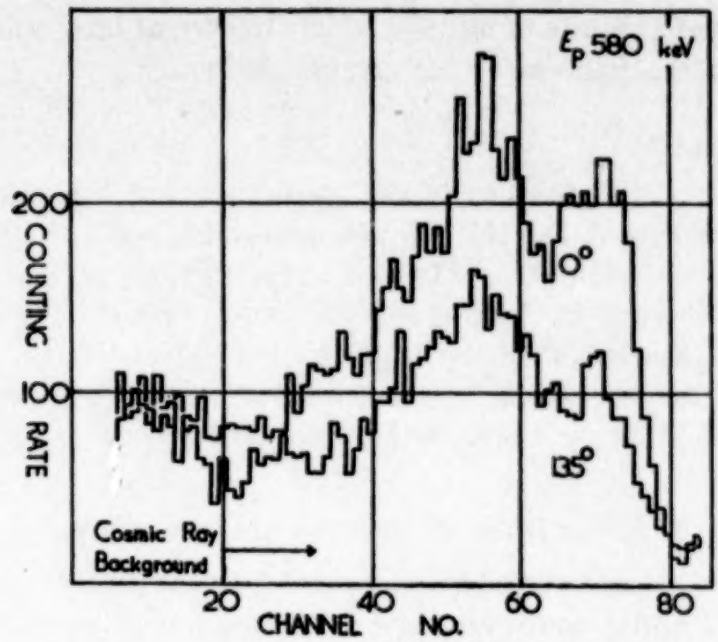

Fig. 3. Same as fig. 2, with $E_p = 580$ keV, target 10 keV thick.

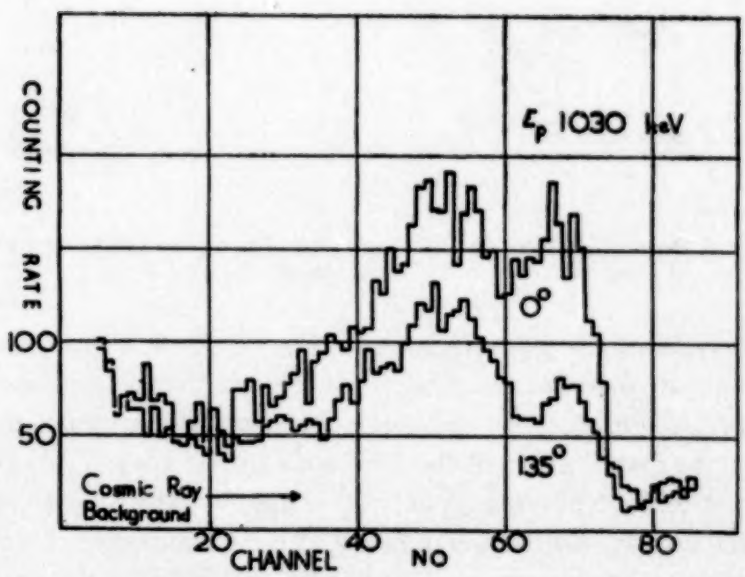

Fig. 4. Same as fig. 2, with $E_p = 1030$ keV, target 10 keV thick.

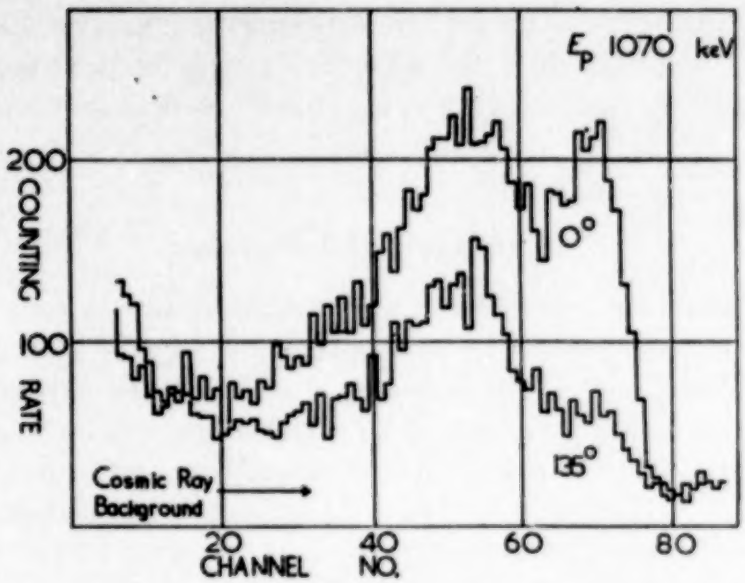

Fig. 5. Same as fig. 2, with $E_p = 1070$ keV, target 10 keV thick.

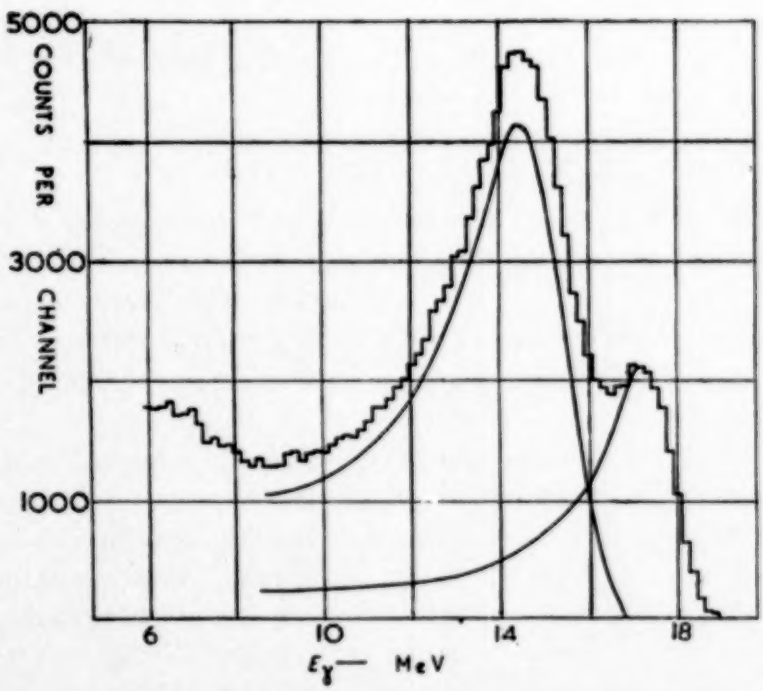

Fig. 6. Line shape of the 14.8 and 17.6 MeV gamma rays detected at 0° by the NaI(Tl) spectrometer ($E_p = 380$ keV, target 200 keV thick).

of the monochromatic 17.6 MeV gamma ray could be re bypresented the pulse height distribution of the 20.3 MeV gamma ray from H^3reac(p, γ)He^4 tion and a separation of the 14.8 and 17.6 MeV gamma rays is shown in fig. 6. The line shape of the lower energy component does not extend beyond 16.9 MeV.

4. Angular Distributions

Measurements of the energy spectra were made at 8 to 10 angles of observation, chosen in random order but at approximately equally spaced intervals of cos θ between 1 and -0.71. The targets were set in a plane perpendicular to the proton beam but for measurements at 90°, the backing was inclined at an angle of 20° to the beam. Targets 10 keV thick were used in the measurements between 450 and 550 keV and 950 and 1100 keV. At the 441 keV resonance, targets less than 5 keV thick were used and below 300 keV they were 40 keV thick. In the remaining energy regions, targets 20 keV thick were used.

The angular distributions of the unresolved gamma rays $W(\theta)_{14.8+17.6}$ were calculated by summing all events between 8.5 MeV and 19.5 MeV for each pulse height distribution. For the 17.6 MeV gamma rays, $W(\theta)_{17.6}$ angular distributions were obtained by summing between 16.9 MeV and 19.5 MeV. The totals, after correction for cosmic ray background, absorption in the target backing, counting loss in the pulse height analyser and normalisation to the same number of monitor counts, were expressed with the angle of observation in the centre of mass system.

Experimental points for $W(\theta)_{14.8+17.6}$ and $W(\theta)_{17.6}$, normalised to unity at cos $\theta = 1$ are shown in figs. 7 and 8.

4.1. ANALYSIS OF THE ANGULAR DISTRIBUTIONS

The distributions are not symmetrical about $\theta = 90°$ and odd powers of cos θ are present, indicating interference between contributions from protons of odd and even parity. Since the resonance is due to odd (p-wave) parity protons, the interference is due to even parity (s, d, g-wave) protons. Because of the centrifugal barrier, only s and d-wave protons need be considered in this energy range.

In this reaction, E1 radiation can arise from s and d wave protons and since it is more probable than magnetic or higher order electric radiation, the interfering radiation is assumed to be E1 in character, limiting the highest order term in the angular distribution function to $\cos^2\theta$. Interference between gamma radiation from d-wave interaction and the E2 radiation in the resonant M1+E2 14.8 MeV gamma ray would introduce a $\cos^3\theta$ term and the coefficient could be of the same order of magnitude as the coefficient of $\cos^2\theta$ (E. Bradford, private communication).

The angular distributions would then be of the form

$$W(\theta)_{14.8} = A_0 + A_1 \cos\theta + A_2 \cos^2\theta + A_3 \cos^3\theta,$$
$$W(\theta)_{17.6} = A_0 + A_1 \cos\theta + A_2 \cos^2\theta.$$

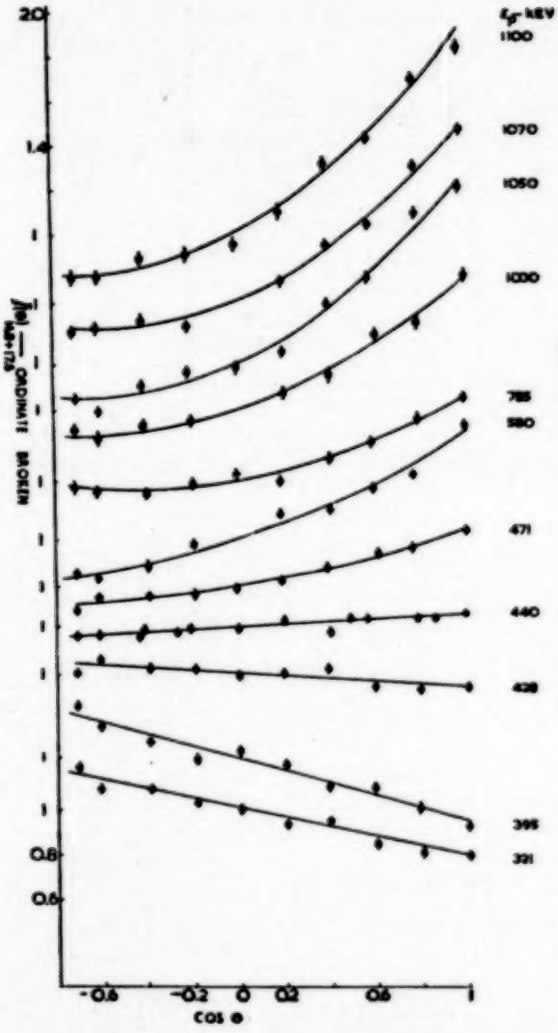

Fig. 7. Angular distributions of the unresolved gamma rays $W(\theta)_{14.8+17.6}$.

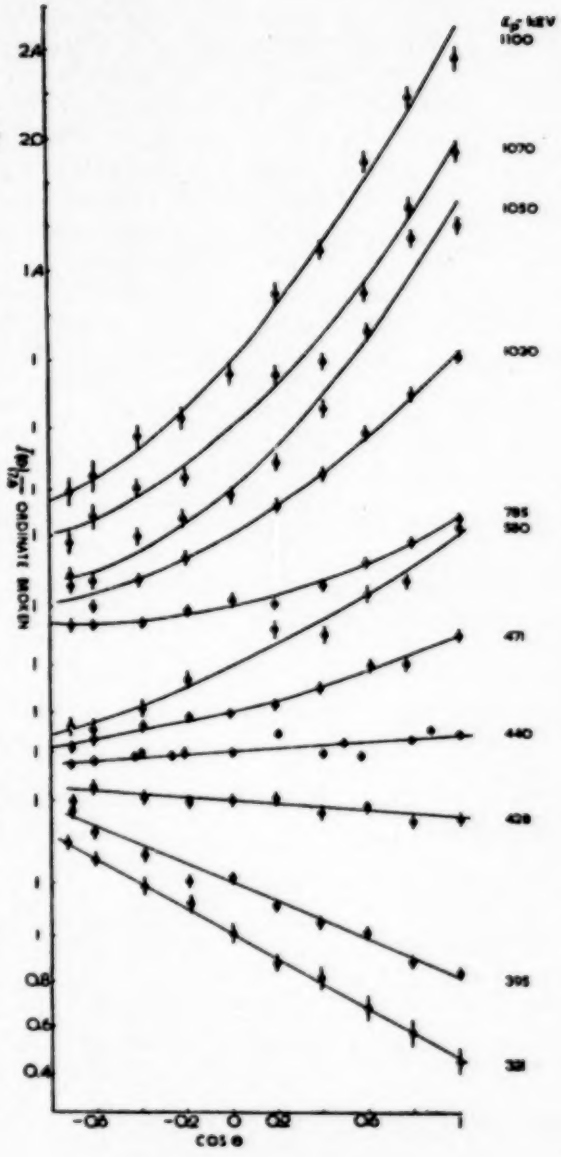

Fig. 8. Angular distributions of the ground state transition $W(\theta)_{17.6}$.

A number of the measurements of $W(\theta)_{14.8+17.6}$ were analysed in the form $A_0 + A_1 \cos\theta + A_2 \cos^2\theta + A_3 \cos^3\theta$, but the errors in A_3 were large and no significance could be attributed to the values.

The solid lines in figs. 7 and 8 show the results of a least squares fit of the

polynomials $A_0+A_1\cos\theta+A_2\cos^2\theta$ to the experimental points. The values of the coefficients used in these figures are given in table 1.

TABLE 1

Values of the coefficients of the angular distributions in figs. 7 and 8

Proton energy (keV)	$W(\theta)_{14.8+17.6}$		$W(\theta)_{17.6}$	
	A_1/A_0	A_2/A_0	A_1/A_0	A_2/A_0
1100	0.52	0.35	1.15	0.4
1070	0.41	0.36	0.90	0.39
1050	0.46	0.36	0.87	0.43
1030	0.31	0.26	0.56	0.23
786	0.18	0.2	0.20	0.17
581	0.33	0.14	0.49	0.10
471	0.17	0.08	0.20	0.07
440	0.056	0.008	0.064	0.015
428	−0.057	−0.029	−0.070	0.004
396	−0.27	−0.02	−0.41	0.04
321	−0.22	0.01	−0.56	0.00

Errors in A_1 and A_2 have been estimated from the statistical and possible geometrical errors.

4.2. THE ANGULAR DISTRIBUTION OF THE GAMMA RAY TRANSITION TO THE 2.9 MeV LEVEL OF Be^8

The function $W(\theta)_{17.6}$ was multiplied by the factor required to satisfy the condition that

$$\frac{A_{0\ 17.6}}{A_{0\ 14.8+17.6}-A_{0\ 17.6}}=\frac{I_{17.6}}{I_{14.8}},$$

the intensity ratio measured at 90° [19]). The functions $W(\theta)_{14.8+17.6}$ and $W(\theta)_{17.6}$ were then subtracted to give the coefficients A_0, A_1 and A_2 of $W(\theta)_{14.8}$.

4.3. EXPERIMENTAL RESULTS

The angular distributions were expressed in the form $A_0(1+a_1\cos\theta+a_2\cos^2\theta)$ and figs. 9, 10, 11 and 12 show the variation with proton energy of a_1 and a_2 for the resolved and unresolved gamma rays. In the case of the angular distributions of the 14.8 MeV gamma ray, the coefficients have been derived from the smoothed values of a_1 and a_2 in $W(\theta)_{14.8+17.6}$ and $W(\theta)_{17.6}$.

Fig. 11 includes the values of a_2 reported by Devons and Hine [13]) and Kraus [3]) and the excitation function at $\theta = 90°$ (Mainsbridge [19]).

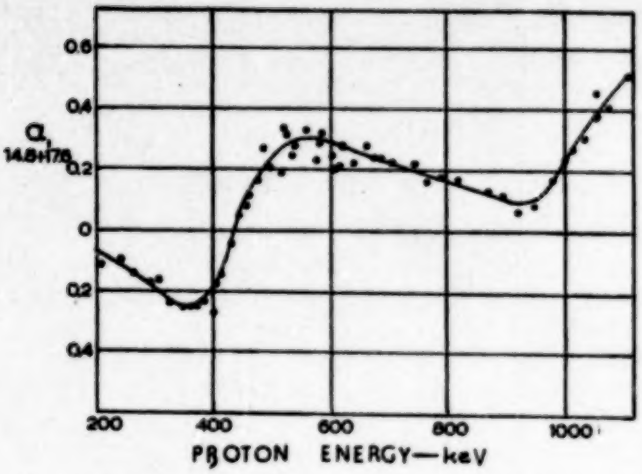

Fig. 9. Variation of a_1 in $W(\theta)_{14.8+17.6}$.

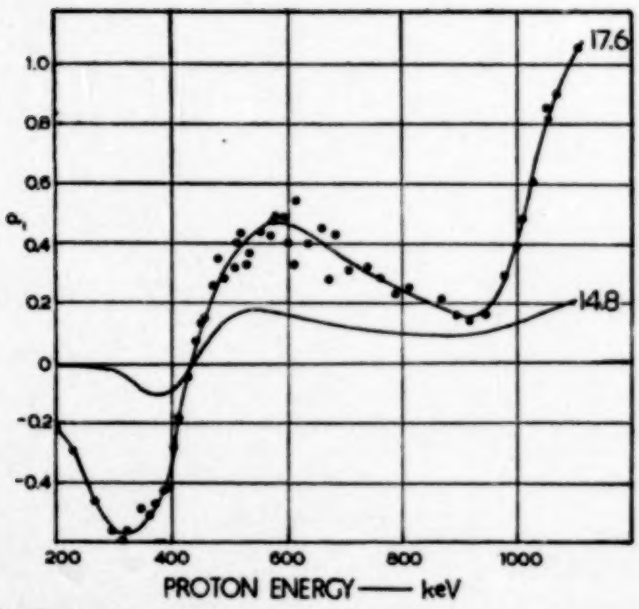

Fig. 10. Variation of a_1 in $W(\theta)_{17.6}$ and $W(\theta)_{14.8}$.

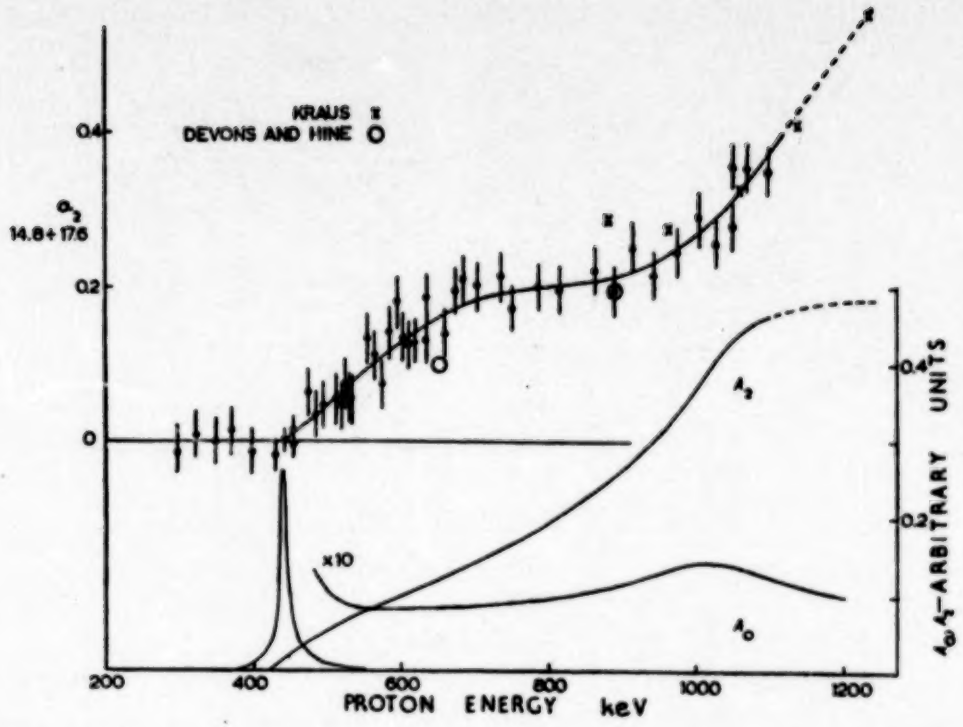

Fig. 11. Variation of a_2, A_0 and A_2 in $W(\theta)_{14.8+17.6}$. Experimental points reported by Kraus [8]) and Devons and Hine [12]) are included.

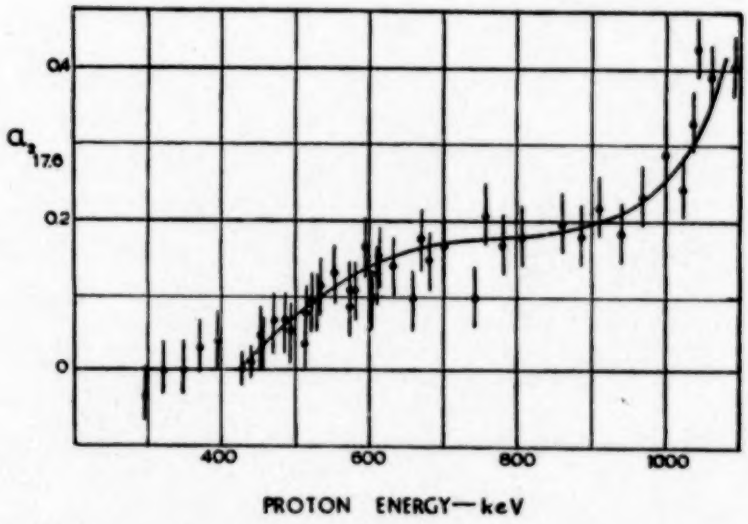

Fig. 12. Variation of a_2 in $W(\theta)_{17.6}$.

5. Discussion

5.1. THE VARIATION OF a_2

Inspection of figs. 11 and 12 shows the values of a_2 to be the same for both gamma rays, within experimental errors.

At the 441 keV resonance, a_2 is approximately zero and, neglecting small

background effects, is consistent with the resonance being p-wave with channel spins 1 and 2 in the ratio of $\frac{1}{5}$ (Devons and Lindsey [20])). The appearance of a_2 immediately above the 441 keV resonance suggests that the background contains some contribution from d-wave protons.

At the 1030 keV resonance, the situation is not immediately clear. If each value of a_2 is multiplied by the value of the excitation function at the corresponding value of E_p, the resulting A_2 is seen to rise steadily through the resonance (fig. 11). Measurements of A_2 up to $E_p = 1240$ keV by Kraus suggest that A_2 continues to rise slowly beyond the resonance and the finite value of A_2 can be attributed entirely to the non-resonant background. If this is correct, the resonant radiation would be isotropic and consistent with the resonance being p-wave ($J = 1^+$) with channel spins 1 and 2 in the ratio of $\frac{1}{5}$.

5.2. THE VARIATION OF a_1

Interference effects have been reported [3, 13]) from measurements of $W(\theta)_{14.8+17.6}$ in the neighbourhood of the 441 and 1030 keV resonances and the present results are in general agreement with those works but the separation of the two components shows the interference to be stronger for the ground state transition than for the transition to the 2.9 MeV level of Be^8. This effect appears to account for the marked difference in the angular distributions of the two components †.

The magnitude of the interference for each gamma ray would depend on the relative intensity of the component at the resonance and in the interfering background ratiation of opposite parity. The undetermined mixing ratios at the resonances of M1+E2 radiation in the transitions to the first excited state would have to be considered as well as the separate interference contributions from s and d wave proton capture in the non-resonant background.

At the 1030 keV resonance, both gamma rays show interference effects and this supports the conclusion that both are resonant at this energy.

Thanks are due to Dr. F. Barker and E. Bradford of the Department of Theoretical Physics for their valuable discussion, to Professor E. W. Titterton for his interest in this work and to Messrs. I. F. Wright and D. S. Gemmell for advice in the design of the experiment. This work was supported by a grant from the Australian Atomic Energy Commission.

† Measurements of the intensity ratio of the two components at $\theta = 90°$ [19]) showed the ratio to be constant from $E_p = 800$ keV to 1030 keV and it is concluded that both are resonant at the 1030 keV resonance.

References

1) F. Ajzenberg-Selove and T. Lauritsen, Nuclear Physics **11** (1959) 1
2) T. W. Bonner and J. E. Evans, Phys. Rev. **73** (1948) 666
3) A. A. Kraus, Phys. Rev. **93** (1954) 130
4) P. C. Price, Proc. Phys. Soc. A **67** (1954) 849

5) R. L. Walker and B. D. McDaniel, Phys. Rev. **74** (1948) 315
6) M. B. Stearns and B. D. McDaniel, Phys. Rev. **82** (1951) 450
7) D. H. Wilkinson, Phil. Mag. **45** (1954) 259
8) S. Devons and G. Goldring, Proc. Phys. Soc. A **67** (1954) 413
9) A. J. F. Boyle, Nuclear Physics **1** (1956) 581
10) W. D. Warters, W. A. Fowler and C. C. Lauritsen, Phys. Rev. **91** (1953) 917
11) D. A. Liberman and R. F. Christy, Phys. Rev. **92** (1953) 1085 A
12) D. A. Liberman, Ph. D. Thesis, Calif. Inst. of Technology (1955)
13) S. Devons and M. G. N. Hine, Proc. Roy. Soc. A **199** (1949) 56
14) H. Neuert and T. Retz-Schmidt, Zeits. f. Naturf. **13a** (1958) 829
15) H. Nabholz, D. Stoll, and H. Waffler, Helv. Phys. Acta **25** (1952) 153
16) E. Fairstein, Rev. Sci. Insts. **27** (1956) 475
17) E. K. Inall and A. J. F. Boyle, Phil. Mag. **44** (1953) 1081
18) E. K. Inall, Phil. Mag. **45** (1954) 768
19) B. Mainsbridge, Aust. J. Phys. **13** (1960)
20) S. Devons, and G. R. Lindsey, Proc. Phys. Soc. A **63** (1950) 1202

2.B

Nuclear Physics **21** (1960) 15—20; © *North-Holland Publishing Co., Amsterdam*

Not to be reproduced by photoprint or microfilm without written permission from the publisher

THE ELASTIC SCATTERING OF 96 MeV NEUTRONS BY NUCLEI

G. L. SALMON

Clarendon Laboratory, Oxford

Received 6 July 1960

Abstract: The differential cross sections for the elastic scattering of neutrons of mean energy 96 MeV, have been measured out to the first diffraction minimum for lithium, beryllium, carbon, aluminium, copper, cadmium, lead and uranium.

1. Introduction

The differential cross sections for the elastic scattering of neutrons from complex nuclei have been measured at 84 MeV by Bratenahl *et al.* [1]), at 136 MeV by van Zyl, Voss and Wilson [2]), at 290 MeV by Ball [3]) and at 350 MeV by Ashmore, Mather and Sen [4]). Because of the limited energy resolution obtainable with neutron counters in this energy range, the measurements are limited to the forward diffraction maximum where the contribution from inelastically scattered neutrons is small. In this experiment, the differential cross sections were measured for the elastic scattering of neutrons with a mean energy of 96 ± 2.5 MeV and width at half height of 24 MeV, by lithium, beryllium, carbon, aluminium, copper, cadmium, lead and uranium. The results are compared with an optical model calculation in the accompanying paper by P. E. Hodgson [5]).

2. Experimental Details

The neutrons were produced in a carbon target which intercepted 136 MeV protons in the Harwell synchrocyclotron. Carbon, with a large Q-value was used because, owing to geometrical reasons, it was not possible to align a beryllium target at a suitable radius to produce a neutron beam below 100 MeV. The beam was defined by a steel collimator 5.4 cm high, 1.9 cm wide and 2.4 m long, set in the concrete shielding wall (fig. 1), and the final 1.2 m of the collimator was increased to 6.35 cm $\times$ 2.54 cm in order to clear the neutron beam. A thin polythene bag containing hydrogen gas, displaced the air from the beam path near the counter.

The scattering elements were in disc form and all but the lithium were of negligible impurity. The lithium was found to contain 5.3 ± 0.3 % by weight of copper and 3.4 ± 0.2 % of zinc, and the results were corrected accordingly.

The detector was a tank of liquid scintillator 7.6 cm wide, 14 cm high and 44.5 cm long which has been described by Thresher *et al.* [6]). A brass plate, 1.3 cm thick, in front of the counter reduced the energy of any protons which were produced by reactions in the scatterer to a value below the threshold of detection. Neutrons were recorded which produced a recoil proton in the scintillator with an energy greater than about 80 MeV. Since the counting rate in such a detector which uses a fixed discriminator bias level is strongly dependent on the stability of the electronics and of the photomultipliers, the pulse height distributions from the counter were recorded on a 100-channel analyser, and the maximum pulse height determined for each measurement. The upper half of the pulse height distribution was approximately triangular,

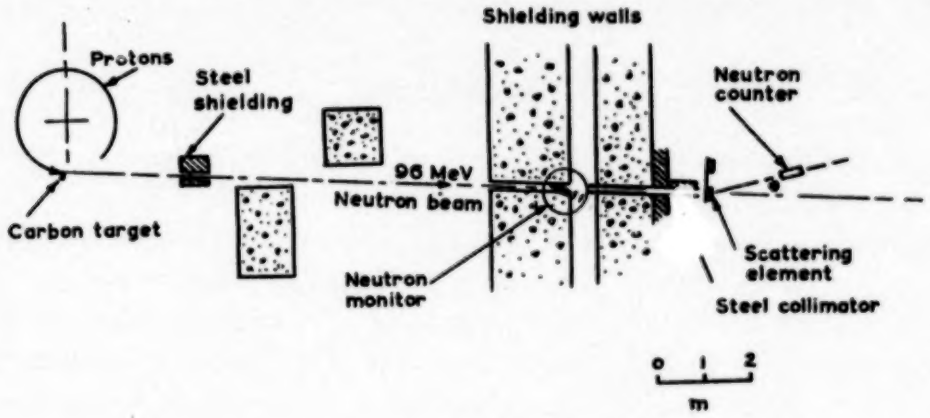

Fig. 1. The apparatus.

and with a small and known non-linearity in the A.E.R.E. type 1049B amplifier, the upper 30 % of the distributions could be fitted by least squares to a straight line. From the intercept of this line with the energy axis, the maximum pulse amplitude was determined, and by accepting only those pulses greater than 70 % of this maximum amplitude, no neutron of energy below 80 MeV could contribute to the data. The maximum error associated with this process, and with the effect of gain shifts, was estimated to be less than 3 %. When the differential cross section was strongly energy dependent, the energy distribution of the scattered neutrons differed from that of the incident beam, and the pulse height distribution was corrected accordingly before its analysis. The effect of this correction on the cross sections was largest near the diffraction minimum, but never exceeded 10 % and introduced an error of less than 4 %.

The neutron beam was monitored by recording with a two counter proton telescope, the recoil protons of energy greater than 50 MeV which were scattered at 15° out of a polythene radiator in the beam path before the collimator. The monitor counting rate was about 500 counts per second so that the beam intensity could be reduced by a factor of 500 for the measurements with the neutron counter in the direct beam. The beam was reduced by decreasing the

vertical aperture of the cyclotron at a small radius, and an observed change in the pulse amplitude from the neutron counter was attributed to an increase in the beam energy by 1 MeV. The uncertainty in the absolute cross section scale due to the correction for this effect was less than 1 %. Counting losses in the monitor were determined experimentally by comparison with the neutron counter over a range of beam intensity.

The neutron background consisted of two parts; that due to neutrons which came directly through the shielding walls and was independent of the counter position, and that which was scattered at small angles out of the neutron beam and out of the collimator. The latter was attenuated with the scatterer in position. The measured background with no scatterer was constant at angles greater than 5° and not altered by closing the collimator; the excess at small angles was reduced by the attenuation of the scatterer before subtraction from the scattering runs. The background was never more than 30 % of a scattering run.

3. The Effective Neutron Spectrum

The energy distribution of the neutrons from the cyclotron target (fig. 2, curve A), was determined from the distribution of recoil protons out of a liquid

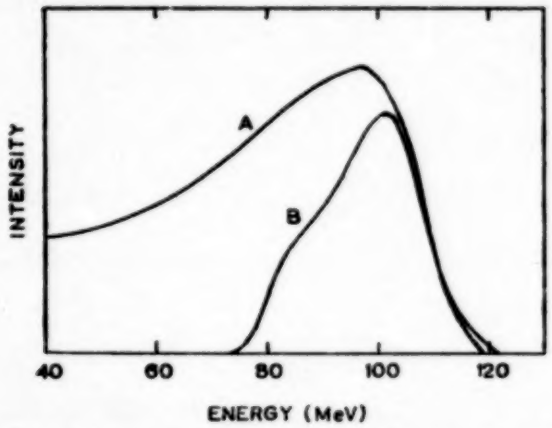

Fig. 2. Curve A shows the incident neutron energy distribution. Curve B is the effective neutron spectrum.

hydrogen scatterer. This was combined with the calculated energy dependence of the counter efficiency to give the effective neutron spectrum shown in curve B, which has a width at half height of 24 MeV. The effective energy for the counter was determined experimentally by measuring the attenuation of carbon in good geometry and using the total cross section measurements of Thresher[15]).

4. Evaluation of the Cross-Sections

Absolute values of the differential cross sections were obtained by measuring the ratio of the scattered neutron flux to the direct beam intensity, with

counting rates C and C_0 respectively. The neutron detection efficiency was not uniform over the area of the counter because of edge effects. Therefore the effective area was determined relative to the area of a collimator 2.34 cm × 6.60 cm, which was the area of the neutron beam at the point where it met the counter in the measurement of C_0. The ratio of the counting rates, C_b for the counter in an uncollimated neutron flux, and C_a for the same flux collimated to 2.34 cm × 6.60 cm, is equal to the ratio of the effective area to 15.43 cm², multiplied by the square of the ratio of the distances of the collimator and counter respectively from the cyclotron target. The effective area A was found to be 83.2±3.3 cm². Then the differential cross section is given by

$$\frac{d\sigma}{d\Omega} = \frac{C}{C_0}\frac{R^2}{NxA}$$

for a thin scatterer with N nuclei per cm³ and of thickness x. The effective radius R of the counter from the scatterer was found experimentally by comparing the counting rates with its front end 185 cm and 85 cm from the scatterers. For the measurements at 1° scattering angle, the value of R was 403 cm, between 3° and 10° it was 203 cm, and at larger angles it was 103 cm.

The observed angular distribution which resulted from all orders of scattering was approximately Gaussian, so that the n-times scattered neutrons were distributed like $d\sigma/d\Omega(\theta/\sqrt{n})$ and the intensity of neutrons scattered at an angle θ into a solid angle $\Omega = A/R^2$ was

$$I(\theta) = \Omega I_0 \sum_{n=1}^{\infty} \frac{1}{n!} (Nx\sigma_e)^n \exp(-Nx\sigma_t) \frac{1}{n\sigma_e} \frac{d\sigma}{d\Omega}\left(\frac{\theta}{\sqrt{n}}\right).$$

No more than double scattering was significant. Therefore from the first two terms, and putting $I(\theta)/I_0 = C/C_0$, we find

$$\frac{d\sigma}{d\Omega} = \frac{C}{C_0}\frac{\exp(Nx\sigma_t)}{Nx\Omega} - \frac{Nx\sigma_e}{4}\frac{d\sigma}{d\Omega}\left(\frac{\theta}{\sqrt{2}}\right),$$

where σ_t is the total cross section and σ_e is the total elastic cross-section. The second term, which is due to double scattering was about $2\frac{1}{2}$ % at small angles, and rose to 10 % near the diffraction minimum.

At 203 cm radius from the scatterer, the counter subtended an angle of 2°. The resultant correction to the data for this finite angular resolution was largest where the cross-sections changed rapidly with angle near the diffraction minima for the heavy elements. A 2 % contribution to the elastic scattering at 1° from the heavier elements was due to the interaction of the magnetic moment of the neutron with the Coulomb field of the nucleus Schwinger [7]), Voss and Wilson [8]). A calculated value was subtracted to yield the nuclear scattering alone.

5. The Contribution from Inelastic Scattering

The effective energy distribution of the neutrons recorded by the counter had a total width of about 40 MeV. Inelastic events, leaving the nucleus with an excitation of up to 20 MeV would contribute appreciably to the scattering measurements. At 96 MeV, the cross-sections for the inelastic scattering of neutrons should be comparable with the corresponding cross-sections for protons. The values shown in table 1 were estimated from the proton data of

TABLE 1

Estimated corrections for inelastic scattering (mb/sr) in laboratory coordinates. Only those values are shown which are greater than 1 % of the differential cross section. The probable error of the corrections is ±50 %.

θ_{lab}	Copper	Aluminium	Carbon	Beryllium	Lithium
3°				10	5
5°				10	5
10°			6	10	6
12.5°	20	10	8		
15°		10	10	12	9
20°			10	15	8
25°					5

Strauch and Titus [9]), Dickson and Salter [10]), Tyren and Maris [11, 12, 13]), and Clegg, Foley, Segel and Salmon [14]), and have been subtracted from the results.

6. The Results

The differential cross sections in the centre of mass system are shown in table 2, together with the relative standard deviations between each point. This uncertainty combines a standard deviation of about 3 % for the counting rate, 1 % at wide angles for the multiple scattering correction, 1 % for the finite angular resolution, and up to 5 % for the estimated contribution from inelastic scattering. There is an additional uncertainty in the absolute scale with a standard deviation of 5.5 %, which includes 2 % in the direct beam measurement of C_0; 4 % for the effective area of the counter; 2 cm in the effective radius; and 2 % for the monitor counting loss. The standard deviation of the effective energy measurement was 2.5 MeV.

The results are shown graphically in the accompanying paper by Hodgson [5]). These differential cross sections lie consistently between those of Bratenahl *et al.* at 84 MeV, and of van Zyl *et al.* at 136 MeV. For lead, where the total cross section is nearly constant below 100 MeV, the results are almost coincident with the 84 MeV data.

The author wishes to thank Mr. B. Rose for his valuable criticism of this work, and the Harwell cyclotron group for their willing co-operation.

TABLE 2

Differential cross sections (b/sr) in the centre-of-mass system. The additional standard deviation on the absolute scale is 5.5 %

Uranium		Lead		Beryllium	
θ_{CM}	$\frac{d\sigma}{d\Omega}$	θ_{CM}	$\frac{d\sigma}{d\Omega}$	θ_{CM}	$\frac{d\sigma}{d\Omega}$
1.00	80.9 ±1.8	1.00	64.1 ±1.4	3.33	0.722±0.022
3.01	65.4 ±1.1	3.01	54.3 ±1.0	5.55	0.612±0.023
4.02	51.9 ±1.4	4.02	43.9 ±1.2	11.10	0.431±0.014
5.02	38.3 ±0.9	5.02	34.2 ±0.8	16.64	0.231±0.009
6.03	29.9 ±1.1	6.03	25.8 ±0.7	22.17	0.077±0.009
7.53	14.2 ±0.5	7.54	13.0 ±0.4		
10.04	2.8 ±0.3	10.05	3.4 ±0.3		
Cadmium		**Copper**		**Lithium**	
1.01	33.6 ±0.9	1.02	14.99 ±0.49	3.43	0.445±0.018
3.03	28.0 ±0.6	3.05	13.24 ±0.31	5.72	0.370±0.018
5.04	20.9 ±0.5	5.08	10.64 ±0.26	11.43	0.266±0.011
7.57	11.0 ±0.4	7.62	7.43 ±0.26	17.14	0.158±0.007
10.09	4.15±0.15	10.16	3.83 ±0.13	22.8	0.068±0.005
12.61	1.16±0.11	12.70	1.59 ±0.08	28.5	0.031±0.004
Aluminium		**Carbon**			
2.07	3.85±0.19	2.17	1.200±0.12		
3.11	3.92±0.11	3.25	1.153±0.033		
5.19	3.28±0.09	5.42	0.991±0.032		
10.37	1.79±0.04	10.83	0.661±0.017		
12.96	1.19±0.04	13.53	0.488±0.014		
15.55	0.63±0.04	16.24	0.313±0.014		
		21.63	0.126±0.010		

References

1) A. Bratenahl, S. Fernbach, R. H. Hildebrand, C. E. Leither and B. J. Moyer, Phys. Rev. **77** (1950) 597
2) C. P. van Zyl, R. G. P. Voss and R. Wilson, Phil. Mag. **1** (1956) 1003
3) W. P. Ball, UCRL Report 1938 (1952) (unpublished)
4) A. Ashmore, D. S. Mather and S. K. Sen, Proc. Phys. Soc. A **71** (1958) 552
5) P. E. Hodgson, Nuclear Physics **21** (1960) 21
6) J. J. Thresher, C. P. van Zyl, R. G. P. Voss and R. Wilson, Rev. Sci. Instr. **26** (1955) 1186
7) J. Schwinger, Phys. Rev. **73** (1948) 407
8) R. G. P. Voss and R. Wilson, Phil. Mag. **1** (1956) 175
9) K. Strauch and F. Titus, Phys. Rev. **103** (1956) 200
10) J. M. Dickson and D. C. Salter, Nuovo Cim. **6** (1957) 235
11) H. Tyren and Th. A. J. Maris, Nuclear Physics **4** (1957) 637
12) H. Tyren and Th. A. J. Maris, Nuclear Physics **6** (1958) 82, 446
13) H. Tyren and Th. A. J. Maris, Nuclear Physics **7** (1958) 24
14) A. B. Clegg, K. J. Foley, R. E. Segel and G. L. Salmon, 1960 (to be published)
15) J. J. Thresher, Nuclear Physics (to be published)

2.E

Nuclear Physics **21** (1960) 21—27; © *North-Holland Publishing Co., Amsterdam*

Not to be reproduced by photoprint or microfilm without written permission from the publisher

OPTICAL MODEL ANALYSIS OF THE SCATTERING OF 96 MeV NEUTRONS BY NUCLEI

P. E. HODGSON

Clarendon Laboratory, Oxford

Received 6 July 1960

Abstract: Total, absorption and small-angle elastic differential cross-sections for Li, Be, C, Al, Cu, Cd, Pb and U are fitted by the optical model.

1. Introduction

Several extensive studies of the scattering of nucleons by nuclei have now been made using the optical model of the nucleus. In general, the agreement between theory and experiment is quite good, but it is noticeable that equally good fits can often be obtained with widely different values of the model parameters. This is partly due to the inherent ambiguities in the model, but also to the incompleteness of the experimental data. Thus, for example, it is easy to fit small-angle elastic scattering, but much more difficult to fit wide-angle elastic scattering, polarisations and absorption cross-sections as well, together with the total cross-section in the case of neutron scattering. The extra data eliminate whole regions of parameter space that fit the more limited data, and consequently if a fit can be obtained the corresponding model parameters are much more meaningful in terms of nuclear structure.

The recent measurements of Salmon [1]) of the differential elastic scattering cross-section out to the first minimum for 96 MeV neutrons, of Bowen *et al.* [2]) of the total neutron cross-sections for a range of energies, together with the measurements of absorption cross-sections in the region of 100 MeV by De Juren and Knable [3]) and by Voss and Wilson [4]) make available fairly complete sets of data for a range of nuclei at 96 MeV. Apart from the polarisations, the only information missing is the shape of the differential elastic cross-section at high angles. Lack of the polarisations is not so important since these are determined largely by the spin-orbit potential, which in turn has only a second order effect on the other measurable quantities.

These sets of data for beryllium, lithium, carbon, aluminium, copper, cadmium, lead and uranium have been fitted by the optical model. As far as possible the results are presented so that as more accurate data becomes available the improved values of the model parameters may be easily found.

2. Optical Model

To facilitate comparison with other work at different energies, the optical model potential was chosen to have the form

$$V(r) = U\rho(r) + iWf(r) + \left(\frac{\hbar}{m_\pi c}\right)^2 (U_s + iW_s)\frac{1}{r}\frac{d\rho}{dr}\mathbf{l}\cdot\boldsymbol{\sigma},$$

where $\rho(r)$ has the Saxon-Woods form with $a = 0.65\times10^{-13}$ cm, $f(r)$ is a Gaussian with $b = 0.98\times10^{-13}$ cm, and the nuclear radius is $1.25A^{\frac{1}{3}}\times10^{-13}$ cm, using the notation of Bjorkland and Fernbach [5]).

The Schrödinger wave equation was separated into partial waves and each partial wave equation integrated outwards numerically by the Fox-Goodwin method until the nuclear field became negligible. These internal solutions were fitted smoothly to the solution of the wave equation in the external region, which can be obtained analytically as a combination of spherical Bessel and spherical Neuman functions. This gives the complex elements of the scattering matrix for each partial wave and spin orientation, from which the measurable quantities can easily be calculated. The whole calculation was carried out on the Oxford University Ferranti Mercury Computer. Details of the methods used will be published separately.

3. The Fitting Procedure

The procedure adopted will be described in detail for carbon. The experimental data consist of:

(1) total cross-section $\sigma_T = 505\pm8$ mb, interpolated from the work of Bowen *et al.* [2]). (2) Ratio [3]) of absorption to total cross-section 0.45 ± 0.015, whence $\sigma_A = 227\pm8$ mb. A correction is necessary to allow for those neutrons inelastically scattered through less than 45°; from the work of Strauch and Titus [6]) and of Tyren and Maris [7]), Salmon estimates this to be ≈ 8 mb. Thus $\sigma_A = 235\pm8$ mb. (3) Salmon's differential cross-sections [1]).

The parameters of the optical model are U and W, the strengths of the real and imaginary parts of the central potential, U_s and W_s the corresponding quantities for the spin-orbit potential, and a, b and r_0 the potential shape parameters. Bjorkland and Fenbach's potential shape parameters and the spin-orbit potentials $U_s = -3.2$ MeV, $W_s = 0$ they used to fit proton scattering were used throughout this work. If later measurements of neutron polarisation require some revision of the spin-orbit potentials, the present work will not be appreciably affected, since the total and differential cross-sections are insensitive to the spin-orbit potential. This leaves only U and W to be determined by the experimental data.

It is possible to fix U and W from σ_T and σ_A alone by a procedure that makes use of the relative insensitivity of σ_A to changes in U. The absorbing part W of

the central potential essentially determines σ_A, and the refracting part U only affects it insofar as increasing U refracts more of the incident neutrons towards the absorbing potential, thus increasing σ_A. The effect is very small, as shown in

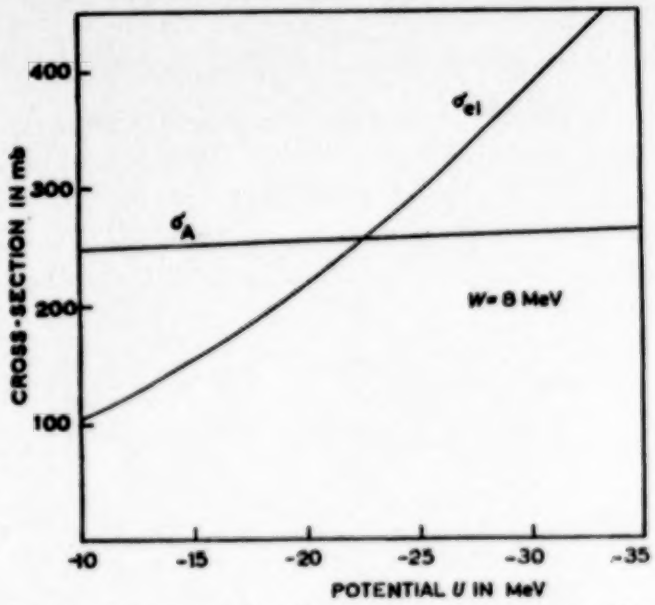

Fig. 1. Absorption and elastic cross-section for 96 MeV neutrons on carbon as a function of U for constant W.

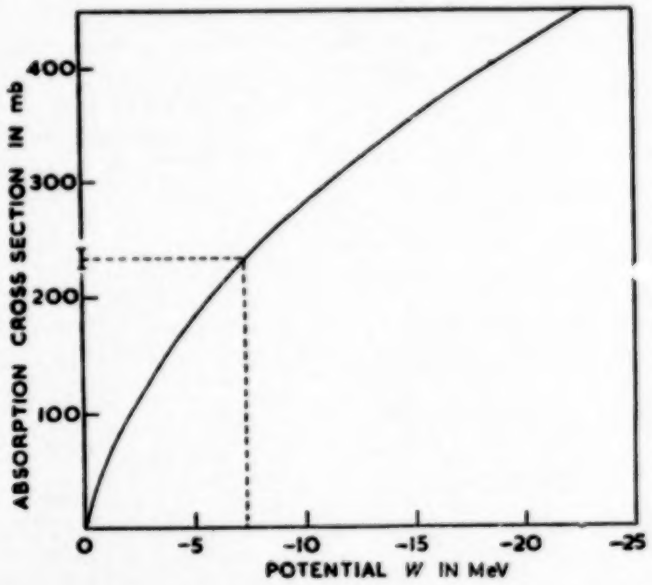

Fig. 2. Absorption cross-section for 96 MeV neutrons on carbon as a function of W.

fig. 1, where σ_A and σ_E are given as functions of U for constant W. The absorption cross-section is practically independent of U. It is therefore possible to construct a graph of σ_A as a function of W only, that is valid for the range of U of practical interest; this is shown in fig. 2. The value of $W = -7.1 \pm 0.5$ MeV corresponding to the measured σ_A can be obtained at once from it. Then,

keeping W to this value, σ_E can be calculated as a function of U, as in fig. 1, and the value appropriate to the measured σ_E obtained from it. This gives $U = -22.8 \pm 1.3$ MeV. In the region of best fit the potentials can be expressed as linear functions of the cross-sections

$$U = a_1\sigma_A + b_1\sigma_E + c_1, \quad W = a_2\sigma_A + b_2\sigma_E + c_2.$$

The values of the constants for carbon are given in table 1.

TABLE 1

Experimental cross-sections and the parameters of the optical model potentials

	Li	Be	C	Al	Cu	Cd	Pb	U
σ_T	294	431	505±8	1025±17	2063±26	3168±45	4666±50	5070±60
σ_A	155	210	235	440	815	1200	1865	2028
σ_E	139	221	270	585	1248	1968	2801	3042
U	−21.6	−24.9	−22.8	−22.6	−20.9	−19.3	−15.6	−14.8
W	−6.2	−7.6	−7.1	−9.0	−10.7	−11.7	−14.0	−14.2
a_1	−0.0091	−0.0105	−0.0574	−0.0034	−0.0069	−0.0064	−0.0036	−0.0040
b_1	−0.0909	−0.0711	−0.0686	−0.0316	−0.0149	−0.0103	−0.0063	−0.0056
c_1	−7.54	−6.95	+9.18	−2.61	+3.35	+8.56	+8.93	+10.33
a_2	−0.0470	−0.0474	−0.0428	−0.0349	−0.0245	−0.0224	−0.0202	−0.0178
b_2	+0.0011	+0.0014	+0.0015	+0.0010	+0.0006	+0.0005	+0.0004	+0.0003
c_2	+0.90	+2.02	+2.53	+5.75	+8.57	+14.20	+22.61	+20.96
L_{max}	10	11	12	14	18	20	23	24

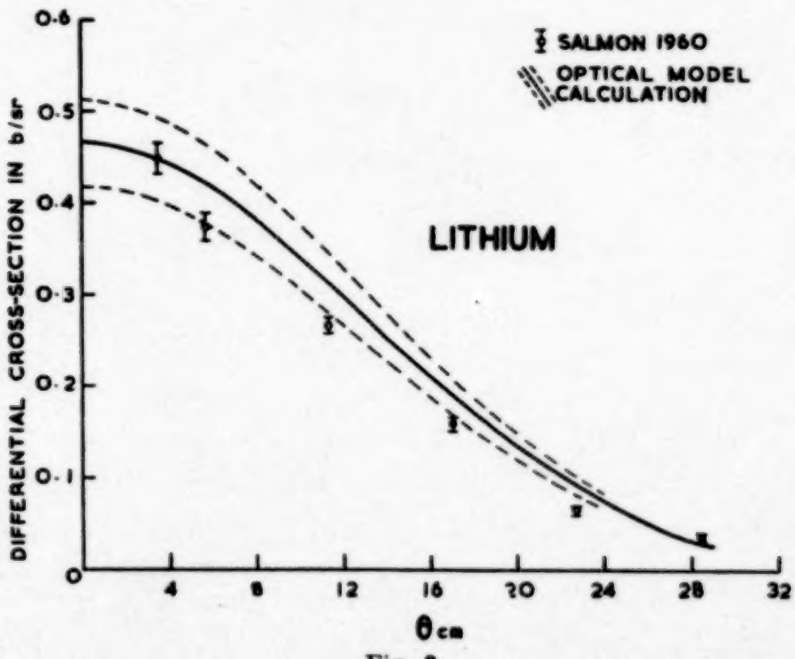

Fig. 3

Figs. 3—7. Differential elastic cross-section for 96 MeV neutrons on a range of nuclei compared with the calculations using the optical model. The dotted lines indicate the limits corresponding to the 10 % uncertainty in the absolute values of Salmon's measurements.

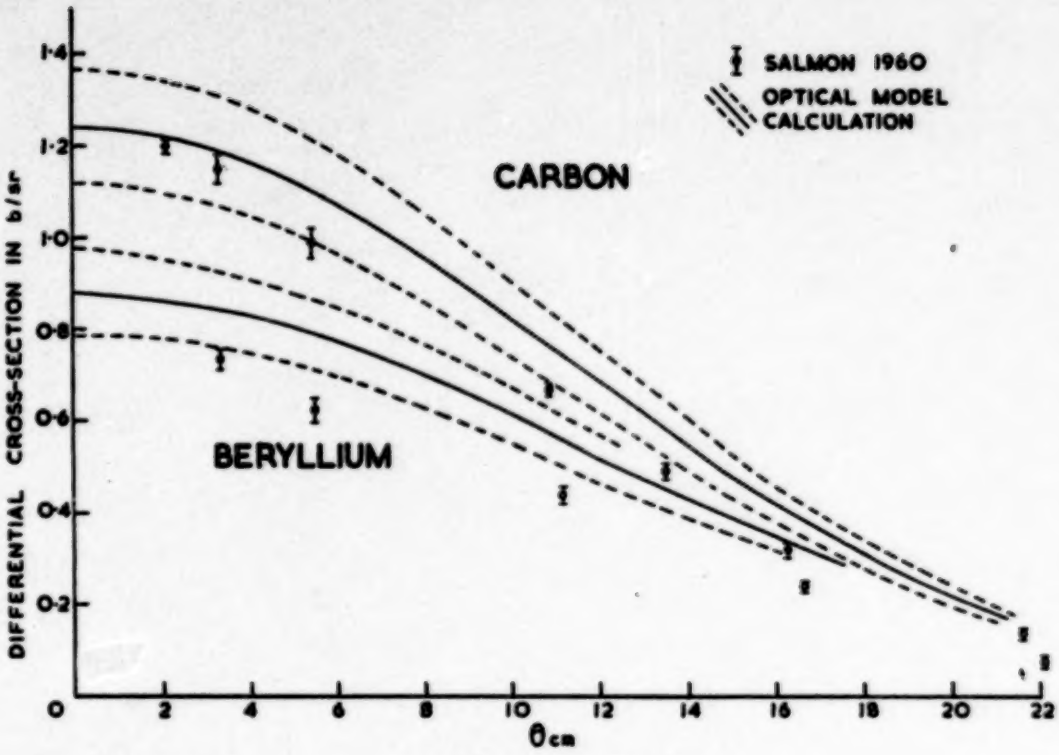

Fig. 4. See caption fig. 3.

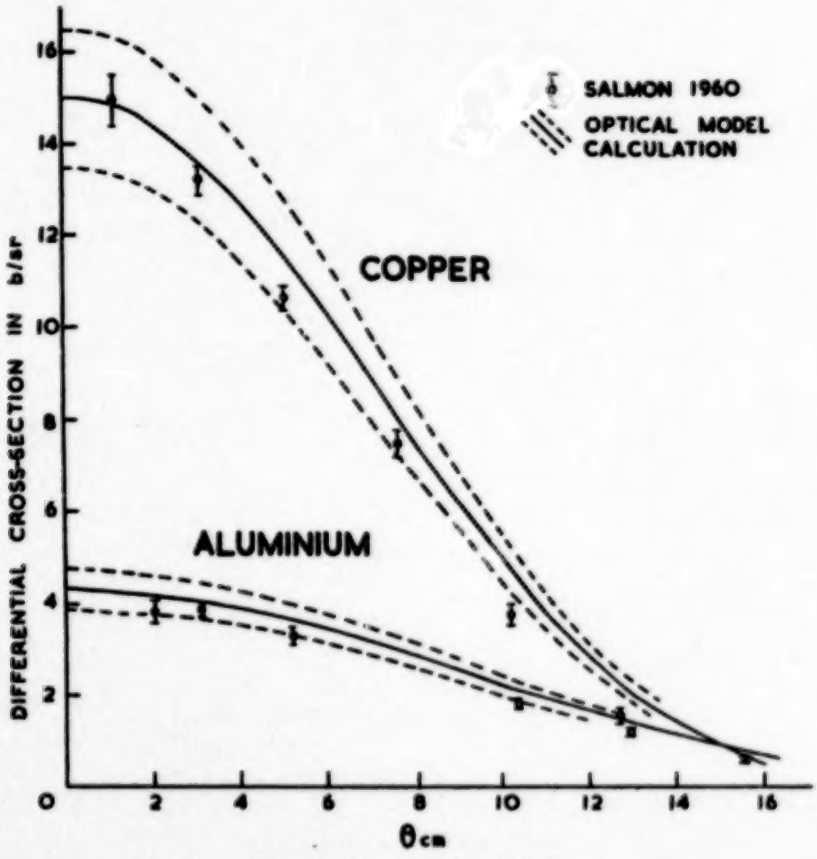

Fig. 5. See caption fig. 3.

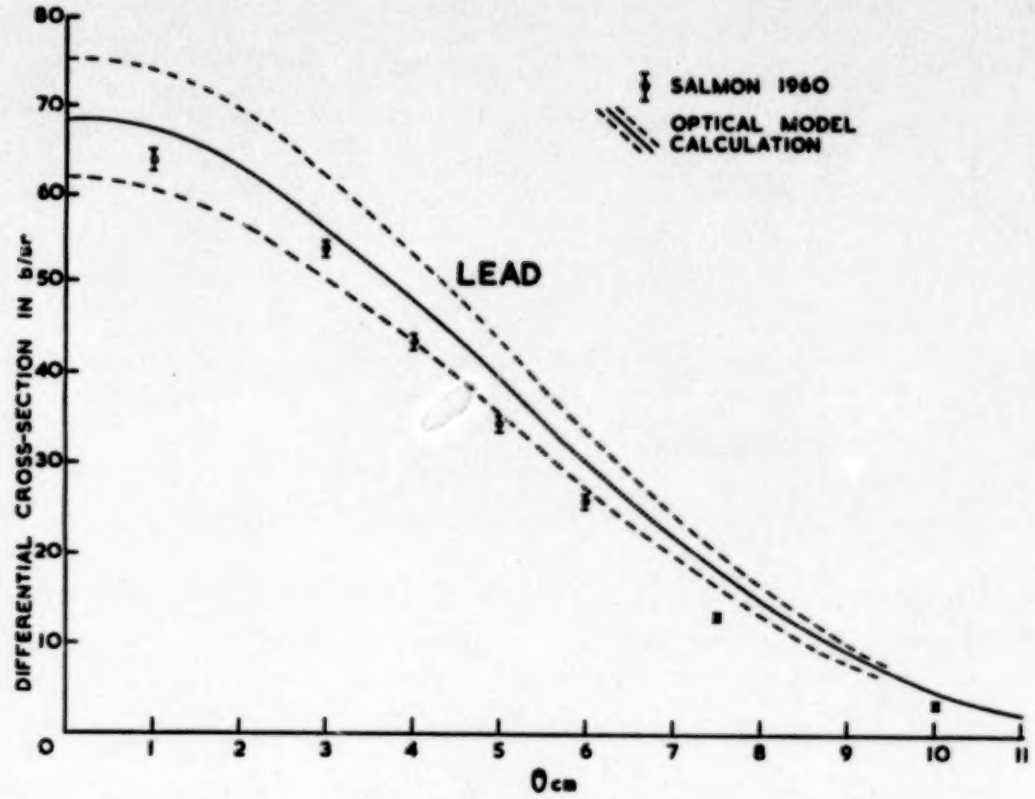

Fig. 6. See caption fig. 3.

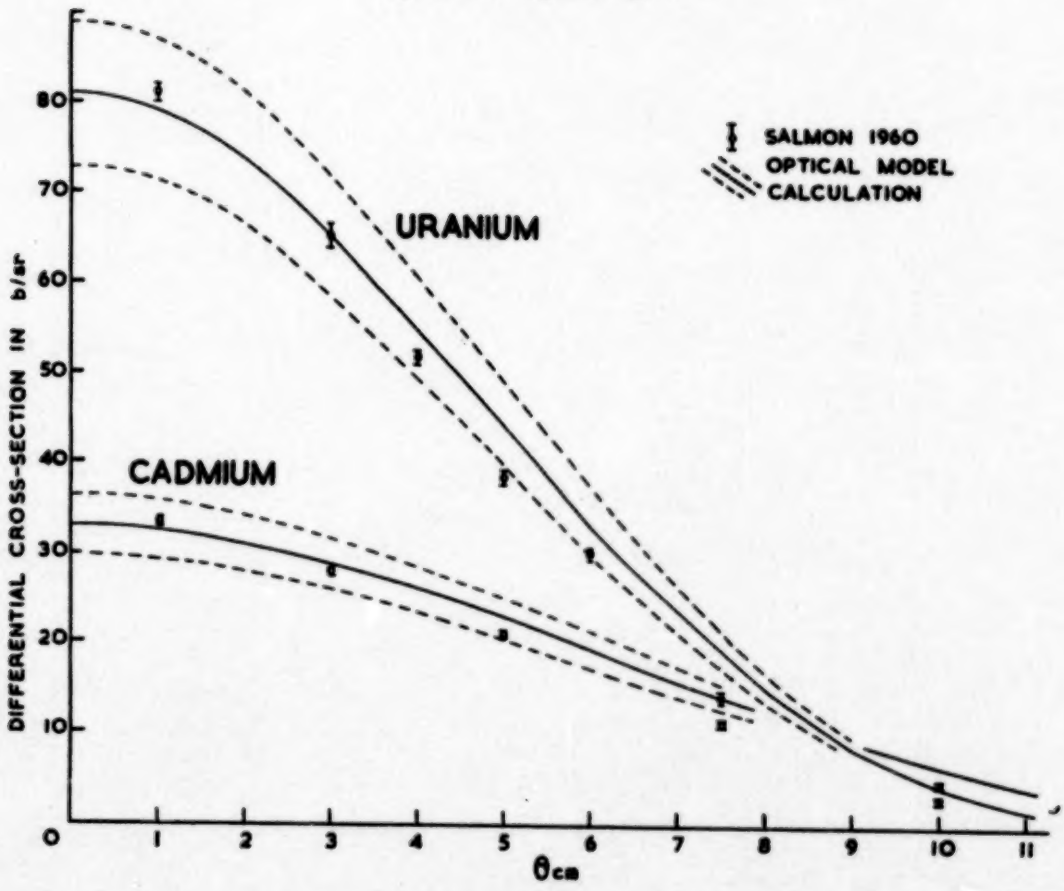

Fig. 7. See caption fig. 3.

The value of W determined by this procedure is unique, but that of U may be only the first of a series of values †. The curve of σ_E against U for constant W (fig. 1) rises to a maximum at higher values of U, and subsequently oscillates; this may give the observed σ_E for a series of values of U. The potentials used here are similar to those found by Bjorklund and Fernbach, but other deeper potentials may have more reasonable variations with energy.

This procedure was repeated for the other elements, and the results are given in table 1. Using these potentials, the differential cross-sectons for elastic scattering were calculated as described in the previous section.

No absorption cross-sections were available for lithium, beryllium and uranium, so in these cases an extrapolated value of σ_T/σ_A was obtained from De Juren and Knable's work. There is some uncertainty in this procedure, especially for lithium and beryllium, so the corresponding optical model parameters are unreliable. Otherwise, the optical model potentials are determined to the same accuracy as for carbon.

In figs. 3—7, the dotted lines indicate only the 10 % uncertainty in the absolute values of the experimental cross sections. There is an additional uncertainty due to the errors in the total and absorption cross-sections from which the optical model parameters were derived. Taking this into account, the figures show general agreement between the optical model calculations and Salmon's measurements. Since the experimental distributions were not used in determining the model parameters, this agreement is a significant test of the model. There is perhaps some tendency for the calculated cross-sections to be higher than the experimental. If this effect is significant, it may indicate that the optical model underestimates the scattering at large angles.

I would like to thank Professor D. H. Wilkinson, F. R. S. for suggesting this work, Dr G. Salmon for communicating and discussing his experimental results, Dr. B. Buck and Mr R. N. Maddison for their work on the computer programme, the Director of the Oxford University Computing Laboratory for the use of the computer, Miss N. Reynolds, Miss S. Tilley and the staff of the Computing Laboratory for their assistance, and the D.S.I.R. for its support.

† This was pointed out to the author by Dr. J. J. Thresher.

References

1) G. L. Salmon, Nuclear Physics **21** (1960) 15
2) P. H. Bowen, J. P. Scanlon, G. H. Stafford, J. J. Thresher and P. E. Hodgson (in preparation)
3) J. De Juren and N. Knable, Phys. Rev. **77** (1950) 606
4) R. G. P. Voss and R. Wilson, Proc. Roy. Soc. **236** (1956) 41
5) F. Bjorklund and S. Fernbach, Phys. Rev. **109** (1958) 1295; Communication to the Second International Conference on the Peaceful Uses of Atomic Energy (1958)
6) K. Strauch and F. Titus, Phys. Rev. **103** (1956) 200
7) H. Tyren and Th. A. J. Maris, Nuclear Physics **4** (1957) 637

2.E

Nuclear Physics **21** (1960) 28—32; © *North-Holland Publishing Co., Amsterdam*

Not to be reproduced by photoprint or microfilm without written permission from the publisher

THE ELASTIC SCATTERING OF HELIUM 3 BY MEDIUM WEIGHT NUCLEI

P. E. HODGSON

Clarendon Laboratory, Oxford

Received 6 July 1960

Abstract: The experimental results of Greenlees and Rowe on the elastic scattering of helium 3 by nickel, palladium, cadmium and tin are analysed by the optical model. The scattering cross-section is found to be more sensitive to the diffuseness of the nuclear surface than to the other parameters of the nuclear potential. The values found for the Saxon-Woods diffuseness factor a are: (Ni) 0.61 ± 0.02, (Pa) 0.61 ± 0.02, (Cd) 0.52 ± 0.03 and (Sn) 0.50 ± 0.02 ($\times 10^{-13}$ cm).

1. Introduction

Previous analyses of the elastic differential cross sections for the scattering of helium 3 by carbon, neon and argon [1]), and by aluminium, copper and vanadium [2]) have shown that the optical model of the interaction is able to give a good account of the observed distributions. It is therefore useful to analyse the recent data of Greenlees and Rowe [3]) on nickel, palladium, cadmium and tin in the same way.

The optical model potential used has the form

$$V = V_C(r)+(U+iW)f(r),$$

where $V_C(r)$ is the Coulomb potential, U and W the refracting and absorbing parts of the nuclear potential, and $f(r) = [1+\exp\{(r-R)/a\}]^{-1}$ is the Saxon-Woods form factor, with nuclear diffuseness a and radius $R = r_0 A^{\frac{1}{3}}$. If suitable numerical values are chosen for the parameters of the potential the corresponding Schrödinger wave equation for the interaction process may be solved to give the observable quantities by the methods described elsewhere [4]). All the calculations were carried out on the Oxford University Mercury computer.

2. Fitting Procedure and Results

The four parameters U, W, r_0 and a were systematically varied to find the minimum value of

$$\Delta_N = \sum_N \left(\frac{(d\sigma/d\Omega)_{Exp}-(d\sigma/d\Omega)_{Th}}{\delta(d\sigma/d\Omega)_{Exp}} \right)^2$$

TABLE 1

Parameters of the best fit potentials, the calculated reaction cross sections and the values of Δ_N for the N measured points. A is the normalisation constant by which the experimental distribution must be multiplied to agree with the theoretical one.

Nucleus	E_{He^3}	$-U$	$-W$	r_0	a	σ_R(mb)	N	Δ_N	A
Ni	29.1	25	23	1.6	0.61	1426	8	15	1.14 ± 0.02
Pa	28.95	20	20	1.6	0.61	1524	10	36†	1.13 ± 0.02
Cd	29.0	25	30	1.6	0.52	1455	16	193†	1.18 ± 0.02
Sn	29.0	25	15	1.6	0.50	1384	12	14	1.10 ± 0.01

† If the last experimental point for cadmium is omitted, Δ is reduced to 80, and if the third experimental point of palladium is omitted, Δ is reduced to 18.

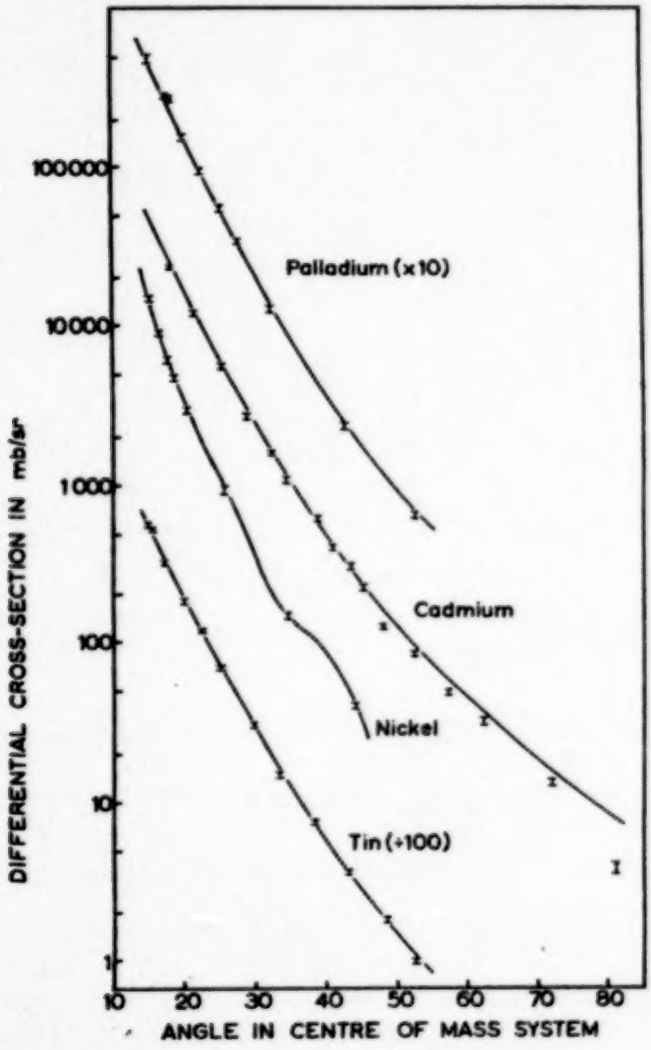

Fig. 1. Differential cross-sections for the elastic scattering of 29 MeV helium-3 by nickel, palladium, cadmium and tin compared with the best optical model curves, using the parameters given in table 1.

the summation being extended over all the experimental points. The procedure used to find the minimum was essentially the same as that used previously [5])

The best values of the potential parameters are given in table 1, and the corresponding differential cross-sections compared with the experimental results in fig. 1. On the whole the agreement is satisfactory, though in the case of cadmium Δ is rather too high. This may be due either to underestimates of the errors on the experimental points, or it may indicate an inadequacy in the model.

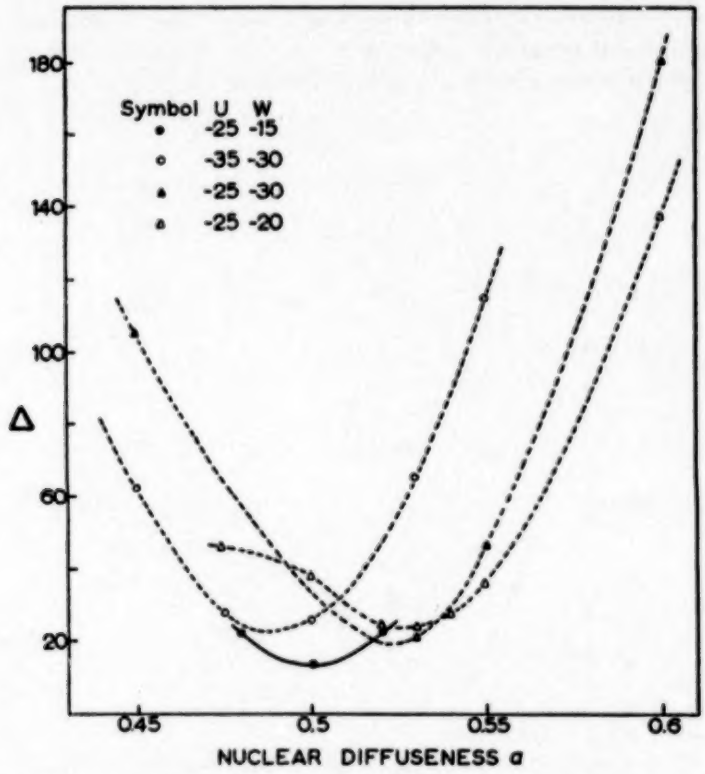

Fig. 2. Δ as a function of nuclear diffuseness for various U and W for 29 MeV helium-3 on tin.

TABLE 2

Variation of Δ with r_0 and a in the region of best fit for tin

a \ r_0	1.59	1.6	1.61
0.48		23	
0.50	17	14	17
0.52		23	

TABLE 3

Variation of Δ with U and W in the region of best fit for tin.

$-W$ \ $-U$	20	25	30
10		23	40
15		14	
20	47	18	18

After the first few calculations had been made, it was found that the experimental points all lay significantly below the calculated curves, indicating an error in the absolute normalisation of the measured cross sections. In each case

the discrepancy was comparable with the 6 % absolute uncertainty quoted by Greenlees and Rowe [3]). Since the fitting could certainly be done more accurately than this, it was decided to normalise the experimental results to the calculated curves by multiplying them by a factor A that minimises Δ for all the experimental points. This normalisation was checked by seeing that the fit was good at small angles where the Coulomb field dominates, and the scattering is insensitive to the nuclear potential. The final values of A, averaged in each case over the best four runs, are given in table 1. This method is more accurate than normalising at small angles to the Coulomb cross section alone, since increasingly accurate account is taken of the nuclear field as the fitting procedure progresses.

It was found that the calculated cross-section is much more sensitive to the diffuseness a than to the other parameters of the nuclear potential. This is shown for tin in fig. 2, where Δ is plotted as a function of a for various U and W, and in tables 2 and 3, which show the variation of Δ in the region of best fit. As a result, the analysis fixes a quite accurately as 0.50 ± 0.02, while proportionately larger uncertainties must be set on the best values of U, W and r_0. For the reasons discussed previously [5]) it is impossible to put firm limits on the best values of the parameters while the reaction cross-sections are unknown and the effects of the spin-orbit forces have not been taken into account.

3. Helium 3 as a Nuclear Probe

The sensitivity of the differential cross sections to the diffuseness of the nuclear surface has a simple physical explanation. It will be recalled from previous work [1, 2]) that the differential cross-sections for the scattering of helium 3 by light nuclei like carbon and aluminium show a pronounced diffraction pattern which becomes progressively weaker through argon and vanadium and has virtually disappeared leaving almost a simple exponential for the heavier nuclei studied in the present work. The reason for this is that the oscillations in the cross sections are due to diffraction effects in the bulk of the nucleus. In the case of helium 3 these are confined to the outer regions of the nucleus due to its low mean free path in nuclear matter. As the nuclear charge increases, the incident helium 3 nuclei are kept farther and farther away from the bulk of the nucleus by the Coulomb field until finally the diffraction effects can no longer occur. The helium 3 nuclei are then passing through only the outer regions of the nuclear field and can be used to study its radial variation. As the nuclear charge is still further increased or, alternatively, as the incident energy is reduced, the incident particle does not feel the nuclear field at all, and the scattering is pure Coulomb. There is thus an intermediate region between bulk nuclear and pure Coulomb scattering where the scattering is sensitive to the fringe of the nuclear field.

The values of the nuclear diffuseness are given in table 1, and show significant variations from nucleus to nucleus. It should be possible to interpret these in terms of nuclear structure. Thus tin and cadmium having their outer shell almost complete have smaller surface diffuseness than nickel and palladium which have less complete outer shells.

Before this work can be accepted as giving reliable knowledge of the outer nuclear surface, it is necessary to see how the measured diffuseness depends on the energy of the incident helium 3 nuclei, and to correlate it with information derived from the scattering of other particles by a range of nuclei. It would also be interesting to obtain independent information on the diffuseness from the spacing of the higher excited states of nuclei, as suggested by Beard [6]).

I would like to thank Professor D. H. Wilkinson, F.R.S., and Professor W. E. Burcham, F.R.S. for valuable discussions, Dr G. W. Greenlees and Mr P. C. Rowe for communicating their experimental results prior to publication, the Director of the Oxford University Computing Laboratory for the use of the Ferranti Mercury Computer, Dr. B. Buck and Mr R. N. Maddison for their work on the computer programme, Miss N. Reynolds, Miss S. Tilley and the Staff of the Computing Laboratory for their assistance, and the D.S.I.R. for its support.

References

1) J. Aguilar, W. E. Burcham, J. B. A. England, P. E. Hodgson, P. V. March, J. S. C. McKee E. M. Mosinger, A. Garcia and W. T. Toner, Proc. Roy. Soc. A **257** (1960) 13
2) J. S. Lilley, P. C. Rowe and P. E. Hodgson (in preparation)
3) G. W. Greenlees and P. C. Rowe, Nuclear Physics **15** (1960) 687
4) B. Buck, R. N. Maddison and P. E. Hodgson, Phil. Mag. (in the press)
5) P. E. Hodgson, J. Aquilar, A. Garcia and J. B. A. England, Nuclear Physics (in the press)
6) D. B. Beard, Phys. Rev. Letters **3** (1960) 432

2.B

Nuclear Physics **20** (1960) 33—37; © *North-Holland Publishing Co., Amsterdam*

Not to be reproduced by photoprint or microfilm without written permission from the publisher

ANGULAR CORRELATION IN $C^{12}(n, n'\gamma)C^{12}$ AT 14 MeV

G. DECONNINCK † and A. MARTEGANI

Centre de Physique Nucléaire de Louvain, Belgium

Received 18 July 1960

Abstract: A method is developed for measuring angular correlation in inelastic scattering of 14 MeV neutrons. Random coincidences are practically suppressed by combining time of flight and fast coincidences techniques. Angular correlation has been measured on the first excited state of C^{12} and the results are in good agreement with Banarjee and Levinson's calculations based on the distorted wave method.

1. Introduction

In recent years it has been found that the statistical theory of nuclear reactions failed to explain angular distributions in inelastic processes such as (p, p'), (α, α') and (n, p) . . . The same conclusion must hold in the case of (n, n') processes but experimental data are practically absent because of the poor efficiency and the lack of resolution of neutron detectors.

The direct interaction theory which is a more realistic picture of these reactions may be tested in two different ways: one can measure the angular distribution and the angular correlation between the products of the reaction.

In previous work [7]) we have extended in the forward direction the measurements of Anderson *et al.* [1]) on the angular distribution in $C^{12}(n, n')C^{12\alpha}(E_\gamma = -4.43$ MeV); in the present work we give results on the correlation between the inelastically scattered neutron and the de-excitation γ-ray.

2. Experimental Arrangement

In this experiment the background plays a dominant role and must be eliminated as completely as possible. This is possible by simultaneous detection of three particles the α-particle of the T(d, n)α reaction, the inelastically scattered neutron and the γ-ray.

The circuits consist of a time of flight based on the associated particle method and a fast coincidence between the neutron and the γ-ray.

This circuit has been described previously [2]). The resolution of the time of flight circuit was 2×10^{-9} sec but in this experiment the dimensions of the neutron detector are considerably larger (9 cm long) and the resolution was reduced to 3.5×10^{-9} sec.

† Chercheur agréé de l'I.I.S.N.

The γ rays are detected in a 10.2 cm $\times$ 10.2 cm NaI coupled to an RCA 6 810 A photomultiplier by a conical lucite guide. The resolution was measured with (n, γ) coincidences of a PoBe source and found to be 4.5×10^{-9} sec. The PoBe source is very convenient, because it gives γ-rays of the same energy as the $C^{12}(n, n')C^{12}$ reaction.

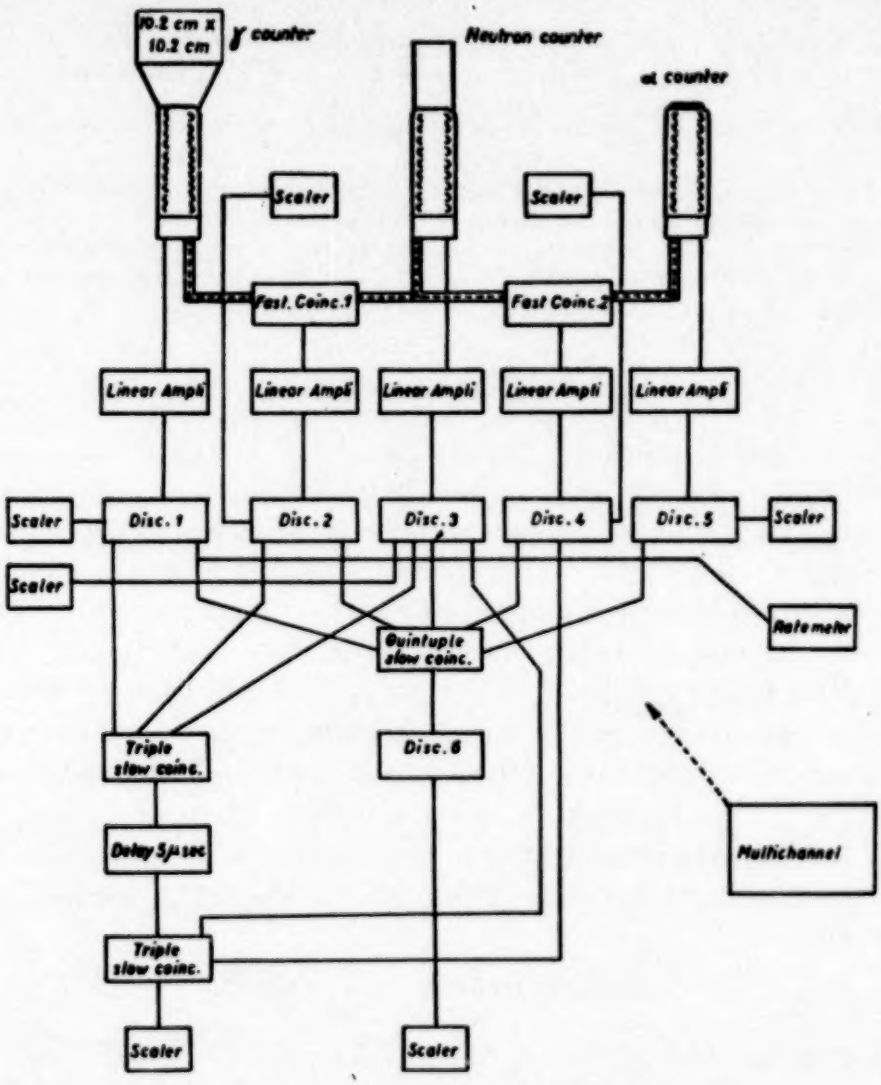

Fig. 1. Block diagram of the electronics.

Because of the high efficiency of NaI for 14 MeV neutrons, special care must be taken in the γ-ray chain, to avoid pile up effects and fluctuations in the dynode voltage. The cathode voltage was fixed at -1750 V, which is the minimum required to obtain normalisation of the anode pulses due to the 4.43 γ-ray photopeak and pair production. A second EHT supply fixed at -950 V fed the 10^{th} dynode in order to maintain constant voltage at this point when the counting rate varies. Moreover, to eliminate this variation and avoid fluctuations

in the pile up, the cadence of the Van der Graaff was regulated to maintain fixed the counting rate in the γ chain.

Fig. 1 shows a block diagram of the electronics. The two fast coincidence circuits are completed by slow channels. In the γ channel, the pulses from the 12th dynode are amplified, and the discriminator 1 accepts pulses from the peak of pair production and photoeffect of the 4.43 MeV γ rays (PoBe source).

The discriminator 3 in the neutron chain was varied for the two experimental methods we used. In the α chain all the pulses are normalised and discriminator 5 adjustment is not critical. The coincidence pulses are also discriminated and the five signals coming from the different chains are taken in coincidence (10^{-5} sec).

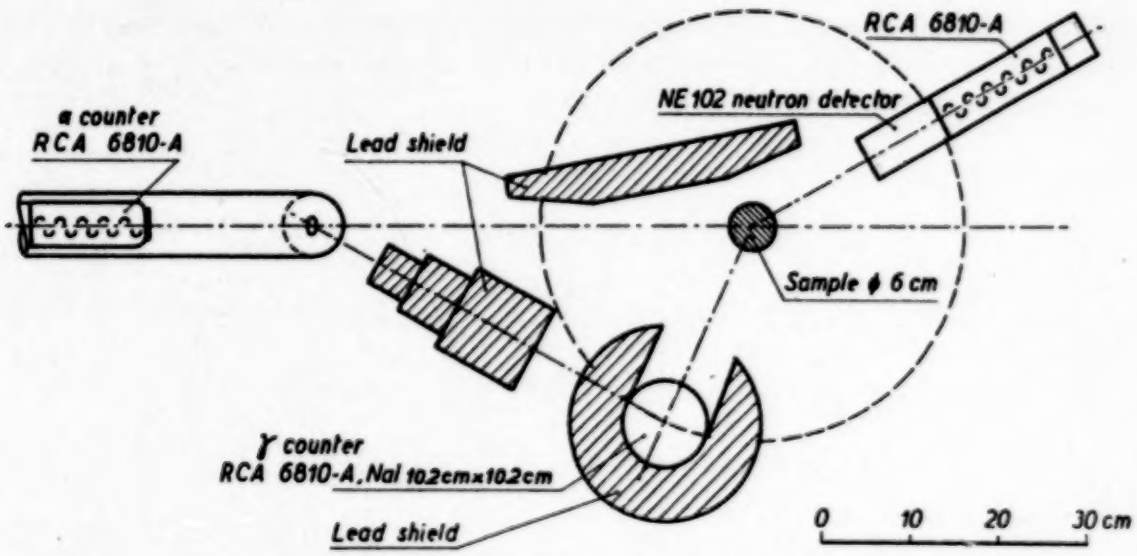

Fig. 2. Geometry of the experimental arrangement.

We should make some remarks about the counting rates: when gated by its two side channels, the (n, γ) coincidence gives one count for 2 sec and the (n, α) coincidence a maximum of three counts per sec.

Owing to the resolution time of the multiple coincidence we obtain about 1 random coincidence per 10 hours and this is quite negligible. A delayed coincidence system has been utilised to measure random coincidences by delaying the (n, γ) events and taking the triple coincidences with the (n, α) events (fig. 1).

The geometry is shown in fig. 2. The sample is a high density pure graphite cylinder (6 cm diam, 7 cm high). The NaI, shielded by lead, is vertically positioned so that it can rotate between 40° and 140° in the incident direction of neutrons. The mean flight path of the neutrons before detection is about 20 cm and this corresponds to a time of flight of 5×10^{-9} sec for 10 MeV neutrons. For a γ ray this time is 0.7 msec, so that the difference in the times of flight is

about 4×10^{-9} sec. It is thus possible to discriminate (n, γ) events and (γ, n) events by time of flight but this method (referred as 1st method) is very sensitive to a jitter of discriminator 4.

A more stable but less efficient method consists of eliminating the γ-ray detection by setting the level of disc. 3 to a higher position (2nd method).

In the two cases the possibility of detecting (n, γ) coincidences due to other levels than the first is negligible. These levels are known to decay mostly by 3α disintegrations [3]).

3. Method of Measurement and Results

The measurements were monitored with an anthracene counter biased to an energy of 3 MeV in order to eliminate the D(d, n) neutrons. We took measurements at intervals of 5 min with and without sample; the different positions were randomly alternated.

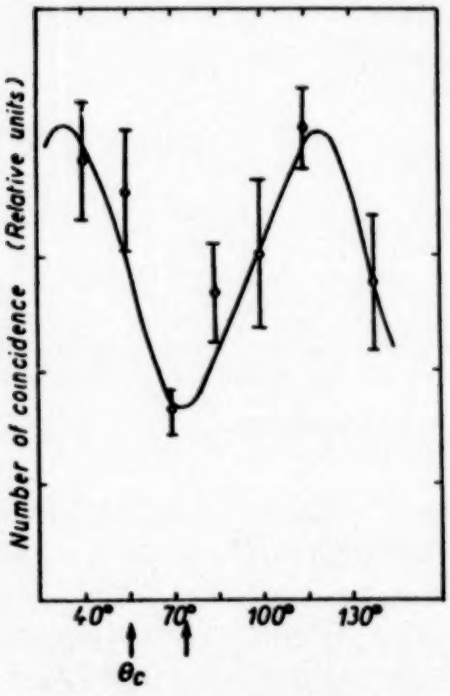

Fig. 3. Angular correlation of the $C^{13}(n, n'\gamma)C^{13}$ reaction (1st method).

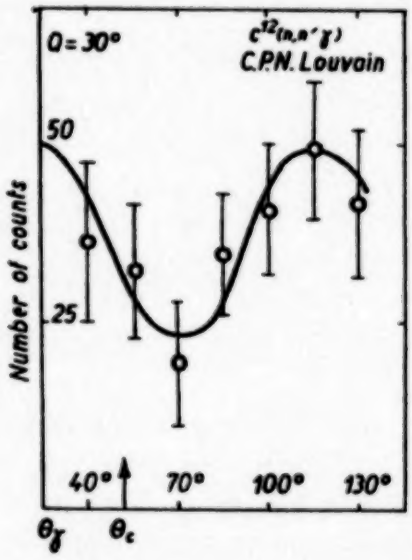

Fig. 4. Angular correlation of the $C^{13}(n, n'\gamma)C^{13}$ reaction (2nd method).

The angle of the neutron detector was fixed to 30°, where the cross section for inelastic scattering is 40 mb/sr.

We first used the first method, which is subject to important fluctuations as we said above. The γ counter was placed at 7 different angles: 40°, 55°, 70°, 85°, 100°, 115° and 140°; the results are given in fig. 3.

In the second method the γ's were detected at the same positions, except for

the 140° position which was replaced by 130°. Fig. 4 shows the results. In this method the stability was very good.

Random coincidences were also detected at the rate of one per day as calculated before.

Moreover, in each measurement we detected about 1 800 elastically scattered neutrons. Taking into account the efficiency of the detectors and the solid angles, we calculated the mean number of coincidences to be about 2 per measurement, corresponding exactly to our results.

4. Conclusions

The analysis of the two curves shows that the shape is exactly the same and that the law $A+B\sin^2 2(\theta_\gamma-\theta_0)$ first predicted by Satchler [4]) is borne out, although the classical recoil angle is 52° and the minimum of our two curves occurs at about 70°. This corresponds to the shift of the recoil axis predicted by Banarjee and Levinson [5]), on the basis of distorted wave method. No attempt can be made to calculate the ratio A/B because the curve is smoothed out by the finite resolution (about 45°) and multiple scattering events in the sample which is one mean free path in length. These results may be compared with those of Sherr and Hornyak on inelastic scattering of 16 MeV protons on C^{12}.

The same experiment of (n, n'γ) angular correlation measurement could be made on a nucleus where the second excited level is well separated from the first (several MeV), as in Li^7 for example.

We are very indebted to Professor M. de Hemptinne for his continued interest in this experiment and to Dr. Macq for helpful discussions of the practical and theoretical aspects of the work. We wish to thank the I.I.S.N. for financial support of this work.

References

1) Anderson, Gardner, McClure, Nakada and Wong, Phys. Rev. **111** (1958) 572
2) Deconninck et Martegani, Ann. Soc. Scient. de Bruxelles **73** No II (1959) 287
3) Singletary and Wood, Phys. Rev. **114** (1959) 1595
4) Satchler, Proc. Phys. Soc. B **68** (1955) 1037
5) Banarjee and Levinson, Ann. Phys. **2** (1957) 499
6) Sherr and Hornyak, Bull. Am. Phys. Soc. **1** (1956) 197
7) Deconninck and Martegani, IISN Groupe de travail des accélerateurs, Réunion du 25 Mai 1960 (to be published)

2.B:2.E

Nuclear Physics **21** (1960) 38—42; © *North-Holland Publishing Co., Amsterdam*

Not to be reproduced by photoprint or microfilm without written permission from the publisher

ELASTIC SCATTERING OF 13 MeV DEUTERONS ON ALUMINIUM

N. CINDRO, M. CERINEO

Institute "Ruđer Bošković", Zagreb, Yugoslavia

and

A. STRZALKOWSKI

Institute for Nuclear Research, Cracow 23, Poland

Received 12 July 1960

Abstract: The angular distribution of 13 MeV deuterons scattered elastically on aluminium was measured by means of the thin scintillation crystal technique. Although not so prominent as at 15 MeV the increase of the differential cross section at backward angles was also observed at the deuteron energy of 13 MeV. The reason for back angles maxima in elastic scattering has not been elucidated so far.

1. Introduction

The elastic scattering of 15 MeV deuterons on a number of elements has been studied by Gove, Wall and Darden, and Cindro and Wall [1]). While the angular distribution of scattered deuterons on all elements investigated showed the usual Rutherford scattering modified by a diffraction-like effect due to nuclear

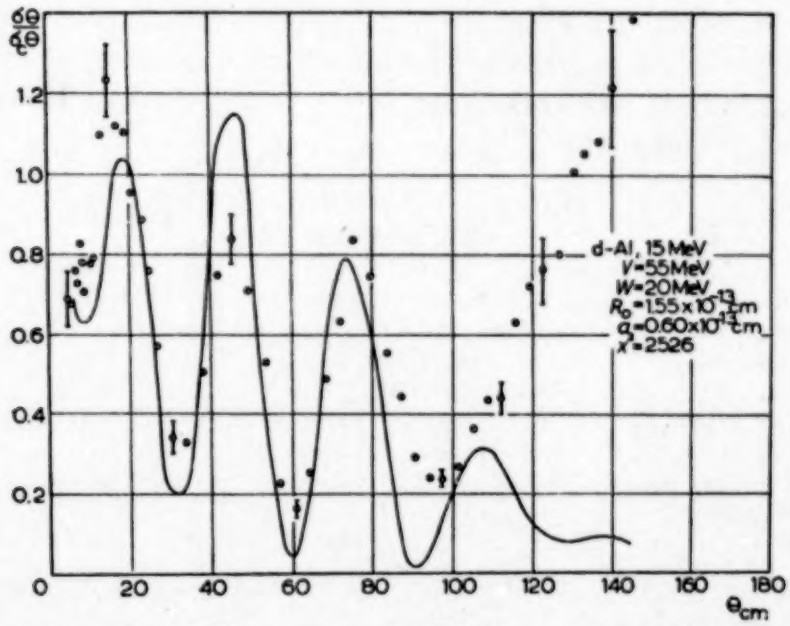

Fig. 1. Ratio of differential cross sections versus Coulomb cross sections for elastic scattering of 15 MeV deuterons on Al. The theoretical curve is an attempted fit with the optical model using the Saxon potential [8]).

scattering [1, 2, 3]), the results on Al were somewhat different. The most interesting feature of the scattering on Al was a steady increase of the differential cross-section at backward angles, especially prominently shown relative to the Rutherford scattering (fig. 1). The reason for such an exceptional behaviour has not been elucidated so far. In order to throw some more light on this problem, the authors have investigated the elastic scattering of deuterons of 13 MeV energy on aluminium.

2. Experimental Arrangement

The 13 MeV deuteron beam of the 120 cm cyclotron of the Centre of Nuclear Physics in Kraków was focused on a 2 mg/cm² Al target. Although the position

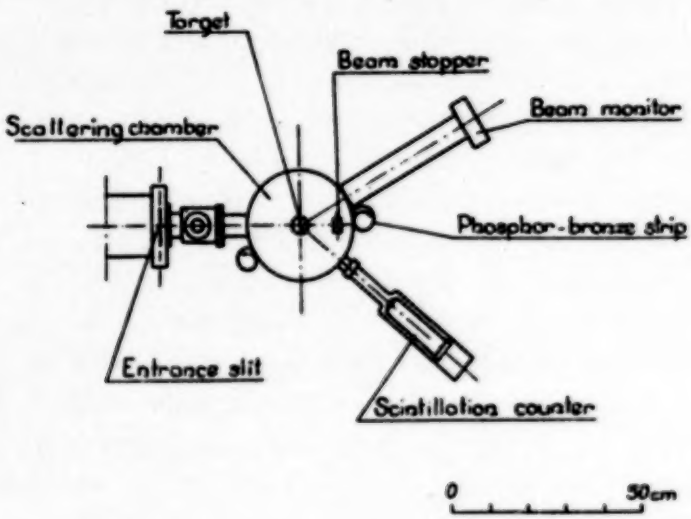

Fig. 2. Experimental arrangement and scattering chamber.

of the beam spot, about 7 mm in diameter, was not always central, the hitting of the frame was avoided by making the target 25 × 25 mm in dimensions. The detection of particles was performed by means of a thin CsI(Tl) crystal scintillation counter placed at a distance of 300 mm from the target on an arm rotating around the axis of the target. The continuous changing of scattering angles was secured by a phosphor-bronze strip which adhered vacuum tightly to the side wall of the scattering chamber, the counter holding arm being mounted on this strip (fig. 2). Two different Al diaphragms 0.5 and 1.5 mm in diameter were placed in front of the crystal in order to regulate the beam intensity which could not be decreased below 0.05 μA having a constant value. The pulses from an EMI 6097 B photomultiplier were fed through standard equipment to a 100-channel amplitude analyser.

The discrimination between elastically scattered deuterons and protons from Al^{27}(d, p) reactions, especially numerous at large angles, was performed by

choosing different thicknesses of CsI(Tl) crystals, ranging from 243 to 177 mg/cm^2, for different angular regions. The respective crystal thickness was always chosen to be exactly sufficient to stop the elastically scattered deuterons, the particles of higher energy being thus discriminated because of their lower specific ionization in passing through the crystal and accordingly lower light output. At all angles the (d, p) protons gave approximately 30 % less energy than the deuterons and could be more or less easily discriminated from them. Possible admixtures of scattered deuterons leaving Al^{27} nuclei in the 1st excited state, could not be completely excluded, especially in the back angle region. A typical energy spacing between the ground and 1st excited state deuterons at 120° laboratory angle for Al^{27} was 0.8 MeV (10.3 and 9.5 MeV respectively) which amounts to about 8 % of the energy of the ground state peak. With the total resolution of the apparatus being about 8 %, the distinction between the ground state and 1st excited state deuteron peaks could not be accomplished in a completely satisfactory way. Admixtures of inelastically scattered deuterons may therefore amount to about 5—15 % of the measured cross section in the region from 100° to 145°.

The absolute cross section measurements were made by means of the beam integrator. From previous measurements [1, 2]) it was known that the cross section for 13.5 MeV deuterons elastically scattered on Au is purely Rutherford up to scattering angles of about 40°. The performance of the integrator was checked by comparing the absolute cross section for Au(d, d) from 25° to 40° using the integrator data with the calculated cross-section. It has been found that the integrator was reliable to better than 5 %. Several runs of measurements of Au(d, d)Au scattering were included in the absolute cross section estimations.

Another scintillation counter was placed additionally as a beam monitor at a fixed angle of 30° with respect to the incident beam and the pulses were biased in such a way that only elastically scattered deuterons and highest energy protons from Al(d, p) reactions were counted by a scaler. There has always been a reasonable agreement (within 5—10 %) between the two ways of monitoring the beam.

3. Results and Discussion

The results for elastic scattering of 13 MeV deuterons on Al^{27} are given in fig. 3. The cross sections are given as ratios to the Rutherford cross section. The errors shown are only statistical ones.

The total errors in the cross section are due to statistics, to the monitoring of the beam, to angle setting, to the incomplete separation of elastically scattered deuterons from the proton edge, especially at large angles, and to a certain amount of inelastically scattered deuterons mixed in the elastic peak. The statistical errors were always smaller than 10 %. The monitoring errors being of

the order of some 5 % were presumably ruled out by performing several runs at each angle. The angle setting were accurate to $\pm 0.5°$. The error due to the incomplete separation of the elastic peak is rather difficult to evaluate for each point. Sampling of several points at a number of different angles showed that an additional error of up to about 10 % could be added to the statistical one.

The general feature of the angular distribution at 13 MeV is similar to that for elastic scattering of 15 MeV deuterons on Al given on fig. 1. A diffraction-like pattern is visible at angles up to 90°, while the rise at backward angles is not so pronounced as at 15 MeV. The diffractional character of the first three peaks is witnessed by the shift of their position at 13 MeV as compared to 15 MeV.

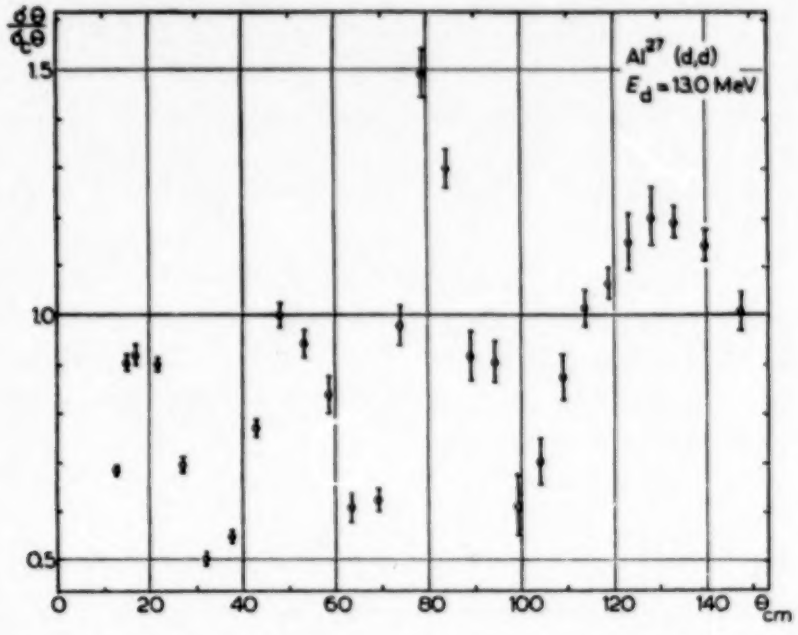

Fig. 3. Ratio of differential cross sections versus Coulomb cross sections for elastic scattering of 13 MeV deuterons on Al.

According to the simple diffraction theory of elastic scattering, the angular distribution is governed by the variable

$$x = 2kR \sin \tfrac{1}{2}\theta,$$

where k is the wave number of the incident particle, R the radius of the scattering nucleus and θ the scattering angle. Larger scattering angles θ are required for the 13 MeV case in order to obtain the same values of x.

The problem of the back angle maxima in elastic scattering is a long standing problem. The fact that elastic scattering of deuterons on Al at 13 MeV reproduces the general features of the scattering at 15 MeV, shows that the reason for the anomalously high back-angle cross sections is probably not the hitting of a broad resonant level of the compound nucleus Si^{29} (compound elastic scattering). The effect is rather inherent in the process, because it is visible also [4, 5]) in the

elastic scattering of 7.5 and 10 MeV protons on Al. From both the data at 15 and 13 MeV, it is, however, not possible to ascertain without any doubt whether the increase in the ratio of the measured cross-section to the Rutherford one at angles from about $\theta = 100°$ to $\theta = 145°$ is only the rising side of a broad peak or it goes on steadily to 180°.

The analysis of 15 MeV data with the Saxon type optical potential [6]) has shown that a potential with the following parameters:

$$V = 55\,\text{MeV}, \quad W = 20\,\text{MeV}, \quad R_0 = 1.55\times10^{-13}\,\text{cm}, \quad a = 0.60\times10^{-13}\,\text{cm},$$

is able (fig. 1) to reproduce more or less correctly the angular region up to 90°, while it fails completely to reproduce the backward angle region. Although the optical model analysis has not been attempted at 13 MeV, it is conceivable that a similar result would be obtained also at this energy. It seems therefore that a mechanism different than the optical diffraction and absorption might be necessary to explain the backward part of the angular distribution of deuterons elastically scattered on Al.

The authors wish to thank Professor H. Niewodniczański for his support and encouragement. We are indebted to the Cyclotron Operation Staff for running the cyclotron. Two of the authors (N. C. and M. C.) express their gratitude to both the Polish and Yugoslav Atomic Energy Authorities for enabling them to stay in the Cracow Centre of Nuclear Physics and perform the experiments.

References

1) H. E. Gove, Phys. Rev. **99** (1955) 1353;
N. S. Wall and C. W. Darden (private communication);
N. Cindro and N. S. Wall (to be published)
2) J. R. Rees and M. B. Sampson, Phys. Rev. **108** (1957) 1289
3) J. L. Yntema, Phys. Rev. **113** (1959) 261
4) W. Waldorf, Thesis, MIT (1957)
5) N. M. Hintz, Phys. Rev. **106** (1957) 1201;
A. E. Glassgold, W. B. Cheston, M. L. Stein, S. B. Schuldt and G. W. Erickson, Phys. Rev. **106** (1957) 1207
6) M. A. Melkanoff and N. Cindro (to be published)

3.A

Nuclear Physics **21** (1960) 43—48; © *North-Holland Publishing Co., Amsterdam*

Not to be reproduced by photoprint or microfilm without written permission from the publisher

GAMMA RADIATIONS FROM EXCITED STATES OF Ne^{20}

T. A. RABSON, W. D. BARFIELD, D. L. BERNARD, T. W. BONNER and W. W. GIVENS

The Rice University, Houston, Texas †

Received 29 July 1960

Abstract: Gamma radiations from excited states of Ne^{20} have been measured with a lens type pair spectrometer. The nuclear reactions which have been used are F^{19}(d, n)Ne^{20} and Na^{23}(p, α) Ne^{20}. Gamma radiation with Doppler corrected energies of 7.26, 8.26, 9.22, 9.98, 10.59 and 11.31 MeV has been attributed to Ne^{20}. The 8.26 MeV and 10.59 MeV γ-rays are believed to be due to cascades: 9.98 → 1.63 and 12.22 → 1.63, and the remainder are due to ground state transitions. Gamma radiation was also observed with an energy of 6.67 MeV which is attributed to F^{20}, and a γ-ray with an energy of 6.17 MeV was observed and attributed to O^{16}. A search was made for nuclear pairs from a 0^+ excited state of Ne^{20} at 4.25 or 4.97 MeV using the Na^{23}(p, α)Ne^{20} reaction. No nuclear pairs were observed which indicates that the 4.25 MeV state is not 0^+.

1. Introduction

Measurements of the γ radiations from the deuteron bombardment of F^{19} were carried out in 1951, by Terrell and Phillips [1]) with a pair spectrometer with a resolution of 10 %. Deuterons with an energy of 1.56 MeV were used in this experiment. Other measurements have been reported (1955) by Bent, Bonner, McCrary, Ranken and Sippel [2]) with a lens type pair-spectrometer with a resolution of 3.6 % and with deuterons with an energy of 3.6 MeV. The second experiment was limited to γ radiations with energies over 9 MeV. The present experiments were undertaken to obtain better information about the high energy γ radiations by substituting the intermediate-image geometry for the ring-focus geometry which was previously used. The γ spectra were also carried to lower energies by an improved technique in absorbing the high energy beta rays from F^{20} which is produced in the reaction F^{19}(d, p)F^{20}.

2. Experimental Arrangement

The earlier experiments with the lens spectrometer [1, 2]) did not make use of the internal pair spectrum as is customary because of the strong beta particle background from F^{20}. Those experiments were carried out by placing an aluminium absorber that was 5 mm thick between the target and a 77 mg/cm² lead converter. This aluminium absorber was of sufficient thickness to reduce

† Work supported in part by the U. S. Atomic Energy Commission.

the beta particle energies so that γ radiation with energies above 9 MeV could be observed. The present experiments made use of improved absorbers of the beta particles. The absorbers were an industrial diamond and a synthetic sapphire each 2.2 mm thick, which were placed between the target and a lead radiator with a mass of 79 mg/cm^2. A portion of the results was obtained with the diamond absorber alone. Diamond (density 3.5 g/cm^3) was selected as the best absorber of electrons per unit thickness, obtainable in the light elements; heavier elements would produce a significant number of pairs in the thick absorber and so limit the sensitivity of the spectrometer to detect weak γ radiations.

The target used in these experiments was made by evaporating 10 mg/cm^2 of CaF_2 on a 26 mg/cm^2 silver foil. The first experiments were carried out with 3.6 MeV deuterons and the diamond absorber. Under these conditions good data were obtained with 3 % energy resolution for γ radiation of 7.9 to 12.5 MeV. The second experiment was carried out with both the diamond and sapphire absorbers and results were obtained as low as 5.8 MeV. With this geometry data were not obtained in the interval 8.8 to 10.5 MeV which had already been adequately covered in the first experiment. A third experiment was carried out with 1.8 MeV deuterons to investigate the possibilities of γ ray cascading in Ne^{20} and to differentiate between reactions, other than the F^{19}(d, n)Ne^{20} reaction, which have different Q values.

An energy calibration of the apparatus was made by observing the 6.14 MeV γ radiation from the reaction F^{19}(p, α)O^{16}. The calibration was accomplished by changing the bombarding beam to protons on the same target.

A fourth experiment was carried out to search for γ radiation or internal pairs from the 4.25 and 4.97 MeV levels in Ne^{20}. A NaI target of 15 mg/cm^2 on a 28 mg/cm^2 gold backing was bombarded with 4.8 MeV protons; excited states of Ne^{20} were populated by the Na^{23}(p, α)Ne^{20} reaction.

3. Results and Discussion

The results of the first two experiments are given in figs. 1 and 2. A compilation of the γ ray energies and the relative intensities is given in table 1. Eight γ rays with uncorrected energies of 6.17, 6.70, 7.29, 8.30, 9.26, 10.02, 10.63 and 11.36 MeV were observed.

The following reactions are energetically possible when F^{19} is bombarded with deuterons:

$$F^{19}(d, n)Ne^{20} \quad \text{with} \quad Q = 10.65 \text{ MeV},$$

$$F^{19}(d, p)F^{20} \quad \text{with} \quad Q = 4.38 \text{ MeV},$$

$$F^{19}(d, \alpha)O^{17} \quad \text{with} \quad Q = 10.04 \text{ MeV}.$$

The Q value of the second reaction is such that only states below 7.7 MeV may be formed. States above 4.2 MeV of excitation in O^{17} can break up by neutron emission and would give weak γ emission above this level. States in Ne^{20}

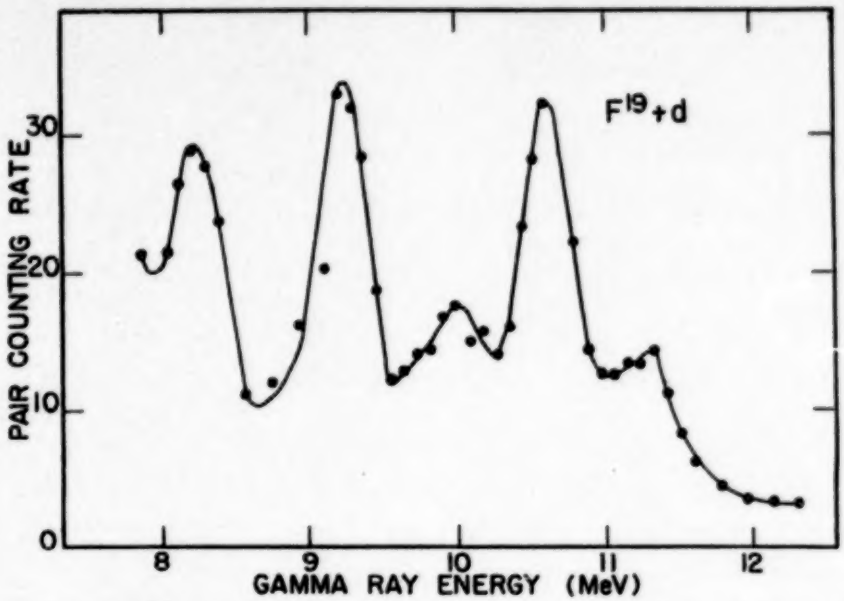

Fig. 1. External pair spectrum from bombarding a 10 mg/cm² CaF_2 target with 3.6 MeV deuterons using a 2.2 mm diamond absorber and a 70 mg/cm² lead converter.

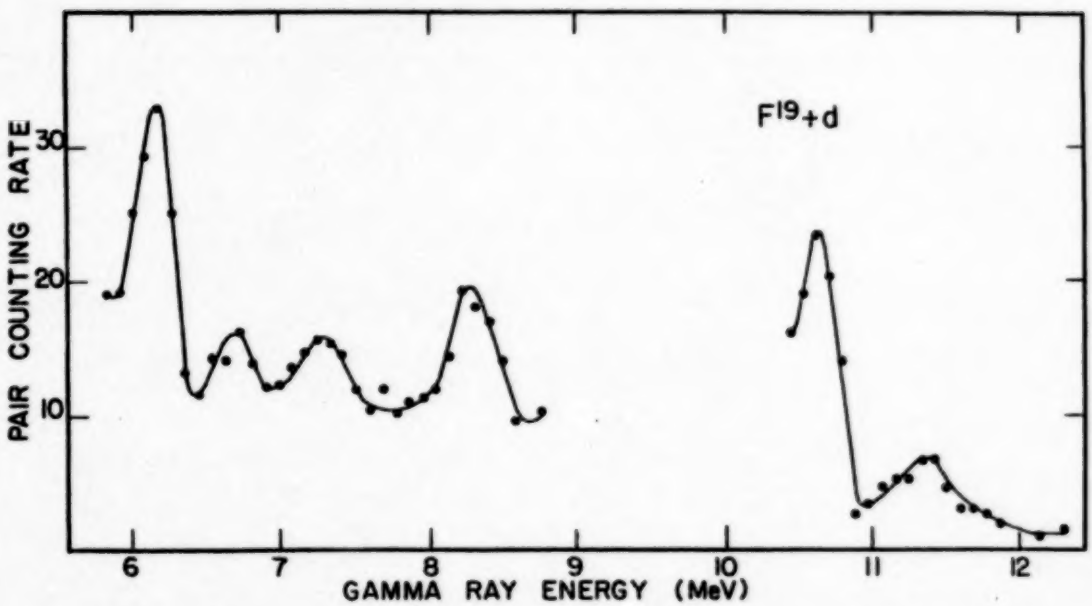

Fig. 2. External pair spectrum from bombarding a 10 mg/cm² CaF_2 target with 3.6 MeV deuterons using a 2.2 mm diamond absorber, a 2.2 mm sapphire absorber and a 79 mg/cm² lead converter.

above about 6 MeV in excitation have a high probability of breaking up by α particle emission to the ground state of O^{16} if they have even spin and parity or odd spin and parity. Higher excited states may break up by α particle emission

TABLE 1

Gamma radiation from $F^{19}+d$

Observed energy (MeV)	Doppler corrected energy (MeV)	Relative yield	Assignment	
6.17±0.05		100	O^{16}	6.14 → 0
6.70±0.07	6.67±0.07	29	F^{20}	6.63 → 0
7.29±0.07	7.26±0.07	27	Ne^{20}	7.26 → 0
8.30±0.05	8.26±0.05	33	Ne^{20}	9.98 → 1.63
9.26±0.05	9.22±0.05	38	Ne^{20}	9.22 → 0
10.02±0.10	9.98±0.10	12	Ne^{20}	9.98 → 0
10.63±0.07	10.59±0.07	32	Ne^{20}	12.22 → 1.63
11.36±0.10	11.31±0.10	11	Ne^{20}	11.31 → 0

to the first excited state (0^+) or the second excited state of O^{16}, a 3^- state. States of Ne^{20} with $T = 1$ are inhibited from decaying by α emission to the 3^- state which is energetically possible for excited states above 10.89 MeV. This isobaric spin selection rule together with the small α particle barrier penetration would allow decay predominantly by γ emission from states as high as 12.2 MeV.

TABLE 2

Energy levels observed in Ne^{20}

$O^{16}(\alpha, \alpha')O^{16}$ Energy (MeV)	$Ne^{20}(p, p')Ne^{20}$ Energy (MeV)	$Na^{23}(p, \alpha)Ne^{20}$ Energy (MeV)	$F^{19}(d, n)Ne^{20}$ Energy (MeV)	Present experiment Energy (MeV)
	1.63*	1.635*	1.5	
	4.26*	4.248*	4.2	
	4.97*	4.969*		
	5.63	5.631	5.4	
6.738(0)				
7.182(3^-)				
7.218(0)				
7.450(2)				
7.861(2)			7.3	7.26*(1^+, 2^-)
8.7 (0)				
8.748(1^-)				
8.8 (2)				
8.898(1)				
9.092(4)				
9.172(3^-)	9.2		9.0	9.22*(1^+, 2^-)
9.570(2)				
10.1 (1^-)	10.0		10.1	9.98*(1^+)
				11.31*(1^+, 2^-)
				12.22*(3^+)

* Gamma radiation has been observed from these states.

Table 2 lists the levels observed in Ne^{20} by α scattering from O^{16} [3, 4, 5]), by inelastic proton scattering from Ne^{20} [6]), by the reaction $Na^{23}(p, \alpha)Ne^{20}$ [7]), and by the reaction $F^{19}(d, n)Ne^{20}$ [8]). The energies given by Schrank and O'Neill are for identification only. The γ rays indicated are those observed in the present work and those reported by Kruse, Bent and Lidofsky [9]) from the reactions $F^{19}(d, n)$ and $Na^{23}(p, \alpha)$. The states that are observed by α particle scattering will emit γ rays with negligible intensity because of their much more probable break up by α emission.

The 11.31 MeV γ ray is most likely from a ground state transition in Ne^{20} because it was also seen at 1.56 MeV bombarding energy by Terrell and Phillips [1]). This is energetically impossible if it is a cascade between a 12.90 MeV state and the 1.63 MeV first excited state of Ne^{20}. The 10.59 MeV transition is undoubtedly a cascade from a state at 12.22 MeV in Ne^{20} to the 1.63 MeV first excited state since it disappears at a deuteron energy of 1.8 MeV. The 9.98 and 9.22 MeV transitions are probably from states in Ne^{20} reported at 9.0 and 10.1 MeV by Bonner [8]) from measurements of the neutron groups from the $F^{19}(d, n)Ne^{20}$ reactions. The 8.26 MeV radiation is probably from a cascade between the 9.98 MeV state and the 1.63 MeV state in Ne^{20}. The 7.26 MeV transition is probably the ground state transition from the level reported at about 7.3 MeV [8]). The 6.67 MeV transition is most likely from F^{20} because there is no energy difference between known states in Ne^{20} of this energy, and a 6.63 MeV γ has been observed from F^{20} [10]) as the strongest capture γ ray from the reaction $F^{19}(n, \gamma)F^{20}$. This γ ray could not possibly be from the 6.74 MeV state in Ne^{20} observed by α particle scattering [3]) because it would break up by α emission. There are no known states around 6.17 MeV in Ne^{20} or states whose cascade would give 6.17 MeV radiation. It is probable that this γ ray is from the second excited state of O^{16} at 6.14 MeV formed by α emission to this state from a highly excited state of Ne^{20}. This γ ray energy should not be Doppler corrected in this case since the state has a life time of 1.2×10^{-11} sec. Further weight is given to the argument that the 6.70 and 6.17 MeV γ radiations are from other nuclei than Ne^{20} by the fact that when the deuteron energy was reduced from 3.6 to 1.8 MeV the total γ radiation as measured by a geiger monitor and the singles register dropped by a factor of six while the 6.17 MeV γ radiation dropped by a factor of 50 or more and the 6.70 MeV radiation by a factor of at least 20. These facts indicate that the effective threshold for making these γ rays is above 1.8 MeV.

The 9.98 MeV state is probably a 1^+, $T = 1$ state or a $T = 0$ state with $J = 1^+$ or 2^-. A cascade between this state and the 1.63 MeV first excited state also would be expected. This transition was observed to have an energy of 8.26 MeV. The most probable assignment of the 12.22 MeV state is 3^+ with isobaric spin $T = 1$. It is probably the $T = 1$ analog of one of the states in F^{20} at 1.97, 2.05 and 2.20 MeV. The 11.31 MeV state must be 1^+ or 2^- in order to

explain its high probability of decay to the ground state. It would have to be a $T = 0$ state if it were 2^- in order for it not to decay principally by an E1 cascade to the first excited state. If it were 1^+ it could be the $T = 1$ analog of either of the excited states in F^{20} at 0.65, 0.83 or 0.99 MeV which have been reported [11]) to have even parity and a spin of 1, 2 or 3. A weak cascade between the 11.31 MeV state and the 1.63 MeV state would be difficult to distinguish from the observed γ ray of 9.98 MeV attributed to a ground state transition. The 9.22 and 7.26 MeV states by the preceding arguments would also be 1^+ or 2^- levels in order not to decay by α emission and to decay by γ emission to the ground state.

The experiment carried out with the reaction $Na^{23}(p, \alpha)Ne^{20}$ failed to detect γ ray peaks at 4.25 or 4.97 MeV. This experiment was quite sensitive to detecting nuclear pairs from a 0^+ state in Ne^{20}. The Q value of the (p, α) reaction is 2.38 MeV and at the bombarding energy that was used a decreasing probability of populating the higher levels is expected because of the reduced barrier penetration of the lower energy α particles. If the 4.25 MeV state is a 0^+ level, the nuclear pair peak of this energy should be easily observable because of the thousand times greater probability of observing nuclear pairs than internal pairs. The height of such a nuclear pair peak was calculated in terms of the height of the 2.62 MeV γ peak and the branching ratios based on an E2 transition. This predicted peak is 100 times as great as the smallest observable effect and so it seems very likely that the 4.25 MeV level is not a 0^+ state. No peak was observed at 4.97 MeV; however, there was no way to know the relative population of this state in our experiment.

References

1) J. Terrell and G. C. Phillips, Phys. Rev. **83** (1951) 703
2) Bent, Bonner, McCrary, Ranken and Sippel, Phys. Rev. **99** (1955) 710
3) J. R. Cameron, Phys. Rev. **90** (1953) 839
4) A. J. Ferguson and L. R. Walker, Phys. Rev. **58** (1940) 666
5) McDermott, Jones, Smotrich and Benenson, Phys. Rev. **118** (1960) 175
6) G. Schrank and G. K. O'Neill, Bull. Am. Phys. Soc. **1** (1956) 29
7) W. W. Buechner and A. Sperduto, Phys. Rev. **106** (1957) 1008
8) T. W. Bonner, Proc. Roy. Soc. A **174** (1940) 339
9) Kruse, Bent and Lidofsky, Bull. Am. Phys. Soc. **2** (1957) 351
10) Kinsey, Bartholomew and Walker, Phys. Rev. **83** (1951) 519
11) Bromley, Bruner and Fulbright, Phys. Rev. **89** (1953) 396

2.G

Nuclear Physics **21** (1960) 49—54; © *North-Holland Publishing Co., Amsterdam*

Not to be reproduced by photoprint or microfilm without written premission from the publisher

STRIPPING ANALYSIS OF THE REACTION Na^{23} (d, p) Na^{24}

F. A. EL BEDEWI

Nuclear Physics Laboratory, Atomic Energy Establishment, Cairo, U.A.R.

and

M. A. EL WAHAB

Faculty of Science, Alexandria University, Egypt

Received 12 July 1960

Abstract: A heavy particle magnetic spectrograph has been used to study the energies and angular distributions of proton groups emitted from a sodium target bombarded with 8.60 MeV deuterons. New excited states in Na^{24} have been observed at 4.74 $\pm$0.04 MeV and 5.13$\pm$0.08 MeV. The angular distributions of some proton groups have been compared with curves calculated from deuteron stripping theories. While an s- or d-wave neutron capture is observed for the low lying levels, a p-wave is found to dominate the higher excited states.

1. Introduction.

In investigating the deuteron stripping in a nuclear reaction, it is necessary to measure accurately the energy levels of the residual nucleus as well as the angular distributions of outgoing particles associated with groups corresponding to certain energy levels. The choice of the target material is quite significant and, accordingly, sodium has been chosen because both the parent and residual nuclei taking place in the reaction Na^{23} (d, p) Na^{24} are of particular theoretical interest. While the odd-proton nucleus Na^{23} has, according to the shell model, a ground state proton configuration $1d_{\frac{3}{2}}$ yet its spin [1]) is known to be $\frac{3}{2}$+. Moreover, theoretical predictions concerning the character of the energy levels of the residual odd nucleus Na^{24} are not yet available on account of the many interactions expected between its odd nucleons. Further experimental investigations are still required for sodium which exists naturally as a single stable isotope Na^{23}.

Up to an excitation energy of 4.558 MeV, Sperduto and Buechner [2]) have accurately measured, by magnetic analysis, the energy levels in Na^{24} and have been able to resolve many close levels with spacing as low as 17 keV. Since this investigation, a few inconsistant results [3–5]) on the nuclear properties of the three low lying excited states are the only data reported. Applying stripping analysis, trials have been made by various authors [5–8]) to fit levels up to 1.341 MeV.

The object of the present work is to search for higher excited states as well as to report angular distributions of a number of proton groups emitted from the bombardment of a thin sodium target by 8.60 MeV deuterons.

2. Procedure.

A thin layer of sodium prepared by evaporating the pure metal on the gold leaf backing of 0.78 mg/cm^2 areal density has been quickly transferred to the target chamber where evacuation of the system was immediately started. A collimated deuteron beam provided by the Liverpool 94 cm cyclotron was used and the outgoing protons were analysed by a heavy particle magnetic spectrograph [9]) with photographic plate detection. The experimental procedure is similar to that previously described by El Bedewi [10]) and El Bedewi and Tadros [11]). The mean value of the incident deuteron energy has been found to be 8.60$\pm$0.03 MeV as given in our previous report [12]) on the elastically and inelastically scattered deuterons from sodium.

3. Results and Discussion.

3.1. ANALYSIS OF ENERGY LEVELS

A typical spectrum of protons for an angle of observation of 20° is shown in fig. 1. The groups leading to states in Na^{24} are numbered in the order given by Sperduto and Buechner [2]) begining with P_0 for the ground state group. Other proton groups arising from possible carbon and oxygen contaminations are labeled with the symbol of the corresponding nucleus and numbered in order of increasing excitation energy. These groups were easily sorted out from those due to sodium on account of the variation of the energy shift with angle and confirmed by their agreeement with their well known Q-values and angular distributions [13]).

The position of arrows shown at P_0, P_1, . . ., P_{19} representing possible groups from Na^{23}(d, p)Na^{24} reaction are derived from the results of Sperduto and Buechner [2]) and they are found to agree well with the observed groups. However, owing to the complexity of the Na^{24} level structure in the region between 3.4 MeV and 4.3 MeV, four groups P_9—P_{12} have been obscured in the presented spectrum by the O_1 group, the groups P_{13}, P_{14} and P_{15} are lumped together in one group P_x and the groups P_{16}, P_{17} and P_{18} are combined together and shown as P_y.

Outside the range of Sperduto and Buechner's [2]) measurements, two new groups denoted by P_{20} and P_{21} have been observed. Although the latter group is found mixed with the C_1 group at some angles of observation yet it is well separated at other angles as shown for angle 35° in fig. 1(B). The corresponding energy levels in Na^{24} are found to be 4.74$\pm$0.04 and 5.13+0.08 MeV and respectively. Recent investigations [3,4]) on thermal neutron capture gamma radiation from sodium indicate the existance of several gamma transitions. But, owing to the lack of information on the level positions between 4.56 MeV and the neutron binding energy at 6.96 MeV and due to the need for coincidence experiments of high precision to clear up some doubtful assignments, it is diffi-

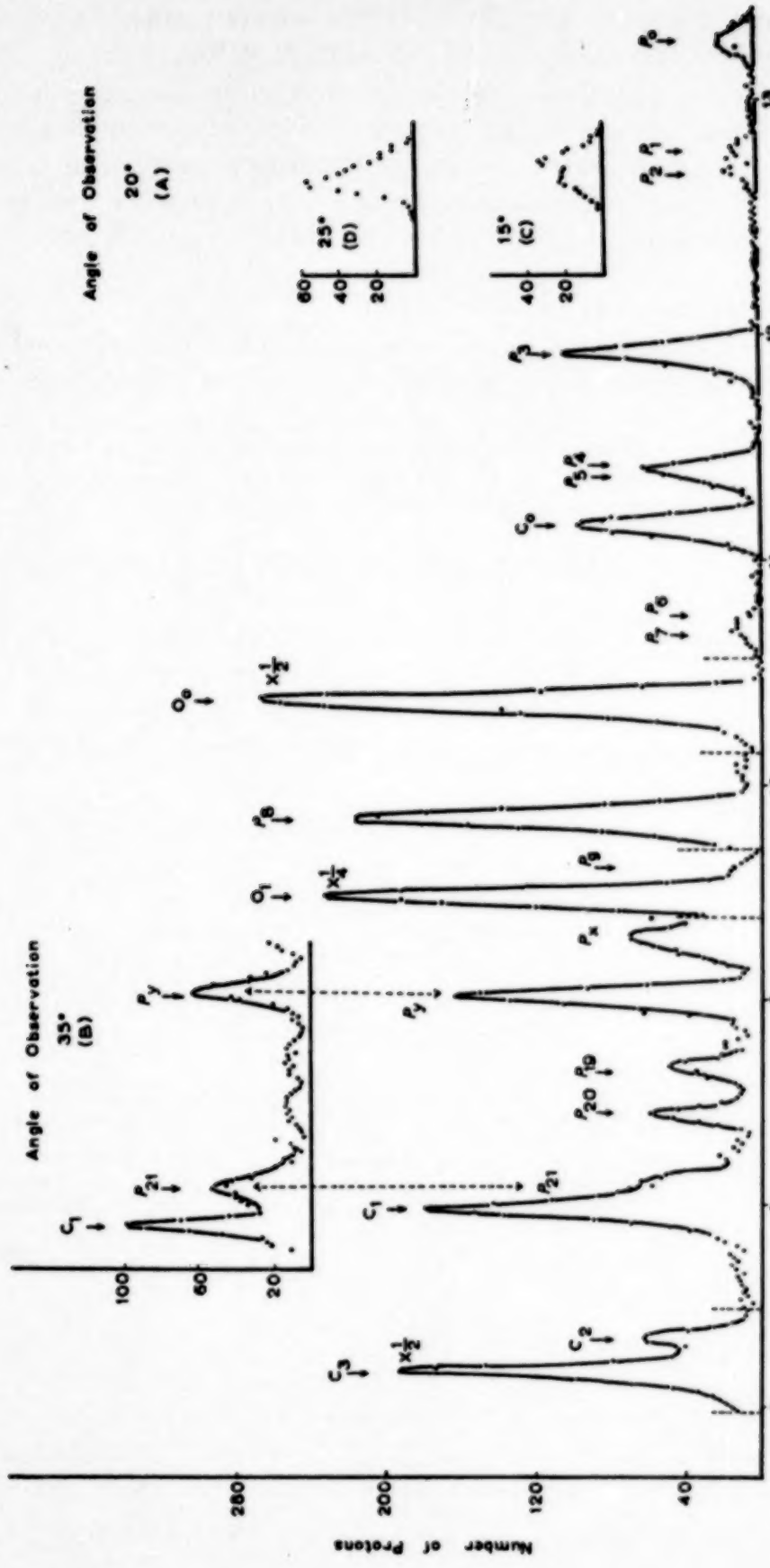

Fig. 1. Spectrum of proton groups from the deuteron bombardment of sodium.

cult to establish a unique decay scheme. Such ambiguity could be represented by the two gamma rays of energies 1.66 MeV and 2.21 MeV observed by Groshev *et al.* [3]) and confirmed by Motz [4]). While the latter author has suggested these transitions to occur between known levels yet the former authors assumed the transitions to take place between the neutron binding energy state and probable levels at 5.30 MeV and 4.75 MeV respectively. The present work confirms the existance of such levels.

3.2. ANGULAR DISTRIBUTION MEASUREMENTS

The angular distributions of proton groups associated to the ground state and various levels in Na^{24} up to an excitation energy of 4.74 MeV (P_{20}) are

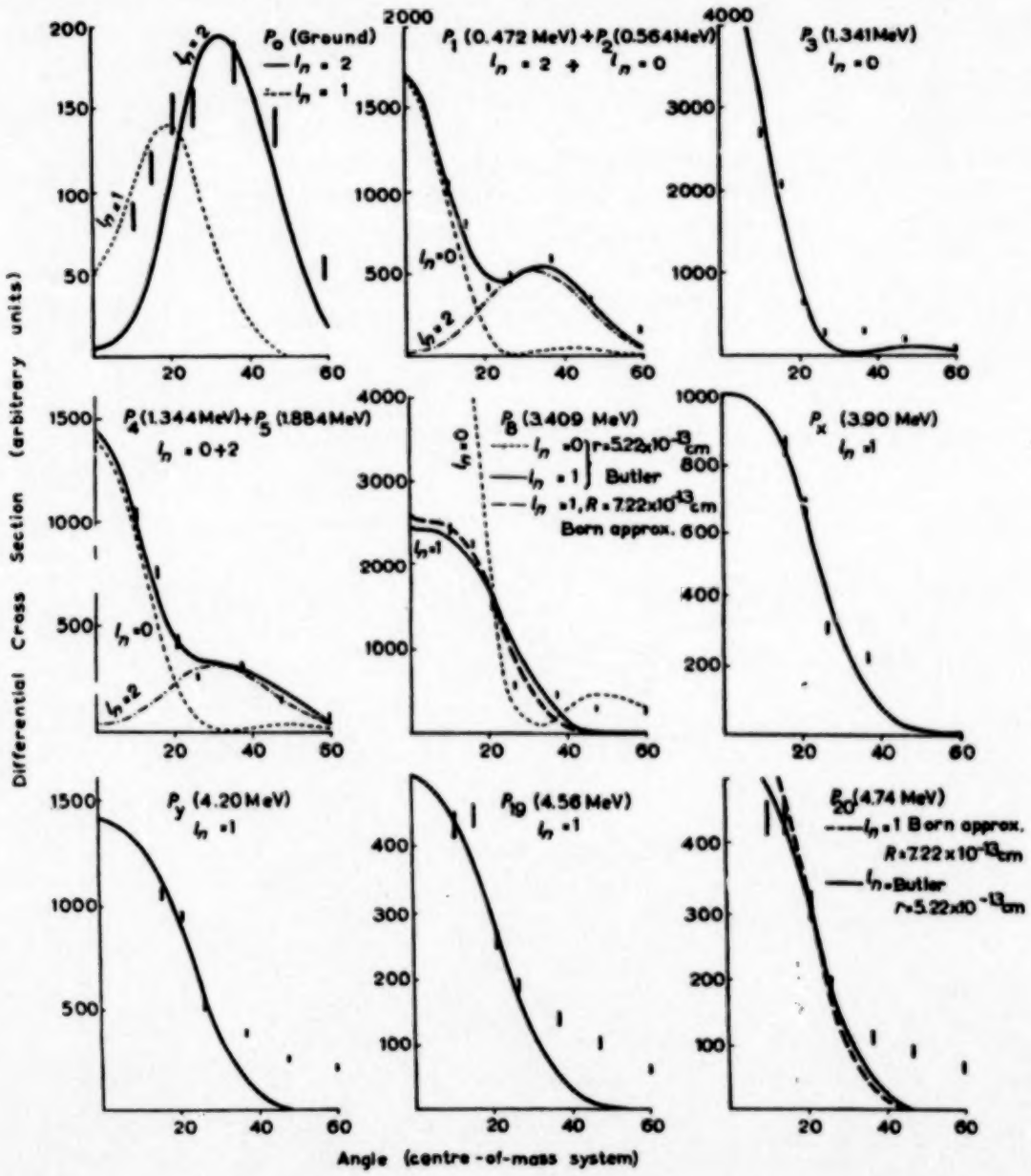
P0 (Ground)
l_n = 2
l_n = 1
P1 (0.472 MeV) + P2 (0.564 MeV)
l_n = 2 + l_n = 0
P3 (1.341 MeV)
l_n = 0
P4 (1.344 MeV) + P5 (1.884 MeV)
l_n = 0+2
P8 (3.409 MeV)
l_n = 0 r = 5.22x10^-13 cm
l_n = 1 Butler
l_n = 1, R = 7.22x10^-13 cm
Born approx.
Px (3.90 MeV)
l_n = 1
Py (4.20 MeV)
l_n = 1
P19 (4.56 MeV)
l_n = 1
P20 (4.74 MeV)
l_n = 1 Born approx. R = 7.22x10^-13 cm
l_n = Butler r = 5.22x10^-13 cm
Differential Cross Section (arbitrary units)
Angle (centre-of-mass system)

Fig. 2. Angular distributions of proton groups emitted from $^{23}Na(d, p)^{24}Na$ reaction.

plotted in the centre-of-mass system as shown in fig. 2. The theoretical curves are calculated from Butler's formula [14]) using a radius of interaction of 5.22×10^{-13} cm and choosing a value for the angular momentum l_n transferred by the captured neutron to give the best fit. The results are consistent with those derived from the Born approximation stripping theory [15]) using a larger radius of interaction 6.22×10^{-13} cm or even 7.22×10^{-13} cm as shown in case of P_8 and P_{20}.

Previous to the present measurements, angular distributions of proton groups P_0 and P_3 corresponding to the ground and third excited state at 1.341 MeV respectively have been reported at 14 MeV incident deuteron energy by Vogelsang and McGruer [8]), at $E_D = 10$ MeV by Bretscher *et al.* [5]) and at $E_D = 3$ MeV by Shapiro [6]). The distributions obtained from all these investigations are in good agreement with those shown in fig. 2 and it is surprising to point out that in case of the ground state angular distribution, the experimental curve is generally found to be broader than the best fitting theoretical one.

Since the ground state of Na^{23} is known [1]) to have spin $\frac{3}{2}^+$ then the value of $l_n = 2$ for the ground state transition indicates that it should have even parity and spin 0, 1, 2, 3, or 4. This result is in agreement with the value of 4^+ for the spin and parity of the Na^{24} ground state as measured by Bellamy and Smith [16]). Also, the value of $l_n = 0$ found for the 1.341 MeV level (P_3) suggests that this state should have even parity and spin 1 or 2. The latter spin is excluded when the Gamow-Teller selection rules are applied to the results of Dropesky and Schardt [17]) on the beta decay of the even nucleus Ne^{24} ground state. These authors have observed a transition to that level in Na^{24} which thus limits its spin to 1^+ or 0^+. It thus follows that the 1.341 MeV level in Na^{24} should have spin 1^+.

With regard to the proton groups P_1 and P_2 corresponding to the closely spaced levels at 0.472 MeV and 0.564 MeV respectively, their combined angular distribution shown in fig. 2 agrees well with that reported by Bretscher *et al.* [5]) and by Shapiro [6]). However, neither of these authors were able to find out the proper l_n value corresponding to each separate group and on account of the intensity of gamma capture transitions, the former authors were unfortunately led to different spin assignment. But, as shown in fig. 1, the relative intensities of these two groups at different angles (15°, 20° and 25°) definitely assign $l_n = 2$ to the transition to the 0.472 MeV state and $l_n = 0$ to the transition to the 0.564 MeV level. It follows that the former state has even parity and spin 0, 1, 2, 3 or 4 while the latter one has even parity and spin 1 or 2. The beta decay of Ne^{24} studied by Dropesky and Schardt [17]) has also shown an allowed transition to the first excited state in Na^{24} but not to the second state. Thus, spins $\geqq 2$ are excluded from the possible assignment for the first state while spin $\geqq 2$ is expected for the second one. In addition, the isomeric life time of 20 ms. for the first state measured by these authors excludes zero spin. So,

definite spin assignments of 1^+ for the 0.472 MeV state and 2^+ for the 0.564 MeV are thus concluded.

The angular distributions for proton groups corresponding to higher excited states have not been measured previously. The groups P_4 and P_5 corresponding to closely spaced levels at 1.844 MeV and 1.884 MeV respectively have been lumped together and their combined distribution represents a mixture of $l_n = 0$ and $l_n = 2$. This result indicates that they should have even parity and spin 1 or 2 for one of them and 0, 1, 2, 3 or 4 for the other. The proton groups P_6 and P_7 corresponding to levels at 2.464 MeV and 2.561 MeV respectively are very weak but their combined angular distribution may be fitted by theoretical curves for $l_n = 1$ and $l_n = 2$.

Finally, a p-wave neutron capture is found for each of the remaining states corresponding to the investigated groups P_8(3.409 MeV), P_{19} (4.558 MeV) and P_{20}(4.74 MeV). This may apply as well to each or better to the dominating component of the combined groups P_x and P_y. As previously mentioned P_x represents the sum of P_{12}(3.850 MeV), P_{13}(3.899 MeV) and P_{14}(3.929 MeV), while P_y represents P_{15}(4.184 MeV), P_{16}(4.202 MeV) and P_{17}(4.219 MeV). It follows that each of these states should have odd parity and spin 0, 1, 2 or 3.

Références.

1) M. H. L. Pryce, Rep. Progr. Phys. **17** (1954) 1
2) A. Sperduto and W. W. Buechner, Phys. Rev. **88** (1952) 574
3) L. V. Groshev, B. P. Adyasevich and A. M. Demidov, International Geneva Conference on the Peaceful Uses of Atomic Energy (1954) Report 8-P-651
4) H. Motz, Phys. Rev. **104** (1956) 1353
5) M. M. Bretscher, J. O. Alderman, A. Elwyn and F. B. Shull, Phys. Rev. **96** (1954) 103
6) F. Shapiro, Phys. Rev. **93** (1954) 290
7) S. Takemoto, T. Dazai and R. Chiba, Phys. Rev. **91** (1953) 1024 (L)
8) W. F. Vogelsang and J. N. McGruer, Phys. Rev. **109** (1958) 1063
9) T. S. Green and R. Middleton, Proc. Phys. Soc. **69** (1956) 28
10) F. A. El Bedewi, Proc. Phys. Soc. **69** (1956) 221
11) F. A. El Bedewi and S. Tadros, International Geneva Conference on the Peaceful Uses of Atomic Energy (1958), Report 15-P-1482
12) F. A. El Bedewi and M. A. El Wahab, Bull. Faculty of Science (Alexandria) **2** (1958) 37
13) F. Ajzenberg and T. Lauritsen, Rev. Mod. Phys. **27** (1956) 77
14) S. T. Butler, Proc. Roy. Soc. A **208** (1951) 559
15) A. B. Bhatia, K. Huang, R. Huby and H. C. Newns, Phil. Mag. **43** (1952) 485
16) E. H. Bellamy and K. F. Smith, Phil. Mag **44** (1953) 33
17) B. J. Dropesky and A. W. Schardt, Phys. Rev. **102** (1956) 426

4.E

Nuclear Physics **21** (1960) 55—65; © *North-Holland Publishing Co., Amsterdam*

Not to be reproduced by photoprint or microfilm without written permission from the publisher

CONTRIBUTIONS TO THE DECAY OF Eu^{152}

WERNER SCHNEIDER †

Department of Physics, Swiss Federal Institute of Technology, Zürich

Received 12 July 1960

Abstract: The spectrum of the β^--particles emitted in the decay of 13 y Eu^{152} has been studied with a magnetic spectrometer of the Züntitype and with a semicircular spectrometer of high resolution. The shape factor proposed by Langer *et al.* for the 1490 keV β^--spectrum was confirmed and the relative intensities of the other β^--transitions were redetermined. Only the intensity of the 1070 keV β^--transition is strongly influenced by the choice of the correction factor applied to the spectrum of the 1490 keV β^--transition. The energies and intensities of internal conversion lines obtained in this experiment are in good agreement with those previously reported. The spin-parity assignment for the highest excited level in Gd^{152} is proposed to be 2−.

1. Introduction

The investigation of the decay scheme of the 13 y Eu^{152} has been the subject of many papers (e.g. ref. [1–6, 8, 11–15])). Whereas the decay mode to Sm^{152} is rather well established, a complete up to date analysis of the continuous β^--spectrum is still lacking. Cork *et al.* [1]) and Bhattacherjee *et al.* [2]) have reported the log *ft* values and the relative contributions of the different β^--transitions to the total disintegration rate of Eu^{152}. Their analysis was based on the assumption that the ground state of Eu^{152} is a 4− state. Paramagnetic resonance measurements [3]), however, have resulted in a spin assignment of 3 to the Eu^{152} ground state. The new spin assignment implies that the 1490 keV β^--transition is not unique as was originally assumed by Cork *et al.* [1]) and Bhattacherjee *et al.* [2]). Recent experiments [4, 5, 6]) showed that this transition to the first excited 2+ level in Gd^{152} is first forbidden and that the contribution of the $\int B_{ij}$ matrix element is unusually large. Langer *et al.* [4]) measured the shape of the 1483 keV β^--spectrum and determined the correction factor as

$$a_1 = (W^2-1)0.791+(W_0-W)^2+5\pm 2, \quad W_0 = 3.902.$$

This factor can only be explained on the basis of a large relative intensity of the $\int B_{ij}$ component.

The measurements presented in this paper confirm the correction factor reported by Langer *et al.* [4]). In addition the relative intensities were redetermined on the basis of this correction factor. As expected, only the determination

† Present address: Institute of Physics, Uppsala University, Uppsala (Sweden).

of the relative intensity of the 1070 keV β^--transition is strongly influenced by the choice of the correction factor, whereas the effect on the other transitions can be neglected.

2. Source Preparation and Experimental Procedure

The Eu^{152} sources were prepared from a pile-irradiated mixture of Eu^{151} and Eu^{153} enriched in Eu^{151} to 91.8 %.

The β^--spectrum was investigated by means of a lens spectrometer of the Zünti-type [7]) and a semicircular spectrometer of high resolution ($\Delta E/E < 8\times10^{-3}$). The lens spectrometer was used in the energy range from 60 keV to 1700 keV. The energy range below 250 keV was covered with the aid of the semicircular spectrometer. The electron spectrum was measured at 650 energy points with a statistical error of less than 1 %.

3. Experimental Results

From the experimental points the Kurieplot was constructed for the energy range $W > 2.4$ (fig. 1). The Kurieplot reveals the existence of a high energy

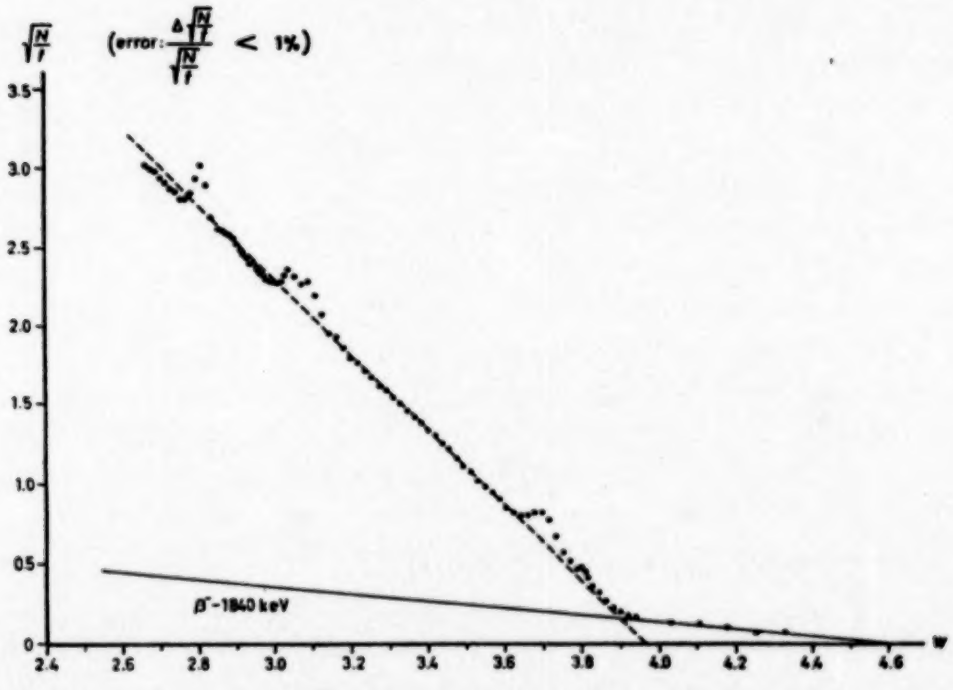

Fig. 1. Kurieplot of the total β^--spectrum for $2.60 < W < 4.40$.

tail, which indicates the presence of a β^--transition with an end point of $W_0 = 4.60\pm0.06$. These high energy electrons cannot be interpreted as Compton electrons, since the highest energy γ-ray involved in the Eu^{152} decay has a quantum energy of only 1409 keV. The possibility of these electrons being

entirely due to the 1840 keV β^--transition of Eu^{154} can be excluded on the basis of the fact that no conversion electrons of the 1280 keV β^--transition of Gd^{154} could be observed. It seems rather improbable that these electrons can be attributed to a third forbidden transition from Eu^{152} to the ground state of Gd^{152}. At present no reasonable explanation for the presence of the 1840 keV β^--spectrum can be offered. It may be worth to mention that a similar high energy tail was observed by Alburger *et al.* [8]), which was, however, interpreted as belonging to Eu^{154}.

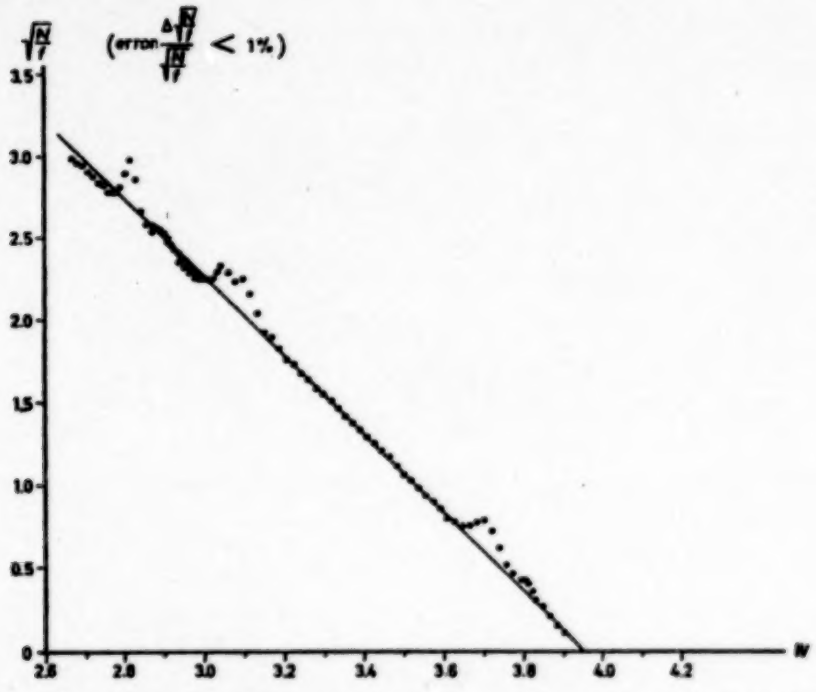

Fig. 2. Kurieplot for $2.60 < W < 4.0$ after subtraction of the 1840 keV β^--spectrum.

The presence of this high energy β^--spectrum gives an uncertainty of about 10 keV in defining the end point of the 1490 keV β^--transition. The Kurieplot, after subtraction of the unexplained 1840 keV spectrum, is presented in fig. 2. The straight line, tentatively drawn, shows clearly that the β^--spectrum does not have the allowed shape.

To investigate the dependence of the analysis of the continuous β^--spectra on the correction factor chosen for the 1490 keV transition, both factors $a_1^1 = (W^2-1)+(W_0-W)^2$ (unique shape) and $a_1^2 = (W^2-1)0.791+(W_0-W)^2+5$ (Langer *et al.* [4])) were applied†. The factor a_1^1 does not yield a straight line Kurieplot over the whole energy range involved, and, in addition, results in a concave Kurieline for the 1070 keV β^--spectrum. The factor proposed by

† Langer *et al.* [4]) found for W_0 a value of 3.902. From fig. 2 we determined a slightly different preliminary value, namely $W_0 = 3.950$. This does not, however, affect the values for the correction factor a_1^2 by more than max. 0.5 % in the energy range considered. Thus we used in the first approximation $W_0 = 3.950$.

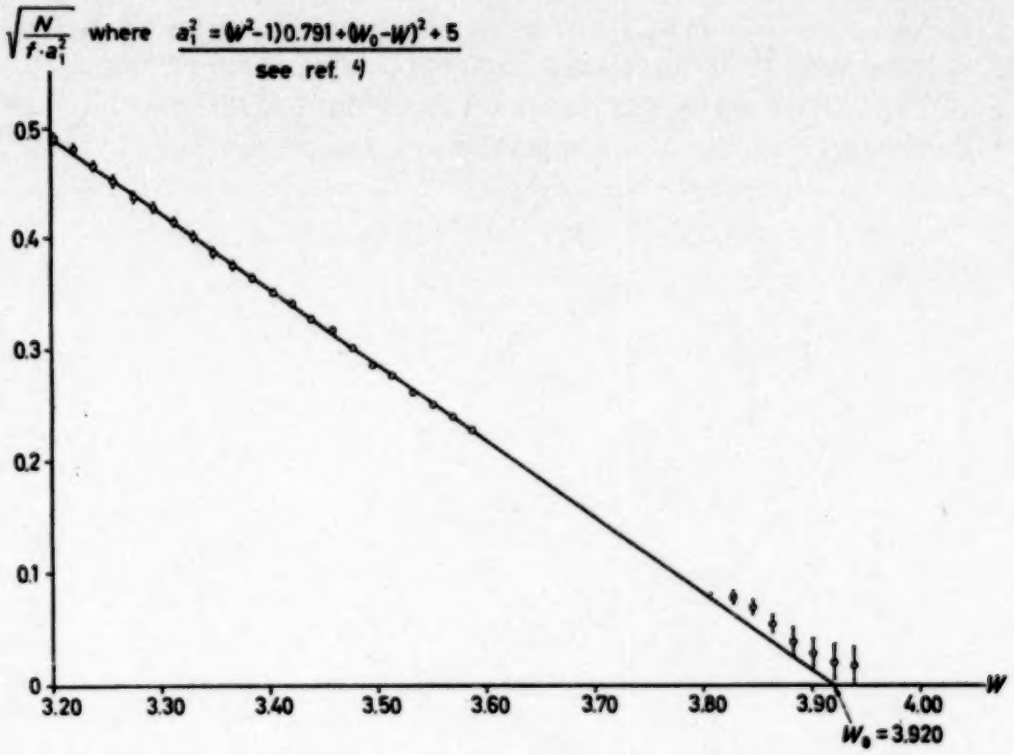

Fig. 3. Kurieplot corrected with the shape factor proposed by Langer *et al.* [4]) for the 1490 keV β^--spectrum.

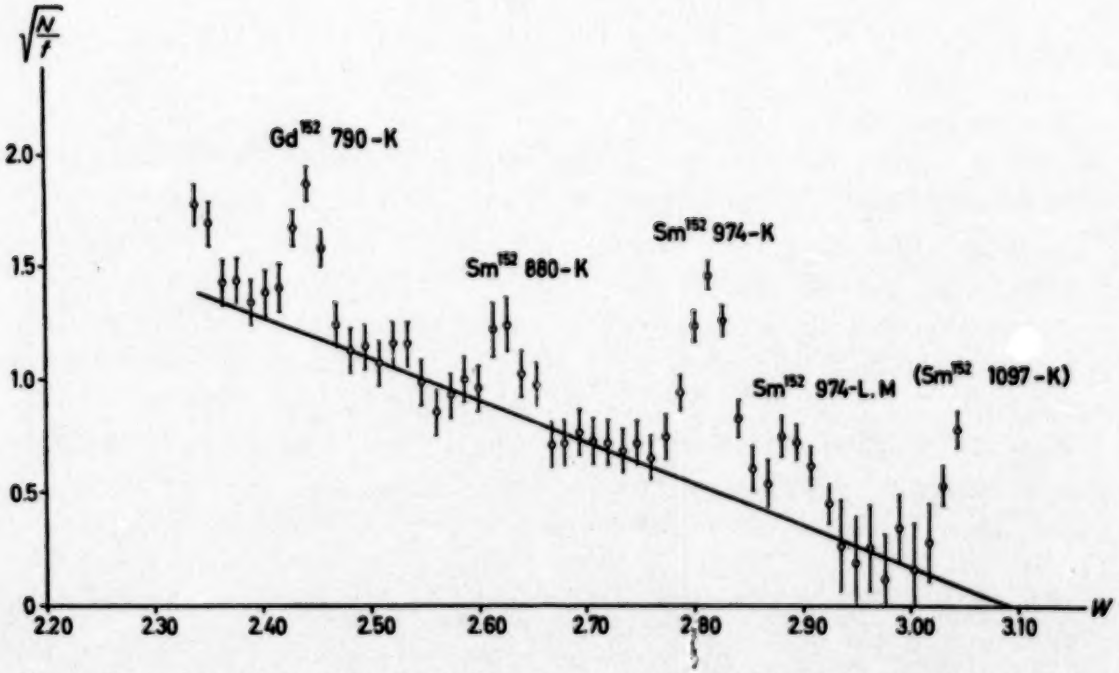

Fig. 4. Kurieplot for $2.30 < W < 3.10$ after subtraction of the 1840 keV and 1490 keV β-spectra.

Langer *et al.* [4]), on the other hand, gives very satisfactory agreement with our data. The Kurieplot of the 1490 keV β^--spectrum obtained with the a_1^2 correction factor is shown in fig. 3. The Kurieplot after subtraction of the 1490 keV β^--spectrum is displayed in fig. 4. The subtraction of the 1490 keV β^--spectrum requires extrapolation of the major part of this spectrum since only the upper

TABLE 1

Energy, relative abundance and log *ft* value for the 1490 keV and the 1070 keV β^--transition obtained with different correction factors applied to the 1490 keV β^--spectrum.

Energy E_0 (keV)		Percentage of total Eu^{152} activity		Log *ft*	
a_1^1	a_1^2	a_1^1	a_1^2	a_1^1	a_1^2
1477±20	1492±20	6.6	7.6	12.2	12.3
1083±20	1072±20	2.7	1.4	12.1	12.5

part of the spectrum could be measured directly. The result of the subtraction is thus very sensitive to the assumed form of the spectrum and therefore depends greatly on the choice of the correction factor. The results obtained by applying the a_1^1 and a_1^2 correction factors are given in table 1 and figs. 5 and 6. As mentioned above, the other transitions ($E_0 = 690$ keV, 360 keV and 190 keV) are not noticeably influenced by the choice of the particular correction factor. The newly determined values of the relative intensities and of the log *ft* values are given in table 2.

TABLE 2

Summary of β^--transitions in Eu^{152}

Energy E_0 (keV)	Percentage of Eu^{152} β^--activity	Percentage of total Eu^{152} activity	log *ft*
1492±20	24.9	7.6	12.3
1072±20	4.6	1.4	12.5
690±20	50.9	15.6	10.8
360±30	12.9	4.0	10.4
190±40	6.2	1.9	9.8
1840±30	0.5	(0.15)	14.3

It is impossible to make statements about the shapes of the 1070, 690, 360 and 190 keV β^--spectra from the measured electron spectrum because of the abundance of superimposed conversion lines. It is possible, however, to draw some conclusions from the decay scheme of Gd^{152} (see next section), namely a) that the 690 keV and probably the 190 keV β^--transition are allowed, and b) that the 1070 keV β^--transition should be first forbidden. The log *ft* values of all β^--transitions involved in the decay of Eu^{152} are much larger than usual. No explanation of this fact can be found at this moment. *K*-forbiddenness cannot

be considered, since it has no meaning to define a K-quantum number for the spherical Gd^{152} nucleus. In any case it seems that in the case of Eu^{152} the first forbidden transitions have log ft values > 12 and the allowed transitions have log ft values between 9.5 and 11.

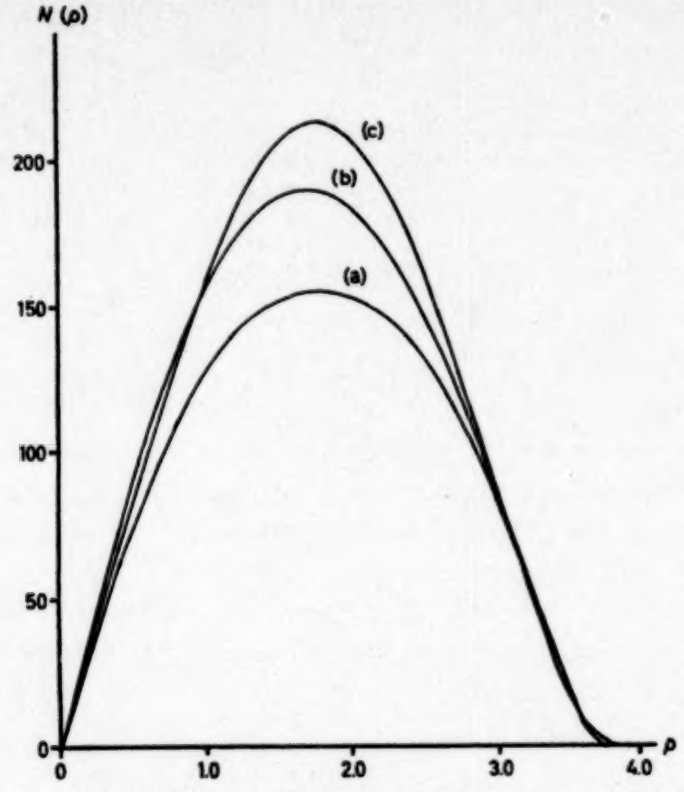

Fig. 5. The shape of the 1490 keV β^--spectrum extrapolated on the basis of different correction factors a_1^k:
(a) $a_1^1 = (W^2-1)+(W_0-W)^2$, (b) $a_1^2 = (W^2-1)0.791+(W_0-W)^2+5$, (c) $a_1^3 = 1$, i.e. for the allowed shape (see straight line in fig. 2)

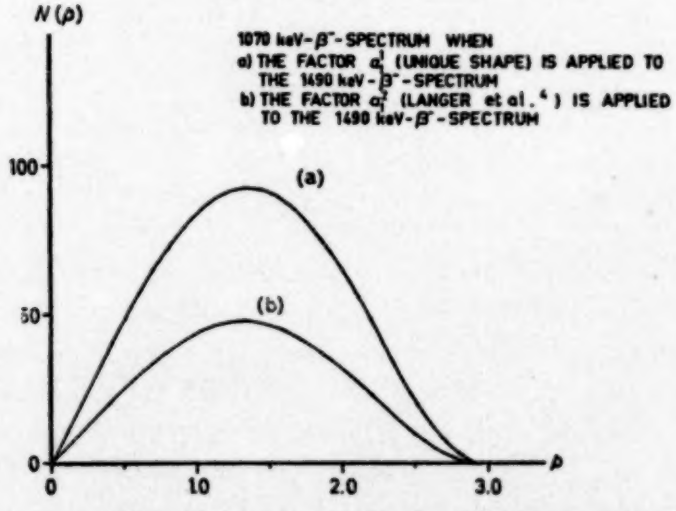

Fig. 6. Dependence of the relative intensity of the 1070 keV β^--spectrum on the correction factor applied to the 1490 keV β^--spectrum.

4. Conversion Spectra

From our measurements some information about the conversion electron spectra was obtained. The results are presented in table 3. The intensities of the conversion lines 1 to 8 are given with an error of less than 5 %, whereas the error of the other conversion lines is about 15 % (for very weak lines about 30%). Using the values of relative γ-ray intensities reported by Marti [11]) it is possible to calculate the conversion coefficients of some γ-transitions from the relative intensities of conversion lines measured in our experiment (table 3).

The measured K/L ratio for the 122 keV γ-ray in Sm^{152} indicates that this transition is a pure E2-transition. From the tables of conversion coefficients presented by Sliv and Band [9]) the theoretical value of the 122-K-conversion coefficient α_2 is then taken. From this value a common factor q is computed which must be applied to the experimentally determined ratios

$$N_{e^-}^{rel}/N_{\gamma}^{rel}$$

in order to get the absolute conversion coefficients a,

$$a = \frac{N_{e^-}}{N_{\gamma}} = q\frac{N_{e^-}^{rel}}{N_{\gamma}^{rel}}, \quad \text{where } q = \frac{\alpha_2(Z = 62,\ 122\,\text{keV}) \times N_{\gamma-122}^{rel}}{N_{e^- - K-122}^{rel}}.$$

In table 4 we present the experimentally determined conversion coefficients of some γ-transitions in Gd^{152}. In the last column we list the multipolarity of these γ-transitions assigned on the basis of a comparison of the theoretical and experimental values.

5. Decay Scheme and Discussion

The data presented in tables 2, 3 and 4 make it possible to set up the decay scheme discussed below (fig. 7).

a) Gd^{152}

The measured K/L ratio of the 345 keV γ-ray of 3.4($\pm$0.2) indicates that this transition is a pure E2-transition. Thus an assignment of 2+ has to be made for the first excited level in Gd^{152} in accordance with the Goldhaber-Sunyar rule.

The experimentally determined conversion coefficient of the 413 keV transition indicates that this transition from the second excited level to the first excited level of Gd^{152} is an E2-transition with a possible small admixture of M1. Thus the following spin assignments to the 757 keV-level are possible: 2+, 4+, 3+, 1+, 0+. The latter three can be excluded, however, by angular correlation measurements [11, 14]). In addition 0+ and 1+ are also excluded on the basis of log ft arguments.

TABLE 3

Energies, relative intensities and K/L+M+ . . . ratios of internal conversion lines. The K/L+M+. ratios were determined by comparing the areas of the K and the corresponding L+M+ . . . conversion lines.

Line nr.	Electron energy (keV)	Relative intensity	Energy sum (keV)	Assignment		Experimental K/L ratio	Theoretical K/L ratio for E2 [9])	Experimental K/L+M ratio	Theoretical K/L+M ratio for E2 [9, 10])	Multipol. assignment
				Sm^{152}	Gd^{152}					
1	74.6	2930	121.5	K-122		1.87	1.85	1.5	1.3	E2
2	115	1570	122.3	L-122						
3	120.8	390	122.3	M-122						
4	198.3	81	245.2	K-245				3.4	2.8	E2
5	238.0	24	245.3	L-245						
6	296.0	100	346.2		K-344			3.4	3.3	E2
7	337.8	29.1	345.6		L-344					
8	362.8	4.5	413		K-413					see table 4
9	401	3.5	448	K-450				5		see table 4
10	445	0.7	452	L-450						
11	543	4.1	590	K-594				(2.2)		see table 4
12	591	1.9	598	L-594						
13	571	3.6								
14	615	3.5								
15	649	7.9	696	K-693				6		see table 4
16	684	1.3	691	L-693						
17	739	2.7	790		K-790					
18	832	1.6	880	K-880						see table 4
19	927	4.6	974	K-974				(2.7)		see table 4
20	968	1.7	975	L-974						
21	1050	2.9	1097	K-1097						see table 4
22	1074	3.6	1121	K-1120				4.5		see table 4
23	1112	0.8	1119	L-1120						
24	1382	1.7	1429	K-1435				4.9		see table 4
25	1433	0.35	1440	L-1435						

TABLE 4

K-conversion coefficients and multipolarity assignments

Isotope [a])	Transition energy (keV)	Rel. γ-line int. [b])	Rel. conv. line int. [c])	Exp. K-conv. coeff.	Theoretical K-conversion coefficients α_K [d])				Multipol. assignm.
					E1	E2	M1	M2	
Gd^{155}	413	6	3.4(−2)	2.2(−2)	6.2(−3)	1.95(−2)	3.5(−2)	1.2(−1)	E2 or E2+M1
	790	44	2 (−2)	1.7(−3)	1.6(−3)	4.1 (−3)	7.4(−3)	2.0(−2)	E1
	1280	8.3	<1.5(−3)	<7 (−4)	6 (−4)	1.5 (−3)	2.2(−3)	5.2(−3)	E1

[a]) The relative conversion line intensities presented in this paper are in good agreement with the results reported by other authors. In the case of Sm^{155} no new multipolarity assignment could be determined. Therefore we refer to the paper of Nathan and Hultberg [18]) for results concerning the decay to Sm^{155}.

[b]) Reported by Marti [11]).

[c]) 3.4(−2) means 3.4×10^{-2}, etc.

[d]) Taken from the tables presented by Sliv and Band [9]).

For the third excited level at 1134 keV spin and parity assignments of 1−, 2−, 3− can be made on the basis of the experimentally determined conversion coefficient. Angular correlation measurements [11, 14]) suggest 3, so a 3− can be assigned to the 1134 keV-level in agreement with the assignment made by O. Nathan and S. Hultberg [13]).

For the highest excited state, the 1625 keV-level, angular correlation measurements [11]) suggest spin assignments of 4, 3 or 2. The conversion coefficient,

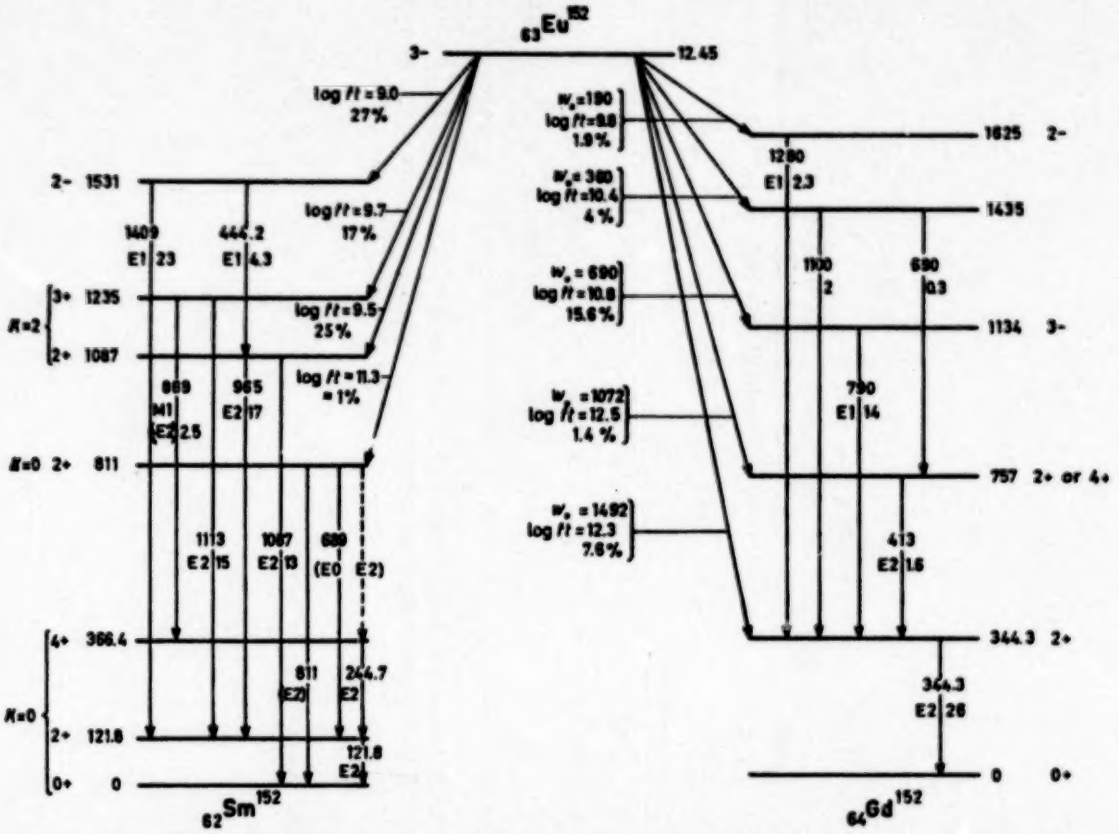

Fig. 7. Decay scheme of 13 y Eu^{152}. (The decay to Sm^{152} as reported by Nathan and Hultberg [13]) is included).

indicating that the 1280 keV transition to the first excited level is an E1-transition, suggests a 1−, 2− or 3− assignment. In addition the log *ft* value for the 190 keV β^--transition from Eu^{152} to this level implies that this β^--transition cannot be second forbidden, excluding spin assignments of 1 and 5. Recent γ-γ angular correlation measurements seem to support a spin 2 assigument (to be published). Thus an assignment of 2− for this 1625 keV level is proposed.

The conversion coefficient of the 1100 keV γ-transition could not be determined and consequently the multipolarity of this γ-ray is not known.

b) Sm^{152}

The results of our experiment are in good agreement with results reported

by other groups [1, 2, 8, 12, 13, 15]). In the decay scheme presented above, the decay to Sm^{152} is included as reported by O. Nathan and S. Hultberg [13]).

7. Auger Lines

Measurements performed by means of the semicircular spectrometer reveal the existence of the Auger electron groups given in table 6.

TABLE 6

Observed Auger electron groups

Energy (keV)	Assignment
32.3	Sm^{152} K-L-L
38.9	Sm^{152} K-L-M, K-L-N, ...
43.8	Sm^{152} K-M-M, K-M-N ...

The 101 keV γ-line in Sm^{152} reported by Bhattacherjee *et al.* [2]) could not be observed.

We like to thank Professor Rolf. M. Steffen, Purdue University, for his kind help and for many stimulating discussions. We are also indebted to Professor Paul Scherrer and Dr. T. R. Gerholm for their interest in this work. The facilities put at our disposal by Professor Kai Siegbahn are greatfully acknowledged.

References

1) J. M. Cork, M. K. Brice, R. G. Helmer and D. E. Sarason, Phys. Rev. **107** (1957) 1621
2) S. K. Bhattacherjee, T. D. Nainan, S. Raman and B. Sahai, Nuovo Cim. **7** (1958) 501
3) M. Abraham, R. Kedzie and C. D. Jeffries, Phys. Rev. **108** (1957) 58
4) L. M. Langer, D. R. Smith and M. P. Klein, Bull. Am. Phys. Soc. **7** (1959) 426
5) J. W. Sunier, P. Debrunner and P. Scherrer, Nuclear Physics **19** (1960) 62
6) H. Dulaney Jr., C. H. Braden and L. D. Wyly, Phys. Rev. **117** (1960) 1092
7) W. Zünti, Helv. Phys. Acta **21** (1948) 179
8) D. E. Alburger, S. Ofer and M. Goldhaber, Phys. Rev. **112** (1958) 1998
9) L. A. Sliv and I. M. Band, Tables of conversion coefficients (Moscow, 1956)
10) M. E. Rose, Internal conversion coefficients (North-Holland Publishing Co., Amsterdam, 1958)
11) J. Marti, Diplomarbeit E. T. H. 1959 and private communications from the angular correlation group at the Physical Institute of E.T.H.
12) O. Nathan and M. A. Waggoner, Nuclear Physics **2** (1956/57) 548
13) O. Nathan and S. Hultberg, Nuclear Physics **10** (1959) 118
14) L. Grodzins and H. Kendall, Bull. Am. Phys. Soc. **1** (1956) 163, 164
15) B. V. Bobykin and K. M. Novik, Izv. Akad. Nauk SSSR Ser. Fiz. **21** (1957) 1556

2.C:3.A

Nuclear Physics **21** (1960) 66—98; © *North-Holland Publishing Co., Amsterdam*

Not to be reproduced by photoprint or microfilm without written permission from the publisher

PARAMETERS AND GAMMA-RAY SPECTRA OF NEUTRON RESONANCES IN THE ISOTOPES OF MERCURY

R. T. CARPENTER and L. M. BOLLINGER

Argonne National Laboratory, Argonne, Illinois †

Received 18 July 1960

Abstract: The Argonne fast chopper has been used to study the neutron resonances of mercury. The neutron transmissions of five samples of normal mercury and six isotopically enriched samples were measured in the energy interval from 10 to 30 000 eV. Twenty-eight resonances were isotopically identified and parameters, including the spin, were determined for most of them. Average values of level spacings, radiations widths, and neutron strength functions were derived from the individual parameters. The spacings and radiation widths exhibit the expected rapid increase as the doubly closed shell is approached. Unexpectedly, the total radiation widths of different resonances of Hg^{201} are found to fluctuate by a larger factor than has been previously observed in any other nuclear species. The gamma-ray spectra and the multiplicity of gamma rays from capture in these resonances were measured and both quantities were found to differ from resonance to resonance in a way that is consistent with the fluctuations in the widths. Seven high-energy gamma rays were resolved in the capture gamma-ray spectra of three resonances in Hg^{201}. The absolute intensities of the transitions were determined by a least-squares fit of the data to an experimentally determined line shape. It was found that these high-energy transitions are on the average enhanced, relative to those of lower energy, by about a factor of 15 beyond the usual E_γ^3 law. The remainders obtained by subtracting the partial widths of the seven high-energy transitions from the total radiation widths are constant, within errors, for the three resonances investigated. This indicates that the fluctuations in the total radiation width are the result of fluctuations in the intensities of the transitions of highest energy. The observed magnitude of the fluctuations is shown to be consistent with that expected from random fluctuations of the partial radiation widths.

1. Introduction

Previous studies of neutron cross sections have shown that the average values of the parameters of resonances in a given nucleide are strongly influenced by the closeness of the nucleide to the major closed shells [1, 2]). The data have tended to be fragmentary in the immediate vicinity of the closed shells, however, since there the wide spacing of nuclear levels made only a few resonances available for study. Recent improvements in the resolution of neutron spectrometers have greatly increased the range of energy over which good measurements can be made, thus making it possible to observe the shell effects in more detail. The measurements reported in this paper were undertaken with this objective in mind.

† Work performed under the auspices of the U. S. Atomic Energy Commission.

One of the more favorable groups of nucleides for an observation of the dependence of neutron resonance parameters on the shell structure of the nucleus is the group of Hg isotopes. Here there are seven target nucleides that lie close to the doubly closed shell of 82 protons and 126 neutrons; with a fixed value of $Z = 80$, the neutron numbers vary from 116 to 124. Because of the wide range of the neutron numbers, marked differences in the characteristics of the resonances in the various isotopes are expected. In particular, both the level spacing and the radiation width are expected to increase rapidly with increasing neutron number.

The experiments described in the present paper were initiated as a set of transmission measurements intended to give quantitative information about the influence of shell structure on the average values of the resonance parameters of the mercury isotopes. However, as the work progressed an unexpected and interesting phenomenon of another kind was uncovered, with a resulting change in the emphasis of the experiment. It was found [3]) that the total radiation widths of the resonances of Hg^{201} differed from resonance to resonance by as much as a factor of 2, a greater variation than had been reported previously in statistically significant results for any nucleide. Thus, in an effort to obtain a better understanding of this effect, the measurements were extended to a study of the gamma-ray spectra resulting from neutron capture in the resonances of Hg^{201} The spectra are found [4]) to differ greatly from resonance to resonance in a manner that is consistent with the differences in the radiation widths. The final section of the paper is devoted to a discussion of various possible interpretations of the observed fluctuations in the radiation widths and the capture gamma-ray spectra.

2. Neutron Cross Sections

2.1. TRANSMISSION MEASUREMENTS

The Argonne fast chopper, the neutron spectrometer used in the present study, has been described previously [5]). The high-resolution rotor (rotor II) of the system was employed in the transmission measurements; it was operated at a speed of 15 000 rot. per min. For the energy range below 150 eV, for which a flight path of 60 m was used, the resolution was 27 nsec/m. When a large sample was available for study, a flight path of 120 m was used above 150 eV, so that the resolution was 12 nsec/m. Neutrons were detected with boron-loaded liquid scintillation detectors similar to type 22, as described by Bollinger and Thomas [6]). Pulses from the detectors were stored in a 1024-channel time analyzer [7]). Above 150 eV the analyzer was operated with $\frac{1}{2}$-μsec channels; it was used with 1-μsec channels below 150 eV. The resolutions quoted above include the effects of finite channel widths, moderation time in the detectors, and the geometrical widths of the detecors, as well as the width of the neutron burst.

The transmissions of five samples of normal mercury were measured. The two thickest samples were of normal mercury metal and had thicknesses of 0.1544 and 0.0516 atoms/barn. Two samples of intermediate thickness were of HgS and had thicknesses of 0.0207 and 0.00500 atoms/barn. The thinnest sample was a mixture of HgS and S and had a thickness of 0.00198 atoms/barn.

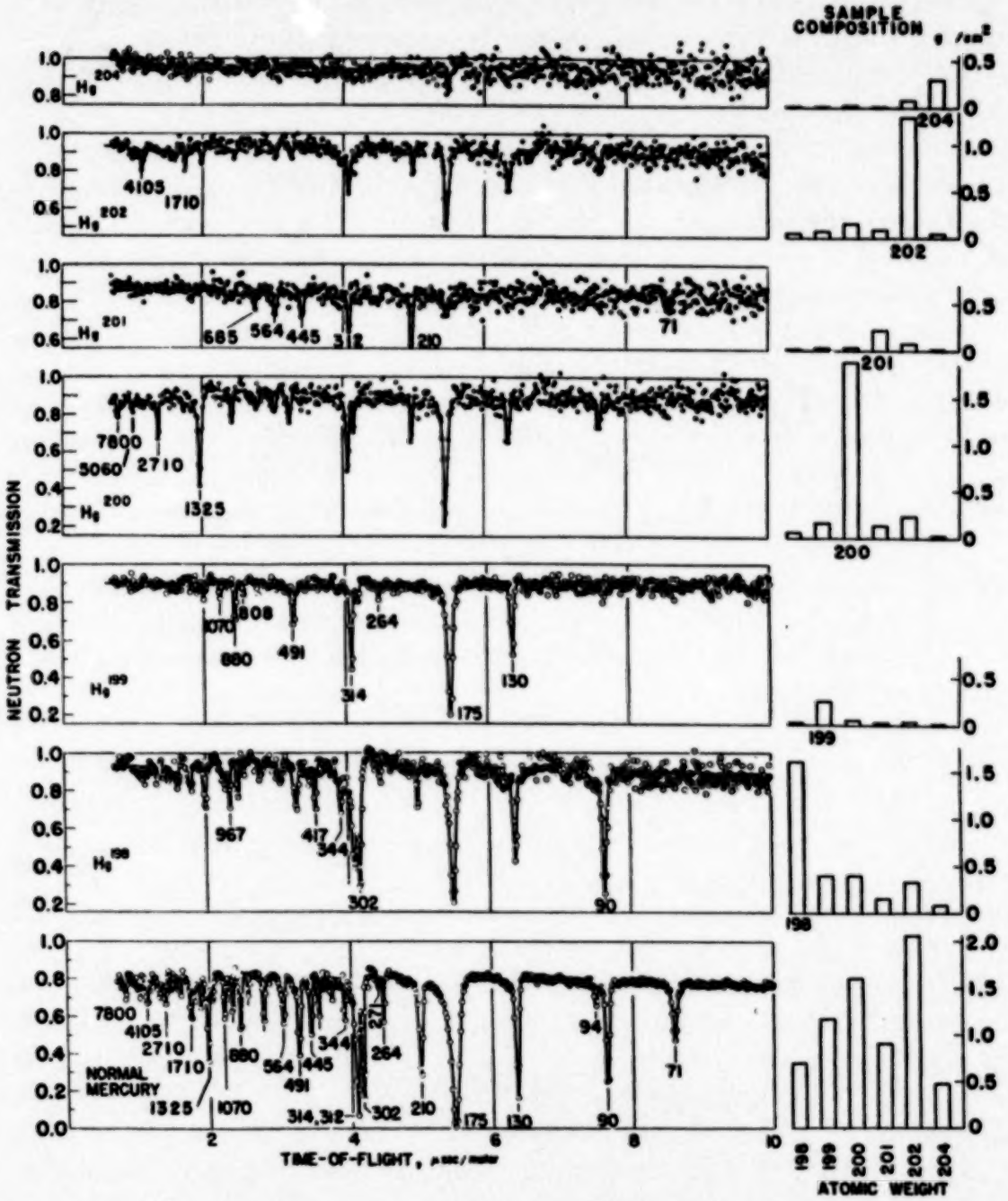

Fig. 1. Neutron transmission of isotopically enriched samples of mercury. The histograms to the right give the isotopic thicknesses of the samples in g/cm². The transmission of a sample of normal mercury is included for comparison. The numbers on the transmission dips are the resonance energies.

Measurements were also made on six samples enriched in the isotopes 198, 199, 200, 201, 202 and 204, respectively. The total and isotopic sample thicknesses of these samples are shown at the right in fig. 1.

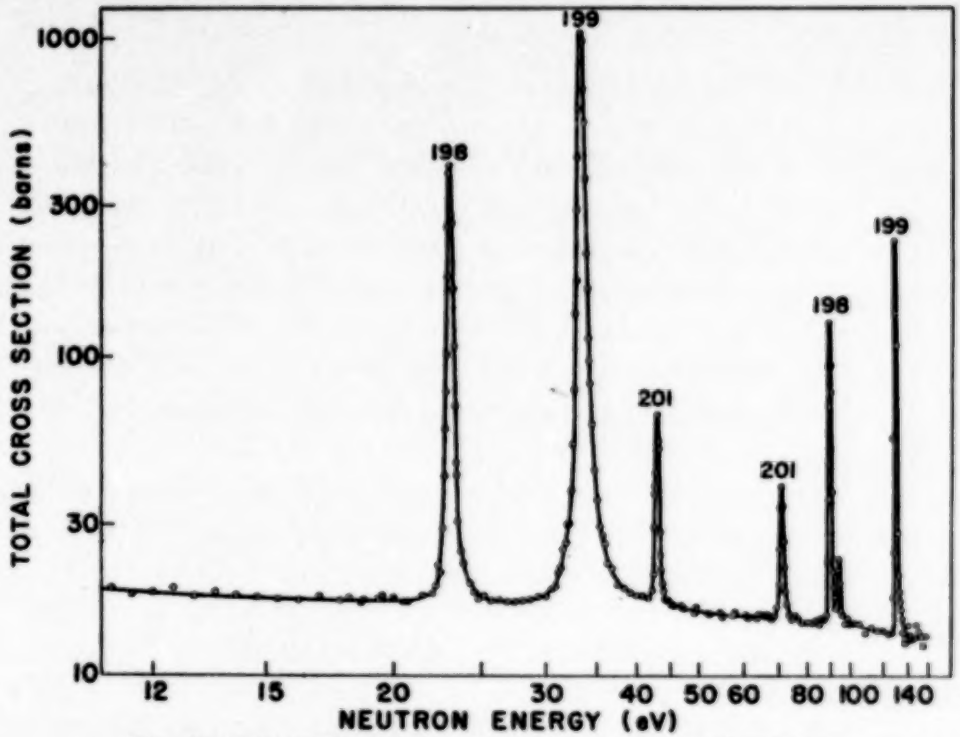

Fig. 2a. The total neutron cross section of normal mercury.

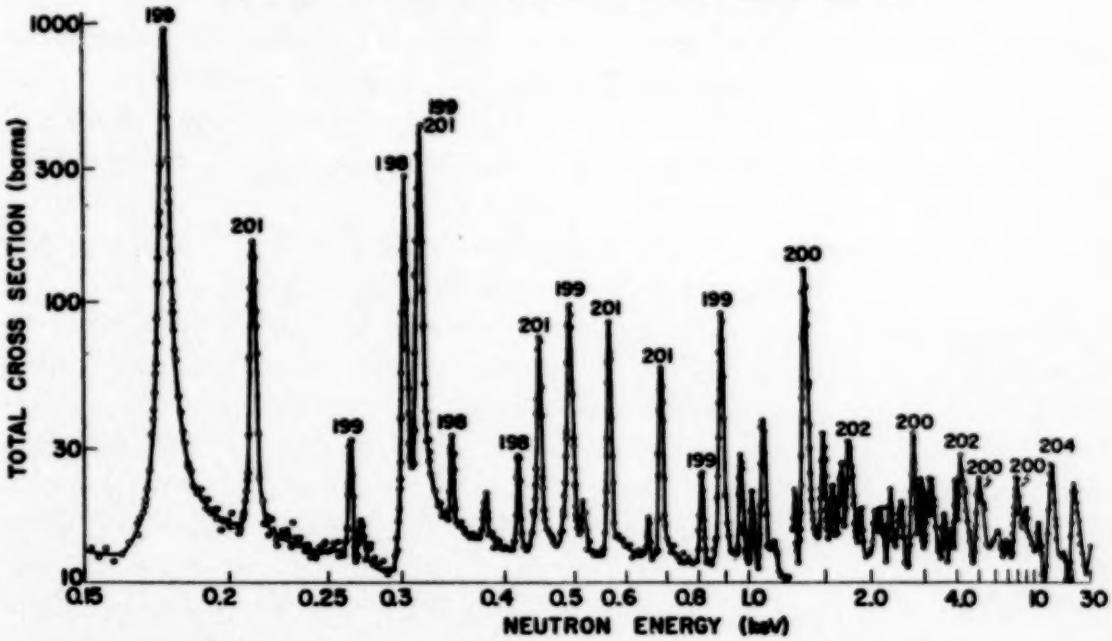

Fig. 2b. The total neutron cross section of normal mercury.

The total cross section of normal mercury, as obtained from the transmission measurements, is shown in fig. 2. The results shown are composites of the data

for all of the samples of normal mercury. The transmission of the enriched samples are shown in fig. 1, where the results for a sample of normal mercury are included for comparison.

2.2. ISOTOPIC ASSIGNMENT OF RESONANCES

The magnitude of the transmission dips observed in the various spectra of fig. 1 are our principal source of information about the isotopes responsible for the resonances of mercury. These data were used in making isotopic identifications by finding, for each resonance, the assignment for which the areas of the transmission dips of all the runs are consistent with a single set of resonance parameters. The results obtained are given in table 1. They are also indicated in fig. 1 by labelling a resonance with its energy only on the curve associated with the isotope to which the resonance is assigned. The results of the present study are consistent with those few assignments [8]) that had been made previously on the basis of transmission measurements.

Although the transmission data for the separated isotopes give a unique and clear-cut isotopic assignment of prominent and well-resolved resonances, some of the weak resonances observed with thick samples of normal mercury did not give transmission dips with a measurable area when the relatively thin enriched samples were studied. Levels of this kind are those at 71 and 93 eV. We have therefore attempted to identify the isotopes responsible for these weak resonances by observing the gamma-ray spectra resulting from resonant capture of neutrons. In another study of this kind, Bird *et al.* [9]) found that capture in the odd-neutron nucleides of mercury resulted in a small but observable line in the low-energy spectrum of single gamma rays, a line which is produced by the decay of the first excited state of the compound nucleus. These gamma-ray lines, at 368 keV from the target Hg^{199} and at 439 keV from the target Hg^{201}, serve as a means of isotopic identification of resonances. However, the spectrum of single gamma rays was not useful for identification of the resonances of the even isotopes of mercury since no lines were observed in their spectra.

In our application of capture gamma-ray spectra for isotopic assignment of resonances, we found that it is advantageous to record the spectra associated with coincident counts in *two* NaI scintillators rather than the spectra of *single* gamma rays. When single gamma rays are recorded, the characteristic lines used for isotopic identification tend to be submerged in a general background of unwanted counts. The relative magnitude of this background is reduced by about a factor of ten by requiring a coincident count in a second crystal. Moreover, some further improvement is achieved by requiring that the height of the coincident pulse should correspond to a gamma-ray energy greater than 600 keV. The principal effect of this latter refinement is to suppress the 511-keV background line from annihilation quanta.

The equipment used in the observation of gamma-ray spectra for isotopic

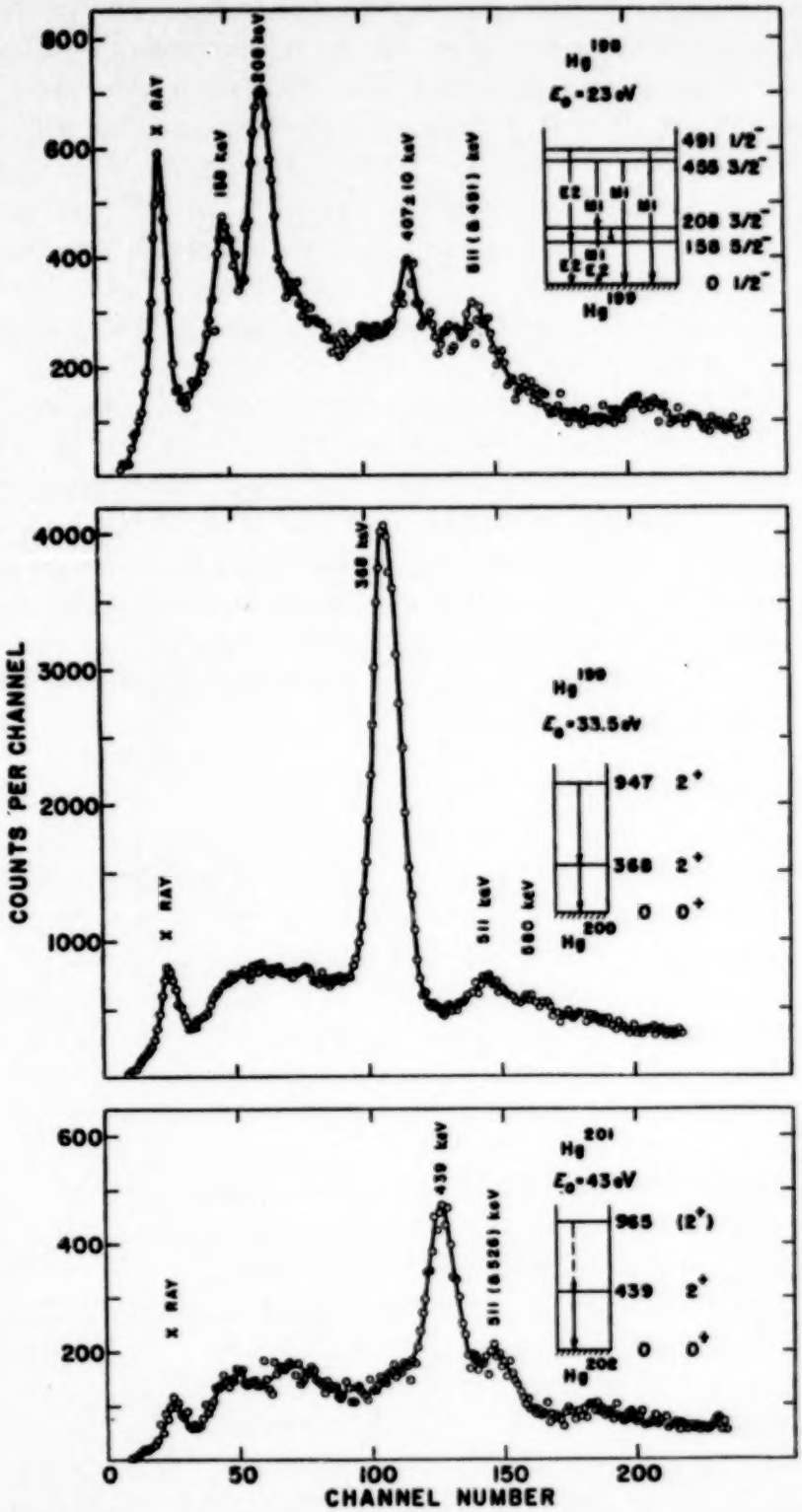

Fig. 3. Spectra of low-energy gamma rays following neutron capture in resonances of Hg^{198}, Hg^{199} and Hg^{201}. No background corrections have been made. Most of the prominent lines arise from transitions between the known levels indicated on the level schemes in the upper right of each figure.

identification is described in section 3 and shown in fig. 4. Illustrative examples of the spectra obtained for isotopic identification are shown in fig. 3. It is seen that the characteristic lines that result from capture in the even-odd isotopes are very prominent. It was particularly impressive to find that the 71-eV resonance, which could not be identified from the results of hundreds of hours of transmission measurements, could be assigned to Hg^{201} (in confirmation of the results of Bird *et al.* [9])), after a running time of only 10 minutes. Moreover, it is seen in the figure that capture in the even isotope Hg^{198} also results in a characteristic line spectrum which is clear enough to be used for isotopic identification.

In addition to the spectra presented in fig. 3, coincidence gamma-ray spectra were measured for the resonances at 71, 90, 130, 175 and 210 eV. In each case the spectrum leads to a positive isotopic assignment that is in agreement with that from the transmission measurements. The weak resonance at 93 eV was also studied, but in this case no identification could be made. However, from the combined results of the transmission and gamma-ray measurements, the 93-eV resonance can be assigned to either Hg^{198} or Hg^{202}, or possibly Hg^{200}. Consideration of the systematics of level densities and neutron widths make Hg^{198} the most probable assignment.

2.3. RESONANCE PARAMETERS

The transmission data presented above were analyzed under the assumption that the cross section may be described as resulting from the sum of contributions from resonances having the single-level Breit-Wigner shape for s-wave neutrons [10]); the effects of both radiative capture and scattering were included. The principal method used to deduce the resonance parameters was that of partial areas [11]) of transmission dips. Briefly stated, in this method one considers the area above a transmission dip in a restricted interval ($E_0-\varepsilon$ to $E_0+\varepsilon$) around a resonance at energy E_0. This interval must include all transmission data points which are affected by resolution; that is, the transmission dip must be completely resolved outside of the energy interval used. In this case, the partial area A'_E is independent of resolution and is determined completely by the resonance width Γ, the Doppler width Δ, and the product $n\sigma_0$ of the sample thickness and the cross section at exact resonance. Curves of A'_E/Δ versus $n\sigma_0$, with Δ/Γ as a running parameter, have been prepared for values of $\delta E/\Delta \equiv 2\varepsilon/\Delta$ ranging from 0.5 to 100. Using these curves, when n is known one may obtain a different relation between σ_0 and Γ for each sample thickness used. Also, independent runs using the same sample thickness may be analyzed with different values of $\delta E/\Delta$ to give different relations between σ_0 and Γ.

Wherever possible, an additional relation between σ_0 and Γ was obtained by curve fitting. The effects of Doppler broadening and interference between

resonance and potential scattering were included in the curve fitting, but resolution broadening was not. Hence the method was applied only to resonances which are rather well resolved. The curve fitting was especially useful as a means of checking on the importance of errors that might arise in the area analysis from the assumption of a symmetrical resonance shape.

Because of the close spacing of the three resonances near 310 eV, a special treatment of the data was required. The energies and shapes of the three resonances were assumed to be known. The parameters σ_0 and Γ for each of the resonances were then varied until the area of the complex transmission dip formed by the three resonances was consistent with the experimental area for each sample. This series of calculations, which was performed on the digital computer GEORGE, takes into account both Doppler broadening and the asymmetry in the shapes of resonances.

To find the best values of the individual resonance parameters, all of the independent relationships obtained by the above methods were combined by the least-squares method described in the Appendix to give solutions for σ_0 and Γ. The quantity $g\Gamma_n$ is then calculated from the well-known equation [10])

$$g\Gamma_n = \frac{\sigma_0 \Gamma}{4\pi\lambda\!\!\!^{-2}_0} = \frac{\sigma_0 \Gamma E_0}{2.603 \times 10^6}. \tag{1}$$

Here g is the statistical factor given by $\frac{1}{2}(2J+1)(2I+1)^{-1}$, where I is the spin of the target nucleus and J that of the compound state that is formed; Γ_n is the scattering width, and $2\pi\lambda\!\!\!^{-}_0$ is the neutron wavelength at the exact resonance energy; E_0 is in eV and σ_0 is in barns. The results for σ_0, Γ, and $g\Gamma_n$ are shown in columns 3, 4 and 5 of table 1 along with the root-mean-square errors associated with them. In the few cases for which resonances could not be isotopically assigned, we list $F\sigma_0$ and $Fg\Gamma_n$, where F is the fractional abundance of the unknown isotope responsible for the resonance.

To obtain values for the radiation width Γ_γ and the scattering width Γ_n of a resonance from the results for σ_0 and Γ, it is necessary to know the spin J of the resonance in question. For the even target nucleides, $I = 0$ and therefore $J = \frac{1}{2}$ if it is assumed that only s-wave neutron interactions are observable at the energies considered here. Thus g has the single value of unity. For the odd-neutron target nucleides, the assignment of spin is more involved since J may assume either of the two values $I \pm \frac{1}{2}$. For clarity of presentation, the discussion of the data available for the spin assignments of resonances of Hg^{199} and Hg^{201} is deferred until the next section. The results of that discussion are listed in column 6 of table 1.

Once the value of J has been determined, values of Γ_n, Γ_γ and $\Gamma_n^0 \equiv \Gamma_n E_0^{-\frac{1}{2}}$ follow immediately. In a few cases the least-squares calculation gives values for σ_0 and Γ that lead to the physically impossible result of a negative radiation width. In all cases this result can be explained as arising from statistical uncer-

TABLE 1

Parameters of the neutron resonances in mercury. The errors listed are standard statistical errors

Target isotope	E_0 (eV)	σ_0 (barns)	Γ (mV)	$g\Gamma_n$ (mV)	J	Γ_γ (mV)	Γ_n (mV)	Γ_n^0 (mV)
196 ($I = 0$)	93.5 [a]	12700±3400	405± 100	184 ± 12	½	221±100	184± 12	19.0 ±1.2
198 ($I = 0$)	23.0	7000± 420	115± 7	7.1 ± 0.3	½	108± 7	7.1 ± 0.3	1.48± 0.05
	89.7	4880± 520	172± 15	28.9 ± 1.2	½	143± 15	28.9± 1.2	3.06 ± 0.06
	302.0	7200± 360	1030± 100	860 ± 110	½	170±100	860 ± 110	49.5 ± 6
	344.0	2800± 690	198± 35	73 ± 10	½	[f]	73 ± 10	3.9 ± 0.5
	417	3200±1380	310± 83	159 ± 27	½	151±109	159 ± 27	7.8 ± 1.3
199 ($I = \frac{1}{2}$)	33.5	8050± 360	335± 9	34.7 ± 0.7	1	289± 10	46.3± 0.9	7.99± 0.15
	129.6	2020± 950	460± 134	46 ± 9	0	275±100	185 ± 34	16.3 ± 3.0
	175.1	8500± 800	1210± 62	692 ± 30	1	288± 76	922 ± 40	69.8 ± 3.0
	263.8	1000±1050	260± 230	26 ± 5	1	225±235	35 ± 7	2.17± 0.4
	314	4700± 470	1370± 70	778 ± 120	1	330±130	1040 ± 160	58.5 ± 8.8
	491	1210± 100	2870± 140	655 ± 21	0	[f]	2620 ± 80	118.3 ± 3.5
	808	1660± 870	848± 271	436 ± 64	1	267±388	581 ± 124	20.4 ± 4.3
	880	1950± 140	3350± 182	2210 ± 80	1	405±172	2945 ± 108	99.3 ± 3.6

200 ($I = 0$)	1325	1830 ± 100	9500 ± 1500	9000 ± 1500	½	[f]	9000 ± 1500	250 ± 40
	2710	920 ± 40	12500 ± 2000	12000 ± 2000	½	[f]	12000 ± 2000	230 ± 40
	3800 [a]				½			
	5060	500 ± 15	18500 ± 2000	18000 ± 2000	½	[f]	18000 ± 2000	250 ± 30
	6650 [a]				½			
	7800	315 ± 15	59000 ± 16000	59000 ± 16000	½	[f]	59000 ± 16000	660 ± 180
201 ($I = \frac{3}{2}$)	43.0	483 ± 25	293 ± 13	2.35 ± 0.10		290 ± 13		0.71 ± 0.03 [e]
	70.8	345 ± 60	465 ± 56	4.58 ± 0.26		456 ± 60		1.09 ± 0.06 [e]
	210.4	2020 ± 130	925 ± 58	156 ± 9	1	509 ± 57	416 ± 24	28.6 ± 1.7
	312.5	2350 ± 940	900 ± 180	250 ± 80				29 ± 10 [e]
	445	2020 ± 330	1180 ± 118	417 ± 27				39.6 ± 2.6 [e]
	564	2530 ± 290	1460 ± 97	799 ± 30	2	182 ± 158	1278 ± 67	53.8 ± 2.8
	685	1860 ± 390	1830 ± 230	893 ± 79	2	401 ± 353	1429 ± 126	54.6 ± 4.8
202 ($I = 0$)	1710	1400 ± 150	6000 ± 2000	5500 ± 2000	½	[f]	5500 ± 2000	130 ± 50
	4105	610 ± 25	18500 ± 6000	18000 ± 6000	½	[f]	18000 ± 6000	280 ± 90
Not known	270.7	18 ± 6 [c]	2300 ± 900	4.4 ± 0.7 [d]				
	380 [b]							
	513	14 ± 19 [c]	1550 ± 2010	4.3 ± 0.5 [d]				
	650			8 ± 6 [d]				

[a]) The isotopic assignment is uncertain.
[b]) There are apparently two or three weak, unresolved resonances at about this energy.
[c]) The quantity listed is $F\sigma_0$ (F = fractional abundance).
[d]) The quantity listed is $Fg\Gamma_n$.
[e]) The quantity listed is $2g\Gamma_n^0$.
[f]) Assumed values of Γ_γ were used in calculating other parameters.

tainties in the experimental data. For these cases, or when the data were not complete enough to obtain a meaningful value of Γ_γ, the parameters σ_0, Γ and Γ_n were calculated for assumed values of Γ_γ.

For some of the resonances in Hg^{201}, the J-value could not be determined. However, the neutron widths of two of these, the levels at 43- and 71-eV, are so small that no significant error is made by calculating Γ_γ from $\Gamma_\gamma = \Gamma - 2g\Gamma_n$.

2.4. ASSIGNMENT OF J-VALUES

In general, there is only one situation that allows the spin of a resonance to be determined by transmission measurements alone. Since Γ is greater than Γ_n, eq. (1) gives

$$g > \frac{\sigma_0 E_0}{2.60 \times 10^6}. \tag{2}$$

Occassionally σ_0 is large enough, when applied in eq. (2), to eliminate the lower of the two values $g = \frac{1}{2}[1 \pm (2I+1)^{-1}]$ that are possible when $I \neq 0$. The limits of g for the resonances of Hg^{199} and Hg^{201} are listed in table 2. These results immediately show that $g \neq \frac{1}{4}$, and hence $J = 1$, for the resonances at 175,

TABLE 2

Spin assignments of the resonances in Hg^{199} and Hg^{201}

Target isotope	E_0	g_{min}	Calculated Γ_γ(mV)		Resonance spin			J-value assignment
			$J = I - \frac{1}{2}$	$J = I + \frac{1}{2}$	Transmission	Single γ rays	2-step cascades [f]	
	−2					(0) [a]	0	0
	34	0.10±0.005	196± 13	289± 10	(1)	1 [b, c, d, e]	1	1
	130	0.10±0.05	275±100	398±135		(0, 1) [e, d]	0	0
	175	0.57±0.06	−1380±132	288± 76	1	1 [d]	1	1
199	263	0.10±0.11	164±230	225±230		1 [e]		1
	314	0.57±0.06	−1740±480	330±170	1			1
	491	0.23±0.030	172±354	1940±250	0			0
	808	0.51±0.27	−895±460	267±388	(1)			(1)
	880	0.66±0.05	−5490±250	405±172	1			1
	43	0.01±0.0004	289± 12	291± 12				
	71	0.01±0.002	453± 56	459± 56				
	210	0.17±0.010	510± 57	676± 60		1		1
201	312	0.28±0.11	223±228	500±151				
	445	0.35±0.06	68±139	513±125				
	565	0.55±0.06	−670±280	182±158	2			2
	685	0.45±0.10	−552±420	401±353	(2)			(2)

[a]) B. B. Kinsey and G. A. Bartholomew, Can. J. Phys. **31** (1953) 1051
[b]) Landon and Rae [12])
[c]) Bird *et al.* [9]).
[d]) Bollinger *et al.* [13])
[e]) M. K. Brussel and R. L. Zimmerman, Bull. Am. Phys. Soc. **4** (1959) 472
[f]) Bollinger and Cote' [14]).

314, 808 and 880 eV in Hg^{199}; also, $g \neq \frac{3}{8}$, and hence $J = 2$, for the resonances at 564 and 685 eV in Hg^{201}.

To make further spin assignments it is necessary to employ some additional piece of information. One possibility is to make use of our knowledge, from this and other experiments, of the general behavior of Γ_γ. This idea has been applied to each resonance of the present data by calculating Γ_γ for the two allowed g-values and examining the results to find an inconsistency between one of the values and our estimate of what values Γ_γ may reasonably be expected to assume. The results of the calculations of Γ_γ are given in table 2. The J-value assignments given by our examination of these data are listed in column 4 of table 2. The assignments in parentheses are suggested by the data but are not quite certain.

Recent studies of the high-energy gamma rays resulting from resonant capture of neutrons have also given information about the spins of the resonances of Hg. As emphasized by Landon and Rae [12]), the observation of a ground-state transition from radiative capture in an odd-neutron target nucleus having spin $\frac{1}{2}$ is conclusive proof that $J \neq 0$ for the compound state, since the $0^{\pm} \rightarrow 0^{+}$ transition is strictly forbidden. However, a failure to observe the ground-state transition does not necessarily imply that $J = 0$ since the transition, although present, may merely be too weak to be observable. The care that must be exercised in this regard is strikingly illustrated by the results for the 175-eV resonance in Hg^{199}. Our transmission data demonstrate conclusively that $J = 1$ for this resonance. Yet the ground-state transition is exceedingly weak, accounting for only about 0.1 % of the primary transitions, as compared to about 3 % in the case of the resonance at 34 eV [13]).

A study of the high-energy gamma-ray spectra following resonant capture in even-odd nucleides with spin $\frac{3}{2}$ also may give strong indications of the spins of its resonances. If the compound nucleus is formed in a 2^{-} state, the ground-state transition would be expected to be either an M2 or E3, and hence very weak, whereas an E1 transition is possible from a 1^{-} state. Thus the observation of a strong ground-state transition in the spectrum is a convincing indication that $J = 1$. The spin of the 210-eV resonance of Hg^{201} is assigned on the basis of information of this kind.

Another kind of gamma-ray measurement for the determination of spin has recently been developed by Bollinger and Cote' [14]). In their method, termed the "2-step cascade method," one measures the total intensity of all gamma-ray cascades that proceed to the groud state in exactly two transitions. It is found that this two-step process is more probable for initial states having $J = 0$ than for those having $J = 1$, when the final (ground) state has $J = 0$.

The J-value assignments that are implied by the gamma-ray data are listed in columns 5 and 6 of table 2. The results of the two gamma-ray methods are in generally good agreement with each other and with the assignments from

the transmission measurements. Our conclusions as to the correct assignments, as judged from the combined results of the three different kinds of determinations, are listed in column 9. Note that one effect of the comparison presented in table 2 is to remove the previous uncertainties, arising from differing interpretations of the high-energy gamma-ray spectra, about the J-value of the resonance at 130 eV in Hg^{199}.

2.5. AVERAGE VALUES OF RESONANCE PARAMETERS

The parameters for individual resonances that are listed in table 1 may be used to deduce average values of parameters for the various isotopes of Hg. In table 3, we summarize the results obtained for the level spacing, the radiation width, and the neutron strength function. For comparison, the values of these quantities for neighboring nucleides of the same character are also given.

TABLE 3

Average values of resonance parameters. The binding energies B_n are known to an accuracy of about 60 keV. The numbers in parentheses associated with the values of $\bar{S}$ and $\bar{\Gamma}_n^0/D$ are estimates of the factor by which the values are uncertain.

Target isotope	I	B_n [a] (MeV)	$\bar{S}$ (eV)	N	$2(2I+1)\bar{S}$ (eV)	$\bar{\Gamma}_n^0/D \times 10^4$	$\bar{\Gamma}_\gamma$ (mV)	Calculated $\bar{\Gamma}_\gamma$ (mV)
$_{74}W^{183}_{109}$	$\frac{1}{2}$	7.44	12(1.2 [b])	5	48		52±11 [b]	61
$_{76}Os^{189}_{113}$	$\frac{3}{2}$	7.88	4.3(1.2)[c]	8	35		85±10 [c]	85
$_{78}Pt^{195}_{117}$	$\frac{1}{2}$	7.90	23(1.2)[d]	5	93		115±20 [b]	103
$_{80}Hg^{198}_{118}$	0	6.67	89(1.2)	4	179	1.7(1.8)	125±20	133
$_{80}Hg^{199}_{119}$	$\frac{1}{2}$	8.07	63(1.2)	5	253	2.7(1.4)	280±20	183
$_{80}Hg^{200}_{120}$	0	6.26	1730(1.4)	5	2460	2.1(1.6)		148
$_{80}Hg^{201}_{121}$	$\frac{3}{2}$	7.76	84(1.3)	4	692	1.8(1.6)	380±90	225
$_{80}Hg^{202}_{122}$	0		2540(1.4)	2	5080	1.7(3)		

[a]) H. E. Duckworth, Revs. Mod. Phys. **29** (1957) 767

[b]) D. J. Hughes and R. B. Schwartz, Brookhaven National Laboratory Report BNL-325, 2nd Ed. (1958)

[c]) H. E. Jackson, private communication (1960)

[d]) Argonne fast chopper group, unpublished (1960)

The average value $\bar{S}$ of the observed level spacing was calculated from the number N of resonances for which the resonance energy E_0 satisfies the requirement $E_1 < E_0 \leqq E_2$. The uncertainties associated with $\bar{S}$ are estimates of probable errors based on the magnitude of N. In the calculation, the spacings between adjacent levels of the same spin and parity are assumed to be governed by the Wigner distribution and the density of states is assumed to be proportional to $(2J+1)$. For each isotope, the upper limit E_2 was chosen as the energy of a resonance at a low enough energy to insure that almost all of the resonances

at lower energy have been detected. For all isotopes except Hg^{199} we let $E_1 = 0$; for Hg^{199} we let $E_1 = -2$ eV, the energy of the state just below the binding energy.

Under the assumption that the density of states is proportional to $(2J+1)$ for small values of J, as all the experimental evidence now tends to confirm, the average spacing may best be discussed in terms of the derived quantity $2(2I+1)\bar{S} = D_0$, a quantity which is independent of J and is such that the spacing of levels of spin J equals $D_0/(2J+1)$. This quantity is listed in column 4 of table 3. As is seen from the results given in the table, the data for Hg help to fill out the picture [1]) of a D_0 that increases rapidly as one approaches the doubly closed shell (82 protons, 128 neutrons). It is noteworthy that this behavior of D_0, like that for the data below the 50-proton shell [15]), cannot be explained on the basis of changes in the excitation energy, since the neutron binding energy is approximately the same for Os^{189}, Pt^{195}, Hg^{199} and Hg^{201}.

The strength function Γ_n^0/D was calculated from the data of table 1 by means of the relationship

$$\frac{\overline{\Gamma}_n^0}{D} = \frac{1}{E_2 - E_1} \sum_r^M (g\Gamma_n^0)_r, \tag{3}$$

where the sum is over all resonances satisfying the condition $E_1 < E_0 \leqq E_2$. The error assigned to $\overline{\Gamma}_n^0/D$ is a probable error dependent on the number M of resonances. The assumptions concerning the limits E_1 and E_2 were similar to those outlined for the calculations of $\bar{S}$, except that the upper limit E_2 was generally greater in calculating $\overline{\Gamma}_n^0/D$, since a failure to detect weak resonances does not have an important effect on the sum in eq. (3). Therefore, since all resonances within the range from E_1 to E_2 may not have been detected, the values of M used in estimating the errors were derived from the relationship $E_2 - E_1 = M\bar{S}$.

The results for the strength function, as given in table 3, are in generally good agreement with those of neighboring nucleides. They tend to be consistent with those obtained by Chase *et al.* [16]) in an optical-model calculation that takes into account the effects of the diffuse surface and the deformation of the nucleus. Only the value $(2.7 \pm 1.0) \times 10^{-4}$ for Hg^{199} appears to be somewhat inconsistent with the calculated value of 1.0×10^{-4}. However, this discrepancy is no greater than that for many other nucleides and, especially in view of the small size of the statistical sample, it is not necessarily significant.

The calculation of average values of the radiation width Γ_γ from the results of table 1 is complicated by the experimental uncertainty of the individual values, since these values are drawn from a distribution having a width that is probably of the same order of magnitude as the experimental errors. Therefore, in table 3 we list as the average a value that is merely consistent with all the individual widths.

Here again for Γ_γ, as for D_0, the results of the present study confirm and expand our previous knowledge [1,2]) that Γ_γ increases steadily as the doubly closed shell is approached from smaller values of A. Once more the effect cannot be explained in terms of changes in the excitation energy. One possible explanation of the systematic variation of the radiation widths is that it results from changes in the relative importance of the so-called "direct transitions" [17]). However, at the present time this process is too incompletely understood to permit a quantitative consideration of the matter.

A second interpretation of the increase in Γ_γ with increasing A might be that it is a shell effect which makes itself felt because of the influence of shell structure on the level density. In the simple statistical model of radiation widths †, the partial widths of individual transitions are assumed to depend only on the energy difference and multipolarity of the transition and the level spacing at the initial compound state. Then the total radiation width Γ_γ, which is approximately equal to the sum of partial widths of the primary E1 transitions, is given [18]) by

$$\Gamma_\gamma = cA^{\frac{2}{3}} \int_0^Q (Q-E)^3 \frac{D(Q)}{D(E)} \, dE, \tag{4}$$

where c is a constant, Q is the excitation energy, E is the energy of the final state involved in the primary transition, and $D(Q)$ and $D(E)$ are te level spacings at energies Q and E, respectively. The quantities A and Q are almost the same for the target nucleides Os^{189}, Pt^{195}, Hg^{199} and Hg^{201}, so that eq. (4) can account for changes in Γ_γ only by means of changes in the energy dependence of D, i.e., in the ratio $D(Q)/D(E)$. For the simple Fermi-gas model of nuclear level densities, Bethe [10]) has shown that the density $\rho \equiv D^{-1}$ is essentially proportional to $\exp(\alpha\sqrt{AE})$, where α is a constant; thus, the ratio $D(Q)/D(E)$ is equal to $\exp[-\alpha\sqrt{A}(\sqrt{Q}-\sqrt{E})]$, which decreases with increasing A for any given energies Q and E. As a consequence Γ_γ would decrease with increasing A, in contradiction to the experimental evidence for the nucleides being considered.

What is needed to explain the experimental behavior of Γ_γ is a change in the energy dependence of the level density as the closed shell is approached. Examining other relationships for the level density, we find that the formula of Rosenzweig [19]), which explicitly takes shell effects into account, again fails to explain the observed behavior of the radiation widths. Another level-density relationship which includes shell effects is that of Newton [20]).

† In section 4 it is shown that the γ-radiation resulting from neutron capture in Hg^{201} cannot be treated as a purely statistical process in that a few high-energy transitions appear to play an exceptionally important role in determining the total radiation width. However, even with the contribution of these high-energy γ rays subtracted, the remainder Γ'_γ is found to be at least twice as great for Hg^{199} and Hg^{201} as for Os^{189}. Thus a statistical treatment involving many transitions is needed to explain the behavior of the widths.

Cameron [21]) has used this relationship in eq. (4) to obtain an expression for Γ_γ. Using his equation, we obtain the widths listed in the last column in table 3; these widths are normalized to the experimental value for Os^{189}. It is seen that the behavior of the calculated widths is in qualitative agreement with that of the experimental data, especially in view of the nonstatistical influence of high-energy transitions from capture in Hg^{201}, a subject to be treated in a later section. It should be stressed that the qualitative similarity in the calculated and experimental results does not necessarily support the form of the energy dependence of Newton's relationship; it only tends to confirm the direction of the predicted *change* in the energy dependence near the closed shell.

2.6. DISTRIBUTION OF RADIATION WIDTHS

Perhaps the most interesting result of the cross-section measurements presented above is the large difference in the radiation widths of the Hg^{201} resonances. In no previous measurement have statistically meaningful fluctuations of a comparable magnitude been reported †. As a result, it had become generally accepted that Γ_γ is almost constant from resonance to resonance in a given nucleide [1, 2]). The widths obtained for the resonances in Hg^{198} and Hg^{199} are consistent with this hypothesis. The widths for Hg^{201} are clearly very different, however. In view of the unique character of this result, a considerable effort was made to find any possible source of errors in the data or in the calculations. Although the magnitudes of some of the widths have been changed from what was originally reported by us [3]), chiefly because of the influence of the results of new transmission measurements with the thickest sample, the basic finding of large fluctuations in the total radiation widths of Hg^{201} remains unchanged. The failure of the Harwell [9]) group to observe differences of a comparable magnitude in their measurements on mercury does not, in the opinions of the authors, cast serious doubt on the existence of these differences, in view of the better resolution, wider range of sample thickness, and smaller statistical errors of the present set of measurements. Moreover, the large difference between the radiation widths for the 43- and 71-eV resonances has recently been confirmed by the Brookhaven group [22]). Thus the wide spread among the radiation widths of Hg^{201} is considered to be real and the remainder of this paper is concerned with the investigation of different aspects of this effect.

3. Gamma Rays from Resonant Capture

Since the total radiation width is the sum of the partial widths for transitions from the initial compound state to all levels of lower energy, large differences in the total radiation widths of resonances should be accompanied by noticeable differences in their capture gamma-ray spectra. In an effort to detect a correlation of this kind between radiation widths and spectra, both the single and

† See *note added in proof*.

coincidence gamma-ray spectra resulting from capture in the Hg^{201} resonances have been measured.

3.1. APPARATUS

The capture gamma-ray spectra were studied with the experimental apparatus shown in fig. 4. To provide a high intensity of neutrons, rotor I [5]) of the chopper was used. Neutron flight paths of both 6.74 and 25 m were used, giving time-of-flight resolutions of about 0.4 and 0.08 μsec/m, respectively.

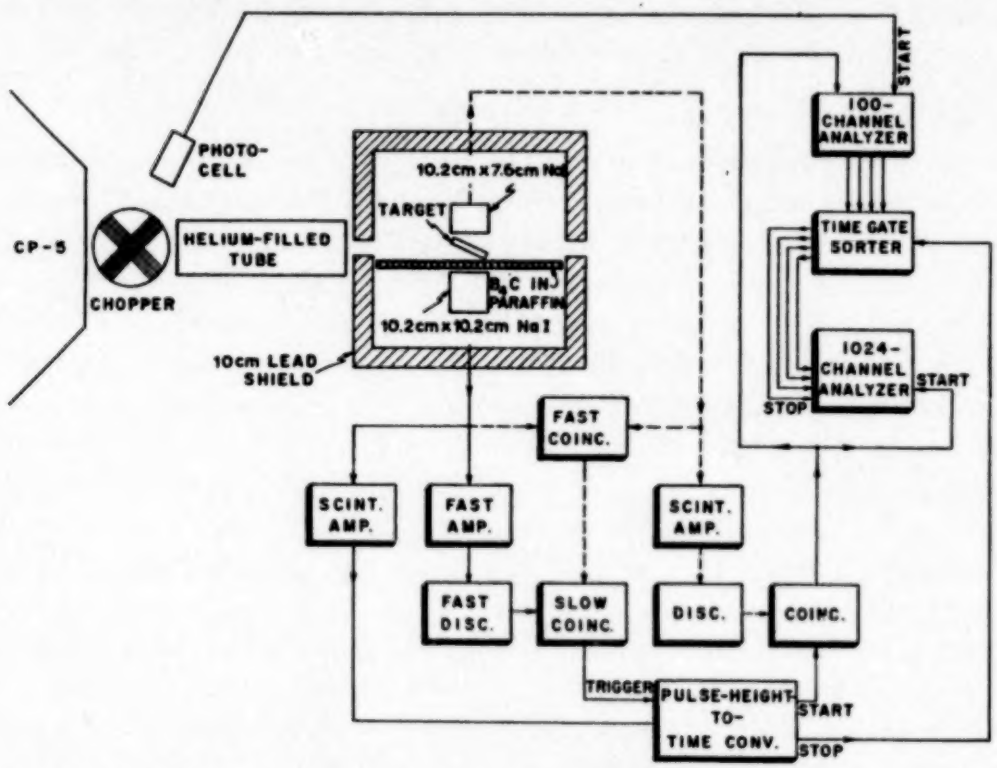

Fig. 4. Experimental arrangement for the observation of resonance-capture gamma-ray spectra. The dashed lines indicate the extra components used for coincidence measurements.

The spectra of single gamma rays were studied with a 10.2 cm × 10.2 cm NaI(Tl) scintillator which was shielded by 3.8 cm of B_4C in paraffin to exclude neutrons scattered out of the target. The coincidence measurements were made with a 10.2 cm × 10.2 cm and a 7.6 cm × 10.2 cm crystal; the coincidence requirement made it unnecessary to use a neutron absorber in front of the crystals.

The electronic circuits shown in fig. 4 were used to record the pulse-height spectra for four different bands of neutron energy in the following manner. A trigger pulse is fed to the pulse-height-to-time difference converter when certain arbitrary conditions on the pulse-height of one or both crystals are satisfied. This trigger permits the height of the amplifier pulse being fed to the converter to be transformed into two output pulses ("start" and "stop"), for which the difference in time is proportional to the height of the input pulse.

The "start" pulse is now required to pass through a gate which may impose a second set of conditions on the scintillation pulse heights. If these conditions are met, the "start" pulse is used to trigger the 1024-channel analyzer. For runs of this kind, the analyzer is split into 4 groups of 256 channels, and the addresses of these four groups advance in parallel. The "start" pulse is also used as the detector input of the 100-channel analyzer, which is triggered by the photocell pulse from the chopper just prior to each burst of neutrons. If the "start" pulse falls within one of four groups of channels in the 100-channel analyzer, a pulse is fed out of that group. This output pulse opens one of four gates through which the "stop" pulse from the converter is allowed to pass into the corresponding portion of the 1024-channel analyzer.

3.2. SPECTRA OF SINGLE GAMMA RAYS

As a by-product of measurements with the experimental arrangement described above, the spectrum of total gamma-ray intensity as a function of neutron

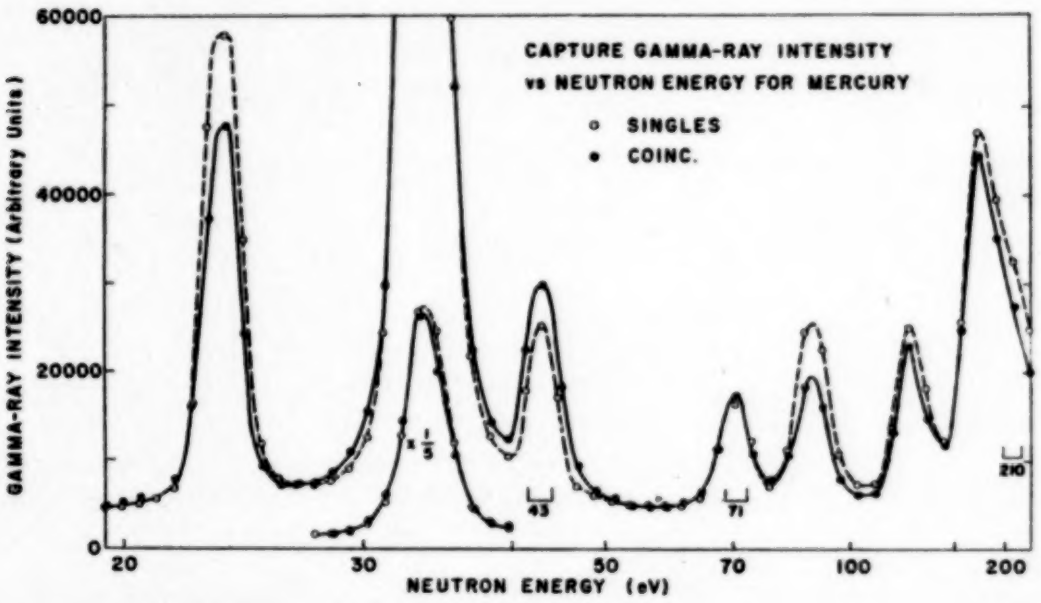

Fig. 5. Total gamma-ray intensity versus neutron time-of-flight for a mercury target. The dashed line shows single gamma-ray intensity while the solid line shows the rate of detected coincidences. The curves are normalized for equal areas under the peaks at 71 eV. Some of the background counts have been subtracted from the data for single gamma rays.

time-of-flight is recorded on the 100-channel analyzer at the same time the pulse-height spectra are recorded in the 1024-channel analyzer. The dashed curve of fig. 5 shows the time-of-flight spectrum obtained with the 6.7-m flight path when single gamma rays from a mercury target were detected. The time intervals during which pulses were accepted for analysis in the 1024-channel analyzer are shown by square brackets. The pulses arriving during the off-resonance intervals between the 43- and 71-eV resonances were recorded as an

approximate measure of the background spectra. The data obtained with the 25-m flight path are similar to those of fig. 5, except that the resonances are much better resolved.

The pulse-height spectra, obtained with the 6.74-m path, for the Hg^{201} resonances at 43, 71 and 210 eV are shown in fig. 6. Background counts have been subtracted from these spectra and the curves were normalized for equal areas, that is, for the total number of detected gamma rays. Even the most qualitative examination of the data of fig. 6 reveals significant differences in the three spectra. For both resonances which have large radiation widths,

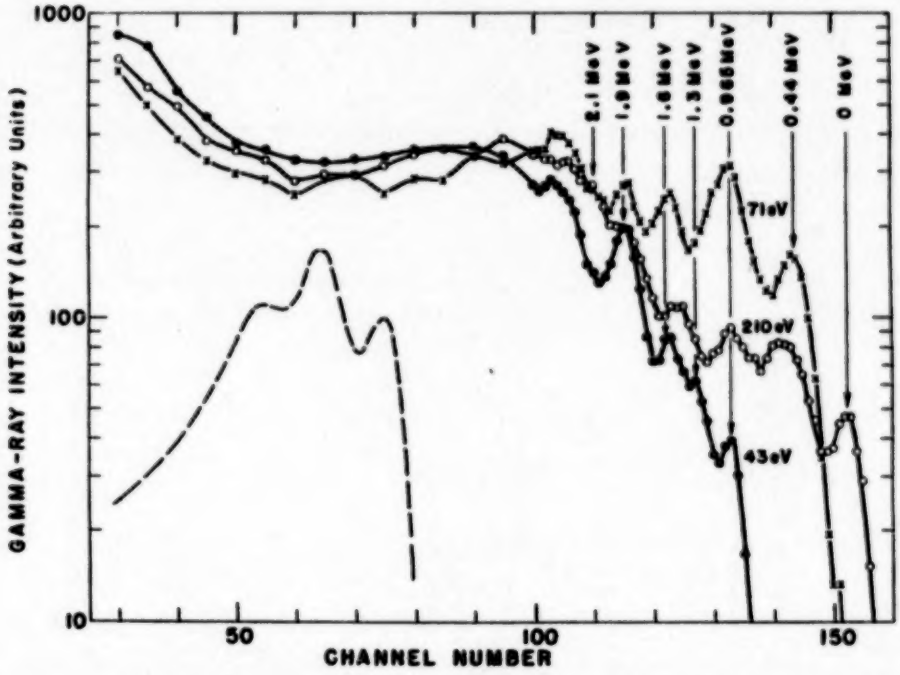

Fig. 6. Spectra of high-energy gamma rays following neutron capture in resonances of Hg^{201}. The spectrometer response to a single gamma ray is shwon as a dashed line at the lower left of the figure.

those at 71- and 210-eV, the spectra contain intense transitions to the levels within 2 MeV of the ground state, whereas these transitions are weak for the 43-eV resonance. Except for the different intensities of these high-energy transitions, the spectra appear quite similar. The data suggest, then, that the fluctuations in the total radiation widths are associated with differences in the intensities of the high-energy transitions.

To arrive at quantitative conclusions concerning the effect of the highest energy transitions on the total radiation width, it is necessary to obtain the absolute intensities of these transitions. The first step in the analysis for the transition probabilities was to locate the excited states to which the transitions proceed. Only the energies of the first two excited states of Hg^{202} were known [23]) from previous experiments. Other levels had to be located by unpeeling the

resonant-capture gamma-ray data. For this purpose, the pulse-height spectrum of a 7.64-MeV gamma ray which follows capture of thermal neutrons in Fe^{56} was used as the line shape of the scintillator; this reference spectrum, which was obtained by correcting the capture γ-ray spectrum of Fe^{56} for contributions from several weaker lines, is shown as a dashed line in the lower left of fig. 6.

In an analysis of the kind indicated above, it was found that at least seven transitions are needed to explain the high-energy transitions directly to states below 2.2 MeV. These transitions, or the low-energy states to which they proceed, are given in fig. 6 and in table 4. The seven transitions indicated are not necessarily a unique or complete description of the spectra since only strong transitions can be observed and the lines that are observed may result from the superposition of two or more unresolved lines. However, this ambiguity in the results of the analysis is of no great importance for the present purpose, in that we are primarily interested in the *sum* of the partial widths for the high-energy transitions, and this sum does not depend sensitively on the decay scheme used to describe the spectra.

After determining a level scheme for Hg^{202}, the next step in the analysis was to find the relative intensities a_{jr} of transition j following capture in the rth resonance. These intensities were determined by a least-squares fit of each measured spectrum to a relationship of the form $y_{ir} = \sum_j a_{jr} R_{ij}$, where y_{ir} is the number of counts in the ith channel for the rth spectrum and R_{ij} is the contribution to the ith channel of a transition of unit intensity and an energy equal to that of the jth transition. The reference spectrum R_{ij} was the corrected 7.64-MeV line of Fe^{56}, which was discussed above. The use of the same line shape for all transitions is not expected to result in significant errors since the range of gamma-ray energies considered is rather small. The procedure followed in making the least-squares fit of the experimental spectra was to find the set of a_{jr} that results in a minimum value for the variance V_r^2, defined by

$$V_r^2 = \sum_i w_{ir}(y_{ir} - \sum_j a_{jr} R_{ij})^2, \tag{5}$$

where w_{ir} is the weight associated with the value y_{ir}. This minimization has been coded for machine computation on the Argonne digital computer GEORGE.

An important aspect of the least-squares method is that the minimum value of V_r^2 provides a measure of the goodness of fit. Specifically, the statistical distribution of the minimum value is approximately a χ^2 distribution with $(n-m)$ degrees of freedom, where n is the number of channels used and m is the number of unknown a_j in the analysis. To find the best values for the energies of the transitions used to describe the capture gamma-ray spectra, as discussed earlier, the energies were adjusted in value until an acceptably small value of V_r^2 was obtained for all three spectra.

Having determined a set of a_{jr}, it remains to find the normalizing constant to convert these relative values into absolute units. Elementary considerations indicate that the probability I_{jr} of emission of the jth gamma ray following capture in the rth resonance, is given by $I_{jr} = Ca_{jr}/N_r$, where N_r is the number of captures at the rth resonance and C is a constant that is independent of j and r if the same detector geometry is used in all measurements. Furthermore, if we neglect the effects of multiple scattering of neutrons, then $N_r = f(E)\phi_r$, where $f(E)$ is the neutron flux and ϕ_r is the fraction of incident neutrons that are captured in the time channels used to study the resonance r. Thus for a dE/E neutron spectrum we have

$$I_{jr} = ka_{jr}E_0\phi_r^{-1}, \tag{6}$$

where k is another constant independent of j and r. The fraction ϕ_r was determined by using the parameters of table 1 in a double numerical integration that takes into account both Doppler and resolution broadening of the resonance. The constant k is determined by making use of the known [13]) intensity (0.033) of the ground-state transition for the 34-eV resonance of Hg^{199}, the spectrum for this resonance having been recorded at the same time as those in Hg^{201}. Note that the intensity of the 34-eV resonance was itself obtained by normalization to the 6.45-MeV line of the thermal spectrum, and that the intensity of this thermal line is somewhat uncertain. Thus the normalization constant k involves a long chain of measurements, with the result that it might be uncertain by as much as a factor of 1.4.

TABLE 4

Intensities of high-energy gamma rays from capture in the resonances at 43, 71 and 210 eV of Hg^{201}.

Energy of final state (MeV)	I_γ (Photons per 100 captures)		
	43 eV	71 eV	210 eV
0	0 ± 0.2	0.6± 0.5	7.2± 0.4
0.44	0.9± 0.2	18.0± 0.8	1.0± 0.7
0.965	0.5± 0.4	1.9± 1.6	2.6± 1.0
1.31	5.4± 0.7	3.7± 2.3	1.6± 0.8
1.61	3.4± 1.0	7.2± 3.0	0.9± 1.2
1.9	1.2± 1.0	8.3± 2.8	17.8± 1.4
2.1	10.0± 1.6	12.3± 4.7	9.5± 1.9
$\sum_{i=1}^{7} I_{\gamma i}$	21.3± 2.1	52.0± 6.8	40.6± 3.1
$\sum_{i=1}^{7} \Gamma_{\gamma i}$(mV)	62 ± 6	234 ±31	210 ± 20
$(\Gamma_\gamma - \sum_{i=1}^{7} \Gamma_{\gamma i})$(mV)	228 ±14	222 ±69	300 ±60

The results of the spectral analysis outlined agove are listed in table 4. The first column gives the energies of the final states involved in the transitions used to describe the high-energy portion of the spectra. The absolute intensities (in units of photons per 100 captures) of the various transitions are listed in the remaining columns; the errors associated with the intensities are those arising only from statistical uncertainties in the gamma-ray spectra. The second from the last line of the table gives the sum of the intensities of the high-energy transitions.

The partial widths Γ_{jr} for the jth transitions are readily obtained from the results of tables 2 and 4 since $\Gamma_{jr} = I_{jr}\Gamma_{\gamma r}$, where $\Gamma_{\gamma r}$ is the total radiation width of the resonance r. The next to the last line of table 4 gives the sum $\sum_j \Gamma_{jr}$ of the partial widths for the seven high-energy transitions. If these sums are subtracted from the total radiation widths, the remainders $\Gamma''_\gamma = \Gamma_\gamma - \sum \Gamma_{jr}$ are found to be 228 ± 14, 222 ± 69 and 300 ± 60 mV. These values are equal within the errors and they are certainly consistent with the degree of fluctuation which has been observed in Γ_γ for other nucleides; the systematic uncertainties in the values of $\sum \Gamma_{jr}$ resulting from uncertainties of the normalizing constant k are not large enough to negate this conclusion.

The relative constancy of Γ''_γ and the large differences in the partial sum $\sum \Gamma_{jr}$ gives quantitative confirmation of our earlier conjecture that the fluctuations in the total radiation width result from fluctuations in the intensities of the transitions of highest energy.

3.3. MULTIPLICITY OF GAMMA RAYS

The measurements described in the last section show that an important fraction of the transitions following capture in the 71- and 210-eVresonances proceed directly to low-lying levels, whereas this fraction is relatively small for the 43-eV resonance. As a consequence, it is to be expected that the average number $\bar{\nu}$ of photons per capture is higher for the 43-eV resonance than for the 71- and 210-eV resonances.

Experimentally, *relative* values of the average gamma-ray multiplicity may be determined as the number of γ rays detected per neutron capture, i.e.,

$$\bar{\nu} \propto \frac{\text{total number of } \gamma \text{ rays detected}}{\text{number of neutrons captured}}. \tag{7}$$

The validity of this relationship depends on the following assumptions: a) the detection efficiency of the scintillator is constant; b) the low-energy discrimination level, set to eliminate room background and the 511-keV annihilation radiation, excludes a constant fraction of the total number of gamma rays detected by the crystal; c) a constant fraction of the gamma rays produced are internally converted or reabsorbed in the sample; d) the detection efficiency is small enough that the probability of detecting more than one gamma ray per capture is negligible.

The recent Monte Carlo calculations by Miller and Snow [24]) show that the detection efficiency of a 10.2 cm × 10.2 cm NaI scintillator does not change much over the range of interest to us. Experiments with different bias settings showed assumptions (b) and (c) to be valid within about 6 % for the resonances at 43- and 71-eV. Rough considerations of the experimental geometry show that certainly less than 5 % of the counts result from accidental sums of two or more gamma rays. Moreover, there is a strong canceling of errors from all the above sources when one considers the *ratio* of two multiplicities. Thus we estimate the total systematic error in such a ratio as less than 5 %, compared to statistical errors of about 13 %.

In making use of eq. (7) to determine $\bar{\nu}$, the number of neutron captures was calculated in the same way as was described above for the determination of partial radiation widths. The mercury sample used in the capture gamma-ray studies had a thickness of 0.0113 atoms/barn in the direction of the beam. The resonance parameters used are those listed in table 1. With these data, the ratio of the number of captures in the resonance at 43 eV to that at 71 eV is calculated to be 1.55 ± 0.14. On the basis of data from several runs, one of which is shown in fig. 5, the ratio of the total number of gamma rays produced is, under the assumptions discussed above, 1.94 ± 0.08. Thus the ratio of the gamma-ray multiplicities for the resonances at 43 and 71 eV is

$$\frac{\bar{\nu}_{43}}{\bar{\nu}_{71}} = \frac{1.94 \pm 0.08}{1.55 \pm 0.14} = 1.25 \pm 0.18.$$

Another measurement of interest is the number of coincident counts in two detectors as a result of resonant capture of neutrons. This quantity is proportional to the average number of pairs of photons produced per capture and the total number of captures. If, following a given capture, there are ν photons produced, there are $\frac{1}{2}\nu(\nu-1)$ pairs of photons and thus $\nu(\nu-1)$ ways in which a coincidence may be recorded. Thus, the number of coincidences per neutron capture is proportional to $\langle \nu(\nu-1) \rangle_{\mathrm{av}}$. This statement implies, in addition to the assumptions made before, that the coincidence efficiency is constant.

The neutron time-of-flight spectrum resulting from a typical coincidence measurement is given in fig. 5. Proceeding in the same way as for the single γ-ray spectra, we obtain the result

$$\frac{\langle \nu_{43}(\nu_{43}-1) \rangle_{\mathrm{av}}}{\langle \nu_{71}(\nu_{71}-1) \rangle_{\mathrm{av}}} = 1.57 \pm 0.19.$$

The largest source of error in the above calculations arises from uncertainties in the resonance parameters used to compute the ratios of the number of captures. This source of error is eliminated if we take the ratio of the above

ratios and obtain

$$\frac{\langle \nu_{43}(\nu_{43}-1)\rangle_{av}/\langle \nu_{43}\rangle_{av}}{\langle \nu_{71}(\nu_{71}-1)\rangle_{av}/\langle \nu_{71}\rangle_{av}} = 1.22\pm 0.08.$$

All the results presented above show that the γ-ray multiplicity is greater for the 43-eV resonance than for the 71-eV resonance. Since this difference is in the direction to be expected from the differences in the γ-ray spectra, it tends to confirm the importance of the high-energy transitions for the decay of the initial compound states formed by capture in the resonances of Hg^{201}.

4. Discussion of Fluctuations in Total Radiation Widths

In the preceding sections it was shown that the total radiation widths and the capture gamma-ray spectra of the resonances of Hg^{201} differ to a greater extent than had been expected on the basis of the results for other nucleides. We now explore several possible explanations of the peculiar characteristics of the Hg^{201} resonances.

4.1. ENHANCEMENT OF HIGH-ENERGY TRANSITIONS

We have seen in the previous section that the fluctuations in the total radiation widths of the resonances in Hg^{201} result almost entirely from differences in the partial widths of the highest energy transitions. Clearly, these differences in the partial widths can produce large fluctuations in the total radiation widths of the resonances in Hg^{201} only because the transitions involved contribute such a large fraction of the total width, namely, an average of about 40 % for the three resonances investigated. Ones intuitive reaction is that 40 % is a much larger contribution than would be expected for the sum of the intensities of seven lines if the radiative de-excitation of the initial compound state were governed by statistical factors alone [18]), i.e., if the primary spectrum were of the form $\rho(E)(Q-E)^3$. It is the purpose of the present section to make a quantitative examination of this question.

The total radiation width is the sum of all the partial widths for transitions from the capture state to all nuclear levels of lower energy. We assume that only E1 transitions contribute appreciably to the primary spectrum, in which case the expectation values of the partial widths are all proportional to the cube of the transition energy. Thus, allowing for the possibility that the seven transitions of highest energy are of a different character than the other transitions, the total radiation width may be expressed as

$$\langle \Gamma_\gamma \rangle_{av} = \alpha \sum_{i=1}^{7} (Q-E_i)^3 + \beta \sum_{i=8}^{n} (Q-E_i)^3, \tag{8}$$

where α and β are constants. The question of whether or not the seven transitions

of highest energy are abnormally strong may be answered by determining whether α is significantly greater than β. The experimental data of table 4 show that the first term of eq. (8) is equal to $0.4\ \langle\Gamma_\gamma\rangle_{av}$ and the second term is equal to $0.6\ \langle\Gamma_\gamma\rangle_{av}$. Thus, the "enhancement factor" $k \equiv \alpha/\beta$, is given by

$$k = \frac{0.4}{0.6} \frac{\sum_{i=8}^{n} (Q-E_i)^3}{\sum_{i=1}^{7} (Q-E_i)^3}. \tag{9}$$

The numerical value of the enhancement factor k depends, of course, on the set of energies E_i used in eq. (9). The first seven energies were taken from table 4. The remaining levels were determined by the relationship

$$E_i = E_{i-1} + \rho^{-1}(E_{i-1}). \tag{10}$$

The level density $\rho(E)$ was assumed to be of the form [10]) $\rho(E) = C_1 \exp\{C_2(E-\delta)^{\frac{1}{2}}\}$. The energy gap parameter [20]) δ was allowed to assume the values $-\infty$, 0, 1.0 and 1.66 MeV, and for each case the constants C_1 and C_2 were fixed by matching $\rho(E)$ with the observed level density at 2.2 MeV and at the binding energy Q, which was taken as 7.85 MeV. Note that the case $\delta \to -\infty$ corresponds to the form $\rho(E) = C_1 \exp\{C_2 E\}$. On the basis of the measured spectra described in the previous section, the density of levels at 2.2 MeV accessible via E1 transitions from the capture state is of the order of 10 MeV^{-1}. However, because of the uncertainty in this value, the calculation was performed for a range of assumed values. The density of levels at the binding energy was computed from the results listed in table 3.

The results of the calculation are shown in fig. 7, where the enhancement factor is plotted versus the assumed spacing at 2.2 MeV for different values of δ.

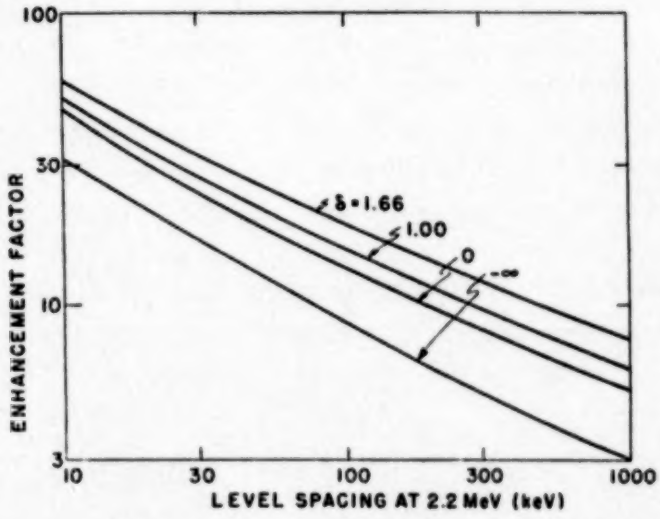

Fig. 7. Calculated values of the enhancement factor for high-energy transitions in Hg^{202}.

Taking δ as the pairing energy, which is on the order of 1 MeV, and the spacing of levels at 2.2 MeV as 100 keV, we see the high-energy transitions are enhanced by about a factor 15 over the predictions of the statistical model. Moreover, k is much greater than unity for all reasonable values of the parameters that determine the density of nuclear energy levels. This behavior of k must be systematic in nature since the magnitude of the expected random fluctuations in the sum of seven partial widths (approximately a factor of 1.5) is much smaller than the observed enhancement factor. Thus, there seems to be no reason to doubt that the high-energy transitions of Hg^{202} are greatly enhanced †, as compared to transitions of lower energy, beyond the E_γ^3 law. A similar behavior [25, 26]) of the γ-ray spectra from capture of thermal neutrons in other heavy nucleides has been interpreted [17]) as resulting from "direct" transitions of the incident s-wave neutron into a lower state characterized by strong p-orbital components.

It is of interest to compare the observed parital widths listed in table 4 with the theoretical estimate of Blatt and Weisskopf [18]). Their calculation, which is based on the independent-particle model modified to approximate the effects of the complexity of the emitting nucleus, predicts a value of 0.00878 D_0^{-1} $(2J+1)^{-1} E_\gamma^3$ for the partial width (in eV) of an E1 transition having energy E_γ in MeV from a resonance of spin J in Hg^{202}. In this expression, D_0 is the spacing (in MeV) of low-lying single-particle levels from which the final state is accessible by E1 transitions. Using the value $D_0 = 15$ MeV, which is predicted by the shell model, we find that the sum of partial widths to the seven final states listed in table 4 is 0.418 eV for resonances with $J = 1$ and 0.251 eV for $J = 2$ resonances. This is to be compared with the observed values of 0.062 eV, 0.234 eV and 0.210 eV for the three resonances studied. The most intense transition observed is the transition from the 71-eV resonance to the first excited state. This transition has a partial width of 0.082 ± 0.004 eV. The expression above gives a value of 0.079 eV if the resonance has spin 1 and 0.048 eV if the resonance has spin 2. In view of the approximate nature [18]) of the theoretical expression, it seems fair to conclude that the observed intensities of the high-energy transitions in Hg^{202} agree in order of magnitude with the predictions of the modified independent-particle calculation.

4.2. RANDOM FLUCTUATIONS IN THE TOTAL RADIATION WIDTH

Having found experimentally that the observed fluctuations in the total radiation widths of the resonances of Hg^{201} result from differences in the intensities of the highest energy transitions and that these transitions are enhanced, relative to lower energy transitions, beyond the E_γ^3 law, it remains for us to

† The alternative possibility of explaining the gamma-ray spectrum in terms of an anomalous dependence of the level density on excitation energy is inconsistent with the value of Γ''_γ of Hg^{201} in comparison with Γ_γ of Hg^{199}, etc.

give a quantitative explanation of the observed fluctuations. Our first inquiry is whether or not purely random fluctuations in the partial radiation widths can account for the observed differences in the total radiation widths. In this consideration we closely follow the approach of Porter and Thomas [27]). On the basis of reasonable assumptions about the complexity and independence of the wave functions describing the highly excited states formed by resonant capture of neutrons, they show that the widths of transitions from the initial state are randomly distributed in a chi-squared distribution with ν degrees of freedom, that is, the partial width $\Gamma_{\gamma i}$ is governed by the frequency function

$$P(x_i)\mathrm{d}x_i = \frac{1}{\Gamma(\frac{1}{2}\nu)}\,(\tfrac{1}{2}\nu x_i)^{\frac{1}{2}\nu-1}\mathrm{e}^{-\frac{1}{2}\nu x_i}\tfrac{1}{2}\nu\mathrm{d}x_i\,, \tag{11}$$

where

$$x_i = \frac{\Gamma_{\gamma i}}{\langle\Gamma_{\gamma i}\rangle_{\mathrm{av}}}$$

and $\Gamma(\frac{1}{2}\nu)$ is the well-known Γ-function. The correct value of ν for high-energy radiative transitions is currently in dispute, the experimental evidence [13]) being somewhat contradictory. However, the majority of the data appear to be consistent with a low value and, since there is at present no firm theoretical reason for a value larger than unity, we will assume $\nu = 1$ in the following discussion.

Given the distribution of partial widths, it is a straightforward problem to calculate the variance in their sum. Such a calculation was performed by Porter and Thomas in the paper mentioned. Their calculation, however, was for a rather special level-density formula. Also, the form of their result gives a misleading impression of the dependence of the variance on the number of effective levels. It was therefore decided to perform the calculations with a variety of level-density formulae.

Before proceeding with our calculation, the question of the statistical independence of transitions from a given initial compound state to the various bound final states needs to be considered. As Porter and Thomas suggest [27]), transitions to highly excited states, whose wave functions are very complex, are probably uncorrelated. On the other hand, there may exist groups of low-lying states which have very similar properties so that transition probabilities to these states may be highly correlated †. The effect of these correlations on the variance may be approximately accounted for by treating these groups as single, independently contributing transitions, i.e., by decreasing the "effective" level density at low excitations.

† The experimental evidence now available, although very limited in extent, does not show the presence of these correlations. See the results of table 1 in Bollinger *et al.* [13]).

Under the assumptions stated above, the total radiation width Γ_γ is a random variable that may be written in the form

$$\Gamma_\gamma = \sum_i \Gamma_{\gamma i} \equiv \sum_i \langle \Gamma_{\gamma i} \rangle_{\mathrm{av}} x_i. \tag{12}$$

The nth moment of Γ_γ may now be computed as

$$\langle \Gamma_\gamma^n \rangle_{\mathrm{av}} = \int_0^\infty \cdots \int_0^\infty \Gamma_\gamma^n \prod_i P(x_i) \mathrm{d}x_i, \tag{13}$$

where the statistical independence of the transition probabilities is assumed. A straightforward calculation using eqs. (11), (12), and (13) shows that the variance is

$$V^2 = \frac{\langle \Gamma_\gamma^2 \rangle_{\mathrm{av}} - \langle \Gamma_\gamma \rangle_{\mathrm{av}}^2}{\langle \Gamma_\gamma \rangle_{\mathrm{av}}^2} = \frac{2}{\nu} \frac{\sum_i \langle \Gamma_{\gamma i}^2 \rangle_{\mathrm{av}}}{\sum_i \langle \Gamma_\gamma \rangle_{\mathrm{av}}^2}. \tag{14}$$

Thus, if we let the average values of the partial widths be described by eq. (8), the expression for the variance becomes

$$V^2 = \frac{2}{\nu} \frac{k^2 \sum_{i=1}^{7} (Q - E_i)^6 + \sum_{i=8} (Q - E_i)^6}{\left[k \sum_{i=1}^{7} (Q - E_i)^3 + \sum_{i=8} (Q - E_i)^3 \right]^2}. \tag{15}$$

In the calculation of the variance of Γ_γ, the energy gap δ and the level spacing at 2.2 MeV were allowed to be free parameters but the enhancement factor k was varied in such a way that the seven transitions of highest energy contributed the experimentally determined 40 % of the total radiation width. The result of the calculation was found to be completely insensitive to the values of δ and the level spacing at 2.2 MeV, that is, the calculated fluctuation of Γ_γ is entirely dominated by fluctuations of the 7 transitions of highest energy. Quantitatively, the coefficient of variance is found to lie within the narrow range $0.20 < V < 0.22$ when the values of δ and the level spacing at 2.2 MeV are allowed to assume the full range of values used in fig. 7. This calculated result is to be compared with the experimentally determined value $V = 0.22 \pm 0.02$, as obtained from the total radiation widths of the 43-, 71- and 210-eV resonances in Hg^{201}. We see that the experimental value is entirely consistent with that expected on the basis of our model. On the other hand, additional calculations show that the expected coefficient of variance is only about 0.07 when $k = 1$, i.e., when the high-energy transitions are not enhanced. The probability of obtaining a value $V = 0.22$ from three numbers drawn at random from a normal distribution for which $V = 0.07$ is only 1.0×10^{-6}. Thus we conclude that the total radiation width cannot be reasonably expected to

fluctuate as much as was observed for the resonances of Hg^{201} unless the probabilities of a small group of transitions are enhanced.

4.3. THE INFLUENCE OF SPIN AND PARITY

As has been pointed out many times in the literature, the total radiation width should be independent of the spin and parity of resonances if certain conditions are satisfied. This result is easily seen from eq. (4). If the density of nuclear states is proportional to $(2J+1)$ and if many final states contribute to the integral, the presence of the ratio $D(Q)/D(E)$ in eq. (4) has the effect of making Γ_γ independent of J; the greater number of states accessible to an initial state of higher J is exactly counterbalanced by the greater transition probability of the initial state of lower J. Conversely, a failure of either of these assumptions to be valid could lead to a dependence of Γ_γ on J.

The $(2J+1)$ law for level densities is well known to be an approximation. More accurately, the density is expected to be proportional to $(2J+1)\exp\{(2J+1)^2/2\sigma_m^2\}$, where σ_m^2 is a constant [28]). This dependence of level density on J implies that resonances with the smaller of the two possible J-values should have smaller radiation widths, if we assume the same law holds at all excitations. The effect is small, however; even for σ_m as small as 3, the predicted difference between the radiation widths for spin 0 and spin 1 resonances is less than 1 %.

The other assumption necessary to make Γ_γ independent of J was that the density of final states be large. This condition is clearly not true below about 1.5 MeV in even-even nuclei, and yet transitions to this region can contribute greatly to the total radiation width. As an example of the influence of the small level density at low energies, consider the reaction $Hg^{199}(n, \gamma)Hg^{200}$. Using the level scheme of Segel [29]) for Hg^{200}, we find that there are 6 levels below 2.5 MeV that are accessible by E1 transitions from a 1^- level; two of these are accessible by E1 transitions from a 0^- level. This ratio is exactly the 3 to 1 ratio predicted by a $(2J+1)$ law. However, the corresponding ratio for $\sum E_{\gamma i}^3$ is 5.3 to 1. If transitions to these 6 levels account on the average for 25 % of the total radiation widths of 1^- initial states, which is probably a conservatively small estimate, then the high-energy transitions contribute only about 14 % to the total radiation widths of $J = 0$ resonances. Thus, unless there is some strange mechanism enhancing the low-energy transitions for $J = 0$ resonances, they would be expected to have total radiation widths about 11 % smaller than the total radiation widths of resonances for which $J = 1$.

The reaction $Hg^{201}(n, \gamma)Hg^{202}$ may be influenced by the spin of the initial compound state in a similar way. Because of the J-dependence of the level density at the initial states, transitions from states with $J = 2$ are expected to be weaker by a factor of $\frac{3}{5}$, on the average, than the corresponding transitions from states with $J = 1$. Normally this factor is exactly balanced by the fact

that there are more 3^+ states, which are accessible by E1 transitions only from 2^- initial states, than there are 0^+ final states, which are accessible only from 1^- initial states. However, it would not be surprising if there are no 3^+ states at low energy in Hg^{202}. In this case, the sum of widths of transitions from a 1^- initial state to the seven lowest states listed in table 4 would be at least twice as great as the corresponding sum for transitions from a 2^- state. Thus, since about half of the total radiation width is contributed by the high-energy transitions, the total radiation widths of 2^- states would be systematically at least 25 % lower than the widths of 1^- states.

Because of the expectation of fluctuations of a statistical nature in the total radiation widths, we cannot be certain that a systematic dependence on the spin can be detected in the experimental data. However, the data are clearly consistent with a dependence on spin. Thus the resonances at 43, 445, 564 and 685 eV could be assigned $J = 2$, and the resonances at 71, 210 and 313 assigned $J = 1$. The $J = 2$ resonances then have radiation widths consistent with a mean value of about 0.30 eV and the $J = 1$ resonances have radiation widths consistent with a mean value of about 0.45 eV.

The parity of the initial compound state would have an even greater influence on the total radiation widths of Hg^{201} than does its spin. However, the neutron widths of the resonances are great enough to make it almost certain that they are excited by s-wave neutrons. Thus, it is highly probable that the initial states are all of negative parity, the case already considered.

4.4. SUMMARY AND CONCLUSIONS

In the preceding sections we have shown that the total radiation widths of Hg^{201} fluctuate by about a factor of two. The capture γ-ray spectra of the resonances having large widths contain unusually intense high-energy transitions. When the partial widths associated with these high-energy transitions are subtracted from the total radiation width, the remainder is roughly the same from resonance to resonance.

A quantitative examination of the experimental data shows that the reduced partial radiation widths $\Gamma^0_{\gamma i} = E_\gamma{}^{-3}\Gamma_{\gamma i}$ of the high-energy transitions are much greater than the average reduced widths of transition of lower energy from the initial state. As a consequence of this enhancement of the high-energy transitions, two mechanisms become available for explaining the observed fluctuations in the total radiation width. One mechanism depends on the systematic influence of the spin of the initial state in relation to the spins of the small number of final states at low energy. An alternative explanation depends on the purely random fluctuations of the partial widths of a few high-energy transitions. Especially if both of these mechanisms are operative, as is expected, our calculations show that the observed fluctuations in Γ_γ are entirely reasonable in magnitude and are in no way anomalous.

The above description of the factors governing the total radiation width offers an explanation of the fact that the widths of Hg^{201} fluctuate more widely than those of other nucleides. The characteristic which results in the unusual behavior of the widths of Hg^{201} is the great strength of a small number of transitions from the initial state formed by neutron capture. We expect a similar correlation between capture γ-ray spectra and the degree of fluctuation of total radiation widths for other nucleides. In an examination of the γ-ray spectra from capture of thermal neutrons in nucleides for which the radiation widths of several resonances are known, no case is found in which a few transitions dominate the spectrum to a degree comparable with that observed in the spectra from capture in Hg^{201}. Thus the approximate constancy of the radiation widths of almost all the nucleides that have been studied is entirely consistent with their capture γ-ray spectra. On the other hand, for many nucleides for which total radiation widths have not been measured the capture γ-ray spectra are dominated by a few strong transitions to an even greater extent than is observed for Hg^{201}. Most of these nucleides are lighter than niobium or near the doubly-closed shell. In the past it has not been possible to determine the total radiation widths of these nucleides because of the small fraction of radiative capture in their resonances. However, as it becomes technically feasible to make more complete measurements we may expect to find other cases for which the total radiation widths exhibit wide fluctuations.

The authors wish to thank Drs. Norbert Rosenzweig and Peter Moldauer for helpful discussions of the theoretical questions involved in this paper.

Appendix

The application of the total-area method yields [30]) a relation between σ_0 and Γ of the form

$$\sigma_0 \Gamma^{\alpha} = f(A), \tag{16}$$

where α and $f(A)$ are very nearly constants, independent of σ_0 and Γ. Also, α varies much more slowly with the area A than does $f(A)$. In fact, α varies only between 1 and 2 for an unlimited variation in the area whereas $f(A)$ is proportional to A for small areas and to A^2 for large areas. Thus the usual plot of log σ_0 versus Γ yields a straight line whose intercept, at $\Gamma = 1$, is strongly area-dependent and whose slope varies only slowly with area. The partial area method [11]) yields relations of the same form as eq. (16) except that now α depends more strongly on σ_0 and Γ. In addition, α and $f(A)$ depend on the energy interval used. The slope α is nearly enough constant, however, that we may assume a linear relation between log σ_0 and log Γ over a fairly large range of these variables. Thus in general we have n relations of the form

$$\sigma_0 \Gamma^{\alpha_i} = F_i, \quad i = 1, \ldots, n, \quad n \geqq 2, \tag{17}$$

one for each sample thickness and/or energy interval used, and possibly one obtained by curve fitting. In logarithmic form these relations are

$$\log \sigma_0 + \alpha_i \log \Gamma = \log F_i \equiv \beta_i. \tag{18}$$

We now treat α_i and β_i as experimentally determined quantities and use the usual weighted-least-squares procedure to find the best solution for $\log \sigma_0$ and $\log \Gamma$. The weights assigned to each pair (α_i, β_i) are the squares of the reciprocals of the errors associated with the β_i due to errors in the areas A_i. We assume that errors in the area will not affect α. The error in β_i due to errors in the area is given by

$$\Delta\beta_i = \frac{\Delta F_i}{F_i} = \left(\frac{A_i}{F_i}\frac{\partial F_i}{\partial A_i}\right)\frac{\Delta A_i}{A_i} \equiv h_i \frac{\Delta A_i}{A_i}. \tag{19}$$

A set of curves has been prepared to facilitate the calculation of the quantity h_i which can be shown formally to be given by

$$h_i = \left(\frac{\partial \log n\sigma_0}{\partial \log A'_E/\Delta}\right)_{\Gamma = \text{const}}. \tag{20}$$

The quantity $\Delta A/A$ includes errors due to statistical errors in the transmission data in the resonance, errors in the backgrounds, and errors in the off-resonance transmission.

Note added in proof: A recent paper by C. Corge, V. D. Huynk, J. Julien, S. Mirza, F. Netter and J. Simic in Le Journal de Physique et le Radium reports large fluctuations in the total radiation widths of Pt^{195}. This reported behavior, which is difficult to understand in the case of platinum, is ignored in the present paper because the data are too briefly reported to allow the reader to judge their reliability.

References

1) L. M. Bollinger, in Nuclear Spectroscopy, edited by F. Ajzenberg-Selove (Academic Press, New York and London, 1960)
2) J. S. Levin and D. J. Hughes, Phys. Rev. **101** (1956) 1328
3) R. T. Carpenter and L. M. Bollinger, Bull. Am. Phys. Soc. **4** (1959) 271
4) R. T. Carpenter and L. M. Bollinger, Bull. Am. Phys. Soc. **4** (1959) 473
5) L. M. Bollinger, R E. Cote' and G. E. Thomas, Proc. 2nd Int. Conf. on the Peaceful Uses of Atomic Energy (United Nations Publication, Geneva, 1958) Vol. 14, p. 239
6) L. M. Bollinger and G. E. Thomas, Rev. Sci. Instr. **28** (1957) 489
7) Robert W. Shumann, Rev. Sci. Instr. **27** (1956) 686
8) R. R. Palmer and L. M. Bollinger, Phys. Rev. **102** (1956) 228
9) J. R. Bird, M. C. Moxon and F. W. K. Firk, Nuclear Physics **13** (1959) 525
10) H. A. Bethe, Revs. Mod. Phys. **9** (1937) 69
11) L. M. Bollinger and J. P. Marion, Argonne National Laboratory Report ANL-5754 (1957) 11
12) H. H. Landon and R. Rae, Phys. Rev. **107** (1957) 1333

13) L. M. Bollinger, R. E. Cote' and T. J. Kennett, Phys. Rev. Letters 3 (1959) 376
14) L. M. Bollinger and R. E. Cote', Bull. Am. Phys. Soc. 5 (1960) 294
15) N. Rosenzweig, L. M. Bollinger, L. L. Lee, Jr., and J. P. Schiffer, Proc. 2nd Int. Conf. on the Peaceful Uses of Atomic Energy (United Nations Publication, Geneva, 1958) Vol. 14, p. 58
16) D. M. Chase, L. Willets and A. R. Edmonds, Phys. Rev. 110 (1958) 1080
17) A. M. Lane and J. E. Lynn, Atomic Energy Research Establishment Report AERE-R 2891 (1959)
18) John M. Blatt and Victor F. Weisskopf, Theoretical Nuclear Physics (John Wiley and Sons, New York, 1952) Chapter 12
19) N. Rosenzweig, Phys. Rev. 108 (1957) 817
20) T. D. Newton, Can. J. Phys. 34 (1956) 804
21) A. G. W. Cameron, Can. J. Phys. 35 (1957) 666
22) H. H. Bolotin, R. E. Chrien and A. P. Jain, Bull. Am. Phys. Soc. 4 (1959) 473
23) P. Born, J. Molenaar and J. Blok, Physica 25 (1959) 326
24) W. F. Miller and W. J. Snow, Rev. Sci. Instr. 31 (1960) 39
25) G. A. Bartholomew, P. J. Campion, J. W. Knowles and G. Manning, Proc. Int. Conf. on Neutron Interactions with the Nucleus, U.S.A.E.C. Tech. Inf. Sercive, TID-7547 (1957) p. 252
26) L. V. Groshev, A. M. Demidov, V. N. Lutsenku and V. I. Pelekhov, Proc. 2nd. Int Conf. on the Peaceful Uses of Atomic Energy (United Nations Publications, Geneva, 1958) Vol. 15, p. 138
27) C. E. Porter and R. G. Thomas, Phys. Rev. 104 (1956) 483
28) C. Bloch, Phys. Rev. 93 (1954) 1094
29) R. E. Segel, Phys. Rev. 111 (1958) 1620
30) E. Melkonian, Proc. Int. Conf. Peaceful Uses of Atomic Energy (United Nations, New York, 1956) Vol. 4, p. 340

1.C

Nuclear Physics 21 (1960) 99—105; © *North-Holland Publishing Co., Amsterdam*
Not to be reproduced by photoprint or microfilm without written permission from the publisher

VALIDITY OF THE TWO-PARTICLE APPROXIMATION IN THE MANY-BODY PROBLEM

KAILASH KUMAR †

Tata Institute of Fundamental Research, Bombay 1

Received 2 June 1960

Abstract: Brenig's method in the many-body problem is shown to be equivalent to a method of superposition of configurations. Compact expressions are obtained for quantities neglected in the two-particle approximation. The magnitude of corrections to the energies is discussed.

1. Introduction

Brenig [1]) has reduced the many-body Schrödinger equation to a set of coupled integro-differential equations for the so-called correlation functions for successively larger numbers of particles. By making a two-particle approximation [1]) on the equations for one and two particle correlation functions Brueckner' theory is obtained in its lowest order. However, as Eden *et al.* [2]) have pointed out there was no way of obtaining corrections to this approximation in Brenig's formalism. In this note it is shown (sect. 2) that Brenig's set of equations is equivalent to a set obtained in the method of superposition of configurations [3]). The connection with the usual perturbation theory then becomes clear. Brenig's choice of basic wave functions and his variational principle interpretation of this choice is discussed in sect. 3. In sect. 4 the correct equation for the two-particle function $\psi_{\rho\sigma}$ is put in a form most suited for making two-particle approximation. The corrections to the single-particle and total energies are obtained and discussed in sect. 5. It is shown that the structure of these terms is the same as that of the first few corrections to Brueckner's theory. A significant formal advantage is that the number of terms is very small. The infinite series of correction terms familiar from the usual forms of Brueckner theory does not occur.

2. Equivalence to the Method of Superposition of Configurations

It is convenient to modify slightly Brenig's notation [1]). We take Latin and Greek indices for particles outside and inside the chosen configuration. The determinant formed by occupied orbitals is D_0, as in Brenig's paper [1]), but determinants belonging to singly, doubly, triply, etc. excited configurations

† Now at the Australian National University, Canberra.

are written respectively as

$$D^{a}_{\mu}, \quad D^{ab}_{\mu\nu}, \quad D^{abc}_{\mu\nu\rho}, \quad \text{etc.}$$

For instance, the determinant D^{a}_{μ} is obtained from D_0 by replacing ϕ^{μ} everywhere in it by ϕ^{a}. Similarly for higher configurations.

Also, let M be the matrix that generates the system eigenfunction Ψ_0 of H from D_0. Thus,

$$\begin{aligned}\Psi_0 &= MD_0 \\ &= (0|M|0)D_0 + \sum_{\mu,a} \binom{a}{\mu}|M|0)D^{a}_{\mu} + \sum_{\mu\nu,ab} \binom{ab}{\mu\nu}|M|0)D^{ab}_{\mu\nu} + \ldots . \end{aligned} \tag{1}$$

The normalised determinantal wave-function is

$$|\cdots) = (N!)^{-\frac{1}{2}} D^{\cdots}_{\cdots}, \tag{2}$$

where N is the number of particles in the system.

Brenig's normalisation

$$(D_0|\Psi_0) = N!(\Pi_0|\Psi_0) = N!$$

requires that

$$(0|M|0) = 1.$$

Here, Π_0 is the product of the diagonal elements of D_0 and Π^{μ}, $\Pi^{\mu\nu}$, etc., are obtained by omitting $\phi^{\mu}(\mu)$, $\phi^{\mu}(\mu)\phi^{\nu}(\nu)$, etc., respectively from Π_0.

The correlation functions ϕ_{μ}, $\psi_{\mu\nu}$, $\psi_{\mu\nu\rho}$, etc., are related to the matrix elements of M. Thus,

$$\binom{a}{\mu}|M|0) = (\Pi^{\mu}\phi^{a}(\mu)|\Psi_0) = (\phi^{a}|\phi_{\mu}). \tag{4a}$$

Similarly,

$$\binom{ab}{\mu\nu}|M|0) = (\phi^{a}\phi^{b}|\psi_{\mu\nu}), \tag{4b}$$

$$\binom{abc}{\mu\nu\rho}|M|0) = (\phi^{a}\phi^{b}\phi^{c}|\psi_{\mu\nu\rho}), \tag{4c}$$

etc.

It follows that

$$\phi_{\mu} = \phi^{\mu} + \sum_{a} \binom{a}{\mu}|M|0)\phi^{a}, \tag{5a}$$

$$\psi_{\mu\nu} = \phi^{\mu\nu} + \sum_{a} \binom{a}{\mu}|M|0)\phi^{a\nu} + \sum_{b} \binom{b}{\mu}|M|0)\phi^{\mu b} + \sum_{ab} \binom{ab}{\mu\nu}|M|0)\phi^{ab}. \tag{5c}$$

Here, ϕ^{ab}, ϕ^{abc} etc., are determinants formed from basic orbitals ab, abc, etc. Eqs. (5) may be further written as

$$\phi_{\mu}(1) = (I_1 + M_1)\phi^{\mu}(1), \tag{6a}$$

$$\psi_{\mu\nu}(12) = (I_{12} + I_1M_2 + I_2M_1 + M_{12})\phi^{\mu\nu}(12), \tag{6b}$$

$$\psi_{\mu\nu\rho}(123) = (I_{123} + \sum_{(123)} I_{12}M_3 + \sum_{(123)} I_1M_{23} + M_{123})\phi^{\mu\nu\rho}(123), \tag{6c}$$

where I_1, I_{12}, etc., are unit operators for appropriate particles. The sum $\sum_{(123\ldots)}$ is over all distinct permutations of these numbers. The operators M_{12}, M_{123}, etc., defined through eqs. (5) and (6) are symmetric in their indices and they do not connect states within the chosen configuration.

For ease of reference we reproduce Brenig's equations [1]):

$$H = \sum_{\mu} T_{\mu} + \tfrac{1}{2} \sum_{\mu\nu} v_{\mu\nu}, \tag{7a}$$

$$E = \sum_{\mu} (\phi^{\mu}|T_{\mu}|\phi_{\mu}) + \tfrac{1}{2} \sum_{\mu\nu} (\phi^{\mu}\phi^{\nu}|v|\psi_{\mu\nu}), \tag{7b}$$

$$E\phi_{\mu} = T_{\mu}\phi_{\mu} + \sum_{\nu} (\phi^{\nu}|v_{\mu\nu}|\psi_{\mu\nu}) + \sum_{\nu} (\phi^{\nu}|T_{\nu}|\psi_{\mu\nu}) + \tfrac{1}{2} \sum_{\nu\rho} (\phi^{\nu}\phi^{\rho}|v_{\nu\rho}|\psi_{\mu\nu\rho}), \tag{7c}$$

$$E\psi_{\mu\nu} = (T_{\mu} + T_{\nu} + v_{\mu\nu})\psi_{\mu\nu} + \sum_{\rho} (\phi^{\rho}|v_{\mu\rho} + v_{\nu\rho}|\psi_{\mu\nu\rho}) + \sum_{\rho} (\phi^{\rho}|T_{\rho}|\psi_{\mu\nu\rho}) + \tfrac{1}{2} \sum_{\rho\sigma} (\phi^{\rho}\phi^{\sigma}|v_{\rho\sigma}|\psi_{\mu\nu\rho\sigma}), \tag{7d}$$

etc.

By multiplying eqs. (7c) *et seq.* respectively by $\phi^{a}(\mu)$, $\phi^{a}(\mu)\phi^{b}(\nu)$, etc., rearranging and using eqs. (4) and (5) one is lead to the following equivalent set of equations:

$$(E - \mathscr{D}^{a'}_{\mu'})(^{a'}_{\mu'}|M|0) = (^{a'}_{\mu'}|H|0) + \sum_{\mu, a} (^{a'}_{\mu'}|H|^{a}_{\mu})_{N}(^{a}_{\mu}|M|0) + \sum_{\mu\nu,\, ab} (^{a'}_{\mu'}|H|^{ab}_{\mu\nu})_{N}(^{ab}_{\mu\nu}|M|0) + \sum_{\mu\nu\rho,\, abc} (^{a'}_{\mu'}|H|^{abc}_{\mu\nu\rho})_{N}(^{abc}_{\mu\nu\rho}|M|0), \tag{8a}$$

$$(E - \mathscr{D}^{a'\nu'}_{\mu'\nu'})(^{a'\nu'}_{\mu'\nu'}|M|0) = (^{a'\nu'}_{\mu'\nu'}|H|0) + \sum_{\mu, a} (^{a'\nu'}_{\mu'\nu'}|H|^{a}_{\mu})_{N}(^{a}_{\mu}|M|0) + \sum_{\mu\nu,\, ab} (^{a'\nu'}_{\mu'\nu'}|H|^{ab}_{\mu\nu})_{N}(^{ab}_{\mu\nu}|M|0) + \text{two more terms}, \tag{8b}$$

where $\mathscr{D}$ is a diagonal operator defined by

$$(n|\mathscr{D}|m) = \delta_{nm}\mathscr{D}_{m} = \delta_{nm}(m|H|m) \quad \text{for any} \quad |m) \equiv |^{ab\ldots}_{\mu\nu\ldots}). \tag{9}$$

The summation in eqs. (8) is such that μ, ν, ρ, etc., are inside the chosen configuration and a, b, c, etc., outside it, while the subscript N signifies that only the non-diagonal elements of H are to be taken.

To show the connection with ordinary perturbation theory define the operator

$$G = (E - \mathscr{D})M. \tag{10}$$

Then, identically,

$$E = (0|H|0) + (0|G|0). \tag{11}$$

With the help of eqs. (8) and (10), $(0|G|0)$ may be expanded. A Brillouin-Wigner (or Rayleigh-Schrödinger) series is obtained in the usual form if the basic orbitals ϕ^{μ}, ϕ^{a} are eigenfunctions of kinetic energy T_{μ}. The set of coup'ed equations for the matrix elements of G have been given by Nesbet [3]), who

discussed their reduction to Hartree-Fock and Brueckner methods in the case in which only singly and doubly excited configurations are considered.

3. Choice of Orbitals

Brenig's choice of orbitals is such that $\phi_\mu = \phi^\mu$. He has related this to a variational principle minimising the angle between the wave functions Ψ_0 and D_0 in the Hilbert space. From eq. (5a) one sees the more concrete meaning of this requirement, viz.

$$(^a_\mu|M|0) = M_1 = (^a_\mu|G|0) = 0, \tag{12}$$

which has the well-known interpretation that the choice of orbitals (i.e. the zero order Hamiltonian) is such that all effects of one-particle excitations are included from the beginning (see also Nesbet[3]).

In discussing the two-particle approximation much simplication results if eq. (12) is supposed to hold, although this is not essential to the argument.

4. Equation for $\psi_{\mu\nu}$

Eqs. (12) and (7b) show that the total energy is entirely determined by $\psi_{\mu\nu}$ which in turn is determined by eq. (7d). In two-particle approximation eq. (7d) reduces to the Bethe-Goldstone equation. If one assumes that the main effects are well represented in this approximation eq. (7d) can be reduced to an integral equation for $\psi_{\mu\nu}$ by following the method of Brenig and making use of eqs. (6) to obtain the corrections †. We have

$$\psi_{\mu\nu}(12) = \phi^{\mu\nu}(12) + \frac{P(1-Q)}{\varepsilon_{\mu\nu} - \mathscr{H}_{12}} v_{12}\psi_{\mu\nu}(12) + \frac{P}{\varepsilon_{\mu\nu} - \mathscr{H}} \mathscr{A}_{\mu\nu}(12), \tag{13}$$

where P is an operator which eliminates the singularities of the propagator, Q is a projection operator which takes care of the Pauli principle,

$$\varepsilon_{\mu\nu} = \varepsilon_\mu + \varepsilon_\nu, \quad \varepsilon_\mu = (\phi^\mu|T+V|\phi_\mu), \tag{14}$$

$$V\phi_\mu = \sum_\nu (\phi^\nu|v_{\mu\nu}|\psi_{\mu\nu}), \tag{15}$$

$$\mathscr{H}_{12} = T_1 + T_2 + V_1 + V_2 \equiv \mathscr{H}, \tag{16}$$

and

$$\mathscr{A}_{\mu\nu} = \mathscr{A}'_{\mu\nu} + \mathscr{A}''_{\mu\nu} + \mathscr{A}'''_{\mu\nu}, \tag{17a}$$

$$\mathscr{A}'_{\mu\nu}(12) = \sum_\rho \int \phi^{\rho*}(3) T_3 (I_1 M_{23} + I_2 M_{13} + M_{123}) \phi^{\mu\nu\rho}(123) \mathrm{d}2, \tag{17b}$$

† For instance, in the third term of eq. (7d) one writes in two-particle approximation $\psi_{\mu\nu\rho}(123) \approx (I_{12} + M_{12})\ \phi^{\mu\nu\rho}(123)$; corrections are then obtained by comparing with eq. (6c) and give rise to the $A'_{\mu\nu}$ term of eq. (17b).

$$\mathscr{A}''_{\mu\nu}(12) = \tfrac{1}{2}\sum_{\rho\sigma}\int \phi^{\rho*}(3)\phi^{\sigma*}(4)v_{34}(I_{13}M_{24}+I_{24}M_{13}+I_{14}M_{23}+I_{23}M_{14} + \sum_{(1234)} I_1 M_{234}+M_{1234}-M_{13}M_{24})\phi^{\mu\nu\rho\sigma}(1234)\mathrm{d}3\mathrm{d}4, \quad (17c)$$

$$\mathscr{A}'''_{\mu\nu}(12) = \sum_{\rho}\phi^{\rho*}(3)v_{13}[(M_{23}M_{123}-M_{13}M_{13})\phi^{\mu\nu}(12)\phi^{\rho}(3) -(M_{13}+M_{123}-M_{23}M_{12})\phi^{\mu\nu}(32)\phi^{\rho}(1) \quad (17d) -(M_{13}+M_{23}+M_{123}-M_{13}-M_{13}^2)\phi^{\mu\nu}(13)\phi^{\sigma}(2)]\mathrm{d}3 + \text{terms with 1 and 2 interchanged.}$$

Let $\psi^{\mathrm{B}}_{\mu\nu}$ be the solution of Brenig's form of Bethe-Goldstone equation which is obtained by omitting the last term in eq. (13). That is, let

$$\psi^{\mathrm{B}}_{\mu\nu} = \phi^{\mu\nu} + \frac{1}{a}v\psi^{\mathrm{B}}_{\mu\nu}; \quad \frac{1}{a} = \frac{P(1-Q)}{\varepsilon_{\mu\nu}-\mathscr{H}}. \quad (18)$$

Then the solution $\psi_{\mu\nu}$ of eq. (13) is given by †, ††

$$\psi_{\mu\nu} = \psi^{\mathrm{B}}_{\mu\nu} + \left(1-\frac{1}{a}v\right)^{-1}\chi_{\mu\nu}, \quad \chi_{\mu\nu} = \frac{P}{\varepsilon_{\mu\nu}-\mathscr{H}}\mathscr{A}_{\mu\nu}. \quad (19)$$

5. Corrections to Total and Single-Particle Energies

The total energy expression (7b) may be rewritten with the help of the single-particle potential V defined in eq. (15).

$$E = \sum_{\mu}(\phi^{\mu}|T+\tfrac{1}{2}V|\phi_{\mu}). \quad (20)$$

In the two-particle approximation we have

$$V\phi_{\mu} \approx V^{\mathrm{B}}\phi_{\mu} \equiv \sum_{\nu}(\phi^{\mu}|v_{\mu\nu}|\psi^{\mathrm{B}}_{\mu\nu}). \quad (21)$$

In terms of the Brueckner K-matrix defined by $v\psi^{\mathrm{B}}_{\mu\nu} = K\phi^{\mu\nu}$, one has

$$V^{\mathrm{B}}\phi_{\mu} = \sum_{\nu}(\phi^{\nu}|K|\phi^{\mu\nu}), \quad (22)$$

so that the correction to the single-particle energy is

$$\Delta V\phi_{\mu} = (V-V^{\mathrm{B}})\phi_{\mu} = \sum_{\nu}(\phi^{\nu}|K|\chi_{\mu\nu}) \quad (23)$$

and that to the total energy is

$$\Delta E = \tfrac{1}{2}\sum_{\mu\nu}(\phi^{\mu}\phi^{\nu}|K|\chi_{\mu\nu}). \quad (24)$$

† A discussion with Dr. S. N. Biswas is thankfully acknowledged.

†† Eq. (18) is actually non-linear in $\psi^{\mathrm{B}}_{\mu\nu}$. One has to use some linearisation approximation or self-consistent method in actually solving it. Some similar procedure is assumed to be applicable to eq. (13), and the solution (19) is to be understood in that sense.

We seem † to have here expressed the correction terms in a reasonably compact form. It may be recalled that in usual theory [6]) the corrections are represented by an infinite series. In the present method also a series expansion for these can be obtained using eq. (8), and expressing v in terms of the K-matrix.

In the nuclear matter case, because of momentum conservation, the contributions from the terms $\mathscr{A}'_{\mu\nu}$ and $\mathscr{A}''_{\mu\nu}$ vanish. The most important contributions arise from the term $\mathscr{A}'''_{\mu\nu}$ of eq. (17d). In order that these corrections be finite for hard core potentials it is required that

$$(M_{23}+M_{123}-M_{13}M_{12}) = (M_{12}+M_{123}-M_{12}M_{23})$$
$$= (M_{12}+M_{23}+M_{123}-M_{13}-M_{13}^2) = 0 \quad \text{for} \quad r_{13} < r_c. \quad (25)$$

Outside this range one has to know the form of the M-functions. To obtain an estimate of the contribution from two-particle correlations one can relate M_{12} with the function $f(r_{12})$ used in Jastrow's variational method [4, 5]). In the notation of ref. [5]) where the un-normalised total wavefunction is written as $\Psi_0 = \prod_{i<j} f(r_{ij}) D_0/N!$ the relation is

$$M_{12} = (f(r_{12})-\langle f\rangle)/\langle f\rangle, \quad (26)$$

where $\langle f\rangle$ represents the average value of $f(r_{12})$ for the state in question and the above definition ensures that M_{12} does not connect states within the chosen configuration.

When this form of M_{12} is used together with some appropriate form for v or K outside the hard-core the structure of the correction term due to $\mathscr{A}'''_{\mu\nu}$ is very similar to that of the third order cluster terms studied by Bethe [6]). Magnitudes are also not expected to differ much.

Higher order corrections arise from terms in M_{123} and $M_{\mu\nu}M_{\nu\rho}$. At the moment it is not possible to give an estimate of these terms. It is, however, significant that no heigher order correlation amplitudes occur directly in these corrections. It may be possible to find the three-particle correlation amplitude M_{123} by a variational method [5]) similar to that used for finding M_{12}.

6. Further Corrections to Single-Particle Energies

Eq. (23) does not include all the corrections to the single-particle energies ε_μ defined by eqs. (14) and (15).

Other corrections arise because the single-particle equation

$$(T+V)\phi_\mu = \varepsilon_\mu \phi_\mu \quad (27)$$

is obtained by making a two-particle approximations [1]) on eq. (7c). This

† See preceding footnote.

neglects the following terms arising respectively from the third and fourth term on the right hand side of eq. (7c):

$$\sum_{\nu}\int \phi^{\nu *}(2)T_2 M_{12}\phi^{\mu\nu}(12)\mathrm{d}2, \tag{28}$$

$$\tfrac{1}{2}\sum_{\nu\rho}\int \phi^{\nu *}(2)\phi^{\rho *}(3)v_{23}(I_2M_{13}+I_3M_{12}+M_{123})\phi^{\mu\nu\rho}(123)\mathrm{d}2\mathrm{d}3. \tag{29}$$

In the nuclear matter case these corrections are unimportant. Indeed for this case (28) vanishes †, because M_{12} does not connect states in the chosen configuration. For reasons given with eq. (25) we must have, from (29),

$$I_2M_{13}+I_3M_{12}+M_{123}=0. \tag{30}$$

Outside this range the contribution from M_{12} and M_{13} is evaluated using (26). The terms from the main diagonal of $\phi^{\mu\nu\rho}$ vanish. The exchange terms are small. Finally although M_{123} is not known it may be expected to have only small effects because it brings in components from outside Fermi-sea which may not be expected to influence the diagonalised energies very much. For finite nuclei, especially light nuclei to which Brueckner's theory is applied [2, 7]), the preceding remarks do not apply. The corrections do not vanish in these cases, but might still be small because the number of states to be summed over are small.

† It may also be made to vanish for finite systems by replacing T by a suitable operator. The same holds for $\mathscr{H}'_{\mu\nu}$, eq. (17b).

References

1) W. Brenig, Nuclear Physics **4** (1957) 363
2) R. J. Eden, V. J. Emery and S. Sampanthar, Proc. Roy. Soc. A **253** (1959) 177
3) R. K. Nesbet, Phys. Rev. **109** (1958) 1632
4) A. De-Shalit and V. F. Weisskopf, Ann. of Phys. **5** (1958) 282
5) R. Jastrow, Phys. Rev. **98** (1955) 1479;
   A. Temkin, Ann. of Phys. **9** (1960) 93
6) H. A. Bethe, Phys. Rev. **103** (1956) 1353
7) H. J. Mang and W. Wild, Z. Phys. **154** (1959) 182

2.C:
6.A.

Nuclear Physics **21** (1960) 106—115; © *North-Holland Publishing Co., Amsterdam*
Not to be reproduced by photoprint or microfilm without written permission from the publisher

ALUMINIUM (p, γ) RESONANCES WITH H_1^+, H_2^+ AND H_3^+ IONS

P. F. DAHL, D. G. COSTELLO AND W. L. WALTERS
University of Wisconsin, Madison, Wisconsin

Received 27 June 1960

Abstract: Aluminium (p, γ) resonances were studied with H_1^+, H_2^+ and H_3^+ ions, under a variety of conditions, to clarify discrepancies between molecular ion results and results with H_1^+ ions. Thick target gamma-ray yield curves from H_2^+ ions are very asymmetric. They are accurately fitted by assuming the electron in the ion is torn away the moment the target is struck. The ensuing Coulomb force pushes the two protons apart. Proton energies in the laboratory system are substantially changed, and some protons pass through the resonance twice. Six resonance energies were measured with protons in terms of the Li(p, n) threshold at 1881.1 keV. Values obtained are (in keV) 632.8±0.2, 923.4±0.3, 937.7±0.3, 992.4±0.3, 1001.7±1.0 and 1213.6±0.5.

1. Introduction

It is customary to extend the proton energy range of electrostatic accelerators by making use of H_2^+ and H_3^+ ions which are available from hydrogen ion sources. Molecular ion beams are also convenient for calibrating the energy scale of the energy selector used in conjunction with the accelerator; thus a (p, γ) resonance or (p, n) threshold reaction furnishes three calibration points when H_1^+, H_2^+ and H_3^+ ions are used.

Recent careful measurements of the resonance energies and widths of narrow (p, γ) resonance reactions have revealed discrepancies in results when thick target gamma-ray yield curves obtained with H_2^+ ions are compared with corresponding curves fr ı protons. The former yield curves are quite asymmetric, which throws doubt on their use in precise reaction studies and calibrations. It has not been entirely clear whether these discrepancies are of instrumental origin, or whether they reflect the anomalous behavior of molecular ions in the target. The present work was undertaken to throw further light on these effects.

2. Experimental Equipment

The ion beam from the electrostatic accelerator [1]) is first deflected in a magnetic field where the desired mass component is sorted out, then traverses a one-meter cylindrical 90° electrostatic energy analyzer before entering the target chamber. For the present work the analyzer was adjusted for an energy resolution of 0.1 %, giving a total theoretical energy spread of 2 keV at 1 MeV

proton energy. The voltage scale of the analyzer is calibrated in terms of the Li(p, n) threshold at 1.881 MeV, and the linearity of the scale over the region of interest has been checked by measurements of several resonances and thresholds with protons. No detectable long-time drift of the voltage scale was encountered over the period of about six months during which the experimental data were taken; reproducibility of extrapolated threshold energies and resonance energies was generally considerably better than 0.05 %.

Gamma rays are detected with a 5 cm × 5 cm NaI(Tl) crystal in conjunction with a photomultiplier tube and standard amplifying and counting circuits.

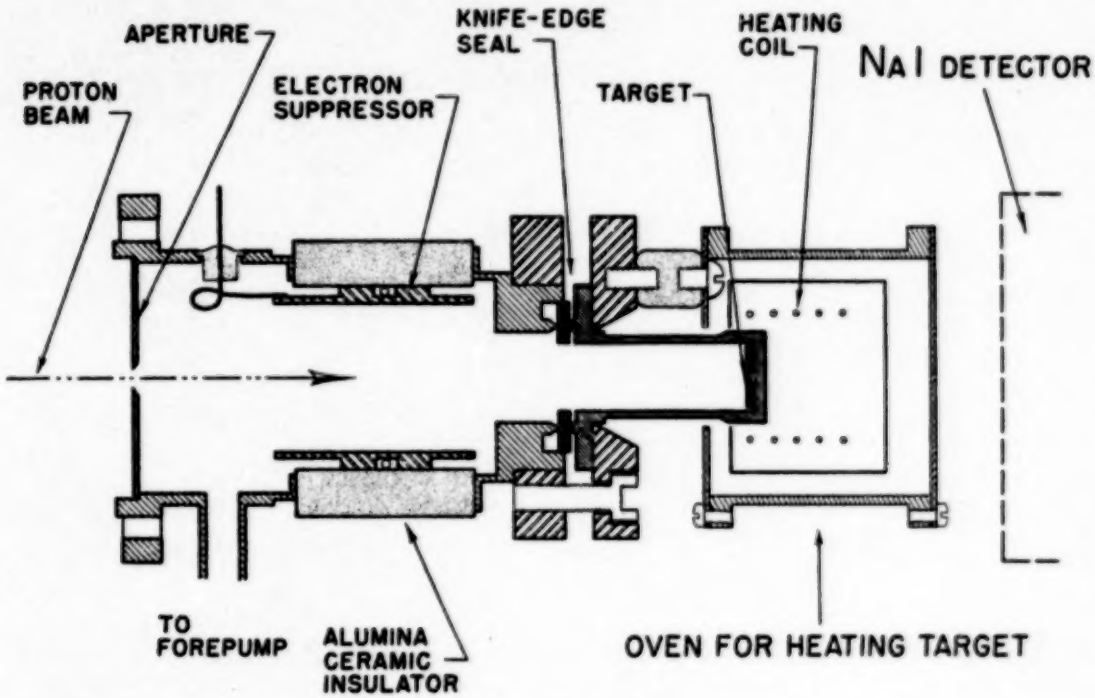

Fig. 1. Target chamber.

The circuitry includes a current integrator for measuring the incident beam current.

The target chamber is illustrated in fig. 1. Part of the work was done with aluminium foil targets approximately 50 keV thick to a 1-MeV proton beam. Thin targets of aluminium and thick targets of lithium were prepared by evaporation of aluminium or lithium fluoride, respectively, in a seprate evaporation chamber. Some thick targets of aluminium were also made in this way. The lithium targets were covered with a fine copper mesh to prevent error in the current measurements due to charge accumulation on the non-conductive targets. For all evaporated targets thin disks of copper were used for target backing.

Considerable trouble was experienced at first with carbon deposits on the targets, which were probably due to vapors originating from a vacuum valve

near the target chamber. This problem was solved by recessing the targets in an "oven" as illustrated. The target chamber was kept at 150° C, and the proton current at the target was restricted to about 0.2 μA. These were found to be optimum conditions for preventing build-up, while at the same time avoiding melting the foil targets by the beam. Under these conditions reproducibility of yield curves was quite good even after prolonged running on the same spot on the target.

3. Experimental Results

3.1. YIELD CURVES FROM H_1^+ AND H_2^+ IONS

Most of the work was concerned with the $Al^{27}(p, \gamma)Si^{28}$ resonance which according to Bondelid's and Kennedy's measurements [2]) is at 992.4 keV.

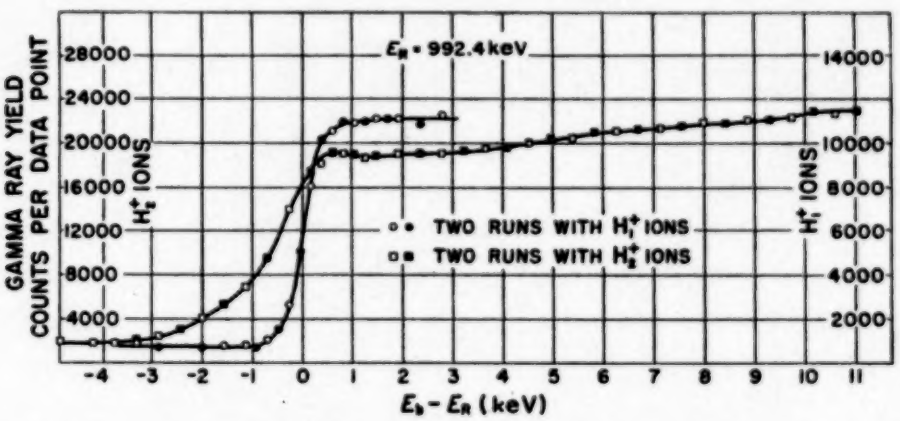

Fig. 2. Yield curves for the resonance at 992.4 keV obtained with H_1^+ and H_2^+ ions, and a target 50 keV thick. Standard deviations in the values of data points are less than the diameter of the circles. Here, E_b denotes the mean incident proton energy, and E_R the resonance energy. Integrated charge per data point was 41μC. Background measured by intercepting the beam near the target chamber entrance was subtracted from target yields. No corrections could be made for background originating in the target backing and two beam-defining apertures.

In fig. 2 is shown a set of typical thick target gamma-ray yield curves, obtained with the proton beam and the H_2^+ beam. The energy corresponding to one-half maximum yield on the curve from protons is taken as the resonance energy, and the interquartile range † on the curve agrees well with that predicted on the basis of the electrostatic analyzer geometry and a theoretical triangular proton energy distribution. Additional sources of broadening, including the natural width of the resonance, are small in comparison to the energy spread in the proton beam.

The leading edge of the resonance step in the curve from H_2^+ ions is very asymmetric, with the yield starting about 3 keV below the resonance. Near the

† Width between ¼ and ¾ maximum yield.

resonance energy the curve flattens out very quickly, and remains relatively flat for several keV before it rises gradually to a maximum yield which agrees approximately with that of the H_1^+ yield. The two curves never fully meet, owing to the presence of an additional weak resonance about 10 keV above the main resonance. It should be noted that targets 5 to 10 keV thick, generally considered thick for resonance investigations in this region, are not sufficiently thick to bring out the full shape of the curve from H_2^+ ions.

3.2. OTHER TARGETS AND INVESTIGATIONS

An attempt was made to establish the shape of the curve from H_2^+ ions when the metallic target was replaced by aluminium oxide. Although results were not very satisfactory, owing to target difficulties, a curve of the same general shape was indicated.

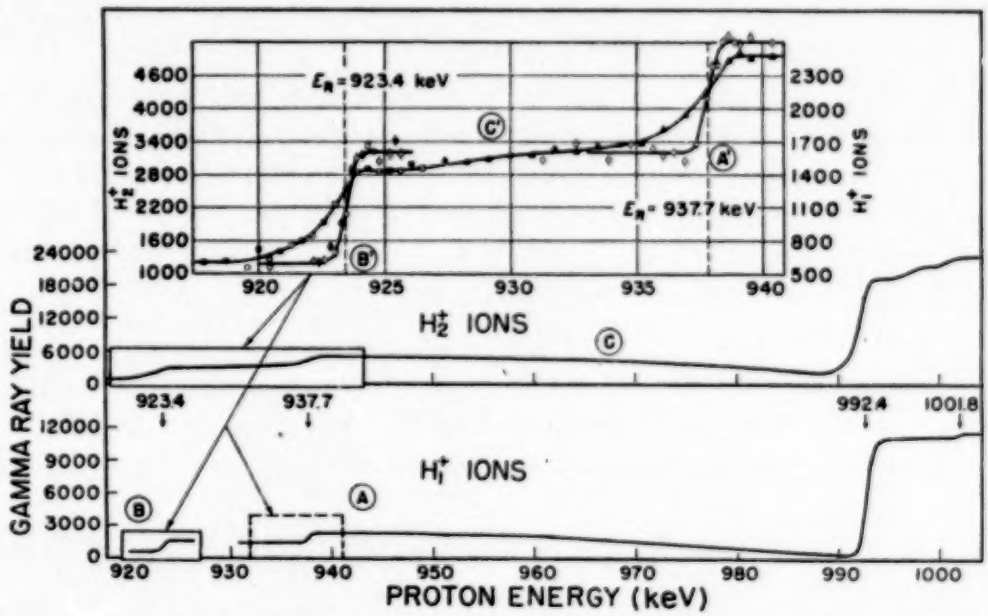

Fig. 3. Yield curves from four adjoining resonances with H_1^+ and H_2^+ ions, and targets 50 keV thick. The insert shows curve B and parts of curve A and C on a larger scale. A slightly higher yield was obtained during runs B and C than during run A which was made a month earlier with a different target and slightly different counter conditions. Yield values in the dashed enclosure of curve A were multiplied by a factor of 1.15 to give the points of curve A'.

Resonances at 633, 923 and 938 keV gave yield curves in quantitative agreement with the curve at 992 keV. In fig. 3 are shown results from a pair of runs across four adjoining resonances with the two beams, and with targets 50 keV thick.

A yield curve obtained with the detector set at 90° to the beam axis agrees with the yield curve obtained with the detector in its usual position at 0°.

To check further on possible quantum effects a run was made with ions from hydrogen gas whose normal para-hydrogen content had been enriched. No

difference in yield was seen, although this result is inconclusive, since the abnormal para-hydrogen content may have been destroyed in the ion source discharge.

3.3. THIN TARGET RESULTS

Owing to the reduced counting rate and problems encountered in preparing satisfactory targets thin target data were less reproducible than thick target data. Peaks of the yield curves obtained from the two different beams appeared to agree, after correcting for target thickness, and correcting for the fact that the H_2^+ ion includes an electron which shares energy with the two protons. The apparent agreement in resonance energy from thin target data has been noted previously by Bondelid and Kennedy, from whicht hey conclude that the observed thick target anomalies are not due to "non-linearity" effects [3]).

3.4. YIELD CURVE FROM H_3^+ IONS

A single run was made with the H_3^+ beam across a resonance at 633 keV. A yield curve was obtained of similar shape to that obtained with the H_2^+ beam. Quantitative information could not be extracted from the curve, however, because of a relatively high background yield, probably due in part to a neutron background from small amounts of deuterium; a small carbon deposit may also have been present during this run.

3.5. INERT SURFACE LAYERS

In fig. 4 are shown a series of yield curves obtained from evaporated targets on top of which thin layers of copper were evaporated, varying from about

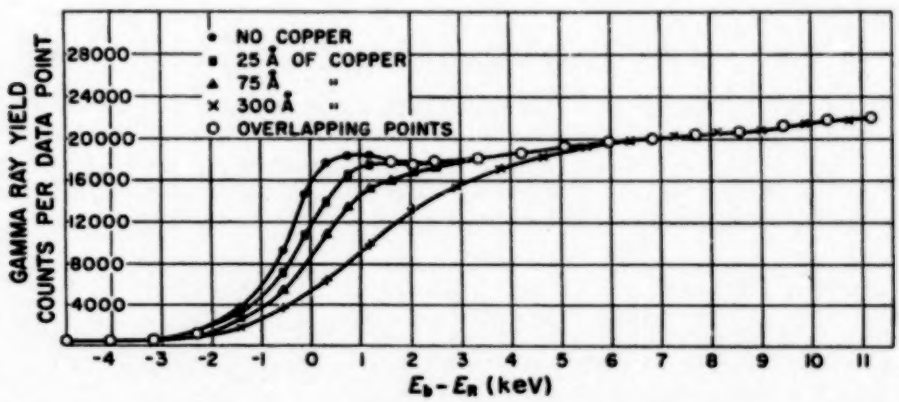

Fig. 4. Yield curves for the resonance at 992 keV from H_3^+ ions and evaporated Al targets covered with evaporated copper layers of different thickness. Thickness values given in Ångstroms are only approximate. Standard deviations in the values of data points are less than the size of the symbols. Here, E_b denotes the mean incident proton energy and E_R the resonance energy. Integrated charge per data point was 41 μC.

25 Å to 200 Å in thickness. The result is a gradual broadening and washing out of the features of the curve, proportional to the amount of copper. Similar progressive changes in shape of the yield curve were encountered before the carbon buildup problem was solved, and served as a convenient and sensitive indicator of the cleanliness of the target surface.

3.6. RESONANCE ENERGY DETERMINATIONS

Results from measurements of six resonance energies with protons, in terms of the 1881.1 keV Li(p, n) threshold standard, are given in table 1. All resonance energy measurements were based on thick target yield curves using H_1^+ ions,

TABLE 1

Resonance energy values

Resonance Energy (keV)		
632.8±0.2	937.7±0.3	1001.7±1.0
923.4±0.3	992.4±0.3	1213.6±0.5

and the average of six measurements of the Li(p, n) threshold. The R.M.S. uncertainties quoted include ±0.02 % uncertainty in the location of the extrapolated Li(p, n) threshold value on our energy scale, ±0.02 % uncertainty in the linearity of the electrostatic analyzer, and an uncertainty in locating the midpoints on resonance yield curve steps varying from 0.005 % for the resonance yield curve steps varying from 0.005 % for the resonance at 992 keV to 0.10 % for the resonance at 1002 keV.

Further details, including a fuller presentation of data referred to, but not included here, are given in a Ph. D thesis by one of the authors [4]).

4. Discussion

Anomalous yield curves from H_2^+ ions have been observed previously, both at this laboratory [5]) and elsewhere, although in most earlier examinations the experimental accuracy was not sufficiently good to reveal the finer details of the curves.

An examination of the problem was undertaken by Anderson *et al.* [6]). They concluded that the discrepancy in resonance energies as deduced from the midpoint of the thick target step was probably due to a non-linearity in the energy scale. The excess broadening of the curves from H_2^+ ions was attributed to internal motion of the protons in the ion.

The problem has also been investigated by Bondelid and Kennedy [3]), who pointed out that the asymmetry of the yield curve below the resonance might be explained by assuming that the H_2^+ ion survives as an ion for a penetration depth in the target of $\frac{1}{2}$ to 1 keV before breaking up. They obtained apparent

confirmation of this explanation by passing the ion beam through a stripping gas of appropriate thickness before it struck the target; in this case a broad but symmetric curve was obtained, with a midpoint in good agreement with the midpoint of the rise of the curve from protons.

The detailed yield curves obtained at this laboratory would seem to exclude any possibility of an explanation from non-linearity of the electrostatic analyzer.

5. Interpretation of Results

5.1. MODEL USED

Computations have been carried out for the following model. The attached electron is torn from the molecular ion the moment the ion strikes the target. The ensuing Coulomb force between the two protons pushes them apart. A proton oriented forward in the ion will receive an impulse in the forward direction, and the trailing proton will feel a retarding impulse. Forward protons from ions with axes (internuclear axes) oriented at small angles with respect to the beam axis at the time of breakup will gain energy more rapidly than they lose energy from ionization, and may pass through the resonance twice. A Coulomb energy of about 6 eV per proton in the centre-of-mass system results in a maximum of about $\pm$ 5 keV in the laboratory system. The forward proton from an ion with its axis oriented at 0° to the beam axis at the moment of break-up will receive a net gain in energy of about 1.5 keV above incident energy, and penetrates to a depth of about 1000 Å in the target before the rate of energy loss becomes normal. If the ion axis is at 70° with respect to the beam, dE/dx for the forward proton is zero at the moment of breakup, and for larger angles dE/dx is always negative.

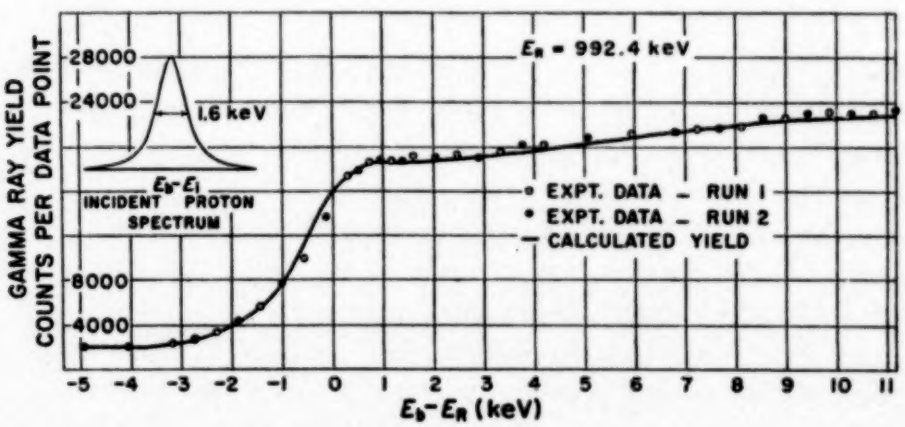

Fig. 5. Analytical fit to the yield from H_3^+ ions at the 992-keV resonance. The insert shows the incident proton energy distribution used in the calculation. Here E_i denotes the incident energy of a proton in a beam of mean energy E_b. The resonance energy is denoted by E_R. Integrated charge per data point was 41 μC.

A calculated yield curve, fitted to the experimental data, is shown in fig. 5. The fit was made by normalizing the maximum yield of the calculated curve to the observed maximum yield of the curve obtained with protons, and by allowing for the 250-eV shift due to the mass of the extra electron. The dielectric constant of the target material was assumed to be unity. For the curve shown the Coulomb effect was cut off rather arbitrarily at a proton separation of about 5 Å, at which point the two protons have penetrated to a depth of 1200 Å in the target. At this separation the Coulomb energy acquired in vacuum would be 90 % of the maximum Coulomb energy.

5.2. INTERNAL ENERGY EFFECTS

A yield curve for a monoenergetic incident beam of H_2^+ ions was first calculated. Internal motion was assumed to be zero in this step. Final curves were obtained using as proton energies at the instant of breakup distributions of various plausible shapes, including a Gaussian and triangular shape. In all cases effects of internal motion were lumped together with the beam energy spread from the electrostatic analyzer. The best over-all fit to the data was provided by a distribution of the Serber [7]) form

$$N(E) = \frac{E_0 a}{[(E-E_0)^2+E_0 a]^{\frac{1}{2}}} \qquad (1)$$

where E_0 represents the mean incident ion energy, a is a constant, and the half-width is given by $E\frac{1}{2} = 1.533\ (E_0 a)^{\frac{1}{2}}$. Most of the observed thin target yield curves are similar to the Serber form, with a narrow width at half-maximum yield and a long tail at the base.

The energy spread from the internal vibrational motion of the two protons in the molecular ion depends on how the ions are distributed in the various excited vibrational states. The zero-point vibrational energy of the H_2^+ ion is known to be 0.14 eV, and its dissociation energy is 2.6 eV [6]). An internal energy of 1 eV corresponds to a maximum classical energy spread of ± 2 keV in the laboratory system, if the energy of the centre-of-mass is 1 MeV. The energy spread resulting from internal motion may therefore be approximately the same as the energy spread passed by the electrostatic analyzer. A half-width of 1.6 keV was used in eq. (1), and the tail was cut off at ± 4 keV. A summary of the calculation is given in the appendix.

5.3. EFFECTS OF ABNORMAL IONIZATION

The theoretical fit was found to be insensitive to the inclusion of small contributions from two other possible effects: the effective stopping power of the target medium may be above normal or below normal for a short distance into the target. Increased stopping power might be expected from the collective behavior of the two protons immediately after the electron is torn away.

Decreased stopping power would result if ions survive as such for a short distance into the target. If these effects do exist they may effectively cancel each other.

5.4. INERT SURFACE LAYERS

The calculation was modified to include various thicknesses of copper layers on the target, and the resulting yield curves are in qualitative agreement with what is observed under these conditions: the sharp bend in the curve near the resonance energy is gradually washed out. Quantitative fits to the experimental data were not attempted in this case, however, since the actual thicknesses of the copper or carbon layers were only poorly known.

5.5. YIELD CURVES WITH HIGHER RESOLUTION

All of the present data were taken with the electrostatic analyzer set for a fixed resolution of 0.1 %, in order to pass a proton beam of reasonable current through the slit system. Our calculations indicate that with higher resolution a broad peak should appear in the yield curves immediately above the resonance energy, rather than the flat plateau observed. Thinner targets may also produce a peak; a slight peak was observed at times, when semi-thick targets of 5 to 10-keV thickness were used. Such a peak may be detected in fig. 4.

No attempt was made to treat the yield from H_3^+ ions analytically.

The authors wish to express their appreciation to Professor R. G. Herb for his continued guidance and encouragement during the present experiment. They are also grateful for helpful discussions with Professor R. G. Sachs, Professor H. W. Lewis and E. A. Silverstein.

This work was supported by the U. S. Atomic Energy Commission and by the Graduate School from funds supplied by the Wisconsin Alumni Research Foundation.

Appendix

A short summary of the computation is given here. The yield may be represented by

$$Y(E_b) = N \int_{x=0}^{\infty} \int_{E=-\infty}^{\infty} \int_{E_1=-\infty}^{\infty} g(E_b, E_1) W(E_1, E, x) \sigma(E) \mathrm{d}E \mathrm{d}E_1 \mathrm{d}x, \quad (2)$$

where N represents the number of atoms per gram in the target, $\sigma(E)$ represents the cross section in cm² per atom, $W(E_1, E, x)\mathrm{d}E$ is the probability that a particle incident on the target with energy E_1 has an energy between E and $E+\mathrm{d}E$ at a depth x grams/cm² in the target, $g(E_b, E_1)\mathrm{d}E_1$ is the probability that a particle in the incident beam of mean energy E_b has an energy between

E_1 and E_1+dE_1 [8]). We assume that $g(E_b, E_1) = g(E_b-E_1)$ and $\sigma(E)$ is taken to be a δ-function, so that the yield becomes

$$Y(E_b) = N \int_{E_1=-\infty}^{\infty} g(E_b-E_1)dE_1 \int_{x=0}^{\infty} W(E_1, E_R, x)dx. \quad (3)$$

Here E_R is the resonance energy. The function $W(E_1, E_R, x)$ was taken as

$$W(E_1, E_R, x) = \int_{\theta=0}^{\pi} \delta\{E_R-[\mathscr{E}(x)\cos\theta-kx+E_1]\}\sin\theta\, d\theta, \quad (4)$$

where $\mathscr{E}(x)\cos\theta$ represents the laboratory energy due to the Coulomb repulsion, θ is the angle the molecular ion axis makes with respect to the beam axis at the time of break-up, and kx is the energy loss in the target at a depth x.

Integration of $W(E_1, E_R, x)$ over x resulted in a yield curve for a monoenergetic beam of incident protons which is discontinuous at $E_1 = E_R$. To overcome this difficulty at the resonance energy, $g(E_b-E_1)$ was assumed to have a narrow rectangular shape of a width negligible compared to that of the energy distribution defined by the electrostatic analyzer, and an approximate value for the monoenergetic yield at the point of singularity was calculated accordingly. Numerical integrations were then performed over various assumed incident proton energy distributions. Details of the calculation are given in ref. [4]).

References

1) Michael, Berners, Eppling, Knecht, Northcliffe and Herb, Rev. Sci. Instr. **30** (1959) 855
2) R. O. Bondelid and C. A. Kennedy, Phys. Rev. **115** (1959) 1601
3) R. O. Bondelid and C. A. Kennedy, NRL Report 5083 (Naval Research Laboratory, Washington, D.C., 1958)
4) P. F. Dahl, Ph. D. Thesis, University of Wisconsin, 1960 (unpublished)
5) Herring, Douglas, Silverstein and Chiba, Phys. Rev. **100** (1955) 1239 (A)
6) Andersen, Gjötterud, Holtebekk and Lönsjö, Nuclear Physics **7** (1958) 384
7) R. Serber, Phys. Rev. **72** (1947) 1008
8) Nuclear Reactions I, edited by P. M. Endt and M. Demeur (North-Holland Publishing Company, Amsterdam, 1959) p. 293

2.B:2.E

Nuclear Physics 21 (1960) 116—127; © *North-Holland Publishing Co., Amsterdam*

Not to be reproduced by photoprint or microfilm without written permission from the publisher

SPIN-ORBIT COUPLING FOR SPIN-1 PARTICLES

G. R. SATCHLER

Oak Ridge National Laboratory, Oak Ridge, Tennessee

Received 8 July 1960

Abstract: A one-body spin-orbit potential for spin-1 particles may contain, in addition to the familiar vector term $\mathbf{l} \cdot \mathbf{s}$ used with spin-$\frac{1}{2}$ particles, certain tensor terms T. The T may be constructed from the position, momentum and angular momentum vectors of the particle. Time reversal invariance cannot be demanded if a complex potential is allowed, but the requirements of parity conservation and symmetry of the scattering matrix allow only three forms of T. Only one of these remains diagonal in the orbital angular momentum. A simple model illustrates the possible origin of a tensor coupling for deuterons. The implications for the scattering and polarization of spin-1 particles is discussed.

1. Introduction

It has become customary to attempt to describe the elastic scattering of particles by atomic nuclei in terms of an optical model [1]). Such a model replaces the interaction between the particle and the nucleus by a simple potential well, in general with an imaginary part to account for inelastic events (whether they occur by absorption into a compound nucleus or by some direct mechanism). Following its initial success in describing the average scattering of nucleons, the optical model has been applied to the scattering of deuterons [2]), alphas [3]), and even nitrogen ions [4]). It was natural to extend this description to the polarization of the scattered particles (if they have spin), or the scattering of polarized particles. Scattering by a central potential will not induce any spin polarization, so it is necessary to include some spin-orbit coupling in the optical model. With spin-$\frac{1}{2}$ particles the only one-body spin-orbit potential we can construct is the familiar vector term $\mathbf{L} \cdot \mathbf{S}$ times some radial dependence. However, with particles of spin-1 we can construct additional operators coupling spin and spatial motion which are scalar products of two second-rank spherical tensors operating on the spin and spatial coordinates respectively. In the next section we consider which tensors are allowed when certain symmetry conditions are imposed. In the following section we discuss the possible origin of the tensor coupling, taking as an example the effect in impulse approximation of the internal D-state of the deuteron. Finally we discuss the effect of these terms on the scattering and polarization of spin-1 particles, using as illustration the Born approximation.

2. Symmetry Conditions and Acceptable Tensors

The first symmetry requirement is that the interaction potential be a scalar under rotations of the coordinate axes. So, provided the scatterer has zero spin or we neglect any coupling to its spin, the optical potential can be written as a series of scalar products

$$V = \sum_k v_k \mathbf{S}_k \cdot \mathbf{R}_k \equiv \sum_{kq} v_k (-)^q S_{kq} R_{k-q}. \tag{1}$$

$\mathbf{S}_k$ is a spherical tensor [5]) of rank k in the spin-space of the particle, while $\mathbf{R}_k$ operates on its space coordinates. Their components transform under coordinate rotations like the spherical harmonics Y_k^q, for example

$$R_{kq'}(x') = \sum_q R_{kq}(x) D^k_{qq'}(\alpha\beta\gamma), \tag{2}$$

where $(\alpha\beta\gamma)$ are the Euler angles of the rotation taking the unprimed coordinate axes into the primed [5]). Spin tensors $\mathbf{S}_k$ can be defined with rank $k \leqq 2s$ for spin-s particles. In spin-space we have only the unit operator $\mathbf{1}$ and the spin operator $\mathbf{s}$, a scalar and vector respectively, so we may put $\mathbf{S}_0 = \mathbf{1}$, and $\mathbf{S}_1 = \mathbf{s}$. Similarly the tensor $\mathbf{S}_2$ can be defined uniquely in terms of the components of $\mathbf{s}$ by contraction with a Clebsch-Gordan coefficient,

$$S_{2q} = \sum_\mu s_\mu s_{q-\mu} \langle 1\mu,\ 1q-\mu | 2q \rangle, \tag{3}$$

where $s_0 = s_z$, $s_{\pm 1} = \mp (s_x \pm i s_y)/\sqrt{2}$. For example, $S_{20} = (3s_z^2 - s(s+1)/\sqrt{6}$. (There is no need to use symmetric combinations like $(s_\mu s_\lambda + s_\lambda s_\mu)$ in (3), since the symmetry of the Clebsch-Gordan coefficient does this automatically even when the s_μ do not commute). When $s = \frac{1}{2}$, the S_{2q} are identically zero.

We have three vectors out of which to construct the coordinate tensors $\mathbf{R}_k$, the position vector $\mathbf{r}$, the momentum $\mathbf{p} = -i\nabla$, and the orbital angular momentum $\mathbf{L} = -i\mathbf{r} \times \nabla$. The number of admissible combinations may be limited by imposing further symmetry conditions, the most obvious of which is parity conservation. Since all the spin terms have even parity, so must the tensors $\mathbf{R}_k$. Invariance under time reversal [6]) cannot be demanded in general when non-elastic channels are open because we use a complex potential to simulate absorption. In other words that part of the scattering matrix which describes elastic scattering need not be unitary by itself [7]). However, the scattering matrix is symmetric, and we wish to preserve this property in the optical model. Coester [8]) has shown that symmetry results from a real hamiltonian if it is also hermitian. A trivial extension of his work shows that a complex potential U leads to a symmetric scattering matrix provided the imaginary part of the potential (that is, that part which is odd under time reversal) is also anti-hermitian. Of course, this condition is satisfied by a simple central

potential $U = V(r)+iW(r)$; we now impose it on the spin-orbit coupling terms also.

The scalar term $k = 0$ of the potential (1) corresponds to the usual central potential and we may normalize so that $\mathbf{S}_0 = \mathbf{R}_0 = 1$. The only vector, $k = 1$, term allowed is the usual $\mathbf{L} \cdot \mathbf{S}$ potential, with a complex radial dependence in general; parity excludes $\mathbf{r} \cdot \mathbf{s}$ and $\mathbf{p} \cdot \mathbf{s}$. Second rank tensors $\mathbf{R}_2$ can be formed by analogy with the spin tensor (3)

$$R_{2q}(\mathbf{a}, \mathbf{b}) = \sum_{\mu} a_\mu b_{q-\mu} \langle 1\mu, 1q-\mu | 2q \rangle, \tag{4}$$

where $\mathbf{a}$, $\mathbf{b}$ are chosen from the vectors $\mathbf{r}$, $\mathbf{p}$ and $\mathbf{L}$. Parity conservation limits $\mathbf{a}$, $\mathbf{b}$ to the pairs $(\mathbf{r}, \mathbf{r})$, $(\mathbf{p}, \mathbf{p})$, $(\mathbf{L}, \mathbf{L})$ and $(\mathbf{r}, \mathbf{p})$. For example, the tensor formed from $(\mathbf{r}, \mathbf{r})$ is essentially a spherical harmonic of the polar angles (θ, ϕ) of $\mathbf{r}$. Taking $\mathbf{a} = \mathbf{b}$ as the unit vector $\hat{\mathbf{r}}$ along $\mathbf{r}$, the expression (4) becomes

$$R_{2q}(\hat{\mathbf{r}}, \hat{\mathbf{r}}) = (8\pi/15)^{\frac{1}{2}} Y_2^q(\theta, \phi). \tag{5}$$

Tensors (4) formed from the pairs with $\mathbf{a} = \mathbf{b}$ are both real and hermitian, hence they may be associated with a complex radial dependence and still preserve the symmetry of the scattering matrix. Hermitian here means the property

$$R_{2q}(\mathbf{a}, \mathbf{b})^\dagger = (-)^q R_{2-q}(\mathbf{a}, \mathbf{b}).$$

The spin tensor has the same property so their scalar product is hermitian in the usual sense, $(\mathbf{R}_2 \cdot \mathbf{S}_2)^\dagger = (\mathbf{R}_2 \cdot \mathbf{S}_2)$. The tensor formed from $\mathbf{r}$ and $\mathbf{p}$ must be rejected because it is imaginary (in the time reversal sense) and also hermitian

$$R_{2q}(\mathbf{r}, \mathbf{p})^\dagger = (-)^q R_{2-q}(\mathbf{p}, \mathbf{r}) = (-)^q R_{2-q}(\mathbf{r}, \mathbf{p}).$$

The second equality holds because only a scalar can be formed from the commutator

$$(r_\mu p_{-\lambda} - p_{-\lambda} r_\mu) = (-)^\mu i \delta_{\lambda\mu},$$

namely,

$$\sum_{\lambda\mu} (-)^\mu \delta_{\lambda\mu} \langle 1\mu, 1-\lambda | k\mu-\lambda \rangle = -\sqrt{3}\, \delta_{k0}.$$

The momentum tensor $\mathbf{R}_2(\mathbf{p}, \mathbf{p})$ must also be discussed further because of the commutation properties of $\mathbf{p}$. When associated with a radial function $U(r)$ the combination is no longer hermitian. Rather,

$$[U(r) R_{2q}(\mathbf{p}, \mathbf{p})]^\dagger = (-)^q R_{2-q}(\mathbf{p}, \mathbf{p}) U(r)^*,$$

and the p_μ do not commute with $U(r)$. However, the symmetric combination

$$U(r)\mathbf{R}_2(\mathbf{p}, \mathbf{p}) + \mathbf{R}_2(\mathbf{p}, \mathbf{p})U(r),$$

has the required property: real part hermitian and imaginary part anti-hermi-

tian. A further hermitian tensor may be formed by sandwiching the radial function between the two momentum operators,

$$R_{2q}(\mathbf{p}, U\mathbf{p}) = \sum_{\mu} \hat{p}_{\mu} U(r) \hat{p}_{q-\mu} \langle 1\mu,\, 1q-\mu | 2q \rangle,$$
$$= (-)^q R_{2-q}(\mathbf{p}, U^*\mathbf{p})^{\dagger}.$$

However, this is not independent of the tensors previously discussed in the sense that

$$\mathbf{R}_2(\mathbf{p}, U\mathbf{p}) = \tfrac{1}{2}[U(r)\mathbf{R}_2(\mathbf{p}, \mathbf{p}) + \mathbf{R}_2(\mathbf{p}, \mathbf{p})U(r)] + f(r)\mathbf{R}_2(\hat{\mathbf{r}}, \hat{\mathbf{r}}),$$

where $f(r)$ is determined by $U(r)$, $f(r)\hat{r}_{\mu}\hat{r}_{\nu} = \frac{1}{2}\nabla_{\mu}\nabla_{\nu}U(r)$. So in a phenomenological analysis it is not necessary to consider both tensors; we choose the former.

We are then left with three acceptable tensor forms. Alternatives for them may be derived by using the recoupling relation

$$\mathbf{S}_2 \cdot \mathbf{R}_2(\mathbf{a}, \mathbf{b}) = (\mathbf{s} \cdot \mathbf{a})(\mathbf{s} \cdot \mathbf{b}) - \tfrac{1}{2} i\mathbf{s} \cdot (\mathbf{a} \times \mathbf{b}) - \tfrac{1}{3}\mathbf{s}^2(\mathbf{a} \cdot \mathbf{b}), \tag{6}$$

remembering that $\mathbf{L} \times \mathbf{L} = i\mathbf{L}$, and $\mathbf{r} \times \mathbf{r} = \mathbf{p} \times \mathbf{p} = 0$. For spin $s = 1$ they become

$$T_r = \mathbf{S}_2 \cdot \mathbf{R}_2(\hat{\mathbf{r}}, \hat{\mathbf{r}}) = (\mathbf{s} \cdot \hat{\mathbf{r}})^2 - \tfrac{2}{3}, \tag{7a}$$

$$T_p = \mathbf{S}_2 \cdot \mathbf{R}_2(\mathbf{p}, \mathbf{p}) = (\mathbf{s} \cdot \mathbf{p})^2 - \tfrac{2}{3}\mathbf{p}^2, \tag{7b}$$

$$T_L = \mathbf{S}_2 \cdot \mathbf{R}_2(\mathbf{L}, \mathbf{L}) = (\mathbf{L} \cdot \mathbf{s})^2 + \tfrac{1}{2}\mathbf{L} \cdot \mathbf{s} - \tfrac{2}{3}\mathbf{L}^2. \tag{7c}$$

The spin tensor $\mathbf{S}_2$ may be thrown into yet another form for deuterons, if we neglect the deuteron internal D-state. For then the deuteron spin is the vector sum of the neutron and protons spins, $\mathbf{s} = \frac{1}{2}(\boldsymbol{\sigma}_N + \boldsymbol{\sigma}_P)$, where the $\boldsymbol{\sigma}$ are Pauli spin operators. Since it is not possible to form a second rank tensor from $\boldsymbol{\sigma}_N$ or $\boldsymbol{\sigma}_P$ by themselves (being spin-$\frac{1}{2}$), it turns out the spin tensor (3) can be rewritten

$$S_{2q} = \tfrac{1}{2} \sum_{\mu} (\sigma_N)_{\mu} (\sigma_P)_{q-\mu} \langle 1\mu,\, 1q-\mu | 2q \rangle, \tag{8}$$

or $\mathbf{S}_2(\mathbf{s}, \mathbf{s}) = \frac{1}{2}\mathbf{S}_2(\boldsymbol{\sigma}_N, \boldsymbol{\sigma}_P)$. Then using eq. (6) we get for example

$$2T_r = (\boldsymbol{\sigma}_N \cdot \hat{\mathbf{r}})(\boldsymbol{\sigma}_P \cdot \hat{\mathbf{r}}) - \tfrac{1}{3}(\boldsymbol{\sigma}_N \cdot \boldsymbol{\sigma}_P), \tag{9}$$

which is the form suggested by Goldfarb [9]). However, the scalar product form (1) remains the most convenient when calculating matrix elements. The matrix elements in an angular momentum representation are given in the appendix, while those in Born approximation are discussed in sect. 4 and the appendix. We note here that the first two tensors (7a) and (7b) are not diagonal in the orbital angular momentum, coupling partial waves with angular momentum differing by two units (not one, because of parity).

3. Deuteron Tensor Coupling

We have no reliable model for deuteron-nucleus interactions at low and medium energies, although we may get some qualitative ideas on the existence and origin of the tensor couplings discussed above. The vector spin-orbit coupling experienced by nucleons in the shell-model and optical model are understood as the average effect of two-body spin-orbit or tensor forces. Such forces, at least in second order, would lead to a deuteron tensor coupling T_L of the form (7c); further, if the internal D-state motion of the deuteron is taken into account a term T_τ of the form (7a) also appears in first order. These effects may be understood in terms of the impulse approximation [10, 11]) which, although presumably only valid at high energies, gives a convenient physical picture.

We adopt Watanabe's approach [10]), using an optical potential (with spin-orbit coupling) for the interaction between each nucleon of the deuteron and the target nucleus. In first order, neglecting the deuteron D-state, Watanabe obtains a central potential and a vector spin-orbit coupling for the deuteron-nucleus interaction. The extension to second order (which would include some polarization of the deuteron) would introduce some tensor coupling T_L arising from the nucleon-nucleus spin-orbit force. However, already in first order we obtain some of the tensor T_τ when we take account of the internal deuteron D-state. We shall now show this with a simple model; the results may have little quantitative significance but do indicate that the tensor terms may be appreciable.

To first order the deuteron-nucleus potential is given by

$$U = \langle\chi|V_N+V_P|\chi\rangle,$$

where χ is the internal wave function for the deuteron, and V_N, V_P are the neutron-nucleus and proton-nucleus interactions repectively. We take for the latter a central plus spin-orbit potential [1])

$$V_i = V_C(r_i)+V_S(r_i)\mathbf{l}_i\cdot\boldsymbol{\sigma}_i, \tag{10}$$

For the deuteron wave function we use the representation which is an operator in spin-space [12])

$$\rho\chi(\rho) = u(\rho)+w(\rho)S_{NP}. \tag{11}$$

S_{NP} is the two-body tensor operator

$$\rho^2 S_{NP} = 3(\boldsymbol{\sigma}_N\cdot\boldsymbol{\varrho})(\boldsymbol{\sigma}_P\cdot\boldsymbol{\varrho})-(\boldsymbol{\sigma}_N\cdot\boldsymbol{\sigma}_P)\rho^2 \tag{12}$$

and $\boldsymbol{\varrho} = \mathbf{r}_N-\mathbf{r}_P$ is the neutron-proton separation. In the nucleon potentials (10) we require $\mathbf{r}_N = \mathbf{r}+\frac{1}{2}\boldsymbol{\varrho}$ and $\mathbf{r}_P = \mathbf{r}-\frac{1}{2}\boldsymbol{\varrho}$, where $\mathbf{r}$ gives the centre of mass

of the deuteron; then they may be expanded in $\mathbf{r}$ and $\boldsymbol{\varrho}$,

$$V_{C,S}(r_i) = \sum_{kq} \varepsilon^k v_{C,S}^{(k)}(\mathbf{r}, \varrho) Y_k^q(\hat{\mathbf{r}}) Y_k^q(\hat{\boldsymbol{\varrho}})^*, \tag{13}$$

where $\varepsilon = +1$ if $i = \mathrm{N}$, $\varepsilon = -1$ if $i = \mathrm{P}$, and a vector appearing as the argument of a spherical harmonic denotes its polar angles. Further, we rewrite the tensor operator (12) and use the relation (8) with $\mathbf{s} = \frac{1}{2}(\boldsymbol{\sigma}_\mathrm{N} + \boldsymbol{\sigma}_\mathrm{P})$

$$S_{\mathrm{NP}} = 4(6\pi/5)^{\frac{1}{2}} \sum_q S_{2q}(\mathbf{s}, \mathbf{s}) Y_2^q(\hat{\boldsymbol{\varrho}})^*. \tag{14}$$

The main, S-state, contribution to the central part of the potential U comes from the $k = 0$ term of eq. (13),

$$U_\mathrm{C}(r) = 2\int_0^\infty u(\rho)^2 v_\mathrm{C}^{(0)}(r, \rho)\mathrm{d}\rho. \tag{15}$$

For the S-state contribution to the vector spin-orbit term we have $\mathbf{l}_\mathrm{N} = \mathbf{l}_\mathrm{P} = \frac{1}{2}\mathbf{L}$, where L is the orbital angular momentum of the deuteron centre of mass. The coefficient of $\mathbf{L} \cdot \mathbf{S}$ in the potential U then becomes

$$U_\mathrm{V}(r) = \int_0^\infty u(\rho)^2 v_\mathrm{S}^{(0)}(r, \rho)\mathrm{d}\rho. \tag{16}$$

The S—D cross-terms, with the nucleon central potentials V_C, give a contribution to the tensor coupling T_r; with eq. (14) they are

$$8(6\pi/5)^{\frac{1}{2}} \sum_q S_{2q}(\mathbf{s}, \mathbf{s}) \int \mathrm{d}\boldsymbol{\varrho} Y_2^q(\hat{\varrho})^* \rho^{-2} u(\rho) w(\rho) [V_\mathrm{C}(r_\mathrm{N}) + V_\mathrm{C}(r_\mathrm{P})]$$
$$= U_\mathrm{T}(r) \mathbf{S}_2(\mathbf{s}, \mathbf{s}) \cdot \mathbf{R}_2(\hat{\mathbf{r}}, \hat{\mathbf{r}}).$$

Only the $k = 2$ term of the expansion (13) is involved, so

$$U_\mathrm{T}(r) = 24\int_0^\infty u(\rho) w(\rho) v_\mathrm{C}^{(2)}(r, \rho)\mathrm{d}\rho. \tag{17}$$

The use of a velocity-dependent or non-local nucleon-nucleus potential V could also give rise to momentum tensors of the form (7b).

To evaluate and compare these three terms we take a gaussian shape for the nucleon optical potential because this has a convenient expansion (13),

$$V_\mathrm{C}(r_i) = -V_0 \exp(-r_i^2/R^2),$$
$$v_\mathrm{C}^{(k)}(r, \rho) = -4\pi V_0 (-i)^k j_k(ir\rho/R^2) \exp -\left(\frac{4r^2 + \rho^2}{4R^2}\right). \tag{18}$$

If we take a Thomas form for the spin-orbit coupling [1]), $V_\mathrm{S}(r_1) = -(\lambda R^2/r_1)(\mathrm{d}V_\mathrm{S}/\mathrm{d}r_1) = 2\lambda V_\mathrm{C}(r_1)$, the same expansion can be applied to this. Further, we approximate the deuteron radial wave functions with oscillator functions

$$u(\rho) = N_0(\rho/a) \exp -(\rho/a)^2, \quad w(\rho) = N_2(\rho/a)^3 \exp -(\rho/a)^2.$$

The justification for this is that it allows the integrals to be done very easily

and we are only interested in order of magnitude results. For the central potential (15) we find

$$U_C(r) = -U_0 \exp -(r/r_0)^2,$$

where

$$U_0 = 2V_0\left(1+\frac{a^2}{8R^2}\right)^{-\frac{1}{2}}, \quad r_0 = R\left(1+\frac{a^2}{8R^2}\right)^{\frac{1}{2}}.$$

As expected, U_C is less strong than $2V_C$ and has a longer tail. The vector spin-orbit potential (16) is just proportional to U_C, $U_V(r) = \lambda U_C(r)$. The radial dependence of the tensor coupling (17) becomes

$$U_T(r) = -U_1(r/r_0)^2 \exp -(r/r_0)^2,$$

where

$$U_1/U_0 = (3P_D/40)^{\frac{1}{2}}\left(\frac{a}{R}\right)^2\left(1+\frac{a^2}{8R^2}\right)^{-1},$$

and P_D is the deuteron D-state probability (about 4 %). In light nuclei (say $A \lesssim 16$) where the gaussian potential may be a reasonable approximation we have λ of the order of $\frac{1}{20}$. For this region $a \approx R$($a \approx 3\times10^{-13}$ cm gives a reasonable fit to the actual wave function) and U_1/U_0 is also of order $\frac{1}{20}$, so the tensor coupling may be appreciable. For heavier nuclei the gaussian potential (18) is misleading because it does not give the constant surface thickness that is found experimentally [1]). A potential like the Woods-Saxon [1]) that does have a constant surface thickness leads to both vector U_V and tensor U_T having strengths proportional to R^{-1}. Thus one anticipates the two terms having the same relative strengths for all nuclei. The important parameter for the tensor coupling (at least in this approximation) is the ratio of the deuteron radius to the surface thickness of the nucleon potentials.

4. Scattering and Polarization

A number of authors have discussed the scattering and polarization of spin-1 particles, and some of this work is summarized in ref. [13]). Although we have reduced the number of admissible tensor spin-orbit couplings to three this is still an uncomfortably large number for a phenomenological analysis such as the optical model attempts. Further, there is no exact correspondence between the vector and tensor couplings, and the vector and tensor types of spin polarization. The vector spin-orbit force $\mathbf{L}\cdot\mathbf{S}$ by itself will in general give rise to some second-rank tensor polarization of the particles it scatters.

An additional complication with the tensors T_r and T_p of eqs. (7a) and (7b) is that both have matrix elements off-diagonal in the orbital angular momentum L of the particle. Partial waves with L differing by 2 units are coupled (not by

1 because they have opposite parity). The wave function corresponding to incident particles with wave vector $\mathbf{k}$ and spin component m along $\mathbf{k}$, scattered by a spinless target, may be expanded in partial waves of total angular momentum J and orbital L

$$\Psi_m = \sum_{JLL'} [4\pi(2L+1)]^{\frac{1}{2}} \langle L0, sm|Jm\rangle (kr)^{-1} f^J_{L'L}(kr) \psi_{JL'm},$$

where ψ is the spin-angle function

$$\psi_{JLm} = \sum_{m'} i^L Y_L{}^{m-m'}(\theta, \phi) \chi_{sm'} \langle Lm-m', sm|Jm\rangle,$$

so that in the absence of any interaction

$$\Psi_m \to \chi_{sm} \exp(i\mathbf{k}\cdot\mathbf{r}).$$

The radial function satisfies the coupled equations

$$\left[\frac{d^2}{dr^2} - \frac{L'(L'+1)}{r^2} + k^2 - \frac{2\eta k}{r} - \frac{2\mu}{\hbar^2} U^J_{L'}(r)\right] f^J_{L'L}(kr)$$
$$= \sum_{L''\neq L'} \frac{2\mu}{\hbar^2} \langle L'J|U|L''J\rangle f^J_{L''L}(kr), \quad (19)$$

where μ is the reduced mass, and η the usual Coulomb parameter. $U_L{}^J(r)$ is the diagonal value of the potential, $\langle LJ|U|LJ\rangle$, while the terms $L' \neq L$ are the transitions between partial waves induced by the tensor spin-orbit couplings T_r or T_p. If these are not present the right hand side of eq. (19) vanishes and $L = L'$ only. Otherwise we have no means of assessing the importance of these coupling terms. There is no obvious reason why the off-diagonal elements of T_r or T_p should be appreciably smaller than the diagonal ones, especially if the interaction were concentrated at the nuclear surface, although the total effect of such terms could be small. The answers to these questions can only be obtained by numerical studies. The tensor T_L avoids this difficulty because it is diagonal in L; of course (because they are scalar products) all three tensors are diagonal in the total angular momentum J.

Goldfarb has discussed the vector coupling, and the tensor (9), in Born approximation [9]); his formulae contain some misprints and the corrected ones are included in the appendix. The Born approximation is only valid at high energies, where probably it is most reasonable to apply an impulse approximation without the intermediary step of an optical potential [11]). However, it can give a feeling for the behavior at lower energies, especially if we treat the scattering by the central potential exactly, taking only the spin coupling terms in Born approximation. The amplitude for scattering through θ from $\mathbf{k}_1$ to $\mathbf{k}_2$ is a matrix in spin space and can be written in general as

$$M(\theta) = A(\theta) + iB(\theta)\mathbf{s}\cdot\mathbf{n} + \sum_\alpha C_\alpha(\theta)\mathbf{S}_2\cdot\mathbf{R}_2(\alpha), \quad (20)$$

where $\mathbf{n}$ is the unit vector along $\mathbf{k}_1 \times \mathbf{k}_2$ and the $\mathbf{R}_2(\alpha)$ are tensors formed as in eq. (4) from pairs of the vectors $\mathbf{k}_1$, $\mathbf{k}_2$ and $\mathbf{n}$. Again, although we cannot demand time reversal invariance for M if inelastic events are possible, the requirements of parity conservation and symmetry only allow two independent tensors, for example $\mathbf{R}_2(\mathbf{n}, \mathbf{n})$ and $\mathbf{R}_2(\mathbf{k}_1, \mathbf{k}_2)$. The Born approximation to M for scattering from a potential U is

$$M_B(\theta) = -(\mu/2\pi\hbar^2)\langle \mathbf{k}_2|U|\mathbf{k}_1\rangle. \tag{21}$$

So the three terms (20) of M become the matrix elements of the corresponding central U_C, vector U_V and tensor U_T parts of U (see appendix). This correspondence still holds in distorted wave Born approximation. For this we treat the scattering from U_C exactly (this gives $A(\theta)$) but treat the vector and tensor and tensor coupling in Born approximation, using for the $|\mathbf{k}\rangle$ in eq. (21) not plane waves but the corresponding waves distorted by scattering from U_C. The expectation value of some observable O after scattering is given by

$$\langle O\rangle = \mathrm{tr}\,(M^+OM)/\mathrm{tr}(M^+M). \tag{22}$$

Hence, in these approximations a tensor coupling U_T by itself leads to zero vector polarization $\mathbf{P} = \langle \mathbf{s}\rangle$ for the scattered particles. Contributions to $\mathbf{P}$ arise from cross-terms between the central and vector potentials, and between the vector and tensor (provided they are not both real); the first will dominate if the spin-orbit coupling is weak. Tensor polarizations $\langle T_{kq}\rangle$ as defined by Lakin [13, 14]) † can arise from the vector or tensor couplings by themselves, or from cross-terms between the vector and tensor or between the tensor and central potentials. The last contribution will be largest if the vector and tensor potentials are weak compared to the central. So, to this approximation, the vector polarization is mainly influenced by the vector spin-orbit coupling and the tensor polarization by the tensor coupling.

One quite general result is that if we choose a z-axis perpendicular to the scattering plane the components $\langle T_{2\pm1}\rangle$ vanish whatever coupling is present.

Appendix

The vector coupling $\mathbf{L}\cdot\mathbf{S}$ for spin-1 particles has the value L if the total angular momentum $J = L+1$, -1 if $J = L$, and $-(L+1)$ if $J = L-1$. It is diagonal in both J and L. Matrix elements of the tensor couplings (7) are readily evaluated by standard techniques [5]), and we soon find the diagonal terms

$$\sqrt{6}\langle LJ|T_r|LJ\rangle = \begin{cases} -L(2L+3)^{-1} & \text{if } J = L+1, \\ 1 & \text{if } J = L, \\ -(L+1)(2L-1)^{-1} & \text{if } J = L-1, \end{cases}$$

† $\langle T_{2q}\rangle$ is proportional to the expectation value of the spin operator (3), $T_{2q} = \sqrt{3}S_{2q}$.

$$\tfrac{3}{2}(2L+1)^{\frac{1}{2}}\langle LJ|T_2|LJ\rangle = \begin{cases} -L(2L+3)^{-1}\nabla^2 & \text{if } J=L+1, \\ -\nabla^2 & \text{if } J=L, \\ -(L+1)(2L-1)^{-1}\nabla^2 & \text{if } J=L-1, \end{cases}$$

$$6\langle LJ|T_L|LJ\rangle = \begin{cases} L(2L-1) & \text{if } J=L+1, \\ -(2L-1)(2L+3) & \text{if } J=L, \\ (L+1)(2L+3) & \text{if } J=L-1. \end{cases}$$

These matrix elements, of course, correspond to integration over angle and spin coordinates only, not the radial coordinate r. Also, ∇^2 takes its value for angular momentum L, namely

$$\nabla^2 = \frac{\mathrm{d}^2}{\mathrm{d}r^2} + \frac{2}{r}\frac{\mathrm{d}}{\mathrm{d}r} - \frac{L(L+1)}{r^2}.$$

The off-diagonal elements between L and $L+2$ can only occur for $J = L+1$. These are

$$(2L+3)\langle L+2, L+1|T_1|L, L+1\rangle = [\tfrac{3}{2}(L+1)(L+2)]^{\frac{1}{2}},$$

$$(2L+3)\langle L+2, L+1|T_2|L, L+1\rangle = -[(L+1)(L+2)]^{\frac{1}{2}}\left[\frac{\mathrm{d}^2}{\mathrm{d}r^2} - \frac{2L+1}{r}\frac{\mathrm{d}}{\mathrm{d}r} + \frac{L(L+2)}{r^2}\right].$$

The Born approximation for the scattering amplitude $M(\theta)$ is given by eq. (21). We use a potential

$$U = U_C(r) + U_V(r)\mathbf{L}\cdot\mathbf{s} + U_T(r)\mathbf{S}_2\cdot\mathbf{R}_2,$$

where the last term may be any of the tensors (7). The central potential U_C gives the term $A(\theta)$ in eq. (20),

$$A(\theta) = -(2\mu/\hbar^2)\int_0^\infty U_C(r) j_0(Qr) r^2 \mathrm{d}r,$$

where the recoil $\mathbf{Q} = \mathbf{k}_1 - \mathbf{k}_2$ with $Q = 2k\sin\frac{1}{2}\theta$. Remembering that $\mathbf{L}\exp(i\mathbf{k}\cdot\mathbf{r}) = (\mathbf{r}\times\mathbf{k})\exp(i\mathbf{k}\cdot\mathbf{r})$, the vector coupling gives

$$B(\theta) = -(2\mu/\hbar^2)k\cos\tfrac{1}{2}\theta\int_0^\infty U_V(r) j_1(Qr) r^3 \mathrm{d}r.$$

The contribution to eq. (20) from the tensor T_2 follows immediately if we use eq. (5), giving $C_2(\theta)\mathbf{S}_2\cdot\mathbf{R}_2(\hat{\mathbf{Q}}, \hat{\mathbf{Q}})$ with

$$C_2(\theta) = (2\mu/\hbar^2)\int_0^\infty U_{T_2}(r) j_2(Qr) r^2 \mathrm{d}r.$$

Since $R_{2q}(\hat{\mathbf{Q}}, \hat{\mathbf{Q}}) = (8\pi/15)^{\frac{1}{2}} Y_2^q(\alpha, \beta)$, where (α, β) are the polar angles of $\mathbf{Q}$, this term becomes diagonal if the z-axis is chosen along $\mathbf{Q}$, so $\mathbf{S}_2\cdot\mathbf{R}_2 = (S_z^2 - \frac{2}{3})$. That is, T_2 causes the spins to precess around $\mathbf{Q}$ without flipping.

Similarly, using $R_{2q}(\mathbf{p}, \mathbf{p}) \exp(i\mathbf{k}\cdot\mathbf{r}) = \exp(i\mathbf{k}\cdot\mathbf{r})R_{2q}(\mathbf{k}, \mathbf{k})$, we find for the symmetrized tensor $U_{T_p}(r)T_p + T_pU_{T_p}(r)$ a term

$$C_p(\theta)\mathbf{S}_2 \cdot [\mathbf{R}_2(\hat{\mathbf{k}}_1, \hat{\mathbf{k}}_1) + \mathbf{R}_2(\hat{\mathbf{k}}_2, \hat{\mathbf{k}}_2)],$$

where

$$C_p(\theta) = -(2\mu/\hbar^2)k^2 \int_0^\infty U_{T_p}(r) j_0(Qr) r^2 \mathrm{d}r.$$

The alternative momentum tensor $\mathbf{S}_2 \cdot \mathbf{R}_2(\mathbf{p}, U\mathbf{p})$ has a matrix element

$$C_p(\theta)\mathbf{S}_2 \cdot \mathbf{R}_2(\hat{\mathbf{k}}_1, \hat{\mathbf{k}}_2).$$

For the simple model discussed in sect. 3 we have

$$\begin{aligned} A(\theta) &= \pi^{\frac{1}{2}}(\mu U_0/2\hbar^2) r_0^3 \exp(-\tfrac{1}{4}Q^2 r_0^2), \\ B(\theta)/A(\theta) &= \tfrac{1}{2}\lambda k^2 r_0^2 \sin\theta, \\ C(\theta)/A(\theta) &= -(U_1/U_0)k^2 r_0^2 \sin^2 \tfrac{1}{2}\theta. \end{aligned}$$

The differential cross-section and polarizations can be calculated from the matrix M according to eq. (22) [11, 13, 14]). The matrix elements of the spin-tensor components S_{2q} between states with spin z-components m and m' are

$$\langle m'|S_{2q}|m\rangle = \sqrt{\tfrac{5}{3}}\langle 1m'|1m, 2q\rangle \delta_{m', m+q}.$$

If, for example,

$$M(\theta) = A(\theta) + iB(\theta)\mathbf{s}\cdot\mathbf{n} + C_r(\theta)\mathbf{S}_2 \cdot \mathbf{R}_2(\hat{\mathbf{Q}}, \hat{\mathbf{Q}}),$$

the differential cross-section, which is $\frac{1}{3}\,\mathrm{tr}\,|M|^2$, becomes

$$\mathrm{d}\sigma/\mathrm{d}\omega = |A|^2 + \tfrac{2}{3}|B|^2 + \tfrac{2}{9}|C_r|^2,$$

and the vector polarization $P(\theta) = \langle \mathbf{s}\cdot\mathbf{n}\rangle$ is

$$3(\mathrm{d}\sigma/\mathrm{d}\omega)P(\theta) = \mathrm{Im}[4AB^* + \sqrt{\tfrac{2}{3}}BC_r^*].$$

For the tensor polarization we choose a z-axis along $\mathbf{k}_2$, and y-axis along $-\mathbf{n}$, when

$$\begin{aligned} 3\sqrt{2}(\mathrm{d}\sigma/\mathrm{d}\omega)\langle T_{20}\rangle &= 3\,\mathrm{Re}\,(BC^*)\sin\theta - |B|^2 + \mathrm{Re}[C^*(A - \tfrac{1}{6}C)](1 - 3\cos\theta), \\ \sqrt{3}(\mathrm{d}\sigma/\mathrm{d}\omega)\langle T_{21}\rangle &= \mathrm{Re}\,[C^*(A\sin\theta + B\cos\theta - \tfrac{1}{6}C\sin\theta)], \\ 2\sqrt{3}(\mathrm{d}\sigma/\mathrm{d}\omega)\langle T_{22}\rangle &= \mathrm{Re}\,[C^*(\mathrm{A} - \tfrac{1}{6}C)](1 + \cos\theta) - |B|^2 - \mathrm{Re}[BC^*)\sin\theta. \end{aligned}$$

These quantities may be used directly in the formulae for double-scattering experiments [13, 14]). The polarization P vanishes if A, B and C_r are all real (as in Born approximation with real potentials) although the $\langle T_{2q}\rangle$ do not.

References

1) A. E. Glassgold, Progress in nuclear physics (Pergamon Press, London, 1959)
2) H. S. Melkanoff, Proc. of the Conference on the nuclear optical model, Florida State University (1959);
I. Slaus and W. P. Alford, Phys. Rev. **114** (1959) 1054
3) W. B. Cheston and A. E. Glassgold, Phys. Rev. **106** (1957) 1215
4) C. E. Porter, Phys. Rev. **112** (1957) 1722;
R. H. Bassel, R. M. Drisko and M. A. Melkanoff, Bull. Am Phys. Soc. **5** (1960) 67
5) M. E. Rose, Elementary theory of angular momentum (John Wiley and Sons, New York, 1957)
6) E. P. Wigner, Group theory (Academic Press, New York, 1959)
7) L. C. Biedenharn, Nuclear Physics **10** (1959) 620;
A. I. Baz, Soviet Phys. JETP **5** (1958) 521
8) F. Coester, Phys. Rev. **84** (1951) 1259; **89** (1953) 619
9) L. J. B. Goldfarb, Nuclear Physics **7** (1958) 622
10) S. Watanabe, Nuclear Physics **8** (1958) 484
11) H. P. Stapp, Phys. Rev. **107** (1957) 605
12) R. Sachs, Nuclear theory (Addison-Wesley Publishing Company, Cambridge, 1953) Ch. 3
13) G. R. Satchler, Oak Ridge National Laboratory Report 2861 (1960)
14) W. Lakin, Phys. Rev. **98** (1955) 139

3.A

Nuclear Physics 21 (1960) 128—132; © *North-Holland Publishing Co., Amsterdam*

Not to be reproduced by photoprint or microfilm without written permission from the publisher

SPINS OF THE ISOMERIC STATES OF Hf^{178} AND Hf^{180}

MARTIN DEUTSCH and RUDOLF W. BAUER

Laboratory for Nuclear Science, Massachusetts Institute of Technology, Cambridge 39, Massachusetts †

Received 25 July 1960

Abstract: The 4.8 sec state of Hf^{178} and the 5.5 h state of Hf^{180} are shown by angular correlation measurements to have spin $J = 8$.

1. Introduction

The odd-parity "intrinsic" excited states of even-mass deformed nuclei have been a subject of extensive semi-empirical theoretical analysis [1]). The isomeric states of Hf^{178} and Hf^{180} with excitation energies near 1 MeV are classified in this category and usually assigned 8^- character [2]). No direct experimental confirmation of the value $J = 8$ has appeared in the literature and other

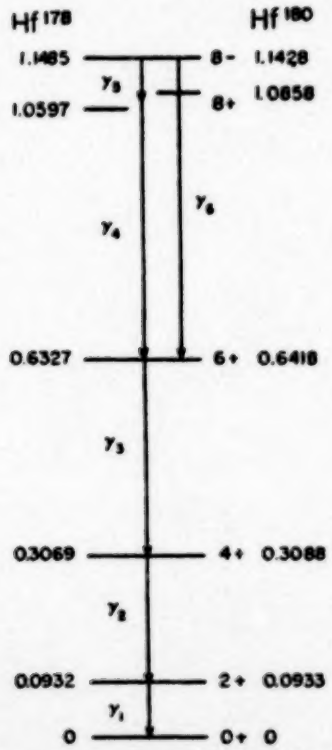

Fig. 1. Decay schemes of the hafnium isomers.

† This work is supported in part through AEC Contract AT (30-1)-2098, by funds provided by the U. S. Atomic Energy Commission, the Office of Naval Research and the Air Force Office of Scientific Research.

assignments have been proposed, e.g. $J = 9$ for Hf^{180} [3,4]) on the basis of internal conversion data. Fig. 1 shows the relevant features of the nuclear level schemes involved.

We have established unambiguously that in each case the state from which γ_5 is emitted has 8^- character. The proof is provided by the angular correlation between γ_5 and the γ rays of the rotational cascade $\gamma_1 \ldots \gamma_4$ together with the observation that the internal conversion coefficient for γ_5 is so small that at least 98 % of the γ ray intensity must be E1 radiation. Accepting the well-established assignment 8^+ for the highest level of the rotational sequence only $J = 7$, 8 or 9 is possible for the state in question. ($J = 7$ is rather improbable in view of the low intensity of the cross-over γ ray leading to the 6^+ level.)

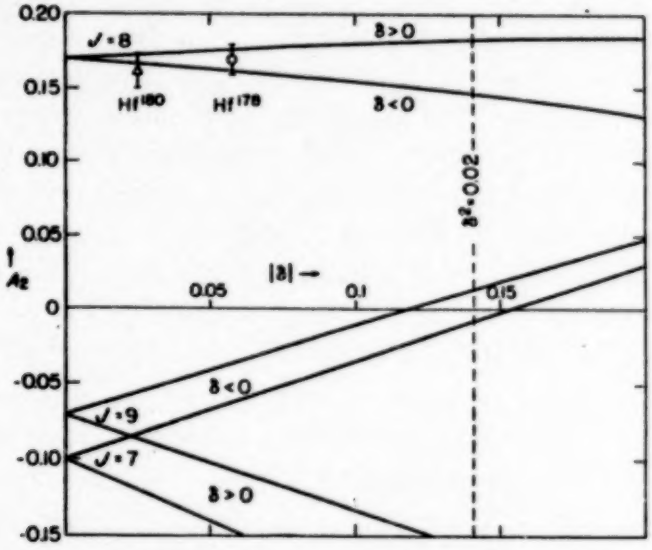

Fig. 2. The coefficient A_2 of the angular correlation $W(\theta) = 1 + A_2 P_2(\cos\theta)$ for the spin sequences 7—8—6, 8—8—6, 9—8—6. The quantity δ is the fractional amplitude of M2 radiation. The dotted line indicates the largest value of $|\delta|$ which could possibly be consistent with internal conversion data.

Fig. 2 shows the theoretical coefficients [5,6]) A_2 of the correlation $W(\theta) = 1 + A_2 P_2(\cos\theta) + \ldots$ for the three spin sequences 7—8—6, 8—8—6, 9—8—6 possible for the cascade γ_5—γ_4. The angular correlation γ_5—γ_3, γ_5—γ_2, γ_5—γ_1 should be identical with γ_5—γ_4 since the four E2 γ rays form a "basic" cascade [7]). We note that only $J = 8$ results in positive values of A_2. Fig. 2 also shows the average experimental values of A_2 for the two cascades studied. Obviously 8 is the only possible spin assignment for the initial state consistent with these data. Following we present some details of our experiments, since their internal consistency provides strong support for the entire decay scheme and because some aspects of the technique may be of interest to specialists.

The only significant difficulty of the experiment arises from the fact that in both decays there occur other radiations with energies so close to that of γ_5 that they cannot be separated by scintillation spectrometry. We have overcome this difficulty by the use of "critical" absorbers with K-absorption discontinuities between the otherwise indistinguishable energies.

2. The Nucleus Hf^{178}

This nucleide was investigated in equilibrium with its parent Ta^{178}(2 hr) since the half-life of the isomeric state (4.8 sec) is too short for convenient experimentation. Ta^{178} was produced by the reaction Lu^{175} (α, n) with 30 MeV α particles in the MIT cyclotron, and separated from lutetium and hafnium by solvent extraction. We confirmed that all of the relevant radiations belong to the decay scheme of the isomeric state [8]) by scintillation spectrometry on the 5 sec hafnium activity "milked" from the tantalum by rapid solvent extraction.

For the angular correlation measurements we used sources dissolved in a few drops of concentrated hydrofluoric acid, since our experience indicates that this chemical form is least likely to show significant perturbation of the intermediate nuclear spin orientations. The 88 keV radiation γ_5 was detected in a 3 mm thick NaI scintillator and was separated from γ_1 (93 keV) by an absorber of about 0.35 g/cm^2 of bismuth which has an absorption discontinuity at 90.5 keV and reduces the intensity of γ_1 by about a factor 10 and γ_5 by about a factor 1.7. A collimating cone with tantalum partitions was used to reduce the effect of secondary K X rays produced in the absorber. The properties of the 88 keV radiation could be isolated completely by performing experiments alternately with bismuth and lead absorbers. The difference between such measurements is entirely due to the radiation falling between 88.0 and 90.5 keV. The counting rate remaining with a lead absorber was approximately 20 % of that with equivalent bismuth absorber.

γ_2, γ_3 and γ_4 were detected in a 7.6 cm $\times$ 7.6 cm NaI scintillator. The angular correlation was measured by recording the pulse height spectrum from this detector in a multi-channel analyzer gated by coincidences with 88 keV pulses from the other counter. Thus the correlation between γ_5 and each of the other three γ rays is obtained in a single measurement. For completeness a similar measurement was performed for γ_1, using a 1.3 cm thick scintillator. The result was consistent with those for the other γ rays but afflicted with considerably greater uncertainties arising from secondary radiations. From the absorption in lead and bismuth and from the relative intensities of the "90 keV" lines in Hf^{178} and Hf^{180}, we deduce the intensity ratio $\gamma_5/\gamma_1 = 3 \pm 0.5$ in Hf^{178}. Using the theoretical conversion coefficient [9]) $\alpha_2 \approx 4$ for γ_1, we deduce for γ_5 the value $\alpha \approx 0.67 \pm 0.25$ .The theoretical values for E1 and M2 transitions of 88 keV are $\alpha_1 \approx 0.45$, $\beta_2 \approx 50$ respectively. This yields, then, the ratio $\delta^2 = (5 \pm 5) \times 10^{-3}$

for the M2 contribution to γ_5. Conservatively we may set $\delta^2 < 2\times10^{-2}$ and this is the limit indicated in fig. 2. The results for the several correlations are summarized in table 1.

TABLE 1

Angular correlation coefficients A_2

	γ_1	γ_2	γ_3	γ_4
Hf^{178}	0.11±0.04	0.165±0.014	0.170±0.012	0.176±0.012
Hf^{180}	0.14±0.04	0.165±0.015	0.162±0.015	0.154±0.015

3. The Nucleus Hf^{180}

Hf^{180m} was produced by the reaction $Hf^{179}(n, \gamma)$ in the MITNR reactor, using enriched (83 %) Hf^{179}. The apparatus used was identical with that used for Hf^{178} except that the tantalum partitions of the collimating cone were replaced by silver. The 57.6 keV γ_5 was separated from the Hf K X rays by the use of thulium and erbium absorbers. The conditions for isolating γ_5 are less favorable for Hf^{180} than in the case of Hf^{178} because both of the critical absorbers *transmit* most of the interfering X radiation. The properties of γ_5 must therefore be determined by subtraction of numbers of comparable magnitude. This disadvantage is compensated by the longer mean life of the source and by the *a priori* knowledge that coincidences with atomic X rays are necessarily isotropic; thus approximately equal precision is obtained for the two isotopes. The K absorption discontinuities of thulium (59.4 keV) and erbium (57.5 keV) both fall between the K_α and K_β lines of Hf. Both materials should therefore reduce the X ray intensity equally. We used absorbers of 0.1 g/cm² of Tm_2O_3 and Er_2O_3 and found the results shown in table 2.

TABLE 2

Observed transmission through critical absorbers

	Tm_2O_3	Er_2O_3
Ta^{177}(Hf X ray)	0.60	0.59
Hf^{180}(X ray+γ_5)	0.68	0.35

From these results and approximate values for absorption coefficients of a 3 cm^2g^{-1} and 16 cm^2g^{-1} on the two sides of the discontinuity, we conclude that γ_5 is about 1.65 ±0.5 times as intense as the KX ray. Using the theoretical E2 conversion coefficients for γ_1—γ_4 and a fluorescent yield of 0.93, we estimate that there are about 0.38 K X rays and therefore 0.63±0.2 57.6 keV γ rays per Hf^{180} disintegration. Assuming the intensity of γ_6 to be 0.15 [3,4]), this yields $\alpha = 0.5\pm0.5$ for γ_5. With $\alpha_1 \approx 0.3$, $\beta_2 \approx 100$ from ref. [9]) we estimate $\delta^2 \doteq (2\pm5)\times10^{-3}$ or again conservatively $\delta^2 < 2\times10^{-2}$. Quite recently

Edwards [10]) has reported an experimental value of $\alpha = 0.67 \pm 0.05$ for γ_8. The excess over the theoretical value is however almost entirely due to L_I and L_{II} conversion (cf. also ref. [3])) and therefore does not indicate an admixture of M2 radiation. Our result for α is less precise than those of ref. [2,4,10]), but it is quite sufficient for our purpose.

The coefficients A_2 for the various γ rays were obtained *mutatis mutandis*, as in the case of Hf^{178} and are summarized in table 1 and in fig. 2.

We wish to thank the staffs of the MIT cyclotron and reactor for their cooperation in preparing the sources.

References

1) Cf. e.g. C. J. Gallagher, Nuclear Physics **16** (1960) 215
2) V. V. Anisovich, JETP (USSR) **34** (1958) 1639; (Soviet Phys. JETP **7** (1958) 1125)
3) G. Scharff-Goldhaber, M. McKeown and J. W. Mihelich, Bull. Am. Phys. Soc. **1** (1956) 206
4) V. S. Gvozdev and L. I. Rusinow, Doklady Ak. Nauk. USSR **112** (1957) 401; (Soviet Phys. Doklady **2** (1957) 35)
5) M. Ferentz and N. Rosenzweig, ANL 5324 (1954)
6) A. H. Wapstra, G. J. Nijgh and R. van Lieshout, Nuclear spectroscopy tables (North-Holland Publishing Co., Amsterdam, 1959)
7) S. Raboy and V. E. Krohen, Phys. Rev. **98** (1955) 24
8) F. I. Felber, F. S. Stephens and Frank Asaro, J. Inorg. and Nucl. Chemistry **7** (1958) 153
9) L. A. Sliv and I. M. Band, Tables of internal conversion coefficients (Izd. Akad. Nauk, Leningrad, 1956 and 1958)
10) W. F. Edwards, Thesis, Calif. Inst. Tech. (1960)

3.A:4.E

Nuclear Physics 21 (1960) 133—136; © *North-Holland Publishing Co., Amsterdam*

Not to be reproduced by photoprint or microfilm without written permission from the publisher

NEW NUCLEIDE ACTINIUM-231

K. TAKAHASHI and H. MORINAGA

Department of Physics, University of Tokyo, Bunkyoku, Tokyo, Japan †

Received 18 July 1960

Abstract: A new nucleide actinium-231 was identified from the reaction of $Th^{232}(\gamma, p)Ac^{231}$ induced by the 25-MeV bremsstrahlung. The activity was chemically separated from fission products with the aid of a recoil method. The half-life of this new isotope was found to be $T_{\frac{1}{2}} = 15 \pm 1$ min and the end-point energy of the beta ray was $E_\beta = 2.1 \pm 0.1$ MeV. Several weak gamma rays were also observed.

There has been no report of the nucleide Ac^{231}, which is expected to be a beta-emitter produced from the (γ, p) reaction on Th^{232}. Encouraged by success in identifying Pa^{237} by producing it through the (γ, p) reaction on U^{238} and separating it with the aid of a recoil method [1]), we have further attempted to discover the previously unknown isotope Ac^{231} by a similar method to that employed in the study of Pa^{237}.

The whole procedure of the experiment was quite similar to that used for the identification of Pa^{237}, except that in the present case the chemical separation following the physical separation by recoil was largely dispensed with. From the experience of the protactinium experiment we know that the physical separation achieved by the 1 : 40 ratio of uranium oxide (thorium oxide in this case) to the oxalic powder was practically perfect. Moreover the (γ, p) cross section should be almost the same for U^{238} and for Th^{232} but the photofission cross section decreases substantially from uranium to thorium. The latter fact makes the danger of contamination by fission products in the thorium experiment less.

The actual procedure taken, therefore, was as follows: the powder mixture ($\leqq 8$ μm in grain size) of thorium oxide and oxalic acid in the ratio of 1 : 40 was irradiated in the internal target [2]) of the Tohoku University betatron with the 25-MeV bremsstrahlung, for approximately 20 minutes most of the time. The use of an internal target was convenient since thorium oxide was not chemically treated. In such a case, with external bombardment, the sample to be counted becomes bulky, and thus quite active because of natural activity of thorium.

After the irradiation, the sample was washed with hot water. The oxalic acid powder was dissolved and the fission product activities in the oxalic acid powder

† Work performed at Department of Physics, Tohoku University, Sendai, Japan.

phase were dissolved into the solution along with the oxalic acid. Then the solution was centrifuged; the precipitate was washed two or three times with a dilute solution of oxalic acid. After the filtration the precipitate of thorium oxide on the filter paper was dried. It took about 8 minutes for the treatment.

Other chemical methods and other bombardment schedules, especially short ones for investigating the shorter-life side, were performed, but the

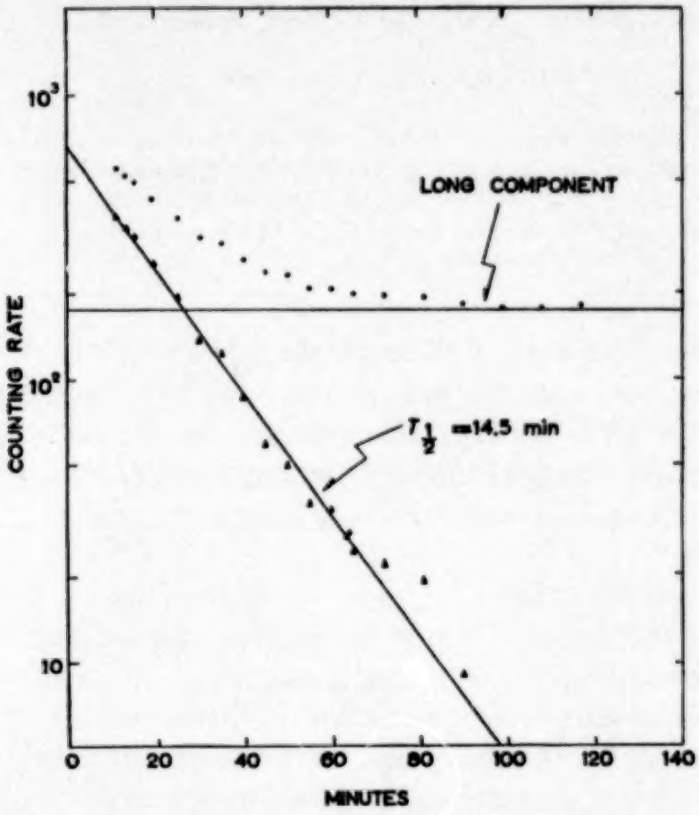

Fig. 1. A typical decay curve of the beta rays higher than 1.5 MeV from the thorium oxide bombarded with the 25-MeV bremsstrahlung.

method described above was found to be the best among those we tried. These include, thorium-nitrate-graphite mixture and their external bombardment followed by specific chemical separation of actinium. They all gave the activity of Ac^{231} which is described below, but with poorer yield or with more contamination of nitrogen or carbon. It would be possible to avoid the latter in the short time available for the chemical treatment but not much effort was made to exploit this method since the mere physical separation proved quite sufficient for our purpose.

The radiations, both gamma and electron, were measured by a scintillation spectrometer with a hundred-channel analyzer, the same one used for the study of Pa^{237}.

The study of beta spectra taken with a plastic phosphor revealed an unknown beta component with a half-life of approximately 15 min and the end-point of

approximately 2 MeV. The latter value is consistent with the expected decay energy of Ac^{231}. The intensity was approximately what is expected from the experiment of Pa^{237}.

Fig. 1 shows the decay curve of the beta components higher than 1.5 MeV. After subtracting the long component, which comes from natural activities of Ac^{228} (or Th^{232}), a 15-min activity is seen. This level discriminates both N^{13} and

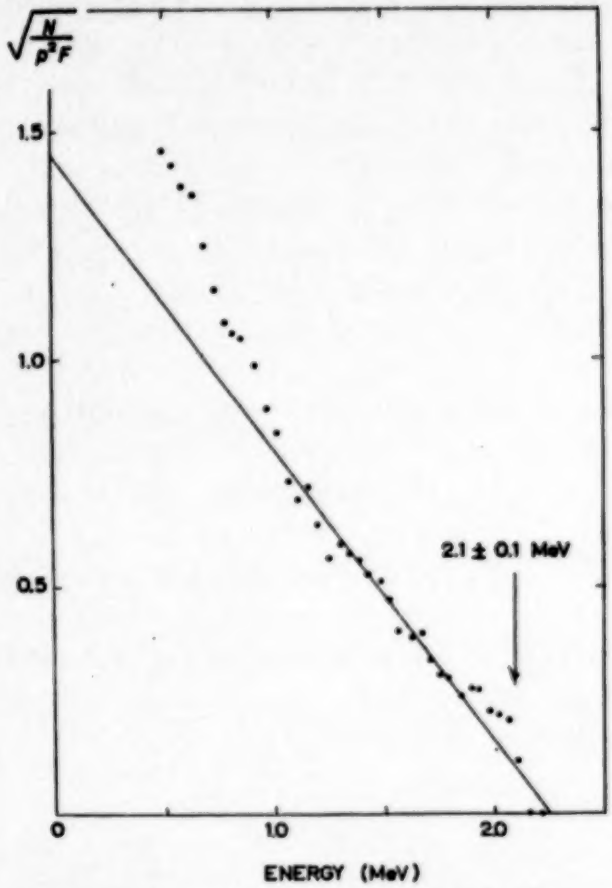

Fig. 2. Kurie plot of the beta ray of Ac^{231}.

C^{11} which could come in. It is not expected that such a single half-life would be observed from a fission fragment. Since the (γ, n) product is the 25-h Th^{231} which has less decay energy, this 15-min component must be assigned to Ac^{231}. Also, as described below, all the radiation characteristics of this 15 min activity are consistent with the assignment of Ac^{231}.

Fig. 2 shows the Kurie plot of this 15-min beta activity. The end-point is determined to be $E_\beta = 2.1 \pm 0.1$ MeV. No correction of the resolution is applied to this plot.

The gamma ray spectrum observed with a 3.8 cm × 3.8 cm NaI(Tl)crystal showed several weak peaks decaying with a half-life of approximately 15 min. Their energies are about 85 keV, 185 keV, 280 keV, 390 keV and 710 keV, respectively. The last three lines are very weak and their existence is not quite

certain. The two lines of 280 keV and 390 keV, however, may correspond to those observed in the alpha decay of U^{235} by Johansson [3]). The 85-keV line is attributed to the KX-ray and the 185-keV line is probably the gamma ray which was observed [3, 4]) in the alpha decay of U^{235}. Most of the beta rays seem to go to the ground state or to very low states, the gamma rays from which are difficult to observe.

The above decay characteristics are quite well explained from the unified model which is found to describe the nuclear decay scheme in this region surprisingly well [5, 6]). The ground state of Th^{231} is most likely to be the $\frac{5}{2}+[633]$ state from the alpha decay of U^{235}. On the other hand the ground state of Ac^{227} is well established to be $\frac{3}{2}+[651]$. Then, one can reasonably expect the ground state of Ac^{231} to be $\frac{3}{2}+[651]$ from the analysis of the Nilsson's diagram. Therefore we can expect an allowed and hindered transition between ground states of Ac^{231} and Th^{231}. The experimental log *ft* value for the beta transition is calculated to be 6.6, which is a very appropriate value for a transition classified as allowed and hindered.

The 185-keV gamma ray is considered to be due to the transition from the 185-keV state to the ground state. From the analysis of the alpha decay of U^{235}, this 185-keV state is expected to be the $\frac{5}{2}-[752]$ intrinsic state. Therefore, a weak beta branching of lower energy feeding this state is expected to exist. Since the transition from $\frac{3}{2}+[651]$ to this state is classified to be first forbidden and unhindered, it is not surprising to expect such a beta branching. It should also be noted that from Nilsson's model no other large beta branching is expected in this decay. These facts completely support the assignment of this newly found activity as nucleide actinium-231.

References

1) K. Takahashi and H. Morinaga, Nuclear Physics **15** (1960) 664
2) H. Morinaga and T. Kuroyanagi, Nuclear Instruments and Methods **6** (1959) 66
3) S. A. E. Johansson, Arkiv Fysik **10** (1956) 97
4) Iu. I. Filimonov and B. V. Pshenichinikov, Soviet Physics JETP **35** (1959) 378
5) F. S. Stephens, F. Asaro and I. Perlman, Phys. Rev. **113** (1959) 212
6) B. R. Mottelson and S. G. Nilsson, Mat. Fys. Skr. Dan. Vid. Selsk. **1**, No. 8 (1959)

8.B

Nuclear Physics **21** (1960) 137—141; © *North-Holland Publishing Co., Amsterdam*

Not to be reproduced by photoprint or microfilm without written permission from the publisher

EFFECTIVE RANGE FOR K^+-NUCLEON INTERACTION FROM DISPERSION RELATIONS

S. N. BISWAS and V. GUPTA

Tata Institute of Fundamental Research, Bombay

Received 8 July 1960

Abstract: An exact formula for the effective range for K^+-P interaction, in the S-wave approximation, has been deduced using dispersion theoretic techniques. It is shown that if the assumption of zero effective range which is generally used for a phenomenological fit of $K-N$ data, is valid then our analysis clearly indicates that the K-meson-hyperon relative parity must be odd (the $\Sigma-\Lambda$ relative parity being even). The contribution of the dispersion integral over the unphysical region has been fully taken into account in the present analysis. A general discussion of the nature of the coupling is given for a non-vanishing but small effective range. The advantage of the use of the effective range formula to determine the sign of the relative parities is also pointed out.

1. Introduction

The experimental data on K-meson-nucleon scattering are quite successfully explained by a phenomenological approach [1]) based on the effective range expansion, with the assumptions that the interaction takes place through S-waves only and further that the range of the interaction is alsmost zero. The isotropic angular distribution of both K^+ and K^- scattering by protons strongly supports the predominance of the S-wave and since the K-meson mass is nearly four times the pion mass it seems reasonable to assume that the range of the K^+-p interaction is zero. The nature of the K-meson coupling to the baryons is not clear though from the phenomenological analysis. In this note the consequences of these assumptions have been explored from the point of view of dispersion theory to predict the parities of the strange particles. To this end we have given a consistent procedure, using dispersion relations, for obtaining the coefficients of powers of k^2 in the effective range expansion of k cot $\delta = -1/a + rk^2 + \ldots$, where δ is the S-wave phase shift and k is the momentum of the K-meson in the centre-of-mass system. In particular, the effective range r has been expressed (cf. sect. 2) in terms of the bound state contributions and dispersion integrals containing experimentally observable cross-sections. The determination of the coefficients of k^4, etc., is of some interest for the nucleon-nucleon singlet scattering [2]).

By making a Taylor's expansion (at an energy ω equal to the K-meson rest mass) of the real part of the forward scattering amplitude, Amati [3]) obtained

the remainder $R(\omega)$ after the first term, which he defined as the 'effective range'. With a definite choice of relative K—Y and Σ—Λ parities in the bound state contributions and estimating the dispersion integrals numerically Amati obtained an upper limit for $R(\omega)$ (at a particular energy) which could be compared with experiment. However, the evaluation of the dispersion integrals presents a little problem because of the presence of an unphysical continuum of the scattering amplitude in the energy region $\frac{1}{2}\mathrm{K} \lesssim \omega < \mathrm{K}$ owing to Σ, Λ production in the K^- absorption processes. In estimating the dispersion integrals Amati assumed a smooth extrapolation of the scattering amplitude into the unphysical region and obtained a negligible contribution to the dispersion integral over the unphysical region. It has been pointed out by Tuan [4]) that this neglect is not quite justified in case of the even K—Y and even Σ—Λ relative parities. In this case quite a large contribution may arise from the cusp-behaviour of the total K^-—p cross-section near the scattering threshold. By making an extrapolation of the experimental curve in the unphysical region and comparing with the perturbation analysis below threshold [4]) one obtains an approximate shape of the curve in the unphysical region. We will take into consideration this contribution from the unphysical region. In case of odd K—Y relative parity, perturbation theory, however, provides simply a smooth extrapolation of the scattering cross-section below threshold. Thus as in earlier works the unphysical region contribution is negligible. The present experimental data on hyperon production due to K^-absorption give roughly the following relative abundances [1]) Σ^-: Σ^+: Σ^0: $\Lambda^0 = 4 : 2 : 2 : \frac{1}{2}$. This indicates relatively small Λ^0-production compared to the Σ-production. Thus in our analysis we will neglect the contribution of Λ^0-production to $\sigma^-_{\mathrm{abs}}(\omega)$ in the dispersion integrals.

In sect. 3 we give a discussion of the effective range formula. We use the units $\hbar = c = 1$ and further use the particle symbol to denote its rest mass.

2. Effective Range Formula

The relativistic dispersion relations [5]) for forward $\mathrm{K}^\pm$—p scattering can be written as

$$D^\pm(\omega) = [\mathrm{B.S.}]^\pm + \frac{P}{\pi}\int \frac{k'\sigma^\pm(\omega')}{\omega'-\omega}\,\mathrm{d}\omega' + \frac{P}{\pi}\int \frac{k'\sigma^\mp(\omega')}{\omega'+\omega}\,\mathrm{d}\omega', \qquad (1)$$

where $D^+(\omega)$ and $D^-(\omega)$ are the real parts of the forward K^+—p and K^-—p scattering amplitudes at energy ω; σ^+ and σ^- are the respective total cross-sections. The lower limit of the integration for σ^+ is K while for σ^- it is $\omega_{\Lambda\pi} = \{(\Lambda+\pi)^2 - \mathrm{N}^2 - \mathrm{K}^2\}/2\mathrm{N}$ owing to the K^--absorption via $\mathrm{K}^- + \mathrm{p} \to \Lambda^0 + \pi^0$. The bound state terms $[\mathrm{B.S.}]^\pm$ depend on the relative N, Σ, Λ and K parities. We tabulate below the eight possible cases.

TABLE 1

The bound state contributions for various relative parities with respect to the nucleons. The relative parity is indicated by the subscript (+ for even and − for odd) on the particle symbol. The superscripts ± in the last column refer to $K^\pm$ scattering by protons.

	Relative parities	$[B.S.]^\pm$
1	$K_+\Sigma_+\Lambda_+$, $K_-\Sigma_-\Lambda_-$	$B_\Lambda^\pm(\omega, 1)+B_\Sigma^\pm(\omega, 1)$
2	$K_-\Sigma_+\Lambda_+$, $K_+\Sigma_-\Lambda_-$	$B_\Lambda^\pm(\omega, \gamma_5)+B_\Sigma^\pm(\omega, \gamma_5)$
3	$K_+\Sigma_-\Lambda_+$, $K_-\Sigma_+\Lambda_-$	$B_\Lambda^\pm(\omega, 1)+B_\Sigma^\pm(\omega, \gamma_5)$
4	$K_-\Sigma_-\Lambda_+$, $K_+\Sigma_+\Lambda_-$	$B_\Lambda^\pm(\omega, \gamma_5)+B_\Sigma^\pm(\omega, 1)$

The $B_Y^\pm$ in table 1 are given by

$$B_Y^\pm(\omega, 1) = g_Y^2 \frac{(Y+N+\omega_Y)}{2Y(\omega\pm\omega_Y)} \tag{2}$$

and

$$B_Y^\pm(\omega, \gamma_5) = -g_Y^2 \frac{(Y-N-\omega_Y)}{2Y(\omega\pm\omega_Y)}, \tag{3}$$

where $\omega_Y = Y^2-N^2-K^2/2N$ and Y is used to denote either Λ or Σ. The 1 and γ_5 refer to the vertex operator occurring in the first Born term needed for the evaluation of B_Y. It should be remarked from table 1 that only four cases are distinguishable. For example, $[B.S.]^\pm$ is the same for all three K, Σ, Λ scalars or pseudoscalars (cf. 1st row, table 1).

We shall only consider K^+-p scattering as the phase shift δ in this case is real. We have at low energy, for small δ and S-wave scattering,

$$D^+(k) = \frac{1}{k\cot\delta},$$

also

$$k\cot\delta = -\frac{1}{a} + \tfrac{1}{2}rk^2 + \ldots,$$

where a (a positive quantity) and r are the scattering length and effective range respectively for the K^+-p interaction. We note here that K^+-p potential is repulsive. We have then from above

$$r = -\frac{1}{K(D^+(K)]^2}\left[\frac{\partial D^+(\omega)}{\partial\omega}\right]_{\omega=K}. \tag{4}$$

By using (1), we obtain from (4)

$$r=-\frac{1}{K[D^+(K)]^2}\left\{\frac{P}{\pi}\int d\omega' k'\left[\frac{\sigma_+}{(\omega'-K)^2}-\frac{\sigma_-}{(\omega'+K)^2}\right]+\left[\frac{\partial}{\partial\omega}[B.S.]^+\right]_{\omega=K}\right\}. \quad (5)$$

The coefficients of higher powers of k^2 may be obtained in an analogous way.

On the basis of the various assumptions already mentioned in the introduction we analyse eq. (5) in the next section to investigate the influence of the cusp-behaviour of the absorption cross section in the unphysical continuum on the effective range and also to point out the possible relative parity assignments consistent with the present experimental data. In this connection it is worth noticing that the present analysis to deduce the sign of the 'strong interaction parity' from the effective range formula (see eq. (5) and note that $D^+(\omega)$'s are connected with the scattering lengths) is independent of the sign of the scattering lengths of the $K^{\pm}$—p scattering. The sign of the parity determined by the subtracted dispersion formula used formerly [6]) strongly depends on the knowledge of the definite sign of the scattering lengths. Hence our analysis based on eq. (5) removes the ambiguity in assigning the sign of the parity caused by the experimental uncertainty in the sign of the scattering lengths.

3. Analysis and Conclusions

From the experimental evidence of the slow variation of $\sigma^+(\omega)$ with energy at low and medium energies and further that $\sigma^-(\omega)$ is considerably larger at low energies, Tuan evaluated the physical integral with a constant value of 48 mb for the difference $\sigma^- - \sigma^+$. However, to take into account properly the near $1/v$-law behaviour of the absorption cross section Amati's approximation has been used here. It is quite interesting to note that the sign of the physical integral is important since purely on the basis of this sign one can rule out some of the parity assignments. In estimating the integrals over the unphysical region we have used Tuan's [4]) extrapolation of the absorption cross section for K^--mesons. A large contribution from the unphysical region arises for the cases given in the first and the fourth rows of table 1. Using the above estimates and the numerical values of the bound state terms from (2) and (3), we obtain from (5)

$$r=-\frac{1}{[D^+(K)]^2K^3}\begin{Bmatrix}-11.6\\0.95\\-11.6\\0.95\end{Bmatrix}\frac{g_\Lambda^2}{4\pi}+\begin{Bmatrix}-10.3\\1.1\\1.1\\-10.3\end{Bmatrix}\frac{g_\Sigma^2}{4\pi}-\begin{Bmatrix}28.4,\\10\ ,\\10\ ,\\28.4,\end{Bmatrix}\begin{matrix}\text{(6a)}\\\text{(6b)}\\\text{(6c)}\\\text{(6d)}\end{matrix}$$

The numbers in the 1st, 2nd row, etc., of the square brackets refer to the four cases listed in the corresponding rows of table 1.

It is clear from (6a) that if the effective range is exactly zero then either one or both of the coupling constants g_Λ and g_Σ are imaginary contrary to what one expects. Thus the parity assignments $K_+\Sigma_+\Lambda_+$ and $K_-\Sigma_-\Lambda_-$ are ruled out. If $r \neq 0$ then again even K—Y relative parity is untenable as the minimum value of rK for extremely weak [KNΛ] and [KNΣ] couplings turns out to be ≈ 37 which is too large compared to a maximum $rK \approx 2$ which one expects if the interaction proceeds via two-pion exchange.

The cases with $\Sigma-\Lambda$ relative parity odd given by (6c) and (6d) could give $r = 0$ and $rK \approx 1$ only if $g_\Sigma^2/g_\Lambda^2 \approx \frac{1}{10}$ or 10 which suggests that one of the couplings [NKΛ] or [NKΣ] is much stronger than the other. But, purely from the hypothesis of charge independence one would expect g_Λ and g_Σ to be nearly equal so as to explain the observed ratio of K^+—n charge exchange to total scattering cross-sections [7]).

Thus the only parity assignments consistent with zero effective range, given by (6b) are $K_-\Sigma_+\Lambda_+$ and $K_+\Sigma_-\Lambda_-$. Assuming $g_\Sigma = g_\Lambda = g$ we can determine the coupling constant from (6b). One finds $g^2/4\pi = 4.9$. For a non-vanishing range of order 1/K we find that $4 \leqq g^2/4\pi \leqq 6$.

Hence we arrive at the conclusion that the analysis of the present experimental data in terms of K—N dispersion relations favours the odd relative K-meson-hyperon parity and even $\Sigma-\Lambda$ relative parity. It should also be pointed out that the use of a smooth extrapolation σ_{abs}^- in the unphysical region instead of Tuan's extrapolation would not affect our conclusions.

References

1) J. D. Jackson, Ravenhall and Wyld, Nuovo Cim. **9** (1958) 834;
R. H. Dalitz and S. F. Tuan, Ann. Phys. **8** (1959) 100
2) J. Shapiro and M. A. Preston, Can. Jour. Phys. **34** (1956) 451
3) D. Amati, Phys. Rev. **113** (1959) 1692
4) S. F. Tuan, Phys. Rev. **113** (1959) 1375
5) P. T. Mathews and A. Salam, Phys. Rev. **110** (1958) 565, 569;
K. Igi, Prog. Theor. Phys. **19** (1958) 238
6) C. Goebel, Phys. Rev. **110** (1958) 572
7) H. Stapp, Phys. Rev. **106** (1957) 135;
L. K. Pandit and S. N. Biswas, Nuclear Physics **12** (1959) 521

1.D.2

Nuclear Physics 21 (1960) 142—156; © *North-Holland Publishing Co., Amsterdam*

Not to be reproduced by photoprint or microfilm without written permission from the publisher

NOTE SUR L'INTERPRÉTATION COLLECTIVE DES DEUX PREMIERS NIVEAUX 2+ DES NOYAUX PAIRS

MAURICE JEAN

Laboratoire de Physique Nucléaire, Faculté des Sciences, BP No 1, Orsay (S. et O.) France †

Reçu le 5 mai 1960

Abstract: It is shown that the qualitative agreement with the experimentally observed ratio of electromagnetic de-excitation probabilities of the first 2+ levels of even nuclei which is exhibited by the theoretical predictions of the Davydov and Filippov asymmetric rotor model, can equally well be obtained for a more conventional model effecting a gradual transition between the quadrupole oscillations of spherical nuclei and the vibrations and rotations of spheroidal ones.

1. Introduction

Davydov et Filippov [1]) ont récemment proposé un modèle remarquablement simple pour décrire systématiquement les bas niveaux excités des noyaux pairs. Ce modèle a fourni pour la première fois la possibilité de confronter les résultats expérimentaux concernant les premiers niveaux excités d'une large classe de noyaux s'étendant des couches magiques aux noyaux déformés avec des prévisions théoriques. Il a par conséquent suscité un vif intérêt chez les spectroscopistes nucléaires, intérêt qui s'est trouvé accru par des succès remarquables [2]) dans l'interprétation des propriétés des niveaux de spin et parité 2+. Le modèle de Davydov et Filippov assimile le noyau à un rotor asymétrique [3]) et peut être considéré comme un cas limite du modèle de Bohr-Mottelson dans lequel le noyau devient infiniment rigide, la déformation étant ainsi caractérisée par les *valeurs fixées* des paramètres β et γ. Les valeurs de γ ne sont pas nécessairement restreintes à 0° ou à un multiple de 60° comme dans le modèle rotationnel à symétrie axiale mais peuvent varier entre les deux limites 0° et 60°. Pour $\gamma = 30°$ le spectre des niveaux excités présente une structure tout à fait différente de celle de la bande rotationnelle familière en $I(I+1)$; il possède alors une certaine similitude avec le spectre vibrationnel des phonons quadrupolaires. Pour $\gamma = 0$ ou $\frac{1}{3}\pi$ on retrouve évidemment le modèle rotationnel usuel. En faisant varier continuement γ entre ces valeurs extrêmes Davydov et Filippov obtiennent une description qui englobe assez bien l'ensemble des spectres observés dans les régions intermédiaires entre le voisinage des couches magiques et les zones de grandes déformations [2]).

† Les résultats de cette étude ont été présentés au Colloque de Physique Nucléaire de la Société Française de Physique (février-mars 1960).

Il semble cependant difficile de comprendre, sauf peut-être dans quelques cas particuliers, pour quelles raisons une aussi large classe de noyaux préfèreraient une déformation asymétrique. Sans vouloir discuter plus avant cette question, qui implique une étude détaillée de l'énergie de déformations des noyaux, nous nous proposons plus simplement, dans cette note, de montrer que l'allure générale des propriétés des deux premiers niveaux 2+ des noyaux pairs peut être également reproduite par un modèle du type que nous appellerons conventionnel parce qu'il assure la transition entre les spectres vibrationnels et les spectres rotationnels usuels en favorisant progressivement une déformation à symétrie axiale. Ce modèle purement phénoménologique n'a cependant pas d'autre ambition que d'avoir la valeur d'un exemple.

2. Formulation Générale

Dans un travail visant à interpréter les propriétés générales des noyaux des régions vibrationnelles de Scharff-Goldhaber et Weneser [4]), Wilets et Jean [5]) ont montré que l'addition à l'hamiltonien libre des phonons quadrupolaires, d'un potentiel „γ instable" permet de lever partiellement la dégénérescence du triplet qui constitue le second niveau des vibrations quadrupolaires purement harmoniques, tout en conservant la règle de sélection interdisant la désexcitation électromagnétique de ce second niveau. Il était toutefois remarqué dans ce même travail que l'introduction d'un potentiel tendant à stabiliser γ autour de $\gamma_0 = 0°$ ou de $60°$ lève complètement la dégénérescence des niveaux dans un ordre convenable pour assurer les transitions vers les spectres rotationnels en même temps qu'elle lève l'interdiction de la transition (E2; $2' \to 0$) †. Ces conclusions s'appuyaient sur un calcul de perturbations portant sur le potentiel „γ stabilisateur". Nous généralisons ici ces considérations en utilisant une méthode échappant aux limitations du calcul des perturbations.

La forme du noyau étant inchangée lorsqu'on effectue la transformation $\gamma \to \gamma + 2\kappa\pi/3$, l'hamiltonien doit être lui-même invariant dans cette transformation, ce qui implique qu'un potentiel „γ stabilisateur" dépendant seulement de la forme du noyau doit être une fonction périodique de 3γ. Si l'on veut progressivement favoriser la symétrie axiale avec la forme allongée le choix le plus simple paraît être un potentiel de la forme

$$V_\gamma = \frac{k'}{\beta^2}(1 - \cos 3\gamma), \tag{1}$$

où k' est un paramètre arbitraire positif. Ce potentiel présente un minimum prononcé pour $\gamma = 0$ ou $2\kappa\pi/3$ et tend donc bien à stabiliser le noyau dans le sens désiré. Cependant sa dépendance en β, qui est choisie de façon à assurer la séparabilité des équations, peut paraître peu réaliste puisqu'on s'attend à ce

† Nous désignerons, comme l'usage s'en est répandu, par 2^+ et $2'$ les deux premiers niveaux $2+$.

que la stabilité de forme s'accroisse avec la déformation. En réalité lorsqu'on considère l'énergie potentielle dans son ensemble,

$$V(\beta, \gamma) = \tfrac{1}{2}C\beta^2 + \frac{k'}{\beta^2}(1-\cos 3\gamma), \tag{2}$$

on observe que la valeur d'équilibre β_0 de β est elle-même fixée par la valeur de k' de telle sorte que finalement la stabilisation de forme augmente bien avec la déformation β_0, quoique trop lentement pour que le modèle soit suffisamment réaliste. Nous reviendrons sur cette question ultérieurement et nous nous contenterons d'utiliser le potentiel défini par (2).

L'hamiltonien du modèle ainsi proposé est donc de la forme

$$H = T_\beta + T_\gamma + T_{\text{rot}} + V(\beta, \gamma), \tag{3}$$

avec

$$T_\beta = -\frac{\hbar^2}{2B}\frac{1}{\beta^4}\frac{\partial}{\partial\beta}\beta^4\frac{\partial}{\partial\beta}, \tag{4a}$$

$$T_\gamma = -\frac{\hbar^2}{2B\beta^2}\frac{1}{\sin 3\gamma}\frac{\partial}{\partial\gamma}\sin 3\gamma\frac{\partial}{\partial\gamma}, \tag{4b}$$

$$T_{\text{rot}} = \frac{\hbar^2}{8B\beta^2}\sum_{\kappa=1}^{3}\frac{Q_\kappa^2}{\sin^2\left(\gamma - 2\kappa\frac{\pi}{3}\right)}, \tag{4c}$$

où les Q_κ sont les opérateurs du moment angulaire. Nous utiliserons les variables réduites

$$r = \beta\sqrt{\frac{B\omega}{\hbar}} \quad \text{et} \quad \varepsilon = \frac{E}{\hbar\omega}, \tag{5}$$

où E est l'énergie et $\omega = (C/B)^{\frac{1}{2}}$ est la fréquence classique associée aux phonons non couplés. Nous poserons par ailleurs

$$L_k = -\frac{1}{\sin 3\gamma}\frac{\partial}{\partial\gamma}\sin 3\gamma\frac{\partial}{\partial\gamma} + \tfrac{1}{4}\sum_{\kappa=1}^{3}\frac{Q_\kappa^2}{\sin^2\left(\gamma - 2\kappa\frac{\pi}{3}\right)} + k(1-\cos 3\gamma), \tag{6}$$

où $k = 2Bk'/\hbar^2$. L'équation de Schrödinger

$$\{T + V(r, \gamma)\}\Psi(r, \gamma, \theta_i) = E\Psi(r, \gamma, \theta_i) \tag{7}$$

devient séparable lorsqu'on fait choix du potentiel (2). En effet, si l'on pose

$$\Psi(r, \gamma, \theta_i) = \frac{\varphi(r)}{r^2}\Phi(\gamma, \theta_i), \tag{8}$$

on a les équations

$$\varepsilon\varphi(r) = \tfrac{1}{2}\left[-\frac{\mathrm{d}^2}{\mathrm{d}r^2} + \frac{\Lambda_k+2}{r^2} + r^2\right]\varphi(r) \tag{9}$$

et

$$\Lambda_k \Phi(\gamma, \theta_i) = L_k \Phi(\gamma, \theta_i). \tag{10}$$

Les propriétés d'invariance [6]) de l'hamiltonien permettent d'écrire les fonctions $\Phi(\gamma, \theta_i)$ sous la forme

$$\Phi^{IM\Lambda_k}(\gamma, \theta_i) = \sum_K g_K^{I\Lambda_k}(\gamma)\mathscr{D}^I_{MK}(\theta_i), \tag{11}$$

où les $\mathscr{D}^I_{MK}$ sont les fonctions de transformation pour les harmoniques sphériques d'ordre I et les fonctions $g_K^{I\Lambda_k}(\gamma)$ sont telles que seules les valeurs paires de K interviennent et que

$$g_K{}^I(\gamma) = (-)^1 g^I_{-K}(\gamma).$$

En introduisant (11) dans (10) cette dernière équation conduit à un système d'équations différentielles couplées pour les fonctions $g_K{}^I$:

$$\left\{\Lambda_k - \mathscr{H}_\gamma - \frac{\sin^2\gamma + 3\cos^2\gamma}{(\sin^2\gamma - 3\cos^2\gamma)^2}[I(I+1)-K^2] - \frac{K^2}{4\sin^2\gamma}\right\} g_K^{I\Lambda_k}(\gamma)$$

$$= \frac{-\sqrt{3}\sin\gamma\cos\gamma}{(\sin^2\gamma - 3\cos^2\gamma)^2}\{\sqrt{(I+K)(I+K-1)(I-K+1)(I-K+2)}\, g^{I\Lambda_k}_{K-2}(\gamma)$$

$$+\sqrt{(I-K)(I-K-1)(I+K+1)(I+K+2)}\, g^{I\Lambda_k}_{K-2}(\gamma)\}, \tag{12}$$

avec

$$\mathscr{H}_\gamma = -\frac{1}{\sin 3\gamma}\frac{\mathrm{d}}{\mathrm{d}\gamma}\sin 3\gamma\frac{\mathrm{d}}{\mathrm{d}\gamma} + k(1-\cos 3\gamma). \tag{13}$$

Ce système se simplifie considérablement si, suivant Bès [7]), on effectue le changement de variable $z = \cos 3\gamma$ et des changements de fonction qui dans le cas des moments angulaires $I = 0$ et $I = 2$ se réduisent à

$$g_0^{0\Lambda_k}(\gamma) = U(z) \quad (I = 0) \tag{14}$$

et

$$\left.\begin{aligned} g_0^{2\Lambda_k}(\gamma) &= w(z)\cos\gamma + v(z)\cos 2\gamma \\ g_2^{2\Lambda_k}(\gamma) &= g_{-2}^{2\Lambda_k}(\gamma) = \frac{1}{\sqrt{2}}(w(z)\sin\gamma - v(z)\sin 2\gamma) \end{aligned}\right\} \quad (I = 2). \tag{15}$$

Dans le cas $I = 0$ l'équation unique qui détermine la seule fonction g s'écrit alors

$$\left[9(1-z^2)\frac{\mathrm{d}^2}{\mathrm{d}z^2} - 18z\frac{\mathrm{d}}{\mathrm{d}z} + kz + (\Lambda_k - k)\right] U(z) = 0. \tag{16}$$

Pour $I = 2$ on a les deux équations couplées

$$\left[9(1-z^2)\frac{d^2}{dz^2} - 24z\frac{d}{dz} + kz + (\Lambda_k - k - 4)\right] w + 12\frac{dv}{dz} = 0,$$
$$\left[9(1-z^2)\frac{d^2}{dz^2} - 30z\frac{d}{dz} + kz + (\Lambda_k - k - 10)\right] v + 6\frac{dw}{dz} = 0. \tag{17}$$

Ces équations aux valeurs propres ne diffèrent évidemment de celles de Bès que par les termes en k. Il ne semble cependant pas que leurs solutions exactes puissent s'obtenir facilement. Dans ce qui suit nous utilisons des solutions approchées obtenues par une méthode variationnelle.

3. Discussion des Solutions pour les Cas Extrêmes $k \to 0$ et $k \to \infty$

Des solutions approchées des équations (16) et (17) s'obtiennent aisément dans les deux cas limites où le paramètre k caractérisant la stabilisation de forme est soit petit ($k \to 0$) soit grand ($k \to \infty$). Nous discuterons rapidement les résultats d'une étude de ces deux cas limites car ce sont eux qui nous ont servi de guide pour faire choix des fonctions d'essai que nous avonsfinalement utilisées.

Pour $I = 0$ l'équation (16) se réduit, si $k = 0$, à l'équation caractéristique des polynomes de Legendre. Lorsque k est suffisamment petit, le traitement comme perturbation du terme en kz consiste à développer la fonction U pour l'état fondamental suivant les polynomes de Legendre. On trouve alors à l'ordre le plus bas (non banal) des perturbations

$$\Lambda^{I=0}_{k\to 0} = k - \frac{k^2}{54}, \quad U \approx 1 + \frac{k}{18}z. \tag{18}$$

D'autre part, dans l'autre cas extrême $k \to \infty$, c'est à dire lorsque la stabilisation de forme est très grande, le changement de variable

$$z = 1 - \sqrt{\frac{9}{2k}}\xi^2 \tag{19}$$

permet de séparer dans l'équation (16) des termes d'ordre zéro et des termes du premier ordre en $k^{-\frac{1}{2}}$. A l'ordre zéro l'équation se réduit à celle d'un oscillateur isotrope à deux dimensions et l'on trouve

$$\Lambda^{I=0}_{k\to\infty} = (2n+1)\sqrt{18k}, \quad U \approx e^{-\frac{1}{2}\xi^2} L_n(\xi^2), \quad (n = 0, 1, 2, \ldots), \tag{20}$$

où L_n est le $n^{\text{ième}}$ polynome de Laguerre. Les termes du premier ordre se traitent aisément par perturbation et l'on trouve pour l'état fondamental

$$\Lambda^{I=0}_{k\to\infty} = \sqrt{18k} - \tfrac{9}{2}, \quad U \approx e^{-\frac{1}{2}\xi^2}. \tag{21}$$

Pour $I = 2$ le traitement se complique un peu. Pour $k = 0$, les solutions ont été données par Bès. Les deux premiers niveaux 2 correspondent à

$$\Lambda_{k=0}^{I=2} = 4, \quad w = 1, \quad v = 0, \tag{22a}$$

$$\Lambda_{k=0}^{I=2'} = 10, \quad w = 0, \quad v = 1. \tag{22b}$$

Lorsque k est différent de zéro, mais petit, ces deux états se superposent linéairement entre eux et avec les autres niveaux de spin 2. Si l'on considère maintenant le cas opposé $k \to \infty$ on vérifie que le changement de variable (19) permet également de séparer dans les équations (17) des termes d'ordre zéro et du premier ordre par rapport à $k^{-\frac{1}{4}}$. Lorsqu'on résout les équations couplées obtenues en négligeant les termes du premier ordre on obtient deux classes de solutions

$$\Lambda_{k\to\infty}^{I=2} = (2n+1)\sqrt{18k}, \quad w = 2v = U_n^{\,0} \approx e^{-\frac{1}{2}\xi^2} L_n^{(0)}(\xi^2), \quad (n = 0, 1, 2, \ldots), \tag{23a}$$

$$\Lambda_{k\to\infty}^{I=2'} = (2n+2)\sqrt{18k}, \quad w = -v = U_n^{\,1} \approx e^{-\frac{1}{2}\xi^2} L_n^{(1)}(\xi^2), \quad (n = 0, 1, 2, \ldots), \tag{23b}$$

où $L_n^{(\alpha)}$ est le polynome associé de Laguerre. Il est encore intéressant de traiter les termes du premier ordre par la méthode de perturbation. On trouve, à l'ordre le plus bas des perturbations, pour le premier niveau $I = 2$

$$\Lambda_{k\to\infty}^{I=2} = \sqrt{18k} - \tfrac{5}{2}. \tag{24}$$

On constate qu'à l'ordre zéro, l'énergie du premier niveau $2+$ coïncide avec celle du niveau fondamental. Une différence n'apparaît qu'à l'ordre suivant et l'on a

$$\Lambda_{k\to\infty}^{I=2} - \Lambda_{k\to\infty}^{I=0} = 2. \tag{25}$$

En remontant à l'équation (9) on voit que si la déformation se trouve stabilisée à une valeur $\beta = \beta_0$ l'énergie correspondant à (25) a pour valeur $E = \hbar^2/B\beta_0^2$, c'est à dire l'énergie de rotation qu'on attend de la relation $E = I(I+1)\hbar^2/6B\beta_0^2$ qui résulte du traitement plus conventionnel de Bohr et Mottelson [6]).

4. Utilisation de la Méthode Variationnelle

De façon à pouvoir interpoler entre les deux cas extrêmes que nous venons d'examiner nous avons utilisé les fonctions d'essai qui nous ont paru les plus simples mais suffisamment flexibles pour reproduire les deux limites $k \to 0$ et $k \to \infty$.

Dans le cas $I = 0$ la fonction choisie pour décrire *l'état fondamental* est de la forme

$$U = N_0^{-\frac{1}{2}} e^{\alpha z}, \tag{26}$$

où N_0 est le facteur de normalisation et α le paramètre à varier. La comparaison

avec (18), (19) et (20) (pour $n = 0$) montre que cette fonction est capable de reproduire les deux limites. En utilisant (10)—(14) on obtient comme équation pour déterminer α

$$\frac{\mathrm{d}\Lambda_k^{I=0}(\alpha)}{\mathrm{d}\alpha} = 0 \quad \text{avec} \quad \Lambda_k^{I=0}(\alpha) = 2\int_{-1}^{+1} \mathrm{d}z U L_z U, \tag{27}$$

où

$$L_z = -9(1-z^2)\frac{\mathrm{d}^2}{\mathrm{d}z^2} + 18z\frac{\mathrm{d}}{\mathrm{d}z} + k(1-z) \equiv \mathscr{L}_z^0 + k(1-z).$$

Avec (26) on a

$$N_0 = \frac{2}{\alpha}\,\mathrm{sh}\,2\alpha, \tag{28a}$$

$$\Lambda_k^{I=0}(\alpha) = (9\alpha - k)\left(\frac{1}{\mathrm{th}\,2\alpha} - \frac{1}{2\alpha}\right) + k. \tag{28b}$$

Il est finalement plus commode de considérer k comme déterminé en fonction de α par l'intermédiaire de (27), qui donne

$$k = 9\alpha^2 \frac{\mathrm{sh}\,4\alpha - 4\alpha}{(\mathrm{sh}\,2\alpha)^2 - 4\alpha^2}. \tag{29}$$

Il est aisé de retrouver les deux résultats (18) et (21) correspondant respectivement à $k \to 0$ et $k \to \infty$.

Pour $I = 2$ nous avons choisi de décrire les deux états qui nous intéressent par les fonctions

$$w = N_2^{-\frac{1}{2}} \mathrm{e}^{\alpha z}, \quad v = N_2^{-\frac{1}{2}} \beta \mathrm{e}^{\alpha z}. \tag{30}$$

Les cas extrêmes qui nous servent de critère sont bien reproduits par ce choix puisque les limites $\alpha \to 0$ et $\beta \to 0$ ou $\alpha \to 0$ et $\beta \to \infty$ redonnent (22a) ou (22b) alors que $\alpha \approx k^{\frac{1}{2}}$, $\beta = \frac{1}{2}$ ou $\alpha \approx k^{\frac{1}{2}}$, $\beta = -1$ redonnent bien (23a) ou (23b) avec $n = 0$. La variation par rapport au paramètre β fournit deux solutions que nous pouvons associer à chacun des deux états $2+$ qui nous intéressent. Des difficultés peuvent être liées à la non-orthogonalité des états ainsi obtenus. Nous avons cependant, dans ce qui suit, négligé de les orthogonaliser, un calcul explicite de leur intégrale de recouvrement ayant révélé qu'au degré de précision souhaité les états correspondants à (30) peuvent être considérés comme orthogonaux.

La norme est donnée par la condition

$$1 = 2\int_{-1}^{+1} (w^2 + 2wvz + v^2)\mathrm{d}z \tag{31}$$

et la quantité à varier est

$$\Lambda_k^{I=2}-k = 2\int_{-1}^{+1} dz \left\{(w+vz)\mathscr{L}_s{}^0 w+(v+wz)\mathscr{L}_s{}^0 v-6v(1-z^2)\frac{dw}{dz}\right.$$
$$\left.-12w(1-z^2)\frac{dv}{dz}+4w^2+10v^2+14wvz-kz(w^2+2wvz+v^2)\right\},$$

ce qui donne en utilisant (30)

$$N_2 = \frac{2}{\alpha}\left\{\left(1+\beta^2-\frac{\beta}{\alpha}\right)\mathrm{sh}\ 2\alpha+2\beta\ \mathrm{ch}\ 2\alpha\right\}, \tag{33a}$$

$$\Lambda_k^{I=2}(\alpha,\beta)-k = \frac{A\beta^2+B\beta+C}{A'\beta^2+B'\beta+C'}, \tag{33b}$$

avec

$$A = \left(\frac{11}{2}+\frac{k}{2\alpha}\right)\mathrm{th}\ 2\alpha+(9\alpha-k), \quad B = \left(18\alpha-2k-\frac{k}{\alpha^2}+\frac{13}{2\alpha}\right)\mathrm{th}\ 2\alpha+\frac{2k}{\alpha}-13,$$

$$C = \left(-\frac{1}{2}+\frac{k}{2\alpha}\right)\mathrm{th}\ 2\alpha+(9\alpha-k), \quad A' = C' = \mathrm{th}\ 2\alpha, \quad B' = \left(2-\frac{\mathrm{th}\ 2\alpha}{\alpha}\right)$$

Les équations fixant α et β pour k donné sont alors

$$\frac{\partial \Lambda_k^{I=2}(\alpha,\beta)}{\partial\alpha} = \frac{\partial \Lambda_k^{I=2}(\alpha,\beta)}{\partial\beta} = 0.$$

La dernière détermine β en fonction de α par une équation quadratique

$$(AB'-A'B)\beta^2+2(AC'-A'C)\beta+(BC'-B'C) = 0. \tag{34}$$

Nous avons admis par la suite que la valeur de α n'est pas sensiblement différente de celle obtenue facilement dans l'étude de l'état fondamental. Cette approximation se trouve bien vérifée dans la limite $k \to \infty$. Elle l'est moins bien dans les cas opposés ($k \to 0$) puisqu'on trouve alors $\alpha_{k\to 0}(I=0) = \frac{1}{18}k$, $\alpha_{k\to 0}(I=2) = \frac{1}{24}k$ et $\alpha_{k\to 0}(I=2') = \frac{1}{30}k$ au premier ordre en k. Nous ne pensons pas cependant que cette approximation introduise une trop grande erreur (Voir figure 2).

Du point de vue pratique, la relation (29) permet d'établir une correspondance biunivoque entre k et α de telle sorte que nous pourrons utiliser indifféremment l'un ou l'autre paramètre. L'expression (28) permet de calculer $\Lambda^{I=0}$ pour toute une série de valeurs de α. De même la relation (34) fournit pour chaque valeur de α deux solutions β et β' qui sont associées aux deux états $2+$ qui nous intéressent. On obtient alors $\Lambda_k^{I=2}$ et $\Lambda_k^{I=2'}$ à l'aide de (33). Les fonctions d'ondes et les valeurs propres Λ se trouvent ainsi déterminées approximativement.

Il reste finalement à déterminer les fonctions radiales et simultanément les niveaux d'énergie par la résolution de l'équation (9). Posant

$$\varphi(r) = r^{\lambda} e^{-\frac{1}{2}r^2} \psi(r), \tag{35}$$

l'équation (9) se réduit à

$$\left\{\frac{d^2}{dr^2} + 2\left(\frac{\lambda}{r} - r\right)\frac{d}{dr} + 2(\varepsilon - \lambda - \tfrac{3}{2})\right\}\psi(r) = 0, \tag{36}$$

si

$$\lambda = \tfrac{1}{2}(1 + \sqrt{4\Lambda + 9}). \tag{37}$$

Le changement de variable $x = r^2$ conduit à l'équation

$$\left\{x\frac{d^2}{dx^2} + (\lambda + \tfrac{1}{2} - x)\frac{d}{dx} + \tfrac{1}{2}(\varepsilon - \lambda - \tfrac{1}{2})\right\}\psi(x) = 0, \tag{38}$$

dont les solutions propres sont données par la série hypergéométrique

$$\psi(x) = {}_1F_1(-\nu; \lambda + \tfrac{1}{2}; x) \quad (\nu = 0, 1, 2 \ldots), \tag{39}$$

avec

$$\varepsilon = 2\nu + \lambda + \tfrac{1}{2} = 2\nu + 1 + \tfrac{1}{2}\sqrt{4\Lambda + 9}. \tag{40}$$

Nous sommes essentiellement intéressés par les bas niveaux, c'est à dire par l'état fondamental des vibrations β nous n'utiliserons donc (40) que pour $\nu = 0$. Les fonctions d'ondes correspondantes sont alors simplement

$$\varphi(r) \propto r^{\lambda} e^{-\frac{1}{2}r^2}. \tag{41}$$

Les résultats numériques en ce qui concerne les niveaux d'énergie ont été condensés dans le rapport

$$X = \frac{\varepsilon_{2'} - \varepsilon_0}{\varepsilon_2 - \varepsilon_0}, \tag{42}$$

TABLEAU 1

Résultats numériques

α	0	0.1	0.3	0.5	0.7	1	1.5	2	3	4
k	0	1.944	5.534	9.608	14.27	22.90	43.38	73.20	162.1	288.8
$X = \frac{\varepsilon_{2'} - \varepsilon_0}{\varepsilon_2 - \varepsilon_0}$	0	2.14	2.49	3.04	3.81	5.21	8.31	11.74	18.9	26.5
$r_0 = \frac{B(E2; 2' \to 0)}{B(E2; 2' \to 2)}$	0	0.00245	0.0236	0.064	0.117	0.196	0.320	0.393	0.488	0.542
$r_1 = \frac{B(E2; 2' \to 2)}{B(E2; 2 \to 0)}$	2	1.76	1.28	0.865	0.605	0.345	0.188	0.118	0.066	0.0445

où ε_2 et ε_3 sont les énergies des deux niveaux 2+ et ε_0 l'énergie du fondamental. La variation de ce rapport en fonction de α est donnée figure 1 alors que la connection entre α et le paramètre de stabilisation de forme k est représentée figure 2 et tableau 1.

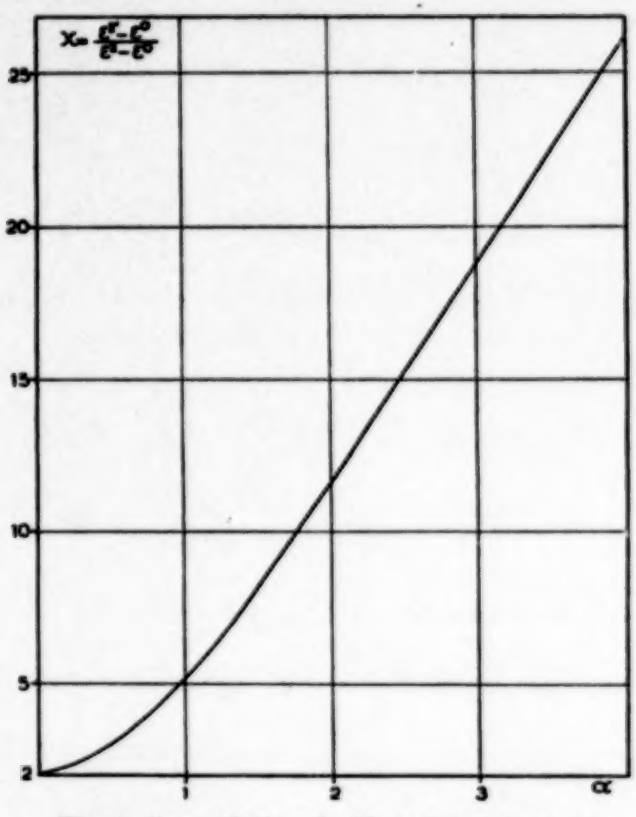

Fig. 1. La variation de X en fonction de α.

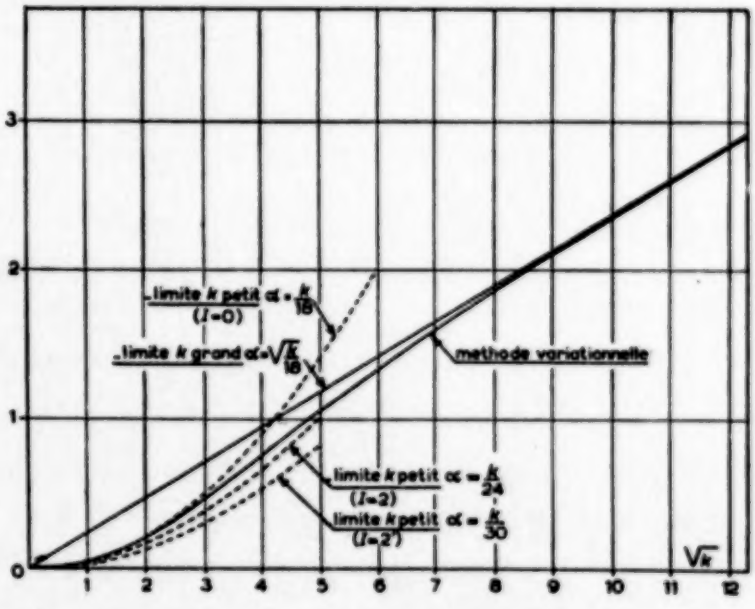

Fig. 2. La connection entre α et k.

5. Les Probabilités de Transition

Du point de vue de la comparaison avec l'expérience ce sont les probabilités de désexcitation par rayonnement électromagnétique E2 qui nous intéressent au premier chef. Les quantités importantes sont les probabilités de transitions réduites

$$B(\mathrm{E2};\, \mathrm{i} \to \mathrm{f}) = \sum_{\mu M_\tau} |\langle \mathrm{i}|\mathscr{M}_e(2;\mu)|\mathrm{f}\rangle|^2, \tag{43}$$

où

$$\mathscr{M}_e(2;\mu) = \frac{3}{4\pi} ZeR_0^2\beta\left\{\mathscr{D}^{2*}_{\mu 0}\cos\gamma + (\mathscr{D}^{2*}_{\mu 2}+\mathscr{D}^{2}_{\mu -2})\frac{\sin\gamma}{\sqrt{2}}\right\}.$$

Introduisant successivement (5), (8), (11) puis (14) et (15) on obtient pour la transition d'un des niveaux 2+ vers le fondamental

$$B(\mathrm{E2};\, 2\Lambda^2\tau^2 \to 0\Lambda^0\tau^0) = \left(\frac{3}{4\pi} ZeR_0^2\right)\frac{\hbar}{B\omega}|\langle\tau^2|r|\tau^0\rangle|^2\tfrac{1}{5}\mathscr{A}^2, \tag{45}$$

avec

$$\mathscr{A} = 2\int_{-1}^{+1}(w+vz)U\,dz, \tag{46}$$

où $\langle\tau^2|r|\tau^0\rangle$ est l'élément de matrice radial

$$\langle\tau^2|r|\tau^0\rangle = \int_0^\infty \varphi^{\tau^2}(r)\,r\,\varphi^{\tau^0}\,dr. \tag{47}$$

Les nombres quantiques caractérisant les fonctions radiales étant désignés par τ.

De même, pour les transitions entre les deux niveaux 2+ on obtient

$$B(\mathrm{E2};\, 2'\Lambda'\tau' \to 2\Lambda\tau) = \left(\frac{3}{4\pi} ZeR_0^2\right)\frac{\hbar}{B\omega}|\langle\tau'|r|\tau\rangle|^2\tfrac{2}{7}\mathscr{B}^2, \tag{48}$$

avec

$$\mathscr{B} = 2\int_{-1}^{+1}\{(w'w+v'v)z+(w'v+v'w)\}\,dz, \tag{49}$$

où les fonctions w' et v sont celles correspondant au niveau 2'.

Nous sommes davantage intéressés par des rapports d'intensité que par les valeurs absolues; aussi nous calculerons le rapport

$$r_1 = \frac{B(E2;\, 2'\Lambda^{2'}\tau^{2'} \to 2\Lambda^2\tau^2)}{B(\mathrm{E2};\, 2\Lambda^2\tau^2 \to 0\Lambda^0\tau^0)} = \frac{10}{7}\frac{|\langle\tau^{2'}|r|\tau^2\rangle|^2}{|\langle\tau^2|r|\tau^0\rangle|^2}\left(\frac{\mathscr{B}}{\mathscr{A}}\right)^2 \tag{50}$$

des probabilités réduites des deux rayonnement E2 en cascade. De même nous évaluerons le rapport d'embranchement

$$r_2 = \frac{B(\mathrm{E2};\, 2'\Lambda^{2'}\tau^{2'} \to 0\Lambda^0\tau^0)}{B(\mathrm{E2};\, 2'\Lambda^{2'}\tau^{2'} \to 2\Lambda^2\tau^2)} = \frac{7}{10}\frac{|\langle\tau^{2'}|r|\tau^0\rangle|^2}{|\langle\tau^{2'}|r|\tau^2\rangle|^2}\left(\frac{\mathscr{A}'}{\mathscr{B}}\right)^2, \tag{51}$$

où $\mathscr{A}'$ est identique à (46) mais exprimé avec les fonctions d'ondes du niveau 2'. En introduisant (26) et (30) on trouve

$$\mathscr{A} = \frac{1}{\alpha(N_0 N_2)^{\frac{1}{2}}} \left\{ \left(1 - \frac{\beta}{2\alpha}\right) \operatorname{sh} 2\alpha + \beta \operatorname{ch} 2\alpha \right\}, \tag{52}$$

où N_0 et N_2 sont donnés respectivement par (28a) et (33a). Le coefficient $\mathscr{A}'$ est donné par une expression identique à (52) mais où β est remplacé par β' et N_2 par $N_{2'}$, obtenu également à l'aide de (33a) par le même remplacement de β par β'. On a de même

$$\mathscr{B} = \frac{1}{\alpha(N_2 N_{2'})^{\frac{1}{2}}} \left\{ \left[(\beta + \beta') - \frac{1 + \beta\beta'}{2\alpha} \right] \operatorname{sh} 2\alpha + (1 + \beta\beta') \operatorname{ch} 2\alpha \right\}. \tag{53}$$

Quant aux éléments de matrices radiaux, ils se calculent analytiquement lorsqu'on tient compte de la forme (41) des fonctions radiales. Ils s'expriment alors à l'aide de la fonction gamma. L'équation (39) nous montre que τ désigne en fait les nombres quantiques ν et λ qui caractérisent complètement la fonction radiale $\varphi(r)$. Comme nous nous sommes limités aux états pour lesquels $\nu = 0$ on a seulement à calculer des éléments de matrice de la forme $\langle \nu = 0, \lambda_1 | r | \nu = 0, \lambda_t \rangle$. On trouve

$$\langle 0\lambda_1 | r | 0\lambda_t \rangle = \frac{\Gamma(\frac{1}{2}\lambda_1 + \frac{1}{2}\lambda_t + 1)}{\sqrt{\Gamma(\lambda_1 + \frac{1}{2})\Gamma(\lambda_t + \frac{1}{2})}}. \tag{54}$$

Les paramètres β et β' ayant été déduits en fonction de α à partir de (34), $\mathscr{A}$, $\mathscr{A}'$ et $\mathscr{B}$ ont été calculés à l'aide de (28a), (33a), (52) et (53). D'autre part,

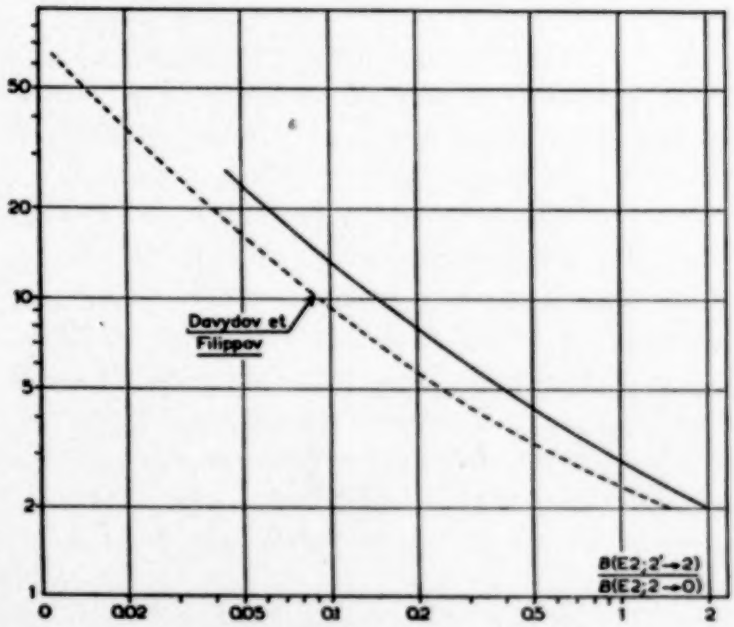

Fig. 3. Résultats numériques pour r_1.

λ est calculé pour chaque valeur de α à partir de (77) par l'intermédiaire de Λ donné soit par (28b), soit par (33b). Les valeurs des éléments de matrice $\langle\tau^1|r|\tau^1\rangle$ se calculent alors avec (54) et l'on peut établir la variation des rapports r_1 et r_2 en fonction de α, c'est à dire finalement en fonction de X. Les résultats numériques sont présentés dans les figures 3 et 4 et le tableau 1.

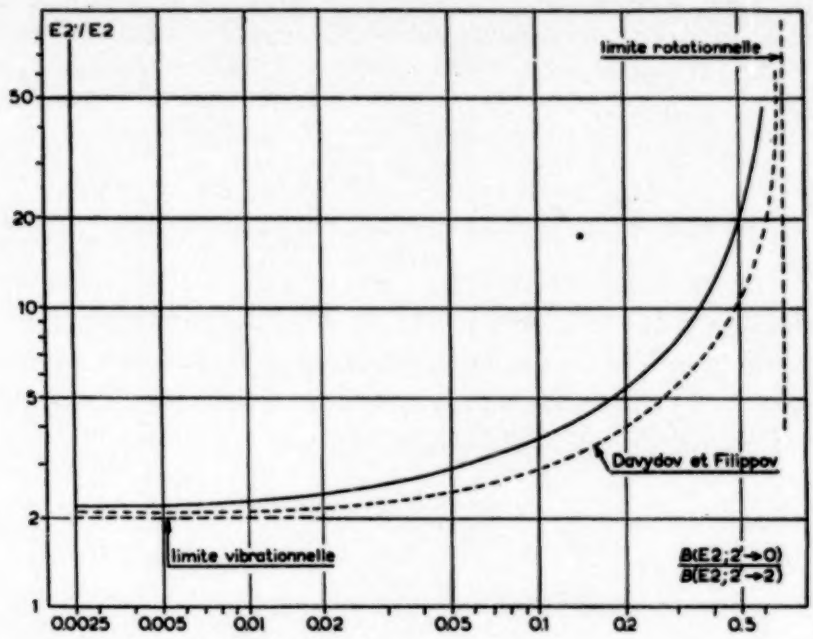

Fig. 4. Résultats numériques pour r_2.

6. Discussion des Résultats et Conclusion

Du point de vue de la confrontation avec l'expérience ce sont les courbes des figures 3 et 4 qui sont intéressantes. Pour faciliter la comparaison avec les données empiriques nous avons reproduit sur ces figures les courbes correspondant aux rapports r_1 et r_2 qui résultent de la théorie de Davydov et Filippov et qui, comme le montrent les figures 1 et 4 de l'article de Van Patter[2]), résument assez bien l'allure générale de la systématique. Nous pouvons conclure que la théorie développée dans cette note permet également de rendre compte de cette allure générale en assurant une transition progressive entre la zone vibrationnelle et la zone rotationnelle à symétrie axiale. Nous devons toutefois admettre que les courbes de Davydov et Filippov fournissent une meilleure interpolation entre les points empiriques. Cependant le traitement utilisé dans ce travail n'est qu'approximatif et la méthode variationnelle se prête difficilement à une estimation des erreurs commises. Il n'est pas impossible qu'un traitement rigoureux, par exemple une résolution exacte analytique ou numérique des équations (16) et (17) améliore la situation. Le modèle est cependant certainement trop simple car il n'est pas évident que la stabilisation de forme et

la déformation puissent être assurées simultanément par un seul paramètre k. On peut penser à adjoindre à l'énergie potentielle (2) un terme γ instable du type $k''\beta$. Les équations restent encore séparables au sens de (8). Les considérations développées précédemment en ce qui concerne la fonction $\Phi(\gamma, \theta_i)$ sont encore valables et seule l'équation (9) est modifiée par la présence d'un terme proportionnel à $(r-r_1)^2$. Une solution approchée de cette équation radiale peut encore être obtenue par la méthode de Wilets et Jean [5]). Les probabilités de transition ne sont pas considérablement modifiées, mais les positions des niveaux d'énergies peuvent être considérablement perturbées. En particulier l'énergie du niveau 2' ne croît plus nécessairement indéfiniment lorsque l'on tend vers la limite rotationnelle, comme c'est le cas en l'absence du terme γ instable et dans le modèle de Davydov et Filippov. Il est possible d'imposer une relation entre k et k'' de façon à ce que $\varepsilon_{2'}-\varepsilon_0$ atteigne une limite finie correspondant aux niveaux de vibration γ des noyaux rotationnels. Le modèle reste néanmoins encore éloigné de la réalité par le fait même qu'il est construit à partir du modèle hydrodynamique de Bohr et Mottelson; les moments d'inertie sont donc du type irrotationnel lorsqu'on atteint la limite de complète stabilisation de forme.

Malgré les inconvénients que nous venons d'énumérer il nous semble intéressant d'avoir attiré l'attention sur la possibilité de rendre compte des tendances générales de la systématique des excitations 2+ des noyaux pairs dans le cadre d'une théorie assurant une certaine continuité entre les vibrations quadrupolaires des noyaux sphériques et les noyaux rotationnels †. La théorie de Davydov et Filippov n'est pas à l'abri des difficultés examinées rapidement plus haut et certaines de ses prédictions dont on pourrait penser faire un test sont également reproduites par le modèle proposé dans cette note. Il en est ainsi, en particulier, de l'égalité de la somme des énergies des deux premiers niveaux 2+ et de l'énergie du premier niveau 3+. On le vérifie aisément †† dans les deux limites $k \to 0$ et $k \to \infty$, et une estimation basée sur la méthode variationnelle décrite au paragraphe 4 conduit à penser qu'il en est bien ainsi dans les régions intermédiaires. Le modèle incluant des oscillations de forme du noyau est certainement plus riche que le modèle de rotor asymétrique et doit permettre d'interpréter davantage de données expérimentales (telles que la présence de niveaux 0+ au voisinage du 2' ou bien l'existence de noyaux tels que $X < 2$). Une meilleure connaissance de l'énergie potentielle de déformation est cependant nécessaire pour permettre de l'exploiter pleinement.

Je remercie Monsieur Robert Arvieu qui m'a aidé au début de ce travail.

† Dans un preprint reçu alors que ce travail était en cours de rédaction T. Tamura et T. Udagawa [9]) atteignent des conclusions analogues aux nôtres en traitant par la méthode de perturbation un potentiel γ stabilisateur généralisant l'expression (1). Voir aussi T. Tamura et L. G. Kowai [10]).

†† Pour $k = 0$ on a $\varepsilon_2 = \hbar\omega$, $\varepsilon_{2'} = 2\hbar\omega$ et $\varepsilon_3 = 3\hbar\omega$. D'autre part pour $k \to \infty$ (noyau rotationnel) on a $\varepsilon_2 = \hbar^2/B\beta_0^2$ et $\varepsilon_3 = \varepsilon_{2'} + \hbar^2/B\beta_0^2$, car le premier niveau 3 devient alors le premier niveau de rotation de la bande construite à partir du niveau 2+ de vibration γ.

References

1) A. S. Davydov et G. F. Filippov, Nuclear Physics **8** (1958) 237
2) D. M. Van Patter, Nuclear Physics **14** (1960) 42
3) cf. aussi C. Marty, Nuclear Physics **1** (1956) 85; **3** (1957) 193
4) G. Scharff-Goldhaber et J. Weneser, Phys. Rev. **98** (1955) 212L
5) L. Wilets et M. Jean, Phys. Rev. **102** (1956) 788
6) A. Bohr, Mat. Fys. Medd. Dan. Vid. Selsk. **26**, No 14 (1952)
7) D. R. Bès, Nuclear Physics **10** (1959) 373
8) A. Bohr et B. Mottelson, Mat. Fys. Medd. Dan. Vid. Selsk. **27** No. 16 (1953)
9) T. Tamura et T. Udagawa, preprint
10) T. Tamura et L. G. Kowai, Phys. Revs. Letters **3** (1959) 344

7.C

Nuclear Physics **21** (1960) 157—160; © *North-Holland Publishing Co., Amsterdam*

Not to be reproduced by photoprint or microfilm without written permission from the publisher

OPTICAL MODEL ANALYSIS OF NEGATIVE PION-PROTON ELASTIC SCATTERING BETWEEN 1.4 AND 6.8 GeV

G. DOMOKOS and A. SEBESTYÉN

Department of Cosmic Rays, Central Research Institute for Physics, Budapest

Received 18 July 1960

Abstract: Elastic scattering of negative pions on protons is analysed in terms of an optical model. The rms radius of the absorptive region is found to be $\langle r^2 \rangle^{\frac{1}{2}} = (0.521 \pm 0.016) \cdot 10^{-13}$ cm.

1. Introduction

The high energy elastic πp scattering amplitude is usually considered as pure imaginary, and is compared with the diffraction pattern from a black sphere [1–3]).

Such analyses result in a value of $\approx 1 \times 10^{-13}$ cm for the radius of the hypothetical black sphere.

These results may be questioned from at least two points of view. First, it is well known from diffraction theory, that for a black sphere the total elastic cross section would be ≈ 20 mb, in contrast with its experimental value of $3 \div 7$ mb. Second, if the nucleon core had indeed such a large size, it would be rather difficult to understand the success of meson theory in explaining the electromagnetic structure of the proton.

A more realistic approach to the problem is that of Blokhintsev and coworkers, who calculated the distribution of the pion absorption coefficient with the ray-optical approximation on the basis of an optical model [4]).

The present work aims at investigating the energy dependence of the absorption coefficient.

2. Method of Analysis and Results

Under the same assumptions as in ref. [4]) (i.e. if the real part of the amplitude is negligible and the ray-optical approximation is valid) the differential cross section and the semi-classical phase shifts $\eta(\rho)$ are connected by the following equation:

$$\eta(\rho) = \tfrac{1}{2} \ln \left\{ 1 + k \int_{-1}^{1} \left(\frac{\mathrm{d}\sigma}{\mathrm{d}\Omega} \right)^{\frac{1}{2}} J_0(2k\rho \sin \tfrac{1}{2}\vartheta) \mathrm{d} \cos \vartheta \right\}, \tag{1}$$

while the absorption coefficient can be expressed as the functional (see ref. [5])) of $\eta(\rho)$,

$$a(z) = -\frac{2}{\pi} \frac{\mathrm{d}}{\mathrm{d}z} \int_{z}^{\infty} \mathrm{d}y \, \eta(y) (y - z)^{-\frac{1}{2}}, \tag{2}$$

where $y = \rho^2$, $z = r^2$ (ρ is the semi-classical "impact parameter").

The function $\eta(\rho)$ for different energies has been calculated from the experimental data of refs. [1–3]) by means of graphical integration.

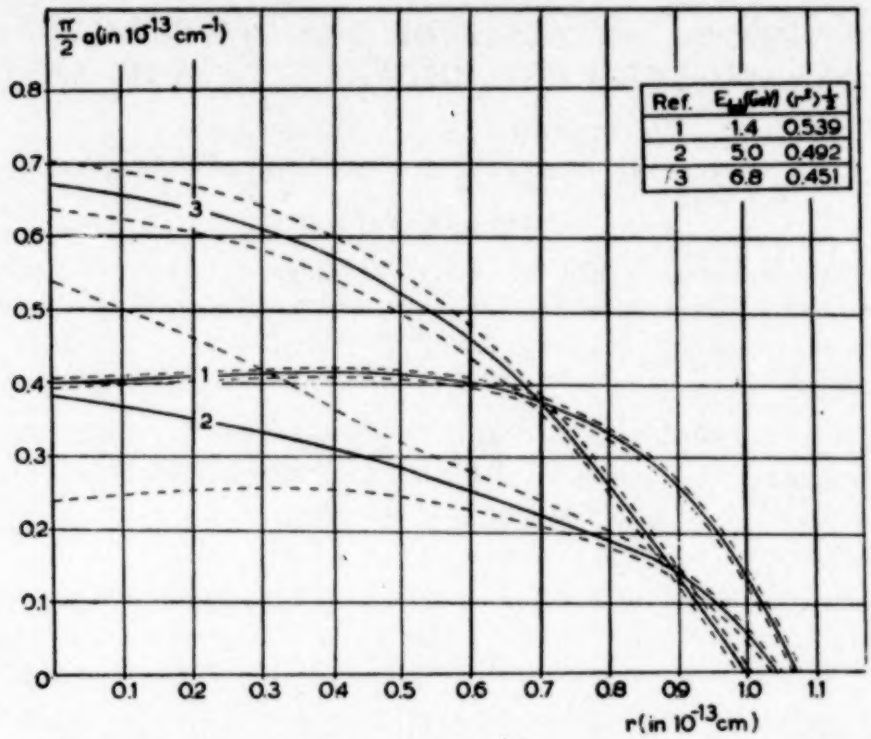

Fig. 1. Absorption curves as calculated from refs. [1–3]). Curves are labelled with the number of the corresponding reference. Rms radii obtained from different curves are indicated. Dotted curves denote one standard deviation.

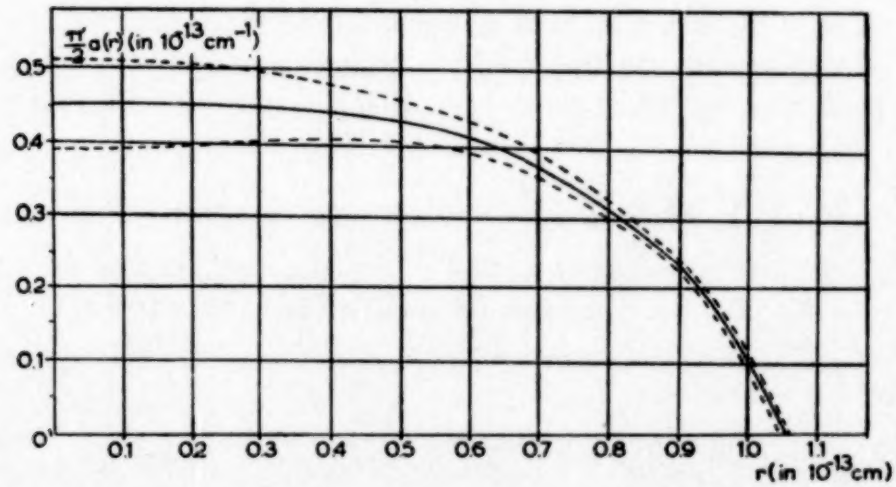

Fig. 2. Weighted average of absorption curves. Dotted curves denote one standard deviation.

In view of the experimental difficulties the values of the differential cross section at small momentum transfer cannot be considered reliable. In order to obtain reasonable results, the value of $d\sigma/d\Omega$ at $\vartheta = 0$ has been calculated

from the optical theorem. (This is consistent with our basic assumptions.)

Having obtained the phase shifts from eq. (1), $a(z)$ was calculated from eq. (2) with the help of a graphical integration followed by numerical differentiation.

The curves $a(r)$ as calculated from the aforementioned data are plotted in fig. 1.

No systematic tendency could be found in the absorption curves regarded as function of energy. In fact, the differences between the absorption curves corresponding to different energy values, are nowhere larger than the threefold standard error, when $0 \leqq r \leqq 0.6 \times 10^{-13}$ cm the tails of the curves being rather uncertain because of possible systematic errors in the experimental data in the low momentum transfer region.

Therefore, assuming all the deviations between the absorption curves to be due to statistical fluctuations of the original data, we tentatively calculated an averaged absorption curve (fig. 2). In the averaging, the curves have been weighted corresponding to the total number of events from which the curve had been calculated. For the weighted average of rms radii of the distributions we obtained

$$\langle r^2 \rangle^{\frac{1}{2}} = (0.521 \pm 0.016) \times 10^{-13} \text{ cm}.$$

As can be seen from fig. 2, the absorption is fairly high and almost constant up to about 0.3×10^{-13} cm decreasing gradually afterwards.

The total elastic and reaction cross sections can be calculated from the following formulas †:

$$\sigma_e = \pi \int_0^\infty dy[1-\exp(-2\eta(y))]^2, \quad \sigma_r = \pi \int_0^\infty dy[1-\exp(-4\eta(y))]. \qquad (3)$$

The cross sections calculated from our phase shifts agree within the statistical errors with those given by refs. [1–3]), thus serving as a check on the internal consistency of our analysis.

3. Discussion

Our results seem to indicate, that there exists a strongly absorbing "core" inside the nucleon with a size about 0.5×10^{-13} cm. Although the absorption coefficient found is rather high, it is important to realize that the "black-sphere approximation" is of rather dubious value, especially because of the long tail of the absorption curve. In spite of the poor statistics of individual measurements, our results suggest that the "optical" properties of the core would be energy independent, at least in the energy region under investigation. From this point of view, too, it is very desirable to increase the statistics of the measurements, especially at higher pion energies.

† Formulas (3) are the semi-classical approximation of the well-known expressions $\sigma_e = 2\pi k^{-1} \Sigma_l (2l+1)|1-\exp 2i\delta_l|^2$ and $\sigma_r = 2\pi k^{-1} \Sigma_l (2l+1)(1-|\exp 2i\delta_l|^2)$, with $\delta_l = i\eta_l$.

Accepting the rms radius as a measure of the "size" of the core, there is an apparent contradiction between the "black-sphere" interpretation and our own.

It is easy to show, however, that with increasing absorption coefficient, the width of the first maximum in the diffraction pattern increases, being maximal in the case of a black sphere. In fact, if we take a sphere with a radius equal to our rms radius and with a constant absorption coefficient the half width of the first maximum equals that of a black-sphere with $R \approx 0.9 \times 10^{-13}$ cm.

This simple example alone shows (apart from the effect of the non-uniformity of a) the importance of the fact that the core is grey.

The authors take pleasure in expressing their indebtedness to Prof. L. Jánossy for his interest in the present work and to Dr. E. Fenyves for fruitful discussions on the subject. They wish to express their sincere thanks to Miss M. Szücs for her valuable aid in the numerical computations.

References

1) M. Chretien, J. Leitner, N. P. Samios, N. Schwartz and J. Steinberger, Phys. Rev. **103** (1957) 383
2) G. Maenchen, W. B. Fowler, W. M. Powell and R. W. Wright, Phys. Rev. **108** (1957) 850
3) Van Gan-Chan, Van-Tzu-Tzen, Din Da-Tzao, V. G. Ivanov, IU. V. Kasisev, E. N. Kladnitskara L. A. Kuliukina, Nguen Din Ti, A. V. Nikitin, S. Z. Otviniovskij, M. J. Soloviev, R. Sosnovskij and M. D. Shafranov, JETP **38** (1960) 4260
4) D. I. Blokhintsev, V. S. Barashenkov and B. G. Grishin, Nuovo Cim. **9** (1958) 249
5) G. Domokos and A. Sebestyén (to be published)

8.B

Nuclear Physics **21** (1960) 161—163; © *North-Holland Publishing Co., Amsterdam*

Not to be reproduced by photoprint or microfilm without written permission from the publisher

MASS DIFFERENCES IN SECOND ORDER PERTURBATION THEORY

A. I. SOLOMON

Peterhouse, Cambridge, England

Received 19 May 1960

Abstract: The results of numerical computations of the mass differences of certain elementary particles on the basis of second order perturbation theory are given. The calculations are based on the assumption that the mass splitting is due to the mass differences of the intermediate particles emitted in the self-energy graphs.

1. Introduction

In a recent article [1]), Bransden and Moorhouse have shown that the assumption of a K^0—K^+ mass difference can be used to explain, in part at any rate, the Σ^-—Σ^+ mass difference within the framework of second order perturbation theory.

This note presents the results of numerical calculations based on second order perturbation theory and arising from the application of this method to the neutron-proton mass difference. The converse procedure is also examined, namely the explanation of the K^0—K^+ and π^+—π^0 mass differences in terms of the mass differences of the intermediate fermions in their second order graphs.

2. Neutron-Proton Mass Difference

In the spirit of the approach of Bransden and Moorhouse, the neutron-proton mass difference is due to the mass differences of the K-mesons appearing as virtual particles in the following interactions:

$$\begin{aligned} &n \to \Sigma^- + K^+, \quad p \to \Sigma^0 + K^+, \\ &n \to \Sigma^0 + K^0, \quad p \to \Sigma^+ + K^0, \\ &n \to \Lambda + K^0, \quad p \to \Lambda + K^+. \end{aligned}$$

Adding these contributions,

$$\Delta M(n-p) = -g^2_{\Sigma Kn}(\Sigma K^0 - \Sigma K^+) + g^2_{\Lambda Kn}(\Lambda K^0 - \Lambda K^+),$$

in an obvious notation, where Σ is the average Σ mass. This calculation gives a very small effect; in fact, it may be noted that, with the "restricted hyperon symmetry", $g^2_{\Sigma Kn} = g^2_{\Lambda Kn}$, and neglect of the $\Sigma - \Lambda$ mass difference, it is zero.

On actual substitution of the experimental masses (in this paper the masses reported by Alvarez [2]) are used) and taking $g^2_{\Sigma Kn} = g^2_{\Lambda Kn} = g^2$, the result is

$$\Delta M(\mathrm{n-p}) = g^2\left(\begin{smallmatrix}0.04\\0.01\end{smallmatrix}\right) \text{ MeV},$$

where the upper figure refers to a scalar, and the lower to a pseudo-scalar K meson. This would require an enormous coupling constant to fit the observed data (≈ 130 for a pseudo-scalar K).

If, however, we further take into account the Σ mass splittings, we find

$$\Delta M(\mathrm{n-p}) = g^2\left(\begin{smallmatrix}-1.04\\0.55\end{smallmatrix}\right) \text{ MeV},$$

and we see that a pseudo-scalar K and a coupling of 1.5 will reproduce the known difference.

3. K^0—K^+ Mass Difference

We now apply the converse procedure, namely that the K^0-K^+ mass difference is due to the mass differences of the intermediate Σ particles. As we must now take the difference of two quadratically divergent graphs, the result is logarithmically dependent on a cut-off. The contributing interactions are

$$K^0 \to \bar{\Sigma}^+ + p, \quad K^+ \to \bar{\Sigma}^- + n,$$
$$K^0 \to \bar{\Xi}^- + \Sigma^-, \quad K^+ \to \bar{\Xi}^0 + \Sigma^+.$$

The mass difference is cut-off sensitive for small values of the cut-off, but its asymptotic behaviour is

$$\Delta M(K^0-K^+) = \{\left(\begin{smallmatrix}0.3\\14.4\end{smallmatrix}\right) g^2_{n\Sigma K} - \left(\begin{smallmatrix}4.6\\16.1\end{smallmatrix}\right) g^2_{\Sigma\Xi K}\} \log\left(\frac{\Lambda}{M}\right)^2$$

for very large cut-off Λ, where the upper figure refers to a scalar coupling and the lower to a pseudo-scalar coupling.

Results computed from the accurate formula show that a cut-off of about 2 nucleon masses will reproduce the experimental mass difference of 4 MeV, if the parities and coupling constants chosen are those of Bransden and Moorhouse i.e., $g^2_{n\Sigma K} = 4$, $g^2_{\Sigma\Xi K} = 3$, and the K—n interaction is pseudo-scalar, while the Ξ—K interaction is scalar.

4. π^+—π^- Mass Difference

We may now attempt to explain the $\pi^+-\pi^-$ mass difference in a similar way to that of the K-mesons, using strange particle mass differences in the self-energy graphs. The neutron-proton mass difference is found to be insufficient to give the required order of magnitude to the mass difference, contributing a difference of the order of 10^{-2} MeV for the usual order of cut-off. The graphs

considered correspond to

$$\pi^+ \to \Sigma^0 + \bar{\Sigma}^-, \quad \pi^0 \to \Sigma^- + \bar{\Sigma}^-,$$
$$\pi^+ \to \Sigma^+ + \bar{\Sigma}^0, \quad \pi^0 \to \Sigma^+ + \bar{\Sigma}^+,$$
$$\pi^+ \to \Lambda^0 + \bar{\Sigma}^-, \quad \pi^0 \to \Lambda^0 + \bar{\Sigma}^0,$$
$$\pi^+ \to \bar{\Lambda}^0 + \Sigma^+, \quad \pi^0 \to \bar{\Lambda}^0 + \Sigma^0.$$

The asymptotic expression is

$$\Delta M(\pi^+ - \pi^0) = \frac{g^2}{2M_\pi \pi}(M_\Sigma - M_\Lambda)(M_{\Sigma^+} + M_{\Sigma^-} - 2M_{\Sigma^0}) \log\left(\frac{\Lambda}{M}\right)^2$$

for a pseudo-scalar pion, and therefore ultimately gives the correct sign for the mass difference. But the coefficient is small, and a cut-off of the order of 20 nucleon masses, much larger than that usually envisaged in these calculations, would be necessary to give the magnitude required by experiment (4.6 MeV).

5. Conclusion

It appears from these calculations that the mass differences of the K^0 and K^+ particles can be used to give a consistent picture of the Σ and nucleon fine splitting, and that the converse procedure, although not cut-off independent, can also be made to explain the K and π meson splitting by choosing suitable cut-offs.

The author wishes to thank Dr. J. C. Polkinghorne for helpful discussions, the Electors to the Robert Gardiner Memorial Scholarship for a maintenance grant, and the Director of the Mathematical Laboratory, Cambridge, for permission to use Edsac II.

References

1) B. H. Bransden and R. G. Moorhouse, Phys. Rev. Lett. **2** (1959) 431
2) L. Alvarez, Report of the Kiev Conference, July, 1959

4.E

Nuclear Physics 21 (1960) 164—169; © *North-Holland Publishing Co., Amsterdam*

Not to be reproduced by photoprint or microfilm without written permission from the publisher

THE DECAY CHAIN $Yb^{164} \rightarrow Tm^{164} \rightarrow Er^{164}$

A. ABDURAZAKOV, K. GROMOV, B. DALKHSUREN, B. DŽELEPOV, I. LEVENBERG, A. MURIN, Yu. NORSEYEV, V. POKROVSKY, V. CHUMIN and I. YUTLANDOV

Laboratory of Nuclear Problems, Joint Institute for Nuclear Research, Dubna, USSR

Received 14 March 1960

Abstract: It has been established that among the spallation products of Ta there is an isotope Yb^{164}($T_{\frac{1}{2}} = 75 \pm 2$ min) which disintegrates into a hitherto unknown isotope Tm^{164} ($T_{\frac{1}{2}} = 2 \pm 0.5$ min). Tm^{164} turns into a stable Er^{164} emitting positons with an end-point energy of 2940 ± 20 keV and 91.5 ± 0.1 keV and 211 ± 2 keV γ-rays.

In 1955 Nervik and Seaborg [1]) discovered an Yb isotope possessing a positon activity ($E_{\beta^+} = 2.4$ MeV) with $T_{\frac{1}{2}} = 75$ min among the products of spallation of Ta by 340 MeV protons. Later similar results ($T_{\frac{1}{2}} = 75$ min. $E_{\beta^+} = 2.9$ MeV) were obtained by Kalyamin *et al.* [2]). These experiments failed to establish reliably the mass number of the above-mentioned isotope Yb. Drawing on indirect considerations, Nervik and Seaborg [1]) supposed that the mass number of the isotope is $A = 167$, while Kalyamin *et al.* [2]) favoured the assumption $A = 161$.

We have tried to obtain more detailed data on the decay of Yb (75 min). A source of Yb was obtained as a spallation product of Ta irradiated by 680 MeV protons. A Ta target weighing 5 g was irradiated for 15 to 20 min in the internal beam of the synchrocyclotron of the Joint Institute of Nuclear Research (Dubna). The sum of rare earth elements was separated from Ta and spallation and fission products by coprecipitation with a small quantity (≈ 1 mg) of lanthanum fluoride. The precipitate of the fluoride was solved in the mixture of boric and nitric acids after which the rare-earth hydrooxides were precipitated by ammonia and solved in a drop of hydrochloric acid as 1 : 4. The rare-earth elements were sorbed from the solution by a small quantity of Dowex-50 cationite and separated chromatographically [3, 4]) in a column filled with the Dowex-50 cationite at a temperature 85° C. The column was 10 cm long and 2 mm in diameter, the resin grains were from 10 to 15μm. Ammonia lactate with $p_H = 4.5$ was used as eluent. In separating the group of rare-earths the elution of various fractions was kept uniform by constantly changing the eluent concentration. The chemical operations (from the end of irradiation and to the moment of the isolation of Yb) lasted for about two hours. The sources for β- and γ-spectrometers were prepared by evaporating drops of eluent containing Yb on aluminium foil.

This method of obtaining Yb sources inevitably led to the presence of other isotopes along with Yb (75 min) in the sample under examination: Yb^{167} (18 min); Yb^{166} (58 h); Yb^{169} (30.6 d) and their daughter isotopes Tm^{167} (9.6 d) and Tm^{166} (7.7 h). This naturally interfered with investigation of the Yb (75 min) spectra.

The γ, β^+ and e^--spectra were investigated using a β-spectrometer with a uniform magnetic field (resolving capacity at the 661 keV Cs^{137} transition K-line 0.8 %), β-spectrograph with a permanent magnet and photographic detection and a scintillation γ-spectrometer with a multi-canal analyzer (the number of canals: 128, the average dead time $\approx$ 80 μ sec, a memory device on the potentialoscope).

The experimental results of investigating the decay chain starting from Yb (75 min) are represented in table 1.

TABLE 1

Experimental data of the decay chain $Yb^{166} \rightarrow Tm^{166} \rightarrow Er^{166}$

Energy (keV)	Intensity †			
	γ	K	L	M
of γ-transitions				
91.5±0.1	8±3		28±5 ††	10±2
211 ±2	weak	0.3	0.16	weak
of positons				
2940± 20			100	
1300±100			4	

† The intensity of the component of positons with $E_0 = 2.94$ MeV is put equal to 100.
†† The ratio L_I+L_{II}/L_{III} is equal to 1.08

The conversion electron spectrum revealed 91.5 keV and 211 keV transition lines, while the γ-spectrum a 90 keV line and a very weak 210 keV line. The 9.15 keV transition energy and relative intensities $(L_I+L_{II}) : L_{III}$ were determined with the constant field β-spectrometer. No 211 keV transition lines were detected. Unfortunately, the instruments used precluded any reliable detection of the 9.15 keV transition K-line.

The intensity of the β^+-spectrum in all sections declined from $T_{\frac{1}{2}} = 75\pm 2$ min. The Fermi analysis shows that the marginal positon energy amounted to 2940±20 keV and there were no deviations from the shape of resolved spectra in the portion of the spectrum above 1300 keV. Such deviations existed at lower energies, and if assumed that they are connected with the presence of the second component in the β^+-spectrum, the latter's end point energy amounts to 1300± 100 and its intensity to 4 % of the rigid component of the β-spectrum (fig. 1).

By comparing the respective intensities we obtain the L-shell conversion

coefficient for the 91.5 keV transition $\alpha_L = 3.5 \pm 1.5$. This value is in satisfactory agreement with the theoretical value 2.16 for the E2 transition multipolarity [5]) and widely differs from other values. The ratio $(L_I + L_{II}) : L_{III}$ is also in good agreement with the theoretical value 1.05 for the E2 transition multipolarity. Furthermore, the ratio 2.3 of the energies of the two transitions discovered is in good agreement with the theoretical value 2.33 for the transition between the first excited levels of the rotation band of the ground state of even nuclei.

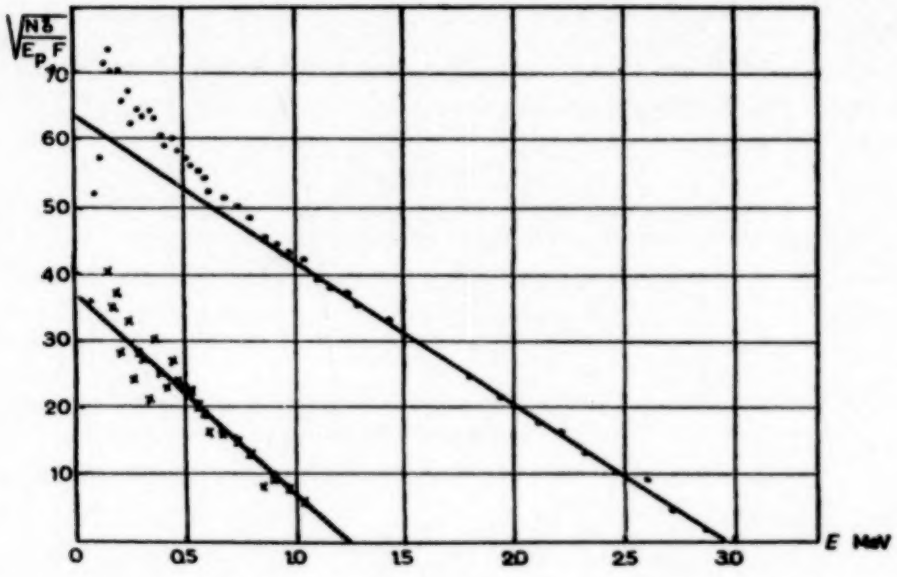

Fig. 1. Kurie graph of the positon spectrum of an equilibrium mixture of Yb^{164} and Tm^{164}. The upper line shows the hard component of the positon spectrum (Tu^{164} : $E_0 = 2940$ keV). The lower line shows the possible soft component of the positon spectrum ($E_0 = 1300$ keV).

Thus, both multipolarity and energy transition ratio favoured the supposition that we were observing the transitions between the levels of an even nucleus (Er^{164} or Er^{162}). The 91.5 keV transition energy within errors coincides with 91.3 keV transition energy found in Er^{164} in the β^--decay of Ho^{164} [6]). The assumption $A = 164$ also agrees well with semi-empirical data on the nucleus masses [7, 8]), if the positon radiation is to be referred to the Tm^{164} decay. According to the above-mentioned tables the difference of the masses of Yb^{164} and Tm^{164} amounts to 1232 keV and 1301 keV, while the difference of the masses of Tm^{164} and Er^{164} amounts to 3785 keV and 3097 keV respectively.

Thus, our results pointed to the existence of the decay chain Yb^{164} (75 min) $\rightarrow Tm^{164} \rightarrow Er^{164}$. This identification was also borne out by the experiments to discover the conversion lines † of the possible daughter activities of Yb (75 min). An hour and a half or two hours after the isolation of the Yb fraction (Yb^{167} disintegrated completely within this time) Tm was isolated from

this fraction. In the purified Yb source the $Tm^{167, 166, 165, 163 \text{ and } 161}$ lines which would be the most conspicuous and convenient for observation were looked for. The results of the research enabled us to reject the possibilities of $A = 167$, 166, 165, 163 or 161 practically completely.

To obtain direct proofs of the existence of Tm^{164} we first of all made an attempt to discover with a scintillation γ-spectrometer the characteristic activity in the daughter Tm isolated from Yb. This search has yielded no reliable results, which was interpreted as a consequence of the shortness of the Tm^{164} half-life period (no less than 15 min elapsed from the moment of the appearance of Yb in the chromatogram and up to the start of measuring the daughter Tm). Nor were attempts at quicker separation of Yb and Tm successful, since the separation would be incomplete in these cases.

For this reason we turned to the establishment of the accumulation of Tm^{164} in Yb. For this purpose a drop of Yb was taken from the advanced edge of the Yb peak of the Yb and Tm separation chromotogram, and the time dependence of the intensity of the 510 keV γ-line (of the peak of the annihilation radiation) was registered. The same was repeated in another series of experiments with a 90 keV γ-line. In both cases measurements began 2 to 3 min after the egress of the drop from the column.

Measuring the 510 keV γ-line was facilitated having no perceptible β^+-radiation in other Yb isotopes and the Yb spectrum having a high intensity of γ(510 keV). In experiments with a 90 keV γ-line account had to be taken of the accumulation of 80 keV pertaining to Yb^{166} and Tm^{166} since γ (80 keV) and γ (90 keV) cannot be resolved by scintillation spectrometers. The accumulation of γ (80 keV) had been investigated before [9]) and verified in our experiments. The results obtained for γ (90 keV) are in good agreement with the results for γ (510 keV).

Fig. 2 shows the result of measuring the accumulation of γ (510 keV). Only the initial section is represented (measurements lasted from 5 to 7 h, so that the 75 min-period could be registered very well). The accumulation is dinstinctly visible; the daughter Tm^{164} period, hence obtained, is equal to 2 min.

The value of the Tm^{164} half-life period, averaged by more than 10 measurements, amounts to 2.0 ± 0.5 min. By our data we could also estimate Yb^{164} positon radiation. It transpired that its intensity does not exceed 10 % of the total positon radiation intensity, or does not exist at all. Comparatively low accuracy of this estimate is due to the impossibility of accurately determining the moment of separation of Yb and Tm in the chromatographic column. Apart from the 91.5 and 211 keV γ-lines, no intense (10 % of positon radiation intensity) lines which could belong to Yb^{164} or Tm^{164} were observed in our experiments. The 91.5 keV (E2) transition intensity amounts to no more than

† It is difficult to solve this problem with a scintillation γ-spectrometer on account of Tm^{166} possessing a complex spectrum.

60 % of the number of positons emitted in Tm^{164} decay. This probably shows that a considerable portion of Yb^{164} and Tm^{164} decays goes into the ground states (see fig. 3). Estimating the values τf for these transitions, we obtain

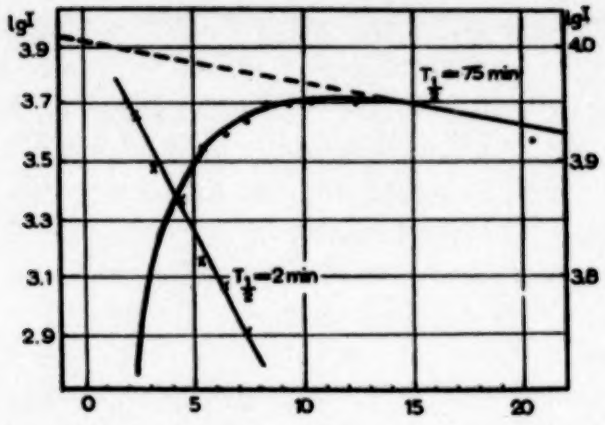

Fig. 2. Tne initial portion of the intensity variation curve of the 510 keV γ-line. The time from the moment of separation of Yb and Tm is marked off on the abscissa and the logarithm of the intensity on the axis of the ordinates. The curved line is an experimental result (right scale), while the straight line is the result of deduction (left scale).

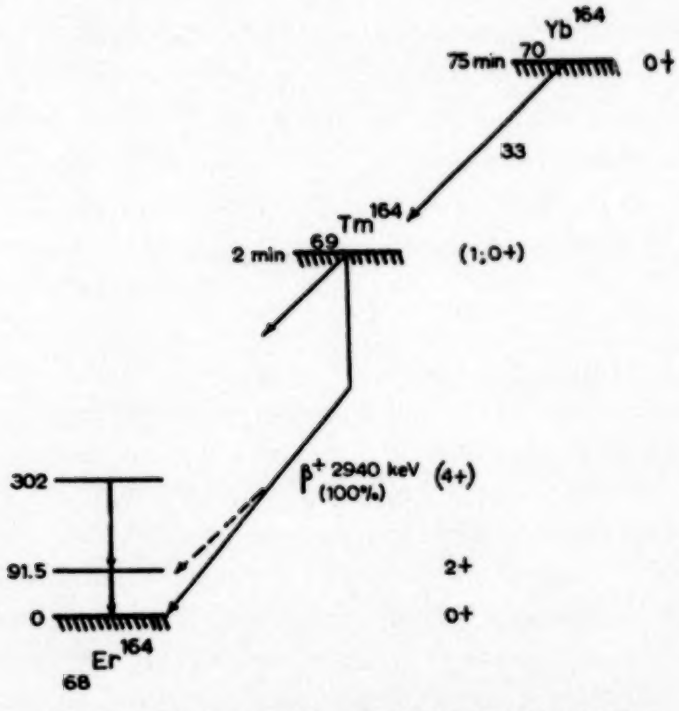

Fig. 3. The decay scheme $Yb^{164} \rightarrow Tm^{164} \rightarrow Er^{164}$.

$\log f\tau \lesssim 5$ for each of them, which obviously points to the allowed character of the transitions.

This might seem to contradict the possible values of the spin ${}_{69}Tm^{164}_{95}$. True enough, according to the theoretical rules [10, 11]), usually well conformed to, the

spin of the odd nucleus ${}_{69}Tm^{164}_{95}$ should be equal to $(\Omega_p \pm \Omega_n)$ where Ω_p and Ω_n are the spins of an even proton and neutron respectively. According to Nilsson's scheme [12]) $\Omega_p = \frac{1}{2}^+$ and $\Omega_n = \frac{5}{2}^-$ so that the spin Tm^{164} may amount to 2^- or 3^-. The choice between these two values according to the rule of Gallagher and Moszkowski [13]) leads to the value 3^-. Neither agrees with the allowed character of the transitions.

It is known, however, that for the 95th neutron the $\frac{5}{2}^+$ state is realizable (for ${}_{66}Dy^{161}_{95}$ see refs. [14, 15])). Furthermore, it is known [14, 15]) that for $Z = 69$, $\frac{1}{2}^+$ state is realizable, but as the number of neutrons decreases the $\frac{7}{2}^+$ state proximates it. Thus, the energy distance between the $\frac{1}{2}^+$ ground state and the $\frac{7}{2}^+$ excited one amounts to 636 keV for ${}_{63}Tm^{171}_{102}$, 316 keV for ${}_{69}Tm^{169}_{100}$ and 179 keV for ${}_{69}Tm^{167}_{98}$. Thus, there is a possibility that in ${}_{69}Tm^{164}_{95}$ the last proton is in the $\frac{7}{2}^+$ state. Then $\Omega_p \pm \Omega_n$ may account to 1^+ or 6^+ and according to ref. [13]), the value 1^+ should be selected.

The question naturally calls for additional research. In particular, we have been searching for weaker γ-transitions belonging to Yb^{164} or Tm^{164}.

Note added in proof: The conversion electron spectrum in the region of $E_e < 900$ keV has been investigated in the subsequent research. A great amount of very weak conversion lines has been observed. In particular, we have observed γ-transitions of 355.5 ± 1, 361 ± 1, 391 ± 1, 773 ± 2.5, 862 ± 3, 907 ± 3 and 930 ± 3 keV.

References

1) W. E. Nervik and G. T. Seaborg, Phys. Rev. **97** (1955) 1092
2) A. V. Kalyamin, I. Yu. Levenberg and V. A. Yakovlev, Atomnaya Energia **5** (1959) 582
3) Z. W. Mayer and E. C. Freiling, Journ. Amer. Soc. **75** (1953) 5647
4) B. K. Preobrazhensky, O. M. Lilova, A. M. Dobronravova and E. Teterin, Inorganic Chemistry Magazine **1** (1956) 2294
5) L. A. Slif and I. M. Band, Tables of γ-Radiation Internal Conversion Coefficients, Part I (K-shell), (USSR Ac. Sci., 1957); Part II (L-shell), (USSR Ac. Sci., 1958)
6) J. W. Mihelich, B. Harmatz and T. H. Handley, Phys. Rev. **108** (1957) 989
7) J. Riddel, A Table of Levy's Empirical Atomic Masses, Chalk River, Ontario, CRP-654 (1957)
8) A. G. W. Cameron, A Revized Semi-Empirical Atomic Mass Formula, Chalk River, Ontario, CRP-690 (1957)
9) V. I. Baranovsky and V. N. Pokrovsky, Izv. Akad. Nauk. SSSR Ser. Fiz. **23** (1959) 819
10) A. Bohr and B. R. Mottelson, Mat. Fys. Medd. Dan. Vid. Selsk. **27**, No. 16 (1953)
11) L. K. Peker, Izv. Akad. Nauk SSSR. Ser. Fiz. **21** (1957) 1029
12) S. G. Nilsson, Mat. Fys. Medd. Dan. Vid. Selsk. **29**, No. 16 (1955)
13) C. J. Gallagher and S. A. Moszkowsky, Phys. Rev. **111** (1958) 1282
14) B. Harmatz, T. H. Handley and J. W. Mihelich, Phys. Rev. **114** (1959) 1082
15) B. R. Mottelson and S. G. Nilsson, Mat. Fys. Skr. Dan. Vid. Selsk. **1**, No. 8 (1959)

7.B

Nuclear Physics **21** (1960) 170—176; © *North-Holland Publishing Co., Amsterdam*

Not to be reproduced by photoprint or microfilm without written permission from the publisher

RELATIONS FOR THE ELECTROMAGNETIC SELF-MASSES OF PARTICLES

W. R. THEIS

Institute for Theoretical Physics, University of Hamburg

Received 15 July 1960

Abstract: Equations for the electromagnetic self-masses of the first order in the fine structure constant are obtained including all non-electromagnetic interactions without approximation.

1. Introduction

The self-masses of charged particles which have only electromagnetic interactions are infinite in relativistic perturbation theory; this does not prevent an interpretation, because within the framework of the renormalization programme self-masses are unobservable and the unexplained experimental masses are regarded as given parameters. But the small mass differences of particles which differ only in their electromagnetic properties are most promising for an attack on the further problem of explaining masses by their interactions. Even these differences are infinite, if one regards them as electromagnetic and neglects other interactions. If one uses, in purely electromagnetic theory, a cut-off which corresponds to the nucleon mass, one gets for the $\pi^+ - \pi^0$ mass difference approximately the experimental value with the right sign [1]). For the neutron-proton mass difference this is not the case: the proton becomes heavier than the neutron. Feynman and Speisman [2]) have shown, that one gets the right order if one takes into account the coupling with the π-mesons by introducing the anomalous point magnetic moments of proton and neutron. Gasiorowicz and Petermann [3]) have estimated the mass difference between K^+ and K^0 with purely electromagnetic interaction and cut-off: they get the wrong sign. In this case the other interactions give no anomalous magnetic moment (spin 0), so that they cannot be partly introduced in such a simple way. But if one takes into account an extended charge, one can choose charge distributions (positive for K^+ and non-vanishing for K^0) which give the observed $K^+ - K^0$ mass difference even in a classical calculation [4, 5]).

An estimate of the mass differences has therefore to include the non-electromagnetic interactions in a more accurate manner. Thereby the mass differences may become finite without cut-off so that there may be a possibility of answering the first question of the mass spectrum in the frame-work of usual relativistic field theories.

Cini, Ferrari and Gatto [6]) have included strong interactions in determining the mass difference of neutron and proton. They insert instead of the free fields the strongly interacting fields into the formal expression for the purely electromagnetic self-masses. After some approximations they get formally the Feynman-Speisman result, only the cut-offs are replaced by form factors which are partly determined from electron-proton scattering leading to a wrong sign of the mass difference. Recently Riazuddin [7]) used similar formulae for the $\pi^+-\pi^0$ mass difference. Soon after that, a derivation of the defining equations was published by Sunakawa and Tanaka [8]) with reference to unpublished work of Sorensen [9]) †. Here the counter terms $\delta m = \delta^{(0)}m + e^2\delta m^{(1)}$ were evaluated to order e^2. A correct calculation of the difference $\delta^{(1)}m_p - \delta^{(1)}m_n$ gives the results of these authors multiplied by a factor, which depends only on the strong interactions. On the other hand the difference $e^2(\delta^{(1)}m_p - \delta^{(1)}m_n)$ is not equal to the mass difference $m_p - m_n = m_{0p} - m_{0n} + \delta^{(0)}m_p - \delta^{(0)}m_n + e^2(\delta^{(1)}m_p - -\delta^{(1)}m_n)$ as assumed in these papers. The bare masses m_0 should be the same for proton and neutron but $\delta^{(0)}m_p - \delta^{(0)}m_n$ is unequal zero showing that $e^2\delta^{(1)}m$ are not the electromagnetic self-masses (to order e^2). Whereas the values $\delta^{(1)}m_i$ are solutions of a system of coupled equations in the case of strongly interacting particles, it will be shown in the present paper that the defining equations of the true electromagnetic self-masses are uncoupled without any approximation, and give to order e^2 (including all non-electromagnetic interactions) the expression for the mass difference of proton and neutron used as a starting point in the previously mentioned numerical calculations [6–9]).

2. Derivation of the Relations for the Self-Masses

The self-masses of particles due to all interactions are given by the mass counter terms. The defining equations are

$$(\Phi_{p'}^{(k)}, (S-1)\Phi_p^{(k)}) = 0 \tag{1}$$

for all one particle states $\Phi^{(k)}$. The left-hand side of eq. (1) is a function of the mass terms x_i, the mass counter terms δx_i and the unrenormalized coupling constants of which only e will be written explicitly:

$$(\Phi_{p'}^{(k)}, (S-1)\Phi_p^{(k)}) \equiv f^{(k)}(x_i, \delta x_i, e). \tag{2}$$

The differences $x_i - \delta x_i$ are the bare mass terms.

Without electromagnetic but including other interactions these equations have the form $f^{(k)}(\tilde{x}_i, \delta\tilde{x}_i, 0) = 0$. The bare masses are equal in both cases since by definition they are independent of all interactions, therefore $x_i - \delta x_i = \tilde{x}_i - \delta\tilde{x}_i$. The mass differences $x_i - \tilde{x}_i = \delta x_i - \delta\tilde{x}_i \equiv \Delta x_i$ are the electro-

† I am indebted to Dr. Sorensen for sending me a copy. Some results of this work were reported by G. C. Wick [10]).

magnetic self-masses. Their defining equations are

$$f^{(k)}(x_i, \delta x_i, e) = 0, \quad f^{(k)}(x_i - \Delta x_i, \delta x_i - \Delta x_i, 0) = 0. \tag{3}$$

The variation of δx_i and e can be evaluated using time dependent canonical transformations, but the variations of x_i change the spectrum of the energy momentum vector; thus if one wants to calculate them unambiguously one has to use the explicit form of the functions $f^{(k)}$ given by perturbation theory to any order.

In the covariant perturbation theory the eqs. (3) are usually written in the form [11])

$$\overset{(k)}{\Sigma}{}^*(p, x_i, \delta x_i, e)|_{p \text{ on } x_k} = 0, \quad \overset{(k)}{\Sigma}{}^*(p, x_i - \Delta x_i, \delta x_i - \Delta x_i, 0)|_{p \text{ on } x_k - \Delta x_k} = 0, \tag{4}$$

where

$$\Sigma^* = S_F^{-1} - S'_F{}^{-1}, \quad \text{resp.} \quad \Delta_F^{-1} - \Delta'_F{}^{-1},$$

are the proper self-energy parts and p on x is an abbreviation for $-ip\gamma = m$, resp. $-p^2 = m^2$. The free propagators are defined as [11])

$$S_F^{-1} = -2\pi i(ip\gamma + m) \quad \text{and} \quad \Delta_F^{-1} = -2\pi i(p^2 + m^2).$$

The essential point now is that the propagators S'_F and Δ'_F depend only on the differences $x_i - \delta x_i$. To see this one first realizes that in the perturbation expansion the dependence on x_i is entirely due to the free propagators. The dependence on δx_i becomes evident if one constructs $S'_F(p, x_i, \delta x_i)$ from $S'_F(p, x_i, 0)$ by inserting in the last expression for the free propagators everywhere the values $\bar{S}_F$, resp. $\bar{\Delta}_F$, defined by

$$\bar{S}_F = S_F + S_F(-2\pi i \delta m)\bar{S}_F \quad \text{and} \quad \bar{\Delta}_F = \Delta_F + \Delta_F(-2\pi i \delta m^2)\bar{\Delta}_F.$$

which leads to

$$\bar{S}_F = S_F(p, x - \delta x) \quad \text{and} \quad \bar{\Delta}_F = \Delta_F(p, x - \delta x).$$

The two eqs. (4) can thus be written

$$\overset{(k)}{\Sigma}{}^*(p, x_i, \delta x_i, e)|_{p \text{ on } x_k} = 0, \quad \overset{(k)}{\Sigma}{}^*(p, x_i, \delta x_i, 0)|_{p \text{ on } x_k - \Delta x_k} + 2\pi i \Delta x_k = 0, \tag{5}$$

showing that to any order in e there are single equations for each Δx_k, which may be discussed separately. The variables x_i, δx_i in Σ^* are the same in both expressions and shall be omitted therefore.

For spin $\frac{1}{2}$ particles eqs. (5) have the explicit form

$$\Sigma^*(-i\gamma p = m, e) = 0, \quad \Sigma^*(-i\gamma p = m - \Delta m, 0) = -2\pi i \Delta m,$$

with [11])

$$\Sigma^*(-i\gamma p, e) = A' - 2\pi i \delta m - 2\pi i(1 - Z^{-1})(i\gamma p + m) + \Sigma_c{}^*.$$

Solving these equations to first order in e^2 one obtains

$$2\pi i \Delta m Z^{-1} = e^2 \frac{\mathrm{d}\Sigma^*}{\mathrm{d}e^2}(m, 0). \tag{6}$$

For the connection with the S-matrix it is convenient to deal with the improper self-energy Σ instead of Σ^*. It is given by

$$\Sigma S_F = \Sigma^* S'_F, \quad S'_F = S_F + S_F \Sigma S_F, \tag{7}$$

or expressed through S-matrix elements:

$$(\Phi_{p'}^{(k)}, (S-1)\Phi_p^{(k)}) = 2m_k \delta^4(p'-p) \overset{(k)}{\Sigma}(m). \tag{8}$$

Differentiation of eqs. (7) with respect to e^2 leads to

$$S_F \frac{\mathrm{d}\Sigma}{\mathrm{d}e^2} S_F = S'_F \frac{\mathrm{d}\Sigma^*}{\mathrm{d}e^2} S'_F$$

and therefore on the mass shell to

$$\frac{\mathrm{d}\Sigma}{\mathrm{d}e^2}(m) = Z \frac{\mathrm{d}\Sigma^*}{\mathrm{d}e^2}(m). \tag{9}$$

Collecting eqs. (6), (8) and (9) one gets

$$2\pi i \, \Delta m \, 2m \, \delta^4(p'-p) = e^2 \frac{\mathrm{d}}{\mathrm{d}e^2}(\Phi_{p'}, (S-1)\Phi_p), \tag{10}$$

where Φ_p is a spin $\frac{1}{2}$ state.

For spin 0 particles one can repeat every step with the result

$$2\pi i \, \Delta m^2 \, \delta^4(p'-p) = e^2 \frac{\mathrm{d}}{\mathrm{d}e^2}(\Phi_{p'}, (S-1)\Phi_p). \tag{11}$$

Here ϕ_p is a spin 0 state. (The differentiation with respect to e^2 in (10) and (11) should not include a differentiation of the mass counter terms).

In order to evaluate the right-hand sides of eqs. (10) and (11) one has to introduce the electromagnetic interactions in detail. This can be done most simply using Dyson's formal representation of the S-matrix:

$$S(H_w(\varphi^{\mathrm{in}})) = \frac{T\mathrm{e}^{-i\int H_w(\varphi^{\mathrm{in}})\mathrm{d}x}}{\langle T\mathrm{e}^{-i\int H_w(\varphi^{\mathrm{in}})\mathrm{d}x}\rangle_0}, \quad H_w = H_\gamma + H_s. \tag{12}$$

The Hamilton operator H_γ stands for the electromagnetic interaction, H_s for the other (usually strong) interactions including the self-mass terms due to these interactions, φ^{in} are free field operators belonging to the experimental masses, $\langle\rangle_0$ is an abbreviation for the expectation value in the vacuum state

of these fields. Eq. (12) can be written as

$$S = S(H_s(\varphi^{in}))S(H_\gamma(\varphi)) \equiv S_s S(H_\gamma(\varphi)), \tag{13}$$

where φ are the unrenormalized Heisenberg fields for $e = 0$. Eq. (13) is easily obtained by considering the differential equation for

$$U(t) = T\exp\left\{-i\int_{-\infty}^{t} H_w(\varphi^{in})dx\right\}, \quad \text{with} \quad U(t) = U_s(t)U'_\gamma(t),$$
$$i\dot{U}_s(t) = H_s(\varphi^{in})U_s(t),$$
$$i\dot{U}'_\gamma(t) = H_\gamma(U_s^{-1}(t)\varphi^{in}U_s(t))U'_\gamma(t) \equiv H_\gamma(\varphi)U'_\gamma(t).$$

Such a separation was already used for β-decay in connection with time reversal and final state interactions[12]). Using formula (13) and observing $S_s\Phi_\beta = \Phi_\beta$ one obtains

$$(\Phi_{\beta'}, S\Phi_\beta) = (\Phi_{\beta'}, Te^{-i\int H_\gamma(\varphi)dx}\Phi_\beta)\{\langle Te^{-i\int H_\gamma(\varphi)dx}\rangle_0\}^{-1}, \tag{14}$$

where

$$H_\gamma = -ej_\mu A_\mu^{in} - e^2 j\{(A_\mu^{in})^2 + (A_4^{in})^2\}$$
$$+ \sum_i \delta\bar{m}_i\bar{\psi}^i\psi^i + \sum_\alpha \delta\bar{m}_\alpha{}^2\varphi^{*\alpha}\varphi^\alpha + \tfrac{1}{2}\sum_\nu \delta\bar{m}_\nu{}^2(\varphi^\nu)^2,$$

with

$$j_\mu = \tfrac{1}{2}i\{\sum_i{}' [\bar{\psi}^i, \gamma_\mu\psi^i]_- + \sum_\alpha{}' [\varphi^{*\alpha}, \overleftrightarrow{\partial_\mu}\varphi^\alpha]_+\},$$
$$j = -\sum_\alpha{}' \varphi^{*\alpha}\varphi^\alpha,$$
$$\Box A_\mu = -(ej_\mu + 2e^2 jA_\mu).$$

Here ψ^i, φ^α, φ^ν are the field operators of the particles of spin $\frac{1}{2}$, the particles of spin 0 which are different from their antiparticles and the self-conjugate particles of spin 0 ($\{\varphi^\nu\}^* = \varphi^\nu$); $\delta\bar{m}_i$, $\delta\bar{m}_\alpha{}^2$, $\delta\bar{m}_\nu{}^2$ represent parts of their self-masses. In the primed sums over i and α one has to omit the particles with vanishing electric charge. (The counter terms with four Boson operators are dropped because they do not contribute to the e^2-approximation. The vacuum expectation values are not subtracted in the mass terms since they cancel in the final result).

The order e^2 and the first order in the mass terms (which will be used in the appendix) of the numerator in eq. (14) is

$$-\tfrac{1}{2}e^2\int dxdy\langle TA_\mu^{in}(x)A_\nu^{in}(y)\rangle_0(\Phi_{\beta'}, Tj_\mu(x)j_\nu(y)\Phi_\beta)$$
$$+ ie^2\int dx\langle(A_\mu^{in})^2 + (A_4^{in})^2\rangle_0(\Phi_{\beta'}, j\Phi_\beta) \tag{15}$$
$$-i\int dx(\Phi_{\beta'}, \{\sum_i \delta\bar{m}_i\bar{\psi}^i\psi^i + \sum_\alpha \delta\bar{m}_\alpha{}^2\varphi^{*\alpha}\varphi^\alpha + \tfrac{1}{2}\sum_\nu \delta\bar{m}_\nu{}^2(\varphi^\nu)^2\}\Phi_\beta).$$

In this approximation ej_μ can be replaced by $-\Box A_\mu$. The relation

$$\Box_x \Box_y T A_\mu(x) A_\nu(y) - T \Box A_\mu(x) \Box A_\nu(y) = \Box_y \delta_{\mu\nu} \delta^4(x-y) - 2ie^2 j \delta^4(x-y)(\delta_{\mu\nu} + \delta_{\mu 4}\delta_{\nu 4}) \quad (16)$$

gives for the first two terms of eq. (15)

$$-\tfrac{1}{2}\int \mathrm{d}x\mathrm{d}y \langle T A_\mu^{\mathrm{in}}(x) A_\nu^{\mathrm{in}}(y)\rangle_0 \cdot \{\Box_x \Box_y (\Phi_{p'}, T A_\mu(x) A_\nu(y) \Phi_p) - \delta_{\mu\nu}(\Phi_{p'}, \Phi_p) \Box_y \delta^4(x-y)\}. \quad (17)$$

Inserting eqs. (15) and (17) into (14) one gets

$$(\Phi_{p'}, (S-1)\Phi_p) = -i(2\pi)^4 \delta^4(p'-p) T, \quad (18)$$

where

$$T = -\tfrac{1}{2} i \int \mathrm{d}x \langle T A_\mu^{\mathrm{in}}(\tfrac{1}{2}x) A_\nu^{\mathrm{in}}(-\tfrac{1}{2}x)\rangle_0 \Box_x \Box_x (\Phi_p, \{T A_\mu(\tfrac{1}{2}x) A_\nu(-\tfrac{1}{2}x) - \langle T A_\mu(\tfrac{1}{2}x) A_\nu(-\tfrac{1}{2}x)\rangle_0\} \Phi_p)$$
$$+ \sum_i \delta \bar{m}_i (\Phi_p, \{\bar{\psi}^i \psi^i - \langle \bar{\psi}^i \psi^i \rangle_0\} \Phi_p) + \sum_\alpha \delta \bar{m}_\alpha^2 (\Phi_p, \{\varphi^{*\alpha} \varphi^\alpha - \langle \varphi^{*\alpha} \varphi^\alpha \rangle_0\} \Phi_p)$$
$$+ \tfrac{1}{2} \sum_\nu \delta \bar{m}_\nu^2 (\Phi_p, \{(\varphi^\nu)^2 - \langle (\varphi^\nu)^2 \rangle_0\} \Phi_p).$$

With this expression and eqs. (10), (11) one obtains the final result for the electromagnetic self-masses including all non-electromagnetic interactions

$$\Delta m^2 = \tfrac{1}{2}(2\pi)^3 i \int \mathrm{d}x \langle T A_\mu^{\mathrm{in}}(\tfrac{1}{2}x) A_\nu^{\mathrm{in}}(-\tfrac{1}{2}x)\rangle_0 \cdot \Box_x \Box_x (\Phi_p, \{T A_\mu(\tfrac{1}{2}x) A_\nu(-\tfrac{1}{2}x) - \langle T A_\mu(\tfrac{1}{2}x) A_\nu(-\tfrac{1}{2}x)\rangle_0\} \Phi_p), \quad (19)$$

where the right-hand side has to be taken to order e^2.

The author would like to thank Drs. H. Lehmann, B. Stech, K. Symanzik and W. Zimmermann for valuable discussions on this subject.

Appendix

Using old fashioned perturbation theory the result for the electromagnetic self-masses to first order (eq. (19)) is obtained in this appendix without the explicit form of the perturbation series for the strong interactions.

Together with the two eqs. (3),

$$\text{(I)}: \quad f^{(k)}(x_i, \delta x_i, e) = 0 \quad \text{and} \quad \text{(II)}: \quad f^{(k)}(x_i - \Delta x_i, \delta x_i - \Delta x_i, 0) = 0,$$

a third equation is regarded as an intermediate step,

$$\text{(III)}: \quad f^{(k)}(x_i, \delta x_i - \delta \bar{x}_i, 0) = 0,$$

which represents a system without electromagnetic interactions but the same masses as in (I).

The quantities $\delta\bar{x}_i$ can be calculated by a canoncical transformation from (I) to (III), since the masses remain constant. The result is given in eq. (18) with $T = 0$.

The transition from (III) to (II) changes only the mass terms from $x_i - \delta x_i$ to $x_i - \delta x_i + \delta\bar{x}_i$. The change in the energy is therefore

$$\begin{aligned}\Delta E(\Phi_{\mathfrak{p}'}, \Phi_{\mathfrak{p}}) &= 2E\Delta E\delta^3(\mathbf{p}'-\mathbf{p}) = \Delta m^2\delta^3(\mathbf{p}'-\mathbf{p}) \\ &= \sum_i \delta\bar{m}_i(\Phi_{\mathfrak{p}'}, \int \mathrm{d}^3x\{\bar{\psi}^i\psi^i - \langle\bar{\psi}^i\psi^i\rangle_0\}\Phi_{\mathfrak{p}}) \\ &+ \sum_\alpha \delta\bar{m}_\alpha{}^2(\Phi_{\mathfrak{p}'}, \int \mathrm{d}^3x\{\varphi^{*\alpha}\varphi^\alpha - \langle\varphi^{*\alpha}\varphi^\alpha\rangle_0\}\Phi_{\mathfrak{p}}) \\ &+ \tfrac{1}{2}\sum_\nu \delta\bar{m}_\nu{}^2(\Phi_{\mathfrak{p}'}, \int \mathrm{d}^3x\{(\varphi^\nu)^2 - \langle(\varphi^\nu)^2\rangle_0\}\Phi_{\mathfrak{p}}),\end{aligned}$$

which together with the vanishing of the expression (18) leads to eq. (19).

References

1) A. Petermann, Helv. Phys. Acta **27** (1954) 441
2) R. P. Feynman and G. Speisman, Phys. Rev. **99** (1954) 590
3) S. Gasiorowicz and A. Petermann, Phys. Rev. Letters **1** (1958) 457
4) Chong Kuang-Chao and V. Ogievetski, Preprint P 352 Dubna (1959)
5) P. T. Matthews and J. L. Uretsky, Phys. Rev. Letters **3** (1959) 297
6) M. Cini, E. Ferrari and R. Gatto, Phys. Rev. Letters **2** (1959) 7
7) Riazuddin, Phys. Rev. **114** (1959) 1184
8) S. Sunakawa and K. Tanaka, Phys. Rev. **115** (1959) 754
9) R. Sorensen, AEC-NYO-7119
10) G. C. Wick, Proc. Seventh Rochester Conference 1957 (Interscience, New York, 1957) Ch. I, p. 41
11) F. J. Dyson, Phys. Rev. **75** (1949) 1736
12) e.g. T. D. Lee and C. N. Yang, Elementary Particles and Weak Interactions (Brookhaven Nat. Lab., 1957) p. 25;
see also K. Symanzik, Seminar notes Oberwolfach 1958

3.A:
4.E

Nuclear Physics **21** (1960) 177—188; © *North-Holland Publishing Co., Amsterdam*

Not to be reproduced by photoprint or microfilm without written permission from the publisher

DISINTEGRATION OF ^{66}Ge

R. A. RICCI †, R. K. GIRGIS †† and R. VAN LIESHOUT

Instituut voor kernphysisch Onderzoek, Amsterdam

Received 22 July 1960

Abstract: The decay of ^{66}Ge has been investigated by scintillation techniques. The beta and gamma ray spectra were measured and the experimental results are given in tables 1 and 2. Gamma-gamma coincidences have also been performed and the results are reported in table 3. On the basis of these data a decay scheme is proposed (see fig. 8) and some features of the ^{66}Ge disintegration are discussed.

1. Introduction

Like ^{67}Ge, the nucleide ^{66}Ge was found by Hopkins [1]) in a spallation reaction; it was reported to decay by positon emission to ^{66}Ga with a half-life of $\approx$ 2.5 hours. No other information was available when a preliminary investigation about the decay of this nucleide was performed at this Institute [2]).

It was found in the course of experiments concerning ^{67}Ge, that a large amount of ^{66}Ge was produced by an (α, 2n) reaction on Zn [2,3]). Its decay was also investigated and gamma rays of 45 ± 1, 70 ± 1, 114 ± 2 and 182 ± 4 keV were found with a half-life of $\approx$ 2.5 hours and assigned to the ^{66}Ge disintegration in the preliminary report [2]).

Subsequently, the decay of this nucleide was investigated in more detail in order to construct a more complete decay scheme.

2. Experimental Procedure and Results

The ^{66}Ge sources were produced by bombarding chemically pure Zn (metallic foil) with 42-MeV alpha particles from the synchro-cyclotron during about 45 min ($\approx 3\ \mu$Ah).

The irradiated targets were dissolved in 6*N* HCl containing Ge and Ga carriers. The Ge fraction was distilled from this solution as the tetrachloride and collected in 6*N* HCl. The distillation was performed at least 3 hours after the end of the irradiation in order to reduce the quantity of ^{67}Ge, which is also produced in large amounts, to negligible proportions. Thereafter Ge was precipitated as the sulphide with H_2S, filtered, dried and measured.

† On leave of absence from the Istitute Nazionale di Fisica Nucleare, Sottosezione di Napoli, and from the Instituto di Fisica Superiore dell' Università di Napoli, Napoli, Italia.

†† On leave of absence from the Faculty of Science, University of Cairo, Giza, Egypt, U.A.R.

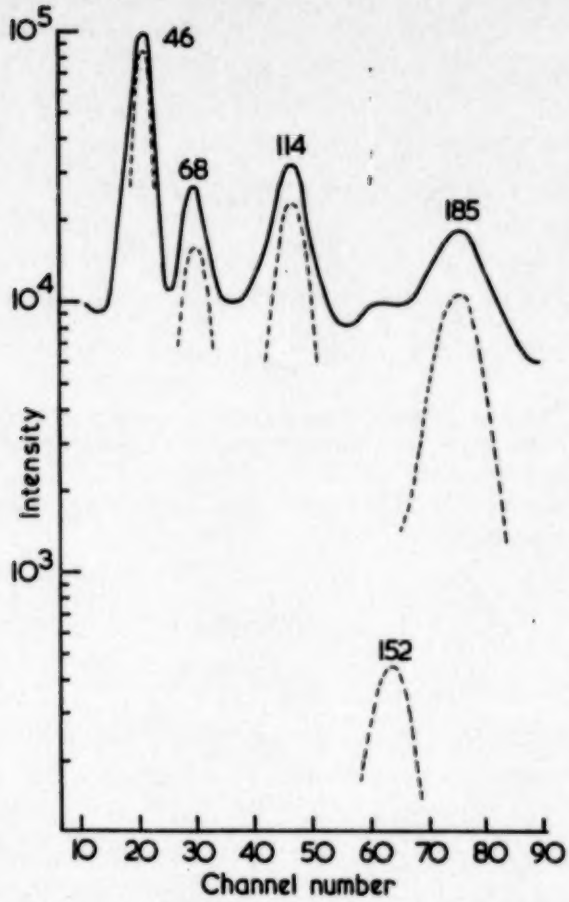

Fig. 1. Gamma ray spectrum of 2.4 hour ^{66}Ge in the energy region below 200 keV. The various analysed peaks (after subtraction of the contribution due to gamma rays of higher energy) are indicated by dashed curves.

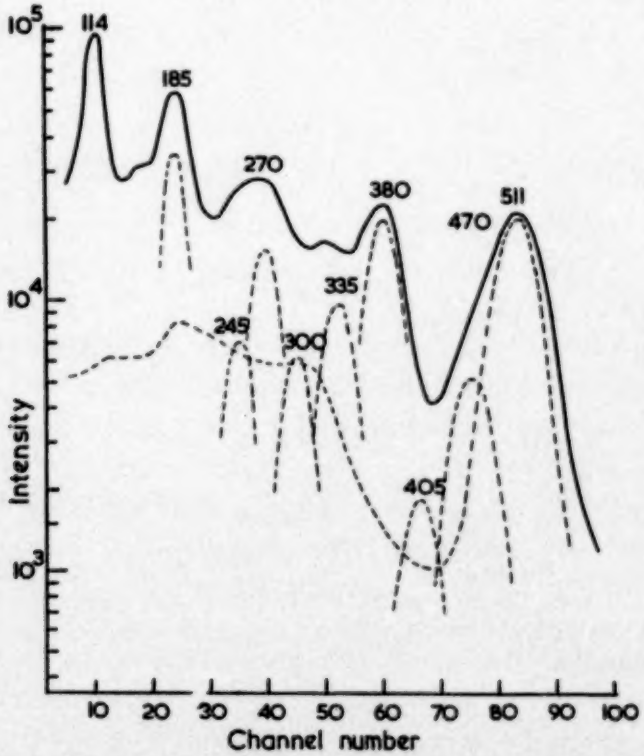

Fig. 2. Gamma ray spectrum of ^{66}Ge in the region from ≈ 100 keV to ≈ 600 keV.

In this manner the contribution of ^{67}Ge and its decay product ^{67}Ga was indeed reduced to negligible proportions. On the other hand, some ^{69}Ge was always present and its contribution led to some difficulties in the analysis of the high energy gamma ray spectrum and in the determination of the positon spectrum.

For this reason the direct gamma and beta ray spectra and the coincidences were also measured with ^{66}Ge sources produced by irradiation of Zn, in the form

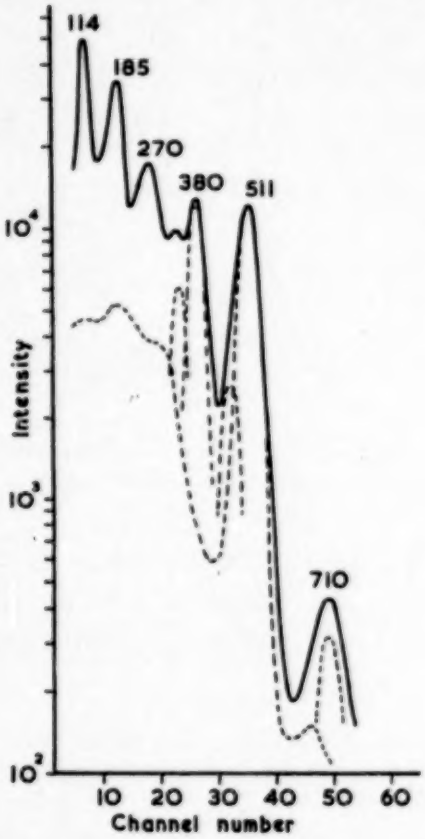

Fig. 3. Part of the gamma ray spectrum of ^{66}Ge involving the weak 710 keV gamma ray. The tail of the 511 keV peak due to annihilation in flight of the positons and the backscattering coincidences (see ref. [4])) is also shown.

of ZnO, enriched in mass 64 (composition: Mass 64 : 96.64 %, 66 : 2.60 %, 67 : 0.06 %, 68 : 0.73; impurities < 0.2 %). In this way the contribution of ^{69}Ge in the energy region of interest was reduced to less than 1 % at the start of the measurements.

The various spectra were measured with scintillation detectors (NaI(Tl) and stilbene crystals) optically coupled to DuMont photomultipliertubes, and displayed on the 100-channel RIDL analyser. Figs. 1, 2 and 3 show the experimental gamma ray spectra for three different energy regions, as obtained with the enriched sources. The analysis was performed in the usual way [4, 5]), taking into account the small contributions of ^{69}Ge and ^{66}Ga. Only one weak gamma ray

due to the decay of ^{66}Ge was found in the region above the annihilation peak, the major part of the analysed spectrum being due essentially to ^{69}Ge and ^{66}Ga (see fig. 3).

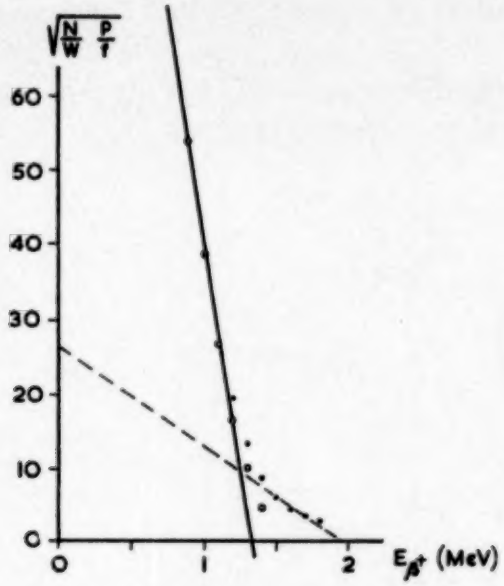

Fig. 4. Fermi-Kurie diagram of the positon spectrum from ^{66}Ge. The contributions due to ^{66}Ga and ^{69}Ge have been subtracted.

Fig. 4 shows the Fermi-Kurie plot of the positon spectrum of a source obtained from enriched ^{64}Zn, as measured with a stilbene crystal (diameter 4 cm, thickness 1 cm). A small initial contribution of ^{66}Ga was taken into

TABLE 1

Gamma rays in the decay of ^{66}Ge

^{66}Ge from ^{64}Zn(42 MeV α, 2n) chem. $T_{\frac{1}{2}} = 2.4 \pm 0.2^{h}$. Scin			
Energy (keV)	Intens. (γ/100 β^+)	Energy (keV)	Intens. (γ/100 β^+)
46± 2	60±5	300±10	10±5
68± 2	18±2	335± 8	31±3
114± 2	36±3	380± 8	78±6
152± 4	≈2	405±10	10±3
185± 4	37±3	470±10	31±3
245± 5	11±3	$\gamma^{\pm}$	200
270±10	31±3	710±10	4±1

TABLE 2

Beta ray branches

Energy (MeV)	Relative intensity
1.3±0.1	100
2.0±0.2	<10

account and subtracted. The total spectrum consists of a strong branch of maximum energy 1.3±0.1 MeV; a higher energy branch is also present with maximum energy of 2.0±0.2 MeV and a relative intensity of less than 10 %. Scattering effects prevent our making definite statements on the possible existence of positon groups with maximum energy below ≈ 800 keV.

The results of these measurements are collected in tables 1 and 2. The half-life reported there is an average value obtained from the decay of the different

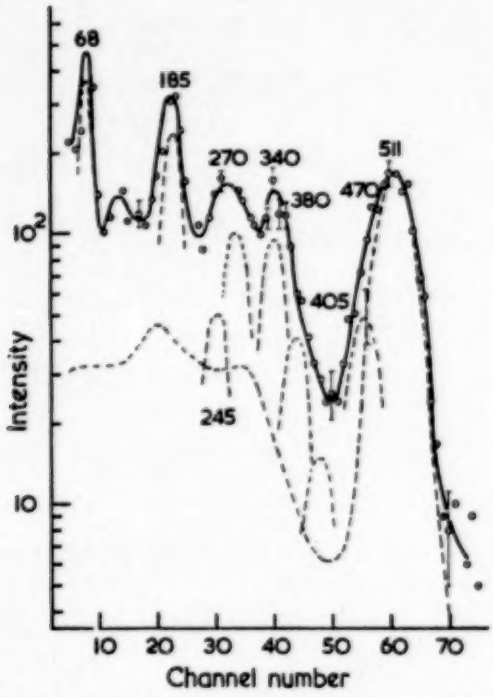

Fig. 5. Pulse height distribution of gamma rays in coincidence with the 46 keV photopeak. The analysed peaks are shown as dashed curves, no corrections have been made in this graph for Compton contributions to the coincidences.

gamma rays and from the beta ray spectrum. The decay was followed for at least 20 hours; and the contribution of ^{66}Ga was calculated at the different times from the known genetic relationship and subtracted.

Gamma-gamma coincidences with ^{66}Ge sources produced from natural Zn and from enriched ^{64}Zn were measured with a conventional fast-slow coincidence set up (fast resolving time $2\tau = 2\times10^{-8}$ sec), by selecting a given photopeak in a single-channel analyser and displaying the gamma ray spectrum in coincidence on the 100-channel analyser. Figs. 5, 6 and 7 show the different gamma ray spectra in coincidence with the selected 46, 68 and 114 keV gamma rays respectively. The results are collected in table 3. Coincidences with the 185 keV gamma ray were also measured, but owing to the fact that this gamma ray is superimposed on the backscattering peak of the annihilation radiation and on the Compton distributions of the strong 380 and 340 keV gamma rays,

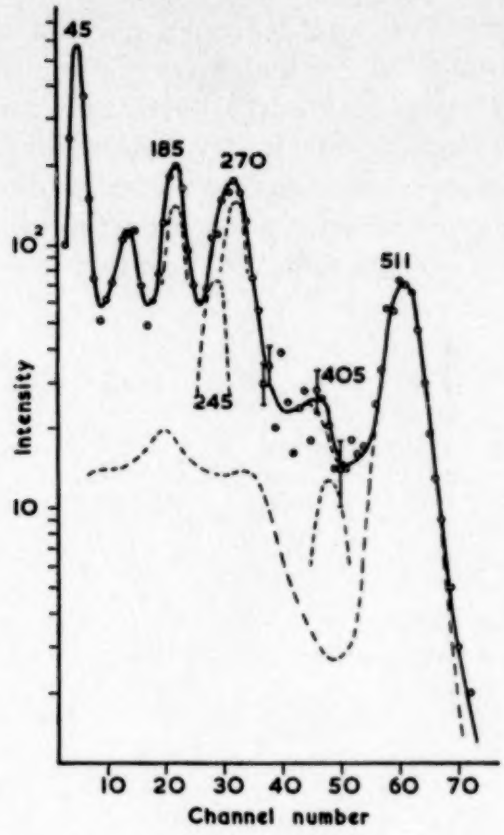

Fig. 6. Coincidences with the 68 keV photopeak.

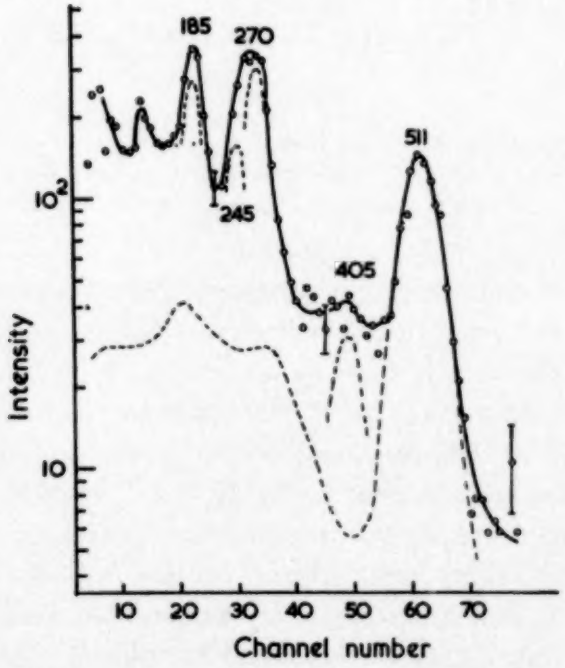

Fig. 7. Coincidences with the 114 keV photopeak.

the interpretation in this case was inconclusive. The results collected in table 3

for this case should be regarded only as indications for possible coincidences.

TABLE 3

Gamma-gamma coincidences [a])

Energy (keV)	46	68	114	185
46	no	30 %	no	yes
68	100 %	no	no	yes
114	no	no	no	yes
185	55±15 %	20± 5 %	27± 8 %	no
245	55±15 %	40± 8 %	60±14 %	
270	45±10 %	35± 6 %	55±12 %	yes
335	88±15 %	no	no	yes
380	20± 7 %	≲15 %	≲15 %	yes?
405	55±10 %	40±10 %	50±10 %	no
470	90±15 %	no	no	no
$\gamma^{\pm}$	61± 7 %	15± 2 %	20± 3 %	yes

[a]) Corrections for Compton contributions have been applied. The percentages refer to the fraction of the intensity of each gamma ray which is in coincidence with the respective gating peaks.

3. Discussion

The spin of the even parent nucleus ^{66}Ge is assumed to be 0^+, while that of the daughter nucleus ^{66}Ga has been measured [6]) to be 0, and the parity is almost certainly even. The total decay energy of ^{66}Ge amounts to $E_e \approx 3.0$ MeV, according to beta decay energy systematics [7]). Therefore the weak positon branch of 2.0±0.2 MeV reported above leads to the ground state of ^{66}Ga or to states with an excitation energy below ≈ 200 keV. The small intensity of this branch ($\log ft = 6.8$) might indicate a first forbidden transition. However, it is known that the direct beta transition between the ^{66}Ga ground state and that of ^{66}Zn, which is also of the type $0^+ \rightarrow 0^+$, has $\log ft = 7.8$. Therefore it seems that the beta transitions between the three respective ground states, which are forbidden both on Gamow-Teller and on Fermi selection rules, proceed only by virtue of small isobaric spin admixtures in the $T = 1$ (^{66}Ge), $T = 2$ (^{66}Ga) and $T = 3$ (^{66}Zn) states.

The strong 1.3 MeV positon group has $\log ft \approx 5$, is evidently allowed and must proceed to levels above ≈ 500 keV with spin 1^+ (or 0^+). Assuming no other positon branches and, at most, weak capture transitions to higher levels, the calculated total capture to positon ratio becomes 1.45±0.20.

The energy values of and the coincidence relations between the three gamma rays of lowest energy prove unambiguously that they form a cascade and cross-over structure originating from a level at 114 keV and branching through a level at 46 keV. In view of the intensities of these gamma rays it is impossible to place this structure anywhere in the decay scheme except directly on the ^{66}Ga ground state.

In order to calculate total transition rates, corrections for internal conversion should be applied. Since the ground state of ^{66}Ga is known to have a spin zero, all transitions ending on this ground state are pure multipoles. It follows that the 46 keV gamma ray is a pure dipole transition ($\alpha_{tot} = 0.62$), since the assumption of a quadrupole transition ($\alpha_{tot} = 12$) would make it completely impossible to establish an intensity balance with the positon and capture intensities. The spin of the 114 keV level can only be 1 or 2. If it is 2, the conversion electron intensity of the 114 keV quadrupole transition ($\alpha_{tot} = 0.43$) is so large that it leads to serious difficulties in establishing an intensity balance for the 114 keV level (some gamma rays are excluded from feeding the 114 keV level on the basis of the coincidence results and population by positons is known to be weak), even if the 68 keV transition is assumed to be a pure dipole.

TABLE 4

Relative intensities of the lower energy transitions corrected for internal conversion

Energy (keV)	Photon intensity	Theoretical α_{tot}		Multipolarity	Total intensity [a])
		M1	E2		
46	60±5	0.62	12.2	M1	97±8
68	18±2	0.20	2.9	(90±10)% M1 + (10±10)% E2	26±6
114	36±3	0.05	0.43	M1	38±3

[a]) Relative to 100 positons, see table 1.

The spin of the 114 keV level is therefore also 1. The 68 keV transition can still be a mixture of dipole and quadrupole, but the same arguments as used above exclude more than 20 % quadrupole admixture. Theoretical and emperical estimates [8]) of the dipole-quadrupole ratio are not conclusive in this case, since some of the possible nucleon configurations for the ^{66}Ga levels (see below) may cause an *l*-forbidden dipole part. It has therefore been assumed that the 68 keV transition contains (10±10) % quadrupole admixture. Nothing can be said about the parities of the two lower excited states from the gamma ray studies, but shell model considerations strongly suggest even parity, limiting the various transitions to M1 and E2. The photon intensities, theoretical conversion coefficients [9]) and total transition intensities for the three lower energy gamma rays are listed in table 4. (Corrections for conversion of the other gamma rays are negligible for dipole and quadrupole transitions).

On the basis of the knowledge about the 46, 68 and 114 keV transitions, the spectra coincident with these three gamma rays can be compared with the total gamma ray spectrum by normalizing the intensity of the relevant gamma ray in the coincident spectrum (corrections for Compton contributions have been applied) to that in the direct spectrum with the appropriate factor (e.g.

the 68 keV gamma ray should be 100 % coincident with the 46 keV one, the 46 keV gamma ray should be 30 % coincident with the 68 keV one, the coincidences with the 114 keV gamma ray can be normalised by means of the relationships in the 270—46 and 270—68 keV coincidences). In this manner the percentage of each gamma ray, coincident with each of the three lower energy gamma rays, was determined; these numerical results ar also collected in table 3. Although the data on the 152, 300 and 710 keV gamma rays are inconclusive, those on the other gamma rays can be interpreted in the following manner. The total intensity of the 68, 245, 270, 335, 405 and 407 keV gamma rays, passing through the 46 and the 114 keV transitions is $\approx$ 100 % of the gamma ray intensity in the direct spectrum (within the error limits). This therefore implies that all of these are involved in gamma ray cascades through intermediate levels which do not show appreciable branching directly to the ground state. The only important transition which does not belong to this structure is the 380 keV gamma ray and its position in the decay scheme will be discussed later.

It is safe to conclude that the 185 keV transition is partly involved in a cascade that reaches the ground state bypassing the 114 and 46 keV levels, while some of the levels fed by the positon branches show a similar behaviour.

The 68, 335 and 470 keV transitions are not present in the coincidences with the 68 and 114 keV gamma rays, so they lead directly to the 46 keV level. The intensity balance with the 46 keV transition requires that the three gamma rays populate the 46 keV level in parallel, since no additional strong positon feeding is observed. Levels are thus present at 380 ± 8 and at 515 ± 10 keV.

The 270 and 405 keV transitions fit between these new levels and the one at 114 keV and their coincident intensities are in agreement with such a position. Although the error on the coincident intensities of the 245 keV transition is somewhat large, it must also be placed in this class of transitions, giving a level at 360 ± 6 keV; this also improves the intensity balance for the 114 keV level. The weak 152 keV line now fits between the 360 and 515 keV levels, although any other position would not affect the above conclusions.

The strong 185 keV transition must be placed between still higher levels since its coincident intensities show that it reaches the 46 and 114 keV levels through a cascade with branching. The most acceptable position is on top of the 380 keV level in view of the branching ratio from this level, although the 515 keV level cannot be completely excluded on this argument alone. However, the coincidences with the 185 keV gamma ray as gating peak exclude the second possibility. (The 185 keV transition is in coincidence with a broad peak at $\approx$ 250 keV, which then should be interpreted as being the 270 keV line).

The level scheme constructed so far (see fig. 8) is almost unambiguously fixed by the energy and intensity values of the gamma rays and the coincidence relations between them. No important change would result from addition of

the weak 300 and 710 keV gamma rays anywhere in the level scheme. The energy balance requires 135 ± 16 units of positons plus capture whereas the amount calculated from the energies and intensities of the two positon branches is 145 ± 20 units. However, the strong 380 keV transition still has to be incorporated into the scheme.

The coincidences with the 185 keV and the 46 keV peaks, show that the 380 keV transition must be at least double. A plausible solution would be to assume a level at 760 keV as the origin of the major part of the 380 keV peak, feeding a

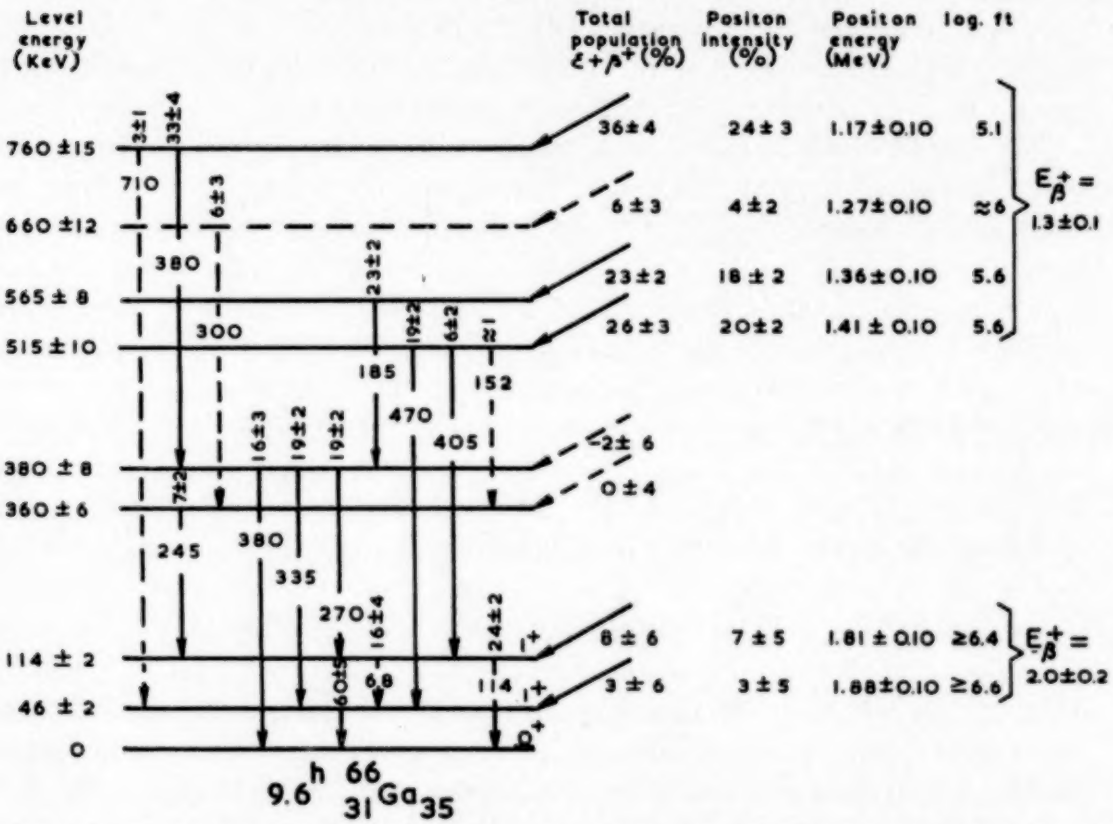

Fig. 8. Proposed level scheme for ^{66}Ga. The numbers at the origin of each gamma ray give the total transition intensity (photons plus conversion electrons) in % per decay.

level at 380 keV, which decays by three parallel gamma rays of 380, 335 and 270 keV. Intensity balance arguments for the 380 keV level (excluding direct feeding of the level by a positon branch) require that the intensity of the upper member be 52 ± 6 units, that of the lower member 26 ± 4 units. This interpretation can explain the number of positons found in coincidence with the three lower energy lines, and it is in agreement with the fact that most of the positons have an energy indicating population of levels above $\approx$ 500 keV. It also explains the fact that coincidences have been observed between the 380 keV gamma ray and the 185 and 46 keV transitions and it yields a satisfactory intensity balance between the number of gamma transitions to the ground state (160 ± 15 units)

and the number of decays of ^{66}Ge calculated from the positon branches (145 ± 20 units). The agreement is less satisfactory if one considers the fractions of the 185 and 380 keV gamma rays passing through the 46 and 114 keV transitions, but this probably reflects the difficulties in the normalization and the analysis of the rather complex coincident spectra.

The decay scheme in fig. 8 has been constructed on the basis of the above discussion. The weak 710 keV transition has been assumed to originate at the 760 keV level, the one of 300 keV has arbitrarily been placed on top of the 360 keV level (for convenience in calculating the beta branches). The percentages of all transitions, as reported on the decay scheme, have been calculated by normalising the total intensity of all transitions ending on the ground state to 100 % of the decays (direct positon feeding of the ^{66}Ga ground state has been neglected). The energies and intensities of the various positon and capture branches have been calculated under the assumption that the observed 1.30 MeV positon group corresponds to the weighted average of the four branches indicated on the decay scheme; theoretical ε/β^+ ratios for allowed transitions have been used in the calculations. A total decay energy of $E_e = 2.95 \pm 0.15$ MeV is derived on the basis of this decay scheme.

The spin of the ground state of ^{66}Ga is known to be 0^+, those of the two lower levels are 1^+, and those of the three levels fed by the three major positon branches must be 0^+ or 1^+.

The 31st proton and the 35th neutron in ^{66}Ga can occupy the $p_{\frac{1}{2}}$ and $f_{\frac{5}{2}}$ single particle states. Two 0^+ and four 1^+ states can be constructed with the two nucleons in these states. Many more states with these same spin values can be expected if the paired nucleons are distributed over the $p_{\frac{1}{2}}$ and $f_{\frac{5}{2}}$ states in various ways or if the $p_{\frac{3}{2}}$ single particle state is involved. If the observed levels in ^{66}Ga belong to these different configurations, the absence of some of the possible gamma ray transitions can be understood, since in some cases these transitions can only take place if more than one nucleon changes its state. Moreover, *l*-forbidden M1 transitions are known to occur in this mass region. Therefore, the decay characteristics of the various levels in ^{66}Ga are not in disagreement with general expectations.

The authors would like to thank Prof. Dr. P. C. Gugelot, Prof. Dr. A. H. W. Aten Jr. and Prof. Dr. A. H. Wapstra for their interest in this work, Mrs. M. Lindner-Groen for performing the chemical separations and the personnel of the synchro-cyclotron for the various irradiations.

This work forms part of the research program of the "Stichting voor Fundamenteel Onderzoek der Materie (F.O.M.)", which is financially supported by the "Nederlandse Organisatie voor Zuiver-Wetenschappelijk Onderzoek (Z.W.O.)". One of the authors (R.K.G.) is indebted to the Egyptian Atomic Energy Commission for a grant.

References

1) H. H. Hopkins Jr. and B. B. Cunningham, Phys. Rev. **73** (1948) 1406;
H. H. Hopkins Jr., Phys. Rev. **77** (1950) 717
2) R. A. Ricci and R. van Lieshout, Nuovo Cim. **4** (1956) 1592
3) R. A. Ricci and R. van Lieshout, Nuclear Physics **10** (1959) 360
4) R. K. Girgis, R. A. Ricci and R. van Lieshout, Nuovo Cim. **11** (1959) 156
5) R. K. Girgis, Thesis, University of Amsterdam (1959);
R. K. Girgis and R. van Lieshout, Physica **25** (1959) 133
6) J. L. Worcester, W. A. Nierenberg, R. Marrus, J. C. Hubbs, Bull. Am. Phys. Soc. **2** (1957) 383, K2
7) K. Way and M. Wood, Phys. Rev. **94** (1954) 119
8) A. H. Wapstra, G. J. Nijgh, R. van Lieshout, Nuclear spectroscopy tables (North-Holland Publishing Company, Amsterdam, 1959)
9) M. E. Rose, Internal conversion coefficients (North-Holland Publishing Company, Amsterdam, 1958)

2.L

Nuclear Physics **21** (1960) 189—195; © *North-Holland Publishing Co., Amsterdam*

Not to be reproduced by photoprint or microfilm without written permission from the publisher

ELASTIC SCATTERING OF 24.4 MeV DEUTERONS BY PROTONS

W. T. H. VAN OERS and K. W. BROCKMAN, Jr.

Instituut voor kernphysisch Onderzoek, Amsterdam

Received 4 July 1960

Abstract: The differential cross section for the elastic scattering of 24.4 MeV deuterons by protons (equivalent to 12.2 MeV p—d scattering) has been measured at angles between 15° and 170° in the centre of mass system with an overall accuracy of the order of 3 %. The measurements stand in good agreement with recent measurements near 10 and 14 MeV and show the same apparent disagreement with the theory of Christian and Gammel in the Coulomb-nuclear interference region.

1. Introduction

Elastic scattering of nucleons by deuterons is by now an oft repeated experiment [1–7]), but the great attention it has drawn is justified by the theoretical importance of the problem. Since only three bodies are involved, it may be hoped that techniques will evolve, which will describe the interaction in detail from the point of view of nucleon-nucleon forces. Then, these experiments may give specific information on the details of nuclear forces. For the kinds of analysis that may be required (for example, determinations of nuclear phase shifts directly from cross section data), it is important that there be an abundance of data from various sources and at various energies.

The interaction has been treated theoretically in the region 1—14 MeV by Christian and Gammel [8]), who were able to obtain good fits to the data existing at the time of their work. For the case of proton-deuteron scattering, the highest energy at which a comparison with experiment was made was for the data at 9.7 MeV [3]). Recent measurements in Japan at 10.14 MeV and 13.93 MeV [8]) show a systematic deviation from the 9.7 MeV work. They also appear to disagree with the theory of Christian and Gammel [8]) in the region of Coulomb-nuclear interference occurring between 15° and 30°. There the theory gives a sharper dip in the cross section than is observed experimentally. The present data, which are at effective proton bombarding energy of 12.2 MeV, seem to agree quite well with the Japanese measurements and thus corroborate the apparent disagreement with theory.

2. Experimental Procedure

The way this experiment is usually done is to use protons as the incident particles and deuterium as the target. We have adopted the reverse procedure

and bombarded a hydrogen target with deuterons. When deuterons are the incident particles, twice the incident energy is required to reach the same centre of mass energy as when protons are incident. Thus, while our incident deuteron energy was 24.4 MeV, our experiment is equivalent to 12.2 MeV p—d scattering.

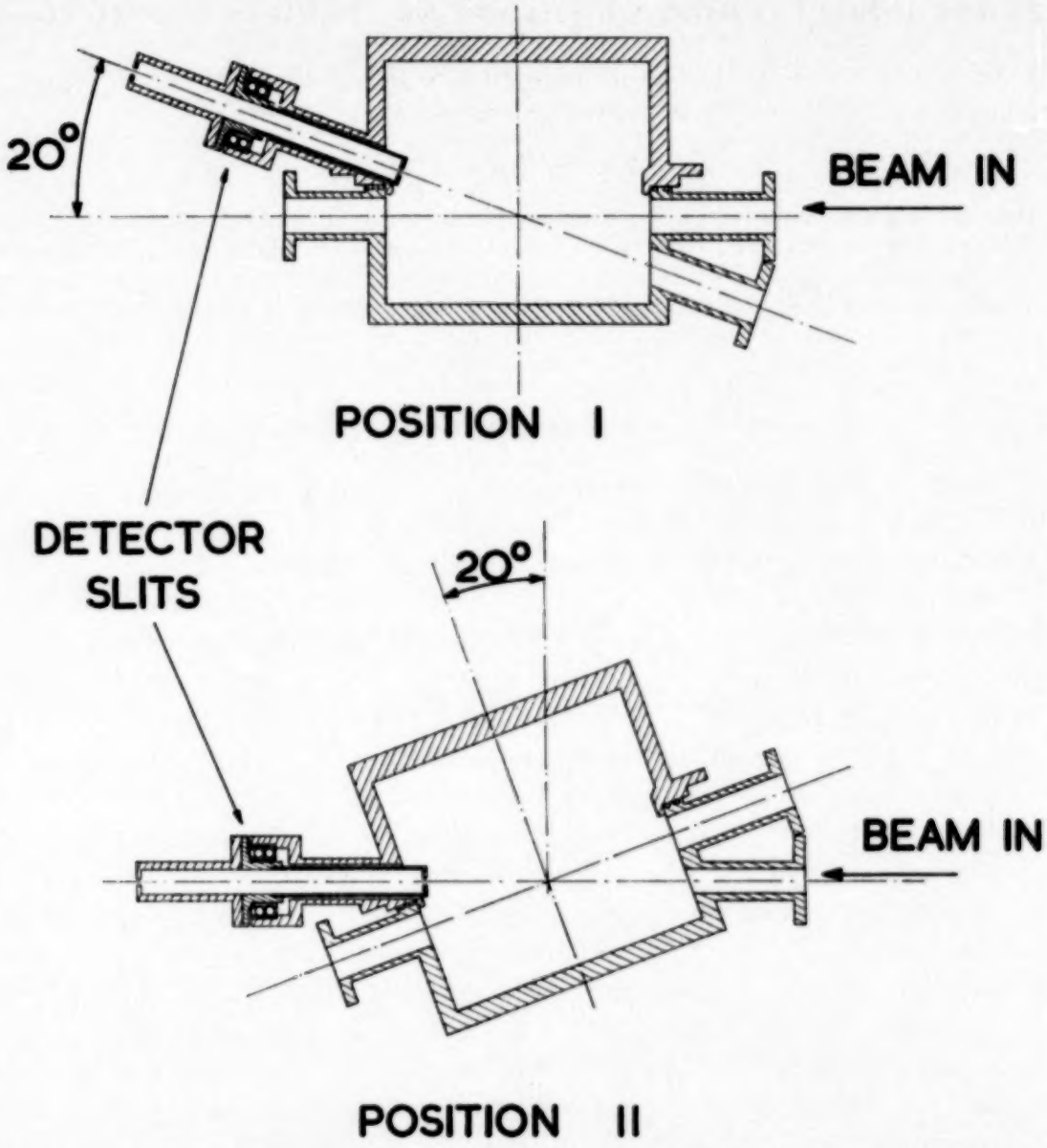

Fig. 1. Scattering chamber. Two orientations of the chamber with respect to the incident beam are shown.

Deuterons of the external beam of the Amsterdam synchrocyclotron were focused by a pair of quadrupole magnets on to the beam defining collimators of a scattering chamber placed about 20 m from the cyclotron. Fig. 1 shows schematically the scattering chamber used. This type of chamber is rather common now-a-days. The particle beam passes across the lower half of the chamber,

while detection apparatus is attached to the upper half or lid. A continuous variation of scattering angle is achieved by rotation of the lid. Normally the chamber is used in position 1, in which the beam emerges from a port at the rear side of the chamber. Using the chamber in this position allows the beam to be caught in a faraday cup for current integration, but the minimum scattering angle is limited to 20°. In the present experiment, where the velocity of the centre of mass is especially large, laboratory angles below 20° are extremely important. Most of the measurements were done therefore with the chamber tilted to position 2, in which one may scatter at any angle down to zero, but in which reliable current integration is not possible. Measurements done in this position were normalized to each other by use of a monitor counter observing scattering from the gas target at a fixed angle of 20°.

With this chamber, the scattering angle could be set with an accuracy of a tenth of a degree. The axis of the particle beam in the chamber could be found with the same accuracy in both horizontal and vertical planes.

The scattering chamber was filled with hydrogen gas at pressures ranging between 20 and 50 cm of mercury. Commercially available hydrogen gas of 99.9 % purity was used. The impurities were oxygen and water vapor, each to the extent of about 0.05 %.

The thickness of the gas target and the counter solid angle were determined in the usual manner by a pair of slits in front of the counter. These slits consisted of a circular hole directly before the counter and a rectangular slit about three quarters of the way to the scattering centre. When a scattering chamber of this type is used, the requirement that the rectangular slit be perpendicular to the plane of scattering requires rotation of this slit as the scattering angle is changed. The system to provide this rotation is indicated in fig. 1.

During the experiment, the distances of these counter slits from the scattering centre were kept constant (41.8 ± 0.1 cm from the circular slit to the centre and 31.3 ± 0.05 cm between the slits), while the widths of the slits were varied to accommodate counting rates and requirements of angular resolution. The diameter of the hole before the detector and the width of the rectangular slit were normally set to be the same; the values used varied from 2 to 15 mm. The slit dimensions were measured with a travelling microscope with an accuracy of the order of 0.25 % or better.

Copper slits were normally used except at the smallest angles, where the rectangular detector slit and the final beam collimation slit were replaced with graphite slits. Using lower Z material for these slits reduced the amount of double slit edge scattering into the detector. This effect provided a serious background problem at very small scattering angles, where it was not possible to construct an efficient anti-scattering baffle and simultaneously satisfy the requirements of gas scattering geometry.

Scattered deuterons and protons were detected in a CsI scintillation counter

and pulse height spectra were recorded with an RCL 256-channel kicksorter. In most runs, background spectra for subtraction were obtained by placing a sufficiently thick absorber in front of the detector to stop protons and deuterons. For small laboratory angles ($\theta \leqq 12°$) the double slit edge scattering previously mentioned also contributed to the background. In order to eliminate this latter background, we observed the spectrum at a particular laboratory angle at two different target gas pressures. From two such runs, the part of the spectrum due to only the target gas could be extracted.

Measurements were made for laboratory angles up to 60°. For greater angles, the recoil proton peak could not be resolved from the background with the desired accuracy. The observation of deuterons was kinematically limited to angles less than 30°. At angles less than 30°, deuterons emerge from the scattering centre at two different energies. The higher energy group consists of deuterons scattered at angles less than 120° in the centre of mass system, while the lower group consists of those scattered at centre of mass angles greater than 120°. Only those deuterons of the higher energy group were observed. The low energy deuterons either fell in the background or stopped in foils on the way to the counter. The smallest laboratory angle at which measurements were made was 5°.

At certain angles the peak of the pulse height spectrum corresponding to the scattered deuterons overlapped that of the recoil protons. In this case, an auxiliary run was made, in which absorbing foils were placed in front of the counter and a separation of the peaks was achieved due to the difference in energy loss of protons and deuterons. The same procedure was used, with account being taken of the spectral distortion introduced by the foils, when the deuteron peak overlapped a part of the proton continuum resulting from disintegration of the deuteron.

As previously stated, most of the runs were done with the chamber in the tilted position (position 2), and using a monitor counter allowed us to obtain a relative differential cross section curve. To obtain the absolute cross section, certain angles greater than 20° were remeasured with the chamber in position 1 and with current integration. For these angles a ratio of the absolute to relative cross section was obtained. A statistically weighted average of the values of this ratio was used as a multiplication factor to convert the relative cross sections to an absolute scale.

During runs, the beam energy was determined by comparing the positions of the elastic proton peak at various angles with the shifted positions of these peaks, when an aluminium absorber was placed in front of the counter[9]). A series of such runs yielded the incident energy with an accuracy of approximately 1 %. The obtained value was in good agreement with the value found by other methods. The mean energy of the beam was found to vary slightly throughout the period of measurements. The magnitude of this effect was estimated to be

of the order of 150—200 keV. Considering this variation and the uncertainty of the energy measurement, the best value to be quoted for the incident deuteron energy is 24.35 ± 0.35 MeV.

3. Results

The absolute differential cross section converted into the centre of mass system is reported in table 1. The third column indicates whether the observed

TABLE 1

Differential cross sections for elastic p—d scattering in the centre of mass system for 24.35 ± 0.35 MeV incident deuterons. The last column of the table gives only the relative error for each point. An estimate of the absolute error is given in the text.

θ (degrees)	$\frac{d\sigma}{d\Omega}$ (mb · sr^{-1})	observed particle	error (%)	θ (degrees)	$\frac{d\sigma}{d\Omega}$ (mb · sr^{-1})	observed particle	error (%)
15.2	126.8	d	4.1	113.9	15.0	p	1.8
18.0	119.8	d	3.8	113.9	14.8	p	1.9
20.8	119.8	d	3.5	119.1	13.0	p	2.4
23.6	120.9	d	3.3	123.0	11.5	p	2.7
26.4	118.0	d	3.2	126.7	12.7	p	3.2
29.2	116.6	d	3.0	126.7	12.9	p	2.7
32.0	115.4	d	3.1	130.5	14.4	p	2.4
35.3	114.5	d	2.5	130.5	14.6	p	3.5
35.3	112.7	d	2.5	134.2	19.7	p	2.2
41.3	101.2	d	2.3	138.0	24.0	p	2.2
47.2	92.5	d	2.1	141.7	34.7	p	2.1
53.2	84.9	d	1.8	145.5	48.5	p	2.0
59.9	76.5	d	1.7	149.3	53.6	p	2.3
66.7	67.0	d	1.6	153.0	66.2	p	2.4
74.2	56.1	d	1.5	156.8	84.1	p	2.5
74.7	57.8	p	1.3	156.8	87.2	p	2.5
76.5	53.4	p	1.4	158.8	91.2	p	3.7
80.3	48.3	p	1.2	160.5	99.1	p	3.0
81.5	44.2	d	1.8	160.5	100.4	p	2.8
81.5	42.5	d	1.4	160.5	100.8	p	2.8
85.8	41.5	p	1.3	160.7	100.9	p	3.3
91.3	34.6	p	1.4	162.5	107.1	p	3.5
96.9	28.6	p	1.5	164.2	114.9	p	4.4
102.5	23.2	p	1.6	164.2	115.2	p	4.4
108.1	18.7	p	1.7	164.3	115.9	p	3.5
108.3	18.0	p	3.9	166.2	123.6	p	3.6
108.3	17.9	p	1.8	168.0	129.7	p	3.9
113.7	15.1	p	1.8	169.9	135.0	p	4.2

particle was a proton or a deuteron and the last column gives the total error for the relative differential cross section. The total error in the multiplying factor used to convert all measurements from relative to absolute cross section is estimated to be 3 %.

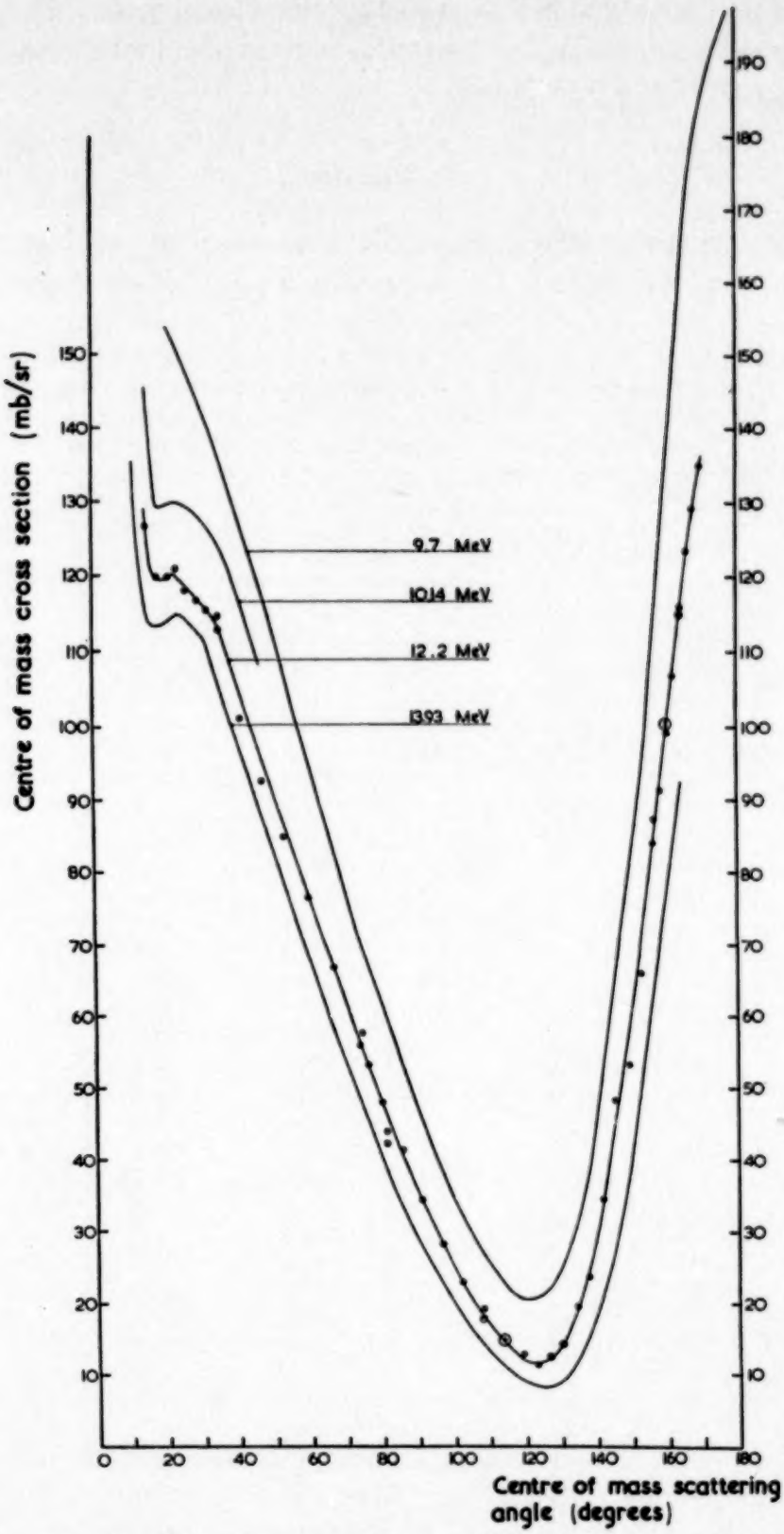

Fig. 2. Centre of mass differential cross section for elastic scattering at several energies. The curve labeled 12.2 MeV shows the results of the present work.

Two additional corrections were applied to the data. The first of these was for the effects of finite geometry using the formula of Critchfield and Dodder [10]). The second correction was to account for the fraction of pulses lying in the tails of the elastic peaks. These tails arise from nuclear reactions of the counted particles in the scintillation crystal. The number of pulses in the tails must be estimated independently since their direct observation is obscured by low energy protons coming from the target. Service [11]) has measured the fraction of the total counts that will be lost from the main elastic peak into the tail for protons of various energies. We have estimated that the effect will be 1.5—2 times as great for deuterons. The correction that is applied increases with the energy of the detected particle, but in our case it amounted to about 0.8 % in the worst case. A rather conservative estimate of the error which might be introduced by an incorrect estimate of this correction was included in the errors quoted for the measured cross sections.

Fig. 2 shows the centre of mass differential cross section along with measurements at nearby energies. We draw attention to the great similarity of the shape of our curve in the Coulomb-nuclear interference region to that of the data at 10.14 and 13.93 MeV.

We would like to thank Prof. P. C. Gugelot for his interest and helpful criticism. The work was performed as part of the research program of the "Stichting voor Fundamenteel Onderzoek der Materie" (F.O.M.), which is financially supported by the "Nederlandse Organisatie voor Zuiver Wetenschappelijk Onderzoek" (Z.W.O.).

References

1) Sherr, Blair, Kratz, Bailey and Taschek, Phys. Rev. **72** (1947) 663
2) L. Rosen and J. C. Allred, Phys. Rev. **82** (1951) 777
3) Allred, Armstrong, Bondelid and Rosen, Phys. Rev. **88** (1952) 433
4) D. O. Caldwell and J. R. Richardson, Phys. Rev. **98** (1955) 28
5) V. J. Ashby, University of California, Radiation Laboratory, Report UCRL-2091 (1953) (unpublished)
6) J. H. Williams and M. K. Brussel, Phys. Rev. **110** (1958) 136
7) Kikuchi, Sanada, Suwa, Hayashi, Nisimura and Fukunaga, J. Phys. Soc. Japan (to be published)
8) R. S. Christian and J. L. Gammel, Phys. Rev. **91** (1953) 100
9) K. W. Brockman Jr. (to be published)
10) L. C. Critchfield and D. C. Dodder, Phys. Rev. **75** (1949) 419
11) D. H. Service, Annual Progress Report, University of Minnesota, (1958) (unpublished)

1.D.3

Nuclear Physics **21** (1960) 196—219; © *North-Holland Publishing Co., Amsterdam*

Not to be reproduced by photoprint or microfilm without written permission from the publisher

EXPERIMENTAL EVIDENCE FOR CLUSTER STRUCTURES IN LIGHT AND MEDIUM WEIGHT NUCLEI

RAYMOND K. SHELINE and KARL WILDERMUTH

Florida State University

Received 18 July 1960

Abstract: The assumption of this paper in accordance with the cluster model is that nuclei may be considered to be composed of clusters (single nucleons, H^2, He^3, H^3, He^4, etc.). Comparison of cluster model predictions and experimental level schemes are made for the nuclei Li^7, Be^7, C^{13}, O^{18}, F^{19}, Ne^{20}, Ca^{40} and Sc^{43}. It is shown that comparisons between the spectra of certain pairs of nuclei are particularly relevant from the viewpoint of the cluster model. Comparisons of the spectra of the following pairs of nuclei are made: N^{16}, O^{17}; F^{19}, Ne^{20}; K^{40}, Ca^{41}; and Sc^{43}, Ti^{44}. In addition the cluster model predicts levels of parity different than the ground state. The relative position of these nuclei are compared in nuclei in which the smallest cluster is varied from a single nucleon to larger clusters. This model further predicts that immediately after double closed-shell structures, nuclei with H^3 or He^3 clusters (e.g., F^{19}) will exhibit a strong decrease in this excitation energy. The negative parity states and first 0+ states in alpha-particle nuclei should decrease with increasing atomic number. These predicted systematics agree with the limited experimental data which are available but suggest the need for considerable additional data to further test the predictions. These results indicate substructures which are often more important than shell-model structures.

1. Introduction

This paper attempts qualitative interpretations and predictions of some of the experimental data for nuclei ($A = 7$—43) from the framework of the cluster model [1, 2, 3]). It is prompted by the belief that the cluster model should have a natural appeal to the experimentalist. It is a model which can be easily visualized because of its similarity to molecular systems, and which at the same time has the versatility which different nuclear models bring to bear on the problem of nuclear structure. The versatility of the cluster model in making more qualitative interpretations and often better quantitative interpretations may be explained as follows:

1) The indistinguishability of the nucleons, described by the antisymmetric character of the cluster wave functions, reduces or in some cases completely eliminates the differences between the different kinds of single particle and collective motions. This is the reason that the shell model with interaction very often contains collective features [4]).

2) The cluster model is formulated in such a way that for every single nuclear level and nuclear reactions, one can introduce a complete eigenfunction system, which is especially suitable for the description of this level or this

reaction. This suitable eigenfunction system can change from level to level and reaction to reaction [1] †.

This suitable choice of eigenfunction systems allows us to get a deeper physical insight into nuclear structure and nuclear reactions. In a very natural way with this method one can often see when and how one has to forsake the usual shell model description of the individual nuclear levels or nuclear reactions. To see this in more detail we shall discuss the low-energy negative parity spectrum of O^{16} from the point of view of the cluster model [3]).

Because it is energetically unfeasible, one assumes that in the low excited states of O^{16} no α-particle clusters are broken up. Therefore it is most convenient to choose a C^{12}—α-particle cluster representation for the description of these levels††.

We will use average oscillator potentials with the same frequency parameter ω for all cluster motions and for all motions of the nucleons inside the clusters †††. The ground state of O^{16} is then described by a 3s oscillation of the α-particle cluster relative to the unexcited C^{12} cluster. The corresponding cluster wave function (after complete antisymmetrization) coincides completely with the usual oscillator shell model wave function for the O^{16} ground state.

The lowest α-particle states of negative parity in O^{16} are described in the single particle oscillator shell model as a superposition of states in which only one nucleon is lifted up to the 2s or 1d subshell. Under these restrictions only three negative parity α-particle states with the spins $I = 3-$, $I = 1-$ and $I = 2-$ exist [3]). In the C^{12}—α-particle cluster representation these levels are described as 3p and 3f oscillations of the α-particle cluster relative to the unexcited and first excited C^{12} cluster. These three states are essentially identical with the three lowest negative parity states of O^{16} in the calculations of Elliot and Flowers [5]). The qualitative agreement with the three lowest experimentally measured negative parity levels of O^{16} is complete with respect not only to spin and parity, but also energy sequence.

It is of interest to consider now the next O^{16} level of negative parity ($I = 1-$). If one wants to describe this state as a superposition of single particle excitation states into the 2s and 1d subshell — as is done in the paper of Elliot and Flowers [5]) — then it necessarily follows that in this state an α-particle cluster is broken up. This is energetically very unfavored ‡.

† One can describe all nuclear levels and nuclear reactions by means of one eigenfunction system — for instance the single particle shell model eigenfunction system. Often the description then becomes extremely complicated and also physical insight into the problem is frequently lost. By using different eigenfunction systems one is doing in effect what is done in analytical geometry in introducing for every special problem the most convenient coordinate system.

†† The C^{12}—α-particle cluster representation is easier to handle than the 4 α-particle cluster representation which one could also use.

††† We will call this assumption "the oscillator assumption". Note that $a = M\omega/\hbar$ is the width parameter of the oscillator potential.

‡ In the calculations of Elliot and Flowers this state is separated by a clear gap from the three lowest O^{16} negative parity states. Therefore, it is impossible in their calculations to describe the 4th negative parity level of O^{16} as a $1-$ state as is indicated by the experiments.

Since this negative parity level lies only 3.44 MeV above the 2— negative parity level we prefer to assume that this is also an α-particle state, but with a higher order oscillation of the α-particle cluster relative to the C^{12} cluster than in the three lowest negative parity states of O^{16}. In the frame of the oscillator model, this negative parity state must have an excitation of three oscillator quanta†. For the lowest α-particle state of three oscillator quanta excitation one expects a 4p oscillation of the α-particle cluster relative to the unexcited C^{12} cluster. The angular momentum of this state must be $I = 1-$. This agrees with the angular momentum of the 4th negative parity level of O^{16}. Similar arguments apply to the negative parity levels of O^{16} of energy less than 12.78 MeV. (The 12.78 MeV level is the first level with $I = 1-$). The description of these levels in the frame of the cluster model also deviates completely from the usual shell model description. The explanations of the low energy spectra which we have sketched for the negative parity levels of O^{16} as a special example can be applied to many other low energy nuclear spectra.

If one calculates the energy distances of the O^{16} negative parity levels from the O^{16} ground state under the assumption that the average oscillator potentials for all cluster motions and internal motions of the nucleons inside the cluster have the same frequency parameter ω as the ground state ($\omega = e\hbar/M = 2.2 \times 10^{22}\text{sec}^{-1}$) and with two body forces which describe the low energy two-nucleon scattering data in a good approximation††, then one gets much too high excitation energies for these levels[3]). For the $I = 3-$ level one gets, for instance, 16.7 MeV excitation energy instead of the experimental value 6.14 MeV. This large discrepancy between calculated and experimental value is essentially due to the following two reasons:

First, the restoring force in the α-particle cluster C^{12} cluster oscillation is anharmonic in such a way that with increasing amplitude the oscillation frequency decreases.

Secondly, if the mean distance between the α-particle cluster and the C^{12} cluster increases, then the radius of the α-particle cluster becomes smaller. This comes from the fact that a free α-particle always has a smaller radius than an α-particle cluster in a nucleus†††. For convenience we will call this "the radius change effect".

Both effects decrease the excitation energy. Both of these effects influence in varying degrees all excitation energies of nuclear levels. To take into account both of these effects quantitatively we must necessarily deviate from the usual shell model calculations with interaction. This is true because in the shell

† In the language of the single particle model this means that one has to consider excitations of nucleons up to the 3s, 2d, 1g oscillator subshells and one, two, and three particle excitations.

†† These forces have no hard core.

††† The width parameter of a free α-particle is 4.7×10^{25} cm^2, whereas the width parameter of an α-particle cluster in O^{16} is 3.57×10^{25} cm^2.

model calculations with interaction one uses only one parameter which is always equal to the ground state frequency parameter. The quantitative consideration of these effects can be done at least approximately for the lowest excited levels of light nuclei ($A \leqq 12$) by a method which is described in ref. [3]).

Calculations have already been carried out for the low energy levels of Be^8, Li^7, and He^5, in spite of considerable complexity†. This complexity which will increase very quickly with increasing atomic weight dramatized the need for qualitative interpretations and predictions of the type we attempt in this research. In this way, without carrying out lengthy calculations we can observe significant cluster structure in nuclei and theoretically predicted effects, such as the deviation from the "oscillator assumption" (anharmonicity), the radius change effect, and the relationship of different cluster structures.

The procedure will be as follows:

I) We shall discuss some of the significant low-energy spectra of nuclei, whose general structure can be predicted by the cluster model by means of qualitative physical arguments.

II) Comparison will be made of parts of nuclear spectra which have similar cluster structures. This comparison depends in a first approximation only the similarity of the cluster structures in the compared states but not on the exact form of the nuclear wave functions. Therefore one can predict in these cases approximately the level distances of a part of the spectrum of a nucleus if one knows the corresponding level distances in the related nucleus. For instance, one can compare the low energy negative parity spectrum of F^{19} with the low energy positive parity spectrum of Ne^{20}. This kind of comparison is a good test for the cluster structure of certain nuclear levels.

III) We shall discuss the first excited levels with different parity than the nuclear ground state. We will be concerned with nuclei with an outside α-particle, triton, He^3, deuteron cluster or an outside neutron or proton††. The relative position of these levels is especially determined by the anharmonicity factor (deviation from the oscillator assumption discussed in the introduction). One expects in general that the anharmonicity effect increases from α cluster to triton cluster . . . to odd-nucleon cluster since the number of correlations which are included in the excitation mode decreases the anharmonicity of the restoring force†††. Another effect which here in general (exception F^{19}) plays a minor role is the radius change effect.

† The calculations are tedious even if one takes the most convenient cluster wave function system for the calculations. On the other hand, if one were to try to carry out these calculations with the usual single particle shell model wave functions, one would get completely lost.

†† We are only interested in states of changed parity in which the parity change comes essentially from the change of the relative oscillations of the α-particle, triton, etc., clusters, and not from the breaking up of these clusters.

††† In the shell model picture without residual interaction the distance of changed parity states above the ground state should be approximately the same regardless of cluster structure for all nuclei of approximately the same atomic weight.

IV) We shall compare the energies of the first excited 0+ levels in even nuclei. We again will observe the influence of the anharmonicity and radius change effect.

2. Spectra of Individual Nuclei

We will begin by indicating the nomenclature which we use for different modes of oscillation. They are schematically represented in fig. 1. The numbers to the left of the harmonic oscillator potential indicate the order of the oscillator

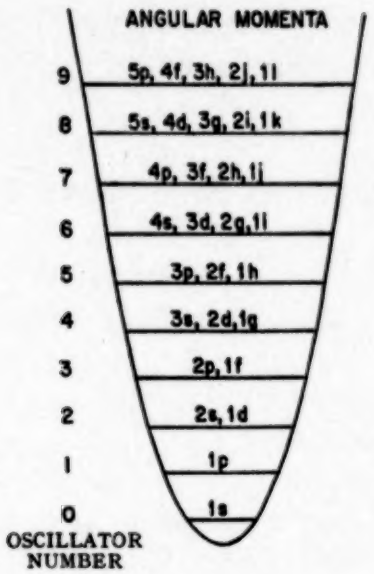

Fig. 1. Notation used in the oscillator assumption. For explanation see text.

excitation. The letters inside indicate the angular momenta and parity possible for a given oscillation. The number inside indicates the number of times this angular momentum has appeared up to this oscillation.

2.1. ENERGY LEVELS OF Li^7 AND Be^7

The experimental data on the nuclear spectra of Li^7 and Be^7 are shown in fig. 2. The cluster model representation of Li^7 and Be^7 is especially simple. It may be thought of as an α-particle cluster and a triton cluster in the case of Li^7, and an α-particle cluster and a He^3 cluster in the case of Be^7. In view of the large binding energy of the last nucleon in free triton (approximately 6.3 MeV) we may attempt to explain all states below 6 or 7 MeV in terms of these two simple undissociated clusters.

We must expect that the low-lying negative parity states in both Li^7 and Be^7 result from the relative motion of the triton or He^3 against the α-particle. This must be an oscillation of third order with $l = 1$ or 3 in accord with the Pauli

principle. (See subsection 2.2). The $l = 1$ configuration should give rise to the lowest state since in this configuration the clusters are closer to each other on the average. Therefore, due to the attractive nature of nuclear forces, the $l = 1$ configuration has a larger negative potential energy than the $l = 3$ configuration. The $l = 1$ configuration should give rise to a $\frac{3}{2}-$ ground state and a $\frac{1}{2}-$ first excited state, and the $l = 3$ configuration should give rise to the

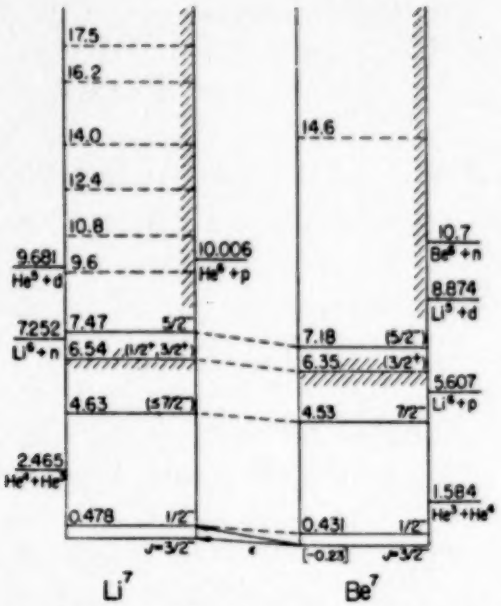

Fig. 2. Energy levels of Li^7 and Be^7. In figs. 2, 3, 4, 5 and 6 we have used the levels directly as presented in "The Light Isobars", by T. Lauritsen and F. Ajzenberg-Selove, (Joint Report of Haverford College and California Institute of Technology August 1959).

higher lying states with angular momentum-parity, $\frac{7}{2}-$ and $\frac{5}{2}-$ † in that order. The fact that the $\frac{3}{2}-$ state is the ground state and the $\frac{1}{2}-$ state, the first excited state, is the direct consequence of the two-body force spin orbit coupling. The splitting is in agreement with the spin orbit coupling splitting in He^5 and Li^6 [3]).

It is to be expected that the spin orbit splitting in Li^7 and Be^7 will be approximately one sixth that of the $I = 1$, $T = 0$ ($E_{exc} = 5.5$ MeV), and $I = 3$, $T = 0$ ($E_{exc} = 2.18$ MeV) levels in Li^6 ††. The spin orbit splitting is known to be

† From measurements of reduced width it appears that in the $\frac{1}{2}-$ state at 7.47 and 7.18 MeV in Li^7 and Be^7 respectively the triton and He^3 clusters are broken up [11]).

†† This can be explained roughly in the following way: in Li^7 and Be^7 the triton cluster moves around the nucleus with $1\hbar$ of relative orbital angular momentum. The odd proton whose spin is responsible for the total spin of the triton cluster therefore has an average angular momentum of $\frac{1}{3}\hbar$. On the other hand in Li^6 the total relative orbital angular momentum of the deuteron cluster in the mentioned states is $2\hbar$. Thus, each nucleon of the deuteron cluster contributes a factor of 3 to the splitting of these levels compared with the spin orbit splitting in Li^7. For a more detailed discussion see ref. [3]), p. 46 and p. 52. and ref. [6]).

3.3 MeV in Li^6. From these considerations we would have expected the splitting to be approximately 0.6 MeV in Li^7. The observed value is 0.48 MeV. Considering the roughness of the assumptions, the agreement is good.

2.2. ENERGY LEVELS IN C^{12}

For the description of the low lying states of C^{12} we can choose either a three α-particle or a Be^8—α-particle cluster representation. These representations are entirely equivalent. For our consideration we will use the last representation, that is a Be^8—α-particle cluster representation. The low lying excited states in C^{12} may be considered to be generated from cluster configurations in which neither the outside α-particle cluster nor the α-particle cluster in Be^8 is broken up. The ground state of C^{12} must then be represented as the Be^8 cluster in its ground state and the α-particle cluster in the 3s oscillation. To understand this we consider this state in C^{12} from the viewpoint of the one particle shell model representation. In this picture 8 nucleons must be in the 1p shell *as demanded by the Pauli principle.* (That means that these 8 nucleons have together 8 quanta of oscillation excitation). In the Be^8—α-particle cluster representation we have a fourth order excitation between the two alpha clusters in Be^8 [3]). Therefore we *must* also have a fourth order oscillation of the outside α-particle cluster relative to the Be^8 cluster. Only in this way can we have 8 quanta of oscillation excitation and therefore the same kinetic energy in both representations. This will give rise to a 0+ ground state for C^{12}. (See fig. 3.) Built on top of the 0+ ground state one expects to find the 2d, 1g oscillations given a 2+ and a 4+ state in this order (the penetrating orbit argument). The energy differences between the levels should approximate that of a ground state rotational band in an even nucleus. (See ref. [3]), p. 61).

One then expects to find a second 0+ level, the 4s oscillation of the α cluster against the Be^8 ground state cluster. Again one expects to find the superimposed 2+, 4+ and 6+ members of the rotational band (6th order oscillations). One is immediately struck by the fact that the second 0+ state is so low lying in C^{12}: 7.66 MeV; this is much lower than the 4+ level of the ground state band. In the framework of the simple shell model one must excite to the next higher oscillator shell with a consequent excitation energy of the order of 20 MeV or more. This large decrease in excitation energy of the second 0+ state is due to two effects as indicated in the Introduction. We repeat: The first effect is the anharmonic nature of the α-particle oscillation against the Be^8 cluster such that with increasing amplitude the oscillation frequency decreases. In the second place, in a higher oscillation state one can expect the mean distance between the α-particle and the Be^8 clusters to increase. This will result in a decrease in the radius of the α-particle cluster, since the α-particle cluster is now more nearly a free α-particle and the free α-particle has a smaller radius than the bound α-particle cluster. Since the interaction energy between the

Be^8 cluster and the α-particle cluster should change much more slowly than the internal energy of the α-particle cluster as its radius decreases, one can expect a considerable lowering in the excitation energy due to this effect.

In addition to the two positive parity rotational bands, one expects to observe a 2+ state which may be thought of as an α-particle cluster in a 4s oscillation against the first excited state of the Be^8 cluster. Such a 2+ level

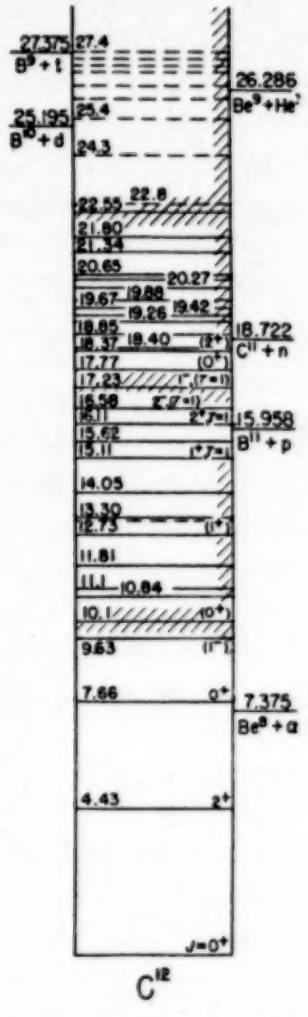

Fig. 3. Energy levels of C^{12}.

should lie approximately 2.9 MeV above the 0+ level of the second rotational sequence, this being the energy of excitation of the first 2+ state in Be^8. One also expects negative parity levels in C^{12}. These will involve 3p, 2f, and 1h oscillations of the α-particle against the ground state of the Be^8 cluster (5th order oscillations). Due to the penetrating orbit argument one expects the 5p 1− oscillation in C^{12} to be the lowest lying, followed by 3− and 5− levels. One might also expect these oscillations to couple with higher excited states of the Be^8 cluster. These configurations will give rise to negative parity states with

even as well as with odd angular momenta. The third broad 0+ level at 10.1 MeV may be explained as a still higher very anharmonic oscillation of the α-particle cluster against the Be^8 ground state cluster.

A detailed look at the spectrum of C^{12} (see fig. 3) shows that many of the states we have predicted have not as yet been found. Nonetheless the states which have been experimentally studied fit the cluster model rather well. It must be remembered that these predictions are less reliable at high energy where the α-particle itself can be broken up. At still higher energies ($E_\alpha \geqq 15$ MeV) one must refine the considerations to take into account also the broken up clusters. Experimentally it would therefore be very valuable to continue the search for the two positive rotational sequences and other positive and negative parity sequences suggested by the cluster model. It is particularly important to determine the spin and parity of the states at 9.63, 10.1, 10.84, 11.1, 11.81, 12.73, 13.30 and 14.05 MeV.

2.3. ENERGY LEVELS OF O^{16}

Fortunately the nuclear spectrum of O^{16} is more complete than the C^{12} spectrum. It is shown in fig. 4. One chooses for the description of the O^{16} state a C^{12}—α-particle cluster representation. Since O^{16} is a double closed shell nucleus, the 4th order oscillation gives rise, however, only to the 3s 0+ ground state and not to 2d and 1g oscillations. This is the result of the action of the Pauli exclusion principle and the indistinquishability of the nucleons. These principles act with a great deal of power for low lying states in which the outside neutron and proton shells are largely occupied, which means that a considerable intercluster penetration is present †‡.

One then expects to see a 2nd 0+ (6.06 MeV) state representing as before a higher order oscillation of the α-particle cluster against the C^{12} cluster. In this higher energy range, however, the Pauli principle is not so restrictive and one now expects to see the superimposed 2+ (6.92 MeV) and 4+ (10.36 MeV) states which were expected in C^{12}. As in C^{12}, one also expects to observe a 2nd 2+ (9.84 MeV) state (in C^{12}, a 3rd 2+ state). As before this represents a higher order α-particle oscillation against the first excited state of the C^{12} cluster. Before leaving the positive parity states we should mention that the 0+ state lies even lower in O^{16} than in C^{12} and is depressed far below what one would expect from the simple shell model. This difference between O^{16} and C^{12} can be anticipated because the radius change effect increases in general with atomic weight (especially with closed shell nuclei). See also ref. [3]), p. 63 and 81.

† For instance, after antisymmetrization the cluster wave function of the O^{16} ground state describes a completely spherically symmetric nucleus. Therefore, a ground state rotational sequence cannot exist.

‡ The fact that a cluster in nuclear matter can have a completely different behaviour than the corresponding free particle is a particularly transparent effect of the indistinguishability of the nucleons. (See ref. [3]), p. 58.)

One would expect the ratio

$$\frac{E(4+;\ 10.36\ \text{MeV})-E(0+;\ 6.06\ \text{MeV})}{E(2+;\ \ 6.92\ \text{MeV})-E(0+;\ 6.06\ \text{MeV})}$$

to be approximately 3 : 1. The experimental ratio actually observed is 5 : 1. The positive parity level sequence observed is however in complete agreement with the cluster model.

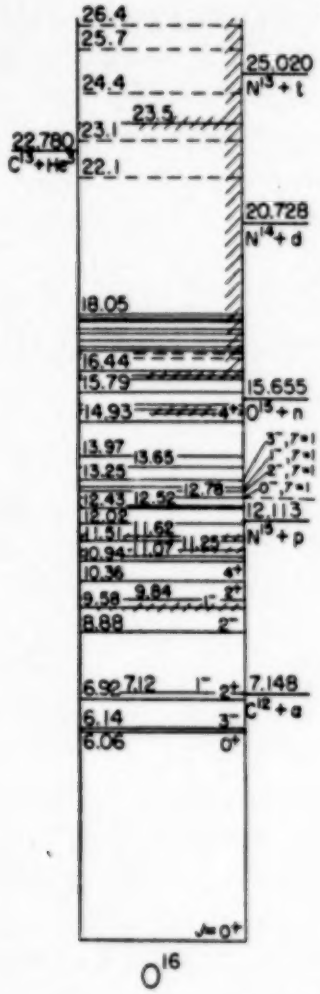

Fig. 4. Energy levels of O^{16}.

Now we come to the very interesting negative parity states of O^{16}. Since these states have been discussed in the introduction we shall only make a comparison with experiment and mention some additional facts. The 3−, 1−, 2−, 1− sequence predicted in the introduction is borne out by experiment. (See fig. 4.)

One would expect due to the penetrating orbit argument that the 1− state (a 3p excitation of the α-particle cluster against the C^{12} cluster ground state) lies lower energetically than the 3− state (a 2f oscillation of the α-particle cluster against the C^{12} ground state cluster). This is contrary to the experimen-

tal facts. The reason for this is that the penetration of the α-particle cluster and the C^{12} cluster is so great that the indistinguishability of the nucleons and the Pauli principle destroy this qualitative penetrating orbit argument. If one calculates in "the oscillator assumption" the excitation energies of these levels with the Serber force, they are degenerate. The spin orbit coupling lowers the 3— states below the 1— states. The negative parity levels of O^{16} afford a very nice example of the use of two or more different representations in considering a level spectrum.

The excitation energies of all these levels are again much lower than one would expect from shell model calculations with interaction due to the cluster model effects previously described. These effects increase with increasing mean distance between the clusters. This explains the larger effect in the lowest positive parity excitation states relative to the lowest negative parity excitation states. (See fig. 4.) In general, the experimental situation in O^{16} is excellent. Perhaps the most valuable additional experiments would be of the type which measures reduced widths of levels. This kind of measurement may determine the relative importance of various cluster configurations in a given state directly [7]).

2.4. ENERGY LEVELS OF F^{19}

We begin with a consideration of the low energy positive parity spectrum of F^{19}. In similarity to the considerations in Li^7 and Be^7, F^{19} may be thought of as an unexcited O^{16} cluster and a triton cluster. In the framework of the "oscillator assumption" we expect a 6th order oscillation of the triton cluster relative to the O^{16} cluster (Pauli principle) with the resulting 4s, 3d, 2g, li oscillations. We get by the penetrating orbit argument the level sequence $\frac{1}{2}+$, $\frac{5}{2}+$, $\frac{3}{2}+$, $\frac{9}{2}+$ . . . if we take into account the spin of the triton cluster and the spin orbit coupling. This is in agreement with the experimental levels. (See fig. 5.) It is particularly interesting to note the doublet nature $(\frac{1}{2}+\ \frac{5}{2}+)$; $(\frac{3}{2}+\ \frac{9}{2}+)$ of the levels in this spectrum. The doublet nature is not fundamental theoretically but arises from the fact that the spin orbit coupling lowers the $\frac{5}{2}+$ state into the $\frac{1}{2}+$ state region without exchanging the sequence. This is also true for the $\frac{3}{2}+\ \frac{9}{2}+$ doublet.

The amount of spin orbit interaction may be estimated by comparison with the splitting in O^{17}. In O^{17} it is measured as 5.08 MeV between the $\frac{5}{2}+$ ground state and the first $\frac{3}{2}+$ level. As a first approximation we might expect that it will be one third (see ref. [3]), p. 92) of 5.08 MeV for the corresponding levels in F^{19}. The measured value is 1.4 MeV to be compared with 1.7 MeV.

The negative parity states of F^{19} can be satisfactorily explained by N^{15} and α-particle clustering because this representation is favored energetically. The oscillation of the α-particle cluster against the N^{15} cluster gives rise to 5s, 4d, 3g, 2i and 1k relative oscillations. The coupling of the N^{15} cluster spin to

these orbital angular momenta gives rise to the following level sequences: $\frac{1}{2}; \frac{5}{2}; \frac{3}{2}; \frac{9}{2}; \frac{7}{2}; \frac{13}{2}; \frac{11}{2}; \ldots$ We would expect that the spin orbit splitting between the $\frac{5}{2}$ and $\frac{3}{2}$ states, for example, will be less than in the corresponding positive parity levels in F^{19}. An important reason for this is that the spin of the odd proton in the triton cluster moves in the field of the entire O^{16} cluster in the positive parity states whereas the N^{15} cluster moves in the field of only the α-particle cluster in the negative parity states. (See also ref. [3]), p. 95.)

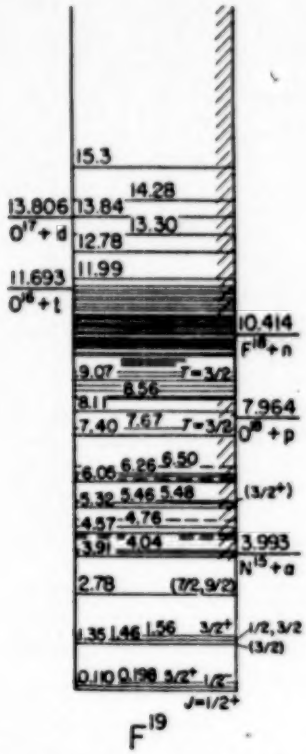

Fig. 5. Energy levels of F^{19}.

The fact that the negative parity states in F^{19} lie so low in the spectrum is of considerable interest. If one breaks up an α-particle cluster in the O^{16} cluster and forms an outside α-particle cluster in going from the positive to the negative parity states, then to a first approximation one expects an increase in the kinetic energy of the system of approximately $\frac{1}{2}\omega\hbar$. This might be 6—10 MeV in this region.

The energy of breakup for the α cluster in O^{16} is smaller than the breakup energy of the outside α cluster (radius change effect — see sect. 1 and subsect. 2.2). Therefore one gets back a lot of internal cluster energy by this nucleon transition. This energy gain compensates almost entirely for the increase of kinetic energy.

We must expect that for excitation energies above $\approx$ 5 MeV our approximation for positive and negative parity low energy excited states gets increasingly

worse with increasing energy because the internal excitation energies for the N^{15}, α-particle and triton clusters are all of this order.

The considerations of Elliot and Flowers [8]) coincide with these considerations for the positive parity low energy spectrum of F^{19}. However, we have chosen a more flexible point of view which also includes the negative parity levels.

Further considerations of the negative parity levels follow in sect. 3.

2.5. ENERGY LEVELS IN Ne^{20}

The experimental spectrum for Ne^{20} is shown in fig. 6. Similar to previous considerations we would expect an O^{16}-α cluster relative oscillation of 8th order with 5s, 4d, 3g, 2i, 1k oscillations and 0+, 2+, 4+, 6+, and 8+ states. In

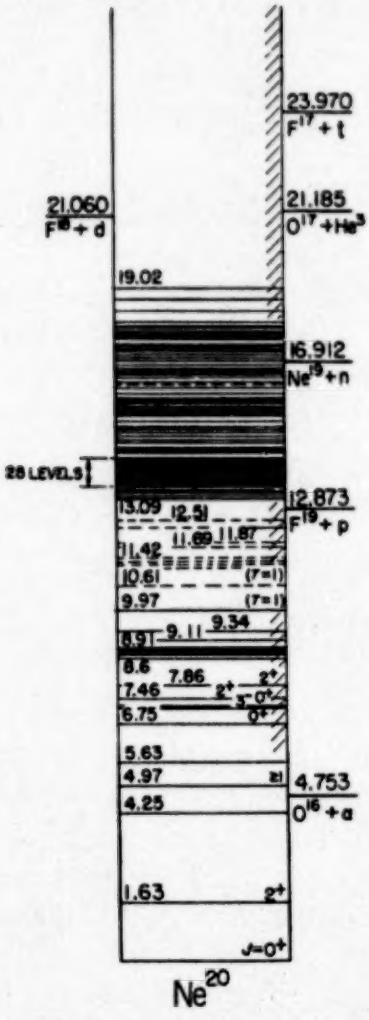

Fig. 6. Energy levels of Ne^{20}.

addition one expects a 2nd 0+ state which is described by the internal positive parity excitation of the O^{16} cluster of Ne^{20}. Also a 1− state would be expected which is a mixture of a 9th order relative oscillation and an internal negative parity excitation of the O^{16} cluster with 8th order relative oscillation.

The states at 4.248, 4.969, 5.631 MeV whose spin and parity have not been experimentally determined are of particular interest. Thus, in the cluster model the most reasonable interpretation of these three states would be that one is a 4+ (possibly the 4.969 MeV state); one is a 0+ and one is a negative parity state.

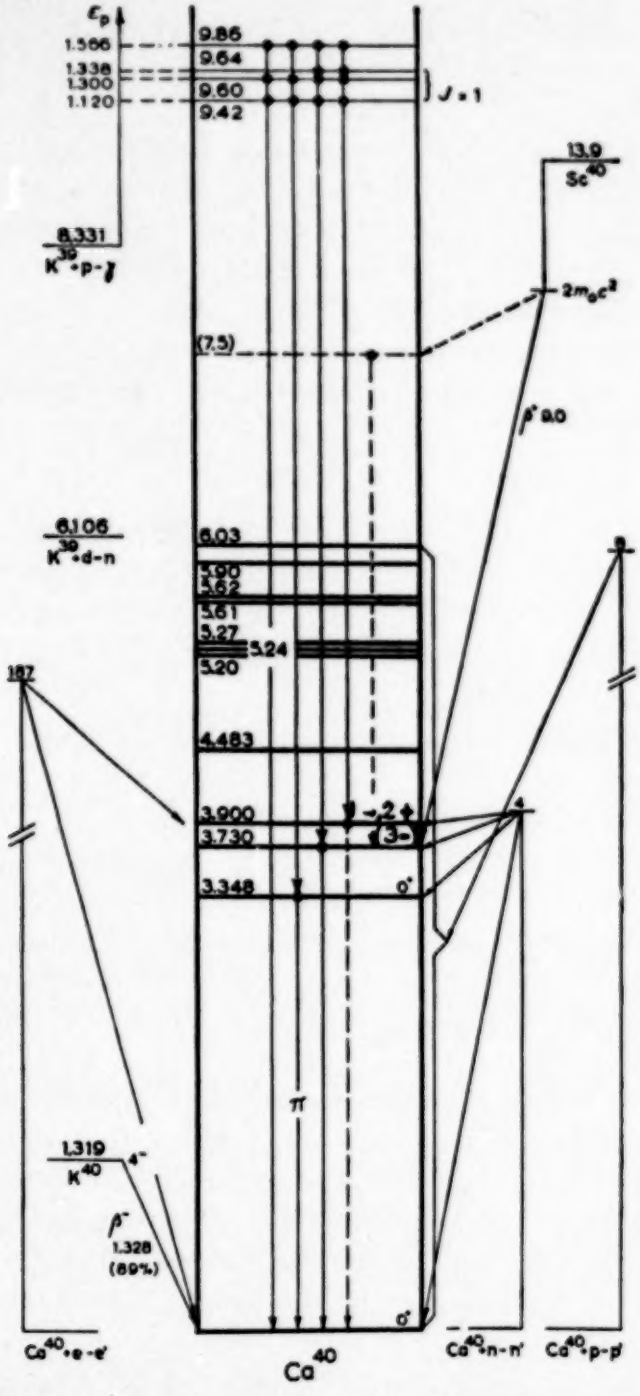

Fig. 7. Energy levels of Ca^{40}. See J. H. Johnson and C. M. Class, Bull. Am. Phys. Soc. **4** (1959) 79. (Assignments for the 3.73- and 3.90-MeV states are 3− and 1−, 2+ respectively. They were incorrectly reported in the publication (private communication from C. M. Class).

In the collective model by analogy with Mg^{24} one would expect to find a very low lying second 2+ state, presumably the 4.248 MeV state (the gamma vibrational band head [9]). These experimental determinations are therefore of great interest.

2.6. ENERGY LEVELS IN Ca^{40}

Although a great deal of additional experimental information should be found for Ca^{40}, the few experimental data which are available (see fig. 7) are interesing and significant.

Ca^{40}, like O^{16}, is an α-particle nucleus with a double closed shell. Consequently by arguments similar to those in O^{16} we know that the 0+ ground state of Ca^{40} will not have superposed 2+, 4+, . . . rotational states. As in O^{16} the first excited state in Ca^{40} should be a 0+ state. This state should have an internal deformation resulting in superposed 2+, 4+ . . . states. Also we expect negative parity states in this same energy vicinity with spin parity 3− and 1−. Thus the expectations are born out by the meager experimental data thus far available.

2.7. ENERGY LEVELS IN Sc^{43}

Since one of the important purposes of this paper is the suggesting of possible experiments testing the validity of the cluster model and an attempt to interest experimentalists in these problems, we have chosen to predict the spectrum for a nucleus for which almost no experimental data are available. The nucleus chosen is Sc^{43} which should be particularly susceptible to a cluster model approach. Furthermore, this nucleus is fairly susceptible to experimental studies; it may be studied by the nuclear reactions $Ca^{40}(\alpha, p)Sc^{43}$, $Ca^{42}(d, n)Sc^{43}$, $Ca^{43}(p, n)Sc^{43}$, $Sc^{45}(p, t)Sc^{43}$ and $Ti^{46}(p, \alpha)Sc^{43}$.

The low lying negative parity states in Sc^{43} may be conveniently described by an unexcited Ca^{40} and triton cluster representation. Due to the Pauli principle the lowest relative oscillation of the triton cluster against the Ca^{40} cluster will be of 9th order with the resulting 5p, 4f, 3h, 2j and 1l oscillations. Each orbital angular momentum splits into doublets due to the spin orbit coupling of the spin of the triton cluster.

To get an estimation of spin orbit coupling, we should use the splitting of the $\frac{7}{2}-$ and $\frac{5}{2}-$ levels in Ca^{41}. As previously indicated the spin orbit splitting in Sc^{43} should be one third that of the corresponding spin orbit splitting in Ca^{41}. Unfortunately the spin orbit splitting in Ca^{41} is not definitely known. By comparison with the expected 2+ level in Ti^{44} ($\approx$ 1.0 MeV; see subsect. 3.4) we may assume that the centre of gravity for the energy splitting (5p, 4f) in Sc^{43} is $\approx$ 1 MeV.

In fig. 8 a proposed spectrum for Sc^{43} is presented. The positive parity states are discussed in the next section; for the calculation of the negative parity levels of this spectrum, we use the following formulas:

For the centre of gravity energies

$$\Delta E = 0.05\{l(l+1)-l_0(l_0+1)\}.$$

For the spin orbit splitting †

$$\Delta E_{so}(I = l-\tfrac{1}{2}) = 0.5(l+1), \quad \Delta E_{so}(I = l+\tfrac{1}{2}) = -0.5l.$$

The sequence of these negative parity levels depends very much on the constants in the above formulas and the complete validity of the equation. Unfortunately, the constants are very poorly known, and it is difficult to know how

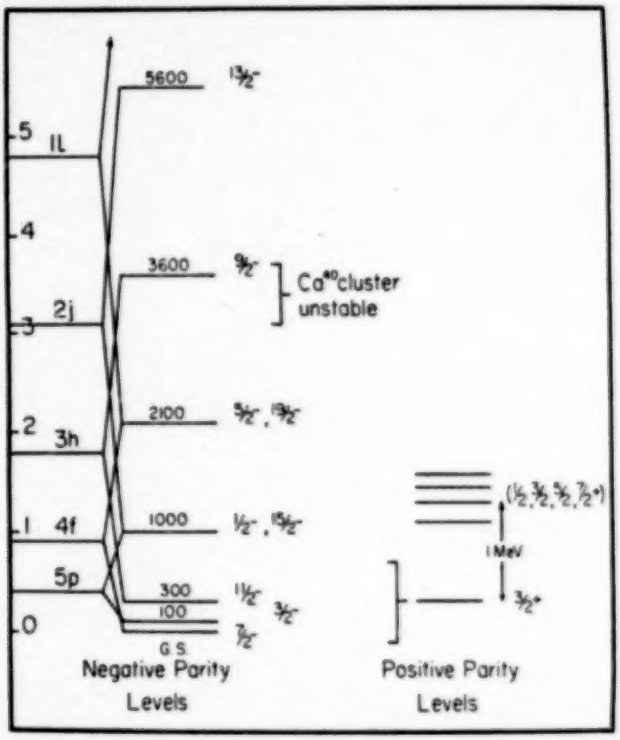

Fig. 8. Predicted levels in Sc^{43}. For the calculations see text.

well the equations will work. Accordingly one must expect that some of the level sequences may be wrong, but the general structure of the low energy levels is not to be doubted. It should be further pointed out that above ≈ 3.5 MeV the predictions are increasingly less valid because this is the energy of excitation of the Ca^{40} cluster.

3. Comparisons of the Spectra of Related Nuclei

3.1. THE SPECTRA OF F^{19} AND Ne^{20}

If we compare the low energy negative parity F^{19} spectrum and the low energy positive parity spectrum of Ne^{20}, then we see that the cluster representations describing them are similar. In the negative parity levels of F^{19} we have

† This gives approximately the right spin orbit splitting of the $\frac{5}{2}+$ and $\frac{3}{2}+$ levels in F^{19}.

an N^{15}, α-particle clustering; whereas in Ne^{20} the positive parity levels result from O^{16} and α-particle clusters. Therefore the 0+, 2+, 4+ . . . levels should split in F^{19} into $\frac{1}{2}-$; $\frac{5}{2}-$, $\frac{3}{2}-$; $\frac{9}{2}-$, $\frac{7}{2}-$ . . . levels due to the spin of the N^{15} cluster. The centre of gravity distances of these doublets should be approximately the energy differences between the 0+, 2+ 4+ states in Ne^{20}. The energy differences may be slightly less in F^{19} than in Ne^{20} because we have 16 nucleons in the big cluster in Ne^{20} but ony 15 in F^{19}. The agreement between the negative parity spectrum of F^{19} and the positive parity spectrum in Ne^{20} is shown in figs. 5 and 6. Additional experimental data are needed for both F^{19} and Ne^{20}.

3.2. THE NUCLEI N^{16} AND O^{17}

O^{17} and F^{17} have the cluster representations O^{16} plus a neutron or a proton, whereas N^{16} may be represented as an N^{15} cluster plus a neutron. Thus we can see that the essential difference we must expect between O^{17} spectra and N^{16} spectra is that the extra neutron in N^{16} can couple to the spin of the N^{15} cluster,

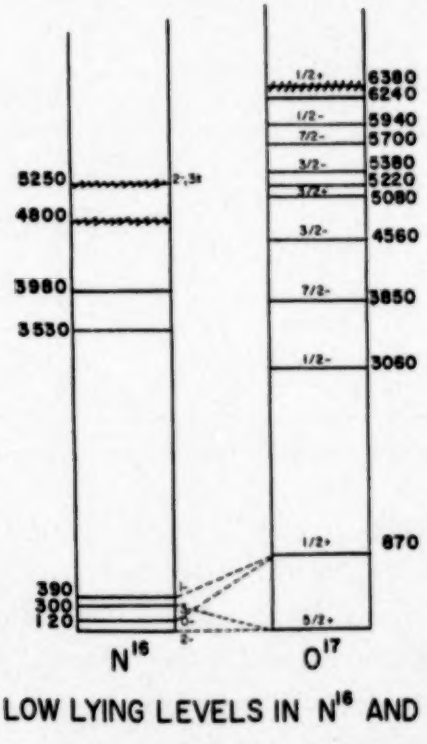

Fig. 9. Comparison of the nuclear spectra of N^{16} and O^{17}. See F. Ajzenberg-Selove and T. Lauritsen, Nuclear Physics **11** (1959) 1.

whereas in O^{17} the extra nucleon couples only with the zero angular momentum of the double closed shell O^{16}. The comparison of the spectra of O^{17} and N^{16} is shown in fig. 9. The two lowest levels in O^{17} are $\frac{5}{2}+$ and $\frac{1}{2}+$. The $\frac{5}{2}+$ state when coupled with the N^{15} cluster should give rise to two levels with spin parity

3− and 2−. The $\frac{1}{2}$+ state when coupled with N^{15} cluster should give rise to two states with spin parity 1− and 0−. All four states should have $T = 1$. It is immediately obvious from fig. 9 that these predictions are satisfactory. The careful determination of the other spin parity in O^{17} and the coupling of these states with the N^{15} cluster to give additional states in N^{16} will provide additional tests for the cluster model.

3.3. THE SPECTRA OF Ca^{41} AND K^{40}

In similarity to the relation of O^{17} and N^{16} it is of special interest to compare the spectra of Ca^{41} and K^{40}. Thus, whereas Ca^{41} can be considered as a Ca^{40} cluster plus a neutron, K^{40} can be described as a K^{39} cluster plus a neutron. The essential differences one can expect then between the Ca^{41} and the K^{40}

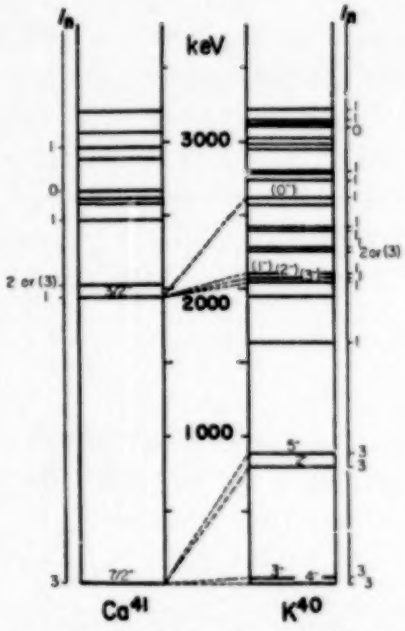

LOW LYING LEVELS IN K^{40} AND Ca^{41}

Fig. 10. Comparison of the nuclear spectra of K^{40} and Ca^{41}. See H. A. Enge, E. J. Irwin, Jr., and D. H. Weaver, Phys. Rev. **115** (1959) 949.

spectra involve the fact that the extra neutron in K^{40} couples with the spin of the K^{39} cluster, whereas in K^{41} the extra neutron couples only with the angular momentum of the double closed shell of Ca^{40}. The comparison of the spectra of Ca^{41} and K^{40} is shown in fig. 10. Only the two lowest levels in Ca^{41} are of interest to us. They have the spins, $\frac{7}{2}$− and $\frac{3}{2}$−. In strict shell model nomenclature these represent the $f\frac{7}{2}$ and $p\frac{3}{2}$ states. The K^{39} cluster has the spin $\frac{3}{2}$+ as seen from the ground state of the nucleus K^{39}. Thus one expects to observe in K^{40} a quartet of near lying states, one of which will be the ground state, which results from the coupling of the $\frac{3}{2}$+ state of the K^{39} cluster with the $\frac{7}{2}$− state of the odd neutron. This would give rise to four states with spins, 5−, 4−, 3− and

2−. The $\frac{3}{2}$− state should couple with the $\frac{3}{2}$+ state to give a quartet of states with spin parity 3−, 2−, 1− and 0−. Furthermore, one would expect that the centre of gravity of these two quartets of states should equal approximately the energy difference between the $\frac{7}{2}$− and $\frac{3}{2}$− states in Ca^{41}, namely, 1.947 MeV. This prediction is borne out as shown in fig. 10. The states at 1.639 and 1.954 MeV do not fit in well with this prediction. It would therefore be worthwhile to investigate especially their spin and parity in more detail. It should, however, be pointed out that the particle-hole theory of the shell model equally well predicts this correlation of states in the pairs O^{17}—N^{16} [5]) and Ca^{41}—K^{40} [10]). In fact, ultimately the two methods must be shown to be equivalent.

3.4. THE SPECTRA OF Sc^{43} AND Ti^{44}

In fig. 8 we have also presented the positive parity spectra of Sc^{43}. In so doing we were anticipating the discussion of this section. Here we must compare the spectra of Ti^{44} and Sc^{43}. Unfortunately the 2+ state is not known for Ti^{44}. However, we can estimate that it lies at $\approx$ 1.0 MeV from the general systematics of the first 2+ state for nuclei in this region. Then the K^{39} cluster with spin $\frac{3}{2}$+ will couple with the 0+ and 2+ states to give a $\frac{3}{2}$+ state and then a quartet of states ($\frac{1}{2}$, $\frac{3}{2}$, $\frac{5}{2}$, and $\frac{7}{2}$+). The centre of gravity of the quartet should lie $\approx$ 1.0 MeV above the $\frac{3}{2}$+ state.

3.5. OTHER CASES

One might expect to make comparisons between a number of other sets of nuclei. In particular we might mention that Na^{23} should have some negative parity levels which mirror the levels in Mg^{24}. One expects that somewhere in the region from 2.5 to 4 MeV one should observe a $\frac{1}{2}$− state. (See sect. 4.) This $\frac{1}{2}$− state should be separated by $\approx$ 1.3 MeV from the centre of gravity of $\frac{5}{2}$− and $\frac{3}{2}$− states. In a similar way it ought to be possible to make comparisons between the spectra in Al^{27} and Si^{28}. Once again one expects a $\frac{1}{2}$− state separated by about 1.8 MeV from the centre of gravity of higher $\frac{5}{2}$− and $\frac{3}{2}$− states.

4. Changed Parity states (A = 8 to A = 40)

In fig. 11 we present the correlation diagram for first excited states with parity opposite to the ground state † for nuclei in the region $A = 8$ to $A = 40$. Lines connecting nuclei which have similar cluster structures are intended to show the correlation. Those cluster structures considered are (1) alpha cluster nuclei, (2) alpha cluster nuclei with an additional triton or He^3 structure, (3) alpha cluster nuclei with or without a triton or He^3 cluster and deuteron,

† For simplicity and brevity we will call these states changed parity states — c.p. states.

dineutron or diproton cluster, (4) alpha cluster nuclei with or without a triton or He^3 cluster and one odd neutron or proton. Let us consider each of these trends individually.

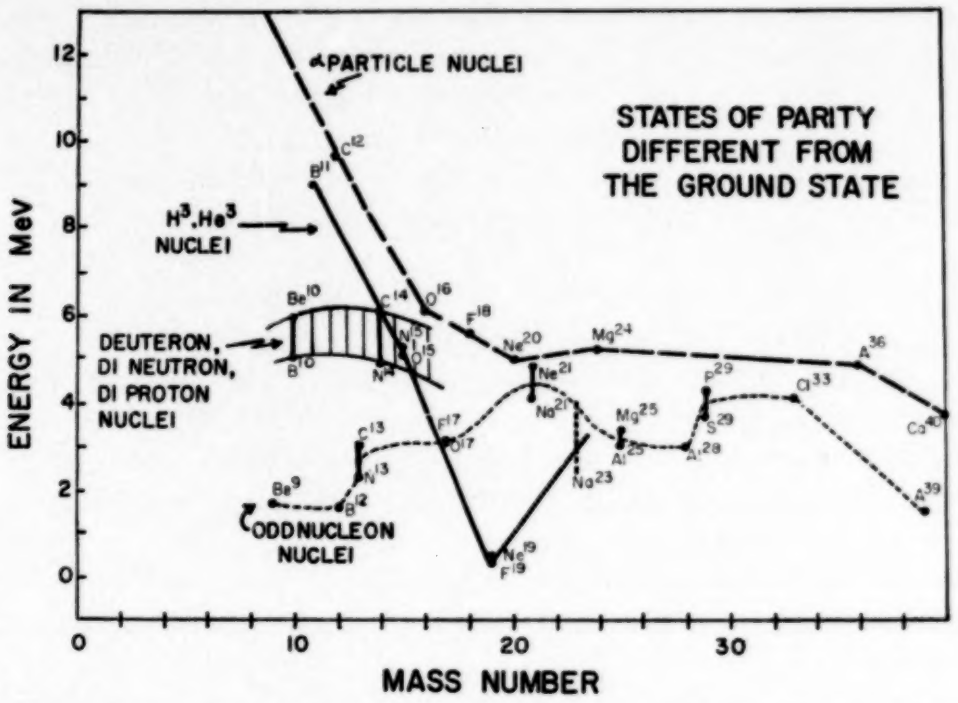

Fig. 11. A plot of the energy of the first changed parity state above the ground state as a function of A. The data are mostly taken from F. Ajzenberg-Selove and T. Lauritsen, Nuclear Physics **11** (1959) 1 and P. M. Endt and C. M. Braams, Rev. Mod. Phys. **29** (1957) 683; Al^{28}—H. Enge and J. Taylor (private communication). Na^{23}—the first c.p. states cannot lie below the region of the dashed line; there are several states of unknown parity in this region. Ca^{40}—see fig. 7.

4.1. ALPHA CLUSTER NUCLEI

Nuclei considered are C^{12}, O^{16}, Ne^{20}, Mg^{24}, Si^{28}, S^{32}, A^{36} and Ca^{40}. As indicated in the introduction the c.p. states of these alpha particle nuclei should in general lie highest because the outside cluster (alpha) has the most nucleons. We will also expect the c.p. states to evidence a general trend downward as A increases. (See subsect. 4.4.) This trend is immediately obvious from fig. 11. It is, of course, important to observe the first negative parity states in Si^{28} and S^{32} so that the trend might be more nearly completed.

4.2. TRITON CLUSTERS

The c.p. states of the triton cluster nuclei should lie below the α cluster nuclei but above those of other cluster nuclei. However, immediately after completing a shell as, for example in F^{19}, a triton cluster can exchange with an α cluster of a lower shell and gain back a considerable amount of internal cluster energy. (See subsect. 2.4.)

Immediately after F^{19} the next triton cluster nucleus is Na^{23}. One already has an additional α cluster outside the O^{16} double closed shell; consequently, the triton α cluster exchange effect observed in F^{19} will not be nearly as marked. Unfortunately, the first negative parity state in Na^{23} it not known but may very well lie in the region from 2.5 to 4 MeV. In general then one will expect relatively high lying negative parity states for triton cluster neuclei, dropping discontinuously very low immediately after closing a shell, then increasing continuously until the next double closed shell is reached. Unfortunately, the data for most triton cluster nuclei are very meager. It is to be urged that additional data on the negative parity states of these nuclei be obtained.

4.3. DEUTERON, DINEUTRON AND DIPROTON CLUSTER NUCLEI

As we would expect, in general the c.p. states of deuteron, dineutron and diproton cluster nuclei lie below both the c.p. states in α cluster and triton cluster nuclei but above those of odd nucleon cluster nuclei. One does not expect to observe the exchange effect with lower shells as in triton cluster nuclei with either the deuteron clusters or the dineutron and diproton clusters because these exchanges would, in effect, represent two particle excitations and should lie very high. Consequently, one does not expect the discontinuity immediately after closed shells for these cluster nuclei which one observes for the triton cluster nuclei.

We have assumed the change of parity comes from the change of the relative motion of the outside cluster and not from the breaking up of the internal structure of the clusters. This assumption is fulfilled approximately for alpha and triton cluster nuclei because for these nuclei the outside clusters are relatively tightly bound (exceptions are Li^7 and Be^7; see ref. [6])). On the other hand this assumption is less valid for deuteron, diproton and dineutron cluster nuclei.

4.4. ODD NUCLEON CLUSTERS

These nuclei should, in general, lie the lowest of all. This is completely borne out by the experimental information now available. One would also expect some variation in the position of the energy of the negative parity states depending on whether the core has simple α clusters or whether there are triton clusters, etc. The irregularity of these low lying negative parity states is in keeping with these conclusions.

We see that in general the c.p. states of the α cluster nuclei decrease in general with A in contrast to the c.p. states of odd nucleon nuclei. This is due to the fact that in general the radius change effect increases with atomic weight. (See also sect. 5).

It should very strongly be stressed that the experimental information used in constructing fig. 11 is very incomplete and that additional information on the negative parity states of light nuclei would be particularly valuable.

5. Low Lying 0+ States in the Light Even Nuclei

It has been known for some time that very often in doubly closed shell nuclei the first excited state is the 0+ state. In fig. 12 we have plotted on a log-log scale the energy of all low lying 0+ states for even nuclei against the mass number of these nuclei. It is of particular interest to note that in the case of C^{12}, O^{16}, Ca^{40} and Zr^{90} a straight line correlation results. The slope of this line agrees very closely with a $A^{-\frac{2}{3}}$ energy dependence. All of these nuclei involve double closed shells (six neutrons and protons in C^{12} have some closed shell characteristics because of spin orbit coupling).

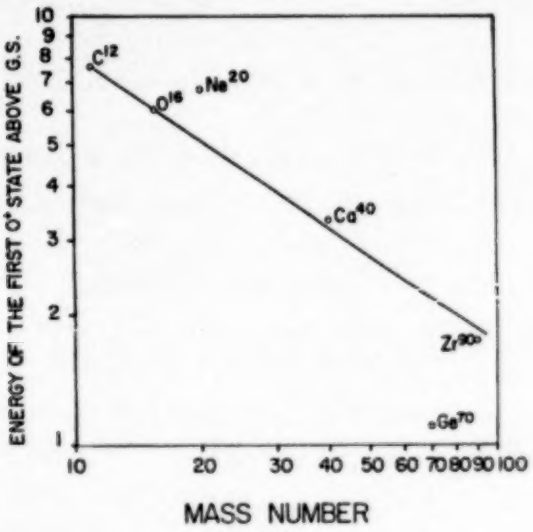

Fig. 12. A plot of the log of energy of the first 0+ excited state against A. The slope of the line indicates an $A^{-\frac{2}{3}}$ energy dependence. Ge^{72} has a first excited 0+ state at 690 keV not shown on the graph.

From simple shell model considerations (oscillator assumption) one would expect an $A^{-\frac{1}{3}}$ energy dependence due to the proportionality of the nuclear volume to the atomic weight. There are two other factors which will effect the A dependence. These are the anharmonicity dependence of the relative cluster motions and the radius change effect. These proportionality factors are difficult to evaluate but will tend to change the $A^{-\frac{1}{3}}$ dependence toward an $A^{-\frac{2}{3}}$ dependence. As explained previously these factors depress very strongly ($\approx$ 10 MeV) the 0+ levels in α cluster nuclei relative to shell model values. As indicated in fig. 12, the 0+ level in Ne^{20} lies considerably above the general trend of the 0+ levels in closed shell nuclei. This is due to the fact that in the second 0+ state in Ne^{20} the excited α particle cluster moves (from the O^{16} cluster) in a region with considerable nuclear matter due to the presence of an outside α particle cluster. This reduces the radius change effect with a consequent increase in the energy of the second 0+ level. A similar and perhaps even larger effect should

be observed in Mg^{24}. Therefore it would be of considerable interest to establish experimentally with certainty the presence of the second 0+ level in this nucleus.

6. Conclusions

In the preceding sections we have attempted to point out some of the comparisons between the experimentally observed levels in the light and medium weight nuclei and the predictions of the cluster model. Simultaneously we have tried to indicate those experiments which have particular value in further comparison with the cluster model. Summarizing, we can say that the agreement between the limited experimental data thus far and the cluster model has been gratifying and seems to affirm the natural physical insight of this model.

As a first approximation we have designed the wave functions of the cluster model states from the viewpoint of the "oscillator assumption." Furthermore the states used in our considerations have always been assumed to be pure. Nonetheless we are aware of the fact that all nuclear states are described by a mixture of different cluster wave functions. Thus, for instance, both the first and second 2+ states in O^{16} are certainly mixtures of states in which one has (in the oscillator notation) a 3d oscillation of the outside alpha cluster against the unexcited C^{12} cluster and a 3s oscillation of this alpha cluster against the C^{12} cluster in its first excited state †. For the lower 2+ state the 3d wave function is most important whereas for the second 2+ state the other wave function is more important.

The main advantage of this model is its versatility. In principle, one can discuss the other models from the point of view of the cluster model. Even in a single nucleus it is useful to describe different states by different cluster wave functions (by different specialized nuclear models). For instance, the low energy positive parity states of F^{19} are most conveniently described as O^{16} triton cluster wave functions, whereas the low energy negative parity states of F^{19} are described as N^{15}—α-particle cluster wave functions. It is important to note again that in general the cluster representations of states get increasingly complex at higher and higher energies as more and more stable clusters are broken up. Nonetheless the usefulness of a simple cluster representation will sometimes reappear at an energy far above the energy of breakup of the involved clusters. It should also be noted again that it is often advantageous to consider a given single state from the point of view of different cluster wave function systems. For the negative parity states of O^{16}, for instance, it was very useful to consider these states together from the point of view of the shell model representation and the α-particle representa-

† In addition, one has considerable deviations from the oscillator assumption.

tion. Every cluster wave function means in some sense an extreme point of view because one uses qualitative arguments which sometimes include only very vaguely the Pauli principle and the indistinguishability of nucleons. However, by comparing the conclusions which one gets from different cluster wave function systems and especially by selecting and discarding the contradictory conclusions, one can often learn about the influence of the Pauli principle and the indistinquishability of the nucleons on nuclear behavior without explicit lengthy calculations. This is true because any nuclear state can always be completely described in principle in every cluster wave function system.

We are grateful to the Atomic Energy Commission and Contract AT-(40-1)-2434, to the Office of Ordnance Research and Contract DA-01-009-ORD-703 and to the Office of Naval Research and Contract NONR 988(09), for their support of this work. We also wish to thank Professors T. Lauritsen and F. Ajzenberg-Selove for the use of some of their level schemes presented in "The Light Isobars".

References

1) K. Wildermuth and Th. Kanellopoulos, Nuclear Physics **7** (1958) 150;
see also G. C. Phillips and T. A. Tombrello, Phys. Rev. (to be published)
2) K. Wildermuth and Th. Kanellopoulos, Nuclear Physics **9** (1958/59) 449
3) K. Wildermuth and Th. Kanellopoulos, The application of the cluster model to nuclear physics (CERN Report 59—23)
4) J. K. Perring and T. H. Skyrme, Proc. Phys. Soc. **69** (1956) 600;
J. P. Elliot and T. H. Skyrme, Proc. Roy. Soc. A **232** (1955) 561;
and especially:
J. P. Elliot, Proc. Roy. Soc. A **245** (1958) 128, 562;
B. F. Bayman and A. Bohr, Nuclear Physics **9** (1958/59) 596;
D. M. Brink, Nuclear Physics **4** (1957) 215
5) J. P. Elliot and B. H. Flowers, Proc. Roy. Soc. A **242** (1957) 57
6) L. D. Pearlstein, Y. C. Tang and K. Wildermuth, Nuclear Physics **18** (1960) 23
7) B. Roth and K. Wildermuth, Nuclear Physics **18** (1960)
8) J. P. Elliot and B. H. Flowers, Proc. Roy. Soc. A **229** (1955) 536;
see also:
E. B. Paul, Phil. Mag. **2** (1957) 311;
G. Rakavy, Nuclear Physics **4** (1957) 375
9) G. Rakavy, ref. [8]);
A. K. Kerman, Ch. 10 in Nuclear Reactions, ed. by P. M. Endt and M. Demeur, Vol. I (North-Holland Publishing Company, Amsterdam, 1959)
10) Enge, Irwin and Weaver, Phys. Rev. **115** (1959) 949
11) P. Miller, private communication

9.A

Nuclear Physics **21** (1960) 220—224; © *North-Holland Publishing Co., Amsterdam*

Not to be reproduced by photoprint or microfilm without written permission from the publisher

REMARKS ON THE ENERGY DISTRIBUTION OF MESONS CREATED IN HIGH-ENERGY NUCLEAR COLLISIONS

E. M. FRIEDLÄNDER

Cosmic Ray Laboratory, Institute of Atomic Physics, Bucharest

Received 13 July 1960

Abstract: It is shown that the assumption of a Heisenberg-type spectrum of the secondaries from high-energy mesons jets is in contradiction with the observed distribution of c.m.s. angles and that of the transverse momenta. Starting from observational data on the latter quantities a rough approximation for the c.m.s. energy spectrum is computed.

1. Introduction

In their investigation of high-energy jets, Edwards *et al.* [1]) have tried to compare the energy spectrum of the secondaries with the theory of multiple production of Heisenberg [2]). In order to obtain this spectrum they have used the experimentally obtained angular distribution in the centre-of-mass system of the colliding nucleons (hereafter referred to as C-system) together with the assumption that the transverse momentum component of the secondaries p_T is a constant. With an observed distribution of the form $f(>z) \propto z^{-1}$, where $z \equiv \operatorname{cosec} \bar{\theta}$, this assumption leads to Heisenberg's momentum spectrum

$$F_C(p)\mathrm{d}p \propto p^{-2}\mathrm{d}p. \tag{1}$$

The same spectrum has been predicted again on entirely new grounds in two recent papers [3, 4]) which tried to interpret multiple meson production by an analogy with Čerenkov radiation. Isotropic emission and a Heisenberg spectrum have also been repeatedly advocated (cf. e.g. refs. [5–7])).

The conclusion drawn in ref. [1]) as to the shape of $F_C(p)$ is in itself questionable since p_T is known not to be strictly constant but to obey (in log p_T coordinates) a Gaussian distribution about an almost constant mean value [8]). The spread of the p_T-values (cf. e.g. fig. 5 of ref. [1])) is large enough to invalidate the $p^{-2}\mathrm{d}p$ spectrum in the C-system †.

Now the problem of physical interest is not so much to find some system (be it even the C-system) in which a p^{-2} spectrum holds, but to investigate the production spectrum in the system of the body which actually emits the mesons.

† One standard deviation of the Gaussian curve which describes accurately fig. 5 of ref. [1]) covers the range of p_T-values from 0.2 to 1.0 GeV/c.

Experimental evidence has been accumulating in the last years [9-12]) in favour of the so-called two-centre model of cosmic-ray jets. Most of these events have been proved to be consistent with the emission of mesons from two bodies, moving away from each other in the C-system, and disintegrating independently and isotropically into mesons, each in its own rest system (hereafter referred to as C*-systems). It is the purpose of this note to investigate the production spectrum of mesons within the framework of the two-centre model. It will first be shown that the experimental facts on transverse momenta † are incompatible with the assumption that in each C*-system the production spectrum is of the form $p^{-2}\mathrm{d}p$. Then we shall try to deduce approximately the true shape of this distribution from observational data.

2. Contradiction between the Observed and Heisenberg's Spectrum

Indeed, let us assume that as a result of a non-central nucleon-nucleon collision, two hot centres have been formed, and that in each centre energy dissipation proceeds via meson production according to Heisenberg's theory. In view of the relatively low inelasticity values [1, 9]), there is even, according to Heisenberg, no reason to expect lack of isotropy in each C*-system for most of the created particles. In fact, the Duller-Walker diagrams [13]) constructed separately for each C-system have been consistently found [9, 10, 12]) to be straight lines of slope 2, thus proving isotropy in C*.

We shall now assume for each C*-system the validity of the main conclusion of Heisenberg's theory, viz. strong energy dissipation with a spectrum

$$F_{C^*}(p)\mathrm{d}p = \begin{cases} p_0 p^{-2}\mathrm{d}p & \text{for} \quad p \geqq p_0, \\ 0 & \text{for} \quad p < p_0, \end{cases} \tag{2}$$

with an arbitrary cut-off value p_0. Given isotropy in C*, the probability of finding in C* a meson with momentum p at an angle θ^* will be

$$W(p, \theta^*)\mathrm{d}p\,\mathrm{d}\theta^* = \begin{cases} \tfrac{1}{2} p_0 p^{-2}\,\mathrm{d}p \sin\theta^*\,\mathrm{d}\theta^* & \text{for} \quad p \geqq p_0, \\ 0 & \text{for} \quad p \leqq p_0. \end{cases} \tag{3}$$

Therefrom one obtains easily the distribution of the transverse momentum component

$$p_T \equiv p \sin\theta^*, \tag{4}$$

viz.

$$G(p_T)\mathrm{d}p_T = \begin{cases} \tfrac{1}{2} p_0 \dfrac{\mathrm{d}p_T}{{p_T}^2}\left[\arcsin\dfrac{p_T}{p_0} - \dfrac{p_T}{p_0}\left(1 - \left(\dfrac{p_T}{p_0}\right)^2\right)^{\frac{1}{2}}\right], & \text{for} \quad p_T < p_0, \\ \tfrac{1}{4}\pi p_0 \dfrac{\mathrm{d}p_T}{{p_T}^2}, & \text{for} \quad p_T \geqq p_0. \end{cases} \tag{5}$$

† Owing to the Lorentz invariance of p_T its distribution observed in the lab. system applies to each of the C*-systems as well.

For the comparison with experiment it is more convenient to use [8]) instead of p_T another variable

$$x \equiv \ln (p_T/\mu), \tag{6}$$

where μ is the pion rest mass. With

$$x_0 \equiv \ln (p_0/\mu), \tag{7}$$

we obtain from (5), (6) and (7) the distribution of x:

$$G_1(x)\mathrm{d}x = \begin{cases} \frac{1}{2}\mathrm{d}x[\mathrm{e}^{-(x-x_0)} \arcsin \mathrm{e}^{(x-x_0)} - (1-\mathrm{e}^{-2(x-x_0)})^{\frac{1}{2}}] & \text{for } x < x_0, \\ \frac{1}{4}\pi \mathrm{e}^{-(x-x_0)}\mathrm{d}x & \text{for } x \geqq x_0. \end{cases} \tag{8}$$

Thus G_1 is a function of $x-x_0$ only, i.e. its shape is invariant with respect to any change of the arbitrary cut-off value p_0; this value affects only the position of the peak located at x_0 (fig. 1).

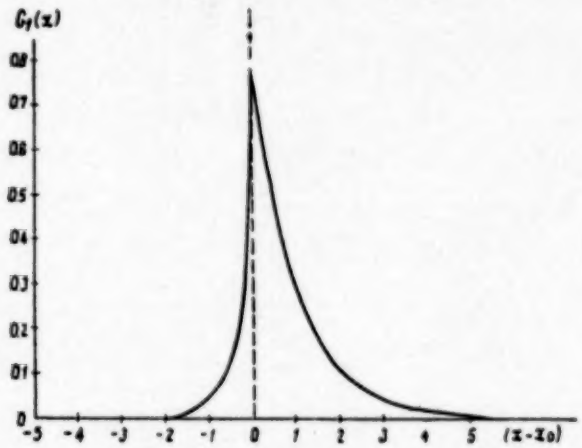

Fig. 1. The distribution function of x.

As can be seen in fig. 1 the distribution of x is strongly asymmetric. From (8) it follows that

$$\int_{x_0}^{\infty} G_1(x)\mathrm{d}x = \tfrac{1}{4}\pi, \tag{9}$$

and hence the ratio of the number of particles with $x > x_0$ to the number of particles with $x < x_0$ is

$$\pi/(4-\pi) \approx 3.66. \tag{10}$$

The average $\bar{x}$ of x is also shifted to the right of the peak by an amount

$$\bar{x}-x_0 \approx 0.69. \tag{11}$$

The standard deviation of this distribution is

$$\sigma_x \approx 1.1. \tag{12}$$

Both $\bar{x}$ and σ have been obtained by numerical integration. All these features of $G_1(x)$ are at variance with the experimental findings. In this compilation of data on transverse momenta. Zhdanov [8]) has shown that at all primary energies the quantity x obeys a Gaussian distribution with no detectable asymmetry The overall standard deviation of x equals [14]) ≈ 0.69, i.e. it is ≈ 1.6 times smaller than the value (12) computed from eq. (8). Both above conclusions are independent of the choice of p_0. It must be stressed that the asymmetry. predicted by eq. (10) is so strong that it would have been detected even with poorer statistics than the ones available in Zhdanov's review.

We must thus conclude that, within the framework of the two-centre model a spectrum of the form $p^{-2}\mathrm{d}p$ is incompatible with the available experimental material.

3. The True Spectrum-Shape

Conversely one may try to deduce the shape of $F_{C^*}(p)$ from the *observed* Gaussian distribution of x and the isotropy in C*. Using again a logarithmic variable

$$y \equiv \ln (p/\mu), \tag{13}$$

it can be shown that the distribution of y is given by

$$F_1(y)\mathrm{d}y = \tfrac{1}{2}\mathrm{d}y \int_0^\infty \frac{1}{\sqrt{2\pi}\sigma} (1-\mathrm{e}^{-2t})^{-\frac{1}{2}} \exp\left[-\frac{(y-a-t)^2}{2\sigma^2}\right] \mathrm{e}^{-2t}\mathrm{d}t, \tag{14}$$

where

$$t \equiv \ln \operatorname{cosec} \theta^* \tag{15}$$

and a and σ are the mean and standard deviation of x. The greatest weight in this integral is borne by the values of t close to zero. Hence the distribution of y must be roughly a Gaussian centred at a value $a+t'$, where

$$t' \approx \ln \frac{4}{\pi} \approx 0.24. \tag{16}$$

Such a narrow distribution of p would be difficult to distinguish in experiment from a sharp line

$$F_{C^*}(p)\mathrm{d}p \approx \delta(p-\mu \mathrm{e}^{a+t'})\mathrm{d}p, \tag{17}$$

in view of the relatively large experimental errors. This may explain the partial success of different special variants of the two-centre model [10-11]), based upon monochromatic emission from the two centres.

Besides, even the evidence for an integral $1/z$ distribution brought forward by the Bristol group [1]) is itself far from conclusive. Recently Nishikawa [15]) has obtained in a high-multiplicity jet a shape quite different from $1/z$. The

same result has been obtained by the author on 9 GeV proton induced meson showers. As will be shown in detail in a forthcoming paper these results are in much better agreement with an almost monokinetic spectrum of the emitted pions than with a $p^{-2}dp$ law.

The author is very much indebted to Mrs. M. Marcu for help in the numerical computations and to Prof. J. Ausländer, Prof. S. Titeica, Dr. G. Domokos, Mr. S. Alper and Miss M. Spîrchez for useful discussions.

References

1) B. Edwards, J. Losty, D. Perkins, K. Pinkau and J. Reynolds, Phil. Mag. **3** (1958) 237
2) W. Heisenberg, Zs. f. Phys. **133** (1952) 65; Kosmische Strahlung (Springer, Berlin 1953)
3) G. Yekutieli, Nuovo Cim. **13** (1953) 446
4) W. Czyz, J. Erikson and S. Glashow, Nuclear Physics **13** (1959) 56
5) R. Marshak, Meson Physics (McGraw-Hill, New York 1952)
6) I. Rosenthal and D. Cernavsky, Fortschr. d. Phys. **4** (1956) 560
7) J. Takibaev, JETP **38** (1960) 1276
8) G. B. Zhdanov, JETP **34** (1958) 856
9) P. Ciok, I. Coghen, J. Gierula, R. Holinsky, A. Jurak, M. Miesowicz, J. Saniewska and J. Pernegr, Nuovo Cim. **10** (1958) 741
10) G. Cocconi, Phys. Rev. **111** (1958) 1699
11) J. Burmeister, K. Lanius and H. Meier, Nuovo Cim. **11** (1959) 12
12) H. Babayan, M. Sarinyan and E. Tumanyan, JETP **38** (1960) 313
13) N. Duller and W. Walker, Phys. Rev. **93** (1954) 215
14) E. M. Friedländer, Nuovo Cim. **12** (1959) 483
15) K. Nishikawa, J. Phys. Soc. Japan **14** (1959) 880

1.A

Nuclear Physics **21** (1960) 225—232; © *North-Holland Publishing Co., Amsterdam*

Not to be reproduced by photoprint or microfilm without written permission from the publisher

STABILITY CONDITIONS AND NUCLEAR ROTATIONS IN THE HARTREE-FOCK THEORY

D. J. THOULESS

Mathematical Physics Department, University of Birmingham

Received 28 July 1960

Abstract: An expression for a general Slater determinant is written in the notation of second quantization. This expression has just the right number of arbitrary coefficients, so no subsidiary conditions are required, and the expression for a particular determinant is unique. This notation is used to study two problems. Firstly, a condition for a particular solution of the Hartree-Fock equations to minimize the expectation value of the Hamiltonian is derived. This condition is equivalent to the condition for stability of collective modes in the random phase approximation. Secondly, the determinant which minimizes the expectation value of the Hamiltonian while giving a particular value to the expectation value of a component of angular momentum is found. In this way, an expression for the moment of inertia of an axially symmetric system is derived within the framework of the Hartree-Fock theory. The expression for a determinant is generalized to include the type of wave functions used in the theory of superconductivity.

1. Introduction

There is a considerable amount of arbitrariness in the representation of a Slater determinant, since any set of linear combinations of the wave functions which make up the determinant gives rise to the same determinant. On the other hand, although the density matrix uniquely determines the determinant, it must satisfy a subsidiary condition in order to be the density matrix of a determinantal wave function [1]). It is convenient to use a representation in which the numbers of coefficients is equal to the number of degrees of freedom of an N-particle determinant, and such a representation is developed in sect. 2 of this paper.

The representation is used to calculate the conditions that a determinant must satisfy in order to minimize the expectation value of the Hamiltonian. The condition that the first derivatives with respect to the coefficients should be zero gives the Hartree-Fock self-consistent field equations, but the condition that the second derivatives should be non-negative gives an additional condition which must be satisfied. This new condition is the same as the condition for collective modes to be stable in the random phase approximation.

The representation is also used to find a determinant which gives a particular value for the expectation value of the angular momentum, and which also minimizes the Hamiltonian. In the first approximation, the additional energy is

proportional to the square of the angular momentum, for a nonspherical system, and the constant of proportionality gives an expression for the moment of inertia.

The representation can be generalized in an obvious way to give the type of wave functions which are used in the theory of superconductivity as a first approximation. This generalization is shown to be equivalent to the usual definitions of such wave functions in terms of quasi-particle operators, but no applications are worked out.

2. Representation of a Slater Determinant

We wish to represent a general Slater determinant $|\Phi\rangle$ for a system of N particles by use of creation and annihilation operators in a particular representation. The operator a_i^+ creates a particle with wave function φ_i and the operator a_i annihilates a particle with wave function φ_i. We denote by $|\Phi_0\rangle$ the configuration in which the first N-levels are occupied, so that

$$|\Phi_0\rangle = (\prod_{i=1}^{N} a_i^\dagger)|0\rangle, \tag{1}$$

where $|0\rangle$ denotes the vacuum, in which no particles are present. Written in this form, $|\Phi_0\rangle$ is normalized to unity.

Theorem. Any N-particle Slater determinant $|\Phi\rangle$ which is not orthogonal to $|\Phi_0\rangle$ can be written in the form

$$\begin{aligned} |\Phi\rangle &= [\prod_{i=1}^{N} \prod_{m=N+1}^{\infty} (1+C_{mi} a^\dagger_m a_i)]|\Phi_0\rangle \\ &= [\exp(\sum_{i=1}^{N} \sum_{m=N+1}^{\infty} C_{mi} a_m^\dagger a_i)]|\Phi_0\rangle, \end{aligned} \tag{2}$$

where the coefficients C_{mi} are uniquely determined. Conversely, any wave function written in the form of eq. (2), with $|\Phi_0\rangle$ defined by eq. (1), is an N-particle Slater determinant.

This theorem is easily proved. We suppose that $|\Phi\rangle$ is a determinant of the wave functions

$$\psi_\alpha = \sum_{i=1}^{\infty} f_{\alpha i} \varphi_i, \tag{3}$$

where α runs from 1 to N. Using second quantization, we can write this Slater determinant as

$$|\Phi\rangle = [\prod_{\alpha=1}^{N} (\sum_{i=1}^{N} f_{\alpha i} a_i^\dagger + \sum_{m=N+1}^{\infty} f_{\alpha m} a_m^\dagger)]|0\rangle. \tag{4}$$

Since we have assumed that this wave function is not orthogonal to $|\Phi_0\rangle$, we can normalize it so that its scalar product with $|\Phi_0\rangle$ is unity. This gives

$$\langle \Phi_0 | \Phi \rangle = \det f_{\alpha i} = 1, \tag{5}$$

where both α and i run from 1 to N. We write the inverse of the $N\times N$ matrix $f_{\alpha i}$ as $F_{i\alpha}$, so that we have

$$\sum_{i=1}^{N} f_{\alpha i}F_{i\beta}=\delta_{\alpha\beta},\quad \sum_{\alpha=1}^{N} F_{i\alpha}f_{\alpha j}=\delta_{ij}, \tag{6}$$

for i and j less than or equal to N. We can then define

$$C_{mi}=\sum_{\alpha=1}^{N} F_{i\alpha}f_{\alpha m} \tag{7}$$

for $i\leqq N$, $m>N$. We can write N linear independent combinations of the wave functions ψ_α, which are, from eqs. (3), (6) and (7),

$$\chi_i=\sum_{\alpha=1}^{N} F_{i\alpha}\psi_\alpha=\varphi_i+\sum_{m=N+1}^{\infty} C_{mi}\varphi_m. \tag{8}$$

The Slater determinant of these must be identical with $|\Phi\rangle$, so that we have

$$\begin{aligned}|\Phi\rangle&=[\prod_{i=1}^{N}(a_i^{\dagger}+\sum_{m=N+1}^{\infty} C_{mi}a_m^{\dagger})]|0\rangle=[\prod_{i=1}^{N}(1+\sum_{m=N+1}^{\infty} C_{mi}a_m^{\dagger}a_i)a_i^{\dagger}]|0\rangle\\&=[\prod_{i=1}^{N}\prod_{m=N+1}^{\infty}(1+C_{mi}a_m^{\dagger}a_i)]|\Phi_0\rangle.\end{aligned} \tag{9}$$

The sum over m can be replaced by a product because all terms in which the same creation operator occurs more than once vanish. For the same reason, the infinite product of eq. (2) can be written as an exponential. The coefficients are uniquely determined because C_{mi} is the ratio of the scalar product of $|\Phi\rangle$ with $a_m^{\dagger}a_i|\Phi_0\rangle$ to its scalar product with $|\Phi_0\rangle$. Thus we have proved the theorem.

The converse is obvious, since $|\Phi\rangle$ defined by eq. (2) is a determinant of the wave functions χ_i defined by eq. (8).

3. Stability of Solutions of the Hartree-Fock Equations

We can use our theorem to find the conditions that $|\Phi_0\rangle$ must satisfy if it minimizes the expectation value of the Hamiltonian, which we take to be

$$H=\sum_{i=1}^{\infty}\sum_{j=1}^{\infty}T_{ij}a_i^{\dagger}a_j+\tfrac{1}{2}\sum_{i=1}^{\infty}\sum_{j=1}^{\infty}\sum_{k=1}^{\infty}\sum_{l=1}^{\infty}V_{ij,kl}a_j^{\dagger}a_i^{\dagger}a_k a_l. \tag{10}$$

We can expand

$$E=\langle\Phi|H|\Phi\rangle/\langle\Phi|\Phi\rangle \tag{11}$$

in powers of the C_{mi}, and we require that the first order term should vanish, while the second order term should be positive definite. The condition for the first order term to vanish is

$$T_{mi}+\sum_{j=1}^{N}(V_{mj,ij}-V_{mj,ji})=0, \tag{12}$$

and this, as is well known [2]), is satisfied if the wave functions φ_i satisfy the Hartree-Fock self-consistent field equations. If eq. (12) is satisfied, there is no loss of generality in assuming that the representation is such that, for all i and j, we have

$$T_{ij}+\sum_{k=1}^{N}(V_{ik,jk}-V_{ik,kj})=\varepsilon_i\delta_{ij}, \tag{13}$$

where ε_i is the Hartree-Fock energy of φ_i. The expectation value of the Hamiltonian for $|\Phi\rangle_0$ is

$$E_0=\langle\Phi_0|H|\Phi_0\rangle=\sum_{i=1}^{N}T_{ii}+\tfrac{1}{2}\sum_{i=1}^{N}\sum_{j=1}^{N}(V_{ij,ij}-V_{ij,ji}). \tag{14}$$

We can substitute eq. (2) into eq. (11) to evaluate the expression up to second order in the C_{mi}. Making use of eqs. (13) and (14), we get

$$\langle\Phi|\Phi\rangle\approx 1+\sum_{i=1}^{N}\sum_{m=N+1}^{\infty}|C_{mi}|^2, \tag{15}$$

and

$$\begin{aligned}\langle\Phi|H|\Phi\rangle\approx{}& E_0\langle\Phi|\Phi\rangle+\sum_{i=1}^{N}\sum_{m=N+1}^{\infty}(\varepsilon_m-\varepsilon_i)|C_{mi}|^2\\&+\sum_{i=1}^{N}\sum_{j=1}^{N}\sum_{m=N+1}^{\infty}\sum_{n=N+1}^{\infty}[(V_{in,mj}-V_{in,jm})C_{nj}^{*}C_{mi}+\tfrac{1}{2}(V_{ij,mn}-V_{ij,nm})C_{mi}C_{nj}\\&+\tfrac{1}{2}(V_{mn,ij}-V_{mn,ji})C_{mi}^{*}C_{nj}^{*}].\end{aligned} \tag{16}$$

Since the normalization factor drops out, the necessary condition for $|\Phi_0\rangle$ to minimize the expectation value of the Hamiltonian is that the quadratic form on the right of eq. (16) should be non-negative definite. This means that the eigenvalues λ of the equation

$$\begin{aligned}(\varepsilon_m-\varepsilon_i)C_{mi}+\sum_{j=1}^{N}\sum_{n=N+1}^{\infty}[(V_{jm,ni}-V_{jm,in})C_{nj}+(V_{mn,ij}-V_{mn,ji})C_{nj}^{*}]&=\lambda C_{mi},\\(\varepsilon_m-\varepsilon_i)C_{mi}^{*}+\sum_{j=1}^{N}\sum_{n=N+1}^{\infty}[(V_{in,mj}-V_{in,jm})C_{nj}^{*}+(V_{ij,mn}-V_{ij,nm})C_{nj}]&=\lambda C_{mi}^{*},\end{aligned} \tag{17}$$

must all be positive or zero. If the self-consistent field has some symmetry, these equations may become much simpler. For example, in the case of an infinite medium where the wave functions φ_i may be plane waves, eq. (17) couples C_{mi} to C_{nj} only if the momentum difference between φ_m and φ_i is equal to the momentum difference between φ_n and φ_j, and to C_{nj}^{*} only if it is equal to the momentum difference between φ_j and φ_n. In the case of a finite system, the self-consistent field may be spherically symmetric, in which case the eigenvectors of eq. (17) must be eigenvectors of angular momentum.

There is a close relation between eq. (17) and the equation for the frequencies of collective modes in the random phase approximation. Using the method of

Sawada [3]), we can derive the equation for frequencies ω of collective modes, which is

$$(\varepsilon_m-\varepsilon_i)x_{mi}+\sum_{j=1}^{N}\sum_{m=N+1}^{\infty}[(V_{jm,ni}-V_{jm,in})x_{nj}+(V_{mn,ij}-V_{mn,ji})y_{nj}]=\hbar\omega x_{ni},$$
$$(\varepsilon_m-\varepsilon_i)y_{mi}+\sum_{j=1}^{N}\sum_{m=N+1}^{\infty}[(V_{in,mj}-V_{in,jm})y_{nj}+(V_{ij,mn}-V_{ij,nm})x_{nj}]=-\hbar\omega y_{mi}. \tag{18}$$

This equation will be discussed in detail in another paper. If eq. (17) has eigenvalue zero, so has eq. (18). If one eigenvalue of eq. (17) is negative, then eq. (18) has imaginary eigenvalues. If no eigenvalue of eq. (17) is negative, then all the eigenvalues of eq. (18) are real. A collective mode with imaginary energy can build up indefinitely, and so the failure of the determinant $|\Phi_0\rangle$ to minimize the expectation value of the Hamiltonian is revealed by a unstable collective mode in the random phase approximation. This is why we refer to the "instability" of the solution of the Hartree-Fock equations. This connection between the random phase approximation and the Hartree-Fock theory is not surprising, since Goldstone and Gottfried have derived the random phase equations by using time-dependent Hartree-Fock theory [4]).

The nature of the instability which is found in a particular representation may give a clue to the nature of the best solution of the Hartree-Fock equations. For example, if quadrupole oscillations are unstable for a spherically symmetric solution, we would conjecture that the shape of the best self-consistent potential would be approximately spheroidal. This situation might occur in a model of deformed atomic nuclei. If $|\Phi_0\rangle$ is a determinant of plane waves, density fluctuations may be unstable, and the best self-consistent potential is likely to be periodic (in one, two, or all three dimensions). This possibility has been discussed by Overhauser [5]).

Unless $|\Phi_0\rangle$ is a determinant of plane waves, there are always Slater determinants which give the same expectation value of a translation-invariant Hamiltonian, because the position of the wave function does not affect the expectation value. If the self-consistent potential is not spherically symmetric, the orientation can also be changed without affecting the expectation value. An infinitesimal displacement $\mathbf{r}$ is generated by putting

$$C_{mi}=\int\varphi_m^*\mathbf{r}\cdot\nabla\varphi_i \tag{19}$$

in eq. (2), and an infinitesimal rotation about the x-axis is generated by putting

$$C_{mi}=\int\varphi_m^*\left(y\frac{\partial}{\partial z}-z\frac{\partial}{\partial y}+i\sigma_x/\hbar\right)\varphi_i, \tag{20}$$

where σ_x is the component of the spin angular momentum operator, in eq. (2). It can easily be verified that eqs. (19) and (20) give eigenvectors of eq. (17) with eigenvalue zero. The right side of eq. (19) is only zero if the self-consistent

field is translation invariant, and the right side of eq. (20) is only zero if the self-consistent field is invariant under rotations about the x-axis. Eq. (19) does not give an eigenvector of eq. (17) when the Hartree-Fock theory is applied to electrons in any atom, since the Hamiltonian is not translation invariant, but the nucleus of the atom provides a natural origin for the coordinate system.

4. The Rotational Problem

There is a natural way of calculating the moment of inertia of a system within the framework of the Hartree-Fock theory. We can try to find what determinant minimizes the expectation value of the Hamiltonian subject to the restriction that the average value of a component of the angular momentum should have a particular value. The expectation value of the Hamiltonian will generally increase as the angular momentum increases, and the rate of increase gives an estimate for the moment of inertia. This method is similar to the method proposed by Gross [6]) but Gross required the exponent on the right of eq. (2) to be a local operator, while we shall not make that requirement.

A similar method certainly gives the right answer for the translational problem. If $|\Phi_0\rangle$ is a determinant which gives zero for the expectation value of the linear momentum,

$$|\Phi\rangle = \exp[(iP/N\hbar)\sum_{i=1}^{N} x_i]|\Phi_0\rangle \tag{21}$$

is a determinant which gives P for the expectation value of the x-component of the linear momentum. The expectation value of the energy increases by $P^2/2NM$, where M is the mass of one particle, so we correctly calculate the total mass of the system to be NM. In this case, our method is identical with that of Gross [6]).

In the rotational problem it is not possible to get an exact answer. We suppose that the determinant $|\Phi_0\rangle$ which minimizes the expectation value of the Hamiltonian gives expectation value zero for all components of angular momentum, but that it has only axial symmetry, not spherical symmetry. The orientation of the axis of symmetry is not determined. If we require that the expectation value of the x-component of angular momentum J_x have a particular very small value, the determinant which minimizes the expectation value of the Hamiltonian is very nearly equal to $|\Phi_0\rangle$ only if its axis is in the yz-plane. We, therefore, choose the axis of $|\Phi_0\rangle$ to be along the z-axis, and use eq. (2) to expand the expectation value of J_x. We get

$$\langle\Phi|J_x|\Phi\rangle \approx \sum_{i=1}^{N}\sum_{m=N+1}^{\infty}[(J_x)_{im}C_{mi}+C_{mi}^{*}(J_x)_{mi}], \tag{22}$$

to first order. The expectation value of the Hamiltonian is given by eq. (16),

to second order. Using the method of undetermined multipliers, we find that the equations for the coefficients C_{mi} are

$$(\varepsilon_m-\varepsilon_i)C_{mi}+\sum_{j=1}^{N}\sum_{n=N+1}^{\infty}[(V_{jm,ni}-V_{jm,in})C_{nj}+(V_{mn,ij}-V_{mn,ji})C_{nj}^*]=\Omega(J_x)_{mi},$$
$$(\varepsilon_m-\varepsilon_i)C_{mi}^*+\sum_{j=1}^{N}\sum_{n=N+1}^{\infty}[(V_{in,mj}-V_{in,jm})C_{nj}^*+(V_{ij,mn}-V_{ij,mn})C_{nj}]=\Omega(J_x)_{im}, \tag{23}$$

provided that Ω, and hence the expectation value of J_x, is sufficiently small.

If we use eqs. (16), (22) and (23) to calculate the moment of inertia, we get

$$\begin{aligned}\mathcal{J}&=(\langle\Phi|J_x|\Phi\rangle)^2/2(\langle\Phi|H|\Phi\rangle-E_0\langle\Phi|\Phi\rangle)\\&=\sum_{i=1}^{N}\sum_{m=N+1}^{\infty}[(J_x)_{im}C_{mi}+(J_x)_{mi}C_{mi}^*]/\Omega,\end{aligned} \tag{24}$$

which is independent of Ω. The solution of eq. (23) is generally quite complicated, but eq. (24) has the structure of the cranking model of Inglis [7]). If we ignore the terms which involve the interaction in eq. (23), we get immediately

$$\mathcal{J}=2\sum_{i=1}^{N}\sum_{m=N+1}^{\infty}|(J_x)_{mi}|^2(\varepsilon_m-\varepsilon_i)^{-1}, \tag{25}$$

which is the simple cranking model formula. This follows from eq. (23) if the exchange terms in the potential are neglected, and so would be correct if the Hartree theory rather than the Hartree-Fock theory were used. In the Hartree-Fock theory corrections to the simple formula will generally be necessary. Our formula is probably rather more difficult to use than that of Gross [6]), but may yield a higher value of the moment of inertia, since the trial wave functions are less restricted.

5. Generalization of the Representation

We can generalize the wave function $|\Phi\rangle$, which is defined by eq. (2), in an obvious way, and get

$$\begin{aligned}|\Phi'\rangle=[\exp[\tfrac{1}{2}\sum_{i=1}^{N}\sum_{j=1}^{N}C_{ij}a_ia_j+\tfrac{1}{2}\sum_{i=1}^{N}\sum_{m=N+1}^{\infty}(C_{mi}-C_{im})a_m^\dagger a_i\\+\tfrac{1}{2}\sum_{m=N+1}^{\infty}\sum_{n=N+1}^{\infty}C_{mn}a_m^\dagger a_n^\dagger)]|\Phi_0\rangle.\end{aligned} \tag{26}$$

This is the type of wave function which is used as a first approximation in the theory of superconductivity, and particular examples of this representation have been used by Bardeen, Cooper and Schrieffer [8]), and by Valatin [9]) in this connection. The comparison of eqs. (2) and (26) shows how this type of wave function can be regarded as a generalized Slater determinant, and why the variational method of determining the wave function is a generalization of the Hartree Fock theory [10]).

This theory is usually developed in terms of quasi-particle operators which are linear combinations of particle creation and annihilation operators. If we have a complete set of quasi-particle annihilation and creation operators α_i, $\alpha_i^\dagger$, then there is a wave function $|\Phi'_0\rangle$ such that

$$\alpha_i|\Phi'_0\rangle = 0 \tag{27}$$

for all i. The determinant $|\Phi_0\rangle$ is a special case of such a wave function. It is easy to show that there is a complete set of quasiparticle annihilation operators β_i which give zero when they operate on the wave function

$$|\Phi'\rangle = [\exp(\tfrac{1}{2}\sum_i\sum_j C_{ij}\alpha_i^\dagger\alpha_j^\dagger)]|\Phi'_0\rangle. \tag{28}$$

One such operator is proportional to

$$\alpha_i+\tfrac{1}{2}\sum_j (C_{ji}-C_{ij})\alpha_j^\dagger,$$

because of the commutation relation

$$[\alpha_i, \exp(\tfrac{1}{2}\sum_j\sum_k C_{jk}\alpha_j^\dagger\alpha_k^\dagger)] = \sum_l (C_{il}-C_{li})\alpha_l^\dagger \exp(\tfrac{1}{2}\sum_j\sum_k C_{jk}\alpha_j^\dagger\alpha_k^\dagger). \tag{29}$$

A complete set of quasi-particle annihilation operators can be chosen in this way.

The methods of this paper could be used to study whether the solution of the variational problem does minimize the expectation value of the Hamiltonian. In a particular case, it has been shown that the condition for a minimum and the condition for the stability of collective modes in the random phase approximation are identical [11]). It would also be possible to use this method to study the rotational problem in a superfluid system of fermions, although it is not obvious that the results would be different from the results obtained by Migdal [12]).

The author wishes to thank Dr. J. J. Griffin and Dr. J. G. Valatin for some helpful discussions which he has had with them.

References

1) P.-O. Löwdin, Phys. Rev. **97** (1955) 1490
2) N. F. Mott and I. N. Sneddon, Wave Mechanics and its Applications (Oxford, 1948), pp. 135-8
3) K. Sawada, Phys. Rev. **106** (1957) 372
4) J. Goldstone and K. Gottfried, Nuovo Cim. **13** (1959) 849
5) A. W. Overhauser, Phys. Rev. Letters **4** (1960) 415
6) E. P. Gross, Nuclear Physics **14** (1960) 389
7) D. R. Inglis, Phys. Rev. **96** (1954) 1059
8) J. Bardeen, L. N. Cooper and J. R. Schrieffer, Phys. Rev. **108** (1957) 1175
9) J. G. Valatin, Nuovo Cim. **7** (1958) 843
10) N. N. Bogoliubov, Doklady Akad. Nauk USSR **119** (1958) 244 [translation in Soviet Phys. Doklady **3** (1958) 292]
11) D. J. Thouless, Annals of Phys. **10** (1960) 553
12) A. B. Migdal, JETP (USSR) **37** (1959) 249 [translation in Soviet Phys. JETP **37** (1960) 176]

1.B

Nuclear Physics **21** (1960) 233—236; © *North-Holland Publishing Co., Amsterdam*

Not to be reproduced by photoprint or microfilm without written permission from the publisher

AN IMPROVED APPROXIMATION FOR SCATTERING PROBLEMS (II)

P. SWAN

Department of Physics, University of Melbourne

Received 19 July 1960

Abstract: A method of calculating scattering phase-shifts developed in a previous paper [1]), hereafter referred to as (I), is improved for long-tailed potentials by using a better form factor $g_l(r)$, which takes into account distortion of the wave function by the potential tail.

A numerical comparison for ^{3}S and ^{1}S neutron-proton scattering is made for wells of gaussian, exponential and Yukawa shape. Comparison of results with those of (I) shows a reduction in error of more than half for non-singular potentials for which satisfactory $g_l(r)$ can be constructed, such as the exponential potential. Singular potentials such as the Yukawa well give the least satisfactory results, as satisfactory $g_l(r)$ cannot be constructed in the usual simple way, due to neglect of logarithmic terms in the distorted wave function.

1. Introduction

In (I) it was shown that an elastic scattering event may be described by the distorted wave function

$$u_l(r) = \mathscr{J}_l(kr)\cos\delta_l - g_l(r)\mathscr{N}_l(kr)\sin\delta_l, \tag{1}$$

where

$$g_l(r) = \begin{cases} f_l(r) & (r \leqq r_a), \\ 1 & (r \geqq r_a), \end{cases} \tag{2}$$

subject to the boundary conditions $g_l(r \to 0) \approx r^{2l+1}$ and $u_l(r_a)$, $u'_l(r_a)$ continuous. This is valid only for very light nuclei, where $\delta_l \leqq \pi$ [2]).

Substitution in the integral equation for the phase-shift,

$$\sin\delta_l = -\frac{1}{k}\int_0^\infty U(r)\mathscr{J}_l(kr)u_l(r)\mathrm{d}r, \tag{3}$$

leads to the new relation

$$\tan\delta_l \approx B_{1l}/(1-B_{2l}), \tag{4}$$

where

$$B_{1l} = -\frac{1}{k}\int_0^\infty U(r)\mathscr{J}_l^2(kr)\mathrm{d}r, \tag{5}$$

$$B_{2l} = \frac{1}{k}\int_0^\infty g_l(r)U(r)\mathscr{J}_l(kr)\mathscr{N}_l(kr)\mathrm{d}r, \tag{6}$$

B_{1l} being the first Born approximation integral.

The cut-off range may be found roughly from the requirement that the potential be negligible for $r \geqq r_a$; however, best results are obtained by choosing r_a to give the correct zero-energy scattering length a.

This procedure is the best for treating a spherical well and is also excellent for wells with short tails, such as the gaussian and Woods-Saxon potentials. However, the idea of a cut-off range is obviously less suitable for wells with longer tails, such as the exponential and Yukawa potentials. Numerical calculations in (I) in fact show that although the latter two wells give good results at low and intermediate energies (due to the zero energy normalization used via a), at high energies (4) may give results no better or even worse than using the first Born approximation B_{1l}. Of course, the error in these cases is already small. Note that that correct value of a is obtainable using Kohn's method[3,4]).

2. Form Factors for Long-tailed Potentials

An improved approximate theory is possible for long-tailed potentials if the condition (2) is dropped and replaced by the boundary conditions

$$g_l(r \to 0) \approx r^{2l+1}, g_l(r \to \infty) \to 1. \tag{7}$$

We take the potential $U(r)$, assumed non-singular at $r = 0$, of form

$$U(r) = -U_0\phi(r), \tag{8}$$

where $\phi(0) = 1$, $1-\phi(r \to 0) \approx r^n$ $(n \geqq 1)$. A convenient form factor is then

$$g_l(r) = Ar^{2l+1}\phi(r)+(1-\phi(r))^{2l+1}, \tag{9}$$

which satisfies (7) and at the same time assumes a direct relation between the radial factor $\phi(r)$ of the potential and the distortion of the wave function. The constant A must be chosen to give the correct zero-energy scattering length a.

If the radial factor $\phi(r)$ of (8) is singular at $r = 0$, then we must replace (9) by

$$g_l(r) = Ar^{2l+1}\phi_1(r)+(1-\phi_1(r))^{2l+1}, \tag{10}$$

where

$$\phi_1(r) = \phi(r)C(r) \tag{11}$$

and $C(r)$ is a factor cutting off the singularity of $\phi(r)$ at $r = 0$:

$$\phi_1(0) = 1, \quad 1-\phi(r \to 0) \approx r^n \quad (n \geqq 1), \quad C(r \to \infty) \to 1.$$

3. Low Energy Neutron-Proton Scattering for Tailed Wells

In this section application of the results of section 2 is made to ^{3}S and ^{1}S n−p scattering at low energies (s-waves only). Gaussian, exponential and Yukawa wells are considered. We use the fact that (4) reduces to the shape-independent formula (28) of (I),

$$k \cot \delta_0 = -\frac{1}{a} + \tfrac{1}{2}r_0k^2 + O(k^4), \tag{12}$$

where the relations (29) of (I) give the zero-energy scattering length a and effective range r_0 as integral functions of $U(r)$ and $g_0(r)$. It is sufficient to test that the value of A in (9) which gives the correct a value also leads to a good value of r_0. Well parameters used are those in section 8 of (I), but $g_0(r)$ is taken from (9) or (10) above.

For the gaussian well we use $\phi(r) = e^{-r^2/b^2}$, for the exponential well $\phi(r) = e^{-r/b}$, and for the Yukawa well $\phi_1(r) = (e^{-r/b}/(r/b))$ arctan r/b, where b is the parameteric range of the well in each case. Experimental values are taken as

^{3}S n−p scattering: $a = 5.38\times10^{-13}$ cm, $r_0 = 1.70\times10^{-13}$ cm;
^{1}S n−p scattering: $a = -23.69\times10^{-13}$ cm, $r_0 = 2.70\times10^{-13}$ cm.

Using the above experimental a values, values of r_0 calculated in papers (I) and (II) respectively are shown in table 1.

TABLE 1

Calculated values of effective range r_0 in units of 10^{-13} cm for n−p scattering as obtained from papers (I) and (II) respectively

Well shape	Spin state	r_0 paper (I)	r_0 paper (II)
Gaussian	^{3}S	1.686	1.711
	^{1}S	2.711	2.635
Exponential	^{3}S	1.667	1.729
	^{1}S	2.852	2.752
Yukawa	^{3}S	2.27	2.186
	^{1}S	3.21	3.089

Table 1 shows that r_0 for the gaussian well is improved by only about 25 %. This is due to the short potential tail involved, so that the cut-off method for $g_0(r)$ in (I) already gives a very good result. However, the exponential well results show a reduction in error by factors of 2.3 and 2.9 for ^{3}S and ^{1}S scattering respectively. This is to be expected owing to the important effect of the long well-tail on $g_0(r)$.

The Yukawa well results of (I) showed much larger errors than any other well shape. The results of (II) give r_0 values about 15 % and 24 % better for ^{3}S and ^{1}S scattering respectively. However, the remaining errors are still unduly large and cannot be mainly due to the tail effect, as alternative expressions for $\phi_1(r)$ all give substantially the same results.

The source of the remaining Yukawa well error may be understood if one remembers that for small r, the Yukawa potential behaves similarly to a Coulomb potential. The regular and irregular solutions of the latter for small r are [5])

$$F_0(r) = C_0 kr(1+r/2R+\ldots), \tag{13}$$

$$G_0(r) = \frac{1}{C_0}\left\{1+\frac{r}{R}\left(\ln\frac{r}{R}+2\gamma-1+h(\alpha)+\ldots\right)\right\}, \tag{14}$$

where

$$C_0^2 = 2\pi\alpha/(e^{2\pi\alpha}-1), \quad \alpha = e^2/\hbar v, \quad R = \hbar^2/me^2,$$

$$h(\alpha) = \mathrm{Re}\{\Gamma'(-i\alpha)/\Gamma(-i\alpha)\} - \ln\alpha, \quad \gamma = \text{Euler's constant}.$$

For small r, $F_0(r)$ behaves like $\mathcal{J}_0(kr)$, but $G_0(r)$ does not behave like $-\mathcal{N}_0(kr)$ due to the logarithmic term in (14). This indicates that (1) is not the correct form for the wave function when the potential has a $1/r$ singularity. An empirical adjustment might be attempted by replacing A in the expression (10) for $g_l(r)$ by $A+B(r/b)\ln(r/b)$; A and B can actually be found to give the correct a and r_0 values; however, this already assumes a knowledge of the low energy scattering and can only be used for prediction of higher energies.

4. Neutron-Proton Scattering at Arbitrary Energies

Calculations over a wide range of energies 0.8—186 MeV ($k = 0.1-1.5$) have been performed for ^{3}S and ^{1}S n—p scattering, using the exponential well. Table 2 compares exact s-wave phase-shifts δ_0, obtained by solution of the wave equation in (I), with the approximate results obtained by using the $g_0(r)$ of papers (I) and (II) respectively.

TABLE 2

Values of s-wave phase-shift δ_0 for n—p scattering by exponential well

k	^{3}S state			^{1}S state		
	Exact	$g_0(r)$ from (I)	$g_0(r)$ from (II)	Exact	$g_0(r)$ from (I)	$g_0(r)$ from (II)
0.1	2.6310	2.5917	2.6279	1.0621	1.0541	1.0551
0.25	2.0672	2.0040	2.0796	1.1093	1.0883	1.0993
0.5	1.5440	1.4751	1.5230	0.9327	0.9091	0.9346
0.75	1.2900	1.1726	1.2239	0.7865	0.7526	0.7572
1.0	1.0890	0.9844	1.0301	0.6645	0.6390	0.6566
1.5	0.8383	0.7639	0.7947	0.5087	0.4936	0.5033

From table 2, we see that the mean errors in δ_0 for ^{3}S and ^{1}S n—p scattering are reduced from 4.9 % to 2.2 % and from 2.5 % to 1.1 % repectively. Thus use of the improved form factor (9) is well justified for long-tailed potentials.

References

1) P. Swan, Nuclear Physics **18** (1960) 245
2) P. Swan, Nature **187** (1960) 585
3) L. Spruch and L. Rosenberg, Phys. Rev. **116** (1960) 1034, **117** (1960) 1095; Nuclear Physics **17** (1960) 30
4) T. Ohmura, Journ. Math. Phys. **1** (1960) 27
5) K. B. Mather and P. Swan, Nuclear Scattering (Cambridge University Press, 1958)

8.B

Nuclear Physics **21** (1960) 237—244; © *North-Holland Publishing Co., Amsterdam*

Not to be reproduced by photoprint or microfilm without written permission from the publisher

DIRECTIONAL CORRELATION OF MESONS IN A CASCADE DECAY OF BARYONS RESULTING FROM A BARYON-BARYON REACTION

A. DELOFF and J. WRZECIONKO

Institute for Nuclear Research, Warsaw

Received 7 July 1960

Abstract: This is a continuation of a preceding work by the same authors [1]). We obtained general expressions of the momentum directional correlation function of mesons resulting from the decay of baryons being products of a baryon-baryon reaction. As a particular case we examined a reaction in which both particles before reaction are unpolarized. Calculations were done assuming that a) particles before the reaction are in the S state only (low energy zero threshold collision), or b) final state baryons are in the S-state only (high threshold reaction). Several experimental possibilities for a determination of the relative intrinsic parity of baryons are discussed.

1. Introduction

In a preceding paper [1]) which will be hereafter referred to as (I) we considered reactions of the type a+b → c+d, where all particles involved are $\frac{1}{2}$ spin baryons. The relative intrinsic parity of these particles was assumed to be even ($I_a I_b = I_c I_d$), or odd ($I_a I_b = -I_c I_d$), both cases being taken into account. We used the phenomenological S-matrix approach and found the corresponding cross sections and polarizations, expressed in terms of the scattering angle θ and some phenomenological parameters, for the two cases of the relative parity. We found further, that, even without assuming a particular interaction there are some possibilities of distinguishing between the relative parities. Assuming that transitions go only from the S state we got different angular dependences of the polarizations for the two values of the relative parity. If the particles in the initial state are unpolarized, the final state particles are a) unpolarized if the relative parity is even, or b) polarized normal to the scattering plane, with the degree of polarization proportional to sin 2θ, if the relative parity is odd. These results can serve as a test for the determination of the relative parity of baryons. In this paper we discuss some other possibilities of the determination of the relative parity.

We will consider the decay of the final state particles (c and d) assuming that they decay by one mode into a baryon and a meson. The shape of the momentum correlation function for mesons emerging in this process depends on the relative parity of the particles occurring in the reaction. We give a

general expression for these correlation functions in both cases of relative parity. As an example we calculate the correlation for transitions in the S-state approximation in which either the a and b particles are in the S-state, or the c and d particles are produced in the S-state only. The measurement of the correlation can give some information about relative parities.

2. The Correlation Function, General Theory

The transition T matrix for the reaction a+b → c+d, where a, b, c, d particles are $\frac{1}{2}$ spin baryons was discussed briefly in (I). Using the phenomenological S-matrix technique we give there the general form of T in the two cases of the relative intrinsic parity. Denoting by $T^{(+)}$ and $T^{(-)}$ the transition matrix in the even ($I_a I_b = I_c I_d$) and odd ($I_a I_b = -I_c I_d$) relative parity case respectively we have according to (I)

$$T^{(+)} = A+B\boldsymbol{\sigma}_1\cdot\mathbf{n}+C\boldsymbol{\sigma}_2\cdot\mathbf{n}+D\boldsymbol{\sigma}_1\cdot\mathbf{n}\boldsymbol{\sigma}_2\cdot\mathbf{n}+E\boldsymbol{\sigma}_1\cdot\mathbf{m}\boldsymbol{\sigma}_2\cdot\mathbf{m}+F\boldsymbol{\sigma}_1\cdot\mathbf{l}\boldsymbol{\sigma}_2\cdot\mathbf{l} + G\boldsymbol{\sigma}_1\cdot\mathbf{l}\boldsymbol{\sigma}_2\cdot\mathbf{m}+H\boldsymbol{\sigma}_1\cdot\mathbf{m}\boldsymbol{\sigma}_2\cdot\mathbf{l}, \quad (1)$$

$$T^{(-)} = A'\boldsymbol{\sigma}_1\cdot\mathbf{l}+B'\boldsymbol{\sigma}_2\cdot\mathbf{l}+C'\boldsymbol{\sigma}_1\cdot\mathbf{l}\boldsymbol{\sigma}_2\cdot\mathbf{n}+D'\boldsymbol{\sigma}_1\cdot\mathbf{n}\boldsymbol{\sigma}_2\cdot\mathbf{l}+E'\boldsymbol{\sigma}_1\cdot\mathbf{m}+F'\boldsymbol{\sigma}_2\cdot\mathbf{m} + G'\boldsymbol{\sigma}_1\cdot\mathbf{m}\boldsymbol{\sigma}_2\cdot\mathbf{n}+H'\boldsymbol{\sigma}_1\cdot\mathbf{n}\boldsymbol{\sigma}_2\cdot\mathbf{m}, \quad (2)$$

where the angular dependence of the scalar functions $A, \ldots, H$ and $A', \ldots, H'$ was given in (I), $\boldsymbol{\sigma}_1$ and $\boldsymbol{\sigma}_2$ are Pauli spin vectors, and three unit vectors $\mathbf{n}$, $\mathbf{m}$, $\mathbf{l}$ are defined as follows

$$\mathbf{n} = \frac{\mathbf{p}_i \wedge \mathbf{p}_f}{\sin\theta}, \quad \mathbf{m} = \frac{\mathbf{p}_i - \mathbf{p}_f}{2\sin\frac{1}{2}\theta}, \quad \mathbf{l} = \frac{\mathbf{p}_i + \mathbf{p}_f}{2\cos\frac{1}{2}\theta},$$

where $\mathbf{p}_i$ and $\mathbf{p}_f$ are unit vectors in the direction of the initial and final c.m. momentum respectively.

We will now consider the decay of the final state baryons assuming that they decay only by one mode into a baryon and a meson. The transition matrix describing the decay of the c-particle has the form $a_1+b_1\boldsymbol{\sigma}_1\cdot\mathbf{k}_1$, where the $\mathbf{k}_1$ vector is a unit vector in the direction of motion of the meson in the rest system of c. Similarly the decay of d is described by a matrix $a_2+b_2\boldsymbol{\sigma}_2\cdot\mathbf{k}_2$, where $\mathbf{k}_2$ is a unit vector determining the momentum of the second meson in the rest system of d.

Having these transition matrices together with expressions (1) and (2) in mind we can write functions $W(\mathbf{k}_1, \mathbf{k}_2)$ describing the correlation of the mesons momenta $\mathbf{k}_1$ and $\mathbf{k}_2$,

$$W(\mathbf{k}_1, \mathbf{k}_2) = \lambda_1\lambda_2\,\mathrm{Tr}\{T\rho T^\dagger(1+\eta_1\boldsymbol{\sigma}_1\cdot\boldsymbol{\varkappa}_1)(1+\eta_2\boldsymbol{\sigma}_2\cdot\boldsymbol{\varkappa}_2)\}/\mathrm{Tr}\{T\rho T^\dagger\}, \quad (3)$$

where

$$\lambda_\alpha = |a_\alpha|^2 + |b_\alpha|^2, \quad \eta_\alpha = \frac{2\,\mathrm{Re}\,(a_\alpha b_\alpha^*)}{|a_\alpha|^2 + |b_\alpha|^2}, \quad (\alpha = 1, 2),$$

and the vectors $\varkappa_1$ and $\varkappa_2$ are defined as

$$\varkappa_1 = \mathbf{k}_1 + \frac{\mathbf{p}_c \cdot \mathbf{k}_1}{(E_c + m_c)m_c}\mathbf{p}_c - \frac{1}{m_c}\mathbf{p}_c \wedge \mathbf{k}_1,$$

$$\varkappa_2 = \mathbf{k}_2 + \frac{\mathbf{p}_d \cdot \mathbf{k}_2}{(E_d + m_d)m_d}\mathbf{p}_d - \frac{1}{m_d}\mathbf{p}_d \wedge \mathbf{k}_2.$$

Furthermore, ρ is the density matrix describing the polarizations of a and b particles, T stands here for $T^{(+)}$ or $T^{(-)}$. For small momenta of the particle c and d respectively, where $p_c/m_c \ll 1$ and $p_d/m_d \ll 1$ the contribution from the motion of these particles can be neglected and we can put $\varkappa_\alpha \approx \mathbf{k}_\alpha$. The correlation function W can be expressed in terms of the polarizations of the c and d particles and the spin correlation tensor. As a matter of fact we get simply from (3)

$$W(\mathbf{k}_1, \mathbf{k}_2) = \lambda_1\lambda_2\{1 + \eta_1 P_{1i}\kappa_{1i} + \eta_2 P_{2i}\kappa_{2i} + \eta_1\eta_2 C_{ij}\kappa_{1i}\kappa_{2j}\}, \tag{4}$$

where, $i, j = x, y, z$, the quantities P_{1i} and P_{2i} are the polarization vectors of the c and d particle respectively, and C_{ij} is the spin correlation tensor; the definitions are

$$P_{1i} = \frac{\mathrm{Tr}\{T\rho T^\dagger \sigma_{1i}\}}{\mathrm{Tr}\{T\rho T^\dagger\}}, \tag{5}$$

$$P_{2i} = \frac{\mathrm{Tr}\{T\rho T^\dagger \sigma_{2i}\}}{\mathrm{Tr}\{T\rho T^\dagger\}}, \tag{6}$$

$$C_{ij} = \frac{\mathrm{Tr}\{T\rho T^\dagger \sigma_{1i}\sigma_{2j}\}}{\mathrm{Tr}\{T\rho T^\dagger\}}. \tag{7}$$

3. The S-State Approximation

The general form of the W function as given by (4) is very complicated especially if the particles a and b occurring in the initial state of our reaction are polarized. Even if one would get the explicit formulae for $P_{1i}^{(\pm)}$, $P_{2i}^{(\pm)}$, $C_{ij}^{(\pm)}$ expressed by the scalar functions $A, \ldots, H$ or $A', \ldots, H'$ it is impossible to draw any conclusion about the relative parities. For both values of the relative parity the expressions for polarizations and C_{ij} are very similar. It is sufficient to know how the $P_{1i}^{(+)}$, $P_{2i}^{(+)}$, $C_{ij}^{(+)}$ depend on the $A, \ldots, H$ functions and one can write at once the dependence of the $P_{1i}^{(-)}$, $P_{2i}^{(-)}$, $C_{ij}^{(-)}$ on the $A', \ldots, H'$ functions by the application of a simple transformation. This is shown in the

appendix. However, it is possible to distinguish between parities by investigating the angular dependence of the polarizations and the correlation tensor. The angular dependence of these quantities should obviously be much influenced by the types of transitions, the latter being determined by the relative intrinsic parity of the particles involved in the reaction. Using the $A, \ldots, H$ and $A', \ldots, H'$ expressed in terms of the scattering angle θ as given in (I) one can find the angular dependence of the polarizations and the correlation tensor for both cases of the relative parity. However, it is rather difficult to get general expressions for them preserving all angular momenta. We will discuss here a simplified case assuming the so called S-state approximation introduced in (I). According to this approximation we assume two special cases: a) the final state particles are only in the S-state and b) the initial state particles are only in the S-state. Besides that we confine ourselves to reactions in which the initial state particles a and b are unpolarized. Putting $\rho = \frac{1}{4}$ we obtain the polarizations and the correlation tensor

$$\sigma^{(+)} P_{1i}^{(+)} = n_i 2[\mathrm{Re}(AB^*+CD^*)+\mathrm{Im}(GE^*+FH^*)], \tag{8a}$$

$$\sigma^{(+)} P_{2i}^{(+)} = n_i 2[\mathrm{Re}(AC^*+BD^*)+\mathrm{Im}(HE^*+FG^*)], \tag{8b}$$

$$\begin{aligned}\sigma^{(+)} C_{ij}^{(+)} &= n_i n_j 2\,\mathrm{Re}(AD^*+BC^*+HG^*-EF^*)\\ &+m_i m_j 2[\mathrm{Re}(AE^*-FD^*)+\mathrm{Im}(CH^*+BG^*)]\\ &+l_i l_j 2[\mathrm{Re}(AF^*-ED^*)+\mathrm{Im}(GC^*+HB^*)]\\ &+l_i m_j 2[\mathrm{Re}(AG^*+HD^*)+\mathrm{Im}(CF^*+EB^*)]\\ &+m_i l_j 2[\mathrm{Re}(AH^*+GD^*)+\mathrm{Im}(F^*B+C^*E)],\end{aligned} \tag{8c}$$

$$\sigma^{(+)} = |A|^2+|B|^2+|C|^2+|D|^2+|E|^2+|F|^2+|G|^2+|H|^2. \tag{8d}$$

The corresponding expressions for the odd relative parity can be obtained using the substitution (A.1) from the appendix. Now let us consider the two particular

TABLE 1

Possible transitions according to assumptions a) and b)

	Parity even		Parity odd	
	transition	amplitude	transition	amplitude
a) Final state particles in the S state	$^1S_0 \to {}^1S_0$	α	$^3P_0 \to {}^1S_0$	α'
	$^3S_1 \to {}^3S_1$	β	$^1P_1 \to {}^3S_1$	β'
	$^3D_1 \to {}^3S_1$	γ	$^3P_1 \to {}^3S_1$	γ'
b) Initial state particles in the S state	$^1S_0 \to {}^1S_0$	a	$^3S_1 \to {}^3P_1$	a'
	$^3S_1 \to {}^3S_1$	b	$^3S_1 \to {}^1P_1$	b'
	$^3S_1 \to {}^3D_1$	c	$^1S_0 \to {}^3P_0$	c'

cases quoted as a) and b) above. If the initial state particles are assumed to be in the S-state we have only three transition amplitudes different from zero, a similar situation results for the final state particles in the S-state. The corresponding transitions are written in table 1.

Using the definitions of $A, \ldots, H$ and $A', \ldots, H'$ given in (I) we express them by the corresponding transition amplitudes and the scattering angle θ. The obtained $A, \ldots, H$ and $A', \ldots, H'$ are next inserted to (8). After a lot of algebra we get finally

$$\begin{aligned} W^{(\pm)}(\mathbf{k}_1, \mathbf{k}_2) = \lambda_1\lambda_2\{&1+\eta_1 \mathbf{P}_1^{(\pm)} \cdot \mathbf{k}_1+\eta_2 \mathbf{P}_2^{(\pm)} \cdot \mathbf{k}_2 \\ &+\eta_1\eta_2[C_{nn}^{(\pm)} \mathbf{n} \cdot \mathbf{k}_1 \mathbf{n} \cdot \mathbf{k}_2+C_{mm}^{(\pm)} \mathbf{m} \cdot \mathbf{k}_1 \mathbf{m} \cdot \mathbf{k}_2+C_{ll}^{(\pm)} \mathbf{l} \cdot \mathbf{k}_1 \mathbf{l} \cdot \mathbf{k}_2 \\ &+C_{lm}^{(\pm)} \mathbf{l} \cdot \mathbf{k}_1 \mathbf{m} \cdot \mathbf{k}_2+C_{ml}^{(\pm)} \mathbf{m} \cdot \mathbf{k}_1 \mathbf{l} \cdot \mathbf{k}_2]\}, \end{aligned} \tag{9}$$

where for the final state particles in the S-state we have

$$\mathbf{P}_1^{(\pm)} = \mathbf{P}_2^{(\pm)} = 0.$$

In that case, we have for parity even

$$\begin{aligned} C_{nn}^{(+)} &\equiv C_{ij}^{(+)} n_i n_j = [|\beta|^2+2|\gamma^2|+2 \operatorname{Re}(\gamma\beta^*)]/16p^2\sigma^{(+)}, \\ C_{ll}^{(+)} &\equiv C_{ij}^{(+)} l_i l_j = \left[\left|\beta-\frac{1}{\sqrt{2}}\gamma\right|^2-|\alpha|^2-\tfrac{3}{2}\cos\theta(|\gamma|^2+2\sqrt{2}\operatorname{Re}(\beta\gamma^*))\right] \Big/ 16p^2\sigma^{(+)}, \\ C_{mm}^{(+)} &\equiv C_{ij}^{(+)} m_i m_j \\ &= \left[\left|\beta-\frac{1}{\sqrt{2}}\gamma\right|^2-|\alpha|^2+\tfrac{3}{2}\cos\theta(|\gamma|^2+2\sqrt{2}\operatorname{Re}(\beta\gamma^*))\right] \Big/ 16p^2\sigma^{(+)}, \\ C_{lm}^{(+)} &\equiv C_{ij}^{(+)} l_i m_j = \tfrac{3}{2}\sin\theta[|\gamma|^2+2\sqrt{2}\operatorname{Re}(\beta\gamma^*)]/32p^2\sigma^{(+)}, \\ C_{ml}^{(+)} &\equiv C_{ij}^{(+)} m_i l_j = C_{lm}, \end{aligned} \tag{10}$$

where $\sigma^{(+)}$ is the cross section

$$\sigma^{(+)} = [|\alpha|^2+3|\beta|^2+3|\gamma|^2]/16p^2.$$

For parity odd we have

$$\begin{aligned} C_{nn}^{(-)} &\equiv C_{ij}^{(-)} n_i n_j = [3|\beta'|^2-|\alpha'|^2]/16p^2\sigma^{(-)}, \\ C_{ll}^{(-)} &\equiv C_{ij}^{(-)} l_i l_j = [\tfrac{3}{2}|\gamma'|^2-|\alpha'|^2+\cos\theta(\tfrac{3}{2}|\gamma'|^2-3|\beta'|^2)]/16p^2\sigma^{(-)} \\ C_{mm}^{(-)} &\equiv C_{ij}^{(-)} m_i m_j = [\tfrac{3}{2}|\gamma'|^2-|\alpha'|^2-\cos\theta(\tfrac{3}{2}|\gamma'|^2-3|\beta'|^2)]/16p^2\sigma^{(-)}, \\ C_{lm}^{(-)} &\equiv C_{ij}^{(-)} l_i m_j = 3\sin\theta[|\gamma'|^2-2|\beta'|^2]/32p^2\sigma^{(-)}, \\ C_{ml}^{(-)} &\equiv C_{ij}^{(-)} m_i l_j = C_{lm}^{(-)}, \end{aligned} \tag{11}$$

where

$$\sigma^{(-)} = (|\alpha'|^2+3|\beta'|^2+3|\gamma'|^2).$$

The corresponding expressions for the case when the S-state is assumed as the initial state are for parity even

$$\begin{aligned}
&\mathbf{P}_1^{(+)} = \mathbf{P}_2^{(+)} = 0,\\
&C_{nn}^{(+)} = [|b|^2-|a|^2-2|c|^2+2\sqrt{2}\,\mathrm{Re}\,(bc^*)]/16p^2\sigma^{(+)},\\
&C_{ll}^{(+)} = [|b|^2-|a|^2+\tfrac{1}{2}|c|^2-\sqrt{2}\,\mathrm{Re}(bc^*)-\cos\theta(3\sqrt{2}\,\mathrm{Re}(bc^*)+\tfrac{3}{2}|c|^2)]/16p^2\sigma^{(+)},\\
&C_{mm}^{(+)} = [|b|^2-|a|^2+\tfrac{1}{2}|c|^2-\sqrt{2}\,\mathrm{Re}(bc^*)+\cos\theta(3\sqrt{2}\,\mathrm{Re}(bc^*)+\tfrac{3}{2}|c|^2)]/16p^2\sigma^{(+)},\\
&C_{lm}^{(+)} = C_{ml}^{(+)} = \sin\theta[3\sqrt{2}\,\mathrm{Re}(bc^*)+\tfrac{3}{2}|c|^2]/16p^2\sigma^{(+)},
\end{aligned} \tag{12}$$

where

$$\sigma^{(+)} = (|a|^2+3|b|^2+3|c|^2)/16p^2,$$

and for parity odd

$$\begin{aligned}
&\mathbf{P}_1^{(-)} = -\mathbf{P}_2^{(-)} = \mathbf{n}3\sqrt{2}\sin 2\theta\,\mathrm{Im}(a'b'^*)/16p^2\sigma^{(-)},\\
&C_{nn}^{(-)} = [3|b'|^2-|c'|^2]/16p^2\sigma^{(-)},\\
&C_{ll}^{(-)} = [3(|a'|^2-2|b'|^2)-(3|a'|^2+2|c'|^2)\cos\theta+6|a'|^2\cos\theta\cos 2\theta]/32p^2\sigma^{(-)},\\
&C_{mm}^{(-)} = [3(|a'|^2-2|b'|^2)+(3|a'|^2+2|c'|^2)\cos\theta-6|a'|^2\cos\theta\cos 2\theta]/32p^2\sigma^{(-)},\\
&C_{lm}^{(-)} = \sin\theta[-(3|a'|^2-2|c'|^2)+6\sqrt{2}\,\mathrm{Re}\,(a'b'^*)\cos\theta+6|a'|^2\cos^2\theta]/32p^2\sigma^{(-)},\\
&C_{ml}^{(-)} = \sin\theta[-(3|a'|^2-2|c'|^2)-6\sqrt{2}\,\mathrm{Re}(a'b'^*)\cos\theta+6|a'|^2\cos^2\theta]/32p^2\sigma^{(-)},
\end{aligned} \tag{13}$$

where

$$\sigma^{(-)} = (|a'|^2+3|b'|^2+3|c'|^2)/16p^2.$$

4. Discussion

First let us discuss processes with the S state taken in the final state. To this category belong reactions with sufficiently high threshold where the kinetic energy of the initial state particles is mostly transformed into the big masses of the final state particles. We can therefore assume that the final state particles are very slow, and are produced really in the S state predominantly. This assumption, at least, is to be checked experimentally if we choose only reactions with isotropic cross section. We will consider here the following examples examined already by Barshay [2]):

$$\mathrm{N}+\bar{\mathrm{N}}\to\Lambda+\bar{\Sigma},\quad \mathrm{N}+\bar{\mathrm{N}}\to\bar{\Lambda}+\Sigma,\quad \mathrm{N}+\bar{\mathrm{N}}\to\Lambda+\bar{\Lambda}.$$

In the meson correlation function obtained by Barshay there was only one direction connected with the reaction, and this was the direction of the ingoing beam. To get more information about the correlation he assumed that the particles in the initial state are polarized. However, if the full kinematics of the reaction is taken into account, i.e. if the directions of the final state particles momenta are included in the correlation, we obtain more information even when

the initial state particles are unpolarized. The dependence of the components of $C_{ij}^{(\pm)}$ on the scattering angle θ does not give any possibility of distinguishing between parities. From the other side we can here think about a full experiment aiming at the determination of the two sets of the scattering amplitudes, defined by the upper part of table 1. We have 5 independent real parameters and 5 conditions for them given by the measurement of the cross section and the four components of $C_{ij}^{(\pm)}$. This could be very important in the determination of the parity.

Consider now the second class of reactions without a threshold. Here the energy is released due to the total rest mass of the particles, bigger before then after the reaction. For low energy collisions we can assume the S-wave in the initial state. In this case the correlation function shows quite interesting features. First of all in the odd parity case the polarization vectors are different from zero. The other important property is the angular dependence of the $C_{ij}^{(\pm)}$ tensor different in each relative parity case. However, we know only two reactions available for the experimental analysis. These are reactions examined by Pais and Treiman [3]) and Treiman [4]):

$$\Sigma^- + \mathrm{p} \to \Lambda + \mathrm{n}, \quad \text{(i)}$$
$$\Xi^- + \mathrm{p} \to \Lambda + \Lambda. \quad \text{(ii)}$$

In the final state of the processes (ii) we have like particles so the results (12), (13) should be corrected by taking Pauli principle into account. Due to this principle the a, a' and c' amplitudes are absent. The components of $C_{ij}^{(+)}$ are not much altered by putting $a = 0$. It is not the same for the odd parity case, where because of the vanishing of two amplitudes a' and c' we have simply

$$\mathbf{P}_1^{(-)} = \mathbf{P}_2^{(-)} = 0, \quad C_{nn}^{(-)} = +1, \quad C_{ll}^{(-)} = C_{mm}^{(-)} = -1, \quad C_{ml}^{(-)} = C_{lm}^{(-)} = 0.$$

The above results are strongly dependent on the relative intrinsic parity of the particles involved in the reaction. The measurement of the correlation of the pion momenta could be a sensitive test for distinguishing between parities. We notice also that in this measurement it is not necessary to have the initial particles polarized.

The authors are much indebted to Professor J. Werle for reading the manuscript and helpful remarks.

Appendix

The $T^{(-)}$ matrix which is a pseudoscalar can be written as a scalar times a pseudoscalar. Excluding from $T^{(-)}$ the $\boldsymbol{\sigma}_2 \cdot \mathbf{m}$ matrix we can write

$$T^{(-)} = (\tilde{A} + \tilde{B}\boldsymbol{\sigma}_1 \cdot \mathbf{n} + \tilde{C}\boldsymbol{\sigma}_2 \cdot \mathbf{n} + \tilde{D}\boldsymbol{\sigma}_1 \cdot \mathbf{n}\boldsymbol{\sigma}_2 \cdot \mathbf{n} + \tilde{E}\boldsymbol{\sigma}_1 \cdot \mathbf{m}\boldsymbol{\sigma}_2 \cdot \mathbf{m}$$
$$+ \tilde{F}\boldsymbol{\sigma}_1 \cdot \mathbf{l}\boldsymbol{\sigma}_2 \cdot \mathbf{l} + \tilde{G}\boldsymbol{\sigma}_1 \cdot \mathbf{l}\boldsymbol{\sigma}_2 \cdot \mathbf{m} + \tilde{H}\boldsymbol{\sigma}_1 \cdot \mathbf{m}\boldsymbol{\sigma}_2 \cdot \mathbf{l})\boldsymbol{\sigma}_2 \cdot \mathbf{m} = \tilde{T}\boldsymbol{\sigma}_2 \cdot \mathbf{m},$$

where the new scalar functions are simply related to the primed quantities

$$\begin{aligned} \tilde{A} &= F', \quad \tilde{B} = H', \quad \tilde{C} = -iB', \quad \tilde{D} = -iD', \\ \tilde{E} &= E', \quad \tilde{F} = iC', \quad \tilde{G} = A', \qquad \tilde{H} = iG'. \end{aligned} \tag{A.1}$$

The $\tilde{T}$ matrix introduced above is of the same form as $T^{(+)}$; this is very useful in many calculations. Consider the $T^{(-)}\rho T^{(-)\dagger}$ matrix, where ρ is given by

$$\rho = \tfrac{1}{4}(1+\boldsymbol{\sigma}_1 \cdot \boldsymbol{\xi}_1)(1+\boldsymbol{\sigma}_2 \cdot \boldsymbol{\xi}_2);$$

here, $\boldsymbol{\xi}_1$ and $\boldsymbol{\xi}_2$ are the polarization vectors of the particles a and b respectively. Introducing $\tilde{T}$ we have

$$T^{(-)}\rho T^{(-)\dagger} = \tilde{T}\rho' \tilde{T}^{\dagger},$$

where ρ' is of the same form as ρ with $\boldsymbol{\xi}_2$ replaced by

$$\boldsymbol{\xi}'_2 = -\boldsymbol{\xi}_2 + 2\mathbf{m}' \cdot \boldsymbol{\xi}_2 \mathbf{m}. \tag{A.2}$$

Due to the same form of $\tilde{T}$ and $T^{(+)}$ any result obtained for the even parity case can be written at once for the odd parity case. One should only apply the transformation $A \to \tilde{A}, \ldots, H \to \tilde{H}, \boldsymbol{\xi}_2 \to \boldsymbol{\xi}'_2$ and next make use of (A.1) and (A.2).

References

1) A. Deloff and J. Wrzecionko, Nuclear Physics (1960)
2) S. Barshay, Phys. Rev. **113** (1959) 349
3) A. Pais and S. B. Treiman, Phys. Rev. **109** (1958) 1759
4) S. B. Treiman, Phys. Rev. **113** (1959) 355

2.C

Nuclear Physics **21** (1960) 245—255; © *North-Holland Publishing Co., Amsterdam*

Not to be reproduced by photoprint or microfilm without written permission from the publisher

DISPERSION FORMULAS IN THE THEORY OF NUCLEAR REACTIONS

V. I. SERDOBOLSKY

P. N. Lebedev Physical Institute, Moscow, USSR

Received 4 March 1960

Abstract: The paper offers a theory of resonances in nuclear reactions, in which the concept of the R-matrix is not used. Under consideration is a certain parameter whose smallness makes it possible to select, out of the total number of formal levels obtained in the theory, the resonance levels attributable to the formation of the long-lived compound nucleus. For the levels which do not overlap the nuclear-reaction thresholds the compound-nucleus resonances are singled out by the poles of a Green's function at complex energies. The dispersion formulas thus obtained are linear with respect to resonances and contain the complex reduced half-widths. These formulas do not depend on auxiliary "hypersurface radii" and take into account the tails of wave functions responsible for multi-particle processes occurring close to the surface of the nucleus.

1. Introduction

The invariably successful application of the Breit-Wigner resonance formulas for the analysis of a great variety of nuclear reactions has contributed to the evolution of a number of general mathematical theories justifying and specifying the simplest resonance formulas. In 1947 Wigner suggested the well-known theory [1]) based on the application of the R-matrix. In a number of subsequent papers this theory was perfected and extended to embrace various particular cases. The success of the theory for the past ten years has been summarized in an extensive paper [2]). Yet at present it has been clear that the Wigner theory is unsatisfactory in many respects. A large number of auxiliary parameters without physical meaning figure in the R-matrix formalism. These are the energy levels and halfwidths of formal "remote levels" and arbitrary "radii of nucleus hypersurface". It is not clear how the processes involving the emission of two or more real or virtual particles should be described. On the other hand, practical computation has shown that in many cases the apparatus of the Wigner theory proves cumbersome and unjustifiably complex.

Accumulation of experimental data has shown that processes occurring without the formation of a compound nucleus bulk large in nuclear reactions. Papers concerned with the "unified theory of nuclear reactions" [3–6]) have appeared. It was found that scattering on an optical potential as well as direct interactions and processes involving the formation of a compound nucleus may conveniently be described by a single mathematical apparatus. Dispersion

formulas in the framework of the unified theory of nuclear reactions have been studied by Feshbach [5]) as well as Sano, Yoshida and Terasawa [6]). The formulas obtained in ref. [5]) have a limited range of application. In ref. [6]) the permeability coefficients in dispersion formulas are represented as infinite series which makes their practical application rather difficult.

The present paper has two basic aims: to overcome the most essential theoretical drawbacks inherent to the current formal theory and to develop a procedure for evolving dispersion formulas with allowances for optical interaction and other processes weakly depending on energy. Sec. 2 introduces a parameter, defined by eq. (3), whose smallness makes it possible to regard the formal quantities E_λ and $\gamma_{\lambda c}$ as compound-state resonance parameters. Sec. 3 investigates the analytic properties of the wave function and the Green's function $(E-H)^{-1}$ of the general problem of collision with rearrangement of particles. The expansion (8) for the Green's function near the poles is established. Sec. 4 discusses a dispersion expansion (11) independent of arbitrary radii and taking account of the possibility of multiparticle decay. Under consideration is the problem of the reality of the quantities $\gamma_{\lambda c}$ included in practical formulas. These quantities prove to be complex as a rule. Sec. 5 demonstrates that the compound-state wave functions in the region of energies far from the threshold form a biorthogonal system. Hence follows eq. (23) for parameters entering into the dispersion formulas. Sec. 6 discusses the problem of correlations in the signs of $\gamma_{\lambda c}$ and allowances for the contribution of the "remote levels".

2. Selection of Compound States

As in the previous papers concerned with the unified theory of nuclear reactions, we shall proceed from the integral equations of the formal theory of rearrangement collisions. Let ϕ be the wave function of free motion of particles of the α type with the spin quantum numbers sv and the momentum $\hbar\mathbf{k}$ in the centre-of-mass system. Let H be the total Hamiltonian of the problem, and H_0 the Hamiltonian of free motion in the channel α, H being equal to H_0+V. Two solutions $\psi^{(+)}$ and $\psi^{(-)}$ are obtained from eq. (4) for Im $E \to \pm 0$. (see below). Let us introduce an optical potential V^0 and the wave functions $\psi_0^{(+)}$ and $\psi_0^{(-)}$ describing scattering on an optical potential in each of the channels. The indices and operators relating to some other channel with other quantum numbers will be designated by dashes. Let $\mathscr{V}$ be equal to $V-V^0$; then the following identity (see refs. [4,6])) can be written:

$$\langle\phi'|V'|\psi^{(+)}\rangle = \langle\phi'|V'|\psi_0^{(+)}\rangle+\langle\psi_0^{(-)'}|\mathscr{V}'|\psi_0^{(+)}\rangle + \langle\psi_0^{(-)'}|\mathscr{V}'(E-H+i\varepsilon)^{-1}\mathscr{V}|\psi_0^{(+)}\rangle. \quad (1)$$

The first term in (1) describes an optical interaction and vanishes for $\alpha' \neq \alpha$. The second term represents the amplitude of direct processes in the distorted

wave approximation method. In ref. [6]) the authors regarded the third term of the right-hand side of eq. (1) as a resonance one and applied the Kapur-Peierls theory [7]). As is well known, only some of an infinite number of formal levels correspond to those really observed. Let us determine a parameter whose smallness allows of regarding a given level as conditioned by the formation and disintegration of a compound nucleus. We shall proceed from the time description of a nuclear reaction suggested in ref. [8]) and isolate compound states by their large lifetimes. Average reaction times are closely connected with the nature of the energy dependence of wave functions and amplitudes: according to the uncertainty principle $\Delta E \approx \hbar/t$, where ΔE is the interval over which the wave functions change essentially. The characteristic periods of potential scattering and direct processes are, in general, determined by the time needed by the particles for their flight across the nucleus R/v. For particles with the highest orbital momenta this time increases, due to slowing down near the centre, by a factor $(kR)/P_c$, where P_c is the permeability coefficient determined in ref. [2]). The decay time of the compound state λ with respect to the channel $\alpha slJM$ (index c) is equal to $\hbar/2P_c|\gamma_{\lambda c}|^2$. The ratio

$$\frac{t_{\text{flight}}}{t_{\text{decay}}} = \frac{|\gamma_{\lambda c}|^2}{E_R}, \quad \text{where } E_R = \frac{\hbar^2}{2mR^2}, \tag{2}$$

is at the same time the ratio of the width of the compound-nucleus level to that of the optical resonance width $P_c E_R$. The parameter describing a compound state may be determined more accurately with the help of wave functions. The ratio of the square of the wave function modulus of a decaying state averaged over the hypersurface of the nucleus to the internal volume average is

$$\frac{(4\pi)^{-1}\sum_c^{\text{open}} |\langle c|\Psi_\lambda\rangle_R|^2}{\tau^{-1}\int_\tau |\Psi_\lambda|^2 d\tau} = \tfrac{1}{3}\sum_c^{\text{open}} \frac{|\gamma_{\lambda c}|^2}{E_R}. \tag{3}$$

The sum over c includes only open channels. The quantity (3) describes a relative time which the system spends in one-particle states possible at the given energy. This time should be small for the compound nucleus. Treatment of experimental data performed in ref. [10]) shows that even for light nuclei the parameter (3) rarely exceeds 0.1.

3. Analytic Properties

Analytic dependence of the wave function of the stationary problem on complex energy calls in principle for special proof. With real E this proof can probably be performed with the aid of general theorems on the regular dependence of the solutions on the form of the equation and the boundary conditions.

With Im $E \neq 0$ the proof of analyticity offers no difficulties. The spectral analysis [1]) shows that the Green's function $G = (E-H)^{-1}$ is analytical with respect to E at all points which do not coincide with the points of the H operator spectrum. The wave function ψ is connected with $(E-H)^{-1}$ through the Gell-Man-Goldberger equation

$$\psi = \phi + (E-H)^{-1}V\phi. \tag{4}$$

The continuous spectrum of the operator lies on the half axis of real energies $E > E_1$. For Im $E \to \pm 0$, $E > E_1$, G passes into the Green's funtions $G^{(\pm)}$, and ψ into the $\psi^{(\pm)}$ of the physical problem. The asymptotic form of the wave functions (by the radiation condition) contains wave numbers proportional to $\sqrt{E-E_n}$, where E_n is the energy of the nth threshold of the reaction. The analytic continuations of $\psi^{(\pm)}$,therefore, are unique analytic functions only of the arguments $\sqrt{E-E_1}, \ldots \sqrt{E-E_n}, \ldots$. The region of determinations of these functions constitutes a system of Riemann sheets with branch points at $E_1, \ldots E_n, \ldots$. From the continuity equation it follows that in the principal Riemann sheet in which all Im $\sqrt{E-E_n} > 0$, the Green's function G may have poles only at real E. These poles describe the stationary states of the system. Apart from them, complex poles lying in other Riemann sheets are possible. If the pole approaches the half-axis $E > E_1$ of the principal sheet on which a continuous spectrum lies, resonances can be observed in the cross sections.

The time reversibility of quantum mechanics leads to a certain symmetry in the analytic continuations G and ψ. Let O be a time reversibility operator, such that

$$H^* = OHO^+. \tag{5}$$

It is convenient to introduce the operation B which, in acting on the point E in the system of Riemann sheets, leads to reflection with respect to the real half-axis of the principal sheet $E < E_1$. For example, the result of the action of B on E is E^*, $B\sqrt{E-E_n}$ is equal to $-(\sqrt{E-E_n})^*$, etc. For real energies it is obvious that

$$OG^{(\pm)}O^+ = BG^{(\pm)*}. \tag{6}$$

The operation B^* changes the signs of all roots in the arguments of analytic functions and consequently does not violate analyticity. The relation (6) therefore holds good for the complex E as well. It is clear that the poles of G are paired, a pole $\tilde{\lambda}$ at the energy BE_λ corresponding to each pole λ at the energy E_λ. Physical meaning can evidently be attributed only to the first order poles. The function $[\mathrm{Res}\,\psi]_{E_\lambda}$ satisfies the Schroedinger equation with complex energy E_λ and contains only divergent waves in all channels; therefore the residue $[\mathrm{Res}\langle JM|\psi\rangle]_{E_\lambda}$ can be regarded, except for a proportionality factor, as the wave function ψ_λ of the quasi-stationary state with given integrals of motion

J and M. The constant phase of ψ_λ should naturally be chosen so that

$$\psi_{\bar{\lambda}}^* = (-)^{J-M} O\psi_\lambda(-M). \tag{7}$$

With the help of the relations (4), (6) and (7) the resonance part of the Green's function can be expanded near the poles over the quasi-stationary state wave functions. In Dirac's notations ψ_λ is a ket $|\lambda\rangle$ and $\psi_{\bar{\lambda}}^*$ the bra $\langle\lambda|$. The expansion has the form

$$G = \sum_\lambda \frac{|\lambda\rangle\langle\lambda|}{E-E_\lambda} + G_{\text{smooth}}. \tag{8}$$

It will be noted that if the compound-nucleus level overlaps the nuclear-reaction threshold, the optical wave function changes essentially over energy intervals of the order of Γ owing to the permeability coefficient. The isolation of compound states according to energy dpendence therefore becomes impossible. In refs. [11]) and [4]) the approximation $\Gamma \ll |E-E_{\text{thresh}}|$ is actually used, where E_{thresh} is the energy of the threshold closest to E. In the same approximation, the second term in (8) which remains after the subtraction of the polar part of G can be regarded as the Green's function of direct and optical processes.

4. Dispersion Expansion

As has been established, the compound-nucleus resonances are contained in the last term of eq. (1). To obtain a dispersion formula it is sufficient to substitute (8) and pass to the representation with quantum numbers $\alpha slJM$. Employing the formulas given in the appendix, we obtain

$$S^J_{c'c} = \frac{i}{\hbar} \sum_\lambda \frac{\langle c' u_{c'}|\mathscr{V}'|\lambda\rangle\langle\lambda|\mathscr{V}|cu_c\rangle}{E-E_\lambda} + (S^J_{c'c})_{\text{smooth}}. \tag{9}$$

With the help of relations like (5), (7) and (25) we can easily see that the resonance part of (9) is symmetrical with respect to the indices c′ and c. For the sake of convenience we introduce the notation

$$u_{\lambda c} = i(2\hbar)^{-\frac{1}{2}}\langle cu_c|\mathscr{V}|\lambda\rangle = i(2\hbar)^{-\frac{1}{2}}\langle\lambda|\mathscr{V}|cu_c\rangle. \tag{10}$$

The expansion (9) assumes the form

$$S^J_{c'c} = (S^J_{c'c})_{\text{smooth}} + 2i \sum_\lambda \frac{u_{\lambda c'} u_{\lambda c}}{E_\lambda - E}. \tag{11}$$

An essential theoretical advantage of eq. (11) is that it was derived without the assumption of the orthogonality of the wave functions of the channels on the nucleus hypersurface. Thus, there arises no "problem of cutting off the tails of wave functions" characteristic of the current theories. It is clear

that multi-particle processes occurring on the nucleus surface do not distort the shape of the dispersion formula and the influence of closed channels (in the energy region far from threshold) is inessential. The decay of the compound nucleus into three or more particles can be described with eqs. (9) and (11) through a proper choice of the function u_c with allowance for a continuous spectrum of outgoing particles. Eq. (11) does not contain the radii of the channels, the choice of which is largely arbitrary. If, on the other hand, it is assumed that there exists a hypersurface on which the wave functions $|c\rangle$ are orthogonal, the usual results will be obtained. In the energy region far from threshold the values of u_c depend weakly on energy and it may be assumed that $u_c = u_c(k_\lambda r)$. Let us replace $\mathscr{V}$ in the brackets by the difference $H-H_0-V^0$ and make use of Green's theorem. We find that

$$u_{\lambda c} = \Omega_c P_c^{\frac{1}{2}} \gamma_{\lambda c}. \tag{12}$$

Here Ω_c and P_c are the same as in ref. [2]).

The amplitudes of the reduced halfwidths are as usual equal to

$$\gamma_{\lambda c} = \left(\frac{\hbar^2 R}{2m}\right)^{\frac{1}{2}} \langle c|\lambda\rangle_R = \left(\frac{\hbar^2 R}{2m}\right)^{\frac{1}{2}} \langle \lambda|c\rangle_R. \tag{13}$$

The quantities $\gamma_{\lambda c}$ are complex, in general. It will be noted that the $\gamma_{\lambda c}$ in the Kapur-Peierls theory [7]) are also complex. In the R-matrix theory, with its procedure of eliminating the infinite background of levels, the dispersion formula contains, not the $\gamma_{\lambda c}$, but certain modified quantities $\alpha_{\lambda c}$ smoothly depending on energy. In the simplest case of the equation with one level (see ref. [2]))

$$\alpha_\lambda = (1-R^0(L-B))^{-1}\gamma_\lambda. \tag{14}$$

If the remaining part of the S-matrix corresponds to scattering on an optical potential, R^0 has only diagonal elements equal to $(L_c^0-B_c)^{-1}$. In the energy region far removed from optical resonances, $|L_c^0| \gg 1$ (an infinitely high potential wall) and $\alpha_{\lambda c}$ reduce to the real $\gamma_{\lambda c}$ of Wigner's theory. Thus, the quantities $\gamma_{\lambda c}$ in (12) are real only when there is one isolated level of the compound nucleus, while other processes are well described by scattering on an infinitely high potential wall.

5. Phases of the Reduced Halfwidths

The complex character of $\gamma_{\lambda c}$ leads to doubling the indefinite parameters and at a first glance considerably depreciates the dispersion equation (11). It turns out, however, that the phases of these values can be determined from certain general considerations.

To begin with, it will be noted that if the halfwidths of levels are considerably less than the distance to the nearest threshold of the nuclear reaction, the wave

functions of the compound states ψ_λ and $\psi_{\tilde{\lambda}}$ form a mutually orthogonal system. To show this, the equations

$$(E_\lambda - H)\psi_\lambda = 0 \quad \text{and} \quad (E_\mu - H^*)\psi_{\tilde{\mu}}^* = 0 \tag{15}$$

are multiplied by $\psi_{\tilde{\mu}}^*$ and ψ_λ, subtracted and integrated over a certain volume τ which contains the compound nucleus. Owing to the smallness of the parameter (3) the wave functions ψ_λ are relatively small outside the nucleus and the corresponding integrals depend weakly on the choice of τ. Due to E_λ being complex, the functions ψ_λ exponentially increase at infinity, $\psi_\lambda \approx \exp(-\mathrm{Im}\, k_\lambda r)$ at $r \to \infty$ in channel α, and therefore the volume τ must be finite. Let us select the radii R_H of the hypersurface limiting τ so that the ratio R/R_H (R is the radius of the nucleus) is of the order of the parameter (3). Then $R \ll R_H$, and at a distance R_H from the nucleus, the tails of wave functions corresponding to the virtual many-particle processes and channels closed at the given energy will make an insignificant contribution. At the same time the modulus of $\mathrm{Im}\, k_\lambda R_H$ will be smaller than unity and in the integrals over $d\tau$ the main contribution will come from the integration over the internal part of the compound system, $r < R$. The application of the Green theorem yields

$$(E_\mu - E_\lambda)\int \psi_{\tilde{\mu}}^* \psi_\lambda \, d\tau = \sum_c^{\text{open}} \gamma_{\mu c}\gamma_{\lambda c}[(L_c)_{E_\lambda} - (L_c)_{E_\mu}]. \tag{16}$$

The quantities γ depend on the radius of the hypersurface and are determined according to (13). The real part of the logarithmic derivatives changes slowly with energy, and the derivative $\partial\, \mathrm{Re}\, L_c/\partial E$ equals, in order of magnitude, E_R^{-1} (see ref. [2]), p. 352). This means that in the approximation of a small parameter (3), in eq. (16) only the imaginary parts P_c of the logarithmic derivatives are essential. It is clear that for the levels not overlapping the thresholds, the functions ψ_λ and $\psi_{\tilde{\lambda}}$ are mutually orthogonal in the approximation $\Gamma/|E - E_{\text{thresh}}| \ll 1$. At $\mu = \tilde{\lambda}$ we obtain the following relation containing the norm of functions ψ_λ:

$$N_\lambda = \int |\psi_\lambda|^2 d\tau = -(\mathrm{Im}\, E_\lambda)^{-1} \sum_c^{\text{open}} |u_{\lambda c}|^2. \tag{17}$$

On the other hand, with the aid of the conventional procedure and applying Green's theorem to the analytic continuation of the functions $\psi^{(-)*}$ and $\partial\psi^{(+)}/\partial E$ near the pole E_λ, the following equality may be established:

$$\int \psi_{\tilde{\lambda}}^* \psi_\lambda \, d\tau = 1 - \sum_c^{\text{open}} \left(\frac{\partial L_c}{\partial E}\right)_{E_\lambda} \gamma_{\lambda c}^2. \tag{18}$$

In the same approximation $L_c = \text{const.}$ and the integral (18) is equal to unity. Now it can easily be found that

$$\tfrac{1}{2}\int |\psi_\lambda - \psi_{\tilde{\lambda}}|^2 d\tau = N_\lambda - 1. \tag{19}$$

It is clear that $N_\lambda \geqq 1$. The equations for ψ_λ and $\psi_{\tilde{\lambda}}$, accurate to the ratio $\Gamma_\lambda/|E-E_{\text{thresh}}|$, coincide, and the dependence of solutions describing compound states on the choice of limiting conditions is weak; therefore, for isolated levels, ψ_λ approximately equals $\psi_{\tilde{\lambda}}$, and $N_\lambda = 1$. If the levels overlap, even small changes in the initial equation and limiting conditions lead to an essential change in the shape of eigenfunctions. Let us assume than n levels of the compound nucleus lie in a small region of energies of the order of Γ. The respective wave functions ψ_λ are linearly independent and in the approximations made satisfy the biorthogonality condition. Variation of limiting conditions will lead to a shift of eigenvalues by a quantity of the order of Γ and to the formation of new eigenfunctions which will be linear combinations of the former. Applying this argument to the functions ψ_λ we come to the equality

$$\psi_\lambda = \sum_\mu a_{\mu\lambda} \psi_{\tilde{\mu}}. \tag{20}$$

The coefficients $a_{\mu\lambda}$ are determined from the biorthogonality condition

$$a_{\mu\lambda} = a_{\tilde{\lambda}\tilde{\mu}} = \int \psi_\mu^* \psi_\lambda \, d\tau, \quad a_{\lambda\lambda} = a_{\tilde{\lambda}\tilde{\lambda}} = N_\lambda. \tag{21}$$

Hence

$$a_{\mu\lambda} = 2i \frac{\sum_c^{\text{open}} u_{\mu c}^* u_{\lambda c}}{E_\mu^* - E_\lambda}. \tag{22}$$

We multiply (20) by $\psi_{\tilde{\nu}}^*$ and integrate the result; the equation thus obtained imposes a relation between the coefficients $a_{\mu\lambda}$:

$$\sum_\mu a_{\mu\lambda} a_{\mu\nu} = \delta_{\lambda\nu}. \tag{23}$$

The relation (20) between the functions ψ_λ is approximately satisfied in the internal region; on the surface of the nucleus, eq. (20) holds good only when the effects connected with the permeability of the potential well are inessential. It is noteworthy that eq. (23) with coefficients (22) can be deduced from the principal equation (11) if it is demanded that the approximate S-matrix with a certain number of selected levels satisfies the unitarity condition. Specific applications and derivation of dispersion formulas for certain particular cases of practical interest is given in a separate paper [12]).

6. Averaged Cross-Sections and Correlations in the Signs of $\gamma_{\lambda c}$

If the signs of $\gamma_{\lambda c}$ do not correlate, it is clear from (23) that the cross terms over levels with $\mu \neq \lambda$ vanish in averaging with respect to levels and to channels alike. The quantities $\gamma_{\lambda c}$ are real and the Γ_λ are equal to -2 Im E_λ.

Recently mention has often been made of the need for taking into account the

correlation in the distribution of the signs of the amplitudes of the reduced halfwidths of the compound-nucleus levels [4, 13]) .Brown and De Dominicis admitted that it is possible to obtain the matrix elements of direct processes by taking account of correlations over sufficiently large energy intervals. Let us assume that the average $\overline{\gamma_{\lambda c'}\gamma_{\lambda c}}$ is not equal to zero. Just as in ref. [6]) we write down the cross-section averaged with respect to energy:

$$\sigma_{c'c} \approx \overline{|S_{c'c}|^2} = |S_{c'c}|^2 + \overline{|S_{c'c}^{\text{comp}}|^2} - \overline{|S_{c'c}^{\text{comp}}|^2}. \tag{24}$$

The diagonal terms with $\mu = \lambda$ in the right-hand side of (24) yield the well-known Weisskopf-Ewing equation for processes passing through the formation of the compound nucleus. The contribution of the remaining terms depends on the correlation of the quantities $\gamma_{\lambda c}$. Analysis of eq. (11) shows that for $\Gamma \gg D$ a certain positive additional term is obtained. This term may be interpreted as a cross-section of a certain rapid process evidently involving a small number of particles. Yet for $\Gamma \ll D$ the correlation addition to the cross-section proves to be negative. This result contradicts the assumption made in ref. [4]) concerning the nature of the terms describing direct interactions. The procedure of summing up the influence of remote levels was used by Bloch [3]), Brown and De Dominicis [4]) as well as Lane [13]). It is characteristic that in all these papers use was made of the closure relation for the wave functions Ψ_λ in the Kapur-Peierls theory. After summation terms of the type (1) were obtained. It can easily be seen, however, that all values connected with the resonances escape from the theory at the moment one uses the closure relation. The fact that, for example, a considerable part of the nuclear interaction is described by the optical potential shows that the system of physical wave functions of the compound nucleus can by no means be regarded as a closed one. Thus, the correlations evolved in refs. [3, 4, 13]) are merely correlations between the amplitudes of the formal mathematical levels of the Kapur-Peierls theory; as for the $\gamma_{\lambda c}$ related to the real compound states of the nucleus, it is natural to retain for them the Bethe assumption.

7. Appendix: Wave Functions ϕ, $\psi^{(\pm)}$, $\psi_0^{(\pm)}$ in the Representation with Quantum Numbers *asLJM*

To simplify the formulas we use the Dirac notations. For the spherical function depending on the radiusvector of the coordinate we shall use the notation $|lm\rangle$. As before [2])

$$\langle lm| = (|lm\rangle)^* = (-)^{l-m}|l-m\rangle. \tag{25}$$

Similar relations hold for the spinor $|s\nu\rangle$ and the spin-angular function of the total momentum. The bracket $|\alpha\rangle$ will designate the wave function of the inter-

nal motion in the channel α normalized so that the integral $\langle\alpha|\alpha\rangle$ with respect to internal variables is unity. The aggregate of the quantum numbers $\alpha slJM$ will be designated by the index c as before. The wave function ϕ describes the motion of non-interacting particles with the quantum numbers αsv and the relative momentum at infinity $\hbar\mathbf{k}$. In normalizing

$$\langle\phi'|\phi\rangle = \delta_{\alpha'\alpha}\delta_{s'v',sv}\delta(\mathbf{k}'-\mathbf{k}), \tag{26}$$

ϕ is equal to

$$|\phi\rangle = i\left(\frac{\hbar}{2\pi mk}\right)^{\frac{1}{2}} \sum_{\substack{lm\\JM}} Y^*_{lm}\left(\frac{\mathbf{k}}{k}\right)(svlm|JM)\frac{J_c-O_c}{v^{\frac{1}{2}}r}|c\rangle. \tag{27}$$

Here the ket $|c\rangle$ designates the ket $|\alpha slJM\rangle$ and the remaining notations are conventional [2]). The interaction leads to the appearance of divergent waves in other channels. Outside the range of forces

$$|\psi^{(+)}\rangle = i\left(\frac{\hbar}{2\pi mk}\right)^{\frac{1}{2}} \sum_{\substack{lm\\JM}} Y^*_{lm}\left(\frac{\mathbf{k}}{k}\right)(svlm|JM)\sum_{c'}\frac{\delta_{c'c}I_{c'}-S^J_{c'c}O_{c'}}{v'^{\frac{1}{2}}r'}|c'\rangle. \tag{28}$$

Acoording to (4)

$$\langle\psi^{(-)}| = i\left(\frac{\hbar}{2\pi mk}\right)^{\frac{1}{2}} \sum_{\substack{lm\\JM}} Y_{lm}\left(\frac{\mathbf{k}}{k}\right)(svlm|JM)\sum_{c'}\frac{\delta_{c'c}I_{c'}-S^J_{c'c}O_{c'}}{v'^{\frac{1}{2}}r'}\langle c'|. \tag{29}$$

The transition amplitude from the state ϕ to state ϕ' is expressed by the matrix element $\langle\phi'|V'|\psi^{(+)}\rangle$, Replacing V' by the difference $(E-H'_0)-(E-H)$, the integration reduces to a surface part, as a result of which

$$\langle\phi'|V'|\psi^{(+)}\rangle = i\hbar^2(2\pi)^{-1}(m'mk'k)^{-\frac{1}{2}}$$
$$\times \sum_{\substack{l'm'lm\\JM}} Y_{l'm'}\left(\frac{\mathbf{k}'}{k'}\right)Y^*_{lm}\left(\frac{\mathbf{k}}{k}\right)(s'v'l'm'|JM)(svlm|JM)(S^J_{c'c}-\delta_{c'c}). \tag{30}$$

In the representation $\alpha slJM$ the wave functions of scattering on the optical potential (central without spin-orbit coupling) are equal to

$$|\psi_0^{(+)}\rangle = i\left(\frac{\hbar}{2\pi mk}\right)^{\frac{1}{2}} \sum_{\substack{lm\\JM}} Y^*_{lm}\left(\frac{\mathbf{k}}{k}\right)(svlm|JM)u_l(kr)|\alpha slJM\rangle, \tag{31}$$

$$\langle\psi_0^{(-)}| = i\left(\frac{\hbar}{2\pi mk}\right)^{\frac{1}{2}} \sum_{\substack{lm\\JM}} Y_{lm}\left(\frac{\mathbf{k}}{k}\right)(svlm|JM)u_l(kr)\langle\alpha slJM|, \tag{32}$$

u_l being equal to $v^{-\frac{1}{2}}r^{-1}(I_l-S_l{}^0O_l)$ outside the region of interaction. Sometimes it is convenient to express the optical scattering S-matrix through the logarith-

mic derivative L^0:

$$S_c^0 = \Omega_c^2 \frac{L_c^0 - L_c^*}{L_c^0 - L_c} = \Omega_c^2 \exp(2i\delta_c^0), \quad L_c^0 = R\left[\frac{\partial(ru_c)}{\partial r} \Big/ ru_c\right]_R. \tag{33}$$

Here Ω_c and L_c are the same as in ref. [2]).

In conclusion I avail myself of the opportunity to thank Professor A. S. Davydov for his attention and stimulating advice.

References

1) E. P. Wigner and L. Eisenbud, Phys. Rev. **72** (1947) 29
2) A. M. Lane and R. G. Thomas, Revs. Mod. Phys. **30** (1958) 257
3) C. Bloch, Nuclear Physics **4** (1957) 503
4) G. E. Brown and De Dominicis, Annals of Physics **6** (1959) 209; and others
5) H. Feshbach, Annals of Physics **5** (1958) 357
6) M. Sano, S. Yoshida and T. Terasawa, Nuclear Physics **6** (1958) 20
7) P. L. Kapur and R. E. Peierls, Proc. Roy. Soc. A **166** (1938) 277
8) F. L. Friedman and V. F. Weisskopf, Niels Bohr and the Development of Physics (Pergamon Press, London, 1955)
9) V. I. Smirnov, A Course of Higher Mathematics (Moscow, 1959) vol. V, p. 576
10) T. Teichman and E. P. Wigner, Phys. Rev. **87** (1952) 123
11) H. Feshbach, C. F. Porter and V. F. Weisskopf, Phys. Rev. **96** (1954) 448
12) V. I. Serdobolsky, JETP **38** (1960) 1903
13) A. M. Lane, Nuclear Physics **11** (1959) 625

Editor's Note: A point of view akin to that of the present paper is outlined, on a somewhat more rigorous basis, in my lectures at the Summer Meeting of Physicists at Hercegnovi (Yugoslavia) (September 1959). This treatment is an extension of an investigation by J. Humblet published in 1952, and will shortly been presented in more detail by J. Humblet and myself in this journal.

2.E

Nuclear Physics **21** (1960) 256—269; © *North-Holland Publishing Co., Amsterdam*

Not to be reproduced by photoprint or microfilm without written permission from the publisher

A MODEL FOR THE CALCULATION OF THE OPTICAL POTENTIAL IN SOME FINITE NUCLEI

B. JANCOVICI

Laboratoire de Physique Théorique et Hautes Énergies, Faculté des Sciences, Orsay (S. et O.), France †

Received 12 July 1960

Abstract: The present paper describes in sect. 2 an explicit calculation of the optical potential, up to the second order in perturbations, in a simple model for the finite nuclei He^4, O^{16}, Ca^{40}, which are pictured as made of nucleons bound in an harmonic oscillator average potential; finite nucleus wave functions are used through the whole calculation, and no results pertinent to the infinite nuclear matter case are used. Numerical results for the imaginary potential are presented in sect. 3. Although our model is very crude, it is interesting to compare the results to those obtained through the Thomas-Fermi approximation, if only to test this approximation: this is done in sect. 4, where the conclusions are stressed. It is found that the imaginary potential at low energy has a maximum in the surface, a conclusion which had been previously derived only in the frame of the Thomas-Fermi approximation.

1. Introduction

The optical potential which describes the propagation of a neutron through infinite nuclear matter has been computed from two-body nucleon-nucleon forces [1]). All numerical studies in the case of finite nuclei [2–5]) use an approximation in which the optical potential, at a point with a given nuclear density, is taken equal to the optical potential in infinite nuclear matter of the same density; this approximation may be called the Thomas-Fermi approximation [2]).

Exact expansions of the optical potential in series of the two-body interaction have been given for finite nuclei [6–7]) and are represented by diagrams [8]). It seems, incidentally, that the prescription for computing the optical potential is not unique, because several potentials are able to reproduce the same elastic scattering amplitudes at a given energy. We anyhow replace in zeroth order the target nucleus by a one-body potential, U; the individual-particle model states are the bound and unbound eigenfunctions of this potential. Up to the second order, the optical potential $\mathscr{V}$ is then given by the diagrams of fig. 1, where the horizontal dotted line represents the two-body interaction v, and where the full lines are particle and holes; the target nucleus model state, which is assumed to be non-degenerate, is taken as the vacuum. These diagrams are to be interpreted as matrix elements of the optical potential between one-particle eigenstates of the zeroth-order potential U. Following the prescription of Bell and Squires [6]),

† Work supported in part by the United States Air Force through the European Office, Air Research and Development Command.

we consider the matrix elements between all occupied and unoccupied eigenstates.

Fig. 1. The first and second order diagrams for the optical potential.

The optical potential which results from the graphs of fig. 1 is a non-local potential $\mathscr{V}(x_1, x_2)$ in coordinate space. We assume that the two-body interaction between two nucleons at points $\mathbf{x}_1$ and $\mathbf{y}_1$ is $\mathcal{O}v(\mathbf{x}_1-\mathbf{y}_1)$, where $\mathcal{O}$ is a spin and isobaric spin dependent operator. We call P_σ and P_τ the spin and isobaric spin exchange operators; $k(\mathbf{x}_1)$, $p(\mathbf{x}_1)$, $q(\mathbf{x}_1)$ are space eigenfunctions of the average potential $U(\mathbf{x}_1)$ and E_k, E_p, E_q are the corresponding energies. With these notations, the contributions of the graphs of fig. 1 are the following †:

$$\mathscr{V}^{(1a)}(\mathbf{x}_1, \mathbf{x}_2) = \tfrac{1}{4}\,\mathrm{Tr}\,\mathcal{O}\sum_{k<}\int k^*(\mathbf{y}_1)v(\mathbf{x}_1-\mathbf{y}_1)k(\mathbf{y}_1)\mathrm{d}\mathbf{y}_1\delta(\mathbf{x}_2-\mathbf{x}_1) \quad (1.1a)$$

($k <$ under the summation sign indicates that this summation runs on all occupied space states k; $>$ would mean a summation on unoccupied states),

$$\mathscr{V}^{(1b)}(\mathbf{x}_1, \mathbf{x}_2) = -\tfrac{1}{4}\,\mathrm{Tr}\,\mathcal{O}P_\sigma P_\tau \sum_{k<} k^*(\mathbf{x}_1)v(\mathbf{x}_1-\mathbf{x}_2)k(\mathbf{x}_2), \quad (1.1b)$$

$$\mathscr{V}^{(2a)}(\mathbf{x}_1, \mathbf{x}_2) = \tfrac{1}{4}\,\mathrm{Tr}\,\mathcal{O}^2$$

$$\times \sum_{\substack{k< \\ p,\,q>}} \frac{\int k^*(\mathbf{y}_2)v(\mathbf{x}_2-\mathbf{y}_2)p(\mathbf{x}_2)q(\mathbf{y}_2)\mathrm{d}\mathbf{y}_2 \int p^*(\mathbf{x}_1)q^*(\mathbf{y}_1)v(\mathbf{x}_1-\mathbf{y}_1)k(\mathbf{y}_1)\mathrm{d}\mathbf{y}_1}{E+E_k-E_q-E_p} \quad (1.2a)$$

(E is the energy of the incident particle),

$$\mathscr{V}^{(2b)}(\mathbf{x}_1, \mathbf{x}_2) = -\tfrac{1}{4}\,\mathrm{Tr}\,\mathcal{O}^2 P_\sigma P_\tau$$

$$\times \sum_{\substack{k< \\ p,\,q>}} \frac{\int k^*(\mathbf{y}_2)v(\mathbf{x}_2-\mathbf{y}_2)p(\mathbf{y}_2)q(\mathbf{x}_2)\mathrm{d}\mathbf{y}_2 \int p^*(\mathbf{x}_1)q^*(\mathbf{y}_1)v(\mathbf{x}_1-\mathbf{y}_1)k(\mathbf{y}_1)\mathrm{d}\mathbf{y}_1}{E+E_k-E_p-E_q}, \quad (1.2b)$$

$$\mathscr{V}^{(2c)}(\mathbf{x}_1, \mathbf{x}_2) = \tfrac{1}{4}\,\mathrm{Tr}\,\mathcal{O}^2$$

$$\times \sum_{\substack{k,\,p< \\ q>}} \frac{\int p^*(\mathbf{x}_2)k^*(\mathbf{y}_2)v(\mathbf{x}_2-\mathbf{y}_2)q(\mathbf{y}_2)\mathrm{d}\mathbf{y}_2 \int q^*(\mathbf{y}_1)v(\mathbf{x}_1-\mathbf{y}_1)p(\mathbf{x}_1)k(\mathbf{y}_1)\mathrm{d}\mathbf{y}_1}{E-E_k-E_p+E_q}, \quad (1.2c)$$

† The traces are meant on spin and isobaric spin states of two particles; Tr 1 = 16.

$$\mathscr{V}^{(2d)}(\mathbf{x}_1, \mathbf{x}_2) = -\tfrac{1}{4} \operatorname{Tr} \mathscr{O}^2 P_\sigma P_\tau$$

$$\times \sum_{\substack{k,\,p< \\ q>}} \frac{\int p^*(\mathbf{x}_2) k^*(\mathbf{y}_2) v(\mathbf{x}_2-\mathbf{y}_2) q(\mathbf{y}_2) d\mathbf{y}_2 \int q^*(\mathbf{y}_1) v(\mathbf{x}_1-\mathbf{y}_1) p(\mathbf{y}_1) k(\mathbf{x}_1) d\mathbf{y}_1}{E-E_k-E_p+E_q}. \quad (1.2d)$$

In the cases (1.2a) and (1.2b) where the energy denominator may vanish, the energy E must have an imaginary part, the result of which will be to perform an average on the resonances [9]); as a consequence (1.2a) and (1.2b) will contribute an imaginary part to the optical potential. Our main interest in the present paper will actually be the imaginary part, for two reasons:

a) The leading term for the real part (1.1a) is a local potential identical to the result of the Thomas-Fermi approximation. On the contrary, the leading terms for the imaginary part are second order graphs, and they are rather different in their structure from the Thomas-Fermi analogous terms. Therefore the finite size of the nucleus, if it has any effect, will mostly be apparent in the imaginary part.

b) The practical computation of the second-order terms is faster for their imaginary part because the imaginary parts of the series (1.2a) and (1.2b) converge more quickly.

We shall now proceed to the actual calculation of this imaginary potential in a simple model.

2. Calculations in the Harmonic Oscillator Model

For actual computations, we shall from now on assume that the average potential U is a harmonic oscillator potential

$$U(\mathbf{x}_1) = \frac{\hbar^2 \nu^2}{2M} x_1^2 \quad (2.1)$$

($\hbar$ is the Planck constant, M the nucleon mass and ν a parameter which decribes the strength of U). Of course, strictly speaking, we are interested in a scattering problem and we would need a zeroth order potential U going to zero at infinity. It would be more correct to say that what we do is to approximate these bound and unbound eigenfunctions and eigenvalues which explicitly appear in (1.1) and (1.2) by those ones of a harmonic oscillator. This is of course a rather crude model, but its comparison with the extreme opposite case of infinite nuclear matter could be of interest.

We furthermore assume that the two-body interaction is gaussian:

$$\mathscr{O}v(\mathbf{x}_1-\mathbf{y}_1) = \mathscr{O}\Lambda e^{-\alpha^2(\mathbf{x}_1-\mathbf{y}_1)^2} \quad (2.2)$$

and it is then rather convenient to perform all calculations with the relative and centre-of-mass variables

$$\mathbf{x}_2-\mathbf{x}_1 = \mathbf{x}, \quad \mathbf{x}_2+\mathbf{x}_1 = 2\mathbf{X}, \quad \mathbf{y}_2-\mathbf{y}_1 = \mathbf{y}, \quad \mathbf{y}_2+\mathbf{y}_1 = 2\mathbf{Y}. \quad (2.3)$$

With these variables, it is shown in the Appendix that a partial summation on one harmonic oscillator shell can be carried for the contribution of this shell to the mixed density function

$$D_n(Y, y) \equiv \sum_{\substack{k \\ E_k = E_n}} k^*(\mathbf{y}_2)k(\mathbf{y}_1) = \left(\frac{\nu}{\pi}\right)^{\frac{3}{2}} e^{-\frac{1}{2}\nu(2Y^2+\frac{1}{2}y^2)} \mathscr{L}_n(Y, y), \tag{2.4}$$

where

$$\mathscr{L}_n(Y, y) = \sum_{h=0}^{n} (-)^h L_h^{(\frac{1}{2})}(2\nu Y^2) L_{n-h}^{(\frac{1}{2})}(\tfrac{1}{2}\nu y^2) \tag{2.5}$$

($L_h^{(\frac{1}{2})}$ denotes a Laguerre associated polynomial [10]). This function D_n happens to depend only on the lengths of $\mathbf{Y}$ and $\mathbf{y}$.

Explicit expressions can then easily be obtained for the first-order contributions (1.1a) and (1.1b). The computation of the second-order contributions is much simplified by adopting the same two-body interaction parameters in (2.2) as in the work of Verlet [1]) on infinite nuclear matter: the exchange dependence $\mathscr{O}$ is such that $\mathrm{Tr}\, \mathscr{O}^2 P_\sigma P_\tau$ vanishes, and so there are no contributions from (1.2b) and (1.2d). The remaining contributions, which are the only ones for which the computation is not trivial, are (1.2a) and (1.2c); (1.2a) is especially important since it is here the only contribution to the imaginary part of the optical potential, due to the imaginary part of E in the denominator.

The product of two-body interactions which appears in (1.2a) and (1.2c) is easily seen to be

$$v(\mathbf{x}_2-\mathbf{y}_2)v(\mathbf{x}_1-\mathbf{y}_1) = \Lambda^2 e^{-\alpha^2[2(\mathbf{X}-\mathbf{Y})^2+\frac{1}{2}(\mathbf{x}-\mathbf{y})^2]} \tag{2.6}$$

and, from (2.4), (1.2a) becomes

$$\mathscr{V}^{(2a)} = \frac{\mathrm{Tr}\, \mathscr{O}^2\Lambda^2}{4\hbar\omega}\left(\frac{\nu}{\pi}\right)^{\frac{3}{2}} e^{-\frac{1}{2}\nu(2X^2+\frac{1}{2}x^2)}$$

$$\times \sum_{\substack{n< \\ m,\, l>}} \frac{\mathscr{L}_l(X, x) \iint e^{-2\alpha^2(\mathbf{X}-\mathbf{Y})^2-\frac{1}{2}\alpha^2(\mathbf{x}-\mathbf{y})^2-\nu(2Y^2+\frac{1}{2}y^2)} \mathscr{L}_n(Y, y)\mathscr{L}_m(Y, y)\mathrm{d}\mathbf{Y}\,\mathrm{d}\mathbf{y}}{\varepsilon+ij-\frac{3}{2}+n-m-l}, \tag{2.7}$$

where the index n runs on all occupied shells ($n = 0, 1, \ldots$), and the indices m and l, on all empty shells. $\varepsilon+ij$ is the energy in units of $\hbar\omega = \hbar\nu/M$ with a small averaging part j; ε is measured from the bottom of the well.

A similar expression, but with no imaginary part, could be given for (1.2c); the only difference would be in a summation on n, l ⟨and m⟩, and in an $\varepsilon-\frac{3}{2}-n-l+m$ in the denominator.

For further calculations, we shall now specialize to given nuclei, and obtain numerical values for the imaginary part of (2.7).

2.1. He^4

In the case of He^4 only one shell ($n = 0$) is occupied; for that shell $\mathscr{L}_0 = 1$, and we obtain from (2.7)

$$\mathscr{V}^{(2a)} = \frac{\mathrm{Tr}\,\mathscr{O}^2\Lambda^2}{4\hbar\omega}\left(\frac{\nu}{\pi}\right)^{\frac{3}{2}} e^{-\frac{1}{2}\nu(2X^2+\frac{1}{2}x^2)} \times \sum_{m,\,l=1}^{\infty} \frac{\mathscr{L}_l(X,x)\iint e^{-2\alpha^2(\mathbf{X}-\mathbf{Y})^2-\frac{1}{2}\alpha^2(\mathbf{x}-\mathbf{y})^2-\nu(2Y^2+\frac{1}{2}y^2)}\,\mathscr{L}_m(Y,y)\,d\mathbf{Y}\,d\mathbf{y}}{\varepsilon+ij-\frac{3}{2}-m-l}. \quad (2.8)$$

Using (2.6), we see that the double integral in (2.8) is a sum of products of integrals [11]) like for instance

$$\int e^{-2(\alpha^2+\nu)Y^2+4\alpha^2\mathbf{X}\cdot\mathbf{Y}} L_h^{(\frac{1}{2})}(2\nu Y^2)\,d\mathbf{Y} = 4\pi\int_0^\infty e^{-2(\alpha^2+\nu)Y^2}\frac{\sinh 4\alpha^2XY}{4\alpha^2XY}L_h^{(\frac{1}{2})}(2\nu Y^2)Y^2\,dY \quad (2.9)$$

$$= \left(\frac{\pi}{2(\alpha^2+\nu)}\right)^{\frac{3}{2}}\left(\frac{\alpha^2}{\alpha^2+\nu}\right)^h e^{\frac{2\alpha^4}{\alpha^2+\nu}X^2} L_h^{(\frac{1}{2})}\left(\frac{\alpha^2}{\alpha^2+\nu}2\nu X^2\right),$$

and we obtain for (2.8)

$$\mathscr{V}^{(2a)}(X,x) = \frac{\mathrm{Tr}\,\mathscr{O}^2\Lambda^2}{4\hbar\omega}\left(\frac{\nu}{\pi}\right)^{\frac{3}{2}}\left(\frac{\nu}{\alpha^2+\nu}\right)^3 e^{-\frac{(3\alpha^2+\nu)\nu}{2(\alpha^2+\nu)}(2X^2+\frac{1}{2}x^2)} \times \sum_{m,\,l=1}^{\infty}\frac{\mathscr{L}_l(X,x;1)\,\mathscr{L}_m\left(X,x;\frac{\alpha^2}{\alpha^2+\nu}\right)\left(\frac{\alpha^2}{\alpha^2+\nu}\right)^m}{\varepsilon+ij-\frac{3}{2}-m-l}, \quad (2.10)$$

where

$$\mathscr{L}_m(X,x;t) = \sum_{h=0}^{m}(-)^h L_h^{(\frac{1}{2})}(t2\nu X^2)L_{m-h}^{(\frac{1}{2})}\left(t\frac{\nu}{2}x^2\right), \quad (2.11)$$

and therefore

$$\mathscr{L}_m(X,x;1) \equiv \mathscr{L}_m(X,x). \quad (2.12)$$

2.2. O^{16}

Two shells ($n = 0, 1$) are now occupied, the contributions of which to (2.7) will be called $\mathscr{V}_0^{(2a)}$ and $\mathscr{V}_1^{(2a)}$:

$$\mathscr{V}^{(2a)} = \mathscr{V}_0^{(2a)} + \mathscr{V}_1^{(2a)}. \quad (2.13)$$

$\mathscr{V}_0^{(2a)}$ is given by (2.10), with the modification that m and l now run from 2 to ∞.

$\mathscr{V}_1^{(2a)}$ is the term of (2.7) with $n = 1$; using

$$\mathscr{L}_1(Y,y) = 2\nu Y^2 - \tfrac{1}{2}\nu y^2, \quad (2.14)$$

and the relation [10])

$$xL_n^{(\frac{1}{2})}(x) = -(n+1)L_{n+1}^{(\frac{1}{2})}(x)+(2n+\tfrac{3}{2})L_n^{(\frac{1}{2})}(x)-(n+\tfrac{1}{2})L_{n-1}^{(\frac{1}{2})}(x), \quad (2.15)$$

one obtains

$$\mathscr{L}_1(Y,y)\mathscr{L}_m(Y,y) = (m+1)\mathscr{L}_{m+1}(Y,y)+2\mathscr{M}_m(Y,y)+(m+2)\mathscr{L}_{m-1}(Y,y), \quad (2.16)$$

where

$$\mathscr{M}_m(Y,y) = \sum_{h=0}^{m}(-)^h(2h-m)L_h^{(\frac{1}{2})}(2\nu Y^2)L_{m-h}^{(\frac{1}{2})}\left(\frac{\nu}{2}y^2\right). \quad (2.17)$$

Using (2.16) in (2.7), and performing the integrals with the help of (2.9), one obtains

$$\mathscr{V}_1^{(2a)}(X,x) = \frac{\mathrm{Tr}\,\mathscr{O}^2\Lambda^2}{4\hbar\omega}\left(\frac{\nu}{\pi}\right)^{\frac{3}{2}}\left(\frac{\nu}{\alpha^2+\nu}\right)^3 e^{-\frac{(3\alpha^2+\nu)\nu}{2(\alpha^2+\nu)}(2X^2+\frac{1}{2}x^2)}$$

$$\times\sum_{m,\,l=2}^{\infty}\frac{\mathscr{L}_l(X,x;1)}{\varepsilon+ij-\frac{1}{2}-m-l}\left[(m+1)\mathscr{L}_{m+1}\left(X,x;\frac{\alpha^2}{\alpha^2+\nu}\right)\left(\frac{\alpha^2}{\alpha^2+\nu}\right)^{m+1}\right. \quad (2.18)$$

$$\left.+2\mathscr{M}_m\left(X,x;\frac{\alpha^2}{\alpha^2+\nu}\right)\left(\frac{\alpha^2}{\alpha^2+\nu}\right)^m+(m+2)\mathscr{L}_{m-1}\left(X,x;\frac{\alpha^2}{\alpha^2+\nu}\right)\left(\frac{\alpha^2}{\alpha^2+\nu}\right)^{m-1}\right],$$

where

$$\mathscr{M}_m(X,x;t) = \sum_{h=0}^{m}(-)^h(2h-m)L_h^{(\frac{1}{2})}(t2\nu X^2)L_{m-h}^{(\frac{1}{2})}\left(t\frac{\nu}{2}x^2\right). \quad (2.19)$$

2.3. Ca^{40}

Three shells ($n = 0, 1, 2$) are now occupied, the contribution of which to (7) will be called $\mathscr{V}_0^{(2a)}$, $\mathscr{V}_1^{(2a)}$, and $\mathscr{V}_2^{(2a)}$:

$$\mathscr{V}^{(2a)} = \mathscr{V}_0^{(2a)}+\mathscr{V}_1^{(2a)}+\mathscr{V}_2^{(2a)}. \quad (2.20)$$

$\mathscr{V}_0^{(2a)}$ is given by (2.10), with the modification that m and l now run from 3 to ∞; similarly $\mathscr{V}_1^{(2a)}$ is given by (2.18) with the same modification.

$\mathscr{V}_2^{(2a)}$ is the term of (2.7) with $n = 2$; using

$$\mathscr{L}_2(Y,y) = \tfrac{3}{2}-\tfrac{1}{2}\nu y^2-2\nu Y^2+\tfrac{1}{2}(\tfrac{1}{2}\nu y^2)^2-\tfrac{1}{2}\nu y^2 2\nu Y^2+\tfrac{1}{2}(2\nu Y^2)^2, \quad (2.21)$$

and the relation (2.15), one obtains

$$\begin{aligned}\mathscr{L}_2(Y,y)\mathscr{L}_m(Y,y) = {}&\tfrac{1}{2}(m^2+3m+2)\mathscr{L}_{m+2}(Y,y)+2m\mathscr{M}_{m+1}(Y,y)\\ &+m(m+1)\mathscr{L}_m(Y,y)+2\mathscr{N}_m(Y,y)\\ &+2(m+2)\mathscr{M}_{m-1}(Y,y)+\tfrac{1}{2}(m^2+3m+2)\mathscr{L}_{m-2}(Y,y),\end{aligned} \quad (2.22)$$

where

$$\mathscr{N}_m(Y, y) = \sum_{h=0}^{m} (-)^h (2h-m)^2 L_h^{(\frac{1}{2})}(2\nu Y^2) L_{m-h}^{(\frac{1}{2})}\left(\frac{\nu}{2} y^2\right). \tag{2.23}$$

Using (2.22) in (2.7), and performing the integrals with the help of (2.9), one obtains

$$\begin{aligned}
\mathscr{V}_2^{(2a)}(X, x) = {} & \frac{\mathrm{Tr}\, \mathscr{O}^2 \Lambda^2}{4\hbar\omega} \left(\frac{\nu}{\pi}\right)^{\frac{3}{2}} \left(\frac{\nu}{\alpha^2+\nu}\right)^3 \mathrm{e}^{-\frac{(3\alpha^2+\nu)\nu}{2(\alpha^2+\nu)}(2X^2+\frac{1}{2}x^2)} \\
& \times \sum_{m,\, l=3}^{\infty} \frac{\mathscr{L}_l(X, x; 1)}{\varepsilon + ij + \frac{1}{2} - m - l} \left\{ \tfrac{1}{2}(m+2)(m+1) \mathscr{L}_{m+2}\left(X, x; \frac{\alpha^2}{\alpha^2+\nu}\right)\left(\frac{\alpha^2}{\alpha^2+\nu}\right)^{m+2} \right. \\
& + 2m \mathscr{M}_{m+1}\left(X, x; \frac{\alpha^2}{\alpha^2+\nu}\right)\left(\frac{\alpha^2}{\alpha^2+\nu}\right)^{m+1} \\
& + \left[m(m+1) \mathscr{L}_m\left(X, x; \frac{\alpha^2}{\alpha^2+\nu}\right) + 2\mathscr{N}_m\left(X, x; \frac{\alpha^2}{\alpha^2+\nu}\right) \right] \left(\frac{\alpha^2}{\alpha^2+\nu}\right)^m \\
& + 2(m+2) \mathscr{M}_{m-1}\left(X, x; \frac{\alpha^2}{\alpha^2+\nu}\right)\left(\frac{\alpha^2}{\alpha^2+\nu}\right)^{m-1} \\
& \left. + \tfrac{1}{2}(m+2)(m+1) \mathscr{L}_{m-2}\left(X, x; \frac{\alpha^2}{\alpha^2+\nu}\right)\left(\frac{\alpha^2}{\alpha^2+\nu}\right)^{m-2} \right\},
\end{aligned} \tag{2.24}$$

where

$$\mathscr{N}_m(X, x; t) = \sum_{h=0}^{m} (-)^h (2h-m)^2 L_h^{(\frac{1}{2})}(t2\nu X^2) L_{m-h}^{(\frac{1}{2})}\left(t\frac{\nu}{2} x^2\right). \tag{2.25}$$

3. Numerical Calculations

The Laguerre polynomials, the functions (2.11), (2.19) and (2.25), and finally the imaginary part of the double series (2.10), (2.18) and (2.24) were evaluated for different values of the variables, using an IBM 650 digital computer.

The value of the harmonic oscillator parameter was adjusted for each nucleus to fit the measured mean square radius [12]), taking into account the centre-of-mass motion [13]). These parameters and those ones of the two-body potential [1]) are listed in table 1.

TABLE 1

The numerical constants

$\alpha = 0.674\, f^{-1}$ ($f = 10^{-13}$ cm), $\Lambda = 72$ MeV, $\mathrm{Tr}\, \mathscr{O}^2 = 8.54$		
He^4	$\nu = 0.463\, f^{-1}$	$\hbar\omega = 19.1$ MeV
O^{16}	$\nu = 0.338\, f^{-1}$	$\hbar\omega = 14.0$ MeV
Ca^{40}	$\nu = 0.242\, f^{-1}$	$\hbar\omega = 10.0$ MeV

The averaging parameter j

In the case of He^4, Im $\mathscr{V}^{(2a)}(0, 0)$ was first computed as a function of the energy $\varepsilon\hbar\omega$ for 3 values $j = 1, 2, 3$ of the averaging parameter. The curves of fig. 2 show how the oscillations of Im $\mathscr{V}^{(2a)}$ are damped when j increases, since

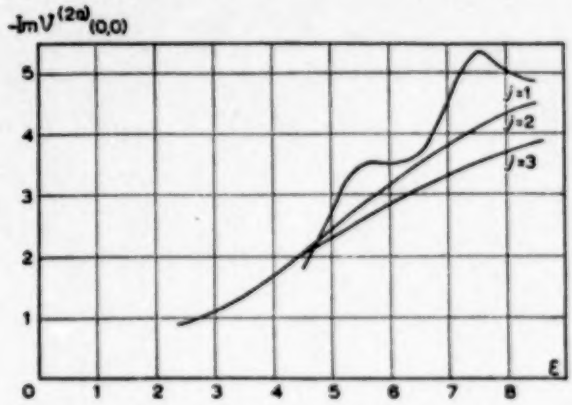

Fig. 2. (He^4) — Im $\mathscr{V}^{(2a)}(0, 0)$ in MeV/f^3 as a function of ε for different values of j ($f = 10^{-13}$ cm). ε is in units of $\hbar\omega = 19.1$ MeV.

the effect of j is to average $\mathscr{V}^{(2a)}$ over an energy interval of the order of $j\hbar\omega$. It is seen that a reasonable damping is obtained for $j \geqq 2$, and the value $j = 2$ will be used in all further calculations.

He^4

The non-local imaginary potential Im $\mathscr{V}^{(2a)}(X, x)$ depends on X and x as defined by (2.3). The values 'at the centre of the nucleus' are obtained for $X = 0$, and the dependence on x then shows the non-local extension of the potential. This function Im $\mathscr{V}^{(2a)}(0, x)$ is plotted on fig. 3 for several values of

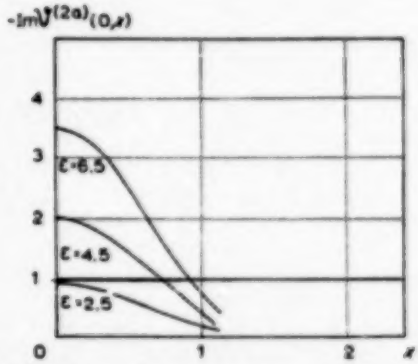

Fig. 3. (He^4) — Im $\mathscr{V}^{(2a)}(0, x)$ in MeV/f^3 as a function of x (in units of f) for different values of ε.

the energy. It is seen that the range of the non-locality (the value of x at which Im $\mathscr{V}^{(2a)}$ is half of its value at $x = 0$) is about 0.6 or $0.7\,f$ ($f = 10^{-13}$ cm).

An 'equivalent local potential' can be defined by

$$\mathscr{V}_{\text{loc}}(X) = 4\pi \int_0^\infty \mathscr{V}(X, x) x^2 \mathrm{d}x \tag{3.1}$$

Im $\mathscr{V}_{\text{loc}}(0)$ is plotted on fig. 4 as a function of the energy.

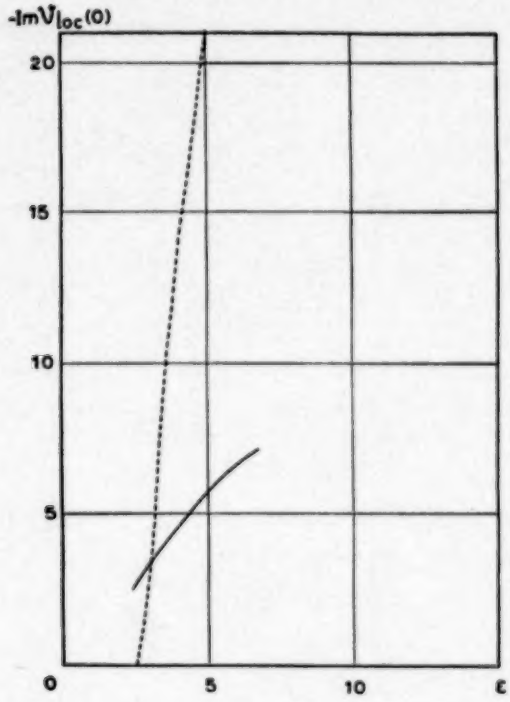

Fig. 4. (He^4) — Im $\mathscr{V}_{\text{loc}}(0)$ in MeV as a function of ε. ε is in units of $\hbar\omega = 19.1$ MeV. The dotted line is the Thomas-Fermi approximation.

O^{16}

Im $\mathscr{V}^{(2s)}(0, x)$ is plotted on fig. 5 and Im $\mathscr{V}_{\text{loc}}(0)$ on fig. 6. It is seen that the range of the non-locality is about $0.9\,f$.

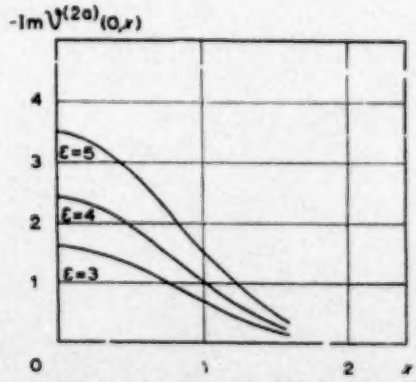

Fig. 5. (O^{16}) — Im $\mathscr{V}^{(2s)}(0, x)$ in MeV/f^3 as a function of x (in units of f) for different values of ε.

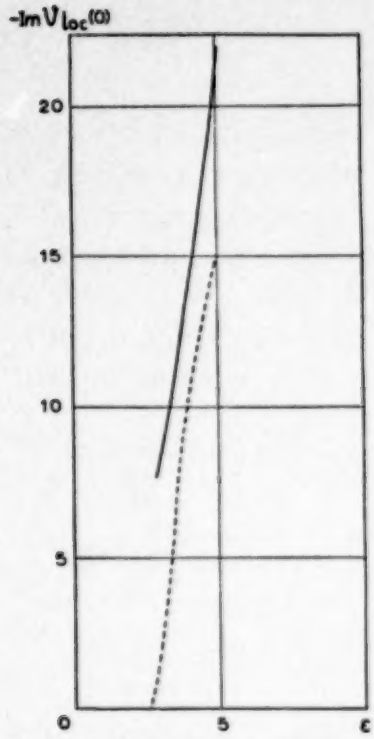

Fig. 6. $(O^{16})-\mathrm{Im}\ \mathscr{V}_{\mathrm{loc}}(0)$ in MeV as a function of ε. ε is in units of $\hbar\omega = 14$ MeV. The dotted line is the Thomas-Fermi approximation.

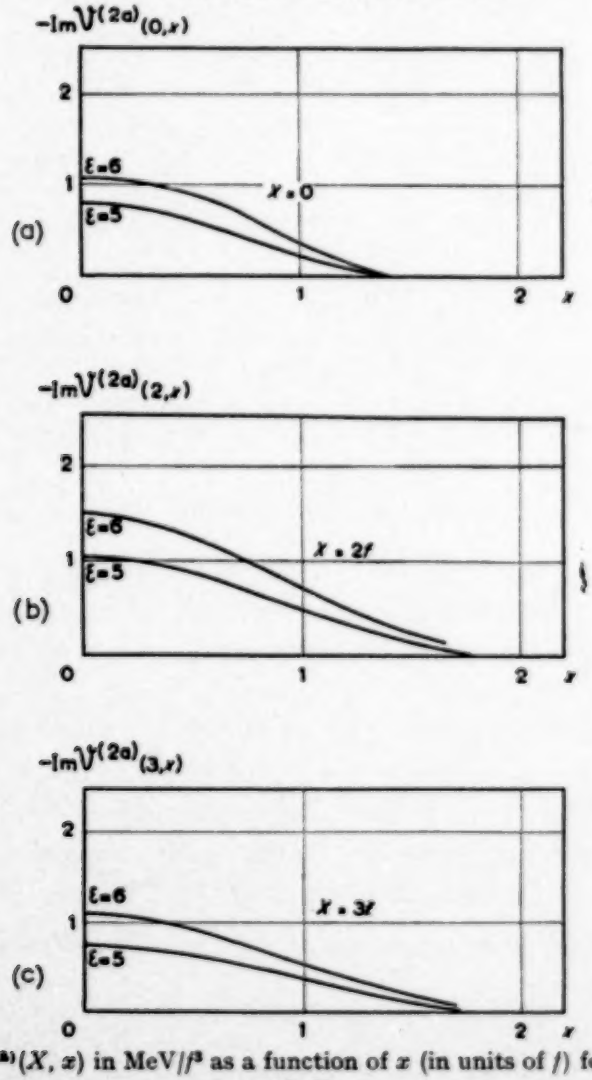

Fig. 7. $(Ca^{40})-\mathrm{Im}\ \mathscr{V}^{(2a)}(X, x)$ in MeV/f^3 as a function of x (in units of f) for different values of ε and X.

Ca^{40}

Im $\mathscr{V}^{(2h)}(X, x)$ is plotted on fig. 7 for the values $X = 0, 2, 3\,f$ respectively. It is seen that the range of the non-locality increases with X, from about $0.8\,f$ for $X = 0$ to $1\,f$ for $X = 3$. The depth also varies with a maximum at $X = 2$. As a result, the imaginary equivalent local potential Im $\mathscr{V}_{loc}(X)$, which is plotted on fig. 8 as a function of X, shows a variation with X and it has a maximum around $X = 2$. The suggestion that the absorbtive potential has a maximum in the surface is once more supported.

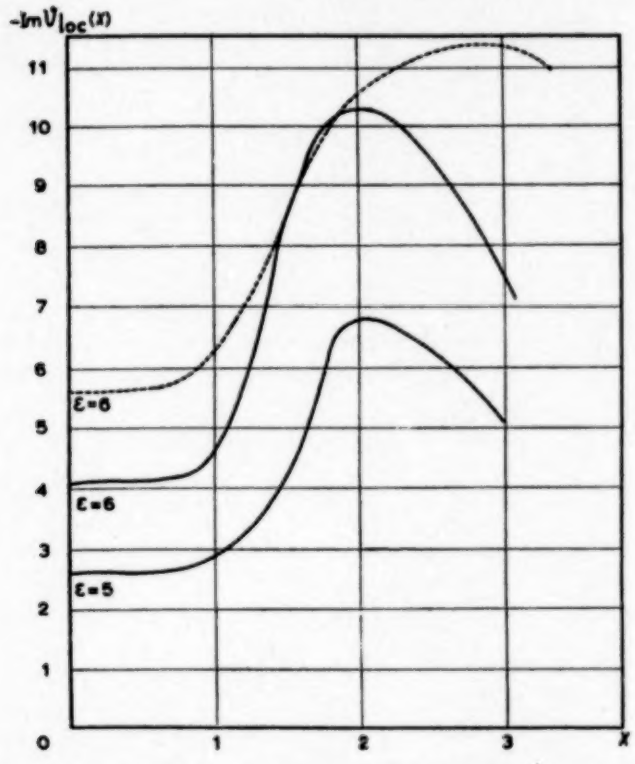

Fig. 8. (Ca^{40}) – Im $\mathscr{V}_{loc}(X)$ in MeV as a function of X (in units of f) for two different values of ε. The dotted line is the Thomas-Fermi approximation.

4. Discussion

We do not intend to carry on here a detailed comparison of our results with the experimental information. We do not look for any qualitative agreement, due to the crudeness of our model. For instance, we know that the convergence of the perturbation expansion is very poor [2]). Furthermore, to our knowledge, there are no available analyses of experiments on the basis of a non-local imaginary potential †. We, however, suggest that such analyses should be made; the rough estimate of the present paper is a non-locality 'range' of about 0.8 to 1 f.

It is more interesting to compare the imaginary equivalent local potential of the present calculation with the results of the Thomas Fermi approximation

† *Note added in proof:* Such an analysis has appeared after the present paper was submitted for publication [14]).

as used by Verlet [1]). (Incidentally, these results are themselves in fair agreement with experiment). To make the comparison precise, we define at each point X a local Fermi momentum k_0 which is related to the density $\rho(X)$ at this point by the customary relation for an infinite medium

$$\rho(X) = (16/3\pi^2)k_0^3; \tag{4.1}$$

we also define an incident particle momentum in the well k_N by the relation

$$\varepsilon\hbar\omega = k_N^2/2M. \tag{4.2}$$

We then follow the prescriptions of Verlet for the second-order computation of $\operatorname{Im} \mathscr{V}_{\text{loc}}(X)$ in infinite nuclear matter, with the above determined values of k_0 and k_N. The results of these calculations are plotted in dotted lines on figs. 4, 6, 8. Fig. 4 shows that He^4 is very poorly described by the Thomas-Fermi approximation, a not very surprising result for a nucleus in which only one space state is occupied. The agreement in the case of O^{16} (Fig. 6) can be considered as fair especially if we remember that the imaginary potential is a very sensitive function of the energy, and that the comparison of the energies between the two models is not obvious to define; the comparison is of course not significant when k_N goes to k_0 ($\varepsilon = 2.5$ in the case of O^{16}), because the Thomas-Fermi model then predicts a vanishing imaginary potential. For this reason, in the case of Ca^{40} (fig. 8), we have plotted the Thomas-Fermi curve only for the case $\varepsilon = 6$. The agreement between the shell model and the Thomas-Fermi approximation is then rather good; in the surface (for $X \approx 3f$), the Thomas-Fermi approximation overestimates the imaginary potential, but this is to be expected because this approximation probably overestimates the effect of the Pauli principle.

Our shell model calculation nevertheless shows that the absorption has a maximum in the surface; this very important effect is therefore not a spurious result of the Thomas-Fermi approximation, and this is the main conclusion of the present paper †.

The possible effect of the clusters in the surface is, however, not yet clarified.

The author is indebted to Miss E. Yeivine for her kind help in the programmation for the IBM 650 computer and to Dr. L. Verlet for interesting discussions.

Appendix

MIXED DENSITY FUNCTION FOR A CLOSED SHELL IN A HARMONIC OSCILLATOR POTENTIAL

We wish to compute the contribution from the nth harmonic oscillator shell ($n = 0, 1, 2 \ldots$) to the mixed density function, for particles in one spin and

† The stronger absorption in the surface would probably be even more enhanced in a calculation beyond the second order [2]).

isobaric spin state. This function is

$$D_n = \sum_{k \text{ in shell } n} k^*(\mathbf{r}_1)k(\mathbf{r}_2), \tag{A.1}$$

where k are the space wave functions. The quantity $k^*(\mathbf{r}_1)k(\mathbf{r}_2)$ may alternatively be thought of as the total wave function for two particles in the states k and k^*; it is well known that such a wave function may be expressed as a finite sum of products of a function of $\mathbf{R} = \frac{1}{2}(\mathbf{r}_1+\mathbf{r}_2)$ by a function of $\mathbf{r} = \mathbf{r}_2-\mathbf{r}_1$. We shall see that D_n is actually rather simple with these variables.

We first notice that

$$D_0 = (\nu/\pi)^{\frac{3}{4}} e^{-\frac{1}{2}\nu(r_1^2+r_2^2)} = (\nu/\pi)^{\frac{3}{4}} e^{-\frac{1}{2}\nu(2R^2+\frac{1}{2}r^2)}. \tag{A.2}$$

D_n for higher shells will now be obtained by the use of appropriate elevation operators. A state $k(\mathbf{r}_i)$ $(i = 1,2)$ of energy $(n+\frac{1}{2})\hbar\omega$ may be separated in cartesian coordinates x_i, y_i, z_i as

$$k(\mathbf{r}_i) = f_a(x_i)g_b(y_i)h_c(z_i), \tag{A.3}$$

where $(a+\frac{1}{2})\hbar\omega$ is, for instance, the energy for the x_i oscillation mode; of course

$$a+b+c = n. \tag{A.4}$$

$f_a(x_i)$ may be obtained from

$$f_0(x_i) = (\nu/\pi)^{\frac{1}{4}} e^{-(\frac{1}{2}\nu x_i^2)} \tag{A.5}$$

with the help of the elevation operator

$$\xi_i = (\tfrac{1}{2}\nu)^{\frac{1}{2}}(\nu x_i - \partial/\partial x_i); \tag{A.6}$$

one has

$$f_a(x_i) = \frac{1}{\sqrt{a!}} \xi_i^a f_0(x_i) \tag{A.7}$$

and similar equations for y_i and z_i with operators η_i and ζ_i respectively. Therefore

$$k(\mathbf{r}_i) = \frac{\xi_i^a \eta_i^b \zeta_i^c}{\sqrt{a!\, b!\, c!}} \left(\frac{\nu}{\pi}\right)^{\frac{3}{4}} e^{-\frac{1}{2}\nu r_i^2} \tag{A.8}$$

and (A.1) may be written

$$\begin{aligned} D_n &= \sum_{a+b+c=n} \frac{(\xi_2\xi_1)^a(\eta_2\eta_1)^b(\zeta_2\zeta_1)^c}{a!\, b!\, c!} D_0 = \frac{1}{n!}(\xi_2\xi_1+\eta_2\eta_1+\zeta_2\zeta_1)^n D_0 \\ &= \frac{1}{n!}(\boldsymbol{\varrho}_2 \cdot \boldsymbol{\varrho}_1)^n D_0, \end{aligned} \tag{A.9}$$

where

$$\boldsymbol{\varrho}_i = (\tfrac{1}{2}\nu)^{\frac{1}{2}}(\nu \mathbf{r}_i - \partial/\partial \mathbf{r}_i). \tag{A.10}$$

We can take the variables **R** and **r**; we obtain

$$\boldsymbol{\varrho}_1 = (1/\sqrt{2})(\mathbf{P}-\boldsymbol{\varrho}), \quad \boldsymbol{\varrho}_2 = (1/\sqrt{2})(\mathbf{P}+\boldsymbol{\varrho}), \tag{A.11}$$

where

$$\mathbf{P} = (\tfrac{1}{4}\nu)^{\frac{1}{2}}[2\nu\mathbf{R}-\partial/\partial\mathbf{R}], \quad \boldsymbol{\varrho} = (1/\nu)^{\frac{1}{2}}[\tfrac{1}{2}\nu\mathbf{r}-\partial/\partial\mathbf{r}], \tag{A.12}$$

and from (A.9) and (A.11)

$$D_n = \frac{1}{n!}\left(\frac{P^2-\rho^2}{2}\right)^n D_0. \tag{A.13}$$

Since **P** is an elevation operator in the **R** space, each term P^{2m} in the expansion of (A.13) must generate, from the factor $\exp(-\nu R^2)$ in D_0, the m^{th}s harmonic oscillator wave function (since P^2 is a scalar, only s states are obtained). These wave functions involve [10]) associated Laguerre polynomials $L_n^{(\frac{1}{2})}(2\nu R^2)$. More precisely, using the definition

$$L_n^{(\alpha)}(x) = \frac{e^x x^{-\alpha}}{n!}\frac{d^n}{dx^n}(e^{-x}x^{n+\alpha}), \tag{A.14}$$

it can be shown that

$$P^2 e^{-\nu R^2} L_{n-1}^{(\frac{1}{2})}(2\nu R^2) = -2n e^{-\nu R^2} L_n^{(\frac{1}{2})}(2\nu R^2) \tag{A.15}$$

and similarly

$$\rho^2 e^{-\frac{1}{2}\nu r^2} L_{n-1}^{(\frac{1}{2})}(\tfrac{1}{2}\nu r^2) = -2n e^{-\frac{1}{2}\nu r^2} L_n^{(\frac{1}{2})}(\tfrac{1}{2}\nu r^2); \tag{A.15'}$$

(A.13) then becomes

$$D_n = (\nu/\pi)^{\frac{3}{2}} e^{-\frac{1}{2}\nu(2R^2+\frac{1}{2}r^2)} \sum_{\lambda=0}^{n} (-)^\lambda L_\lambda^{(\frac{1}{2})}(2\nu R^2) L_{n-\lambda}^{(\frac{1}{2})}(\tfrac{1}{2}\nu r^2). \tag{A.16}$$

It is interesting to notice that D_n does not depend on the angle between **R** and **r**.

References

1) L. Verlet, Nuovo Cim. **7** (1958) 821; Ann. de Phys. **4** (1959) 643. (Earlier references are given there)
2) L. Verlet and J. Gavoret, Nuovo Cim. **10** (1958) 505
3) K. Harada and N. Oda, Prog. Theor. Phys. **21** (1959) 260
4) G. L. Shaw, Ann. of Phys. **8** (1959) 509
5) L. C. Gomes, Phys. Rev. **116** (1959) 1226
6) J. S. Bell and E. J. Squires, Phys. Rev. Letters **3** (1959) 96
7) L. M. Frantz and R. T. Mills, Nuclear Physics **15** (1960) 16
8) J. Goldstone, Proc. Roy. Soc. A **239** (1957) 267
9) G. E. Brown, C. J. De Dominicis and J. S. Langer, Ann. of Physics **6** (1959) 209
10) W. Magnus and F. Oberhettinger, Formulas and theorems for the functions of mathematical physics (Chelsea Publishing Co., 1954) p. 84
11) A. Erdélyi *et al.*, Tables of Integral Transforms (Mc Graw Hill, 1954), vol. II, p. 43
12) D. G. Ravenhall, Rev. Mod. Phys. **30** (1958) 430
13) L. J. Tassie and F. C. Barker, Phys. Rev. **111** (1958) 940
14) Wyatt, Wills and Green, Phys. Rev. **119** (1960) 1031

2.F

Nuclear Physics **21** (1960) 270—275; © *North-Holland Publishing Co., Amsterdam*

Not to be reproduced by photoprint or microfilm without written permission from the publisher

THE INTERACTION RADIUS IN DIRECT REACTIONS

LEONARD S. RODBERG †

Los Alamos Scientific Laboratory, University of California, Los Alamos, New Mexico

and

Physics Department, University of Maryland, College Park, Maryland ††

Received 18 July 1960

Abstract: In the direct interaction theory of nuclear reactions a parameter appears which describes the radius of the surface region in which the direct interaction takes place. Fits to experimental data using Born approximation theories lead to interaction radii which are considerably larger than nuclear radii determined by other means. It is suggested here that this is a simple consequence of the distortion of the incident and outgoing waves, described in terms of an optical potential. This potential increases the relative momentum in the region of interaction, leading to smaller interaction radii for a given angular-momentum transfer. The energy independence of observed direct reaction angular distributions can also be understood in terms of the modified momentum inside the nuclear potential.

1. Introduction

The direct interaction theory [1–6]) of nuclear reactions has been successfully applied to numerous reactions in the medium energy region. This theory postulates a single-step process which is induced by an interaction between a medium-energy incident particle and a nucleon or collective mode of the target nucleus, leaving the residual nucleus in a low-lying excited state. Most applications of this idea have assumed that the direct interaction takes place at the surface of the target, and have described the wave function outside the surface by a simple plane wave (cut-off Born approximation). In spite of this crude approximation, the theory has had remarkable success in describing the diffraction-type angular distributions observed in these reactions, and in relating these distributions to the shell structure of the target nucleus. This success is attributable to the fact that the angular distribution is determined primarily by the angular momentum transferred to the target, and by the restriction of the region of interaction to the surface of the target [2, 3, 5]). The gross features of the distribution are thus fixed by the kinematics of the process. The particular interaction mechanism appears to have little effect upon it, and little has been determined about the various mechanisms (nucleon-nucleon collisions, collective excitations, etc.) which may be responsible for the excitation.

† Present address: Physics Department, University of Maryland, College Park Maryland.

†† Work performed under the auspices of the United States Atomic Energy Commission.

A common feature [1,5,7]) of all attempts to fit these reactions using the cut-off Born approximation is that the interaction radius is uniformly larger than the radius of nuclear matter [8]) (the "Hofstadter radius") or the radius of the nuclear optical potential determined from elastic scattering data [9]). In this note we want to suggest that this discrepancy is a simple consequence of the distortion of the incident and outgoing waves. Detailed numerical calculations [4]) show that agreement with experiment can be obtained using correct radius parameters when this distortion is included.

2. Description in terms of an Optical Potential

A convenient description of the distortion is obtained by means of the optical model. In this model the *elastic* scattering of a particle by the nucleus is described by a complex single-particle potential. This model has been quite successful [10]) in describing medium- and high-energy scattering cross sections and angular distributions.

In a recent publication [11]) we have pointed out that there is a simple approximate relation between the positions of the maxima and minima in *elastic* scattering angular distributions, and the range and depth of the optical potential. The relation is obtained by replacing the optical potential with a real square well, and approximating the single-particle wave function inside the well by $\psi \approx e^{i\mathbf{K}_1 \cdot \mathbf{r}}$. Here $\mathbf{K}_1$ is a vector having a magnitude equal to the wave number *inside* the optical well ($K = \sqrt{2M(E+V)}/\hbar$), and having the direction of the incident wave. This approximation is analogous to a WKB approximation in which the refraction due to the curvature of the nuclear surface is neglected. While the details of the angular distribution may depend on this curvature, it appears that the gross interferences necessary to produce the maxima and minima are dependent only on the *size* of the scatterer, and not on its detailed shape (optical model calculations [12]) indicate that the positions of the maxima and minima are insensitive to the fall-off distance of the real potential or to the presence of an imaginary potential.)

Using this approximation, the angular distribution is proportional to $j_1^2(qR)$ where $q^2 = k^2+K^2-2kK\cos\theta$, k is the wave number outside the well, θ is the scattering angle, R is the nuclear radius, and $j_1(x)$ is the spherical Bessel function. For large x, $j_1(x)$ is proportional to $\cos x$, so that the minima occur when $qR = \frac{1}{2}(2n+1)\pi$, $(n = 1, 2, \ldots)$. This gives a relation between the energy, well depth, radius, and angle of the minima. If Born approximation (replacing K by k) is used, complete disagreement with experiment is found. The success of the present model suggests that the most important effects of the refracting medium are represented simply by the change in wave number, or relative momentum.

We would now like to see how this idea may be applied to direct-interaction

inelastic scattering. In an approximation which neglects multiple inelastic scattering inside the target nucleus, the matrix element for inelastic scattering can be written [4])

$$T_{fb,ia} = \int d\xi d\mathbf{r} \psi_f^{(-)*}(\mathbf{r}) \varphi_b^*(\xi) t(\mathbf{r}, \xi) \psi_i^{(+)}(\mathbf{r}) \varphi_a(\xi), \tag{1}$$

where $\varphi_a(\zeta)$ and $\varphi_b(\xi)$ are the initial and final states of the target, $\psi_i^{(+)}(\mathbf{r})$ and $\psi_f^{(-)}(\mathbf{r})$ are the initial and final distorted wave functions of the projectile, and $t(\mathbf{r}, \xi)$ is the interaction between the projectile and the target nucleus. The coordinate of the projectile is denoted by $\mathbf{r}$, while ζ represents the variables of the target. The notation of eq. (1) is particularly appropriate to a simple inelastic reaction, such as (p, p'); however, with slight modifications which will not affect the ensuing argument, it can easily be adapted to rearrangement processes, such as (d, p), (α, p), etc.

In the Born approximation theory the single particle functions $\psi_i^{(+)}(\mathbf{r})$ and $\psi_f^{(-)}(\mathbf{r})$ are replaced by unmodified plane waves, $e^{i\mathbf{k}_i \cdot \mathbf{r}}$ and $e^{i\mathbf{k}_f \cdot \mathbf{r}}$, respectively. The Butler form [2]) of the theory is obtained if these plane waves are set equal to zero for $r < R$, while the interaction $t(\mathbf{r}, \zeta)$ is assumed to have a short range but to be independent of radial position. The Bhatia [13]) form is obtained if the interaction is assumed to act only at the radius R, i.e., $t(\mathbf{r}, \zeta) = t_0 \delta(r - R)$. The restriction of the interaction to the surface region represents a basic assumption of the direct interaction theory, which attempts to describe reactions leading to low excited states of the residual nucleus, as distinguished from the highly-excited states to which compound-nucleus, or volume-interaction, processes will usually contribute.

3. Discussion

In either form of the theory, R, which we shall call the interaction radius, becomes a parameter which is varied in order to fit experimental data. In most cases there is very little difference in the predictions of these theories †, each yielding an oscillatory angular distribution which is characterized by $j_l(pR)$, where l is the angular momentum transferred and $p = |\mathbf{k}_i - \mathbf{k}_f|$. In

† We believe that there are theoretical reasons to favor the Bhatia form. The single particle functions $\psi_i^{(+)}$ and $\psi_f^{(-)}$ damp out toward the interior of the target with a mean free path [10, 14]) that is of the order of 1 to 3×10^{-13} cm (depending on the energy and the nature of the projectile). The exponential fall-off of φ_a and φ_b towards the outside of the nucleus is characterized by a length of about 2×10^{-13} cm (for a binding energy per particle of 5 to 8 MeV). Hence, if $t(\mathbf{r}, \xi)$ is a short-range interaction, the oscillating part of $\psi_i^{(+)}$ and $\psi_f^{(-)}$ (which is associated with the positive kinetic energy, and is, in Born approximation, just $j_l(pr)$) appears in the integral of eq. (1) multiplied by a function which falls off rather symmetrically about some radius R'. If one performs a Taylor expansion of this oscillating part about $r = R'$, the first term is $j_l(pR')$ while the second term is approximately zero; this is just the Bhatia form. The Butler form, on the other hand, assumes that the inner cut-off is much sharper than the outer one; this seems to be in conflict with the fall-off parameters discussed above.

general the value of R which is required to fit the data is significantly larger than the radii determined by other methods, such as electron scattering, optical-model fits to elastic nucleon scattering, etc.

Multiple-scattering theory [15]) suggests that the distortion of the incident and outgoing waves may be included by using a complex optical potential to determine $\psi_i^{(+)}$ and $\psi_f^{(-)}$; this has been done successfully in several cases [4]). If we approximate these optical model wave functions using the approach described earlier, we find $\psi_i^{(+)}(\mathbf{r}) \approx e^{i\mathbf{K}_i \cdot \mathbf{r}}$ and $\psi_f^{(-)}(\mathbf{r}) \approx e^{i\mathbf{K}_f \cdot \mathbf{r}}$, where $\mathbf{K}_i$ and $\mathbf{K}_f$ are constant vectors which have the directions of $\mathbf{k}_i$ and $\mathbf{k}_f$, respectively, but magnitudes determined by the real part of the optical potential:

$$|\mathbf{K}_i| = \frac{\sqrt{2M_i(E_i+V_i)}}{\hbar}, \quad |\mathbf{K}_f| = \frac{\sqrt{2M_f(E_f+V_f)}}{\hbar}. \tag{2}$$

It should be realized that this relation is very crude since the potential is actually not constant, so that V_i and V_f represent only average well depths in the surface region for the initial and final states. If this approximation is made, one obtains a form identical with the Born approximation result, except that $p = |\mathbf{k}_i - \mathbf{k}_f|$ is replaced by $P = |\mathbf{K}_i - \mathbf{K}_f|$, the momentum transfer inside the target †. The Butler and Bhatia forms may be obtained exactly as before, with only the definition of momentum transfer changed. Comparison of this modified theory with various experiments shows that the presence of the potential has the following interesting effects:

a). If R is set equal to the nuclear radius determined in electron scattering experiments (with appropriate corrections for the size of the projectile) one finds that fits to the angular distribution minima in various experiments [1, 16]) are obtained if both V_i and V_f are set equal to 25 MeV. This is a satisfying result, since the interaction radius now has a well-defined physical significance, while the mean depth found for the optical potential is about one-half the central depth, as expected for a surface interaction (the potential for all light projectiles has a central depth of about 50 MeV.)

The physical reason for this is clear. The momentum transfer P is larger than the free-particle momentum transfer p since the particle is moving through an attractive well. Since the angular distribution is determined by the angular momentum transfer which is, classically, $l = PR$, the larger momentum transfer permits the interaction to take place at a smaller radius. In other words, the large interaction radius which has been obtained previously is simply a

† In low-energy low-Q stripping reactions the result takes a slightly different form. Here one assumes that only the stripped-off particle (for instance, the neutron in a (d, p) reaction) enters the nuclear field, while the residual part of the projectile remains always outside. The interaction radius in this case is related to the coordinate of the stripped-off particle, which is incident on the target with a momentum p (which it is transferring from the projectile to the target). Thus one should treat p as an incident momentum, so that P becomes the momentum of the stripped-off particle inside the target, that is, $P = \sqrt{2M_i(E_p+V_i)}/\hbar$, where $E_p = \hbar^2 p^2/2M_i$.

reflection of the fact that the momentum transfer which was assumed was too small.

b). In most cases the shape of the angular distribution is unchanged by this modification. If the Q-value of the reaction is considerably smaller than the incident energy, $k_1 \approx k_f$, $p \approx 2k_1 \sin \frac{1}{2}\theta$, and the angular distribution depends on $pR \approx 2k_1 R \sin \frac{1}{2}\theta$. If this form of the theory is fit to experiment, a radius R_p is determined. If the modified form is used, k_1 is replaced by K_1, and a new radius R_P will be found. But these are related by $k_1 R_p = K_1 R_P$, so that the angular distribution is not altered. For a stripping-type reaction, the absorption of a nucleon (reducing the mass of the outgoing particle) leads to a positive Q-value (increasing the kinetic energy of the outgoing particle). Thus in many cases of this kind we also find $k_1 \approx k_f$. When this condition holds,

$$P \approx \sqrt{\frac{E_1+V}{E_1}}\, p \text{ and } R_P \approx \sqrt{\frac{E_1}{E_1+V}}\, R_p.$$

c). Experiments [17]) have shown that the angular distributions in direct reactions are remarkably independent of energy, remaining constant over energy ranges of the order of 10 MeV. In the old theory this necessitated making the interaction radius a function of energy; in the present form R can be kept fixed since P is a slowly-varying function of E_1 (for $E_1 \lesssim V$). The relevant momentum is now the momentum inside the nuclear potential, which is nearly constant for low energies.

In the simplified model used here the form of the matrix element is unchanged by the introduction of the optical potential. This suggests that the most important effects of the distortion are already contained in the Born approximation theories, and may provide one clue to the great success of these theories. The apparent restriction to the surface region which is required in these theories and the relation of this to compound nucleus formation should be investigated using more rigorous models.

References

1) R. Huby, in Progr. in Nuclear Physics (Academic Press, New York, 1953) Vol. 3 and references therein;
Austern, Butler and McManus, Phys. Rev. **92** (1953) 350
2) S. T. Butler, Phys. Rev. **106** (1957) 272
3) H. Ui, Progr. Theoret. Phys. **18** (1957) 163
4) C. A. Levinson and M. K. Banerjee, Ann. Phys. N.Y. **2** (1957) 471, 499; **3** (1958) 67;
L. S. Rodberg, Ann. Phys. N.Y. **9** (1960) 373;
N. K. Glendenning, Phys. Rev. **114** (1959) 1297;
W. Tobocman, Phys. Rev. **115** (1959) 98 and earlier work referred to therein
5) J. S. Blair and E. M. Henley, Phys. Rev. **112** (1958) 2029
6) J. S. Blair, Phys. Rev. **115** (1959) 928
7) W. W. Daehnick and J. M. Fowler, Phys. Rev. **111** (1958) 1309 and many others
8) R. Hofstadter, Rev. Mod. Phys. **28** (1956) 214

9) S. Fernbach, Rev. Mod. Phys. **30** (1958) 414;
A. E. Glassgold, Rev. Mod. Phys. **30** (1958) 419
10) Proc. of the International Conference on the Nuclear Optical Model, Florida State Univ. Tallahassee, Florida (1959)
11) L. S. Rodberg, Nuclear Physics **15** (1960) 72
12) For instance, A. E. Glassgold and P. J. Kellogg, Phys. Rev. **107** (1957) 1372
13) A. B. Bhatia, K. Huang, R. Huby and H. C. Newns, Phil. Mag. **43** (1952) 485
14) G. Igo and R. M. Thaler, Phys. Rev. **106** (1957) 126
15) N. C. Francis and K. M. Watson, Phys. Rev. **92** (1953) 291:
K. M. Watson, Phys. Rev. **105** (1956) 1388
16) For instance:
H. E. Wegner and W. S. Hall, Phys. Rev. **119** (1960) 1654;
H. J. Watters, Phys. Rev. **103** (1956) 1763
17) For instance:
J. E. Brolley, Jr., T. M. Putnam and L. Rosen, Phys. Rev. **107** (1957) 820;
Nonaka, Yamaguchi and Mikumo, Journal of the Phys. Soc. of Japan **14** (1959) 1260;
L. Stewart, J. E. Brolley, Jr., and L. Rosen, Phys. Rev. **119** (1960) 1649

7.A

Nuclear Physics **21** (1960) 276—299; © *North-Holland Publishing Co., Amsterdam*

Not to be reproduced by photoprint or microfilm without written permission from the publisher

ON CONSERVATION OF PROBABILITY IN THE LEE MODEL

PHILIPPE DENNERY † and NORMAN M. KROLL

Columbia University, New York, New York ††

Received 18 July 1960

Abstract: Heisenberg's treatment of the Lee model in an indefinite metric with "dipole" or "complex" ghosts is extended to include more than one heavy particle and to include heavy particle motion. It is shown that with this extension new bound states of negative norm and real energy appear, which can, via a scattering process, lead to a failure of unitarity in the theory.

1. Introduction

Pauli and Källén [1]), in their analysis of the Lee model [2]), have shown that this model fails to conserve probability for a finite renormalized coupling constant in the point source limit. Heisenberg [3]), and later Pauli and Glaser [4]), showed that this conclusion could be modified by dealing with the model in a manner which bears some analogy with Heisenberg's quantization of the spinor model.

Heisenberg's treatment of the Lee model was restricted to the case of a single, stationary heavy particle and an arbitrary number of light bosons. The hope is expressed, in Heisenberg's original work, that the prescription used will automatically insure conservation of probability when more than one heavy particle is present.

In the present work, we investigate this question by extending Heisenberg's treatment to the case of two heavy particles, endowed with kinetic energies. We will show how to renormalize the model in this case. In sections 4 and 5, we will show that if we fix the constants of the theory so that the roots of the V particle in the one heavy particle sector correspond to a dipole ghost, there will always exist a bound state of an N and a V that has a real energy and a negative norm, in the two heavy particles sector. In section 6 we will show that the S-matrix for the scattering of 3 N's and a θ is not unitary since one of the possible final states contains the aforementioned bound state of negative norm. The first two sections are concerned with general considerations on the static version of the model.

† Work supported in part by the United States Atomic Energy Commission and submitted in partial fulfillment of the requirements for the degree of Doctor of Philosophy, in the Faculty of Pure Science, Columbia University.

†† A preliminary report on this problem was given by N. Kroll at the CERN Conference (1958).

2. The Lee Model

In this section we will give a brief review of the Lee model adapting it to a notation that will be used throughout the paper, and using from the start, an imaginary coupling constant.

The Lee model has three kinds of particles: two infinitely heavy particles (usually thought of as fermions), the V- and the N-particle, and one light boson, the θ-particle. Only the following reactions are allowed:

$$V \rightleftarrows N+\theta.$$

The Lee model may be divided into sectors, each having a given baryon (b) and charge (q) number. Therefore we make the following assignments:

	V	N	θ
b	1	1	0
q	0	1	−1

and study now the sector characterized by $b = 1, q = 0$. To this end we introduce the τ matrices which operate on the heavy particles as follows:

$$\tau_+N = 0, \quad \tau_-N = V, \quad \tau N = 0, \quad \tau_3 = (1-2\tau), \quad \tau_+V = N, \quad \tau_-V = 0, \quad \tau V = V.$$

The Hamiltonian for this sector may be written as a sum of a free part and an interaction part:

$$H = H_0+\mathscr{H},$$
$$H_0 = m\tau+\int \mathrm{d}\mathbf{k}n(k)\mathrm{d}\omega_k, \tag{1a}$$

$$\mathscr{H} = (4\pi)^{\frac{1}{2}}if\int \frac{\mathrm{d}\mathbf{k}}{\sqrt{2\omega_k}}[\tau_+a^*(k)v(k)+\tau_-a(k)v^*(k)]. \tag{1b}$$

Here, $a^*(k)$ and $a(k)$ are respectively creation and destruction operators for the bosons; $v(k)$ is a cutoff factor which we may eventually set equal to 1; m is the unrenormalized energy of the V-particle; ω_k is the energy of the θ-particle, $\omega_k = \sqrt{k^2+\mu^2}$; $n(k) = a^*(k)a(k)$ is the occupation number of the bosons. We have fixed the energy scale so that the energy of the N can be taken to be zero.

Since the coupling constant is imaginary, the Hamiltonian can be self-adjoint only in the sense of the indefinite metric; that is, we may have

$$\langle H\psi, \eta\psi\rangle = \langle\psi, \eta H\psi\rangle,$$

where η is the metric operator.

From (1a) and (1b), we see that the operator η which will make H self-adjoint is $\eta = \tau_3$. It has the property $\tau_3|\mathrm{V}\rangle = -|\mathrm{V}\rangle$.

The wave function in the sector may be written

$$\psi = a|\mathrm{V}\rangle + \int \mathbf{dk}\, a^*(k)g(k)|\mathrm{N}\rangle,$$

where the kets denote bare particle states and the θ vacuum. Solving the steady state Schrödinger equation gives simply:

$$g(k) = \frac{(4\pi)^{\frac{1}{2}} if v^*(k)}{\sqrt{2\omega_k}(E-\omega_k)}$$

and

$$S^0(E) = 0, \tag{2}$$

where

$$S^0(E) = E - m + 2\pi f^2 \int \mathbf{dk}\, \frac{|v(k)|^2}{\omega_k(E-\omega_k)}. \tag{3}$$

We shall be interested in the case in which (2) has two roots, or a double root. (It can be shown that only in this case is it possible to go to the point source limit $v(k) = 1$.) Designating these two roots by m_1 and m_2, it is convenient to re-express $S^0(E)$ in terms of m_1 and m_2, rather than in terms of m and f. m_1 and m_2, if real, are chosen less than μ.

The condition that m_1 should be a root yields the following expression for m:

$$m = m_1 + 2\pi f^2 \int \frac{\mathbf{dk}}{\omega_k(m_1-\omega_k)}. \tag{4}$$

Inserting (4) into (3) and using the identity

$$\frac{1}{E-\omega_k} = \frac{1}{m_1-\omega_k} + (m_1-E)\frac{1}{(m_1-\omega_k)(m_2-\omega_k)} + \frac{(m_1-E)(m_2-E)}{(m_1-\omega_k)(m_2-\omega_k)(E-\omega_k)}$$

yields

$$S^0(E) = (E-m_1)\left[1 - 2\pi f^2 \int \frac{\mathbf{dk}}{\omega_k(m_1-\omega_k)(m_2-\omega_k)}\right] + (E-m_1)(E-m_2)2\pi f^2 \int \frac{\mathbf{dk}}{\omega_k(\omega_k-m_1)(\omega_k-m_2)(E-\omega_k)}.$$

In order that m_2 also be a root of (3), we must choose f^2 in such a way that

$$1 - 2\pi f^2 \int \frac{\mathbf{dk}}{\omega_k(m_1-\omega_k)(m_2-\omega_k)} = 0. \tag{5}$$

We then define a renormalized function

$$S_R^0(E) = \frac{S^0(E)}{f^2} = (E-m_1)(E-m_2)2\pi \int \frac{\mathbf{dk}}{\omega_k(\omega_k-m_1)(\omega_k-m_2)(E-\omega_k)}, \quad (6)$$

which remains well defined in the point source limit when, according to (5), $f \to 0$. It is of interest to note that for real m_1, m_2,

$$\langle \psi_{V_1}, \tau_3 \psi_{V_2} \rangle = N\left[-1+2\pi f^2 \int \frac{\mathbf{dk}}{\omega_k(\omega_k-m_1)(\omega_k-m_2)}\right] = 0, \quad (7)$$

N being a normalization factor. Hence, in the case of real and unequal roots m_1, m_2, (5) expresses the orthogonality of the states corresponding to these root.

If $m_1 = m_2$, then $\psi_{V_1} = \psi_{V_2}$ together with (5) indicate that the double root has a vanishing norm. In the case of complex roots with $m_2 = m_1^* = m_V$ we have

$$\langle \psi_{V_1}, \tau_3 \psi_{V_1} \rangle = \langle \psi_{V_2}, \tau_3 \psi_{V_2} \rangle = N\left[-1+2\pi f^2 \int \frac{\mathbf{dk}}{\omega_k|(\omega_k-m_V)|^2}\right] = 0,$$

which expresses the vanishing of the norm of states with complex eigenvalues. Eq. (7) also guarantees that Im $m = 0$, as seen from (4). This condition was of course assumed from the start, and is consistent with a positive and real value for f^2. In general, the norm of the V-state is given by

$$\eta = \langle \psi, \tau_3 \psi \rangle = -a^2 \frac{\partial S_R^0(E)}{\partial E},$$

and it is evident that if, in the case of real roots, one of the roots has a positive norm, then the other root must have a negative norm.

The case of real and unequal roots is that discussed by Pauli and Källén [1]). When $m_1 = m_2$ (real) we have the Heisenberg case [3]), while the case $m_1 = m_2^*$ (complex) is the one considered by Pauli and Glaser [4]).

When $m_1 \neq m_2$ (real) we have two discrete solutions of the Schrödinger equation. However, when $m_1 = m_2$ we have only one such solution of the Schrödinger equation. In this latter case the solutions of the Schrödinger equation do not form a complete set. The set can be completed by adding another such vector of zero norm, orthogonal to all solutions of the Schrödinger equation (i.e., the continuum states to be discussed) except the discrete state at m_1. This extra state is called the dipole ghost by Heisenberg. While it is not a solution of the steady state Schrödinger equation, it does appear in connection with the general solution of the time-dependent Schrödinger equation.

Besides discrete states, there exist also continuum states in this sector. These correspond to the scattering of a θ-particle by an N, and lead, in all cases, to a unitary S-matrix.

We turn now to a consideration of the higher sectors, consisting of one N and two or more θ's. Pauli and Källén showed that unitarity failed in the sector $N+2\theta$, when the V particle in the sector $b = 1, q = 0$ had two real and distinct eigenvalues. If we consider the case of complex conjugate roots in the $b = 1$, $q = 0$ sector, then it can easily be shown that unitarity is preserved. This is connected with the fact that it is not possible to have energy-conserving transitions to states with a complex energy.

The case of the double root in the $b = 1$, $q = 0$ sector, requires a special discussion. If one starts with complex roots and lets

$$\operatorname{Im} m_1 = \operatorname{Im} m_2 \to 0,$$

then clearly unitarity will be preserved. However, if one starts with real distinct roots m_1, m_2 and then lets

$$m_1 \to m_2,$$

then unitarity will again fail. Heisenberg achieves unitarity in the double root case by imposing a special boundary condition on the reaction equations. We shall note at the appropriate place that this condition is equivalent to the first mentioned limiting process.

3. Two Fixed Heavy Particles

We consider in this section the case of two fixed heavy particles. Since the particles are fixed, the distance between them enters simply as a parameter. This problem has been considered by Weinberg [5]) for the case of real m_1 for both real and imaginary unrenormalized coupling constants (in his notation, a renormalized coupling constant less than or greater than the critical coupling constant). He shows that with an imaginary coupling constant, states of complex energies can appear. We shall be interested in the question of whether in the case of real coincident, or complex conjugate roots, there exists states of real energy and negative norm †. We examine the sector $b = 2$, $q = 1$. The interaction part of the Hamiltonian is written in a slightly different way:

$$\mathscr{H} = (4\pi)^{\frac{1}{2}} if \int \mathrm{d}\mathbf{k}[\tau_+^{(1)} a^*(k)v^*(k)\mathrm{e}^{-\frac{1}{2}i\mathbf{k}\cdot\mathbf{r}} + \tau_-^{(1)} a(k)v(k)\mathrm{e}^{+\frac{1}{2}i\mathbf{k}\cdot\mathbf{r}} + \tau_+^{(2)} a^*(k)v^*(k)\mathrm{e}^{+\frac{1}{2}i\mathbf{k}\cdot\mathbf{r}} + \tau_-^{(2)} a(k)v(k)\mathrm{e}^{-\frac{1}{2}i\mathbf{k}\cdot\mathbf{r}}.$$

Here, $\tau_\pm^{(1)}$, $\tau_\pm^{(2)}$ are the $\tau_\pm$ matrices defined previously. The superscript (1) and (2) indicate that they operate only on the 1st or 2nd particle of the state vector. The heavy particles are fixed at the points $+\mathbf{r}$ and $-\mathbf{r}$. We let the state vector of the sector be

$$\psi_\pm = A[|\mathrm{VN}\rangle \pm |\mathrm{NV}\rangle] + \int \mathrm{d}\mathbf{k}\, g_\pm(k) a^*(k) |\mathrm{NN}\rangle.$$

† This question has also been investigated by G. Källén (private communication).

The symmetrical and antisymmetrical combination reflect the symmetry of the Hamiltonian under the exchange of particles labelled (1) and (2). Solving the Schrödinger equation gives

$$g_{\pm}(\mathbf{k}) = \pm g_{\pm}(-\mathbf{k}) = \frac{2(4\pi)\,if A^{\frac{1}{2}}}{\sqrt{2\omega_k}(E-\omega_k)} \begin{pmatrix} \cos \frac{1}{2}\mathbf{k}\cdot\mathbf{r} \\ i \sin \frac{1}{2}\mathbf{k}\cdot\mathbf{r} \end{pmatrix}$$

and

$$S_{\pm}^{0}(E) = 0,$$

where

$$S_{\pm}^{0}(E) = E - m + 2\pi f^2 \int \frac{\mathrm{d}\mathbf{k}}{\omega_k(E-\omega_k)} \pm 2\pi f^2 \int \frac{\mathrm{e}^{i\mathbf{k}\cdot\mathbf{r}}}{\omega_k(E-\omega_k)}\,\mathrm{d}\mathbf{k}.$$

Proceeding as before, we re-express $S_{\pm}^{0}(E)$ in terms of m_1, m_2, define $S_{\mathrm{R}\pm}^{0}(E) = S_{\pm}^{0}(E)/f^2$, and then, after an angular integration, we obtain

$$S_{\mathrm{R}\pm}^{0}(E) = S_{\mathrm{R}}^{0}(E) \pm \frac{1}{\pi i r} \int_{-\infty}^{\infty} \frac{\mathrm{e}^{ikr} k\,\mathrm{d}k}{\omega_k(E-\omega_k)},$$

where $S_{\mathrm{R}}^{0}(E)$ is given by (6). Transforming the above integral to a more useful form, we find

$$S_{\mathrm{R}\pm}^{0}(E) = S_{\mathrm{R}}^{0}(E) \pm \frac{E}{\pi r} \int_{0}^{\infty} \frac{\mathrm{e}^{-(\mu^2+\mathscr{E}^2)^{\frac{1}{2}}r}}{E^2+\mathscr{E}^2}\,\mathrm{d}\mathscr{E} \mp \frac{1}{r}\,\mathrm{e}^{-(\mu^2-E^2)^{\frac{1}{2}}r}\theta(E), \qquad (8)$$

where $\theta(E) = 1$ if $E > 0$ and $\theta(E) = 0$ if $E < 0$. From equations (6) and (8) we conclude

(a) $S_{\mathrm{R}+}^{0}(E)$ has no real roots.

(b) For sufficiently small r, $S_{\mathrm{R}-}^{0}(E)$ always has two real roots with energies less than μ, corresponding to real discrete states. In the case of the dipole ghost ($m_{\mathrm{V}} = m_{\mathrm{V}}^{*}$), this is true for any r; one of the two roots always has a negative norm.

One can easily see that, as in the Pauli-Källén case, the presence of the two real roots would lead to a failure of unitarity, that is, with m_{V}, m_{V}^{*}, and r chosen so that real roots are present, an initial state of the form NN and two incoming θ-particles can make transitions to the discrete state (NV) of negative norm and one outgoing θ-particle. It is therefore evident that the case $m_{\mathrm{V}} = m_{\mathrm{V}}^{*}$, especially emphasized by Heisenberg, always fails.

One may take the view †, however, that inasmuch as r enters as a parameter rather as a dynamical variable, that one should choose m_{V}, m_{V}^{*}, after r has been fixed, in such a way as to guarantee complex or double roots only for $S_{\pm\mathrm{R}}^{0}(E)$. In this case the $q = 0$ sector and the scattering part of the $q = 1$ sector are satisfactory. However, the higher q sectors no longer remain satisfactory.

† W. Heisenberg (private communication)

We have considered the $q = 0$, $b = 2$ sector in some detail, especially in the large r limit. There one finds states of real energy and negative norm corresponding to two V-particles, even if m_V and m_V^* are chosen in accordance with the prescription proposed above. This result is not surprising in view of the fact that as r goes to infinity one would expect a pair of states with energy $m_V+m_V^*$. It is easy to see that the norm of one of these states will be negative.

It may be anticipated that this result would lead to a breakdown of unitarity in the $q = -1$, $b = 2$ sector. An explicit demonstration based upon a reaction cross-section calculation is complicated to carry out, but the results which we obtain in subsequent sections indicate strongly that such a failure would occur.

4. Particles with Finite Mass

To obtain a more realistic theory, we must allow the heavy particles to have a finite mass. Moreover, if we want to study the scattering of one heavy particle upon another, as we will want to do, it becomes essential to incorporate the kinetic energies of the heavy particles into the theory. We again look at the first sector characterized by $q = 0$, $b = 1$, and we write the Hamiltonian as

$$H = H_0+\mathscr{H},$$

$$H_0 = \tau_N N_p+\tau_V V_p+\int \mathrm{dk}\, \eta(k)\omega_k,$$

$$\langle p|\mathscr{H}|q\rangle = (4\pi)^{\frac{1}{2}} i \int \frac{\mathrm{dk}}{\sqrt{2\omega_k}} [f(q)\tau_+ a^*(k)v^*(k)\delta(p+k-q) + \tau_- f(p)a(k)v(k)\delta(p-k-q),$$

with

$$\tau_N|\mathrm{N}\rangle = |\mathrm{N}\rangle, \quad \tau_V|\mathrm{V}\rangle = |\mathrm{V}\rangle, \quad \tau_N|\mathrm{V}\rangle = 0, \quad \tau_V|\mathrm{N}\rangle = 0.$$

N_p is the kinetic energy of the N-particle, $N_p = (\sqrt{m^2+p^2}-m)$ and m_N is its mass. V_p is the unrenormalized kinetic energy of the V-particle. Its form so far is completely arbitrary. It will be determined by the form of the renormalized kinetic energy function which we will choose in such a manner that it will exhibit a physically reasonable behavior. The interaction part of the Hamiltonian is written as a matrix element in the heavy particle momentum variables; only the θ-operators are shown explicitly. For a finite source radius it is necessary (or at least convenient) to take the coupling constant momentum dependent. In the point source limit the momentum dependence disappears.

As before, we solve the Schrödinger equation, giving

$$S(E, p) = 0,$$

where

$$S(E,p) = E - V_p + 2\pi f^2(p) \int \frac{\mathbf{dk}\,|v(k)|^2}{\omega_k(E-\omega_k-N_{p-k})}. \tag{9}$$

We shall confine our attention to the complex root case, regarding the double root as a limit of this case. As in our treatment of the fixed source, we express $V_p, f(p)$ in terms of the roots in E of $S(E,p)$, which we designate by Q_p, Q_p^*. Thus,

$$V_p = Q_p + 2\pi f^2(p) \int \frac{\mathbf{dk}\,|v(\mathbf{k})|^2}{\omega_k(Q_p-\omega_k-N_{p-k})}. \tag{10}$$

The requirement that $\operatorname{Im} V_p = 0$, or equivalently that Q_p^* alwo be a root, yields

$$2\pi f^2(p) \int \frac{\mathbf{dk}\,|v(k)|^2}{\omega_k|(Q_p-\omega_k-N_{p-k})|^2} = 1. \tag{11}$$

The momentum dependence of Q_p can be chosen arbitrarily and the above equations used to compute the required momentum dependence of V_p and $f(p)$. If Q_p and N_p are not chosen in a way which affects the convergence of the integral in (11), then $f \to 0$ for all p in the point source limit.

From (9), (10), and (11) we obtain the renormalized S-function:

$$S_R(E,p) = \frac{S(E,p)}{2\pi f^2} = |(E-Q_p)|^2 \int \frac{\mathbf{dk}}{\omega_k|(Q_p-\omega_k-N_{p-k})|^2(E-\omega_k-N_{p-k})}. \tag{12}$$

We have thus arrived once more at the result that we may choose a coupling constant such that the only solutions in this sector are either complex ghosts, or dipole ghosts.

While Q_p is arbitrary, we shall choose the presumably reasonable form (for small p) $Q_p = Q_0 + p^2/2K$. To avoid peculiarities in the total momentum dependence of the two heavy particle bound states which we will study in the next section, we choose K to be real.

5. Two Heavy Particle Bound States

We have seen in section 3 that, however we may choose the roots of the V-particle in the sector $b = 1$, $q = 0$, there will always exist for sufficiently small r real roots of negative norm in the sector $b = 2$, $q = 1$. Of course, up to now, we have only considered the case when the heavy particles were at rest. In analogy to the Born-Oppenheimer treatment of molecular problems, the energies of these discrete states, as functions of r, can be thought of as corresponding to an interaction potential of finite range. We might expect therefore, that it would be possible to choose Q_0 and K such that there would be no bound

states at all when the particles are allowed to move. We now investigate this possibility.

Following previous notations, we write the Hamiltonian for the sector $q = 1$, $b = 2$ as

$$\begin{aligned} H_0 &= \tau_N^{(1)} N_{p_1} + \tau_V^{(1)} V_{p_1} + \tau_N^{(2)} N_{p_2} + \tau_V^{(2)} V_{p_2} + \int \mathbf{dk} \eta(k) \omega_k \langle p_1, p_2 | \mathscr{H}_B | q_1, q_2 \rangle \\ &= (4\pi)^{\frac{1}{2}} i \int \frac{\mathbf{dk}}{\sqrt{2\omega_k}} [f(q_1)\tau_+^{(1)} a^*(k) v^*(k) \delta(p_1 + k - q_1)\delta(p_2 - q_2) \\ &\quad + f(p_1)\tau_-^{(1)} a(k) v(k) \delta(p_1 - q_1 - k)\delta(p_2 - q_2) \\ &\quad + f(q_2)\tau_+^{(2)} a^*(k) v^*(k) \delta(p_2 + k - q_2)\delta(p_1 - q_1) \\ &\quad + f(p_2)\tau_-^{(2)} a(k) v(k) \delta(p_2 - q_2 - h)\delta(p_1 - q_1). \end{aligned} \tag{13}$$

We may write the wave function for this sector as

$$\psi(p_1, p_2) = \varphi_1(p_1, p_2)|\mathrm{VN}\rangle + \varphi_2(p_1, p_2)|\mathrm{NV}\rangle + \int \mathbf{dk}\, g(p_1, p_2, k) a^*(k)|\mathrm{NN}\rangle.$$

Since $H = H_0 + \mathscr{H}_B$ is invariant under the interchange of the particles labelled 1 and 2, the amplitudes obey the relations

$$\varphi_2(p_1, p_2) = \pm \varphi_1(p_2, p_1), \quad g(p_1, p_2, k) = \pm g(p_2, p_1, k). \tag{14}$$

Using (13) to solve the Schrödinger equation, we find

$$\begin{aligned} H_0 \psi(p_1, p_2) &= (V_{p_1} + N_{p_2})\varphi_1(p_1, p_2)|\mathrm{VN}\rangle + (V_{p_2} + N_{p_1})\varphi_2(p_1, p_2)|\mathrm{NV}\rangle \\ &\quad + \int \mathbf{dk}(N_{p_1} + N_{p_2} + \omega_k) g(p_1, p_2, k) a^*(k)|\mathrm{NN}\rangle, \end{aligned}$$

$$\begin{aligned} \mathscr{H}\psi(p_1, p_2) &= (4\pi)^{\frac{1}{2}} i \int \frac{\mathbf{dk}}{\sqrt{2\omega_k}} [(v^*(k) f(p_1 + k)\varphi_1(p_1 + k, p_2) \\ &\quad + v^*(k) f(p_2 + k)\varphi_2(p_1, p_2 + k) a^*(k)|\mathrm{NN}\rangle \\ &\quad + v(k) f(p_1) g(p_1 - k, p_2, k)|\mathrm{VN}\rangle + v(k) f(p_2) g(p_1, p_2 - k, k)|\mathrm{NV}\rangle], \end{aligned}$$

whence we find, from $H\psi = E\psi$,

$$g(p_1, p_2, k) = \frac{(4\pi)^{\frac{1}{2}} i v^*(k)}{\sqrt{2\omega_k}} \left[\frac{f(p_1 + k)\varphi_1(p_1 + k_1, p_2) + f(p_2 + k)\varphi_2(p_1, p_2 + k)}{E - \omega_k - N_{p_1} - N_{p_2}} \right]$$

and

$$S(E - N_{p_2}, p_1)\varphi_1(p_1, p_2) = \int \frac{\mathbf{dk}|v(k)|^2 f(p_2 + k)\varphi_2(p_1 - k, p_2 + k)}{\omega_k(\omega_k + N_{p_2} + N_{p_1 - k} - E)},$$

where $S(E, P)$ is given by (9). Here we will make the replacement $S(E, P) \rightarrow$

$f^2 S_R(E, P)$ with $S_R(E, P)$ given by (12) and then rescale φ_1 so that $\varphi_1 \to f^{-1}\varphi_1$ then, taking the point source limit, we obtain

$$S_R(E-N_{p_2}; p_1)\varphi_1(p_1, p_2) = \pm \int \mathrm{d}\mathbf{k}\, \frac{\varphi_1(-p_2-k, -p_1+k)}{\omega_k(\omega_k+N_{p_2}+N^{\circ}_{p_1-k}+E)}, \tag{15}$$

with

$$S_R(E-N_{p_2}; p_1) \equiv |(E-Q_{p_1}-N_{p_2})|^2 \int \frac{\mathrm{d}\mathbf{k}}{\omega_k Q_{p_1}-\omega_k-N_{p_1-k})|^2(\omega_k+N_{p_2}+N_{p_1-k}-E)}. \tag{16}$$

In (15) we have made use of the symmetry conditions (14).

It is necessary to investigate whether the equation (15) has in fact a solution at all, and if it does, whether this solution, which would represent a bound state, has a positive or a negative norm. To make calculations easier, we let the system have zero total momentum. Equation (15) may then be written, letting

$$\varphi(p) \equiv \varphi_1(p, -p),$$

$$S_R(E-N_p; p)\varphi(p) = \int K_{\pm}(p, k)\varphi(p-k)\mathrm{d}\mathbf{k},$$

where

$$K(p, k) = \pm[\omega_k(N_p+N_{p-k}+\omega_k-E)]^{-1}.$$

In the case of zero total momentum, the wave function for the sector is

$$\psi_{\pm}(p_1, p_2) = \varphi_{\pm}(p_1, p_2)\chi_{\pm}\delta(p_1+p_2)+\int \mathrm{d}\mathbf{k} g_{\pm}(p_1, p_2, k)a^*(k)\delta(p_1+p_2+k)|\mathrm{NN}\rangle, \tag{17}$$

where we introduced $\chi_{\pm} = \frac{1}{2}(|\mathrm{NV}\rangle \pm |\mathrm{VN}\rangle)$.

In this case, only even or odd solutions may enter, but not both. The norm of the state vector is

$$\begin{aligned}
N &= \langle \psi_{\pm}, \tau_3^{(1)}\tau_3^{(2)}\psi_{\pm}\rangle \\
&= -\tfrac{1}{2}\int \mathrm{d}\mathbf{p}_1\mathrm{d}\mathbf{p}_2|\varphi_{\pm}(p_1, p_2)|^2\delta^2(p_1+p_2)+\int \mathrm{d}\mathbf{k}\int \mathrm{d}\mathbf{p}_1\mathrm{d}\mathbf{p}_2|g(p_1, p_2, k)|^2\delta^2(p_1+p_2+k) \\
&= -\tfrac{1}{2}\delta(0)\left[\int \mathrm{d}\mathbf{p}|\varphi(p)|^2-\pi\int \mathrm{d}\mathbf{k}\int \mathrm{d}\mathbf{p}\,\frac{|v(k)|^2}{\omega_k(E-\omega_k-N_p-N_{p-k})^2}\right] f^2(-p)|\varphi(p)|^2 \\
&\quad +f^2(p)|\varphi(p+k)|^2 \pm f(-p)f(p+k)(\varphi^*(p)\varphi(p+k)+\varphi^*(p+k)\varphi(p))\Big] \\
&= -\tfrac{1}{2}\delta(0)\left\{\int \mathrm{d}\mathbf{p}\left[\left(1-2\pi\int \frac{\mathrm{d}\mathbf{k}}{\omega_k(E-\omega_k-N_p-N_{p-k})^2}|\varphi(p)|^2\right.\right.\right. \\
&\quad \left.\left.\left. \mp\pi\int \mathrm{d}\mathbf{p}\int \mathrm{d}\mathbf{k}\,\frac{|v(k)|^2 f(p)f(p-k)}{\omega_k(E-\omega_k-N_p-N_{p-k})^2}(\varphi^*(p)\varphi(p-k)+\varphi^*(p-k)\varphi(p))\right]\right\} \\
&= -\tfrac{1}{2}\delta(0)\left[\int \mathrm{d}\mathbf{p}\frac{\partial S_R}{\partial E}|\varphi(p)|^2-\int \mathrm{d}\mathbf{k}\int \mathrm{d}\mathbf{p}\,\frac{\partial K_{\pm}}{\partial E}(\varphi^*(p)\varphi(p-k)+\varphi^*(p-k)\varphi(p))\right].
\end{aligned} \tag{18}$$

The last line follows from the replacement $\partial S/\partial E \to f^2 \partial S_R/\partial E$. ($\varphi(p)$ has been rescaled as assumed previously so that N is now independent of f).

If we assume that N_p and N_{p-k} are negligible compared to ω_k, then $K(p, k)$ becomes independent of p; the second term inside the brackets in (18) may be written in terms of the Fourreir transform of $\varphi(p)$ as

$$2\int \frac{\partial \Omega_\pm(r)}{\partial E} |\varphi(r)|^2 \mathrm{d}\mathbf{r},$$

$$\Omega_\pm(r) \equiv \int K_\pm(k) \mathrm{e}^{-i\mathbf{k}\cdot\mathbf{r}} \mathrm{d}\mathbf{k} = \frac{2\pi}{ir} \int_{-\infty}^{\infty} K_\pm(k) \mathrm{e}^{ikr} k \mathrm{d}k.$$

We will show first that $\Omega_-(r)$ will lead to a state of negative norm. The above integral is similar to the one appearing in (8). We find for $E < 0$

$$\frac{\partial \Omega_-(r)}{\partial E} = -4\pi |E| \int_0^\infty \eta^2 \mathrm{d}\eta \frac{\mathrm{e}^{-(\mu^2+E^2\eta^2)^{\frac{1}{2}}r}}{(1+\eta^2)(\mu^2+E^2\eta^2)^{\frac{1}{2}}},$$

while for $0 < E < \mu$

$$\frac{\partial \Omega_-(r)}{\partial E} = -4\pi E \int_0^\infty \frac{\eta^2 \mathrm{d}\eta \mathrm{e}^{-(\mu^2+E^2\eta^2)^{\frac{1}{2}}r}}{(1+\eta^2)(\mu^2+E^2\eta^2)^{\frac{1}{2}}} - 2\pi^2 E \frac{\mathrm{e}^{-(\mu^2-E^2)^{\frac{1}{2}}r}}{(\mu^2-E^2)^{\frac{1}{2}}}.$$

In both cases the contribution of these terms to the norm is negative. Since $S_R(E)$ has only a single maximum in E, $\partial S_R/\partial E > 0$ for E less than the value at which $S_R(E)$ has its maximum. For the case of real Q_p, this occurs whenever $E < Q_p + N_p$.

We shall now show that for real Q_0, the equation with the kernel $K_-(k)$ has a solution with $E < Q_0 < Q_p + N_p$. This solution will therefore have a negative norm.

We first rewrite this equation in coordinate space by expanding Q_p as $Q_p = Q_0 + p^2/2K$ and neglecting $N_p = p^2/2m_N$ and $p^2/2K$ as compared to ω_k. We then obtain for the dipole case (Q_0 real)

$$(-\nabla^2+\gamma^2)^2 \psi(r) = V(r)\psi(r),$$

where

$$\gamma^2 \equiv 2M(Q_0 - E), \quad M \equiv \frac{m_N k}{m_N + k}$$

and

$$V(r) \equiv 4M^2 \left[\int \frac{\mathrm{d}\mathbf{k}}{\omega_k (Q_0-\omega_k)^2 (E-\omega_k)}\right]^{-1} \Omega_-(r).$$

This reduces to

$$\left(-\frac{d^2}{dr^2}+\gamma^2\right)^2 \phi_0(r) = V(r)\phi_0(r) \tag{19}$$

for S-states, with $\phi_0(r) = r\psi(r)$.

If equation (19) is to have a discrete solution, it must have associated with it certain boundary conditions derivable from its integral equation. But if $\varphi(p)$ is assumed to be square integrable, then by using equation (15) it may be shown that $\varphi(p) \sim p^{-6}$ for large p. Therefore its Fourier transform

$$\psi(r) = \int d\mathbf{p}\, \varphi(p) e^{-i\mathbf{p}\cdot\mathbf{r}}$$

has the property that $\psi(r)$ and $\nabla^2\psi(r)$ are finite at the origin. This means that we must have $\phi_0(0) = \phi_0''(0) = 0$.

The potential $V(r)$ in equation (19) has the property of being everywhere positive and similar in form to the Yukawa potential. It has a rather complicated analytic expression, and we shall not attempt to solve (19) explicitly. It is not difficult to show, however, that (19) must give rise to at least one bound state.

We first investigate the case of an infinitesimally narrow square well of width ξ, of height V_0, at a distance a from the origin.

A long but straight-forward calculation presented in Appendix 1, shows that at least one bound state exists with

$$\xi = \frac{2(t+1)^2\gamma^3}{-at\gamma^5+at^2\gamma^5+V_0t^2a\gamma-V_0a\gamma+V_0t^2+V_0t}. \quad (t \equiv \tanh \gamma a)$$

Taking into account the fact that small ξ implies small γ, this may be simplified to

$$\gamma = \tfrac{1}{2}a^2V_0\xi.$$

We next assert the following theorem:

THEOREM

If a potential $V(r)$ gives at least one bound state, a potential $V'(r)$ that is everywhere positive and greater than $V(r)$ will always give at least one bound state.

This theorem, which is the analogue of a similar theorem valid for the ordinary second order Schrödinger equation, is proved in Appendix 2.

From the above results we may conclude that (19) has at least one bound state for an arbitrary, everywhere positive $V(r)$. It may be wondered why, in contrast to the Schrödinger equation, one obtains a bound state even for an arbitrarily weak potential. The reason may be illustrated as follows: outside the range of the potential, an asymptotic solution is $\phi_0(r) = re^{-\gamma r}$. This function

satisfies the boundary condition $\phi_0(0) = 0$ but fails to satisfy the curvature condition $\phi_0''(0) = 0$ by terms of the order of γ. Since γ can be as small as necessary, it can therefore be surmised that one can obtain a bound state with an arbitrarily weak potential.

Eq. (19) referred to the case of the dipole ghost. In the more general case when $\mathrm{Im}\, Q_p \neq 0$, this equation becomes

$$\left(-\frac{\mathrm{d}^2}{\mathrm{d}r^2}+\mathrm{Re}\, \Gamma\right)^2 \phi_0(r) = [V(r)-(\mathrm{Im}\, \Gamma)^2]\phi_0(r),$$

$$\Gamma \equiv 2M(Q_0-E).$$

For a given $\mathrm{Re}\, \Gamma$, and with $\mathrm{Im}\, \Gamma = 0$, we will always have a bound state of negative norm as first seen. If $\mathrm{Im}\, \Gamma$ becomes too large there will be no bound states. Hence bound states in this sector can always be avoided by taking $\mathrm{Im}\, Q_0$ large enough. On the other hand, there will always be a range of $\mathrm{Im}\, Q_0$ about zero within which there will exist at least one bound state of negative norm, the bounds of this region depending on $\mathrm{Re}\, Q_0$ and M.

Equation (19) may also be generalized to the case of non-zero total momentum. If one writes non-relativistically

$$Q_{p_1}+N_{p_2} = Q_0+\frac{p_1^2}{2k}+\frac{p_2^2}{2m_N} = Q_0+\frac{p^2}{2M}+\frac{P^2}{2(m_N+k)},$$

where M is the reduced mass ($M = m_N k/(m_N+k)$), P the momentum of the centre of mass of the bound state, and p the momentum relative to the centre of mass, then in the bound state equation (19) one must make the replacement

$$\gamma^2 \to \gamma'^2 \equiv 2M\left(Q_0-E+\frac{P^2}{2(m_N+k)}\right).$$

6. Non-Unitarity of the *S*-Matrix

In the previous section, we have shown that if we specify the roots of the V-particle in the one heavy particle sector to be real and coincident, then there will always exist a bound state of an N and a V that has a real energy and a negative norm.

Now the question of interest is whether such a bound state may occur as a fragment in the scattering of particles in the higher sectors of the Lee model. For example, one may ask whether the scattering of $3\mathrm{N}+\theta$ can lead to a final state comprising a bound state of an N and a V that has a negative norm, together with a free N.

To answer this question, we derive first the scattering equations of the sector $3\mathrm{N}+\theta$. The Hamiltonian is

$$H_0 = \tau_N^{(1)} N_{p_1} + \tau_V^{(1)} V_{p_1} + \tau_N^{(2)} N_{p_2} + \tau_V^{(2)} V_{p_2} + \tau_N^{(3)} N_{p_3} + \tau_V^{(3)} V_{p_3}$$
$$+ \int \mathbf{dk}\, n(k)\omega_k \langle p_1, p_2, p_3 | \mathscr{H} | q_1, q_2, q_3 \rangle$$
$$= (4\pi)^{\frac{1}{2}} i \int \frac{\mathbf{dk}}{\sqrt{2\omega_k}} [f(q_1)\tau_+^{(1)} a^*(k) v^*(k) \delta(p_1 + k - q_1)\delta(p_2 - q_2)\delta(p_3 - q_3)$$
$$+ f(p_1)\tau_-^{(1)} a(k) v(k) \delta(p_1 - q_1 - k)\delta(p_2 - q_2)\delta(p_3 - q_3) \qquad (20)$$
$$+ f(q_2)\tau_+^{(2)} a^*(k) v^*(k) \delta(p_2 + k - q_2)\delta(p_1 - q_1)\delta(p_3 - q_3)$$
$$+ f(p_2)\tau_-^{(2)} a(k) v(k) \delta(p_2 - q_2 - k)\delta(p_1 - q_1)\delta(p_3 - q_3)$$
$$+ f(q_3)\tau_+^{(3)} a^*(k) v^*(k) \delta(p_3 + k - q_3)\delta(p_1 - q_1)\delta(p_2 - q_2)$$
$$+ f(p_3)\tau_-^{(3)} a(k) v(k) \delta(p_3 - k - q_3)\delta(p_1 - q_1)\delta(p_2 - q_2)].$$

The derivation of the scattering equations proceeds in a now familiar way. We let

$$\psi_\alpha(p_1, p_2, p_3) = \varphi_0(p_1, p_2, p_3; k_0) a^*(k_0) |\mathrm{NNN}\rangle$$
$$+ \phi_1(p_1, p_2, p_3) |\mathrm{VNN}\rangle + \phi_2(p_1, p_2, p_3) |\mathrm{NVN}\rangle + \phi_3(p_1, p_2, p_3) |\mathrm{NNV}\rangle \qquad (21)$$
$$+ \int \mathbf{dk}\, G(p_1, p_2, p_3, k) a^*(k) |\mathrm{NNN}\rangle.$$

φ_0 is an arbitrary incoming state of $3\mathrm{N}+\theta$ and obeys the free equation

$$H_0 \varphi_0 = E\varphi_0.$$

We obtain, by solving the Schrödinger equation,

$$S_R(E - N_{p_2} - N_{p_3}; p_1)\phi_1(p_1, p_2, p_3)$$
$$= \int \frac{\mathbf{dk}\, \phi_2(p_1 - k, p_2 + k, p_3) + \phi_3(p_1 - k, p_2, p_3 + k)}{\omega_k(\omega_k + N_{p_1 - k} + N_{p_2} + N_{p_3} - E)} + \varphi_1, \qquad (22a)$$

$$S_R(E - N_{p_1} - N_{p_3}; p_2)\phi_2(p_1, p_2, p_3)$$
$$= \int \frac{\mathbf{dk}\, \phi_1(p_1 + k, p_2 - k, p_3) + \phi_3(p_1, p_2 - k, p_3 + k)}{\omega_k(\omega_k + N_{p_2 - k} + N_{p_1} + N_{p_3} - E)} + \varphi_2, \qquad (22b)$$

$$S_R(E - N_{p_1} - N_{p_2}; p_3)\phi_3(p_1, p_2, p_3)$$
$$= \int \frac{\mathbf{dk}\, \phi_1(p_1 + k, p_2, p_3 - k) + \phi_2(p_1, p_2 + k, p_3 - k)}{\omega_k(\omega_k + N_{p_3 - k} + N_{p_1} + N_{p_2} - E)} + \varphi_3. \qquad (22c)$$

The inhomogeneous terms are

$$\varphi_1 = \frac{(4\pi)^{\frac{1}{2}} i}{\sqrt{2\omega_{k_0}}} \varphi_0(p_1 - k_0, p_2, p_3, k_0),$$

$$\varphi_2 = \frac{(4\pi)^{\frac{1}{2}} i}{\sqrt{2\omega_{k_0}}} \varphi_0(p_1, p_2 - k_0, p_3; k_0),$$

$$\varphi_3 = \frac{(4\pi)^{\frac{1}{2}} i}{\sqrt{2\omega_{k_0}}} \varphi_0(p_1, p_2, p_3 - k_0; k_0).$$

Equations of this form in the double root case have been discussed by Heisenberg with reference to the single fixed N, Nθ scattering problem. He points out that the usual outgoing wave boundeary condition yields, on account of the double root in, for example, $S_R(E-N_2-N_3, p_1)$ at $E-N_2-N_3 = Q_1$, an unacceptable asymptotic behavior for large spatial separation of the particles. This behavior can be avoided by requiring that the right hand sides of (22) vanish at the critical points $E-N_2-N_3 = Q_1$, etc. In order to impose this condition, it is necessary to write ϕ_1, for example, in the form

$$\phi_1(p_1, p_2, p_3) = a_1(p_1, p_2, p_3)\delta(E - Q_{p_1} - N_{p_2} - N_{p_3}) + \frac{\chi_1(p_1, p_2, p_3)}{E - Q_{p_1} - N_{p_2} - N_{p_3} - i\varepsilon}, \tag{23}$$

where χ_1 is regular at the critical point. Similar expressions are written for ϕ_2, ϕ_3. The functions a_1, a_2, a_3 are to be determined by the requirement that the right hand sides of (22) vanish at the critical point. The form (23) corresponds, of course, to the addition of an incoming flux of VNN to the NNNθ flux in just the amount necessary to cancel out the unacceptable outgoing form.

It is worth observing that Heisenberg's specification appears quite naturally if one considers the double root case as arising from the limit

$$\text{Im } Q_p = -\text{ Im } Q_p^* \equiv \Gamma \to 0.$$

We show first that any solution of (22) leads to the vanishing of the right hand sides of (22) in the limit Im $Q_p \to 0$. For, assume it does not. Then, in the vicinity of the critical point, we have, e.g.,

$$\phi_1(p_1, p_2, p_3) \approx \frac{F(p_1, p_2, p_3)|_{\text{critical point}}}{(E - N_{p_2} - N_{p_3} - \text{Re } Q_{p_1})^2 + \Gamma^2}.$$

The contribution of this region to the integral on the right hand side of (22b) is of order Γ^{-1} over a domain of values not restricted by Re $Q_1+N_2+N_3-E \approx 0$. Hence as $\Gamma \to 0$ the right hand side of (22b) becomes infinite at values of p_1, p_2, p_3 where the left hand side does not, and ϕ_1 cannot be a solution. Q.E.D.

The extra incoming wave contained in (23) appears only in the limit $\Gamma = 0$. For $\Gamma \neq 0$ the incoming wave is weakly but exponentially damped as $r \to \infty$.

Heisenberg has also pointed out that the occurrence of a bound state of energy E_B among the reaction products should be indicated by a pole in the ϕ's.

This means that, for example, in the vicinity of the pole in p_3,

$$\phi_i(p_1, p_2, p_3) \approx \frac{\bar{\phi}_i(p_1, p_2)}{E-E_B-N_{p_3}}, \quad (i = 1, 2, 3).$$

Insertion of this expression in (22) yields the bound state equation (15) for $\bar{\phi}_1$ and $\bar{\phi}_2$ studied in sect. 5. We wish to show that the imposition of the boundary condition (23) does not affect this conclusion.

We take

$$\begin{aligned}
\chi_1(p_1, p_2, p_3) &\approx \frac{f(p_1, p_2)g(p_3)}{E-E_B-N_{p_3}} (E-Q_{p_1}-N_{p_2}-N_{p_3}) + \text{smaller terms},\\
\chi_2(p_1, p_2, p_3) &\approx \frac{f_2(p_1, p_2)g(p_3)}{E-E_B-N_{p_3}} (E-Q_{p_2}-N_{p_1}-N_{p_3}) + \text{smaller terms}, \quad (24)\\
\chi_3(p_1, p_2, p_3) &\approx \frac{f_3(p_1, p_2)g(p_3)}{E-E_B-N_{p_3}} (E-Q_{p_3}-N_{p_1}-N_{p_2}) + \text{smaller terms},
\end{aligned}$$

and also

$$\begin{aligned}
a_1(p_1, p_2, p_3) &\approx \frac{b_1(p_1, p_2)c(p_3)}{E-E_B-N_{p_3}} + \text{smaller terms},\\
a_2(p_1, p_2, p_3) &\approx \frac{b_2(p_1, p_2)c(p_3)}{E-E_B-N_{p_3}} + \text{smaller terms}, \quad (25)\\
a_3(p_1, p_2, p_3) &\approx \frac{b_3(p_1, p_2)c(p_3)}{E-E_B-N_{p_3}} + \text{smaller terms}.
\end{aligned}$$

Inserting expression (23) for ϕ_1, ϕ_2, ϕ_3 into (22a) and using (24) and (25), we obtain

$$\begin{aligned}
&\frac{S_R(E-N_{p_2}-N_{p_3}; p_1)f_1(p_1, p_2)g(p_3)}{E-E_B-N_{p_3}}\\
&\quad = \int \frac{d\mathbf{k}\, f_2(p_1-k, p_2+k)g(p_3)}{\omega_k(\omega_k+N_{p_1-k}+N_{p_2}+N_{p_3}-E)(E-E_B-N_{p_3})}\\
&\quad + \int \mathbf{dk} \frac{f_3(p_1-k, p_2)g(p_3+k)}{\omega_k(\omega_k+N_{p_1-k}+N_{p_2}+N_{p_3}-E)(E-E_B-N_{p_3+k})} \quad (26)\\
&\quad + \int \frac{\mathbf{dk}\, b_2(p_1-k_1p_2+k)c(p_3)\delta(E-Q_{p_2+k}-N_{p_1-k}-N_{p_3})}{\omega_k(\omega_k+N_{p_1-k}+N_{p_2}+N_{p_3}-E)(E-E_B-N_{p_3})}\\
&\quad + \int \mathbf{dk} \frac{b_3(p_1-k_1p_2)c(p_3+k)\delta(E-Q_{p_3+k}-N_{p_1-k}-N_{p_2})}{\omega_k(\omega_k+N_{p_1-k}+N_{p_2}+N_{p_3}-E)(E-E_B-N_{p_3+k})}\, \mathbf{dk}+\varphi_1.
\end{aligned}$$

In the limit as $E \to E_B+N_3$, the third term on the right of (26) vanishes since

the argument of the δ-function is negative. The second, fourth and inhomogeneous terms are regular in that limit. Therefore, we obtain

$$S_R(E_B - N_{p_2}; p_1) f_1(p_1, p_2) = \int d\mathbf{k} \frac{f_2(p_1 - k, p_2 + k)}{\omega_k(\omega_k + N_{p_1 - k} + N_{p_2} - E_B)},$$

which is precisely the bound state equation (15) †.

We consider now the transition amplitude from an incoming state represented by the state vector (21) to an outgoing state containing a bound NV fragment and a free N. This latter state may be written ††

$$\psi_\beta^{(\mp)}(p_1, p_2, p_3; \bar{p}_3) = \psi_\beta(p_1, p_2)\delta(p_3 - \bar{p}_3) + \frac{1}{E - H \mp i\varepsilon}(\mathcal{H} - \mathcal{H}_B)\psi_\beta(p_1, p_2)\delta(p_3 - \bar{p}_3) \quad (27)$$

and obeys the steady-state Schrödinger equation. E is the total energy of the system; $\mathcal{H}_B$ is the interaction Hamiltonian given by equation (13); $\psi_\beta(p_1, p_2)$ is the state vector of the bound NV, and has a negative norm. It may be written as

$$\psi_\beta(p_1, p_2) = \varphi_{\beta_1}(p_1, p_2)|\mathrm{VN}\rangle + \varphi_{\beta_2}(p_1, p_2)|\mathrm{NV}\rangle + \int d\mathbf{k}\, g_\beta(p_1, p_2, k) a^*(k)|\mathrm{NN}\rangle \quad (28)$$

and is normalized to -1,

$$\langle \psi_\beta, \tau_3 \psi_\beta \rangle = -1.$$

The S-matrix element from a free $3N+\theta$ state at $t = -\infty$ to a bound NV+ free N state at $t = +\infty$ is given by

$$S_{\alpha\beta} = \langle \phi_\alpha^{(+)}, \tau_3 \psi_\beta^{(-)} \rangle. \quad (29)$$

Using the orthogonality relation [6])

$$\langle \psi_\beta^{(-)}, \tau_3 \phi_\alpha^{(-)} \rangle = 0$$

and (27), we obtain from (29)

$$S_{\alpha\beta} = \langle \phi_\alpha^{(+)}, \tau_3(\psi_\beta^{(-)} - \psi_\beta^{(+)}) \rangle = 2\pi i \langle \phi_\alpha^{(+)}, \tau_3(\mathcal{H} - \mathcal{H}_B)\psi_\beta(p_1, p_2)\delta(p_3 - \bar{p}_3)\delta(E_\alpha - E) \rangle.$$

† Considering the analogous case of fixed N, Nθ's, Heisenberg concludes that the boundary condition (23) modifies the associated bound state equation and leans upon this conclusion to show that unitarity is saved in the case when bound states are found. We will show in Appendix 3 that the associated bound state equation is in fact not modified. This does not affect the conclusions reached with respect to the one heavy particle sectors, as Heisenberg subsequently showed that there are no solutions to the bound state equations in this sector. This observation, however, should make the failure of the argument for our case less surprising.

†† We will treat the heavy particles as distinguishable. In a realistic theory the heavy particles would typically have spins as well as statistics, and symmetry dependent selection rules would not hold for all possible spin states.

Using (13), (20), and (28) we find

$$S_{\alpha\beta} = 4\pi^2 i \iiiint \mathrm{d}\mathbf{k}\, \mathrm{d}\mathbf{p}_1\, \mathrm{d}\mathbf{p}_2\, \mathrm{d}\mathbf{p}_3 \frac{g_\beta^*(p_1, p_2, k)}{\sqrt{\omega_k}} \delta(p_3 - k - \bar{p}_3)\phi_3(p_1, p_2, p_3)\delta(E_\alpha - E)$$

$$= 4\pi^2 i \iiint \mathrm{d}\mathbf{p}_1\, \mathrm{d}\mathbf{p}_2\, \mathrm{d}\mathbf{k}\, \frac{g_\beta^*(p_1, p_2, k)}{\sqrt{\omega_k}} \phi_3(p_1, p_2, \bar{p}_3 + k)\delta(E_\alpha - E). \quad (30)$$

We have set

$$E_\alpha \equiv E_B + N_{\bar{p}_3},$$

E_B being the energy of the bound state. We wish to discuss now the contribution of (30) to the unitarity condition on the S-matrix. We introduce the projection operator P into the continuum states of the total Hamiltonian H. If we assume that the in and out states each form a complete set of states with respect to E, then we may write

$$P \equiv \sum_\beta |\psi_\beta^{(+)}\rangle\langle\psi_\beta^{(+)}|\tau_3\eta_\beta \equiv \sum_\beta |\psi_\beta^{(-)}\rangle\langle\psi_\beta^{(-)}|\tau_3\eta_\beta. \quad (31)$$

η_β is the signature of the norm of the state vector $|\psi_\beta^{(\pm)}\rangle$. It is either $+1$ or -1 according as to whether $|\psi_\beta^{(\pm)}\rangle$ has a positive or a negative norm. Written in this fashion, P has the correct properties of a projection operator: P is self-adjoint in the sense of the indefinite matric and $P^2 = P$. If we extract from (31) its α^{th}-diagonal element, we obtain the relation

$$\sum_\beta |S_{\alpha\beta}|^2 \eta_\beta = \eta_\alpha = 1, \quad (32)$$

since the incoming state α has a positive signature. Now, if the theory is to allow an interpretation in terms of probabilities, it is necessary that (32) be identical to the condition

$$\sum_\beta |S_{\alpha\beta}|^2 = 1, \quad (33)$$

for it is this condition alone which guarantees that transitions with negative probabilities may not occur. However, (30) would contribute negatively to (32) on account of the negative norm of the bound state. Therefore, in order that the unitarity condition (33) hold, it would be necessary that (30) vanish identically for all possible incident states. There does not appear to be any reason why this should be the case. Of course, an explicit demonstration based on approximate solutions of eqs. (22) and (30) would be desirable. However, the absence of a coupling constant, together with the double roots in S_R in eqs. (22) make the usual iterative approximations inapplicable. The situation does not impress us as sufficiently promising to warrant a lengthy investigation of this rather remote possibility.

7. Conclusion

The foregoing considerations have indicated that in order to insure conservation of probability in a higher sector, namely the sector $q = 2$, $b = 3$, one cannot choose the roots of the V-particle in the one heavy particle sector to be real and coincident. Of course, we are still free to choose the roots of the V-particle in the lowest sector to be complex. In this way we may avoid altogether the bound states of an N and a V and preserve unitarity in the $q = 2$, $b = 3$ sector. However, as we have already pointed out, the specification of complex roots in the lowest sector leads to states of two V's of real energy and of negative norm. It is very probable that these states would be created in the scattering of say $3N+2\theta$, and thereby destroy unitarity. The underlying premise in Heisenberg's treatment of the Lee model, and more generally of the indefinite metric, has been the hypothesis that unitarity can be guaranteed by prescriptions referring to the one particle states only. It seems very unlikely that this hypothesis can hold.

Appendix

A.1. THE EXISTENCE OF AT LEAST ONE BOUND STATE

We will show that equation (19) has a solution when $V(r)$ is an infinitesimally narrow square well of width ξ and height $V_0 = P^4$. Outside the well we have

$$\frac{d^4y}{dx^4} - 2\gamma^2 \frac{d^2y}{dx^2} + \gamma^4 y = 0, \tag{A.1}$$

with the general solution

$$y_R = (D+Ex)e^{-\gamma x} \quad \text{(to the right)},$$

and

$$y_L = (B+Cx)e^{\gamma x} + (-B+Cx)e^{-\gamma x} \quad \text{(to the left)},$$

the left-side solution satisfying

$$y_L(0) = y_L''(0) = 0.$$

Inside the well the equation is

$$\frac{d^4y}{dx^4} - 2\gamma^2 \frac{d^2y}{dx^2} - (p^4-\gamma^4)y = 0. \tag{A.2}$$

The general solution is

$$y_i(x) = A_1 \sin \alpha x + A_2 \cos \alpha x + A_3 \sinh \beta x + A_4 \cosh \beta x,$$

with

$$\alpha = (p^2-\gamma^2)^{\frac{1}{2}}, \quad \beta = (p^2+\gamma^2)^{\frac{1}{2}}.$$

We may expand the functions and their derivatives at b in terms of a. Since $b-a \equiv \xi$ is infinitesimal. For example

$$y_R(b) = y_R(a)+\xi y'_R(a), \quad y_i(b) = y_i(a)+\xi y'_i(a).$$

By continuity we obtain

$$y_R(a)+\xi y'_R(a) = y_i(a)+\xi y'_i(a) = y_L(a)+\xi y'_L(a).$$

Similarly:

$$y'_R(a)+\xi y''_R(a) = y'_L(a)+\xi y''_L(a), \quad y''_R(a)+\xi y'''_R(a) = y''_L(a)+\xi y'''_L(a).$$

The fourth continuity equations is obtained by making use of the equations (A.1) and (A.2); it gives

$$y'''_R(a)+\xi[2\gamma^2 y''_R(a)-\gamma^4 y_R(a)] = y'''_L(a)+\xi[2\gamma^2 y''_L(a)+(p^4-\gamma^4)y_L(a)].$$

There will be a solution to equations (1b) and (1b) if the determinant $\Delta \equiv e^{-2\gamma a}\cosh^2\gamma a\Delta'$ vanishes. Δ' is given by the following array ($t \equiv \tanh \gamma a$):

$1-\xi\gamma$	$a-\xi\gamma a+\xi$	$-t-\xi\gamma$	$-a-\xi-\xi\gamma at$
$-\gamma+\xi\gamma^2$	$-\gamma a+1+\xi\gamma^2 a-2\xi\gamma$	$-\gamma-\xi\gamma^2 t$	$-1-\gamma at$ $-2\xi\gamma t-\xi\gamma^2 a$
$\gamma^2-\xi\gamma^3$	$\gamma^2 a-2\gamma-\xi\gamma^3 a$ $+3\xi\gamma^2$	$-\gamma^2 t-\xi\gamma^3$	$-2\gamma t-\gamma^2 a$ $-3\xi\gamma^2-\xi\gamma^3 at$
$-\gamma^3+\xi\gamma^4$	$-\gamma^3 a+3\gamma^2+2\xi\gamma^4 a$ $-4\xi\gamma^3-\xi\gamma^4 a$	$-\gamma^3-2\xi\gamma^4 t$ $-\alpha\xi t$	$-3\gamma^2-\gamma^3 at$ $-4\xi\gamma^3 t-2\xi\gamma^4 a$ $-\alpha^2\xi a$

The vanishing of Δ' yields the following relation

$$\xi = \frac{2(t+1)^2\gamma^3}{-at\gamma^5+at^2\gamma^5+V_0t^2a\gamma-V_0a\gamma+V_0t^2+V_0t}.$$

A.2. PROOF OF THE THEOREM OF SECT. 5

To prove the theorem stated in the paper, we introduce an auxiliary quantity λ into (19), and replace $\phi_0(r)$ by $\phi(r)$ as follows:

$$\left(-\frac{d^2}{dr^2}+\gamma^2\right)^2 \phi(r) = \lambda V(r)\phi(r). \tag{A.3}$$

For a given $V(r)$ and γ^2, (A.3) can be regarded as an eigenvalue equation for λ. We shall take λ_0 to be the minimum eigenvalue and $\phi_0(r)$ the associated eigenfunction. Evidently λ_0 will depend upon the value γ^2 and the potential $V(r)$. It is clear from the hypothesis that for $V(r)$ as specified, there exists, for a

properly chosen γ^2, at least one possible λ (viz. $\lambda = 1$) and hence a minimum λ equal to λ_0. As γ^2 and $V(r)$ are varied, λ_0 will vary with them.

The theorem is now proved with the aid of three lemmas.

Lemma 1:

$$\lambda_0(\gamma^2, V'(r)) \leqq \lambda_0(\gamma^2, V(r)).$$

Proof: Consider the everywhere positive functional

$$\Lambda(\gamma^2, \phi(r), V(r)) = \frac{\int_0^\infty (\phi''^2(r) + 2\gamma^2\phi'^2(r) + \gamma^4\phi^2(r))\mathrm{d}r}{\int_0^\infty V(r)\phi^2(r)\mathrm{d}r}. \tag{A.4}$$

This has a stationary value with respect to $\phi(r)$ which occurs when $\phi(r)$ is a solution of the equation:

$$\left(-\frac{\mathrm{d}^2}{\mathrm{d}r^2} + \gamma^2\right)^2 \phi(r) = \Lambda(\gamma^2, \phi(r), V(r))V(r)\phi(r).$$

Call this solution $\phi_0(r)$ and the corresponding minimum eigenvalue (for a given γ^2)

$$\Lambda(\gamma^2, \phi_0(r), V(r)) \equiv \lambda_0(r^2, V(r)).$$

Then $\lambda_0(\gamma^2, V(r))$ is equal to expression (A.4) when $\phi_0(r)$ is substituted for $\phi(r)$. The lemma is then proved by inspection.

Lemma 2: For a given $V(r)$, $\lambda_0(\gamma^2, \phi_0(r), V(r))$ is a monotone increasing function of γ^2.

Proof: From equation (2b), keeping $V(r)$ fixed, we have

$$\frac{\mathrm{d}\lambda_0(\gamma^2, \phi_0(r), V(r))}{\mathrm{d}\gamma^2} = \frac{\partial\lambda_0}{\partial\gamma^2}\bigg|_{\phi_0(r)} + \int \mathrm{d}r \, \frac{\delta\lambda_0(\gamma^2, \phi_0(r), V(r))}{\delta\phi_0(r)} \, \frac{\partial\phi_0(r)}{\partial\gamma^2}.$$

The last term vanishes since λ_0 is stationary and the first term is positive. This proves the lemma.

Lemma 3:

$$\lambda_0(\gamma^2, \phi(r), V(r)) \to \infty \quad \text{as} \quad \gamma^2 \to \infty.$$

Proof: Introduce a new functional $\Gamma(\gamma^2, \eta(r), V(r))$ that is also everywhere positive,

$$\Gamma(\gamma^2, \eta(r), V(r)) = \frac{\int_0^\infty (2\eta'^2(r) + \gamma^2\eta^2(r))\mathrm{d}r}{\int_0^\infty V(r)\eta^2(r)\mathrm{d}r}. \tag{A.5}$$

The value $\eta_0(r)$ of $\eta(r)$ which makes Γ a minimum satisfies the Schrödinger equation:

$$-2\eta_0''(r) + \gamma^2\eta_0(r) = \lambda'_0(\gamma^2, \eta_0(r), V(r))V(r)\eta_0(r),$$

where

$$\lambda'_0(\gamma^2, \eta_0(r), V(r)) \equiv \Gamma(\gamma^2, \eta_0(r), V(r)).$$

Now upon comparing eqs. (A.4) and (A.5) we see that

$$\lambda_0 \geqq \frac{\gamma^2 \int_0^\infty (2\phi_0'^2(r) + \gamma^4 \phi_0^2(r)) \mathrm{d}r}{\int_0^\infty V(r)\phi_0^2(r)\mathrm{d}r} \geqq \frac{\gamma^2 \int_0^\infty (2\eta_0'^2(r) + \gamma^4 \eta_0^2(r)) \mathrm{d}r}{\int_0^\infty V(r)\eta_0^2(r)\mathrm{d}r},$$

since the last term is the minimum of the second term. Hence

$$\lambda_0(\gamma^2, \phi_0(r), V(r)) \geqq \gamma^2 \lambda'_0(\gamma^2, \eta_0(r), V(r))$$

But, the well-known properties of the Schrödinger equation imply $\lambda'_0 \to \infty$ as $\gamma^2 \to \infty$. Hence also $\lambda_0 \to \infty$.

The consequences of the three lemmas may be exhibited in a graph (fig. 1).

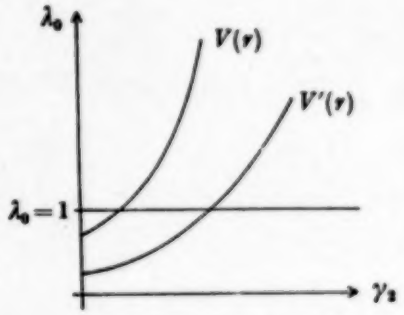

Fig. 1.

If we assume that eq. (19) has a bound state for the specified $V(r)$, this implies that the $\lambda_0(V(r))$ versus γ^2 curve intersects the line $\lambda_0 = 1$. Then the $\lambda_0(V'(r))$ curve must also intersect that line and the theorem is proved.

A.3. REDERIVATION OF HEISENBERG'S SUBSIDIARY EQUATION

We wish to derive here, for the case of a fixed N and three θ-particles, the subsidiary equation which should replace Heisenberg's equation (126) [3]).

The Schrödinger equation for the scattering states is given by (Heisenberg's equation (122))

$$S(E-\omega_1-\omega_2)\varphi(\omega_1, \omega_2) = \frac{1}{4\pi}\int \frac{k_3\omega_3 \mathrm{d}\omega_3}{\sqrt{\omega_3}(E-\omega_1-\omega_2-\omega_3)}\left(\frac{\varphi(\omega_3, \omega_2)}{\sqrt{\omega_1}} + \frac{\varphi(\omega_1, \omega_3)}{\sqrt{\omega_2}}\right) - \varphi_0(\omega_1, \omega_2), \quad \text{(A.6)}$$

where

$$\varphi_0(\omega_1, \omega_2) = \frac{2}{g_0\sqrt{4\pi}}\int \frac{k_3\omega_3 \mathrm{d}\omega_3}{\sqrt{\omega_3}} \psi_0(\omega_1, \omega_2, \omega_3)\delta(E-\omega_1-\omega_2-\omega_3),$$

ψ_0 being the incoming N+3θ state. Evidently ϕ_0 vanishes unless

$$\omega_1+\omega_2 \leqq E-\mu.$$

We write

$$\varphi(\omega_1, \omega_2) = a(\omega_1, \omega_2)\delta(E-E_0-\omega_1-\omega_2)+\frac{\chi(\omega_1, \omega_2)}{E-E_0-\omega_1-\omega_2+i\varepsilon}.$$

The functions $a(\omega_1, \omega_2)$ and $\chi(\omega_1, \omega_2)$ are symmetrical under the interchange of their arguments. One then requires that the right hand side of (1) vanish at the critical point where

$$\omega_1+\omega_2+E_0-E = 0.$$

Since at that point $\varphi_0 = 0$, this condition leads to

$$a(\omega_1, \omega_2) = \tag{A.7}$$
$$-\left(\frac{k_1}{E_0-\omega_1}+\frac{k_2}{E_0-\omega_2}\right)^{-1}\int\frac{k_3\sqrt{\omega_3}\,d\omega_3}{E_0-\omega_3}\left(\frac{\chi(\omega_3, \omega_2)}{\sqrt{\omega_1}(\omega_1-\omega_3+i\varepsilon)}+\frac{\chi(\omega_1, \omega_3)}{\sqrt{\omega_2}(\omega_2-\omega_3+i\varepsilon)}\right).$$

This expression differs from Heisenberg's eq. (125) [3]).

We may now re-express (A.6) in terms of χ, by making use of (A.7). The result is

$$\frac{S(E-\omega_1-\omega_2)\chi(\omega_1, \omega_2)}{E-E_0-\omega_1-\omega_2+i\varepsilon} = \tfrac{1}{2}\int k_3\sqrt{\omega_3}\,d\omega_3\left[\left\{\frac{\chi(\omega_3, \omega_2)}{\sqrt{\omega_1}(\omega'_1-\omega_3)(E-\omega_1-\omega_2-\omega_3)}\right.\right.$$
$$-\frac{k'_1\theta(\omega'_1-\mu)}{(E_0-\omega_1)(E_0-\omega_3)}\left[\frac{k'_1}{E_0-\omega'_1}+\frac{k_2}{E_0-\omega_2}\right]^{-1}$$
$$-\frac{\chi(\omega_3, \omega'_2)}{\sqrt{\omega_1}(\omega_1-\omega_3)}\,\frac{k'_2\sqrt{\omega'_2}}{(E_0-\omega_2)\sqrt{\omega_2}}\,\frac{\theta(\omega'_2-\mu)}{E_0-\omega_3}\left[\frac{k_1}{E_0-\omega_1}+\frac{k'_2}{E_0-\omega'_2}\right]^{-1}\Bigg\} \tag{A.8}$$
$$+\left\{\frac{\chi(\omega_1, \omega_3)}{\sqrt{\omega_2}(\omega'_2-\omega_3)}\,\frac{1}{E-\omega_1-\omega_2-\omega_3}-\frac{k'_2}{E_0-\omega_2}\,\frac{\theta(\omega'_2-\mu)}{E_0-\omega_3}\left[\frac{k_1}{E_0-\omega_1}+\frac{k'_2}{E_0-\omega'_2}\right]^{-1}\right.$$
$$\left.\left.-\frac{\chi(\omega'_1, \omega_3)}{\sqrt{\omega_2}(\omega_2-\omega_3)}\,\frac{k'_1}{E_0-\omega_1}\sqrt{\frac{\omega'_1}{\omega_1}}\,\frac{\theta(\omega'_1-\mu)}{E_0-\omega_3}\left[\frac{k'_1}{E_0-\omega'_1}+\frac{k_2}{E_0-\omega_2}\right]^{-1}\right\}\right].$$

We have set $\omega'_1 \equiv E-E_0-\omega_2$, $\omega'_2 \equiv E-E_0-\omega_1$, and $\theta(x) = 1$ for $x > 0$, while $\theta(x) = 0$ for $x < 0$. This equation has a quite different form from the corresponding one given by Heisenberg (eq. (126) in ref. [3])).

It is now an easy matter to see what bound states may occur in the scattering of N+3θ. If there occurs, as a final state, an outgoing discrete state of N+2θ of energy E_B together with a free θ of energy ω_1, we may write the wave function

in the neighborhood of $E = E_B+\omega_1$ as

$$\chi(\omega_1, \omega_3) \approx \frac{f(\omega_1)\psi(\omega_3)}{E-E_B-\omega_1}(\omega'_2-\omega_3),$$

once we have noted that the term in $a(\omega_1, \omega_3)$ does not contribute in the region

$$E_B < E_0+\mu.$$

In the limit $\omega_1 \to E-E_B$, the only term on the right hand side of (A.8) which contributes is the one in $\chi(\omega_1, \omega_3)$. Therefore we find in this limit

$$\psi(\omega_2)S(E_B-\omega_2) = \tfrac{1}{2}\int \frac{k_3\omega_3 d\omega_3\psi(\omega_3)}{\sqrt{\omega_2\omega_3}(E_B-\omega_2-\omega_3)},$$

which is precisely the Schrödinger equation for the discrete states of the sector $N+2\theta$. Therefore, the subsidiary equation of the sector $N+3\theta$ gives rise to the same discrete states of the subsector $N+2\theta$, as the Schrödinger equation. Since Heisenberg has shown that this equation has no solutions, this result does not affect his conclusions with respect to the one heavy particle sector.

This result generalizes easily to the case of more than three θ's.

References

1) G. Källén and W. Pauli, Mat. Fys. Med. Dan. Vid. Selsk. **30**, No. 7 (1955)
2) T. D. Lee, Phys. Rev. **95** (1954) 1329
3) W. Heisenberg, Nuclear Physics **4** (1957) 522
4) W. Pauli and V. Glaser, CERN Symposium (1958)
5) S. Weinberg, Phys. Rev. **102** (1956) 285
6) J. M. Jauch, Helv. Phys. Acta **31** (1958) 661

7.A

Nuclear Physics **21** (1960) 300—309; © *North-Holland Publishing Co., Amsterdam*

Not to be reproduced by photoprint or microfilm without written permission from the publisher

EXTRA SOLUTIONS OF THE DISPERSION RELATIONS AND RESONANCE SCATTERING

A. O. BARUT and K. H. RUEI †

Physics Department, Syracuse University, Syracuse 10, *New York* ††

Received 14 June 1960

Abstract: The connection between the extra solutions of the dispersion relations plus the unitary condition and the existence of unstable intermediary states is discussed. It is shown for the potential scattering that both lead to a resonance behaviour in the cross-section. The dispersion relation and the unitarity condition describe, therefore, a quantal system whose spectrum is enlarged by the inclusion of unstable intermediate states.

1. Introduction

A program under current investigation in quantum field theory, as suggested by Gell-Mann [1]), is the calculation of all measurable quantities, in particular scattering amplitudes, from dispersion relations and unitarity, without the intruduction of a Lagrangian. Since the dispersion relations employ some very general principles (Lorentz invariance, microscopic causality, the existence of a complete set of states of positive energies), these principles would then determine the quantum field theory uniquely in terms of some measurable parameters without any renormalization procedures of the usual theories. Some definite progress has been made in this direction [2]).

It is, therefore, indicated to look at the solutions of the system of dispersion relations and unitarity. In the case of the static-source meson theory in one meson approximation it is well known that the dispersion-type equation of this theory has an infinite number of solutions [3]). This type of ambiguity has been found in other situations. In particular, Norton and Klein [4]) have shown in a particular model that the infinitely many solutions of the Low equation are physical and correspond to the internal degrees of freedom of the system. In other words there are a class of Hamiltonians which give rise to the same Low equation and there is a one-to-one correspondance between the solutions of the Low equation and the Hamiltonians.

† Now at Department of Physics, Essex College, Assumption University Windsor, Ontario, Canada.

†† Work supported by the Air Force Office of Scientific Research under Contract No. AF 49(638)-801.

It is in this spirit that we consider in this paper the extra solutions of the dispersion relations and unitarity. We refer to the solution of the dispersion relations which is also a solution of the Hamiltonian as the "true" solution, in contrast to the remaining "extra" solutions. We would like to establish a relation between these extra solutions and the dispersive or resonance behaviour of the scattering. In other words, our contention is that the system of dispersion relation and unitarity is, like the Low equation, a larger system, that all their solutions have physical meaning and that it is insensitive to the existence of resonance producing intermediary unstable states.

To have a definite and simple case, we shall consider in this first paper the dispersion relation for potential scattering[5]). The extra solutions of this equation together with the unitarity will be shown to have indeed the resonance behaviour. On the other hand, an S-matrix formalism with the assumption of the existance of unstable intermediary states gives also rise to a resonance scattering. Now the argument that there should be a connection between these two situations runs as follows. Consider a situation where one observes resonances and the dispersion relations "check" for these resonances. By checking the dispersion relations we cannot decide obviously whether or not we have to do with the true or the extra solutions. Now since the true solution in the case of, say, potential scattering cannot give rise to any resonances, they must be due to the extra solutions. In other words, the dispersion relations and unitarity describe a larger system than the Schrödinger equation, a system involving arbitrary unstable intermediate states.

Our hope is to extend the above relation between the extra solutions of the dispersion relations and the unstable intermediate states to, say, pion-nucleon scattering (or even to unstable particles) and using the experimental information to determine the properties of unstable states which in turn will give us information about the interactions.

Some examples of the extra solutions of the dispersion relations for potential scattering in the case of a square well potential have already been reported by S. Gasiorowicz and H. A. Ruderman[6]) and found completely unphysical †. The true solution is unique and can be constructed, in principle, starting with the inhomogeneous term (see appendix) especially with the help of the double dispersion relations. We study the general structure of the extra solutions and the corresponding cross-sections. This discussion is preceeded by the derivation of the cross-section formula in the case of the existence of unstable intermediate states. Finally we compare the two expressions to prove that the extra solutions may be connected with the unstable states. If such states do not exist, the solution of the system of dispersion relations and unitarity is unique and is the true solution.

† Actually the examples given by these authors for the square well potential do not satisfy their condition C, hence they are not the proper extra solutions of the dispersion relations.

It is well known that in the nuclear reaction or scattering the resonance phenomena are explained by the assumption of the existence of unstable intermediate states which have to be put into the theory. We see that the dispersion relations refer actually to this larger group of systems which contain the possibility of unstable intermediate state. We also extend this idea to elementary processes. The question arises whether even any field theory can account for the observed resonances in the scattering or elementary particles, or the existence of intermediary states has to be put into the theory in some form or another.

Since the Schrödinger equation enlarged by the intermediate states is already a field theory (creation and annihilation of particles) the complete consistency or our approach can be proved only in a field theoretical model. Such a model will be given in a subsequent paper where we prove the dispersion relation in the presence of intermediary states and discuss further the question raised in the previous paragraph.

2. S-Matrix for Processes involving Unstable States

We consider † the time-independent Hamiltonian H_0+H_1. The undisturbed part H_0 is assumed to have a continuous spectrum E corresponding to eigenstates $|q\rangle$ of the incident particles (including scatterer), and a discrete spectrum E_α corresponding to unstable states $|\alpha\rangle$. We assume that H_0+H_1 has the same continuous spectrum E as H_0 corresponding to eigenstates $|Q\rangle$. Those states $|Q\rangle$ can be expanded into the complete set of states comprising $|q\rangle$ and $|\alpha\rangle$ states. Forming the matrix elements $\langle q'|H_0+H_1|Q\rangle$ and $\langle\alpha'|H_0+H_1|Q\rangle$ we obtain the equations

$$\begin{aligned}(E-E')\langle q'|Q\rangle &= \sum_{\alpha'}\langle q'|H_1|\alpha'\rangle\langle\alpha'|Q\rangle+\int dq''\langle q'|H_1|q''\rangle\langle q''|Q\rangle,\\ (E-E'_\alpha)\langle\alpha'|Q\rangle &= \sum_{\alpha''}\langle\alpha'|H_1|\alpha''\rangle\langle\alpha''|Q\rangle+\int dq''\langle\alpha'|H_1|q''\rangle\langle q''|Q\rangle.\end{aligned} \tag{1}$$

We decompose $|Q\rangle$ into incident and scattered parts by

$$|Q\rangle = |q\rangle+|\chi\rangle \tag{2}$$

and solve for $\langle q'|\chi\rangle$ and $\langle\alpha'|\chi\rangle$.

$$\langle q'|\chi\rangle_\pm = \frac{1}{E-E'\pm i\varepsilon}[G_\pm(q'q)+J_\pm(q'q)], \tag{3a}$$

$$\langle\alpha'|\chi\rangle = \frac{1}{E-E'_\alpha}[L(\alpha'q)+M(\alpha'q)], \tag{3b}$$

† The discussion of this section parallels those of P.A.M. Dirac, and J. M. Jauch and F. Rohrlich [8]).

where G, J, L, M satisfy the following integral equations

$$\begin{aligned}
G_{\pm}(q'q) &= \langle q'|H_1|q\rangle + \int \frac{dq''\langle q'|H_1|q''\rangle G_{\pm}(q''q)}{E-E''\pm i\varepsilon}, \\
J_{\pm}(q'q) &= \sum_{\alpha''}\langle q'|H_1|\alpha''\rangle\langle\alpha''|\chi\rangle + \int \frac{dq''\langle q'|H_1|q''\rangle J_{\pm}(q''q)}{E-E''\pm i\varepsilon}, \\
L(\alpha'q) &= \langle\alpha'|H_1|q\rangle + \sum_{\alpha''}\frac{\langle\alpha'|H_1|\alpha''\rangle L(\alpha''q)}{E-E''_{\alpha}}, \\
M(\alpha'q) &= \int dq''\langle\alpha'|H_1|q''\rangle\langle q''|\chi\rangle + \sum_{\alpha''}\frac{\langle\alpha'|H_1|\alpha''\rangle M(\alpha''q)}{E-E''_{\alpha}}.
\end{aligned} \tag{4}$$

The $\pm$ solutions correspond to asymptotic outgoing and ingoing waves, respectively. The S-Matrix between two stable states q' and q is given by [8])

$$S_{\pm}(q'q) = \delta(q'q) \mp 2\pi i\delta(E-E')(G_{\pm}(q'q)+J_{\pm}(q'q)). \tag{5}$$

Here G is entirely due to the $|q\rangle$ states, whereas J contains contributions from the $|\alpha\rangle$ states.

We make now the essential assumption that

$$\langle\alpha'|H_1|\alpha\rangle = 0. \tag{6}$$

That is to say, there are no first order transitions between two unstable states.

We are interested in the contribution of the $|\alpha\rangle$ states to the scattering cross-section. For this purpose we solve J_+ in eq. (4) by iteration starting with the inhomogeneous term

$$J_+^{(1)} = \sum_{\alpha''}\langle q'|H_1|\alpha''\rangle\langle\alpha''|\chi\rangle \tag{7}$$

and obtain

$$J_+ = \sum_{n=1}^{\infty} J_+^{(n)},$$

with

$$J_+^{(n)} = \sum_{\alpha}\int \frac{dq''\ldots dq^{(n)}\langle q'|H_1|q''\rangle\ldots\langle q^{(n)}|H_1|\alpha\rangle\langle\alpha|\chi\rangle}{(E-E''+i\varepsilon)\ldots(E-E^{(n)}+i\varepsilon)} \equiv \sum_{\alpha} j_+^{(n)}(q'\alpha)\langle\alpha|\chi\rangle, \tag{8}$$

where we have introduced the expressions $j_+^{(n)}(q'\alpha)$. On the other hand $\langle\alpha|\chi\rangle$ satisfies eq. (3a), which with eqs. (6), (4) and (3b) becomes

$$\begin{aligned}
(E-E'_{\alpha})\langle\alpha'|\chi\rangle_{\pm} = \langle\alpha'|H_1|q\rangle &+ \int \frac{dq''\langle\alpha'|H_1|q''\rangle G_{\pm}(q''q)}{E-E''\pm i\varepsilon} \\
&+ \sum_{n}\sum_{\alpha=1}^{N}\int \frac{dq''\langle\alpha'|H_1|q''\rangle j_{\pm}(q''\alpha)\langle\alpha|\chi\rangle}{E-E''\pm i\varepsilon}.
\end{aligned} \tag{9}$$

These are N coupled equations for $\langle\alpha|\chi\rangle$ if we have N $|\alpha\rangle$ states. For $N=1$ we have

$$\langle\alpha|\chi\rangle^{\pm}=\frac{1}{E-E_\alpha-(A+iB)}\left(\langle\alpha|H_1|q\rangle+\int\frac{dq''\langle\alpha|H_1|q''\rangle G_\pm(q''q)}{E-E''\pm i\varepsilon}\right), \quad (10)$$

where

$$A+iB=\int\frac{\langle\alpha|H_1|q''\rangle\ldots\langle q^{(n)}|H_1|\alpha\rangle dq''\ldots dq^{(n)}}{(E-E''+i\varepsilon)\ldots(E-E^{(n)}+i\varepsilon)}. \quad (11)$$

Hence

$$J_+(q'q)=\sum_n j^{(n)}(q'\alpha)\frac{1}{E-E_\alpha-(A+iB)}\cdot\left(\langle\alpha|H_1|q\rangle+\int\frac{dq''\langle\alpha|H_1|q''\rangle G_+(q''q)}{E-E''+i\varepsilon}\right). \quad (12)$$

The contribution of the $|\alpha\rangle$ states to the cross-section — if we omit the G-part of the amplitude completely — is given by

$$\Delta\sigma=\frac{16\pi^4 m}{k}\int|J_+(q'q)|^2\delta(E-E')dq',$$

where k is the momentum of the incident particle.

We first evaluate this expression up to the second order in the iteration near the resonance:

$$J_+=\frac{\langle q'|H_1|\alpha\rangle\langle\alpha|H_1|q\rangle}{E-E_\alpha-(a+ib)}, \qquad a+ib=\int\frac{dq''\langle\alpha|H_1|q''\rangle\langle q''|H_1|\alpha\rangle}{E-E''+i\varepsilon}. \quad (13)$$

We split the second integral into a principal part $P\int$ and a part containing $i\pi\int\delta(E-E')$ and take the imaginary part which gives

$$b=\pi\int dq''\delta(E-E'')|\langle\alpha|H_1|q''\rangle|^2.$$

This expression occurs in $\Delta\sigma$ and we get the resonance formula

$$\Delta\sigma=\frac{16\pi^3 m}{k}\frac{|\langle\alpha|H_1|q\rangle|^2 b}{(E-E_\alpha-a)^2+b^2}. \quad (14)$$

The parameters a and b of the resonance are connected by (11) or (13) to the unstable states $|\alpha\rangle$. In the spcial case that $\langle\alpha|H_1|q\rangle$ depends only on the magnitude of momentum k (i.e. for example, if $|\alpha\rangle$ is a pure angular momentum state) then $\delta(E-E')$ in the expression for $\Delta\sigma$ implies $q'=q$ and we get the simpler

expression

$$\Delta\sigma = \frac{C}{k^2}\,\frac{b^2}{(E-E_\alpha-a)^2+b^2}, \tag{14'}$$

where C is a constant number. (For s-wave resonance, $C = 4\pi$).

Coming back now to the general expression (3a) for the scattering amplitude $G+J$ we want to show that (a) it does not admit, in the presence of $|\alpha\rangle$ states, a series expansion in powers of the coupling constant g^2 and (b) that the J-part, hence the total amplitude $G+J$ satisfies the dispersion relation. The first assertion follows from the existence of denominators of the form $1/(E-E_\alpha-A-iB)$. Here A and B contain the coupling constant g^2 and if we expand this factors again by binomial expansion, we get factors like $1/(E-E_\alpha)$, $1/(E-E_\alpha)^2$, etc.; thus, higher order poles are introduced on the real axis. No such terms appear in G-part of the amplitude.

To prove that the J-part satisfies the dispersion relation we have to show that it does not have a complex pole in the first Riemann sheet of the energy plane. It is sufficient to show that the function

$$h(z) = z-E_\alpha-\sum_n \int \frac{\mathrm{d}q''\langle\alpha|H_1|q''\rangle j^{(n)}(q''\alpha)}{z-E''+i\varepsilon}$$

does not have a zero. Following Levy [9]) we see that the imaginary part of $h(z)$ is non-zero for Im $z \neq 0$; the dominant term of Im $h(z)$ for example, is of the form

$$\mathrm{Im}\ (z) \int \frac{\mathrm{d}q''|\langle\alpha|H_1|q''\rangle|^2}{|z-E''|^2} \neq 0 \quad \text{for} \quad \mathrm{Im}\ (z) \neq 0.$$

$h(z)$ can have zeros, however, on the real axis, which correspond to stable bound states.

The remaining analytical properties of the J-amplitude depends on the type of $|\alpha\rangle$ states. The analyticity will be proved for a particular field theoretical model in a subsequent paper.

Thus, the theory with the inclusion of $|\alpha\rangle$ states gives rise to a resonant scattering and satifies the dispersion relation. In the next section we look at these states from the point of view of the extra solutions of the dispersion relation.

3. Structure of the Extra Solutions of the Dispersion Relations

We first consider two solutions differing in one phase shift only. The partial wave amplitudes are identical except for a particular l for which

$$f_l(k) = \frac{1}{2ik}(2l+1)(\mathrm{e}^{2i\eta_l}-1), \qquad f'_l(k) = \frac{1}{2ik}(2l+1)(\mathrm{e}^{2i\eta'_l}-1), \tag{15}$$

where η_l and η'_l are the only distinct phase shifts. We introduce the reciprocal functions $g_l(k) \equiv 1/f_l(k)$ and $g'_l(k) \equiv 1/f'_l(k)$ and define

$$g'_l(k) = g_l(k) + y_l(k). \tag{16}$$

From the unitarity and the symmetry of the S-matrix, i.e.

$$(e^{2i\eta'_l(k)})^*(e^{2i\eta'_l(k)}) = 1, \quad (e^{2i\eta'_l(k)})^* = e^{2i\eta'_l(-k)},$$

it follows that $y_l(k)$ is a real and even function of k:

$$y_l(k) = y_l^*(k) \quad \text{for} \quad k \geqq 0, \quad y_l(k) = y_l(-k) \quad \text{for all } k. \tag{17}$$

The total scattering amplitude as a function of the momentum k of the incident particle and the momentum transfer τ satisfies the dispersion relation[5])

$$\operatorname{Re} f(k, \tau) = \frac{2}{\pi} \int_0^\infty \frac{\operatorname{Im} f(k', \tau) k' \, dk'}{k'^2 - k^2} + V(\tau) + \text{res. at bound states}, \tag{18}$$

provided $|V(r)| < M/r^2$, where M is a finite positive number, $\int_0^\infty dr r|V(r)| < \infty$ and $\int dr r^2|V(r)| < \infty$. The quantity $V(\tau)$ is the Fourier transform of $V(r)$,

$$V(\tau) = \int e^{i\boldsymbol{\tau}\cdot\mathbf{r}} V(r) d\mathbf{r}.$$

If for a given potential hence given $V(\tau)$ there are two solutions of eq. (18), the difference of the two solutions must be regular and approach zero as $|k| \to \infty$ in the upper k-plane. Otherwise the two solutions would generate different inhomogenous terms in eq. (18). The difference of the two solutions is just

$$(f'_l(k) - f_l(k)) P_l(\cos\theta) = -\frac{y_l(k) f_l^2(k)}{1 + f_l(k) y_l(k)} P_l(\cos\theta). \tag{19}$$

First of all $P_l(1 - \tau^2/2k^2) \sim 1/k^{2l}$ as $k \to 0$. Hence $y_l(k)$ must behave at $k \to 0$ at least as k^{2l} to make the difference (19) regular at the origin. For potentials with arbitrary large cutoff the S-matrix hence $f_l(k)$ has an essential singularity at infinity [10]) in the upper half plane of the form e^{-2iCk}, where C is a positive number. Thus from (17) and (19) $y_l(k)$ must contain a factor at least e^{k^2} (which for $k = i\chi$ is $e^{-\chi^2}$); then the difference (19) goes to zero in all directions as $|k| \to \infty$. In the upper half plane $y_l(k)$ can take any value except $y_l(k) = -1/f_l(k)$.

If there is a bound state for the particular l we are considering, $f_l(k)$ has a factor $1/(k - ik_0)$ at this pole, and in order to make the difference (19) finite, $y_l(k)$ according to (17) must behave at least as $(k^2 + k_0^2)^2$.

This completes the discussion on the form of the functions $y_l(k)$. To summarize it must contain factors at least like $k^{2l}e^{k^2}$ and be an even function of (complex) k, and real for $k \geqq 0$. Given a function $y_l(k)$ having the above properties the

extra solution is given by

$$f'_l = \frac{f_l}{1+y_l f_l}.$$

f_l and f'_l are identical at the poles and at the essential singularity at ∞. Everywhere else they are both regular.

Next we consider the contribution of the extra solutions to the total scattering cross-section σ, anticipating that they have physical meaning. Since

$$\sigma = \frac{4\pi}{k^2}\sum_l (2l+1)\sin^2\eta_l = 4\pi \sum_l \frac{1}{2l+1}|f_l|^2,$$

the contribution of f'_l to the cross-section is given by

$$\Delta\sigma = (|f'_l|^2 - |f_l|^2)\frac{4\pi}{2l+1}.$$

Assuming that the resonance is due to f'_l we replace

$$|f'_l|^2 - |f_l|^2 \approx |f'_l - f_l|^2 = \left|\frac{y_l f_l^2}{1+f_l y_l}\right|^2.$$

Putting further $f_l = f_l^{(1)} + i f_l^{(2)}$ we get

$$\Delta\sigma = \frac{4\pi}{2l+1}\,\frac{y_l^2|f_l^2|^2}{(1+f_l^{(1)}y_l)^2+(f_l^{(2)}y_l)^2}. \tag{20}$$

This expression will give rise to a resonance, if $1+f_l^{(1)}y_l$ is very small. Let us assume in the idealized case that for a certain k, $1+f_l^{(1)}(k)y_l(k) = 0$, then the unitarity of $f_l(k)$ gives

$$f_l^{(2)^2} = \frac{k^2}{(2l+1)^2}|f_l^2|^2, \tag{21}$$

hence

$$\Delta\sigma = \frac{4\pi}{k^2}(2l+1),$$

independent of f'_l. This formula, however, corresponds to a sharp resonance of phase shift $\frac{1}{2}\pi$. In reality $1+f_l^{(1)}y_l$ is never zero.

Eqs. (20) and (14) or (14′) can now be compared. Letting $(f_l^{(1)}+1/y_l) = E-E_a-a_l$ and $f_l^{(2)} = b_l$, eq. (20) becomes

$$\Delta\sigma \approx \frac{4\pi}{k^2}(2l+1)\,\frac{b_l^2(k)}{(E-E_a-a_l(k))^2+b_l^2(k)}. \tag{22}$$

The theory can be generalized to solutions differing in more than one phase shift, say in N phase shifts, then (19) is replaced by

$$\sum_l (f'_l - f_l) P_l = -\sum_l \frac{y_l f_l^2}{1+f_l y_l} P_l. \tag{23}$$

This whole expression must be now regular everywhere and approach zero as $|k| \to \infty$. Each $y_l(k)$ again satisfies eq. (17). In this case we put (using $\tau^2 = 2k^2(1-\cos\theta)$)

$$f_l(k', \tau) = \sum_l f_l(k') P_l\left(1 - \frac{\tau^2}{2k'^2}\right)$$

$$= \sum_{l,l'} f_l(k') A_{ll'}\left(\frac{k^2}{k'^2}\right) P_{l'}(\cos\theta),$$

where $A_{ll} = 0$ if $l < l'$. We obtain from the dispersion relation (18)

$$\operatorname{Re} f_l(k) = \frac{2}{\pi}\int_0^\infty \frac{\operatorname{Im}\sum_{l'} A_{l'l}\left(\frac{k^2}{k'^2}\right) f_{l'}(k') k' \, dk'}{k'^2 - k^2} + \mathscr{V}_l(k) + \text{res. at } l,$$

where

$$V(\tau) = \sum_l \mathscr{V}_l(k) P_l(\cos\theta).$$

Inserting (23) into this equation we get N coupled equations for the functions $y_l(k)$,

$$\operatorname{Re}\frac{y_l(k) f_l^2(k)}{1+f_l(k) y_l(k)} = \frac{2}{\pi}\int_0^\infty \frac{\operatorname{Im}\sum_{l'} A_{l'l}\left(\frac{k^2}{k'^2}\right) \frac{y_{l'}(k') f_{l'}^2(k')}{1+f_{l'}(k') y_{l'}(k')} k' \, dk'}{(k'^2 - k^2)},$$

which together with the unitarity eq. (17) are the requirements on $y_l(k)$ and hence the extra solutions.

Appendix

UNIQUENESS OF THE TRUE SOLUTION

Given a potential we must distinguish the "true" solution of the dispersion relations from the extra solutions. We first show that there is a *unique* solution of dispersion relation and unitarity which can be expanded in a power series of the coupling constant $\lambda (H_1 = \lambda V)$. Let

$$f(k, \tau) = \sum \lambda^n f^{(n)}(k, \tau)$$

and choose $f^{(1)}(k, \tau) = V(\tau)$ hence $\operatorname{Im} f^{(1)}(k, \tau) = 0$. We write the unitarity

condition in the form

$$\operatorname{Im} f(k,\tau) = \frac{1}{2\pi}\int \mathrm{d}^3\tau'\,\delta(\tau'^2+2\mathbf{k}\cdot\boldsymbol{\tau}')f^*(k,|\boldsymbol{\tau}-\boldsymbol{\tau}'|)f(k,\tau')$$

and compare coefficients of λ^2. Then

$$\operatorname{Im} f^{(2)}(k,\tau) = \frac{1}{2\pi}\int \mathrm{d}^3\tau'\,\delta(\tau'^2+2\mathbf{k}\cdot\boldsymbol{\tau}')f^{(1)}(k,|\boldsymbol{\tau}-\boldsymbol{\tau}'|)f^{(1)}(k,\tau').$$

Now we use the dispersion relation (18) to determine $\operatorname{Re} f^{(2)}$. The integral in (18) extends also over the unphysical region $\tau > 2k$. The function $f(k,\tau)$ can be defined in this region if $\tau < 2\alpha$, where α is defined by the inequality [5])

$$\int_0^\infty r^2\mathrm{d}r|V(r)|\mathrm{e}^{\alpha r} < \infty.$$

We remark that if one introduces a cutoff at arbitrarily large distances as is required in the formulation of the S-matrix starting from the so called complex Schrödinger equation [10]), the analytical continuation into the unphysical region is well defined.

Continuing this process we generate the unique true solution and as we have noted above, the extra solutions cannot be generated by this process.

References

1) M. Gell-Mann, Proc. of the 6th Annual Rochester Conference on High Energy Physics, 1956 (Interscience, New York), sect. III, p. 30
2) S. Mandelstam, Phys. Rev. **112** (1958) 1344; **115** (1959) 1741, 1752
3) L. Castillejo, R. H. Dalitz and F. J. Dyson, Phys. Rev. **101** (1956) 453
4) R. Norton and A. Klein, Phys. Rev. **109** (1958) 991
5) N. Khuri, Phys. Rev. **107** (1957) 1148
6) S. Gasiorowicz and H. A. Ruderman, Phys. Rev. **107** (1957) 868
7) Blankenbeder, Goldberger, Khuri and Treiman, Ann. Phys. **10** (1960) 62
8) P. A. M. Dirac, Principles of quantum mechanics (Oxford University Press, 1958), p. 52; J. M. Jauch and F. Rohrilich, The theory of photons and electrons (Addison and Welsley, 1955), Ch. 7
9) M. Levy, Nuovo Cim. **13** (1959) 115
10) A. O. Barut and K. H. Ruei, Journ. Math. Phys. (in publication)

1.D.3

Nuclear Physics **21** (1960) 310—326; © *North-Holland Publishing Co., Amsterdam*

Not to be reproduced by photoprint or microfilm without written permission from the publisher

ENERGY LEVELS OF Be^9 AND B^9

R. R. SPENCER,† G. C. PHILLIPS and T. E. YOUNG††

The Rice University, Houston, Texas†††

Received 8 August 1960

Abstract: The low lying energy levels of Be^9 and B^9 have been investigated by means of magnetic analysis of the $Be^9(p, p')Be^9$ and $B^{10}(He^3, \alpha)B^9$ reactions, respectively. Several distinctive features of the data result in a model being proposed to describe the low lying energy level structure of these mirror nuclei. The model describes the mass nine nuclei as two-body cluster states of $Be^8(0^+)$ + nucleon and $Be^8(2^+)$ + nucleon and gives quantitative agreement with the experimental width of the states. A generalized density of states function is employed to describe the continuum spectra, and allows a description of the cusp effects in the spectra of the two nuclei as aspects of two-body cluster spatial localization, and many-body decay occurring as a sequence of two-body separations.

1. Introduction

The low lying energy levels of Be^9 have been the subject of extensive investigation. On the basis of a theoretical analysis of photo- and electrodisintegration of Be^9, Guth and Mullin [1]) deduced an $S_{\frac{1}{2}}$ state for this nucleus at about 1.5 MeV excitation and a broad $D_{\frac{3}{2}}$ state at an excitation considerably above 2.5 MeV. Van Patter *et al.* [2]) reported a state at 2.422 ± 005 MeV in Be^9 from a study of the $B^{11}(d, \alpha)Be^9$ reaction. Moak *et al.* [3]) observed protons from the $Li^7(He^3, p)Be^9$ reaction and reported states in Be^9 at 1.8, 2.43, 3.2 and 4.2 MeV. Magnetic analysis of the alpha particles from the $B^{11}(d, \alpha)Be^9$ reaction indicated two relatively broad states in Be^9 at 1.75 MeV and 3.02 MeV in addition to the narrow state at 2.43 MeV, according to Lee and Inglis [4]). Gossett *et al.* [5]) made a study of the low lying Be^9 states by means of magnetic analysis of the $Be^9(p, p')Be^9$ reaction. These authors observed a broad distribution of protons with a well-defined high momentum edge occurring at an energy corresponding to 1.675 ± 0.002 MeV excitation in Be^9. This distribution rose to a peak in an energy interval that was greater than the target thickness, and decreased slowly to yield an asymmetric, cusp like, distribution with an approximate width at half-height of 150 keV. They suggested that this distribution might be the result of a three-body break-up of the compound system since the high momentum edge of the distribution occurred at an excitation very near to that required for the neutron decay of Be^9, (the γ, n threshold for Be^9 has

† Now with the Phillips Petroleum Company, Idaho Falls, Idaho.

†† Now at Trinity University, San Antonio, Texas.

††† Work supported in part by the U. S. Atomic Energy Commission.

been measured to be 1.666 ± 0.002 MeV by Mobley and Laubenstein [6]). Gossett *et al.* [5]) also observed a proton group corresponding to a state in Be^9 at 2.432 ± 0.004 MeV. The centre-of-mass width of this state was determined perhaps to be no greater than 1 keV; however, an absolute upper limit of 3 keV may be asserted. Rasmussen *et al.* [7]) obtained values of 1.74 ± 0.1 and 3.01 ± 0.1 MeV for the broad Be^9 states by magnetic analysis of alpha particles and deuterons that were inelastically scattered from a Be^9 target. These authors were able to fit the observed deuteron and alpha particle distributions for the 1.74 MeV effect by assuming a three-body break-up of the compound nucleus in which the neutron and Be^8 interact by means of a final state S-wave potential scattering. It was assumed that the outgoing alpha particle or deuteron experienced no interaction with either of the other particles. They could not, however, eliminate the possibility that the 1.74 MeV effect is a state in the usual sense. Bockelman *et al.* [8]) studied the $Be^9(p, p')Be^9$ reaction by magnetic analysis of the scattered protons and obtained excitation energies of 1.664 ± 0.005 for the high momentum edge of the broad distribution and 2.434 ± 0.005 and 3.03 ± 0.03 MeV for the two states in Be^9. These authors determined the minimum width of the 3.03 MeV state to be 280 keV. They also studied the $B^{11}(d, \alpha)Be^9$ reaction, obtaining similar results. Following the technique and assumptions used by Rasmussen *et al.* [7]) they were able to fit the observed proton and alpha particle distributions with a three-body mechanism.

The low lying energy levels of B^9 have not previously been extensively investigated. Stelson and Preston [9]) observed neutrons corresponding to the ground state of B^9 from the $Be^9(p, n)B^9$ reaction. They estimated the width of this state to be less than 2 keV. Almqvist *et al.* [10]) reported a state at 2.58 ± 0.13 MeV in B^9 from a study of the $B^{10}(He^3, \alpha)B^9$ reaction. Marion *et al.* [11]) observed thresholds in the $Be^9(p, n)B^9$ reaction, by the counter-ratio method, corresponding to the ground state of B^9 and to a state at 2.326 ± 0.006 MeV excitation. The latter threshold rose to a peak in approximately 70 keV of bombarding energy although the target used was much thinner than 70 keV, thus suggesting that the 2.3 MeV level may have an appreciable width. These authors also observed a broad anomaly in the ratio which would correspond to a state at about 1.4 MeV in B^9 if interpreted as a threshold. However, there has been no other evidence for a B^9 state at this energy.

The present experiments were carried out in an attempt to clarify the nature of the low lying states of the mirror nuclei, Be^9 and B^9. Due to some changes in the vacuum tube of the Rice 180° magnetic spectrometer which reduced the background for inelastic scattering experiments, it appeared profitable to re-examine the $Be^9(p, p')Be^9$ reaction in order to define more clearly the shape of the broad proton distribution corresponding to 1.7 MeV excitation in Be^9. A study of the B^9 levels, by means of the $B^{10}(He^3, \alpha)B^9$ reaction, was then undertaken in an attempt to locate the mirror levels to those observed in Be^9

and to determine their widths, if possible. This paper reports these experimental results and suggests an interpretation of the low excited states of Be^9—B^9 in terms of the two-body interaction of a nucleon with the 0^+ and 2^+ excited states of Be^8. The cusp like effect in the spectrum of Be^9 is described as an aspect of two-body cluster spatial localization.

2. Experimental Procedure

The Rice University 180° magnetic spectrometer was used in conjunction with the Rice 5.5 MeV Van de Graaff accelerator to obtain the spectra of charged particles. The spectrometer has been described in detail by Gossett *et al.* [12]). In general, Ilford nuclear track plates were used to detect the particles, although a scintillation counter was used for a portion of one spectrum where a high resolution was not required.

For the Be^9 experiment a thin, self-supporting foil of Be^9 was bombarded with protons from the Van de Graaff accelerator. The scattered protons were analyzed in momentum by the spectrometer. The bombarding energy was calculated from the momentum of the proton group corresponding to the ground state of Be^9. The excitation energies corresponding to other groups of protons were calculated from the bombarding energy and the momenta of these groups.

The B^{10} target used to study the levels of B^9 was prepared by evaporating a sample of boron enriched to 96 % in B^{10} onto a carbon foil. This target was then bombarded with He^{3+} ions from the Van de Graaff accelerator. The charged particles emitted by nuclear reactions in the target were analyzed in momentum by the spectrometer. The bombarding energy was calculated from the momentum of a deuteron group corresponding to the ground state of C^{11} which results from the $B^{10}(He^3, d)C^{11}$ reaction. The Q values corresponding to other groups of charged particles were calculated from the momenta of the groups and the bombarding energy.

3. Experimental Results

3.1. $Be^9(p, p')Be^9$

The observed spectrum of protons scattered inelastically from the Be^9 target is shown in fig. 1. In this figure, the number of protons in a 1.5 mm by 10 mm strip on the photographic plate has been plotted *versus* the magnetic rigidity of the particles, $B\rho$. The spectrum on photographic plates was incomplete in the region of the broad peak, (50), so the missing portion of the data was supplemented by a spectrum taken with the scintillation counter at the same bombarding energy. The counter data appear as crosses in fig. 1. The exposure for each of the photographic plates was 1000 μC of protons incident on the target. This figure clearly shows a broad distribution of protons beginning at a $B\rho$ of about 197 kG$\times$cm. The extrapolated high momentum edge of this

group corresponds to an excitation of 1.674 MeV in Be^9. This broad distribution rises from a very low background to a peak in about 30 keV. The narrow proton group occurring at a $B\rho$ of approximately 162 kG × cm corresponds to an excitation of 2.43 MeV in Be^9. The broad proton group centred about $B\rho$ of 132 kG × cm corresponds to an excitation of about 3.04 MeV.

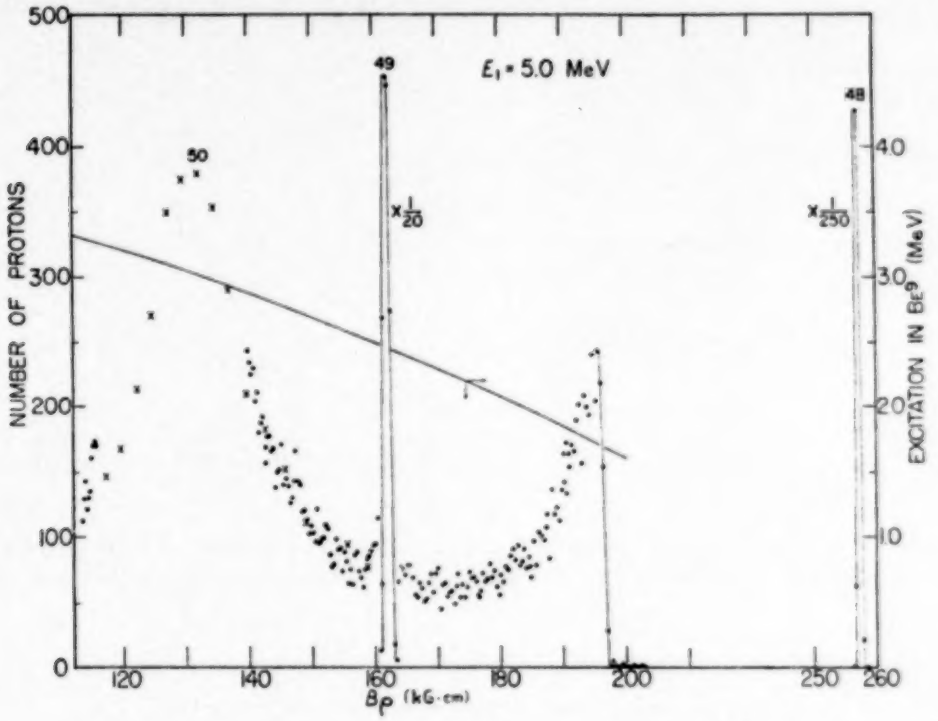

Fig. 1. Partial spectrum of protons scattered from a thin Be^9 foil target. Dots represent data taken with photographic plates. Crosses represent data taken with a scintillation counter. The peaks marked 48, 49 and 50 correspond respectively to the elastic group, and inelastic proton groups to the 2.43 and 3.04 states in Be^9. The strange anomaly at about 195 kG × cm is discussed in detail in the text.

2.2. $B^{10}(He^3, \alpha)B^9$

Figs. 2 and 3 show the spectra of alpha particles, deuterons, and protons obtained from bombarding the B^{10} target with He^{3+} ions at two different energies. The exposure for each photographic plate was 500 μC of He^{3+} ions incident on the target. The observed reaction products have been plotted as number of particles counted in a 0.25 mm × 10 mm strip on the photographic plate *versus* the magnetic rigidity $B\rho$. In these two figures the number of particles in every fourth strip have been plotted; hence, these figures represent only one-fourth the data available. The groups of alpha particles, (51) and (52), in figs. 2 and 3 correspond to the ground state and a 2.33 MeV excited state in B^9, respectively. Alpha particle group, (53), in fig. 3 corresponds to the ground state of O^{15} resulting from the $O^{16}(He^3, \alpha)O^{15}$ reaction in an oxygen contaminant. In addition to these discrete groups of alpha particles, a continuum of alpha particles beginning in the neighborhood of the B^9 ground state group,

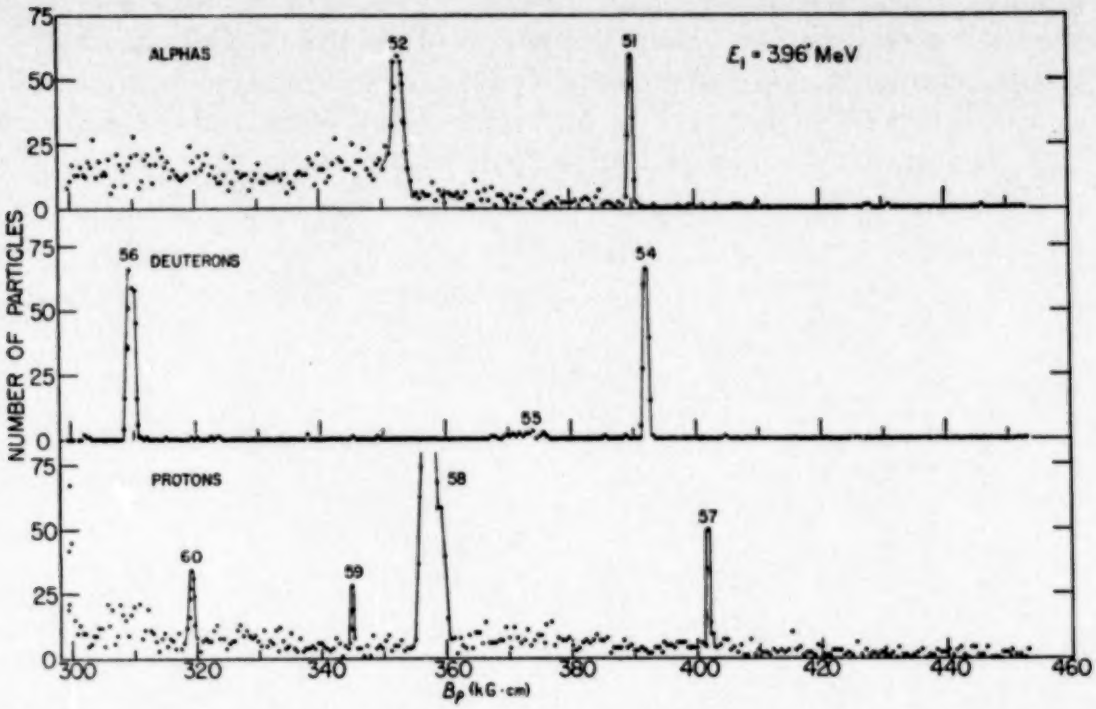

Fig. 2. Partial spectra of alpha particles, deuterons, and protons emitted from a target of B^{10} bombarded with He^{3+} ions. The target was made from a sample of boron enriched to 96 % in B^{10}.

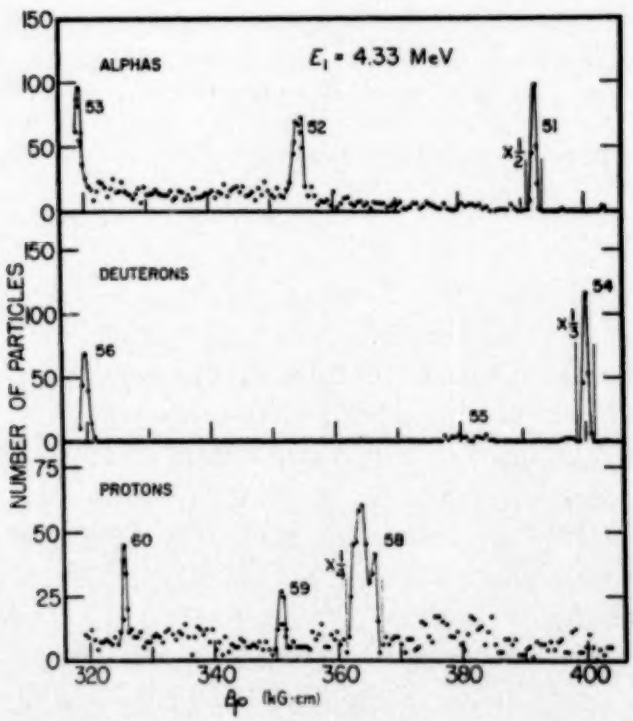

Fig. 3. Partial spectra of alpha particles, deuterons, and protons emitted from a target of B^{10} bombarded with He^{3+} ions. The target was made from a sample of boron enriched to 96 % in B^{10}.

(51), and persisting throughout the spectra of these figures is readily apparent. The alpha particle spectra of figs. 2 and 3 cover the region of B^9 excitation from 0 to 5 MeV. In order to examine the shape of the continuum all of the available

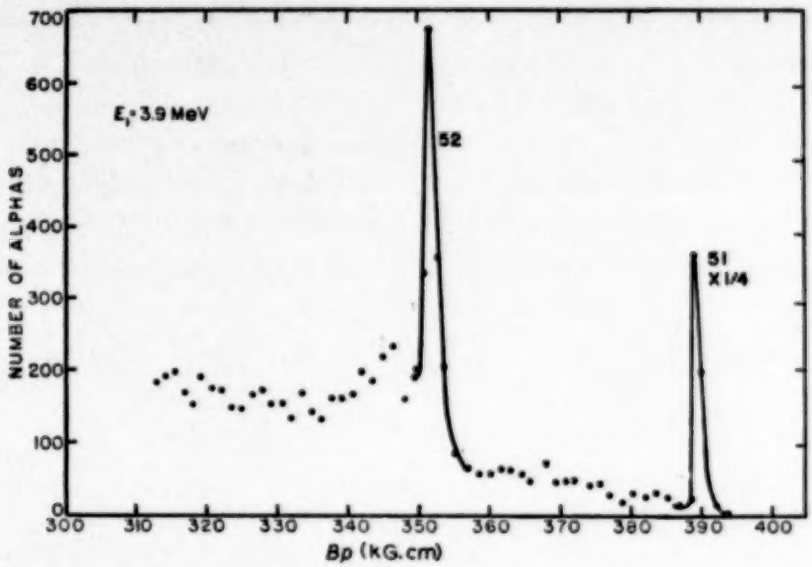

Fig. 4. Alpha particle spectrum of fig. 2 replotted to show the shape of the alpha particle continuum more clearly.

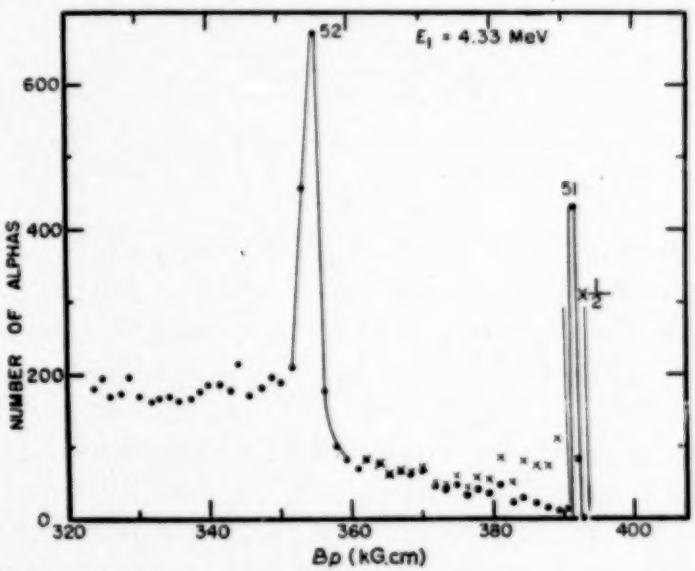

Fig. 5. Alpha particle spectrum in fig. 3 replotted to show the shape of the alpha particle continuum more clearly. A portion of the spectrum has been divided by the penetrability for decay of the B^9 nucleus by S wave proton emission and is plotted as crosses.

data were utilized. The alpha particles in each 3 mm × 10 mm strip on the photographic plate were plotted *versus* the magnetic rigidity. The resulting plots are shown in figs. 4 and 5. As before, the alpha particle groups, (51) and (52), correspond to the ground state and 2.33 MeV state in B^9 respectively. It is

evident from these figures that there exists a comparatively broad group of alpha particles centered at a $B\rho$ of about 346 kG × cm. This broad group corresponds to an excitation of approximately 2.79 MeV in B^9. The region of excitation in B^9 covered by the above spectra is about 0 to 5 MeV. It is of considerable interest to note that none of the above spectra show evidence for a broad state in B^9 in the region of 1.4 MeV excitation. Such a state might be inferred to exist from the data of ref. [11]).

In order to study the shape of the alpha particle continuum at higher B^9 excitations, a spectrum was taken at 4.88 MeV bombarding energy which covered the region of excitation in B^9 from 4.8 to 7.8 MeV. Fig. 6 shows the resulting data. This spectrum exhibited no narrow groups of alpha particles;

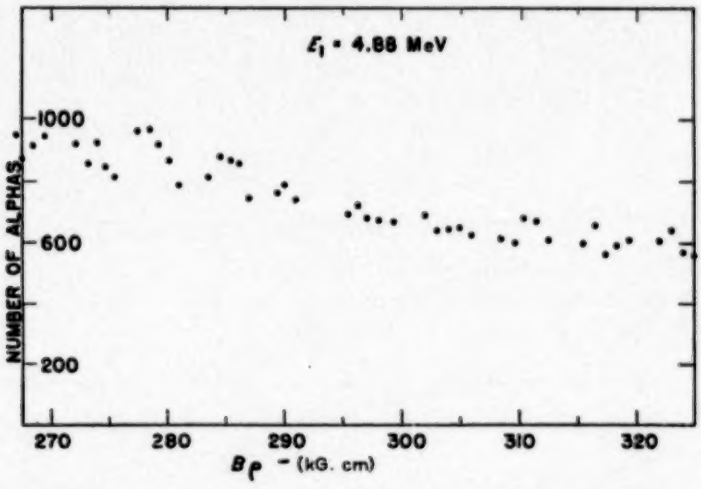

Fig. 6. Alpha particles from a B^{10} target bombarded with He^{3+} ions. The spectrum represents excitation of B^9 in the energy region 4.8 to 7.8 MeV.

however, a narrow group with less than one-fourth the intensity of the group corresponding to the 2.33 MeV state in B^9 would not have been discerned.

In addition to obtaining the energies of low lying states in B^9, the C.M. width of the 2.33 MeV state was determined. Using a target of natural boron, (81.2 % B^{11} and 18.8 % B^{10}), a single photographic plate was exposed to include the region of excitation of the 2.33 MeV state in B^9. An alpha particle group corresponding to the B^{10} ground state, from the $B^{11}(He^3, \alpha)B^{10}$ reaction, also appeared on this plate as is shown in fig. 7. The width at half-height of this latter group was used as a measure of the energy spread due to the spectrometer, target thickness, beam spread, and any other external factors that may exist. Assuming Gaussian distributions for the total width of the group corresponding to the 2.33 MeV state and the width due to the above mentioned external factors, the C.M. width of the 2.33 MeV state in B^9 was computed to be 0.083 MeV.

The bombarding energies for the spectra of figs. 2 and 3 were calculated from the energies of the deuteron group, (54), in these figures. This group corresponds

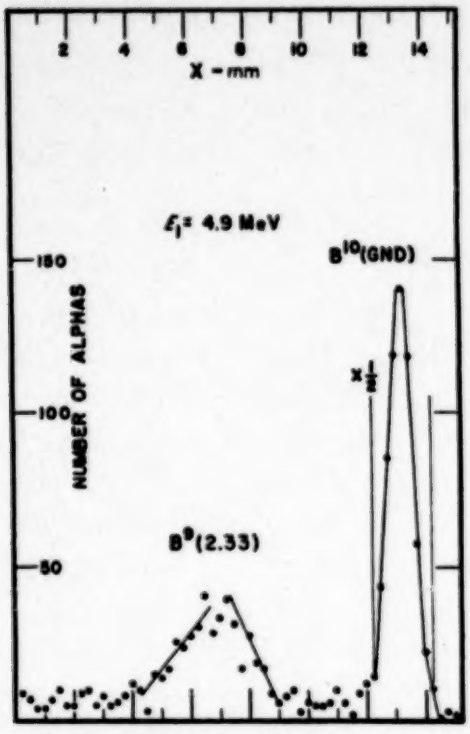

Fig. 7. Alpha particle data from a single photographic plate showing the B^9(2.33 MeV) state and the B^{10} ground state for determination of the width of the B^9(2.33 MeV) state. The target was natural boron. The exposure was approximately 1500 μC of He^{3+} ions incident on the target.

TABLE 1

Reaction Q values, excitation energies, and centre-of-mass widths for the reactions listed at the bombarding energies E_1 given

Reaction	E_1 (MeV)	Q (MeV)	Mean excitation (MeV)	C. M. Width (keV)
$Be^9(p, p')Be^9$	4.972	−1.674	1.674±0.005 [a])	175±25
	4.972	−1.70	1.70 ±0.015 [b])	
	4.951	−2.430	2.430±0.005	≤3
	5.0	−3.04	3.04 ±0.050 [b])	250±50
$B^{10}(He^3, \alpha)B^9$	3.958	12.135		
	3.959	12.131		
	4.330	12.122		
	4.732	12.134		
	4.882	12.129	0	<37
$B^{10}(He^3, \alpha)B^9$	3.958	9.805		
	3.959	9.800		
	4.330	9.791		
	4.732	9.808	2.330±0.002 [a])	83± 9
	4.401	9.797	2.39 ±0.010 [b])	
$B^{10}(He^3, \alpha)B^9$	3.959	9.34	2.79 [b])	500 to 900

[a]) Calculated for the high momentum edge of the group.
[b]) Corrected to the centre of the group.

to the ground state of C^{11} resulting from the $B^{10}(He^3, d)C^{11}$ reaction. A second deuteron group, (56), was also observed in the spectra of these two figures and was determined to correspond to a state at 2.005 MeV in C^{11}. The present results are summarized in table 1.

4. Discussion

In examining all the data concerning the low lying levels of the mirror nuclei Be^9 and B^9, four distinctive and somewhat disturbing features are observed: (A) the "cusp" in the Be^9 spectra at about 1.7 MeV excitation and the lack of similar anomaly in the B^9 spectra; (B) the relative widths of the mirror states, Be^9(2.43 MeV) and B^9(2.33 MeV) and (C) Be^9(3.1 MeV) and B^9(2.79 MeV); (D) the broad rise in the counter-ratio for the $Be^9(p, n)$ reaction [11]). The proposed explanation of these four unusual features will be discussed below.

It was found that these features may be explained by considering the mass nine nuclei in terms of a simple model. This model, which seems to be necessary to give agreement with the experimental facts, is that of a weakly interacting nucleon moving about a Be^8 core. It is necessary to consider the core as either $Be^8(0^+)$ or $Be^8(2^+)$ corresponding, respectively, to the ground state or first excited state of Be^8. The model was used primarily in predicting the decay properties of the low lying Be^9 and B^9 levels, but allows a somewhat more complete understanding of other properties of the nuclei.

Since approximately the same spectral shape has been observed for $Be^9(p, p')Be^9$, $B^{11}(d, \alpha)Be^9$, and $Li^7(He^3, p)Be^9$, it will be assumed that the spectral shape is independent of the mode of excitation of Be^9. Similarly the $B^{10}(He^3, \alpha)B^9$ reaction will be assumed to give the spectral shape of B^9. This amounts to assuming that the matrix elements that govern the emission of the observed particles are independent of the type of particle emitted and the energy of the emission and that the spectral shape is determined by the properties of the mass nine system alone. Although these remarks are not rigorously proved none of the reported experiments are in disagreement with these assumptions.

According to the cluster model [13]) the sharp, or semi-sharp, states of any nuclear system are primarily of the form of two-body cluster interactions. Furthermore, any state tends to have a wave function whose most important two-body amplitudes are of the type whose free two-body parents lie nearby in energy. In the case of the low energy mass nine nuclei the only nearby free parents are (a) nucleon $+Be^8(0^+)$, (b) nucleon $+Be^8(2^+)$, and (c) alpha particle + mass five $(\frac{3}{2}^-)$. It is thus expected that the low energy states of Be^9—B^9 will likely be rather pure states of one or the other of these two-body configurations. These two-body parents of the mass nine nuclei are shown in the energy level diagrams of fig. 8. In what follows the α+mass five configurations will be neglected on two grounds: (1) they do not seem to be necessary to

describe the data, and (2) the configurations α+mass 5 and Be^8+nucleon are likely to be very similar in the nature of their wave functions. Henley and Kunz [14]) have made model-dependent calculations including the α+mass 5 decay channel. Because of the nature of their assumptions they were forced to the conclusion that only the α+mass 5 channel is important. In the discussion to be presented below no such restrictions will be employed, the maximum allowed widths will be deduced, and the mirror states of the nuclei compared.

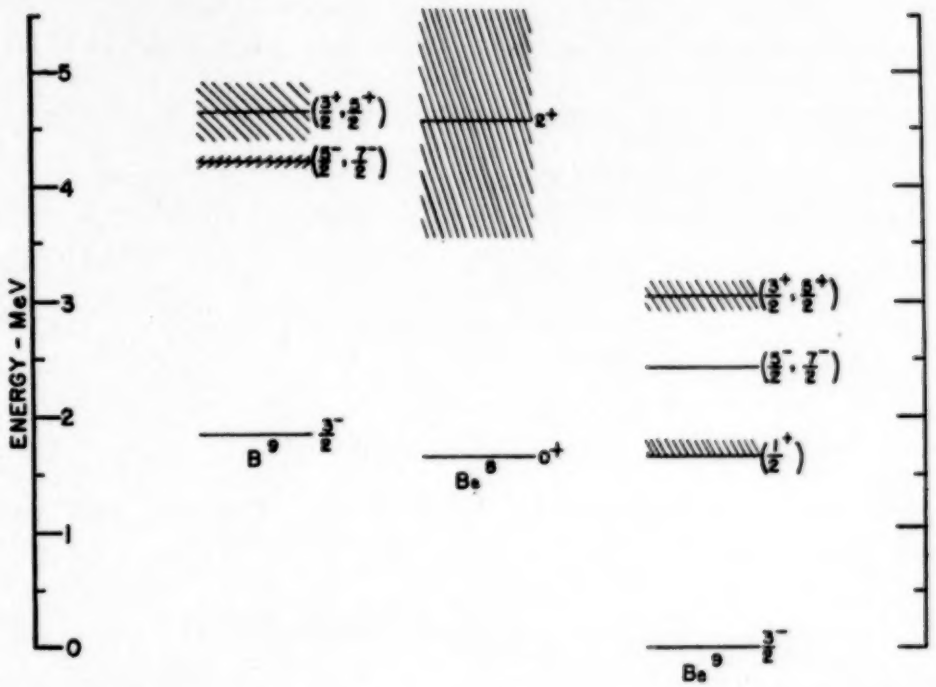

Fig. 8. Energy level diagram of the mass nine nuclei. The available low lying two-body parents involving states in Be^8 are indicated. The graphs are plotted so that a nucleon mass-energy has been added to states in the Be^8 system to obtain the adjacent energies in the mass nine nuclei.

4.1. THE "CUSP" EFFECTS IN Be^9—B^9

In terms of this model the 1.7 MeV effect in Be^9 may be described as an S-wave neutron plus a $Be^8(0^+)$ core. Applying the Wigner sum rule [15]) with a channel radius of 4.35×10^{-13} cm, the experimental C.M. width of the 1.7 MeV effect indicates the neutron decay of Be^{9*} (1.7 MeV) proceeds dominately by S-wave emission. The apparent lack of a similar effect in the alpha particle spectra leading to B^9 poses a difficult problem, however. The spectra of figs. 4 and 5 suggest that the same effect may exist in the region of excitation between the threshold for proton emission by B^9 and the ground state of B^9, (i.e. below what is termed the ground state). Such an effect might not have been observed due to the low yield or to concealment by the B^9 ground state group. This suggestion is strengthened by considering the curve that is the result of removing the S-wave proton penetrability from the present data on the $B^{10}(He^3,$

α)B^9 reaction. This has been done for the data of fig. 5 and is represented by the crosses in that figure. The corrected data reveal a curve rising towards low excitation energies in B^9 and indicate that the "cusp" effect of Be^9 may occur for B^9 but at an energy *below* the "ground state". This type of threshold behavior may be predicted for spectra that yield a system of two weakly interacting particles [16]), and while similar to the interpretation given by Rasmussen *et al.* is actually of a different physical motivation.

The cusp effects that seem to occur in both Be^9 and B^9 may be described by employing the concept of the generalized density of states [13,16]). This model treats reactions such as the decay of an excited nucleus D*,

$$D^* \rightarrow b+\alpha+\alpha+\text{nucleon}, \tag{1}$$

where b is the particle observed in a spectrogram, and $\alpha+\alpha+$nucleon is the final, continuum state of excited states of Be^9 and B^9. The cluster model [13]) supposes that the reactions occur as a sequence of two-body steps:

$$D^* \rightarrow b+\text{mass } 9, \tag{2}$$

$$\text{mass } 9 \rightarrow \text{nucleon}+Be^8, \tag{3}$$

$$Be^8 \rightarrow \alpha+\alpha. \tag{4}$$

Each two-body step in the decay can be shown to proceed with an intensity that is proportional to

$$\rho_{l,a}^{(b)}(E) = \frac{1}{\pi}\frac{d}{dE}(\delta_l(E)+\phi_l(E, r = a)), \tag{5}$$

where $\delta_l(E)$ is the scattering phase shift of $l\hbar$ orbital waves, $\phi_l(E, r = a) = = \tan^{-1} F_l/G_l|_{r=a}$ is the hard sphere phase shift corresponding to the radius of interaction a, and E is the centre-of-mass energy of the two-body system that is left by the emission of the particle.

Since the spectrograms corresponding to reaction (2) are so similar, and since the 0^+ ground state of Be^8 is so narrow [17]), it will be supposed that only reaction (3) determines the behavior of the mass nine spectra near to the nucleon $+Be^8(0^+)$ threshold. Thus it will be assumed that the spectrograms, near threshold, are of shapes determined entirely by aspects of the coupling of a nucleon to the 0^+ ground state of Be^8. Eq. (5) should describe the spectra. If it is further assumed that (a) the nucleon and Be^8 are in an S state of relative motion and (b) that there is a negligible interaction between the two bodies, then it follows that

$$\rho_{0,a}^{(b)}(E) = \frac{1}{\pi}\frac{d\phi(E, a)}{dE}, \tag{6}$$

since $\delta_0(E) \approx 0$.

For Be^9 eq. (6) gives explicitly

$$\rho_{0,a}^{(\text{neutron})}(E) = (a/\pi)(\mu/2\hbar)^{\frac{1}{2}} E^{-\frac{1}{2}}, \tag{7}$$

which may be employed to account for the cusp like behavior of the Be^9 spectrum near the $n+Be^8(0^+)$ threshold. When the effects of the measured target thickness of about 30 keV are included the resulting fit to the experimental data is shown in fig. 9. The excellence of the fit would imply that this anomalous feature of Be^9 *is not a "state" in the usual sense* of representing an energy situation of Be^9 that is unusually stable due to attractive forces. Rather

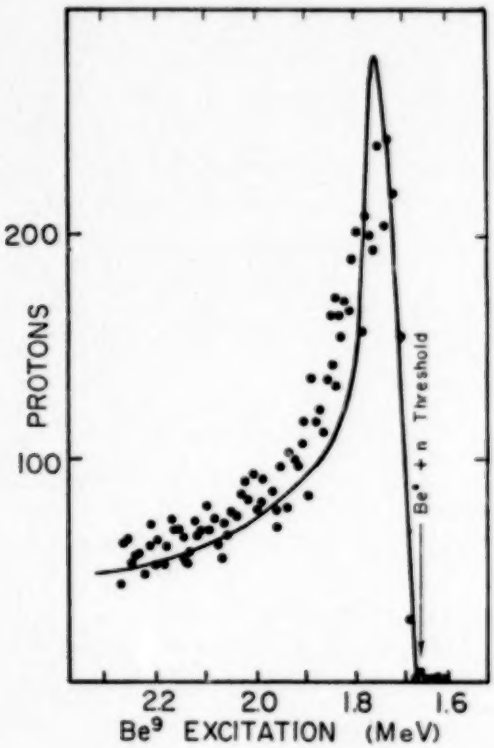

Fig. 9. The spectrum of Be^9 near the Be^8+n threshold. The experimental points are from fig. 1. The curve was calculated from eq. (7) and is discussed in the text. The peak is not a state in the usual sense, but is an aspect of spatial localization produced by a sequence of two-body reactions.

the agreement implies that the Be^8 and neutron are produced in a spatically localized arrangement by the emission of the inelastically scattered proton, that the dispersion of energy is an aspect of the spatial localization, and that the peak near threshold is due to the slowness with which the non-interacting neutron and Be^8 decay when there is little energy available for decay.

Similarly eq. (6) may be employed to seek a fit to the spectrum of B^9. The results are shown in fig. 10. The statistical inaccuracies of the data prohibit a careful comparison of the data and calculations. However, the fact that the variations of the spectrogram are reasonably well reproduced by eq. (6) tends to confirm the analysis of Be^9 given above and serves to show that there is no

"state", in the usual sense, in either Be^9 or B^9 corresponding to the 1.7 MeV anomaly in Be^9.

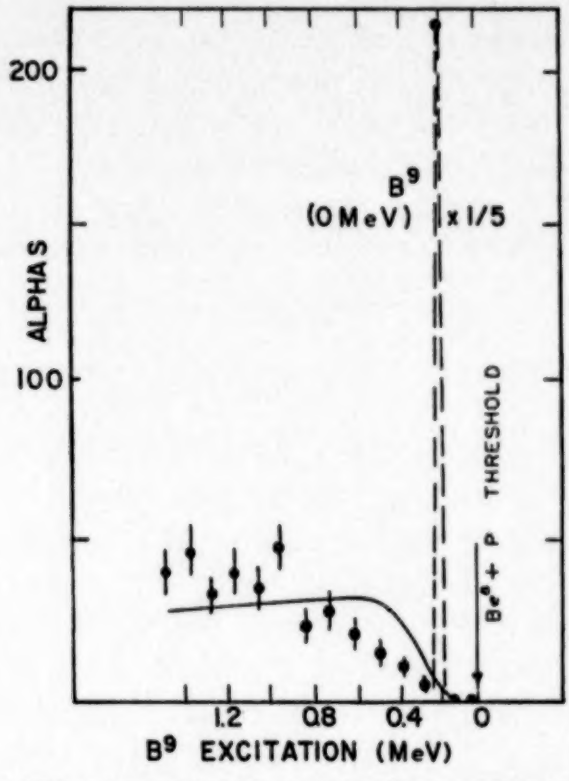

Fig. 10. The spectrum of B^9 at low excitation energies. The experimental points are from fig. 4. The curve was calculated from eq. (6). The Coulomb interaction of p+Be^8 has suppressed the peak that would otherwise have occurred at the Be^8+p threshold.

4.2. THE 2.43—2.33 MeV STATES IN Be^9—B^9

The particular configuration which appears to give the best agreement with the experimental data for the 2.43—2.33 MeV mirror pair is that of a P-wave nucleon moving about a $Be^{8*}(2^+)$ core. This configuration was first determined by comparison of R_c and R_e, where R_c is the calculated ratio of the C.M. width of the B^9(2.33 MeV) state to the width of the Be^9(2.43 MeV) state, and R_e is the experimental ratio of widths. R_c was calculated by assuming that the probability of decay of a given excited state of a mass 9 system depends on the product of the probability of formation of the Be^8 product state and the penetrability of the emitted nucleon, integrated over the possible energies of the emitted nucleon. An approximate estimate of the probability of formation of Be^8 at any energy E was taken to be the number of alpha particles observed in the B^{10}(d, α)Be^8 reaction with energy corresponding to the residual Be^8 nucleus being left at an excitation energy E. The B^{10}(d, α)Be^8 data were taken from a report by Holland [18]). The ratio of C.M. widths of the two mirror mass nine states for particular modes of decay, (i.e. different values of l, the angular momentum of the emitted nucleon, or different residual Be^8 states), were then obtained from the decay probabilities. It should be noted that this technique

would be expected to predict too small a ratio of proton to neutron widths for the mass 9 system decaying to $Be^{8*}(2^+)$. The results of these calculations are summarized in table 2 for the 2.43—2.33 MeV mirror pair. These results are in accord with the experimentally assigned negative parity [19, 20]), and the favored spin of $\frac{5}{2}^-$ for this pair of states.

TABLE 2

Ratio of widths R of proton decay of B^9 to neutron decay of Be^9 for the 2.43—2.33 MeV mirror states. R_c gives the calculated width for decay to the 0^+ or 2^+ states of Be^8 and for different values of l, the angular momentum of the emitted nucleon (see text). R_e is the experimental ratio.

	Decay to $Be^8(0^+)$		Decay to $Be^{8*}(2^+)$
l	1	3	1
R_c	0.9	11	$\geqq 20$
R_e			$\geqq 30$

These results may be considered in more detail by employing the generalized density of states method to calculate the partial energy width for the decay of a state in a particular channel λ where the residual nucleus is in the continuum. Thus the decay of either of the 2.43—2.33 MeV mirror pair of states has a partial width

$$\Gamma_\lambda = 2\gamma_\lambda^2 \int_0^{E_{max}} \theta_\lambda^2(E) P_\lambda(E) dE, \tag{8}$$

where $\gamma^2_{W.L.,\lambda}$ is the Wigner limit reduced width $3\hbar^2/2\mu_\lambda a_\lambda^2$, $P_\lambda(E)$ is the penetrability, ka/A_λ^2, of the emitted nucleon and the energy dependent fractional parentage coefficient $\theta_\lambda^2(E)$ is given by

$$\theta_\lambda^2(E) = \vartheta_\lambda^2 \rho_\lambda(E). \tag{9}$$

ϑ_λ^2 is the energy independent fractional parentage coefficient and $\rho_\lambda(E)$ is the generalized density of states function. In this case $\rho_\lambda(E)$ refers to the final state of the $\alpha+\alpha$ system comprising Be^8. The function $\rho_\lambda(E)$ was calculated for $a = 8\times 10^{-13}$ cm and by using the experimental $\alpha+\alpha$ scattering phase shifts [17]). The coulomb functions of Bloch *et al.* [21]) were employed for obtaining the proton penetrabilities.

Figs. 11 and 12 show $\rho_2(E)$ for D states in Be^8 plotted along with S, P and D wave nucleon penetrabilities $P_l(E)$. Similar calculations have been made for the configurations nucleon+$Be^8(0^+)$. All of the results for the Be^9—B^9 mirror states at 2.43—2.33 MeV are given in table 3.

Examination of table 3 reveals that there is no possible explanation of the width of the 2.43—2.33 MeV states in Be^9—B^9 by decay processes to $Be^8(0^+)$. However, it is noted that either S or P wave emission to $Be^8(2^+)$ will explain the observed ratio of widths and will also satisfy the Wigner limit. Since there is

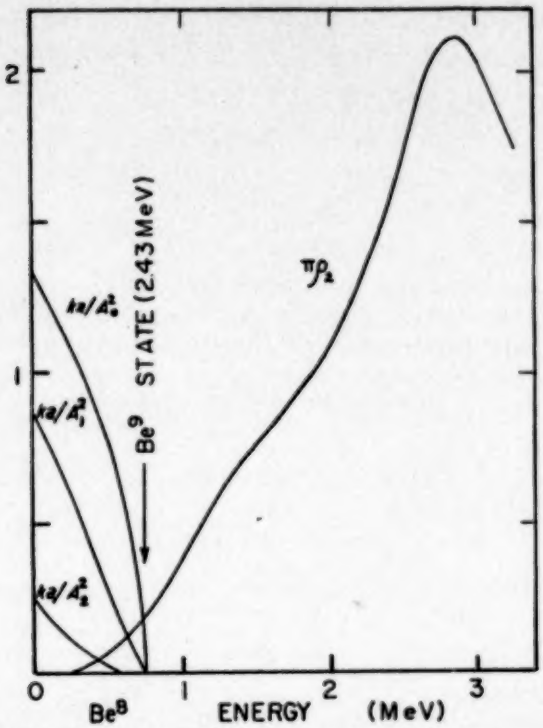

Fig. 11. Decay of Be^9(2.43 MeV) by neutron emission to the continuum states of $Be^8(2^+)$. The penetrabilities $P_l(E)$ of the neutrons and the generalized density of states function $\rho_2(E)$ are shown as functions of the excitation in Be^9. The small amount of density function available to the decay produces very small partial widths for neutron emission.

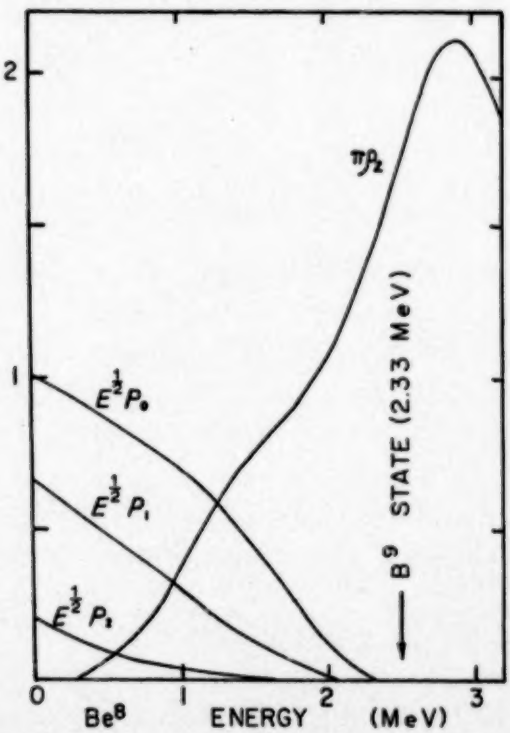

Fig. 12. Decay of B^9(2.33 MeV) by proton emission to the continuum states of $Be^8(2^+)$. The penetrabilities $P_l(E)$ of the protons and the generalized density of states function $\rho_2(E)$ are shown as functions of the excitation in B^9. The considerable amount of density function available to the decay produces rather large reduced widths for proton emission.

TABLE 3

Level parameters of the 2.43—2.33 MeV states of Be^9—B^9. The calculated Wigner limit width Γ_{max} for the two nuclei are shown, along with the fractional parentage coefficient $\theta^2 = \Gamma_{exp}/\Gamma_{max}$. Also given is $R_c = \Gamma_{max}(B^9)/\Gamma_{max}(Be^9)$. The experimental value of R is $R_e \geq 30$. The experimental values of the widths are $\Gamma_{exp}(B^9) = 83$ keV, $\Gamma_{exp}(Be^9) \leq 3$ keV.

		Pure $Be^8(0^+)$ parentage					Pure $Be^8(2^+)$ parentage				
l	Nucleus	Γ_{max} (MeV)	R_c	R_c allowed	θ_l^2	θ_l^2 allowed	Γ_{max} (MeV)	R_c	R_c allowed	θ_l^2	θ_l^2 allowed
0	Be^9 B^9	3.8 3.4	1.1	no	9×10^{-4} 4×10^{-2}	yes yes	0.015 0.41	27	yes	$\leqq 0.2$ 0.2	yes
1	Be^9 B^9	2.6 2.1	1.2	no	10^{-3} 4×10^{-2}	yes yes	0.004 0.13	32	yes	$\leqq 0.75$ 0.7	yes
2	Be^9 B^9	0.9 0.9	1.0	no	3×10^{-3} 9×10^{-2}	yes yes	3×10^{-4} 0.01	40	yes	$\leqq 10$ 8	no
3	Be^9 B^9	0.13 0.007	18.5	yes	3×10^{-2} 12	yes no					

reason to believe that the states are of negative parity, the P wave emission case will be chosen. Marion [22]) has observed that no more than about 10 % of the neutron decays of the 2.43 MeV Be^9 state populate the ground state of Be^8. If it is assumed that these states are $\frac{5}{2}^-$ in character, it follows that they are almost purely of the form $Be^8(2^+)+P$ wave nucleon, and have a fractional parentage coefficient of less than 10^{-3} for the configuration $Be^8(0^+)+F$ wave nucleon.

4.3. THE 3.04—2.79 MeV STATES IN Be^9—B^9

Similar calculations were carried out for the 3.04—2.79 MeV mirror pair employing experimental data, and the results are summarized in table 4. Due to the uncertainty in the C.M. width of the 2.79 MeV B^9 state it appears that either of two configurations may be suitable: an S wave nucleon moving about a $Be^{8*}(2^+)$ core or a D wave nucleon moving about a $Be^8(0^+)$ core.

TABLE 4

Ratio of widths R of proton decay of B^9 to neutron decay of Be^9 for the 2.79—3.04 MeV mirror states (see table 2)

	Decay to $Be^8(0^+)$			Decay to $Be^{8*}(2^+)$	
l	0	1	2	0	1
R_c	0.8	0.9	1.7	2.4	3.7
R_e	2.5 ± 0.5				

4.3. THE SLOW NEUTRON ANOMALY IN B^9

The broad rise in the neutron counter-ratio curve of ref. [11]) may now be explained by the decay of the 2.43 MeV and/or the 3.04 MeV states following their formation by proton inelastic scattering. The broad nature of the anomaly is undoubtably due to the centre-of-mass motion of the decaying nucleus and the broad nature of the $Be^{8*}(2^+)$ residual state.

Thus the unusual features of the low energy spectra of the mass nine nuclei can be interpreted by considering the system as primarily composed of the configurations $Be^8(0^+)$+nucleon and $Be^8(2^+)$+nucleon. The "cusp" effects of these nuclei are viewed as an aspect of spatial localization of S wave nucleons due to the two-body nature of nuclear states. The 2.43—2.33 MeV mirror pair clearly show a two-body interaction of a nucleon with $Be^8(2^+)$, of the type predicted by the cluster model.

The authors wish to thank Dr. J. B. Marion for stimulating discussions.

References

1) E. Guth and C. J. Mullin, Phys. Rev. **76** (1949) 234
2) Van Patter, Sperduto, Huang, Strait and Buechner, Phys. Rev. **81** (1951) 233
3) Moak, Good and Kunz, Phys. Rev. **96** (1954) 1363
4) L. L. Lee and D. R. Inglis, Phys. Rev. **99** (1955) 96
5) Gossett, Phillips, Schiffer and Windham, Phys. Rev. **100** (1955) 203
6) R. C. Mobley and R. A. Laubenstein, Phys. Rev. **80** (1950) 309
7) Rasmussen, Miller, Sampson and Gupta, Phys. Rev. **104** (1956) 456
8) Bockelman, Leveque and Buechner, Phys. Rev. **104** (1956) 456
9) P. H. Stelson and W. M. Preston, Phys. Rev. **83** (1951) 469L
10) Almqvist, Allen and Bigham, Phys. Rev. **99** (1955) 631A
11) Marion, Bonner and Cook, Phys. Rev. **100** (1955) 91
12) Gossett, Phillips and Eisinger, Phys. Rev. **98** (1955) 724
13) T. A. Tombrello and G. C. Phillips, Nuclear Physics **20** (1960) 648
14) E. M. Henley and P. D. Kunz, Phys. Rev. **118** (1960) 248
15) T. Teichmann and E. P. Wigner, Phys. Rev. **87** (1952) 123
16) G. C. Phillips, T. A. Griffy and L. C. Biedenharn, Nuclear Physics **21** (1960) 327
17) N. P. Heydenburg and G. M. Temmer, Phys. Rev. **104** (1956) 123;
Russell, Phillips and Reich, Phys. Rev. **104** (1956) 135;
Jones, Phillips and Miller, Phys. Rev. **117** (1960) 525
18) Holland, Inglis and Malm, Phys. Rev. **99** (1955) 92
19) F. L. Ribe and J. D. Seagrave, Phys. Rev. **94** (1954) 934
20) J. B. Reynolds and K. G. Standing, Phys. Rev. **101** (1956) 158
21) Bloch, Hull, Broyles, Bouricius, Freeman and Breit, Revs. Mod. Phys. **23** (1951) 147
22) J. B. Marion, private communication;
see also Bodansky, Eccles and Halpern, Phys. Rev. **108** (1957) 1019

1.D.3

Nuclear Physics **21** (1960) 327—339; © *North-Holland Publishing Co., Amsterdam*

Not to be reproduced by photoprint or microfilm without written permission from the publisher

THE SIGNIFICANCE OF THE GENERALIZED DENSITY OF STATES FUNCTION FOR NUCLEAR SPECTRA

G. C. PHILLIPS, T. A. GRIFFY and L. C. BIEDENHARN

The Rice University, Houston, Texas †

Received 8 August 1960

Abstract: The cluster model of the nucleus suggests that three- (or more-)body decay may be treated as a time sequence of two-body interactions. The cross section for particle emission into a spectrum of energies may be calculated if it assumed that the reaction $a+A \rightarrow D^* \rightarrow$ $\rightarrow b+C+c$ occurs as a sequence of two-body decays: $D^* \rightarrow B^*+b$; $B^* \rightarrow c+C$. If B^* is produced in a localized state of radius a and decays only via the single two-body channel $c+C$ whose phase shift is known, then the cross section for emission of particles b is largely determined by a density of states factor $\rho = (1/\pi)\mathrm{d}/\mathrm{d}E_B(\delta_l(E_B)+\varphi_l(a, E_B))$. This result is discussed and compared both to experiments and to other treatments of the same problem.

1. Introduction

In a typical nuclear spectroscopic experiment an excited state of a nucleus D of energy E_D is observed to decay by emission of particles b with a total release of energy Q_1:

$$a+A \rightarrow D^* \rightarrow b+B+Q_1. \tag{1}$$

In general, when the yield of particles b *versus* the energy (or momentum) is observed, a complex spectrogram $N_{D^*}(E_b)$ *versus* E_b results. Here $N_{D^*}(E_b)$ is the number of particles of type b whose energy is between E_b and $E_b+\mathrm{d}E_b$. The distribution extends from zero to an energy determined by Q_1 and the kinetics of the process. If the decay of D^* is as indicated in (1), i.e. the decay involves the separation of the two body system b+B, then there is a linear relationship between the energy E_b and the energy of excitation E_B of the system B. Thus the experimental data may be used to derive a distribution function $N_{D^*}(E_B)$ *versus* E_B. In cases where $N_{D^*}(E_B)$ consists of very narrow peaks at energies E_B, and is zero elsewhere, it is customary to interpret such a diagram as giving the sharp energy eigenvalues of the system B. In cases where the maxima of $N_{D^*}(E_B)$ exhibit measurable energy widths Γ_n, it is customary to associate these observable widths with the non-zero decay half life τ_n of the nuclear state of system B by

$$\tau_n \approx \hbar/2\Gamma_n. \tag{2}$$

In such a case the width of the state is due to its ability to decay, and the assump-

† Work supported in part by the U. S. Atomic Energy Commission.

tion of the two-body nature of process (1) must be questioned; when

$$B \rightarrow c+C+Q_2, \tag{3}$$

the proper description of the transformations may be a three- (or more-)body process such as

$$D^* \rightarrow b+c+C+(Q_1+Q_2). \tag{4}$$

For such a process as (4) the measurement of N_{D^*} *versus* E_b may not consistute enough information to determine the dynamics of the reaction; the beta decay process is an example of a type (4) transformation. Nevertheless, there is considerable reason to believe that (1) is an accurate model for many nuclear transformation processes involving heavy particle emission even when the system B quickly decays. The success of the two-body cluster model [1]) of the nucleus in describing many aspects of nuclear dynamics would imply that the sequence of reactions (1) and (3) is a proper description of the processes and that (4) is of little importance. Other authors have considered this model [2]); the purpose of the present paper is to investigate further the consequences of such a model.

Thus it will be supposed that a three-body decay may be considered as a well separated time sequence of two-body decays. This model of process (1) may certainly be employed in cases where the emission only excites sharp states of B. It is convenient to treat this latter decay process by perturbation theory which gives the result that the cross section is [3])

$$\sigma_{D^*}(\theta, \phi, k_b) = (\mu_a \mu_b k_a / 4\pi^2 \hbar^4 k_b) |\langle B+b, E_b | H' | A+a, E_a \rangle|^2, \tag{5}$$

where $|a+A, E_a\rangle$ represents the initial state vector, $|B+b, E_b\rangle$ the final state vector, and H' is the interaction Hamiltonian for the process (1). In this expression k_a and k_b are the initial and final wave numbers for the reaction (1). $\sigma_{D^*}(\theta, \phi, k_b)$ then gives the observed distribution $N_{D^*}(E_B)$.

Frequently, when different reactions are studied that produce the nucleus B,

$$F^* \rightarrow f+B+Q_3, \tag{6}$$

the distribution function $N_{F^*}(E_B)$ *versus* E_B derived from the data may be very similar to $N_{D^*}(E_B)$ *versus* E_B. Since the square of the matrix elements occurring in σ_{D^*} and σ_{F^*} are not obviously the same, the experimental observation may seem surprising at first sight. However, it is clear, in the case where only sharp states of B occur at a set of energies E_n, that the result is a simple one since the very stable system B cannot exist at any other energy than in its sharp states. This fact determines the sharp nature of $N_{D^*}(E_B)$ and $N_{F^*}(E_B)$ and accounts for their similarity. This information may be included by rewriting (5) as

$$\sigma_{D^*}(E_B) = (\mu_a \mu_b k_a / 4\pi^2 \hbar^4 k_b) |\langle B+b, E_B | H' | A+a, E_a \rangle|^2 \rho(E_B), \tag{7}$$

where $\rho(E_B)$ may be called a *generalized density of states* function for B and for the case of B having only a set of sharp states at energies E_n,

$$\rho(E_B) = \sum_n \delta(E - E_n). \tag{8}$$

E_b may now be considered a *continuous* variable with the vectors $|B+b, E_b\rangle$ defined for all E_b. It is noted that ρ contains a great deal of the information about the shape of the spectrum in that it contains *all* of the information about the energy positions of the sharp lines in the spectrum. It should be emphasized that the nuclei b and B in the above calculations are usually treated as *particles* and *localized* in the sense that they interact only inside a small volume where the nuclear forces, corresponding to H', are strong.

To treat the case when the state B is unstable is more complicated. In particular, it is of interest to consider if a knowledge, from experiment, of the details of the decay of B, as in (3), is sufficient to determine some of the features of the spectra $N_{D^*}(E_B)$ and $N_{F^*}(E_B)$. It is reasonable that such a construction is possible. For example, resonances at a set of energies E_n shown by the inverse of (3) in elastic scattering,

$$c+C \rightarrow B^* \rightarrow c+C, \tag{9}$$

are evidence for semi-stable states of B. It is expected that $N_{D^*}(E_B)$ by process (1) may reveal these same semi-stable states of B as regions of enhanced transition in a continuous spectrum. If the phase-shifts or the scattering matrix for process (9) are experimentally determined then the general structure of $N_{D^*}(E_B)$ may be calculated in some cases.

If the sequence of two two-body emissions, given in (1) and (3), are the important mechanism for the processes then the system B may be considered to be produced in a *localized decaying state* due to the short range nature of the forces. The spectrum of particles b is just a manifestation of the energies of excitation of B that are necessary to produce the localization of B. If the transition probability rate $W(E_b)$, of producing particle b with energy E_b is multiplied by the life-time $T(E_b)$ for decay of the localized system B with energy $(E_{total} - E_b)$, then $W(E_b)T(E_b)$ is just the desired transition probability. This argument shows there are *two* ways in which structure may appear in the spectra of particles b: (1) the structure of W or (2) the structure of $T(E_b)$. This reasoning also shows that $T(E_b)$ and the density of states function $\rho(E_B)$ are very closely related. The comparison of these two quantities is another purpose of this paper.

Watson [4]) has made different but similar arguments and concluded that the desired spectral function should be similar to the cross section for producing B by reaction (9). It will be shown that Watson's argument neglects certain essential properties of ρ and T (in particular the effect of long range forces and spatial localization).

The density of states function employed in (7) and (8) seems to be the most reasonable definition for treating a set of discrete final states where each final (bound) wave function is normalized. However, for treating the case of continuum final wave functions two methods seem possible: (1) the method employed for discrete bound states may be extended to include continuum states by treating these latter states as discrete; (2) the energy variation of the matrix element in (5) associated with the continuum nature of the final state may be extracted by renormalizing the final state wave function. This amounts to calculating the probability that the final continuum state has c+C within the volume of interaction. Both of these methods will be discussed below.

2. The Generalized Density of States Function in the Continuum

2.1. LOCALIZED PRODUCTION OF THE FINAL STATE

In the usual employment of (5) or (7) and (8) the final (bound) state of B is normalized but *not necessarily inside the volume of interaction defined by the short range interaction* H'. The set of discrete states, at energy E_n', have a *number of states function* $n(E) = \int_0^E \rho(E')\mathrm{d}E'$, where $\rho(E)$ is given by (8). $n(E)$ may be associated with the number of loops of the wave function representing B. This argument may be extended to continuum states of B. However, it should be noted that the form of the wave function of B external to a, the range of H', is immaterial. Thus the wave function of B may be chosen so as to converge rapidly to zero for $r \geqq a$ and the number of loops of the function may be associated only with the internal number of loops.

In this paper the physical assumption is made that the processes (1) and (3) proceed in a step wise, two-body fashion. Thus it is supposed that the decay of D* first occurs to *all* states of system B that are energetically allowed by the emission of the observed particles b. Later the excited, localized system B may decay to c+C. The separation of the three-body decay into a sequence of two-body interactions allows the calculation of some features of the spectrum of the particles. The fact that the nucleus B may be unstable is then of no unusual significance; it is only required that the two clusters of nucleons c and C that comprise nucleus B be localized for a time slightly longer than is required for particle b to escape. Thus it is necessary to calculate the number of ways that B may be left somewhat localized in space at any particular energy of excitation.

It was noted by the definition of $\rho(E_B)$ given in (8) that the perturbation theory for the reaction cross section may be extended to include the case of a *set* of discrete states. Similarly, the continuum states of B will be trated as a set of discrete states by the technique of supposing that the wave function of B is confined inside a small sphere of radius a. This sphere will be taken to correspond to the localized nature of system B when it is produced by the short range interactions of the composite system D*. The localized size of B in this

process does *not* necessarily correspond to the size of a system B derived by scattering c and C as in (9) since the volume in which B is produced in (1) must reflect the effects of the forces of the other nucleons that comprise system b.

To calculate the energy density of the discrete states of the localized system B three steps will be employed [5]): (a) $\rho_R(E_B)$, the number of discrete states of B in unit energy interval, will be calculated when B is supposed to consist of the purely two-body system c+C confined inside a very large sphere of radius R. (b) $\rho_{a,R}(E_B)$, the number of discrete states per unit energy interval of B, will be calculated when B is supposed to consist purely of the two-body system c+C *excluded* from the small sphere of radius a and confined inside the large sphere of radius R. (c) The *generalized density of states* of B, $\rho_a(E_B)$, will be defined as

$$\rho_a E_B = \lim_{R\to\infty} [\rho_R(E_B) - \rho_{a,R}(E_B)].$$

$\rho_a(E_B)$ is always a function of two aspects of the transformation: firstly, the *interaction* of c and C to produce B will enter into $\rho_a(E_B)$ through the term $\rho_R(E_B)$ and secondly, the *localization* of B will influence the results through the term $\rho_{R,a}(E_B)$. The evaluation of these quantities is given below.

(a) The free (unconfined) states of B have wave functions that for $r \geqq a$ are

$$\psi_{B,l}(E) = (kr)^{-1}[\cos\delta_l F_l(k,r) + \sin\delta_l G_l(k,r)], \tag{10}$$

where F_l and G_l are appropriate external partial wave solutions to the scattering process (9). Eq. (10) defines $\delta_l(k)$ to be the usual scattering phase shift.

Using box normalization it is required that each partial wave $\psi_{B,l}(r = R)$, of the total wave function representing B must vanish. Thus

$$\begin{aligned} 0 &= kR\psi_{B,l}(E,R) \\ &= [\cos\delta_{l,R} F_l(k,R) + \sin\delta_{l,R} G_l(k,R)] \approx \sin(kR + \delta_{l,R} - \tfrac{1}{2}l\pi), \end{aligned} \tag{11}$$

since

$$F_l(k,r) \approx \sin(kr - \tfrac{1}{2}l\pi), \quad G_l(k,r) \approx \cos(kr - \tfrac{1}{2}l\pi).$$

Thus

$$n\pi = kR + \delta_{l,R}(k_n) - \tfrac{1}{2}l\pi \tag{12}$$

and the sharp, allowed, energies are given by those values k_n of k that satisfy (12) for integers n. n represents the number of loops, or half-waves, of the partial wave function extending from the origin to $r = R$. Also n represents the number of (discrete) states of the system whose energy is less than or equal to the energy $E_n = \hbar^2 k_n^2/2\mu_B$.

On varying n, corresponding to a change from state n to state $n+1$,

$$\frac{\Delta n}{\Delta k_n} = \frac{1}{\pi}\left[R + \frac{\Delta\delta_{l,R}}{\Delta k_n}\right]\delta(k - k_n). \tag{13}$$

This expression gives the change of the number of loops of the wave function in

the spherical box for a change of the wave number by unity and it is equal to the number of states in that unit wave number interval corresponding to the system B existing somewhere in the box of radius R.

(b) If the two-body system c+C comprising B were confined in the box of radius R, but excluded from the small volume of radius a, then the solutions $\psi^{(ex)}_{B,l}(E, r)$ of the wave equation obey

$$kR\psi^{(ex)}_{B,l}(E, R) = 0 \tag{14}$$

and also

$$ka\psi^{(ex)}_{B,l}(E, a) = 0. \tag{15}$$

This system will have a set of discrete states of energy $E_{n'}$, and the number of such states per unit wave-number interval will be

$$\frac{\Delta n'}{\Delta k_{n'}} = \frac{1}{\pi}\left[R - \frac{\Delta\phi_{R,l}(E, a)}{\Delta k_{n'}}\right]\delta(k-k_{n'}), \tag{16}$$

where

$$\phi_{R,l}(E, a) = \tan^{-1}[F_l(k, a)/G_l(k, a)]. \tag{17}$$

(c) The number of discrete states of B that correspond to the system being entirely inside the small volume of radius a and whose wave numbers lie between k and $k+\mathrm{d}k$ may be associated with the number of loops of the wave function with $r \leqq a$, which is given by

$$\frac{\Delta N}{\Delta k} = \frac{\Delta n}{\Delta k} - \frac{\Delta n'}{\Delta k}$$

$$= \frac{1}{\pi}\left\{\frac{\Delta\delta_{l,R}}{\Delta k}\delta(k-k_n) + \frac{\Delta\phi_{l,R}(k, a)}{\Delta k}\delta(k-k_{n'}) + R[\delta(k-k_n) - \delta(k-k_{n'})]\right\}. \tag{18}$$

In the limit as $R \to \infty$ the phase shifts approach their usual values

$$\delta_{l,R}(k_n) \to \delta_l(k), \quad \phi_{l,R}(k_{n'}, a) \to \tan^{-1}[F_l(k, a)/G_l(k, a)],$$

while the last term in (18) vanishes. Also the limit of (18) defines a *generalized density of states* function, $\rho_l(k_B)$ for the system B, in the sense that

$$\rho_l(k_B) = \frac{1}{\pi}\frac{\mathrm{d}}{\mathrm{d}k_B}\left(\delta_l(k_B) + \phi_l(k_B, a)\right) \tag{19a}$$

is the number of continuum states of B lying between k_B and $k_B+\mathrm{d}k_B$. Similarly

$$\rho_l(E_B) = \frac{1}{\pi}\frac{\mathrm{d}}{\mathrm{d}E_B}\left(\delta_l(E_B) + \phi_l(E_B, a)\right) \tag{19b}$$

is the number of continuum states of B having energy between E_B and $E_B+\mathrm{d}E_B$. Since the quantity of (19a) is always positive definite it follows that

$$\left|\frac{\mathrm{d}\delta_l}{\mathrm{d}k}\right| \leqq \frac{\delta\phi_l}{\mathrm{d}k}, \tag{20}$$

which is similar to a result that has been derived by Wigner [6]) if one supposes that a must be greater than or equal to the range of forces between c and C.

Suppose that the scattering process (9) exhibits a resonance whose phase shift is well described by the single level dispersion theory [7]). Then

$$\delta_l = \beta_l - \phi_l, \tag{21}$$

where

$$\beta_l = \tan^{-1}[\tfrac{1}{2}\Gamma_\lambda/(E_\lambda + \Delta_\lambda - E)] \tag{22}$$

with

$$\tfrac{1}{2}\Gamma_\lambda = \rho\gamma_\lambda^2/(F_l^2+G_l^2) = \rho\gamma_\lambda^2/A_l^2,$$

and

$$\Delta_\lambda = -[\gamma_\lambda^2/\rho][(\rho/A_l)(\mathrm{d}A_l/\mathrm{d}\rho)+l]$$

with $\rho = ka$, and γ_λ^2 the reduced width. Thus

$$\rho(E_B) = \sin^2(\delta_l+\phi_l)/\pi\gamma_\lambda^2 P_l, \tag{23}$$

if it is assumed that Γ_λ and Δ_λ are slowly varying with E. Here P_l is the penetrability

$$P_l = \rho A_l^{-2} = \rho[F_l^2+G_l^2]^{-1}.$$

This result is the same as (41) and suggests that the single level approximation amounts to assuming a localization of the type of (38). This form of the density of states function has been applied by several authors [4, 8]).

2.2. RENORMALIZATION OF THE FINAL STATE WAVE FUNCTION

A second method of calculating the generalized density of states function is by means of renormalizing the final state function. The final state function ψ representing c+C in (5) may be first normalized inside a large box of radius $R(\to\infty)$. Write

$$\psi = N(E)[U(E,r)/r]Y_l^m(\theta,\varphi). \tag{24}$$

Then the generalized density of states function may be reasonably defined as

$$\rho(E) = \rho_0(E)N^2(E), \tag{25}$$

when $\int_0^a |U/r|^2\mathrm{d}v = 1$ and $\int_0^R |\psi|^2\mathrm{d}v = 1$, and ρ_0 is the *usual* density of final states of c+C given by

$$\rho_0 = \mu R/\pi\hbar^2 k. \tag{26}$$

Thus

$$N^2(E) = \int_0^a |\psi|^2\mathrm{d}v = N^2\int_0^a |U|^2\mathrm{d}r. \tag{27}$$

Now by employing the result (derived from the Wronskian) that

$$\int_0^a |U|^2\mathrm{d}r = \frac{\hbar^2}{2\mu}\left[\frac{\partial U^*}{\partial r}\frac{\partial U}{\partial E} - U^*\frac{\partial^2 U}{\partial r\,\partial E}\right]_0^a, \tag{28}$$

which holds for any central potential of c+C scattering, it follows that

$$N^2 = \frac{1}{2k}\left[\frac{\partial U}{\partial r}\frac{\partial U}{\partial E} - U\frac{\partial^2 U}{\partial r\,\partial E}\right]^a = -\frac{U^2}{2k}\frac{\partial}{\partial k}\left(\frac{\partial U}{\partial r}\Big/ U\right)\Big|_a. \tag{29}$$

Here the fact that $U(k, r=0)=0$ has been used, and U has been taken real. The appropriate normalized U, for $r \geqq a$, is

$$U = (2/R)^{\frac{1}{2}} A(k, r)\sin(\phi+\delta), \tag{30}$$

where ϕ is defined by (17) and $A = (F^2+G^2)^{\frac{1}{2}}$. Thus

$$\rho = \frac{\mu}{\pi\hbar^2 k}\left[\frac{\mathrm{d}}{\mathrm{d}k}(\delta+\phi) - \tfrac{1}{2}\left(\frac{1}{k} - 2\frac{\partial A}{\partial k}\Big/ A\right)\sin 2(\phi+\delta) - \frac{1}{k}\left(A\frac{\partial^2 A}{\partial r\,\partial k} - \frac{\partial A}{\partial r}\frac{\partial A}{\partial k}\right)\sin^2(\delta+\phi)\right]. \tag{31}$$

In the special case when U for $r \leqq a$ may be taken as independent of the energy

$$U(a, E) = \zeta = \text{constant}, \tag{32}$$

then

$$\rho = [2\mu a/\pi\hbar^2\zeta^2][\sin^2(\phi+\delta)]/P, \tag{33}$$

where $P \equiv ka/A^2$ is the penetrability.

3. The Generalized Density of States Function

Process (1) will in general lead to both a set of discrete states and a continuum of states. This general case may be treated by combining the results given in sections 1 and 2. In what follows the method of subsect. 2.1 will be used to define ρ. Thus the system B, normalized in a box of radius R, has a set of eigenstates that allow the wave fuction of the state to satisfy the boundary conditions. The total number of states of the system may be associated with the number of loops of the wave function, and the net number of states available to the decay may again be associated with the net number of loops of the wave function inside the interaction radius a. Expressions (8) and (19) give, respectively, the appropriate density of states function for the discrete energy states and the states defined for a continuous range of the energy. Thus generally

$$\rho_l(E_B) = \sum_n \delta(E_B - E_n) + \frac{1}{\pi}\frac{\mathrm{d}}{\mathrm{d}E_B}(\delta_l+\phi_l(a)) \tag{34}$$

and

$$\sigma_l(E_B) = \left\{\sum_n \delta(E_B - E_n) + \frac{1}{\pi}\frac{\mathrm{d}}{\mathrm{d}E_B}(\delta_l+\phi_l(a))\right\} \times (\mu_a\mu_b k_a/4\pi^2\hbar^4 k_b)|\langle B+b, E_B|H'|A+a, E_a\rangle|^2 \tag{35}$$

for each partial wave of decay into the single channel c+C. Eqs. (34) and (35) give the most general prescription for calculating the defined density of states function and the cross section in the case of only one decay channel for B being open. It should be noted that (34) gives the proper relative normalization of this density of states function for decay to both discrete and continuum states of B. This statement does not exclude an energy variation of the matrix element.

4. Other Interpretations of the Density of States Function

4.1. LOCALIZATION OF THE INTERACTIONS

In a two-body nuclear transition, such as (1), the transition occurs so as to produce system B in a fairly well defined spatial region of radius a. This localization of the interaction, and of B, produces an indetermination of the energy of the transition; i.e. a spectrum of particles b will be produced, and this spectrum is just a manifestation of the localized nature of the interaction. Thus the density of states function may be viewed as the probability that the system B is localized in the interaction volume of radius a.

There is, in general, some wave function $F_l(r)$ that describes each partial wave of the system B = c+C just as it is produced and before it decays. Thus

$$f_l(k) = \int_0^a F_l(r)\psi_l(r, k)\mathrm{d}r \tag{36}$$

gives the projections of $F_l(r)$ on the energy eigenstates $\psi_l(k, r)$ of relative motion of c+C, and the density of states function may be reasonably defined as proportional to $f_l(k)^2$,

$$\rho_l(E) = \alpha|f_l(k)|^2. \tag{37}$$

In particular suppose that the situation before the decay may be described by

$$F_l(r) = \delta(r-a). \tag{38}$$

Thus employing (36) and (38)

$$f_l(k) = \psi_l(k, a) \tag{39}$$

and by (37) and (39)

$$\rho_l(E) = \alpha|\psi_l(k, a)|^2. \tag{40}$$

Now on using (11), (17) and (40)

$$\rho_l(E) = \alpha A_l^2 \sin^2(\delta_l+\phi_l(a))/a^2k^2, \tag{41}$$

where $A_l^2 = F_l^2+G_l^2$. This is a result similar to that obtained by other writers [4]), and applied to a number of interesting problems.

4.2. TIME-DEPENDENT CONSIDERATIONS

In sect. 1 it was pointed out that the transition probability P for leaving system B excited to energy E_B should be given by

$$P(E_B) = W(E_B)T(E_B), \tag{42}$$

where $W(E_B)$ is the square of a matrix element and $T(E_B)$ is the lifetime of the localized system B. This result follows from the following considerations: the decay of an excited nucleus D* between time t and $t+dt$ to leave B excited in the interval dE'_B is given by

$$dP_l(E'_B, t) = W_l(E'_B)P_{l,a}(E'_B, t)dt, \tag{43}$$

where

$$W_l(E'_B) = (2\pi/\hbar)|\langle B, b|H'|A, a\rangle|^2\rho_{b,B}(E_{B,b}) \tag{44}$$

is the transition probability calculated using time independent, normalized initial and final state vectors and $P_a(t, E_B)$ is the time dependent probability that the final system B+b of energy E_B is within the volume of interaction of H' whose radius is a. $\rho_{b,B}$ is the *usual* density of final states function for the particles b+B. Now Smith [9]) has shown that the time delay T_l of each partial wave of a two-body system c+C whose scattering may be described by phase shifts δ_l is

$$T_l = \hbar \frac{d\delta_l}{dE_B}.$$

This time is the time delay with respect to the time delay of the same scattering problem but with no short range forces. Another, similar, time delay may be defined as

$$T'_{l,a} = -\hbar \frac{d\phi_l(a)}{dE_B},$$

where $\phi_{l,a}$ is defined by (17). This time is the time dealy (actually it is always negative!) for a partial wave of c+C scattering where the waves are *excluded* from the small sphere of radius a.

When the system c+C is initially enclosed in the small sphere each partial wave will have a time delay in decaying given by

$$\Delta T_{l,a} = T_l - T'_{l,a} = \hbar \frac{d}{dE_B}(\delta_l + \phi_l(a)). \tag{45}$$

Thus, if the system B is considered as an initially localized, normalized, wave packet that decays with the characteristic time, $\Delta T_{l,a}$, then the probability that B, excited to E_B, is within the interaction distance of b is given by

$$P_{a,l}(t, E_B) = \exp(-t/\Delta T_{l,a}). \tag{46}$$

Equations (43) and (46) give, upon integration over the time,

$$P = \hbar W_l(E_B) \frac{d}{dE_B}(\delta_l + \phi_l(a)). \tag{47}$$

This equation clearly leads to the same scattering cross section results of (7) and (19), and suggests that the density of states and life time of the localized state are related by

$$\rho_{l,\mathrm{a}}(E_\mathrm{B}) = (2/\hbar)\Delta T_{l,\mathrm{a}}(E_\mathrm{B}) = \frac{1}{\pi}\frac{\mathrm{d}}{\mathrm{d}E}(\delta_l + \phi_l(\mathrm{a})). \tag{48}$$

5. Applications

There seem to be several cases of special interest in the application of this model to particular experimental situations. These will be discussed below.

5.1. PREDICTION OF SPECTRAL SHAPES

The cross section given in (7) may be generalized to (22) for transitions to the sharp and continuum states of B if ρ is given the value of (21). Thus if the system B can only decay into one channel, c+C, for which the scattering phase shifts δ_l can be measured then the density of states functions ρ can be calculated. If the matrix element in (7) is slowly varying the spectrum of (1) may be deduced. This method has been successfully applied to the Be^9(p, d)Be^8; $Be^8 \rightarrow \alpha+\alpha$ reaction [10]).

5.2. SPECTRAL ANOMALIES DUE TO LOCALIZATION

Consider the case where there are no nuclear forces between c and C; then $\delta_l = 0$ and

$$\rho_l(E_\mathrm{B}) = \frac{1}{\pi}\frac{\mathrm{d}\phi_l(\mathrm{a})}{\mathrm{d}E_\mathrm{B}}. \tag{49}$$

In general $\mathrm{d}\phi/\mathrm{d}E_\mathrm{B}$ has a maximum at a certain low energy. This maximum of ρ may be expected to be evidenced in spectra even in those cases where the produced nucleus B has either small, or no nuclear forces stabilizing it, and thus small values of $\mathrm{d}\delta/\mathrm{d}E_\mathrm{B}$ for channel c+C.

This simple case exemplifies what is perhaps the only really new result of this paper: *one may expect anomalies of yield in certain energy regions of spectra where the anomalies do not correspond to metastable states of the final system produced by internal forces but rather correspond to the final system being left localized.*

For example consider two non-interacting particles c and C that comprise B. If S wave states are considered $\delta_0 = 0$, $\phi_0 = ka$ and

$$\rho_0(E_\mathrm{B}) = (a/\pi)(\mu/2\hbar)^{\frac{1}{2}} E_\mathrm{B}^{-\frac{1}{2}}. \tag{50}$$

This result predicts that the spectrum of particles b due to producing S states in the final system B will have a high peak at the maximum energy of particles b which leave c+C with very small energy. This is a reasonable result since the

cross section should be proportional to the "life time" of system B inside the small sphere. Classically this time is $a/V_{c,C}$ where $V_{c,C}$ is the relative velocity of c and C and so the time is proportional to $E_B^{-\frac{1}{2}}$. A different result is predicted by employing (31): the high peak at threshold is suppressed although a low energy peak remains.

There seem to be a number of experimental examples of these "localization anomalies"; in the preceding paper [11]), Spencer has discussed an example in the mirror nuclei Be^9—B^9.

It should be pointed out that the results (31) and (33) do not seem to be capable of describing properly the aspects of spatial localization considered in this case.

5.3. CONSTRUCTION OF PHASE SHIFTS FROM SPECTRA

Suppose the spectrum of (1) is measured; i.e. $\sigma(E_B)$ is measured. If (3) is the only channel available to B then the phase shift for (9) may be deduced if the matrix element is assumed to be constant. Thus (7) and (19) becomes

$$\frac{d\delta_l}{dE_B} = (2\pi\hbar^2/\mu)^2\sigma(E_B)(k_b/k_a)|M|^2 - \frac{d\phi_l(a)}{dE_B}, \tag{51}$$

where $M = \langle B+b, E_B|H'|A, E_a\rangle$, and

$$\delta_l(E) = (2\pi\hbar^2/\mu k_a^{\frac{1}{2}})^2 \int_0^E \sigma(E_B)k_b|M|^2 dE_B - \phi_l(E, a). \tag{52}$$

If $|M|^2$ may be assumed a constant then $\delta(E)$ may be calculated. In some cases this assumption is reasonable: when $\sigma =$ constant $\times F(E_B)$, independent of the energy of the first transition, and the type of particle b, then it is possible to associate $F(E_B)$ with $\rho(E_B)$ and to use this result to *deduce* the scattering phase shifts.

5.4. ENERGY VARIATION OF THE MATRIX ELEMENTS

There seems to be another interesting application of these ideas: if the scattering phase shifts are measured then a density of states function, $\rho(E)$ may be constructed and compared to the form of spectrograms which gives $\sigma =$ (constant) $\times$ (matrix element)$^2 \times \rho(E_B)$. Thus information about the energy variation of the matrix elements may be obtained.

6. Conclusions

The treatment of many-body decay as a sequence of two-body decays allows the prediction of many features of spectral shapes provided the phase shifts of the produced composite particle are known. These ideas allow obvious extensions to the more complicated cases where a phase shift description is inadequate

and an S-matrix representation is required. Since the emphasis is upon using one set of experimental data (phase shifts) to predict some properties of another set of data (spectra) and since no S-matrices are really well measured primary quantities, extensions of the method do not seem called for at the present. Instead, the interest in the model should properly be focused upon its application to simple experimental situations so as to investigate its applicability to nuclear problems.

References

1) G. C. Phillips and T. A. Tombrello, Nuclear Physics **20** (1960) 648
2) A. M. Lane and R. G. Thomas, Rev. Mod. Phys. **30** (1958) 257;
G. C. Phillips and L. C. Biedenharn, Bull. Am. Phys. Soc. II, **5** (1960) 44
3) L. I. Schiff, Quantum mechanics (McGraw-Hill, New York, 1949) p. 195
4) Kenneth M. Watson, Phys. Rev. **88** (1952) 1163
5) These arguments are similar to those of several authors:
L. Gropper, Phys. Rev. **51** (1937) 1108;
E. Beth and G. E. Uhlenbeck, Physica **4** (1937) 915;
Kilpatrick, Keller, Hammel and Metropolis, Phys. Rev. **94** (1954) 1103
6) E. P. Wigner, Phys. Rev. **98** (1955) 145
7) E. P. Wigner and L. Eisenbud, Phys. Rev. **72** (1947) 29
8) E. W. Hamburger and J. R. Cameron, Phys. Rev. **117** (1960) 781;
T. A. Griffy and L. C. Biedenharn, Nuclear Physics **15** (1960) 636
9) Felix T. Smith, Phys. Rev. **118** (1960) 349
10) Beckner, Jones and Phillips, to be published.
11) Spencer, Phillips, and Young, Nuclear Physics **21** (1960) 310

3.A

Nuclear Physics **21** (1960) 340—343; © *North-Holland Publishing Co., Amsterdam*

Not to be reproduced by photoprint or microfilm without written permission from the publisher

RADIOACTIVE DECAY OF Tm^{167}

H. NARASIMHAIAH † and M. L. POOL

Department of Physics, Ohio State University, Columbus, Ohio

Received 29 July 1960

Abstract: Erbium oxide enriched in the mass number 167 was irradiated with 12-MeV deuterons and 6-MeV protons. An activity with a half-life of 9.58 days was produced and ascribed to Tm^{167}. The spectrum consisted of Er K X-radiations and gamma rays of 57, 208 and 532 keV and the observed relative intensities were 100, 5.4, 56.6 and 3.18 respectively. None of the gamma rays was in coincidence with another. Transition probabilities and branching ratios are shown in a proposed energy level diagram.

1. Introduction

A half-life of 9.6 days was assigned to Tm^{167} following bombardments of holmium with alpha particles and erbium with protons [1]). Nervik and Seaborg showed the presence of gamma rays with energies of 49, 115, 202, 515 and 720 keV in the Tm^{167} spectrum [2]). However later, only the Er K X-radiation and gamma rays with energies of 57 and 207 keV were observed [3]). The earlier observed 115-keV peak in the gamma-ray spectrum can be attributed to the back scatter from the 207-keV gamma ray and to the summation of the Er K X radiation and the 57-keV gamma ray. Coulomb excitation of rare earth nuclei [4]) resulted in the detection of levels at 80 and 172 keV, presumably in the erbium nucleide of mass number 167. The spin of Er^{167} was measured [5]) to be $\frac{7}{2}$. The existence of a 208-keV E3 isomeric transition with a half-life of 2.5 sec has been established [6]). The spectrum of Tm^{167} based on internal conversion data consists of transitions of 57.1, 208.2 and 532.2 keV [7]). The 57-keV transition has a multipole order of 87 % M1+13 % E2 and there exists the possibility that the 264-keV level is the first excited rotational level $(\frac{3}{2}-)$ of the intrinsic level at 208 keV.

The purpose of this paper is to investigate the high energy spectrum of Tm^{167} by coincidence scintillation spectrometry.

2. Experimental Results

Erbium oxide enriched to 58.8 % in the mass number 167 was bombarded with 12-MeV deuterons and 6-MeV protons. The following were the percents of

† Now at the National College, Bangalore, affiliated to the University of Mysore, India.

other isotopes present in the sample: Er^{166}, 14; Er^{168}, 25.3; and Er^{170}, 1.93.

The spectrum of the bombarded sample consisted of the Er K X-radiations and gamma rays of 57, 80, 208, 448, 532, 640, 730, 820, 1016, 1280 and 1464 keV. Comparison of the above spectrum with the 88-day spectrum of Tm^{168} showed that all the gamma rays [8]), except those with energies of 57, 208 and 532 keV, belonged to Tm^{168}. The high energy portion of the spectrum is represented in fig. 1. The pure Tm^{168} spectrum used for comparison was obtained by bombard-

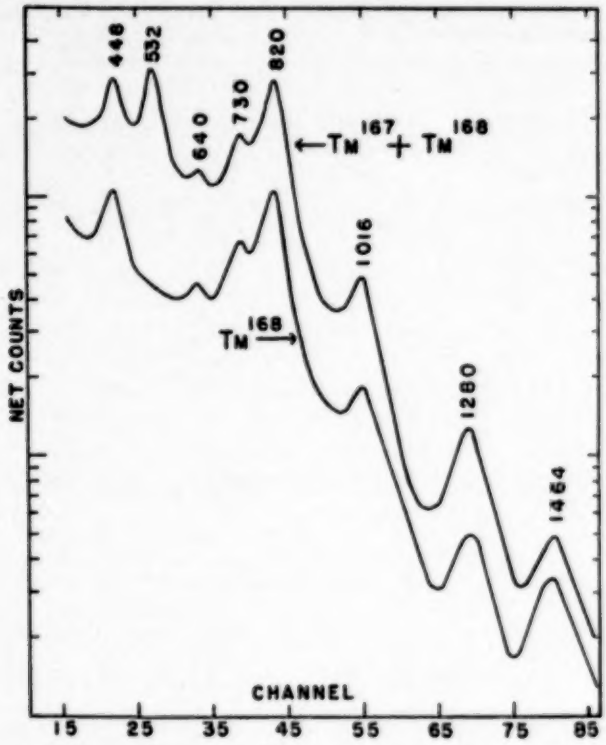

Fig. 1. Comparison of the high energy portion of the composite spectrum with that of Tm^{168}.

ing enriched Er^{168} with 6-MeV protons. The 7.7-hour spectrum [9]) of Tm^{166} was also present in the early portion of the decay of the activity. The presence of Er^{168} and Er^{166} in the enriched Er^{167} sample accounts for the appearance of the respective Tm^{168} and Tm^{166} activities. The gamma rays with energies 57, 208 and 532 keV as well as the Er K X-radiations decayed with a half-life of 9.58 ± 0.05 days as measured over four half-lives. The assignment of the activity to Tm^{167}, previously made on internal conversion data, is thus confirmed [7]).

Gamma-gamma coincidence measurements show that none of the gamma rays is in prompt coincidence. The relative intensities N_γ and the transition probabilities N_T of the radiations have been calculated and are shown in table 1.

The 57-keV gamma ray was not observed directly in the spectrum because of its closeness to the intense Er K X-radiation of 49 keV. However, the presence of the gamma ray was evident in the coincidence measurements.

From the spectrum of the bombarded enriched Er^{167} sample the spectrum of Tm^{168} was completely subtracted by means of the 100-channel analyzer. The

net Tm^{167} spectrum was then used to determine the number of counts under the 208- and 532-keV gamma -ray peaks. From the 17×10^5 counts obtained under the composite K X-radiation and the 57-keV gamma-ray peaks, the counts in the two separate components were calculated by using the conversion electron data and the multipole order of the 57-keV gamma ray. The results are shown in column two of table 1.

TABLE 1

Transition probabilities N_T and radiation intensities N_γ

Energy (keV)	No. of counts[a])	Crystal efficiency	N_γ intensity	Multipole order	$\frac{N_T}{N_\gamma}$ [b])	N_T	N_K [c])
49	15.8	0.5	44.2 [d])				
57	1.2	0.5	2.40	87 % M1+ 13 % E2	20.38	48.3	28.8
208	12.5	0.5	25.0	E3	2.67	66.7	12.4
532	0.56	0.4	1.4	73 % E1+ 27 % M2	1.03	1.44	0.034

[a]) Number of counts in the spectral distributon in units of 10^3.
[b]) Obtained by using the data from M. E. Rose [10]).
[c]) Number of K X-radiations of 49-keV produced because of internal conversion.
[d]) Obtained after applying the crystal efficiency, fluorescence yield (0.932), and the absorption by the 0.25 cm aluminium covering (1.3).

3. Discussion

Fig. 2 shows the proposed energy level diagram. Since the 532-keV gamma ray is not in coincidence with the 57-keV gamma ray, the 532-keV transition is either to the ground state or to the 208-keV metastable level. The latter choice would result in a $\frac{1}{2}+$ or a $\frac{3}{2}+$ for the spin for a 740-keV level, and a heavy population of the level. The latter prediction conflicts with the observed weak intensity of the 532-keV gamma ray. Such a choice would also tend to favor transitions that have not been observed. However, a 532-keV level with a spin of $\frac{5}{2}-$ is consistent with all the experimental scintillation results and with the 73 % E1+27 % M2 multipole order [7]) of the 532-KeV transition. The $\frac{5}{2}-$ spin explains the weakness in intensity of the 532-keV gamma ray. Also the unobserved transitions to the 208-keV and the 265-keV levels would be expected exceedingly weak because of the large change in K, $\frac{5}{2} \rightarrow \frac{1}{2}$. The symbol K used here and in fig. 2 represents the component of the total angular momentum quantum number along the axis of nuclear summetry.

The number of emitted K X-radiations is 44.2, in units of 10^5, and is arrived at by dividing the observed 15.8 counts, as shown in table 1, by the efficiency of the crystal, 0.5, and the fluorescence yield, 0.932, and by multiplying by 1.3 to compensate for the aluminium absorption on the NaI crystal. The number of X-radiations, resulting from the internal conversion of 48.3 57-keV transitions that yielded 1.20 observed 57-keV gamma rays, is 28.8. The conversion coeffi-

cient used in the calculation was $\alpha_K = 12.09$. The numbers of X-radiations similarily obtained from the 208- and 532-keV gamma rays are 12.4 and 0.03

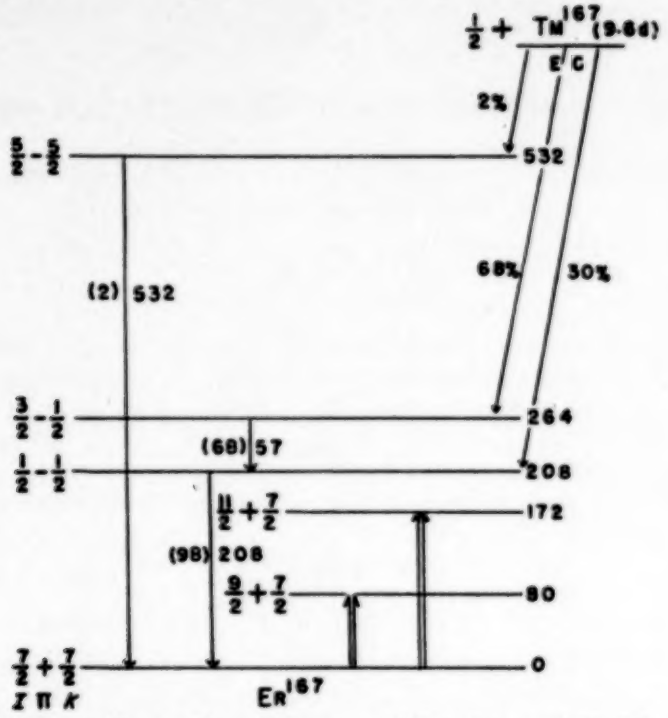

Fig. 2. Energy level diagram of the decay of Tm^{167}.

respectively. Hence, the total number of emitted X-radiations, 44.2, is approximately equal to that calculated from the gamma ray internal conversions; namely, $28.8+12.4+0.036 = 41.2$. Therefore, Tm^{167} appears to decay to the 208- and 264-keV levels essentially by L or M electron capture.

An expression of appreciation is extended to R. P. Sullivan for the technical help in the maintenance of the electronic equipment used in this investigation and to the Office of Naval Research for support in obtaining the enriched isotopes. One of us (H. N.) is grateful to the United States Educational Foundation for the award of a Fulbright Travel Grant.

References

1) G. Wilkinson and H. G. Hicks, Phys. Rev. **75** (1959) 1377
2) W. E. Nervik and G. T. Seaborg, Phys. Rev. **97** (1955) 1092
3) G. M. Gorononskii, A. Murin, V. N. Pokrovskii and B. J. Preobrazhenskii, Bull. Acad. Sc. USSR **21**, No. 7 (1957) 1005
4) N. P. Heydenberg and G. M. Temmes, Phys. Rev. **100** (1955) 150
5) B. Bleaney and H. E. D. Scovil, Proc. Phys. Soc. A **64** (1951) 204
6) J. W. Mihelich. B. Harmatz and T. H. Handley, Phys. Rev. **108** (1957) 989
7) B. Harmatz, T. H. Handley and J. W. Mihelich, Phys. Rev. **114** (1959) 1082
8) K. P. Jacob, J. W. Mihelich. B. Harmatz and T. H. Handley, Phys. Rev. **117** (1960) 1102; R. G. Wilson and M. L. Pool, Phys. Rev. **118** (1960) 227
9) R. G. Wilson and M. L. Pool, Bull. Am. Phys. Soc. **5** (1960) 255
10) M. E. Rose, Internal conversion coefficients, (North-Holland Publishing Company, Amsterdam, 1958) p. 88

2.A.1

Nuclear Physics **21** (1960) 344—346; © *North-Holland Publishing Co., Amsterdam*

Not to be reproduced by photoprint or microfilm without written permission from the publisher

NEUTRON CROSS SECTIONS IN CHLORINE

G. S. MANI, T. A. TOMBRELLO and D.A.A.S.N. RAO †

The Rice University, Houston, Texas ††

Received 25 July 1960

Abstract: An upper limit of 5 mb has been obtained for the Cl^{37}(n, p)S^{37} reaction cross section at a neutron energy of 17.5 MeV. The cross section for the Cl^{35}(n, 2n)Cl^{34m} reaction has been measured for neutron energies between 17 MeV and 22 MeV.

The measurement of Cohen and White [1]) of the Cl^{37}(n, p)S^{37} reaction ($Q = -3.4$ MeV) indicated an anomalous behavior in the variation of the cross section with the energy of the incident neutron. Their experiment showed that the reaction seems to start at about 10 MeV of neutron energy and the cross section increases to ≈ 70 mb at 17.0 MeV of neutron energy. Their results also seem to indicate that the competing (n, 2n) reaction ($Q = -10.5$ MeV) does not reduce the cross section at higher neutron energies.

Cohen and White used NaCl as a target and measured the S^{37} activity by counting the betas. Since (n, p), (n, α) and (n, 2n) reactions of sodium and of Cl^{35} may introduce a large background of unwanted activities, we have repeated their experiment using LiCl as a target and have looked for the 3.09 MeV γ ray in the decay of S^{37} to Cl^{37}. Since neutron reactions in lithium yield no activity except the short-lived He^6 and Li^8, by looking at a specific γ ray in the decay of the residual nucleus we eliminate the background due to other activities. We have compared the S^{37} activity obtained from γ ray measurement with the 843 keV and 1015 keV γ rays from the Al^{27}(n, p)Mg^{27} reaction. A 5.1 cm by 5.1 cm NaI (Tl) crystal was used for the γ ray measurements, and the neutron flux was monitored with a 2.5 cm by 1.3 cm stilbene crystal. The cross section for the Al^{27}(n, p)Mg^{27} reaction is known up to 22.8 MeV of neutron energy [2]). Our experiment was done at a neutron energy of 17.5 ± 0.25 MeV, and we found that the upper limit on the (n, p) cross section in chlorine at this energy is 5 mb. In fig. 1 the γ spectra from the Al^{27}(n, p)Mg^{27} and the Cl^{37}(n, p)S^{37} reactions are shown. It can be seen from these curves that the chlorine reaction is not detectable above the background. The magnitude of this background provides the upper limit on the cross section that is given above. This upper limit for the (n, p) reaction at 17.5 MeV is consistent with the value of 10 mb

† Texas Southern University, Houston, Texas.

†† Work supported by the U. S. Atomic Energy Commission.

obtained by Paul and Clark[3]) at 14 MeV. It is interesting to note that other nuclei with a neutron excess like A^{40} and Ca^{44} also have a low (n, p) cross section.

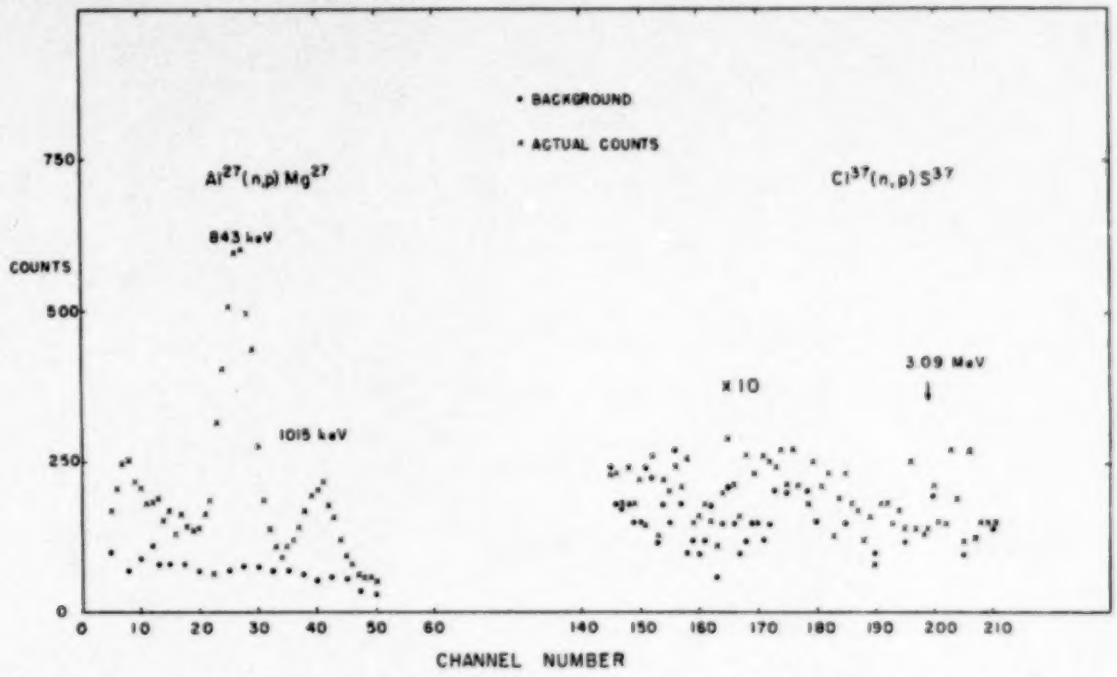

Fig. 1. Comparison of the γ ray spectra for the (n, p) reaction in Cl^{37} with that in Al^{27} at 17.5 MeV of neutron energy.

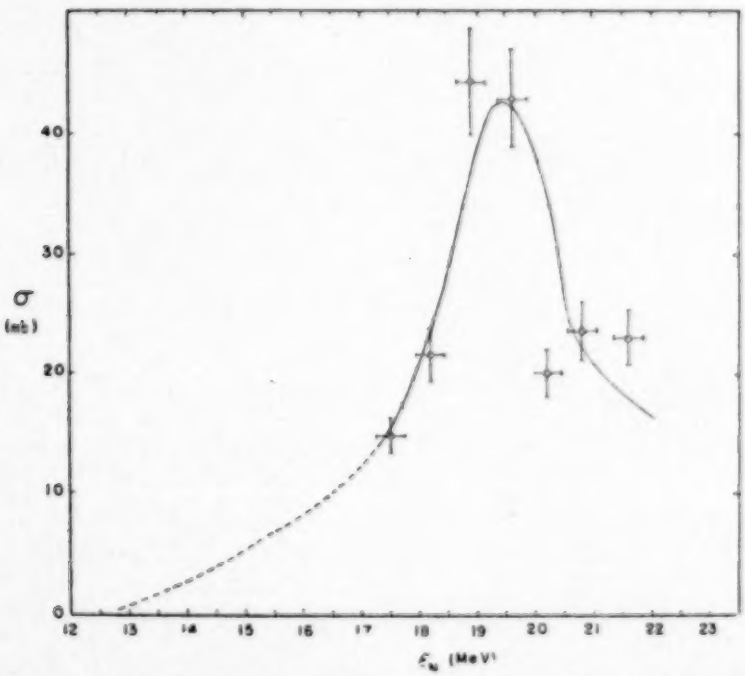

Fig. 2. The cross section for the Cl^{35}(n, 2n)Cl^{34m} reaction as a function of the neutron energy.

We have also measured the Cl^{35}(n, 2n)Cl^{34m} reaction going to the isomeric state in Cl^{34}. Fig. 2 gives the variation of the (n, 2n) cross section with the neu-

tron energy. The absolute cross section was obtained by comparison with the $Al^{27}(n, p)Mg^{27}$ cross section at two neutron energies. The absolute cross section is accurate to $\pm 20\,\%$, and the statistical uncertainty at each data point is $\pm 10\,\%$.

References

1) A. G. Cohen and P. H. White, Nuclear Physics **1** (1956) 73
2) Mani, MacCallum and Ferguson (to be published)
3) E. B. Paul and R. L. Clark, Can. J. Physics **31** (1953) 267

1.E.5

Nuclear Physics **21** (1960) 347—352; © *North-Holland Publishing Co., Amsterdam*

Not to be reproduced by photoprint or microfilm without written permission from the publisher

ISOTOPE SHIFT CALCULATIONS FOR NON-UNIFORM CHARGE DISTRIBUTIONS

A. R. BODMER

Department of Theoretical Physics, University of Manchester, Manchester, England

Received 20 June 1960

Abstract: It is shown that recent calculations by Meligy of the charge dependent isotope shift for the special case of a trapezoidal nuclear charge distribution are in agreement with previous results, obtained by the author, which are applicable to any charge distribution whatever its shape, both sets of calculations allowing for the distortion of the electron wavefunction by the nuclear charge distribution. A discussion of Meligy's numerical results is given which indicates that previous conclusions about the isotope shift discrepancy remain essentially unchanged.

1. Introduction

Recently two papers, by Meligy [1]) and by Meligy *et al.* [2]), have appeared in which calculations of the charge dependent isotope shift (I. S.) are made, allowing for the distortion of the electron wavefunction by the nuclear charge distribution which is taken to have a trapezoidal shape. Meligy's results appear to have a very different form from the results of calculations [3, 4]) made by the author and in addition there is a difference as regards the actual numerical results. The calculations of refs. [3, 4]) also allowed for distortion of the electron wavefunction but are much more general than Meligy's, being applicable to any charge distribution, which enters the results only through the root-mean-square radius $\langle r^2\rangle^{\frac{1}{2}}$ and through its change $\delta\langle r^2\rangle^{\frac{1}{2}}$ between the two isotopes considered. In view of the basic importance of such calculations for the understanding and analysis of the I. S. data it is important to be clear about their status. Furthermore it is instructive to compare a calculation, such as Meligy's, for a special form of charge distribution with the corresponding results obtained from our more general expressions.

We wish to point out in this note that the results of refs. [3, 4]) although simpler and more general than Meligy's are at the same time also more exact than the results of Meligy's first paper and as exact as those of Meligy's second paper. Furthermore we shall also discuss the discrepancy of Meligy's numerical results with ours which can then only arise from the use of different magnitudes for the parameters characterising the charge distribution.

2. Isotope Shift Calculations

In ref. [3]) the following, essentially exact, result was obtained for the difference ΔE in the energy of an s-electron (the only important case) moving in the field

of a point charge and an extended nuclear charge distribution, both of total charge Ze,

$$\Delta E = \frac{N}{4\sigma\Gamma^2(2\sigma)} \frac{a+(1+\sigma)K(x_1)}{a+(1-\sigma)K(x_1)} x_1^{2\sigma}. \tag{1}$$

Here, $\sigma = \sqrt{1-a^2}$, $a = Z\alpha$, $\alpha = e^2/\hbar c$, Γ denotes the Γ-function, $x_1 = 2Zr_1/a_H$ (where a_H is the Bohr radius and the distance r_1 corresponds to a point outside the charge distribution). The quantity $K(r) = f(r)/g(r)$ is the ratio of the small to the large Dirac radial functions appropriate to the potential of the charge distribution being considered. The normalisation factor N is given by

$$N = \left(\frac{4\pi R}{Z}\right) a_H^3 \psi_S^2(0), \tag{2}$$

where R is the Rydberg constant and $\psi_S(0)$ is the Schrödinger wavefunction at the origin with the nucleus considered as a point charge. With $\psi_S^2(0) = Z^3/\pi a_H^3 n^3$, appropriate to an unscreened Coulomb potential, n being the principal quantum number, eq. (1) is just Meligy's general expression for an s-electron. Because of screening effects on $\psi_S^2(0)$ (see ref. [5]) for a discussion of these) it is more realistic to write ΔE in the form of eq. (1) with N given by eq. (2). It is interesting and satisfactory that Meligy has obtained eq. (1) by an essentially quite distinct method from that used in ref. [3]).

It was shown in ref. [3]) that in virtue of the equation satisfied by K this quantity could be obtained by an iterative procedure which corresponds to an expansion of K in powers of a. Thus for a uniform charge distribution of radius R the second iteration gives

$$K(R) = K(a) = -\tfrac{2}{5}a(1+0.106a^2), \tag{3}$$

this depending only on a. The third and higher iterations differ only negligibly from eq. (3) for all elements. Further, it was shown that eq. (1) could then be written for any charge distribution as

$$\Delta E = \frac{N}{4\sigma\Gamma^2(2\sigma)} \frac{a+(1+\sigma)K(a)}{a+(1-\sigma)K(a)} x_u^{2\sigma}, \tag{4}$$

where $K(a)$ is given by eq. (3) and R_u is the radius of the equivalent uniform charge distribution and is given by

$$\tfrac{3}{5}ZR_u^2 = \langle r^2 \rangle, \tag{5}$$

where $\langle r^2 \rangle$ is the mean-square radius of the charge distribution being considered.

For the I.S. $\delta(\Delta E)$ one obtains similarly as for ΔE

$$\delta(\Delta E) = \frac{N}{2\Gamma^2(2\sigma)} \frac{a+(1+\sigma)K(a)}{a+(1-\sigma)K(a)} x_u^{2\sigma} \frac{\delta R_u}{R_u} = 2\sigma\Delta E \frac{\delta R_u}{R_u}. \tag{6}$$

Here δR_u is the change in the radius of the equivalent uniform charge distribution between the two isotopes considered and is thus, from eq. (5), determined by the corresponding change $\delta\langle r^2\rangle^{\frac{1}{2}}$ between the two isotopes. The normalisation factor N is again given by eq. (2). The use of eqs. (4) and (6) together with the equivalence relation (5) and eq. (3) for $K(a)$ was shown in refs. [3,4]) to be of the same accuracy as eq. (3) for $K(a)$ and thus to be essentially exact for all elements.

We now apply the above results to the special case of a trapezoidal charge distribution used by Meligy:

$$\rho(r) = \begin{cases} \rho(0) & \text{for } 0 < r < c-\zeta, \\ \rho(0)\,\dfrac{(c+\zeta-r)}{2\zeta} & \text{for } c-\zeta < r < c+\zeta, \\ 0 & \text{for } r > c+\zeta, \end{cases} \tag{7}$$

with

$$\rho(0) = \frac{3Ze}{4\pi c^3}\,(1+y^2)^{-1} \text{ and } y = \zeta/c.$$

Here $\rho(0)$ is the central charge density, c is the half-density radius and 2ζ is the surface thickness. From eqs. (5) and (7) one obtains

$$R_u^2 = c^2(1+y^2)^{-1}(1+\tfrac{10}{3}y^2+y^4) \tag{8}$$

and

$$\frac{\delta R_u}{R_u} = \frac{\delta c}{c}\left[1 - \left(\frac{c^2}{R_u^2}\right) y^2\,(1+y^2)^{-2}(\tfrac{7}{3}+2y^2+y^4)\right], \tag{9}$$

assuming, as Meligy does, that only c changes (i.e. assuming a constant nuclear surface thickness). If, using eq. (8), $R_u^{2\sigma}/(c+\zeta)^{2\sigma}$ is expanded in powers of a one obtains,

$$R_u^{2\sigma} = (c+\zeta)^{2\sigma}[1-2y(1+y)^{-2}(1+y^2)^{-1}(1-\tfrac{2}{3}y+y^2)+\mathrm{O}(a^2)]. \tag{10}$$

If now only the terms independent of a^2 in the square brackets are retained in eq. (10) and if for $K(a)$ only the leading term in eq. (3) is used, the expressions so obtained for ΔE and $\delta(\Delta E)$ agree with the corresponding expressions in Meligy's first paper to the *lowest* order in a; the terms in a^2 are, however, different. The disagreement for the higher order terms in a arises because in his first paper Meligy obtains K for the distribution (7) only to the lowest order in a (by direct integration of the Dirac radial equations). In Meligy's second paper, K for the distribution (7) is obtained to the next order in a corresponding to eq. (3) for a uniform distribution. The corresponding results then agree with ours also to higher order in a. As shown in ref. [3]) the higher order terms in a can contribute more than 10 % to $\delta(\Delta E)$ for heavy elements.

It is thus a very satisfactory confirmation of our very general results for

ΔE and $\delta(\Delta E)$ that these results, which are valid for any charge distribution, agree exactly with the results of quite independent calculations for the particular case of a trapezoidal distribution.

3. Discussion of Numerical Results

As regards Meligy's numerical results it is clear from the above discussion that these must agree with those obtained from eqs. (4) and (6) if in these expressions the values of R_u and $\delta R_u/R_u$ are related through eqs. (8) and (9) to the values of c and ζ used in Meligy's equivalent expressions. Meligy uses the values $c = 1.05\, A^{\frac{1}{3}} f$ and $\zeta = 1.53 f$ (with $f = 10^{-13}$ cm), where these values have been obtained from those for a Fermi distribution used in analyses of the electron scattering data [6]). Numerical values given below will be for $A = 165$, which represents an appropriate mean for those nuclei for which I.S. data are available. Using eqs. (8) and (9), Meligy's values then give $R_u = 1.13\, A^{-\frac{1}{3}} f$ and $(3A/R_u)\mathrm{d}R_u/\mathrm{d}A = 0.87$, where the latter quantity is the change of radius relative to that for a uniform distribution with $R_u \propto A^{\frac{1}{3}}$. These values are to be compared with the values $R_u = 1.2\, A^{\frac{1}{3}} f$ and $(3A/R_u)\mathrm{d}R_u/\mathrm{d}A = 0.88$, used in ref. [4]) which were directly based on the value $R_u = 1.115\ A^{\frac{1}{3}} + 2.151\, A^{-\frac{1}{3}} - -1.742\, A^{-1}$ obtained by Elton [7]) from his analysis of the electron scattering data. It should be observed that $(3A/R_u)\mathrm{d}R_u/\mathrm{d}A = 1$ if $R_u \propto A^{\frac{1}{3}}$, the deviation from unity being due to the lack of proportionality of R_u to $A^{\frac{1}{3}}$ which, according to Elton, may be interpreted as a consequence of the constant nuclear surface thickness together with a constant, or almost constant, total central density assuming the neutron and proton distributions to be the same.† We consider the ratios

$$\gamma_{el} = \frac{(\Delta E)_{el}}{(\Delta E)_{std}} \text{ and } \eta_{el} = \frac{(\delta(\Delta E))_{el}}{(\delta(\Delta E))_{std}},$$

where $(\Delta E)_{std}$ and $(\delta(\Delta E))_{std}$ are the shifts for a uniform distribution of radius $R \propto A^{\frac{1}{3}}$, considered as a standard, and where the suffix $_{el}$ denotes that the corresponding shifts are predicted on the basis of the electron scattering data. Numerical values of γ_{el} and η_{el} for the distribution (7) with the above values of c and ζ are given in ref. [1]). To allow for the higher order effects in a, which were not consistently treated in this paper, one should multiply Meligy's values for γ_{el} and η_{el} by 0.943 and 0.964 respectively. Meligy's values then become (for $A = 165$), $\gamma_{el} = 0.613$ and $\eta_{el} = 0.53$, where $R_{std} = 1.5\, A^{\frac{1}{3}} f$. These corrected values are essentially the ones used in Meligy's analysis [2]) of the I.S. data. With $R_{std} = 1.2\, A^{\frac{1}{3}} f$ these values become $\gamma_{el} = 0.90$ and $\eta_{el} = 0.78$. These are then to be directly compared with our values [4]), $\gamma_{el} = 1$ and $\eta_{el} = (3A/R_u)\mathrm{d}R_u/\mathrm{d}A = 0.88$, where in our case $R_{std} = R_u = 1.2\, A^{\frac{1}{3}} f$. The differ-

† It may be noted that if the neutron and proton distributions are assumed to be the same, eq. (7) will not quite give a constant central density as was assumed in Elton's analysis.

ence in the values of R_u and $(3A/R_u)\mathrm{d}R_u/\mathrm{d}A$ used by Meligy and ourselves then accounts for the remaining difference in the two sets of values, nearly all the difference in η_{el} coming from the difference in the values of R_u. We consider our values of γ_{el} and η_{el} to be essentially the best available at present, since these are based rather directly on the electron scattering data through eqs. (4) and (6).

In ref. [2]) Meligy makes an analysis of the recent compilation of I.S. data given by Brix and Kopfermann [8]). Meligy calculates the contributions to the I. S. due to differences of intrinsic deformation between isotopes [9–13]) using an expression [11]) for this contribution which allows for the distortion of the electron wavefunction and obtaining the intrinsic deformations from the relevant E2 transition probabilities and the expression for these appropriate to rotational states. From Meligy's tabulated results one can then obtain the corresponding values of $(\delta(\Delta E))_{vol}$ and η_{vol}, where these are the "experimental" values due to only the "volume" effect after allowance has been made for the contribution due to intrinsic deformations. With $\eta_{el} = 0.88$, the average of Meligy's values for all those cases where this contribution can be obtained then gives for the I.S. discrepancy

$$\frac{\eta_{vol}}{\eta_{el}} = \frac{(\delta(\Delta E))_{vol}}{(\delta(\Delta E))_{el}} \approx 0.82 \pm 0.1, \tag{11}$$

while using Meligy's value of $\eta_{el} = 0.78$ gives instead $\approx 0.93 \pm 0.1$. Allowing for the rather large errors, the value of eq. (11) is essentially consistent with the value 0.74 ± 0.1 used for the I. S. discrepancy in ref. [4]).

It must be pointed out that effects of nuclear polarisation [14]) may have to be taken into account when allowing for the contribution due to intrinsic deformations, since quadrupole polarisation effects [13]) may not be negligible for rotational, or even vibrational, nuclei. Such dynamic effects would be expected to have an effect in the opposite direction to the static effect of intrinsic deformations considered in refs. [9–13]) and thus to make these estimates of the effects of deformation somewhat uncertain. If only those nuclei are considered for which the intrinsic deformations are small, and for which any deformation-dependent contributions to the I. S. are thus in any case expected to be small, the I. S. discrepancy, for just these nuclei, becomes $\approx 0.75 \pm 0.1$. It thus seems reasonable to try to relate a discrepancy of this sort of value to the effects of nuclear compressibility [4, 10]) which would in any case be expected to give an effect of the right order of magnitude.

References

1) A. S. Meligy, Nuclear Physics **14** (1959/60) 248
2) A. S. Meligy, S. Tadros and M. A. El-Wahab, Nuclear Physics **16** (1960) 99
3) A. R. Bodmer, Proc. Phys. Soc. A **66** (1953) 1041
4) A. R. Bodmer, Nuclear Physics **9** (1958/1959) 371

5) G. Breit, Revs. Mod. Phys. **30** (1958) 507
6) R. Hofstadter, Revs. Mod. Phys. **28** (1956) 214; Ann. Rev. Nucl. Sci. **7** (1957)
7) L. R. B. Elton, Nuclear Physics **5** (1957) 173; **8** (1958) 396
8) P. Brix and H. Kopfermann, Revs. Mod. Phys. **30** (1958) 517
9) P. Brix and H. Kopfermann, Z. Physik **126** (1949) 344
10) L. Wilets, D. L. Hill and K. W. Ford, Phys. Rev. **91** (1953) 1488
11) A. R. Bodmer, Proc. Phys. Soc. A **67** (1954) 622
12) D. L. Hill, Handbuch der Physik (Springer-Verlag, Berlin, 1957), Vol. 39
13) A. S. Reiner, Thesis (University of Amsterdam, 1958)
14) G. Breit, G. B. Arfken and W. W. Clendenin, Phys. Rev. **78** (1950) 390

2.J

Nuclear Physics **21** (1960) 353—366; ©*North Holland Publishing Co., Amsterdam*

Not to be reproduced by photoprint or microfilm without written permission from the publisher

AN APPROACH TO THE SYSTEMATICS OF DELAYED NEUTRON PRECURSORS

ALEXIS C. PAPPAS

Department of Chemistry, University of Oslo, Blindern, Norway

and

GÖSTA RUDSTAM †

The Gustaf Werner Institute for Nuclear Chemistry, Uppsala, Sweden

Received 8 August 1960

Abstract: A review of the theory of delayed neutron emission probabilities is given and the expectations critically surveyed. The upper Z limits of the region where delayed neutron emission is energetically favoured are estimated throughout the table of nucleides and has led to a systematics of delayed neutron precursors. The average distance of the delayed neutron precursor (Z, N) from the stable charge Z_{N-1} of the isotones of the delayed neutron emitter $(Z+1, N-1)$, i.e. $(Z_{N-1}-Z)$ increases from light to heavy nucleides. The effect of closed nucleon shells is very pronounced. Just above neutron shell edges the upper Z limit is drawn towards stability. This effect increases with higher neutron shells.

1. Introduction

Soon after the discovery of nuclear fission, Roberts, Meyer and Wang [1]) found that a small percentage of the fission neutrons were emitted about 10 sec after the fission act itself. Bohr and Wheeler [2]), in their theoretical interpretation of the fission process, explained the emission of these neutrons as a result of β-decay from fission fragments leaving the daughter nucleus in a state of excitation above the binding energy of the last neutron. Then there is a possibility that this neutron may be emitted in the subsequent de-excitation process. Thus the total β-decay energy of the precursor and the neutron binding energy in the daughter enter as major parameters in studies of delayed neutron emission.

On the basis of this picture the first approach to an estimate of delayed neutron emission probabilities for nucleides in the fission product region was given by Pappas [3]). The results, although inherently crude, proved valuable in interpreting some of the characteristics and phenomenae associated with the delayed neutron emission in fission [3, 4]). These original calculations have since been improved independently by Keepin [5]) and by Pappas [6]).

Due to the influence of closed shells in lowering nucleon binding energies it

† Present address: SC-Division, European Organization for Nuclear Research, CERN, Geneva, Switzerland.

has generally been assumed that the delayed neutron precursors are limited to regions just beyond closed neutron shells [3, 7, 8]). The probability curves given by Pappas were therefore used for the development of a "systematics" of delayed neutron precursors beyond the 50 and the 82 neutron closed shells [6]).

In the present paper the systematics is extended to cover the whole region of nucleides with a view to getting a method of deciding whether delayed neutron precursors can be expected to be found also outside closed shell regions. Ultimately an investigation of the influence of closed nucleon shells on the general trends of the systematics was also aimed at.

Together with yield calculations of nucleides formed in fission [3]) and spallation [9]) such systematics would be valuable for the identification of short-lived nucleides showing the characteristics of delayed neutron precursors by using different nuclear reactions for their production.

2. Theory of Delayed Neutron Emission Probability

In their comprehensive treatment of nuclear fission Bohr and Wheeler [2]) discuss emission of delayed neutrons on the basis of the liquid drop model nucleus and the Fermi β-decay theory.

When departing from the β-stability line into the neutron rich region of the valley of nuclear stability the total β-decay energy — ground to ground state transition — will, on the average, increase while the binding energy of the last neutron will decrease.

Thus from a certain distance the β-decay energy Q_Z^β of a nucleide (Z, N) is expected to exceed the neutron binding energy B_{N-1} in the daughter nucleide $(Z+1, N-1)$. In this region the product nucleus after the β-decay can be left in excited states which have energies above the neutron binding energy. The probability for this to occur will necessarily increase in the neutron rich region or in regions just above closed neutron shells where nuclei show anomalously low neutron binding energies. In the latter regions $Q_Z^\beta > B_{N-1}$ rather close to stability. As already emphazised it is in these regions where the delayed neutron precursors have been expected to occur and where they have also been experimentally found, except for the 4.1 sec ^{17}N and the 1.3 min ^{210}Tl.

The de-excitation of the excited daughter nucleide $(Z+1, N-1)$ can take place either by γ-emission to lower states or by evaporation of a neutron. In the latter case the neutron emitting state is populated by decay from the parent while the neutron emission from the daughter is instantaneous. Thus the neutrons will be delayed for the observer showing the half-life of the precursor † as illustrated in fig. 1.

† In the nomenclature proposed by Keepin [10]) and now generally adopted, the parent nucleide (Z, N) and the daughter nucleide $(Z+1, N-1)$ are termed delayed neutron precursor and delayed neutron emitter, respectively.

The arguments given above form the basis of the theory of delayed neutron emission probability as developed just above the 50 and the 82 closed neutron shells [3,5,6]). In short, the results show that delayed neutron precursors in fission must be nucleides having closed shell plus 2 or a few more neutrons. The main features of this theory will now be outlined and the basis laid for an extension of the systematics to cover the whole table of nucleides.

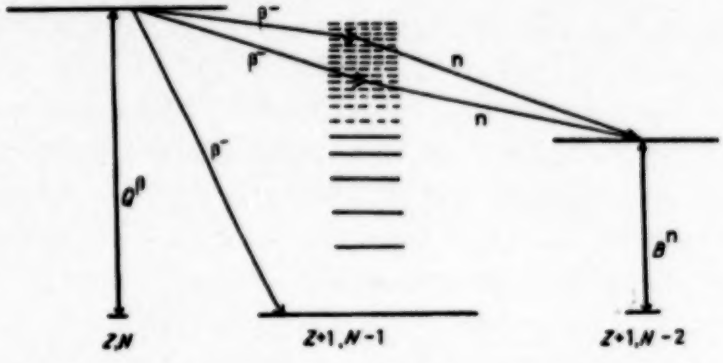

Fig. 1. Schematic representation of delayed neutron emission.

According to the Fermi theory of β-decay the probability for a transition to a state in the daughter nucleide with energy E above the ground state depends on the energy available, i.e. on $(Q_Z^{\beta}-E)$, and on the matrix element M of the transition involved. If $\rho_{Z+1}(E)$ gives the level density of the daughter at the excitation energy E then the probability for reaching a state within the energy interval E to $E+\mathrm{d}E$ is given by

$$W(E)\mathrm{d}E = \text{const.}\ |M|^2 f(Z+1, Q_Z^{\beta}-E)\rho_{Z+1}(E)\mathrm{d}E. \tag{1}$$

Here $f(Z+1, Q_Z^{\beta}-E_{Z+1})$ is the Fermi function.

The subsequent de-excitation of this state by neutron or by gamma emission will depend on the partial widths Γ_n and Γ_γ for these processes and their energy dependence. The neutron emission probability is given by

$$p(\mathrm{n}) = \frac{\Gamma_n}{\Gamma_n+\Gamma_\gamma}, \tag{2}$$

which multiplied with eq. (1) gives the fraction of the excited states decaying by neutron emission only. The total number of neutron emitting states is obtained by integration between B_{N-1} and Q_Z^{β}. Normalizing this to the total number of excited states in $(Z+1, N-1)$ one gets

$$P(\mathrm{n}) = \frac{\int_{B_{N-1}}^{Q_Z^{\beta}} \frac{\Gamma_n}{\Gamma_n+\Gamma_\gamma} |M|^2 f(Z+1, Q_Z^{\beta}-E)\rho_{Z+1}(E)\mathrm{d}E}{\int_0^{Q_Z^{\beta}} |M|^2 f(Z+1, Q_Z^{\beta}-E)\rho_{Z+1}(E)\mathrm{d}E} \tag{3}$$

which is the probability for delayed neutron emission from the delayed neutron precursor (Z, N) [3, 5, 6]. This formula can, however, not be straightforwardly evaluated.

No detailed information is available about the matrix elements involved and only general conclusions can be drawn about the degree of forbiddeness of the involved transitions. It has, however, been shown by Batchelor and Hyder [11]) and also by others that the energy spectra of the delayed neutrons emitted are essentially continuous. This points towards a high density of levels in the neutron emitter above the neutron binding energy. Thus the β-decay can be assumed to proceed by a high multiplicity of branches, and from a classical point of view the probability of allowed transitions should be expected to be high. The simplest assumption that can be made then, is that the matrix elements do not show any systematic variation with the energy of the final state in the β-decay. M can then be replaced by a constant value.

The Fermi function is a non-analytic integral which has been evaluated numerically by Moszkowski [12]) and by Feenberg and Trigg [13]). As a first approximation this function is proportional to the fifth power of the energy difference involved. On the basis of the uncertainties inherent in the estimate of the parameters in eq. (3) as discussed later one of the present authors chose in previous treatments [3, 6]) to replace the Fermi' function by this fifth power dependence, i.e.

$$f(Z+1, Q_Z^{\beta}-E) \approx \text{const.}\ (Q_Z^{\beta}-E)^5. \tag{4}$$

Keepin [5]), however, with access to an electronic computer used the true Fermi function and arrived at essentially the same results.

The partial width for neutron emission Γ_n equals zero at an excitation energy equal to the neutron binding energy. At higher excitation it increases rapidly with energy. The gamma width Γ_γ varies little and is essentially constant from level to level in a given nucleide [14]). Only crude values of Γ_n and Γ_γ are available, but sufficiently is known [15]) to conclude that for s- or p-wave neutrons the ratio in eq. (2) increases from zero to unity when the excitation energy goes from B_{N-1} to $B_{N-1}+50$ keV. The energies involved, however, cannot at present be estimated to better than 0.1—0.2 MeV. Therefore, no significant error is introduced by setting the width factor equal to unity.

The level density function is usually represented by a formula of the following type [16]):

$$\rho_{Z+1}(E) = C \exp 2(aE)^{\frac{1}{2}}, \tag{5}$$

where the constants C and a depend on the nucleus under consideration. Using empirically determined values of C and a ($a \approx 10/A$ [17])) this formula is expected to give the right order of magnitude of the level density for stable and near stable nucleides in regions away from closed shells [16]). Newton [18]) and

others have shown that it is preferable to use a fictitious excitation energy in eq. (5) in order to correlate nuclear pairing and closed shell effects. Thus it is recommended to express the level density by

$$\rho_{Z+1}(E) = C \exp a(E-E_c)^{\frac{1}{2}} \tag{6}$$

where E_c is a characteristic level free of even-odd and closed shell effects; or even by more improved formulas [19]). Considering the crudeness of our approach the validity of introducing this refinement in a general treatment of the present problem can be questioned. Moreover, very little is known about the real shape of the nuclear energy surface in the region far from stability which is of interest for the estimate of the parameter E_c and we do not know if the level density variation is the same as for near stable nucleides from which the eq. (6) is deduced. Nevertheless one should presume that such refinements just above closed shell where the nucleides concerned are closer to stability would make the results more reliable. That the probability curves, however, given in ref. [3]) without and in ref. [6]) with the introduction of the characteristic level, but otherwise based on similar estimates of Q_Z^β and B_{N-1} are much alike can be ascribed to the large partial weight of the energy parameters Q_Z^β and B_{N-1} in the final results. These parameters occur approximately in the sixth power in $P(\mathrm{n})$ depressing the other ones to a very large extent.

The parameter in which $P(\mathrm{n})$ should finally be expressed in order to compare various precursors and emitters should be characteristic of each precursor. For this parameter Pappas [3]) introduced the distance of the delayed neutron precursor (Z, N) from the most stable charge † Z_{N-1} corresponding to the neutron number $N-1$ of the delayed neutron emitter $(Z+1, N-1)$, i.e. $Z_{N-1}-Z_\beta$.

Using this parameter both Q_Z^β and B_{N-1} can be given as simple functions on the basis of energies measured, extrapolated or calculated from mass formulas.

3. Delayed Neutron Precursors in Fission

The first evaluation [3]) of eq. (3) in a somewhat simplified form was done by using neutron binding energies estimated by extrapolation from values measured in the vicinity of stability. The β-decay energies involved were taken from β-decay systematics using the shell modified liquid drop formulation of the nuclear energy surface as given by Brightsen, Coryell and Pappas [20]).

On the basis of a thorough study of different mass formulas and their expectations Pappas [6]) was able to conclude that the mass formula recently given by Cameron [21]) is the most preferable one in studies of the present kind. It predicts first and second mass differences to a high degree of reliability. This formula was

† The values of Z_{N-1} are given by the crossing of the isotone lines $(N-1)$ with the lines of maximum stability (Z_A) [3]) and Z_β is identical with Z in the delayed neutron precursors.

therefore selected to compute the energies involved in the evaluation of eq. (3) just above closed neutron shells in the more refined treatment given in ref. [6]).

A more elaborate treatment of the same regions was made by Keepin [5]) who with access to an electronic computer used the unsimplified eq. (3). He obtained

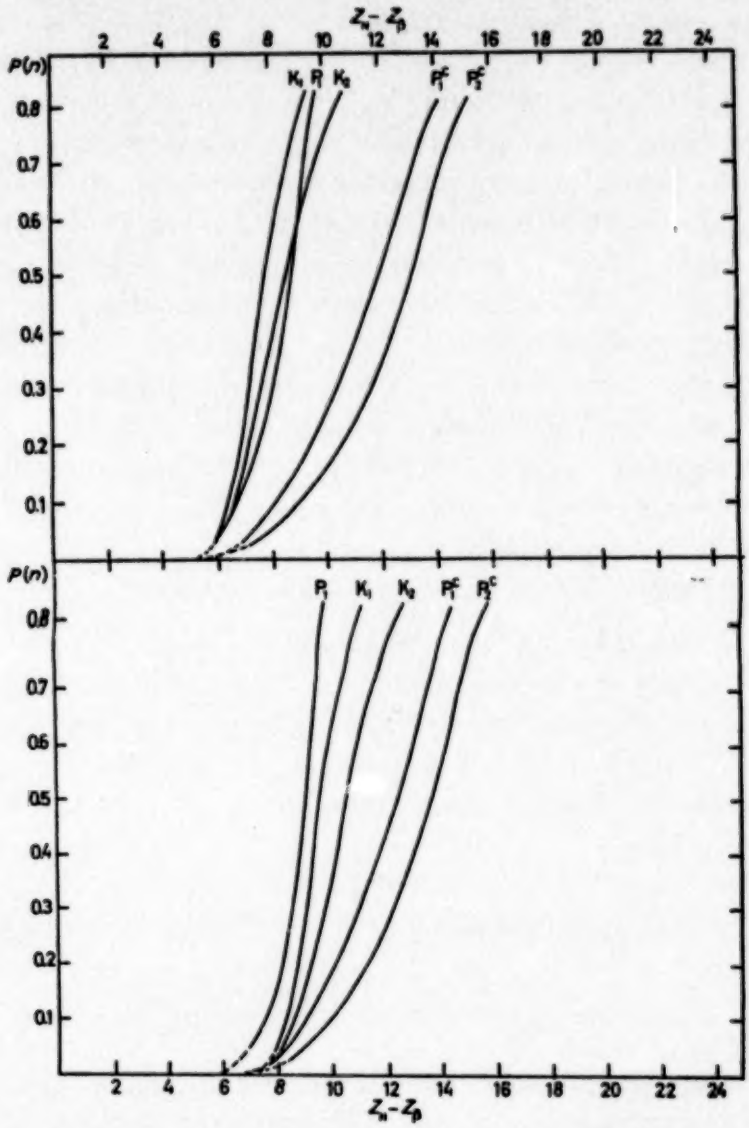

Fig. 2. Delayed neutron emission probabilities for nucleides just above the 50 neutron shell (Upper curves: odd Z precursors; lower curves: even Z precursors. P = Pappas [6]), K = Keepin [5]), P^c = Pappas [6]). Indices 1: even N; indices 2: odd N).

the energies involved partly as in (3) and partly using the Levy mass formula [22]). The latter is, however, not as well suited as the Cameron formula to treat regions influenced by closed nucleon shells [6]), i.e. those regions where previous delayed neutron studies have been performed.

The probability curves obtained by Keepin turned out to be quite similar to those given in ref. [3]) for odd Z precursors while for even Z precursors the results

in ref. [3]) give higher probabilities. All these results seem, however, to predict too optimistic values as compared with the results obtained in ref. [6]).

A comparison between the results of these three estimates [3, 5, 6]) can be made from figs. 2 and 3. The true probabilities should presumably be found between the curves of refs. [3, 5]) and those of ref. [6]).

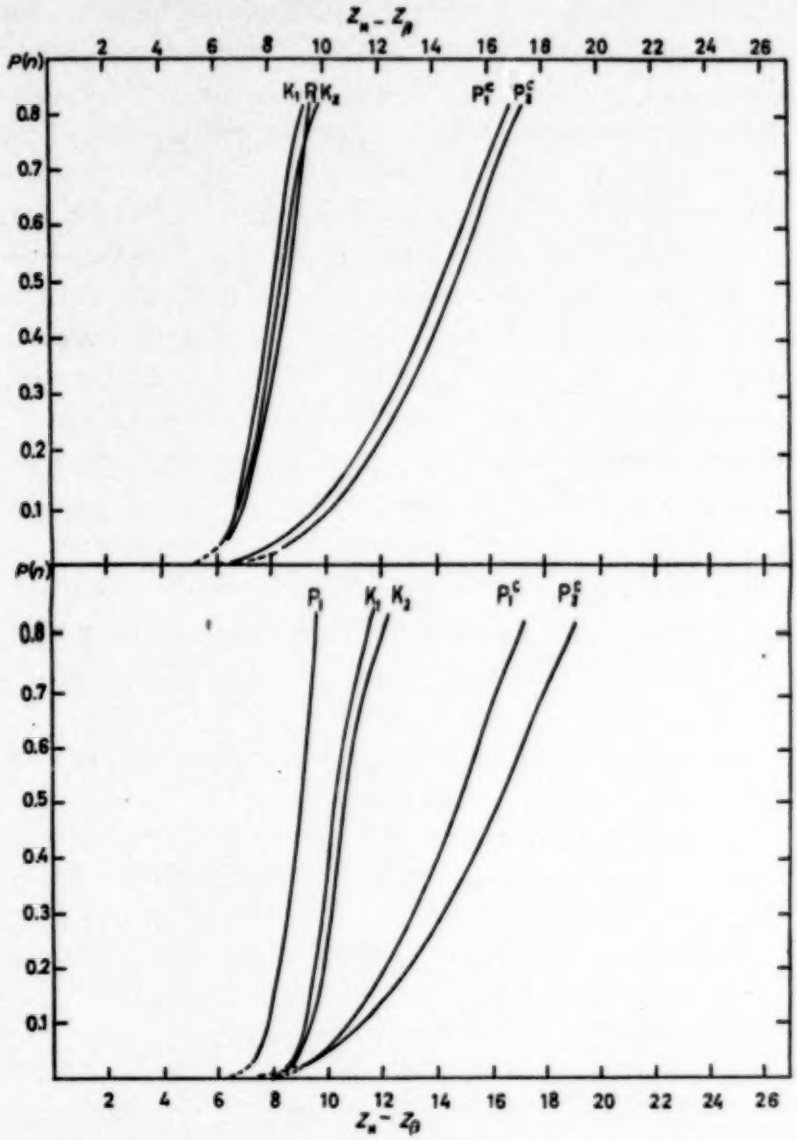

Fig. 3. Delayed neutron emission probabilities for nucleides just above the 82 neutron shell. (Upper curves: odd Z precursors; lower curves: even Z precursors. P = Pappas [3]), K = Keepin [5]), P^c = Pappas [6]). Indices 1: even N; indices 2: odd N).

From the latter curves a systematics of delayed neutron precursos has been developed for nucleides just above the 50 and the 82 neutron shells [6]). The results of this systematics will be discussed in connection with the general systematics developed later in this paper.

The maximum number of possible delayed neutron precursors expected in

thermal neutron induced fission of uranium is according to Pappas [6]) about 50. These nucleides are grouped into two parts having neutron numbers equal to or higher than 52 and 84, respectively, and will of course show up in highly different yields.

The number of precursors expected seems high and considerably exceeds the six generally accepted previously [4]). The excistence of only six has, however, been questioned [6]) on the basis of the spread in half-lives and yields as given by different authors, and in the spread in delayed neutron emission probabilities as calculated from "observed" delayed neutron yields and estimated fission yields of the respective precursor nucleides.

Using a pre-selection in addition to theoretical estimates based on four criteria † governed by the properties of the six "known" delayed neutron groups[4]) Keepin [5]) reduces the number of the possible delayed neutron precursors in fission by about one half. By further use of this approach Keepin is able to make predictions for each of the six "known" delayed neutron groups. He concludes that only some isotopes of bromine and iodine should contribute to the total delayed neutron yields.

The feasibility of the prediction of delayed neutron precursors on the basis of experimental information of the six delayed neutron groups can be doubted, but whatever treatment is accepted the prospective delayed neutron precursors is much larger than six. This was suggested by Pappas [3]) already in the first treatment of this problem, an idea now shared with Coryell [23]) and with Cameron [24]).

Until recently, however, no experimental support for this point of view has been available.

Parallel with the refined theoretical approaches to the problem Perlow and Stehney [25, 26]) have experimentally identified new delayed neutron precursors in fission. Using very fast techniques they were able to prove chemically that each of the four longest of the "known" delayed neutron periods contains one isotope of bromine and one of iodine, except the longest one which is due to an isotope of bromine only. The probability that this dualty holds also for the two shorter periods seems to be supported from half-life systematics. The experiments of Perlow and Stehney, however, show without doubt that the previously accepted and "accurately known" delayed neutron half-lives are composites of at least two components with different or similar half-lives and that the analysis of the gross delayed neutron decay curve into six components is artifical.

This conclusion is also supported by the delayed neutron studies in spontaneous fission of ^{252}Cf by Cox and collaborators [27]). Due to the displacement of the light peak in the yield mass curve of about 15 mass numbers with respect to

† Those criteria are: 1). Half-life must be within the range of "known" delayed neutron periods. 2). $Q_{Z^\beta} > B_{N-1} - 1$ MeV to allow for uncertainties in Q_{Z^β} and B_{N-1}. 3). Constancy of observed P(n) values. 4). Reasonable agreement between experimental and theoretical P(n) values.

the light peak in the curve for thermal neutron fission of ^{235}U only the heavy fragments will contribute to delayed neutron precursors in ^{252}Cf. The results found can therefore only be explained that in addition to isotopes of iodine more heavy fragment precursors must contribute to the delayed neutrons; these precursors should also be present in ^{235}U fission. An indication along the same lines may also be found in the work by Cowan and Orth [28]). These authors studied the diffusion and volatilization of fission products, and conclude that most of the delayed neutron precursosrs are isotopes of bromine and iodine but they do not exclude the possibility of significant admixtures of isotopes of other elements.

That only isotopes of bromine and iodine are identified may support the limitations introduced by Keepin by use of selection criteria. It does not, however, exclude also isotopes of other elements as contributors. It is well known that chemical isolation of bromine and iodine can be done exceedingly fast due to the volatility of these elements while the chemical isolation of the other elements proposed (except for krypton and xenon) is very tedious compared to the half-lives of interest in these studies, the order of seconds or less †.

The work of Perlow and Stehney [26]) gives therefore experimental support to the validity of the theoretical approach to the delayed neutron emission probabilities, as well as to the systematics developed. Thus it seems feasible to extend this systematics to cover also the regions outside closed neutron shells, i.e. the whole table of nucleides.

During the course of this work John and Lombard [29]) made a partial survey of the known nucleides for delayed neutron precursors using energy systematics coupled with strong selection criteria ††. Their results, however, do not go any further than previous estimates [3, 5, 6]).

4. Delayed Neutron Precursor Systematics

The nuclear energy surface is well known only for stable and near stable nuclei [20]). On this basis it is ordinarily assumed that the parabolic surfaces in the configuration space for the mass of a nucleide as a function of its mass number and proton number extend far into the neutron rich and neutron deficient regions.

When nuclear level densities are concerned the formula given by eq. (5) is only expected to give order of magnitude estimates in nuclei not to near closed shells. The improved equations are better approximations, but their validity far into the neutron rich region is not established. Consideration of the possible

† When half-lives shorter than few seconds are concerned even bromine and iodine chemistry is long.

†† These criteria are: 1). The precursor should have odd Z. 2). The neutron number should exceed one of the closed shells by either two or three. 3). A reasonable amount of information on the β^- emitter should be available.

limitations of both the parabolic energy surface and the level density formula is therefore important in the following approach to a general systematics. This approach concerns nucleides which are neutron rich to a much higher degree than those discussed in the previous section.

It was therefore found appropriate to base the general systematics mainly on energy considerations. As basis the Cameron mass formula [21]) is chosen because this is known [6]) to represent first and second order mass differences to a high degree of accuracy. In this formula nucleon pairing and shell correction terms are built in independent of how far from stability a nucleide is found. The isobaric curves turn out not to be purely parabolic as the nuclear energy surface near stability would predict. With the discussed limitations in mind, it is felt, however, that an approach as indicated is with our present knowledge the best one for an evaluation of $P(\mathrm{n})$ far into the neutron rich region where no experimental data are available.

The neutron binding energy of isotones decreases with decreasing number of protons in the nuclei. Therefore delayed neutron precursors can only be expected in the neutron rich region of the stability valley †.

The main step in the development of the delayed neutron precursor systematics is according to the previous discussion in this paper a comparison of the β-decay energy of the precursor with the neutron binding energy of the emitter, i.e. Q_Z^{β} with B_{N-1} and the use of this in equation (3) to estimate the delayed neutron emission probability $P(\mathrm{n})$.

In this way the upper Z limit in fig. 4 is obtained for isotones that may be delayed neutron precursors. The lower Z limit is governed by the spontaneous emission of neutrons.

The results obtained in fig. 4 give the general delayed neutron systematics and the influence of closed nucleon shells on this.

The general results can be summarised as follows:

1) The delayed neutron precursors must possess very short half-lives except in regions beyond closed shells where the half-lives might be long.

2) The probability for delayed neutron emission from a given (odd, even) type of precursor nucleide increases with increasing distance $(Z_{N-1}-Z_{\beta})$ from stability.

3) The minimum value of $(Z_{N-1}-Z_{\beta})$ for which a nucleide might show the characteristics of delayed neutron precursors depends mainly on the eveness and oddeness of Z_{β}.

This is caused by the pairing energies involved in Q_Z^{β} and B_{N-1} which result in favouring odd Z nucleides above even Z nucleides ††. Thus for a given probability

† In the neutron deficient region delayed proton emitters could be expected if it were not for the potential barrier, i.e. $Q_Z^{\beta} > B^{\mathrm{p}}{}_{Z-1} + B_{\mathrm{c}}$. Thus only in the lightest nuclei where the potential barrier B_{c} is small, can delayed proton precursors be expected to have measurable half-lives.

†† Note that even-proton (neutron), odd-neutron (proton) precursors give odd-proton (neutron), even-neutron (proton) emitters.

odd Z precursors are about two units in $(Z_{N-1}-Z_\beta)$ closer stability than even Z precursors.

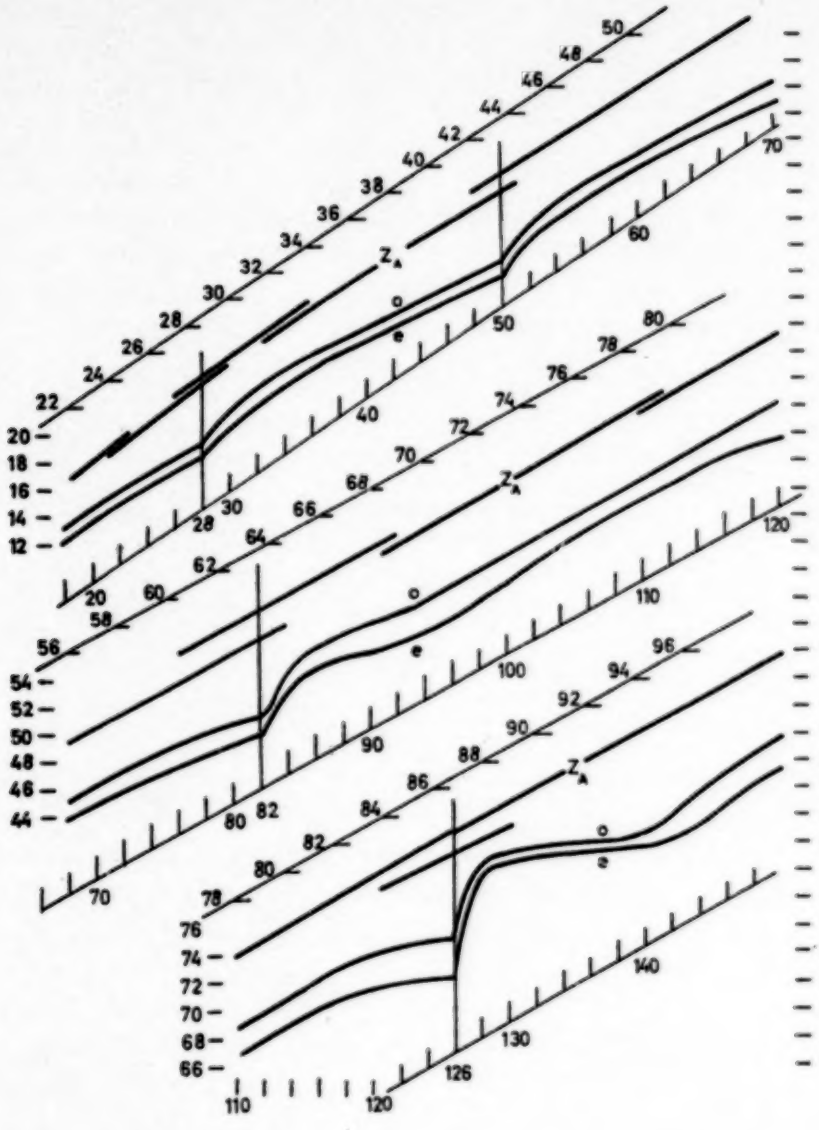

Fig. 4. Systematics of delayed neutron precursors and the influence of closed neutron shells on this systematics. (Z_A: β-stability line [20]). Ordinate: charge number; abcissa: neutron number. Curve o: upper limit for odd Z nucleides showing characteristics of delayed neutron precursors; curve e = = upper limit for even Z nucleides showing characteristics of delayed neutron precursors).

4) The average minimum distance from stability $(Z_{N-1}-Z_\beta)$ for odd Z delayed neutron precursors increases from about 3 for light nuclei to about 8 for heavy nuclei. This is due to the opening of the valley of stability with mass number which lowers the β-decay energy to a greater extent than the neutron binding energy.

These general trends of the delayed neutron precursor systematics are influenced by closed neutron shells as clearly shown in fig. 4:

1) Just above closed shells the upper limit for delayed neutron emission is moved towards stability. This effect increases with higher shell numbers and is roughly 1, 2, 3 and 5 charge units at the 28, 50, 82 and 126 neutron shell respectively.

2) With increasing distance from the shell the influence of the shell effect diminishes as follows: For a given type of nucleides the probability curves are displaced 0.2 and 0.4 charge units on the average towards larger $Z_{N-1}-Z_\beta$ values for each increase of 2 in the neutron number for even and odd N precursors, respectively.

All delayed neutron precursors identified among the fission products, i.e. the isotopes of bromine with mass numbers 87—92 and the isotopes of iodine with mass numbers 137—141 are in fig. 4 found under the curve giving the upper limit for delayed neutron precursors of odd Z nucleides in accordance with what one should expect. Also ^{210}Tl known as a delayed neutron precursor is given as such in fig. 4.

As pointed out in earlier papers [3, 6, 23, 24]) and shwon by Perlow and Stehney [25, 26]) the delayed neutron precursors should be more frequent present among the fission products with neutron numbers just above closed neutrons shells than previously anticipated. This view is also supported by fig. 4.

The results of the systematics developed in the present paper show moreover that the properties of delayed neutron precursors might frequently be present also among nucleides outside closed shell regions. As these prospective delayed neutron precursors necessarily must possess very short half-lives, their identification is entirely based on the development of new experimental techniques which should be coupled with half-life systematics of neutron rich nucleides.

The authors are indepted to Drs. A. G. W. Cameron and A. F. Stehney for prepublication information of their work.

The authors are glad to expres their sincere thanks to the Nansenfondation in Norway for supporting grants, which made the collaboration in this work possible.

Note added in proof: In a recent letter to Nature, Rudstam, Svanheden and Pappas report new delayed neutron precursors in the mass region below copper.

Appendix

TABLE 1

Upper Z limits for nucleides showing characteristics of delayed neutron precursors. The A values given are the highest integer mass number above the limits given in fig. 4. These nucleides will necesserily have quite different $P(n)$ values (cf. eq. (3)).

Odd-proton precursors				Even-proton precursors			
Z	A	Z	A	Z	A	Z	A
11	27	57	145	12	30	58	154
13	31	59	152	14	35	60	159
15	36	61	158	16	40	62	164
17	41	63	163	18	46	64	169
19	47	65	169	20	50	66	174
21	51	67	175	22	54	68	180
23	55	69	180	24	59	70	186
25	60	71	186	26	65	72	196
27	65	73	191	28	71	74	201
29	72	75	201	30	77	76	203
31	78	77	204	32	83	78	206
33	83	79	206	34	86	80	209
35	87	81	210	36	91	82	224
37	91	83	224	38	95	84	230
39	96	85	229	40	101	86	234
41	102	87	233	42	107	88	240
43	107	89	238	44	112	90	244
45	113	91	244	46	119	92	249
47	119	93	249	48	125	94	255
49	125	95	255	50	133	96	261
51	133	97	261	52	136	98	267
53	137	99	267	54	139	100	274
55	140			56	147		

References

1) R. Roberts, R. C. Meyer and P. Wang, Phys. Rev. **55** (1939) 510
2) N. Bohr and J. A. Wheeler, Phys. Rev. **56** (1939) 426
3) A. C. Pappas, American Report LNS-MIT-63, AECU-2806 (1953), Part IV; Inaugural Dissertation, University of Oslo
4) G. B. Keepin and T. F. Wimett, Proc. Intern. Conf. on the Peaceful Uses of Atomic Energy, Geneva 1955 (United Nations, New York, 1956) Vol. **4**, p. 162
5) G. R. Keepin, J. Nucl. Energy **7** (1958) 13
6) A. C. Pappas, Proc. Sec. Intern. Conf. on the Peaceful Uses of Atomic Energy, Geneva 1958 (United Nations, Geneva, 1958) Vol **15**, p. 373
7) M. G. Mayer, Phys. Rev. **74** (1948) 235
8) C. D. Coryell and N. Sugarman, Editors note in Paper 52, National Nuclear Energy Series, Div. IV, **9** (McGraw-Hill, New York, 1951)
9) G. Rudstam, Inaugural Dissertations, University of Uppsala (1956)
10) G. R. Keepin, Progr. Nucl. Energy **1** (1956) 191
11) R. Batchelor and H. R. Mck. Hyder, J. Nucl. Energy **3** (1956) 7
12) S. A. Moszkowski, Phys. Rev. **82** (1951) 35

13) E. Feenberg and G. Trigg, Rev. Mod. Phys. **22** (1950) 399
14) D. J. Hughes and R. L. Zimmerman, in Nuclear Reactions I, ed. by P. M. Endt and M. Demeur North-Holland Publishing Co., Amsterdam, 1959) Chapter VIII, § 4
15) J. Feshbach, C. E. Porter and V. F. Weisskopf, Phys. Rev. **96** (1954) 448
16) J. M. Blatt and V. F. Weiskopf, Theoretical Nuclear Physics (John Wiley and Sons, New York, 1952)
17) J. B. Lang and K. J. LeCouteur, Proc. Phys. Soc. A **67** (1954) 586
18) T. D. Newton, Can. J. Phys. **34** (1956) 804
19) A. G. W. Cameron, Can. J. Phys. **36** (1958) 1040
20) R. A. Brightsen, C. D. Coryell and A. C. Pappas, see C. D. Coryell, Ann. Rev. Nucl. Sci. **2** (1953) 305
21) A. G. W. Cameron, Canadian Report CRP-690/AECL-433 (1957)
22) H. B. Levy, American Report UCRL-4588 (1955)
23) C. D. Coreyell, personal communication to A. C. Pappas (1957)
24) A. G. W. Cameron, personal communication to A. C. Pappas (1958)
25) G. J. Perlow and A. F. Stehney, Phys. Rev. **107** (1957) 776
26) A. F. Stehney and G. J. Perlow, Proc. Sec. Intern. Conf. on the Peaceful Uses of Atomic Energy, Geneva 1958 (United Nations, Geneva, 1958) Vol. **15**, p. 384; see also Phys. Rev. **113** (1959) 1269
27) S. Cox, P. Fields, A. Friedman, R. Sjoblom and A. Smith, Phys. Rev. **112** (1958) 960
28) G. A. Cowan and C. J. Orth, Proc. Sec. Intern. Cont. on the Peaceful Uses of Atomic Energy, Geneva 1958 (United Nations, Geneva, 1958) Vol. **7**, p. 328
29) W. John and F. J. Lombard, J. Inorg. Nucl. Chem. **11** (1959) 81

3.A

Nuclear Physics **21** (1960) 367—382; © *North-Holland Publishing Co., Amsterdam*

Not to be reproduced by photoprint or microfilm without written permission from the publisher

GROUND STATE GAMMA TRANSITIONS FROM STATES AT 10.09 AND 10.24 MeV in N^{14} AND REINVESTIGATION OF THE 9.17- AND 10.43-MeV GAMMA RAY DISTRIBUTIONS

H. J. ROSE, F. RIESS and W. TROST

Physikalisches Institut der Universität Freiburg, Freiburg i. Br., Germany †

Received 25 July 1960

Abstract: The angular distributions of the ground state transitions from the N^{14} 9.17- and 10.43-MeV levels have been reinvestigated using the reaction $C^{13}(p, \gamma)N^{14}$ at the 1.75- and 3.11-MeV resonances. From the value obtained for the anisotropy of the $9.17(J^\pi = 2^+) \rightarrow 0(J^\pi = 1^+)$ transition limits on the quadrupole-dipole mixture are obtained. The 10.43-MeV state is assigned $J = 2$ using the results of previous investigations. From a distribution measurement limits are set on the quadrupole-dipole mixture in the $10.43 \rightarrow 0$ transition. A strong, energy dependent $\cos\theta$ term was observed in the angular distribution of the ground state gamma rays for proton bombarding energies between 2.7 and 3.2 MeV. For this energy range the (p, γ) excitation functions have been determined at angles of 0°, 90° and 140° with respect to the proton beam and additional distribution measurements have been made in the neighbourhood of the 3.11-MeV resonance. The theoretical fits of these data present evidence that the $\cos\theta$ term mainly arises from interference between the 10.43-MeV level and "non-resonant background" caused by the "long tailed" 0.55-MeV resonance corresponding to the 8.06-MeV, $J^\pi = 1^-$, $T = 1$ state. In as much as this explanation of the $\cos\theta$ term is likely the 10.43-MeV level must have even parity. Rather marked variations of the strength of the $\cos\theta$ term at proton bombarding energies of 2.75 and 2.90 MeV show the presence of levels at 10.09- and 10.24-MeV excitation energy in N^{14} which decay extremely weakly to the ground state. The 10.09-MeV state is also clearly observed in the excitation functions. Estimates of the total widths and gamma widths of both these states are obtained from the excitation functions. Gamma rays from states at 10.09 and 10.24 MeV have not been reported previously.

1. Introduction

A detailed investigation of the decay modes of the 9.17-MeV excited state in N^{14} has been made recently [1, 2]. Comparison of the results of this investigation with shell model calculations [3, 4] leads to the conclusion that the 9.17-MeV $J^\pi = 2^+$ state arises in part from the p^{-2}(i.e. s^4p^{10}) configuration as a $(J, T) = (2,1)$ state. Furthermore, the gamma width and the proton reduced width of the 9.17-MeV state give evidence [4]) that this state cannot be purely p^{-2}. Another (2,1) state arising from $p^8(s, d)$ is expected around 10-MeV excitation energy and it has been pointed out in ref. [4]) that this configuration probably contributes appreciably to the eigenfunction of the 9.17-MeV state. However, as a consequence of these considerations it appears that in the group of levels

† Work supported in part by the German Ministerium für Atomkernenergie.

known experimentally between 8 and 10.5 MeV another $T = 1$ state with $J^\pi = 2^+$ is likely to be expected besides the one at 9.17 MeV and this other (2,1) state also should arise from p^{-2} and $p^8(s, d)$. Preliminary results of the present authors on the decay scheme of the 10.43-MeV state indicate that this state shows decay modes quite similar to the ones observed from the decay of the 9.17-MeV $J^\pi = 2^+$ state. Further arguments have been advanced in ref. [4]) that — if there is another (2,1) state in the group of levels known experimentally between 8 and 10.5 MeV which also arises (partially) from p^{-2} — it seems that it must be the 10.43-MeV state.

The anisotropy of the $9.17 \rightarrow 0$ gamma ray distribution has been measured previously by Woodbury *et al.* [5]) who obtained $A = -(0.48 \pm 0.03)$, while in the case of the $10.43 \rightarrow 0$ transition the angular distribution has been determined by Willard *et al.* [6]) who obtained $W(\theta) = 1-(0.50 \pm 0.03)\cos^2\theta$ at a proton bombarding energy corresponding to maximum yield from a $C^{13}(p, \gamma)N^{14}$ resonance at (3.11 ± 0.01) MeV using a thin target (thickness smaller than 5 keV at a proton bombarding energy $E_p = 3.11$ MeV). The gamma width of the $9.17 \rightarrow 0$ transition and the total width have been determined by Hanna and Meyer-Schützmeister [7]) from gamma resonance scattering experiments as $\Gamma_\gamma = (8.7 \pm 1.5)$ eV and $\Gamma = (77 \pm 12)$ eV, respectively. The gamma width of the $10.43 \rightarrow 0$ transition, $(2J+1)\Gamma_\gamma = 85$ eV, was obtained from absolute cross section measurements by Willard *et al.* [6]).

Present available experimental and theoretical information on M1 transitions in self-conjugate nuclei [8]) shows that no conclusion about E1 character of the $9.17 \rightarrow 0$ transitions should be drawn from the observed gamma widths of these transitions. In fact, calculations of Elliott [9]) and Warburton and Pinkston [4]) show that a gamma width of approximately 25 eV for M1 should be expected if one of these states were arising purely from p^{-2} as (2,1) state. However, it can be concluded from the values obtained for Γ_γ that both the transitions ($9.17 \rightarrow 0$ and $10.43 \rightarrow 0$) must be mainly dipole in character.

The values reported for the total width of the 10.43-MeV level differ: from $C^{13}(p, \gamma)N^{14}$ a value $\Gamma = (30 \pm 3)$ keV has been obtained [6]) while from $C^{13}(p, p)C^{13}$ a value $\Gamma = (80 \pm 10)$ keV is reported by Zipoy *et al.* [10]) who located the resonance at (3.12 ± 0.03) MeV corresponding to a level at 10.44 MeV. The only reported branch in the decay of the 10.43-MeV state leads to the 6.44-MeV excited state with a relative intensity of 10 % [6]).

A conclusive spin assignment to the 10.43-MeV state can be given on the basis of present available experimental knowledge: the 6.44 MeV state has been recently assigned [2]) $J = 3$. Using the value of 10 % for the intensity of the branch from the 10.43-MeV to the 6.44 MeV state and the gamma width $(2J+1)\Gamma_\gamma = 85$ eV of the $10.43 \rightarrow 0$ transition Weisskopf matrix elements $|M(E2)|^2 > 300$ and $|M(M2)|^2 > 10^4$ are obtained if the $10.43 \rightarrow 6.44$ transition were quadrupole in character. Therefore, the transition must be predominantly

dipole in character, or — in turn — the 10.43-MeV state must have $J = 2$ †.

This assignment is in agreement with recent results of Kashy *et al.* [11]) obtained from $C^{13}(p, p)C^{13}$ which indicate that the 10.43-MeV level most probably has $J^\pi = 2^+$. Furthermore, Kashy *et al.* [11, 12]) observed a level corresponding to 10.24-MeV excitation energy in N^{14} ††.

The possible assignments of this state as obtained from preliminary analysis of the $C^{13}(p, p)C^{13}$ data are $J^\pi = 1^-$ or 0^- with 1^- more likely than 0^- ††† (an indicated assignment of $J^\pi = 1^-$ is reported in ref. [11]). The presence of a level at 10.24-MeV excitation energy in N^{14} ($E_p = (2.90 \pm 0.04)$ MeV) was formerly reported by Zipoy *et al.* [10]) from $C^{13}(p, p)C^{13}$. As a further level in the neighbourhood of the 10.43-MeV state a level at 10.51 MeV excitation energy in N^{14} is reported by Kashy *et al.* which also is indicated to have $J^\pi = 1^-$ [11]). This level has not been reported by Zipoy *et al.* [10]).

In the present paper an investigation of the angular distribution of the gamma rays from the $9.17 \rightarrow 0$ transition will be described together with a rather extensive study of the $10.43 \rightarrow 0$ distribution at proton bombarding energies on and off the 3.11-MeV resonance in the reaction $C^{13}(p, \gamma)N^{14}$. The observation of a strong $\cos\theta$ term in the angular distribution of the ground state gamma rays at bombarding energies slightly below and above the 3.11-MeV resonance leads to a detailed investigation of the (p, γ) excitation functions throughout the range of bombarding energies from 2.7—3.2 MeV. The excitation functions were measured at 0°, 90° and 140° with respect to the proton beam in order to determine the energy dependence of the $\cos\theta$ term over a wide range of bombarding energies. These investigations give evidence that the $\cos\theta$ term mainly arises from interference between the 10.43-MeV level and nonresonant "background" caused by the long "tail" of the 8.06-MeV, $J^\pi = 1^-$, $T = 1$ state. A state of extremely small gamma width at approximately 10.24 MeV influences the interference term. Furthermore, a ground state transition from a level at 10.095 MeV excitation energy in N^{14} is detected. This level and the 10.24-MeV level have not been reported previously from (p, γ) work. Results of Miller

† Preliminary results of the present authors about the decay modes of the 10.43-MeV state using three crystal pair spectrometer techniques indicate a further transition to the 7.02 MeV excited state of comparable strength. The angular distribution of this transition shows positive anisotropy. This is in agreement with both the 10.43-MeV and the 7.02-MeV level having $J = 2$.

†† Actually Kashy *et al.* report a level at 10.20-MeV excitation energy. However, they also give (in their latest report, ref. [11]) for the 10.43-MeV state an excitation energy of 10.415 MeV. Since the most accurate determination of this state seems to be the one obtained by Willard *et al.* [6]) from $C^{13}(p, \gamma)N^{14}$ (error ± 10 keV, using an analyser of the proton beam with an energy resolution better than 0.1 %) the value of 10.43 MeV has been adopted in the present paper. For the 10.24- (or 10.20-) MeV state an excitation energy of 10.24 MeV (corresponding to $E_p = 2.90$ MeV) has been used throughout this paper. The energy location of the 10.24-MeV state relative to the 10.43-MeV state as obtained from the present investigations is $-(200 \pm 30)$ keV, or (10.24 ± 0.035) MeV. A value (10.24 ± 0.04) MeV has been obtained previously by Zipoy *et al.* [10]).

††† E. Kashy, private communication. The authors are indebted to E. K. Warburton for communicating these results to them.

et al. [13]) obtained from $N^{14}(\alpha, \alpha')N^{14}$ have indicated a level corresponding to 10.05-MeV excitation energy in N^{14} and a level at 10.08 MeV with an indicated assignment of $J^\pi = 2^+$ has been recently reported from $C^{13}(p, p)C^{13}$ by Kashy *et al.* [11]).

The investigation of the $9.17 \rightarrow 0$ transition was made as a preliminary study to the detailed investigation of the 9.17-MeV state [1]) and yields information about the quadrupole contribution in the 9.17 $(J^\pi = 2^+) \rightarrow 0(J^\pi = 1^+)$ transition. The investigation of the angular distribution of the $10.43 \rightarrow 0$ transition and the study of the (p, γ) excitation functions for proton bombarding energies between 2.7 and 3.2 MeV yields further information about the parity of the 10.43-MeV state and about the level parameters of the states at 10.09 and 10.24 MeV. Limits on the quadrupole contribution in the $10.43 \rightarrow 0$ transition will be set.

2. The $9.17 \rightarrow 0$ Transition

The angular distribution of the 9.17-MeV gamma rays was obtained from 37 spectra taken at 7 different angles between 0° and 150° with respect to the proton beam. Detection of the gamma rays was accomplished using a 7.6 cm by 7.6 cm NaI(Tl) crystal mounted on a Dumont 6363 photomultiplier tube. The detector was mounted to rotate around the target a ta distance of (22.5 ± 0.1) cm from it. The spectra were recorded on a RIDL Model 3300 100-channel pulse height analyser. The counting rates at different angles were obtained from these spectra (of which each one corresponded to a fixed number of monitor counts) by summing up a certain number of channel counts of the 9.17-MeV radiation full energy loss, one and two quantum escape peaks. This method of evaluation automatically corrects for angle dependent gain shifts. Corrections for absorption were made. These corrections were in the order of 3 to 4 % except for one critical angle (120°) for which the correction was found to be in the order of 10 % (because the target was placed at 45° relative to the proton beam). Solid angle corrections were found to be negligible. The measurements were made at one (fixed) proton bombarding energy corresponding to maximum yield from the 1.75-MeV $C^{13}(p, \gamma)N^{14}$ resonance. The target was the same as described in ref. [1]). The protons were accelerated in the Freiburg University 5.5-MeV Research van de Graaff accelerator. Off resonance contributions were found to be smaller than 1.5 %.

A least squares fit of the data obtained in this manner for the angular distribution of the 9.17-MeV gamma rays gave $W(\theta) = 1 - (0.55 \pm 0.02) \cos^2 \theta$ with a limit on a possible $\cos^4 \theta$ term of $|a_4| < 0.02$ †. The error quoted is three times the least squares error of the fit. No indications for the presence of a

† In view of the experimental errors centre of mass corrections have been neglected throughout this paper.

$\cos\theta$ term have been found by comparison of corresponding counting rates relative to the plane perpendicular to the proton beam. This is not surprising in view of the extremely small proton width of the 9.17-MeV state. The anisotropy $A = -(0.55 \pm 0.02)$ obtained in the present investigation is slightly larger than the value $-(0.48 \pm 0.03)$ obtained previously by Woodbury *et al.* [5]).

Since the transition must be mainly dipole in character (see introduction) the spin of the 9.17-MeV level cannot be greater than 2 units. The theoretical angular distributions about the beam were calculated for the possible reaction and level parameters (inclusive of interference effects). Comparison with the experimentally determined value of A shows that the spin-parity assignments permitted by the anisotropy measurement are $J^\pi = 1^+$, 2^+ or 2^-, for which the experimental value of A can be fitted using suitable mixtures of channel spins and p—f-waves and reasonable limits on the quadrupole admixture in the gamma transition †. From other experimental information [2, 14]) the 9.17-MeV state recently has been assigned to $J^\pi = 2^+$.

The resonant reduced proton widths θ_p^2 were calculated using the value of the level width Γ of the 9.17-MeV state (see the Introduction). The values obtained are given in table 1. Corrections were made for the Thomas shift [16]).

TABLE 1

Proton reduced widths θ_p^2 (defined as in ref. [20])) of the 1.75-, 2.75-, 2.90- and 3.11-MeV resonances in the reaction $C^{13}(p, \gamma)N^{14}$. The values were calculated using $\Gamma = 77$ eV, 12 keV, 120 keV and 36 keV as total widths of the 9.17-, 10.09-, 10.24- and 10.43-MeV levels, respectively. Corrections for the Thomas shift have been made. The Wigner sum rule places an upper limit $\theta_p^2 < 4$. The 9.17- and 10.43-MeV states have $T = 1$, the 10.09- and 10.24-MeV level is assumed $T = 0$ (compare ref. [4])). Interaction radius $R = 4.7 \times 10^{-13}$ cm.

E_p (MeV) \ l	0	1	2	3	4
1.75	4×10^{-5}	8.8×10^{-5}	5.3×10^{-4}	8×10^{-3}	0.31
2.75	3.9×10^{-3}	6.4×10^{-3}	2.4×10^{-2}	0.36	∞
2.90	0.037	0.059	0.22	∞	∞
3.21	0.011	0.016	0.051	0.58	∞

† The experimental value of A excludes a spin-parity assignment of $J^\pi = 1^-$ to the 9.17-MeV level. In this case the 9.17-MeV state would have to be formed by d-wave protons or by a mixture of s- and d-waves. The effects of s- and d-wave interference terms were investigated together with quadrupole-dipole interference by calculating the angular distributions in terms of the relative matrix element $\delta = \pm|M(\mathrm{M2})|/|M(\mathrm{E1})|$ of quadrupole and dipole radiation for different mixing parameters $\varepsilon \cos\xi$ of s-and d-waves, where $\varepsilon = \pm|M(\mathrm{d})|/|M(\mathrm{s})|$ is the relative matrix element and ξ is the relative phase of s- and d-waves which is determined by the Coulomb field and the centrifugal barrier. For the formation of the 9.17-MeV state $\cos\xi$ is calculated to be -0.23 (interaction radius $R = 4.7 \times 10^{-13}$ cm). It is seen from this calculation that the only agreement between the experimentally determined A and theoretically possible values for A can be obtained for a certain region of ε values ($1 < \varepsilon < \infty$) with $|\delta| > 0.5$. In the case of $J^\pi = 1^-$ the gamma transition would have to be a mixture of E1 and M2 radiation. From the known gamma width of the $9.17 \rightarrow 0$ transition (introduction) a Weisskopf matrix element for M2 radiation of 1700 is calculated which clearly excludes $|\delta| > 0.5$.

The Wigner sum rule [17]) places an upper limit of 4 on θ_p^2, therefore partial waves with $l > 4$ are excluded, which — in turn — means that the 9.17-MeV $J^\pi = 2^+$ state could be formed by p- and f-waves. Also the limit placed on $|a_4|$ (combined with the value for A) does not exclude f-wave admixtures in the formation of the 9.17-MeV state by proton capture †. Assuming p-wave formation ($\varepsilon = 0$) of the 9.17-MeV state, limits on δ can be obtained. Comparison of the experimentally determined value for A and the values for A obtained from the formula given in the footnote yields $-0.07 < \delta < -0.04$. The choice of phase factors in the reduced matrix elements is that of Biedenharn and Rose [18]).

3. The 10.43 → 0 Transition and the Ground State Gamma Rays following Proton Bombardment between 2.7 and 3.2 MeV

The detection equipment used for the distribution measurements on the 10.43 → 0 transition and the evaluation of the data was the same as described in the previous section. For some of the measurements described in this section it was found necessary to use extremely thin and uniform targets which were prepared by cracking of 60 % enriched methyl iodide onto 0.2 mm platinum foils ††.

Fig. 1 shows the relative yield of gamma rays of energies greater than 9 MeV as a function of proton bombarding energy. A detailed discussion of the curves will be given later. From the resonance curves shown in fig. 1 a total width $\Gamma = (36 \pm 2)$ keV of a level at 10.43 MeV excitation energy in N^{14} is determined. An excitation curve for gamma rays of energies greater than 2.2 MeV (emitted in the forward direction) has been observed previously by Willard *et al.* [6]) who located the resonance at (3.11 ± 0.01) MeV corresponding to a level at 10.43-MeV excitation energy in N^{14}.

Angular distributions were measured at five different bombarding energies as indicated by the arrows in fig. 1. To determine the angular distributions at proton energies corresponding to the arrows (c) and (e) in fig. 1 very thin and uniform targets (thickness smaller than 3 keV) have been used. To obtain angular distributions corresponding to (a) and (b) a thicker target (45 keV) was used in order to assure reasonable counting rates. Therefore the arrows (a) and (b) label the average energy the protons had in this target. The angular distribution corresponding to (d) and using a thin target (thickness between 1 and 5

† For $J^\pi = 2^+$ the theoretical angular distribution function $W(\theta) = (1+\delta^2)(1+\varepsilon^2) - 0.350\,(1 - 0.700\,\varepsilon\cos\xi + 1.143\,\varepsilon^2)(1 - 4.472\delta - 0.714\delta^2)P_2(\cos\theta) + 0.381\,\varepsilon\delta^2(\varepsilon - 4.898\cos\xi)P_4(\cos\theta)$ is obtained, with $\varepsilon = \pm|M(\mathrm{f})|/|M(\mathrm{p})|$ and $\delta = \pm|M(\mathrm{E2})|/|M(\mathrm{M1})|$ being the relative matrix elements of f- and p-waves and quadrupole and dipole contributions, respectively. $\cos\xi = -0.78$ (explanation of ξ as in the preceding footnote). It is seen from this formula that, if $\delta \to 0$, a_4 vanishes as δ^2. Furthermore, it turns out that A obtained for pure f-wave formation is not much different from A obtained for pure p-wave formation.

†† The authors are indebted to F. Uihlein for the preparation of these targets.

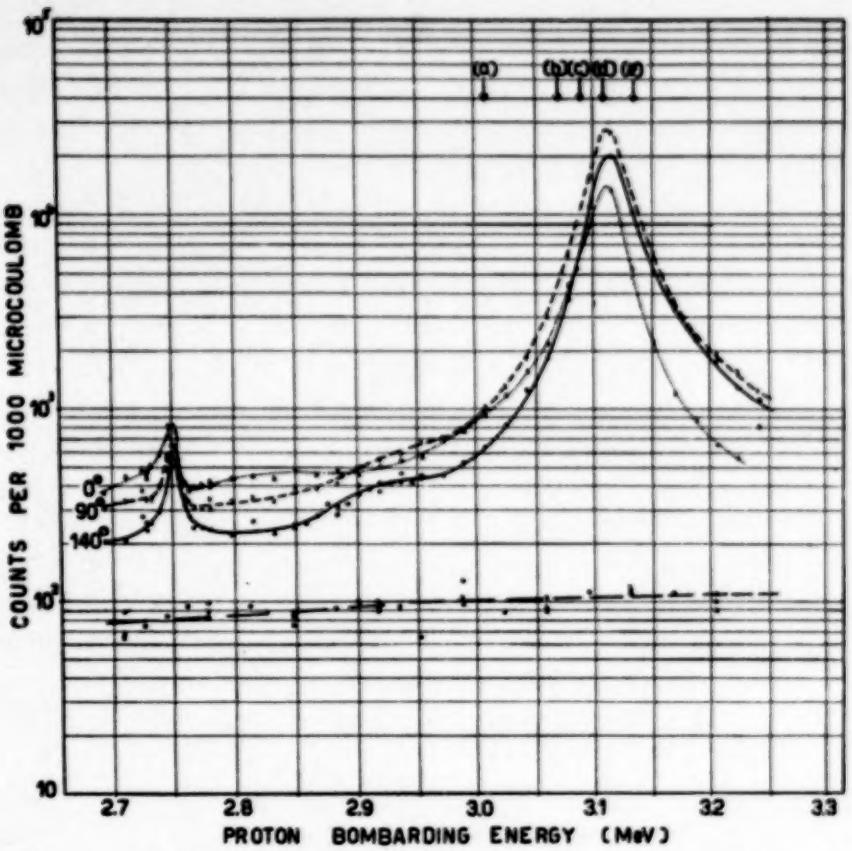

Fig. 1. The $C^{13}(p, \gamma)$ excitation functions as obtained with a 5 keV thick, 60 % enriched C^{13} target. A detailed explanation of this figure is given in sect. 3.

TABLE 2

The coefficients a_1 and a_2 of the angular distribution $W(\theta) = 1 + a_1 \cos\theta + a_2 \cos^2\theta$ of the 10.43-MeV gamma rays at different proton bombarding energies.

Measurement [a])	Bombarding energy (MeV)	a_1	a_2
(a)	3.01	$+(0.32\pm0.10)$	$-(0.29\pm0.10)$
(b)	3.07	$+(0.15\pm0.03)$	$-(0.41\pm0.03)$
(c)	3.09	$+(0.08\pm0.06)$	$-(0.40\pm0.10)$
(d)	3.11	$+(0.03\pm0.03)$ [b])	$-(0.50\pm0.03)$ [b])
		$+(0.02\pm0.02)$ [c])	$-(0.47\pm0.03)$ [c])
		$+(0.03\pm0.03)$ [d])	$-(0.47\pm0.03)$ [d])
(e)	3.135	$-(0.10\pm0.04)$	$-(0.46\pm0.08)$

With the exception of measurement (d) the errors quoted are due mainly to counting statistics and were evaluated using three standard deviations as uncertainty in a single determination. In measurement (d) the errors are least squares errors.

[a]) Compare fig. 1.

[b]) The values have been re-evaluated from the data displayed in ref. [6]) in order to check on a possible $\cos\theta$ term.

[c]) Obtained with 45 keV thick target.

[d]) Obtained with a 5 keV thick target from measurements at 0° 90° and 140°.

keV) has been obtained previously by Willard *et al.* [6]) This measurement has been repeated in the present investigation using a 45 keV thick target and adjusting the proton energy such that the average energy in the target is given by (d). A further determination of the distribution at (d) has been obtained from measurements using a 5 keV thick target.

The results of these distribution measurements are displayed in table 2. The coefficients a_1 and a_2 given in column 3 and 4 of table 2, respectively, were obtained from least squares fits of the data using the expansion $W(\theta) = 1 + a_1 \cos\theta + a_2 \cos^2\theta$. A limit on $|a_4| < 0.1$ is set from the data obtained on-resonance.

It appears from table 2 that a strong cos θ term is present in the angular distribution of the ground state gamma rays which changes sign when going with the proton bombarding energy over the 3.11-MeV resonance. In order to gain further information about the energy dependence of this cos θ term over a wide range of bombarding energies the (p, γ) excitation functions have been measured at different angles with respect to the proton beam. These curves — which have been displayed in fig. 1 — were obtained using a 7.6 cm by 7.6 cm NaI(Tl) crystal which was mounted to rotate about the target at 12 cm distance and which was irradiated at 0°, 90° and 140° for each of the bombarding energies picked (curves 0°, 90° and 140° of fig. 1). Each determination corresponded to a definite integrated charge. Absorption corrections and a check on the symmetry of the detection equipment was made using the annihilation radiation from C^{13}(p, n)N^{13}. In order to obtain reasonable counting rates from the high energy radiation it was found necessary to cut off the spectrum below 3 MeV by using a fast diode discriminator. This discrimination was made before the pulses entered the 100-channel analyser which was used to display the spectrum. The gain of the system was monitored and corrections were made for shifting of the gain with time and position by comparison with the 2.62-MeV gamma rays from the decay of RaTh. The height of the pulses from this radiation was adapted by using a 4 : 1 precision attenuator. When evaluating the data, i.e. summing up a certain number of channels below and above an energy, which was defined by the "monitor" peak, corrections have been made for the energy variation of the ground state transition with bombarding energy. The target used had a thickness of 5 keV at $E_p = 3$ MeV. A check on the 0° curve was made using a 500 eV thick target. The background caused by the platinum backing of the target etc. was determined from the bombardment of a clean platinum foil and was found to be isotropic. The results of these measurements have been also included in fig. 1.

Assuming an angular distribution of the form $W(\theta) = 1 + a_1 \cos\theta + a_2 \cos^2\theta$ the coefficients a_1 and a_2 may also be determined from the excitation functions shown in fig. 1. The experimentally determined background (as obtained from the bombardment of the clean platinum foil) has been taken into account in this evaluation. The results are plotted in fig. 2. Also have been included in

fig. 2 the values obtained for a_1 and a_2 from the distribution measurements as displayed in table 2. It is seen from fig. 2 that — apart from changes at around 2.75 and 2.90 MeV (which will be discussed later) — the cos θ term stays almost constant over a wide range of bombarding energies below $E_p = 3$ MeV. No change of the sign of a_1 is observed in this energy region. The constancy of the cos θ term and the sudden change of the sign of a_1 at $E_p = 3.11$ MeV suggest that the cos θ term is mainly due to interference between the 10.43-MeV level and non-resonant background. Using the $C^{13}(p, \gamma)N^{14}$ cross section obtained by Seagrave [15]) in the proton energy region between 0.4 and 2.8 MeV it appears

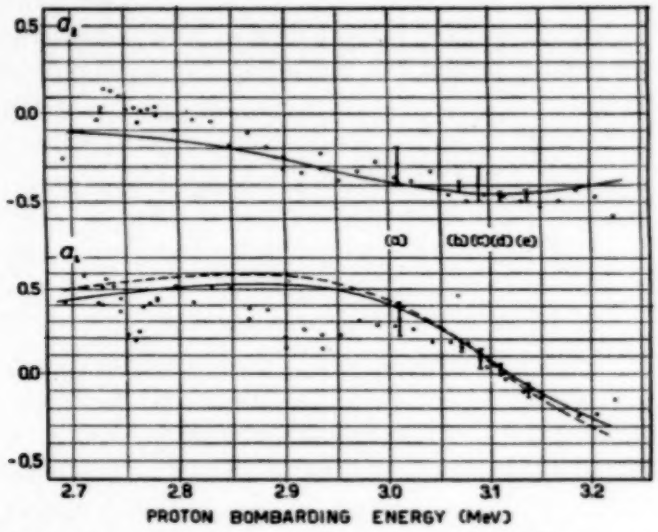

Fig. 2. The coefficients a_1 and a_2 of the angular distribution $W(\theta) = 1 + a_1 \cos\theta + a_2 \cos^2\theta$ as determined from the experiments described in sect. 3. The solid line gives the theoretical fit assuming interference between the 10.43-MeV state and background due to the 8.06-MeV level. The curve was calculated using the formulae of the appendix. The values of the parameters chosen for this calculation are given in the text. The broken line is obtained using a s-wave phase shift 16° larger than the one calculated with $R = 4.7 \times 10^{-13}$ cm from the hard sphere scattering condition. This slight increase of the s-wave phase shift is suggested by comparison of the hard sphere phases with the phases used by Zipoy *et al.* to fit the $C^{13}(p, p)C^{13}$ data.

that the 8.06- and 8.70-MeV levels — which both decay to about 80 % to the N^{14} ground state — should be expected to account for most of the "non-resonant" background between $E_p = 2.7$ and $E_p = 3.1$ MeV. The extrapolation of the cross section curves quoted by Seagrave [15]) for the 8.06- and 8.70-MeV levels yields cross sections of 6.2 μb and 2.8 μb at $E_p = 2.7$ MeV and of 4.2 μb and 1.3 μb at $E_p = 3.2$ MeV for the production of ground state gamma rays due to the 8.06- and 8.70-MeV levels, respectively. Taking a value of 700 μb for the maximum cross section of the 3.11-MeV resonance [6]) to adapt the 90° curve of fig. 1 to absolute units these estimates turned out to be actually too large and had to be decreased by a factor of 0.54 to give a good description of the 90° curve at $E_p = 2.7$ MeV. The values obtained this way are believed to be

reliable estimates and have been used for the cross sections of the 8.06- and 8.70-MeV levels at $E_p = 2.7$ and 3.2 MeV in the remainder of this paper.

Both, the 8.06-MeV ($J = 1$) and the 8.70-MeV ($J = 0$) states have odd parity and are formed by s-wave protons. If — for the moment — it is assumed that the general course of the $\cos\theta$ term in the region of bombarding energies between 2.7 and 3.2 MeV can be described by interference between the 10.43-MeV state and non-resonant background due to the 8.06-MeV or 8.70-MeV (or both) states (which later on will be proved to yield a good over-all fit of a_1 and a_2) the 10.43-MeV state must have even parity. It was shown in the introduction that the 10.43-MeV state must have $J = 2$ which concludes about p- or f-wave formation of this state with channel spin $s = 1$. Since interference takes place for overlapping resonances through the same channel spin s only, the $\cos\theta$ term then must be due to interference between the 10.43-MeV and the 8.06-MeV states. Using the cross sections quoted above for the production of ground state gamma rays at $E_p = 2.7$ MeV and 3.2 MeV the coherent and incoherent (regarding the possibility of interference with the 10.43-MeV state) contributions to the background from the 8.06 and 8.70 MeV levels, respectively, were estimated by linear interpolation. The slightly decreasing functions obtained in this manner were used in the following calculations.

A test of the assumption of level interference can be obtained from a comparison of the experimental data (as displayed in fig. 2) with the results of calculations which were based on the assumption of overlapping levels. The theoretical formula which describes the angular distribution of the gamma rays emitted from a compound nucleus after formation by particle capture is given in the appendix †. In this formula the state of the compound nucleus is interpreted in terms of two overlapping resonances. The formula is given in the mixed (s, Ω) representation, since the entrance channel is represented by a plane wave of (charged) particles incident upon the target nucleus while the exit channel contains gamma quanta. The appearence of a phase factor $\cos\xi$ in the interference term of formula (1) of the appendix is due as well to the fact that the nuclear reaction is initiated by (charged) particles as to the assumption that the state of the compound nucleus is to be described in terms of two (overlapping) single resonances. In the present reaction the proton energy is not well below the barrier height. Consequently, the numerical values of $\cos\xi$ are not determined by the energies and orbital momenta of the protons and the respective widths of the two (overlapping) resonances alone but will also depend on the choice of interaction radius R which determines the phase shift $-\tan^{-1}(F_l(R)/G_l(R))$ due to the hard sphere scattering. However, the uncer-

† A similar formula has been given by Devons and Goldfarb [19]) in the (s, s) representation. Thus it does not apply to a (p, γ) reaction. Therefore, it was felt worthwhile to give the formula applying to charged particle capture with successive emission of gamma quanta explicitely in the appendix.

tainty in the choice of R is small. The theoretical work of Thomas [16]) on the N^{13} levels indicates a preference for a value in the range $(4.4—4.9)\times 10^{-13}$ cm. For the present calculations $R = 4.7\times 10^{-13}$ cm is considered to be a reliable estimate (compare ref. [20])). Thus, once the level parameters and angular momenta are known (or have been chosen), the only arbitrary parameter at our disposal is the sign of the interference term. Of course, this implies the assumption that each of the two interfering levels is formed by one partial wave only (definite l and l') and that the gamma transitions are of pure multipole order. Otherwise further (mixing) parameters would occur in formula (1) together with summations over l, l', L and L'. Furthermore, the way formula (1) is written, implies that only one entrance channel of definite s is open. If different s are possible their contributions add incoherently and certain amplitudes $A(s)$ are to be introduced in the usual way. Corrections on the resonance energies E_0 and E'_0 due to the Thomas shift have been neglected, i.e. E_0 and E'_0 are identified with the maxima of the resonances. Since in our case one of the interfering levels (the 8.06-MeV state) is located far below the energy region to be considered it is convenient to replace the Breit-Wigner function $f'^2(E)$ of this state by a constant or slightly linearly decreasing function. An estimate of this function was obtained from an extrapolation of the cross-section curve of the 8.06-MeV level as described above. As a further consequence of the energy location of the 8.06-MeV state and its total width the resonance phase of this state can be considered to be constant, i.e. arc tan $\Gamma/2(E'_0-E) = \pi$.

The theoretical fit of the experimental data which is obtained using equations (4) and (4a) of the appendix is given by the solid lines in fig. 2. These lines give the values of a_1 and a_2 using $J^\pi = 2^+$, $\Gamma = 36$ keV and $\Gamma_\gamma = 17$ eV as level parameters for the 10.43-MeV state. Furthermore, it has been assumed that the state is formed by p-wave protons. The "incoherent" background as due to the 8.70 MeV state has been taken into consideration using the estimates for the contributions from the 8.70-MeV level as described above. In order to adapt cross section values quoted in microbarns to the arbitrary units in which the excitation functions are obtained, a value of 700 μb has been used for the maximum cross section of the 3.11-MeV resonance [6]).

It is seen from fig. 2 that a good over-all fit of a_1 and a_2 is obtained on the basis of the assumptions made above. Therefore, it is believed that the cos θ term mainly arises from interference between the 10.43-MeV and the 8.06-MeV level. Introducing into equation (1) of the appendix the same parameters as used to fit the experimental values of a_1 and a_2 reasonable over-all fits of the experimental excitation functions are obtained.

From fig. 2 it appears that only a description of the general course of the energy dependence of the cos θ term can be obtained using two level interference. There are rather marked variations of the strength of the cos θ term at proton bombarding energies around 2.75 and 2.90 MeV. From fig. 1 it is seen that the

variations of a_1 at $E_p = 2.75$ MeV are caused by a resonance in the reaction $C^{13}(p, \gamma)N^{14}$ at this proton bombarding energy which corresponds to a level at (10.095 ± 0.015) MeV excitation energy in N^{14}. This energy determination is obtained using $E_p = (3.11 \pm 0.01)$ MeV for the location of the 3.11-MeV resonance. The error includes the uncertainty in the location of the 3.11-MeV resonance. Furthermore, a total width $\Gamma = (12 \pm 3)$ keV and a gamma width $(2J+1)\Gamma_\gamma = (0.5 \pm 0.2)$ eV (using $\Gamma_\gamma = 17$ eV for the 10.43-MeV level) is obtained from the excitation functions shown in fig. 1. It has been pointed out in the introduction that a level at 10.05 MeV has been formerly reported from $N^{14}(\alpha, \alpha')N^{14}$. The level also has been recently observed from $C^{13}(p, p)C^{13}$ at 10.084 MeV (see introduction). The spin assignment indicated by the $C^{13}(p, p)C^{13}$ experiments, namely $J^\pi = 2^+$ is not in agreement with the positive value for a_2 obtained from the excitation functions in fig. 1 unless high quadrupole admixtures are assumed in the $10.09 \rightarrow 0$ transition. It can be shown that an interference between a $J = 2$, 10.09-MeV, the 10.43-MeV level and the "background" from the 8.06-MeV level cannot yield $a_2 > 0$ as long as pure gamma transitions are assumed. Furthermore, the excitation functions displayed in figl 1 give some evidence that this level also is formed — at least partially — with channel spin $s = 1$, i.e. its gamma ray contributions add coherently. This is, because there still remains a $\cos\theta$ term in the angular distribution of the $10.09 \rightarrow 0$ transition even if background subtractions are made in very different ways.

From the energy dependence of a_1 around $E_p = 2.90$ MeV it is concluded that further resonance is present at this bombarding energy which corresponds to an excitation energy of (10.24 ± 0.03) MeV in N^{14}. This conclusion is confirmed by the excitation functions shown in fig. 1. The shape of these functions shows an appreciable dependence on the angle of observation for the range of bombarding energies between 2.8 and 3.0 MeV. This gives evidence that also the contributions from the $10.24 \rightarrow 0$ transition add coherently to the cross sections of the 8.06- and 10.43-MeV levels. An attempt has been made to fit the experimental excitation curves under the assumption of three interfering levels. The extension of formula 1 of the appendix to describe the energy dependence of the distribution of gamma rays emitted from a state which is interpreted in terms of three overlapping levels is straightforward. From these calculations a rough estimate of the gamma width and total width of the 10.24-MeV level is obtained. Using $J^\pi = 1^-$ for the 10.24-MeV level (which is the assignment indicated by the $C^{13}(p, p)C^{13}$ experiments, see introduction) and assuming s-wave formation a value 80 keV $< \Gamma <$ 160 keV for the total width is obtained while a gamma width $\Gamma_\gamma = 0.3$ eV is obtained with an uncertainty of a factor of 3 in either direction.

Because a_1 vanishes at a proton bombarding energy corresponding to maximum yield from the 3.11-MeV resonance (see fig. 2 and table 2) the anisotropy A of the gamma ray distribution at this proton energy is given by a_2. Since the

cross section for the production of gamma rays at $E_p = 3.11$ MeV is 700 μb which is to be compared to a background contribution of a few microbarns it can be shown from formula (4a) of the appendix that an influence on a_2 due to level interference can be neglected, i.e. with respect to a determination of A at $E_p = 3.11$ MeV the 10.43-MeV level can be treated as a well isolated level. Comparison of $a_2 = A = -(0.50 \pm 0.03)$ with the value $A = -(0.55 \pm 0.02)$ obtained for the anisotropy of the $9.17 \rightarrow 0$ transitions and considering that the gamma widths of the $10.43 \rightarrow$ and $9.17 \rightarrow 0$ transition are quite similar the possible spin-parity assignments of the 10.43-MeV level permitted by the anisotropy of the ground state transition are the same as for the 9.17-MeV state; however, it has been shown in the introduction that the 10.43-MeV state must have $J = 2$. From the value of a_2 obtained at $E_p = 3.11$ MeV limits on the quadrupole-dipole mixture in the $10.43 \rightarrow 0$ transition $-5 \times 10^{-2} < \delta < 0$ can be obtained (compare section 2).

The resonant proton reduced widths θ_p^2 of the 10.43-MeV state have been calculated using $\Gamma = 36$ keV. The values obtained are given in table 1. It is seen from this table that the 10.43-MeV level must be formed by protons with $l \leqq 3$, which — considering the even parity assignment — leads to p- or f-wave formation. Although the reduced proton width obtained for f-wave formation does not definitely exclude f-waves it is assumed that the 10.43-MeV state is formed by p-wave protons. The value of θ_p^2 obtained for p-wave formation is rather close to the one expected if the 10.43-MeV state were arising from p^{-2} (compare ref. [4])). The proton reduced widths of the 10.24 and the 10.09-MeV states were calculated using $\Gamma = 120$ keV and $\Gamma = 12$ keV respectively. The values also have been included in table 1. It is seen that the 10.24-MeV state must be formed by protons with $l \leqq 2$.

As to the 10.51 MeV level reported from $C^{13}(p, p)C^{13}$ (see introduction) there is little indication for the presence of a level at this energy which decays to the ground state. The deviations of the experimental values of a_1 an a_2 from the over-all fit may indicate a broad level of extremely small gamma width (for decay to the ground state) at approximately $E_p = 3.2$ MeV.

4. Summary

The angular distributions of the ground state transitions from the 9.17-MeV and 10.43-MeV excited states in N^{14} have been investigated using the reaction $C^{13}(p, \gamma)N^{14}$ at the 1.75-MeV and 3.11-MeV resonances, respectively. The distribution of the $9.17 \rightarrow 0$ transition was found to be $W(\theta) = 1 - (0.55 \pm 0.02) \cos^2\theta$. The anisotropy slightly deviates from the value obtained previously by Woodbury *et al.* [5]). No indidation for a possible $\cos\theta$ term was found and the limit on a possible $\cos^4\theta$ term is $|a_4| < 0.02$. The distribution agrees with the 9.17-MeV state having $J^\pi = 2^+$. Assuming p-wave formation the anisotropy

limits the possible values of the ratio of the reduced matrix elements of quadrupole and dipole contributions in the 9.17 → 0 transition $-0.07 < \delta < -0.04$.

It was shown that — as a consequence of the branch from the 10.43-MeV to the 6.44-MeV state observed by Willard *et al.* [6]) and the spin assignment given recently to the 6.44-MeV state by the present authors [2]) — the 10.43-MeV state must have $J = 2$. The total width of the 3.11-MeV resonance (which corresponds to the 10.43-MeV excited state in N^{14}) was determined to be $\Gamma = (36 \pm 2)$ keV. The resonant reduced proton widths which are obtained using this value for Γ show that the 10.43-MeV state must be formed by proton capture with $l \leq 3$, however, it is assumed that the level is formed by p-wave protons. The angular distribution of the ground state gamma rays was determined at different proton bombarding energies between 2.9 and 3.2 MeV. The distribution obtained at a proton energy corresponding to maximum yield from the 3.11-MeV resonance was found in good agreement with the result obtained previouly by Willard *et al.* [6]). The presence of a strong $\cos\theta$ term in the angular distribution was established at proton bombarding energies slightly below and above the maximum of the 3.11-MeV resonance using extremely thin and uniform targets.

The energy dependence of this $\cos\theta$ term was determined over a wide range of bombarding energies (from $E_p = (2.7-3.2)$ MeV) by measuring the (p, γ) excitation function at different angles with respect to the proton beam. The $\cos\theta$ term changes sign when going through the 3.11 MeV resonance and stays almost constant below the 3.11 MeV resonance throughout the range of bombarding energies. It was shown that a good over-all fit of the energy dependence of the observed $\cos\theta$ term can be obtained if it is assumed that this term arises from interference between the 10.43 MeV $J = 2$ state and the "long tailed" 8.06 MeV $J^\pi = 1^-$ state. In as much as this explanation of the $\cos\theta$ term is likely the 10.43 MeV level must have even parity. From the observation of rather marked variations of the strength of the $\cos\theta$ term at $E_p = 2.75$ and 2.90 MeV bombarding energy the presence of levels at 10.09 MeV and 10.24 MeV is concluded which decay weakly to the N^{14} ground state. This conclusion is supported by the (p, γ) excitation functions. A total width $\Gamma = (12 \pm 3)$ keV and a gamma width $(2J+1)\Gamma_\gamma = (0.5 \pm 0.2)$ eV was obtained for the 10.09 MeV level, while rather rough estimates 80 keV $< \Gamma <$ 160 keV and $\Gamma_\gamma = 0.3$ eV (with an uncertainty of a factor 3 in either direction) were obtained for the 10.24 MeV state †. Using a spin parity assignment $J^\pi = 2^+$ for the 10.43 MeV state limits $-5 \times 10^{-2} < \delta < 0$ are obtained from the anisotropy of the angular distribution observed at a proton bombarding energy $E_p = 3.11$ MeV.

Appendix

The theoretical formula which describes the angular distribution of the gam-

† The gamma widths quoted — of course — are the gamma widths of the ground state transitions.

ma rays emitted from a compound nucleus formed by particle capture into a state which is interpreted in terms of two (overlapping) single resonances can be derived using the general formalism which applies to nuclear reactions and which has been sufficiently presented in several articles, as — for instance — by Blatt and Biedenharn [21]), Lane and Thomas [22]) and Devons and Goldfarb [19]). In the case of a single level resonance an explicit treatment has formely been made by Seed and French [23]) who investigated the interference terms appearing in the angular distributions of gamma rays following the capture of (charged) particles with different angular momenta.

In the case of two overlapping levels which are formed by (charged) particle capture with channel spin s and angular momenta l and l', respectively, the angular distribution of the successive gamma rays is obtained to be

$$\begin{aligned} W(\theta) = \frac{\text{const}}{E} \sum_{\mathrm{K}} \{ & Z(lJlJ; sk) Z_\gamma(LJLJ; Ik) f^2(E) \\ & + Z(l'J'l'J'; sk) Z_\gamma(L'J'L'J'; Ik) f'^2(E) \\ & + 2Z(lJl'J'; sk) Z_\gamma(LJL'J'; Ik) f(E) f'(E) \cos\xi \} P_k(\cos\theta). \end{aligned} \tag{1}$$

A brief discussion of this formula and further explanations have been given in sect. 3. Primes refer to the second level. J denotes the spin of a level after formation by proton capture, l the angular momentum of the captured proton, L the multipolarity of the emitted gamma rays (pure transitions are assumed) and I the spin of the final state. The coefficients Z and Z_γ are defined as

$$Z(lJl'J'; sk) = i^{l'-l+k} \hat{l}\hat{l}' \hat{J}\hat{J}' (ll'00|k0) W(lJl'J'; sk)$$

and

$$\begin{aligned} Z_\gamma(LJL'J'; Ik) = \text{Real Part of } & i^{L'-\pi'-L+\pi+k+2} \hat{L}\hat{L}' \hat{J}\hat{J}' \\ & \cdot (LL'-11|k0) W(LJL'J'; Ik), \end{aligned}$$

with $\hat{a} = (2a+1)^{\frac{1}{2}}$, and $\pi = 0$ or 1 for electric or magnetic radiation, respectively.

The quantity $f(E)$ is defined by

$$f(E) = \pm \left\{ \frac{\Gamma_\mathrm{p} \Gamma_\gamma}{(E_0 - E)^2 + \frac{1}{4}\Gamma^2} \right\}^{\frac{1}{2}}, \tag{2}$$

with $\Gamma =$ total width, $\Gamma_\mathrm{p} =$ proton width, $\Gamma_\gamma =$ gamma width, $E_0 =$ resonance energy and $E = E_\mathrm{p} =$ proton bombarding energy. The relative phase ξ is given by

$$\begin{aligned} \xi = \Big\{ & -\tan^{-1}\left(\frac{F_l(R)}{G_l(R)}\right) + \sigma_l - \tfrac{1}{2} l\pi + \tan^{-1} \frac{\Gamma}{2(E_0 - E)} \\ & + \tan^{-1}\left(\frac{F_{l'}(R)}{(R) G_{l'}}\right) - \sigma_{l'} + \tfrac{1}{2} l'\pi - \tan^{-1} \frac{\Gamma'}{2(E_0 - E)} \Big\}, \end{aligned} \tag{3}$$

where the quantities have their usual significance, *viz.*, F_l, G_l are the regular and irregular solutions of the Coulomb wave equation and $\sigma_l = \arg \Gamma(l+1+i\eta)$, $\eta = (Z_1 Z_2 e^2/\hbar v)$, R = channel radius. The choice of the sign of $f(E)$ is arbitrary. No explicite choice of phase factors in the reduced matrix elements has been made. For $s = 1, l = 1, J = 2, L = 1, I = 1, l' = 0, J' = 1$ and $L' = 1$ (the case concerned in the present paper) the coefficients a_1 and a_2 of the angular distribution $W(\theta) = 1+a_1 \cos\theta+a_2 \cos^2\theta$ are calculated to be

$$a_1 = +\frac{20\sqrt{6}}{47f^2+24f'^2} f(E)f'(E)\cos\xi, \quad a_2 = -\frac{21f^2(E)}{47f^2+24f'^2}. \tag{4}$$

For the numerical evaluation of the F_l and G_l the tables of Bloch *et al.* [24]) have been used.

References

1) H. J. Rose, Nuclear Physics **19** (1960) 113
2) H. J. Rose, W. Trost and F. Riess, Nuclear Physics **12** (1959) 510
3) J. P. Elliott, Phil. Mag. **1** (1956) 503
4) E. K. Warburton and W. T. Pinkston, Phys. Rev. **118** (1960) 733
5) H. H. Woodbury, R. B. Day and A. V. Tollestrup, Phys. Rev. **92** (1953) 1199
6) H. B. Willard, J. K. Bair, H. O. Cohn and J. D. Kington, Phys. Rev. **105** (1957) 202
7) S. S. Hanna and L. Meyer-Schützmeister, Phys. Rev. **115** (1959) 986
8) E. K. Warburton, Phys. Rev. **113** (1959) 595
9) J. P. Elliott, private communication
10) D. Zipoy, G. Freier and K. Famularo, Phys. Rev. **106** (1957) 93
11) E. Kashy, R. R. Perry and J. R. Risser, Bull. Am. Phys. Soc. **5** (1960) 108
12) E. Kashy, R. R. Perry and J. R. Risser, Bull. Am. Phys. Soc. **4** (1959) 96
13) D. W. Miller, B. M. Carmichael, U. C. Gupta, V. K. Rasmussen and M. B. Sampson, Phys. Rev. **101** (1956) 740
14) A. A. Strassenburg, R. E. Hubert, R. W. Krone and F. W. Prosser, Bull. Am. Phys. Soc. **3** (1958) 372
15) N. Jarmie and J. D. Seagrave, Charged Particle Cross Sections, Los Alamos Report 2014
16) R. G. Thomas, Phys. Rev. **88** (1952) 1109
17) T. Teichmann and E. P. Wigner, Phys. Rev. **87** (1951) 123
18) L. C. Biedenharn and M. E. Rose, Rev. Mod. Phys. **25** (1953) 729
19) S. Devons and L. J. B. Goldfarb, Handbuch der Physik (Springer Verlag, Berlin, 1957) Vol. 42, eq. (36.9), p. 460
20) E. K. Warburton, H. J. Rose and E. N. Hatch, Phys. Rev. **114** (1959) 214
21) J. M. Blatt and L. C. Biedenharn, Rev. Mod. Phys. **24** (1952) 258
22) A. M. Lane and R. G. Thomas, Rev. Mod. Phys. **30** (1958) 257
23) J. Seed and A. P. French, Phys. Rev. **88** (1952) 1007
24) I. Bloch, M. H. Hull, Jr., A. A. Broyles, W. G. Bouricius, B. E. Freeman and G. Breit, Rev. Mod. Phys. **23** (1951) 147

2.B:2.E

Nuclear Physics **21** (1960) 383—392; © *North-Holland Publishing Co., Amsterdam*

Not to be reproduced by photoprint or microfilm without written permission from the publisher

THE ELASTIC SCATTERING OF 160 MeV PROTONS FROM LITHIUM, ALUMINIUM, INDIUM AND GOLD

A. JOHANSSON and G. TIBELL †,

The Gustaf Werner Institute for Nuclear Chemistry, University of Uppsala

K. PARKER

A.W.R.E., Aldermaston, England

and

P. E. HODGSON

Clarendon Laboratory, Oxford, England

Received 26 July 1960

Abstract: The differential cross-sections and asymmetries of protons scattered elastically from lithium, aluminium, indium and gold have been measured in the angular range 3—30°. The results are compared with calculations using the optical model, and overall agreement is found.

1. Experimental

1.1. GENERAL

The experiment was designed to determine the asymmetries in the scattering of a polarized beam of protons from various nuclei but, of course, a relative measure of the differential cross-sections for the scattering of an unpolarized proton beam could be obtained by taking the mean values of right and left scattering counting rates. The apparatus was of the conventional double scattering type with a range telescope of three scintillation counters and it has been described in detail in connection with the study of the scattering from carbon [1]). Values of the asymmetry in the scattering from carbon, oxygen, calcium, iron, nickel, and copper obtained with the same apparatus have been published [2, 3]). The only significant change from the previously described set-up was that the angle of the first scattering was decreased from 16.2° to 14.2°. The reduced value of the polarisation of the once scattered beam was well compensated for by the higher beam intensity obtained at the second scatterer. The energy of the protons incident on the second target was 161 MeV; the mean energies of the second scattering varied somewhat due to different target thicknesses (see table 1).

1.2. ENERGY RESOLUTION

The energy spread of the polarized beam was less than 1 MeV full width at half height. Consequently, the resolution was limited almost completely by

† Now at SC Division, CERN, Geneva.

range straggling in the counter telescope which was equivalent to an energy spread of about 2.7 MeV full width at half height. The thicknesses of the absorbers were chosen to correspond to the mean range of protons with an energy that was 1.7 MeV less than the full energy of the elastically scattered particles. The lowest inelastic levels of the studied nuclei are

for Li^7 at 0.478 and 4.63 MeV,
for Al^{27} at 0.842, 1.013, 2.213 and 2.732 MeV,
for In^{115} at 0.335, 0.595, ... MeV and
for Au^{197} at 0.077, 0.268, ... MeV.

The energy resolution was, therefore, not sufficient to separate the elastically scattered protons from those scattered inelastically from the very lowest excited states in any of the nuclei studied. However, the relative inelastic contribution is believed to be small for the angles in question.

1.3. ANGULAR RESOLUTION

The angular resolution function was approximately a gaussian mainly resulting from two different sources, one purely geometrical and the other originating

TABLE 1

Target thicknesses and angular resolutions

Element	Angular region (°)	Target thickness (g/cm²)	Rms angular resolution (°)		
			Geom.	Mult. sc.	Total
Lithium	3–27	0.69	0.55	0.19	0.58
Aluminium	3– 5	0.60	0.34	0.35	0.49
	6–27	2.49	0.55	0.76	0.94
Indium	3– 4	0.20	0.34	0.35	0.49
	5–20	0.60	0.55	0.64	0.84
	24–27	1.19	0.55	0.93	1.08
Gold	4– 7	0.39	0.34	0.63	0.71
	8–27	1.08	0.55	1.09	1.22

from multiple Coulomb scattering. In table 1 are listed the different target thicknesses used and the corresponding rms angular resolutions.

1.4. RESULTS

In tables 2 and 3 are given the asymmetries that would have been obtained if the incoming beam had been 100 % polarized and also values for the differential cross-section in the C.M. system for the scattering of an unpolarized beam. The errors given are computed from counting statistics only (standarddeviations). In addition, there is a 2 % possible systematic error in all asymmetries

TABLE 2

Differential cross sections and asymmetries for lithium and aluminium

Lithium			Aluminium		
C.M. angle (degrees)	Cross section (mb/sr)	Asymmetry (%)	C.M. angle (degrees)	Cross section (mb/sr)	Asymmetry (%)
3.43	535 ±23	10± 5	3.11	13300 ±370	2± 3
4.58	237 ±15	22± 7	4.15	4780 ±290	20± 6
5.72	167 ±12	44±10	5.19	2250 ±190	33± 9
6.86	157 ±10	53± 8	6.22	1741 ± 48	42± 3
8.01	235 ±10	40± 5	7.26	1489 ± 38	43± 3
9.15	211 ± 8	48± 5	8.30	1327 ± 35	47± 3
10.29	178 ± 7	47± 5	10.37	941 ± 26	49± 3
11.43	166 ± 8	53± 5	12.44	519 ± 18	65± 3
12.58	141 ±10	56± 9	13.48	421 ± 18	67± 3
14.29	113.8 ± 4.6	55± 4	14.51	313 ± 13	77± 3
16.00	90.1 ± 5.4	72± 4	16.59	124.0± 7.5	81± 3
17.14	71.7 ± 3.9	74± 4	18.66	49.9± 4.9	87± 5
19.98	39.9 ± 2.5	79± 4	20.73	18.8± 2.5	78± 9
22.82	22.1 ± 1.3	82± 4	22.80	18.3± 1.0	38± 6
26.23	10.8 ± 1.2	86±10	24.35	16.7± 1.1	24± 8
28.49	6.50± 0.86	88±12	24.86	15.3± 0.7	23± 6
30.75	5.82± 0.55	70± 7	27.96	13.1± 1.8	73±10

TABLE 3

Differential cross sections and asymmetries for indium and gold

Indium			Gold		
C.M. angle (degrees)	Cross section (mb/sr)	Asymmetry (%)	C.M. angle (degrees)	Cross section (mb/sr)	Asymmetry (%)
3.03	139800 ±4700	2± 3	4.02	153200 ±3000	0± 2
4.03	41600 ±2100	16± 4	5.03	58700 ±1200	16± 2
5.04	18990 ± 350	23± 2	6.03	32550 ± 890	28± 3
6.05	11940 ± 330	35± 3	7.04	18530 ± 580	31± 4
8.07	4620 ± 170	45± 4	8.04	10430 ± 160	28± 2
9.08	2590 ± 110	47± 4	9.05	4500 ± 130	24± 3
10.09	1215 ± 47	42± 4	10.05	2139 ± 89	25± 5
11.10	554 ± 19	47± 4	11.06	1043 ± 35	21± 4
12.10	258 ± 11	40± 5	12.06	688 ± 27	25± 5
13.11	135.7± 6.5	25± 5	13.07	604 ± 27	22± 5
14.12	158.1± 7.1	35± 5	14.07	646 ± 24	43± 4
15.13	158.1± 8.2	42± 5	15.08	561 ± 21	40± 4
16.14	194 ± 20	40±11	16.58	373 ± 16	46± 4
18.15	182 ± 17	80± 7	18.09	165.2± 8.3	50± 5
20.17	102 ± 13	75± 6	20.10	64.8± 4.2	21± 8
24.20	19.3± 2.0	3±12	22.11	66.6± 6.0	47± 9
27.23	15.7± 2.0	36±15	24.12	64.8± 7.1	47±12
			27.13	31.5± 6.0	60±20

due to the uncertainty of the polarization of the once scattered beam. Misalignment errors should be negligible. In the case of the relative values of the cross-sections an additionalerror might arise from the long time variation of the monitor and range tele scope efficiencies. These errors are difficult to estimate but should not exceedabou t5 %. The absolute scale is not known better than 30 %.

2. Optical Model Analysis

The experimental results were compared with calculations using the optical model of the interaction, with a two-body potential of the form

$$V = V_{\text{Coul}} + (U + iW) f(r) + \left(\frac{\hbar}{m_\pi c}\right)^2 (U_s + iW_s) \frac{1}{r} \frac{\mathrm{d}f(r)}{\mathrm{d}r} \mathbf{l} \cdot \boldsymbol{\sigma},$$

where $f(r)$ has the Saxon-Woods form $(1+\exp((r-R)/a))^{-1}$ and the nuclear radius $R = r_0 A^{\frac{1}{3}}$, using a notation equivalent to that of Bjorklund and Fernbach [4]). All potentials are in MeV, and lengths in $f = 10^{-13}$ cm.

To facilitate comparison with previous work, the same radial form factors were used, viz. $a = 0.65f$, $r_0 = 1.25f$, and only the central and spin-orbit potentials U, W, U_s and W_s were varied. The calculations were made with the nine sets of parameters given in table 4, and those giving the best fits are plotted

TABLE 4

The central and spin-orbit potentials used in the analysis

Run	U	W	U_s	W_s
1	−14.5	−17.3	1.5	−1
2	−12	−15	1.5	−1
3	−16	−15	1.5	−1
4	−12	−20	1.5	−1
5	−16	−20	1.5	−1
6	−14	−11	2.5	−1
7	−14	−15	2.5	−1
8	−18	−11	2.5	−1
9	−18	−15	2.5	−1

together with the experimental results in figs. 1—8. This comparison shows that the model reproduces the main trends of the experimental results, with some notable discrepancies. Thus, the measurements in the region of the minima in the differential cross-sections for indium and gold tend to be high. This is probably due to the finite angular resolution of the detecting apparatus, which has not been taken into account in the calculations. This could also account for the discrepancies at small angles, where the differential cross-section is falling rapidly.

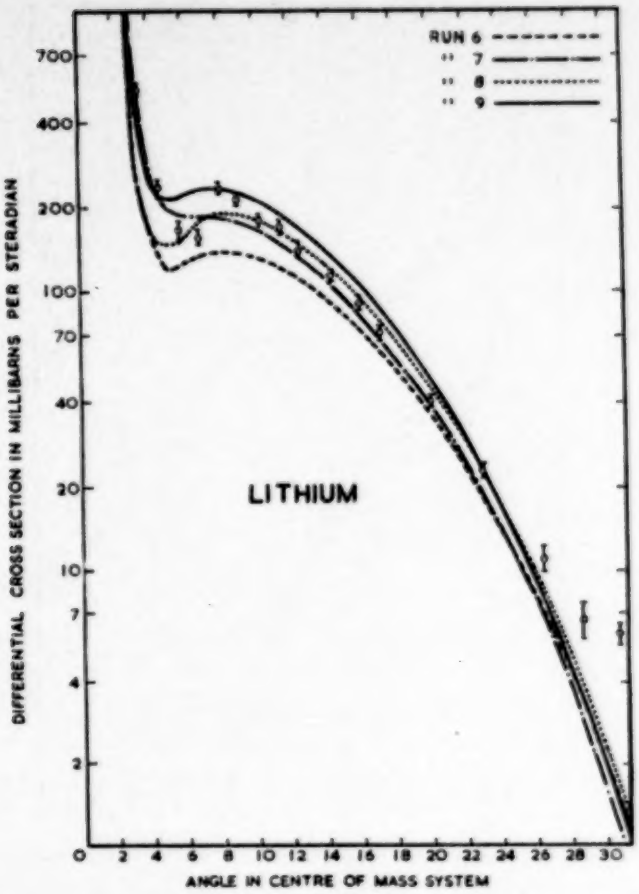

Fig. 1. Differential cross-section for 160 MeV protons on lithium compared with optical model calculations. The parameters of the various runs are given in table 3.

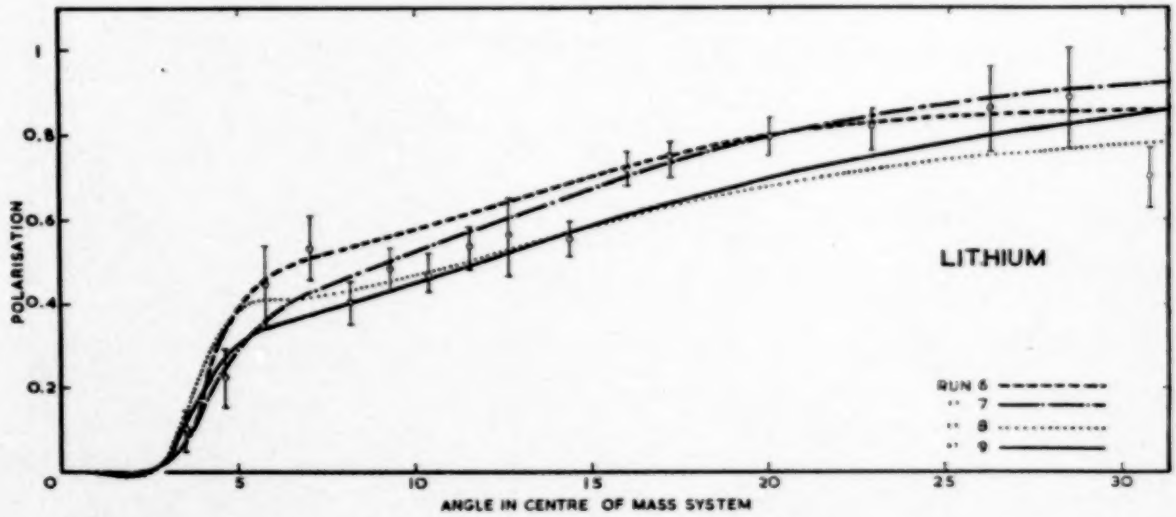

Fig. 2. Polarisation for 160 MeV protons on lithium compared with optical model calculations. The parameters are given in table 3.

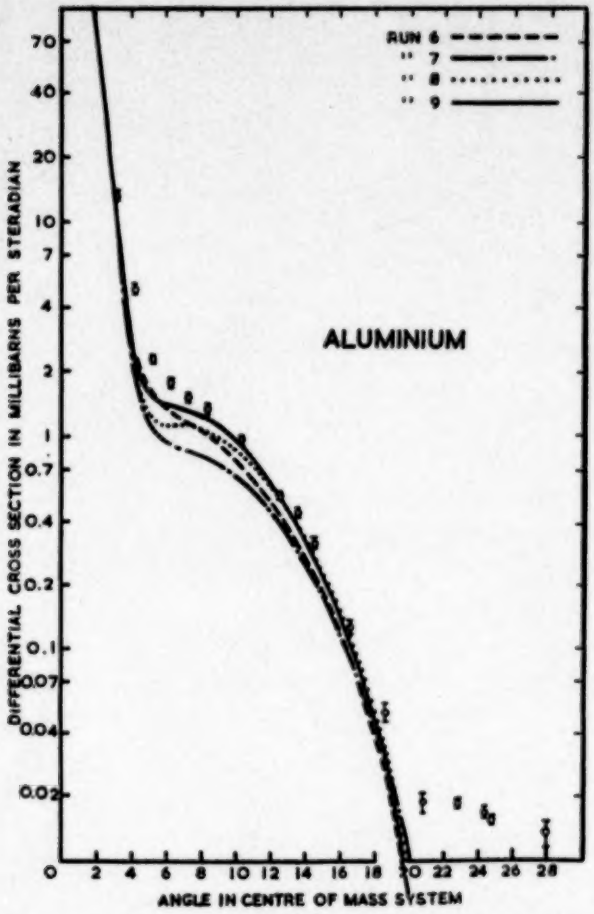

Fig. 3. Differential cross-section for 160 MeV protons on aluminium compared with optical model calculations. The parameters are given in table 3.

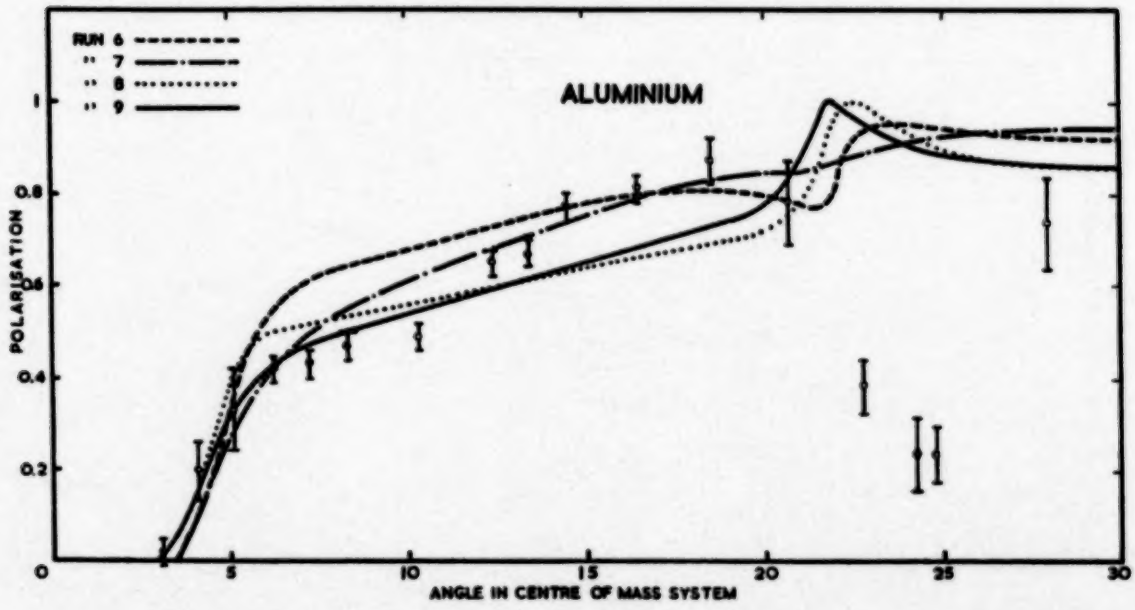

Fig. 4. Polarisation for 160 MeV protons on aluminium compared with optical model calculations. The parameters are given in table 3.

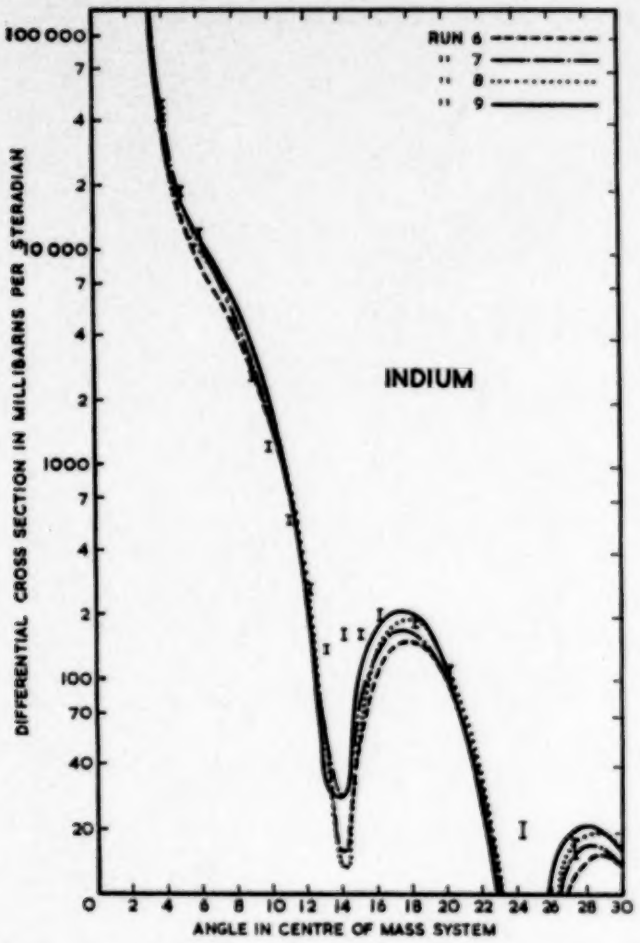

Fig. 5. Differential cross-section for 160 MeV protons on indium compared with optical model calculations. The parameters are given in table 3.

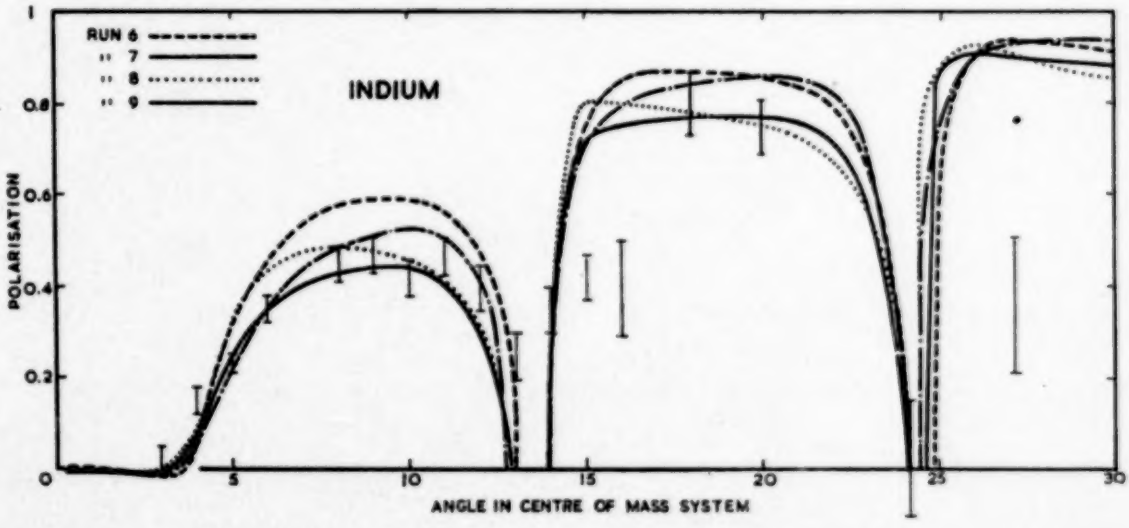

Fig. 6. Polarisation for 160 MeV protons on indium compared with optical model calculations. The parameters are given in table 3.

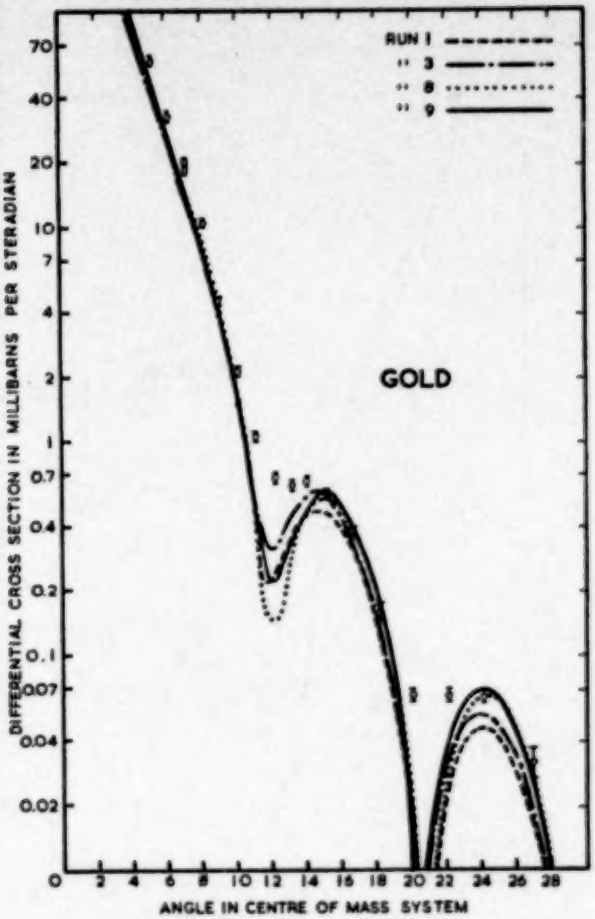

Fig. 7. Differential cross-section for 160 MeV protons on gold compared with optical model calculations. The parameters are given in table 3.

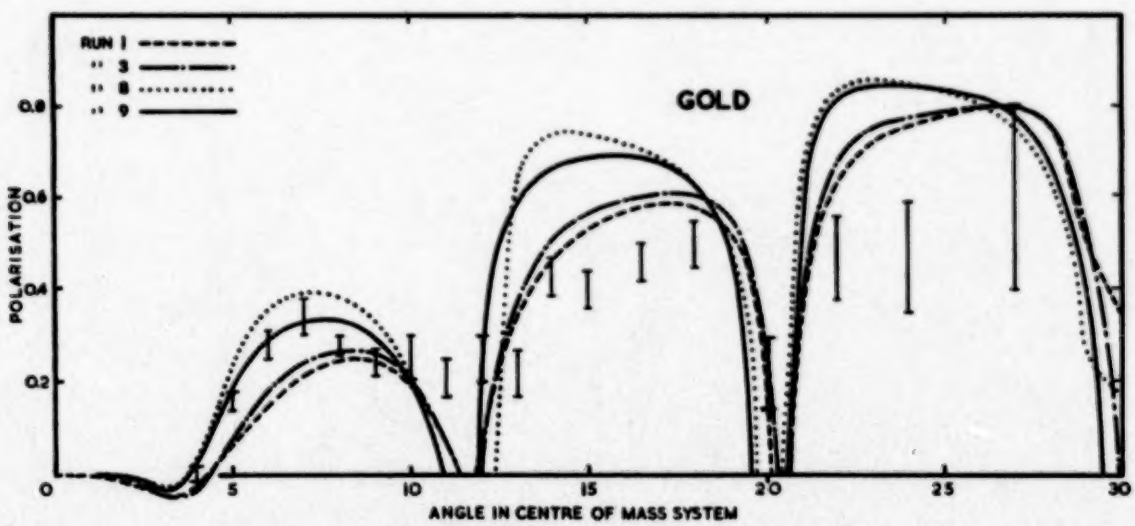

Fig. 8. Polarisation for 160 MeV protons on gold compared with optical model calculations. The parameters are given in table 3.

The polarisations on the whole show satisfactory agreement also, except for aluminium, where a marked minimum in the measured polarisation around 25° is not reproduced by the model. To investigate this in more detail, a series of runs were made for aluminium taking $U = -16$, $W = -16$ and a mesh of values of the spin-orbit potentials $U_s = 0, 1, 2, 3$; $W_s = 0, \pm 1, \pm 2$. Negative values of U_s were not investigated since they correspond to the spin-orbit splitting opposite in sign to that found experimentally. The results of these calculations are given in fig. 9. In no case is the observed form of the polarisa-

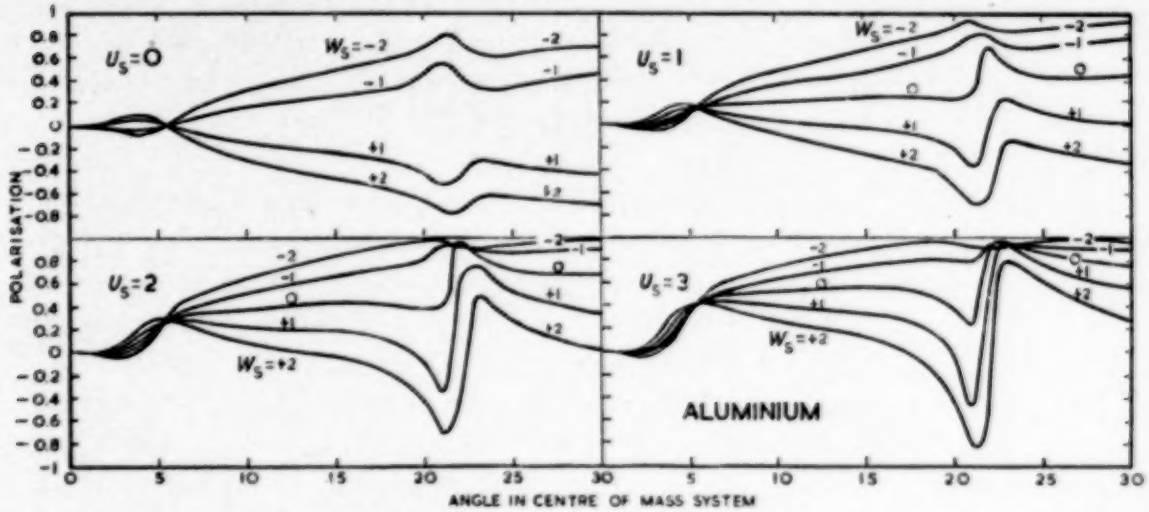

Fig. 9. Polarisations for 160 MeV protons on aluminium for a series of values of the spin-orbit potential.

tion obtained. The polarisation is sensitive to the radial variation of the potential and it is likely that the experimental results could be reproduced with suitable forms. Preliminary investigations show that increased absorption at the nuclear surface has the correct effect, and more detailed calculations are in progress. It is noteworthy that in fig. 9 the polarisations are almost independent of W_s at about 6°.

TABLE 5

Calculated reaction cross-sections in mb for the potentials given in table 4

Run	Lithium	Aluminium	Indium	Gold
1	212.0	495	1247	1753
2	190.3	454	1172	1663
3	191.3	457	1182	1680
4	233.9	533	1306	1818
5	235.2	537	1317	1834
6	149.7	372	1021	1484
7	190.5	455	1179	1669
8	150.1	374	1030	1500
9	191.6	439	1190	1691

The calculated reaction cross-sections are given in table 5; when experimental values are available they will be useful in finding more accurate values of the optical model parameters.

A detailed parameter search to find the best overall fit to the data is not justified until the absolute normalisation of the cross-sections is more accurately known. A series of more accurate measurements is approaching completion, and a more detailed analysis will be made of these results.

The calculations were carried out partly on the IBM 709 computer at AWRE, Aldermaston, and partly on the Ferranti Mercury at the Oxford University Computing Laboratory. The analytical and numerical methods used to solve quantum mechanically the problem of the scattering of a particle by a potential of the above form are described elsewhere [5]).

We would like to thank Professor The Svedberg for his kind interest and encouragement. The help of Mr. R. Alphonce during part of the measurements was very valuable, and the cyclotron crew under Mr. Å. Svanheden was most helpful. The experimental work was supported by the Swedish Atomic Energy Commission.

We are also grateful to Dr. F. Bjorklund for supplying a copy of his programme for the IBM 709 computer, to Mr. J. A. Pether and Mr. B. R. S. Buckingham for their work on this programme, to the operating staff of the A.W.R.E. IBM 709 computer for their assistance, to the Director of the Oxford University Computing Laboratory for the use of the Ferranti Mercury Computer, to Mr. B. Buck and Mr. R. N. Maddison for their work on the computer programme, and to Miss N. Reynolds, Miss S. Tilley and the staff of the Computing Laboratory for their assistance.

References

1) R. Alphonce, A. Johansson and G. Tibell, Nuclear Physics **3** (1957) 185
2) R. Alphonce, A. Johansson and G. Tibell, Nuclear Physics **4** (1957) 643
3) R. Alphonce, A. Johansson and G. Tibell, Nuclear Physics **4** (1957) 672
4) F. Bjorklund and S. Fernbach, Phys. Rev. **109** (1958) 1295
5) B. Buck, R. N. Maddison and P. E. Hodgson, Phil. Mag. (London), in the press

3.A:4.E

Nuclear Physics **21** (1960) 393—396; © *North-Holland Publishing Co., Amsterdam*

Not to be reproduced by photoprint or microfilm without written permission from the publisher

THE HALF-LIFE OF THE FIRST EXCITED STATE OF Tl^{203}

E. C. B. PEDERSON † and R. E. BELL

Radiation Laboratory, Department of Physics, McGill University, Montreal

Received 27 July 1960

Abstract: The half-life of the 279 keV excited state of Tl^{203} has been measured from the logarithmic slope of a delayed coincidence curve. This method is preferable to the centroid shift method which was used for previous delayed coincidence measurements, since it is much less sensitive to systematic effects and to drifts in the apparatus. The half-life was found to be $T_{\frac{1}{2}} = (2.41 \pm 0.10) \times 10^{-10}$ sec, in agreement with previous results from resonance fluorescence, but in moderate disagreement with most recent Coulomb excitation results.

The half-life of the 279 keV excited state of Tl^{203} has been measured by a delayed coincidence technique, with a time resolution sufficient to enable the half-life to be read from the slope of the delayed coincidence curve. This half-life has been measured many times in the past by the delayed coincidence (centroid shift) method [1, 2, 3, 4]), by Coulomb excitation [5, 6]), and by resonance fluorescence [7]). Some of the values obtained, converted to half-lives, are shown in table 1. The value of half-life for the Coulomb excitation measurements was

TABLE 1

Authors	Method	$T_{\frac{1}{2}}$ (in 10^{-10} sec)
Barloutaud *et al.* [5])	Coulomb excitation	3.6 ±1.2
McGowan and Stelson [6])	Coulomb excitation	3 2 ±0.4
Metzger [7])	Resonance Fluorescence	2.7 ±0.5
Azuma and Lewis [1])	Del. Coin. (Centroid Shift)	2.1 ±0.7
Berlovich and Dubinkin [2])	Del. Coin. (Centroid Shift)	2.9 ±0.3
Ewan and Graham [3])	Del. Coin. (Centroid Shift)	2.5 ±0.7
Bashandy, Gerholm and Lindskog [4])	Del. Coin. (Centroid Shift)	2.9 ±0.2
Present work	Del. Coin. (Slope)	2.41±0.10

calculated by Bashandy, Gerholm and Lindskog [4]) from the data of the original investigators [5, 6]), using the E2/M1 mixing ratio $\delta^2 = 2.25 \pm 0.25$ obtained from polarization and angular correlation measurements [6]).

In the present measurement, coincidences were counted between the beta particles from Hg^{203} leading to the 279 keV first excited state in Tl^{203}, and the 279 keV gamma rays from the de-excitation to the ground state. The "fast-slow"

† Now at the Department of Physics, Queen's University, Kingston, Ontario, Canada.

scheme of Bell, Graham and Petch [8]) was used, with the addition of a time-to-amplitude converter similar to that previously described by Green and Bell [9]). The resulting pulse height spectrum was analyzed on a 128-channel analyzer.

The source was ≈ 0.1 μc of Hg^{203} deposited on a 2.5 cm steel disc and covered with 60 $\mu g/cm^2$ of polyvinyl chloride acetate copolymer in four layers. The source was placed between two scintillation counters, each consisting of a 2.5cm $\times$ 2.5 cm $\times$ 1.3 cm diphenylacetylene crystal coupled on a large face to a 6342A photomultiplier. To exclude light and to admit beta particles to one counter, its crystal was covered with four layers of 1 mg/cm^2 mylar, each layer having an aluminium coating on both surfaces. The other crystal, which counted the gammas, was mounted in an aluminium can. The thickness of the can and the source backing was sufficient to exclude beta particles from the gamma counter.

The pulse height selector on the gamma counter was set to accept the high energy end of the Compton distribution from the 279 keV gamma rays, and the pulse height selector on the beta counter was set to accept the high energy end of the beta spectrum. These settings were left unchanged when the prompt curve was taken. The annihilation radiation from Na^{22} positrons annihilating in aluminium was used as a prompt source. The spectrum from the prompt source covered the energy regions accepted by the pulse height selectors, approximating the conditions under which the delayed curve was taken. In addition, the prompt source gave greater counting rates than the Hg^{203} source, so that any broadening of the prompt curve due to spurious counting rate effects would be seen.

The slight tail on the right hand side of the prompt curve is due to delayed coincidences between one annihilation quantum and the 1.28 MeV gamma ray from Ne^{22} accompanying the production of the positron. Because of its energy, this gamma ray contributes about 20 % of the events accepted by the pulse height selectors, and thus would be expected to contribute to the prompt curve a tail having the mean life of positrons in the aluminium surrounding the Na^{22} source. This mean life has been measured as $(1.9 \pm 0.2) \times 10^{-10}$ sec [10]), about 30 % greater than the "instrumental mean life" of the upper part of the prompt curve. The tail is therefore not due to any instrumental fault; in any case its presence does not interfere with the measurement. The Na^{22} prompt curve is adequate to show the instrumental time resolution. It is shown in fig. 1. normalized to the same area as the delayed coincidence curve.

A time calibration was obtained by means of delay cables before and after the three day run on Tl^{203}, and a 2 % change in the calibration constant was found. The prompt curve was taken in a five hour run.

The results for Tl^{203} show an exponential decay over four decades, having a half-life $T_{\frac{1}{2}} = (2.41 \pm 0.10) \times 10^{-10}$ sec. This value was obtained both from the logarithmic slope and by the third moment method of Weaver and Bell [11]). The third moment method requires only the normalized third moment N_3

of the delayed curve about its own centroid and the normalized third moment ε of the prompt curve about its own centroid. Then the mean life $\tau = [\frac{1}{2}(N_3 - \varepsilon)]^{\frac{1}{3}}$. ε is usually small and frequently negligible compared with N_3, so only a rough knowledge of the prompt curve is required. In the present case, ε is 2 % of N_3 and thus an error of 0.7 % would be made in neglecting it completely. The statistical error in the value of τ evaluated from the third moments was calculated from functions given by Weaver and Bell [11]) and is 0.75 %. Calculations

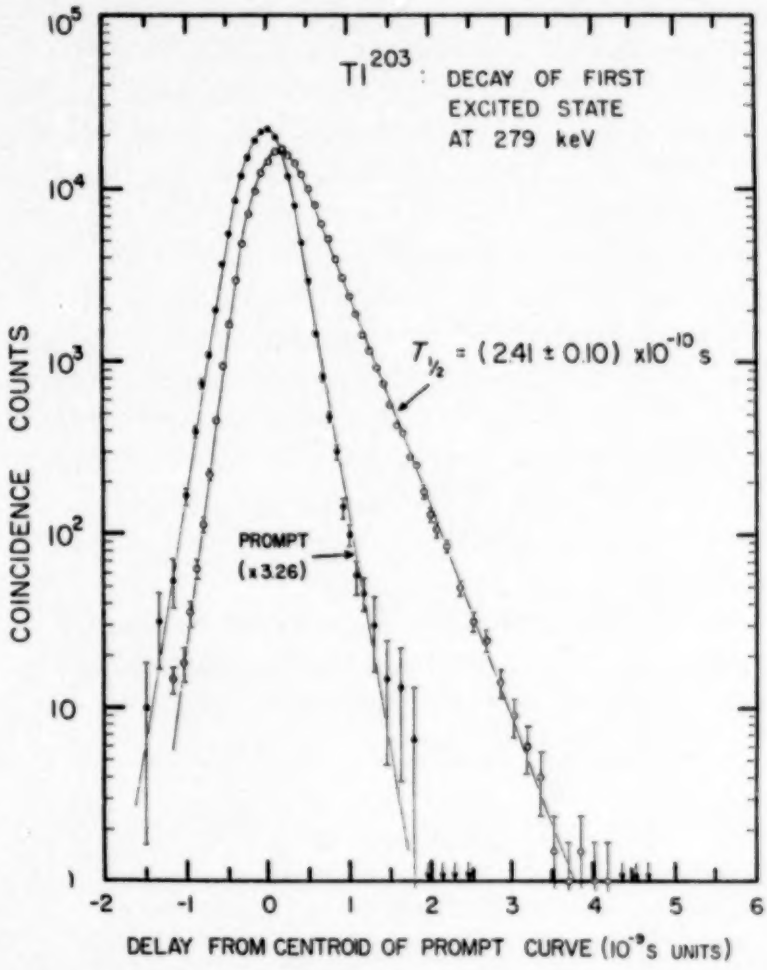

Fig. 1. Time distribution of coincidences between the beta rays leading to the 279 keV first excited state of Tl^{203}, and the de-excitation gamma rays. The prompt curve was obtained from the annihilation radiation coincidences due to positrons from Na^{22}, annihilating in aluminium, and was taken with the same counter biases as the delayed coincidence curve. The "instrumental half-life" of the exponentially decaying portion of the prompt curve is 1.0×10^{-10} sec. For comparison, the prompt curve is shown normalized to the same area as the delayed curve. The small arrows on the time axis represent zero counts.

of the moments were done on an IBM 650 computer using a program written by R. S. Weaver. The total error of 4 % assigned to the half-life determination is mainly to allow for the uncertainty in the time calibration. The value of the half-life obtained from the logarithmic slope of the delayed curve is within 1 %

of the value obtained by the third moment method. However, the value obtained from the shift of the centroid of the delayed curve from the centroid of the prompt curve is 11 % lower than the value obtained by the third moment method, showing the presence of a significant centroid shift due to instrumental effects. This shift does not affect the value for the half-life calculated from logarithmic slope or from the third moments.

The present value of $(2.41\pm0.10)\times10^{-10}$ sec for the half life is in moderate disagreement with the value of $(2.9\pm0.2)\times10^{-10}$ sec found by Bashandy, Gerholm and Lindskog [4]) using a centroid shift method. It is in moderate disagreement with the half-life which they calculate from the Coulomb excitation measurements of McGowan and Stelson [6]), $T_{\frac{1}{2}} = (3.2\pm0.4)\times10^{-10}$ sec.

The present value is in agreement with the nuclear resonance scattering measurement of Metzger [7]), who found that the radiative mean life $\tau_\gamma = (4.7\pm0.8)\times10^{-10}$ sec. The half-life $T_{\frac{1}{2}}$ is related to τ_γ by the relation $\tau_\gamma = T_{\frac{1}{2}}(1+\alpha)/\ln 2$, where α is the total conversion coefficient. If one assumes $\alpha = 0.225\pm0.006$ from the data of Nordling *et al.* [12]), and of Nijgh *et al.* [13]), then $T_{\frac{1}{2}} = (2.7\pm0.5)\times10^{-10}$ sec, in agreement with the results of the present work.

Recent work by B. I. Deutch [14]) on resonance fluorescence by the centrifuge method has yielded a preliminary value for $\tau_\gamma = (5.15\pm0.25)\times10^{-10}$ sec. This value is subject to a correction which will reduce τ_γ, but probably not down as low as 4.7×10^{-10} sec.

The authors wish to thank Professor L. Yaffe for providing the Hg^{203} source, and Mr. G. Grant, who deposited the source. Thanks are also due to Dr. F. R. Metzger, who, during a visit to this laboratory, urged that the half-life be re-measured.

References

1) R. E. Azuma and G. M. Lewis, Phil. Mag. **46** (1955) 1034
2) E. E. Berlovich and G. V. Dubinkin, Soviet Physics JETP **5** (1957) 164
3) G. T. Ewan and R. L. Graham, private communication to ref. [7])
4) E. Bashandy, T. R. Gerholm and J. Lindskog, Arikiv för Fysik **17** (1960) 421
5) R. Barloutaud, T. Grjebine and M. Riou, Physica **22** (1956) 1129
6) F. K. McGowan and P. H. Stelson, Phys. Rev. **109** (1958) 901
7) F. R. Metzger, J. Franklin Inst. **261** (1956) 216
8) R. E. Bell, R. L. Graham and H. E. Petch, Can. J. Phys. **30** (1952) 35
9) R. E. Green and R. E. Bell, Nuclear Instruments **3** (1958) 127
10) R. E. Bell and M. H. Jørgensen, Can. J. Phys. **38** (1960) 652
11) R. S. Weaver and R. E. Bell, Nuclear Instruments **9** (1960) (to be published)
12) C. Nordling, K. Siegbahn, E. Sokolowski and A. H. Wapstra, Nuclear Physics **1** (1956) 326
13) G. J. Nijgh, A. H. Wapstra, L. Th. M. Ornstein, N. Salomons-Grobben, J. R. Huizenga and O. Almén, Nuclear Physics **9** (1958/59) 528
14) F. R. Metzger (private communication)

1.D.1:
4.C

Nuclear Physics **21** (1960) 397—405; © *North-Holland Publishing Co., Amsterdam*
Not to be reproduced by photoprint or microfilm without written permission from the publisher

SHELL MODEL CALCULATIONS FOR MASS 12 NUCLEI, PERTINENT TO A TEST OF THE CONSERVED VECTOR CURRENT THEORY

HANS A. WEIDENMÜLLER †

W. K. Kellogg Radiation Laboratory, California Institute of Technology, Pasadena, California ††

Received 1 August 1960

Abstract: Results of shell-model calculations are being reported, which determine whether two proposed experiments with mass 12 nuclei serve as good tests of the conserved vector current theory of β-decay. The measurement of the β-spectra in the decays of B^{12} and N^{12} to the ground state of C^{12} seems to give a very good test of the conserved vector current theory. As a by-product; calculations are reported for various transition probabilities within the mass 12 nuclei: those involving the first excited state of C^{12} are in poor agreement with experiment.

1. Introduction

The conserved vector current theory (C.V.C.T.) of β-decay [1, 2]) predicts that certain second order contributions to allowed, $\Delta T = 1$ transitions are given by the electromagnetic matrix elements of the analogous γ-transition. It is possible to detect these second order contributions to β-decay either by a careful measurement of the β-spectrum, which should show deviations from the allowed form, or by a measurement of the angular correlation between the β-particle and a subsequently emitted γ- or α-particle. The anisotropy of such a correlation should be proportional to second order matrix elements.

Since the C.V.C.T. applies only to the vector part of the β-interaction, and makes no statements about axial vector second forbidden matrix elements, it has been proposed [1]) that a good way to test this theory should be a simultaneous measurement of β^+- and β^--spectra (or angular correlations) from the $T = 1$, $T_z = \pm 1$ levels of two isobaric nuclei to a low-lying state with $T = 0$ of the nucleus with the same mass number. A comparison of the results eliminates the unknown axial vector contributions and gives a statement about the vector matrix elements, which should then be compared with the analogous γ-transition matrix elements.

As an example, Gell-Mann [1]) considered the β-decays of N^{12} and B^{12} to the ground state of C^{12}. The analogous γ-transition is pure M1 and proceeds from

† On leave of absence from Institut für Theoretische Physik der Universität, Heidelberg, Germany.

†† Work supported in part by the joint program of the Office of Naval Research and the U. S. Atomic Energy Commission.

the first $J = 1$, $T = 1$ level in C^{12} at 15.11 MeV. Both the strength of this transition Γ and the log ft of the allowed β-decay are known [3]; they are $\Gamma = 54.3 \pm 9.3$ eV and $\log ft = 4.1 \pm 0.05$. The $\log ft$ is inversely proportional to the square of the reduced Gamow-Teller matrix element $\langle||\sigma\tau||\rangle$, and Γ is proportional to the square of the reduced M1-matrix element,

$$\langle||\mathrm{M1}||\rangle = \langle||l\tau||\rangle + (\mu_p - \mu_n)\langle||\sigma\tau||\rangle \cong \langle||l\tau||\rangle + 4.70\langle||\sigma\tau||\rangle.$$

From the numbers given above for Γ and $\log ft$, one infers that

$$(4.70\langle||\sigma\tau||\rangle)^2 \cong \langle||\mathrm{M1}||\rangle^2. \tag{1}$$

Since the second forbidden vector contributions for the C.V.C.T. are proportional to the M1-matrix element $4.7\langle||\sigma\tau||\rangle + \langle||l\tau||\rangle$, from the knowledge of Γ one can immediately predict the deviation of the spectra from the allowed form. However, the theory of β-decay in its usual form with no π-mesonic corrections (henceforth referred to as Fermi-theory, F.T.), also gives second forbidden vector contributions, which are proportional to $\langle||\sigma\tau||\rangle + \langle||l\tau||\rangle$, and a good test of the C.V.C.T. is possible only if the prediction of C.V.C.T. and F.T. differ, that is if $\langle||\sigma\tau||\rangle \gg \langle||l\tau||\rangle$. Eq. (1) has the two solutions $|\langle||l\tau||\rangle| \ll |\langle||\sigma\tau||\rangle|$, and $\langle||l\tau||\rangle = -9.4\langle||\sigma\tau||\rangle$. Gell-Mann [1]) assumed the first possibility, in which case the experiment is very well suited for a test since the deviations from allowed form for F.T. and C.V.C.T. differ by a factor 4.70. If, on the other hand, the second solution should be the right one, there should be second-order-corrections of considerable size, no matter whether the vector current is conserved or not, and the proposed experiment would hardly be able to test the theory. The question therefore comes up whether one can determine the ratio $\langle||l\tau||\rangle/\langle||\sigma\tau||\rangle$ in this transition.

As was pointed out to the author [4]) a measurement of the β—γ-angular correlation in the β-decay of B^{12} and N^{12} to the first excited state in C^{12} might give another possibility to test the C.V.C.T. Here, the M1/E2-mixing ratio is unknown, and so is the ratio $\langle||l\tau||\rangle/\langle||\sigma\tau||\rangle$ in the M1 width. Also, the transition probability itself is not known very accurately.

This paper reports on the results of intermediate coupling calculations which try to determine these quantities. Since mass 12 nuclei are not too well described by previously reported intermediate coupling calculations [5, 6]), we will give full account of our results wherever necessary. As a by-product, the calculated $\log ft$ values for the decay of B^{12} to the first three states in C^{12} and various transition probabilities which relate to the first three states in C^{12} will be reported. In the discussion of the β—γ-angular correlation experiment we will be concerned only with the contributions from the vector interaction and not consider electromagnetic corrections due to the fact that the B^{12} and N^{12} ground states differ in energy by almost 4 MeV. This was done by Gell-Mann [7]) for the ground state transition.

2. Results of the Calculation

We carried through the calculations for central forces of Serber, Rosenfeld and Kurath exchange type, for values of $L/K = 5.3$, 6.8 and 8.3 and for values of a/K between 0 and 8. (The notation is standard, see e.g. ref. [8])). Most of the results obtained are similar to the ones reported by Kurath [5, 6]).

2.1. THE LEVEL SPECTRUM

For all types of forces and all values of L/K, the spectrum is similar to the one given by Kurath [5]). In all cases, the $J = 1$, $T = 1$ level lies below the $J = 2$, $T = 1$ level only for values of a/K close to zero; the point of intersection of the two curves for the position of the $J = 1$, $T = 1$ and $J = 2$, $T = 1$ level as a function of a/K moves from $a/K \approx 5.5$ for $L/K = 5.3$ to $a/K \approx 3$ for $L/K = 8.3$ for Kurath and Rosenfeld force mixtures, and is at $a/K \approx 2 \ldots 3$ for Serber forces and all values of L/K. In neither case is it possible to choose a/K such that the position of both these levels and the rest of the data, particularly the transition widths, is brought into agreement with experiment. It should be noted, too, that the experimental statement that the 4^+ level is certainly above 9 MeV excitation gives a lower limit on a/K which is usually larger than the a/K corresponding to the point of intersection of the curves for the $J = 1$, $T = 1$ and $J = 2$, $T = 2$ levels. On the other hand, from an analysis of inelastic electron scattering data, various authors (e.g. ref. [11])) have concluded that the first 2^+ level in C^{12} contains a certain amount of collective or two-quantum excitation, in which case its position calculated from the p-shell model alone should be above the experimental position. From these remarks, it becomes apparent that a choice of a/K can hardly be made from the comparison of the experimental and theoretical spectrum alone; this comparison gives only some limitation on the values of a/K to be used.

In all cases calculated, and with a/K chosen so that the 4^+ level was above 9 MeV excitation, there were no other levels between 0 and 9 MeV excitation, in particular, the second 0^+ level was situated around 15 MeV.

2.2. TRANSITIONS TO THE GROUND STATE OF C^{12}

The E2-width from the $J = 2$, $T = 1$ level has for all cases roughly the magnitude and dependence on a/K as discussed by Kurath [6]); it turns out to be about 0.75 eV and is in agreement with the experimental finding, $\Gamma < 3$ eV. These numbers make use of the choice of $\langle r^2 \rangle$ indicated by the elastic electron scattering experiments [16]), which is roughly a factor of 2 smaller than the value chosen by Kurath [6]), and so do all the E2-widths given subsequently. The E2-width from the first $J = 2$, $T = 0$ level falls slowly from its L—S-coupling-value of 0.006 eV; at values of a/K as indicated by the spectrum it turns out to be about 0.005 eV and is therefore lower than the experimental number

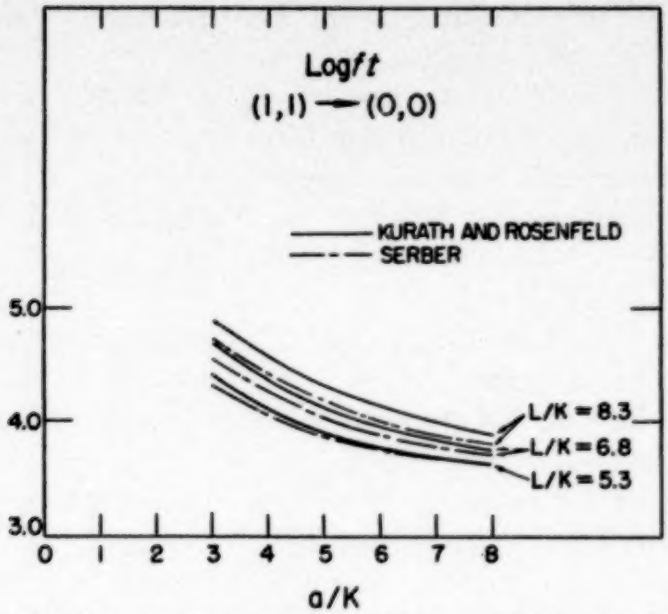

Fig. 1. Log ft for the B^{12} β-decay to the ground state of C^{12} as a function of a/K for various exchange force mixtures and values of L/K as indicated.

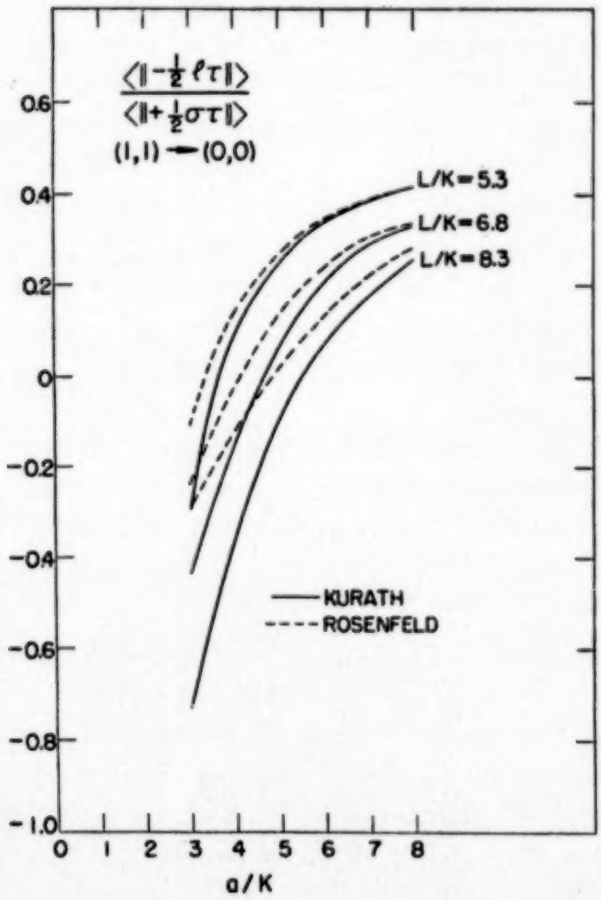

Fig. 2. The ratio $-\langle||l\tau||\rangle/\langle||\sigma\tau||\rangle$ for the $J = 1$, $T = 1$ to $J = 0$, $T = 0$ transition in C^{12} as a function of a/K for various exchange mixtures and values of L/K as indicated. The case of Serber forces in not shown in order not to obscure the picture, it remains, however, within the lines drawn for the other forces.

0.01 ... 0.02 eV [3]). It should also be noticed that according to ref. [11]) the calculated value cannot account for the inelastic electron scattering data †.

The M1-width of the $J = 1$, $T = 1$ state as a function of a/K was given by Kurath [6]), it is practically the same for all three force types, and for $L/K = 6.8$. In order to get the corresponding curves for $L/K = 5.3$ and 8.3, it has, roughly speaking, to be multiplied by 1.5 and by 0.6 respectively. The $\log ft$ as a function of a/K is shown for all cases in fig. 1, and $-\langle||l\tau||\rangle/\langle||\sigma\tau||\rangle$ in fig. 2. As pointed out in ref. [9]), we feel that the Gamow-Teller operator is better known than the magnetic moment operator; we therefore use fig. 1 to determine best values for a/K. It turns out, that $|\langle||l\tau||\rangle/\langle||\sigma\tau||\rangle| \leqq 0.1$ for these values, and $\Gamma(\mathrm{M1}) \approx 40$ eV. This is not quite in agreement with the experimental number; if we want to fit $\Gamma(\mathrm{M1})$, $\log ft \approx 4.0$. In view of the uncertainty of the magnetic moment operator, we consider this a fairly good agreement and can conclude that a has the magnitude assumed by Gell-Mann: $a \approx 1.15 \times 10^{-3}$. Here a is the number which measures the deviation of the spectrum from its allowed form [1]).

2.3. TRANSITIONS TO THE FIRST EXCITED STATE IN C^{12}. THE $\beta-\gamma$ ANGULAR CORRELATION FUNCTION

The most serious difficulty here is provided by the transition from the $J = 2$, $T = 1$ state which has an experimental width of about 70 eV, and is mostly M1 [19]). Its calculated E2 width is around 0.07 eV for all cases, and therefore neglible compared to the calculated M1 width, which for all cases (except again for factors of ≈ 1.5 or 0.6) has the behaviour shown by Kurath [6]) and never actually rises above 20 eV, the value for the best choice of a/K being 10 eV. There is no apparent reason to doubt the experimental information, so this discrepancy must be considered real and serious.

The second 0^+ state has a calculated width of about 10^{-3} eV. Ferrell, from his model of the 0^+ state [11, 12]), has calculated this width and found a similar number. Unless the two parts of the wave function presumably existing in the 0^+-state — the two quantum excitations and the p-shell wave function — contribute to the E2 transition in such a way that the parts cancel each other, these numbers seem to give a fairly reliable estimate on the width of this transition.

Kurath [6]) has also given the M1 width of the $J = 1$, $T = 1$ state, the calculated E2 width of which turns out to be negligible. The modifications introduced here by the various forces and values of a/K are about the same ones as described under 2.2 for the ground state transition. The calculated E2 width is a smooth function of a/K and is about 3×10^{-2} eV. Fig. 3 gives $\log ft$ for the β-decay, and in fig. 4 the ratio $-\langle||l\tau||\rangle/\langle||\sigma\tau||\rangle$ is plotted versus a/K. Although this transi-

† It should be pointed out in this connection, that the calculation of the form-factor for inelastic electron scattering to the first excited state of C^{12} as done by Ferrell and Visscher [11]) contains an assumption: their statement that the wave function for the 2^+state which they call the "collective" wave function is orthogonal on all 2^+-wave functions constructed from the $(1s)^4(p)^8$ configuration is true only for harmonic oscillator wave functions.

tion, too, reveals an apparently quite general pattern — decreasing value of this ratio with increasing mass number in the p-shell, — it is not quite as favourable for a test of the conserved vector current theory as is the ground state transition. The M1-width determined from the calculations turns out to be $\Gamma(\mathrm{M1}) = 2 \ldots 3$ eV, in good agreement with observation [3]), whereas $\log ft_{\mathrm{calc.}} = 4.6$ is in disagreement with the experimental finding [3]) 5.1 ± 0.2. This disagreement is

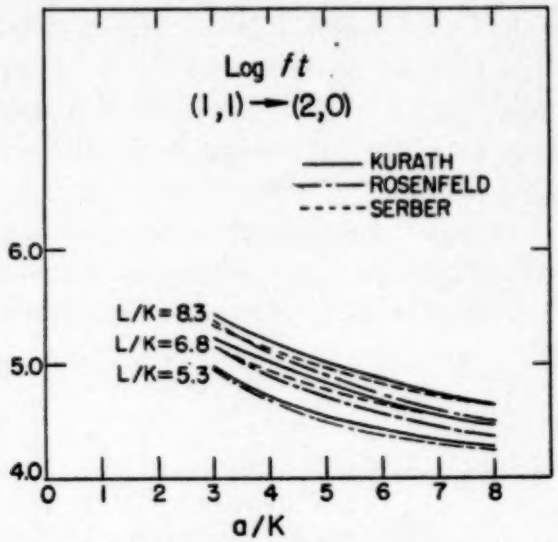

Fig. 3. Log ft for the B^{12} β-decay to the first excited state in C^{12} as a function of a/K for various exchange force mixtures and values of L/K as indicated.

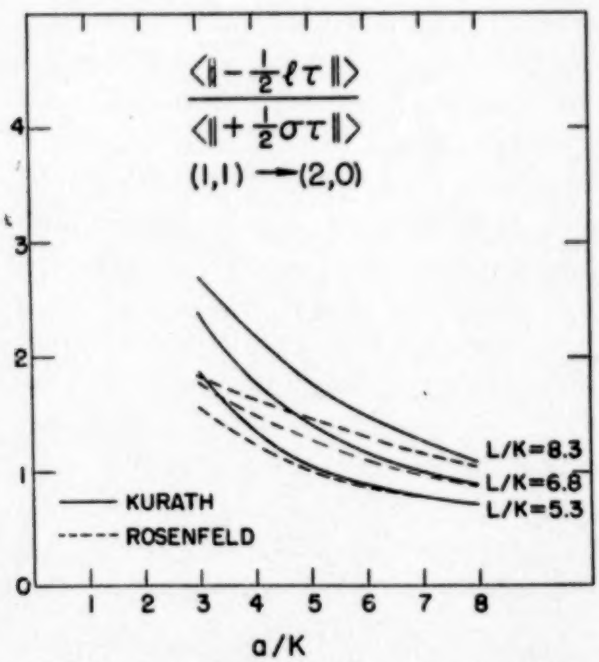

Fig. 4. The ratio $-\langle\|l\tau\|\rangle/\langle\|\sigma\tau\|\rangle$ for the $J = 1$, $T = 1$ to $J = 2$, $T = 0$ M1 transition in C^{12} as a function of a/K for various exchange mixtures and values of L/K as indicated. The case of Serber forces in not shown in order not to obscure the picture, it remains, however, within the lines drawn for the other forces.

rather serious for our purposes, since the ratio $-\langle||l\tau||\rangle/\langle||\sigma\tau||\rangle$ as given in fig. 4 cannot be right unless we assume that a fair part of the (1.1) → (2.0) transition is E2. In the discussion of the β—γ angular correlation function we have, therefore, to be rather careful.

Besides these difficulties, Levinson and Banerjee [17]) have observed that the proton-γ-angular correlation function, in the reaction $C^{12}(p, p^*)C^{12*}(\gamma)C^{12}$, as measured by Sherr *et al.* [20]), indicates that the wave functions of C^{12} are rather close to j—j-coupling, which demonstrates the necessity to enhance the E2 transition from the first excited state by some collective type of transition (compare, e.g. [11])). That the first excited state cannot be excited as easily in a (d, p) reaction with B^{11} as should be expected from the intermediate coupling model was observed by Bennett [18]) who found for the ratio of the two widths ≈ 1, whereas the theoretical value is around 2.0. This has to be taken rather cautiously, of course, since the analysis of these ratios faces serious difficulties.

The introduction of an admixture of collective excitation to the 2^+ state in the form proposed by Ferrell and Visscher [11])

$$\psi_{2^+} = N(\sum_i Y_2^m(i)r_i^2)\phi_0,$$

where ϕ_0 is the ground state wave function in intermediate coupling, might remove many of these difficulties: it enhances the E2 width sufficiently, and numerical calculations carried through by the author show that it itself gives only negligible contributions to the transitions to this state, whereas it reduces these transitions because of the normalization of the wave function. Thus, an admixture of 50 % of this excitation mode to the 2^+ states which is not in disagreement with inelastic electron scattering data, would bring the log ft value in agreement with experiment and reduce the M1 width from the $J = 1$, $T = 1$ state to about 1 eV which is not outside the experimental errors. It would also provide a better understanding of the observations of Levinson and Banerjee and of Bennett. It must be noted, however, that the $J = 2$, $T = 1$ transition width remains a problem.

From an inspection of the transition matrices it can be inferred that it is possible to construct wave functions in intermediate coupling such that all the transition probabilities come into agreement with experiment. Such a procedure seems not very promising, however, because of the large number of unknowns, and the situation remains puzzling.

If one assumes zero anisotropy for B^{12} and neglects E2 contributions for the moment, the β—γ angular correlation function for N^{12} has the form

$$W(\theta) = 1 - \tfrac{8}{3}a \times 0.598 \times 0.418 \times \frac{p^2}{W} P_2(\cos\theta),$$

where p and W are elecron momentum and energy and a is either the quantity

defined by Gell-Mann or its analogue in the F.T. of β-decay (see ref. [9])). This function differs from the corresponding one in the Li^8—B^8 decay by two factors. The average end-point energy is lower by a factor 1.5, and the different coupling of angular momenta reduces the anisotropy by another factor of two. Even with the same a, we obtain, therefore, only $\frac{1}{3}$ of the effect for mass 8 nuclei. Using the experimental log ft and $\Gamma = 3.5 \pm 2.5$ eV, we find

$$a = +(1.8 \pm 1.0) \times 10^{-3}$$

and an angular correlation function

$$W(\theta) = 1 - \alpha P_2(\cos\theta) \quad \text{at the end point energy,}$$

where $0.012 \leqq \alpha \leqq 0.04$ for the C.V.C.T. Here, use has been made of our calculations to determine the sign of a and α. Using the results of our calculations carefully, we presume that $-0.02 \leqq \alpha \leqq 0.02$ for the F.T. If, on the other hand, we use only our calculations and assume that both β-decay and M1-transition width are equally attenuated by a collective admixture to the 2^+ state as discussed above, we obtain $a = 10^{-3}$ and $\alpha \approx 0.014$ for C.V.C.T., and $a = 0 = \alpha$ for F.T. This needs, however, clarification by measurements.

The E2 contribution, as a result or our calculations, is small; its form was given in ref. [9]), and we obtain consistently $\langle ||\mathrm{E2}||\rangle / \langle ||\mathrm{M1}|,\rangle \cong 0.1$, which results in a negligible correction to the angular correlation function. It should be pointed out, however, that from the difficulties encountered in this section and because of the remarks made in subsections 2.1 and 2.2. a measurement of the mixing ratio of E2/M1 in the γ-transition seems necessary. Also, a more precise measurement of the width in question would be interesting.

2.4. THE SECOND 0^+ STATE IN C^{12}

The log ft value for the β-decay to this state is [3]) log $ft = 4.2 \pm 0.3$, its calculated value is around 3.65. This can be understood by the necessity to introduce two quantum-excitations in this state in order to explain its pair-width [14]); these excitations would not contribute, of course, to the allowed β-decay. If one assumes the $T = 1$, $J = 1$ state to contain a rather small admixture of two quantum excitations, which seems reasonable, then the log ft of the β-decay shows, of course, that the 0^+ level cannot be merely composed of two quantum excitations.

3. Conclusion

The overall agreement of the intermediate coupling model with experiment for mass 12 nuclei is such that all the qualitative features of these nuclei (except for the (2.1) → (2.0) transition width) are predicted properly, whereas it seems almost impossible to achieve a quantitative agreement with the forces used for

other nuclei. This is in contrast to the findings for $A = 8$ nuclei. Particularly, the disagreement of the calculated transition width of the $J = 2$, $T = 1$ state with the experimental value may cast some doubt on the validity of the estimates of the corresponding transition for mass 8 nuclei reported on in ref. [9]).

Among the various experiments in nuclear physics proposed so far as a test of the C.V.C.T., the measurement of the spectra of the ground state decays of B^{12} and N^{12} seems to offer the best possibility. The β—γ-angular correlation experiment seems to encounter difficulties similar in nature to the measurement of the β—α-angular correlation in mass = 8 nuclei [15, 9]) and should be accompanied by a measurement to find out the mixing ratio of M1 and E2 radiation in the (1.1) → (2.0) transition, and by a more precise determination of the width of the transition. A measurement of the magnetic moment of B^{12} might also give useful information in this connection.

The author is greatly indebted to Professor C. A. Barnes, Professor F. Boehm, Professor R. F. Christy and Professor W. A. Fowler for discussions on the various aspects of this work. He would like to thank Barbara Zimmerman for her help in the machine calculations. The hospitality of the Kellogg Radiation Laboratory is gratefully acknowledged.

References

1) M. Gell-Mann, Phys. Rev. **111** (1958) 362
2) R. P. Feynman and M. Gell-Mann, Phys. Rev. **109** (1958) 193
3) F. Ajzenberg-Selove and T. Lauritsen, Nuclear Physics **11** (1959) 1
4) C. A. Barnes, private communication
5) D. Kurath, Phys. Rev. **101** (1956) 216
6) D. Kurath, Phys. Rev. **106** (1957) 975
7) M. Gell-Mann and S. M. Berman, Phys. Rev. Lett. **3** (1958) 99
8) F. P. Elliott and A. M. Lane, Encyclopedia of Physics Vol. 39, p. 241 (Springer, Berlin, 1957)
9) H. A. Weidenmüller, Phys. Rev. Lett. **4** (1960) 299
10) G. Morpurgo, Phys. Rev. **110** (1958) 721
11) R. A. Ferrell and W. M. Visscher, Phys. Rev. **104** (1956) 475;
D. Kurath, Nuclear Physics **14** (1960) 398
12) R. A. Ferrell, private communication to Professor W. A. Fowler
13) E. E. Salpeter, Phys. Rev. **107** (1957) 516
14) F. P. Elliott, Phys. Rev. **101** (1956) 1212
15) E. Nordberg, C. A. Barnes and B. Povh, Phys. Rev. Lett. **4** (1960) 23
16) F. H. Fregeau and R. Hofstadter, Phys. Rev. **99** (1960) 1503
17) M. K. Banerjee and C. A. Levinson, Annals of Physics **2** (1957) 499
18) E. Bennett, cited in ref. [17])
19) D. S. Craig, W. Cross and R. Farris, Phys. Rev. **103** (1956) 1414
20) R. Sherr, see ref. [17])

3.B

Nuclear Physics **21** (1960) 406—437; © *North-Holland Publishing Co., Amsterdam*

Not to be reproduced by photoprint or microfilm without written permission from the publisher

LEVELS IN Th^{228} EXCITED IN THE ELECTRON CAPTURE DECAY OF Pa^{228}

E. ARBMAN †, S. BJØRNHOLM and O. B. NIELSEN

Institute for Theoretical Physics, University of Copenhagen

and

Gustaf Werners Institute for Nuclear Chemistry, University of Uppsala

Received 16 June 1960

Abstract: 22h Pa^{228} was produced by (p, 5n) reactions on Th^{232}. The decay was studied by means of a double-focusing high-resolution β-spectrometer, a six-gap high-transmission β-spectrometer, scintillation spectrometers, and coincidence techniques.

More than 200 conversion lines were found. Of these, 153 were ascribed to the Pa^{228} decay on the basis of their half-lives and assigned to 72 γ-transitions in Th^{228}. Numerous coincidence relations between conversion lines and γ-rays were measured.

A decay scheme comprising 22 excited states, ranging from 57.5 keV to 1943 keV, is presented and discussed with respect to the quantum numbers (K, I, π). In addition to the ground-state rotational band, the level structure indicates the presence of 3 or 4 rotational bands, built on intrinsically excited states. The possible collective vibrational character of the lower lying intrinsic states is discussed. Theoretical branching ratios and selection rules associated with the quantum number K are compared with experiment and discussed.

1. Introduction

Levels in Th^{228} excited by radioactive decay have been the subject of numerous investigations. The α-decay leading to Th^{228} has been studied by Asaro *et al.* [1]) and by Scharff-Goldhaber *et al.* [2]), who found the existence of a ground-state rotational band and a low lying negative parity band. The β-decay of Ac^{228} has been studied by several authors [3, 4, 5, 6]). Bjørnholm *et al.* [6]) have presented a decay scheme comprising a $(K, I, \pi) = (2, 2, +)$ band at 966 keV, a (2, 2, −) level at 1118 keV and higher lying states. Measurements [7, 8, 9, 10]) made on the 22 h electron-capture decay of Pa^{228} have revealed that a large number of levels up to about 1900 keV are excited, including most of those populated in the Ac^{228} decay. An interesting study of the 2% α-decay branch of Pa^{228} has also been made [10]). However, many details of the electron capture decay have been left open to question.

A new investigation of the Pa^{228} activity seemed worth while in view of the interest in the modes of excitation of nuclei with deformed equilibrium shape which arise from the progress made in the theoretical description of these excitations. Apart from the rotational levels one would thus expect to find

† Permanent address: Folkskoleseminariet, Falun, Sweden.

intrinsic excitations, some of collective vibrational nature [11,12]), others of single-particle nature [13]). It was hoped that the present study would add to our knowledge about the occurrence and properties of these intrinsic excitations. Experimentally, the difficulties caused by the complexity of the decay were to some extent compensated by the fact that one could take over the information gathered from studies of the α- and β-decay. In addition, a nucleide decaying by electron capture offers special advantages with respect to e—γ coincidence measurements, because one can focus on the conversion lines separately, without interference from a general β-background. The absence of a β-background also facilitates the identification of weak conversion lines. An extensive application of e—γ coincidence techniques, involving the six-gap β-spectrometer, turned out to be essential in the present study.

2. Experimental

2.1. ACTIVITY

300 mg of thorium metal powder were pressed into a section made in an aluminium block. The section, of dimensions $3 \times 10 \times 1$ mm, was open on two sides, displaying the thorium powder directly to the cyclotron beam. The powder was easily pressed into a pellet, which showed no sign of flaking off under the bombarding conditions used. The target was bombarded with 65 MeV protons in the Uppsala synchro-cyclotron. The bombardments lasted 4 to 6 hours with a current of about 1 μA. In all, six bombardments were carried out.

With a proton energy of 65 MeV the production of 0.9 d Pa^{228} by the (p, 5n) reaction is optimized [9]). But also 1.6 d Pa^{229} (E.C.), 17 d Pa^{230} (85 % E.C., 15 % β^-), 1.3 d Pa^{232} (β^-), 27 d Pa^{233} (β^-) and abundant amounts of fission activities are produced.

2.2. SOURCE PREPARATION

The protactinium was separated from the target material and fission products by chemical means. The procedure, which involved three successive absorptions and elutions of protactinium on anion exchange columns, is briefly described in ref. [14]). Hill has given a more detailed description of a method similar to ours [10]). In two cases, use was also made of an extraction of protactinium into di-isopropyl ketone. The column volume of the three ion exchange columns employed was 10, 0.1 and 0.001 ml, respectively. In this way, the activity was concentrated at the same time as the purification went on. The activity was eluted from the last column in a volume of about 0.001 ml and could readily be picked up on a 30 $\mu g/cm^2$ plastic foil, and dried. The β-spectrometer sources produced in this way had a thickness of 30 $\mu g/cm^2$ or less and an area of about 0.1 by 0.5 cm. The overall yield was 25 %—50 %, representing 0.4 to 2 mc of Pa^{228}. Weaker sources of about 5 μc were made for the coincidence experiments. No trace of other than protactinium activities could be found in

the freshly prepared sources. At the beginning of an experiment, the activity due to Pa^{228} was at least ten times stronger than each of the contaminating protactinium activities, Pa^{230}, Pa^{232} and Pa^{233}. (Pa^{229} fortunately decays [15]) to the ground state of Th^{229} and thus does not interfere with the conversion-line spectra, except for the Auger lines).

In one case, a source of isotopically pure Pa^{228} was prepared with the Copenhagen isotope separator [16]). The protactinium was mixed with a few milligrams of thorium oxide and placed in the ion source of the separator at a temperature of about 1000° C. Carbon-tetrachloride gas was let in through a needle valve. This leads to the formation of volatile chlorides, and a beam of thorium and protactinium ions could be extracted from the ion source. After passing the analysing magnet the ions strike into a collector plate from which one can cut out samples corresponding to the various mass numbers. The source prepared in this way had an activity of about 3 μc.

2.3. β-RAY SPECTROMETERS

The more important parts of the conversion-line spectrum (figs. 1 and 2) were measured with a 18.5 cm double focusing spectrometer [17]) adjusted to a resolution of 0.2 % and a transmission of 0.2 %. This instrument has recently been provided with an arrangement for automatic point-by-point recording of spectra, which very much facilitated the time-consuming high resolution measurements [18]).

The entire spectrum was measured with a six-gap orange-type spectrometer which is essentially an enlarged version of that described earlier [19]). Most of the spectrum was measured with the spectrometer adjusted to a resolution of 0.4 % and a transmission of 1 %. The high energy spectrum was measured with a resolution of 1.1 % and 9 % transmission (cf. table 1 and fig. 3). In e—γ coincidence experiments the resolution was 1.5 %, and the transmission almost 10 %.

2.4. ELECTRONIC EQUIPMENT

Spectra of the γ-rays were measured with a 7.6 cm $\times$ 7.6 cm sodium iodide scintillation spectrometer in connection with a 100-channel kicksorter of the Wilkinson type, developed in Harwell and manufactured by Philips.

The electronic equipment used for e—γ and γ—γ coincidence experiments is described in ref. [20]) where one will also find an account on methods for the quantitative determination of coincidence frequencies. (See also fig. 4 and caption to table 4). The coincident circuit had a resolving time of $\approx 5 \times 10^{-8}$ s.

3. The Measurements

3.1. INTERNAL CONVERSION LINES

The conversion-line spectrum was studied from 15 keV to 1900 keV electron energy. Duplicate runs under identical conditions were made with intervals of

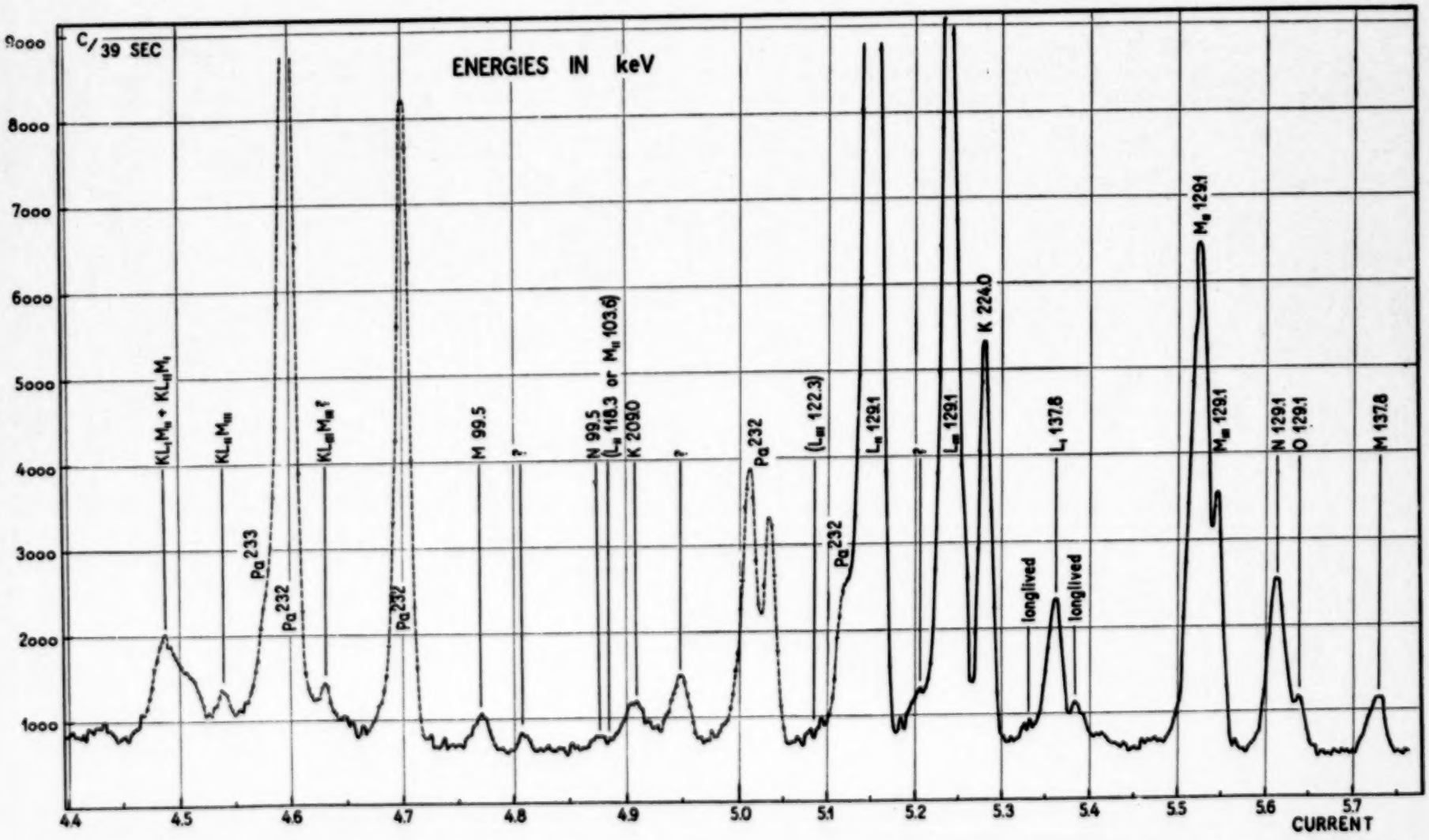

Fig. 1. Section of low energy conversion-line spectrum recorded with the double-focusing β-spectrometer. Resolution 0.4 to 0. 3%. Transmission 0.2 % Lines having half-lives longer than the 22 h Pa^{228} activity are dotted. The expected positions of conversion lines from rotational E2 transitions between members of rotational bands built on excited levels are given in parentheses (L_{II} 118.3 or M_{II} 103.6 and L_{III} 122.3).

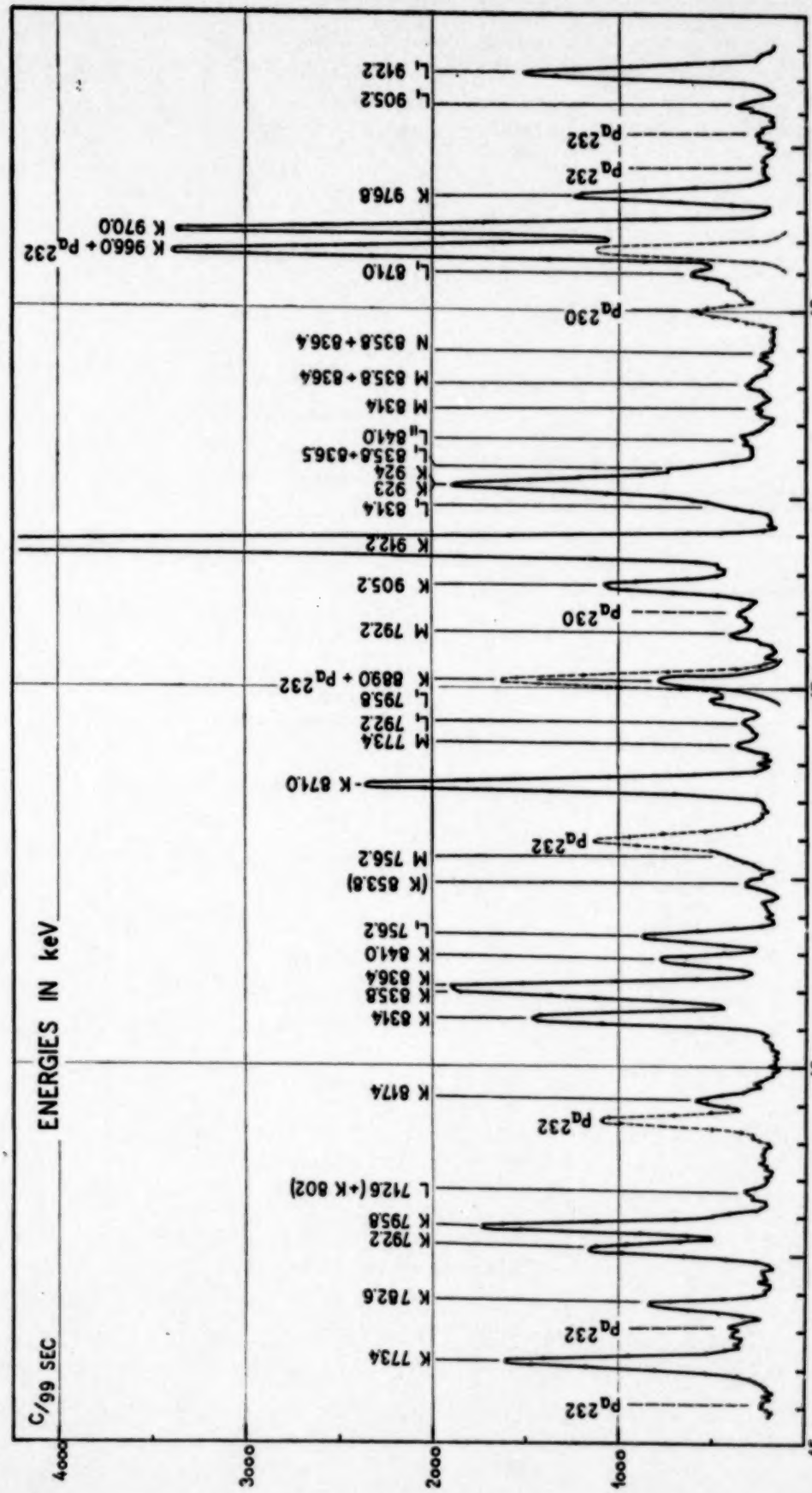

Fig. 2. Section of medium energy conversion-line spectrum recorded with the double-focusing β-spectrometer. Resolution 0.2 %. Transmission 0.2 %. Lines having half-lives longer than 22 h are dotted. In two cases, K 889.0 and K 966.0, lines have been resolved into components belonging to Pa^{233} and Pa^{232}, respectively. This has been achieved by comparison with the conversion-line spectrum of an isotopically pure source of Pa^{233}.

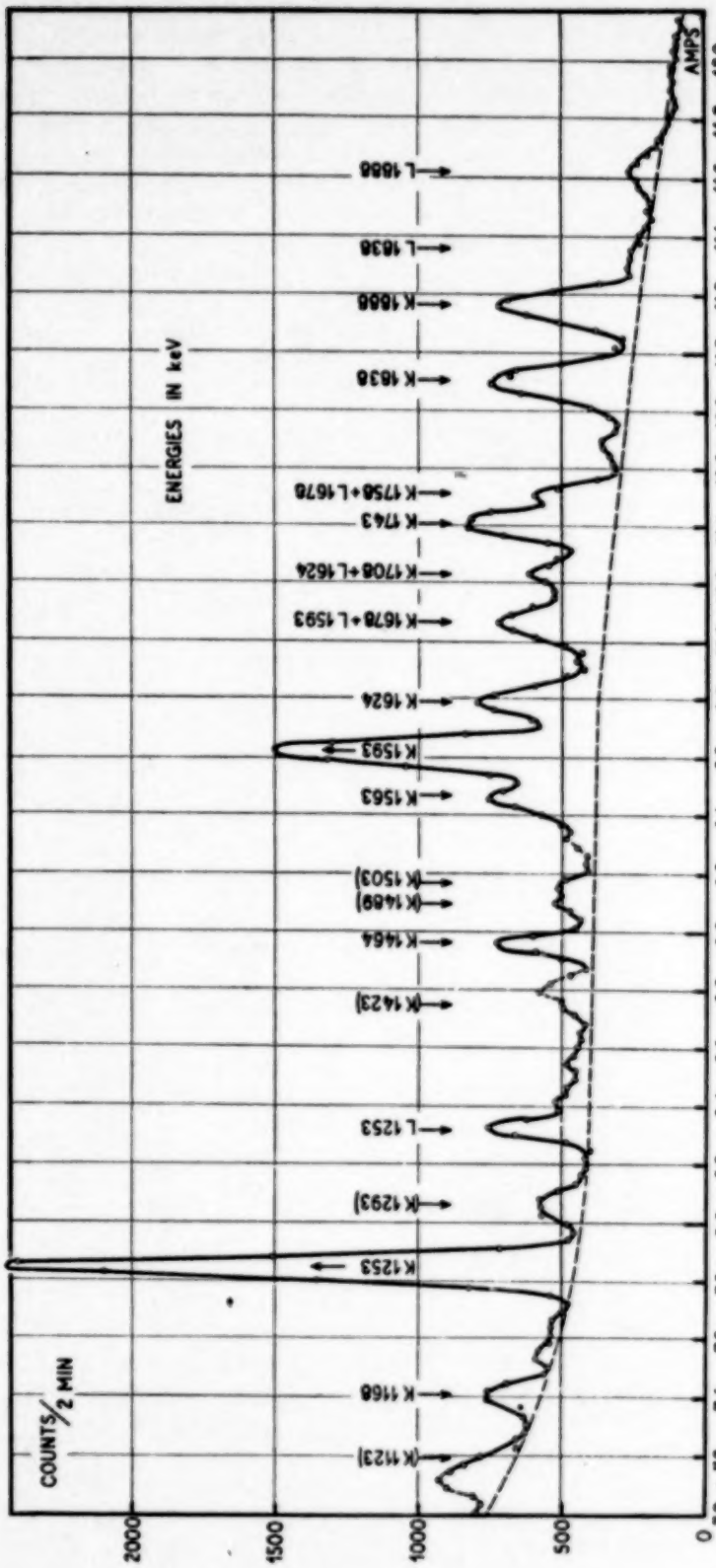

Fig. 3. High energy conversion-line spectrum recorded with the six-gap β-spectrometer. Resolution 1.1 %. Transmission ca. 9 %.
Lines having half-lives longer than 22 h are dotted.

TABLE 1. Conversion lines of Ac^{228} and Pa^{228}.

The first two columns list the energy and intensity of conversion lines observed in the investigation of the β^--decay of Ac^{228} published in ref. [8]). The following two columns give the same quantities observed in the Pa^{228} electron capture decay. The fifth column lists the measured half-life of each conversion line. The assignment of the lines is given in column 6. Part of the weaker lines not assigned may be associated with the 2 % α-decay branch of Pa^{228} leading to excited states in Ac^{224} and, subsequently, Ra^{224} (ref. [10])). In the next column, lines or groups of lines, whose coincident γ-spectra have been recorded, are marked. Column eight indicates which lines have been accounted for by the decay scheme (fig. 5). The last column refers to the spectrometer conditions. The accuracy of the energy determination varies with the spectrometer conditions. In general, the energies are believed to be accurate to 0.1 % on an absolute scale and somewhat better relatively. The intensities are given in per cent of all electron capture decays. The relative accuracy of the intensities is believed to be 5 % for the stronger lines. The absolute accuracy is not better than 10 %.

Ac^{228}		Pa^{228}						
Energy (keV)	Abs. int. (%)	Energy (keV)	Abs. int. (%)	Half-life (days)	Assignment	Coin. pref.	Placed in dec. scheme	Spectrometer
38.3	14.3	37.5	32.0	0.7–1.0	$L_{I\text{-}II}$ 57.5	++	+	Six gap
41.8	12.7	40.1	28.0		L_{III} 57.5	+++	+	Resl. ≈ 1 %
53.5	5.6	52.9	16.2		M 57.5		+	
57.5	2.5	56.5	5.3		N 57.5		+	
		65.2	0.4	0.96	Ra 224?			
		67.1	0.2	0.92				
68.6	0.35	68.3	1.5	0.98	K 178.0, Auger			Double focusing
74.6	2.75	74.7	1.3		K 184.5	+	+	Resl.
79.0	2.02	78.9	0.4		$L_{I\text{-}II}$ 99.4		+	0.33—0.25 %
		84	0.9	1.2	Auger?	+		
		85.8	0.2	1.1	Auger?			
		89.1	0.2	1	Auger?		+	
94.3	0.71	94.3	0.2	0.83	M 99.4		+	
		95.7	0.1	0.8				
		98.3	0.07	1	N 99.4		+	
99.1	0.17	99.4	0.22	0.92	K 209.0		+	
109.2	3.30	109.5	8.10	0.95	$L_{I\text{-}II}$ 129.1	+++	+	
		111.2	0.10	0.80	Ra 224?			
112.8	1.70	112.7	5.00	0.85	L_{III} 129.1	+	+	
		114.3	1.95	0.85	K 224.0	+	+	
117.8	0.03	117.6	0.90	0.95	$L_{I\text{-}II}$ 137.8	+		
124.6	1.28	124.5	3.10	0.80	M 129.1		+	
128.2	0.39	128.0	1.10	0.70	N 129.1		+	
		132.6	0.31	1.00	M 137.8			
		136.6	0.09	0.80	N 137.8			
		137.9	0.04	1				
		138.5	0.03	1				
157.5	0.10	157.6	0.13	0.90	$L_{I\text{-}II}$ 178.0			
161.0	0.11	160.4	0.12	0.75	K 270.0	+	+	
164.2	0.86	164.0	0.35	0.95	$L_{I\text{-}II}$ 184.5	+	+	
169	0.03	169.0	0.06		(K 278)			
172.4	0.07	172.3	1.28	0.90	K 282.2	+++	+	
		175.0	0.08		(L_{III} 191.3)		(+)	
179.2	0.22	179.3	0.07	1.00	M 184.5		+	
		183.3	0.02	1	N 184.5		+	
		186.6	0.06	0.80	(M 191.3)		(+)	

TABLE 1 (continued)

Ac^{228}		Pa^{228}						
Energy (keV)	Abs. int. (%)	Energy (keV)	Abs. int. (%)	Half-life (days)	Assignment	Coin. pref.	Placed in dec. scheme	Spectrometer
189.0	0.04	189.1	0.05	0.80	L_{I-II} 209.0		+	
		200.3	0.03	1	Ra 224?			
		201.4	0.02	1				
		203.4	0.38	0.81	L_I 224.0		+	
		218.1↑	0.13	0.85	M 224.0		+	
218.2	0.07	218.1↑	0.08	0.85	K 327.5 E1	+	+	
		218.1↑	0.13	0.85	K 327.5 E2		+	
		218.1↑	0.08	0.85	K 327.5 E1		+	
		221.4	0.01	1	Ac 224?			
		222.7	0.04	0.85	N 224.0		+	
228.1	0.19	228.9	0.17	0.80	K 338.5	+	+	
		231.5	0.14	0.80	K 341.1	+	+	
		237.5	0.01	1				
		241.6	0.01	1	Ac 224?			
250.2	0.026	250	0.03		L_{I-II} 270.0	+	+	
		257.8	0.09	0.75	(L_{I-II} 278)			
261.5	0.022	262.0	0.31	0.85	L_{I-II} 282.2	+	+	
		265.4	0.022		L_{III} 282.2		+	
		277.0	0.070	0.80	M 282.2		+	
		281.0	0.033		N 282.2		+	
		287.0	0.040		(K 397)			
298.4	0.083	300.1	0.540	0.88	K 409.7	+	+	
306.4	0.012	307.0↑	0.015		L_{I-II} 327.5 E1	+	+	
		307.0↑	0.120		L_{I-II} 327.5 E2		+	
		307.0↑	0.015		L_{I-II} 327.5 E1		+	
		311.2	0.050		L_{III} 327.5		+	
317.4	0.038	318.3	0.050		L_{I-II} 338.5		+	
		321.5	0.090	0.96	L_{I-II} 341.1		+	
		324.6	0.030		L_{III} 341.1		+	
		336.3						
350.9	0.110	353.7	0.870	0.75	K 463.3	+	+	
		359.6	0.020	1	(K 469.2)			
387.6	0.035	390.0	0.210		L_{I-II} 409.7		+	
		393.0	0.046		L_{III} 409.7		+	
		404	0.070	0.7—1.0	M 409.7		+	
		409	0.015		N 409.7		+	
		444	0.330		L_{I-II} 463.3		+	
		447	0.075		L_{III} 463.3		+	
		459	0.095		M 463.3		+	
		507	0.005		(K 617)			
		512	0.015		(K 622)			Six gap
		531	0.030	0.95	K 641			
		552	0.012		K 662			Resl. 0.4 %
		556	0.018	1.00	K 666			
		560	0.004		(K 670)			
		570	0.010		K 680			
		584	0.030	0.85	K 694			

TABLE 1 (continued)

Ac^{228}		Pa^{228}						
Energy (keV)	Abs. int. (%)	Energy (keV)	Abs. int. (%)	Half-life (days)	Assignment	Coin. pref.	Placed in dec. scheme	Spectrometer
		594	0.024		K 704		(+)	
		602	0.017		K 713		+	
		622	0.020		K 732			
		629.7	0.007	1.1	K 739.6		(+)	
		636.0	0.016	0.80	K 745.6			
642	0.050	646.8	0.124	0.90	K 756.2	+	+	Double focusing
659	0.025	663.6	0.042	0.85	K 773.4	+	+	
670	0.010	673.0	0.015	0.88	K 782.6		+	
		682.5	0.031	0.90	K 792.2		+	
681	0.052	686.1	0.053	0.80	K 795.8	+	+	Resl. 0.2 %
		692.2	0.005	1	L_{II} 713		+	
		707.8	0.010	0.90	K 817.4			
		721.6	0.038	0.87	K 831.4		+	
		726.1	0.020		K 835.8			
723	0.017	726.7	0.050	0.87	K 836.4	+	+	
		731.4	0.020	0.80	K 841.0		+	
730	0.013	735.6	0.025	0.80	L 756.2		+	
		744.2	0.005	1	(K 853.8)		(+)	
		761.5	0.080	0.90	K 871.0	+	+	
		768.2		1	M 773.4		+	
		771.9		1	L_I 792.2		+	
		775.5		1	L_I 795.8		+	
		779.4	c. 0.020		K 889.0			
		786.8		1	M 792.2		+	
		795.5	0.027	0.75	K 905.2	(+)	+	
801	0.210	802.3	0.250	0.90	K 912.2	+	+	
		809.4			L_I 831.4		+	
		813.0	0.047	0.90	K 923		+	
812	0.025	813.0	0.025	0.90	K 924	+	+	
		816.0			L_I 835.8	+	+	
					L_I 836.4		+	
		821.6			L_{II} 841.0		+	
		826.5			M 831.4		+	
		830.6			M 835.8			
		835.5			N 836.4		+	
		850.6			L_I 871.0		+	
		855.9	0.146	0.85	K 966.0	+	+	
859	0.130	860.4	0.135	0.80	K 970.0		+	
		867.1	0.050	0.90	K 976.8	+	+	
		884.7			L 905.2		+	
890	0.038	891.9	0.057	0.80	L_I 912.2		+	
895	0.027	902.2	0.012	0.90	L 923, 924		+	
907	0.015	907.2	0.012	0.90	M 912.2		+	
		911.0			N 912.2		+	
		918.4			M 923, 924		+	
		924.5	0.006		K 1034.1		+	

TABLE 1 (continued)

Ac^{228}		Pa^{228}						
Energy (keV)	Abs. int. (%)	Energy (keV)	Abs. int. (%)	Half-life (days)	Assignment	Coin. pref.	Placed in dec. scheme	Spectrometer
951	0.034	945.5	0.033	0.90	L_1 966.0		+	
		940.2	0.033	0.80	L_1 970.0		+	
965	0.011	956.5 / 961.5	0.015	0.80	MN 966, 970		+	
		1013	0.0020	1.50	K 1123		(+)	Six gap Resl. 1.1 %
		1058	0.0020	0.85	K 1168			
		1102	0.0005		L 1123		(+)	
		1143	0.0190	0.9	K 1253			
		1183	0.0015	1.2	K 1293			
		1231	0.0035	0.9	L 1253			
		1250	0.0010		MN 1253			
		1277	0.0008		L 1293			
		1312	0.0006		(K 1423)			
1359	0.0030	1354	0.0025	1.3	K 1464		+	
		1379	0.0008		(K 1489)			
		1393	0.0008		(K 1503)		(+)	
		1453	0.0030	1.0	K 1563		(+)	
1494	0.0120	1483	0.0130	1.0	K 1593		+	
		1514	0.0050	0.9	K 1624		(+)	
		1543	0.0007		L 1563		(+)	
		1568	0.0030	0.9	K 1678			
		1568	0.0025	0.9	L 1593		+	
		1599	0.0020	1.0	K 1708		+	
		1599	0.0010	1.0	L 1624		(+)	
		1634	0.0060	0.8	K 1744			
		1648	0.0015	0.8	K 1758		+	
		1648	0.0006		L 1678			
		1688	0.0007		L 1708		+	
		1728	0.0060	0.9	K 1838		+	
		1778	0.0060	0.9	K 1888		+	
		1816	0.0009		L 1838		+	
		1870	0.0011	1.0	L 1888		+	

†) Unresolved lines analyzed, taking into account the L conversion line intensities and the branching ratios known from Ac^{228}.

2 or 3 days in order to establish the half-life of the conversion lines separately. After the decay of Pa^{228} and Pa^{232}, a third run up to 1000 keV electron energy was made, thus identifying the conversion lines of Pa^{230} and Pa^{233}. Finally, a source of isotopically pure Pa^{232} (made by neutron activation of Pa^{231}) has been measured under the same conditions in the six-gap β-spectrometer.

More than 200 lines were found. Of these, 153 have been ascribed to the decay of Pa^{228} and assigned to 72 γ-transitions in Th^{228}. A few weak conversion lines were not assigned. They may be associated [10]) with the 2 % α-branch of

TABLE 2. Multipolarities and intensities of γ-transitions.

Column 1 lists the energy of the gamma transitions. Column 2 gives the multipolarity, assigned to each transition on the basis of the data given in the following columns. Square brackets indicate that the evidence is not considered conclusive; at least considerable admixtures are not excluded. The following four columns list the evidence that can be extracted from the relative intensities of the conversion lines. In the next three columns, the intensities of the γ-rays, determined from 1) the total γ-spectrum, 2) the e—γ coincidences or 3) calculated from the conversion-line intensities (assuming the multipolarity given in column 2) are compared. Column 11 lists the sum of conversion-line and γ-ray intensities. In the last column the transitions placed in the decay scheme (fig. 5) are marked. The intensities are in per cent of all electron capture decays.

E_γ (keV)	Multi-polarity	L_{I-II}/L_{III}		K/L		γ-intensity (%)				Total intensity (%)	Placed in decay scheme
		exp.	theor.	exp.	theor.	total γ-spectrum	coinc. γ-spectra	calculated from conversion data	adopted value		
57.5	E2	1.15	1.17					0.4		82	+
99.4	M1	>9	200					0.12		0.7	+
129.1	E2	1.62	1.70			2—5		3.9		21	+
137.8	M1	>10	210					0.7		2.0	
178.0	M1	>5	220	≈4	5.0			0.15		0.85	
184.5	M1	>10	220	≈4	5.0			0.50		2.2	+
(191.3)	[E2]					8.5 [a]		≈0.5 } 5.9		(≈1)	(+)
209.0	E1			≦4.5	5.3			≈3.5		3.8	+
224.0	M1	>20	225	5.1	4.8			1.2		3.6	+
270.0	E1			4	5.4			3.0		3.2	+
(278)	(E2)			0.6	0.8	5.1		0.7 } 6.0		(0.9)	
282.2	M1+		230	4.9	4.9			1.4		4.0	+
	E2 [b]		3.3		0.8			0.9			+
327.5	E1		8		5.4			3.2		3.3	+
327.5	[E2]	2.7	3.9	1.0	1.1			2.2		2.5	+
327.5	E1′		8		5.4	17.5		3.2 } 18.6		3.3	+
338.5	E1	>6	8.5	3.0	5.4			7.5		7.8	+
341.1	E2	3.0	4.0	1.2	1.2			2.5		2.8	+
(397)								<2.0			
409.7	E2	4.5	5.0	2.1	1.6	13		13.5	13.0	14	+
(462)	[E2]						2.8		2.8	≈3	+
463.3	E2	4.4	5.8	2.1	1.9	32	25	25	25	26	+
(469.2)											
(617)											

(469.2)											
(617) (622) 641 662 666 (670) 680 694						≈10		<17 % = 17 % if all E1			
704	[M1]							0.35		0.4	(+)
713	E2						1.3	1.2	1.2	1.2	+
732								0.12			
739.6	[M1]							<5		0.13	(+)
745.6								2.1			
756.2	M1			5.0	4.7		2.2	3.4	2.1	2.3	+
773.4	E2					≈10	3.6	1.2 } 11—17	3.4	3.5	+
782.6	[E2]							0.62		1.2	+
792.2	M1						≈0.7	4.5	0.6	0.7	+
795.8	[E2]						≦6		4.5	4.6	+
817.4											
831.4	E2						3.6	3.5	3.5	3.5	+
835.8											
836.4	E2					6.5	7	4.7 } 11	5.9	6.0	+
841.0	E2						1.6	1.9	1.9	1.9	+
853.8	[E2]							0.5		0.5	(+)
871.0	[E2]						5	8.0	8.0	8.0	+
889.0											
905.2	E2						3	2.9	3.0	3.0	+
912.2	E2			4.4	3.8	44	30	27 } 46	27	27	+
923	[E2]			5	3.8		5		5	5	+
924	[E2]						4	7.8	3	3	+
966.0	E2						21	17.5	17.5	17.5	+
970.0	E2			4.2	3.8			15.5 } 40		15.5	+
976.8	E2					49	6	6		6	+
1034.1	[E2]							0.8		0.8	+
(1123)	[E2]			≈4	4			0.3		0.3	(+)
1168						3.5					

TABLE 2 (continued)

E_γ (keV)	Multi-polarity	L_{I-II}/L_{III}		K/L		γ-intensity (%)				Total intensity (%)	Placed in decay scheme
		exp.	theor.	exp.	theor.	total γ-spectrum	coinc. γ-spectra	calculated from conversion data	adopted value		
1253	[M1]			5.4	4.5			1.1			
(1293)				≈2		2	0.8				
(1423)											
1464	[E2]					5	1.5	0.6	0.6	0.6	+
(1489)											
(1503)	[E2]							0.2		0.2	(+)
1563	[E2]			≈3			0.15	0.9		0.9	(+)
1593	[E2]			5.2	5	7	6	3.8	4	4	+
1624	[E2]			5				1.4		1.4	(+)
1678											
1708	[E2]			3	≈5			0.7	0.7	0.7	+
1744	[E2]					3	2.2	2.0 } 3.2			
1758	[E2]							0.5	0.5	0.5	+
1838	[E2]			7	≈5			2.5 } 5.0	2.5	2.5	+
1888	[E2]			5	≈5	4	4	2.5	2.5	2.5	+

[a]) Intensity corrected for sum effect, due to KX-rays.
[b]) The ratio of M1 to E2 determined on the basis of the relative intensities of the K, the L_{I-II} and the L_{III} conversion lines.

TABLE 3. Theoretical conversion coefficients for E1, M1 and E2 transitions ($Z = 90$).

The table is based on the conversion coefficients calculated by Rose [28]), and by Sliv and Band [29]), taking into account the effect of finite nuclear size. In all cases of interest to the present study, the results of these authors are found to agree within a few per cent.

E_γ (keV)	L_{I-II}/L_{III}			K/L			α_L			α_K		
	E1	M1	E2	E1	M1	E2	E1	M1	E2	E1	M1	E2
25.6	0.702	110	0.77				1.98	152	5626			
51	1.64	175	1.15				0.481	22.5	215			
77	2.26	190	1,25				0.165	6.97	29.4			
102	2.27	200	1.48				0.0657	3.06	7.77			
204	5.05	220	2.32	5.3	4.8	0.42	0.0135	0.429	0.355	0.0722	2.04	0.149
306	7.6	237	3.48	5.4	4.9	1.00	0.00534	0.140	0.0707	0.0291	0.686	0.0708
408	9.6	255	5.03	5.4	4.8	1.60				0.0154	0.309	0.0402
511	12.3	268	6.88	5.4	4.8	2.14				0.00987	0.172	0.0265
767				5.5	4.4	3.23				0.00460	0.0583	0.0125
1022				5.5	4.5	3.87				0.00277	0.0274	0.0075
1533										0.00140	0.0090	0.0036
2044										0.00086	0.0042	0.0022

Pa^{228}. The assignment of the conversion lines to γ-transition energies followed without much ambiguity from the energy fits and the relative intensities. (See, however, footnote †) of table 1). The results are listed in table 1.

3.2. γ-TRANSITIONS

The energies of the γ-transitions are listed in table 2 together with the experimental evidence leading to multipole assignment of a number of the transitions. From the table it is seen that the multipolarity of most of the transitions below 500 keV can be determined on the basis of the L_{I-II}/L_{III} and K/L conversion ratios alone. Table 3 gives a list of theoretical conversion coefficients and ratios. From this, one can see to which extent the measured ratios allow a unique multipole assignment. Once the multipole order is known, one can calculate the γ-intensities relative to the conversion-line intensities. The γ-intensities can also be calculated relative to the intensity of the 98 keV K X-ray peak of the scintillation spectrum (fig. 4, above). On this basis, absolute intensities have been determined, although not with very great accuracy. One can now estimate the combined frequency of emission of conversion electrons and nuclear γ-rays. The result is 3.4 transitions per electron capture. This necessarily implies that each transition on the average is accompanied by, and — unless long lived isomeric states are populated — coincident with two to three other transitions, in addition to the K X-rays.

3.3. INTERNAL CONVERSION-LINE—γ-RAY COINCIDENCE MEASUREMENTS

The experimental set-up makes it possible to select the conversion line of a definite γ-transition or a small group of such transitions and measure the entire γ-scintillation spectrum coincident with this, or these few transitions. In view of the abundant number of transitions it is not possible immediately to understand the scintillation spectra in terms of the known γ-energies. A certain iterative procedure is required before an interpretation of the composition and the precise energy of the observed photo-peaks can be made. In this procedure, one is greatly helped by the fact that several of the prominent lines also appear in the Ac^{228} decay (see table 1), where their place in the decay scheme is determined and their coincidence relations are understood. One is also helped by knowing already the multipolarities and intensities of the transitions of energies less than 500 keV. Finally, the requirement that the transition energies should fit within relative errors with differences of the level energies will rule out many erroneous interpretations.

Fig. 4 gives two examples of the measured coincidence spectra. The upper one displays the γ-rays coincident with the 57.5 keV E2 transition which deexcites the first rotational state. It is immediately seen that almost all decays pass through this transition, as should also be expected, since it has an intensity of 82 % (table 2). At 950 keV and 300 keV, there appear to be transitions not

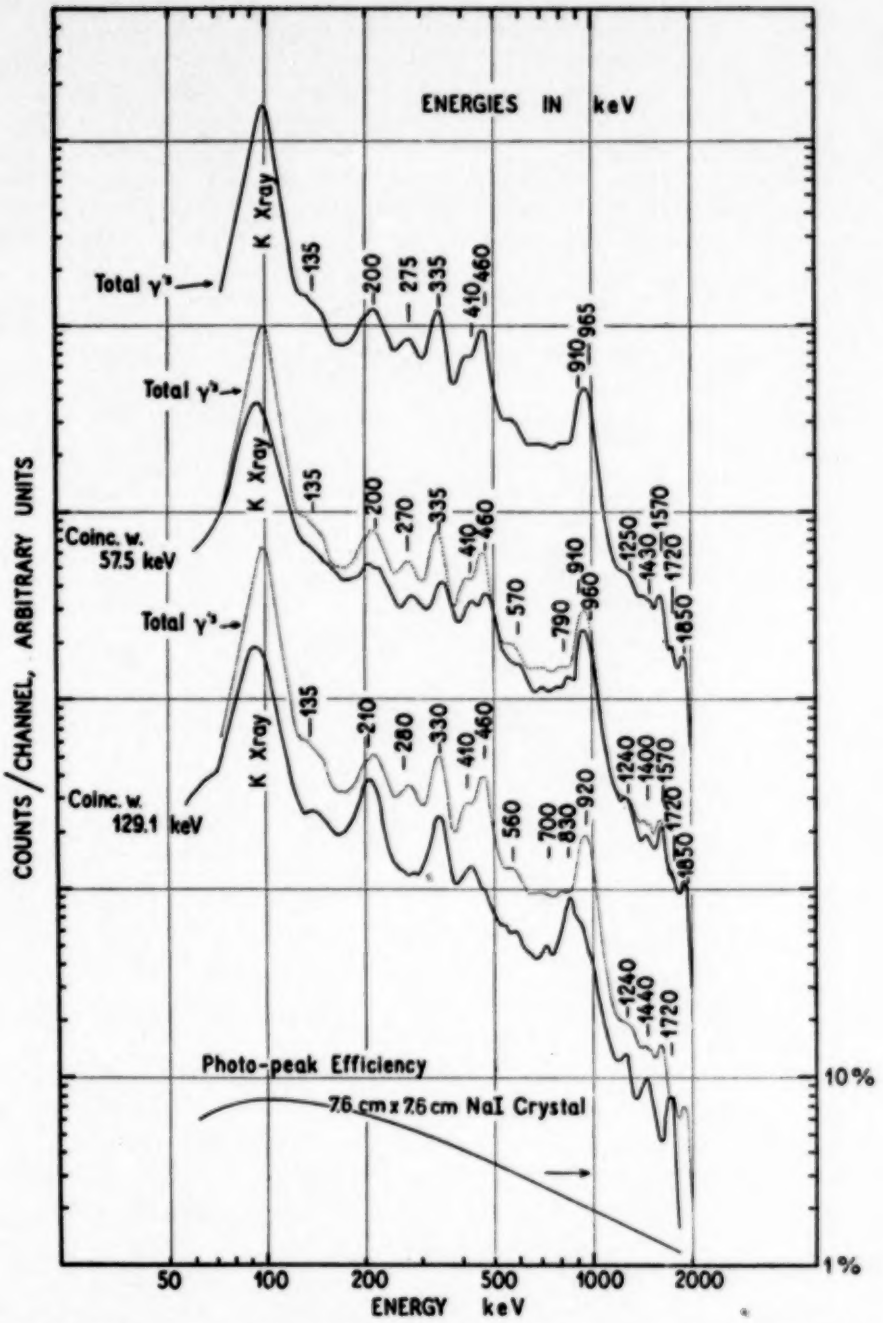

Fig. 4. Double-logarithmic plot showing above the γ-ray spectrum, recorded by a 7.6 cm × 7.6 cm sodium iodide crystal, of an isotopically pure source of Pa^{228}, prepared by the Copenhagen isotope separator. The following curves show the γ-ray spectra obtained in coincidence with conversion electrons of the 57.5 keV E2 (2+ to 0+) and the 129.1 keV E2 (4+ to 2+) ground state rotational transitions, respectively. Below, referring to the ordinate at the right-hand side of the figure, the photo-peak yield curve is shown. This curve gives, with about 5 % accuracy, the percentage of γ-rays recorded in the photo-peak at various energies of the γ-rays, and in the standard source-crystal geometry used for e—γ coincidence measurements with the six-gap β-spectrometer.

TABLE 4. Internal conversion line γ-ray coincidences.

Column 2 indicates the transition energy of the conversion line to which the β-spectrometer has been adjusted in the e—γ coincidence experiment. In these experiments, the β-spectrometer was operated at maximum transmission (c. 10 %) and, consequently, poorer resolution (1.5 %). In several cases, it has therefore not been possible to select one single transition, but rather a group of lines. The next column lists the peak energies found in the sodium iodide scintillation spectrum when gating with the conversion-electron pulses. In the subsequent column, an interpretation of the γ-peaks in terms of the transition energies found in table 2 is given. The coincidence yields in column 5 are corrected for solid angle and photo efficiency of the 7.6 cm × 7.6 cm sodium iodide crystal (see fig. 4), however, not for internal conversion. Corrections for sum effects due to the abundant coincidences with K X-rays have also been included. The energy of levels, established or indicated by the measured coincidence relations, are given in the last column.

Group No.	Selected transition (keV)	γ-rays found in coincidence with conversion electrons of selected transition			Levels established at: (keV)
		Peak energy (keV)	Interpretation (keV)	No. of γ-coincidences per electron (%)	
1a	57.5	100	K X-ray	70	
		135	129	6	
		200		12	
		270		8.3	
		335		15	
		410		11	
		460		15	
		570	?	4	
		690	?	4	
		790		14	
		910	912	37	969
		960	966	25	1023
		1240		1	
		1400		2	
		1570	1593	7	1650
		1720	1708+1744+1758	2.3	1894
		1850	1838+1888	3.6	1946
1b	129.1	100	K X-ray	122	
		135	(138)	10	
		210		30	
		280	282	4.5	
		330		27	
		410	410	14	
		460	463	5	
		560	?	6	
		700	713	8	
		760		7	
		830	836	40	1023
		920		27	
		1240		4	
		1440	1464	7	1650
		1550		1	1894
		1720	1708+1744+1758	10	1946

TABLE 4 (continued)

Group No.	Selected transition (keV)	γ-rays found in coincidence with conversion electrons of selected transition			Levels established at: (keV)
		Peak energy (keV)	Interpretation (keV)	No. of γ-coincidences per electron (%)	
2a	912 (+905)	330	341	2.5	
		460	463	45	1433
		750	756	$\leqq 5$	1894
		950 (broad)	924+977	15	1946
2b	966 +970	410	410	27	
		460	463	17	
		750	756	<4	1433
		840	871	7	
		900	923+924	10	1894
		960	977	9	1946
3a	341	440	462	No quantitative estimate possible	1894
		900	905		1092
3b	410	460	462		
		830	836	20	
		960	966	60	1433
3c	463	460	462	10	(1894)
		900	912	50	1433
		960	970	30	
4a	871 (+783L)	330	?	13	
		450	463	7	
		660	?	12	
		825	836	20	
		950	966	60	1894
4b	923+924	450	410+463 from 836L+912	50	1894
	(+836L +912)	950	912+966+970	55	1946
4c	977 (+970)	460	463 from 970	36	
		920	912+970	90	1946
5	756	900	912	55	
		960	970	40	1726
6	184	780	792	25	1154
		920	912+970	100	1946

TABLE 4. Internal conversion line γ-ray coincidences.

Column 2 indicates the transition energy of the conversion line to which the β-spectrometer has been adjusted in the e—γ coincidence experiment. In these experiments, the β-spectrometer was operated at maximum transmission (c. 10 %) and, consequently, poorer resolution (1.5 %). In several cases, it has therefore not been possible to select one single transition, but rather a group of lines. The next column lists the peak energies found in the sodium iodide scintillation spectrum when gating with the conversion-electron pulses. In the subsequent column, an interpretation of the γ-peaks in terms of the transition energies found in table 2 is given. The coincidence yields in column 5 are corrected for solid angle and photo efficiency of the 7.6 cm × 7.6 cm sodium iodide crystal (see fig. 4), however, not for internal conversion. Corrections for sum effects due to the abundant coincidences with K X-rays have also been included. The energy of levels, established or indicated by the measured coincidence relations, are given in the last column.

Group No.	Selected transition (keV)	γ-rays found in coincidence with conversion electrons of selected transition			Levels established at: (keV)
		Peak energy (keV)	Interpretation (keV)	No. of γ-coincidences per electron (%)	
1a	57.5	100	K X-ray	70	
		135	129	6	
		200		12	
		270		8.3	
		335		15	
		410		11	
		460		15	
		570	?	4	
		690	?	4	
		790		14	
		910	912	37	969
		960	966	25	1023
		1240		1	
		1400		2	
		1570	1593	7	1650
		1720	1708+1744+1758	2.3	1894
		1850	1838+1888	3.6	1946
1b	129.1	100	K X-ray	122	
		135	(138)	10	
		210		30	
		280	282	4.5	
		330		27	
		410	410	14	
		460	463	5	
		560	?	6	
		700	713	8	
		760		7	
		830	836	40	1023
		920		27	
		1240		4	
		1440	1464	7	1650
		1550		1	1894
		1720	1708+1744+1758	10	1946

TABLE 4 (continued)

Group No.	Selected transition (keV)	γ-rays found in coincidence with conversion electrons of selected transition			Levels established at: (keV)
		Peak energy (keV)	Interpretation (keV)	No. of γ-coincidences per electron (%)	
2a	912 (+905)	330	341	2.5	
		460	463	45	1433
		750	756	$\leqq 5$	1894
		950 (broad)	924+977	15	1946
2b	966 +970	410	410	27	
		460	463	17	
		750	756	<4	1433
		840	871	7	
		900	923+924	10	1894
		960	977	9	1946
3a	341	440	462	No quantitative estimate possible	1894
		900	905		1092
3b	410	460	462		
		830	836	20	
		960	966	60	1433
3c	463	460	462	10	(1894)
		900	912	50	1433
		960	970	30	
4a	871 (+783L)	330	?	13	
		450	463	7	
		660	?	12	
		825	836	20	
		950	966	60	1894
4b	923+924 (+836L +912)	450	410+463 from 836L+912	50	1894
		950	912+966+970	55	1946
4c	977 (+970)	460	463 from 970	36	
		920	912+970	90	1946
5	756	900	912	55	
		960	970	40	1726
6	184	780	792	25	1154
		920	912+970	100	1946

TABLE 4 (continued)

Group No.	Selected transition (keV)	γ-rays found in coincidence with conversion electrons of selected transition			Levels established at: (keV)
		Peak energy (keV)	Interpretation (keV)	No of γ-coincidences per electron (%)	
7a	270	340	328	No quantitative estimate possible	
		800 (broad)	796+841		(1123)
		1150 (broad)	1123		(1169)
7b	328 (E1 +E2+E1' +224 (M line)	200		10	
		270	270+282	25	
		330		30	
		450	?	25	
		800	796+841	55	
		930	?	20	
		1100	1123	10	
7c	338	220	224	No quantitative estimate possible	
		300	282		
		460	?		(1169)
		800 (broad)	773+831		(1227)
8a	773	200	209	15	
		280	282	28	1169
		340	338	55	(1451)
		650	Background?	10	
		750	do.	18	
		930	do.	19	
8b	796+ (792)	200	184	9	
		280	270	40	1123
		340	328(E2+E1)	80	(1451)
		630	?	14	
		920	912+970	28	
8c	831+	210 (broad)	209+224	35	1169
	836+ 841	260	270+282	7	1227
		330	328+338	25	(1451)
		410	410	33	
		660	?	16	
		900	871+923	25	
9a	224	200	209	25	
		340	328+338	60	1451
		450	?	5	1227
		700	713	15	514
		825	831	45	
		960		18	

TABLE 4 (continued)

Group No.	Selected transition (keV)	γ-rays found in coincidence with conversion electrons of selected transition			Levels established at: (keV)
		Peak energy (keV)	Interpretation (keV)	No. of γ-coincidences per electron (%)	
9b	282	100	K X-ray	180	
		140	?	26	
		200	209	33	
		270	270	12	
		340	328+338	45	
		450	?	25	1451
		780	773	38	1169
		860	841	36	
		960	Background?	40	
		1100	?	10	
10	178	690	?	No quantitative estimate possible	?
		1160	?		

passing through the first rotational state. The lower spectrum shows coincidence with the 4+ to 2+ transition in the ground-state band. This transition has an intensity of 21 %. Accordingly, a substantial part of the total spectrum has disappeared from the coincidence spectrum. One notes, for instance, that the 1850 keV peak has disappeared, while the 1720 keV peak is still present.

About 50 coincidence spectra were recorded, involving the conversion lines of 32 transitions and the photo-peaks of 50 different γ-rays. In most cases, the scintillation spectra only covered the energy interval 120—1200 keV. Table 4 summarizes the results.

Group one in table 4 deals with the transitions also shown in fig. 4. Here, the evidence for placing the high-energy transitions (> 1000 keV) in the decay scheme is presented. The following groups refer to the states at 969 keV, 1023 keV and 1092 keV. The lower two of these states are known from the decay of Ac^{228}. The three levels will be referred to as the γ-vibrational band. Group 2 contains the γ-rays coincident with the transitions de-exciting this band and thus indicate the transitions feeding the γ-vibrational band. Group 3 represents three strong transitions feeding the band. The groups 4, 5 and 6 have the same characteristic coincidence spectra as group 3, and represent weaker transitions feeding the γ-vibrational band. In group 7, the coincidence relations of the E1 transitions de-exciting the well-known negative parity band at 327.5 keV and 396 keV are given. It is seen that this band, referred to as the octupole vibrational band, is fed by groups of γ-rays of 700—850 keV and 200—350 keV. Groups 8 and 9 list the coincidences of these two groups of transitions. The measurement in group 10 has not been interpreted in an unambiguous way.

In the process of interpreting the coincidence measurements, the sequence of the transitions in the cascades is determined and the level scheme is built up. Using the measured coincidence frequencies it is then possible to calculate the γ-ray intensities of the transitions [20]). The results are found in table 2. It is seen that the multipole order of a major part of the transitions has been determined in this way. The total transition intensities are obtained at the same time.

3.4. γ—γ COINCIDENCE MEASUREMENTS

The γ-ray spectrum coincident with the group of γ-rays of 900—970 keV (fig. 4) has been recorded. The measurement confirms the E2 multipole assignment to the transitions from the levels at 1894 keV and 1946 keV to the γ-vibrational band.

4. The Decay Scheme

4.1. GENERAL

The decay scheme resulting from the measurements described in sect. 3 is presented in fig. 5. The scheme accounts for 47 of the 72 transitions found. The intensity of this fraction of the transitions amounts to 310 per 100 electron capture decays. 25 transitions are not included, representing about 30 per 100 decays. The measurements indicate that the unexplained transitions belong to a set of weakly populated states not included in fig. 5.

The quantitative coincidence experiments have allowed numerous cross-checks of the many cascades. The level energies can be calculated from the transition energies in up to five different ways, and the discrepancies found are within the relative experimental uncertainty which, in the majority of cases, is 0.3 keV. Finally, the intensity balance for the flow of transitions through the excited states to the ground state comes out in a consistent way. We therefore believe that the essential parts of the decay scheme cannot be subject to systematic errors.

4.2. INTENSITY BALANCE AND log ft VALUES

Table 5 gives a list of the levels and the intensity of feeding and de-exciting each level. By difference, the electron capture intensities are determined and log ft values calculated. (The log ft values found in the β^--decay are given for comparison.) It should be emphasized that the log ft values determined in this way are very uncertain, except for the strongly populated levels.

4.3. SPIN AND PARITY ASSIGNMENT AND BRANCHING RATIOS

The spins and parity of the ground-state rotational band are considered established *a priori*.

In a few cases, the assignment is unambiguously determined by the multipolarity of the de-exciting transitions. This is true for the levels at 327.5 keV

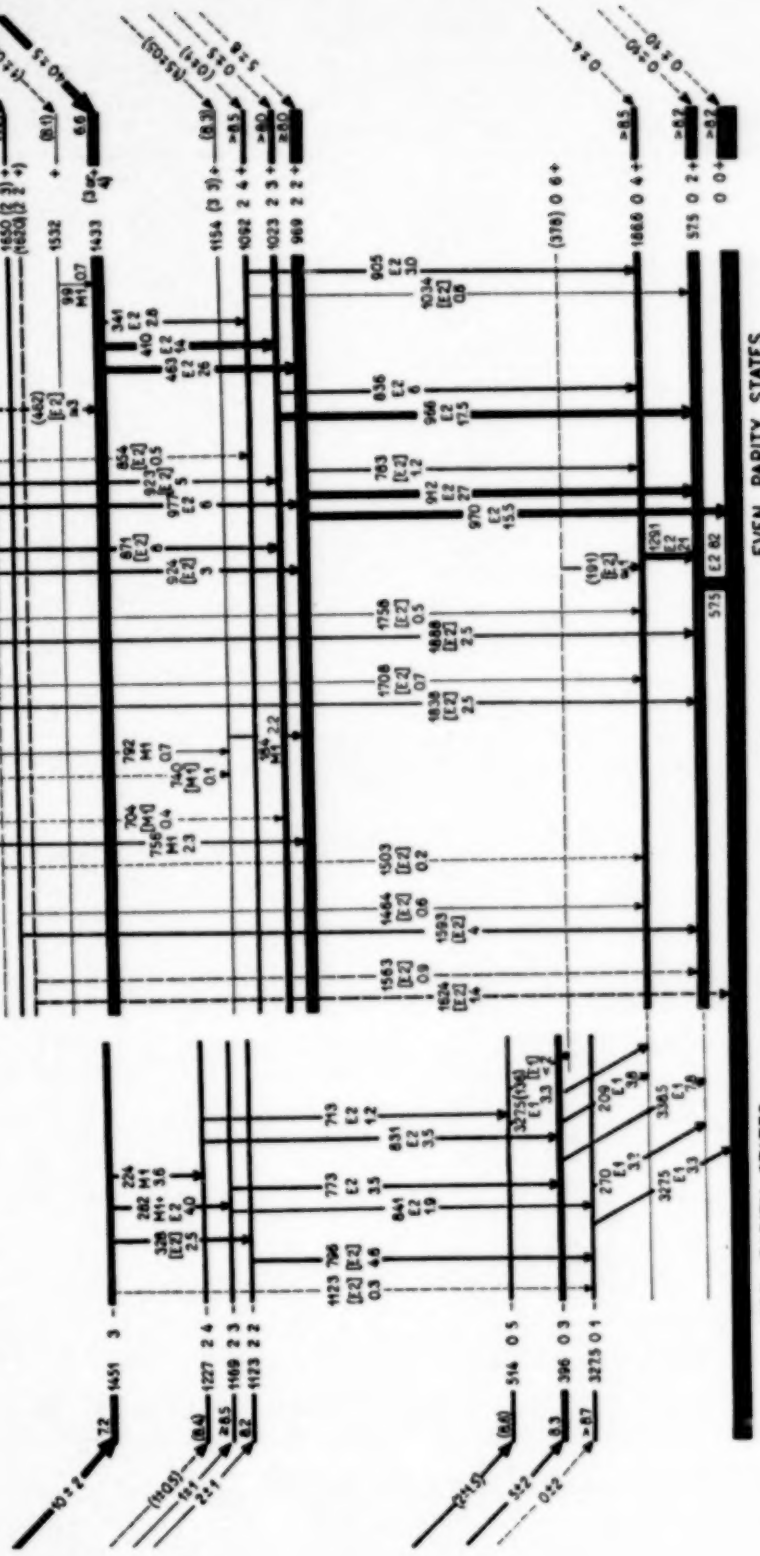

Fig. 5. The decay scheme $Pa^{228} \rightarrow Th^{228}$. The thickness of the lines reflects roughly the intensity of the transitions or the extent to which each level is populated. The odd-parity levels have been separated from those of even parity. The electron capture transitions are therefore seen to come in from both sides. (No β^--transitions are shown). Transitions and levels, for which only tentative evidence is obtained, are dotted. Similarly, numbers in parentheses are tentative, and could be subject to systematic errors. Multipolarities given in square brackets indicate that considerable admixture of other multipolarities cannot be excluded. In some cases, the multipolarity is arbitrarily assumed and the intensity calculated on this basis. For details, see tables 2 and 3.

TABLE 5. Total intensities of internal transitions feeding and de-exciting the levels in Th^{228} together with electron-capture intensities and log *ft* values.

The value $t_{\frac{1}{2}} = 22 \pm 1$h for the half life of Pa^{228} is taken from the Table of Isotopes [15]). It agrees with an average of our measurements (table 1, column 5). The electron capture decay energy $Q_{0EC} = 2.10 \pm 0.05$ MeV is found by closed cycle calculations [30]). Assigning a greater error to this quantity will result in a larger uncertainty on the log *ft* values of the upper two to three levels.

Numbers given in parentheses are tentative and could be subject to systematic error.

Level (keV)	K, I, π	Pa^{228}				Ac^{228} [a])
		Internal transitions		EC directly feeding level (%)	log *ft*	log *ft*
		feeding level (%)	de-exciting level (%)			
0	0, 0, +	101	0	0 ±10	>8.2	>8.8
57.5	0, 2, +	86	82	0 ±10	>8.2	8.8
186.6	0, 4, +	20	21	0 ± 4	>8.5	
327.5	0, 1, −	6.8	6.5	0 ± 2	>8.7	>9.5
395.8	0, 3, −	7.0	11.6	5 ± 2	8.3±0.3	8.5
514.1	0, 5, −	1.2	3.3	(2 ± 1.5)	(8.6±0.4)	
969.5	2, 2, +	39.5	43.7	5 ± 8	≧8.0	7.3
1023.2	2, 3, +	27.5	23.5	0 ± 5	>8.0	≧8.0
1091.8	2, 4, +	3.3	3.8	0 ± 1	>8.5	
1123.4	2, 2, −	2.5	4.6	2 ± 1	8.2±0.3	8.0
1168.8	2, 3, −	4.0	5.4	1 ± 1	≧8.5	
1227.0	2, 4, −	(3.6)	4.7	(1 ± 0.5)	(8.4±0.3)	
1154.0	(3, 3), +	(0.8)	2.2	(1.5± 0.5)	(8.3±0.3)	7.7
1432.8	(4), +	3.7	42.8	40 ± 5	6.6±0.1	>8.0
1451.0	(3), +	0	10.1	10 ± 2	7.2±0.1	≧8.3
1532.2	(4), +	0	0.7	(1 ± 0.5)	(8.1±0.4)	7.1
(1620)	(2, 2, +)	(0)	(2.3)	(2 ± 1)	(7.6±0.5)	
1650	(2, 3, +)	0	4.6	(5 ± 2)	(7.2±0.3)	6.8
(1690)	(2, 4, +)	(0)	(0.2)	(0.2± 0.1)	(8.5±0.5)	
1726	(3, 3, +)	0	2.7	(3 ± 1)	(7.2±0.3)	
1894.0		0	17	17 ± 4	6.0±0.4	
1946.3	(3, 3), +	0	15	15 ± 3	5.8±0.4	
Total		206	307	111 ±20		

[a]) Ref. [6]) and unpublished results of the authors of the same reference.

(1−), 396 keV (3−), and 969 keV (2+). In the remaining cases, the parity is uniquely determined and the spin value is restricted to one of a few possibilities. The rotational description of the nucleus, however, implies that unique quantum numbers can be assigned to several more levels, viz., on the basis of the observed branching ratios. In addition to the total spin one ascribes to the nucleus the quantum number K (the projection of the total angular momentum on the intrinsic nuclear symmetry axis). The transitions from an excited state to the members of a lower lying rotational band will be governed by simple geometrical selection rules [21, 22]). In fig. 6, the reduced relative theoreti-

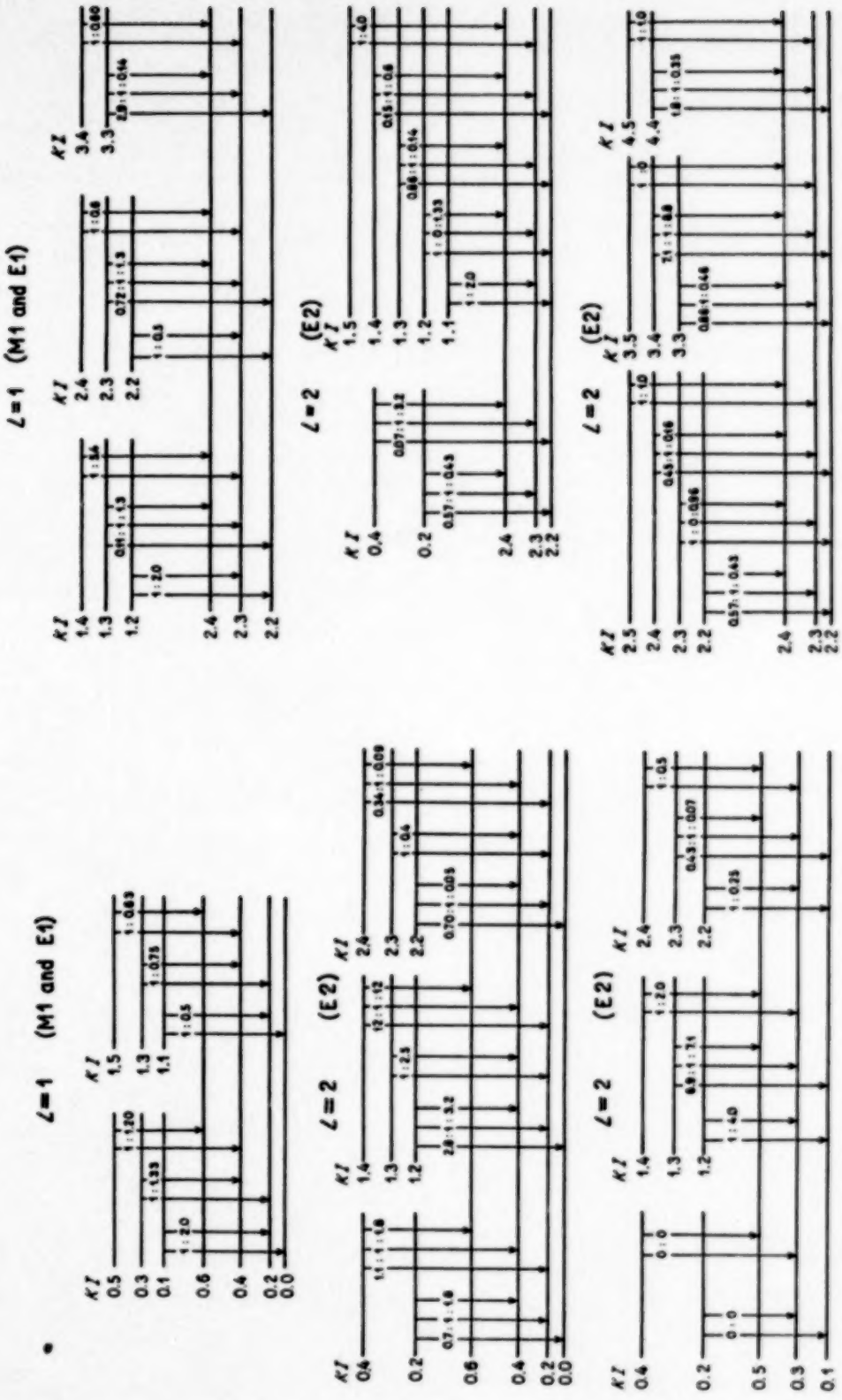

Fig. 6. Theoretical relative reduced branching intensities of transitions from one level to levels in a rotational band [21, 22]. One of the intensities in each branching has been normalized to unity.

TABLE 6. Reduced branching ratios.

The table gives the reduced intensities of the γ-transitions from the upper level listed in column 1 to the lower levels in column 4, the reduction factor being $(E_\gamma)^{2L+1}$, where L is the multipole order. One of the intensities in each branching has been normalized to unity. The experimentally determined branching intensities are given in columns 6 and 7 for Pa^{228} and Ac^{228}, respectively. The theoretical relative reduced branching intensities calculated directly from the Clebsch-Gordan coefficients are listed in column 8. In the last column a correction for the possible rotation-vibration mixing of states has been added to the numbers of column 8 (see text).

Upper level		Mul-tip.	Lower levels		Exp. branching intensity		Theor. branching intensity [b]	
(keV)	K, J, π		(keV)	K, J, π	Pa^{228}	Ac^{228} [a]	$z = 0$	$z = 0.03$
327.5	0, 1, −	E1	57.5	0, 2, +	(1.7) [c]	1.7	2.0	
			0	0, 0, +	1	1	1	
396	0, 3, −	E1	186.6	0, 4, +	2.0 ±0.6	1.8 ±0.3	1.33	
			57.5	0, 2, +	1	1	1	
514	0, 5, −	E1	378	0, 6, +	<9		1.2	
			186.6	0, 4, +	1		1	
969	2, 2, +	E2	186.6	0, 4, +	0.09±0.02	≦0.07	0.05	0.07
			57.5	0, 2, +	1	1	1	1
			0	0, 0, +	0.43±0.05	0.45	0.70	0.59
1023	2, 3, +	E2	186.6	0, 4, +	0.66±0.08	≈0.5	0.40	0.59
			57.5	0, 2, +	1	1	1	1
1092	2, 4, +	E2	378	0, 6, +	≦0.25		0.09	0.15
			186.6	0, 4, +	1		1	1
			57.5	0, 2, +	0.16±0.02		0.34	0.22
1123	2, 2, −	E2	396	0, 3, −	<0.5	<0.3	0.25	0.33
			327.5	0, 1, −	1	1	1	1
1169	2, 3, −	E2	514	0, 5, −	<0.3		0.07	0.11
			396	0, 3, −	1		1	1
			327.5	0, 1, −	0.36±0.04		0.43	0.32
1227	2, 4, −	E2	514	0, 5, −	0.75±0.20		0.50	0.83
			396	0, 3, −	1		1	1
1433	(3, 3), +	E2	1092	2, 4, +	0.46±0.05		0.46	
			1023	2, 3, +	1	1	1	
			969	2, 2, +	1.0 ±0.1	0.8 ±0.1	0.86	
do.	(4, 4), +	E2	do.	do.	0.46±0.05		0.35	
					1	1	1	
					1.0 ±0.1	0.8 ±0.1	1.8	
1451	?, 3, −	M1	1227	2, 4, −	1.72±0.3			•
			1169	2, 3, −	1			
			1123	2, 2, −	≪0.01			

TABLE 6 (continued)

Upper level		Multip.	Lower levels		Exp. branching intensity		Theor. branching intensity [b]	
(keV)	K, J, π		(keV)	K, J, π	Pa^{228}	Ac^{228} [a]	$z = 0$	$z = 0.03$
do.	—	E2	do.	do.	<2 1 1.3 ±0.4			
1650	2, 3, +	E2	186.6 57.5	0, 4, + 0, 2, +	0.24±0.05 1	0.36 1	0.40 1	0.59 1
1726	(3, 3), +	M1	1092 1023 969	2, 4, + 2, 3, + 2, 2, +	<0.4 1 5.0 ±1.5		0.14 1 2.9	
1894	+	E2	1092 1023 969	2, 4, + 2, 3, + 2, 2, +	<0.1 1 0.25±0.10			
do.		do.	186.6 57.5	0, 4, + 0, 2, +	0.4 ±0.1 1			
1946	(3, 3), +	E2	1092 1023 969	2, 4, + 2, 3, + 2, 2, +	0.25±0.1 1 0.9 ±0.3		0.46 1 0.86	
do.	(2, 3), +	do.	186.6 57.5	0, 4, + 0, 2, +	0.3 ±0.1 1		0.40 1	0.59 1

[a]) ref. [8])
[b]) cf. fig. 6.
[c]) see footnote [†]), table 1.

cal transition intensities are given for a number of cases which may be expected to occur in the decay of Pa^{228}. Table 6 gives a comparison of experimental and theoretical branching ratios and the assignments of quantum numbers K and I made on this basis. Comparison with fig. 6 shows to which extent the assignments are unique.

5. The Odd Nuclei Ac^{228} and Pa^{228}

A look at the decay scheme (fig. 5) and at the spin values, parities and log ft values in table 3 leads to the conclusion that Pa^{228} as well as Ac^{228} most probably have spin 3 and positive parity. How does this compare with a single-particle description of a nucleus having a deformed equilibrium shape?

From the diagrams of the calculated energies of neutron and proton states as a function of the deformation [13]) one finds for Ac^{228} (139 neutrons, 89 protons) the orbits n [631] $\frac{3}{2}+$, p [651] $\frac{3}{2}+$ and for Pa^{228} (137 neutrons, 91 protons)

the orbits n [752] $\frac{5}{2}-$, p [530] $\frac{1}{2}-$, when entering the diagrams at the experimentally measured [14]) deformation, $\beta = 0.225$. Using the spin-coupling rule suggested by Gallagher and Moszkowski [23]), one arrives in both cases at the desired value 3+. In this way, the all-over similarity in the two decays is explained by the fact that the parent nuclei have the same spins and parities, and the individual discrepancies are understood in terms of the different intrinsic configurations of the two nuclei.

It should be kept in mind that the experimental assignments are made on the basis of very poor evidence, and that a 3+ configuration can theoretically be constructed in other, less straightforward, ways. The above conclusions are thus likely to represent an oversimplification.

6. The Level Structure

6.1. ROTATIONAL BANDS

The level structure clearly points at the presence of rotational bands. In addition to the ground-state band, others are built on the 327.5 keV (0, 1, −), the 969 keV (2, 2, +), the 1123 keV (2, 2, −) and possibly on a 1620 keV (2, 2, +) state. Three members of each band are excited and the energy differences, with the exception of the 1620 keV band, are known to within 0.2 keV. It is therefore possible to calculate the parameters A and B in the expression for the rotational energy

$$E_{\text{rot}} = A\,I(I+1)+B\,I(I+1)^2. \tag{1}$$

A is proportional to the reciprocal of the effective moment of inertia

$$A = \frac{\hbar^2}{2\mathscr{I}}. \tag{2}$$

The second order terms represent the effect of perturbations of the intrinsic structure produced by the rotational motion. If the main effect can be attributed to a rotation-vibration interaction, it is convenient to define an effective energy E'_{vib} by means of an expression of the form

$$B = -2\left(\frac{1}{E'_{\text{vib}}}\right)^2\left(\frac{\hbar^2}{\mathscr{I}}\right)^3. \tag{3}$$

The eq. (3) is derived from the hydrodynamical model [24]), where E'_{vib} more specifically represents a weighted average of the energies of the β- and γ-vibrations, but it is only expected to be a qualitative relationship, since the hydrodynamical approximation is found not to account in a quantitative way for observed nuclear properties [11]).

The bands are arranged in the order of increasing energy of excitation. It should at first be noted that the moments of inertia exhibit variations of until

40 %. (In view of the experimental uncertainty attached to the existence of the 1620 keV band, this will not be included in the discussion). The values of B vary by a factor of three. The figures in the last column, E'_{vib}, show a small and apparently fairly smooth variation with the energy of the intrinsic excitation. Although this last result can only be considered a qualitative one, it supports the assumption of a rotation-vibration interaction as the main cause of the deviations from the simple rotational formula ($B = 0$). It should further be noted that there seems to be a systematic tendency for the E'_{vib}-values to decrease with increasing energy of excitation.

6.2. LIFETIMES

The present study does not include direct measurements of lifetimes of any of the levels encountered. However, Bell *et al.* [14]) have measured the lifetime of the first excited 57.5 keV (0, 2, +) state. They found the value $t_{\frac{1}{2}} = 4.0\times10^{-10}$ s, and from this calculated the intrinsic electric quadrupole moment, $Q_0 = (8.5\pm0.3)10^{-24}$ cm^2. The transition probability is enhanced by a factor of 200 compared to the single-particle estimate and represents a typical rotational transition. Similar E2 transitions should occur between members of the higher-lying rotational bands, where they have to compete with the high energy transition de-exciting the same levels. Such rotational transitions have not been found, but it is possible to give limits of their intensity (see fig. 1). Making the assumption that the quadrupole moment has the same value in the ground state and in the intrinsically excited states, one can determine upper limits for the lifetimes of these excited states. We have done this in three cases, and obtained the following limits:

$$t_{\frac{1}{2}} < 0.8\times10^{-11}\text{ s}\ (0.5\times10^{-14}\text{ s})\quad\text{for}\quad 514\text{ keV}\ (0, 5, -),$$
$$t_{\frac{1}{2}} < 4\ \times10^{-11}\text{ s}\ (1\ \times10^{-11}\text{ s})\quad\text{for}\quad 1092\text{ keV}\ (2, 4, +),$$
$$t_{\frac{1}{2}} < 1.3\times10^{-11}\text{ s}\ (2\ \times10^{-11}\text{ s})\quad\text{for}\quad 1227\text{ keV}\ (2, 4, -).$$

The numbers in parentheses are single-particle estimates of the partial lifetime of the competing high energy transition [22]). No corrections for spin dependence have been made.

6.3. VIBRATIONAL STATES

Nuclei having a deformed, ellipsoidal equilibrium shape are expected to exhibit several types of collective vibrational excitations [11]).

Two types of quadrupole vibrations are possible: β-vibrations having $(K, I, \pi) = (0, 0, +)$ and γ-vibrations with $(K, I, \pi) = (2, 2, +)$. Levels with these quantum numbers are in fact found in many deformed nuclei at excitation energies 700 to 1200 keV. Coulomb excitation studies have revealed that transitions between such states and the ground state occur with probabilities which are a few times enhanced compared to the single-particle estimate [25, 26])

In the present case, the (2, 2, +) band at 969 keV might well represent a γ-vibration. As can be seen above, the limit on the lifetime of the 1092 keV state unfortunately does not yield any decisive evidence in support of this assumption. No level that can be interpreted as a β-vibration has been observed. In view of the high spin of Pa^{228}, however, the population of a state of $K = 0$ may not be very likely.

In addition to the quadrupole vibrations, the occurrence of octupole vibrations having negative parity and $K = 0$, 1, 2 or 3 has been suggested. The $K = 0$ band at 327.5 keV fits in very well with the systematics of the neighbouring region and will not need further discussion. A possible interpretation of the (2, 2, −) band at 1123 keV would be that this band represents the $K = 2$ octupole vibration. However, the decay of this band by fast E2 transitions to the $K = 0$ octupole band represents a parallel to the decay of the γ-vibrational band to the ground-state band. An interpretation in terms of a γ-vibration superposed on the $K = 0$ octupole band is therefore equally or maybe even more likely. In sect. 6.5, we shall see that the branching ratios for the transitions between the two bands deviate from the theoretical ones in a way which seems characteristic of bands that are mixed by a rotation-vibration interaction. This feature thus lends additional support to the latter interpretation. In discussing these two possibilities, it should be kept in mind that the actual state may be a mixture of both.

The occurrence of states representing two-phonon vibrational excitations is a straightforward consequence of a description in terms of collective vibrations of the nucleus. In the case studied here, one might look for the (4, 4, +) two-phonon γ-vibrational level which would be expected to have approximately twice the energy of the γ-band, i.e., 1938 keV, and to decay by E2 cascades through the γ-band. Possible candidates are the levels at 1894 keV and 1946 keV, which both de-excite by E2 transitions to the γ-band. The two states, however, cannot represent the 4+ and 5+ members of such a band, since the maximum spin for both levels is four and the branching ratios for the E2 transitions going to the γ-band do not support a 4+ assignment to either of them. The two levels might conceivably represent mixtures of a (4, 4, +) single-particle state with the expected (4, 4, +) two-phonon γ-vibration.

The log ft values for the transitions to the vibrational states with $K = 2$ seem to be somewhat higher than to the levels above, which probably represent single-particle excitations. A forbiddenness due to the K quantum number is unlikely. Therefore, the apparent reduction of the transition probability seems to be associated with the intrinsic structure of the vibrational states.

6.4. K-SELECTION RULES

A look at the decay scheme makes it clear that selection rules other than those only depending on total spin and parity are in operation. First of all, the states

having quantum number $K = 0$ are only scarcely or not at all populated by direct electron capture (or β-) transitions. Secondly, the high energy states predominantly decay by multiple cascades instead of going by direct, and energetically favoured transitions to appropriate levels in the ground-state band. These effects are believed to be due to the K selection rule. For example, the 1946 keV (3+) level decays by a 6 %, 977 keV, E2 transition to the (2, 2, +) level at 969 keV, and by a 2.5 %, 1888 keV, E2 transition to the (0, 2, +) level in the ground-state band. The relative retardation factor is equal to the reduced branching ratio: $(6/2.5)(1888/977)^5 \approx 60$. Taking those transitions which may be thought to be once forbidden, we find for the 1123 keV E2 transition from the 1451 keV (3−) state a retardation factor $\approx 3\times10^3$, whereas the same factor from the 1894 keV state is ≈ 40, and for the 1946 keV state ≈ 60. Transitions which may be twice forbidden are not observed, but the following two limits can be computed: $> 5\times10^3$ for 1154 keV (3, 3, +), (M1) and $> 3\times10^4$ for 1433 keV (4, 4, +), (E2).

These findings do not warrant any lengthy discussion. It should be noted, however, that the transitions from the two highest energy levels have relatively small retardation factors.

6.5. ROTATION-VIBRATION INTERACTION

The relative branching intensities, fig. 6, are proportional to the squared Clebsch-Gordan coefficients

$$\langle I_1, L, K_1, K_f-K_1|I_1, L, I_f, K_f\rangle^2.$$

However, since the K quantum numbers are not exact, we may expect to find experimental deviations from these theoretical branching intensities. A study of table 6 reveals that this is so. In some cases it is not even possible to give a definite K assignment.

Hansen *et al.* [20]) have discussed the deviations observed in the branchings from the γ-vibrational band to the ground-state band of Gd^{156} and several other even nuclei in terms of a rotation-vibration interaction causing a mixing of the two bands. A perturbation calculation [27]) leads to a set of correction factors to the theoretical branching intensities expressed in terms of a parameter z, proportional to the admixed amplitude. It is found [20]) that the observed deviations of the branching intensities lead to values of z, which in magnitude and sign are in qualitative agreement with what one should expect if the mixing were due to a rotation-vibration interaction. In table 6 we have listed a number of theoretical branching intensities corresponding to $z = 0$ and $z = 0.03$, using the tables given in ref. [20]). From these one can easily obtain an estimate of the z-values which will correspond to the observed intensities. In the case of the (2, 2, +) band at 969 keV, the γ-vibrational band, the observed intensities lead to a value of $z = 0.050\pm0.010$ %. In the case of the other,

possibly vibrational, band with $K = 2$ at 1123 keV, there are only two corrected intensities which can be compared with experiment. They yield a value of $z = 0.020 \pm 0.008$.

Corrected branching intensities have been included in table 6 at the levels 1650 keV and 1946 keV, which might both have $K = 2$ and which decay to the ground-state band. It is seen that z-values with negative sign are indicated.

7. Conclusion

The present study gives a contribution to a systematic investigation of the occurrence and properties of the higher lying intrinsic levels in nuclei having a non-spherical equilibrium shape.

As a major result, the measurements of log ft values, branching ratios, and relative retardation factors have contributed evidence with respect to the exactness of a description in terms of the quantum number K.

Also, evidence has been presented, demonstrating that the systematics of rotational excitations, known from ground-state rotational bands in even nuclei, can be extended to the lower lying intrinsic states.

The authors wish to express their gratitude to Professor Niels Bohr for the excellent working conditions at this institute and to Professor The Svedberg for his kind interest in this work. One of us (E. A.) wishes to express his sincere thanks to Professor Niels Bohr for hospitality and financial support during a one-month stay at the Institute for Theoretical Physics. Thanks are due to Mr. Åke Svanheden who has arranged the cyclotron bombardments, and Mr. O. Skilbreid for the preparation of an isotope-separated source of Pa^{228}. The very able assistance of Mrs. Helle Nordby throughout all the phases of this work is greatly appreciated. We are indebted to Professor Å. Bohr, Dr. B. R. Mottelson and Dr. Bès for stimulating discussions, and to Mrs. S. Hellmann for invaluable help in preparing the manuscript.

References

1) F. Asaro and I. Perlman, Phys. Rev. **99** (1955) 38
2) G. Scharff-Goldhaber, E. der Mateossian, G. Harbottle and M. McKeown, Phys. Rev. **99** (1955) 180
3) O. H. Black, Proc. Roy. Soc. A **106** (1924) 632
4) J. Kyles, C. G. Campbell and W. J. Henderson, Proc. Phys. Soc. A **66** (1953) 519
5) H. C. Box and G. S. Klaiber, Phys. Rev. **95** (1954) 1247
6) S. Bjørnholm, O. Nathan, O. B. Nielsen and R. K. Sheline, Nuclear Physics **4** (1957) 313
7) W. W. Meinke, A. Ghiorso and G. T. Seaborg, Phys. Rev. **81** (1951) 782
8) T. O. Passell, UCRL-2528 (1954)
9) Ong Ping Hok and E. Arbman, Arkiv för Fysik **11** (1956) 193
10) M. W. Hill, UCRL-8423 (1958)
11) K. Alder, A. Bohr, T. Huus, B. R. Mottelson and Å. Winther, Revs. Mod. Phys. **28** (1956) 432

12) D. Bès, to be published
13) B. R. Mottelson and S. G. Nilsson, Mat. Fys. Skr. Dan. Vid. Selsk. **1**, no. 8 (1959)
14) R. E. Bell, S. Bjørnholm and J. S. Severins, Mat. Fys. Medd. Dan. Vid. Selsk. **32**, no. 12 (1960)
15) D. Ströminger, J. M. Hollander and G. T. Seaborg, Revs. Mod. Phys. **30** (1958) 585
16) K. O. Nielsen and O. Skilbreid, Nuclear Instruments **1** (1957) 159
17) E. Arbman and N. Svartholm, Arkiv för Fysik **10** (1955) 1
18) E. Arbmann, to be published
19) O. B. Nielsen and O. Kofoed Hansen, Mat. Fys. Medd. Dan. Vid. Selsk. **29**, no. 6 (1955)
20) P. G. Hansen, O. B. Nielsen and R. K. Sheline, Nuclear Physics **12** (1959) 389
21) G. Alaga, K. Alder, A. Bohr and B. R. Mottelson, Mat. Fys. Medd. Dan. Vid. Selsk. **29**, no. 9 (1955)
22) G. J. Nijgh, A. H. Wapstra and R. van Lieshout, Nuclear spectroscopy tables (North-Holland Publishing Company, Amsterdam 1959)
23) C. J. Gallagher and S. A. Moszkowski, Phys. Rev. **111** (1958) 1282
24) A. Bohr and B. R. Mottelson, in Beta- and Gamma-ray Spectroscopy, ed. by K. Siegbahn (North-Holland Publishing Company, Amsterdam, 1955), Ch. XVII
25) P. H. Stelson, private communication
26) F. S. Stephens, private communication
27) B. R. Mottelson, private communication to the authors of ref. [20])
28) M. E. Rose, Internal conversion coefficients (North-Holland Publishing Company, Amsterdam, 1958)
29) Sliv and Band, privately distributed tables of conversion coefficients edited in USSR
30) B. M. Foreman, Jr., UCRL-8223 (1958)

3.B

Nuclear Physics **21** (1960) 438—449; © *North-Holland Publishing Co., Amsterdam*

Not to be reproduced by photoprint or microfilm without written permission from the publisher

THE DECAY OF NEPTUNIUM-238

R. G. ALBRIDGE and J. M. HOLLANDER

Lawrence Radiation Laboratory and Department of Chemistry, University of California, Berkeley, California

Received 18 July 1960

Abstract: A study has been made of the energy levels of Pu^{238} which are populated by Np^{238} beta decay, by an examination of the Np^{238} conversion electron spectrum in high-resolution beta spectrographs. The general features of the level scheme as previously given are unchanged but several new transitions are observed, with energies 119.8, 871, 943, 989 and 1034 keV, and two new levels are postulated at 915 and 1034 keV which accommodate all but the 943-keV transition. A possible assignment of the 943-keV transition to the (0+, 0) state of the beta vibrational band is discussed. In addition, the weak 885-keV transition from the 2+ state of the gamma-vibrational band to the 4+ state of the ground band is seen and its relative intensity determined. Comparisons are made of the experimental relative transition intensities of the three photons depopulating this band with those predicted from the rules of Alaga *et al.*; only fair agreement is noted.

A discussion is given of the beta decay branchings and log *ft* values of Np^{238} decay in terms of the postulated characters of the Pu^{238} states and the measured spin of Np^{238}.

1. Introduction

The energy levels of Pu^{238} have been studied extensively from the decay [1–3]) of Cm^{242} and the decay [4–8]) of Np^{238}. The alpha decay of Cm^{242} leads to a well-defined ground-state rotational band, a state of 605 keV which has been assigned [2]) as (1−, 0) †, and a state of 941 keV. The high energy states of Pu^{238} are populated by only a very small fraction of the total alpha decay and (selection rules permitting) are studied more easily through the beta decay of Np^{238}. The spectroscopic studies of this nucleide by Rasmussen *et al.* [4, 5]) and by Baranov and Shlyagin [8]) have defined levels at about 988, 1030 and 1076 keV; these levels are of theoretical interest because of their interpretation [1, 5]) as vibrational states. The spin of Np^{238} has been determined to be 2 by the atomic-beam magnetic-resonance method, in an experiment reported by Albridge, Hubbs and Marrus [10]).

Certain features of the decay scheme suggested further experimental work. In the earlier studies, the two prominent transitions of about 1030-keV energy had not been completely resolved and the transition between the (2+, 2) and (4+, 0) states had not been reported; therefore, it had not been possible to make a complete comparison of the experimental transition intensities with

† This is the Bohr-Mottelson notation for $I\pi, K$.

those predicted by theory. In addition, the tentative assignments of vibrational levels in this nucleus offered the hope of finding additional data concerning this mode of excitation.

2. Sample Preparation

The Np^{238} sample was prepared by a 5-hour neutron irradiation of approximately 200 μg of Np^{237} in the Materials Testing Reactor at Arco, Idaho.

The sample was dissolved in concentrated HCl, and the neptunium co-precipitated with $Zr_3(PO_4)_4$ after reduction to the +4 state by Fe^{++}. Further purification was effected by co-precipitations with LaF_3 and $La(OH)_3$. To separate the neptunium from lanthanum and other rare earths, the solution was passed through a Dowex A-1 anion column at high chloride concentration and the neptunium subsequently eluted with 1 *M* HCl. This sample was electroplated onto a 0.25 mm platinum wire which served as the source for the spectrographs. Used in the experiment were three photographic recording permanent magnet spectrographs with field strengths of 50, 100 and 340 g and resolving power ($\Delta\rho/\rho$) of approximately 0.1 % [3]).

3. Experimental Results

The experimental results are summarized in table 1. The reported transition energies (E_γ) are weighted averages of the results of several exposures.

Since no internal standard was used, absolute errors are not given; however, except for very weak lines the relative precision of the energies should be $\approx$ 0.1 %. The value 44.11 keV listed in parentheses has been used in the decay scheme instead of the value 44.00 keV obtained in this experiment, because the former value was obtained [3]) with use of several internal standards, and is considered the more accurate.

The more certain features of the decay scheme are shown in fig. 1(a). This scheme is similar to those given by Rasmussen *et al.* [5]) and by Baranov and Shlyagin, [8]) with small differences in the energies of some of the states. Fig. 1(b) shows the levels of Pu^{238} populated [2]) by the alpha decay of Cm^{242}.

The transition intensities shown in fig. 1(a) are those deduced from a consideration of the relative intensities of the conversion electrons together with previous information on the beta-decay branchings; these data are discussed below. The relative conversion-electron intensities listed in table 1 are the results of six determinations made by a visual comparison method. For purposes of comparison the intensities are normalized to a value of 0.20 for the K line of the 985.7-keV transition. They are probably accurate to about 25 % for the stronger lines and to a factor of 2 for the weaker lines. Intensities reported by the other investigators are also listed for comparison. Note that the relative

TABLE 1

Np^{239} Conversion electron data

Electron energy (keV)	Conversion shell	Transition energy [a] (keV)	Selected transition energy [b] (keV)	Abundances per 100 beta disintegrations			Relative intensites [c]	
				Freedman *et al.* [6]	Slätis *et al.* [7]	Rasmussen *et al.* [4]	Baranov and Shlyagin [8]	This work
21.76	L_{II}	44.01		38	28.7		23.1	
25.96	L_{III}	44.02		20	21.0		21.1	
38.44	M_{II}	44.00		14			11.6	
39.40	M_{III}	43.96					5.72	
42.58	N_{II}	43.96			15.2		3.71	
42.84	N_{III}	43.97		3.2				
43.71	O	≈44.0						
			(44.11)[d]					
79.52	L_{II}	101.8		1.9	1.4		1.21	
83.74	L_{III}	101.8			0.9		0.64	
96.20	M_{II}	101.8		1.2	0.7		0.40	
97.17	M_{III}	101.7					0.36	
100.3	N_{II}	101.7						
101.4	O	101.7						
			101.7					
96.79	L_I	119.9						
113.9	M_I	119.8						
118.1	N_I	119.7						
			119.8					
99.22	K	221.0	221.0					0.09
170.8	K	292.6	292.6					(?)
748.8	K	870.6	870.6					<0.01
762.8	K	884.6	884.6					0.014
803.6	K	925.4	925.4		0.05	0.04		0.034
818.8	K	940.6			0.10	0.07	0.09	0.072
917.9	L_I, L_{II}	940.2			0.06			0.021
934.4	M_I, M_{II}	940.0						0.0075
			940.4					
821.3	K	943.1	943.1					0.0093
864.0	K	985.8		0.3	0.26	0.20	0.20	0.20
963.1	L_I, L_{II}	985.4			0.13	0.06	0.06	0.059
967.8	L_{III}	985.9						0.010
980.2	M_I, M_{II}	985.8						0.020
985.3	N	≈986						0.0090
			985.7					
867.3	K	989.1	989.1					0.012
905.6	K	1027.4		0.3 [e]	0.22 [e]	0.20 [e]	0.16 [e]	0.048
1005.1	L_I, L_{II}	1027.4			0.08	0.04	0.03	0.018
1021.7	M	≈1027			0.06	0.02		extremely weak
			1027.4					
908.1	K	1029.9					0.08	0.15
1007.3	L_I, L_{II}	1029.6					0.03	0.039
1024.8	M	≈1030						0.011
			1029.9					
912.1	K	1033.8	1033.8					<0.01
973.5	K	1095.3	1095.3					?

For footnotes see next page.

intensities reported in this work for components of the ≈ 1030-keV doublet, which are completely resolved, disagree with the results of Baranov and Shlyagin [8]), who report that the lower-energy (1027-keV) component is more

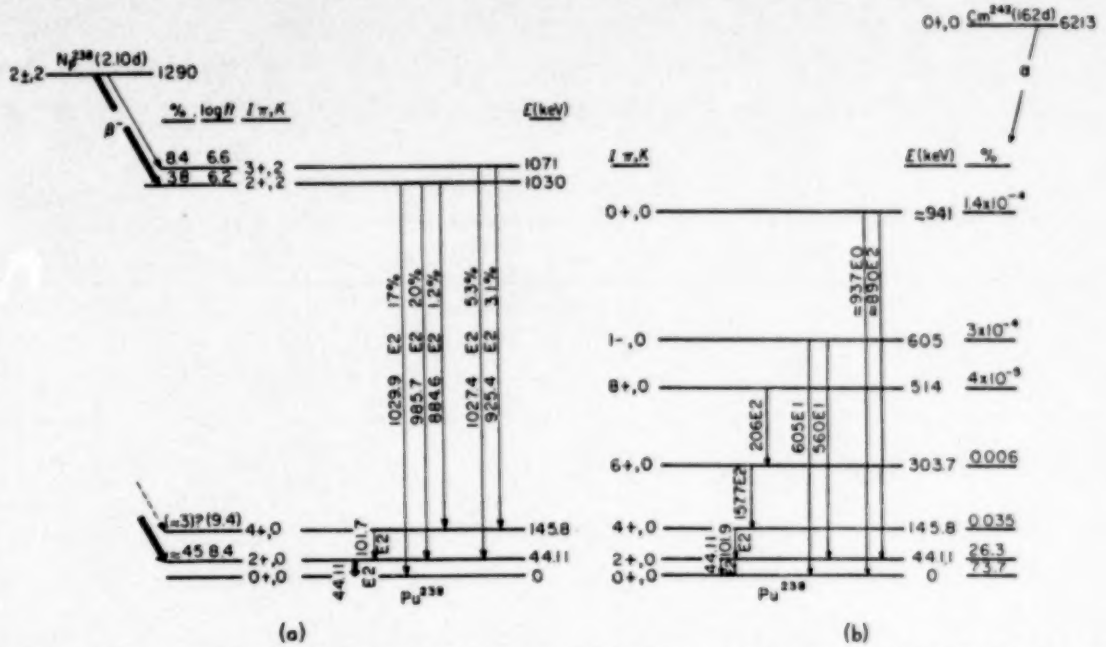

Fig. 1. The energy levels of Pu^{239}. The more certain features of the decay of Np^{239}. (b) Levels populated by the decay of Cm^{242}.

intense than the higher-energy (1030-keV) component, whereas this work shows the opposite result. The other investigators reported a composite intensity without attempting to divide it between the two transitions.

4. Branching-Ratio Comparisons

From the experimental K-conversion coefficients measured by Rasmussen *et al.* [4, 5]) and by Baranov and Shlyagin [8]), it is fairly certain that the 1030- and 986-keV transitions are predominantly electric quadrupole. It is not unreasonable to assume that the 925-keV transition is also electric quadrupole, with the possibility of some magnetic dipole admixture [4, 5]).

---

[a]) Electron binding energies were taken from Hill, Church and Mihelich, Revs. Sci. Instr. **23** (1952) 523

[b]) The selected values are weighted averages of the experimental values.

[c]) For purposes of comparison, the relative intensities from Baranov and Shlyagin and from the work reported here were normalized to Rasmussen's value of 0.20 for the K line of the 985-keV transition. In the last column question marks indicate uncertainty as to the actual existence of the lines.

[d]) The weighted average is 44.00. The value 44.11 had been reported previously by Smith and Hollander [3]) and is considered more accurate.

[e]) The intensities listed for the 1027-keV transition by Freedman, Slätis and Rasmussen include those of the unresolved 1030-keV transition. The division of intensities by Baranov and Shlyagin between 1027 and 1030 is reported as only approximate.

On the assumption that all transitions depopulating the (2+, 2) and (3+, 2) states are electric quadrupole, the experimental relative reduced photon-transition probabilities have been calculated from the observed K-electron intensities by dividing by the theoretical E2 K-conversion coefficients [11]) and correcting for the fifth-power energy dependence. The experimental and theoretical intensities are compared in table 2. These data tend to support

TABLE 2

Pu^{238} experimental and theoretical relative reduced E2 photon transition probabilities (Final states are all in $K = 0$ ground-state band)

Init. st. (keV)	E_γ/E'_γ	$\frac{B(I_1 \to I_f)}{B(I_1 \to I_{f'})}$	Experimental		Theoretical [24])		
			Rasmussen *et al.* [5])	This work	$K_1 = 0$	$K_1 = 1$	$K_1 = 2$
1030	$\frac{986}{1030}$	$\frac{B(2 \to 2)}{B(2 \to 0)}$	1.3	1.5	1.4	0.36	1.4
	$\frac{885}{1030}$	$\frac{B(2 \to 4)}{B(2 \to 0)}$	<0.3	0.15	2.6	1.1	0.071
1071	$\frac{1027}{925}$	$\frac{B(3 \to 2)}{B(3 \to 4)}$		1.0		0.4	2.5

the assignment made by Rasmussen *et al.* [5]) of $K = 2$ as the major K value of the upper band, but because of the relatively poor agreement of experimental and theoretical branching ratios, admixtures of other K values cannot be ruled out. It is interesting to note that Nathan [12]) reports an experimental value of 1.3 for the ratio $B(3 \to 2)/B(3 \to 4)$ for the depopulation of the (3+, 2) level in Dy^{160}. That this value is nearly the same as our value of 1.0 for the analogous transition in Pu^{238} may be coincidental or may indicate a systematic deviation, perhaps arising from admixtures of M1 radiation. The theoretical value of $B(3 \to 2)/B(3 \to 4)$ for $K = 2$ is 2.5. If the 1027-keV transition were pure E2 and the 925-keV transition had a 40 % admixture of M1 radiation, then the experimental branching ratio (1027—E2)/(925—E2) would be 2.5, in agreement with the theoretical value. There are no experimental data that rule out the possibility of 40 % M1 admixture in the 925-keV transition.

5. Discussion of Other Transitions

In addition to those considered above, a number of other — mostly much weaker — conversion lines were observed (table 1). If only one conversion line of a transition was seen, it was assigned as a K line. Of the transitions to be discussed here (at 119.8, 221.0, 292.6, 870.6, 940.4, 943.1, 989.1, 1033.8 and 1095.3 keV) only the one of 940 keV has been reported previously. These

transitions cannot be fitted uniquely into the level scheme; therefore, the interpretations ventured here are speculative.

Fig. 2 is a tentative interpretation of the new data. The two weak transitions of energies 989.1 and 1033.8 keV differ by 44.7 keV, approximately the energy of the first excited state; hence these transitions are used to define a level at 1033.5 keV. The sum 870.6+119.8 = 990.4 keV is within approximately 0.13 % of the energy 989.1 keV. Although energy differences observed with these instruments between lines lying close in energy are usually much better than 0.13 % (see, for example, fig. 1(a)), it is possible that the precision of

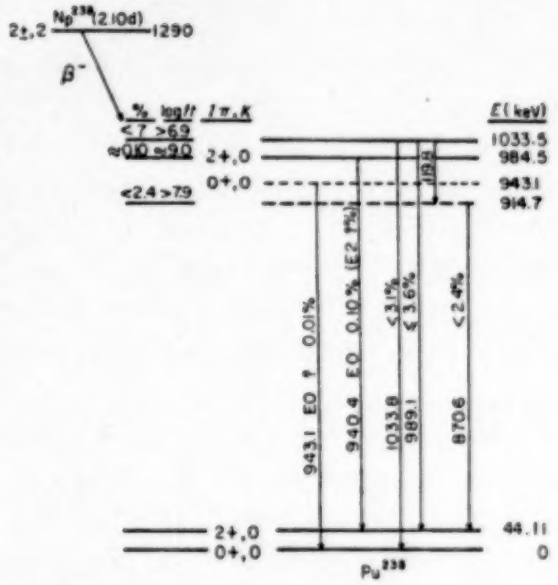

Fig. 2. Tentative assignments of the less prominent transitions in the decay of Np^{238}.

energy measurements of extremely weak lines is no better than this. The above sum may be used, therefore, to assign a level at 914.7 keV. The observation of only L_I, M_I and N_I lines of the 119.8-keV transition suggests that the multipolarity is M1 and not E1; E2 is certainly ruled out. We know nothing of the multipolarities of the other transitions. It is possible that one, or both, of these levels is associated with an octopole vibrational [13,14]) band with the base state (2−, 2) as is postulated, for example, in W^{182} [15]), Dy^{160} [12,16]) and Th^{228} [17]).

Of the remaining transitions one stands out in intensity, the 940.4-keV transition of which K, L and M lines are seen. That this transition should occur without a partner of similar strength appears at first strange, for almost any type of state at this excitation is expected to decay by at least two competing transitions to members of the ground rotational band. It is possible to suggest an interpretation within the framework of a beta-vibrational ($K = 0$) band, following upon earlier work [1,18]) that suggested that levels in Pu^{238} at 937 and 988 keV are the first two states of the $K = 0$ band.

The relative populations of the states of the $K = 0$ band depends upon the parity of Np^{238}, which is unknown (see sect. 6). Therefore it is necessary to consider both possibilities. (a) If the parity is even (2+), one would not expect the first member of the beta vibrational band (0+, 0) to receive direct population by beta decay because the beta transition would be second forbidden. On the other hand, the second member (2+, 0) of the band should be reached by an allowed (though K-forbidden) beta transition, and it is to the de-excitation of this state that we assign the moderately strong 940.4-keV gamma transition, which then places the energy of the (2+, 0) state at 984.5 keV. An explanation of the lack of observation in the electron spectrum of a parallel transition de-exciting this state could be that there is a large amount of E0 character in the 940.4-keV transition. Perlman *et al.* [19]) have found from Cm^{242} alpha decay that the E0 transition from the (0+, 0) level to ground ($\approx$ 940 keV) is about one-half as intense as the E2 transition ($\approx$ 890 keV) from this level to the (2+, 0) state at 44 keV. Because of the great difference in conversion coefficients ($e_K/\gamma(E2) \approx 1\ \%$; $e_K/\gamma(E0) = \infty$), the K line of the E0 transition is 50 times as strong as that of the E2 transition. Such a result is consistent with the theoretical studies by Reiner [20]), Peaslee [21]) and Rasmussen [22]) concerning E0 transition probabilities. If a similar competition exists between E0 and E2 radiation in the depopulation of the 984.5-keV state, then the much weaker electron lines of the E2 transition (984.5 keV) would not be observable in this work. For example, a line 1/50 as intense as the 940-keV K line would have an intensity of only 0.001. In this situation we would probably not expect to see the (0+, 0) state at all, because the intra-band E2 transition from the (2+, 0) state to the (0+, 0) state ($\approx$ 41 keV) must compete with an E2 of 940 keV, and the energy dependence alone discriminates against it by a factor of 6×10^6.

(b) If the parity of Np^{238} is odd (2−), both the (0+, 0) and (2+, 0) states may be populated directly by first-forbidden type beta decay, and we might expect to see the E0 transition between the (0+, 0) beta vibrational state and ground. Asaro *et al.* [23]) have observed, from Cm^{242} alpha decay, a transition of 941.4 ± 2 keV which they assigned as this E0 transition, and it is quite possible that this is the same transition as the one we measure to be 943.1-keV. The two observations were however carried out on different spectrographs, and the lines were very weak in both cases, so one cannot be certain of their identity. This would be an interesting point to settle, for evidence that Np^{238} beta-decays directly to a (0+) state in the daughter would of course rule out an even parity assignment.

Other possible transitions seen at 221.0, 292.6 and 1095.3 keV have not been placed in the decay scheme. Two weak electron lines observed at $\approx$ 106 and $\approx$ 156 keV were without doubt the K lines of the strong 228- and 278-keV transitions in Np^{239} decay, and therefore are not listed in table 1.

6. Beta-Decay Branchings

Information regarding the total intensity of the soft beta component has been obtained by Freedman et *al.* [6]), Rasmussen *et al.* [4]) and Baranov and Shlyagin [8]); their respective values, in fairly good agreement, are 53 %, 55 % and 59 %. In order to obtain intensities of the individual transitions, the measured (relative) electron intensities of this work were converted to transition intensities by use of Rose's theoretical E2 conversion coefficients [11]) and placed on an absolute scale by requiring that the total equal 56 % (average of above determinations). The values so obtained are compared in table 3 with those obtained directly from the absolute electron intensity measurements of Slätis *et al.* [7]) and of Rasmussen *et al.* [4]). The agreement is good.

TABLE 3

Intensities of high-energy transitions in Np^{238} decay

E_γ (keV)	K-electron intensities (percent of disintegrations)			α_K [11]) (Theoretical)	Transition intensity (percent of disintegrations)		
	Slätis [7])	Rasmussen [4])	This work		Slätis [7])	Rasmussen [4])	This work
871			<0.01	4.2×10^{-3} [a])			<2.4 [a])
885			0.014	1.2×10^{-2}			1.2
925	0.05	0.04	0.034	1.1×10^{-2}	5	4	3.1
940	0.10	0.07	0.072	∞	0.10 [b])	0.07 [b])	0.10 [b])
943			0.009	∞			0.013
986	0.26	0.20	0.20	1.0×10^{-2}	26	20	20
989			0.012	3.3×10^{-3} [a])			≦3.6 [a])
1027	0.22	0.20	0.048	0.91×10^{-2}	22	20	5.3
1030			0.15	0.91×10^{-2}			17
1034			<0.01	3.2×10^{-3} [a])			<3.1 [a])

[a]) In order to establish the *maximum* possible transition intensities for the 871-, 989- and 1034-keV transitions, the theoretical E1 conversion coefficients have been used. Their use is consistent with the postulate made in the text that these transitions may originate from states of odd parity.

[b]) This is the E0 transition intensity only. The total transition intensity will be higher if there is substantial E2 mixing.

TABLE 4

Np^{238} beta-decay branchings and log *ft* values

Final state ($I\pi$, K)	Final state (keV)	Percent of beta decay	log *ft*
2+, 0	44.11	≈45	8.4
4+, 0	145.8	(≈3)?	(9.4)
− − −	914.7	<2.4	>7.9
2+, 0	984.5	0.10	9.0
2+, 2	1030	38	6.2
− − −	1034	<7	>6.9
3+, 2	1071	8.4	6.6

From the above information, along with the beta populations to the low-lying levels given by Rasmussen *et al.* [4]) and by Baranov and Shlyagin [8]), log *ft* values of beta decay to the various levels were calculated, and are given in table 4. It is to be emphasized that these calculations are not independent of the present assignment of the multipole orders of the various transitions; however, the only *ft* value which is affected strongly is that of the beta decay to the 984-keV level. If the transition which de-excites this state should prove to be M1 or E2 instead of E0, then the log *ft* value would decrease by approximately one unit or two units, respectively.

The log *ft* value for decay to the 146-keV level is also listed as uncertain because of the experimental difficulties involved in determining the beta population of this level (see below). The multipolarities of the transitions that depopulate the 915- and 1034-keV levels are unknown, but some assumption must be made regarding them in order that the transition intensities can be calculated from the electron data. In order to establish the *maximum* intensities of these transitions (and thus the maximum beta populations of the 915- and 1034-keV levels) we have assumed that these transitions are electric dipoles. This assumption is consistent with the postulate made in the preceding section that these transitions may arise from odd-parity levels.

The log *ft* values are of importance as an indication of the parity of Np^{238}. The more reasonable choice, based upon the existing data, seems to be even parity. The log *ft* values of 6.2 and 6.6 to the 1030- and 1071-keV levels, respectively, indicate either slow allowed transitions ($\Delta I = 0$ or 1, no) or rather fast first-forbidden transitions ($\Delta I = 0$ or 1, yes). As pointed out by Rasmussen *et al.* [5]), the nuclear rearrangement accompanying the decay to the vibrational levels may tend to hinder these transitions; thus the interpretation of the transitions as slow allowed, with even parity for Np^{238}, is preferred.

The reported observance [8]) of $\approx 3\,\%$ primary beta decay to the (4+, 0) level at 146 keV (log $ft = 9.4$) is in contradiction to an assignment of even parity to Np^{238}, because with this assignment the transition should be second-forbidden. However, because of the following theoretical considerations, it would be surprising if as much as 3 % primary beta decay occurs, regardless of the parity assignment. The relative reduced beta-decay transition probabilities for decay to the ground-state and 146-keV level can be calculated by means of vector addition coefficients [24]). The result listed in table 5, is $B(2 \rightarrow 0)/B(2 \rightarrow 4) = 14$. The ratio of the *ft* values for decay to these levels should be just the inverse of this number, or $ft(2 \rightarrow 0)/ft(2 \rightarrow 4) = \frac{1}{14}$. Thus, if $\log ft(2 \rightarrow 4) = 9.4$, calculated from the 3 % beta branching, the value $\log ft(2 \rightarrow 0) = 8.3$ is indicated for decay to the ground state, which corresponds to approximately 60 % beta population. The prediction of such a large percentage of decay to the ground state is inconsistent with the conclusion of Rasmussen *et al.* [5]) that approximately 100 % of the hard betas go directly to the 44-keV level. In

consideration, also, of the fact that the experimental difficulties of measuring a small percentage of beta decay to the 146-keV level are large, we seriously doubt the measurement of direct beta decay to this level [8]).

The predicted and observed reduced transition-probability ratios for beta decay to the gamma vibrational band, also listed in table 5, are in reasonably

TABLE 5

Np^{238} experimental and theoretical relative reduced beta-decay transition probabilities (initial state is the (2,2) ground state of Np^{238})

	$\frac{B(I_1 \to I_f)}{B(I_1 \to I_{f'})}$	Experimental [a])	Theoretical
Ground-state rotational band $L = 2$	$\frac{B(2 \to 0)}{B(2 \to 4)}$	?	14
Gamma vibrational band $L = 1$	$\frac{B(2 \to 2)}{B(2 \to 3)}$	2.5	2.0

[a]) The experimental values are the inverse of the ratio of the experimental *ft* values for decay to the states.

close agreement, which is an indication of the K purity of these states. The beta decay to the 2+, 2 level can proceed by either $L = 1$ or $L = 0$ decay. Since the theoretical branching ratio was calculated for $L = 1$ decay, the agreement between the theoretical and experimental ratios is also an indication that the $2+ \to 2+$ beta transition is predominantly $L = 1$.

The log *ft* value of 9.0 for decay to the (2+, 0) level at 984 keV is consistent with an interpretation of a *K*-forbidden allowed transition as required by the level assignments. The log *ft* values for decay to the levels at 1034 and 915 keV are not in disagreement with the suggestion that these levels may be associated with an octopole vibrational band.

7. Proton and Neutron States in Np^{238}

The measured spin of Np^{238} is 2. Knowledge of the parity of Np^{238} is of interest because it can shed light on the nature of the single-particle states that comprise the ground state of this nucleus.

The coupling rules for the angular momentum of individual particle states in odd nuclei, originally presented by Nordheim [25]), have recently been modified by Gallagher and Moszkowski [26]) to apply to the particle states of deformed nuclei. Within the asymptotic quantum description of these states $[Nn_z\Lambda\pm]\Omega\pi$, where the $\pm$ in the brackets indicates $\Omega = \Lambda \pm \frac{1}{2}$ [27]), the rules predict which of the two possibilities $I = |\Omega_p \pm \Omega_n|$ lies lower, as follows:

$$I = \begin{cases} \Omega_p + \Omega_n & \text{for } \Omega_p = \Lambda_p \pm \frac{1}{2} \text{ and } \Omega_n = \Lambda_n \pm \frac{1}{2}, \\ |\Omega_p - \Omega_n| & \text{for } \Omega_p = \Lambda_p \pm \frac{1}{2} \text{ and } \Omega_n = \Lambda_n \mp \frac{1}{2}. \end{cases}$$

Here, N is the principal quantum number (total number of nodes in the wave function); n_z is the number of planar nodes perpendicular to the nuclear symmetry axis; Λ is the projection of orbital angular momentum on the symmetry axis; $\pm$ is the projection of the intrinsic spin on the symmetry axis; Ω is the projection of the total spin on the symmetry axis; and π is the parity.

It is simplest to assume at first that the ground states of the odd proton and neutron in Np^{238} are the same as in the nearest isotopes and isotones; that is, that the 93rd proton is in the $[642+]\frac{5}{2}+$ state as in the Np^{239} and Np^{237} ground states [28]), and that the 145th neutron is in the $[631-]\frac{1}{2}+$ state, as in the Pu^{239} ground state [28]). It is also possible that the proton is in the $[523-]\frac{5}{2}-$ state, found in Np^{237} at 60 keV [29]) and in Np^{239} at 75 keV. Although the $(\frac{1}{2}-)$ spin assignment of U^{237} is less certain [30]), we must consider also the neutron state $[501-]\frac{1}{2}-$. According to the above coupling rules the possible combinations of these states that give a ground-state of spin 2 are as shown below.

Proton	Neutron	Final state
$[642+]\frac{5}{2}+$	$[631-]\frac{1}{2}+$	$2+$
$[642+]\frac{5}{2}+$	$[501-]\frac{1}{2}-$	$2-$

Thus, the coupling rules predict for the proton state in Np^{238} the unique assignment $[642+]\frac{5}{2}$, while the neutron state depends upon the choice of parity of Np^{238}.

We are indebted to Professors J. O. Rasmussen, I. Perlman, and Dr. F. Asaro for stimulating discussions.

References

1) For a review of previous work see I. Perlman and J. O. Rasmussen, Handbuch der Physik **42** (Springer-Verlag, Berlin, 1957)
2) Asaro, Thompson and Perlman, Phys. Rev. **92** (1953) 694;
Asaro, Harvey, Stephens and Perlman, unpublished data
3) W. G. Smith and J. M. Hollander, Phys. Rev. **101** (1956) 746
4) Rasmussen, Slätis and Passell, Phys. Rev. **99** (1955) 42
5) Rasmussen, Stephens, Strominger and Åström, Phys. Rev. **99** (1955) 47
6) Freedman, Jaffey and Wagner, Phys. Rev. **79** (1950) 410
7) Slätis, Rasmussen and Atterling, Phys. Rev. **93** (1954) 646
8) S. A. Baranov and K. N. Shlyagin, Atomnia Energia **1** (1956) 52
9) (omitted)
10) Albridge, Hubbs and Marrus, Phys. Rev. **111** (1958) 1137
11) M. E. Rose, Internal conversion coefficients (North-Holland Publishing Co., Amsterdam, 1958)
12) O. Nathan, Nuclear Physics **4** (1957) 125
13) Alder, Bohr, Huus, Mottelson and Winther, Revs. Mod. Phys. **28** (1956) 433
14) R. K. Sheline, in Nuclear Structure (Proceedings of the University of Pittsburgh Conference, edited by Sidney Meshkov, June 1957)

15) C. J. Gallagher, Thesis, University of California UCRL-3928, Sept. 1957
16) Bäckström, Lindskog, Bergman, Bashandy and Bäcklin, Arkiv Fysik **15** (1959) 121
17) Bjørnholm, Nathan, Nielsen and Sheline, Nuclear Physics **4** (1957) 313
18) F. S. Stephens, Jr. (private communication)
19) Perlman, Asaro, Harvey and Stephens, Bull. Am. Phys. Soc. **2** (1957) 394
20) A. S. Reiner, Thesis, University of Amsterdam, 1958 (unpublished)
21) D. C. Peaslee, Nuclear monopole matrix elements, UCRL-3523, 1957 (unpublished)
22) J. O. Rasmussen, Theory of E0 transitions in spheroidal nuclei, UCRL-9084, Feb. 1960
23) F. Asaro and I. Perlman, unpublished data (May, 1960)
24) Alaga, Alder, Bohr and Mottelson, Mat. Fys. Medd. Dan. Vid. Selsk. **29**, No. 9 (1955)
25) L. A. Nordheim, Revs. Modern Phys. **23** (1951) 322
26) C. J. Callagher and S. A. Moszkowski, Phys. Rev. **111** (1958) 1282
27) For a discussion of the asymptotic quantum numbers see B. R. Mottelson and S. G. Nilsson, Mat. Fys. Skr. Dan. Vid. Selsk. **1**, No. 8 (1959)
28) Jack M. Hollander, Phys. Rev. **105** (1957) 1518
29) D. Strominger and J. O. Rasmussen, Nuclear Physics **3** (1957) 197
30) Rasmussen, Canavan and Hollander, Phys. Rev. **107** (1957) 141

3.A. *Nuclear Physics* **21** (1960) 450—455; © *North-Holland Publishing Co., Amsterdam*
Not to be reproduced by photoprint or microfilm without written permission from the publisher

GAMMA-GAMMA ANGULAR CORRELATIONS IN Rh^{103}

B. P. SINGH †
Physics Department, Muslim University, Aligarh

Received 18 June 1960

Abstract: The angular correlations of gamma-rays in Rh^{103} have been studied for the 555 keV—55 keV and 440 keV—55 keV cascades. The correlation functions thus obtained are for the 555keV—55 keV cascade:

$$W(\theta) = 1-(0.152\pm0.011)P_2(\cos\theta)-(0.042\pm0.017)P_4(\cos\theta),$$

and for the 440 keV—55 keV cascade:

$$W(\theta) = 1+(0.049\pm0.013)P_2(\cos\theta)-(0.016\pm0.017)P_4(\cos\theta).$$

The spins of the excited levels 650 keV, 535 keV and 95 keV in Rh^{103} have been discussed in the light of these correlation studies. The various possibilities of the spin values for these levels have been summarized.

1. Introduction

The decay of Ru^{103} has been studied by many workers [1]). Recently the investigations of the decay of Ru^{103} by Saraf [2]) revealed two gamma cascades of 555 keV—55 keV and 440 keV—55 keV. He further measured the conversion coefficient of the 55 keV radiation and found it to be 1.2 ± 0.3, which he attributed to an M_1 transition. He proposed a decay scheme and assigned the spins and parities on the basis of the shell model. A study of the directional correlation measurements of gamma-rays may facilitate the spin assignments.

In the present study, two single-channel scintillation spectrometers in coincidence with a resolving time of the order of 10^{-7} s were used. The size of the NaI(Tl) crystals was 3.8 cm in diameter and 2. 5 cm in thickness. The crystals were placed at 7 cm from the source.

The energies of gamma radiations were found to be 55 keV, 495 keV and 610 keV, using a single-channel scintillation spectrometer. The existence of two gamma cascades, 555 keV—55 keV and 440 keV—55 keV, was confirmed by measuring the coincidences between gamma-rays in the 55 keV photo-peak and high energy spectrum. Also the measurements of coincidences between all the high energy gamma-rays and low energy spectrum revealed peaks corresponding to 20 keV and 55 keV.

When this work on angular correlation was complete, Flack and Mason [3]) reported similar work. The difference in their experiment and the present one is that they measured the angular correlation between the gamma-rays of the

† Present address: Physics Department, Roorkee University, Roorkee (India).

cascades by selecting a part of the photo-peaks of respective gamma-rays, while in the present measurements one angular correlation, between gamma-rays in the photo-peak of 55 keV and all the gamma-rays above 505 keV was measured, and the other between gamma-rays of the photo-peak of 55 keV and all the gamma-rays above 400 keV; i.e., combined gamma-rays in the photo-peaks of 440 keV and 555 keV. This method helped us to improve the statistics.

2. Angular Correlation Results

The directional correlation function $W(\theta)$ obtained for the 555 keV —55 keV gamma-ray cascade by the method of least squares, after applying the solid angle correction following Rose [4]) is as follows:

$$W(\theta) = 1-(0.152\pm0.011)P_2(\cos\theta)-(0.042\pm0.017)P_4(\cos\theta).$$

In a similar manner, the correlation function was obtained for (555 keV+440 keV)−55 keV. The angular correlation of the 555 keV−55 keV cascade was subtracted from this, taking the intensity ratio of 555 keV and 440 keV as 1 : 1 as reported by Saraf. The correlation function thus obtained is as follows:

$$W(\theta) = 1+(0.049\pm0.013)P_2(\cos\theta)-(0.016\pm0.017)P_4(\cos\theta).$$

On the other hand, if the data are fitted by the method of least squares to the function $W(\theta) = 1+A_2P_2(\cos\theta)$, then the correlation function for the 555 keV−55 keV cascade is

$$W(\theta) = 1-(0.159\pm0.011)P_2(\cos\theta),$$

and for the 440 keV−55 keV cascade

$$W(\theta) = 1+(0.030\pm0.013)P_2(\cos\theta).$$

3. Discussion

Saraf has proposed a tentative level scheme by energy and coincidence considerations which has been adopted in the present work. The spin and magnetic moment of the ground state of Rh^{103} have been measured by Kuhen and Woodgate [5]), assigning a spin of $P_{\frac{1}{2}}$ to the ground state of Rh^{103}. The 40 keV transition, which is due to a 57 min isomeric state, has been classified by Goldhaber and Hill [6]) as an E3 transition, which means that the 40 keV level is a $\frac{7}{2}+$ state. The conversion coefficient of 55 keV radiation as measured by Saraf is 1.2 ± 0.3. Thus the two extreme values are 0.9 and 1.5. On the other hand, the value of the conversion coefficient as obtained from the tables of Rose [7]) for M1 is 1.65 and for E1 is 0.67. Thus the limits are quite near E1 and M1, for which the value ΔI is zero or one. If we assume transition to be a mixture of E1+M2, the mixing coefficient can be of the order of 0.01 to 0 03.

Thus the spin of the level 95 keV may be $\frac{9}{2}$ or $\frac{7}{2}$ or $\frac{5}{2}$. Saraf and also Flack and Mason have taken the spin value to be $\frac{9}{2}$ for the 95 keV level, basing their arguments on the nuclear shell model. The 495 keV gamma-ray is either an M1 or E2 transition, from various early measurements [1]).

The spin of the ground level of Ru^{103} has been taken by previous workers to be $\frac{7}{2}$ or $\frac{5}{2}$ on the basis of the shell model. Mason, Flack and Parry [8]) have investigated the spin value of the ground state of Ru^{103} by deuteron stripping measurement and have ruled out the spin value of $\frac{7}{2}$. The beta-ray groups of maximum energies of 227 ± 4 and 119 ± 4 keV as measured by Robinson and Langer [9]) give allowed shapes. Thus the spin value of $\frac{7}{2}$, $\frac{5}{2}$, $\frac{3}{2}$ may be considered for the 535 and 650 keV levels of Rh^{103}.

The angular correlation results have been analysed for all the various possibilities for the cascades, mixture or pure, etc. This analysis has been done by the method given by Arns and Weidenback [10]). In this analysis of angular correlation, the following cases may occur:

(i) all the transitions in the cascades are pure, (ii) all the transitions in the cascades are mixtures, (iii) one transition is pure and the other two are mixtures or two transitions may be pure and the other one a mixture.

The 95 keV level can have three spin values i.e. $\frac{9}{2}$, $\frac{7}{2}$, $\frac{5}{2}$. First let us take the 95 keV level to be $\frac{9}{2}$. If we take $\frac{3}{2}$ to be the spin for both the 650 keV and 535 keV levels, then the 440 and 555 keV transitions will have to be E3 or M3, which is contradicted by the coincidences found between β and γ-rays as measured by Robinson and Langer [9]) using a coincidence circuit of the order of 10^{-6}s. Thus only $\frac{5}{2}$ and $\frac{7}{2}$ spin values are left for the 650 keV and 535 keV levels.

If all the transitions in the cascades are pure, then the spin assignment of $\frac{5}{2}$ for the 650 keV level fits with our angular correlation data, but on the other hand, none of the spin values fit data for the 535 keV level. If all the transitions in the cascades are mixtures, then spin values of $\frac{5}{2}$ and $\frac{7}{2}$ can be fitted to the angular correlation data for the 535 keV level for certain mixture values and none of the spin values can be fitted to the 650 keV level as shown in fig. 1. Thus both possibilities can be ruled out. A certain assignment, however, may be considered, if we take one transition to be a mixture and the other two as pure or two transitions to be mixture and the other one as pure. Suppose the 55 keV transition is pure and the 555 keV and 440 keV transitions are dipole and quadrupole mixtures. It is concluded by the analysis of the data as shown by fig. 2 that the spin value of $\frac{7}{2}$ is possible for the 535 keV level and $\frac{7}{2}$ and $\frac{5}{2}$ can be assigned to the 650 keV level for certain values of the mixtures. Next suppose the 55 keV transition is a mixture of dipole and quadrupole and that the other two transitions are pure. In this case if a certain value of the mixture in the 55 keV transition satisfies the experimental data for one of the cascades as for example 555 keV—55 keV cascade, then the same value of the mixture should satisfy the other cascade, i.e. 440 keV—55 keV cascade. Referring to the

fig. 2, if the spin value of $\frac{7}{2}$ can be assigned to the 535 keV level, then the spin value of $\frac{5}{2}$ can be assigned to the 650 keV level. And if $\frac{5}{2}$ can be assigned to the 535 keV level, then $\frac{5}{2}$ is possible for the 650 keV level by taking 55 keV as

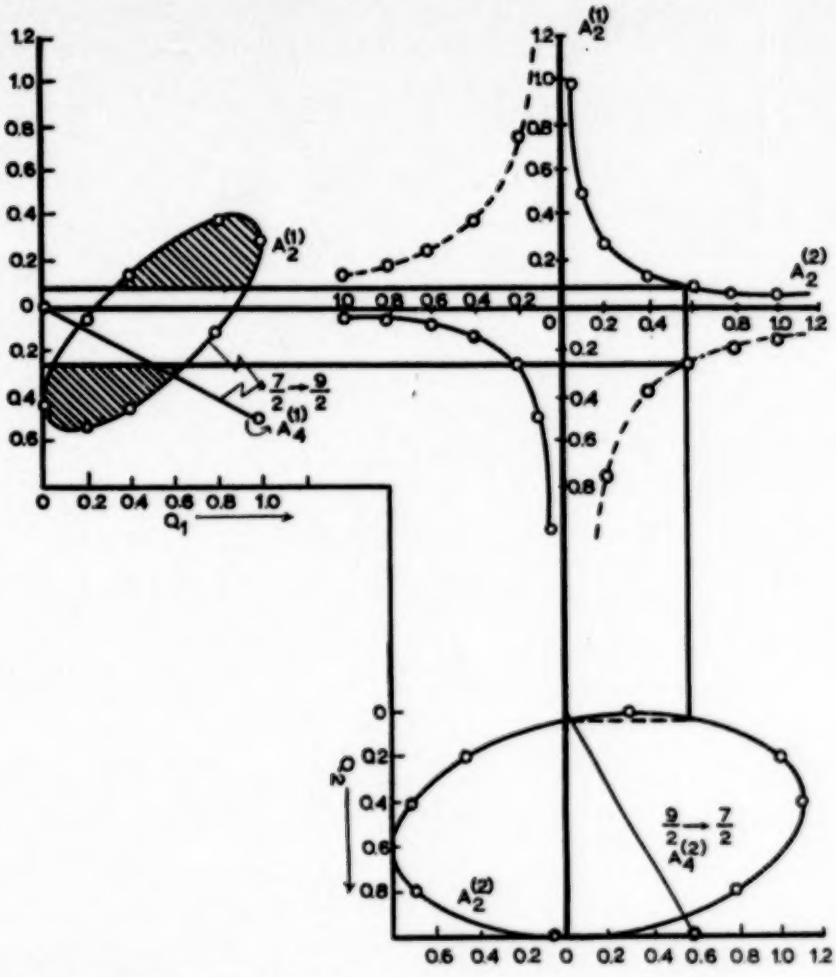

Fig. 1. Analysis of experimental data according to the method given by Arns and Weidenbeck, when both the transitions in the cascades are mixtures. The plots $A_2^{(1)}$ and $A_4^{(1)}$ versus Q_1 (fraction of quadrupole contents in dipole transition) are for the transition $\frac{7}{2} \xrightarrow[440 \text{ keV or } 555 \text{ keV}]{\gamma_1} \frac{9}{2}$ and plots $A_2^{(2)}$ and $A_4^{(2)}$ versus Q_2 (fraction of quadrupole contents in dipole transition) are for the transition $\frac{9}{2} \xrightarrow[55 \text{ keV}]{\gamma_2} \frac{7}{2}$. The range of the value Q_2 is fixed by conversion coefficient data. A_2^{expt} for both cascades is shown by hyperbolas in the diagram. The solid curve indicates A_2^{expt} for the transition $\frac{7}{2} \xrightarrow[440 \text{ keV}]{\gamma_1} \frac{9}{2} \xrightarrow[55 \text{ keV}]{\gamma_2} \frac{7}{2}$ and the dotted curve indicates A_2^{expt} for the transition $\frac{7}{2} \xrightarrow[555 \text{ keV}]{\gamma_1} \frac{9}{2} \xrightarrow[55 \text{ keV}]{\gamma_2} \frac{7}{2}$. The range of Q_1 for $A_2^{(1)}$ in 440 keV transition is indicated by hatched area in upper portion of the ellipse and in 555 keV transition in lower portion of the ellipse. These mixture ranges should also satisfy the correlation coefficient values for A_4^{expt}.

mixture of dipole and quadrupole. Further taking the 55 keV and 555 keV transitions as pure, the spin value of $\frac{5}{2}$ can be assigned to the 650 keV level, but in that case the 440 keV transition will have to be taken as mixture, so the spin

value of $\frac{7}{2}$ is suitable for the 535 keV level. But on the other hand, if we take the 440 keV and 55 keV transitions as pure, none of the spin values suits the 535 keV level. Further taking 55 keV and 440 keV transitions as mixtures, the spin values of $\frac{5}{2}$ and $\frac{7}{2}$ are suitable for the 535 keV level and in that case the 555 keV transition will have to be pure and the spin value to the 650 keV level will be $\frac{5}{2}$.

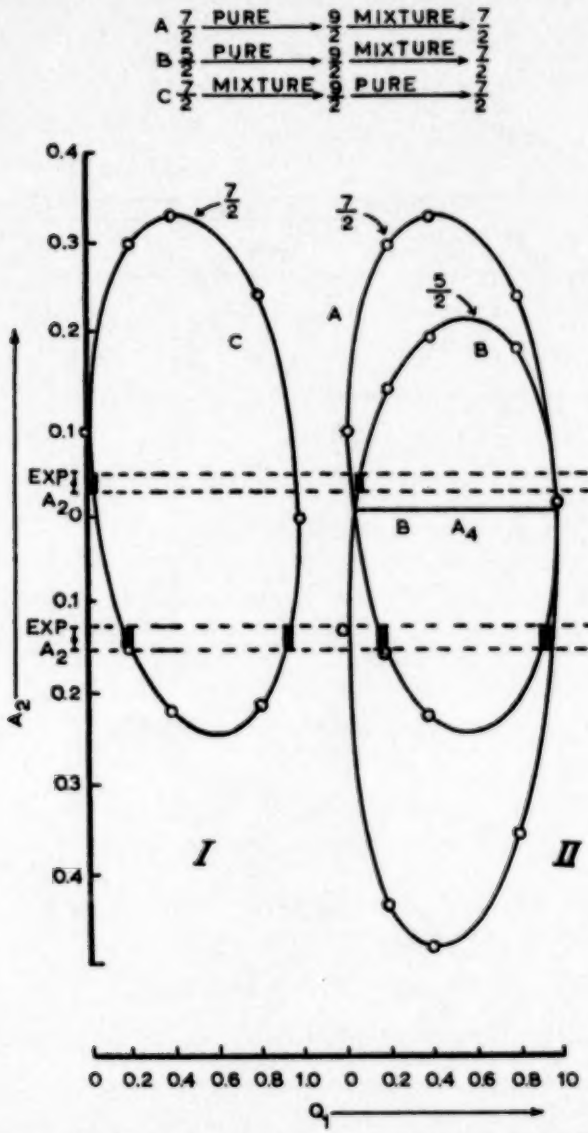

Fig. 2. The curves show $A_2^{expt} = A_2^{(1)} A_2^{(2)}$ versus Q_1 (fraction of quadrupole contents in dipole transition) for the cascades 555 keV−55 keV and 440 keV−55 keV indicated by A, B, C for various spin assignments for the levels according to the method given by Arns and Weidenbeck. The dotted lines indicate the experimental values for the correlation coefficient for the cascades.

But on the other hand, if we take the 555 keV and 55 keV transitions as mixtures, none of the spin values suits the 650 keV level.

By a similar analysis, if we take the spin value $\frac{7}{2}$ to the 95 keV level then three cases can be ruled out, i.e. (i) when all the transitions are pure, (ii) when all the transitions are mixtures, (iii) when the 55 keV transition is mixture and

the 555 keV and 440 keV are pure. But spin value of $\frac{5}{2}$ is favourable for the 535 keV and 650 keV levels, when 55 keV transition is pure and 555 keV and 440 keV are mixtures and also when the 440 keV transition is mixture and 555 keV transition is pure.

Further, taking the spin value of $\frac{5}{2}$ for the 95 keV level, two cases can be ruled out, i.e. when all the transitions are pure or mixtures. If the 55 keV transition is pure and the 440 keV and 555 keV transitions are mixtures, all the spin values are suitable for the 535 keV level and $\frac{3}{2}$ for the 650 keV level for certain mixture values. When the 55 keV transition is mixture and other two are pure, then spin value $\frac{5}{2}$ is suitable for the 650 keV level and the spin value of $\frac{7}{2}$ is possible for the 535 keV level or if spin value of $\frac{7}{2}$ is suitable for the 650 keV level then $\frac{5}{2}$ is suitable for the 535 keV level. If the 55 keV and 440 keV transitions are pure then spin value of $\frac{3}{2}$ is suitable for the 535 keV level and in that case the 650 keV level can have spin value of $\frac{3}{2}$ with mixture in the 555 keV transition. Similarly if the 55 keV and 440 keV transitions are mixtures, the 535 keV level can have spin values of $\frac{5}{2}$ and $\frac{3}{2}$ and in that case the 555 keV transition should be pure and spin values for the 650 keV level should be $\frac{5}{2}$ and $\frac{7}{2}$.

Summarizing, it is evident from the above discussion that quite a few possibilities exist for various combinations of the spins. Further considerations both experimental and theoretical, other than those discussed above are required to decide the actual assignment of the spins. One such consideration is by means of the shell model. If, as is normally considered by other workers, the spin assignment of $\frac{9}{2}$ is most suitable for the 95 keV level, then certain possibilities are ruled out for the 535 keV and 650 keV levels as mentioned above.

The author wishes to express his sincere gratitude to Professor P. S. Gill for his continuous help and guidance in this work. The author is also grateful to Dr. H. S. Hans for helpful discussions during the course of this work. The support of the Council of Scientific and Industrial Research, Government of India, for the award of senior research fellowship is thankfully acknowledged.

References

1) D. Strominger, J. M. Hollander and G. T. Seaberg, Rev. Mod. Phys. **30** (1958)
2) B. Saraf, Phys. Rev. **97** (1955) 715
3) F. C. Flack and P. Mason, Proc. Phys. Soc. **71** (1958) 247
4) M. E. Rose, Phys. Rev. **91** (1953) 610
5) H. Kuhen and G. K. Woodgate, Proc. Roy. Soc. A **64** (1951) 1090
6) M. Goldhaber and R. D. Hill, Rev. Mod. Phys. **24** (1952) 198
7) M. E. Rose, in Beta-gamma ray spectroscopy ed. by K. Siegbahn (North-Holland Publishing Co., Amsterdam, 1955) 906
8) F. C. Mason, P. Flack and G. Parry, Proc. Phys. Soc. **74** (1959) 138
9) R. L. Robinson and L. M. Langer, Phys. Rev. **109** (1958) 1255
10) R. G. Arns and M. L. Weidenbeck, Phys. Rev. **111** (1958) 1631

1.C:
2.E

Nuclear Physics **21** (1960) 456—461; © *North-Holland Publishing Co., Amsterdam*

Not to be reproduced by photoprint or microfilm without written permission from the publisher

IMAGINARY PART OF THE OPTICAL MODEL POTENTIAL IN NUCLEAR MATTER

J. SAWICKI
University of California, Berkeley, California
and
S. A. MOSZKOWSKI
University of California, Los Angeles, California

Received 8 August 1960 †

Abstract: The imaginary part of the optical model potential in nuclear matter has been calculated for various values of the energy, assuming Gammel-Thaler nucleon-nucleon interactions. The calculations were made using the separation method in which the interaction is separated into a short range and long range part, the former giving zero phase shift. To a good approximation, only the long range component contributes to the imaginary part of the optical potential.

1. Introduction

In an other paper by J. Dąbrowski and one of us [1]), the imaginary part of the nuclear potential has been treated in terms of free nucleon-nucleon scattering operators t_0. An equation relating the exact nucleon-nucleon t-matrix with the exclusion principle taken into account to the t_0-matrix is utilized by iterating that equation and retaining only the first few terms of the expansion. The exact antisymmetry of the entire $A+1$ particle system (the scattering nucleon and the target particles) is not taken into account both in ref. [1]) and in the present treatment. Rather we only antisymmetrize the t-matrix and use the Fermi gas model for the target nucleus. Some corrections to this approximation of the "target exchange" type have been estimated by one of us [2]) and found to be small. The procedure of ref. [1]) is only applicable to medium and high energies of the projectile as at low energies the convergence of the iteration series is poor. The reason for that is that t_0, being proportional to $e^{i\delta} \sin \delta/k$ for the S-states, increases greatly as k decreases. On the other hand, the separation method developed by B. Scott and one of us [3]) leads to the expansion of the t-matrix converging rather rapidly. Indeed it proved useful for the problem of the ground state of nuclear matter where low momenta are involved.

† This work was supported in part by the United States Air Force, under contract number AF 49(638)-327 monitored by the Air Force Office of Scientific Research of the Air Research and Development Command, and in part by the Office of Ordnance Research.

2. The t-Matrix Formalism and the Separation Method

Our t-matrix here differs from the reaction matrix for nuclear matter by the outgoing wave boundary condition. The procedure of the present paper is, in general, simpler than that utilizing the Lippman-Schwinger equation relating the t-matrix to the reaction matrix adopted for the calculation of the imaginary potential by Shaw [4]).

Let the t-matrix for the interacting pair of the particles "0" (projectile) and "1" (a target particle) be in the notation of ref. [3])

$$t = v + v\frac{Q}{e+i\eta}t, \tag{1}$$

where Q is the exclusion principle operator and $+i\eta$ stands for the outgoing wave boundary condition. We separate the potential v as $v = v_s + v_1$, where the separation distance c is a function of the relative momentum k. The short range part v_s produces zero phase-shift and therefore the corresponding t-matrix is

$$t_s = v_s + v_s\frac{1}{e_0}t_s, \tag{2}$$

which involves no outgoing wave boundary condition (the equation may be defined with the principle value condition). If we adopt $t_1 = t_s + v_1$ to be the zero order t-matrix, we can expand eq. (1) in this quantity. Retaining only the second order terms we can express t as follows:

$$t = t_1 + t_2, \tag{3a}$$

$$t_2 = t_1\frac{Q}{e+i\eta}t_1 - t_s\frac{1}{e_0}t_s. \tag{3b}$$

In our calculation for nuclear matter (infinite medium) we shall consider only the diagonal components.

The imaginary part of t originates from the $+i\eta$ term in the energy denominator. As the on-energy-shell component of t_s vanishes, the only surviving term is

$$\mathrm{Im}\left(v_1\frac{Q}{e+i\eta}v_1\right) = -\pi(v_1 Q\delta(e)v_1), \tag{4a}$$

and thus

$$\mathrm{Im}\,\langle\mathbf{k}|t|\mathbf{k}\rangle_{\mathbf{K}} = \frac{-\pi kM}{2\hbar^2}\int \mathrm{d}\Omega_{k''}\,Q\left(\frac{\mathbf{K}}{2}\pm k\frac{\mathbf{k}''}{k''}\right)\frac{M^*(k,K)}{M}\left\langle k\frac{\mathbf{k}''}{k''}\middle|v_1\middle|\mathbf{k}\right\rangle^2, \tag{4b}$$

where $\mathbf{k}$ and $\mathbf{k}''$ are the initial and the intermediate state relative momenta, $\mathbf{K}$ is the total momentum, $M^*(k,K)$ is the "effective mass" in a general form†. In

† We have used here the usual approximation of assuming $M^*(k,K)$ to be real, i.e. of neglecting the small contribution of the imaginary nuclear potential to e. This approximation seems reasonable particularly at amall energies.

the following we shall use the approximation $M^* = M$. Eq. (4) is the form of the usual "frivolous model"[5]), however, with the interaction operator represented by the long range potential v_1.

As a realistic nuclear force depends on the angular momentum, spin, and isobaric spin state we shall be using a properly averaged and weighed antisymmetryzed form for the expression $\langle v_1 \rangle^2$.

One possible approximate expression can be obtained if we utilize the fact that Q is important for S-states only. We can then use the free nucleon-nucleon t-matrix t_0 for all the angular momentum states with $L > 0$. If we denote by v_1 the long range part of the S-state potentials, we can have an approximation for the imaginary part of the t-matrix in the form

$$\mathrm{Im}\,\langle \mathbf{k}|t|\mathbf{k}\rangle_{\mathbf{K}} = \mathrm{Im}\langle \mathbf{k}|t_0|\mathbf{k}\rangle_{L>0} - \frac{\pi k M}{2\hbar^2}\int \mathrm{d}\Omega_{k''} Q\left(\frac{\mathbf{K}}{2} \pm k\frac{\mathbf{k}''}{k''}\right)\left\langle k\frac{\mathbf{k}''}{k''}\middle|v_1\middle|\mathbf{k}\right\rangle^2. \quad (5)$$

Now for small k, the matrix elements of v_1 are much smaller than those of t_0. However, calculations made with a standard potential [3]), consisting of a hard core followed by an exponential attractive well, show that the difference becomes small above $k \approx 0.7 \times 10^{13}\ \mathrm{cm}^{-1}$. The detailed calculations discussed below show that relative momenta below $0.7 \times 10^{13}\ \mathrm{cm}^{-1}$ contribute only little to except when the incident energy is very small †. If we replace v_1 by t_0, even for S states, then we obtain essentially just the usual frivolous model [5]), in which Im V is related directly to total nucleon-nucleon cross sections.

3. Details of Calculations

Recently Scott [6]) has computed the long range potentials from the Gammel-Thaler potentials for the singlet states $^1S_0$, $^1P_1$, $^1D_2$, $^1F_3$, $^1G_4$, the triplet tensor-coupled states $^3S_1$, $^3D_1$, $^3D_3$, $^3G_3$, $^3P_2$, $^3F_2$, and the triplet uncoupled states: $^3P_0$, $^3P_1$, $^3D_2$, $^3F_3$, $^3G_4$. We have utilized these results and thus avoided any additional approximation for the $L = 0$ states as well as for the S-state potentials in the framework of the separation method and eq. (4b). Regarding v_1 as an operator in the spin space of the (0, 1)-pair we can write the appropriate antisymmetrized average $\langle v_1 \rangle^2$ over the isobaric spin states T as

$$A\left(\mathbf{k}, k\frac{\mathbf{k}''}{k''}\right) = \tfrac{1}{4}\mathrm{Tr}_{(\sigma_0,\sigma_1)}\left[\tfrac{3}{4}\langle v_1\rangle^2_{T=1} + \tfrac{1}{4}\langle v_1\rangle^2_{T=0}\right]. \quad (6)$$

The function A of eq. (6) can be expanded as

$$A\left(\mathbf{k}, k\frac{\mathbf{k}''}{k''}\right) = \sum_L A_L(k, k) P_L(\cos\theta),$$

† This statement does not seem to hold, however, when non singular nucleon-nucleon interactions are used. For example, for a purely attractive exponential well (no core) which fits the same low energy data as the standard potential, the matrix elements of v_1 and t_0 are significantly different up to $k \approx 1 \times 10^{13}\ \mathrm{cm}^{-1}$.

where θ is the angle between $\mathbf{k}$ and $\mathbf{k}''$. We shall retain only the (largest) isotropic term.

In our approximation the imaginary potential can be written as

$$\operatorname{Im} V(k_0) = 4 \int_{k_1 \leq k_F} \operatorname{Im} \langle \mathbf{k} | t | \mathbf{k} \rangle_{\mathbf{K}} \mathrm{d}^3\mathbf{k}_1, \tag{7}$$

where $\mathbf{k}_0$ and $\mathbf{k}_1$ are the momenta of the projectile and the target particle respectively; k_F is the Fermi momentum.

Following ref. [1]) we shall introduce the variables of integration k and $u = \frac{1}{2}|\mathbf{K}|$. We have $\int \mathrm{d}^3\mathbf{k}_1 = (16\pi/k_0) \int k \mathrm{d}k \int u \mathrm{d}u$.

Following closely the method of ref. [1]) we find †

$$\operatorname{Im} V(k_0) = -4 \left(\frac{16\pi}{k_0}\right)\left(\frac{2\pi^2 M}{\hbar^2}\right) \int_{\frac{1}{2}(k_0+k_F)}^{\frac{1}{2}(k_0+k_F)} \mathrm{d}k k^2 A_0(k) \int_{\max[(k^2-k^2)^{\frac{1}{2}},\, k_0-k]}^{[\frac{1}{2}(k_0^2+k_F^2)-k^2]^{\frac{1}{2}}} \frac{u^2+k^2-k_F^2}{2ku} u \,\mathrm{d}u. \tag{8}$$

The integral over u can be worked out analytically. Using the dimensionless notation $x = (k/k_F)$ and $y = (k_0/k_F)$, we obtain the final result as a single integral over x,

$$\operatorname{Im} V(k_0) = \frac{-128\pi^3}{y} \left(\frac{\hbar^2 k_F^2}{M}\right)^{-1} \int_{\frac{1}{2}(y-1)}^{\frac{1}{2}(y+1)} x \mathrm{d}x \, k_F^6 A_0(k_F x) F(x, y), \tag{9}$$

where $F(x, y)$ is given by

$$\tfrac{1}{3}(\tfrac{1}{2}(1+y^2)-x^2)^{\frac{1}{2}}(\tfrac{1}{4}(y^2-5)+x^2)+\tfrac{1}{6}y(3-y^2)+\tfrac{1}{2}(y^2-1)x-\tfrac{1}{2}yx^2+\tfrac{2}{3}x^3$$

$$\text{if} \quad y \geqq \sqrt{2} \tag{10a}$$

$$\text{or} \quad y \leqq \sqrt{2} \quad \text{and} \quad \tfrac{1}{2}(2-y^2)^{\frac{1}{2}} \leqq |x-\tfrac{1}{2}y| \leqq \tfrac{1}{2},$$

and by

$$\tfrac{1}{3}(\tfrac{1}{2}(1+y^2)-x^2)^{\frac{1}{2}}(\tfrac{1}{4}(y^2-5)+x^2)+\tfrac{1}{3}(1-x^2)^{\frac{3}{2}}$$

$$\text{if} \quad y \leqq \sqrt{2} \quad \text{and} \quad |x-\tfrac{1}{2}y| \geqq \tfrac{1}{2}(2-y^2)^{\frac{1}{2}}. \tag{10b}$$

It may be verified that the function $F(x, y)$ vanishes at both ends of the integration interval. This provides a useful check of our calculation.

We have numerically computed $\operatorname{Im} V(k_0)$ for several values of y and for a nuclear density $k_F = 1.4 \times 10^{13}\ \mathrm{cm}^{-1}$ corresponding to a nuclear radius $R = 1.09\, A^{\frac{1}{3}} \times 10^{-13}$ cm. The long-range Gammel-Thaler potentials computed by Scott [6]) have been used. Unfortunately, the corresponding lab. system energies E_0 of the scattering nucleon cannot be given exactly as we do not know the real single particle potential consistently. Instead, we used the single particle potential of ref. [3]). This is admittedly somewhat inconsistent, but recent work

† We are using the normalization of $\langle \mathbf{k}|v_1|\mathbf{k}\rangle$ corresponding to $\langle \mathbf{k}|t_0|\mathbf{k}\rangle = -(4\pi\hbar^2/(2\pi)^3 M) f(\theta)$, where $f(\theta)$ is the usual scattering amplitude.

of Scott [6]) indicates that the G—T and standard interaction give nearly the same single particle potentials. The numerical results are presented in table 1.

TABLE 1

The imaginary part of the optical potential as a function of k_0 and E_0 for the Gammel-Thaler interaction ($k_F = 1.4 \times 10^{13}$ cm^{-1}).

k_0/k_F	1.2	1.5	1.75	2.0
E_0 (MeV)	14	65	110	160
Im V (MeV)	2.8	12.3	18.7	23.6

4. Discussion of Results

The numbers of table 1 are in quite reasonable agreement with experiment (compare e.g. Glassgold [7]). For $k_0 \geqq 1.5\, k_F$ they are also in essential agreement with the numbers of tables 1 and 2 of ref. [1]) corresponding to the frivolous model with t_0 replacing t_s+v_1.

Note that our Im V increases monotonically with energy. This is directly connected with the fact that the total nucleon-nucleon scattering cross sections fall off only very slowly above 150 MeV in the lab system, though they vary approximately as E^{-1} at lower energies. In the calculations of Lane and Wandel and Clementel and Villi the cross sections were assumed to vary essentially as E^{-1} even at high energies and consequently Im V starts to decrease again above 100 MeV.

We wish to emphasize that our calculated Im V refers to nuclear matter, i.e. the interior of actual nuclei. We have not attempted to make detailed calculation of Im V in the region of the nuclear surface. A crude calculation made assuming $k_F = 1.2 \times 10^{13}$ cm^{-1} indicates, however, that Im V is even larger here than in the nuclear interior [4]). In the framework of the Thomas-Fermi approximation, we can say that since the density is lower at the nuclear surface, the Pauli Principle is less effective there in suppressing collisions.

We have verified that interactions in states with $L > 0$ play a decisive role for the magnitude of Im V, especially at high energies. The S state part of the interaction contributes only 1.2 MeV, 3.5 MeV, 3.1 MeV and 1.9 MeV to the magnitude of Im V at $k_0/k_F = 1.2$, 1.5, 1.75 and 2.0. It is evident that the real part of the potential depends on a weighted sum of t. Considerable cancellation takes place here among contributions from higher L states [6]). However, in the determination of Im V_0, the sum is essentially over $\langle v_1 \rangle^2$ and here all contributions are additive.

5. Higher Order Corrections

In the work discussed above we have considered only terms up to second order in t_s and v_1. In particular we used the fact that only the term $v_1(Q/e+i\eta)v$

cf. eq. (4a) contributes an imaginary part to t and therefore to V. There are, however, many higher-order terms which have an imaginary part, and these must be relatively small in order for our method to converge. For example, the following third order terms appear in our expansion for t_3:

$$t_3 = t_1 \frac{Q}{e+i\eta} t_1 \frac{Q}{e+i\eta} t_1 - t_1 \frac{Q}{e+i\eta} t_s \frac{1}{e_0} t_s - t_s \frac{1}{e_0} t_s \frac{Q}{e+i\eta} t_1 + t_s \frac{1}{e_0} t_s \frac{1}{e_0} t_s. \quad (11)$$

We have not investigated this convergence in detail. However, for the purpose of making a crude estimate, let us assume no possible imaginary component of t_s. Then the imaginary part of t_3 can be written as

$$\operatorname{Im} t_3 = -\pi \left[t_1 Q \delta(e) t_1 \frac{Q}{e+i\eta} t_1 - t_1 Q \delta(e) t_s \frac{1}{e_0} t_s + \text{herm. conj.} \right] \quad (12a)$$

$$= -2\pi [t_1 Q \delta(e) t_2]. \quad (12b)$$

Now since

$$\operatorname{Im} t_2 = -\pi [t_1 Q \delta(e) t_1], \quad (13)$$

we have

$$\frac{\operatorname{Im} t_3}{\operatorname{Im} t_2} = \frac{2t_2}{t_1}, \quad (14)$$

which we estimate to be 10—20 % for the range of energies of interest here.

We are grateful to Dr. Bruce Scott for communicating his results to us before publication and for stimulating discussions.

References

1) J. Dąbrowski and J. Sawicki, Nuclear Physics (to be published)
2) J. Sawicki, Nuovo Cim. **15** (1960) 606
3) S. A. Moszkowski and B. L. Scott, Annals of Phys. **11** (1960) 65
4) G. L. Shaw, Annals of Phys. **8** (1959) 609
5) A. M. Lane and C. F. Wandel, Phys. Rev. **98** (1955) 1524;
E. Clementel and C. Villi, Nuovo Cim. **2** (1955) 176;
L. Verlet and J. Gavoret, Nuovo Cim. **10** (1958) 505
6) B. L. Scott, Ph. D. Dissertation UCLA, June 1960
7) A. E. Glassgold, Rev. Mod. Phys. **30** (1958) 419

2.B:2.F:
2.G

Nuclear Physics 21 (1960) 462—473; © *North-Holland Publishing Co., Amsterdam*
Not to be reproduced by photoprint or microfilm without written permission from the publisher

SELECTION RULES AND CORRELATIONS FOR POLARIZATION IN STRIPPING AND DIRECT PROCESSES

L. J. B. GOLDFARB and R. C. JOHNSON

Theoretical Physics Department, The University, Manchester

Received 27 June 1960

Abstract: Various selection rules for polarization and correlations between effects of incoming polarization and the polarization arising from unpolarized incoming beams are found for a variety of direct nuclear processes. Use is made of the distorted-wave Born approximation, with allowance made for spin-dependent distortion. The results are found without explicit evaluation of the parameters that are involved, but with attention given to the separate effects of the assumptions of parity conservation and the invariance of the interaction under time-reversal.

1. Introduction

In a previous paper [1]), to be referred to as (I), there were established several selection-rules for polarization, which apply to a wide class of nuclear reactions. In addition, several correlations were found between the effects on angular distributions, owing to incoming beams with polarization, as compared to the outgoing polarization using unpolarized incoming beams. These results were found within the framework of the distorted-wave Born approximation (Austern [2])) and were meant to apply to the stripping of deuterons, tritons, He^3 and alpha particles, to the associated pick-up processes, and also to the inelastic scattering of nucleons and heavier particles. They arose mainly as a by-product in the explicit evaluation of the various polarization parameters; yet, their simple form and apparent independence of most of the features of the processes lead one to suspect that they may be derived in a more straightforward manner. It is also of interest to see to what extent these rules depend on the invariance of the interaction under the parity transformation and/or that of time reversal.

We shall concern ourselves, as in (I), with a general class of processes, involving a direct transfer of angular momentum which we specify by a limited set of quantum numbers l, s and j, where $\mathbf{l}+\mathbf{s}=\mathbf{j}$. This transfer is between the initial and final nuclear system and the system of incoming and outgoing particles, each of the latter being of arbitrary spin and complexity. We denote the spin states (total spin and component) of the nuclei by ax and cy, and those of the incoming and outgoing radiations by $s_1\sigma_1$, and $s_2\sigma_2$, respectively. We

further designate the linear momenta of the latter particles by $\mathbf{k}_1$ and $\mathbf{k}_2$, as measured in the centre-of-mass system of the process. With this notation, we write for the matrix element, connecting initial and final states

$$\langle \mathbf{k}_2 s_2 \sigma_2 c\gamma | R | \mathbf{k}_1 s_1 \sigma_1 a\alpha \rangle = \sum_{jls\zeta} (a\alpha, j\zeta | c\gamma) \theta_{j(ls)} \langle \mathbf{k}_2 s_2 \sigma_2, j(ls)\zeta | R | \mathbf{k}_1 s_1 \sigma_1 \rangle. \quad (1.1)$$

The quantity $\theta_{j(ls)}$ arises on integration over that part of the nuclear configuration not involved in the transfer process. If the transfer is taken to be the absorption of nucleons, as occurs in stripping, $\theta_{j(ls)}$ can be interpreted as a reduced-width amplitude for a particle specified by $j(ls)$ in the residual nucleus. For inelastic scattering processes, where there is no real transfer of particles, the interaction may be written in terms of sums of products of terms, one of which acts on the nuclear configuration, giving rise to $\theta_{j(ls)}$, while the other term is represented by $\langle j(ls)\zeta | \rangle$. Exchange effects are neglected here. A fuller discussion with application to specific processes is to be found in (I).

The matrix element on the right-hand side if (1.1), if calculated in the distorted-wave Born approximation, is proportional to the matrix element of the direct-interaction potential, V. This is assumed to be spin-independent for stripping phenomena. The matrix still has a weak dependence on the nuclear system through the optical-model parameters used to describe the effective distortion of the incident and outgoing radiations by the nuclear fields.

In the next section, we shall examine polarization effects according as the distortion is spin-dependent in either of the two stages (incoming or outgoing) of the process, or in neither stage. No general rules seem to be apparent, except if the restriction is made to processes with $l = 0$, or to arbitrary processes, but with spin-dependent distortion in neither stage. If we make the assumptions of invariance of the interaction under the parity transformation and time-reversal, these lead to several conclusions concerning polarization. This is dealt with in sect. 3.

2. General Selection Rules and Correlations for Polarization

We shall restrict ourselves to measurement of either the polarization of the outgoing radiation or to the angular distribution arising from polarized incident beams, but with polarization-insensitive detectors. In the former case, we are concerned with the evaluation of the tensors [3] †

$$\rho_{k_{\mathrm{in}}\kappa}(s_2) \equiv T_{k_{\mathrm{in}}\kappa}(s_2),$$

where $T_{k\kappa}$ is a spin-operator having matrix elements

$$\langle s\sigma' | T_{k\kappa}(s) | s\sigma \rangle = (-)^{s-\sigma'} (s\sigma, s-\sigma' | k\kappa). \quad (2.1)$$

In the latter case, we find the efficiency tensor, $\varepsilon_{k\kappa}(s_1)$, for measurement of the

† In the subsequent discussion we shall use spin tensors of rank k_{in} or k_{ex} according as the radiations are incoming or outgoing.

incoming polarization specified by $\rho_{k\kappa}(s_1)$. These efficiency tensors are so defined that if $(d\sigma/d\Omega)_0$ is the angular distribution with no polarization, the corresponding angular distribution for incoming polarized radiation is given by (cf. (I))

$$\frac{d\sigma}{d\Omega} = \left(\frac{d\sigma}{d\Omega}\right)_0 \sum_{k_{1s}\kappa} \rho_{k_{1s}\kappa}(s_1)\varepsilon^*_{k_{1s}\kappa}(s_1). \tag{2.2}$$

We assume that there is no preparation or detection of the polarization of the target or residual nucleus.

The calculation is most readily done by means of the density-matrix formalism. The density matrix for the outgoing system $\rho^{(f)}$ is related to that for the incoming system, $\rho^{(i)}$, by

$$\rho^{(f)} = R\rho^{(i)}R^\dagger \tag{2.3}$$

where R has matrix elements as in (1.1).

Proceeding as in (I), we find that for unpolarized incident radiation the outgoing polarization is given by

$$\rho_{k_{2s}\kappa}(s_2) = \frac{1}{X}\sum_{jll'ss'}\frac{1}{\hat{j}^2}\theta_{j(ls)}\theta^*_{j(l's')}\sum_{\sigma_1\sigma_2\sigma'_2\zeta}(-)^{s_2-\sigma'_2}(s_2\sigma_2, s_2-\sigma'_2|k_{2s}\kappa)$$
$$\times\langle \mathbf{k}_2 s_2\sigma_2, j(ls)\zeta|V|\mathbf{k}_1 s_1\sigma_1\rangle\langle \mathbf{k}_2 s_2\sigma'_2, j(l's')\zeta|V|\mathbf{k}_1 s_1\sigma_1\rangle^*, \tag{2.4a}$$

while for incoming polarization, the efficiency tensor for detection of this polarization is given by

$$\varepsilon^*_{k_{1s}\kappa}(s_1) = \frac{1}{X}\sum_{jll'ss'}\frac{1}{\hat{j}^2}\theta_{j(ls)}\theta^*_{j(l's')}\sum_{\sigma_1\sigma'_1\sigma_2\zeta}(-)^{s_1-\sigma'_1}(s_1\sigma_1, s_1-\sigma'_1|k_{1s}\kappa)$$
$$\times\langle \mathbf{k}_2 s_2\sigma_2, j(ls)\zeta|V|\mathbf{k}_1 s_1\sigma_1\rangle\langle \mathbf{k}_2 s_2\sigma_2, j(l's')\zeta|V|\mathbf{k}_1 s_1\sigma'_1\rangle^*, \tag{2.4b}$$

where

$$X = \sum_{j\sigma_1\sigma_2\zeta}\left|\sum_{ls}\frac{1}{\hat{j}}\langle \mathbf{k}_2 s_2\sigma_2, j(ls)\zeta|V|\mathbf{k}_1 s_1\sigma_1\rangle\theta_{j(ls)}\right|^2. \tag{2.4c}$$

Factors like $\sqrt{2j+1}$ are abbreviated here and elsewhere by the symbol $\hat{j}$ (stat j).

We now consider the consequences of spin-dependent distortion of the radiations.

2.1. NO SPIN-DEPENDENT DISTORTION OF INCOMING AND OUTGOING RADIATIONS

In addition to the neglect of the spin-dependent distortion of the incoming and outgoing waves, we make the further idealization that there is no coupling of the spin to the internal motion for all the transferred radiations concerned. This description of the internal configuration in terms of purely spatial coordi-

nates means, for example, that in dealing with incoming and outgoing deuterons, the d-state contributions are neglected.

We write for the tensor describing the transferred radiation

$$\langle j(ls)\zeta| \rangle = \sum_{\lambda\sigma} (l\lambda, s\sigma|j\zeta) T^{\lambda\dagger}_{(ls)j}(\mathbf{r}, \xi) T_s^{\sigma\dagger}(s), \tag{2.5a}$$

where ξ represents the spatial coordinates describing the internal motion and $\mathbf{r}$ denotes the coordinates of the centre-of-mass of the radiation referred to the centre-of-mass system of the process. Thus, for example, in deuteron stripping,

$$T^{\lambda}_{(ls)j}(\mathbf{r}, \xi) = u_{(ls)j}(r) i^l Y_l^{\lambda}(\mathbf{r}/r), \quad T_s^{\sigma} = \chi_{\frac{1}{2}}^{\sigma}, \tag{2.5b}$$

where $u_{(ls)j}(r)$ is the radial function of the captured nucleon in the residual nucleus and $\chi_{\frac{1}{2}}^{\sigma}$ is the spin-$\frac{1}{2}$ eigenvector.

Similarly, the eigenfunctions of the incoming and outgoing radiations may be written as

$$\langle\ |\mathbf{k}_1 s_1 \sigma_1\rangle = \phi^{(+)}(\mathbf{k}_1, \mathbf{r}_1, \xi_1)\chi^{\sigma_1}_{s_1}, \tag{2.6a}$$

$$\langle\ |\mathbf{k}_2 s_2 \sigma_2\rangle = \phi^{(-)}(\mathbf{k}_2, \mathbf{r}_2, \xi_2)\chi^{\sigma_2}_{s_2}, \tag{2.6b}$$

where $\phi^{(\pm)}$ are the stationary solutions of the Schrödinger equations containing optical-model potentials which characterize the elastic scattering by the target and residual nuclei, respectively. The superscripts $(\pm)$ refer to the usual boundary conditions of the spherical-wave components which arise by satisfying the conditions of invariance with respect to time-reversal. No explicit use of these boundary conditions will be made in this section. The quantities $\phi^{(\pm)}$ are functions of the coordinates of the centres-of-mass of the radiations $\mathbf{r}_1$ and $\mathbf{r}_2$ as well as of the internal coordinates, denoted symbolically in each case by ξ_1 and ξ_2.

We now assume that the direct-interaction potential is spin-independent, provided that we deal with stripping processes. For inelastic-scattering processes, on the other hand, the term $\langle j(ls)\zeta| \rangle$ represents that part of the interaction which acts between the states of the incoming and outgoing radiation, and incorporates the various tensor components of the interaction for different values of j, l and s. Hence, for these processes the interaction is, in fact, spin-dependent because of the different weighting given to the factors $\langle j(ls)\zeta| \rangle$ in the matrix elements of V. The matrix V may now be transformed by use of (2.5a), (2.6a) and (2.6b) so that

$$\langle \mathbf{k}_2 s_2 \sigma_2, j(ls)\zeta|V|\mathbf{k}_1 s_1 \sigma_1\rangle = \sum_{\lambda\sigma} (l\lambda, s\sigma|j\zeta)(s_2\sigma_2, s\sigma|s_1\sigma_1) V_{(ls)j\lambda}(\mathbf{k}_1, \mathbf{k}_2), \tag{2.7a}$$

where

$$V_{(ls)j\lambda}(\mathbf{k}_1, \mathbf{k}_2) = \langle s_1||T_s|s_2\rangle \langle \phi^{(-)}(\mathbf{k}_2, r_2, \xi_2) T^{\lambda}_{(ls)j}(\mathbf{r})|V|\phi^{(+)}(\mathbf{k}_1, \mathbf{r}_1, \xi_1)\rangle. \tag{2.7b}$$

Substituting (2.7a) into (2.4a) and (2.4b) and using the relation

$$\sum_{\sigma\sigma'\sigma_2\sigma'_2\sigma_1\zeta} (-)^{s_2-\sigma'_2}(s_2\sigma_2,\ s_2-\sigma'_2|k_{2s}\kappa)(s_2\sigma_2,\ s\sigma|s_1\sigma_1)(s_2\sigma'_2,\ s'\sigma'|s_1\sigma_1)$$
$$(l\lambda,\ s\sigma|j\zeta)(l'\lambda',\ s'\sigma'|j\zeta)$$
$$= \hat{s}_1^2\hat{j}^2 W(l'jk_{2s}s;\ s'l)W(ss_1k_{2s}s_2;\ s_2s')(-)^{l'-\lambda'}(l\lambda,\ l'-\lambda'|k_{2s}\kappa), \quad (2.8)$$

we find

$$\rho_{k_{2s}\kappa}(s_2) = \frac{1}{Y}\sum_{jls l's'} W(ss_1k_{2s}s_2;\ s_2s')\theta_{j(ls)}\theta^*_{j(l's')}W(l'jk_{2s}s;\ s'l)$$
$$\times \sum_{\lambda\lambda'}(-)^{l'-\lambda'}(l\lambda,\ l'-\lambda'|k_{2s}\kappa)V_{(ls)j\lambda}V^*_{(l's')j\lambda} \quad (2.9a)$$

and

$$\varepsilon^*_{k_{1s}\kappa}(s_1) = \frac{1}{Y}(-)^{k_{1s}}\sum_{jls l's'}\hat{s}_1^2 W(ss_2k_{1s}s_1;\ s_1s')(-)^{s-s'}\theta_{j(ls)}\theta^*_{j(l's')}$$
$$\times W(l'jk_{1s}s;\ s'l)\sum_{\lambda\lambda'}(-)^{l'-\lambda'}(l\lambda,\ l'-\lambda'|k_{1s}\kappa)V_{(l's')j\lambda'}V^*_{(ls)j\lambda}, \quad (2.9b)$$

where the tensors refer to common coordinate axes and

$$Y = \sum_{jls\lambda}\left|\frac{1}{l\hat{s}}\theta_{j(ls)}V_{(ls)j\lambda}\right|^2.$$

There immediately follow the selection rules

$$0 \leqq \frac{k_{1s}}{k_{2s}} \leqq 2s_{\max}, \quad 0 \leqq \frac{k_{1s}}{k_{2s}} \leqq 2l_{\max}, \quad (2.10)$$

and the correlation †, applicable if there is a unique value of s,

$$\varepsilon_{k_{1s}\kappa}(s_1) = (-)^{k_{1s}}\hat{s}_1^2\frac{W(ss_2k_{1s}s_1;\ s_1s)}{W(ss_1k_{1s}s_2;\ s_2s)}\rho_{k_{1s}\kappa}(s_2). \quad (2.11)$$

2.1. THE CASE $l = 0$

As shown in eq. (2.10) no polarization effects arise when $l = 0$, provided that (1) the optical model potentials are spin-independent, (2) V is spin-independent for stripping processes and (3) there is no coupling of the spin to the internal configuration of the incoming or outgoing radiations and the transferred radiation.

We shall now consider the effects of lifting restriction (1). No simple relations can be found even for $l = 0$ if there is spin-dependent distortion in both stages; however, if the distortion is limited to one stage, simple results are obtained.

† The correlations discussed in this article refer to separate experiments which are performed under identical conditions, except for the preparation and detection of the states of polarization.

Consider a spin-dependent distortion of the outgoing radiation. The associated wave function, instead of as in (2.6b), becomes

$$\langle\ |\mathbf{k}_2 s_2 \sigma_2\rangle = \sum_{\sigma'_2} \phi^{(-)}_{\sigma_2\sigma'_2}(\mathbf{k}_2, \mathbf{r}_2, \xi_2)\chi^{\sigma'_2}_{s_2}. \tag{2.12}$$

We then find

$$\rho_{k_{1s}\kappa}(s_2) = \frac{1}{Z}\sum_{s\sigma_2\sigma'_2\sigma''_2} (-)^{s_2-\sigma'_2}(s_2\sigma_2, s_2-\sigma'_2|k_{2s}\,\kappa) \times V^{(s)}_{\sigma_2\sigma''_2}(\mathbf{k}_1, \mathbf{k}_2)V^{(s)*}_{\sigma'_2\sigma''_2}(\mathbf{k}_1, \mathbf{k}_2) \tag{2.13a}$$

$$\varepsilon_{k_{1s}\kappa}(s_1) = \frac{1}{Z}\sum_{s} \hat{s}_1^2\hat{s}_1^2 W(s_2 s k_{1s} s_1; s_1 s_2) \sum_{\sigma_2\sigma'_2\sigma''_2} (-)^{s_2-\sigma'_2}(s_2\sigma_2, s_2-\sigma'_2|k_{1s}\kappa) \times V^{(s)}_{\sigma''_2\sigma_2}(\mathbf{k}_1, \mathbf{k}_2)V^{(s)*}_{\sigma''_2\sigma'_2}(\mathbf{k}_1, \mathbf{k}_2), \tag{2.13b}$$

where

$$Z = \sum_{s\sigma_2\sigma'_2} |V^{(s)}_{\sigma_2\sigma'_2}(\mathbf{k}_1, \mathbf{k}_2)|^2$$

with

$$V^{(s)}_{\sigma_2\sigma'_2}(\mathbf{k}_1, \mathbf{k}_2) = \langle s_1||T_s|s_2\rangle\langle\phi^{(-)}_{\sigma_2\sigma'_2}(\mathbf{k}_2, \mathbf{r}_2, \xi_2)T_0{}^0(\mathbf{r})|V|\phi^{(+)}(\mathbf{k}_1, \mathbf{r}_1, \xi_1)\rangle. \tag{2.13c}$$

By the properties of the Clebsch-Gordan coefficient in (2.13b) we are immediately led to the selection rule

$$k_{1s} \leqq 2s_2. \tag{2.14}$$

It is also possible to establish a correlation between the tensors in (2.13a), (2.13b). This requires that we deal with the structure of the functions $\phi^{(\pm)}$ in (2.13c).

The eigenfunction $\langle\ |\mathbf{k}_1 s_1 \sigma_1\rangle$, in the absence of spin-dependent distortion, involves the product of a distorted plane-wave describing the motion of the centre-of-mass of the radiation, a function describing the internal configuration and a spin-eigenfunction. Thus, we write

$$\begin{aligned}\langle|\mathbf{k}_1 s_1 \sigma_1\rangle &= 4\pi \sum_{l_1\lambda_1} [f_{l_1}(k_1, r_1)Y^{\lambda_1*}_{l_1}(\mathbf{k}_1)i^{l_1}Y^{\lambda_1}_{l_1}(\mathbf{r}_1)]\psi_1(\xi_1)\chi^{\sigma_1}_{s_1} \\ &\equiv \phi^{(+)}(\mathbf{k}_1, \mathbf{r}_1, \xi_1)\chi^{\sigma_1}_{s_1},\end{aligned} \tag{2.15a}$$

where $\psi_1(\xi_1)$ represents the dependence on the internal configuration, and $f_{l_1}(k_1, r_1)$ is the radial function representing the motion of the centre-of-mass of the incident radiation, normalized so that in the absence of distortion or Coulomb interaction, it reduces to the spherical Bessel function $j_{l_1}(k_1 r)$.

For the outgoing radiation, we have

$$\langle|\mathbf{k}_2 s_2 \sigma_2\rangle = 4\pi \sum_{j_2 l_2 \zeta_2 \lambda_2} Y^{\lambda_2*}_{l_2}(\mathbf{k}_2)(l_2\lambda_2, s_2\sigma_2|j_2\zeta_2)\psi^{\zeta_2}_{j_2(l_2 s_2)}(\mathbf{r}_2)g^{(-)}_{j_2 l_2}(k_2, r_2)\psi_2(\xi_2), \tag{2.15b}$$

where the radial function depends on j_2 as well as on l_2, because of the spin-

orbit interactions. The spin-angular eigenfunction $\psi^{\zeta_2}_{j_2(l_2 s_2)}(\mathbf{r}_2)$ is defined as

$$\psi^{\zeta_2}_{j_2(l_2 s_2)}(\mathbf{r}_2) = \sum_{\lambda_2 \sigma_2} (l_2 \lambda_2, s_2 \sigma_2 | j_2 \zeta_2) i^{l_2} Y^{\lambda_2}_{l_2}(\mathbf{r}_2) \chi^{\sigma_2}_{s_2}. \tag{2.15c}$$

It therefore follows that

$$\phi^{(-)}_{\sigma_2 \sigma'_2}(\mathbf{k}_2, \mathbf{r}_2, \xi_2) = 4\pi \sum_{j_2 l_2 \lambda_2 \lambda'_2 \zeta_2} (l_2 \lambda_2, s_2 \sigma_2 | j_2 \zeta_2)(l_2 \lambda'_2, s_2 \sigma'_2 | j_2 \zeta_2) \times Y^{\lambda_2 *}_{l_2}(\mathbf{k}_2) i^{l_2} Y^{\lambda'_2}_{l_2}(\mathbf{r}_2) g^{(-)}_{j_2 l_2}(k_2, r_2) \psi_2(\xi_2). \tag{2.15d}$$

If we now substitute the above expressions for $\phi^{\pm}$ into (2.13c), we find

$$V^{(s)}_{\sigma_2 \sigma'_2}(\mathbf{k}_1, \mathbf{k}_2) = \sum_{j_2 l_2 \lambda_1 \lambda_2 \zeta_2} Y^{\lambda_2}_{l_2}(\mathbf{k}_2) Y^{\lambda_1 *}_{l_2}(\mathbf{k}_1) (l_2 \lambda_2, s_2 \sigma_2 | j_2 \zeta_2) \times (l_2 \lambda_1, s_2 \sigma'_2 | j_2 \zeta_2) R_0(j_2, l_2, s), \tag{2.16}$$

where $R_0(j_2, l_2, s)$ is an integral over the internal coordinates and the radial coordinates of the projectiles. The matrix element of V takes on the forms V^{I}, V^{II} according as the z-axis is chosen along $\mathbf{k}_1$ or $\mathbf{k}_2$ with the y-axis, in both cases, along $\mathbf{k}_1 \times \mathbf{k}_2$. In particular, we find

$$V^{(s)\mathrm{I}}_{\sigma_2 \sigma'_2}(\mathbf{k}_1, \mathbf{k}_2) = \sum_{j_2 l_2 \lambda_2} Y^{\lambda_2}_{l_2}(\theta, 0) \frac{\hat{l}_2}{\sqrt{4\pi}} (l_2 \lambda_2, s_2 \sigma_2 | j_2 \sigma'_2)(l_2 0, s_2 \sigma'_2 | j_2 \sigma'_2) R_0(j_2, l_2, s) \tag{2.16b}$$

while

$$V^{(s)\mathrm{II}}_{\sigma_2 \sigma'_2}(\mathbf{k}_1, \mathbf{k}_2) = (-)^{\sigma_2 - \sigma'_2} V^{(s)\mathrm{I}}_{\sigma'_2 \sigma_2}(\mathbf{k}_1, \mathbf{k}_2). \tag{2.16c}$$

If we now define the tensor for outgoing radiation with respect to a z-axis along $\mathbf{k}_2$ and the tensor for incoming radiation with a z-axis along $\mathbf{k}_1$, then we must use V^{II} in (2.13a) and V^{I} in (2.13b). There then follows from (2.16c) the correlation

$$\varepsilon^*_{k\kappa}(s_2) = (-)^{\kappa} \hat{s}_1^{\,2} \hat{s}_2^{\,2} W(s_2 s k s_1; s_1 s_2) \rho_{k\kappa}(s_1). \tag{2.17}$$

A similar reasoning when applied to the case of spin-dependent distortion of the incoming radiation only, leads to the selection rule

$$k_{2s} \leqq 2 s_1, \tag{2.18}$$

and the correlation

$$\rho_{k\kappa}(s_2) = (-)^{\kappa} W(s_1 s k s_2; s_2 s_1) \varepsilon^*_{k\kappa}(s_1), \tag{2.19}$$

where the axes used to define the tensors are defined as in (2.17).

Finally, as an example of the above considerations, we apply the preceding formulae to deuteron stripping processes. We find that unless there is spin-dependent distortion acting on the incoming deuterons, there will be no second-rank polarization effects. In addition, we can relate the asymmetry arising from deuterons having first-rank polarization $P_{\mathrm{in}}(1)$ with the polariza-

tion $P_{\text{out}}(\frac{1}{2})$, exhibited by the outgoing nucleons in a second experiment with unpolarized incident deuterons. We find for $l = 0$

$$\frac{d\sigma}{d\Omega} = \begin{cases} \left(\frac{d\sigma}{d\Omega}\right)_0 & \text{(no spin-dependent distortion)} \quad (2.20a) \\ \left(\frac{d\sigma}{d\Omega}\right)_0 [1+\frac{3}{2}P_{\text{in}}(1)P_{\text{out}}(\frac{1}{2})+\text{second-rank polarization effects}], & \text{(no nucleon-spin-dependent distortion).} \quad (2.20b) \\ \left(\frac{d\sigma}{d\Omega}\right)_0 [1+P_{\text{in}}(1)P_{\text{out}}(\frac{1}{2})] & \text{(no spin-dependent distortion of the deuteron),} \quad (2.20c) \end{cases}$$

while for $l \neq 0$

$$\frac{d\sigma}{d\Omega} = \left(\frac{d\sigma}{d\Omega}\right)_0 [1+3P_{\text{in}}(1)P_{\text{out}}(\frac{1}{2})] \quad \text{(no spin-dependent distortion).} \quad (2.20d)$$

In these formulae, $(d\sigma/d\Omega)_0$ is the angular distribution associated with unpolarized deuterons, while $(d\sigma/d\Omega)$ refers to angular distributions, where the incoming deuterons are of arbitrary polarization, but, where in particular $P_{\text{in}}(1)$ denotes the component of vector polarization along $\mathbf{k}_1 \times \mathbf{k}_2$. The quantity $P_{\text{out}}(\frac{1}{2})$ can only be along $\mathbf{k}_1 \times \mathbf{k}_2$ for incident unpolarized deuterons.

3. Considerations Based on Invariance under the Parity Transformation and Time-Reversal

We note that the above rules do not depend on the symmetry character of the interaction. To discuss the implications of parity-conservation and invariance under time-reversal, we cast the matrix elements of V into a convenient form. Noting that the quantity $\langle \mathbf{k}_2 s_2 \sigma_2 j(ls)\zeta | V | \mathbf{k}_1 s_1 \sigma_1 \rangle$ is essentially the matrix element of a tensor operator of rank j acting between states $|s_1\sigma_1\rangle$ and $|s_2\sigma_2\rangle$, we write (see e.g. Ritus [4]))

$$\langle \mathbf{k}_2 s_2 \sigma_2, j(ls)\zeta | V | \mathbf{k}_1 s_1 \sigma_1 \rangle = \langle s_2\sigma_2 | \sum_{j_2 j_1 l_2 l_1 \zeta_1 \zeta_2} S^{j(ls)}_{j_2 l_2, j_1 l_1}(k_1, k_2) \times \psi^{\zeta_2}_{j_2(l_2 s_2)}(\mathbf{k}_2) \psi^{\zeta_1 \dagger}_{j_1(l_1 s_1)}(\mathbf{k}_1) | s_1 \sigma_1 \rangle (j_2 \zeta_2, j\zeta | j_1 \zeta_1), \quad (3.1)$$

where the spin-dependence of V is ignored for stripping, as well as the coupling of the spins to the internal configurations of the radiations. The quantity $S^{j(ls)}_{j_2 l_2, j_1 l_1}$ is a scalar function of the magnitudes of $\mathbf{k}_1$ and $\mathbf{k}_2$, while the quantities $\psi^{\zeta_i}_{j_i(l_i s_i)}(\mathbf{k}_i)$ are spin-angular functions, defined so that

$$\psi^{\zeta_i}_{j_i(l_i s_i)}(\mathbf{k}_i) = \sum_{\lambda_i \sigma_i} (l_i \lambda_i, s_i \sigma_i | j_i \zeta_i) Y^{\lambda_i}_{l_i}(\mathbf{k}_i) \chi^{\sigma_i}_{s_i}, \quad i = 1,2. \quad (3.2)$$

The matrix element of V, therefore takes on the form:

$$\langle \mathbf{k}_2 s_2 \sigma_2, j(ls)\zeta | V | \mathbf{k}_1 s_1 \sigma_1 \rangle = \sum_{j_1 l_1 j_2 l_2 \lambda_1 \lambda_2 \zeta_1 \zeta_2} S^{j(ls)}_{j_2 l_2, j_1 l_1}(k_1, k_2)(l_1 \lambda_1, s_1 \sigma_1 | j_1 \zeta_1) \times (l_2 \lambda_2, s_2 \sigma_2 | j_2 \zeta_2)(j_2 \zeta_2, j\zeta | j_1 \zeta_1) Y^{\lambda_2}_{l_2}(\mathbf{k}_2) Y^{\lambda_1 *}_{l_1}(\mathbf{k}_1). \quad (3.3)$$

It is to be noted that the quantity $S^{j(ls)}_{j_2 l_2, j_1 l_1}$ is identical to the reduced matrix element $\langle j_2(l_2 s_2) | j(ls) || j_1(l_1 s_1) \rangle$ used in (I).

3.1. PARITY-CONSERVATION

Choosing a coordinate system with the y-axis normal to the reaction plane along $\mathbf{k}_1 \times \mathbf{k}_2$, we easily find from (3.3) and the properties of the Clebsch-Gordan coefficients, that

$$\langle \mathbf{k}_2 s_2 - \sigma_2, j(ls) - \zeta | V | \mathbf{k}_1 s_1 - \sigma_1 \rangle = (-)^{j+l-\zeta+s_2+s_1-\sigma_2-\sigma_1} \langle \mathbf{k}_2 s_2 \sigma_2, j(ls)\zeta | V | \mathbf{k}_1 s_1 \sigma_1 \rangle, \quad (3.4a)$$

provided that parity is conserved in the reaction, i.e.,

$$(-)^{l+l_1+l_2} = 1. \quad (3.4b)$$

If now, we use the Hermitian property of the spin tensors (I) and rearrange the expressions (2.4a) and (2.4b) using (3.4a) we find

$$\rho^*_{k_{12}\kappa}(s_2) = (-)^{k_{12}} \rho_{k_{12}\kappa}(s_2), \quad (3.5a)$$

$$\varepsilon^*_{k_{12}\kappa}(s_1) = (-)^{k_{12}} \varepsilon_{k_{12}\kappa}(s_1). \quad (3.5b)$$

Thus, for spin-$\frac{1}{2}$ particles and the particular choice of coordinate system used here, we find only imaginary spin-tensors are effective. This leads to the well-known result that only the polarization normal to the reaction plane contributes to the angular distribution, and likewise for incident unpolarized-radiation, the outgoing polarization is normal to the reaction plane. These statements also apply to particles of higher spin provided that we limit ourselves to only "vector" polarization.

3.2. INVARIANCE UNDER TIME-REVERSAL

Invariance of the interaction under time-reversal requires for consistency that the spin-angular functions be of proper phase so that they satisfy

$$K \psi^{\zeta}_{j(ls)}(\mathbf{r}) = (-)^{j+\zeta} \psi^{-\zeta}_{j(ls)}(\mathbf{r}), \quad (3.6)$$

where K is the time-reversal operator (Wigner [5]). With these choices of phase

we require

$$\langle \mathbf{k}_2 s_2 \sigma_2 c\gamma | R | \mathbf{k}_1 s_1 \sigma_1 a\alpha \rangle$$
$$= (-)^{a+\alpha+c+\gamma+s_2+\sigma_2+s_1+\sigma_1} \langle -\mathbf{k}_1 s_1 - \sigma_1 a - \alpha | R | -\mathbf{k}_2 s_2 - \sigma_2 c - \gamma \rangle \tag{3.7}$$
$$= \sum_{jls\zeta} (a\alpha, js\zeta | c\gamma) \langle a | j(ls) || c \rangle (-)^{j+\zeta+s_1+\sigma_1+s_2+\sigma_2} \langle -\mathbf{k}_1 s_1 - \sigma_1 | V | -\mathbf{k}_2 s_2 - \sigma_2, j(ls) - \zeta \rangle,$$

where we have written for $\theta_{j(ls)}(c, a)$ the reduced matrix element $\langle c || j(ls) | a \rangle$. The latter quantity, corresponds to the emission of radiation $j(ls)$ by the "final" nucleus and, by a choice of phases, consistent with (3.6), together with a choice of real radial functions, it can satisfy

$$\langle c || j(ls) | a \rangle = \langle a | j(ls) || c \rangle. \tag{3.8}$$

Hence time-reversal invariance imposes the condition

$$\langle -\mathbf{k}_1 s_1 - \sigma_1 | V | j(ls) - \zeta, -\mathbf{k}_2 s_2 - \sigma_2 \rangle$$
$$= (-)^{j+\zeta+s_1+\sigma_1+s_2+\sigma_2} \langle \mathbf{k}_2 s_2 \sigma_2, j(ls)\zeta | V | \mathbf{k}_1 s_1 \sigma_1 \rangle. \tag{3.9}$$

Insertion of the above relation in (2.4a) and (2.4b) allows us to relate the tensors of one process I, to those of the inverse process II.

$$\rho^{\mathrm{II}}_{k\kappa}(s_1) = \frac{(-)^k}{\hat{s}_1^{\,2}} \varepsilon^{\mathrm{I}}_{k\kappa}(s_1), \tag{3.10}$$

where the tensors refer to the same coordinate axes in space. This gives for example, the relation of polarization effects in stripping and pickup processes, and is a special case of the general result found by Satchler [6])

We finally consider inelastic-scattering processes with $s = 0$ only. In these cases, the transferred angular momentum is not associated with a real particle. We use optical-model potentials for incoming and scattered radiations which we assume do not differ in an essential manner because of the different energies and nuclei that are involved. We also neglect exchange effects and changes in the internal configuration so that $\mathbf{r}_1 = \mathbf{r}_2 = \mathbf{r}$ and $\xi_1 = \xi_2 = \xi$.

The matrix element of V is now of the form

$$\langle \mathbf{k}_2 \sigma_2 l\lambda | V | \mathbf{k}_1 \sigma_1 \rangle = \sum_{\sigma} \langle \phi^{(-)}_{\sigma_2 \sigma}(\mathbf{k}_2, \mathbf{r}, \xi) | T_l^{\lambda\dagger}(\mathbf{r}) | \phi^{(+)}_{\sigma_1 \sigma}(\mathbf{k}_1, \mathbf{r}, \xi) \rangle, \tag{3.11a}$$

where, because of time-reversal invariance,

$$\phi^{(+)}_{\sigma\sigma'}(\mathbf{k}, \mathbf{r}, \xi) = (-)^{\sigma-\sigma'} \phi^{(-)}_{-\sigma-\sigma'}(-\mathbf{k}, \mathbf{r}, \xi), \tag{3.11b}$$

It therefore follows that

$$\langle \mathbf{k}_2 \sigma_2 l\lambda | V | \mathbf{k}_1 \sigma_1 \rangle = (-)^{\sigma_1 - \sigma_2} \langle -\mathbf{k}_1 - \sigma_1 l\lambda | V | -\mathbf{k}_2 - \sigma_2 \rangle. \tag{3.12}$$

We now make two choices of coordinate axes. In one case, the z-axis is along

$\mathbf{k}_2$ and the y-axis is along $\mathbf{k}_1\times\mathbf{k}_2$, so that

$$\langle \mathbf{k}_2\sigma_2 l\lambda|V|\mathbf{k}_1\sigma_1\rangle = \sum_{j_1 l_1 j_2 l_2 \lambda_1 \zeta_2} S^l_{j_2 l_2, j_1 l_1}(k_1, k_2) \times (l_1\lambda_1, s_1\sigma_1|j_1\zeta_1)(l_2 0, s_1\sigma_2|j_2\alpha_2)(j_2\sigma_2, l\lambda|j_1\zeta_1)\frac{\hat{l}_2}{\sqrt{4\pi}}Y^{\lambda_1}_{l_1}(\theta,\pi); \quad (3.13)$$

whereas in the other case, the z-axis is along $\mathbf{k}_1$ and the y-axis is still along $\mathbf{k}_1\times\mathbf{k}_2$, so that,

$$\begin{aligned}\langle -\mathbf{k}_1-\sigma_2 l-\lambda|V|-\mathbf{k}_2-\sigma_1\rangle &= \sum_{j_1 l_1 j_2 l_2 \lambda_1 \zeta_2} S^l_{j_2 l_2, j_1 l_1}(k_2, k_1)(l_1\lambda_1, s_1\sigma_1|j_1\zeta_1) \\ &\quad\times (l_2 0, s_1\sigma_2|j_2\sigma_2)(j_2\sigma_2, l\lambda|j_1\zeta_1)\frac{\hat{l}_2}{\sqrt{4\pi}}(-)^l Y^{\lambda_1}_{l_1}(\theta,\pi) \\ &\equiv (-)^l\langle \mathbf{k}_2\sigma_2 l\lambda|\bar{V}|\mathbf{k}_1\sigma_1\rangle. \end{aligned} \quad (3.14)$$

We now consider the statistical tensor in (2.4a). Since $s_1 = s_2$ and σ_1, σ_2 and σ'_2 are parameters over which summation is to be performed, we may rewrite the tensor as

$$\rho_{k\kappa}(s_1) = \sum_{\sigma_1\sigma'_1\sigma_2\lambda}(-)^{s_1-\sigma'_1}(s_1\sigma_1, s_1-\sigma'_1|k\kappa) \times \frac{\langle \mathbf{k}_2\sigma_1 l\lambda|V|\mathbf{k}_1\sigma_2\rangle\langle \mathbf{k}_2\sigma'_1 l\lambda|V|\mathbf{k}_1\sigma_2\rangle^*}{X} \quad (3.15a)$$

$$= (-)^\kappa \sum_{\sigma_1\sigma'_1\sigma_2\lambda}(-)^{s_1-\sigma'_1}(s_1\sigma_1, s_1-\sigma'_1|k\kappa) \times \frac{\langle -\mathbf{k}_1-\sigma_2 l\lambda|V|-\mathbf{k}_2-\sigma_1\rangle\langle -\mathbf{k}_1-\sigma_2 l\lambda|V|-\mathbf{k}_2-\sigma'_1\rangle^*}{X} \quad (3.15b)$$

where the last equation follows from (3.11b) and X is defined as

$$X = \sum_{\sigma_1\sigma_2\lambda}|\langle \mathbf{k}_2\sigma_1 l\lambda|V|\mathbf{k}_1\sigma_2\rangle|^2. \quad (3.15c)$$

If we introduce the function $\bar{V}$ in (3.14), we have

$$\rho_{k\kappa}(s_1) = (-)^\kappa \sum_{\sigma_1\sigma'_1\sigma_2\lambda}(-)^{s_1-\sigma'_1}(s_1\sigma_1, s_1-\sigma'_1|k\kappa) \times \frac{\langle \mathbf{k}_2\sigma_2 l\lambda|\bar{V}|\mathbf{k}_1\sigma_1\rangle\langle \mathbf{k}_2\sigma_2 l\lambda|\bar{V}|\mathbf{k}_1\sigma'_1\rangle^*}{\sum_{\sigma_1\sigma_2\lambda}|\langle \mathbf{k}_2\sigma_2 l\lambda|\bar{V}|\mathbf{k}_1\sigma_1\rangle|^2}. \quad (3.15d)$$

In (3.15d) the z-axis is along $\mathbf{k}_2$ instead of along $\mathbf{k}_1$, as in (3.15a); however, the y-axis is the same in both cases. Comparing (3.15d) with the expression for $\varepsilon^*_{k\kappa}(s_1)$ in (2.4b), we note that the latter is equal to $\rho_{k\kappa}(s_1)$, except that V must be replaced by $\bar{V}$. These two quantities differ by an interchange of k_1 and k_2 in the quantity $S^l_{j_2 l_2, j_1 l_1}(k_1, k_2)$ by the choice of z-axes, and by a phase factor which is of no importance here. Thus, except for the different z-axes, we find

that in the limit where $k_1 \to k_2$,

$$\varepsilon^*_{k\kappa}(s_1; \text{in}) = \hat{s}_1^2(-)^\kappa \rho_{k\kappa}(s_1; \text{out}). \tag{3.16}$$

This corresponds to the well-known result in the double elastic-scattering of spin-$\frac{1}{2}$ particles, that the polarization arising from the first experiment is equal to the left-right asymmetry in the second scattering, for common scattering angles, using fully polarized incident particles (Wolfenstein and Ashkin, Dalitz [7])). It is interesting to observe that (3.16) is "almost" true for inelastic scattering provided that $S^I_{j_2 l_2, j_1 l_1}(k_1, k_2)$ is not too sensitive to the interchange of k_1 and k_2. In fact, if a common optical-model potential is used for the incoming and scattered radiation and if the transferred energy is a small fraction of the incident energy, so that $k_1 = k_2$, this assumption may not be too unreasonable. The "almost" equality in this case is a direct consequence of invariance of the interaction under time-reversal and is independent of parity-conservation. A similar fact was already noted by Bell and Mandl [8]) in the limiting case of elastic scattering where the "true" equality, expressed by (3.16) holds.

References

1) L. J. B. Goldfarb and R. C. Johnson, Nuclear Physics (in press)
2) N. Austern, in Fast neutron physics, ed. by J. B. Marion and J. L. Fowler (Interscience, New York 1960) Vol. II, Ch. V
3) L. J. B. Goldfarb, Nuclear Physics **7** (1958) 622
4) I. Ritus, JETP **33** (1957) 1264; Soviet Phys. JETP **6** (1958) 972
5) E. P. Wigner, Göttinger Nachrichten **31** (1932) 546
6) G. R. Satchler, Nuclear Physics **8** (1958) 65
7) L. Wolfenstein and J. Ashkin, Phys. Rev. **85** (1952) 947;
R. H. Dalitz, Proc. Phys. Soc. A **65** (1952) 175
8) J. S. Bell and F. Mandl, Proc. Phys. Soc. **71** (1958) 272, 867

8.C

Nuclear Physics 21 (1960) 474—491; © *North-Holland Publishing Co., Amsterdam*

Not to be reproduced by photoprint or microfilm without written permission from the publisher

WEAK INTERACTIONS IN THE THEORY OF ELEMENTARY PARTICLES WITH FINITE SPACE

I. S. SHAPIRO

Theoretical and Experimental Physics Institute of the USSR Academy of Sciences, Moscow, USSR

Received 15 May 1960

Abstract: A variant of the theory put forth by H. R. Coish [1]) is considered. Two additional quantum numbers are shown to arise in this theory. The selection rules obeyed by them make it possible to forbid the conversion of barions into leptons and the neutrino-less decay of muons into electrons. Combined inversion is found to be the only possible law of transformation of wave functions in the case of space reflections, provided Wigner's transformation law is accepted for time inversions. The spinor field theory proves to be essentially two-component. These results as well as the quantization of electric charge obtained in ref. [1]) are a consequence solely of the finiteness of the space-time manifold, ruling out divergencies.

1. Introduction

Apart from the principal difficulty in eliminating divergences, which is especially formidable in the case of non-renormalised four fermion interactions, the theory of elementary particles also presents us with the problem of accounting for the properties of symmetry. To put it briefly, the physics of the elementary particles contains far more different symmetry relations than we are able to understand and predict, proceeding from the properties of space and time symmetry (or, what amounts to the same thing, from the properties of the symmetry of macroscopic experiments). This holds even when we deal with weak interactions, i.e., when we consider only rigorous conservation laws and ignore the approximate conservations like those of isobaric spin.

As is well known, the general type of four-fermion interaction Hamiltonian presupposes five variants and is described by ten constants (or 20 constants unless lepton charge conservation is postulated). If this state were actually realisable it would mean that there are no additional restrictions imposed by unknown symmetry properties. Actually, the reverse is the case: there are serious experimental grounds to believe that of the total manifold of permissible Hamiltonians, the interactions of the type $(C_V V+C_A A)(C_{V'}V'+C_{A'}A')$ where $|C_A|/|C_V| = |C_A'|/|C_V| = 1$ are realised, or at any rate these quantities are rather close to each other (if we leave out non-local corrections arising due to strong interactions). Heuristically, it is scarcely expedient to regard this universality and distinction of vector interaction as accidental. On the contrary, it is more fruitful to think that this is a manifestation of selection principles unknown to us and general for this class of phenomena.

Another precise law unaccounted for by modern theory is the quantization of electric charge. Since the interaction between a charge and an electromagnetic field is vectorial, it can be supposed that the quantization of the electric charge is caused by the same factors that give rise to the properties of symmetry of weak interactions.

No adequate explanation has yet been given of the connection between space reflection and charge conjugation manifest in the invariance of the Lagrangians with respect to combined inversion. A successful study of this problem will most likely lead to an understanding of why parity is not conserved.

Finally, it will be noted that the forbiddenness of the conversion of barions into leptons and probably of the decay $\mu \to e+\gamma$ are also likely to be explained in a consistent weak interaction theory.

The viewpoint that the problem of divergences and that of symmetry properties are unrelated is quite justified. Yet there can be another approach assuming a close relation between these two problems so that the above-listed symmetry properties become necessary consequences of the absence of divergences. For tentative research the second viewpoint seems more attractive since definite qualitative dependences can be used for orientation in this case.

The present paper investigates the concept suggested by H. R. Coish [1]) according to which the configurational space of field theory consists of a finite number of points. This idea is attractive because the absence, trivial in the present case, of divergences (all integrals become finite sums) leads, as is partially shown in ref. [1]), to the appearance of a number of symmetry properties caused by the very fact of finiteness of space and independent of the number of points in it. The entire scheme admits no arbitrariness except for the assignment of a number of points, the concrete value of which is inessential in the investigation of symmetry properties. Since the concept under consideration is new and the mathetmatical apparatus applied has scarcely been used in physics, it seems worthwhile to recapitulate the principles of the theory and the results obtained by H. R. Coish (the existence of only vector spin tensors and quantization of an electric charge) and, whenever possible, to analyse them in physical terms. This is all the more necessary since, at certain points (the correspondence principle), the present paper is based on a viewpoint differing from that of ref. [1]) New major results obtained in this paper are: a) deduction of a combined inversion law from Wigner's wave function transformation rule with time reflections on the basis of a connection between space and time reflections in finite space † left unused in ref. [1]), and b) the derivation of two new quantum numbers, the selection rules for which forbid the conversion of barions into leptons and the neutrinoless decay of a muon into an electron (i.e., the processes like $\mu \to e+\gamma$, $\mu \to 3e$ etc.). These results do not involve introduction of any

† In this connection it will be noted that the remarks of ref. [1]) concerning combined inversion are hardly correct.

new additional assumptions but are determined only by the symmetry properties of the finite space time manifold.

2. Mathematical Apparatus

By the point x of finite space is understood an aggregate of four quantities $(x_0, x_1, x_2 x_3)$. A multitude of values of each x_μ is assumed, finite and closed with respect to two commutative operations referred to as addition and multiplication. The connection of these two operations is determined by the distribution requirement $(a(b+c) = ab+ac)$. Both operations possess associative properties $(a+b)+c = a+(b+c)$, $a(bc) = (ab)c$. Other requirements are the existence of a unit element and zero $(a \cdot 1 = a, a+0 = a)$ as well as a solution of the unique linear equation $ax+b = c$ with arbitrary a, b, c (this requirement implying the existence for each $a \neq 0$ of the sole reverse element a^{-1} and the element $(-a) : aa^{-1} = 1$, $a+(-a) = 0$). Thus, the multitudes of values of coordinates x_μ are strictly analogous, in the sense of the operations determined in them, to the usual multitude of real numbers with the only essential difference that those multitudes are finite. The requirement of the existence of the above-listed operations is dictated by the desire to have some minimal algorithm of mathematical operations in the new theory, lacking which, no development of the latter is possible. Bearing in mind the correspondence principle, it seems natural to construct this algorithm on the pattern of the usual numerical field. The finite multitudes with two operations possessing the above-mentioned properties are known as Gallois fields. Distinction is made between primitive and non-primitive Gallois fields. The primitive fields do not contain fields of lesser order. The non-primitive fields lack this property, but it can be shown (see ref. [2]) that they contain only one primitive subfield. The number of elements of the primitive field is always equal to a prime. The order (the number of elements) of the non-primitive field is equal to a power of a prime, which is the order of its primitive subfield. Gallois fields are designated as $GF(p^n)$ where p is a prime equal to the number of elements of the subfield, n — any integer and p^n the order of the entire field (the symbol $GF(p)$ obviously corresponding to a simple field). Below, there will occur $GF(p)$ and $GF(p^2)$. The latter, with $p = 4m-1$ (m is any integer) are not dissimilar to the complex number field (the primitive root of the fourth power of a unit element exists in $GF(p^2)$). A peculiarity of Gallois fields is that the assignment of an order of a field entirely determines its structure and properties. In other words, all fields of the same order are isomorphous — there are no different Gallois fields of the same order. It is precisely this fact that makes the entire scheme very rigid and free from arbitrary assumptions, though at first glance it might seem that the construction of finite and consequently discrete space is not unlike that of various space lattice theories. In this connection it will be noted that there

exist no discrete but infinite algebraic fields (any primitive field whose elements form a denumerable multitude is isomorphous to the rational number field, but the latter contains infinitely close elements: see ref. [2])). Once we resolve, in constructing a consistent theory, to change the macroscopic concepts of space and time, there are only two alternatives: either finite space with properties determined rather rigidly by the very fact of finiteness, or the conventional number field. In the latter case, there is much room for variation since, as Riemann already noticed [3]) ,"in the case of a discrete manifold the principle of metric relations is contained in the very concept of this manifold, whereas in the case of continuous manifold it should be sought elsewhere".

2.1. REAL "NUMBERS"

Owing to the isomorphism of Gallois fields of a given order we can confine ourselves to one realisation. Consider first primitive fields. The Gallois primitive field $GF(p)$ is a field of residues † of the prime p. Thus, the elements of $GF(p)$ are the numbers

$$0, 1, 2 \ldots (p-1).$$

The addition and multiplication are determined "modulo p". This means that if $a, b \varepsilon GF(p)$ then $a+b$, ab are the residues of division of the results of conventional arithmetical operations by the number p. It can be easily seen that the residues modulo p form a field only when p is a prime ††. The following relations, the deduction of which exists in mathematical literature, see for example ref. [2]) are essential for the following.

1) If $q = p^n$ is the order of the field, then for any element $a \neq 0$ we have

$$a^{q-1} = 1. \tag{1}$$

2) Among the solutions of eq. (1) there is a primitive root, i.e., $a = a_0$ such that all powers of it up to a_0^{q-1} are different:

$$a_0 \neq a_0^2 \neq a_0^3 \ldots \neq a_0^{q-1}. \tag{2}$$

Since the field contains q elements, the elements exhaust the whole field and consequently any element $a \neq 0$ can be represented in the form

$$a = a_0^k \quad (1 \leqq k \leqq q-1). \tag{3}$$

3) It follows from the above that the equation

$$x^m = 1, \tag{4}$$

where m is an integer has a solution different from $x = 1$ if m is a divisor of $q-1$. A primitive root always exists in this case. In particular, for a primitive

† A residue of p is a remainder on division of an integer by p.

†† If p resolves into multiples m and n, $m \cdot n = 0$, though $m \neq 0$, $n \neq 0$. Therefore, there are no inverse elements for the residues m and n.

root of the fourth power of unity to exist, it is necessary and sufficient that $q-1$ be divisible by 4. This fact is important for introducing complex numbers and will be used in the following.

Let us now consider the problem of formalism of algebraic operations in $GF(p)$. For this formalism to be analogous to the usual algebra (which is necessary for a consistent realisation of the correspondence principle accepted in 2) it is necessary to introduce positive and negative numbers so that the usual rules of signs be conformed to in algebraic operations. It turns out that division of $GF(p)$ (exclusive of the element 0) into two equal parts (positive and negative "numbers") satisfying this requirement is by no means a trivial procedure. The simplest method of this division might seem to be as follows. Let us arbitrarily take $\frac{1}{2}(p-1)$ non-zero residues and call them "positive". If a is a residue of this group, the residue $(-a)$ complementing a to 0 (i.e. up to p) will be called negative. The rule of signs in transposing nominals from one side of an equality to the other will be fulfilled, i.e., from

$$a+b=c$$

it follows that

$$a=c+(-b)\equiv a-b.$$

Yet in such arbitrary division the multiplicative rule of signs $(\pm)\cdot(\pm)=+$, $(\pm)\cdot(\mp)=-$ will not, generally, be fulfilled. This can easily be seen by any example say, $GF(7)$. The general rule of dividing $GF(p)$ into two classes satisfying the requirements imposed was pointed out by Kustaanheime [4]). This rule consists in the classification of the elements of $GF(p)$ according to "quadratic residue" ("square"). The residue is called "square" if it is the residue of the square of an integer. Proceeding from 1), 2) and 3) it is easy to obtain a necessary and sufficient condition for the given element $a\in GF(p)$ to be or not to be a square. The residue a is a square if

$$a^{\frac{1}{2}(p-1)}=1. \tag{5}$$

Inversely, a is not a square † if

$$a^{\frac{1}{2}(p-1)}=-1\equiv p-1. \tag{6}$$

Thus $GF(p)$ (exclusive of 0) is divided according to (5) or (6) into two classes

† Relations (5) and (6) are obtained in the following manner. From (3) it follows that for a square this equation holds

$$a=a_0^{2k}. \tag{5a}$$

Using then (1), at $q=p$, we obtain eq. (5), $a^{\frac{1}{2}(p-1)}=a_0^{k(p-1)}=1$. From 3) it follows that the number of different solutions of eq. (5) is equal to $\frac{1}{2}(p-1)$. The condition (6) is obtained by using (1) and (5),

$$(a^{\frac{1}{2}(p-1)}+1)(a^{\frac{1}{2}(p-1)}-1)=a^{p-1}-1=0. \tag{6a}$$

If a is not a square, (6) follows from (6a).

with an equal number of elements in each. If the squares satisfying (5) are called positive, and all remaining elements (except for 0) satisfying (6) negative, it is easy to establish the fulfilment of the multiplicative rule of signs by using (5) and (6). For an arbitrary p, however, it may happen that the multiplicative rule of signs cannot be combined with the rule of signs when transposing nominals from one side of an equality to the other. This will occur if $p-1 \equiv (-1)$ is a square, i.e., a "positive number" (for example, $p=5$, $\frac{1}{2}(p-1)=2$, $(p-1)^{\frac{1}{2}(p-1)} = 4^2 = 1$). According to (6), a sufficient condition for (-1) not to be a square is the relation

$$(-1)^{\frac{1}{2}(p-1)} = -1. \tag{7}$$

Hence it follows that the prime p must have the form

$$p = 4m-1. \tag{8}$$

A prime like (8) will be understood by the number p in the following. So in $GF(p)$ all the formalism of algebraic operations proves to be completely analogous to conventional algebra. The following distinction is essential, however. The sum of squares is, generally, not a square. In other words, a sum of "positive numbers" may be a "negative number" (for example, for $p = 7$, $2+4 = 6 \equiv -1$). This important fact leads to $GF(p)$ having equalities but no inequalities. The consequences of this are analysed in detail in subsect. 2.3.

From 3) of this section it follows that in $GF(p)$ there is no primitive root of the fourth degree of 1, since $p-1 = 4m-2$ is not divisible by four. In other words, in $GF(p)$ there is no $\sqrt{-1}$. In this sense $GF(p)$ may be called a finite analogue of the field of real numbers.

2.2. COMPLEX "NUMBERS"

Yet an imaginary unity exists in $GF(p^2)$ since $p^2-1 = 8m(2m-1)$ is divisible by four. Any element of $GF(p^2)$ can be represented in the form

$$z = x+iy,$$

where x and y are elements of $GF(p)$. The field $GF(p^2)$ can be called a finite analogue of the field of complex numbers. The fact of finiteness leads, however, to the following distinctive peculiarities. First, designating the element complex conjugate to z by $\bar{z}$,

$$\bar{z} = x-iy$$

and noticing that, by virtue of (8),

$$i^p = -i,$$

we find that

$$z^p = \bar{z} \tag{9}$$

since if $a, b \in GF(p)$, then †

$$(a+ib)^p = a^p+(ib)^p = a-ib. \tag{10}$$

Eq. (9) can be written in the form

$$\bar{z}z = x^2+y^2 = z^{p+1}. \tag{11}$$

Second, as has been noted above, a sum of two squares is not, generally, a square. For this reason, $|z|^2 \equiv \bar{z}z$ is not a positive definite quantity. This essentially affects the properties of a representation of the finite analogue of the Lorentz group. This also means that the norm $\phi^+\phi$ of the state ϕ of the quantum system in the new theory cannot be positive definite. In other words, if it proves possible to transfer an adequately modified apparatus of the linear operators into the new theory, we shall have something not dissimilar to indefinite metrics, though metrics in the case of finite space can be referred to only in highly conventional terms, as will be shown below.

2.3. ORDERING AND GEOMETRY IN $GF(p)$

Hitherto we have treated $GF(p)$ as a certain algebraic manifold without discussing the possibility of introducing geometric concepts, and, particularly, metric relations. These latter call, above all, for the ordering of a multitude of points. That is to say, if the quantities x_μ are given the meaning of the Cartesian coordinates, the concepts "more" and "less" should be defined, without which it is impossible to introduce the concept of a distance of a point on the axis of the coordinates from the origin of the coordinates. The sign of an inequality must be transitive, i.e., from $a > b$, $b > c$, it should follow that $a > c$. The transitivity of inequalities is a consequence of the fact that inequalities can be added, while the concept of ineqaulity involves the existence of positive and negative numbers. We state that $a > b$ if $a-b > 0$. Adding the inequalities $a-b > 0$ and $b-c > 0$ we obtain, as a consequence, $a-c > 0$, i.e., by definition, $a > c$. Hence it is clear that $GF(p)$ cannot be ordered since it is impossible to establish the transitive concept of inequalities in $GF(p)$: from $a > 0$, $b > 0$ it does not follow that $a+b > 0$ since according to the above, a sum of positive definite quantities is not positive definite ††. As was made clear in ref. [4]) $GF(p)$ allows, however, partial ordering if p has the form

$$p = 8lq_1 \ldots q_k-1,$$

where l is an odd number and $q_1, \ldots q_k$ are the first k prime numbers. Then we find that all consecutive residues up to a certain maximal one (containing

† In the polynomial $(a+ib)^p$ the coefficients of the nomials $a^{p-r}(ib)^r$ at $r \not\equiv 0 \pmod p$ are equal to $0 \pmod p$ since they are divisible by p.

†† It will be noted that the impossibility of ordering $GF(p)$ is a corollary of the general theorem that the only ordered simple field is a field of rational numbers (or the fields isomorphous to it, for which see ref. [2])).

q_{k+1} as a multiple) are also squares. Thus, the first N residues are positive and all sums which do not exceed N are likewise positive. This ordered region can be called geometric, since metrics can formally be introduced into it. It should be borne in mind, however, that the geometric region is not an algebraic field and is not closed with respect to algebraic operations. Therefore, it is not invariant under linear transformations and particularly rotations. It can be shown † that a point $\mathbf{x}$ lying in a geometric region ($|\mathbf{x}_j| < \sqrt{\frac{1}{3}N}, j = 1, 2, 3$) is transferred by rotation into a non-geometric region since in $GF(p)$ from the inequality $\mathbf{x}'^2 < N$ it does not follow that $|x'_j| < N$ ($\mathbf{x}'$ are the coordinates of the point after rotation). Thus, in a geometric region there is actually no group of movements. This suggests that the use of a geometric region for obtaining the correspondence principle and investigating the problem of the transition from a new theory to the old one is scarcely possible. On this issue the viewpoint developed in the present paper essentially differs from the propositions contained in refs. [1,5]) in which the geometric region is identified with the conventional space of classical physics. In the following we shall proceed from the impossibility of introducing metric relations into $GF(p)$ to any satisfactory degree, and therefore, the "smallest" and the "greatest" distances do not figure anywhere in the concept evolved below, since no distances at all exist in $GF(p)$. Consequently, the estimates of the number p by the relation of the dimensions of the universe to "nuclear length" [5]) seem likewise unwarranted. We believe that the concept under consideration cannot have a direct bearing on the problems of gravitation and cosmology. It cannot be taken for granted that the suggestion to use a space-time manifold devoid of metrical properties is wrong, for in the microcosmos the classical space-time concepts lose their direct physical content [6]) and exist, inasmuch as there exists a theory inherently consistent and in agreement with experiment.

3. Finite Lorentz Group

It is clear from the above that no matter how much we increase the number p as long as we leave it finite, we shall not approach the properties of usual metrical space. It is sensible, therefore, to search for the correspondence principle by establishing the general features of the old and the new theories which are not connected directly with the metrical properties of the space-time manifold. Bearing this in mind, it will be noted that in finite space there are groups of linear transformations since owing to the solubility of any linear equation in $GF(p)$, there are non-singular matrices. At the same time one of the basic postulates of the old theory is the requirement of invariance of the equations with respect to the Lorentz group ††. It is natural to require the invariance of the

† For the elucidation of this problem the author is indebted to V. S. Popov and E. I. Dolinsky.

†† By the Lorentz group we mean a group consisting of the proper Lorentz group and space and time reflections. The proper Lorentz group contains rotations and the transition into the moving coordinate system.

new theory with respect to the finite analogue of the Lorentz group. It is this postulate, used in the following as a corollary of the correspondence principle, which will have to be formulated qualitatively.

The following method will be used to find the finite analogue of the Lorentz group. Let us find sufficient conditions singling out the Lorentz group along with the requirement of continuity out of all groups of linear transformations. This done, we shall relax the requirement of continuity, and if the remaining conditions determine a certain group of transformations in finite space, we shall demand co-variance of all quantities of the new theory with respect to this finite group.

It is common knowledge that the Lorentz group is determined by the following requirements: a) invariance of the light cone $x'^2 = x_0'^2 - \mathbf{x}'^2 = 0$ if $x^2 = 0$ ($x' = Lx$, L is a transformation of the Lorentz group), b) the requirement that all transformations should form a group, c) isotropy of space leading to the equality

$$\det L = \pm 1 \tag{12}$$

and d) requirement of continuity. Apart from that, it is assumed that the matrices L are real. From a), b) and c) it then follows that for all L

$$x^2 = \Lambda x'^2, \tag{13}$$

$$\Lambda^2 = (\det L)^2 = 1, \quad \Lambda = \pm 1. \tag{14}$$

The requirement of continuity singles out the value $\Lambda = +1$ (since for $L = 1$, $\Lambda = 1$). Sometimes the requirement of continuity is not put forth explicitly, but it manifests itself in the properties of the field of real numbers: in the field of ordinary members there are no real matrices L which satisfy (14) and for which $\Lambda = -1$. In finite space, there are no a priori grounds, in virtue of the absence of continuity, to exclude the values $\Lambda = -1$, matrices being found in $GF(p)$ which satisfy the conditions a), b) and c) in the form (12) and for which $\Lambda = -1$. The finite analogue of the Lorentz group consequently consists of linear transformations which have a determinant equal to ± 1 and which reverse or do not reverse the sign of $x^2 (x^2 \to \pm x^2)$. This group will be referred to as the finite Lorentz group.

Thus, "space-like" and "time-like" intervals in finite space actually do not differ from each other, since these concepts are not invariant with respect to the group of transformations on the basis of which the entire theory is constructed. This by no means implies that superlight signals and violation of causality are admitted in the latter. The quadratic form x^2 has no metric meaning in finite space, nor have the variables x_μ. Therefore, there are no concepts such as the velocity of distribution of a signal: it is impossible to introduce them, the manifold of $GF(p)$ being immetricisable.

The matrix L_- of any transformation $x^2 \to -x^2$ has the form

$$L_- = gL_+ = L'_+ g, \tag{15}$$

where L_+, L'_+ are the matrices leaving x^2 invariant, and g is the matrix reversing the sign of x^2 given in ref. [1]).

$$g = \begin{pmatrix} -\alpha & \beta & 0 & 0 \\ \beta & \alpha & 0 & 0 \\ 0 & 0 & 0 & -1 \\ 0 & 0 & 1 & 0 \end{pmatrix}, \quad \alpha^2+\beta^2 = -1, \quad \det g = +1 \tag{16}$$

An even number of g-transformations does not change x^2 and yet is not, generally, a proper Lorentz transformation ($x'_0/|x'_0| = x_0/|x_0|$, $\det L = +1$) in the accepted sense of this term.

It can easily be seen that

$$g^2 = T \cdot R = -1, \tag{17}$$

where T and R are the matrices of time and space reflections. The product

$$\prod_{i=1}^{i=m} g_i \tag{18}$$

is a proper Lorentz transformation only when

$$m = 4k \quad (k = 0, 1, 2 \ldots). \tag{19}$$

Eq. (17) determines a connection between time and space reflections absent in the conventional Lorentz group. This fact is very important for the theory of representations of the finite Lorentz group. It is precisely from eq. (17) that it follows that combined inversion is the only possible law of transformation of covariant quantities in the case of space reflections, provided Wigner's rule is accepted for time reflections.

4. Spinor Representations of the Finite Lorentz Group

4.1. GENERALISED PROPER FINITE LORENTZ GROUP (det $L_+ = +1$)

As is shown in ref. [1]), two dimensional representations of the generalised proper finite Lorentz group are $p+1$ valued (i.e., the homomorphism is $p+1$ to one). The matrices of a representation a made up of "complex numbers", i.e., the elements of the field $GF(p^2)$, satisfy the requirement

$$\overline{\det a} \cdot \det a = (\det a)^{p+1} = \pm 1. \tag{20}$$

The value $+1$ is found for the matrices $a(L_+)$ corresponding to the "normal" transformations $x^2 \to x^2$, and the value -1 for the matrices $a(L_-)$ corresponding to the transformations reversing the sign of x^2. In particular, the matrix $a(g)$

has the form

$$a(g) = \begin{pmatrix} 0 & \zeta \\ -1 & 0 \end{pmatrix}, \quad \bar{\zeta}\zeta = \zeta^{p+1} = -1, \quad \zeta = \alpha + i\beta. \tag{21}$$

It proves impossible, because of the matrices (21), to impose the requirement $\det a = +1$ on the matrices a, as is the case in the conventional theory, and thus obtain a two-valued spinor representation. Eq. (20) shows that any matrix can be written with an uncertainty in the phase factor ω

$$\bar{\omega}\omega = \omega^{p+1} = 1. \tag{22}$$

Eq. (22) determines the $p+1-$ valuedness of the representation. Indeed, to $L = 1$ correspond $p+1$ matrices $\omega_0, \omega_0^2 \ldots \omega_0^{p+1}$ where ω_0 is the primitive root of eq. (22) †. Since for every transformation $L \equiv L \cdot 1$. the number of matrices $a(L)$ also amounts to $p+1$ and they all differ by factors $\omega_0^r (1 \leqq r \leqq \leqq p+1)$. The matrices $a(L)$ are found from the relation

$$X' = a^+ X a, \tag{23}$$

where

$$X = \sigma_\mu x_\mu = x_0 \cdot 1 - \mathbf{x} \cdot \boldsymbol{\sigma} \tag{24}$$

($\boldsymbol{\sigma}$ are the Pauli matrices), and X' is the matrix (24) for $x' = Lx$. Instead of (24) use could also be made of the equation

$$Y' = b^+ Y b, \tag{25}$$

where

$$Y = \varepsilon \bar{X} \varepsilon^{-1}, \quad \varepsilon = -i\sigma_2, \tag{26}$$

$$b = \varepsilon \tilde{a} \varepsilon^{-1} \equiv (\det \tilde{a})(a^+)^{-1}. \tag{27}$$

Matrices b determine a representation contragradient to a (in conventional spinor formalism a transforms non-dotted indices, while b dotted indices). Designating the spinors transformed by the representations (23) and (25) through φ and χ, it is possible to form a four-component spinor

$$\psi = \begin{pmatrix} \varphi \\ \chi \end{pmatrix},$$

an analogue of the Dirac bispinor. The difference, however, consists in that the matrix of transformation

$$A(L) = \begin{pmatrix} a(L) & 0 \\ 0 & b(L) \end{pmatrix} \tag{28}$$

is determined not uniquely, but with an uncertainty of the diagonal matrix

$$\Omega = \begin{pmatrix} \omega & 0 \\ 0 & \bar{\omega} \end{pmatrix}. \tag{29}$$

† Since $p+1$ is a diviser of p^2-1, the primitive root exists according to 3 of sect. 2.

In the conventional theory this corresponds to the assignment of $A(L)$ with uncertainty of the matrices $e^{i\alpha\gamma_5}$ (the matrix γ_5 being supposed diagonal).

Though there is no way of eliminating multivaluedness of $a(L)$, it is possible to discriminate, when the wave functions of two particles are considered simultaneously, the matrices $a(L)$ and $a_Q(L)$, where

$$a_Q(L) = (\det a)^Q a(L). \tag{30}$$

Here Q is an integer which cannot be interpreted otherwise than a difference of the electric charges of particles with wave functions φ and φ_Q transformed by the matrices $a(L)$ and $a_Q(L)$ respectively. Indeed, assigning $a(1)$ with uncertainty $\omega_0{}^r$ shows that the spinor φ is also assigned to $\omega_0{}^r$ while φ_Q is assigned to $\omega_0{}^{(2Q+1)r}$. Consequently, the assignments of φ and φ_Q differ by a factor $\omega_0{}^{Q\alpha}$ where $\alpha = 2r$. This exactly corresponds to a situation in the gauge transformation of the conventional theory when phase multipliers acquired by the wave functions of particles with a difference of charges Q differ by a factor $\exp(iQ\alpha)$ †. It is important to emphasise that the coincidence with the gauge transformation holds for two-component spinors φ or χ. A different situation arises in the case of a bispinor assigned with uncertainty to Ω. In the conventional theory such multivaluedness corresponds to the Pauli-Gursey transformation, with respect to which the Dirac spinor field Lagrangian with a non-zero mass is not invariant. Thus, it becomes possible to impart a physical meaning of the multivaluedness of the spinor representation of the generalised proper finite Lorentz group only if the spinor field theory can be formulated in two-component form. A prerequisite of this is the possibility of determining the transformation of spinors under reflection without resorting to doubling the number of components. In b) of this section it is shown that the antilinear transformation of wave functions coinciding with combined inversion corresponds to the transformation of the reflection R of space coordinates. With this transformation of wave functions (the only possible one in the present theory ††) there is no need to introduce bispinors. In other words, the spinor field in finite space proves two-component. From the viewpoint of the dynamic principles, the two-component spinor field is sufficient for describing four-fermion vector interactions and spinor electrodynamics (see sect. 6).

The above-listed spinor representations of the generalised proper Lorentz group are incomplete since the following circumstance was left unused: with the same matrices $a_Q(L_+)$ corresponding to the proper finite Lorentz group †††.

† There is a difference in determining the quantum number of an electric charge in the present paper and in ref. [1]). The quantum number Q' introduced in ref. [1]) is equal to $2Q+1$, assuming not only integral but also semi-integral values. The latter requires an expansion of $GF(p^2)$ at least up to $GF(p^4)$, since $\zeta^{\frac{1}{2}(2m+1)}$, where m is an integer and ζ satisfies (21), does not exist in $GF(p^2)$. This difference, however, is not essential for the following.

†† If Wigner's rule of transformation of wave functions with space reflections T is accepted.

††† The proper finite Lorentz group, unlike the generalised one, does not contain g-transformations and TR transformations.

there is certain freedom in assigning the matrices $a_Q(g)$. This freedom is limited by the requirement that the matrices $a_Q(g_1 \ldots g_m)$ with m satisfying (19) coincide with the matrices corresponding to the transformation of the proper finite Lorentz group. This means that the matrices $a_Q(g)$ for two different particles with the same Q can differ also by the factor

$$i^\eta. \quad (1 \leqq \eta \leqq 4). \tag{31}$$

Thus a complete set of quantum numbers determining the spinor representation of the generalised finite Lorentz group has the following form

$$(j_1, j_2), \quad Q, \quad \eta, \tag{32}$$

where (j_1, j_2) are the usual characteristics of the representations of the Lorentz group: $j_1 = \frac{1}{2}$, $j_2 = 0$ correspond to the nor-dotted spinors (matrices a) and $j_1 = 0$, $j_2 = \frac{1}{2}$ to the dotted spinors (matrices b). The same quantum numbers determine the representations in the case of higher spins. A pair of numbers (j_1, j_2) determines the spin and order of a representation (as well as the division into "particles" and "anti-particles" in the case of two-component spinor theory), Q is the electric charge and η is a new quantum number whose role will be made clearer in sect. 5.

4.2. SPACE AND TIME REFECTIONS

In constructing representations of the finite Lorentz group the relation (7) is something new as compared with the conventional theory. Let us designate the representation operators corresponding to the reflections T and R through $\hat{a}(T)$ and $\hat{a}(R)$ respectively. Obviously, the following relation holds:

$$a(g^2) = \hat{a}(T)\hat{a}(R). \tag{33}$$

If Wigner's rule under which the field operators pass into Hermitian conjugates, is accepted for time reflections, then

$$\hat{a}(T) = \tau K, \tag{34}$$

where τ is a certain matrix and K is the Hermitian conjugation operator †

$$K\psi_\lambda = \psi_\lambda^*. \tag{35}$$

From (33) it then follows that the operator $\hat{a}(R)$ must also have the form

$$\hat{a}(R) = \rho K, \tag{36}$$

where ρ is a matrix. This means that the transformation of wave functions under reflections inevitably involves the operation of Hermitian conjugation. The

† Here and in the following * denotes the Hermitian conjugation of q-numbers, and the complex conjugation of c-numbers. The sign + denotes additionally transposition by spinor indices so that $\psi^+ = \psi^{*T}$.

matrix ρ can be found as in the conventional theory from the following commutation relations:

$$a(U)(\hat{a}(R)\psi) = \hat{a}(R)(a(U)\psi), \tag{37}$$

$$a(\mathscr{L})(\hat{a}(R)\psi) = \hat{a}(R)(a(\mathscr{L}^{-1})\psi), \tag{38}$$

corresponding to the relations to be found in the group itself

$$UR = RU, \tag{39}$$

$$\mathscr{L}R = R\mathscr{L}^{-1}, \tag{40}$$

where U are the space rotations (unitary subgroup of L) and $\mathscr{L}$ is a monoparametric Lorentz transformation †. It can be easily seen that (37) and (38) are fulfilled for two-by-two matrices a, ρ if ††

$$\rho = \theta\varepsilon. \tag{41}$$

The scalar factor θ is found from the condition

$$(\hat{a}(R))^2 = \bar{\rho}\rho = \omega_0^{\tau}, \tag{42}$$

or using (41) we obtain

$$\bar{\theta}\theta = \pm 1. \tag{43}$$

Hence it follows that

$$\theta = \zeta_0^{\lambda}, \quad \bar{\zeta}_0\zeta_0 = -1 \quad (1 \leqq \lambda \leqq 2p+2), \tag{44}$$

where ζ_0 is the primitive root ††† of a unity of the degree $2p+2$. The matrix τ can now be determined from (33)

$$\tau = \zeta_0^{1-\lambda}\omega_0^{\tau}\varepsilon, \tag{45}$$

since, according to (21),

$$a(g^2) = -\zeta \equiv \zeta_0\omega_0^{\tau}. \tag{46}$$

† In the final Lorentz group the matrix $\mathscr{L}$ is written

$$\mathscr{L} = \begin{pmatrix} 1 & 0 & 0 & 0 \\ 0 & 1 & 0 & 0 \\ 0 & 0 & a & b \\ 0 & 0 & b & a \end{pmatrix}, \quad a = \tfrac{1}{2}(\varepsilon^2+\varepsilon^{-2}), \quad b = \tfrac{1}{2}(\varepsilon^2-\varepsilon^{-2}), \quad \varepsilon\varepsilon GF(p),$$

$$a(\mathscr{L}) = \omega_0^{\tau}\begin{pmatrix} \varepsilon & 0 \\ 0 & \varepsilon^{-1} \end{pmatrix}, \quad 1 \leqq \tau \leqq p+1.$$

†† In obtaining (41) from (37) and (38) it will be remembered that the matrices $a(U)$ are unitary and have the form

$$a(U) = \begin{pmatrix} \alpha & \beta \\ -\bar{\beta} & \bar{\alpha} \end{pmatrix} = \tfrac{1}{2}(\alpha+\bar{\alpha})1 + \tfrac{1}{2}(\beta-\bar{\beta})\sigma_1 - \tfrac{1}{2}i(\beta+\bar{\beta})\sigma_2 + \tfrac{1}{2}(\alpha-\bar{\alpha})\sigma_3 \bar{\alpha}\alpha + \bar{\beta}\beta = \omega_0^{\tau}.$$

††† A primitive root like this exists in $GF(p^2)$ since $2p+2$ is a divisor of p^2-1.

The number λ evidently does not depend on Q and η since the operator $\hat{a}(R)$ cannot be represented as a product of the matrices $a(L)$. Thus, λ is an additional characteristic of the spinor representation of the finite Lorentz group. The presence of the quantum numbers η and λ makes it possible, as is shown in sect. 5, to forbid the conversion of barions into leptons and the neutrinoless decay of muons into electrons. It should be emphasised that the enumeration

$$(j_1, j_2), Q, \eta, \lambda \tag{47}$$

exhausts all independent quantum numbers which can be obtained from the theory of representations of the finite Lorentz group.

It can easily be seen that the above law of transformation of spinor wave functions in the case of reflection of space coordinates corresponds to combined inversion in the conventional theory. Indeed, under combined inversion

$$\psi \to \theta' C\gamma_0 \psi^*, \quad \theta'^2 = \pm 1, \tag{48}$$

where C is the matrix of charge conjugation. In a representation in which γ_2 is real and $\gamma_0 = \left(\begin{smallmatrix} 0 & 1 \\ 1 & 0 \end{smallmatrix}\right)$, $C = \gamma_2$. From (48) it then follows

$$\varphi \to \theta' \epsilon \varphi^*, \quad x \to -\theta' \epsilon \chi^*, \tag{49}$$

which coincides with what has been obtained above, the only difference being that relation (49) is valid for θ' and not (48) as for θ. In ref. [1]) the transformation of wave functions with reflection was postulated in the conventional four-component form

$$\psi \to \gamma_0 \psi$$

or

$$\varphi \to \chi, \quad \chi \to \varphi.$$

This transformation was interpreted in ref. [1]) as combined inversion on the strength of the fact that φ and χ are transformed by the representations whose matrices are complex conjugated and therefore the signs of the quantum numbers Q are different. This interpretation is hardly correct since, first, in the four-component theory the number Q cannot be interpreted as a charge (see subsect. 4.1a) and, second, combined inversion presupposes the transition from the operators ψ to the operators ψ^*. From the above it must be clear that combined inversion appears in the present theory as a consequence of (17) and Wigner's rule of transformation of wave functions in the case of the time reflections.

5. Four-Fermion Processes

We shall assume that the possibility of a four-fermion process is determined, as in the conventional theory, above all by the possibility of constructing, from the four spinor wave functions of particles involved in the process, an invariant

under the transformations L_+ of the finite Lorentz group (and reversing the sign at g-transformations, i.e., behaving just as the scalar x^2). As a result of the multi-valuedness of the spinor representation of the finite Lorentz group the following quantities of the required type can only be formed (if both dotted and non-dotted spinors are considered):

$$H_\varphi = \varphi_1^+\sigma_\mu\varphi_2\varphi_3^+\sigma_\mu\varphi_4+\text{h.c.}, \tag{50}$$

$$H_\chi = \chi_1^+\sigma_\mu\chi_2\chi_3^+\sigma_\mu\chi_4+\text{h.c.}, \tag{51}$$

$$H_{\chi\varphi} = g^{\mu\nu}\chi_1^+\sigma_\gamma\chi_2\varphi_3^+\sigma_\mu\varphi_4+\text{h.c.}, \tag{52}$$

$$H_{\varphi\chi} = g^{\mu\nu}\varphi_1^+\sigma_\mu\varphi_2\chi_3^+\sigma_\nu\chi_4+\text{h.c.}, \tag{53}$$

where

$$g^{\mu\nu} = 0 \quad (\mu \neq \nu), \quad g^{00} = -g^{11} = -g^{22} = -g^{33} = 1,$$

or their linear combination (with real coefficients)

$$H = aH_\varphi+bH_\chi+cH_{\chi\varphi}+dH_{\varphi\chi}. \tag{54}$$

Thus the general four-fermion Lagrangian of interaction depends only on four constants. In the conventional four-component notation this corresponds to the Lagrangian of the type $(C_V V+C_A A)(C_{V'}V'+C_{A'}A')$, the relation between the constants a, b, c, d and $C_\alpha C_\beta \equiv C_{\alpha\beta}$ being as follows

$$\begin{aligned} a &= C_{VV'}+C_{VA'}+C_{AV'}+C_{AA'}, \quad c = C_{VV'}+C_{VA'}-C_{AV'}-C_{AA'}, \\ b &= C_{VV'}-C_{VA'}+C_{AV'}+C_{AA'}, \quad d = C_{VV'}-C_{VA'}-C_{AV'}-C_{AA'}. \end{aligned} \tag{55}$$

Only such Lagrangians, containing the quantities of the type $\varphi^+\chi$ or $\chi^+\varphi$, are possible as are obained from the two last terms of (54) by the permutation of the spinos φ and χ with the indices of the same parity

$$cH_{\chi\varphi}+dH_{\varphi\chi} = \tfrac{1}{2}[(c+d)(SS'-PP')+(c-d)(SP'-PS')], \tag{56}$$

$$S = \bar\psi_1\psi_4, \quad S' = \bar\psi_3\psi_2, \quad P = \bar\psi_1\gamma_5\psi_4, \quad P' = \bar\psi_3\gamma_5\psi_2, \tag{57}$$

where $\bar\psi = \psi^+\gamma_0$.

It should be borne in mind, however, that the quantities (57) do not exist in the theory independently as covariant quantities: among the spin-tensors of the finite Lorentz group there are no scalars, pseudo-scalars and antisymmetric tensors [1]). Only linear combinations (56) of quantities (57) with two independent coefficients have a certain meaning.

For the invariance of (54) with regard to the proper finite Lorentz group the following condition should be satisfied

$$Q_1+Q_3 = Q_2+Q_4, \tag{58}$$

expressing the conservation of electric charge in four-fermion processes. From

the requirement of the invariance (54) with respect to space reflections the equation,

$$\lambda_1+\lambda_3=\lambda_2+\lambda_4 \tag{59}$$

follows, which also indicates charge conservation.

Finally, the requirement that (54) reverse the sign in g-transformations and consequently remain invariant under $g^2=TR$ transformations leads to the condition

$$\eta_1+\eta_3=\eta_2+\eta_4 \pmod 4. \tag{60}$$

The selection rules (59) and (60) make it possible to forbid the four-fermion processes of the conversion of nucleons (and in general, barions) into leptons and, the neutrinoless μ-meson decay if for example, we put

$$\lambda_p=\lambda_n=\lambda_{e^-}=\lambda_{\nu_1},\quad \lambda_{\mu^-}=\lambda_{\nu_2}\neq\lambda_{e^-}, \tag{61}$$

$$\eta_p=\eta_n=1 \pmod 4,\quad \eta_e=\eta_\mu=\eta_{\nu_1}=\eta_{\nu_2}=0 \pmod 4. \tag{62}$$

It stands to reason that prior to the construction of a consistent dynamic scheme, a concrete assignment of quantum numbers contains a certain element of arbitrariness. What is not arbitrary, however, is the fact that apart from charge and spin, two new quantum numbers inevitably arise in the theory, and the selection rules for these numbers make it possible to forbid the non-observable processes in principle.

6. Concluding Remarks

As was pointed out above, the spinor field in the variant of the theory under consideration is actually two-component, which stems from three causes:

a) Combined inversion proves to be a consequence of Wigner's rule of transforming wave functions with time reflections which obviates the need for doubling the number of spinor components in considering spinor reflections.

b) All new quantum numbers Q, η, λ, which appear in the theory of representations of the finite Lorentz group belong to two-component spinors. It will be emphasised that the number Q can be interpreted as an electric charge only if the spinor field is two-component.

c) There are only such spin tensors which can be constructed from two-component spinors $(V+A+C(V-A))$.

In connection with the above, there arises a problem of to what extent the modern field theory demands the use of four-component spinors if we exclude the requirement of linear transformations of spinors with space reflection. The requirement is not obligatory due to the existence of combined inversion. Weak four-fermion interactions do not, by virtue, of their character, require the use of four-component spinors. The same and for the same reason, applies, as was noted by Gell-Mann and Feynman [7]), to spinor electrodynamics. In the latter case the problem actually reduces itself to the fact that there is a *unique*

local connection between the spinors $\varphi(x)$ and $\chi(x)$,

$$\chi(x) = \frac{1}{m}\sigma_\mu(p_\mu - A_\mu)\varphi.$$

The components χ in this sense differ little from, say, the additional components

$$U_\mu = \frac{\partial\phi}{\partial x_\mu}$$

of the wave function of a particle with zero-spin, introduced for writing first-order equations. Therefore, a closed differential equation of the second order, totally equivalent in its consequences to Dirac's equation for two-component spinors can be written quite similarly to the case of scalar fields. The situation is different for the intercation between a spinor field and a pseudo-scalar boson field. In this case, there is no local connection between φ and χ (if φ is assigned, χ is determined accurately to within an arbitrary solution of homogeneous differential equation) and therefore it is impossible to write a closed local equation (i.e., a differential equation of the finite order) for the two-component spinor φ (or χ). In this sense the theory of strong interactions represents a totally different class of phenomena in which the spinor field is essentially four-component. It is scarcely possible, therefore, to count on finding an adequate mathematical apparatus for the theory of such interactions within the scheme of finite space. True, there exists a possibility of using a pseudo-vector coupling (non-renormalisability in the theory with finite space is of no account). But then the attempts to construct boson fields from fermions have to be given up.

The above-listed difficulties in the theory of strong interactions probaly testify to the fact that if the scheme under considerations has any bearing on reality at all, the model of finite space reflects only a part of the properties of the space-time manifold of the authentic theory. Yet a striking feature of the scheme under consideration is the automatic appearance of symmetry properties known from experiment, these properties arising from one cause: finiteness of the space-time manifold, ruling out divergences. It stands to reason that the destiny of this scheme will be decided, above all, by the possibility of introducing sufficiently simple dynamic principles determining the algorithm of computation of the amplitudes of the real processes.

References

1) H. R. Coish, Phys. Rev. **114** (1959) 383
2) B. L. van der Waarden, Sovremennaya Algebra (GTTI, 1934)
3) B. Riemann, On Hypotheses Underlying Geometry (GITTL, 1956) .
4) P. Kustaanheimo, Soc. Sci. Fennica, Commentations Phys. Math. **15** (1950) 9
5) G. Jarnefelt, Ann. Acad. Sci. Fennicae, Ser. A, **1**, no. 96 (1951);
P. Kustaanheimo, Ann. Acad. Sci. Fennicae, Ser. A, **1** no. **129** (1952)
6) L. Landau and R. Peierls, Zs. f. Phys. **69** (1931) 56
7) R. P. Feynman and M. Gell-Mann, Phys. Rev. **109** (1957) 193

7.B

Nuclear Physics **21** (1960) 492—507; © *North-Holland Publishing Co., Amsterdam*

Not to be reproduced by photoprint or microfilm without written permission from the publisher

ASYMPTOTIC CONDITIONS IN QUANTUM ELECTRODYNAMICS

L. E. EVANS and T. FULTON

The Johns Hopkins University, Baltimore, Maryland †

Received 1 August 1960

Abstract: The applicability to quantum electrodynamics of the asymptotic condition of Lehmann, Symanzik, and Zimmerman (LSZ) is considered. The Coulomb gauge formulation of the theory is examined and it is shown that the LSZ formalism can be used with this form, but not with the Lorentz gauge form. Formal aspects of the renormalization program in the Coulomb gauge are discussed. It is found that the renormalization of the electron requires momentum-dependent factors, and hence that the renormalized electron field violates local commutativity. The *S*-matrix is briefly discussed. To illustrate charge renormalization, a calculation of the charge of the state of a single electron is given.

1. Introduction

Since the first paper of Lehmann, Symanzik, and Zimmermann [1]) in 1955, much use has been made of reduction formulas derived from the so-called "asymptotic condition." These reduction formulas have provided a basis for analyses of the analytic properties of *S*-matrix elements leading to dispersion relations. Most of the problems attacked in this way have involved the strong interactions; little use has been made of these methods in the treatment of radiation problems, largely because of the success of perturbation theory in that area. Little attention has therefore been paid to the difficulties encountered in applying the LSZ methods to the usual formulation of quantum electrodynamics.

The source of the difficulties is the Coulomb interaction, which is conventionally described by means of fictitious quanta of the electromagnetic field [2]). One finds (as will be shown below) that the states of these quanta do not fit into the LSZ scheme. It is therefore natural to look for a form of quantum electrodynamics which avoids the use of fictitious states in the description of the Coulomb interaction. Such a form has been examined by several authors [3,4,5]); it corresponds in the classical limit to the use of the so-called Coulomb or radiation gauge for the potentials. We shall exhibit the use of the LSZ formalism in this theory, and we shall discuss the *S*-matrix briefly.

The remainder of this paper is devoted to an analysis of the renormalization program for this theory, following the methods employed by Källén [2]) in his analysis of the conventional ("Lorentz" gauge) formulation. Because we

† Work supported in part by the National Science Foundation.

incorporate the Coulomb interaction into the electron field, we shall find renormalization factors which are not constants, and the renormalized electron operator will turn out to violate the widely assumed postulate of local commutativity or "causality." We shall nevertheless see that no violation of the postulates of special relativity is implied.

Some of the features of the Coulomb gauge formulation described here have been used by Johnson [6,7] in recent papers concerning the consistency of quantum electrodynamics. We shall not concern ourselves with that question, although we shall confirm and amplify some of Johnson's statements.

2. The Lorentz Gauge and the Asymptotic Condition

In the most common form of quantum electrodynamics, the components of the vector potential are treated symmetrically, resulting in four types of quanta: there are two photons with transverse polarization and two fictitious photons with "longitudinal" and "scalar" polarization. A subset of "physical" states is selected from the set of states in the Hilbert space. It is defined by the requirement that the Lorentz condition

$$\langle \Phi | \partial_\mu A_\mu(x) | \Phi \rangle = 0 \tag{1}$$

hold for expectation values in these states. This set is obviously not complete: the addition of, say, one "scalar" photon to a state in the set yields a state not in the set. Thus, while the fictitious photons are not involved in initial or final states of a scattering problem, they appear in any expansion over intermediate states.

We shall now see that the use of these unphysical states violates the asymptotic condition of LSZ. It is a consequence of that condition that for any kind of field $\varphi(x)$

$$\langle 0 | \varphi(x) | \alpha^{\text{in}} \rangle = \langle 0 | \varphi^{\text{in}}(x) | \alpha^{\text{in}} \rangle, \tag{2}$$

where $|\alpha^{\text{in}}\rangle$ is the state of a single particle of the type created by φ^{in}. (In renormalization theory, the statement of (2) is taken to define $\varphi(x)$ as the renormalized field operator). But in the Lorentz gauge theory of the photon field one can show [2]) that the relevant matrix element must be written

$$\langle 0 | A_\mu(x) | k^{\text{in}} \rangle = (\delta_{\mu\lambda} - k_\mu k_\lambda M) \langle 0 | A_\lambda{}^{\text{in}}(x) | k^{\text{in}} \rangle,$$

where M vanishes only in the trivial free-field case, and $|k^{\text{in}}\rangle$ is the state of a single photon. It is significant that if the polarization of the photon in (3) is transverse, we obtain agreement with (2) because for such states $k_\lambda \langle 0 | A_\lambda{}^{\text{in}} | k^{\text{in}} \rangle = 0$. We thus see that we can maintian consistency with the asymptotic condition of LSZ only if we confine ourselves to physical states; this we are unable to do in the Lorentz gauge theory because the set of such states is not complete.

It is therefore natural to seek a form of quantum electrodynamics where the set of physical states is complete. Such a form is given in the next section. The Coulomb interaction, no longer described by "photons," is treated as a property of the electron field. Because of this the description of the electron field is more complicated than usual, but the applicability of the LSZ methods to that field [8]) is maintained.

3. The Coulomb Gauge

We start with a brief exposition of the fundamentals of Coulomb gauge quantum electrodynamics.

The usual field equations are assumed for the renormalized fields:

$$(\hat{\partial}+m)\psi(x) = f(x), \quad (\hat{\partial} \equiv \gamma^\mu \partial_\mu), \tag{4}$$

$$(\delta_{\mu\lambda}\Box - \partial_\mu\partial_\lambda)A_\lambda(x) = -j_\mu(x), \tag{5}$$

where the exact form of $f(x)$ and $j_\mu(x)$ will be determined when renormalization is discussed. We write the vector potential operator as the sum of a transverse part $\mathscr{A}_\lambda$ representing photons and a longitudinal part $\mathfrak{A}_\lambda$ representing the Coulomb interaction. The condition of transversality is written

$$\partial_\mu \mathscr{A}_\mu(x) = n_\mu \mathscr{A}_\mu(x) = 0,$$

where n_μ is the normal to an arbitrary spacelike plane. In order to accomplish this breakup, we introduce the projection operator [5]) †

$$T_{\mu\lambda} = \delta_{\mu\lambda} + (n_\mu\Box - \partial_\mu\partial)\frac{n_\lambda}{\Box+\partial^2} - (n_\mu\partial+\partial_\mu)\frac{\partial_\lambda}{\Box+\partial^2}, \tag{7}$$

where $\partial \equiv n_\mu\partial_\mu$.

Then applying the operator $T_{\mu\lambda}$ to (5) we obtain

$$T_{\mu\lambda}A_\lambda(x) = \mathscr{A}_\mu(x), \quad T_{\mu\lambda}\mathscr{A}_\lambda(x) = \mathscr{A}_\mu(x), \tag{8}$$

$$\Box\mathscr{A}_\lambda(x) = -j_\lambda(x) - (n_\lambda\Box - \partial_\lambda\partial)\frac{n\cdot j(x)}{\Box+\partial^2}, \tag{9}$$

$$(\delta_{\mu\lambda}\Box - \partial_\mu\partial_\lambda)\mathfrak{A}_\lambda(x) = (n_\mu\Box - \partial_\mu\partial)\frac{n\cdot j(x)}{\Box+\partial^2}. \tag{10}$$

Associated with $\mathscr{A}_\lambda$ we introuce the "incoming" field $\mathscr{A}_\lambda^{\text{in}}$ which obeys the free-field equation and commutation relation

$$\Box\mathscr{A}_\lambda^{\text{in}}(x) = 0, \tag{11}$$

$$[\mathscr{A}_\mu^{\text{in}}(x), \mathscr{A}_\lambda^{\text{in}}(x')] = i\mathrm{d}_{\mu\lambda}D(x-x'), \tag{12}$$

$$\mathrm{d}_{\mu\lambda} \equiv \delta_{\mu\lambda} - \partial^{-2}\partial_\mu\partial_\lambda - n_\mu\partial^{-1}\partial_\lambda - n_\lambda\partial^{-1}\partial_\mu. \tag{13}$$

† In this and succeeding expressions, the inverse differentiation is defined by means of the corresponding Fourier transforms.

Defining the "transverse" current by the right side of (9),

$$j_\lambda{}^{\mathrm{T}}(x) = j_\lambda(x) + (n_\lambda \Box - \partial_\lambda \partial) \frac{n \cdot j(x)}{\Box + \partial^2}, \tag{14}$$

we can write a formal solution for $\mathscr{A}_\lambda$

$$\mathscr{A}_\lambda(x) = \mathscr{A}_\lambda{}^{\mathrm{in}}(x) + \int \mathrm{d}x'\, \mathrm{d}_{\lambda\nu} D^{\mathrm{R}}(x-x') j_\nu{}^{\mathrm{T}}(x'). \tag{15}$$

Using the fact that $j_\lambda{}^{\mathrm{T}}$ obeys the transversality conditions (6) one can put this into the more convenient form

$$\mathscr{A}_\lambda(x) = \mathscr{A}_\lambda{}^{\mathrm{in}}(x) + \int \mathrm{d}x'\, \mathscr{D}^{\mathrm{R}}_{\lambda\nu}(x-x')\, j_\nu{}^{\mathrm{T}}(x'), \tag{16}$$

where $\mathscr{D}^{\mathrm{R}}_{\lambda\nu}(x) = -\theta(x)\mathrm{d}_{\lambda\nu} D(x)$.

A solution for $\mathfrak{A}_\lambda$ is †

$$\mathfrak{A}_\lambda(x) = -n_\lambda \int \mathrm{d}x'\, \delta(\tau-\tau')\partial^{-1} D(x-x') n \cdot j(x'), \quad (\tau \equiv -n \cdot x). \tag{17}$$

We note from this that $\mathfrak{A}_\lambda$ is not an independent dynamical variable, since we are able to express it as a spatial integral of the charge density, which is given by the electron field. Thus the time-development of the longitudinal field is completely determined by the time development of the electron field ††. The only independent dynamical variables are therefore those of the electron and transverse photon fields. It is these, and only these, which we quantize.

Because only physical photon states occur now in the theory, it is a simple matter to apply the asymptotic condition of LSZ. We define †††

$$\tilde{\mathscr{A}}^{\mathrm{T}}(k, s) \equiv -\frac{i}{\sqrt{2\omega}} \int \mathrm{d}\sigma e^{ik\cdot x} \overleftrightarrow{\partial}\, \mathscr{A}_\lambda(x) \varepsilon_\lambda{}^{(s)}(k), \tag{18}$$

where

$$\omega \equiv -n \cdot k, \quad f(x) \overleftrightarrow{\partial}\, g(x) \equiv f(x)(\partial g(x)) - (\partial f(x))\, g(x),$$

and $\varepsilon_\lambda{}^{(s)}(k)$ is the polarization vector of the transverse photons, satisfying the conditions

$$k \cdot \varepsilon^{(s)}(k) = n \cdot \varepsilon^{(s)}(k) = 0, \quad \varepsilon^{(s)}(k) \cdot \varepsilon^{(s')}(k) = \delta_{ss'}, \tag{19}$$

$$\sum_{s=1}^{2} \varepsilon_\mu{}^{(s)}(k) \varepsilon_\lambda{}^{(s)}(k) = \delta_{\mu\lambda} + \frac{1}{\omega}\left[n_\mu k_\lambda + n_\lambda k_\mu - \frac{k_\mu k_\lambda}{\omega}\right]. \tag{20}$$

† To the expression (17) we can add any gauge function $\partial_\lambda \Lambda(x)$ as well as an expression of the form $n_\lambda \varphi(x)$ where $\varphi(x)$ satisfies Laplace's equation $(\Box + \partial^2)\varphi(x) = 0$. The latter we set to zero in order to obtain correct free-field results, and we neglect the gauge function, choosing to work in a particular gauge.

†† In this connection we point out that (10) is not an equation of motion for $\mathfrak{A}_\lambda$. In the frame where $n_\mu = (0, 0, 0, i)$, $\mathfrak{A}_\lambda$ has only a scalar component. If we use this frame in (10), it is easy to see that no *time* derivatives of $\mathfrak{A}_\lambda$ appear.

††† In writing (18) we have anticipated that we will use only eigenstates of energy-momentum. Clearly we can replace the plane wave by any solution of the homogeneous wave equation.

The asymptotic condition is written [1])

$$\lim_{\tau\to-\infty}\langle\Phi|\tilde{\mathscr{A}}^{\tau}(k,s)\Phi'\rangle=\langle\Phi|\tilde{\mathscr{A}}^{\mathrm{in}}(k,s)|\Phi'\rangle, \tag{21}$$

where $\tilde{\mathscr{A}}^{\mathrm{in}}$ is defined from (18) by replacing $\mathscr{A}_\lambda$ by $\mathscr{A}_\lambda{}^{\mathrm{in}}$. The operator $\tilde{\mathscr{A}}^{\mathrm{in}}(k,s)$ is simply the creation operator for an incoming photon with momentum k and polarization state s. Similar statements for $\tau\to+\infty$ define "outgoing" operators and states.

Using this asymptotic condition, it is easy to derive reduction formulas for photon states †. For example, if Q is any field operator, we have

$$\langle\Phi|Q(0)\tilde{\mathscr{A}}^{\mathrm{in}}(k,s)|\Phi'\rangle$$
$$=\langle\Phi|\tilde{\mathscr{A}}^{\mathrm{out}}(k,s)Q(0)|\Phi'\rangle-\frac{i}{\sqrt{2\omega}}\int\mathrm{d}x\mathrm{e}^{ik\cdot x}\Box\langle\Phi|T\mathscr{A}_\lambda(x)Q(0)|\Phi'\rangle\varepsilon_\lambda{}^{(s)}(k). \tag{22}$$

The role of the Coulomb field in this formulation can be explicitly shown by a perturbation-theoretic treatment of the S-matrix, which is given in Appendix 1.

4. Renormalization of the Electron Field

We shall now analyse the renormalization program and determine what form the source terms $f(x)$ and $j_\mu(x)$ in (4) and (5) must have in order to accomplish this program. The analysis will follow closely the work of Källén [2]).

We begin with the electron field. Following (2) we write for the definition of the renormalized field operator, $\psi(x)$,

$$\langle0|\psi(x)|q\rangle=\langle0|\psi^{\mathrm{in}}(x)|q\rangle, \tag{23}$$

where $|q\rangle$ is the state of a single electron with momentum q. The unrenormalized electron field $\psi'(x)$ is chosen to satisfy the equation of motion

$$(\hat{\partial}+m)\psi'(x)=\tfrac{1}{2}ie\{\hat{A}'(x),\psi'(x)\}, \tag{24}$$

and commutation relation

$$\delta(\tau-\tau')\{\psi'(x),\bar{\psi}'(x')\}=-i\hat{n}\delta^4(x-x'). \tag{25}$$

First we examine the commutation relations of the renormalized field. Introducing spectral functions in the usual way, and using charge-conjugation invariance, we find

$$\langle0|\{f(x),\bar{f}(x')\}|0\rangle=\frac{1}{(2\pi)^3}\int\mathrm{d}k\mathrm{e}^{ik\cdot(x-x')}\varepsilon(k)$$
$$\times[\Sigma_1(k,n)+(i\hat{k}+m)\Sigma_2(k,n)+i\hat{n}(n\cdot k)\Sigma_3(k,n)], \tag{26}$$

† We emphasize again that the use of the LSZ methods for the electron field is unchanged by our use of the Coulomb gauge.

where

$$\sum_{p_n=k} \langle 0|f|n\rangle\langle n|\bar{f}|0\rangle = \Sigma_1(k,n)+(i\hat{k}+m)\,\Sigma_2(k,n)+i\hat{n}(n\cdot k)\Sigma_3(k,n). \quad (27)$$

It follows from parity and time-reversal invariance that the Σ_i are functions of k^2 and $(n\cdot k)^2$ only. Then we use the timelike character of the momenta of the states to write

$$\Sigma_i(k^2,(n\cdot k)^2) = \int_0^\infty da\,\delta(a+k^2)\Sigma_i(-a,(n\cdot k)^2). \quad (28)$$

Finally, making use of the formal solution

$$\psi(x) = \psi^{\text{in}}(x) - \int dx'\,S^{\text{R}}(x-x')f(x'), \quad (29)$$

and (23) we obtain for the anticommutator of ψ and $\bar{\psi}$

$$\delta(\tau-\tau')\{\psi(x),\bar{\psi}(x')\} = -i\hat{n}\delta(\tau-\tau')\,\frac{1}{(2\pi)^3}\int d\sigma_\kappa e^{i\kappa\cdot(x-x')} \times\left[1+\int_0^\infty da\left[\frac{2m}{(a-m^2)^2}\Sigma_1(-a,a+\kappa^2)-\frac{\Sigma_2}{(a-m^2)}+\frac{a+m^2+2\kappa^2}{(a-m^2)^2}\Sigma_3\right]\right]. \quad (30)$$

In (30) the following notation has been introduced:

$$\chi_\mu \equiv x_\mu - n_\mu\tau \quad (\tau=-n\cdot x), \quad \kappa_\mu \equiv k_\mu - n_\mu\omega \quad \omega=-n\cdot k,$$
$$\int d\sigma_\kappa g(k) \equiv \int dk\,\delta(\omega)g(k). \quad (31)$$

Next we define

$$\frac{1}{N^2(\kappa^2)} \equiv 1+\int_0^\infty da\left[\frac{2m}{(a-m^2)^2}\Sigma_1(-a,a+\kappa^2)-\frac{\Sigma_2}{a-m^2}+\frac{a+m^2+2\kappa^2}{(a-m^2)^2}\Sigma_3\right], \quad (32)$$

and obtain

$$\delta(\tau-\tau')\{\psi(x),\bar{\psi}(x')\} = -i\hat{n}\delta(\tau-\tau')\,\frac{1}{(2\pi)^3}\int d\sigma_\kappa e^{i\kappa\cdot(x-x')}\,\frac{1}{N^2(\kappa^2)}. \quad (33)$$

We observe in connection with (33) that in this formulation it is impossible to maintain the assumption of local commutativity for the renormalized electron field, since the right side of (33) certainly does not vanish for arbitrary spacelike values of $x-x'$.

We shall now see that the factor N in (32) plays the role of the wave function renormalization "constant" in the Coulomb gauge theory. In order to do this, we express the relation between the renormalized and unrenormalized field in terms of their Fourier transforms

$$\psi'(k) = N(\kappa^2)\psi(k). \quad (34)$$

We can write this in position space as follows:

$$\psi'(x) = \int dx' N(x-x')\psi(x'), \tag{35}$$

where

$$N(x) = \frac{1}{(2\pi)^4}\int dk e^{ik\cdot x} N(\kappa^2). \tag{36}$$

One can show without difficulty that $N(\kappa^2)$ is real, and we see from (32) that it is independent of ω. Therefore we have the following properties:

$$N^*(x) = N(-x), \tag{37}$$

$$N(x) = \delta(\tau)\ \frac{1}{(2\pi)^3}\int d\sigma_\kappa e^{i\kappa\cdot x} N(\kappa^2); \tag{38}$$

also

$$\bar{\psi}'(x) = \int dx' N(x'-x)\bar{\psi}(x'). \tag{39}$$

The inverse relation to (35) we write

$$\psi(x) = \int dx' N^{-1}(x-x')\psi'(x'), \tag{40}$$

where

$$N^{-1}(x) = \delta(\tau)\,\frac{1}{(2\pi)^3}\int d\sigma_\kappa e^{i\kappa\cdot x}\,\frac{1}{N(\kappa^2)}. \tag{41}$$

It follows that

$$\int dx' N(x-x')N^{-1}(x'-x'') = \delta^4(x-x''). \tag{42}$$

Using these relations, we can derive (25) from (33) or vice versa. Finally, to demonstrate that $\psi(x)$ satisfies the defining relation (23), we can use the reduction formula to represent $\langle 0|\psi(x)|q\rangle$. Then direct application of (26), (29), (32) and (33) verifies (23).

Mass renormalization can be carried out in a similar fashion. Spectral representations for the required terms are obtained from the requirement that

$$(\hat{\partial}+m)\langle 0|\psi(x)|q\rangle = 0, \tag{43}$$

which is a direct consequence of (23). We shall not give the details here [9]).

5. Renormalization of the Photon Field

We now apply the procedure just used to the photon field. The definition of the renormalized photon field is

$$\langle 0|\mathscr{A}_\lambda(x)|k\rangle = \langle 0|\mathscr{A}_\lambda^{\text{in}}(x)|k\rangle,$$

where $|k\rangle$ is the state of a single photon of momentum k. The unrenormalized vector potential $A'_\lambda(\lambda)$ satisfies the field equation

$$(\delta_{\mu\lambda}\Box-\partial_\mu\partial_\lambda)A'_\lambda(x) = -\tfrac{1}{2}ie[\bar{\psi}'(x), \gamma^\mu\psi'(x)], \tag{45}$$

and the unrenormalized transverse photon field $\mathscr{A}'_\lambda(x)$ satisfies the same commutation relations as does $\mathscr{A}_\lambda^{\text{in}}(x)$, namely, (12).

To analyse the commutation relations of the renormalized field, we start by introducing spectral functions again. Making use of the properties of the transverse current,

$$\partial_\lambda j_\lambda^{\text{T}}(x) = n_\lambda j_\lambda^{\text{T}}(x) = 0, \tag{46}$$

one can obtain

$$\langle 0|[j_\mu^{\text{T}}(x), j_\lambda^{\text{T}}(x')]|0\rangle = \frac{1}{(2\pi)^3}\int \mathrm{d}k\mathrm{e}^{ik\cdot(x-x')}\varepsilon(\omega)\Pi(k, n)\left[\delta_{\mu\lambda}+n_\mu n_\lambda-\frac{\kappa_\mu\kappa_\lambda}{\kappa^2}\right], \tag{47}$$

where

$$\sum_{p_n=k}\langle 0|j_\mu^{\text{T}}|n\rangle\langle n|j_\lambda^{\text{T}}|0\rangle = \Pi(k, n)\left[\delta_{\mu\lambda}+n_\mu n_\lambda-\frac{\kappa_\mu\kappa_\lambda}{\kappa^2}\right], \tag{48}$$

$$\Pi(k, n) = \Pi(k^2, (n\cdot k)^2), \tag{49}$$

using the notation of (31). From (48) it follows that $\Pi(k, n) \geqq 0$. To see this, we merely set $\mu = \lambda = 1$ and obtain, in the frame where $n = (0, 0, 0, i)$,

$$\Pi(k, n)\left[1-\frac{k_1^2}{k^2}\right] = \sum_{p_n=k}|\langle 0|j_1^{\text{T}}|n\rangle|^2 \geqq 0. \tag{50}$$

Before proceeding further, we shall establish that our spectral function $\Pi(k, n)$ is independent of n and is in fact essentially the funcion introduced by Källén [2]). From (14) and the following property of $D(x)$:

$$\int \mathrm{d}x'\,\delta(\tau-\tau')\partial^{-1}D(x-x')\mathrm{e}^{ik\cdot x'} = \frac{\mathrm{e}^{ik\cdot x}}{\kappa^2}, \tag{51}$$

we can show directly that

$$\langle 0|j_\lambda^{\text{T}}(x)|n\rangle|_{p_n=k} = \langle 0|j_\nu(x)|n\rangle|_{p_n=k}\times\left[\delta_{\nu\lambda}+n_\nu n_\lambda+\frac{\omega}{\kappa^2}n_\nu\kappa_\lambda\right], \tag{52}$$

from which we have

$$\begin{aligned}\sum_{p_n=k}\langle 0|j_\lambda^{\text{T}}|n\rangle\langle n|j_\lambda^{\text{T}}|0\rangle &= 2\Pi(k, n)\\ &= \sum_{p_n=k}\langle 0|j_\mu|n\rangle\langle n|j_\nu|0\rangle\left[\delta_{\mu\nu}+n_\mu n_\nu\left(1+\frac{\omega^2}{\kappa^2}\right)+\frac{\omega}{\kappa^2}(n_\mu\kappa_\nu+n_\nu\kappa_\mu)\right].\end{aligned} \tag{53}$$

The renormalized current is an observable; therefore the expectation value

$$\langle 0|j_\mu(x)j_\nu(x')|0\rangle,$$

of which the sum on the right side of (53) is simply a Fourier component, must be independent of the particular formulation of quantum electrodynamics chosen. This means that we can write

$$\sum_{p_n=k} \langle 0|j_\mu|n\rangle\langle n|j_\nu|0\rangle = \Pi'(k^2)[k_\mu k_\nu - k^2\delta_{\mu\nu}], \tag{54}$$

because this sum must not depend on n_μ, a characteristic of the particular method of quantization we have used. The function Π' is Källén's spectral function [2]). Inserting (54) into (53) we find

$$\Pi(k, n) = -k^2\Pi'(k^2). \tag{55}$$

This establishes the connection of our spectral function with that of Källén [2]), and at the same time shows that Π is in fact independent of n_μ. The latter has a significance which we shall point out presently.

Now we are in a position to obtain the commutation relations of the field $\mathscr{A}_\lambda$. Starting from the formal solution (15), making use of (44) and (47) and writing

$$\Pi(k^2) = \int_0^\infty \mathrm{d}a\, \delta(a+k^2)\Pi(-a), \tag{56}$$

we obtain

$$\begin{aligned}\langle 0|[\mathscr{A}_\lambda(x), \mathscr{A}_\mu(x')]|0\rangle = \frac{1}{(2\pi)^3}\int \mathrm{d}k \mathrm{e}^{ik(x-x')}\varepsilon(\omega) \\ \times\left[\delta_{\mu\lambda}+n_\mu n_\lambda-\frac{\kappa_\mu\kappa_\lambda}{\kappa^2}\right]\int_0^\infty \mathrm{d}a\,\delta(a+k^2)\left[\delta(a)+\frac{\Pi(-a)}{a}\right].\end{aligned} \tag{57}$$

From this follow the equal-time commutation relations ($\dot{a} \equiv \partial a$):

$$[\mathscr{A}_\lambda(x), \mathscr{A}_\mu(x')]\delta(\tau-\tau') = 0, \tag{58}$$

$$[\dot{\mathscr{A}}_\lambda(x), \mathscr{A}_\mu(x')]\delta(\tau-\tau') = 0, \tag{59}$$

$$\begin{aligned}[\dot{\mathscr{A}}_\lambda(x), \mathscr{A}_\mu(x')]\delta(\tau-\tau') \\ = -\frac{i}{1-L}\frac{1}{(2\pi)^3}\int \mathrm{d}\sigma_\kappa \mathrm{e}^{i\kappa\cdot(x-x')}\left[\delta_{\mu\lambda}+n_\mu n_\lambda-\frac{\kappa_\mu\kappa_\lambda}{\kappa^2}\right]\delta(\tau-\tau'),\end{aligned} \tag{60}$$

where

$$\frac{1}{1-L} = 1+\int_0^\infty \mathrm{d}a\,\frac{\Pi(-a)}{a^2}. \tag{61}$$

It is clear that the fact that Π is independent of n_μ has the consequence that L is a constant and that (58), (59), and (60) all vanish when $x-x'$ is spacelike. Thus the photon field in the Coulomb gauge does not violate local commutativity. This is to be expected on physical grounds, in view of the analysis of Bohr and Rosenfeld on the measurability of the electromagnetic fields.

The commutation relations for the unrenormalized field $\mathscr{A}'_\lambda$, given by (12) differ from the above only by the factor $(1-L)$. It is thus clear that the relation between the renormalized and unrenormalized photon fields is

$$\mathscr{A}'_\lambda(x) = \sqrt{1-L}\,\mathscr{A}_\lambda(x). \tag{62}$$

In order to maintain (9) and (10) as the equations for the electromagnetic field, we must then renormalize only the transverse part of the current. This is accomplished by writing the renormalized current in the form

$$j_\lambda(x) = j'_\lambda(x) + L j_\lambda^{\mathrm{T}}(x), \tag{63}$$

where j'_λ is the current before renormalization:

$$j'_\lambda(x) = \tfrac{1}{2} ie[\bar{\psi}'(x), \gamma^\lambda \psi'(x)]. \tag{64}$$

Using the operator $T_{\mu\lambda}$ we can solve (64) for the transverse current in terms of j'_λ:

$$j_\lambda^{\mathrm{T}}(x) = \frac{1}{1-L}\, T_{\lambda\nu} j'_\nu(x). \tag{65}$$

Thus the renormalized current is completely determined from j'_λ, i.e., from the *unrenormalized* electron field ψ'. It then follows from the local commutativity of the ψ'-field that the commutator of two currents vanishes for spacelike separation. Since the current is observable, this commutator must vanish if no interaction is to be propagated at a speed exceeding the speed of light, i.e., if special relativity is to be maintained.

A direct verification of (44) can be carried out using the reduction formula (22), together with (57) and (19). In a similar way, one can show that

$$\langle 0 | j_\lambda^{\mathrm{T}}(x) | k \rangle = 0, \tag{66}$$

which is consistent with (44) and (9). This result is of some interest in connection with a paradoxical result of the Lorentz gauge formulation. In that theory, the equation of motion is

$$\Box A_\lambda(x) = -j_\lambda(x), \tag{67}$$

and in place of (44) we have (3). Using translational invariance, one concludes that

$$\Box \langle 0 | A_\lambda(x) | k \rangle = -k^2 \langle 0 | A_\lambda(x) | k \rangle = 0. \tag{68}$$

However, a direct calculation of $\langle 0 | j_\lambda(x) | k \rangle$ from (22) gives a non-zero result if the polarization state of the photon $|k\rangle$ is "longitudinal" or "scalar." The term which arises has been called a "mass-renormalization" of the unphysical "photons." The origin of this paradox lies in the more basic result discussed recently [10]) concerning the commutator of two total currents, which seems to be a very puzzling inconsistency in quantum electrodynamics. We shed no light

on this problem; we merely point out that the paradox does not occur at this point in the Coulomb gauge formulation.

In closing, we mention that the correctness of the charge renormalization introduced here can be shown by a direct, exact calculation of the charge of the state of a single electron. This is given in Appendix 2.

6. Discussion

Of the two descriptions of quantum electrodynamics which we have considered here, the Coulomb gauge form adheres more closely to the physical situation. Unfortunately, in electrodynamics, the physical situation is rather complicated, so that in actual computations one does not always gain by using the more physical formulation; the symmetry introduced by the Lorentz condition makes for considerable simplification of S-matrix calculations even though one is obliged to introduce unphysical quanta and an indefinite metric. But in examining general properties of quantum electrodynamics, there are reasons to prefer the more physical Coulomb gauge formulation. As we have indicated, one of these is that the LSZ formalism fits naturally into this formalism. The reason is clear. As given by LSZ, the asymptotic condition yields the operators which create the entire Hilbert space of states. It is a physical condition, stating in precise terms the requirement that in a scattering experiment the interacting system should behave, in remote past and future, like a system of non-interacting particles. A theory which introduces states of quanta which have no role in a non-interacting system must be expected to violate such a condition. Thus the Coulomb gauge form of quantum electrodynamics fits the LSZ scheme, while the Lorentz gauge form does not.

But we introduce the Coulomb gauge formalism at a price. In order to preserve covariant-looking expressions, we are obliged to introduce an arbitrary spacelike plane, defined by the normal vector n_μ. The result is a theory in which the electron field is not causal in the sense of the local commutativity of the renormalized fields. (We do not speculate as to the possible consequences of this situation in the proofs of dispersion relations.) A corollary of this is that the renormalization terms associated with the electron field are not constants, but momentum-dependent †. In the case of the mass renormalization, it seems that any physical interpretation of the so-called "bare" mass in this theory is impossible, since such a "mass" would necessarily be momentum-dependent.

As we have seen, especially in the calculation of the charge of the one-electron state, it is not possible to write an expression for the current vector operator entirely in terms of renormalized fields. This is well-known, and is one

† The momentum-dependence of the wave-function renormalization factor N is used by Johnson[6]) in his criticism of the generality of Källén's[2]) work, on the consistency of quantum electrodynamics.

of the reasons why explicit equations of motion are foreign to the spirit of the LSZ program. Actually, it is due to the fact that the unrenormalized electron field appears in the current that the latter is causal in the Coulomb gauge theory.

Finally, we comment briefly on the use of the term "gauge" to specify the formalisms we have discussed. Both the Coulomb gauge theory and the Lorentz gauge theory describe the same physical phenomena, but they handle one aspect of the physical situation, the Coulomb interaction, in fundamentally different ways: in the former theory the interaction is incorporated into the electron field, while in the latter theory it is pictured as being caused by the emission and absorption of quanta. The interaction involves no observable quanta, hence the freedom of choice. But the term "gauge" in this context is perhaps misleading. There is at present some disagreement among various authors as to what transformations should properly be admitted as gauge transformations. If we admit as a gauge transformation any change in the photon Green's function which leaves unaffected the physical results [11]), then of course the two formalisms we have discussed must be classed simply as different gauges. On the other hand, if we insist that the transformed fields remain invariant under translations [12]), we find the set of transformations somewhat restricted. And if we require the Hilbert space to remain unchanged, there is obviously no transformation to connect the Coulomb gauge theory with the Lorentz gauge theory. Since the Hilbert space seems important for the use of the asymptotic condition, we have emphasized the latter view. It is at least conceivable that the question of consistency will provide support for this restricted view. That is, it is possible that the Coulomb gauge theory will turn out to be consistent (because perhaps, of the momentum-dependence of the electron renormalization factors [6])) while the Lorentz gauge theory will be found to be inconsistent, as claimed by Källén [2]). In this regard we point out that even so restricted a definition of gauge transformation for the quantized theory still yields all possible gauge transformations in the classical limit.

Appendix

A.1. THE *S*-MATRIX IN THE COULOMB GAUGE

In this appendix we shall exhibit perturbation theory approximations to the *S*-operator to second order. We shall thus see explicitly the role of the Coulomb field in the Coulomb gauge formalism.

The definition of the *S*-operator is given by

$$\psi^{\text{out}}(x) = S^{-1}\psi^{\text{in}}(x)S, \tag{A.1}$$

$$\mathscr{A}_\lambda{}^{\text{out}}(x) = S^{-1}\mathscr{A}_\lambda{}^{\text{in}}(x)S. \tag{A.2}$$

Using formal solutions of the type (16) we can obtain the well-known expression

$$\psi^{\text{out}}(x) = \psi^{\text{in}}(x) + \int \mathrm{d}x' \, S(x-x') f(x'), \tag{A.3}$$

$$\mathscr{A}_\lambda{}^{\text{out}}(x) = \mathscr{A}_\lambda{}^{\text{in}}(x) - \int \mathrm{d}x' \, \mathrm{d}_{\lambda\nu} D(x-x') j_\nu(x'), \dagger \tag{A.4}$$

and combining these with (A.1) and (A.2) we arrive at

$$[S, \psi^{\text{in}}(x)] = -S \int \mathrm{d}x' \, S(x-x') f(x'), \tag{A.5}$$

$$[S, \mathscr{A}_\lambda{}^{\text{in}}(x)] = S \int \mathrm{d}x' \, \mathrm{d}_{\lambda\nu} D(x-x') j_\nu(x'). \tag{A.6}$$

These form the basis for an expansion of S in powers of e. We write

$$S = 1 + eS^{(1)} + e^2 S^{(2)} + \ldots, \tag{A.7}$$

$$\psi(x) = \psi^{\text{in}}(x) + e\psi^{(1)}(x) + \ldots, \tag{A.8}$$

$$\mathscr{A}_\lambda(x) = \mathscr{A}_\lambda{}^{\text{in}}(x) + e\mathscr{A}_\lambda{}^{(1)}(x) + \ldots, \tag{A.9}$$

$$\mathfrak{A}_\lambda(x) = 0 + e\mathfrak{A}_\lambda{}^{(1)}(x) + \ldots, \tag{A.10}$$

where, because of (17), we see that $\mathfrak{A}_\lambda$ has no zeroth order term.

The first order contribution to (A.5) and (A.6) is therefore

$$[S^{(1)}, \psi^{\text{in}}(x)] = -i \int \mathrm{d}x \, S(x-x') \hat{\mathscr{A}}^{\text{in}}(x') \psi^{\text{in}}(x'), \tag{A.11}$$

$$[S^{(1)}, \mathscr{A}_\lambda{}^{\text{in}}(x)] = \tfrac{1}{2} i \int \mathrm{d}x' \, \mathrm{d}_{\lambda\nu} D(x-x') [\bar{\psi}^{\text{in}}(x'), \gamma^\nu \psi^{\text{in}}(x')]. \tag{A.12}$$

It is then easy to show that these equations are satisfied by

$$S^{(1)} = -\tfrac{1}{2} \int \mathrm{d}x [\bar{\psi}^{\text{in}}(x), \hat{\mathscr{A}}^{\text{in}}(x) \psi^{\text{in}}(x)]. \tag{A.13}$$

(To this we can add a c-number which contributes only a constant phase to the S-matrix and is thus of no interest.) By the usual momentum-energy arguments, this can be shown not to contribute to any physical processes.

The next approximation is obtained by keeping terms up to second order in f and j_λ. The algebra involved in rather lengthy, so we shall quote only the result:

$$\begin{aligned} S^{(2)} = {} & \tfrac{1}{4} \int \mathrm{d}x \, \mathrm{d}x' \, \theta(x-x') [\bar{\psi}^{\text{in}}(x'), \hat{\mathscr{A}}^{\text{in}}(x') \psi^{\text{in}}(x')] [\bar{\psi}^{\text{in}}(x), \hat{\mathscr{A}}^{\text{in}}(x) \psi^{\text{in}}(x)] \\ & + \tfrac{1}{16} \int \mathrm{d}x \, \mathrm{d}x' \, \delta(\tau-\tau') \partial^{-1} D(x-x') \{ [\bar{\psi}^{\text{in}}(x'), \hat{n} \psi^{\text{in}}(x')], [\bar{\psi}^{\text{in}}(x), \hat{n} \psi^{\text{in}}(x)] \}. \end{aligned} \tag{A.14}$$

† To justify the use of j_λ instead of $j_\lambda{}^{\tau}$ here, one can take (16) and show (most easily in momentum space) that the same replacement can be made in that equation because the longitudinal part of the current does not contribute.

The first term above is just the part of the S-operator describing second order processes involving two transverse photons (Compton effect) and also gives the photon-exchange part of Møller scattering. The second term gives the Coulomb scattering contribution to Møller scattering. Both terms have the familiar structure of a term in the expansion

$$S = 1 + \sum_{n=1}^{\infty} \frac{(-i)^n}{n!} \int dx_1 \dots dx_n T[H_1(x_1) \dots H_1(x_n)], \tag{A.15}$$

where the first term in (A.14) is a second order term with

$$H_1^{\text{Trans.}}(x) = -\tfrac{1}{2} ie[\bar{\psi}(x), \hat{\mathscr{A}}^{\text{in}}(x)\psi^{\text{in}}(x)], \tag{A.16}$$

and the other term in (A.14) is a first order term with

$$H_1^{\text{Coul.}}(x) = \frac{e^2}{16} \int dx' \, \delta(\tau - \tau') \partial^{-1}(x - x') \{[\bar{\psi}^{\text{in}}(x'), \hat{n}\psi^{\text{in}}(x')], [\bar{\psi}^{\text{in}}(x), \hat{n}\psi^{\text{in}}(x)]\}. \tag{A.17}$$

The last expression is simply a covariant form of the Coulomb energy density operator for two electron charge densities.

A.2. THE CHARGE OF THE ONE-ELECTRON STATE

In this appendix we give an exact calculation (independent of perturbation theory) of the charge of the state of a single electron. That is, we shall give a direct calculation of $\langle p|Q|p\rangle$ where $|p\rangle$ is the state of a single electron and Q is the charge operator, given by

$$Q = -\int d\sigma n \cdot j(x). \tag{A.18}$$

We begin by obtaining from the reduction formulas a representation of the following matrix element:

$$\langle p_1|j_\lambda(x)|p_2\rangle = -\int dx' \, dx'' \, e^{-ip_1 \cdot x'} e^{ip_2 \cdot x''} \bar{u}(p_1)(\overrightarrow{\partial}' + m)\langle 0|T\psi(x')\bar{\psi}(x'')j_\lambda(x)|0\rangle(-\overleftarrow{\partial}'' + m)u(p_2). \tag{A.19}$$

In (A.19) the arrows indicate how the differentiations of the terms in the T-product are to be performed. After considerable rearranging, and dropping terms which give no contribution, we can put the right side of (A.19) into the following form:

$$\begin{aligned} &-\bar{u}(p_1) \int dx'' \, dx' \, e^{-ip_1 \cdot x'} e^{ip_2 \cdot x''} \\ &\times [\theta(01)\theta(12)\langle 0|\{\bar{f}(2), [j_\lambda(0), f(1)]\}|0\rangle + \theta(02)\theta(21)\langle 0|\{f(1), [\bar{f}(2), j_\lambda(0)]\}|0\rangle \\ &+ \delta(01)\theta(02)\langle 01\{\bar{f}(2), [j_\lambda(0), \hat{n}\psi(1)]\}|0\rangle - \delta(02)\theta(01)\langle 0|\{f(1), [\bar{\psi}(2)\hat{n}, j_\lambda(0)]\}|0\rangle \\ &- \delta(02)\delta(12)\langle 0|\{\hat{n}\psi(1), [\bar{\psi}(2)\hat{n}, j_\lambda(0)]\}|0\rangle]u(p_2), \end{aligned} \tag{A.20}$$

where the notation for the arguments of the functions is $j_\lambda(0) \equiv j_\lambda(x)$, $f(1) = f(x')$, $\theta(01) \equiv \theta(x-x')$, etc.

Now we can integrate over x to obtain the matrix element of the charge operator. To proceed, we need the following commutation relations:

$$[Q, \psi(x)] = -e\psi(x), \tag{A.21}$$

$$[Q, \bar{\psi}(x)] = e\bar{\psi}(x). \tag{A.22}$$

These are easily obtained from expressions (63) and (64) for the current and the commutation relations for the electron field. It is now straightforward to show that the last three terms on the right side of (A.20) give a contribution

$$e\left[2-\frac{1}{N^2(P^2)}\right], \quad (P_\mu \equiv p_\mu - n_\mu \eta, \quad \eta \equiv -n\cdot p), \tag{A.23}$$

to the matrix element $\langle p|Q|p\rangle$. In order to handle the other terms in (A.20), it is convenient to avoid ambiguities by first equating only the spatial parts of the momenta of the two electron states $\langle p_1|$ and $|p_2\rangle$. The energies will be equated after the integrations have been performed. We combine the terms by using the identity $\theta(01)\theta(02) = \theta(01)\theta(12)+\theta(02)\theta(21)$. Then introducing the representation (26) we can put the contribution of the terms into the form

$$\begin{aligned} e\bar{u}(p_1)\int_0^\infty da \int_{-\infty}^\infty d\omega\, \varepsilon(\omega)\delta(P^2+a-\omega^2)\frac{1}{\eta_1-\omega}\,\frac{1}{\eta_2-\omega} \\ \times[\Sigma_1(-a, P^2) + (i\hat{P}+i\hat{n}\omega+m)\Sigma_2 - i\hat{n}\omega\Sigma_3]u(p_2), \end{aligned} \tag{A.24}$$

where $\eta_1 \equiv -n\cdot p_1$ and $\eta_2 \equiv -n\cdot p_2$. Now setting $\eta_1 = \eta_2$ and performing the ω-integration, we obtain

$$e\bar{u}(p)\int_0^\infty da\left[\frac{2\eta\Sigma_1}{(a-m^2)^2} + i\hat{n}\frac{\Sigma_2}{a-m^2} - i\hat{n}\frac{\Sigma_3}{a-m^2} + i\hat{n}\frac{2\eta^2\Sigma_3}{(a-m^2)^2}\right]u(p). \tag{A.25}$$

This is easiest to compute in the frame where $n_\mu = (0, 0, 0, i)$. Using the spinor normalizations

$$\bar{u}(p)u(p) = \frac{m}{p_0}, \quad \bar{u}(p)\gamma^4 u(p) = 1, \tag{A.26}$$

and the definition (32) we obtain finally for the contribution of the first two terms in (A.20):

$$e\left[\frac{1}{N^2(P^2)} - 1\right]. \tag{A.27}$$

Adding this to (A.23) we obtain the desired result

$$\langle p|Q|p\rangle = e. \tag{A.28}$$

This result shows that the renormalization of the charge has been properly accomplished, even though it involves use of renormalization factors which are not constants. It also provides a check on the form we have given for the electric current, justifying the use of the unrenormalized electron field in (64).

References

1) H. Lehmann, K. Symanzik and W. Zimmermann, Nuovo Cim. **11** (1955) 205
2) See e.g.: G. Källén, Handbuch der Physik (J. Springer Verlag, Berlin, 1958) Vol. 5, part 1
3) J. Schwinger, Phys. Rev. **91** (1953) 713
4) J. G. Valatin, Mat. Fys. Medd. Dan. Vid. Selsk. **26**, No. 13 (1951)
5) S. Ozaki, Prog. Theor. Phys. **14** (1955) 511
6) K. Johnson, Phys. Rev. **112** (1958) 1367
7) K. Johnson, preprint (1960)
8) See e.g.: Goldberger, Nambu and Oehme, Ann. Phys. **2** (1957) 226
9) L. E. Evans, Thesis, The Johns Hopkins University (1960)
10) J. Schwinger, Phys. Rev. Letters **3** (1959) 296
11) B. Zumino, Jour. Math. Phys. **1** (1960) 1
12) L. Evans, G. Feldman and P. T. Matthews, preprint (1960)

1.D.1

Nuclear Physics **21** (1960) 508—525; © *North-Holland Publishing Co., Amsterdam*

Not to be reproduced by photoprint or microfilm without written permission from the publisher

A METHOD FOR THE ELIMINATION OF SPURIOUS STATES IN THE NUCLEAR HARMONIC OSCILLATOR SHELL MODEL

B. J. VERHAAR

Instituut voor Theoretische Physica, Universiteit van Amsterdam

Received 12 August 1960

Abstract: A group-theoretical method is used for a classification of the nuclear eigenstates in the harmonic oscillator shell model. This classification turns out to be intimately connected with the distinction between good and spurious states. In fact it provides a procedure for the elimination of spurious states. The method makes use of the invariance properties of the system Hamiltonian for several groups of transformations. In particular a group U_3 formerly used for the study of collective rotational effects in the nuclear shell-model is of importance. This group is related to the degeneracy of the 3-dimensional isotropic harmonic oscillator states. Some special examples, illustrating the method, are given.

1. Introduction

A nuclear model, suitable for explicit calculations and displaying rather well certain features, particularly of light nuclei, is the harmonic oscillator shell model. In this picture of the nucleus all nucleons are assumed identical and supposed to move in a harmonic potential field which is fixed in space. The Hamiltonian defining this system reads (in appropriate units):

$$H_0 = \tfrac{1}{2}\sum_{i=1}^{A}(\mathbf{p}_i^2+\mathbf{r}_i^2), \tag{1}$$

where A is the number of particles having $\mathbf{p}_i$ and $\mathbf{r}_i$ as momentum and position vectors respectively. Introducing the centre-of-mass vector $\mathbf{R} = \sum_i \mathbf{r}_i/A$, we define an intrinsic Hamiltonian H_{intr} by

$$H_0 = H_{\text{intr}} + \frac{\mathbf{P}^2}{2A} + \tfrac{1}{2}A\mathbf{R}^2, \tag{2}$$

where $\mathbf{P} = \sum_i \mathbf{p}_i$ is the total momentum vector. It is clear that in this model the centre-of-mass will "move" in a harmonic potential field while in a more realistic picture one should like the centre-of-mass to move freely in space. The latter situation can e.g. be described by a Hamiltonian

$$H = \tfrac{1}{2}\sum_{i=1}^{A}\{\mathbf{p}_i^2+(\mathbf{r}_i-\mathbf{R})^2\}, \tag{3}$$

where the centre of the force field is assumed to coincide with **R**. This Hamiltonian can be rewritten as

$$H = H_{\text{intr}} + \frac{\mathbf{P}^2}{2A}, \tag{4}$$

where, as is easily checked, H_{intr} is identical with H_{intr} of formula (2) and the centre-of-mass motion is free. Solutions of the Schrödinger equation with the Hamiltonian (4) can be written as $\psi = \psi_{\text{intr}} \exp i\mathbf{K}\cdot\mathbf{R}$. These, however, can easily be obtained from the solutions of the simpler Hamiltonian H_0 if we require that the centre-of-mass is in its groundstate, i.e. the solutions $\psi_0 = \psi_{\text{intr}} \exp(-\frac{1}{2}A\mathbf{R}^2)$. Then it follows that $\psi = \psi_0 \exp(\frac{1}{2}A\mathbf{R}^2) \exp(i\mathbf{K}\cdot\mathbf{R})$.

The problem therefore is to find eigenstates for the model defined by (1) for which $H_{\text{coll}} = \mathbf{P}^2/2A + \frac{1}{2}A\mathbf{R}^2$ has its lowest eigenvalue. These states are called good states. The eigenstates of H_0 with higher centre-of-mass energy $\lambda+\frac{3}{2}$ are called λ times spurious. These states with a certain centre-of-mass energy can be obtained by combining degenerate eigenfunctions of H_0, i.e. states of equal excitation. The linear combinations follow from a diagonalization of the H_{coll} matrix between equally excited states. Elliott and Skyrme [1]) show that for the lowest energy states of H_0 the centre-of-mass is always in a 1s state. Consequently the ground-states in the harmonic-oscillator shell model are always good states. However, for excited states this is no longer true and one has to eliminate the spurious ones amongst them.

In section 2 a certain classification of wave functions is described. The classification method has been introduced by Elliott [2]) for groundstates. It is shown in section 2 that it can also be applied to excited states. The classification is based on the invariance properties of the model Hamiltonian H_0 for several groups of transformations: the permutation group of identical particles, the rotation group and a group following from the symmetry between position and momentum operators. The Hilbert-space of the system under consideration can therefore be split up into irreducible subspaces which are invariant under the above-mentioned transformations. In this way a classification of wave functions is obtained by finding the irreducible representations of the transformation groups.

In section 3 we show that this classification is closely connected with the distinction between good and spurious states. In some cases it gives directly the good and spurious states.

Some special examples are given in section 4. Some mathematical statements are discussed in Appendices 1 and 2.

2. A Classification of Harmonic-Oscillator Wave Functions

First we will pay attention to a classification scheme for states of ν particles in the same shell (energy level), indicated by the quantum number N, corre-

sponding to a one-particle energy of $N+\frac{3}{2}$. The Hamiltonian H_0 is invariant under S_ν, the permutation group of ν particles. Therefore it is possible to classify the H_0 eigenstates according to the representations of the group S_ν. A complete orthogonal basis for such a representation can be obtained by coupling the ν one-particle states to ν-particle states with a certain symmetry $[f]$ under permutations of the ν particles. Each state of this basis can be represented by a Young-diagram $[f](r)$, where (r) denotes the sequence of the particle numbers which defines the role of each particle in the process of coupling. The irreducible space of a representation of S_ν can thus be denoted by $[f]$. In the following often a particular state $[f](r)$ of the basis occurs and for the sake of simplicity we will drop the symbol (r). Unless a different meaning is mentioned explicitly we understand by $[f]$ a particular state of the basis of the subspace with a certain symmetry. In this way the space of H_0 eigenstates is split up into symmetry-classes, i.e. spaces of states with equal $[f](r)$ or in our simplified notation $[f]$. For a more detailed consideration of this so-called Wigner supermultiplet-classification, we refer to Elliott and Lane [4]).

The one-particle Hamiltonian $\frac{1}{2}(\mathbf{p}^2+\mathbf{r}^2)$ is invariant under rotations in phase-space, because it is proportional to the square length of a six-dimensional vector (x, y, z, p_x, p_y, p_z). The requirement that these rotations correspond to unitary transformations in Hilbert-space is equivalent to demanding that the commutation relations between the components of position and momentum vectors shall be invariant. This restricts the rotations in phase-space to a subgroup corresponding to a unitary group U_3. Elliott [2]) introduced this group by means of its nine generating infinitesimal operators, which are constants of the motion of the 3-dimensional isotropic harmonic oscillator.

A further classification of H_0 eigenstates thus consists of splitting up the symmetry-classes $[f]$ into the subspaces which belong to irreducible representations of the group $[U_3]^\nu$ of simultaneous U_3-transformations for the ν particles. The simultaneity of the transformations guarantees that $[U_3]^\nu$ commutes with the group S_ν. The so-defined subspaces may be characterized by the label $(\lambda\mu)$. For a detailed treatment of the physical significance of this so-called U_3-classification we refer to Elliott [2, 3]). Symmetry-classes, corresponding to Young-diagrams with equal symmetry but different sequences of the particles, contain equivalent sets of $(\lambda\mu)$ spaces.

A subgroup of U_3 is the rotation group R_3. A subsequent classification is therefore possible by the total angular momentum quantum numbers L and M.

A wave function of ν_N particles in the same N-shell may thus be denoted by

$$\psi\big((N)^{\nu_N}[f](\lambda\mu)\alpha LM\big), \tag{5}$$

where α is a quantum number which can distinguish between states in a subspace $(\lambda\mu)$, which have equal angular momentum quantum numbers. We can always define α in such a way that states with different α are orthogonal. For

convenience we define the quantum numbers α in $(\lambda\mu)$ spaces having equal λ and μ, in an equivalent way. This procedure of classification was introduced by Elliott [2]) for the ground states, where it is sufficient to consider particles in one shell, as we will presently show.

Now we proceed by defining a classification scheme for the eigenstates of an A particle system in a *general* configuration, i.e. the configuration $(0)^{\nu_0}$, $(1)^{\nu_1}$, $(2)^{\nu_2}, \ldots, (i)^{\nu_i}, \ldots$, where this notation means that there are ν_i particles in the $N = i$ shell. Using the method of Elliott and Skyrme [1]) and Elliott and Lane [4]), we classify the A-particle eigenstates according to the Young-symmetry $[f]$ by the following procedure. Within each shell i we couple the particle states to a shell symmetry $[f]_i$ and after that we couple the several shells to a total symmetry $[f]$.

The spaces, each characterized by $(0)^{\nu_0}[f]_0, (1)^{\nu_1}[f]_1, (2)^{\nu_2}[f]_2, \ldots; [f]$ are then orthogonal. It should be noted that in this notation the labels $[f]_i$, denoting the shell-symmetries, stand for Young-diagrams without a special number sequence. The total symmetry $[f]$ according to the notation convention of section 2 does imply a special number sequence of the particles.

It is possible to split up the defined symmetry-classes into subspaces which correspond to irreducible representations of $[U_3]^A$. This possibility was already mentioned for the case of particles in the same shell, i.e. the symmetry-class $(i)^{\nu_i}[f]_i$ of ν_i particles in the $N = i$ shell is a direct sum of $(\lambda\mu)$ spaces:

$$(i)^{\nu_i}[f]_i = \sum (i)^{\nu_i}[f]_i(\lambda\mu)_i. \tag{6}$$

However, the same statement is valid for the total system of A particles. This follows from a theorem we discuss in Appendix 1. The theorem states that the space $(0)^{\nu_0}[f]_0, (1)^{\nu_1}[f]_1, (2)^{\nu_2}[f]_2, \ldots; [f]$ is equal to a direct sum of $(\lambda\mu)$ spaces, which follows from the reduction of the direct product

$$\prod_i \sum (i)^{\nu_i}[f]_i(\lambda\mu)_i \tag{7}$$

of U_3-representations.

This reduction to $(\lambda\mu)$ spaces, as well as that of $\prod_i (i)^{\nu_i}[f]_i$ to symmetry-classes of A particles, may be performed with the help of the tables of Murnaghan [5]). It should be noted that the set of $(\lambda\mu)$ spaces resulting from the above-mentioned reduction does not depend on the total symmetry $[f]$, but only on the shell-symmetries $[f]_i$. Examples are given in section 4.

Also in the case of these more general configurations it is possible to add the quantum numbers αLM in order to get the following classification of A-particle harmonic-oscillator states:

$$\psi\big((0)^{\nu_0}[f]_0, (1)^{\nu_1}[f]_1, \ldots; [f](\lambda\mu)\alpha LM\big). \tag{8}$$

The effectiveness of the foregoing classification in distinguishing the states is restricted by the multiple occurrence, first of the same $[f]$ in the direct product

$\prod_i (i)^{\nu_i}[f]_i$ and secondly of the same $(\lambda\mu)$ in the direct product $\prod_i \sum (i)^{\nu_i}[f]_i\,(\lambda\mu)_i$. The characterization of states within a subspace $(\lambda\mu)$ by the quantum numbers αLM is unique. For the conclusions in this paper it is irrelevant whether the classification is unique or not.

So far we have considered the nucleons as identical particles without spin. We now introduce the isobaric spin and the spin of the nucleons in order to specify a neutron or proton state and two independent spin states. Retaining the Hamiltonian H_0 which does not contain spin dependent terms, we can consider separately the orbital wave functions and the spin wave functions. It can be proved that a completely antisymmetric total wave function may be formed by taking a suitable linear combination of products of orbital wave functions from a symmetry-class $[f]$ with spin-isobaric-spin wave functions of the so-called adjoint symmetry $[\tilde{f}]$ only [4]). This restricts the number of admissible orbital symmetries $[f]$. The number of rows of $[\tilde{f}]$, which equals the number of columns of $[f]$, is at most equal to the number of independent one-particle spin-isobaric-spin states, i.e. four.

As a consequence a space of ground configuration orbital wave functions of the A-particle harmonic-oscillator system will be characterized by

$$(0)^4[4]_0,\ (1)^{12}[444]_1,\quad (2)^{24}[444444]_2, \ldots, (N)^{\nu_N}[f]_N;\ [f](\lambda\mu), \tag{9}$$

where there are a number of closed shells with definite shell-symmetries $[f]_i = [4^{\frac{1}{2}\nu_i}]$ and one partially filled N-shell. The direct sum (6) for the closed shells consists of the representation (00) only. Therefore $[f]$ and $(\lambda\mu)$ are determined by the particles in the partially filled shell. For this reason a classification of ground states requires a treatment of the case of ν_N particles in one N-shell only.

3. The Elimination of Spurious States

The good states have been defined as those eigenstates of H_0 for which H_{coll} has its lowest eigenvalue. The operator H_{coll} is symmetric in the A particles and therefore invariant under the A-particle permutation-group S_A. Moreover

$$H_{\text{coll}} = \frac{1}{2A}\,(\mathbf{P}^2 + A^2\mathbf{R}^2) = \frac{1}{2A}\,\{(\sum_i \mathbf{p}_i)^2 + (\sum_i \mathbf{r}_i)^2\} \tag{10}$$

is invariant under simultaneous U_3 transformations of the A particles, since it is the square length of the six-dimensional vector $(A\mathbf{R}, \mathbf{P})$ in six-dimensional phase-space. As a consequence the $[U_3]^A$-group is a symmetry group of H_{coll}. This means that H_{coll} is diagonal in the scheme $[f](\lambda\mu)\alpha LM$. Therefore the classification discussed in section 2 diagonalizes H_{coll} to a certain extent. To a certain extent, because there are often equivalent $[f](\lambda\mu)$ spaces. These may differ in configuration or shell-symmetries and can in principle be connected

by H_{coll}, provided they are of equal excitation. (In examples III and IV of section 4 there are only inequivalent spaces). The matrix of H_{coll} has to be calculated only in the direct sum of these spaces. Since H_{coll} is diagonal in αLM, a matrix may be constructed for each αLM, but as a consequence of the invariance of H_{coll} under the $[U_3]^A$-group, these matrices are all equal. Therefor the unitary transformation that makes H_{coll} diagonal may be performed for each αLM separately with the same coefficients. The linear combinations of spaces with equal $[f](\lambda\mu)$ have again the labels $[f](\lambda\mu)$. We can therefore find $[f](\lambda\mu)$ spaces that are entirely good and other $[f](\lambda\mu)$ spaces that are entirely spurious (they are called λ times spurious if the eigenvalue of H_{coll} equals $\lambda+\frac{3}{2}$).

We will here pay some attention to the diagonalization of H_{coll}. H_{coll} is equal to

$$\frac{\mathbf{P}^2}{2A}+\tfrac{1}{2}A\mathbf{R}^2=\frac{(\sum_i \mathbf{p}_i)^2+(\sum_i \mathbf{r}_i)^2}{2A}=\frac{H_0}{A}+\sum_{i>k}\frac{\mathbf{p}_i\cdot\mathbf{p}_k+\mathbf{r}_i\cdot\mathbf{r}_k}{A} \tag{11}$$

The first term gives rise to a constant multiple of the unit matrix. The second term is a sum of two-particle operators of equal form, of which matrix elements may therefore be reduced by fractional parentage techniques to two-particle matrix-elements [4]). The values of the latter will now be given. In Appendix 2 we prove, that properties of irreducible tensor operators, together with the reduction

$$\begin{aligned}(\lambda_1 0)\times(\lambda_2 0)&=\sum(\lambda\mu)=\\&=(\lambda_1+\lambda_2,0)+(\lambda_1+\lambda_2-2,1)+(\lambda_1+\lambda_2-4,2)+\ldots+(\lambda_1-\lambda_2,\lambda_2),\end{aligned} \tag{12}$$

in case $\lambda_1>\lambda_2$, lead to the formula

$$\begin{aligned}&\langle(\lambda'_1 0)(\lambda'_2 0);(\lambda\mu)\alpha LM|\tfrac{1}{2}(\mathbf{p}_1\cdot\mathbf{p}_2+\mathbf{r}_1\cdot\mathbf{r}_2)|(\lambda_1 0)(\lambda_2 0);(\lambda\mu)\alpha LM\rangle\\&=\tfrac{1}{4}\{(\lambda+\lambda'_1-\lambda'_2)(\lambda+\lambda_2-\lambda_1)\}^{\frac{1}{2}}\delta_{\lambda'_1,\lambda_1+1}\delta_{\lambda'_2,\lambda_2-1}\\&+\tfrac{1}{4}\{(\lambda+\lambda'_2-\lambda'_1)(\lambda+\lambda_1-\lambda_2)\}^{\frac{1}{2}}\delta_{\lambda'_2,\lambda_2+1}\delta_{\lambda'_1,\lambda_1-1},\end{aligned} \tag{13}$$

where e.g. $|(\lambda_1 0)(\lambda_2 0);(\lambda\mu)\alpha LM\rangle$ denotes a state-vector in the $(\lambda\mu)$ space, resulting from reduction of the directly multiplied spaces $(\lambda_1 0)$ and $(\lambda_2 0)$ of particle 1 and 2 respectively.

The foregoing method for the elimination of spurious states consists of a U_3-classification of H_0 eigenstates with certain shell- and total symmetries, followed by a diagonalization of H_{coll} (or H_{intr}). There is another way to end up with the same classification and it is advantageous to consider this procedure in some detail. This alternative method starts with H_{coll} and H_{intr} eigenstates which are subsequently classified according to irreducible U_3-representations. For that purpose it is necessary to see how the group $[U_3]^A$ works upon H_{coll} and H_{intr} eigenstates.

The group of simultaneous rotations of the A particles in six-dimensional phase-space, commutes with a transformation in this same phase-space that changes the six-dimensional $(\mathbf{r}_i, \mathbf{p}_i)$ vectors into A independent linear combinations. The requirement that the simultaneous rotations correspond to unitary transformations in Hilbert-space, i.e. that the commutation relations are invariant, has been seen to restrict the rotation-group to a subgroup corresponding to the group $[U_3]^A$ in Hilbert-space. In the same way, the requirement that the linear transformation of $(\mathbf{r}_i, \mathbf{p}_i)$ vectors gives rise to a unitary transformation S in Hilbert-space, is fulfilled by choosing for the A new position-momentum vectors orthogonal linear combinations of $(\mathbf{r}_i, \mathbf{p}_i)$ vectors. If, in particular, one of the new vectors is equal to the centre-of-mass position-momentum vector, the orthogonal linear combinations yield intrinsic position-momentum vectors. The A-particle Hilbert-space is not only a direct product of A one-particle Hilbert-spaces, but also a direct product of A spaces of which $A-1$ belong to intrinsic degrees of freedom and one to the centre-of-mass. An element of the group $[U_3]^A$ has after the unitary transformation S the form $S[U_3]^A S^{-1}$, which according to the above-mentioned argument is equal to $[U_3]^A$ again, where now $A-1$ groups U_3 consist of transformations in the intrinsic Hilbert-spaces and one U_3-group operates in the centre-of-mass Hilbert-space. Because H_{intr} commutes with the "intrinsic group" $[U_3]^{A-1}$, it is possible to split up the H_{intr} eigenspaces into subspaces corresponding to irreducible representations of the intrinsic group $[U_3]^{A-1}$. These are denoted by $(\lambda\mu)_{\text{intr}}$ and are equivalent to the representations of the group $[U_3]^{A-1}$ of $A-1$ particles. In the same way it can be shown that the collective Hilbert-space can be split up into subspaces corresponding to irreducible representations of the "centre-of-mass group" U_3. These invariant subspaces coincide with subspaces of definite centre-of-mass energy. The above mentioned U_3-representations are equivalent to the representation of U_3 in a single-particle Hilbert-space, namely $(\lambda 0)$. We denote them by $(\lambda 0)_{\text{coll}}$.

Irreducible representations of $[U_3]^A$ in the total A-particle Hilbert-space, can be constructed from those of $[U_3]^{A-1}$ and U_3 by reducing the direct product

$$(\lambda\mu)_{\text{intr}} \times (\lambda 0)_{\text{coll}} = \sum (\lambda\mu). \tag{14}$$

It is possible to give the intrinsic wave functions a definite symmetry in the A particles, because the intrinsic group $[U_3]^{A-1}$ is symmetric under permutations of the particles. This follows from the property that both the $[U_3]^A$ and the centre-of-mass U_3-group are symmetric under permutations of the particles. Consequently, it is possible to construct $(\lambda\mu)_{\text{intr}}$ spaces with a definite symmetry $[f]$ of the A particles, denoted by $[f](\lambda\mu)_{\text{intr}}$. The centre-of-mass spaces $(\lambda 0)_{\text{coll}}$ are always totally symmetric, because $\mathbf{R}$ is itself symmetric. Therefore

$$[f](\lambda\mu)_{\text{intr}} \times [A](\lambda 0)_{\text{coll}} = [f] \sum (\lambda\mu), \tag{15}$$

i.e. total symmetry is equal to intrinsic symmetry.

In this way the reduction of directly multiplied intrinsic and collective spaces leads to $[f](\lambda\mu)$ spaces which correspond to one definite centre-of-mass energy. We have thus arrived at the same result as that obtained by the first method of this section, since the spaces

$$[f](\lambda\mu)_{\text{intr}} \times [A](00)_{\text{coll}} = [f](\lambda\mu), \tag{16}$$

are entirely good, while the spaces (15) for $\lambda_{\text{coll}} \neq 0$ are entirely λ_{coll} times spurious.

4. Examples

In this section we want to illustrate how the considerations of the preceding sections can be used to decide which states of the harmonic-oscillator shell model are adequate for the nucleus and which states must be eliminated as being spurious. Before giving a few examples we outline the general procedure. First we apply the classification scheme of section 2 to the configurations of the nucleus under consideration. For a given excitation there may be more than one space with equal labels $[f](\lambda\mu)$. Next we determine the labels $[f](\lambda\mu)$ of the spurious spaces in the following way. With the help of the second method described in section 3 all spurious spaces of given excitation may be found from the good spaces of lower excitations. In this way we find for each excitation how many good spaces of certain $[f](\lambda\mu)$ exist. This leads immediately to a classification according to good and spurious states if for given excitation and $[f](\lambda\mu)$ all spaces are spurious or none. If, however, both good and spurious spaces exist it remains to determine the linear combinations of the $[f](\lambda\mu)$ spaces which are good and those which are spurious. This means that a diagonalization of H_{coll} is then still necessary. In this way we obtain the spaces of good states with certain excitation and labels $[f](\lambda\mu)$ in terms of the states $\psi((0)^{p_0}[f]_0(\lambda\mu)_0,\ (1)^{p_1}[f]_1(\lambda\mu)_1, \ldots;\ [f](\lambda\mu)\alpha LM)$. It is of course possible to express these good states in wave functions of another orthogonal basis, e.g. the wave functions

$$\varphi((0)^{p_0}[f]_0(\lambda\mu)_0\alpha_0 L_0,\ (1)^{p_1}[f]_1(\lambda\mu)_1\alpha_1 L_1, \ldots; [f]LM), \tag{17}$$

where the shell quantum-numbers $\alpha_i L_i$ are used in stead of the labels $(\lambda\mu)\alpha$ of the states ψ. If each shell symmetry $[f]_i$ determines the labels $(\lambda\mu)_i\alpha_i$ uniquely, as is the case in our examples, the wave functions φ are identical with those used by Elliott and Skyrme [1]). The unitary transformation between the sets φ and ψ, if only two shells are involved, can be written in abbreviated notation as

$$\psi((\lambda\mu)\alpha LM) = \sum_{\alpha_i L_i} C^{(\lambda\mu)\alpha L}_{(\lambda\mu)_1\alpha_1 L_1,\,(\lambda\mu)_2\alpha_2 L_2}\ \varphi((\lambda\mu)_1\alpha_1 L_1, (\lambda\mu)_2\alpha_2 L_2; LM), \tag{18}$$

where the coefficients are independent of M and are called fractional parentage coefficients (f.p.c.) for U_3-representations. For any other number of shells the

unitary transoformation may be found by repeated application of the above-mentioned formula. We have calculated the relevant f.p.c. with the help of the group-theoretical techniques, developed by Elliott [3]). In each of the following examples we will use the results of this calculation to represent the good and spurious states in the same way as Elliott and Skyrme. This makes a comparison possible. Examples I(a, b), I(c), II(a, b), III(a, b) deal with the same nuclei as examples I, II, III and IV of Elliott and Skyrme. In addition two new examples (IV, V) are given.

I. THE NUCLEUS $_2He_2^4$

(a) According to the harmonic-oscillator model the α-particle ground-state is given by the configuration $(0)^4$, i.e. $(1s)^4$. This state has particle-symmetry $[f] = [4]$ and belongs to the U_3-representation $(\lambda\mu) = (00)$. Therefore in the notation of section 2 it is denoted by $(0)^4[4](00)$. As mentioned in section 1, the ground-configuration of each nucleus contains only good states. Consequently, in the light of formula (16),

$$(0)^4[4](00) = [4](00)_{\text{intr}} \times [4](00)_{\text{coll}}. \tag{19}$$

(b) The once excited α-particle configuration is $(0)^3(1)^1$, i.e. $(1s)^3(1p)^1$. The three 1s-particles have symmetry [3] and belong to U_3-representation (00). The single 1p-particle has symmetry [1] and U_3-classification (10). Possible total symmetries are therefore given by

$$[3] \times [1] = [4] + [31]. \tag{20}$$

It follows from formula (7), that both [4] and [31] contain a $(00) \times (10) = (10)$ space. Consequently, the first excited α-particle configuration consists of the subspaces

$$\begin{aligned} &(0)^3[3],\ (1)^1[1];\ [4](10) \\ \text{and} \qquad &\qquad\qquad ;\ [31](10). \end{aligned} \tag{21}$$

On the other hand one may also find a once excited space by coupling the $[4](00)_{\text{intr}}$ space, belonging to the ground state, to a $(10)_{\text{coll}}$ centre-of-mass space, as pointed out in section 3, formula (15):

$$[4](00)_{\text{intr}} \times [4](10)_{\text{coll}} = [4](10). \tag{22}$$

This must be identical to the [4](10) space which we already found. The $(0)^3[3]$, $(1)^1[1]$; [4](10) space therefore contains only once spurious states. The less symmetric [31](10) space is entirely good.

(c) Twice excited configurations of the α-particle are

$$(0)^3(2)^1 \text{ i.e. } (1s)^3(1d, 2s)^1 \quad \text{and} \quad (0)^2(1)^2 \text{ i.e. } (1s)^2(1p)^2.$$

The first configuration consists of the spaces

$$(0)^3[3](00),\ (2)^1[1](20);\ [4](20)$$
$$;\ [31](20), \tag{23}$$

and

whereas the second configuration contains

$$(0)^2[2](00),\ (1)^2[2](20);\ [\ 4](20) \tag{24}$$
$$;\ [31](20)$$
$$;\ [22](20)$$
$$(0)^2[2](00),\ (1)^2[11](01);\ [31](01)$$
$$;\ [211](01).$$

Starting from the results of Ia and Ib, we are led to the following spurious spaces

$$[\ 4](00)_{\text{intr}} \times [4](20)_{\text{coll}} = [4](20)$$
$$[31](10)_{\text{intr}} \times [4](10)_{\text{coll}} = [31](20) + [31](01). \tag{25}$$

It follows that a definite linear combination of the two [4](20) spaces found by the classification method is twice spurious and may be determined by diagonalization of H_{coll}. The orthogonal linear combination is an entirely good space. A special linear combination of the two [31](20) spaces is once spurious. The orthogonal linear combination is a good space. The [31](01) space is entirely once spurious. The [22](20) and [211](01) spaces are entirely good.

Diagonalization of H_{coll} leads to

$$\sqrt{\tfrac{3}{4}}\{(1s)^3(1d, 2s)^1;\ [4](20)\} - \sqrt{\tfrac{1}{4}}\{(1s)^2(1p)^2;\ [4](20)\}$$
$$\text{and} \quad \sqrt{\tfrac{1}{4}}\{(1s)^3(1d, 2s)^1;\ [4](20)\} + \sqrt{\tfrac{3}{4}}\{(1s)^2(1p)^2;\ [4](20)\} \tag{26}$$

as good and twice spurious space respectively. This holds for the S- as well as for the D-states of [4](20). For the [31](20) spaces we find

$$\sqrt{\tfrac{1}{2}}\{(1s)^3(1d, 2s)^1;\ [31](20)\} - \sqrt{\tfrac{1}{2}}\{(1s)^2(1p)^2;\ [31](20)\}$$
$$\text{and} \quad \sqrt{\tfrac{1}{2}}\{(1s)^3(1d, 2s)^1;\ [31](20)\} + \sqrt{\tfrac{1}{2}}\{(1s)^2(1p)^2;\ [31](20)\} \tag{27}$$

as good and once spurious space respectively. This, too, applies to the S- as well as to the D-states of [31](20). As in the case of two particles, treated in Appendix 2, we have made the following choice for the relative phases of corresponding states in the two [4](20) spaces belonging to different configurations. The matrix-elements of H_{coll} connecting corresponding states in the two spaces are prescribed to be real and non-negative. The same convention is made for the two [31](20) spaces.

II. THE NUCLEI $_6C_7^{13}$ AND $_7N_6^{13}$

In this example we only consider the states of highest orbital symmetry [4441].

(a) For the ground-configuration $(0)^4(1)^9$ i.e. $(1s)^4(1p)^9$ a [4441] space only results from the 1p-shell symmetry [441]. This space is according to the classification-method of section 2 denoted by

$$(0)^4[4](00),\ (1)^9[441](03);\ [4441](03) \tag{28}$$

and may be written as the following direct product of intrinsic and collective spaces:

$$[4441](03)_{\text{intr}} \times (00)_{\text{coll}}. \tag{29}$$

(b) Once excited configurations are

$$\begin{aligned} &(0)^4(1)^8(2)^1 \quad \text{i.e.} \quad (1s)^4(1p)^8(1d, 2s)^1 \\ \text{and} \quad &(0)^3(1)^{10} \quad \text{i.e.} \quad (1s)^3(1p)^{10} \end{aligned} \tag{30}$$

These configurations consist of the following subspaces of total symmetry [4441]:

$$\begin{aligned} &(0)^4[4](00),\ (1)^8[44](04),\ (2)^1[1](20) \quad ;[4441](24) \\ &\qquad\qquad\qquad\qquad\qquad\qquad\quad ;[4441](13) \\ &\qquad\qquad\qquad\qquad\qquad\qquad\quad ;[4441](02) \\ &(0)^4[4](00),\ (1)^8[431](12),\ (2)^1[1](20) \quad ;[4441](32) \\ &\qquad\qquad\qquad\qquad\qquad\qquad\quad ;[4441](21) \\ &\qquad\qquad\qquad\qquad\qquad\qquad\quad ;[4441](10) \\ &\qquad\qquad\qquad\qquad\qquad\qquad\quad ;[4441](13) \\ &\qquad\qquad\qquad\qquad\qquad\qquad\quad ;[4441](02) \\ &(0)^3[3](00),\ (1)^{10}[442](02) \quad ;[4441](02). \end{aligned} \tag{31}$$

It should be noted, that according to Murnaghan's tables [5]), [44] and [431] are the only possibilities to give [4441] in combination with [4] and [1]. Both [442] and [4411] give combined with [3] the symmetry [4441]. However, the symmetry [4411] is not possible in the 1p-shell.

Now again starting from the ground-configuration, we find with the help of the intrinsic space of fomula (29) the spurious spaces as follows:

$$\begin{aligned} [4441](03)_{\text{intr}} \times (10)_{\text{coll}} = &[4441](13) \\ &[4441](02). \end{aligned} \tag{32}$$

Consequently, the earlier found spaces

$$[4441](24),\ [4441](32),\ [4441](21) \quad \text{and} \quad [4441](10)$$

of the once excited configurations are good, as well as one linear combination of the [4441](13) spaces and two linear combinations of the [4441](02) spaces. The orthogonal linear combinations are once spurious. We have not calculated these linear combinations. On the other hand we did determine the ratio of the coefficients of ψ_1 and ψ_2 in the spurious state mentioned by Elliott and Skyrme[1]) in their formula (18). The linear combination of ψ_1 and ψ_2 calculated by Elliott and Skyrme represents the single state

$$\psi((1s)^4[4](00), (1p)^8[44](04), (1d, 2s)^1[1](20); [4441](02)S) \tag{33}$$

in our formalism. This wave function is according to formula (18) of this section equal to

$$c^{(02)S}_{(04)S,\,(20)S}\varphi((00)S, (04)S, (20)S; S)+c^{(02)S}_{(04)D,\,(20)D}\varphi((00)S, (04)D, (20)D; S). \tag{34}$$

It should be noted that the use of a quantum number α is not necessary in this connection. The φ functions are identical to the ψ_1 and ψ_2 used by Elliott and Skyrme. The absolute values of the f.p.c. are $\frac{1}{3}\sqrt{2}$ and $\frac{1}{3}\sqrt{7}$ respectively, which is in agreement with the results of Elliott and Skyrme [1]).

III. THE NUCLEUS ${}_8O_8^{16}$

(a) The only possible symmetry for the ground-configuration $(0)^4(1)^{12}$ i.e. $(1s)^4(1p)^{12}$ is [4444]. This can only result from a symmetry [4] in the 1s-shell and a symmetry [444] in the 1p-shell. The ground-configuration thus consists of a one-dimensional space, namely

$$(1s)^4[4](00), (1p)^{12}[444](00); [4444](00). \tag{35}$$

This space may be written as $[4444](00)_{\text{intr}}\times(00)_{\text{coll}}$.

(b) The spaces of symmetry [4444] belonging to the once excited configuration $(0)^4(1)^{11}(2)^1$ or $(1s)^4(1p)^{11}(1d, 2s)^1$ are according to formula (7)

$$\begin{aligned}(1s)^4[4](00), (1p)^{11}[443](01), (1d, 2s)^1[1](20); [4444](21)\\ ; [4444](10).\end{aligned} \tag{36}$$

Starting from the $[4444](00)_{\text{intr}}$ space of the ground-configuration we get the following spurious space:

$$[4444](00)_{\text{intr}}\times(10)_{\text{coll}} = [4444](10). \tag{37}$$

Consequently, the earlier mentioned [4444](10) space is entirely once spurious and the [4441](21) space is entirely good. We see that in this case U_3-classification leads immediately to the identification of good and spurious spaces. The only admissible P-states are:

$$\begin{aligned}&\psi((1s)^4[4](00), (1p)^{11}[443](01), (1d, 2s)^1[1](20); [4444](21)PM)\\ &= c^{(21)P}_{(01)P,\,(20)S}\,\varphi((1s)^4, (1p)^{11}[443], (2s)^1; [4444]PM)\\ &+ c^{(21)P}_{(01)P,\,(20)D}\varphi((1s)^4, (1p)^{11}[443], (1d)^1; [4444]PM).\end{aligned} \tag{38}$$

The f.p.c. in this linear combination are in absolute value $\sqrt{\frac{5}{6}}$ and $\sqrt{\frac{1}{6}}$ respectively, which is in agreement with the results of Elliott and Skyrme [1]). The spurious space [4444](10)P is equal to the orthogonal linear combination.

IV. THE NUCLEUS $_{20}Ca^{40}_{20}$

(a) The only possible symmetry for the ground-configuration $(0)^4(1)^{12}(2)^{24}$ i.e. $(1s)^4(1p)^{12}(1d, 2s)^{24}$ is $[4^{10}]$. The shell-symmetries are [4], $[4^3]$ $[4^6]$ for the $N = 0$, 1 and 2 shells respectively. The ground-configuration consists of a one-dimensional space, namely

$$(1s)^4(00),\ (1p)^{12}[4^3](00),\ (1d, 2s)^{24}[4^6](00);\ [4^{10}](00). \tag{39}$$

This space is equal to the direct product $[4^{10}](00)_{\text{intr}} \times (00)_{\text{coll}}$.

(b) The spaces of symmetry $[4^{10}]$ belonging to the once excited configuration $(0)^4(1)^{12}(2)^{23}(3)^1$ i.e. $(1s)^4(1p)^{12}(1d, 2s)^{23}(1f, 2p)^1$ are

$$\begin{aligned}(1s)^4[4](00),\ (1p)^{12}[444](00),\ (1d, 2s)^{23}[4^5 3](02),\ (1f, 2p)^1[1](30);\ &[4^{10}](32)\\ &;\ [4^{10}](21)\\ &;\ [4^{10}](10).\end{aligned} \tag{40}$$

Starting from the ground-configuration the following spurious space is found:

$$[4^{10}](00)_{\text{intr}} \times (10)_{\text{coll}} = [4^{10}](10). \tag{41}$$

Consequently, the above-mentioned $[4^{10}](10)$ space is entirely once spurious and the spaces $[4^{10}](32)$ and $[4^{10}](21)$ are entirely good. Therefore, as in example III, U_3-classification gives directly a separation between good and spurious states. The spurious P-states are

$$\begin{aligned}&\varphi\big((1s)^4[4],\ (1p)^{12}[4^3],\ (1d, 2s)^{23}[4^5 3],\ (1f, 2p)^1;\ [4^{10}]PM\big)\\ &\quad = c^{(10)P}_{(02)S,\,(30)P}\,\varphi\big((2s)^{-1}(2p)^1;\ PM\big) + c^{(10)P}_{(02)D,\,(30)P}\,\varphi\big((1d)^{-1}(2p)^1;\ PM\big)\\ &\quad + c^{(10)P}_{(02)D,\,(30)F}\,\varphi\big((1d)^{-1}(1f)^1;\ PM\big),\end{aligned} \tag{42}$$

where we denote a hole in the same way as Elliott and Skyrme. The f.p.c. in this linear combination are in absolute value $\sqrt{\frac{1}{6}}$, $\sqrt{\frac{2}{15}}$ and $\sqrt{\frac{7}{10}}$ respectively. Both orthogonal P-spaces belong to the spaces $[4^{10}](32)$ and $[4^{10}](21)$ and are consequently good.

V. THE NUCLEUS $_6C_6^{12}$

In this example we only consider the states of highest orbital symmetry [444].

(a) For the ground-configuration $(0)^4(1)^8$ i.e. $(1s)^4(1p)^8$ a space [444] can only result from the shell-symmetries [4] and [44] in the 1s- and 1p-shells

respectively. Thus the ground-configuration contains the following [444] space:

$$(1s)^4[4](00),\ (1p)^8[44](04);\ [444](04). \tag{43}$$

Since this is a good space, it may be written as $[4^3](04)_{\text{intr}} \times (00)_{\text{coll}}$.

(b) The [444] spaces in the once excited configurations $(0)^4(1)^7(2)^1$ and $(0)^3(1)^9$ are

$$\begin{aligned}(1s)^4[4](00),\ (1p)^7[43](13),\ (1d, 2s)^1[1](20);\ &[444](33)\\ &;\ [444](22)\\ &;\ [444](11)\\ &;\ [444](14)\\ &;\ [444](03)\\ (1s)^3[3](00),\ (1p)^9[441](03)\quad\ &;\ [444](03).\end{aligned} \tag{44}$$

Starting from the ground-configuration the following spurious spaces are found

$$[4^3](04)_{\text{intr}} \times (10)_{\text{coll}} = [4^3](14) + [4^3](03). \tag{45}$$

As a consequence, the above-mentioned spaces $[4^3](33)$, $[4^3](22)$ and $[4^3](11)$ are good. The space $[4^3](14)$ is once spurious. Only in the case of the two $[4^3](03)$ spaces, a subsequent diagonalization of H_{coll} is necessary. With the help of f.p.c. it is possible to find expressions for the following good states

$$\begin{aligned}&(33)\ L = 1, 2, 3(2\times), 4(2\times), 5, 6,\\ &(22)\ L = 0, 2(2\times), 3, 4,\\ &(11)\ L = 1, 2,\end{aligned}$$

and the following once spurious states

$$(14)\ L = 1, 2, 3, 4, 5.$$

E.g. the good state $\psi((33)\mathrm{DM})$ or in a more complete notation

$$\psi((0)^4[4](00),\ (1)^7[43](13),\ (2)^1[1](20);\ [444](33)\mathrm{DM})$$

is equal to

$$\begin{aligned}&c^{(33)\mathrm{D}}_{(13)\mathrm{D},\,(20)\mathrm{S}}\psi((00)\mathrm{S},\ (13)\mathrm{D},\ (20)\mathrm{S};\mathrm{D}M) + c^{(33)\mathrm{D}}_{(13)\mathrm{P},\,(20)\mathrm{D}}\psi((00)\mathrm{S},\ (13)\mathrm{P},\ (20)\mathrm{D};\mathrm{D}M)\\ &+c^{(33)\mathrm{D}}_{(13)\mathrm{D},\,(20)\mathrm{D}}\psi((00)\mathrm{S},\ (13)\mathrm{D},\ (20)\mathrm{D};\mathrm{D}M) + c^{(33)\mathrm{D}}_{(13)\mathrm{F},\,(20)\mathrm{D}}\psi((00)\mathrm{S},\ (13)\mathrm{F},\ (20)\mathrm{D};\mathrm{D}M)\\ &+c^{(33)\mathrm{D}}_{(13)\mathrm{G},\,(20)\mathrm{D}}\psi((00)\mathrm{S},\ (13)\mathrm{G},\ (20)\mathrm{D};\mathrm{D}M).\end{aligned} \tag{46}$$

The absolute values of the f.p.c. in this linear combination are respectively $\sqrt{\frac{10}{21}}$, $\sqrt{\frac{2}{5}}$, $\sqrt{\frac{10}{147}}$, $\sqrt{\frac{1}{210}}$ and $\sqrt{\frac{5}{98}}$.

This work is part of the research programme of the "Stichting voor Fundamenteel Onderzoek der Materie" (F.O.M.), which is financially supported by the "Nederlandse Organisatie voor Zuiver Wetenschappelijk Onderzoek" (Z.W.O.). The author is indebted to Dr. J. A. M. Cox for his constant help and many valuable criticisms.

Appendix 1

Consider the direct product of spaces

$$(0)^{\nu_0}[f]_0(r)_0 \times (1)^{\nu_1}[f]_1(r)_1 \times (2)^{\nu_2}[f]_2(r)_2 \times \ldots . \tag{A.1}$$

In this appendix we will make use of the symbol (r) besides $[f]$. Each space $(i)^{\nu_i}[f]_i(r)_i$ is a direct sum of $(\lambda\mu)$ spaces. Therefore we may reduce the beforementioned direct product to a direct sum of $(\lambda\mu)$ spaces, corresponding to irreducible representations of U_3. An arbitrary $(\lambda\mu)$ space occurring in the direct sum is denoted by

$$(0)^{\nu_0}[f]_0(r)_0,\ (1)^{\nu_1}[f]_1(r)_1, \ldots ;\ (\lambda\mu). \tag{A.2}$$

We can find with the help of this space one with a definite total symmetry $[f](r)$ by taking a certain linear combination of spaces that result from the unsymmetrized $(\lambda\mu)$ space by exchange of the particles. S_A commutes with $[U_3]^A$. As a consequence, the linear combination either vanishes or is a $(\lambda\mu)$ space again. Next we will see, in what cases the linear combination vanishes. Each permutation P of S_A may be written as a product of a so-called regular permutation [6]) P_R and a permutation $P_{\nu_0}P_{\nu_1}P_{\nu_2}\ldots$, where P_{ν_i} is a permutation of the ν_i particles in the $N = i$ shell. The permutations $P_{\nu_0}P_{\nu_1}P_{\nu_2}\ldots$ constitute a subgroup of S_A, viz. the direct product of the symmetric groups S_{ν_0}, S_{ν_1}, S_{ν_2}, ... belonging to the different shells. We consider the linear combination of permutations P, which when operating on a general function leads to a function with a certain symmetry $[f](r)$. It can be written as a product of a certain linear combination of permutations $P_{\nu_0}P_{\nu_1}P_{\nu_2}\ldots$ and a linear combination of permutations P_R. The first factor gives a non-vanishing result only in the case of certain symmetries $[f]$. An irreducible representation $[f]$ of S_A is in general a reducible representation of $S_{\nu_0} \times S_{\nu_1} \times S_{\nu_2} \times \ldots$ and may with the help e.g. of Murnaghan's tables [5]) be reduced to a direct sum of irreducible representations of $S_{\nu_0} \times S_{\nu_1} \times S_{\nu_2} \times \ldots .$. If $[f]_0 \times [f]_1 \times [f]_2 \times \ldots$ is among the latter, it may be shown that $[f]$ is one of the symmetries for which the symmetrization of the unsymmetrized $(\lambda\mu)$ space leads to a non-vanishing result, viz. to a space with the same symmetries $[f]_0, [f]_1, [f]_2, \ldots$ in the several shells. The linear combination of regular permutations P_R always gives a non-vanishing result, because spaces resulting from each other by a regular permutation are orthogonal.

As a consequence, all of the $(\lambda\mu)$ spaces (A.2) may be combined with the same set of symmetries $[f](r)$. Therefore each of the possible $[f](r)$ spaces contains the same set of $(\lambda\mu)$ spaces. This set may be obtained by reduction of the direct product $\prod_i \sum (\lambda\mu)_i$, where we write $\sum(\lambda\mu)_i$ for the direct sum of formula (6).

Appendix 2

The matrix-element $\langle(\lambda'_1\,0)(\lambda'_2 0);\,(\lambda\mu)\alpha LM|H_{\text{coll}}|(\lambda_1 0)(\lambda_2 0);(\lambda\mu)\alpha LM\rangle$ is independent of αLM. Therefore we may use for this matrix-element instead of the set αLM the set of quantum numbers $\varepsilon\Lambda K$, introduced by Elliott [3]). These quantum numbers also define an orthogonal basis in a $(\lambda\mu)$ space. By definition ε is the eigenvalue of one of the infinitesimal operators of U_3, mentioned by Elliott [2]), whereas Λ is an integral or half-integral quantum number labeling the irreducible representations of a subgroup R'_3 of U_3, which is isomorphic to the group R_3 of three-dimensional rotations. The states belonging to each representation are labeled like angular momentum substates by the eigenvalue K of one of the infinitesimal operators of R'_3, which may therefore take the values

$$K = \Lambda, \Lambda-1, \Lambda-2, \ldots, -\Lambda. \tag{A.3}$$

It should be noted that the quantum number K according to this definition differs from that of Elliott by a factor 2. For details concerning the quantum numbers ε, Λ and K we refer to Elliott [3]).

The direct product $(\lambda_1 0)\times(\lambda_2 0)$ gives the direct sum $(\lambda_1+\lambda_2, 0)+(\lambda_1+\lambda_2-2, 1)+(\lambda_1+\lambda_2-4, 2)+\ldots+(\lambda_1-\lambda_2, \lambda_2)$, in case $\lambda_1 > \lambda_2$. Consequently, in the notation of Elliott, $\varepsilon_{\min}$ is equal to $\varepsilon_{1\,\min}+\varepsilon_{2\,\min}$, for each $(\lambda\mu)$ resulting from $(\lambda_1 0)\times(\lambda_2 0)$. This means that one can construct the states $|(\lambda\mu)\varepsilon_{\min}\Lambda K\rangle$ from states $|(\lambda_1 0)\varepsilon_1\Lambda_1 K_1\rangle$ and $|(\lambda_2 0)\varepsilon_2\Lambda_2 K_2\rangle$ with $\varepsilon_1 = \varepsilon_{1\,\min}$ and $\varepsilon_2 = \varepsilon_{3\,\min}$ only. As in any $(\lambda\mu)$ space the value $\varepsilon_{\min}$ for ε is compatible only with $\Lambda = \frac{1}{2}\lambda$, it follows that apart from a phase-factor $|(\lambda\mu)\varepsilon_{\min}\Lambda K\rangle$ is equal to

$$\sum_{K_1 K_2} |(\lambda_1 0)\varepsilon_{1\,\min}\Lambda_1 K_1\rangle|(\lambda_2 0)\varepsilon_{2\,\min}\Lambda_2 K_2\rangle\times\langle\Lambda_1 K_1\Lambda_2 K_2|\Lambda_1\Lambda_2\Lambda K\rangle, \tag{A.4}$$

where $\langle\Lambda_1 K_1\Lambda_2 K_2|\Lambda_1\Lambda_2\Lambda K\rangle$ is a Clebsch-Gordan coefficient. A particular choice for the phase-factor will be made presently. We will calculate the matrix-element of H_{coll} for such a state $|(\lambda\mu)\varepsilon_{\min}\Lambda K\rangle$, which has a simple expression in single particle states. H_{coll} may be written as $\frac{1}{4}\{(\sum_i \mathbf{c}_i^\dagger)(\sum_i \mathbf{c}_i)+(\sum_i \mathbf{c}_i)(\sum_i \mathbf{c}_i^\dagger)\}$ in terms of the vector-operators $\mathbf{c}_i^\dagger$ and $\mathbf{c}_i$, standing for creation and annihilation operators for particle i of harmonic-oscillator quanta in the directions x, y and z. As already noticed in formula (11), H_{coll} consists of two terms, namely

$$\tfrac{1}{2}H_0+\tfrac{1}{2}(\mathbf{p}_1\cdot\mathbf{p}_2+\mathbf{r}_1\cdot\mathbf{r}_2) = \tfrac{1}{2}H_0+\tfrac{1}{4}(\mathbf{c}_1^\dagger\cdot\mathbf{c}_2+\mathbf{c}_2^\dagger\cdot\mathbf{c}_1), \tag{A.5}$$

in the case of two particles. The contribution of the first term to the matrix-element of H_{coll} is equal to

$$\tfrac{1}{2}\{(\lambda_1+\tfrac{3}{2})+(\lambda_2+\tfrac{3}{2})\}\delta_{\lambda'_1,\lambda_1}\delta_{\lambda'_2,\lambda_2}). \tag{A.6}$$

The second term gives a non-vanishing contribution only if $\lambda'_1 = \lambda_1 \pm 1$ and $\lambda'_2 = \lambda_2 \mp 1$. Without loss of generality we will treat the case $\lambda'_1 = \lambda_1+1$, $\lambda'_2 = \lambda_2-1$. Then only $\mathbf{c}_1^\dagger \cdot \mathbf{c}_2$ has a non-vanishing matrix-element. Introducing the operators

$$c_{i+}^\dagger = c_{ix}^\dagger + ic_{iy}^\dagger,\ c_{i-}^\dagger = c_{ix}^\dagger - ic_{iy}^\dagger,\ c_{i+} = c_{ix} - ic_{iy} \quad \text{and} \quad c_{i-} = c_{ix} + ic_{iy}, \tag{A.7}$$

we may write $\mathbf{c}_1^\dagger \cdot \mathbf{c}_2$ as

$$c_{1x}^\dagger c_{2x} + c_{1y}^\dagger c_{2y} + c_{1z}^\dagger c_{2z} = c_{1+}^\dagger c_{2+} + c_{1-}^\dagger c_{2-} + c_{1z}^\dagger c_{2z}. \tag{A.8}$$

It is easily shown, that under the group R'_3 the operators $c_{iz}^\dagger$ and c_{iz} transform as scalars. Under the same group $c_{i+}^\dagger$ and $c_{i-}^\dagger$ are the components of an irreducible tensor-operator with $\Lambda = \frac{1}{2}$ and $K = \frac{1}{2}$ and $-\frac{1}{2}$ respectively. In the same way c_{i-} and c_{i+} are the components of an irreducible tensor-operator, also with $\Lambda = \frac{1}{2}$ and $K = \frac{1}{2}$ and $-\frac{1}{2}$ respectively. Therefore $c_{1z}^\dagger c_{2z}$ does not contribute to the matrix-element

$$\langle(\lambda_1+1,\,0)(\lambda_2-1,\,0);\,(\lambda\mu)\varepsilon_{\min}\Lambda K|\mathbf{c}_1^\dagger \cdot \mathbf{c}_2|(\lambda,\,0)(\lambda_2 0);\,(\lambda\mu)\varepsilon_{\min}\Lambda K\rangle. \tag{A.9}$$

Furthermore, the contribution of $c_{1+}^\dagger c_{2+} + c_{1-}^\dagger c_{2-}$ may be derived with the help of the reduced matrix-element [7]) of the tensor-operator of which $c_+^\dagger$ and $c_-^\dagger$ are components, viz.

$$\langle(\lambda+1,\,0),\,\varepsilon'_{\min} = -\lambda-1,\,\Lambda' = \tfrac{1}{2}(\lambda+1)||c_\pm^\dagger||(\lambda 0),\,\varepsilon_{\min} = -\lambda,\,\Lambda = \tfrac{1}{2}\lambda\rangle$$
$$= \{(\lambda+1)(\lambda+2)\}^{\frac{1}{2}}. \tag{A.10}$$

This matrix-element is positive by an appropriate choice of relative phases of the states $|(\lambda 0)\varepsilon_{\min}\Lambda K\rangle$ for different λ. From this formula follows the reduced matrix-element of the tensor-operator with components c_+ and c_-.

Apart from a phase-factor the matrix-element (A.9) is then equal to

$$(-1)^{\frac{1}{2}(\lambda_1+\lambda_2+2)} \times \begin{Bmatrix} \Lambda & \frac{1}{2}(\lambda_2-1) & \frac{1}{2}(\lambda_1+1) \\ \frac{1}{2} & \frac{1}{2}\lambda_1 & \frac{1}{2}\lambda_2 \end{Bmatrix}$$
$$\times\langle(\lambda_1+1,\,0),\,\varepsilon'_{1\,\min} = -\lambda_1-1,\,\Lambda'_1 = \tfrac{1}{2}(\lambda_1+1)||c_{1\pm}^\dagger||(\lambda_1 0),\,\varepsilon_{1\,\min} = -\lambda_1,\,\Lambda_1 = \tfrac{1}{2}\lambda_1\rangle \tag{A.11}$$
$$\times\langle(\lambda_2-1,\,0),\,\varepsilon'_{2\,\min} = -\lambda_2+1,\,\Lambda'_2 = \tfrac{1}{2}(\lambda_2-1)||c_{2\pm}||(\lambda_2 0),\,\varepsilon_{2\,\min} = -\lambda_2,\,\Lambda_2 = \tfrac{1}{2}\lambda_2\rangle.$$

The expression between braces is a $6j$-symbol [7]). The phase-factor of formula (A.4) will now be given that value which makes the phase-factor of formula (A.11) equal to $(-1)^{\frac{1}{2}(\lambda_1+\lambda_2+2)}$.

Then we find

$$\langle(\lambda_1+1, 0)(\lambda_2-1, 0); (\lambda\mu)\varepsilon_{\min}\Lambda K|\mathbf{c}_1^{\dagger}\cdot\mathbf{c}_2|(\lambda_1 0)(\lambda_2 0); (\lambda\mu)\varepsilon_{\min}\Lambda K\rangle$$
$$= \{(\lambda+\lambda_1-\lambda_2+2)(\lambda+\lambda_2-\lambda_1)\}^{\frac{1}{2}}.$$

By exchanging the roles of particles 1 and 2, we find formula (13).

References

1) J. P. Elliott and T. H. R. Skyrme, Proc. Roy. Soc. A **232** (1955) 561
2) J. P. Elliott, Proc. Roy. Soc. A **245** (1958) 128
3) J. P. Elliott, Proc. Roy. Soc. A **245** (1958) 562
4) J. P. Elliott and A. M. Lane, Handbuch der Physik, Vol. 39 (Springer-Verlag, Berlin, 1957)
5) F. D. Murnaghan, Amer. Journal of Math. **59** (1937) 483
6) E. C. Halbert, Thesis University of Rochester (1956)
7) A. R. Edmonds, Angular momentum in quantum mechanics (Princeton University Press, 1957)

9.A

Nuclear Physics **21** (1960) 526—527; © *North-Holland Publishing Co., Amsterdam*

Not to be reproduced by photoprint or microfilm without written permission from the publisher

A MONTE-CARLO CALCULATION OF THE PRODUCTION SPECTRUM OF MESONS IN JETS

M. MARCU and M. SPÎRCHEZ

Cosmic Ray Laboratory, Institute of Atomic Physics, Bucharest

Received 13 July 1960

Abstract: A sample of 200 values of the momentum of the secondaries in high-energy meson jets has been computed by means of a Monte-Carlo procedure, starting from experimental observed facts such as the Gaussian distribution of log p_T and the isotropy in the emitting centre system. The shape of the spectrum of p-values does not agree with dp/p^2.

In a previous paper [1]) a method has been given for computing the distribution of momenta of mesons created in high energy nuclear collisions. This method was based on experimental facts such as isotropic distribution of angles θ^* in the frame of the emitting centre and a Gaussian distribution of the quantity $x = \ln p_T$, which is invariant with respect to Lorentz transform. The final shape of the spectrum obtained in [1]) cannot be put into simple analytical expressions. The rough approximation given there yields only the general behaviour of the spectrum, which is compatible with a Gaussian shape.

The purpose of the present note is to obtain by means of a Monte-Carlo method the explicit shape of this spectrum, using the same experimental facts as in [1]). Thus we have computed a sample of 200 values of the quantity

$$p = p_T \operatorname{cosec} \theta^*. \tag{1}$$

The p_T values have been chosen imposing the condition that the distribution of x be a Gaussian one [2]) with a mean $\langle x \rangle = 0.25$ and a standard deviation $\sigma = 0.685$ [3]). We have also computed a sample of isotropically distributed angles θ^*, using a table of random digits and normal deviates [4]).

The final distribution led us to the value

$$\bar{p} = 0.34 \pm 0.03 \text{ GeV}, \tag{2}$$

which is in good agreement with the value of ≈ 0.4 GeV required by Ciok *et al.* [5]) for the two-centre model.

The distribution of log p is a very narrow one, as can be seen from fig. 1, and is in good agreement with the results obtained in [1]). The integral distribution (fig. 2) is incompatible with a dp/p^2 shape of this spectrum, shown in fig. 2 by a

straight line of slope −1. A similar bent shape of the integral spectrum has also been observed by Nishikawa [6]).

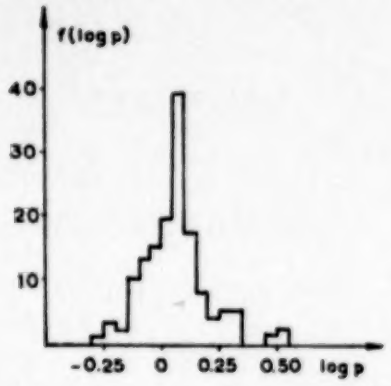

Fig. 1. The distribution function of log p obtained by Monte-Carlo calculation.

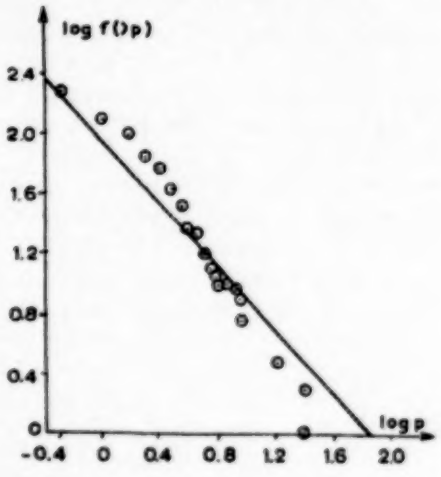

Fig. 2. The integral distribution of the p-spectrum obtained from the Monte-Carlo results.

The authors are indebted to E. M. Friedländer for suggesting the problem and to I. Calogheri for help in the numerical computations.

References

1) E. M. Friedländer, Nuclear Physics **21** (1960) 220
2) G. B. Zhdanov, JETP, **34** (1958) 856
3) E. M. Friedländer, Nuovo Cim. **14** (1959) 796
4) Rand Corporation, A million random digits with 100.000 normal deviates (The Free Press, Glencoe, 1955)
5) P. Ciok, I. Coghen, J. Gierula, R. Hołynsky, A. Jurak, M. Mięsowicz, J. Saniewska and J. Pernegr, Nuovo Cim., **10** (1958) 741
6) K. Nishikawa, J. Phys. Soc. Japan, **14** (1959) 880

10.A

Nuclear Physics **21** (1960) 528; © *North-Holland Publishing Co., Amsterdam*

NEWS ITEM

FIRST ANNUAL REPORT OF O.E.E.C. "DRAGON" HIGH-TEMPERATURE REACTOR PROJECT

The first annual report of the O.E.E.C. high-temperature reactor project (the Dragon Project) was today published by the European Nuclear Energy Agency.

The report covers the period from the start of the project on 1st April, 1959 until 31st March this year. Highlights are the very rapid build-up of project staff, the considerable progress made in the first year (the design of the reactor experiment to be built at A.E.E., Winfrith, United Kingdom, has been finalised and construction work has started), and the negotiation of an agreement with the U. S. Atomic Energy Commission for a full exchange of information between the project and a similar project at Peach Bottom in Pennsylvania.

The report is in three sections of which the first (Introduction and Organisation) surveys briefly the historical background and structure of the Project, and gives a general statement on its present status, including finance.

The remaining two sections cover, in considerable technical detail, the first year's progress in research, development, and reactor design and construction. It is stated in the introduction that this has been done because the Board of Management feels that "this first report should be somewhat more extensive in scope than future annual reports and should be published so that a full picture of the Dragon Project might be made available to a broad public".

Copies of the full report (in English) are available on application to the Public Relations Office of the O.E.E.C. European Nuclear Energy Agency, 38 Boulevard Suchet, Paris 16, France, or to the Public Relations Branch of the UKAEA, 11 Charles II Street, London S.W.1. A French translation will be available later.

2.C:3.A

Nuclear Physics **21** (1960) 529—541; © *North-Holland Publishing Co., Amsterdam*

Not to be reproduced by photoprint or microfilm without written permission from the publisher

RESONANCES IN THE REACTIONS $Si^{28}+p$

J. O. NEWTON †

AERE, Harwell, England

Received 19 August 1960

Abstract: Resonances in the gamma ray yield have been observed at bombarding energies in MeV of 1.653 ± 0.005, 2.09 ± 0.015 and 2.30 ± 0.015. They correspond to energy levels in P^{29} at 4.320 ± 0.015, 4.74 ± 0.022 and 4.94 ± 0.022 MeV with total observed widths of 55.2 ± 2 keV, 14 ± 2 keV and less than 4 keV respectively. Capture gamma radiation proceeding predominantly to the ground state of P^{29} was observed from the two lower resonances. The 4.94 MeV resonance showed only radiation corresponding to that from the first excited state of Si^{29}. The angular distribution of the gamma rays at the 1.65 MeV resonance shows that the 4.320 MeV state has spin $\frac{3}{2}$. Considerations of reduced widths indicate that it has odd parity and is of the "single particle" type. Strong interference effects were observed in the angular distributions at off resonant energies. It seems likely that this interference occurs mainly with the hard sphere part of the direct electric dipole capture process. A cross section of (1.3 ± 0.4) μ barns is obtained for this process at 1.65 MeV bombarding energy on the assumption that all of the interference arises from this source. A value of 1.75 ± 0.35 eV was obtained for the radiative width Γ_γ of the 4.320 MeV state. The angular distribution of the gamma rays at the 2.09 MeV resonance was also shown to be anisotropic but the anisotropy may still be consistent with the previously reported spin of $\frac{1}{2}+$ for the 4.74 MeV state. A value of 0.9 ± 0.4 eV was obtained for the radiative width $(2J+1)\Gamma_\gamma$ of this state.

1. Introduction

This work was originally undertaken in 1954 at the instigation of A. M. Lane to look for states of the single-particle type in light nuclei. Such states are usually characterised by the large values of their reduced widths.

The Q values for proton capture in light nuclei are all greater than 5.5 MeV with the exception of those for the $N = Z$ even nuclei for which they are usually of order 2 MeV. The low Q values for the latter make it possible to study directly the low lying excited states of the nuclei formed by proton capture in these particular cases.

This paper describes some measurements on the reactions $Si^{28}+p$. At the time when these measurements were made there was no information on the excited states of P^{29}. Recently however information on them has been published by a number of groups [1, 2, 3]). The ground state of P^{29} is known to have angular momentum $\frac{1}{2}$ with even parity from the (d, n) reaction on Si^{28} and from the $\log_{10} ft$ value of the β^+ decay of P^{29} [3, 4]). Some of the results given here were reported in the review article of Endt and Braams [4]).

† Present address: The Physical Laboratories, University of Manchester, England.

2. General Method of Measurement

Targets both of natural silicon and of separated Si^{28} in the form of the dioxide were bombarded with protons from the Harwell Van de Graaff generator. They were prepared by evaporation on to 0.13 mm platinum foil; platinum was found to be the most satisfactory target backing from the point of view of background radiation. The gamma rays were observed with a 5.1 cm by 4.4 cm diameter sodium iodide crystal together with a thirty-channel kicksorter.

The background from target impurities was very much higher with the separated Si^{28} targets than with the natural silicon targets. Thus in spite of the numerous strong resonances in the $Si^{29}(p, \gamma)$ and $Si^{30}(p, \gamma)$ reactions observed with the natural silicon targets, it was found better to search for $Si^{28}(p, \gamma)$ resonances with them rather than with the separated targets. The separated targets were used to make sure that the assignments were correct.

For the angular distribution measurements at the 1.65 MeV resonance the proton beam was collimated by a vertical slot of dimensions 2 mm × 7 mm. The counter was initially set up to rotate as accurately as possible in the horizontal plane about the target as centre; the distance from the front of the crystal to the target was 9.5 cm. In the measurements of the variation of anisotropy with bombarding energy and of the angular distribution at the 2.09 MeV resonance the distance to the front of the counter was 4.2 cm. In all cases the apparatus was calibrated by measuring the angular distribution of the 6.1 MeV gamma rays from the 340 keV resonance of the reaction $F^{19}(p\alpha\gamma)O^{16}$. This angular distribution is known to be isotropic [5]).

For the measurements of the absolute yield of the gamma rays it was necessary to estimate a value for the overall detection efficiency of the NaI crystal. This was done by a method of graphical integration taking into account the geometry of the system and the published absorption coefficients for gamma radiation in sodium iodide [6]). In the case of high energy gamma rays, about 4.3 MeV in this case, there is some difficulty in assessing the correct shape of the pulse height spectrum down to zero pulse height. The pulse height spectrum consists of three peaks, corresponding to the full energy of the gamma ray and to the full energy less that due to the escape of one and two annihilation quanta, and a low energy tail. In this case it was assumed that the tail was flat down to 0 eV. The 4.47 MeV gamma ray of C^{12} derived from a Po-Be source was a useful standard for these considerations.

This method for measuring the overall gamma ray detection efficiency was checked by measuring the yield in the same geometry with (a) a Co^{60} source (1.17 + 1.33 MeV) whose strength had been measured by the coincidence method and (b) the 6.1 MeV gamma rays from a thick target of calcium fluoride bombarded with protons exciting the 340 keV resonance in the reaction $F^{19}(p, \alpha\gamma)O^{16}$. The yield per proton of the 6.1 MeV gamma rays for this resonance has been

given by Chao, Tollestrup, Fowler and Lauritsen [7]). They in fact give two values for this quantity, one derived from direct measurements on the gamma rays with Geiger counters, and the other, 12 % lower, from measurements on the alpha group leading to the 6.1 MeV state in O^{16}. The values which we obtained with the Co^{60} gamma rays lay within 10 % of those expected but those with the 6.1 MeV gamma rays varied from approximately the expected value to 30 % less than this. This appeared to be mainly due to target difficulties; the yield from a given target showed a rapid initial fall off with bombarding time and not all targets gave the same initial results. The reason for this was not clear. In view of this it is felt that the standard error on the total gamma ray yield can only be quoted as $\pm$ 20 %.

3. Experimental Results

In the range of bombarding energy from 1.0 to 2.5 MeV, three resonances which could be assigned to the reactions $Si^{28}+p$ were observed. These occurred at bombarding energies in MeV of 1.653 ± 0.005, 2.09 ± 0.015 and 2.30 ± 0.015. They correspond to levels in P^{29} at 4.320 ± 0.015, 4.74 ± 0.02 and 4.94 ± 0.02 MeV if we assume that the Q value of the $Si^{28}(p, \gamma)P^{29}$ reaction is 2.724 ± 0.015 MeV [8]). Most of the work reported in this paper was on the 1.65 MeV resonance.

3.1. THE 1.65 MeV RESONANCE

(a) *Mode of decay.* At this resonance a single gamma ray was observed. The energy of this gamma ray at the peak of the resonance was found to be 4.336 ± 0.015 MeV. It was measured relative to that of 4.433 ± 0.005 MeV [9]) for the gamma ray from the first excited state of C^{12}; this gamma ray was derived from a Po-Be source. If we take the binding energy of a proton in P^{29} to be 2.724 ± 0.015 MeV and the measured bombarding energy, a value of 4.320 ± 0.015 MeV is obtained for the energy of the excited state in P^{29}. This value is consistent with the value obtained for the energy of the gamma ray and strongly indicates that the state decays to the ground state of P^{29}. An upper limit of 20 % of the intensity of the ground state transition can be put to any other radiative decay mode of the level provided that at least one of the gamma rays in the cascade has an energy greater than 1 MeV.

(b) *Measurement of widths.* The resonance was found to be broad and three measurements of its width were made, two with natural silicon targets of thickness 45 $\mu g/cm^2$ and 154 $\mu g/cm^2$ and one with a separated target of thickness 100 $\mu g/cm^2$. In the case of the natural silicon targets it was possible to measure directly the target thickness by measuring the excitation function for two narrow resonance at 1.47 and 1.49 MeV which probably arise from (p, γ) reactions in the other silicon isotopes. The measurements were made by observing the yield of the 4.3 MeV gamma ray with the pulse height analyser for a range of bombarding energies. A mean value for the full width at half height of 55.2 ± 2

keV was obtained after correction for target thickness and angular distribution (see subsection 3.2). The shape of the resonance followed the Breit-Wigner form within the errors of measurement down to a value of the cross section which was approximately 1/30th of the maximum value.

Two measurements were made of the partial cross section $\sigma(p,\gamma)$ for gamma ray emission at the peak of the resonance. Targets of thickness 153 $\mu g/cm^2$ and 98 $\mu g/cm^2$ were used and the gamma rays detected in a counter at 12 cm distance. The method of estimating the counter efficiency was given in section 2. The target thicknesses were estimated both by weighing and from measurements on the narrow resonances at 1.47 and 1.49 MeV, surprisingly good agreement being found between these two methods. The range-energy data of Allison and Warshaw [10]) was used in this estimation. If one assumes that the total width of the state Γ is equal to the width for the incident protons Γ_p and much greater than Γ_γ, then Γ_γ can be calculated from the relation

$$\sigma(p,\gamma) = \frac{\lambda^2}{\pi} \frac{2J+1}{(2S+1)(2I+1)} \frac{\Gamma_\gamma}{\Gamma_p},$$

where S, I and J are the spins of the incident nucleon, target nucleus and compound state respectively. The assumptions are almost certain to be well justified in this case. Using the value of $\frac{3}{2}$ for J (see subsection 4.1) a value of 1.75 ± 0.35 eV was obtained for the partial width for gamma ray emission to the ground state.

(c) *Angular distributions.* A careful measurement of the angular distribution of the 4.3 MeV gamma ray was made at the peak of the resonance using a target of natural silicon of thickness 93 $\mu g/cm^2$. The greatest difficulty in these measurements lies in the assessment of the backgrounds under the peaks. Fig. 1(a) shows a typical spectrum of the 4.3 MeV gamma ray. Fortunately the 4.43 MeV gamma ray of C^{12}, which can be obtained virtually without background from a Po-Be source, has very nearly the same energy as the one of interest here. A very good guide to the shape of the 4.3 MeV gamma ray can therefore be obtained and this considerably reduces the freedom in the choice of background. Some idea of the shape of the background can also be obtained by observing the spectrum off resonance. The procedure adopted was to draw two linear 'extreme' backgrounds under the peaks and to take the error in the background estimation as one quarter of the difference in integrated counts between them. This error was then combined with the various statistical errors in the usual way. The estimation of an error by such a method as this is of course to some extent subjective but is probably the best one can do in the circumstances.

In fig. 1(b) the experimental angular distribution is shown plotted against $\cos^2\theta$. The straight line is the least squares fit to the points. It is clear that the points are consistent with an angular distribution of the form $A + B\cos^2\theta$.

The value of $I(0°)/I(90°)$ is 0.432 ± 0.018, where $I(\theta)$ is the intensity at $\theta°$.

Further measurements were made to see whether the angular distribution varied across the resonance. For these measurements the counter had to be moved nearer to the target in order to obtain an adequate yield and discrimination against background from other sources such as the resolving magnet of the machine. A target of natural silicon rather than separated Si^{28} was used because it produced a lower background. At most bombarding energies the

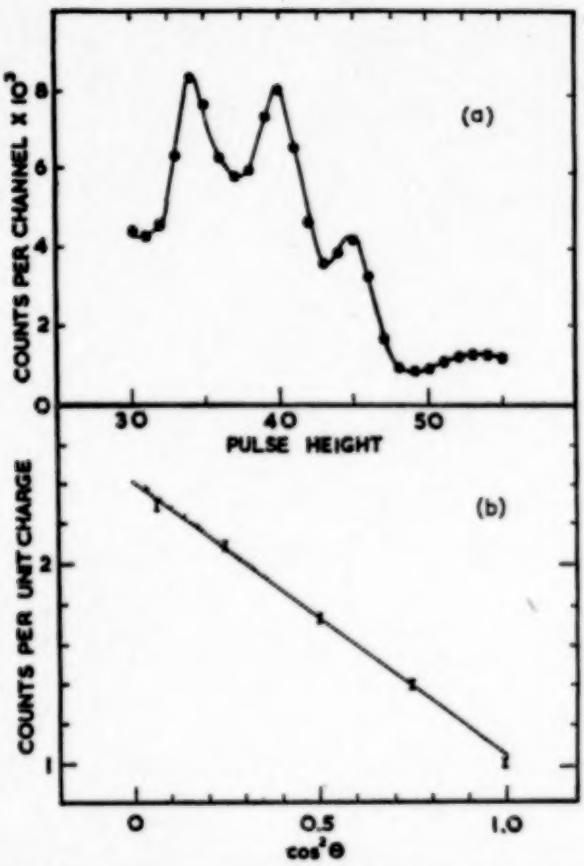

Fig. 1. (a). Typical pulse height spectrum of the 4.33 MeV gamma ray at a bombarding energy of 1.65 MeV. (b). Angular distribution of the 4.33 MeV gamma rays at the peak of the 1.65 MeV resonance. The full line is the least squares fit to the points.

measurements were made at two angles only but for two energies, one on each side of the resonance, complete angular distributions were measured. This was done in order to ascertain whether the interference term causing the variations in angular distributions was an even or an odd function of $\cos\theta$; even and odd functions lead to angular distributions which are symmetrical and asymmetrical respectively about 90°. Unfortunately, owing to the fact that the counter had to be rather close to the target, 120° was the maximum angle which could be obtained.

In these measurements the assessment of background under the 4.3 MeV peak was more difficult than that for the angular distribution at resonance.

This was mainly because the peak to background ratio was much smaller and the counting statistics poorer. In measurements such as these it is necessary to have some consistent way of subtracting off the background. The procedure adopted was as follows. For the complete angular distributions the pulse height spectra for all the angles were summed and extreme backgrounds drawn as for

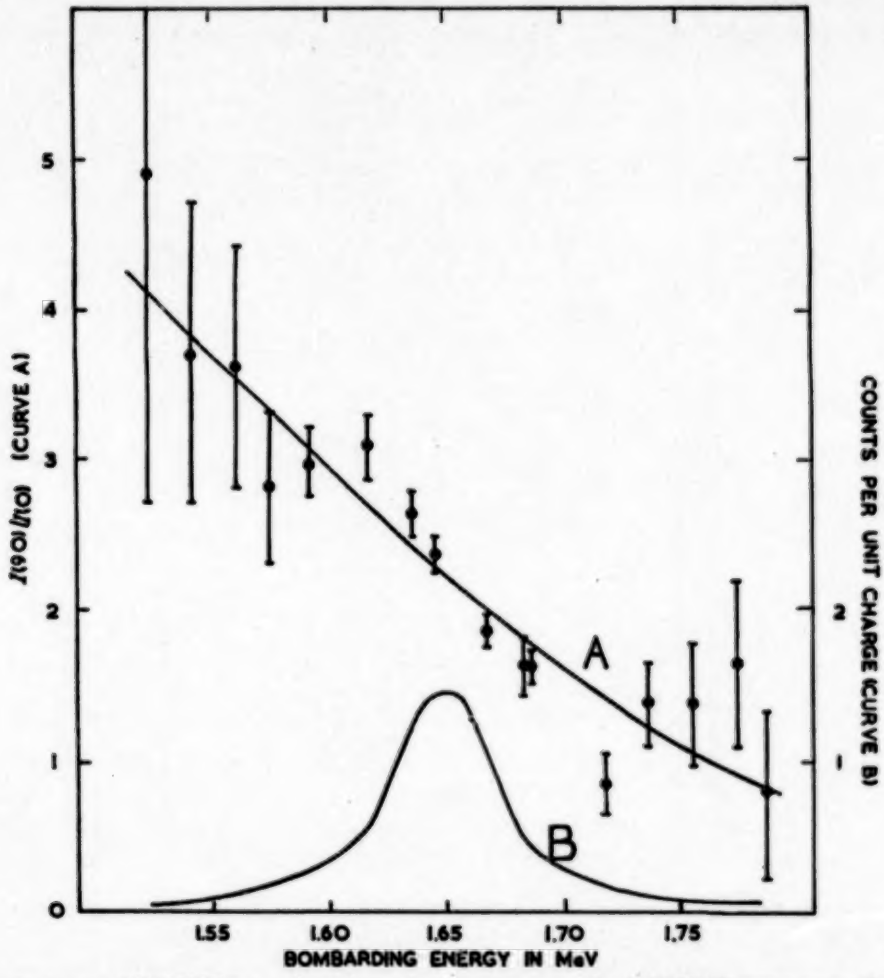

Fig. 2. Anisotropy $I(90)/I(0)$ as a function of energy across the 1.65 MeV resonance. Curve A is a theoretical curve calculated on the assumptions given in the text. Curve B shows the yield at 120° as a function of energy.

the angular distribution at the peak of the resonance; account was taken of the shape of the 4.43 MeV gamma ray of C^{12}. By summing the curves together a curve with good statistics was obtained and this made the shape comparison meaningful. The background count for an individual angle was then taken to have the same ratio to the count in the six or seven channels above the peak as it did in the summed curve. This method assumes of course that the shape of the background does not change with angle; this assumption could be incorrect. In order to minimise any errors arising from the incorrectness of this assumption and from the assumption that the background was linear under the peak it was

usual only to use the full energy peak (and sometimes part of the one-photon escape peak) for the angular distribution measurements. A similar and perhaps slightly more dubious procedure was adopted for the measurements at two angles only. In this case the pairs of curves for three or four adjacent energies were summed in order to assess the background.

In fig. 2 the anisotropy $I(90)/I(0)$ is shown plotted against the bombarding energy. It is seen that there is a very marked variation across the resonance.

In fig. 3 is shown the complete angular distribution taken below the resonance where the anisotropy is relatively stronger. If the interference term causing the variation in anisotropy arises from a state of opposite parity from the 1.65 MeV

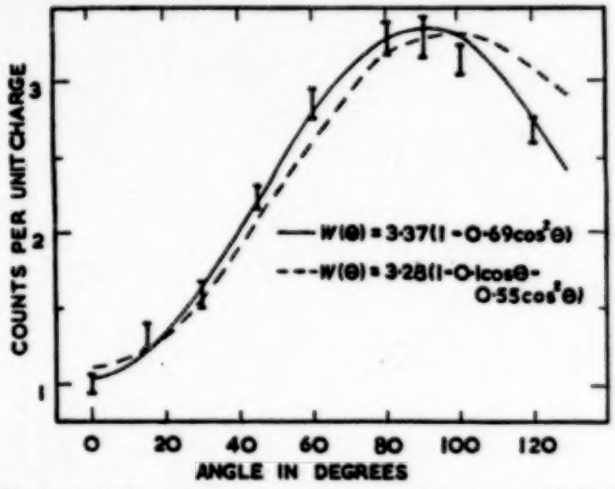

Fig. 3. Angular distribution of the gamma rays at a proton energy of 1.59 MeV. The full line is of the form $1-A\cos^2\theta$ whilst the broken line is of the form $1-B\cos\theta-0.55\cos^2\theta$ (see text).

state, then the angular distribution will have the form $1+A\cos\theta-0.55\cos^2\theta$, where we have allowed for the geometry of the measuring apparatus. If the interference is with a state of the same parity the angular distribution will be of the form $1+B\cos^2\theta$; in both cases it has been assumed that the intensity arising from the other state is negligible. In fig. 3 the full line shows the best fit with a curve of the form $1+A\cos^2\theta$. It can be seen that this curve gives a much better fit than that involving a $\cos\theta$ term, shown by the broken line. It does not seem possible to get a good fit with curves involving $\cos\theta$. This suggests strongly that the interference term arises from a state of the same parity. This conclusion might have been made much more definite if it had been possible to reach greater angles than 120°. This could be done if it were possible to obtain Si^{28} targets free of impurity and if the experiment were performed in a room shielded from radiation arising from the resolving magnet, energy stabilising slits etc. of the machine.

3.2. THE 2.09 MeV RESONANCE

This resonance was observed both with natural silicon and separated Si^{28} targets. The principal mode of decay appeared to be by a gamma ray of energy

4.71±0.02 MeV. The energy calculated for the excited state from the observed bombarding energy is 4.74±0.02 MeV. Thus we may conclude that the state decays mainly to the ground state of P^{29}. The width of the resonance was found, after correcting the target thickness, to be 14±2 keV. This is in agreement with the value of 14 keV reported by Val'ter, Malakhov, Sirokin and Tavarov [1]) and in disagreement with the value of 25 keV reported by Vorona, Olnees, Haeberli and Lewis [2]). No attempt to get an accurate value for the radiative width of the level was made. The value obtained for $(2J+1)\,\Gamma_\gamma$ is 0.9±0.4 eV, where J is the angular momentum of the decaying state.

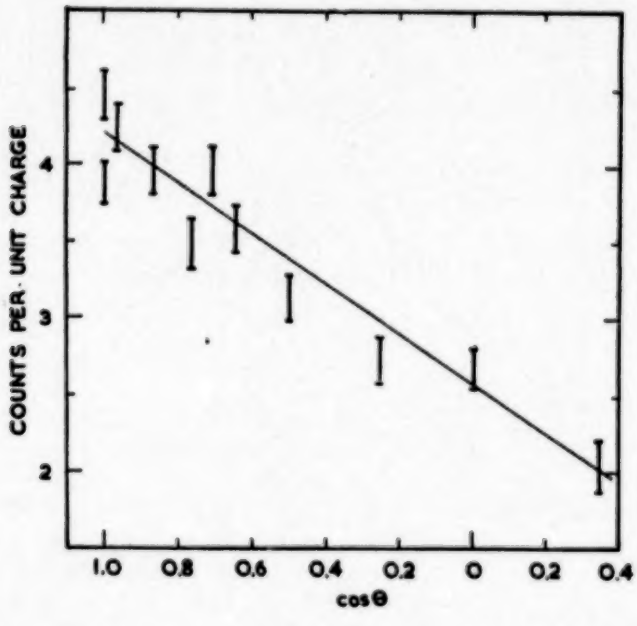

Fig. 4. Angular distribution of the 4.7 MeV gamma rays taken at the peak of the 2.09 MeV resonance.

The angular distribution was measured at the proton energy corresponding to maximum yield. The target of natural silicon had a thickness of about 9 keV to the incident protons. There were again considerable difficulties in background subtraction and the procedure adopted was similar to that used in measuring the angular distributions across the 1.65 MeV resonance. The result is shown in fig. 4 where the results are plotted against cos θ. It can be seen that the points are best fitted by a line of the form $1+(0.65\pm0.1)\cos\theta$. Nevertheless it is difficult to assess the errors in the measurements accurately owing to the difficulty of background subtraction. It therefore would perhaps be unwise to exclude entirely the possibility that the correct angular distribution is of the form $1+A\cos^2\theta$ even though the $1+A\cos\theta$ line still fits the points best when the point at 110° is excluded. It is certainly not possible to say that no term in $\cos^2\theta$ is present.

Owing to the much higher background in the region of the 2.09 MeV resonance as compared with that in the region of the 1.65 MeV resonance it was not practicable to do a large series of angular distribution measurements across the resonance. Two measurements of $I(0°)/I(110°)$ were made at bombarding energies 7 keV below and 10 keV above the peak of the resonance. Values of 2.3 ± 0.4 and 1.7 ± 0.4 respectively were obtained and these are to be compared with the value of 2.1 ± 0.2 obtained at the peak. Thus with the rather large errors of measurement it is not possible to say whether the angular distribution does or does not change across the resonance.

3.3. THE 2.30 MeV RESONANCE

This resonance was observed with both natural silicon and separated Si^{28} targets. The only radiation observed which could be definitely assigned to a reaction with Si^{28} had an energy of 1.767 ± 0.01 MeV. This energy is in good agreement with that of 1.774 MeV [4]) for the first excited state of Si^{28}. Thus the observed radiation is likely to be due to inelastic scattering in Si^{28}. The width of the resonance was observed to be less than 4 keV.

4. Interpretation

4.1. THE 1.65 MeV RESONANCE

Consider first the angular distribution taken at the peak of the resonance. The fact that there is an angular distribution with terms in $\cos^2\theta$ excludes spin $\frac{1}{2}$ for the state and the absence of terms in $\cos^4\theta$ etc. eliminates spin $\frac{5}{2}$ and higher spin. The value of $I(0)/I(90)$ obtained theoretically for spin $\frac{3}{2}$, formation by incident p or d wave protons and decay by dipole emission is 0.40. After correcting for the finite geometry a value of 0.422 is obtained. This is consistent with the experimental value of 0.432 ± 0.018 and hence we may deduce that the state has angular momentum $\frac{3}{2}$.

We may gain further information by considering the reduced width of the state for the incident protons. The incident proton channel is the only major channel available at 1.65 MeV bombarding energy; thus the reduced width γ_p^2 may be calculated from the observed width if the penetrability factor is known. The relation used to calculate γ_p^2 was

$$\Gamma_p = 2kR(F_l^2+G_l^2)^{-1}\gamma_p^2,$$

where k is the wave number of the incident proton in centre-of-mass space, R is the nuclear radius and F_l and G_l are the regular and irregular Coulomb functions for angular momentum l evaluated at the nuclear radius. The quantities required in the evaluation of this relation may be derived from the tables of Bloch *et al.* [11]) or of Sharpe, Gove and Paul [12]). It is convenient to consider a dimensionless reduced width $\Theta^2 = \gamma^2(\hbar^2/MR^2)^{-1}$, where M is the reduced mass of the emitted particle. Then for a given level Θ^2 is most unlikely to exceed

unity [13]) and in fact is unlikely to even approach unity except for a single-particle level i.e. a level in which the emitted nucleon is moving approximately independently of the other nucleons.

The angular distribution does not distinguish between the compound state being formed by $l = 1$ protons or $l = 2$ protons. In table 1 are shown the computed values of Θ^2 for $l = 1$ and 2 protons and for two nuclear radii.

TABLE 1

Values of Θ^2 for protons with $l = 1$ and 2 and two nuclear radii.

l	Nuclear radii	
	$1.465\,A^{\frac{1}{3}}$	$1.465\,(1+A^{\frac{1}{3}})$
1	0.72	0.36
2	11.3	3.6

It can be seen that Θ^2 is greater than unity for $l = 2$ protons and both radii; the actual radius is hardly likely to exceed the larger of the two values taken. On this basis therefore we can say that the formation of the state by $l = 2$ protons is improbable. Hence the excited state is likely to have odd parity. Moreover the fact that the values of Θ^2 are of order unity for $l = 1$ protons and both radii suggests strongly that the excited state in P^{29} is a "single-proton state".

The observed radiation width leads to a value for $|M|^2$, the ratio of observed to single-particle (Weisskopf) transition probabilities, of $(2.1 \pm 0.2) \times 10^{-2}$. This value is close to the average value of $|M|^2$ for E1 transitions in light nuclei.

The ground state of P^{29}, which is known to have angular momentum $\frac{1}{2}$ with even parity, might be expected to approximate to the shell model configuration $(1d_{\frac{5}{2}})^6(2s_{\frac{1}{2}})$ for the protons. Thus energy levels having approximately single-particle character with angular momentum $\frac{3}{2}^-$ and $\frac{1}{2}^-$ corresponding to the shell model states $2p_{\frac{3}{2}}$ and $2p_{\frac{1}{2}}$ would be expected in P^{29} at moderate excitation energies. It seems plausible that the 4.32 MeV level is to be identified with the $2p_{\frac{3}{2}}$ shell model state. The level corresponding to the $2p_{\frac{1}{2}}$ state might be expected to have an energy of order 1 MeV higher than that of the $2p_{\frac{3}{2}}$ state and to have reduced widths of the same order of magnitude as those for the $2p_{\frac{3}{2}}$ state. In fact Vorona *et al.* [2]) have reported a resonance at about 2.9 MeV proton energy corresponding to an excitation of 5.5 MeV in P^{29}. This has a width of about 600 keV and may well correspond to the $2p_{\frac{1}{2}}$ state.

It is interesting to consider the origin of the strong interference terms which come into the gamma ray angular distributions off resonance. It is likely, as explained in subsection 3.1(c), that this interference arises largely from processes involving ingoing and outgoing waves of the same parity as those required in the formation and decay of the 4.32 MeV level. Two processes seem

most likely. These are (a) interference with the tail of the $2p_{\frac{1}{2}}$ state, and (b) interference with the hard sphere part of the direct capture reaction involving incident p wave protons and emission of electric dipole gamma rays.

A number of measurements have been made on the hard sphere part of the process of direct proton capture in various nuclei and these suggest an order of magnitude of 10 P μb for the total cross section, where P is the penetrability factor for the incident protons (e.g. Meyerhoff, Tanner and Hudson [14]). This rough estimate gives a value of about 6×10^{-7} b for the hard sphere direct capture cross section at a bombarding energy of 1.65 MeV. If one assumes for the $2p_{\frac{1}{2}}$ level (*a*) a simple one-level Breit-Wigner formula for the shape, (*b*) that the reduced proton and gamma-ray widths are the same as those for the $2p_{\frac{3}{2}}$ level and (*c*) that its resonance energy is 1 MeV higher than that of the $2p_{\frac{3}{2}}$ level, one obtains a rough estimate for the (p, γ) cross section due to the tail of the $2p_{\frac{1}{2}}$ level at 1.65 MeV bombarding energy of 3×10^{-8} barns. From these estimates it appears that the hard sphere direct capture process is likely to be the most important process of the two. However, since the amplitudes rather than the intensities of these processes are of importance in interference effects they may both produce significant effects. The variations of anisotropy with energy arising from these two particular cases are not distinguishable from these experimental results.

It can be shown that the angular distribution arising from the resonant process and the hard sphere direct capture process is given by the following expression if one assumes that no spin flip takes place in hard sphere direct capture:

$$W(\theta) = (3\sin^2\theta+2)+24z\left[\sqrt{\tfrac{2}{3}}\frac{\Delta E}{\Gamma}\cos\delta+\sqrt{\tfrac{1}{6}}\sin\delta\right]\sin^2\theta + 24z^2\left[\left(\frac{\Delta E}{\Gamma}\right)^2+\tfrac{1}{4}\right]\sin^2\theta, \tag{1}$$

where z^2 is the intensity of the hard sphere direct relative to that of the resonant process at resonance, δ is the phase difference between the two processes at energies well above the resonance, Γ is the width of the resonance and $\Delta E = E-E_r$ is the difference between the bombarding and resonant energies.

Absence of spin flip for the hard sphere part of the direct capture cross section seems plausible; it also seems to be in accord with the limited experimental information on angular distributions in other cases of hard sphere direct capture. From this expression, the observed variation of anisotropy across the resonance and the assumption that all the interference arises from the hard sphere direct capture process, it is possible to deduce that the cross section for the latter is (1.3 ± 0.4) μb at 1.65 MeV bombarding energy. The phase difference δ has to be taken to be 180° with an uncertainty of about $\pm$ 20°. This value for the cross section is in fairly good accord with the rough estimate of 0.6 μb

obtained above. The full line in fig. 2 shows the variation of anisotropy calculated from (1) with the values above.

It can be shown that if the interference arises entirely from the tail of the $2p_{\frac{1}{2}}$ level then the angular distribution is given by the expression

$$W(\theta) = (3\sin^2\theta+2)+8z\frac{\Delta E}{\Gamma}(3\cos^2\theta-1)+32z^2\left[\left(\frac{\Delta E}{\Gamma}\right)^2+\tfrac{1}{4}\right], \qquad (2)$$

where z^2 is the intensity of the $2p_{\frac{1}{2}}$ level relative to that of the $2p_{\frac{3}{2}}$ level at resonance and ΔE and Γ have the same meaning as in eq. (1). The relative amplitude z is a real quantity which can be positive or negative; to fit the experimental data it has to be taken to be positive. It will of course very slowly across the resonance and this was taken into account by assuming a simple Breit-Wigner single-level formula. With the assumptions listed above for the properties of the $2p_{\frac{1}{2}}$ state and the assumption that all of the interference arises from it a cross section of (0.26 ± 0.06) μb for the excitation of the $2p_{\frac{1}{2}}$ level at 1.65 MeV is obtained. This value is much higher than that of 0.03 μb estimated above. It is not easy to see how the value of 0.03 μb can be increased very much. Thus it appears that the interference cannot arise solely from the tail of the $2p_{\frac{1}{2}}$ resonance and in fact is likely to arise largely from the hard sphere part of the direct capture process. If, however, the cross section for excitation of the $2p_{\frac{1}{2}}$ tail is as much as 0.03 μb then the cross section for the hard sphere part of the direct reaction is reduced to (0.7 ± 0.4) μb.

4.2. THE 2.09 MeV RESONANCE

The 2.09 MeV resonance has been reported to be $\frac{1}{2}+$ by Vorona *et al.* [2]) though it was also indicated to be "complex" by Val'ter *et al.* [1]). The angular distribution of the gamma rays was observed to be anisotropic in the present work but if it does indeed contain no higher powers of $\cos\theta$ than the first, then this result can be consistent with the $\frac{1}{2}+$ assignment. The anisotropy could perhaps arise from interference with the tails of the $\frac{3}{2}-$ and $\frac{1}{2}-$ levels, though it seems rather difficult to get quantitative agreement on these assumptions. In view of the uncertainties in the data it does not seem worth while to pursue this point at present.

On the assumption that $r_0 = 1.46\times10^{-13}$ cm and that the state is $\frac{1}{2}+$, the reduced proton width is given by $\Theta^2 = 0.07\pm0.01$. This is considerably lower than unity and indicates that the state is not of predominantly single-particle character. The observed value of 0.9 ± 0.4 eV for $(2J+1)\,\Gamma_\gamma$ leads to a value for $|M|^2$, the ratio of observed to single-particle transition probabilities (Weisskopf) of 0.2 ± 0.1 on the assumption of $J=\frac{1}{2}+$. This is close to the average value of this quantity for M1 transitions in light nuclei.

I should like to thank A. M. Lane for suggesting that this problem might be of interest and for comments.

References

1) A. K. Val'ter, I. Ya. Malakhov, P. V. Sorokin and Ya. Tarenov, Izvest. Akad. Nauk SSSR, Ser. Fiz. **22** (1958) 871
2) J. Vorona, J. W. Olnees, W. Haeberli and H. W. Lewis, Bull. Am. Phys. Soc. **2** no. 1 (1959)
3) J. M. Calvert, A. A. Jaffe and E. E. Maslin, Proc. Phys. Soc. A **70** (1957) 78
4) P. M. Endt and C. M. Braams, Revs. Mod. Phys. **29** (1957) 683
5) S. Devons and M. G. N. Hine, Proc. Roy. Soc. A **199** (1949) 56
6) R. L. Caldwell and S. E. Turner, Nucleonics **12** no. 12 (1954) 47
7) C. Y. Chao, A. V. Tollestrup, W. A. Fowler and C. C. Lauritsen, Phys. Rev. **79** (1950) 108
8) P. M. Endt and J. C. Kluyver, Revs. Mod. Phys. **26** (1954) 95
9) F. Ajzenberg-Selove and T. Lauritsen, Nuclear Physics **11** (1959) 1
10) S. K. Allison and S. D. Warshaw, Revs. Mod. Phys. **25** (1953) 779
11) I. Bloch, M. H. Hall ,A. A. Broyles, W. G. Bouricius, B. E. Freeman and G. Breit, Revs. Mod. Phys. **23** (1951) 147
12) W. T. Sharpe, H. E. Gove and E. B. Paul, Atomic Energy Canada Ltd. Report AECL **268** (1955)
13) E. Vogt, in Nuclear Reactions (Vol. I), edited by P. M. Endt and M. Demeur (North-Holland Publishing Co., Amsterdam 1959)
14) W. E. Meyerhof, N. W. Tanner and C. M. Hudson, Phys. Rev. **115** (1959) 1227

1.E.2:
1.E.5.

Nuclear Physics **21** (1960) 542—554; © *North-Holland Publishing Co., Amsterdam*
Not to be reproduced by photoprint or microfilm without written permission from the publisher

COULOMB ENERGIES OF MIRROR NUCLEI

S. SENGUPTA

Physics Department, Mohsin College, Hooghly, West Bengal, India

Received 25 July 1960

Abstract: A semiclassical expression for Coulomb energies of the mirror nuclei has been derived. The exchange part in the above expression is derived on a statistical model which gives in addition to the usual term, a pairing effect of magnitude 0.33. Inconsistencies in some of the earlier expressions have been pointed out. The radius parameter r_0 from this formula agrees very well with the electron scattering values. A more detailed calculation of the Coulomb energies in LS-coupling shell model with constant values of the parameters within a shell gives least squares fit with an r.m.s. deviation of nearly 4 % in both p and d−s shells. The least squares fit parameters are not satisfactorily reproduced by the harmonic oscillator wave function. The variation of the h.o. strength parameter $\alpha = \sqrt{\omega M/\hbar}$ within p and d−s shell has been studied. A comparison of the r.m.s. radius from Coulomb energies and electron scattering shows a discrepancy of about 8 % in case of Be^9. The vanishing of the second difference of Coulomb energy and its negative value at a shell crossing are found to agree with the detailed shell model calculation.

1. Introduction

Considerable interest has recently been aroused in the Coulomb energy calculation of mirror nuclei [1–7]). Experimental results are now available to an accuracy of 1 % or more. Theoretical calculations are not handicapped by uncertainties of the potential. As energy calculations are not particularly sensitive to the form of wave functions, a reasonable choice of the latter is expected to give fairly accurate results.

A simple calculation of mirror nucleus Coulomb energies on a classical model of uniform charge distribution was previously thought to fit the data well [8]). The small odd-even variation which has a mean value of 0.50 MeV in the p shell and 0.28 MeV in the d shell was, of course, regarded as a specific quantum mechanical effect [8, 9]). This could not be incorporated within the classical calculation because exchange Coulomb energy has no classical analogue. If a uniform density radius R is defined by $R = [\frac{5}{3}\langle r^2\rangle]^{\frac{1}{2}} = r_0 A^{\frac{1}{3}}$, then a value of $r_0 = 1.47 \times 10^{-13}$ cm was determined from mirror nuclei.

The discrepancy of the above value of r_0 with that recently determined from mesic atom X-rays and high energy electron scattering has led to a reexamination of the mirror nuclei formula by many authors [2, 4, 6, 7]). It has been shown that if one takes account of the exchange effect by a separate term subtracted from the classical Coulomb energy then the above discrepancy is removed to a great extent. In sect. 2 we have examined in detail the quantum mechanical

basis of this semiclassical formula. It is shown there that the correction term we are to subtract from the classical Coulomb energy calculated from a uniform or nonuniform charge density consists of two separate terms (1) self energy and (2) exchange energy. Thus a pure self energy interpretation of the correction term [4]) is wrong. Moreover it is pointed out that the self energy term cannot be accounted for in an arbitrary manner [6, 7]). It is to be calculated using the same model of charge distribution as has been assumed for determining the main Coulomb energy. Bethe's [10]) evaluation of the combined correction term, which has been used by Cooper and Henley [2]) and Cherry [7]), is shown to be approximate to the extent that it neglects the pairing effect. If we take account of this term, then the corrected classical Coulomb energy formula not only gives a r_0 much more consistent with the mesic atom and electron scattering data, but also explains the pairing effect exhibited by the mirror nuclei.

In sect. 3 we take up a more detailed calculation for the p and d—s shell nuclei. Carlson and Talmi [1]) and Unna [11]) have calculated mirror nuclei Coulomb energies in the *jj*-coupling shell model. Kofoed-Hansen's [12]) calculations in *LS*-coupling are based on a simplified statistical model. We consider, in detail, the mirror nucleus Coulomb energy in *LS*-coupling. From a study of the least squares fit to the Coulomb energy data it is concluded that the parameters defining the shell model wave functions must vary even within a shell. The same conclusion is arrived at from a study of second differences of Coulomb energy. It is further shown that the vanishing of the second difference observed by Kofoed-Hansen [6]) is really the effect of a major shell crossing and is completely consistent with the detailed shell model calculation. Finally the r.m.s. radius determined from Coulomb energies using harmonic oscillator wave functions is compared with that obtained from an analysis of the electron scattering data assuming a h.o. charge distribution.

2. Semiclassical Expression for Coulomb Energy

Many authors have used the simple classical expression for the Coulomb energy corresponding to a uniform charge distribution, because it leads to a particularly simple estimate of the spatial extension of the charge distribution. Except for the absence of an exchange term such a distribution is consistent with the quantum mechanical statistical model of the nucleus. In the following discussion, however, we consider a more general distribution described by a wave function in the Hartree approximation. For Z protons we write

$$\psi_Z = \frac{1}{\sqrt{Z!}} \sum_P (-)^p P \chi_Z, \tag{1}$$

where

$$\chi_Z = \prod_Z \phi_i,$$

ϕ_i being one of the individual wave functions of the Z protons, and p the parity of the permutation P. We do not consider the neutron wave function as it does not affect the present discussion. For the present we neglect the spin of the proton, the effect of which we shall consider later. Thus ϕ_i is defined by spatial quantum numbers only. The Coulomb energy for Z protons is given by

$$E_C(Z) = \tfrac{1}{2}\sum_{i\neq j} \frac{e^2}{r_{ij}}. \tag{2}$$

The average value of E_C in the state defined by (1) is

$$E_C(Z)=\tfrac{1}{2}\sum_{i\neq j}\int |\phi_i(1)|^2|\phi_j(2)|^2\frac{e^2}{r_{12}}\,dv_1\,dv_2-\tfrac{1}{2}\sum_{i\neq j}\int \bar{\phi}_i(1)\bar{\phi}_j(2)\phi_j(1)\phi_i(2)\frac{e^2}{r_{12}}\,dv_1\,dv_2. \tag{3}$$

Let us introduce ordinary and mixed densities,

$$\rho(1) = \sum_{i=1}^{Z}|\phi_i(1)|^2, \quad \rho(12) = \sum_{i=1}^{Z}\bar{\phi}_i(1)\phi_i(2), \tag{4}$$

where $\rho(11) \equiv \rho(1)$. We add the term

$$E_p = \tfrac{1}{2}\sum_{i=1}^{Z}\int |\phi_i(1)|^2|\phi_i(2)|^2\frac{e^2}{r_{12}}\,dv_1\,dv_2 \tag{5}$$

to both the direct and the exchange integral in eq. (3). Interpreted classically the integral in eq. (5) represents that part of the Coulomb energy which results from the interaction of a charge density $e|\phi_i|^2$ with itself. Therefore it is the self energy of a proton in the ith state. E_p represents the total self energy of the Z protons. Eq. (3) can now be transformed to

$$E_C(Z) = \tfrac{1}{2}\int \rho(1)\rho(2)\frac{e^2}{r_{12}}\,dv_1\,dv_2-\tfrac{1}{2}\int |\rho(12)|^2\frac{e^2}{r_{12}}\,dv_1\,dv_2. \tag{6}$$

The first term above is same as the classical Coulomb energy of a charge distribution defined by $e\rho$ and the second term is a sum of the self energy term (5) and the exchange term in (3). Writing $|\rho(12)|^2$ explicitly,

$$|\rho(12)|^2 = \sum_i |\phi_i(1)|^2|\phi_i(2)|^2+\sum_{i\neq j}\bar{\phi}_i(1)\bar{\phi}_j(2)\phi_j(1)\phi_i(2), \tag{7}$$

we get

$$\int |\rho(12)|^2 dv_1 = \rho(2), \quad \int |\rho(12)|^2 dv_2 = \rho(1). \tag{8}$$

The above result has lead Peaslee [4]) to interpret the second term in (6) as the self energy of the protons. But it may be seen that the relation (8) is valid only because the exchange term in (7) vanishes on integration. Thus (8) reflects the presence of the self energy term only in $|\rho(12)|^2$, while that of the exchange term is suppressed. Cooper and Henley [2]) on the other hand interpreted the second term in (6) as a purely exchange term, overlooking its self energy content. Their equation is thus doubly corrected for self energy and therefore wrong.

The above analysis shows that a classical calculation of the Coulomb energy is quantum mechanically consistent in the Hartree approximation provided we subtract the self energy and the exchange energy from it. It should, however, be clearly pointed out that the self energy term here is not to be interpreted as that of an isolated proton. In the present context self energy is defined by (5) and as such depends on the nature of the charge distribution assumed. If we determine the self energy term arbitrarily [6, 7]) then the consistency of the model is lost.

In all classical calculations of Coulomb energy, the charge distribution is generally taken as spherically symmetric. Strictly this assumption is valid only for protons in a closed shell. If we expand the Coulomb interaction in the usual way [13]) in terms of Legendre polynomials

$$\frac{e^2}{r_{12}} = \sum_{k=0}^{\infty} e^2 \frac{r_<^k}{r_>^{k+1}} P_k(\cos\omega),$$

where ω is the angle between the directions of r_1 and r_2 and substitute this in the first term in (6), then for $k = 0$ the angular part of the integral average out and the resulting spherically symmetrical integral is denoted by the Slater symbol F^0. Thus the assumption of spherically symmetric charge distribution is equivalent to neglecting that part of the Coulomb energy which depend on F^k, $k \geqq 2$. It is known [13]) that the F^k's are decreasing functions of k, so that to a first approximation we can neglect all but F^0. From the detailed calculation of sect. 3, table 2, we see that the spherically symmetric part accounts for about 90 to 95 % of the Coulomb energy difference in mirror nuclei.

Up to now we have been considering protons without spin. If we introduce spin, then ϕ_i will have to be defined by both the spatial and spin quantum numbers and the integration in (3) will include summation over spin coordinates. When this summation is carried out, the first term remains unaffected. The second term is multiplied by $\delta(m_s^i, m_s^j)$. If we now add $i = j$ terms i.e. the self energy terms (5) to both the direct and the exchange integrals and assume that an even number of protons in an incomplete shell is achieved by filling in pairs having the same spatial state and spin states given by $m_s = \pm\frac{1}{2}$, then it is easily seen that for each m_s^i in (3) we get interaction with two states with identical space part and the spin part given by m_s^i and $-m_s^i$. This gives an average contribution of $\frac{1}{2}$ from each space state. Thus for even Z, the effect of proton spin is to multiply the second term in (6) by $\frac{1}{2}$. For Z odd, the situation is the same except when both i and j are the quantum number of the last unpaired proton. In this case the additional factor $\frac{1}{2}$ does not occur and thus we get

$$E_C(Z) = \tfrac{1}{2}\int \rho(1)\rho(2)\frac{e^2}{r_{12}}\,dv_1 dv_2 - \tfrac{1}{4}\int |\rho(12)|^2 \frac{e^2}{r_{12}}\,dv_1 dv_2 - p, \qquad (9)$$

where

$$p = \begin{cases} 0 & \text{for } Z \text{ even,} \\ \frac{1}{4}\int |\phi_Z(1)|^2 |\phi_Z(2)|^2 \frac{e^2}{r_{12}} dv_1 dv_2 & \text{for } Z \text{ odd.} \end{cases}$$

ϕ_Z is the wave function of the last unpaired proton and p is half the self energy of this proton. If we assume the charge distribution of all protons to be the same, and uniform within a sphere of radius R and utilize Bethe's [10]) evaluation on the basis of the statistical model for the second term in (9), we then get

$$E_C(Z) = [0.60Z^2 - 0.460Z^{\frac{4}{3}} - \{1-(-)^Z\}0.30] \frac{e^2}{R}. \tag{10}$$

For the Coulomb energy difference in mirror nuclei one gets

$$\Delta_1(Z) = E_C(Z+1, Z) = [0.60(2Z+1) - 0.613Z^{\frac{2}{3}} - (-)^Z 0.30] \frac{e^2}{R}, \tag{10a}$$

and for the second difference

$$\Delta_2(Z) = \Delta_1(Z) - \Delta_1(Z-1) = \left(1.2 - \frac{0.204}{Z^{\frac{1}{3}}} - (-)^Z 0.60\right) \frac{e^2}{R}. \tag{10b}$$

Eq. (10b) shows the familiar pairing effect for the second difference. The second term in (10b) is a very small correction for all but the first two or three nuclei. Neglecting it and writing (10b) in the usual form $\Delta_2(Z) = a \pm b$ for Z odd (even) we get the pairing effect

$$\frac{\Delta_2(\text{even})}{\Delta_2(\text{odd})} = \frac{a-b}{a+b} = 0.33. \tag{10c}$$

Reference to table 4 shows that this value of the pairing effect represents the average experimental value in both p and d shell much better than either jj-coupling or LS-coupling shell model values. Variations of the individual values and the vanishing of the second difference at shell crossing, however, cannot be explained on the simple model used above.

In the above derivation we have neglected possible coupling between protons in the incomplete shell. But in the approximation of spherical symmetry where we confine ourselves to Slater integrals of zero order only, such couplings will not affect the result. The assumption of a uniform density, however, might be thought to be unrealistic. It is known [2, 14]) that the uniform density gives a lower bound of the Coulomb energy provided we keep $\langle r^2 \rangle$ of the charge distribution fixed. Using a more realistic charge distribution such as a hollow exponential or a modified exponential, the factor in the first term of (10) is changed from 0.60 to 0.65 and 0.67 respectively. The Coulomb energy therefore is not uniquely determined by the r.m.s. radius of the charge distribution. The same is true for the electron scattering results. It may be seen from the analysis of

Meyer-Berkhout *et al.* [15]) that the same electron scattering data for C^{12} can be fit with r.m.s. radii of $2.72f$ and $2.41f$ for two different models of the charge distribution ($f = 10^{-13}$ cm). This fact should particularly be remembered when radius parameters $r_0 = R/A^{\frac{1}{3}}$ deduced from different models are compared. In table 1 we have listed the r_0 values calculated from (10a), along with those calculated by Sood and Green [5]) using a diffuse boundary charge distribution and by Carlson and Talmi [1]) using the *jj*-coupling shell model. Some values of ref. [1]) have been recalculated in view of the modified experimental data †.

TABLE 1

Uniform radius parameter r_0 in units of 10^{-13} cm from (10a). Values in column four from Sood and Green [5]), column five from Carlson and Talmi [1]), in the last column from the electron scattering data [16]).

A	Z	From eq. (10a)	From SG	From CT	From electron scattering
5	2	2.0		2.0	
7	3	1.66	1.55	1.45	1.49
9	4	1.54	1.45	1.54	1.37
11	5	1.38	1.37	1.28	1.33
13	6	1.28	1.33	1.34	
15	7	1.34	1.34	1.28	1.35
17	8	1.34	1.33	1.26	
19	9	1.40	1.35	1.26	
21	10	1.35	1.30	1.26	
23	11	1.34	1.30	1.22	1.33
25	12	1.30	1.29	1.23	
27	13	1.30	1.28	1.20	1.29
29	14	1.28	1.27	1.27	
31	15	1.28	1.27	1.24	1.30
33	16	1.26	1.27	1.25	
35	17	1.28	1.27	1.22	
37	18	1.26	1.27	1.24	
39	19	1.28	1.27	1.22	

The agreement between the results from eq. (10a) and those of Sood and Green is surprisingly good. It may be because of the fact that in a diffuse boundary model the greater part of the charge is distributed uniformly over the nucleus, diffuseness being introduced only at the boundary. The *jj*-coupling values appear to be consistently smaller. The *LS*-coupling values also give almost similar results, so we have not listed them in the table. Electron scattering values of r_0

† We had initially done all our calculations with experimental E_C's compiled by Kofoed-Hansen [6]). But it was realized later that his method of extrapolation of the $n+2$ nuclei data is open to serious objection because of large variation of r_0 in the light nuclei. We have therefore modified his compilation for two mass numbers. For $A = 5$, we take $E_C = 0.80$ MeV, for $A = 9$, $E_C = 1.853$ MeV both obtained from adjusted Q values and binding energy table given by Mattauch *et al.* [17]). For other mass numbers, differences are less than 1 % as is seen from a comparison of the values in ref. [6]) with those of a more recent β-spectroscopic measurement by Wallace and Welch [18]), and we retain the former values.

do not in most cases correspond to any mass number of the mirror nuclei. But they indicate the general trend of variation of r_0 which agrees quite well with that given by equation (10a). The mesic atom r_0 value [2]) determined near or above $A = 50$ is $1.2f$. This value agrees better with the shell model. At present, however, we do not know how far it is permissible to extrapolate the mesic atom value in the mirror nuclei region.

3. *LS*-Coupling Shell Model Calculations

Carlson and Talmi [1]) have made an analysis of the mirror nuclei Coulomb energies in the *jj*-coupling model. Although it is known that the two coupling schemes give broadly similar results in the region of light nuclei, finer differences are known to exist. For example, the pairing effect in the Coulomb energy has significantly different values in the two schemes. We shall consider only proton wave functions. Unna's calculation [11]) with complete neutron proton wave functions show that the differences with Carlson and Talmi's [1]) proton wave function calculations are less than 1 % in all cases. We shall further assume that an even number of l^n protons couple to an ^1S, seniority zero ground state and an odd number to a ^2l, seniority one ground state. For our calculations we shall require three types of interaction energies.

1) *Coulomb interaction in* $(\alpha l)^n$ *configuration*

For our ground state this energy is given by Racah's general formula [1]), in terms of Slater integrals $F^k(\alpha l, \alpha l) = F^k(\alpha l)$. For the special cases of p and d shells we get

$$E_C[(\alpha p)^n, {}^2P \text{ or } {}^1S] = \tfrac{1}{2}n(n-1)F^0(\alpha p) - \{\tfrac{1}{4}n(n-1) - \tfrac{3}{2}[\tfrac{1}{2}n]\}\tfrac{2}{5}F^2(\alpha p), \quad (11)$$

$$E_C[(\alpha d)^n, {}^2D \text{ or } {}^1S] = \tfrac{1}{2}n(n-1)F^0(\alpha d) - \{\tfrac{1}{4}n(n-1) - \tfrac{5}{2}[\tfrac{1}{2}n]\}\tfrac{1}{7}(F^2(\alpha d) + F^4(\alpha d)),$$

where $[\frac{1}{2}n]$ is the largest integer not exceeding $\frac{1}{2}n$.

2) *Coulomb interaction of* $(\alpha l)^n$ *protons with a closed* $(\alpha' l')^{n'}$ *shell*

The formula for the interaction of a single αl-proton with a closed shell is given in Condon and Shortley [13]). As this interaction does not depend on m or m_s, it is easily proved that the interaction for $(\alpha l)^n$ protons will be independent of the coupling among n particles,

$$E_C[(\alpha l)^n; (\alpha' l')^{4l'+2}] = n(4l'+2)[F^0(\alpha l, \alpha' l') - \tfrac{1}{4}\sum_k C_{ll'k}(\alpha l, \alpha' l')], \quad (12)$$

where the coefficients $C_{ll'k}$ are tabulated in Shortley and Fried [19]).

3) *The Coulomb interaction between* $(\alpha l)^n$ *and* $(\alpha' l')^k$ *protons,* k *even*

For the even configuration we assume an ^1S, zero seniority state. From Wigner's angular momentum vector addition formula (see Racah [20])) we can

easily construct the $(\alpha' l')^2\ {}^1S$ wave function

$$\psi[(\alpha' l')^2\ {}^1S] = \frac{1}{(2l'+1)^{\frac{1}{2}}} \sum_{-l'}^{l'} (-)^{l'-m}\{m^+, -m^-\}, \tag{13a}$$

where $\{m^+, -m^-\}$ is a two particle normalized antisymmetric wave function. For $(\alpha' l')^k$, where $k = 2y$, we can generalize

$$\psi[(\alpha' l')^{2y}\ {}^1S] = \frac{1}{\binom{2l'+1}{y}^{\frac{1}{2}}} \sum_{m_1>m_2>m_3\cdots} (-)^{yl'-m_1-m_2\cdots}\{m_1^+ - m_1^-, m_2^+ - m_2^-, \ldots..\} \tag{13b}$$

The summation extends over the $\binom{2l'+1}{y}$ possible sets $(m_1\, m_2 \ldots m_y)$, which do not violate the antisymmetry condition. By operating with spin and spatial angular momentum operators $S_x+iS_y(=\sum_j(s_{xj}+is_{yj}))$ and L_x+iL_y it can be verified that (13b) is a ${}^1S$ state. That its seniority is zero can also be proved. The seniority operator for two particles is defined by [21])

$$\langle l^2 LM|q_{12}|l^2 LM\rangle = \delta(L, 0)(2l+1).$$

From (13a) we get

$$\langle\{m^+ - m^-\}|q_{12}|\{\mu^+ - \mu^-\}\rangle = (-)^{m+\mu}. \tag{13c}$$

For the $(l')^{2y}$ configuration we get a non vanishing matrix element for q_{12} in only two cases, i.e.
the diagonal element

$$\langle\{m_1^+ - m_1^- \ldots\}\ |q_{12}|\{m_1^+ - m_1^- \ldots\}\rangle = \frac{1}{(2y-1)}, \tag{13d}$$

and the nondiagonal element

$$\left\langle \begin{Bmatrix} m_1^+ - m_1^- \ldots \\ \ldots m_i^+ - m_i^- \ldots \end{Bmatrix} |q_{12}|\{m_1^+ - m_1^- \ldots \mu_j^+ - \mu_j^- \ldots\} \right\rangle = \frac{(-)^{m_i+\mu_j}}{y(2y-1)}. \tag{13d}$$

We can now easily calculate the expectation value of the total seniority operator $Q = \sum_{i>j} q_{ij}$ in the state (13b):

$$\langle Q\rangle = y(2l+2-y). \tag{13e}$$

Comparing with Racah's [21]) general expression for $\langle Q\rangle$ in a l^n-configuration state with seniority v,

$$\langle Q\rangle_{nv} = \tfrac{1}{4}(n-v)(4l+4-n-v),$$

we notice that (13b) has seniority zero. We can now use this wave function to calculate the Coulomb interaction and get,

$$E_C[(\alpha L)^n;\ (\alpha' l')^k\ {}^1S] = nk[F^0(\alpha l, \alpha' l') - \tfrac{1}{4}\sum C_{ll'k} G^k(\alpha l, \alpha' l'). \tag{13}$$

That E_C will be proportional to nk could be more easily proved by using Racah's formula for tensor operators [22]). But then the explicit expression of the constant in terms of Slater integrals could not be obtained.

With the help of the formulae (11) to (13) all Coulomb energy differences for

the p and d—s shells can be written down in terms of nineteen Slater integrals. Some of these occur in fixed combinations and finally we get in six p shell nuclei three parameters and in twelve d—s shell nuclei six parameters. Instead of making specific assumptions about the nuclear wave functions in order to evaluate these parameters we, at first, determine them by a least squares fit of the data. The result is shown in table 2. There are considerable r.m.s. deviations in both p and d—s shells. The r.m.s. deviation is calculated in the usual way by $\{\sum \Delta_i^2/N-k\}^{\frac{1}{2}}$, where Δ_i is the difference between the calculated and the experimental value, N is the number of data and k is the number of parameters. The result is expressed as percentage of the energy width adjusted. Adjusted

TABLE 2

Comparison of experimental Coulomb energies with values from LS-coupling where the parameters are adjusted by a least squares fit. The last column gives the percentage contribution of the spherically symmetric charge to E_C, calculated with h.o. wave functions

A	Z	E_C in MeV (experimental)	E_C in MeV (calculated)	r.m.s. deviation	Percentage r.m.s. deviation	Contribution of sph. sym. charge to E_C in per cent
5	2	0.80	0.861			91
7	3	1.646	1.624			100
9	4	1.853	1.886			90
11	5	2.761	2.649	0.12	4.4	96
13	6	3.006	2.911			90
15	7	3.539	3.674	p-shell		94
17	8	3.550	3.667			90
19	9	4.027	4.105			97
21	10	4.266	4.309			94
23	11	4.841	4.776			97
25	12	5.062	4.965			95
27	13	5.584	5.432			97
29	14	5.749	5.710			85
31	15	6.220	6.181	0.12	3.2	86
33	16	6.360	6.302			94
35	17	6.760	6.769	d—s shell		96
37	18	6.920	6.958			94
39	19	7.294	7.425			96

values of the parameters are given in table 3, along with their values calculated with harmonic oscillator wave functions. Both F^k and G^k are easily evaluated in closed forms by using the formula

$$\int_0^\infty e^{-Sx^2} x^{2\beta-1} \left[\int_0^x e^{-y^2} y^{2\alpha-1} dy\right] dx = \frac{\Gamma(\alpha+\beta)}{\alpha(1+S)^{\alpha+\beta}} {}_2F_1\left(1, \alpha+\beta; \alpha+1; \frac{1}{1+S}\right), \tag{14}$$

and the following values of the hypergeometric functions:

$$
\begin{aligned}
&{}_2F_1(1, b; b; \tfrac{1}{2}) = 2, \qquad {}_2F_1(1, b+1; b; \tfrac{1}{2}) = 2+\frac{2}{b}, \\
&{}_2F_1(1, b+2; b; \tfrac{1}{2}) = 2\,\frac{(b+4)}{b} - \frac{4}{b+1}.
\end{aligned}
\tag{14a}
$$

TABLE 3

Least squares fit values of the parameters in p and d−s shell. Column three gives the same calculated with h.o. wave functions, in terms of the constant $\alpha = \sqrt{\omega M/\hbar}$ where ω is the classical frequency of the oscillator. The last column gives α calculated from adjusted values of the parameters

	Parameters in terms of Slater integrals	adjusted values (MeV)	Values in h.o. model in units of $\alpha e^2/\sqrt{2\pi}$	$\alpha(10^{13}\,\mathrm{cm}^{-1})$
p shell	$X = 2F^0(1s1p) - \frac{1}{3}G^1(1s1p)$	0.8614	3.000	0.500
	$F^0(1p)$	0.5958	1.500	0.692
	$F^2(1p)$	0.4172	0.833	0.872
d−s shell	$A = 2F^0(1d1s) - \frac{1}{5}G^2(1d1s) + 6F^0(1d1p) - \frac{2}{5}G^1(1d1p) - \frac{9}{35}G^3(1d1p)$	3.6527	10.350	0.615
	$B = 2F^0(2s1s) - G^0(2s1s) + 6F^0(2s1p) - G^1(2s1p)$	3.6674	10.135	0.630
	$C = 2F^0(2s1d) - \frac{1}{5}G^2(2s1d)$	0.6807	2.413	0.491
	$F^0(1d)$	0.3559	1.258	0.493
	$F = \frac{1}{7}F^2(1d) + \frac{1}{7}F^4(1d)$	0.0557	0.183	0.529
	$F^0(2s)$	0.4710	1.365	0.601

As has been already pointed out in sect. 2, $F^0(\alpha l, \alpha' l')$ is the same as the Coulomb energy of interaction of two spherically symmetric charge distributions defined by the radial parts of the (αl) and $(\alpha' l')$ wave functions. We have calculated the relative contribution to $E_C(Z+1, Z)$ from spherically symmetric part in each of the mirror pair. The result is in the last column of table 2. It is seen that almost in all cases the contribution is greater than 90 %. This result justifies the semiclassical calculations with spherically symmetric charge distributions.

We notice from table 3 that values of α vary rather widely. Particularly in the p shell, the assumption of constant α appears to be completely wrong. That this is not due to the inadequacy of the one parameter h.o. wave functions is more clearly seen from a study of the second difference $\Delta_2(Z)$ (eq. (10b)). From our calculation, we get

in p shell:
$$
\Delta_2(Z) = \begin{cases} F^0(1p) + \frac{2}{5}F^2(1p) & (Z \text{ odd}), \\ F^0(1p) - \frac{4}{5}F^2(1p) & (Z \text{ even}), \end{cases}
\tag{15}
$$

$$\text{in d shell:} \quad \Delta_2(Z) = \begin{cases} F^0(1d)+\frac{2}{7}F^2(1d)+\frac{2}{7}F^4(1d) & (Z \text{ odd}), \\ F^0(1d)-\frac{3}{7}F^2(1d)-\frac{3}{7}F^4(1d) & (Z \text{ even}). \end{cases} \tag{15a}$$

Table 4 shows the experimental values of $\Delta_2(Z)$ for p and d shells. Some atomic numbers in the d shell do not appear in the table because we encounter s shell mirror transitions in these cases, and $\Delta_2(Z)$ is not given by the pure d shell expression (15a). We have also given in the last two columns the theoretical and experimental values of the pairing effect. We do not see the fact mentioned by Kofoed-Hansen [6]) of vanishing pairing effect near the end of a shell. Such an effect is seen only in those $\Delta_2(Z)$ which do not refer to a single shell. For example, the most striking illustration of this effect is $\Delta_2(8)/\Delta_2(7)$, for which experimental value is $0.002 \approx 0$ within experimental error. Here $\Delta_2(8) = = E_C(9.8)-E_C(8.7)$. The first term refers to the d—s shell while the second refers to p shell. Theoretical calculations in LS-coupling with h.o. wave functions give for this ratio a value -0.022 which agrees with the experiment within the limits of error. A negative value of the second difference is actually noticed for $Z = 20$, at the d → f shell crossing [18]). From table 4 we see that the assump-

TABLE 4

The second difference of Coulomb energy and the pairing effect for p and d shell nuclei

Z	$\Delta_2(Z)$—Expt. (MeV)		Pairing effect (expt.)		Pairing effect (theo.)	
	Z odd	Z even	$\frac{\Delta_2(\text{even})}{\Delta_2(\text{odd})}$	mean	LS	jj
3	0.846					
4		0.206	0.244			
5	0.909		0.227	0.300	0.45	0.60
6		0.245	0.270			$p_{\frac{3}{2}}$
7	0.533		0.460			
11	0.575					
12		0.221	0.384			0.55
13	0.522		0.423			$d_{\frac{5}{2}}$
17	0.400			0.409	0.44	
18		0.160	0.400			0.40
19	0.374		0.428			$d_{\frac{3}{2}}$

tion of a constant value of F^k in a shell is clearly violated. According to (15) and (15a) we expect the entries in the second and the third columns of table 4 to be constant within a shell. Assuming h.o. wave functions again we can determine the values of the oscillator parameter $\alpha = \sqrt{\omega M/\hbar}$ for each nuclei from the corresponding Coulomb energies. The result is shown by the full line graph of fig. 1. jj-coupling values calculated from Carlson and Talmi [1]) are shown by the dotted line. The general trend is seen to be a decrease in α with increasing A.

Apparent irregularities superposed on this general tendency may be understood, to some extent, in terms of the shell structure. In the p shell region $5 \leqq A \leqq 15$, α shows wide fluctuation particularly for $A < 11$. In the d−s shell region $17 \leqq A \leqq 39$, there is a more or less uniform and steady decrease in α. The two small irregularities at $A = 17$, 19 and 29, 31 exactly coincide with the region where the s shell is being filled in preference to the d shell. No $d\frac{3}{2}$ subshell effect is noticeable. *jj*-coupling results runs close to the *LS*-coupling values except in the region $A = 29$, 31.

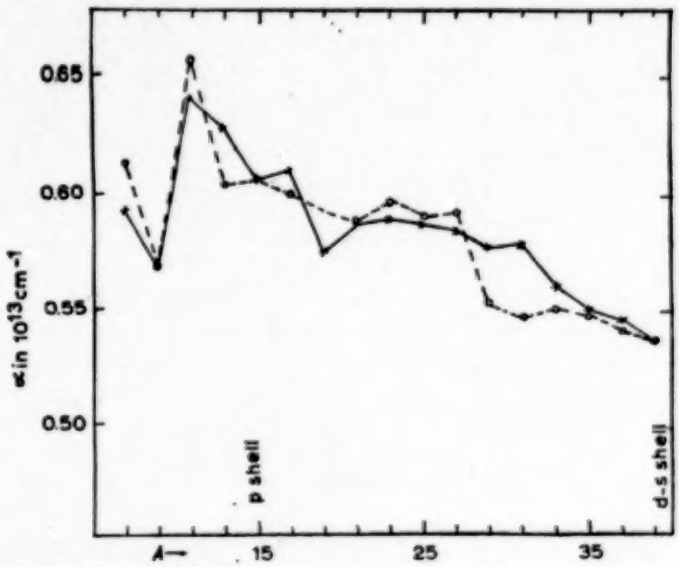

Fig. 1. Variation of the harmonic oscillator parameter $\alpha = \sqrt{\omega M/\hbar}$ in the p and d−s shells. The full line corresponds to *LS*-coupling and the dotted line to *jj*-coupling calculations.

In the h.o. model the r.m.s. radius of the charge distribution of a nucleus is given by

$$\langle r^2 \rangle^{\frac{1}{2}} = \left[\frac{1}{Z} \Sigma \frac{2l+3}{2\alpha^2} \right]^{\frac{1}{2}},$$

where the summation extends over all the protons. While comparing the r.m.s. radius obtained from the Coulomb energy with that from electron scattering, we should remember that the analysis of the electron scattering result should be made on the assumption of a h.o. charge density. Otherwise, the comparison loses much of its significance. In table 5 we have collected four p shell nuclei where such a comparison is possible. The electron scattering r.m.s. radius is taken from Meyer-Berkhout *et al.* [15]) who have analysed the p shell nuclei electron scattering on the basis of various models of charge distribution. In table 5 we notice quite good agreement in three cases. The large discrepancy in the case of Be^9, however, remains unexplained. The mirror decay energy indicates a sharp change in the charge distribution (as is also seen from the large

change in α from fig. 1) as we pass from Be^9 to B^{11}. The electron scattering data, however, do not indicate any such abrupt change.

TABLE 5

Comparison of the r.m.s. radius in units of 10^{-13} cm from electron scattering data and from mirror nuclei Coulomb energies

Nucleus	r.m.s. radius from electron scattering	r.m.s. radius from Coulomb energies
Li^6	2.82	2.91
Be^9	2.26	2.48
B^{11}	2.25	2.26
N^{14}	2.46	2.40

References

1) B. C. Carlson and I. Talmi, Phys. Rev. **96** (1954) 436
2) L. N. Cooper and E. M. Henley, Phys. Rev. **92** (1953) 801
3) B. G. Jancovici, Phys. Rev. **95** (1954) 389
4) D. C. Peaslee, Phys. Rev. **95** (1954) 717
5) P. C. Sood and A. E. S. Green, Nuclear Physics **4** (1958) 274
6) O. Kofoed-Hansen, Rev. Mod. Phys. **30** (1958) 448
7) R. D. Cherry, Phys. Rev. **115** (1959) 1243
8) E. Feenberg and G. Goertzel, Phys. Rev. **70** (1946) 597
9) L. Rosenfeld, Nuclear forces (North Holland Publishing Co., Amsterdam, 1948)
10) H. Bethe, Rev. Mod. Phys. **8** (1936) 82
11) I. Unna, Nuclear Physics **8** (1958) 468
12) O. Kofoed-Hansen, Nuclear Physics **2** (1956/57) 441
13) E. U. Condon and G. H. Shortley, The theory of atomic spectra (Cambridge University Press, N.Y., 1957)
14) F. Bitter and H. Feshback, Phys. Rev. **92** (1953) 837
15) U. Meyer-Berkhout *et al.*, Ann. Phys. **8** (1959) 119
16) R. Hofstadter, Ann. Rev. Nucl. Sc. **7** (1958) 231
17) J. Mattauch *et al.*, Ann. Rev. Nucl. Sc. **6** (1956) 179
18) R. Wallace and J. A. Welch, Phys. Rev. **117** (1960) 1297
19) G. H. Shortley and B. Fried, Phys. Rev. **54** (1938) 739
20) G. Racah, Phys. Rev. **62** (1942) 438
21) G. Racah, Phys. Rev. **63** (1943) 367
22) N. Zeldes, Nuclear Physics **2** (1956/57) 1

2.G

Nuclear Physics **21** (1960) 555—581; © *North-Holland Publishing Co., Amsterdam*

Not to be reproduced by photoprint or microfilm without written permission from the publisher

REACTION MECHANISM STUDIES ON $Si^{28}(d, p)Si^{29}$
(II) Interference Effects

J. A. KUEHNER, E. ALMQVIST and D. A. BROMLEY

Atomic Energy of Canada Limited, Chalk River, Ontario, Canada

Received 1 August 1960

Abstract: Measurements bearing upon the mechanism for the $Si^{28}(d, p)Si^{29}$ reaction, including measurements of differential and total excitation functions and of angular distributions for the proton groups leading to the lowest three states of Si^{29}, have been made for incident deuterons of energy 6—10.7 MeV and for proton detector angles 0°—155°. These measurements have demonstrated a dominant direct interaction amplitude, with, however, a small residual compound system amplitude reflected in interference terms in the cross section. The effects of this interference are displayed by prominent resonance structure in the excitation curves, particularly for proton angles off the forward stripping peak. Upper limits of $< 15\,\%$ and $< 30\,\%$ have been established on the intensity of the compound system contributions to the reaction cross sections to the ground state and first two excited states of Si^{29}, respectively. Angular distributions were found to have similar features over the energy range studied and to display diffraction structure which persists even at large angles. The angular positions of the structural features are well fitted by Butler theory, but with the observed envelope decreasing much less rapidly with angle than does the prediction. Empirically it has been demonstrated that adequate fits are obtained by removing the angle dependence contained in the deuteron factor which appears in the Butler expression for the angular distribution. Reduced widths have been obtained using the methods of Amado and of Bowcock. A comparison of these reduced widths with values obtained by the usual peak-fitting technique has demonstrated that the same relative reduced widths are given by the three methods but that the absolute value obtained using the Amado extrapolation is approximately a factor of two less than that obtained with the other two techniques.

1. Introduction

The great success of simple stripping theory [1]) in interpreting measurements of the nucleon differential and total cross sections and in determining values of the orbital angular momentum transferred by the captured nucleon and reduced widths for both (d, p) and (d, n) reactions has in general been marred by the inability of this theory to correctly predict the details of the measurements and in particular its inability to adequately predict the observed large values for the differential cross sections at large angles. More recently attempts have been made to include refinements to the theory in the form of both Coulomb and nuclear distortion of the incident deuteron wave and the outgoing nucleon wave [2]). These attempts have met with some success in describing some of the data but have been hampered in part by the lack of appropriate measurements bearing on the details of the reaction mechanisms.

In many of the early investigations of (d, p) reactions the principal motivation was that of determining nuclear spectroscopic assignments for the residual states involved: consequently angular distributions rarely were examined at angles removed from the main stripping peaks where other than stripping amplitudes might be expected to play a more significant role. Measurements have in general been carried out at isolated energies determined by the accelerating facilities available, although the cross sections for the reactions $C^{12}(d, p)C^{13}$ [3, 4]), $N^{14}(d, n)O^{15}$ [5, 6, 7]), $O^{16}(d, p)O^{17}$ [8, 9, 10]) and $Ca^{40}(d, p)Ca^{41}$ [11]) have been examined as functions of the incident deuteron energy over restricted ranges. Again, for instrumental reasons, these investigations have been limited to deuteron energies less than 5 MeV, where Coulomb and nuclear forces result in significant distortion of the simple stripping process and greatly complicate any analysis of the data. The results obtained for these reactions can perhaps be summarized by the statement that, while the angular position of the dominant peak of the stripping pattern does not change appreciably as the energy is varied over resonant structure in the excitation curve, the secondary structure does vary rapidly, both in angle and in intensity.

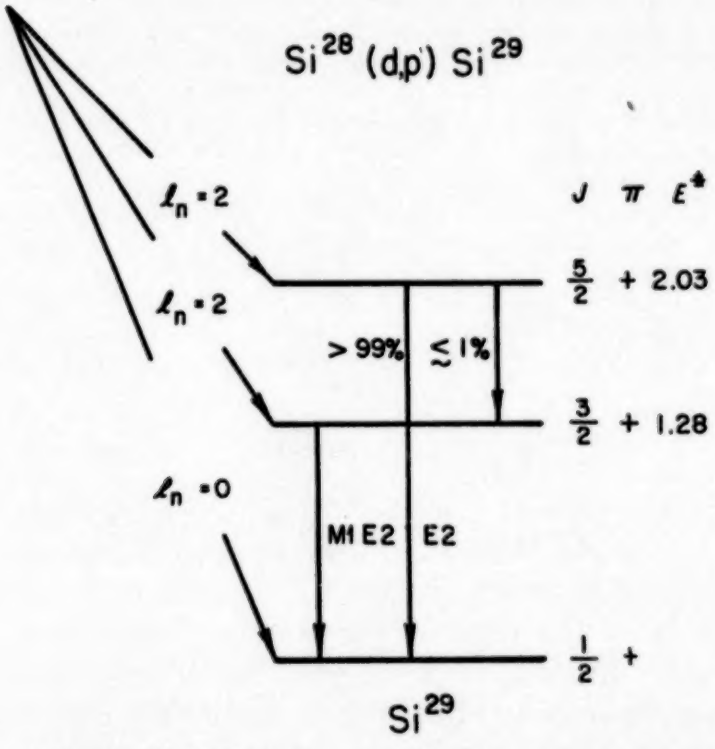

Fig. 1. Level diagram for Si^{29} showing the relevant transitions and assignments.

With the availability of deuteron beams of precisely controlled energy in the energy range below $\approx$ 12 MeV from the tandem accelerator a more detailed study of the dp reaction mechanism becomes possible. This, and a companion paper [12]), present the results of such a study on the $Si^{28}(d, p)Si^{29}$ reactions

involving the ground and first two excited states of Si^{29}. Fig. 1 shows the appropriate assignments as obtained from studies on the $Si^{29}(p, p'\gamma)Si^{29}$ reaction [13]); the multipole mixture for the 1.28 MeV radiation was obtained from gamma radiation linear polarization measurements on this same reaction[14]).

This particular reaction was selected for study for several reasons. Because of the high Q value ($Q_0 = 6.246$ MeV) it permits the study of an $l_n = 0$ and two $l_n = 2$ neutron capture situations, in the latter case with $j_n = l_n \pm \frac{1}{2}$, respectively, under essentially identical kinematic conditions and thus permits more direct study of the non-kinematic features of the mechanism. As well, the deuteron binding energy of 11.759 MeV in P^{30} is not sufficiently high to preclude the possibility of observing resonant effects in the compound system interaction, Another additional reason for the selection of this reaction for study is that the multipolarities and branching in the gamma de-excitation of the residual states is known, facilitating the interpretation of the dpγ angular correlations through both the first and second excited states of Si^{29} by a distorted wave formalism developed by Huby *et al.* [15]). The dpγ angular correlation measurements together with an analysis of them are presented in ref. [12]).

The present paper reports measurements of differential excitation functions for the proton groups leading to the ground and first two excited states of Si^{29} in the $Si^{28}(d, p)Si^{29}$ reaction for $\theta_p = 35°$ and $90°$ and for $6.0 \leqq E_d \leqq 10.7$ MeV and, in addition, reports measurements of angular distributions of these proton groups at 10 energies in this range of deuteron energies.

The differential cross section for the A(d, p)B reaction can be written [15])

$$\frac{d\sigma}{d\Omega} = \frac{\mu_p \mu_d}{8\pi^2 \hbar^4} \frac{(2J_B+1)}{(2J_A+1)} \frac{k_p}{k_d} \sum_{jl} \theta_{jl}^2 \Big(\sum_m |B_{lm}|^2 \Big), \tag{1}$$

where j, l and m are the total and orbital momentum and the component of l along the quantization axis, respectively, for the captured neutron. Subscripts p and d refer to the emitted proton and incident deuteron, respectively. θ_{jl}^2 is the reduced width and B_{lm} is the matrix element given by [15])

$$B_{lm}^2 = \frac{1}{(2l+1)^{\frac{1}{2}}} \int \{\psi_p [u_l (r_n) {}^l Y_l{}^m]_n\}^* V_{np} \psi_d \, d^3 r_p \, d^3 r_n . \tag{2}$$

If these expressions are evaluated using plane waves for the incident and outgoing particles, the usual Butler formalism is obtained. In this, if it is assumed that only one l value is allowed by the selection rules (i.e. the possibility of collective effects mixing in additional l values [16]) is ignored) eq. (2) can be conveniently rewritten as

$$\frac{d\sigma}{d\Omega} = \frac{4\pi \mu_p \mu_d R^3}{\mu_n \hbar^2} \frac{(2J_B+1)}{(2J_A+1)} \frac{k_p}{k_d} \theta^2 \left\{ \frac{1}{\alpha^2 + k_d{}^2} - \frac{1}{\beta^2 + k_d{}^2} \right\}^2 W_l{}^2, \tag{3}$$

where α and β are the constants in the Hülthén deuteron wave function and W_l

is the well known Wronskian tabulated for example by Lubitz [17]) and by Enge and Graue [18]). The term in parentheses is the so-called "deuteron factor",

$$D_{k_d} = \left\{ \frac{1}{\alpha^2 + k_d^2} - \frac{1}{\beta^2 + k_d^2} \right\}^2. \tag{4}$$

Essentially all of the nuclear structure information in this formalism is carried by the reduced width θ^2, and it is of considerable interest, apart from any question of reaction mechanisms, to obtain experimental data on this reduced width for direct comparison with the predictions of specific nuclear models [19]).

A later section of this paper reports on extraction of the reduced widths using several of the techniques which have been suggested to date and compares the results thus obtained. It is concluded that none of the more sophisticated techniques gives significantly better results than those obtained by simply fitting a Butler curve to the dominant stripping maximum.

In using eq. (3) to fit the angular distribution data (using θ^2 in this case as a normalization parameter) it has been found that excellent agreement can be obtained between the predicted and observed diffraction structure using reasonable interaction radii. However, the predicted envelope of these diffraction oscillations, which is determined in large measure by the deuteron factor, is not in accord with the experimental data; empirically it has been found that very creditable fits result when this factor is arbitrarily removed from the expression both for $l_n = 0$ and $l_n = 2$ cases.

2. Experimental Equipment and Procedure

Targets prepared † from blown quartz bubbles (SiO_2) of thickness 5.1 μm were mounted at 45° to the incident deuteron beam. The equivalent deuteron energy loss varies from $\approx$ 150 keV to $\approx$ 100 keV in the range 6 to 10.7 MeV incident energy.

A cylindrical target chamber of height 5.1 cm and radius 5.1 cm used a 12.7 μm Ti window (−25° to 155°) of height 1.9 cm cemented to the chamber wall (using Araldite Type 1 Cement ††) permitting detection of the protons outside the vacuum system. A second Ti window at 270° served as a beam monitor port. A system of four 0.32 cm gold apertures served to define the deuteron beam, which was stopped in a gold foil placed 3.8 cm behind the target. A negatively biased grid structure placed in front of the foil permitted the beam current delivered to the stopper to be integrated. In general, currents of $\approx 3 \times 10^{-7}$ A were employed.

The protons were detected in thin ($\approx$ 3 mm) NaI or CsI crystals using apertures to restrict the angular acceptance to $\approx$ 1° half angle. Sufficient absorber

† The authors are indebted to Mr. R. Bailey for preparation of the targets.

†† Manufactured by Aero Research Ltd., Duxford, Cambridge, England.

was used in front of the counters to stop scattered deuterons and to optimize the separation of the proton groups from the dp reaction. Dual electronic channels terminating in two 100-channel analyzers allowed the simultaneous measurement of excitation functions at two angles. Fig. 2 shows typical spectra obtained at 35° and 90° for $E_d = 8$ MeV. The strong $O^{16}(d, p)O^{17}$ groups from the SiO_2 targets caused no difficulty because of their lower energies.

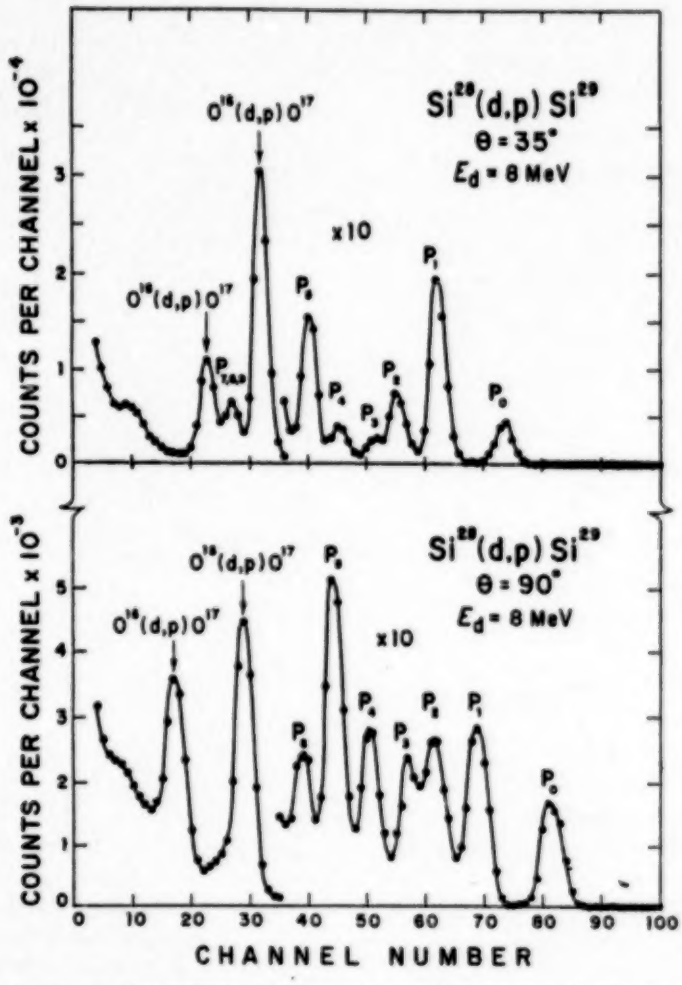

Fig. 2. Proton spectra from the $Si^{28}(d, p)Si^{29}$ reaction at $E_d = 8.0$ MeV, obtained using a 3 mm NaI scintillator and 5.1 μm SiO_2 target. The detection angles were 35° and 90°.

The gold beam stopper was removed for measurements of angular distributions to zero degrees. For these measurements a suitable thickness of high-Z foil was placed directly over the scattering chamber window to stop the deuteron beam. The incident beam was monitored in these cases with a second detector mounted at the monitor port.

3. Excitation Functions

The differential excitation functions for proton groups to the ground and first two excited states of Si^{29} were measured for $6.0 \leqq E_d \leqq 10.7$ MeV, both

at 90° and 35° to the incident beam. This range of bombarding energies corresponds to excitations in the compound nucleus P^{30} of from 17.5 to 21.9 MeV. An angle of 35° was selected for study on the maxima of the $l_n = 2$ stripping patterns for the p_1 and p_2 proton groups where the relative contribution from non-stripping amplitudes is minimized; the cross section at 90°, on the other hand, would be expected to be dominated to a much greater extent by any non-stripping amplitudes present.

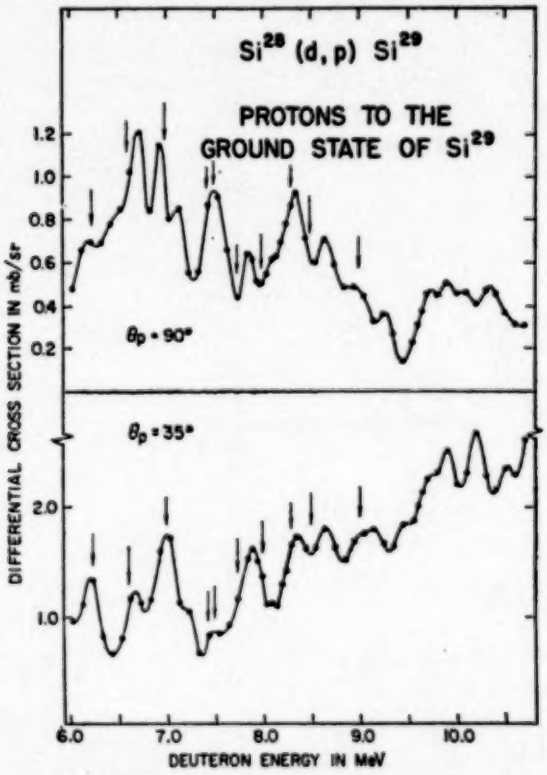

Fig. 3. Proton excitation functions for the ground state proton group from Si^{28}(d, p)Si^{29} measured at laboratory angles of 35° and 90°. The target thickness corresponded to ≈ 120 keV energy loss for 8 MeV deuterons. The arrows indicate energies at which angular distributions have been measured.

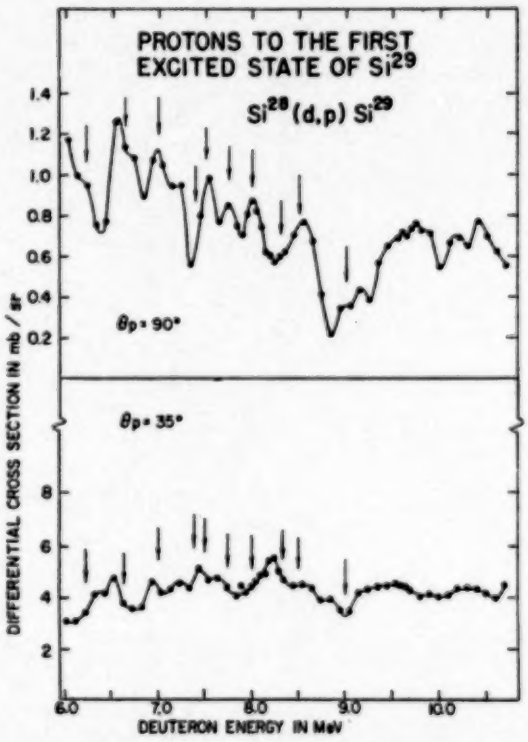
PROTONS TO THE FIRST EXCITED STATE OF Si²⁹
Si²⁸(d,p) Si²⁹
θp = 90°
θp = 35°
DIFFERENTIAL CROSS SECTION IN mb / sr
DEUTERON ENERGY IN MeV

Fig. 4. Proton excitation functions for the first excited state proton group from Si^{28}(d, p)Si^{29} measured at laboratory angles of 35° and 90°. The target thickness corresponded to ≈ 120 keV energy loss for 8 MeV deuterons. The arrows indicate energies at which angular distributions have been measured.

Figs. 3, 4 and 5 show the results of these measurements for the ground state, first excited state (1.28 MeV) and second excited state (2.03 MeV), respectively. It is immediately apparent that all of these excitation functions include compound nucleus resonant effects. The 35° excitation curves for p_1 and $p_2(l_n = 2)$ show an essentially constant envelope with 10—20 % fluctuations from resonant effects; the 90° excitation curves for these two states, in contrast, show much more marked resonant phenomena; yield fluctuations of 30 % and more being observed. The observed decreases of the envelopes with increasing incident energy for these two 90° curves are shown in a later section to result from the

change in the diffraction structure of the angular distribution with energy such that the detector, at a fixed angle, observes differing regions of the oscillatory structure. When this effect is removed the envelope is essentially constant; i.e., the integrated total excitation function changes much less rapidly with energy than does the 90° differential excitation function shown.

The ground state excitation curves, on the other hand, show large fluctuations for both the 35° and 90° cases. This results almost certainly from the fact that,

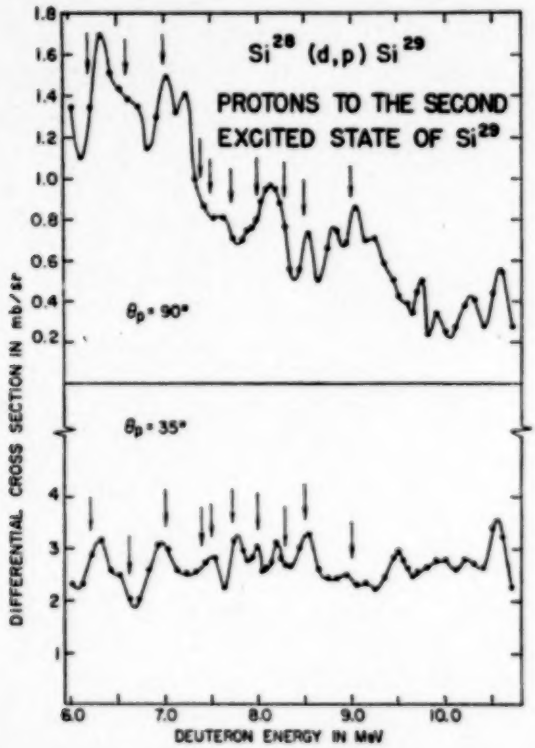

Fig. 5. Proton excitation functions for the second excited state proton group from Si^{28}(d, p)Si^{29} measured at laboratory angles of 35° and 90°. The target thickness corresponded to ≈ 120 keV energy loss for 8 MeV deuterons. The arrows indicate energies at which angular distributions have been measured.

for the ground state reaction, $l_n = 0$, and the main stripping peak is contained in the angular range less than 35°; in this case non-stripping amplitudes are significant at both 35° and 90°. The overall decrease of the 90° excitation function and the increase of the 35° excitation function as the energy is raised from 6 to 10.7 MeV again reflects a kinematic trend with energy of the diffraction structure.

The structure in the differential excitation curves, as shown, in many instances shows widths comparable with the target thickness used (≈ 100 keV) suggesting that the actual resonances responsible may have widths which are significantly less than this. There is essentially no correlation between the structural features of the excitation curves for different residual states nor in fact for different angles of observation and the same residual state. This

behaviour immediately suggests that the structure is caused by interference of the compound amplitudes with each other or with the direct interaction background, as discussed in greater detail later in this paper in connection with the integrated total excitation functions.

4. Angular Distributions

Proton angular distributions have been measured for the ground and first two excited states of Si^{29} at 10 energies in the range $6.2 \leqq E_d \leqq 9.0$ MeV. The energies used are indicated by arrows on the excitation curves of figs. 3, 4 and 5. These were selected not only to span the range of deuteron energies studied but also to examine the behaviour both on and off the resonant structure in the excitation curves.

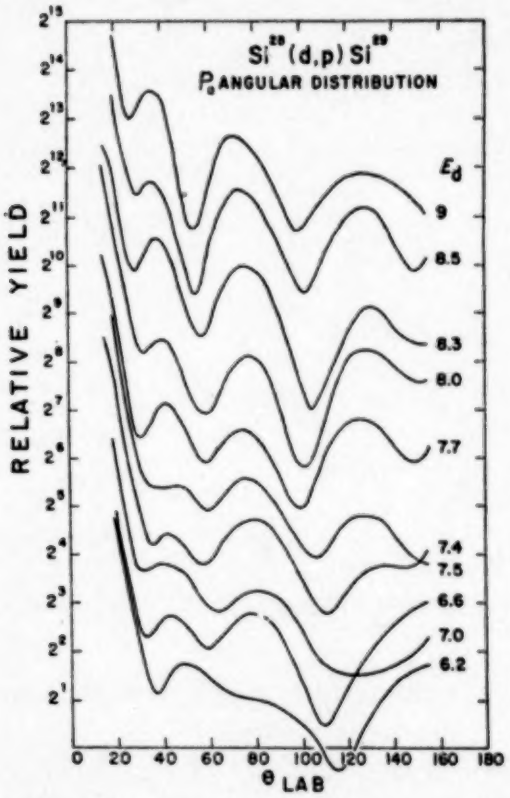

Fig. 6. Proton angular distributions for the ground state proton group from Si^{28}(d, p)Si^{29} ($l_n = 0$). The incident energies used are given and are indicated by arrows in fig. 3. The ordinate is logarithmic and the normalization between the curves at different energies is arbitrary.

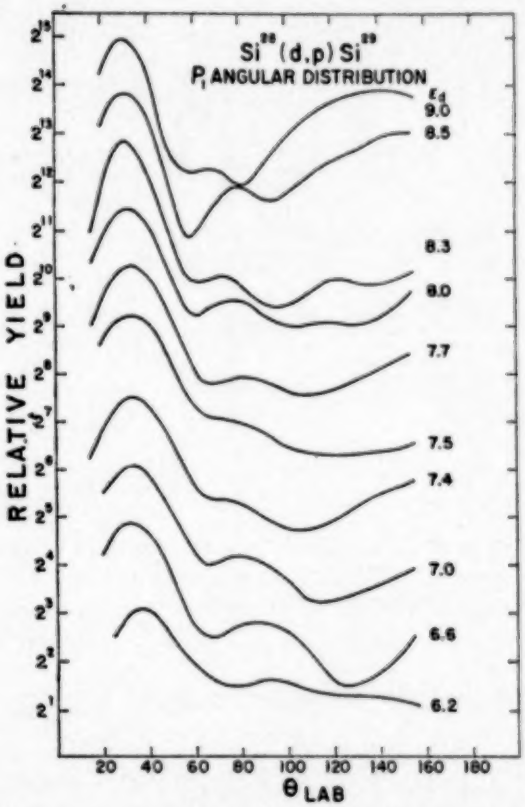

Fig. 7. Proton angular distributions for the first excited state proton group from Si^{28}(d, p)Si^{29}($l_n = 2$). The incident energies used are given and are indicated by arrows in fig. 4. The ordinate is logarithmic and the normalization between the curves at different energies is arbitrary.

Figs. 6, 7 and 8 present the results of these measurements for the ground state ($l_n = 0$), first excited state ($l_n = 2$), and second excited state ($l_n = 2$), respec-

tively. In these figures it should be emphasized that the ordinate is logarithmic; a factor of 2 is represented by the distance between the scale markings. This presentation has been chosen to display the structure at large angles rather than the more usual presentation which focusses attention on the primary peak. The normalization among the curves at different energies is arbitrary.

For comparison, the more familiar linear presentation is used in fig. 9 to display the angular distribution of the ground state proton group for $E_d = 8$ MeV.

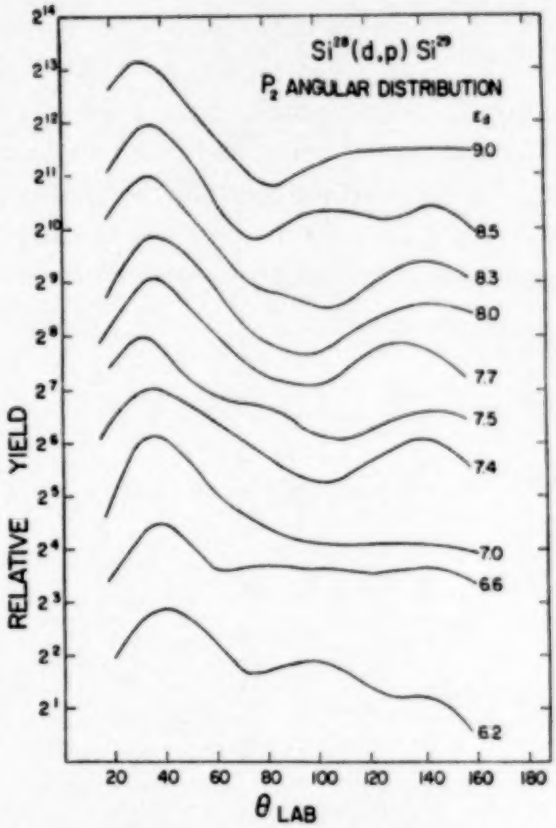

Fig. 8. Proton angular distributions for the second excited state proton group from Si^{28}(d, p)Si^{29} ($l_n = 2$). The incident energies used are given and are indicated by arrows in fig. 5. The ordinate is logarithmic and the normalization between the curves at different energies is arbitrary.

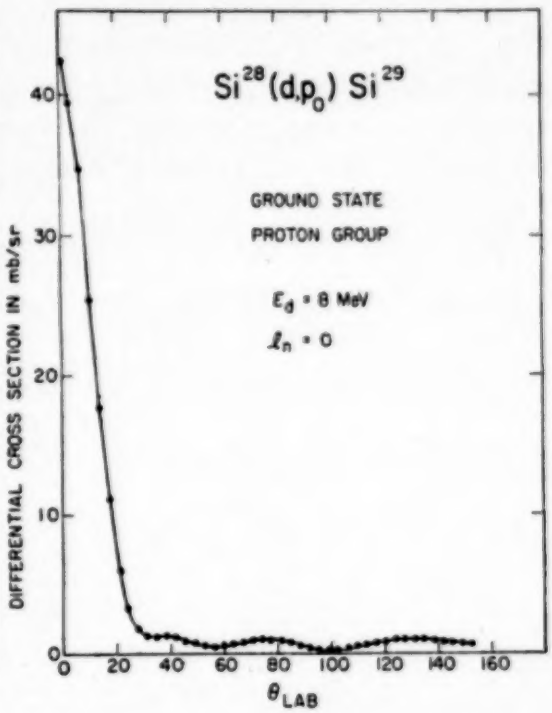

Fig. 9. Proton angular distribution for the ground state proton group from Si^{28}(d, p)Si^{29} ($l_n = 0$) and for $E_d = 8$ MeV. The curve passing through the data points is included as a guide to the eye.

One of the most striking features of these curves, especially in view of the resonant features of the excitation functions, is their similarity over the entire range of energies and angles studied. Greater deviations, however, are noted as the incident energy is decreased, especially at large angles in the case of the p_0 angular distributions and, to a lesser extent, the p_1 and p_2 angular distributions.

The regular diffraction shape which persists even at large angles strongly suggests a dominant direct interaction mechanism.

The observed energy dependence of the envelope of the 35° and 90° excitation data for the p_0 proton group as shown in fig. 3 is readily explicable in terms of the behaviour of the angular distributions shown in fig. 6. In the case of the 35° detector, for example, it is clear that over the energy range considered, the kinematic contraction of the angular distribution sweeps a maximum in the distribution across the counter acceptance angle with consequent tilting of the differential excitation function envelope.

5. Discussion

5.1. CROSS SECTIONS

Having the excitation functions and angular distributions at these 10 energies it is of course possible to integrate the differential cross section for each of the proton groups at each energy to obtain the total rather than the differential excitation function. The total cross sections resulting from these calculations are shown in figs. 10, 11 and 12 for the p_0, p_1 and p_2 proton groups respectively.

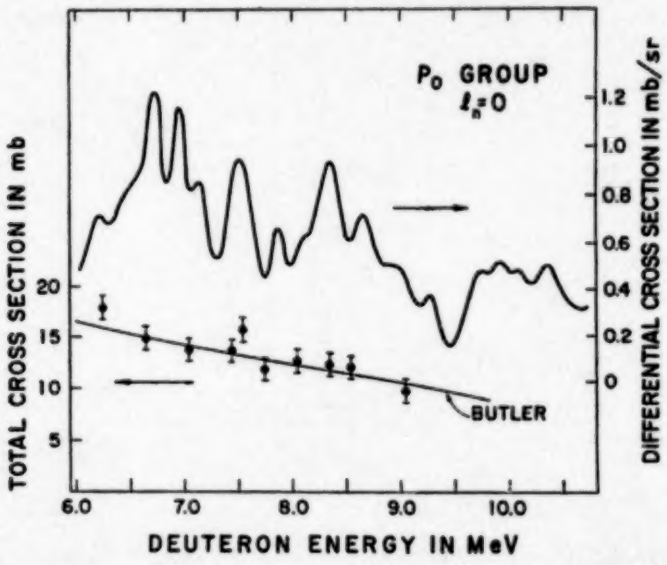

Fig. 10. Values of the total cross section obtained by integration of the differential cross sections are shown as data points for the ground state proton group from $Si^{28}(d, p)Si^{29}$. The magnitude of the errors was estimated from the observed scatter in values obtained using the 35° and 90° differential cross section data. The curve through the data and labelled 'Butler' was computed using eq. (3), choosing a reduced width to give the best fit. The upper curve is the corresponding differential cross section for 90°.

The errors indicated on these data were estimated from the observed scatter in values obtained using the 35° and the 90° excitation function data. The solid curves, shown for comparison, are the corresponding differential excitation functions at 90° in each case.

It is immediately obvious that the large fluctuations which appear in the excitation functions do not persist in the total cross sections; the data are

consistent with a smoothly varying total cross section showing no resonances, although it is not possible to preclude the existence of residual resonant struc-

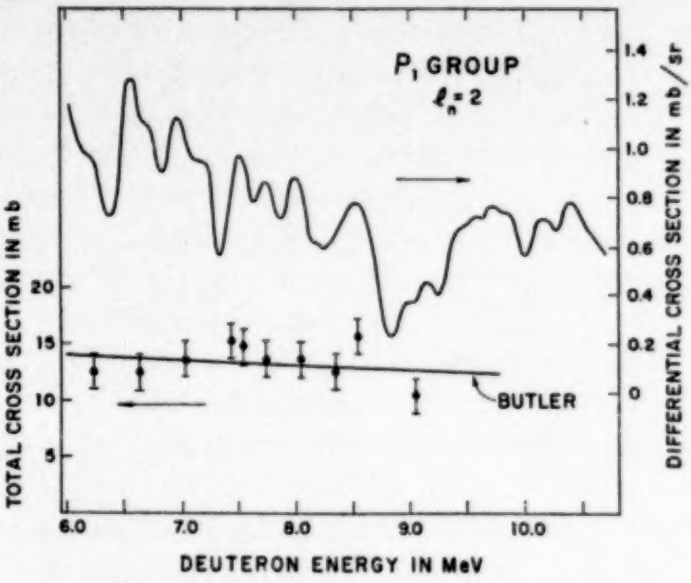

Fig. 11. Values of the total cross section obtained by integration of the differential cross sections are shown as data points for the first excited state proton group from Si^{28}(d, p)Si^{29}. The magnitude of the errors was estimated from the observed scatter in values obtained using the 35° and 90° differential cross section data. The curve through the data and labelled 'Butler' was computed using eq. (3), choosing a reduced width to give the best fit. The upper curve is the corresponding differential cross section for 90°.

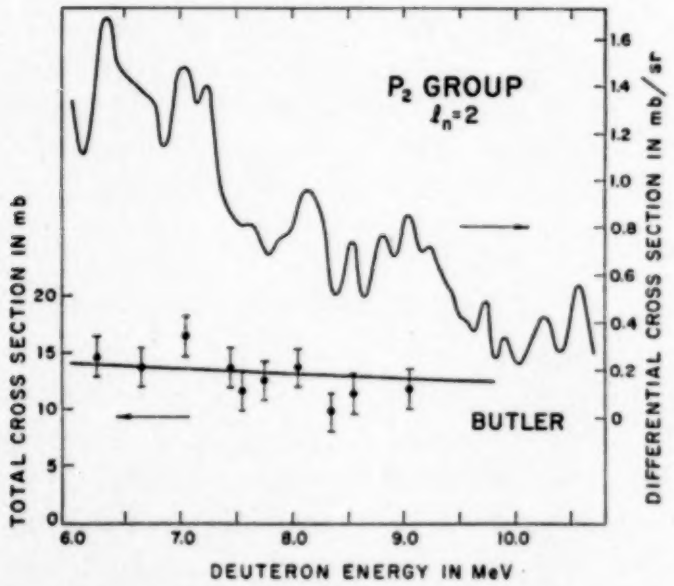

Fig. 12. Values of the total cross section obtained by integration of the differential cross sections are shown as data points for the second excited state proton group from Si^{28}(d, p)Si^{29}. The magnitude of the errors was estimated from the observed scatter in values obtained using the 35° and 90° differential cross section data. The curve through the data and labelled 'Butler' was computed using eq. (3), choosing a reduced width to give the best fit. The upper curve is the corresponding differential cross section for 90°.

ture in the total excitation curve of the order of 10 %. The facts that the fluctuations are observed to be much stronger in the differential excitation functions than in the total cross section and that there is no apparent correlation relating the structure at different angles of observation suggest that they result largely from interference. Other data, namely the angular distributions, which do not change their characteristic diffraction shape over the range of energies studied, imply a dominant direct interaction amplitude. Thus it is strongly suggested that the interference effects observed reflect interference between direct interaction and compound nuclear amplitudes; it is clear that whenever the intrinsic beam energy spread together with the energy spread introduced by the target thickness is small compared to the widths of the local compound states, residual interference effects are expected. The disappearance of the resonance structure in the total cross section then implies that the interfering compound system levels are formed in the main via orbital momentum partial waves in the incident flux which do not correspond to the range of partial waves which dominate the direct interaction process. This is entirely consistent with the well established result that the direct interaction or surface reactions characteristically involve large impact parameters, hence large l values, whereas the compound system levels which most readily participate in reactions such as this, involving low initial and residual angular momenta, are those corresponding to absorption of low order partial waves.

The curves through the data for the total cross section in figs. 10, 11 and 12 are computed using equation (3) and choosing a reduced width θ^2 for each state to give the normalization. The energy variation for the $l_n = 2$ cases is almost entirely due to the factor k_p/k_d which occurs in the expression for the stripping cross section; the energy variation resulting from integration over angles is negligible for these cases. In the $l_n = 0$ case an additional variation results from the evaluation of the integral over angles. The agreement with the experimental energy variation is striking.

5.2. LIMIT ON CONTRIBUTION FROM COMPOUND NUCLEUS FORMATION

An attempt has been made to set a limit on the contribution to the reaction cross section from compound nucleus formation using statistical theory arguments [20]) and the results of a detailed calculation of Vogt [21]). It is possible, by comparison of the calculated form of the angular distributions with the measured angular distributions, to place a limit on the contribution to the reaction cross section from compound nuclear amplitudes. Since this comparison can be made at a number of energies it is possible to average out the effects of interference and obtain a limit for the compound intensity by itself. The comparison is made, quite simply, by subtracting from the measured differential cross section an appropriate contribution of the form predicted for compound nucleus formation such that the difference becomes zero at its lowest point. The amount

subtracted is then assumed to be the maximum possible contribution due to compound nuclear processes. The limit obtained in this manner for the Si^{28}(d, p)Si^{29} compound system intensity to the ground state of Si^{29} is $< 15\,\%$. For the reactions to the first and second excited states of Si^{29}, because of the less marked minima for these $l_n = 2$ angular distributions, a less stringent limit of $< 30\,\%$ in intensity is obtained.

The assumed form of the differential cross sections for compound nucleus formation is

$$\frac{\mathrm{d}\sigma(\theta)}{\mathrm{d}\Omega} = \sum_{n\ \mathrm{even}} a_n P_n(\cos\theta). \tag{5}$$

Only even orders of polynomial appear as a result of the random phase assumption [20]) used. Values of the coefficient ratios in (5), calculated in [21]) for 6 MeV incident deuterons, are listed in table 1.

TABLE 1

Calculated coefficient ratios in the expansion $\mathrm{d}\sigma/\mathrm{d}\Omega = \Sigma\, a_n P_n(\cos\theta)$ (n even) for the differential cross sections due to compound nucleus formation for the reactions Si^{28}(d, p)Si^{29} to the ground and first two excited states of Si^{29} performed for an incident deuteron energy of 6 MeV. See ref. [20]) for further details.

State formed in Si^{29}	a_2/a_0	a_4/a_0	a_6/a_0
Ground state	0.55	0.13	0.003
First excited state	0.36	0.03	0.005
Second excited state	0.06	−0.07	−0.01

It should be noted that the form of (5) is based on very general statistical arguments only and that the values obtained for the limits of the compound nucleus contribution to the reaction cross sections are thus not sensitive to the detailed assumptions used in ref. [21]).

5.3. STATISTICAL MODEL CALCULATIONS

The limits set in the preceding section on the contributions to the reaction cross sections from compound nucleus formation can be compared with the results of a statistical theory calculation of Vogt [21]). In the statistical theory the expressions for the average over resonances of the differential cross section $\langle \mathrm{d}\sigma_{\alpha\alpha'}/\mathrm{d}\Omega \rangle$ and of the partial cross section $\langle \sigma_{\alpha\alpha'} \rangle$ integrated over all angles are [22])

$$\left\langle \frac{\mathrm{d}\sigma_{\alpha\alpha'}}{\mathrm{d}\Omega} \right\rangle = \frac{1}{k_\alpha^2 (2I+1)(2i+1)} \sum_{\substack{s,s',L \\ l,l',J}} (-)^{s-s'} P_L(\cos\theta) Z(lJlJ, sL)$$

$$\times Z(l'Jl'J, s'L) \frac{T^{\alpha}_{sl} T^{\alpha'}_{s'l'}}{\sum_{\alpha''s''l''} T^{\alpha''}_{s''l''}} \tag{6}$$

and

$$\langle \sigma_{\alpha\alpha'} \rangle = \frac{\pi}{k_\alpha{}^2} \sum_{\substack{s,s',L \\ l,l',J}} \frac{2J+1}{(2I+1)(2i+1)} \frac{T^{\alpha}_{sl} T^{\alpha'}_{s'l'}}{\sum_{\alpha''s''l''} T^{\alpha''}_{s''l''}}, \tag{7}$$

where the unprimed quantities refer to the entrance channel and the primed quantities to the reaction channels. For a given channel, α labels the pair of particles and their state of excitation, s is their channel spin (vector sum of the intrinsic spins I and i of the pair), l their relative angular momentum and J the total angular momentum. k_α is the wave vector of the entrance channel, P_L the usual Legendre polynomial and $Z(lJlJ, sL)$ an angular momentum recoupling coefficient [23]). The transmission functions T^{α}_{sl} are defined by

$$T^{\alpha}_{sl} \equiv 4\pi P_{\alpha l} S_{\alpha sl}, \tag{8}$$

where $P_{\alpha l}$ is the penetrability of the channel αsl and $S_{\alpha sl}$ is the strength function for that channel.

The statistical theory results [21]) discussed below were obtained from (6) and (7). A number of approximations were employed. At the deuteron energies of interest a large number of incoming and outgoing waves are involved. Because of this fact and because, at the energy of interest, most of the channels have a strength function corresponding to a strongly absorptive well, the black nucleus value of the strength function was used:

$$S_{\alpha sl} = (\pi K_\alpha R)^{-1}, \tag{9}$$

where R is the nuclear radius and K_α a wave vector for the incoming particle inside the nucleus. With (9) the transmission functions of (6) and (7) reduce to simple penetrabilities — the angular distributions of (6) are then very similar to those of Hauser and Feshbach [20]). Since most of the outgoing channels in the Si^{28} plus d reactions involve nucleon emission the nucleon strength function cancels out in both (6) and (7). For deuterons a radius of 6.3×10^{-13} cm, corresponding to $K_D R \approx 12$, was used. The nucleon penetrabilities of (6) and (7) were evaluated at a radius of 5.8×10^{-13} cm. Although the energies of most of the outgoing channels are known, the estimates of the denominators in (6) and (7) required some reasonable assumptions about the distributions of spins and parities in the large number of channels involving proton and neutron emission. It is estimated that the compound nucleus contributions, evaluated as above, should be reliable to within a factor of about two.

Calculated values of the integrated total cross section for the ground and first two excited states of Si^{29} performed for two incident deuteron energies are listed in table 2. A comparison shows that these cross sections, calculated for the compound nucleus process, are almost twice as large as the experimentally observed cross sections of approximately 10—15 mb (see figs. 10, 11 and 12), in

direct conflict with the limits set in the last section on the contribution from compound nucleus processes. It thus appears that these theoretical estimates of the compound nucleus cross sections are considerably too large.

TABLE 2

Calculated values of the cross section due to compound nucleus formation for the reactions Si^{28}(d, p)Si^{29} to the ground and first two excited states of Si^{29} performed for incident deuterons of energy 6 and 8 MeV. See ref. [21]) for further details.

State formed in Si^{29}	$\sigma_{6\ MeV}$(mb)	$\sigma_{8\ MeV}$(mb)
Ground state	18	13
First excited state	25	18
Second excited state	28	22

To check on the estimates and assumptions involved in the calculations a second comparison has been made between the calculated and experimental cross sections for a group of six states [24]) near an excitation of 6.3 MeV in Si^{29}. A combined cross section of approximately 90 mb is calculated, almost independent of the assumptions which are made regarding the spins and parities of the six states, whereas experimentally only approximately 15 mb is measured. At this excitation one would anticipate that compound amplitudes would be dominant; it thus appears that the theoretical estimates of the compound nucleus cross sections are at least a factor of six too large. It should be noted that if significant stripping amplitudes are still involved in these higher residual state reactions the theoretical estimates are too large by an even greater factor. If a factor of six reduction is arbitrarily applied to all of the theoretical estimates they become consistent with the previously set limit on the contribution to the reaction cross sections from compound nuclear processes for the three lowest levels of Si^{29} in the Si^{28}(d, p)Si^{29} reaction of $< 30\ \%$.

The tendency of the calculated compound nucleus cross section to be too large by a factor of six or more may have a simple explanation. First of all the nuclear radius used in the calculation for formation of a compound nucleus by deuterons, $R = 1.4(A_1^{\frac{1}{3}}+A_2^{\frac{1}{3}})$, may be too large. If the deuteron radius is omitted from the nuclear radius all of the theoretical estimates are reduced by a factor of two or three. An additional small effect, resulting from isobaric spin considerations, tends to inhibit proton emission relative to deuteron and alpha particle emission; however, even if isobaric spin mixing is ignored the effect is only 20 %. Thirdly, depletion of the incoming deuteron beam by the stripping process may decrease the probability of compound nucleus formation significantly. This beam depletion effect appears reasonable since a crude estimate based on the experimental data of the total dp reaction cross section suggests that this cross section is approximately equal to that for the absorption of a deuteron by a black sphere of this radius. Thus it appears reasonable that a significant

fraction of the incident deuterons undergoes stripping before entering close enough to the interior of the nucleus to form a normal compound system.

5.4. ANGULAR DISTRIBUTION FITTING

The form of the proton angular distribution predicted on the assumption of a plane wave mechanism is given in eq. (3). Fig. 13 shows a typical attempt at

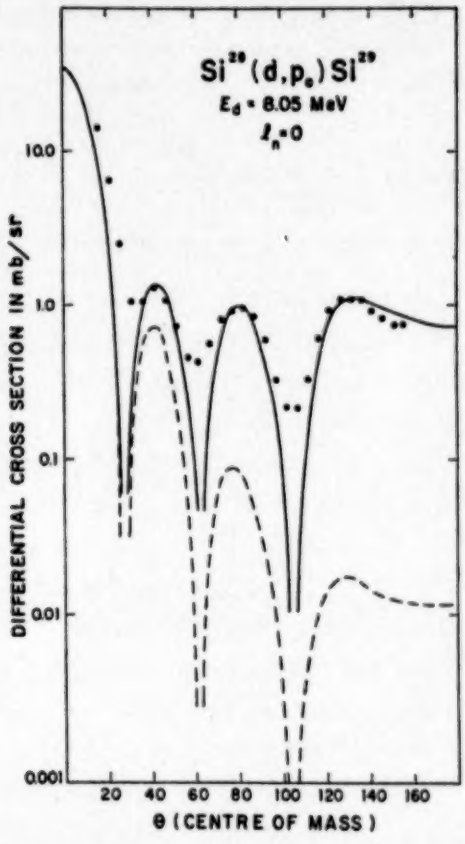

Fig. 13. Angular distribution for the ground state proton group from Si^{28}(d, p)Si^{29}($l_n = 0$) for $E_d = 8.05$ MeV. The dashed curve is that predicted by equation (3) using an interaction radius of 6.6×10^{-13} cm. The solid curve is obtained in the same way from eq. (3) but setting the deuteron factor D_{kd} equal to a constant.

fitting the experimental data for one of the $l_n = 0$ angular distributions using this formalism. The dashed curve is that predicted by equation (3) using an interaction radius of 6.6×10^{-13} cm; as usual the envelope of this curve decreases much more rapidly with angle than do the experimental data. In much of the reported (d, p) work it has been customary either to ignore this discrepancy or to attribute it to one or more of the following causes:

(a) background, presumed due to non-stripping mechanisms and thus relatively independent of angle;

(b) heavy particle stripping contributions [25]) which characteristically show augmented cross sections at back angles;

(c) "mirror imaging" [26]) of the normal forward stripping peak, through

reflection in the nuclear surface, into a more diffuse backward cross section increase;

(d) the effects of Coulomb and nuclear distortions [2]), since the available calculations, albeit rather few as yet, do predict a higher cross section at back angles in general.

During the course of these measurements it was noted that a remarkably good fit can be obtained to the experimental data by modifying the envelope

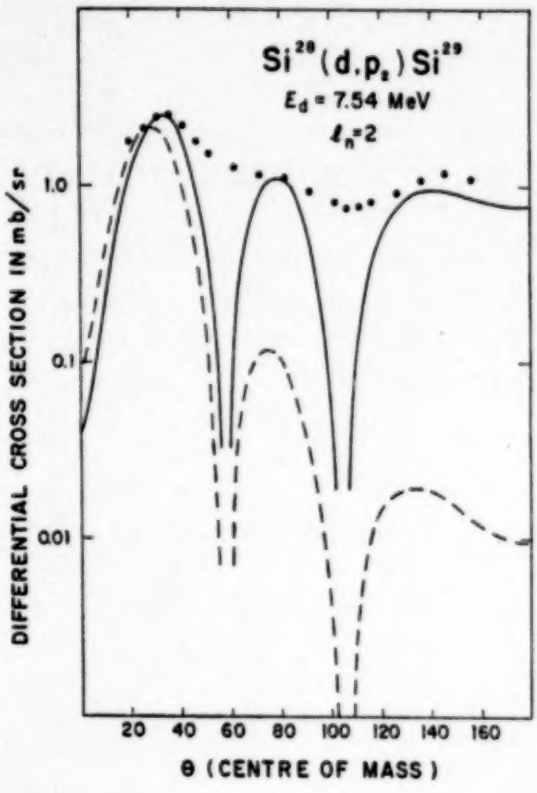

Fig. 14. Angular distribution for the second excited state proton group from Si^{28}(d, p)Si^{29}($l_n = 2$) for $E_d = 7.54$ MeV. The dashed curve is that predicted by eq. (3) using an interaction radius of 6.6×10^{-13} cm. The solid curve is obtained in the same way from eq. (3) but setting the deuteron factor D_{k_d} equal to a constant.

of the diffraction oscillations predicted by eq. (3) and, moreover, that the required modification factor is very closely equal to (within 50 % over the entire angular range) the inverse of the deuteron factor D_{k_d}. The solid curve of fig. 13 was obtained in this way assuming a constant deuteron factor; for comparison the unmodified Butler angular distribution is included as a dashed line. It is interesting to note that not only does this curve give an excellent fit to all the diffraction oscillations but also it reproduces the experimentally observed shape at large angles. The discrepancies at the minima are not attributable to experimental resolution effects; however, it has been demonstrated that only a very small amount of distortion or of absorption [2, 26]) introduced into

the theoretical treatment predicts just such a filling of the deep diffraction minima as is observed.

The empirical approach of setting the deuteron factor constant provides quite acceptable fits to all of the $l_n = 0$ angular distributions measured. Fig. 14 shows a corresponding case for $l_n = 2$ (p_2, $E_d = 7.5$ MeV). The calculated curves correspond to an interaction radius of 6.6×10^{-13} cm as used for the $l_n = 0$ case shown in fig. 13. It is clear that the solid curve gives an acceptable fit in this case as well, although the diffraction minima appear to be filled to a greater extent. As yet unpublished measurements of the Al^{27}(d, p)Al^{28} reaction [27]) show similar agreement between experiment and prediction using a constant deuteron factor.

It may also be of significance that in using eq. (3) unmodified, interaction radii of 6.6×10^{-13} cm and 5.0×10^{-13} cm are required to fit the diffraction structure for the $l_n = 0$ and 2 curves, respectively, whereas when modified, a single radius of 6.6×10^{-13} cm suffices for both cases.

Further work is necessary in order to allow any decision as to whether this agreement, obtained using a constant deuteron factor, is fortuitous or whether there is a more fundamental significance (see also the *Note added in proof*).

5.5. DEUTERON AND PROTON *l*-VALUES

An interesting aspect of the stripping process arises in the interpretation of Legendre polynomial expansion fits of the angular distribution data. It was

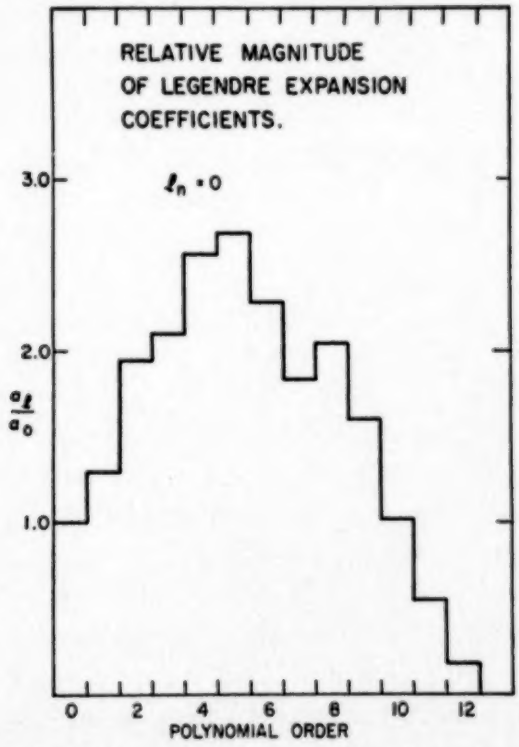

Fig. 15. Relative magnitudes of the average of the coefficients in the expansions of $\Sigma a_n P_n(\cos\theta)$ for the ten $l_n = 0$ angular distributions of fig. 6.

found that for the angular distribution to the ground state of $Si^{29}(l_n = 0)$ the expansion required about 12 terms in even and odd Legendre polynomials to obtain adequate fits. Also, the polynomials with largest coefficients were those of order approximately 4 to 6. Fig. 15 is a plot of the average of the coefficients in such expansions for the ten $l_n = 0$ angular distributions of fig. 6. This can be interpreted as evidence that the incident and outgoing partial waves are important up to and including those with $l = 6$.

5.6. REDUCED WIDTHS

Essentially all of the nuclear structure information is included in the reduced width θ^2 and it is of considerable interest to obtain experimental values for direct comparison with the predictions of specific nuclear models. Unfortunately, the extraction of reduced widths from stripping data is not always straightforward and the values obtained may not be unique. In this subsection an examination is made of several of the techniques for reduced width extraction and a comparison is made of the results obtained.

5.6.1. Fitting forward peak

The method normally used in extracting a reduced width from a stripping reaction is to fit the differential cross section at the first maximum with a Butler curve, adjusting l_n, R and θ^2, to obtain the best fit over a small region near the peak of the angular distribution. This method gives a unique value for the reduced width but it has always been open to question whether or not this value was a good representation of the actual reduced width. The most obvious reason for this doubt is that one uses a theory which does not in general give a good fit to the angular distribution, particularly at large angles. This is, of course, the reason for using the angular region near the maximum cross section, where the theory is best able to fit the experiment.

5.6.2. Amado Technique

It has been pointed out by Amado [28]) that it may be possible to avoid some of these difficulties by utilizing the fact that the cross section expression of eq. (3) has two poles corresponding to $k_d^2 = -\alpha^2$ and $-\beta^2$, respectively. The first of these corresponds to an unphysical momentum transfer $q^2 = -k_n^2$, where k_n is the wave number of the neutron outside the nucleus but bound to it in the specific state considered. This is interpretable as a scattering angle such that $\cos\theta > 1$. The second pole $k_d^2 = -\beta^2$ is ignored because $\beta^2 \gg \alpha^2$ and the equivalent scattering angle is further removed from the physical region, i.e. larger $\cos\theta$. Amado's suggestion stems from the assumption that at a pole of eq. (3) all competing and perturbing processes such as compound nucleus processes and Coulomb and nuclear distortion of the deuteron and proton waves are finite. Thus, at the pole, the Butler theory is exact and one would

hope that an extrapolation of the expression for the reduced width derived from eq. (3) in terms of the measured cross section to this pole would result in an unambiguous value of the reduced width. The extrapolation is conveniently carried out by plotting

$$\theta^2 = \left\{\frac{\mu_n \hbar^2}{4\pi\mu_p\mu_d R^3}\,\frac{(2J_A+1)}{(2J_B+1)}\right\}\frac{k_d}{k_p}\,W_l^{-1}D_{k_d}^{-1}\,\frac{d\sigma}{d\Omega} \tag{10}$$

as a function of $\cos\theta$, with θ the scattering angle in the centre of mass system. If the pole corresponds to $\cos\theta$ near 1 the extrapolation may be carried out graphically with little uncertainty. However, in the cases studied here, the pole corresponds to $\cos\theta \approx 1.3$ and the extrapolation is by no means an obvious one. The curves of fig. 16 in the region of $\cos\theta > 1$ represent an attempt at

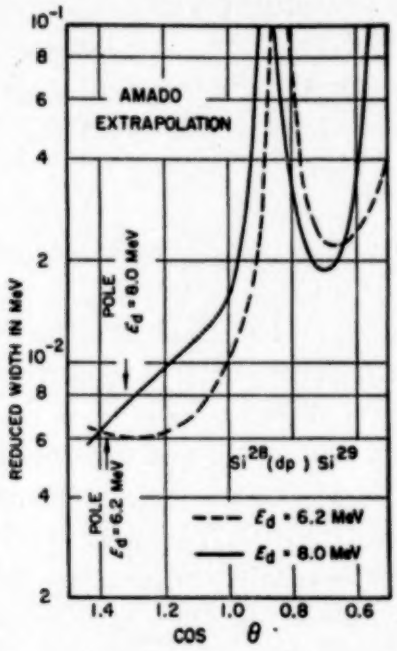

Fig. 16. Amado extrapolation of the reduced width for the ground state ($l_n = 0$) differential cross section for Si^{28}(d, p)Si^{29}. The dashed curve is for $E_d = 6.2$ MeV and the solid curve is for $E_d = 8.0$ MeV. The extrapolation into the region $\cos\theta > 1$ has been carried out using the Legendre polynomial extrapolation described in the text.

obtaining an objective method for carrying out this extrapolation. In obtaining these curves the quotient $\{D_{k_d}^{-1}\,d\sigma/d\Omega\}$ was formed at each angle where $d\sigma/d\Omega$ was measured and the resultant curve was fitted to an expansion of the form

$$\left\{D_{k_d}^{-1}\,\frac{d\sigma(\theta)}{d\Omega}\right\} = \sum_{n=0}^{n_{max}} b_n P_n(\cos\theta). \tag{11}$$

Using the b_n thus determined and the polynomial expressions in $\cos^n\theta$ the quotient curve was extended into the non-physical region to the pole; in so doing its value increased by 2 orders of magnitude. Similarly the Wronskian

was extrapolated into the non-physical region (this corresponds to the transition from circular to hyperbolic trigonometric functions); since it similarly increased, the calculated reduced width from eq. (10) is roughly constant and gives a reasonable extrapolated value. This process is clearly open to the objection that it extrapolates the Legendre polynomials beyond their normal range (in particular the high order polynomials become large for large cos θ with the possible consequence of extreme sensitivity on the maximum order of polynomial used), however, it has the *a postiori* justification of having given internally consistent results (within a factor of two generally) for two deuteron energies and for several different polynomial order cutoffs both for $l_n = 0$ and $l_n = 2$ cases. Typical results obtained using this technique are included in tables 3 and 4.

TABLE 3

Reduced widths in MeV for Si^{28}(d, p)Si^{29} to the Si^{29} ground state ($l_n = 0$).

Method used	6.2 MeV	8.0 MeV
Peak fitting	0.012	0.017
Amado	0.006	0.008
Bowcock	0.012	0.019
Total σ	0.051	0.045

TABLE 4

Reduced widths in MeV for Si^{28}(d, p)Si^{29} to the first excited state of Si^{29} ($l_n = 2$).

Method used	6.2 MeV	8.0 MeV
Peak fitting	0.015	0.017
Amado	0.006	0.007
Total σ	0.034	0.037

5.6.3. *Bowcock technique*

Further techniques for reduced width extraction which are equivalent to a partial wave decomposition of the reaction amplitudes (or intensities) have been suggested by Bowcock [29]). If the predicted cross section of eq. (3), with θ^2 set equal to unity, is expanded as

$$\left[\left(\frac{d\sigma}{d\Omega}\right)_{\text{theor}}\right]^{\frac{1}{2}} = \sum_{n=0}^{n_{max}} a_n P_n(\cos\theta) \tag{12}$$

and similarly the experimental data are expanded as

$$\left[\left(\frac{d\sigma}{d\Omega}\right)_{\text{exp}}\right]^{\frac{1}{2}} = \sum_{n=0}^{n_{max}} b_n P_n(\cos\theta), \tag{13}$$

Bowcock has noted that the reduced width may be obtained from a plot of

b_n/a_n versus n. *A priori* it would be expected that non-stripping amplitudes would most affect this ratio for low n values, but that at higher n values the ratio should tend toward a constant value. The reduced width is then obtained directly as the square of this constant since θ^2 appears as a multiplicative constant in eq. (3). This particular method has the advantage that each term corresponds uniquely to a particular orbital momentum in the incident wave; it has the disadvantage, however, of implying a zero cross section where the amplitude changes sign, in contrast to experiment.

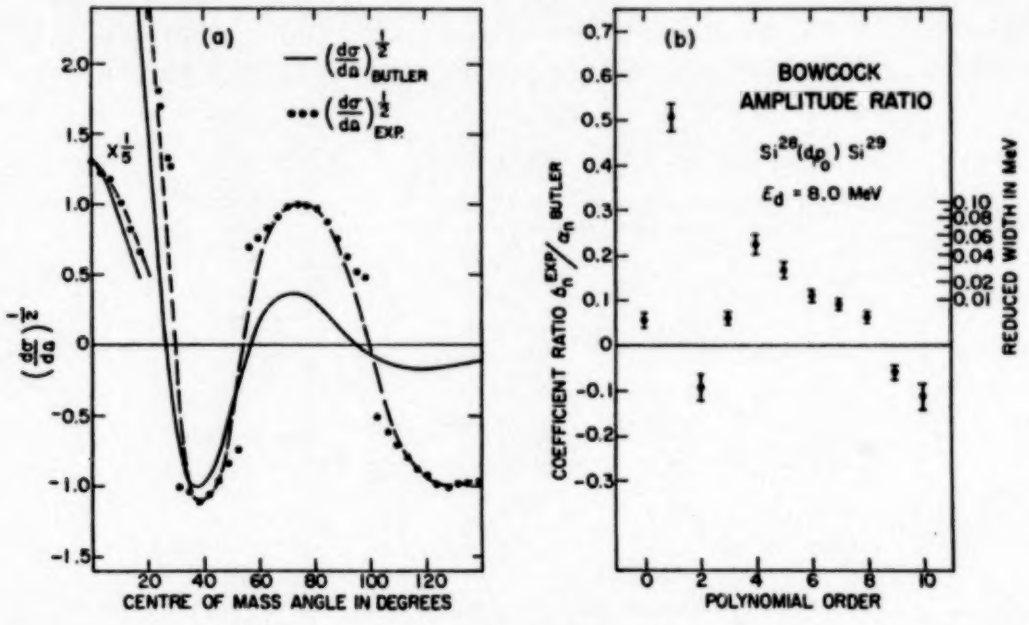

Fig. 17. Bowcock amplitude ratio technique for reduced width extraction. The data are for the ground state ($l_n = 0$) differential cross section for Si^{28}(d, p)Si^{29} for $E_d = 8.0$ MeV. In (a) the solid line is the square root of the Butler differential cross section and the points are the square root of the observed differential cross section. The dashed curve is used in the analysis as a real approximation of the complex reaction amplitude. In (b) values of the ratio b_n/a_n are plotted as a function of the polynomial order.

Fig. 17 shows the results of such an analysis for the ground state group angular distribution for $E_d = 8$ MeV. In (a) the solid line is the square root of the Butler differential cross section and the points are the square root of the observed differential cross section. The dashed curve is used in the analysis as a real approximation of the complex reaction amplitude. In (b) values of the ratio b_n/a_n are plotted as a function of the polynomial order.

The scatter of the points in fig. 17(b) is typical of all the analyses carried out with the Si^{28}(d, p_0)Si^{29} data. The erratic behaviour for low order polynomials is to be expected and reflects the presence of non-stripping amplitudes, but the trend to negative values for the high orders demonstrates the inadequacies of the analysis. However, there is a region, from $n = 3$ to 8, where the ratios have nearly the same value. The reduced width implied by the ratios in this region is

of the order 0.01 to 0.02 MeV. It is of interest that Tobocman [30]) found a similar region of good agreement in an analysis of some calculated [31]) stripping cross sections. In this case good agreement was obtained for polynomial orders in the range $n = 6$ to 9.

In fig. 17(a) the assumed normalization is $\theta^2 = 0.017$ MeV, which corresponds to the value obtained by the peak fitting technique; thus the solid curve passes through the data points near zero degrees scattering angle. It can be seen from the curves that one would obtain essentially the same reduced width by comparing the second maximum (near 40° in this case) in the differential cross section with the Butler cross section. This is rather interesting since the same result obtained in the analysis of Tobocman [30]).

To avoid the approximation inherent in assuming a real reaction amplitude, Bowcock has also noted that expansions of the differential cross section, equivalent to eqs. (12) and (13), rather than its square root, lead to the same conclusions, but without the simple identification of polynomial order. Figs. 18(a) and (b) show such plots carried out for the $l_n = 0$ data for 6.2 and 8.0

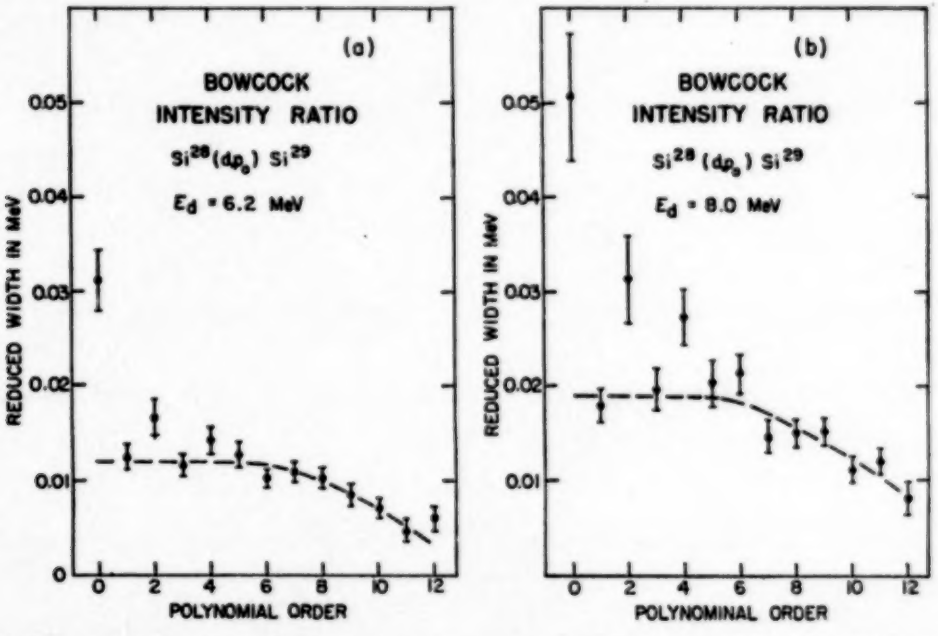

Fig. 18. Bowcock intensity ratio technique for reduced width extraction. The data are for the ground state ($l_n = 0$) differential cross section for Si^{28}(d, p)Si^{29} for (a) $E_d = 6.2$ MeV and (b) $E_d = 8.0$ MeV. Values of the ratio b_n/a_n are plotted as a function of the polynomial order. The magnitudes of the errors are estimated by the scatter in values obtained, using different methods of weighting the points in the least squares fits to expansions in Legendre polynomials. The dashed lines are included to show the trend of the ratios.

MeV, respectively. The decrease in the ratios at large values reflects the fact that the minima in the experimental angular distributions are filled in to some extent; the zeros in the Butler angular distribution require large high order polynomials, with the result that the ratio b_n/a_n becomes small for large n.

It is of particular interest to note that while the ratios for lower, odd n values are essentially constant, those for $n = 0$, 2 and 4 are significantly higher. As noted above, the statistical theory calculation of these angular distributions is expressible as

$$W(\theta) = 1 + \frac{a_2}{a_0} P_2(\cos\theta) + \frac{a_4}{a_0} P_4(\cos\theta). \tag{14}$$

Consequently the deviation of the $n = 0$, 2, 4 points from the dashed lines in fig. 18 may be interpreted as reflecting the presence of such a contribution adding incoherently to the characteristic stripping angular distribution. The magnitude of this contribution, however, which may be identified with the magnitude of an incoherent compound nucleus contribution, is larger than the limit set previously for this contribution and it would thus appear that this simple interpretation involving completely incoherent addition is not valid.

Values of the reduced widths obtained from these analyses are included in table 3.

5.6.4. Fitting total cross section

It was noted in subsection 5.1 above (see figs. 10, 11 and 12) that a satisfactory fit to the total cross section could be made using eq. (3) and adjusting the reduced width to give the correct normalization. This process, then, is an additional method of obtaining a reduced width and, while it may not be based on elegant theoretical ideas, gives values in reasonable agreement with those obtained using other techniques (see tables 3 and 4).

Reduced width values obtained using the various techniques described above are listed in table 3 for the ground state reaction ($l_n = 0$) and in table 4 for the first excited state reaction ($l_n = 2$). Relative reduced widths averaged for the two incident energies are collected in table 5 for the $l_n = 0$ and 2 cases. These

TABLE 5

Averaged relative reduced widths for Si^{28}(d, p)Si^{29} to the ground state ($l_n = 0$) and the first excited state ($l_n = 2$) of Si^{29}.

Method used	$l_n = 0$	$l_n = 2$
Peak fitting	1.0	1.1
Amado	0.5	0.5
Bowcock	1.1	
Total σ	3.3	2.5

tabulations reveal that no method appears any better than the others in its ability to yield reduced widths which are independent of energy. Also, a comparison of the relative values of table 5 shows that the ratios of reduced widths obtained for the two states are closely the same independent of the method of

extraction. This applies even to the relatively crude total cross section method. However, differences in absolute magnitude of up to factors of approximately two are obtained using the different techniques. One can, of course, discount the total cross section method for absolute values since this method places relatively large weight on the large angle cross section where it is well established that the Butler theory breaks down. This leaves good agreement between the normal peak fitting technique and the Bowcock "intensity" method with the Amado extrapolation yielding values a factor of two smaller.

It is of interest to note that the Amado extrapolation achieves the result of the Bowcock technique, namely, to place large weight on the higher order Legendre polynomials in the polynomial fit. It is thus not surprising that they give roughly the same answer.

These results support the contention of Macfarlane and French [19]) that if the simple Butler formula provides an adequate fit to the observed angular distribution near the peak, the reduced width obtained by the simple peak fitting method is not significantly different from that obtained by the techniques of Amado or of Bowcock.

The reduced widths obtained in this investigation agree well with previously determined values obtained for the Si^{28}(d, n)P^{29} reaction [32]) and for the Si^{28}(d, p)Si^{29} reaction [33]).

6. Conclusions

From measurements on the total and differential cross sections for the Si^{28}(d, p)Si^{29} reaction in the energy range $6 \leqq E_d \leqq 10.7$ MeV it has been demonstrated that the reaction mechanism is predominantly a direct one; however, significant interference terms between the direct amplitudes and compound system amplitudes are observed. Upper limits of $< 15\,\%$ and $< 30\%$ have been established on the intensity of the compound system contributions to the reaction cross sections to the ground state and first two excited states of Si^{29}, respectively. It is of interest to note that this is similar to the results of Schiffer and Lee [34]) for dp reactions carried out for $E_d = 3.8-4.5$ MeV and for target nuclei between Ti and Ni, suggesting that the ratio of the contributions from direct and compound system amplitudes is essentially independent of energy over a range of deuteron energies both below and above the ordinary Coulomb barrier. This is a somewhat unexpected result and it would be of considerable interest to discover how general this conclusion may be.

The energy dependence of the total dp reaction cross section has been shown to be well reproduced by the simple plane wave stripping formalism. On the other hand this formalism does not predict the angular distributions measured at other than the regions of the prominent stripping maxima. Empirically it has been demonstrated that adequate fits are obtainable by removing the

angle dependence contained in the deuteron factor; this has been shown to be true for both $l_n = 0$ and $l_n = 2$ cases. Further measurements are again required to delineate the range of validity of this empirical approach.

It has been demonstrated that the four different techniques applied for the extraction of reduced widths from the experimental data give the same relative reduced widths for the dp reactions leading to different final states, even when different values of l_n are involved. In absolute magnitude the usual method of fitting the forward peak with Butler theory and the method of Bowcock were found to give the same result, while the Amado extrapolation technique was found to yield a value a factor of two smaller. This is perhaps not surprising since all methods implicitly assume that a Butler type formalism of the sort given by eq. (3) adequately fits the data. Of the various approaches, that involving simple fitting of the forward maximum has the advantage of simplicity; that suggested by Bowcock provides perhaps the greatest insight into the reaction mechanisms involved in addition to providing the reduced width determination.

Detailed measurements on the Si^{28}(d, pγ)Si^{29} reactions carried out in conjunction with those reported herein are presented in a preceding paper [12]) where they are analysed in terms of distorted wave formalism. These correlation data again provide convincing evidence for a dominant direct reaction mechanism.

The authors wish to thank Drs. E. Vogt, H. McManus and L. G. Elliott for helpful discussions.

Note added in proof: It has been found impossible to sufficiently alter the deuteron form factor using any reasonable deuteron potential (see e.g. Bromley, Kuehner and Almqvist [35])). Alternatively, it has been found by Buck and Satchler [36]) that reasonably good fits are obtained to these angular distributions in a distorted wave calculation which also provides good agreement with the statistical tensors derived by Kuehner, Almqvist and Bromley [12]).

We should like to point out that in the last mentioned article, the forelast paragraph of the Introduction (starting with "It should be noted . . .", on p. 616) needs some correction. The end of the first sentence (beginning with "as will be the case . . .") should be canceled. The statements in this paragraph apply only to the case $l_n = 2$. The number of real theoretical parameters is $2l_n$; thus for $l_n = 1$ a single (d, pγ) angular correlation measurement is sufficient to determine the statistical tensors.

References

1) S. T. Butler, Proc. Roy. Soc. A **208** (1951) 559
2) See for example, W. Tobocman, Phys. Rev. **115** (1959) 98
3) Bonner, Eisinger, Kraus and Marion, Phys. Rev. **101** (1956) 209
4) McEllistrem, Jones, Chiba, Douglas, Herring and Silverstein, Phys. Rev. **104** (1956) 1008

5) Nonaka, Morita, Kawai, Ishimatsu, Takashita, Nakajima and Takano, J. Phys. Soc. Japan **12** (1957) 841
6) S. Morita, J. Phys. Soc. Japan **13** (1958) 126
7) J. L. Weil and K. W. Jones, Phys. Rev. **112** (1958) 1975
8) Stratton, Blair, Famularo and Stuart, Phys. Rev. **98** (1955) 629
9) E. Baumgartner and H. W. Fulbright, Phys. Rev. **107** (1957) 219
10) Berthelot, Cohen, Cotton, Faraggi, Grjebins, Leveque, Naggiar, Roclawski-Conjeaud and Szteinsznaider, Compt. Rend. **238** (1954) 1312
11) L. L. Lee and J. P. Schiffer, Phys. Rev. **107** (1957) 1340
12) Kuehner, Almqvist and Bromley, Nuclear Physics **19** (1960) 614
13) Bromley, Gove, Litherland, Paul and Almqvist, Can. Jour. Phys. **35** (1959) 1042
14) G. J. McCallum, to be published;
G. J. McCallum and A. E. Litherland, Bull. Am. Phys. Soc. **5** (1960) 56
15) Huby, Refai and Satchler, Nuclear Physics **9** (1958) 94
16) J. Sawicki and G. R. Satchler, Nuclear Physics **7** (1958) 289
17) C. R. Lubitz, Numerical table of Butler-Born approximation stripping cross sections, University of Michigan (1957) (unpublished)
18) H. A. Enge and A. Graue, Naturv. rekke, Nr. **13** (1955) 1
19) M. H. Macfarlane and J. B. French, Rev. Mod. Phys. **32** (1960) 567
20) W. Hauser and H. Feshbach, Phys. Rev. **87** (1952) 366
21) E. Vogt, to be published
22) A. M. Lane and R. E. Thomas, Rev. Mod. Phys. **30** (1958) 257
23) Sharp, Kennedy, Sears and Hoyle, Chalk River Report CRT-556, (1954) (unpublished)
24) S. Hinds and R. Middleton, in press
25) L. Madansky and G. E. Owen, Phys. Rev. **99** (1955) 1608;
G. E. Owen and L. Madansky, Phys. Rev. **105** (1957) 1766
26) Butler, Austern and Pearson, Phys. Rev. **112** (1958) 1227
27) Almqvist, Bromley and Kuehner, unpublished measurements
28) R. D. Amado, Phys. Rev. Letters **2** (1959) 399
29) J. E. Bowcock, Proc. Phys. Soc. A **68** (1955) 512
30) W. Tobocman, Phys. Rev. **102** (1956) 588 (L)
31) W. Tobocman and M. H. Kalos, Phys. Rev. **97** (1955) 132
32) Calvert, Jaffe and Maslin, Proc. Phys. Soc. A **70** (1957) 78
33) J. R. Holt and T. N. Marsham, Proc. Phys. Soc. A **66** (1953) 467
34) J. P. Schiffer and L. L. Lee, Phys. Rev. **115** (1959) 1705
35) Bromley, Kuehner and Almqvist, Proc. Intern. Conf. on Nuclear Structure, ed. by D.A. Bromley and E. W. Vogt (University of Toronto Press, 1960), p. 349
36) Buck and Satchler, Proc. Intern. Conf. on Nucler Structure, ed. by D. A. Bromley and E. W. Vogt (Uneversity of Toronto Press, 1960), pp. 44, 285, 289; and private communication

1.C

Nuclear Physics **21** (1960) 582—594; © *North-Holland Publishing Co., Amsterdam*

Not to be reproduced by photoprint or microfilm without written permission from the publisher

ENERGY OF A LOW DENSITY NEUTRON GAS

P. C. SOOD † and S. A. MOSZKOWSKI

University of California, Los Angeles, California ††

Received 25 July 1960

Abstract: The energy of a neutron gas is calculated in the low density limit using the singlet S state shift corresponding to the Gammel-Thaler potential. The corrections to this energy are evaluated assuming a factorable interaction (i.e. a separable potential). The correction due to the Pauli exclusion principle and the pairing correction, i.e., depression of the ground state energy due to pair correlations (similar to that in the theory of superconductivity) are calculated. It is concluded that a pure neutron gas is unbound even at very low densities.

1. Introduction

Recently some calculations have been made by Brueckner, Gammel and Kubis [1]) (hereafter referred to as BGK) on the binding energy of a neutron gas following some earlier speculations [2,3]) on the subject. They applied the methods of Brueckner and Gammel [4]), developed earlier for discussing the properties of nuclear matter, to determine the energy of a pure neutron gas as a function of density; the change in energy from a superconducting type of level inversion was also estimated and shown to be negligible. They also looked at the low density limit by calculating the interaction energy using the so-called phase shift approximation [5]), the relevant singlet S state phase shift being derived from the effective range formula. In the latter case no corrections were included except pointing out that the singlet scattering phase shift, and hence the interaction energy, is expected to be markedly reduced through the effect of the Pauli exclusion principle. It was concluded that a neutron gas is not bound at any density.

In the present paper we treat the low density region, but include two important corrections. Besides the correction due to the Pauli exclusion principle we must consider the pairing effect, i.e., the depression of the ground state energy associated with an energy gap (similar to that in the theory of superconductivity). This second correction is particularly important at low densities where the potential and kinetic energies (assuming a degenerate Fermi gas) are small. These corrections are estimated assuming a factorable interaction. The results point to a system unbound even at very low densities, although they are somewhat sensitive to the magnitude of the energy gap.

† Present address — Physics Department, Panjab University, Chandigarh, India.

†† This work was supported in part by the Office of Ordnance Research U. S. Army.

2. Phase Shift Approximation

In the low density limit the diagonal element of the reaction matrix is given by the phase shift approximation [5])

$$t^{N}(k, k) = -\frac{4\pi\hbar^2}{m}\frac{\delta}{k}, \tag{1}$$

the phase shift δ referring to the singlet S state interaction. In this limit the higher partial waves (with $L \neq 0$) are unimportant due to the centrifugal barrier and the triplet S state cannot occur for a pair of neutrons because of the Pauli exclusion principle. The potential energy per particle is obtained by multiplying the reaction matrix for a given relative momentum k by the probability of finding a pair of particles with that relative momentum, and is given by [1,6])

$$\frac{\text{P.E.}}{N} = \tfrac{1}{2}\int_0^{k_F} t^{N}(k, k)\left(1-\tfrac{3}{2}\frac{k}{k_F}+\tfrac{1}{2}\frac{k^3}{k_F{}^3}\right)\frac{4\pi k^2 \mathrm{d}k}{(2\pi)^3}. \tag{2}$$

The statistical factor is $\frac{1}{2}$ in this case because each neutron can interact with only half the neutrons, i.e., those with opposite spin. It should be noted that for a neutron gas

$$N = 2\left(\frac{4\pi}{3}k_F{}^3\right)\frac{\Omega}{(2\pi)^3},$$

where Ω is the volume of the system. Thus we obtain

$$\frac{N}{\Omega} = \frac{k_F{}^3}{3\pi^2} \tag{3}$$

and

$$k_F = \frac{1.912}{r_0}, \tag{4}$$

r_0 being the radius of the mean volume per neutron.

The phase shift may be calculated, as in BGK, using the effective range formula

$$k\cot\delta = -\frac{1}{a}+\tfrac{1}{2}bk^2, \tag{5}$$

with

$$a = -23.6\times10^{-13}\,\text{cm}, \quad b = 2.65\times10^{-13}\,\text{cm} \tag{6}$$

for the singlet S state. Alternatively it can be obtained for the Gammel Thaler potential (Yukawa well with a repulsive core at 0.4×10^{-13} cm; $V_0 = 434$ MeV and $\mu = 1.45$ for the singlet S state interaction). The potential energy in the two cases differs by only 1—2 %. We have used the latter approach since the

results could be easily obtained with an existing code for numerical calculations (prepared for studying the nuclear matter problem [6]) using the IBM 709 at the Western Data Processing Center at UCLA).

The results obtained for the potential and the total energy per particle are given in table 1. Evidently the system does not lead to a bound state or a

TABLE 1

Energy of a neutron gas in the low density limit (phase shift approximation)

k_F	r_0	K.E./N	P.E./N	E/N
0.1	19.12	0.12	−0.07	+0.05
0.2	9.56	0.50	−0.39	+0.11
0.3	6.37	1.12	−0.96	+0.16
0.4	4.78	1.99	−1.75	+0.24
0.5	3.82	3.11	−2.75	+0.36
0.6	3.19	4.48	−3.92	+0.56
0.64	3.0	5.10	−4.43	+0.67

minimum in the energy density curve. The interaction energy is cut down by the effect of the Pauli exclusion principle whereas the pairing effect serves to push the ground state farther down. Now we consider these two effects separately assuming a factorable interaction. In the following section we derive the parameters of such an interaction.

3. Factorable Interaction

Since we are dealing with the region of momenta rather small compared to the range of the potential, it does not make much difference what form of the potential we choose. The momenta considered are small enough such that the system can only feel the overall effect of the potential but not its details, i.e., only the low energy parameters are important. Thus the potential that we use does not have to have a repulsive core. Indeed it does not have to be local and it seems simplest for the purposes of the present paper to assume a factorable (or separable) interaction. We define the latter as one for which $V(k, k')$ can be written in the form

$$V(k, k') = -V_0 g(k) g(k'). \tag{7}$$

Such a potential was considered by Yamaguchi [7] for the two nucleon problem and the form

$$g(k) = \frac{1}{1+\dfrac{k^2}{\mu^2}} \tag{8}$$

was found to be quite satisfactory. The potential $V(k, k')$ is then a "pseudo-Yukawa" type of potential.

The diagonal matrix elements for the reaction matrix are then given by

$$t(k, k) = V(k, k) + \int_0^\infty V(k, k')G(k', k)t(k', k)\mathrm{d}k', \tag{9}$$

where $G(k', k)$ is the sine transform of the Green's function

$$G(k', k) = \frac{-Q(k')}{e(k')-e(k)} \frac{4\pi k'^2}{(2\pi)^3}, \tag{10}$$

the quantity $Q(k')$ being the projection operator which takes into account the effect of the Pauli exclusion principle and is unity if in the intermediate state both neutrons are outside the Fermi sea and zero otherwise; e denotes the sum of the single particle energies of a pair, and, since the density is quite low, we can neglect the dispersion effect [6]) (modification of the energy momentum relation due to the presence of the other particles) and write $e(k) = \hbar^2 k^2/m$.

For the factorable interaction given in eq. (7) we obtain

$$t(k, k) = \frac{-V_0 g^2(k)}{1+V_0 \int_0^\infty g^2(k')G(k', k)\mathrm{d}k'}. \tag{11}$$

In order to evaluate the parameters of the factorable interaction we consider the scattering of free particles. In this case we know that

$$t^{\mathrm{F}}(0, 0) = + \frac{4\pi\hbar^2}{m} a, \tag{12}$$

$$t^{\mathrm{F}}(k, k) = - \frac{4\pi\hbar^2}{m} \frac{\tan\delta}{k}, \tag{13}$$

where the phase shift δ and the scattering length a can be obtained from the effective range formula (5). It may be noted that eq. (13) is different from the result in the phase shift approximation as given in eq. (1) since the boundary conditions at infinity are different in the two cases. This has been pointed out by Riesenfeld and Watson [5]). For free particles we have $Q = 1$ and

$$G(k', k) = -\beta \frac{k'^2}{k'^2-k^2}, \tag{14}$$

where

$$\beta = \frac{m}{2\pi^2\hbar^2}. \tag{15}$$

Then we can write the integral in eq. (11) as

$$\begin{aligned} \int_0^\infty g^2(k')G(k', k)\mathrm{d}k' &= -\beta\mu^4 \int_0^\infty \frac{k'^2\mathrm{d}k'}{(k'^2+\mu^2)^2(k'^2-k^2)} \\ &= -\beta\mu^4 J(k). \end{aligned} \tag{16}$$

For $k = 0$, we can evaluate J by changing the variable as $k' = \mu \tan \theta$ and obtain

$$J(0) = \frac{\pi}{4\mu^3}. \tag{17}$$

Hence from eq. (11) we get

$$t^{\mathrm{F}}(0, 0) = \frac{-V_0}{1-\frac{1}{4}\beta V_0 \pi\mu}. \tag{18}$$

For $k \neq 0$, the integral $J(k)$ can be evaluated as a contour integral in the complex k plane and the result is

$$J(k) = \frac{\pi}{4\mu} \frac{\mu^2-k^2}{(\mu^2+k^2)^2}, \tag{19}$$

and

$$t^{\mathrm{F}}(k, k) = -\frac{V_0\mu^4}{(\mu^2+k^2)^2}\left[1-\frac{mV_0}{\hbar^2}\frac{\mu^3}{8\pi}\frac{(\mu^2-k^2)}{(\mu^2+k^2)^2}\right]^{-1}. \tag{20}$$

Comparing the results in eqs. (12), (13) and (18), (20) we get

$$b = \frac{2+s}{\mu s}, \quad a = -\frac{2s}{\mu(1-s)}, \quad V_0 = s\frac{8\pi\hbar^2}{\mu m}, \tag{21}$$

where s is the strength parameter [8]) for the potential. Substituting for a and b from eq. (6), we obtain

$$\mu = 1.186, \quad s = 0.933, \quad V_0 = 820\ \mathrm{MeV}. \tag{22}$$

4. Pauli Effect

We have seen that for free particles we have

$$t^{\mathrm{F}}(k, k) = \frac{V(k, k)}{1-\beta V_0 \int_0^\infty g^2(k')\left(\frac{k'^2}{k'^2-k^2}\right)\mathrm{d}k'}. \tag{23}$$

For convenience we suppress the indices (k, k) in following. Including the effect of the Pauli exclusion principle (denoted by the superscript X) and assuming the center of mass momentum to be zero we have

$$t^{\mathrm{X}} = \frac{V}{1-\beta V_0 \int_{k_{\mathrm{F}}}^\infty g^2(k')\left(\frac{k'^2}{k'^2-k^2}\right)\mathrm{d}k'}. \tag{24}$$

The integral in the denominator of eq. (24) is similar to the integral I_2 in eq.

(A.1) (see appendix) and can be evaluated similarly to give

$$\beta V_0 \int_{k_F}^{\infty} g^2(k') \left(\frac{k'^2}{k'^2-k^2}\right) \mathrm{d}k'$$

$$= \tfrac{1}{2}\beta V_0 g^2(k) \left[\left(1-\frac{k^2}{\mu^2}\right)\frac{\pi\mu}{2} - 2k_F\left(1-\frac{2}{3}\frac{k_F^2}{\mu^2}\right) - k\log\frac{k_F-k}{k_F+k}\right] \quad (25)$$

$$= \beta V_0 g^2(k) \left[\left(1-\frac{k^2}{\mu^2}\right)\frac{\pi\mu}{4} - \tfrac{1}{2}kf\left(\frac{k}{k_F}\right)\right],$$

where

$$f\left(\frac{k}{k_F}\right) = \frac{2k_F}{k}\left(1-\frac{2}{3}\frac{k_F^2}{\mu^2}\right) + \log\frac{1-\dfrac{k}{k_F}}{1+\dfrac{k}{k_F}}. \quad (26)$$

Now we note from eq. (23) that

$$\beta V_0 \int_0^{\infty} g^2(k') \left(\frac{k'^2}{k'^2-k^2}\right) \mathrm{d}k' = 1 - \frac{V}{t^F}, \quad (27)$$

while from eq. (16) and (19) we get

$$\beta V_0 \int_0^{\infty} g^2(k') \left(\frac{k'^2}{k'^2-k^2}\right) \mathrm{d}k' = \beta V_0 g^2(k) \left(1-\frac{k^2}{\mu^2}\right)\frac{\pi\mu}{4}. \quad (28)$$

Combining the results in eqs. (24)—(28) we obtain

$$t^X = \frac{V}{1-\left(1-\dfrac{V}{t^F}\right) - \tfrac{1}{2}\beta V k f\left(\dfrac{k}{k_F}\right)}$$

$$= \frac{t^F}{1-\tfrac{1}{2}\beta t^F k f\left(\dfrac{k}{k_F}\right)}.$$

Also we note that

$$\tfrac{1}{2}\beta t^F k = -\frac{1}{2}\frac{m}{2\pi^2\hbar^2}\frac{4\pi\hbar^2}{m}\frac{\delta(k)}{k}k = -\frac{\delta(k)}{\pi},$$

so that we get

$$t^X = \frac{t^F}{1+\dfrac{\delta(k)}{\pi} f\left(\dfrac{k}{k_F}\right)}. \quad (29)$$

Now the relative momentum k of a pair of particles inside the Fermi sea can

have all the values from zero to k_F. Thus including the effect of the Pauli principle we may write

$$\text{P.E.}^X = \frac{\text{P.E.}^F}{1+\frac{\delta(\bar{k})}{\pi} f\left(\frac{\bar{k}}{k_F}\right)}, \tag{30}$$

where $\bar{k}$ is a suitable "average" relative momentum. Now it is seen that the probability of finding a pair of particles with relative momentum k(see eq. (2)) is peaked about $k \approx \frac{1}{2}k_F$, and hence we take

$$\bar{k} = \tfrac{1}{2}k_F$$

which gives

$$f\left(\frac{\bar{k}}{k_F}\right) = 2.9014 - 1.90k_F^2. \tag{31}$$

To obtain an order of magnitude estimate we note that the phase shift is about 1 and also $f(\bar{k}/k_F)$ is of the order of π, such that the Pauli exclusion principle cuts down the potential energy to about one half. The correction factor is a slowly varying function of k, and a different choice for average momentum near $\frac{1}{2}k_F$ will not change the results significantly.

The results obtained using eqs. (30)—(31) are given in columns 4 and 5 of table 2. It is seen that we get farther away from any minimum in the energy density curve.

TABLE 2

Energy of a neutron gas; the superscript X denotes the inclusion of the Pauli effect. The index (1) gives the results corresponding to eq. (39) and the index (2) corresponding to eq. (47) for the pairing correction.

k_F	$\frac{\text{K.E.}}{N}$	$\frac{\text{P.E.}}{N}$	$\frac{\text{P.E.}^X}{N}$	$\frac{E^X}{N}$	$\frac{W_0^{(1)}}{N}$	$\frac{E^{(1)}}{N}$	$\frac{W_0^{(2)}}{N}$	$\frac{E^{(2)}}{N}$
0.1	0.12	−0.07	−0.04	+0.08	−0.06	+0.02	−0.02	+0.06
0.2	0.50	−0.39	−0.20	+0.30	−0.34	−0.04	−0.08	+0.22
0.3	1.12	−0.96	−0.49	+0.63	−0.57	+0.06	−0.16	+0.47
0.4	1.99	−1.75	−0.91	+1.08	−0.66	+0.42	−0.23	+0.85
0.5	3.11	−2.75	−1.49	+1.62	−0.63	+0.99	−0.28	+1.34

5. Pairing Effect

5.1. INTRODUCTION

It has been shown by Bardeen, Cooper and Schrieffer [9]) that the energy difference between the superconducting and the normal states is given by

$$W_0 = -\tfrac{1}{2}N(0)\varepsilon_0^2 = \frac{-2N(0)(\hbar\omega)^2}{\exp\left(-\frac{2}{N(0)V}\right)-1}, \tag{32}$$

where

$$2\varepsilon_0 = \Delta E \tag{33}$$

is the minimum excitation energy required to break up a pair, and is, therefore, the width of the energy gap in the excitation spectrum associated with a highly correlated ground state; $N(0)$ is the density of the states of given spin at the Fermi surface. We know that

$$N(0) = \left.\frac{\mathrm{d}n}{\mathrm{d}E}\right|_{E=E_F} = \left.\frac{\mathrm{d}n}{\mathrm{d}T}\right|_{T=T_F} = A\sqrt{T_F}.$$

The proportionality constant A can be determined from the condition

$$\int_0^{T_F} \frac{\mathrm{d}n}{\mathrm{d}T}\,\mathrm{d}T = \tfrac{1}{2}N.$$

This gives

$$\frac{N(0)}{N} = \frac{3}{4T_F} = \frac{3m}{2\hbar^2 k_F^2}. \tag{34}$$

Also substituting for N from eq. (3) we get

$$N(0) = \beta k_F \Omega. \tag{35}$$

A rough estimate of the pairing effect can be obtained by considering the matrix elements of the potential V with properly normalized S state wave-functions. Thus we obtain

$$N(0)V = \beta k_F V(k_F, k_F). \tag{36}$$

In the low density limit we may replace this by

$$\begin{aligned} N(0)V &= \beta k_F t^F(k_F, k_F) \\ &= -\frac{2\tan\delta}{\pi}. \end{aligned} \tag{37}$$

As in BGK we take the characteristic energy to be the kinetic energy at the Fermi surface, i.e.,

$$\hbar\omega = \frac{\hbar^2 k_F^2}{2m}. \tag{38}$$

Under these assumptions we obtain the energy shift per particle as

$$\frac{W_0}{N} = -\frac{\frac{3}{4}\frac{\hbar^2 k_F^2}{m}}{\exp(\pi\cot\delta) - 1}. \tag{39}$$

The results obtained using this expression are shown in column 6 of table 2, and the resulting total energy per particle in the following column. It is seen

that in this approximation the pairing correction at very low densities is even larger than the corrected potential energy and we get a system with energy very close to zero at rather low densities. However the assumptions made in eqs. (36)—(38) are rather arbitrary. A more accurate evaluation of this effect can be made using factorable interaction. Such an approach has also been considered by Mottelson and Glassgold [10]).

5.2. EVALUATION OF THE ENERGY GAP

As pointed out by Cooper [11]), the basic feature of the Bardeen-Cooper-Schrieffer theory is that the correlated states involve single particle excitations only in a small shell near the Fermi surface, and, if we restrict ourselves to pair correlations, (which are assumed to be responsible for the qualitative features of superconductivity) we are interested in the interaction which takes a pair of particles from one state to another state in this shell near the Fermi surface. The two-body correlations are assumed to have a very strong preference for singlet zero momentum pairs.

Consider two particles of equal but opposite momenta equal to the Fermi momentum, i.e.,

$$k_1 = -k_2 = k_F.$$

These particles can interact as shown in fig. 1(a); actually the particles may end up anywhere on the Fermi surface, but we consider the simplest case shown.

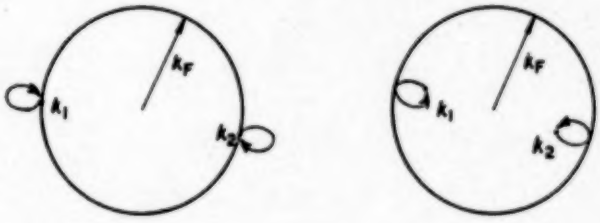

(a) (b)

Fig. 1. (a) The particle-particle interaction. (b) The hole-hole interaction.

For this process (particle-particle interaction) we have

$$G = -\beta \frac{k'^2}{k'^2 - k_F^2} \qquad (k' > k_F).$$

Also we can have a process of the type shown in fig. 1(b); the case shown is identical to the one where a hole starts at the surface, scatters into the Fermi sea and then back out (hole-hole interaction). For the holes we have negative energy and hence

$$G = +\beta \frac{k'^2}{k'^2 - k_F^2}.$$

Combining both of these processes we get

$$G = -\beta \frac{k'^2}{|k'^2 - k_F^2|}.$$

In addition we include the effect of the energy gap by assuming

$$G = -\beta \frac{k'^2}{|k'^2 - k_F^2| + \alpha^2}, \tag{40}$$

where

$$\varepsilon_0 = \frac{\hbar^2 \alpha^2}{m}. \tag{41}$$

We find from eq. (11) that a bound state is determined by the condition

$$1 + V_0 \int_0^\infty g^2(k) G(k, k_F) \mathrm{d}k = 1 - \beta V_0 I = 0. \tag{42}$$

At this point the reaction matrix has a singularity. The evaluation of the integral I (see appendix) leads to the relation

$$1 - \beta V k_F \left[\log \frac{\eta \alpha^2}{4 k_F^2} + \frac{1}{\beta V k_F} \left(1 - \frac{V}{t^F} \right) \right] = 0, \tag{43}$$

where

$$\eta = \exp \left[2 - \frac{4}{3} \frac{k_F^2}{\mu^2} \right]. \tag{44}$$

Thus we obtain

$$\begin{aligned} \varepsilon_0 = \frac{\hbar^2}{m} \alpha^2 &= \frac{4}{\eta} \frac{\hbar^2 k_F^2}{m} \exp \left[\frac{1}{\beta k_F t^F} \right] \\ &= \frac{4}{\eta} \frac{\hbar^2 k_F^2}{m} \exp(-\tfrac{1}{2} \pi \cot \delta). \end{aligned} \tag{45}$$

5.3. COMPARISON WITH OTHER CALCULATIONS

Emery and Sessler [12]) have also calculated the magnitude of the energy gap in nuclear matter. In the low density limit they give

$$\Delta E = 2\varepsilon_0 = \frac{8 \hbar^2 k_F^2}{m^*} \exp \left[-\tfrac{1}{2} \pi \frac{m}{m^*} \cot \delta \right]. \tag{46}$$

For densities of interest in our case m^* is very nearly equal to m. Thus we find that their value is $\eta (\approx e^2)$ times, i.e. about 7 times, larger than our result. We tabulate some results in table 3. It is clearly seen that their low density limit result is very much an overestimate, and, moreover, does not join on to their results from detailed calculations at somewhat higher densities. Our result

seems to be quite reasonable in these respects, and is derived on the basis of

TABLE 3

Values of the energy gap $\Delta E = 2\varepsilon_0$ as obtained by Emery and Sessler [13]) and from our eq. (45).

k_F	Emery and Sessler [13])		$\Delta E = 2\varepsilon_0$ from eq. (45)
	Detailed calc.	Low density limit	
0.1		1.35	0.18
0.2		6.10	0.85
0.3	1.50	12.27	1.81
0.4	2.38	18.21	2.87
0.5	3.22	22.79	3.91

plausible assumptions (validity of the factorable interaction in the region of momenta small compared to the range of the potential, and neglecting terms of the fourth and higher order in k_F and α).

5.4. PAIRING CORRECTION

The pairing energy per particle is now given by

$$\frac{W_0}{N} = \frac{N(0)}{N}\,\frac{\varepsilon_0^2}{2} = \frac{12}{\eta^2}\,\frac{\hbar^2 k_F^2}{m}\exp(-\pi\cot\delta). \tag{47}$$

The results obtained by using this expression for the pairing energy and total energy per particle are given in the last two columns of table 2. The energy remains positive even at the lowest densities considered.

6. Conclusions and Discussion

We conclude that a neutron gas is not bound at even quite low densities. The estimated contribution from the pairing effect is too small to shift the balance towards binding or an energy minimum.

It may be argued that this is a consequence of the strength of the basic nucleon nucleon interaction. It is well known that the potential in the singlet S state does not give a bound state (e.g., the virtual singlet S state in the deuteron). Keeping this in view we have calculated the energy and the correction terms for the so-called "standard potential" (of ref. [6])) with the strength parameter $s = 1$. In the phase shift approximation we get a bound system with an energy minimum at $k_F = 0.5 (r_0 = 3.7 \times 10^{-13}$ cm), the binding energy being 0.36 MeV. However the phase shift for this potential is larger with the result that the Pauli correction factor cuts down the interaction energy by a larger factor; consequently even with the inclusion of the pairing effect we still get an unbound system.

Note added in proof: It may be pointed out that the approximate expression given in eq. (46) neglects (i) the dispersive property and (ii) the exclusion

effect; both these effects vanish as $k_F \to 0$ and the expression should hold in the limit. It is expected to be good for $k_F \ll 0.04$ whereas we have considered $k_F \geqq 0.10$. Thus the comparison in subsection 5.3 is not to be taken seriously. The authors are grateful to Dr. V. J. Emery for these comments.

We are very grateful to Professor A. M. Sessler for suggesting this problem and for stimulating discussions. One of us (P. C. S.) wishes to thank Mr. M. S. Cheema for helpful discussions. We would also like to express our appreciation to the Western Data Processing Center for making computation time available for use on the IBM 709 at UCLA.

Appendix

We evaluate the integral in eq. (42) as follows:

$$\begin{aligned} I &= -\frac{1}{\beta}\int_0^\infty g^2(k)G(k,k_F)\mathrm{d}k = \int_0^\infty \frac{\mu^4}{(\mu^2+k^2)^2}\,\frac{k^2}{|k^2-k_F^2|+\alpha^2}\,\mathrm{d}k \\ &= \int_0^{k_F} \frac{\mu^4}{(\mu^2+k^2)^2}\,\frac{k^2\,\mathrm{d}k}{[(k_F^2+\alpha^2)-k^2]} + \int_{k_F}^\infty \frac{\mu^4}{(\mu^2+k^2)^2}\,\frac{k^2\,\mathrm{d}k}{[k^2-(k_F^2-\alpha^2)]} \qquad \text{(A.1)} \\ &= I_1+I_2. \end{aligned}$$

Let us denote

$$k_F^2+\alpha^2 = a^2.$$

Then we have

$$\begin{aligned} I_1 &= \frac{a^2\mu^4}{(a^2+\mu^2)^2}\int_0^{k_F} \mathrm{d}k\left[\frac{1}{a^2-k^2}+\frac{1}{\mu^2+k^2}-\frac{\mu^2(a^2+\mu^2)}{a^2(\mu^2+k^2)^2}\right] \\ &= \frac{a^2\mu^4}{(a^2+\mu^2)^2}\left[\frac{1}{2a}\log\frac{a+k_F}{a-k_F}+\frac{1}{\mu}\,\frac{a^2-\mu^2}{2a^2}\tan^{-1}\frac{k_F}{\mu}-\frac{(a^2+\mu^2)k_F}{2a^2(\mu^2+k_F^2)}\right]. \qquad \text{(A.2)} \end{aligned}$$

We note that

$$\mu^2 \gg k_F^2 \gg \alpha^2,$$

so that we may neglect α^2 as compared to μ^2; also we neglect terms involving fourth and higher powers of α and k_F. This gives

$$\tan^{-1}\frac{k_F}{\mu} \approx \frac{k_F}{\mu}\left(1-\frac{1}{3}\,\frac{k_F^2}{\mu^2}\right), \quad a^2\pm\mu^2 = k_F^2+\alpha^2\pm\mu^2 \approx k_F^2\pm\mu^2.$$

With these approximations we can rewrite eq. (A.2) as

$$I_1 = -\tfrac{1}{2}k_F g^2(k_F)\left[\left(2-\frac{4}{3}\,\frac{k_F^2}{\mu^2}\right)+\left(1+\frac{\alpha^2}{2k_F^2}\right)\log\frac{\alpha^2}{4k_F^2+2\alpha^2}\right], \qquad \text{(A.3)}$$

where we have substituted

$$g^2(k_F) = \frac{\mu^4}{(\mu^2+k_F^2)^2}.$$

Similarly we get

$$I_2 = -\tfrac{1}{2}k_F g^2(k_F)\left[\left(2-\frac{4}{3}\frac{k_F^2}{\mu^2}\right)+\left(1-\frac{\alpha^2}{2k_F^2}\right)\log\frac{\alpha^2}{4k_F^2-2\alpha^2}-\frac{\pi\mu}{2k_F}\left(1-\frac{k_F^2}{\mu^2}\right)\right]. \tag{A.4}$$

Thus we obtain

$$I = -k_F g^2(k_F)\left[\left(2-\frac{4}{3}\frac{k_F^2}{\mu^2}\right)+\log\frac{\alpha^2}{4k_F^2}-\frac{\pi\mu}{4k_F}\left(1-\frac{k_F^2}{\mu^2}\right)\right], \tag{A.5}$$

where we have neglected the term

$$\frac{\alpha^2}{2k_F^2}\log\frac{4k_F^2-2\alpha^2}{4k_F^2+2\alpha^2},$$

which is of the order of $(\alpha/k_F)^2$.
Now from eq. (27), (28) we have

$$\frac{\pi\mu}{4}\left(1-\frac{k_F^2}{\mu^2}\right) = -\frac{1}{\beta V(k_F, k_F)}\left[1-\frac{V(k_F, k_F)}{t^F(k_F, k_F)}\right]. \tag{A.6}$$

Substituting this result in eq. (A.5) we obtain

$$I = -\bar{k}_F g^2(k_F)\left[\log\frac{\eta\alpha^2}{4k_F^2}+\frac{1}{\beta k_F V}\left(1-\frac{V}{t^F}\right)\right], \tag{A.7}$$

where

$$\eta = \exp\left(2-\frac{4}{3}\frac{k_F^2}{\mu^2}\right). \tag{A.8}$$

References

1) K. A. Brueckner, J. L. Gammel and J. T. Kubis, Phys. Rev. **118** (1960) 1095
2) E. E. Salpeter, Bull. Am. Phys. Soc. **4** (1959) 256
3) K. W. Chun, Ph. D. Thesis, University of Pennsylvania (1959)
4) K. A. Brueckner and J. L. Gammel, Phys. Rev. **109** (1958) 1023
5) W. B. Riesenfeld and K. N. Watson, Phys. Rev. **104** (1956) 492
6) S. A. Moszkowski and B. L. Scott, Annals of Physics (1960), to be published; B. L. Scott, Ph. D. Thesis, University of California, Los Angles (1960)
7) Y. Yamaguchi, Phys. Rev. **95** (1954) 1628
8) J. M. Blatt and V. M. Weisskopf, Theoretical nuclear physics (Wiley, New York, 1952) p. 52
9) J. Bardeen, L. N. Cooper and J. R. Schrieffer, Phys. Rev. **108** (1957) 1175
10) B. R. Mottelson and A. E. Glassgold, private communication
11) L. N. Cooper, Am. J. Phys. **28** (1960) 91
12) V. J. Emery and A. M. Sessler, Phys. Rev. **119** (1960) 248

8.A

Nuclear Physics **21** (1960) 595—598; © *North-Holland Publishing Co., Amsterdam*

Not to be reproduced by photoprint or microfilm without written permission from the publisher

HYPERNUCLEI PRODUCED BY K⁻ INTERACTIONS IN NUCLEAR EMULSIONS

(I) Mesic Decays

MILAN M. NIKOLIĆ

Institute of Physics, University of Bern

Received 19 August 1960

Abstract: 2 and 9 hypernuclei decaying according to the π^- mesic mode were found in examining 415 K^- interactions in flight and 1104 K^- absorptions at rest, respectively. 9 of these hypernuclei were uniquely identified while for the remaining 2 there are more possible interpretations.

The results of an analysis on hyperfragments decaying according to the π^- mesic decay mode and arising from K^- interactions are reported. A following paper [1]), henceforth referred to as (II), has been devoted to a study of the general characteristics of hypernuclei produced in K^- interactions at rest and in flight [2,3]) and to an analysis of the non-mesic decay mode.

Data regarding exposure, scanning and event selection as well as those concerning the profile measurements on tracks by the Poohstrolino method are given in (II). We adopted the range-energy relation of Barkas [4]) for the determination of energies of singly charged particles, and the R—E curve of Wilkins [5]) for the determination of energies of multiply charged particles. The stopping power of the stack was established by the measurement of the ranges of 100 muons from π^+ decays.

Because of the very short ranges of most of the hypernuclei and some of the decay products, it was often not possible to make measurements from which they could be identified. Consequently, we had in such cases to infer identities of the hyperfragments on the basis of the decay dynamics.

In all decays, which according to collinearity, coplanarity and other criteria involved no neutral particles, the determination of the recoil energy was made by considering the momentum balance [6]).

For the evaluation of binding energies we used Wapstra's ion masses [7]), converted by means of Cohen's conversion factor, as well as Barkas' and Rosenfeld's masses of elementary particles [8]). The value of (37.58 ± 0.15) MeV was adopted for the Q-value of the free Λ^0 particle [9]).

Most of the standards used here are the same as those employed by the Chicago group [9]), the report of which should be referred to as the main source of

information in hypernuclei decaying according to the π^- decay mode and arising from K^- captures.

The binding energy error was derived from the uncertainty in the total kinetic energy released in a hyperfragment decay and in a Λ^0 decay. In the estimation of the uncertainty in kinetic energy of a particle emitted in a decay of a hypernucleus, the following were taken into consideration: a) measurement errors, b) range straggling, c) the error in the shrinking factor due to

TABLE 1

Description of 11 hypernuclei

Event no.	Kinetic energy of K^-	Track	Range (μ)	Energy (from range)	Azimuth (deg.)	Dip angle (deg.)
J-111	$T_K \approx 120$ MeV	π^-	41820	54.48	0	−72.4
		He^4	8.9		180	71.4
J-2	$T_K \approx 100$ MeV	π^-	17045	31.51	0	−21
		$H^{1,2,3}$	119.2		156.7	15.7
H-74	K^- capture at rest	π^-	11403	24.86	0	−75
		p	562	9.92	312	77.8
		H^3	6.3		147	−48.1
B-256	K^- capture at rest	π^-	10349	23.49	0	55.6
		p	634	10.63	5	−68.5
		He^3	14		179.5	+39
B-454	K^- capture at rest	π^-	15096	29.34	0	− 7.8
		p	163.5	4.73	149	17.1
		He^4	≈2		249	
J-155	K^- capture at rest	π^-	14400	28.53	0	36.5
		p	43.6	2.08	343.7	7.3
		He^4	10.6		166.7	−27.7
J-302	K^- capture at rest	π^-	14765	28.96	0	−2.8
		p	50.9	2.29	38	−33
		He^4	11.1		192	12.1
J-133	K^- capture at rest	π^-	20152	34.83	0	+14
		Be^7	≈1.5		180	
K-71	K^- capture at rest	π^-	31571	45.76	0	−66
		He^4	4.6	1.52	183	−14.7
		He^4	9.2		4.5	67.3
B-338	K^- capture at rest	π^-	10749	24.02	0	−5.3
		p	231	5.85	169.8	53.4
		He^4	3.2	0.71	86.7	−32.7
		He^4	4.1		253.5	−25
B-292	K^- capture at rest	π^-	15381	29.67	0	13.7
		$H^{1,2,3}$	169		164.9	−19

TABLE 2

Uniquely identified hypernuclei

Event no.	Decay scheme	Q (MeV)	B_Λ (MeV)	δB_Λ (MeV)	P (MeV/c)	r_i (μ)	r_0 (μ)^0
J-111	${}_\Lambda H^4 \rightarrow He^4+\pi^-$	56.92	0.47	1.1	135	8.8	8.9
H-74	${}_\Lambda H^4 \rightarrow H^3+p+\pi^-$	35.61	1.97	0.6	68	8	6.3
B-256	${}_\Lambda He^4 \rightarrow He^3+p+\pi^-$	36.56	1.02	1.0	117	9.4	14.0
B-454	${}_\Lambda He^5 \rightarrow He^4+p+\pi^-$	34.43	3.15	0.6	52	2	2
J-155	${}_\Lambda He^5 \rightarrow He^4+p+\pi^-$	33.63	3.95	0.6	150	11.4	10.6
J-302	${}_\Lambda He^5 \rightarrow He^4+p+\pi^-$	34.17	3.41	0.6	147	11 .	11.1
J-133	${}_\Lambda Li^7 \rightarrow Be^7+\pi^-$	35.67	7.51	0.7	105	1.3	1.5
K-71	${}_\Lambda Li^8 \rightarrow He^4+He^4+\pi^-$	50.22	4.70	1.0	148	11.1	9.2
B-338	${}_\Lambda Be^9 \rightarrow He^4+He^4+p+\pi^-$	31.60	6.11	0.6	85	4	4 2

Notations used in tables 2 *and* 3: Q is the sum of the kinetic energies of the decay products, B_Λ the binding energy of the Λ^0 hyperon in the hypernuclei, δB_Λ as defined in the text, P the resultant momentum of all decay products except recoil, r_i the range of the recoil inferred from P and r_0 the observed recoil range.

TABLE 3

Non uniquely identified hypernuclei

Event no.	Decay scheme	Q (MeV)	B_Λ (MeV)	δB_Λ (MeV)	P (MeV/c)	r_i (μ)	r_0 (μ)
J-2	${}_\Lambda H^4 \rightarrow H^3+p+\pi^-$	35.69	1.89	0.7	39	2.2	0
	${}_\Lambda He^4 \rightarrow He^3+p+\pi^-$	35.69	1.89	0.7	39	1.5	0
	${}_\Lambda He^5 \rightarrow He^4+p+\pi^-$	35.62	1.96	0.7	39	1.5	0
	${}_\Lambda He^7 \rightarrow He^6+p+\pi^-$	35.55	2.03	0.7	39	1	0
B-292	${}_\Lambda H^4 \rightarrow H^3+p+\pi^-$	34.63	2.95	0.7	26	1	0
	${}_\Lambda He^4 \rightarrow He^3+p+\pi^-$	34.63	2.95	0.7	26	1	0
	${}_\Lambda He^5 \rightarrow He^4+p+\pi^-$	34.60	2.98	0.7	26	1	0
	${}_\Lambda He^7 \rightarrow He^6+p+\pi^-$	34.57	3.01	0.7	26	1	0

the uncertainty in the original pellicle thickness, d) the error in the stopping power correction factor due to the uncertainty in emulsion density, and d) the error in the adopted range-energy relation. In evaluation of d) we also took into account Barkas' uncertainty in estimating the standard emulsion density.

The hypernuclei analysed on the basis of the decay kinematics were also run on the Computer "Bull Gamma 3" in a similar way to the non-mesically decaying hypernuclei, in order to control the decay analysis and the computer program (see Appendix in (II)).

Two and nine π^- mesonically decaying hypernuclei were found in examining

415 K^- interactions in flight and 1100 K^- absorptions at rest, respectively.

The observed data describing the events, as well as energies of particles, derived from their ranges, are shown in table 1. Interpretations of the events are given in tables 2 and 3. In table 2 uniquely identified hypernuclei are presented, while in table 3 those cases are given which could not be uniquely interpreted.

As can be seen from table 3, the events I-2 and B-292 could be interpreted as the hyperfragment decay only on the condition that an unvisible recoil was also emitted. However, the possibility that the event I-2 is due to the K^- re-emission could not be excluded.

The observed schemes of decays as well as the values of the binding energies of the Λ^0 hyperon are in agreement with those already published.

All other results related to hypernuclei, which were obtained in the course of this work, are presented in (II), except already published description and interpretation of an unusual double star [10]).

References

1) V. Gorgé, W. Koch, W. Lindt, M. Nikolić, S. Subotić-Nikolić and H. Winzeler, Nuclear Physics **21** (1960) 599
2) M. Nikolić, Y. Eisenberg, W. Koch, M. Schneeberger and H. Winzeler, Helv. Phys. Acta **3** (1960) 221;
W. Koch, Y. Eisenberg, M. Nikolić, M. Schneeberger and H. Winzeler, Helv. Phys. Acta **3** (1960) 237
3) Y. Eisenberg, W. Koch, E. Lohrmann, M. Nikolić, M. Schneeberger and H. Winzeler, Nuovo Cim. **9** (1958) 745
4) W. H. Barkas, P. H. Barrett, P. C. Cüer, H. Heckman, F. M. Smith and H. K. Ticho, Nuovo Cim. **8** (1958) 185;
W. H. Barkas, Nuovo Cim. **8** (1958) 201
5) J. J. Wilkins, A.E.R.E. S/R **664** (1952)
6) W. E. Slater, Suppl. Nuovo Cim. **10** (1958) 1
7) A. H. Wapstra, Physica **21** (1955) 367
8) W. H. Barkas and A. H. Rosenfeld, UCRL-8030 (1958)
9) R. Ammar, R. Levi-Setti, W. E. Slater, S. Limentani, P. E. Schlein and P. H. Steinberg, Nuovo Cim. **15** (1960) 181
10) M. Nikolić, W. Koch, M. Schneeberger and H. Winzeler, Nuclear Physics **15** (1960) 519

8.A

Nuclear Physics **21** (1960) 599—623; © *North-Holland Publishing Co., Amsterdam*

Not to be reproduced by photoprint or microfilm without written permission from the publisher

HYPERNUCLEI PRODUCED BY K⁻ INTERACTIONS IN NUCLEAR EMULSIONS

(II) General Characteristics and Non-Mesic Decays

V. GORGÉ, W. KOCH, W. LINDT, M. NIKOLIĆ, S. SUBOTIĆ-NIKOLIĆ and H. WINZELER

Physikalisches Institut und Seminar für theoretische Physik der Universität, Bern

Received 19 August 1960

Abstract: 60 possible hypernuclei produced in 1104 K⁻ interactions at rest and 415 K⁻ interactions in flight, were analysed. The hypernucleus charge distribution was determined and the non-mesic to π^- mesic ratio was given as a function of the hyperfragment charge. The stimulated decay was discussed. The hypernucleus formation probability was estimated.

1. Introduction

The discovery of hyperfragments by Danysz and Pniewski [1]) stimulated a number of investigations on these nuclear configurations [2,3,4]). However, it is mainly during the last few years that a systematic investigation of hypernuclei has been developed [5,6,7,8,9,10]).

Binding energies of Λ^0 hyperons in lighter hypernuclei are well known, based on the mesic decay analyses of hypernuclei produced by the π^- and K⁻-interactions in nuclear emulsions [6,7,9]). Mesic decays of the hypernuclei produced by 4.5 GeV π^- mesons were the subject of a systematic investigation [7]). Some papers were devoted to the mesic decays of hyperfragments produced by K⁻ interactions [11,12,13,14]). The π^0 decay mode of the hypernuclei arising from K⁻ interactions was also studied [10]).

However, after the work of the Wisconsin group [5]), the only systematic investigation on non-mesic decays of hypernuclei of which we are aware has been published by Silverstein [8]). The work was based on an analysis of hypernuclei produced by high energy negative pions. In this connection one should also mention a special study by Baldo-Ceolin *et al.* [15]) on the stimulated decay of the Λ^0 hyperon.

To our knowledge, no study devoted to non-mesic decays of hyperfragments produced by K⁻ mesons has been published. There is only a particular investigation of two-prong secondary stars with connecting tracks longer than 50μm[16]), and the report by Sacton [17]), who gives some general information but no analyses of non-mesic decays of hyperfragments from K⁻ captures at rest.

This work represents an effort to analyze the hypernuclei detected in a systematic investigation of K⁻ interactions in flight [18]) (the mean energy of the

K^- particles was 85 MeV), and K^- absorptions at rest [19,20]). It covers the general characteristics of the hypernuclei as well as a detailed investigation of non-mesic decays. The kinematic analysis of the non-mesic decays was made by means of the digital computer "Bull Gamma 3". The hypernuclei decaying according to the π^0 decay mode and the actual non-mesic decays were analyzed together, because the latter cannot be distinguished from the former prior to the final analysis.

In view of the small statistics and great difficulties in the analysis of these hypernuclei, the results obtained are to be considered as semi-quantitative.

A study of hypernuclei decaying with the emission of a negative pion is reported in the preceding publication [21]).

2. Experimental

2.1. EXPOSURE AND SCANNING

The non-enriched K^- beam having a momentum of 435 MeV/c upon entrance into the stack, was used in exposing plates at the Berkeley Bevatron [22]). The stack consisted of 150 Ilford G-5 stripped emulsions, each having an area 15 cm $\times$ 17.5 cm and thickness 600 μm. The K^- interactions were found by scanning "along the track". At pick-up the K^- mesons had a mean kinetic energy of 130 MeV. All secondary tracks accompanying K^- absorptions at rest and in flight were traced and most could be identified due to the large dimensions of the stack.

Special attention was paid to all many-prong K^- stars and to possible double stars. Possible hyperfragments, Σ^--absorptions, K^- reemissions and baryonic interactions in flight were selected. Every case which could represent a hyperfragment decay was carefully examined by at least three different observers under a magnification of 100×10 and 100×20. In the case of very nearly centered double stars (the so-called G.O.K.), it was sometimes difficult to establish which was the primary star and which the secondary one, and which tracks belonged to each of them. As a rule, a combination on the basis of the drawings of 3—4 observers was chosen and analyzed. (In 10 out of 46 cases more than one combination was considered as possible by different observers). Although in the final analysis of K^- interactions [19]) 2 events recorded were not included as hyperfragments, they are analyzed in the present work.

2.2. MEASUREMENTS AND STANDARDS

The shrinkage factors used in this work were estimated on the basis of the thickness measurements of each of the 150 plates before exposure and again at the time of hyperfragment measurements.

The emulsion density was not determined directly. The correction of the observed particle range to that in the emulsion of the standard density was made by comparison of ranges of 100 muons from the π^+ decays in our stack with

those of muons in the emulsion of the normal density according to Barkas [23]).

Tracks of all hyperfragment decay products ended in emulsion, so that the range of all of them could be determined.

Only a few decay products could be identified by means of the standard ionization measurements on their tracks (mean gap length), or by determination of the $p\beta$ values of the particles on the basis of multiple scattering measurments.

In order to establish the mass and charge of the decay products, both the constant sagitta scattering method and the Poohstrolino track profile method [24]) were applied whenever possible. An unambiguous hyperfragment identification could sometimes not be made in view of very short track lengths or large dip angles, which permitted no charge or mass measurements. Most tracks being insufficiently long for good statistics in the constant sagitta scattering measurements, the mass assignments inferred from the latter were not always conclusive.

There are various procedures for elaboration of the raw track thickness data [24, 25, 26, 16]), but the results are not always mutually consistent. Taking into account that local calibrations are very time consuming and that, according to Schlein [16]), no regular pattern was observed for the dependence of the profile of tracks on their depth location, we did not make these calibrations. This was found to be justified by our observation that the results obtained by the constant sagitta and profile methods (in the cases when both methods could be used on the same tracks) were mostly mutually consistent. However, the profile measurement is not quite reliable in every individual case, although it is the most suitable method for the charge determination of hyperfragments.

The elaboration of the data obtained by the profile measurements was made in the following manner:

a) The mean thickness was computed in the track length intervals of 10 μm beginning from the track end. After the residual range of 30 μm, the mean thickness was computed from all remaining profile measurements, irrespective of the track length observed.

b) These data were corrected for dip by applying the Milano group correction formula (private communication). (However, our experience indicate that this correction may be somewhat too small for large dip angles).

c) The results for each residual range were compared with the thickness from the calibration curves at the same residual range. Calibration curves for thickness versus residual range were deduced from a certain number of known protons and α particles.

The Barkas R—E relation was used for the determination of energies or singly charged particles [23]). For multiply charged particles the computer used polynomials representing the best fit to the R—E relations given by Demers [27]) and based on Barkas and Papineau curves [28]).

All other standards and conventions are the same as those employed in the

preceding work [21]).

The computation of errors was made in the same manner as described in the study on mesic decays [21]).

2.3. ANALYSIS OF EVENTS WITH COMPUTER

The kinematic analysis of HF decays and the computation of binding energies and their errors were performed by means of the Bull Gamma-3 Electronic Computer (see Appendix). The code was in principle similar to that developed by Inman [11]). It was first controlled by applying it to the well identified mesic decays. The memory-storage of the computer contained the above mentioned polynomials, the range straggling as a function of the normalized range [29]), and the table of mass values [30, 31]). The polynomials giving the energy for each Z were a function of both the range and mass, so that the machine computed the proper energy for each assumed prong identity. The maximum assumed Z values of the hyperfragments were sometimes as high as that of oxygen. The charge of decay products was considered with rather wide limits in order to take into account all possible combinations. The computer ran each possible combination under each of the following assumptions: 1) no neutral particle is emitted, 2) a π^0 meson is emitted or 3) a neutron is emitted.

The machine was instructed to derive the binding energy error by taking into account the experimental errors punched on each prong card as well as all other uncertainties which the computer evaluated on the basis of the given data and the information stored in its memory.

We restricted the combinations to be computed to those giving Λ^0 binding energies between -25 MeV and $+40$ MeV. Of course, only combinations having binding energies within the limits of error of those well known from mesic decays, were finally taken into consideration. One should mention that some combinations involving two or more neutral particles are perhaps mistaken for one-neutral-particle combinations in view of this criterion. The combinations involving the emission of two or more neutrons were also considered, but only for the possible hypernuclei giving two-prong stars. In this case it was necessary to take into account also those combinations which, under the assumption of one-neutron emission, gave a binding energy greater than 40 MeV.

2.4. SELECTION OF HYPERNUCLEI

A Λ^0 or Σ hyperon is produced in any interaction of a K^- meson with one or more nucleons. As a result of the strong interaction with nucleons, Σ particles can be transformed into Λ^0 hyperons. Moreover, Σ^0 can decay into Λ^0 and γ. Hence any K^- interaction can directly or indirectly lead to the production of a Λ^0 hyperon, which in turn may form a hypernucleus. A certain fraction of trapped Λ^0 particles does not give rise to visible hypernuclei, but to the formation of the so-called kryptofragments. (A kryptofragment is a hyperfragment with extremely short range, which cannot be distinguished from the K^- star).

A one-prong non-mesic decay of a hypernucleus was registered only if it was possible to establish that the charge of the hypernucleus was greater than 1. We were also searching for two-body decays of hydrogen hypernuclei. For this purpose all cases of single scatterings (with projected angles greater than 20°) of particles producing black prongs and emitted from K^- stars were registered. Their ranges after the scattering were measured and compared to that to be expected in two-body decays of hydrogen hypernuclei. We found only one possible ${}_{\Lambda}H^3$ hyperfragment.

Accordingly all our results are biassed in the sense that most of the non-mesic decays of hydrogen hyperfragments and some heavier hypernuclei giving only one prong escaped detection.

Double stars connected by very short tracks can arise also from the following processes:

1) K^- reemission. — As was reported in [18]), the probability for a K^- meson to be reemitted is rather low, especially if it has a very low energy. In an analysis of 415 K^- interactions in flight, only 10 cases of K^- reemission were detected. The lowest energy recorded for a reemitted K^- meson was 7 MeV.

2) Collisions in flight leading to nuclear interactions. — All interactions of secondary particles in flight at distances greater than 40 μm were individually analyzed. Only 14 such interactions were detected out of all secondary particles produced by 1600 K^- mesons.

Hence one can conclude that K^- inelastic scatterings as well as interactions in flight are processes which are rather unlikely to produce G.O.K. events. Accordingly, the events 1) and 2) can be neglected as appreciable contaminations.

3) Absorptions of π^- mesons having a very low energy. — We found that only 1 out of 58 and 4 out of 200 negative pions in flight [18]) and at rest [20]), respectively, have an energy lower than 5 MeV. These values are approximately those to be expected from an extrapolation of known π energy spectra. Accordingly, the possible contribution of π^- stars to nearly centered double stars is also small.

4) Σ^- captures. — As can be deduced from the energy spectra of Σ^- hyperons and their times of flight, one might expect a small Σ^- contamination in the region of very short ranges (up to 40 μm).

The discrimination between possible hypernuclei and Σ^- stars can in addition be based on the following criteria:

a) The energy balance of a K^- star rules out the possibility of a hyperon emission. With regard to possible multinucleon reactions, or pion absorptions, this criterion can be useful in the very limited number of cases where a very high energy release takes place in K^- stars. In our analysis 2 such hyperfragments, emitted together with a $\pi^{\pm}$ and satisfying this condition were detected and denoted as "definite".

b) Σ^- capture has a Q-value of about 80 MeV and is rarely accompanied by fast protons, in contrast to the hyperfragment decay. About 60 % of Σ^- captures give zero- or one-prong stars having prongs shorter than 200 μm [19]). However, since Σ^- captures can form kryptofragments via Λ^0 trapping, this criterion does not provide a strong discrimination. (We found 2 kryptofragments among 34 Σ^- stars.)

c) In contrast to hyperfragments, Σ^- captures are accompanied by Auger-electrons. We found that 22 % of Σ^- stars and only 2 possible hyperfragments were accompanied by Auger-electrons.

5) Chance coincidence. — This is rather improbable.

All above mentioned processes can form stars which could be mistaken as the hyperfragment decays. Hence it is not always possible to state definitely that one is dealing with a decay of an actual hypernucleus in each individual case. However, those hyperfragments which decay by the π^- mode can be taken as "definite". Those hyperfragments which are produced along with negative pions in K^- interactions may be taken also as "definite" since the charge-exchange scattering of π mesons and Σ hyperons is very small [19]). We found 5 and 8 such hypernuclei in K^- interactions in flight and at rest, respectively, in addition to the 2 already mentioned as "definite". In figs. 1 and 2, these events are denoted as "definite" hyperfragments. In addition to this, one can also consider those hyperfragments as "definite", the interpretation of which is possible only in terms of the hyperfragment decay (which is the case for most of the interpretable hypernuclei).

However, a rather small contamination from these processes is also evident from the range distributions of connecting tracks of double stars.

3. Results and Discussion

3.1. RANGE DISTRIBUTION OF CONNECTING TRACKS

The range distribution of all possible hyperfragments is shown in figs. 1 and 2. One can see that most hypernuclei have very short ranges (shorter than 40 μm). By comparing the range distribution of all hyperfragments with that of other particles the interactions of which could be mistaken for hyperfragment decays, it can be seen that all contaminations are rather small. (For energy spectra of pions and Σ hyperons see refs. [18, 19, 20]).

3.2. YIELD OF HYPERNUCLEI

In a search for connected stars from 1104 K^- interactions at rest, 43 possible hypernuclei were observed, 9 of which decayed according to the π^- mesic mode. In 3 cases of these double stars it was not possible to distinguish the primary star from the secondary one, and therefore these cases were not analyzed. 17 hypernuclei found in a series of 415 K^- interactions in flight were also analyzed. Two of this group decayed according to the π^-mesic mode.

The yield of the hypernuclei was found to be about 4 % for K^- interactions both at rest and in flight.

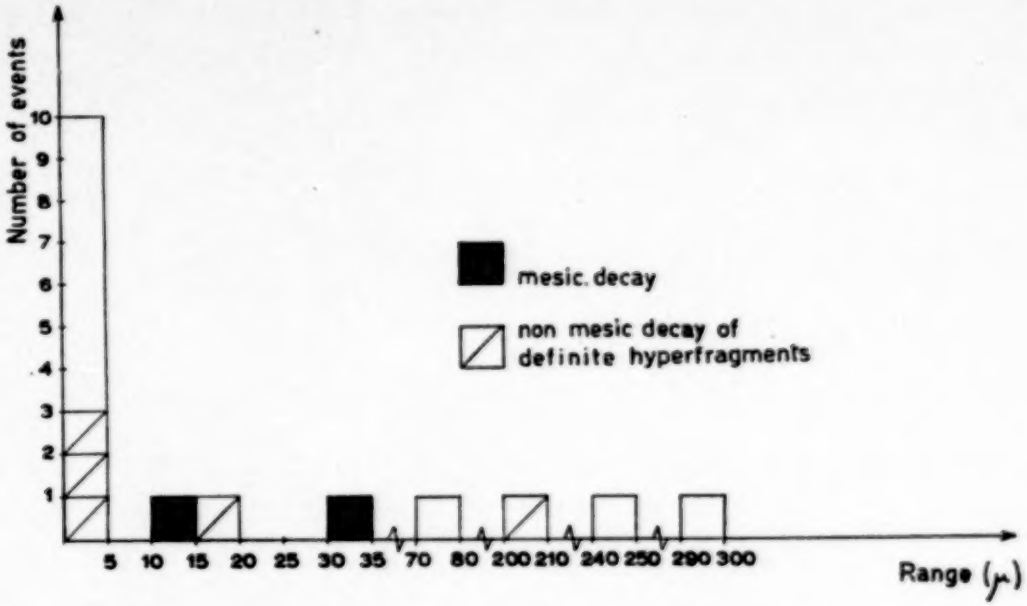

Fig. 1. Range distribution of hypernuclei produced by K^- interactions in flight.

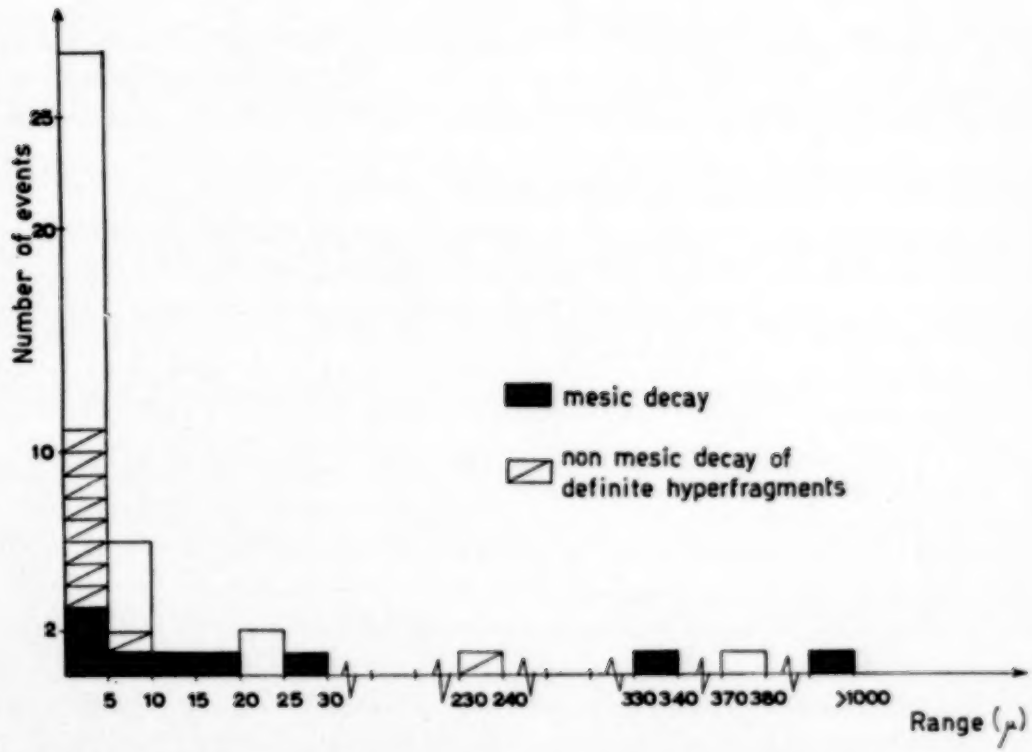

Fig. 2. Range distribution of hypernuclei produced by K^- interactions at rest.

3.3. ANGULAR DISTRIBUTION OF HYPERNUCLEI PRODUCED BY K⁻ INTERACTIONS IN FLIGHT

The angular distribution of the hypernuclei relative to the direction of flight of K^- mesons is shown in fig. 3. (The mean energy of the K^- particles was about

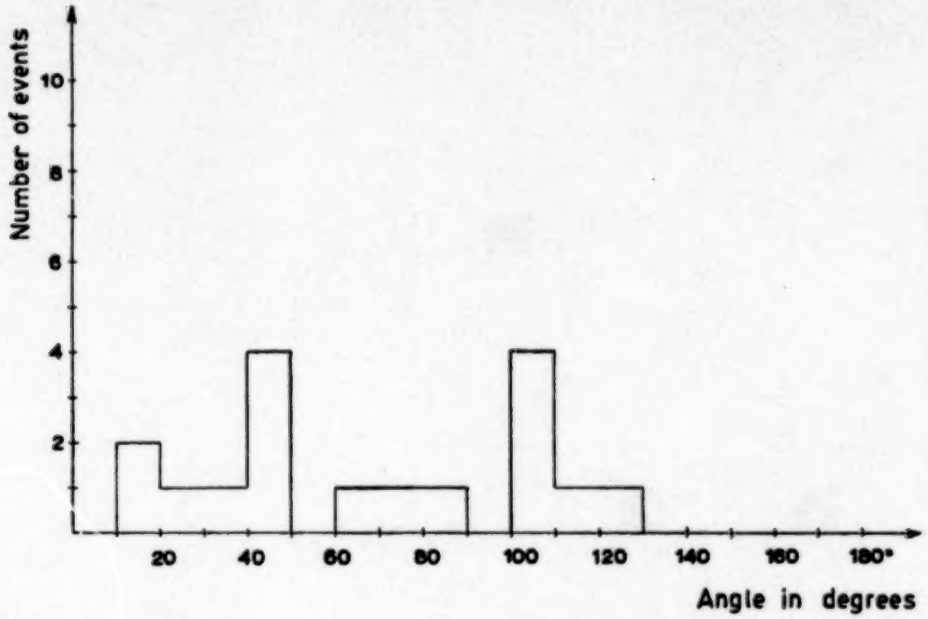

Fig. 3. The angular distribution of hypernuclei with respect to the direction of flight of the K^- meson.

85 MeV). A ratio of the forward to the backward emission (F/B) was found to be $11/6 = 1.8$. In the case of the hypernuclei produced by interactions of π^- mesons having an energy of 4.5 GeV, a F/B value of 2.2 ± 0.5 was stated [8]).

3.4. HYPERFRAGMENT DECAY-PRONG DISTRIBUTION

The decay-prong distribution for hypernuclei produced by K^- interactions in flight and at rest is shown in fig. 4. The largest number of prongs observed in the present experiment is 5. Hence a hypernucleus at least as large as boron was found.

3.5. NON-MESIC AND π^0 DECAY MODES

Results for each event based on both the measurements and the computer analysis (described in 'Experimental') are given in table 1 for hyperfragments produced in K^- interactions in flight, and in table 2 for hyperfragments produced in K^- interactions at rest.

As "interpretable" hypernuclei were considered those satisfying one of the following conditions:

1) The computer analysis gave a unique value for the charge, and the measurements on the decay products (or on the hyperfragment) confirmed the given combinations, or at least were not in a discrepancy with the latter.

TABLE 1

Hypernuclei produced by K^- interactions in flight

Event No.	Decay prong number	Hyper-fragment range (μm)	Interpretable as the hypernucleide	Decay products	$B_\Lambda \pm \Delta B_\Lambda$ (MeV)	Neutral particle energy (MeV)	Fast proton energy (MeV)	Pion from K^- star	Remarks
B-384	1	18	$_\Lambda He^5$	He^3, n, n				π^-	D
B-102	2	202	$_\Lambda He^4$	H^1, H^3, π^0	2.1± 2.6	30.9		π^-	D
B-334	2	3.5	$_\Lambda He^{4,5}$	$H^{1,2}$, H^1, n, n			24.4	π^-	D
Lo-89	2	3	$_\Lambda Be^{9,10}$	He^3, $He^{4,6}$, n	9.1±11.4 2.0±11.3	92.5 78.7		π^-	D
B-30	2	299	$_\Lambda Li^{8,9}$	$H^{1,2}$, He^6, n					in flight
H-99	2	71	$_\Lambda He^5$, $_\Lambda Li^6$	H^1, $H^3(He^4)$, n	5.3± 4.8 0.6± 6.8	71.8 90.5	74.5		$_\Lambda He(1)_\Lambda Li(1)$
I-137	2	3.7	$_\Lambda Be^{10}$ $_\Lambda B^{11,12}$	$He^3(Li^7)$, $He^{6,3,4}$, n	14.1± 9.6 16.6± 9.1 13.0± 7.3	109.7 112.0 111.6			$_\Lambda Be(1)_\Lambda B(2)$
K-97	2	242	$_\Lambda Li^{8,9}$, $_\Lambda Be^{11}$	H^3, $He^{3,4}(Li^6)$, n, n					$_\Lambda Li(2)_\Lambda Be(1)$
M-41	2	2	$_\Lambda Li^6$	H^1, He^4, n	9.2±13.9	67.8	70.7		
H-12	3	2	$_\Lambda Li$, $_\Lambda Be$, $_\Lambda B$					π^-	D, many combinations
B-34	3	4.5	$_\Lambda B^{11}$	H^3, $He^{4,3}$, $He^{3,4}$, n	0.1± 9.8 16.4± 8.9	109.7 94.3			
B-437	3	2.8	$_\Lambda Be^8$, $_\Lambda B^{10}$	H^1, He^4, $H^2(He^4)$, n	13.8± 6.0 14.6± 5.7	108.6 89.6	39.0		$_\Lambda Be(1)_\Lambda B(1)$
Ch-70	3	2	$_\Lambda Be^9$	He^4, H^3, H^1, n	4.1± 7.1	119.9			
K-123	4	2.5	none			92.4			
B-8	5	2	none						

D denotes "definite" hypernuclei

TABLE 2

Hypernuclei produced by K^- interactions at rest

Event No.	Decay prong number	Hyper-fragment range (μm)	Interpretable as the hypernucleide	Decay products	$B_\Lambda \pm \Delta B_\Lambda$ (MeV)	Neutral particle energy (MeV)	Fast proton energy (MeV)	Pion from K^- star	Remarks
I-134	1	4.5	$({}_\Lambda H^3)$	H^2, n	4.5± 3.5	111.8			a)
B-554	1	379	${}_\Lambda He^4$	He^4, π^0	0.9± 6.4	58.0			range of $He^4 \approx 8.5$ μm
Ch-134	2	2.5	${}_\Lambda Be^{5,6}$	He^4, $He^{3,4}$, n	7.4± 9.1 10.0± 9.9	98.8 95.6		π^-	D
Ch-231	2	3	${}_\Lambda Be^8$	H^1, Li^6, n	−2.2± 8.5	138.2	20.2	π^-	D
K-90	2	2	${}_\Lambda He^4$	H^1, H^1, n, n			39.4 21.9	π^-	D
Ch-243	2	4.5	none					$\pi^\pm$	D
K-216	2	1.5	${}_\Lambda He {}_\Lambda Li {}_\Lambda Be \geqq {}_\Lambda B$					π^-	D, many combinations
B-238	2	4	${}_\Lambda He^5$	H^1, H^2, n, n			41.3		
Ch-44	2	4.5	${}_\Lambda Li^{8,9}$	$He^{3,4}$, H^3, n, n					
H-55	2	1.5	${}_\Lambda Li^7$	He^4, H^1, n, n			75.0		
I-92	2	2.5	${}_\Lambda He^{4,5}$	H^1, $H^{1,2}$, n, n			22.1		
M-17	2	4	$\geqq {}_\Lambda N$						
T-45	2	3	${}_\Lambda Li^6$	He^6, H^1, n	10.7± 6.0	133.3			
T-67	2	3	none						
H-104	3	2.9	${}_\Lambda Li {}_\Lambda Be {}_\Lambda C$					π^-	D, Li(2)Be(1)C(2)
Lo-31	3	234	${}_\Lambda Be^8$	He^4, H^2, H^1, π^0	3.1± 4.9	14.1		π^-	D
R-269	3	6.2	$\geqq {}_\Lambda B$				37.2	$\pi^\pm$	D
Ch-147	3	1.5	${}_\Lambda Be^8$	He^3, H^2, H^1, n	12.5± 6.5	91.0			

R-269	3	6.2	$\geqq {}_{\Lambda}B$				37.2	$\pi^{\pm}$	D
Ch-147	3	1.5	${}_{\Lambda}Be^{8}$	He^{3}, H^{3}, H^{2}, n	12.5± 6.5	91.0			
H-48	3	10	${}_{\Lambda}Li^{6,7}$	H^{3}, H^{1}, $H^{1,2}$, n	1.5± 4.8 6.4± 4.8	105.9 104.3	39.4		
I-12	3	8	${}_{\Lambda}Be^{9,10,11}$	$He^{3,6}$, $H^{3,1,2}$, H^{2}, n	9.6± 6.4 3.1± 7.4 5.9± 7.2	64.7 82.6 74.8			
I-193	3	25	${}_{\Lambda}Li^{7,8,9}$	$H^{2,3}$, H^{2}, $H^{2,3}$, n	9.7± 6.3 12.1± 6.4 −0.6± 7.4	77.3 71.6 87.6			
K-149	3	9	${}_{\Lambda}B^{11}$	H^{3}, He^{4}, He^{4}, n	16.2±10.8	100.4			
Lo-66	3	6	${}_{\Lambda}B^{12}$	He^{4}, He^{4}, H^{3}, n	17.5± 7.0	126.4			
Lo-84	3	24							[b]
Lo-119	3	3	${}_{\Lambda}C$	$He^{3,4}$, $He^{4,3}$, $He^{3,4,6}$, n					5 possible combinat.
B-512	4	2	$\geqq {}_{\Lambda}B$					π^{+}	[c]
B-305	4	2	$\geqq {}_{\Lambda}B$						
Ch-102	4	2	$\geqq {}_{\Lambda}B$						
H-86	4	5	${}_{\Lambda}B^{11,12}$	H^{1}, He^{6}, H^{1}, $H^{2,3}$, n	14.3± 6.2 5.1± 7.3		22.5		
K-257	4	4.5	$\geqq {}_{\Lambda}B$						[c]
Ch-254	5	4	$\geqq {}_{\Lambda}B$				86.0	$\pi^{\pm}$	D
I-17 I-301 K-220								π^{-}	K⁻ star and HF-star not clearly separated D

D denotes "definite" hypernuclei

[a]) The binding energy of Λ^{0} in this case exceeds somewhat the limits of error. However, this is a single combination found by the computer and measurement, and if one admits that this event is an actual hyperfragment, then only this combination is available for its interpretation. (A possible case of nonmesic hydrogen (${}_{\Lambda}H^{4}$)) HF-decay has been reported by Blau [32]).

[b]) Only one of decay products of this possible hyperfragment could be identified. Combinations which could be taken into account for this case include the emission of a π^{0} (no n), and the corresponding hypernucleide with the lowest Z is Be, decaying as follows: ${}_{\Lambda}Be^{8} \rightarrow {}_{1}H^{3} + {}_{1}H^{1} + {}_{2}He^{4} + \pi^{0}$ (B = 10.0 MeV±3.3 MeV).

[c]) In a publication on K⁻ interactions at rest [19]), these hypernuclei were taken, on the basis of the visual criterion, as possible Σ^{-} stars.

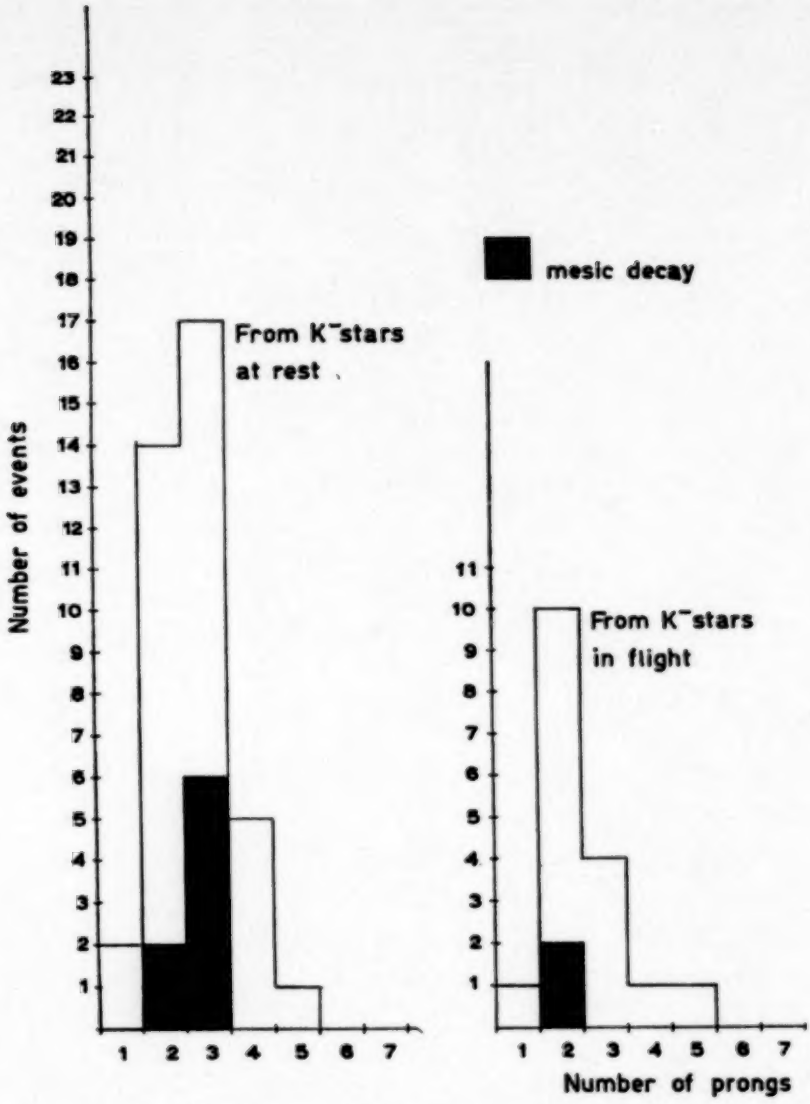

Fig. 4. Distribution of the decay prongs of hypernuclei.

2) The computer analysis suggested no unique charge, but it was possible to determine the charge of the decay products and of the hyperfragment by means of the measurements.

3) The charge of the hyperfragment or of its decay products was determined on the basis of measurements. There were no corresponding combinations with the emission of one neutron which gave the Λ^0 binding energy in the limits of error, but there were possible combinations with the emission of two or more neutrons.

The charge of the hypernuclei could not be uniquely determined in most cases starting from the ${}_{\Lambda}B$. In such cases we restricted our analysis to the deter-

mination of the number of possible hypernuclei compatible with $Z \geqq 5$.

In tables 1 and 2 besides the hyperfragments having uniquely interpretable charge, there are also the hypernuclei given which could be interpreted in terms of different charges (see section on non-mesic to mesic ratio.).

As can be seen from table 1, of the 15 analyzed hyperfragments produced in K^-interactions in flight, 1 decayed according to the π^0 decay mode: ${}_\Lambda He^4 \rightarrow H^1 + H^3 + \pi^0$. (Since 2 hyperfragments were found to decay according to the π^- decay mode, it is to be expected that 1 hyperfragment would decay with the emission of a π^0). 7 interpretable hypernuclei were found to consist of the following hypernuclides: $2\,{}_\Lambda He$, $2\,{}_\Lambda Li$, $2\,{}_\Lambda Be$ and $1 \geqq {}_\Lambda B$. One of these hypernuclei (${}_\Lambda Li^{8,9}$) is compatible with the hyperfragment decay in flight. 4 further hypernuclei could be interpreted in terms of two different charges, while for 3 remaining hyperfragments nothing certain could be said (for two of the latter no admissible combination could be found).

Of hypernuclei produced in K^- interactions at rest and shown in table 2, 2 are compatible with the π^0 decay mode: ${}_\Lambda He^4 \rightarrow He^4 + \pi^0$ and ${}_\Lambda Be^8 \rightarrow He^4 + H^3 + H^1 + \pi^0$ (for third one see footnote [b]) of table 2). (The number of hypernuclei from all analyzed K^- captures, which decay according to the π^0 decay mode, is expected to be about 4 or 5). 24 interpretable hypernuclei were found to consist of the following hypernucleides: $1\,{}_\Lambda H$, $3\,{}_\Lambda He$, $5\,{}_\Lambda Li$, $4\,{}_\Lambda Be$ and $11 \geqq {}_\Lambda B$. There is one HF to which 3 possible charges could be ascribed, while for 6 HF's (2 of which without admissible combinations) it was not possible to make any statement regarding the charge.

Of 14 interpretable two-prong events, 7 were compatible only with the emission of 2 neutrons. The compatibility of more-prong events with combinations involving only one neutron could be fortuitous, since for most of them the admissible combinations involving 2 or more neutrons could be found in principle.

Combinations corresponding to unknown hypernuclei were in general not sought for. One hyperfragment was interpretable only as ${}_\Lambda Li^6$, while some others could be interpreted also as ${}_\Lambda Li^6$, ${}_\Lambda B^9$ and ${}_\Lambda B^{10}$. About the possible example of the nonmesic decay of ${}_\Lambda H^3$, see footnote [a]) of table 2.

3.6. NON-MESIC TO MESIC DECAY RATIO *R*

One of the most significant results of an analysis on hyperfragments is an experimentally found non-mesic to mesic ratio R of various hyperfragment charges. From the comparison of its value with the calculated one, the spin of Λ^0 hyperon can be inferred [33]).

Our results on the charge distribution of the hypernuclei decaying according to the non-mesic decay mode are given in table 3. For the sake of the better statistics and in view of a rather low energy of K^- mesons interacting in flight, the results on hypernuclei produced in K^- interactions both in flight and at

rest are shown together. The numbers in parentheses are obtained when only hypernuclei produced in K^- interactions at rest are taken into account.

TABLE 3

Charge distributions

	Z (charge)				
	1	2	3	4	5
decay prong number distribution	3(2)	20(12)	15(11)	6(5)	2(1)
charge distribution determined by applying Silverstein's procedure	1.5(1)	11.5(7)	17.5(11.5)	10.5(8)	5(4.5)
upper limit for each Z determined by applying Silverstein's procedure	3(2)	23(14)	35(23)	41(28)	23(17)
our "best" charge distribution	1(1)	5.5(3)	8.6(5.4)	7.4(4.2)	13.5(11.4)

The first row of table 3 gives the decay prong number distribution.

The next two rows show the values obtained by applying the procedures proposed by Silverstein [8]).

The second row shows the charge distribution determined by assuming that half of all events have Z equal to the number of prongs and that the remaining events have Z equal to one plus the number of prongs.

The third row gives the upper limits for each Z, obtained by assuming that the charge of each prong is one or two and by calculating the maximum number of events for each Z on the basis of the prong number distribution.

The fourth row gives our "best "charge distribution, i.e. the results based on the complete analysis which are shown in table 1 and 2. The π^0 decay mode was not taken into account in this connection (row 4).

For the 5 hyperfragment decays yielding more possible charge interpretations, we count the number of interpretations leading to different Z and normalize this distribution for the event (see Remarks in tables 1 and 2). The fractions appear because of these hyperfragment decays. In the remaining 2 cases this procedure is not reasonable because of the large number of possible interpretations. These two hyperfragments are therefore not included in our "best" charge distribution, shown in table 3. However, they and those 3 hyperfragments which could not be clearly separated from K^- stars, must be taken into account in determining the non-mesic ratio R as a function of charge. For farther 5 events (4 "none" and Lo-84 in tables 1 and 2) no admissible decay schemes could be found, but because they are probably hyperfragments, they were also taken into consideration in determining the ratio R (table 4). These 10 possible hypernuclei are divided at each hypernucleus charge, according to the proportions of interpreted hypernuclei of the same charge (e.g. according

to the "best" charge distributions in table 3). In this division we took into consideration the minimum possible hyperfragment charge.

2 hypernuclei produced in K^- interactions in flight and 9 hypernuclei produced in K^- absorptions at rest, all decaying according to the π^- decay mode, are described in the preceding publication [21]).

We found the overall non π^- mesic to π^- mesic ratio to be 7.5 ± 5.6 for the K^- stars in flight and 3.8 ± 1.4 for the K^- stars at rest. After the elimination of possible π^0 decays, one obtains the following non mesic to π^- mesic ritio: 7 ± 5.3 for the K^- interactions in flight and 3.6 ± 1.3 for K^- absorptions at rest. The comparison of the both values is very interesting, but in our case a discussion is senseless because of the large statistical errors.

To determine the non-mesic to mesic ratio R as a function of Z, we use the best estimation of the charge distribution which can be made on the basis of published results, instead of using the observed charge distribution of the small number of hypernuclei decaying according to the π^- decay mode and detected in our analysis of K^- interactions.

In a study of hypernuclei arising from K^- captures and decaying according to the π^- decay mode, the Chicago group [9]) found that the 133 uniquely identified hypernuclei (detected by area scanning) consisted of the following hypernucleides: 24.8 % of ${}_{\Lambda}H$, 56.5 % of ${}_{\Lambda}He$, 15 % of ${}_{\Lambda}Li$, 2.3 % of ${}_{\Lambda}Be$ and 1.5 % of ${}_{\Lambda}B$. In systematic analyses of K^- interactions at rest, the certain number of hypernuclei decaying according to the π^- decay mode was registered and uniquely identified. Mora and Ortalli [12]), Sacton [13]) and Nikolić [21]) found all together $10\,{}_{\Lambda}H$, $21\,{}_{\Lambda}He$, $7\,{}_{\Lambda}Li$ and $1\,{}_{\Lambda}Be$ i.e. 25.6 % of ${}_{\Lambda}H$, 53.8 % of ${}_{\Lambda}He$, 18 % of ${}_{\Lambda}Li$ and 2.6 % of ${}_{\Lambda}Be$ as constituents of these hypernuclei. As can be seen, there are no differences between the hypernuclei detected by area scanning and the hypernuclei detected in the systematic analyses of K^- interactions. Therefore we use the values by the Chicago group in the determination of the non-mesic to mesic ratio R as a function of Z. To obtain the latter value, these results are normalized to the total number of observed π^- mesic hyperfragment decays, i.e. 11 for all hyperfragments (produced in K^- interactions both at rest and in flight) or 9 if only hyperfragments arising from K^- interactions at rest are taken into account (values in parentheses).

Table 4 shows the non-mesic to mesic ratio R as a function of Z, obtained on the basis of variously inferred charge distributions (table 3), as well as other already published values. Table 4 gives also the Ruderman-Karplus estimates [33, 5, 37]), computed at the time when the parity non-conservation in the Λ^0 decay was as yet unknown. They were obtained under the assumption of the incoherence between π^- and π^0 virtual intermediate states, which was later shown by Cerulus [34]) to be incorrect. However, as was shown by Dalitz [35]), in the case of the coherence between π^- and π^0 internal conversion processes, the values of the non-mesic to mesic ratio remain essentially those of Karplus and

TABLE 4

Non π^- mesic to π^- mesic ratio R' and non-mesic to π^- mesic ratio R as a function of Z

	Z(charge)				
	1	2	3	4	5
R' estimated from the prong number distribution, determined by applying Silverstein's procedure	0.5(0.4)	1.9(1.4)	10.6(8.5)	42(38)	29(35)
upper limit of R', determined by applying Silverstein's procedure	1.1(0.9)	3.7(2.8)	21(17)	164(133)	135(131)
R from our "best" charge distribution [a])	0.4(0.4)	1.2(0.9)	6.6(5.4)	38(29)	106(97) 64(56)
Schneps-Fry-Swami results [5]) [b])	$R^1 = 0$	$R = 2.3$	$R' = 15.5$	$R' = 70$	
R' by Silverstein [8])	0.2	$0.6 < R' < 1.4$	15	21	
upper limit of R^1 by Silverstein [8])	0.6	2.8	30	55	
R by Schlein [16]) [c])		1.5 ± 0.4			
Revised Ruderman-Karplus estimates of R [d]) for pion angular momentum $l = 0$	0.5	1.2 (for ${}_\Lambda$He^4) ($B_\Lambda = 2.36$)		50	
for pion angular momentum $l = 1$		22 (for ${}_\Lambda$He^4) ($B_\Lambda = 2.36$)		800	

[a]) We detected only a part of the one-prong non-mesic hyperfragment decays, and therefore the real values of R may be in fact (especially in the case of ${}_\Lambda$H and ${}_\Lambda$He) somewhat higher.

[b]) The Schneps-Fry-Swami results are to be taken as upper limits, since a certain number of π^- interactions may have been taken as non-mesic decays.

[c]) Since Schlein [16]) did not include one-prong non-mesic hyperfragment decays in his analysis, his value of R must be considered as a lower limit.

[d]) In comparing all above experimental values for R with the revised Ruderman-Karplus estimates taken from refs. [5, 37])), one should multiply the experimental R by the factor of $\frac{4}{3}$ to correct for the fact that about $\frac{1}{4}$ of the non-mesic decays are due to the conversion of virtual neutral pions [37]).

Ruderman for a Λ^0 particle whose spin is randomly oriented relative to the initial nucleon spins.

In view of the parity non-conservation in the decay of the Λ^0 hyperon, the emission of both s and p channel pions becomes possible in the decay of spin $\frac{1}{2}\Lambda^0$ particles. Therefore the expected theoretical value of the non-mesic to π^- mesic ratio R (which is a function of the ratio p/s of the p and s channel amplitudes in the decay of a free Λ^0 particle) will lie between the values obtained for the outgoing pion angular momentum of 0 and 1 [35]).

Dalitz [35]) previously estimated that R should lie between 4.1 and 10 for ${}_\Lambda$He, and between 170 and 420 for heavier hypernuclei, but there are many uncertainties in these estimates. For an extensive discussion of the subject, see also ref. [36]). Although attempts to obtain the detailed information about the free

Λ^0 decay by means of the experimental non-mesic to mesic ratio R may be unjustified [36, 38]), the observed low values of R (obtained by us too) show that the ratio p/s of the p and s channel amplitudes cannot appreciably exceed unity.

3.7. Λ^0 STIMULATED DECAY

Cheston and Primakoff [39]) and Fowler [40]) suggested the stimulated decay of Λ^0 hyperon to explain the mechanism of the non-mesic de-excitation of Λ^0 particle and the observed nonmesic to mesic ratio as the function of Z.

As was shown by Baldo-Ceolin *et al.* [15]), it is possible, in the case of light hypernuclei, to distinguish the proton stimulated decay from that of the neutron, by means of the energy distribution and the frequency of emitted fast nucleons. Assuming the one-nucleon stimulated decay of Λ^0 hyperon [15]), it is to be expected that each of the interpretable light hypernuclei the decay of which is accompanied by the emission of only one neutral particle should have a fast proton as a decay product. We found that only 10 and 6 hypernuclei out of 31 interpretable hypernuclei decaying according to the non-mesic decay mode had as a decay product a proton with an energy higher than 20 MeV and 30 MeV, respectively. Besides, one of these interpretable hypernuclei had a proton with the energy of 30 MeV and a proton with the energy of 20 MeV among its decay products. There are, in addition (tables 1 and 2), only 3 fast protons, all having the energy higher than 30 MeV. (Two of them were emitted during the decay of hypernuclei which could be interpreted as having two possible charges and one of them was involved in an event having no admissible interpretations).

In 6 cases (4 of which are interpretable) it was found that the particles which according to their ranges could be protons with an energy > 30 MeV, are actually deuterons.

All interpretable hypernuclei decaying according to the non-mesic decay mode had a fast neutron as a decay product.

Energies of fast protons are given in tables 1 and 2. Energies of fast neutrons are also given in the cases when it appeared to be reasonable.

As can be seen, the mean energy of fast neutrons is appreciably higher than that of fast protons.

As is mentioned above, if one assumes the one-nucleon stimulated decay, each of the interpretable hypernuclei decaying with the emission of one neutron should have a fast proton as a decay product. When light hypernuclei from ${}_{\Lambda}$He to ${}_{\Lambda}$Be are considered, then only 3 out of 11 interpretable hypernuclei decaying with the emission of one neutron have a fast proton ($T_p > 20$ MeV) as a decay product. Of 7 interpretable light hypernuclei the decay of which is compatible with the emission of two neutrons, 5 had a proton as a decay product. (The energy of this proton was always higher than 20 MeV). In the latter case, one of the neutrons may not be fast, so that we considered these decays to be also proton stimulated.

These 18 light hypernuclei give the following neutron to proton stimulation ratio: $N/P = \frac{10}{8} = 1.25 \pm 0.6 (1.3 \pm 0.6)$ for the nucleons with the kinetic energy higher than 20 MeV, and $N/P = 2.6 \pm 1.4 (2.3 \pm 1.1)$ for the nucleons with the kinetic energy higher than 30 MeV. The values in parentheses are obtained if one takes into account also the hypernuclei which could be interpreted in terms of different charges.

The number of available hypernuclei in this experiment is too small to allow the consideration of the neutron to proton stimulation ratio as a function of the hyperfragment charge.

Even if the certain number of our hypernuclei was uncorrectly interpreted as the decay involving one neutron instead of two or more neutrons, the N/P stimulation ratio with a cut-off at $T_p = 30$ MeV would remain higher than 1 in view of the relatively small number of observed fast protons.

Baldo-Ceolin *et al.* [4, 15]) found the neutron to proton stimulation ratio from a total of 79 events to be 1.2. Silverstein obtained this ratio to be 0.9 ± 0.2 on the basis of 185 events, and we found it to be 2.3 ± 1.1 on the basis of 22 events. The mean value of these results is 1.09 ± 0.13. The N/P stimulation ratio for the one-nucleon process (under the assumption that the decay branching ratio for the stimulated bound Λ^0 hyperon is the same as for the free Λ^0), which is the function of the relative parity of hyperons and nucleons, has the upper limit of 1. However, still better statistics of events is required in order to state whether the experimental N/P stimulation ratio is higher than 1.

The stimulation process may be not in every case simple. (Of our 11 interpretable hypernuclei involving the emission of one neutron, 4 had no proton as a decay product). The fact that we found only one decay accompanied by two fast protons points out that the multi-nucleon stimulation is relatively unimportant, in accordance with the statement by Baldo-Ceolin *et al.* [15]). As was emphasized by Ferrari and Fonda [41]), it is possible to obtain the N/P stimulation ratio higher than 1, in the case when the stimulated decay of Λ^0 hyperon involves the virtual Σ state. May be this process is of high importance, since the binding of Λ^0 particle in the hypernucleus is not possible by the process involving only one virtual pion [42, 43]).

3.8. HYPERNUCLEUS FORMATION PROBABILITY

In 15 out of 43 hypernuclei produced by the K^- interactionsat rest, at π meson was emitted together with a hypernucleus from the K^- star. 6 pions were identified to have a negative charge and 3 to have a positive charge. The charge sign of other 6 pions could not be established. Two of the latter had an energy higher than 100 MeV. Since they arise from reactions producing Λ^0 hyperons, they consequently must be negative. From the π^+/π^- ratio in K^- interactions at rest [20]), it can be concluded that the remaining 4 pions are probably also negative.

Taking into account a possible observation loss of pions, the pion emission probability and charge independence, and assuming that the reabsorption probabilities for Σ^+, Σ^- and Σ^0 hyperons produced in one-nucleon reactions are mutually equal, one obtains that 25 to 27 out of 43 hypernuclei arise from K^- one-nucleon reactions at rest. We do not know in how many cases the Σ hyperon does a charge exchange, and therefore we assume that the Σ's are all converted into Λ^0's. The remaining 37 %—42 % of hypernuclei are produced in K^- multi-nucleon reactions. Nikolić *et al.* [19]) found that multi-nucleon capture mode takes place in 37 %±5 % of K^- absorptions at rest. This indicates that hypernuclei are produced with the same probability in one- and multi-nucleon captures of K^- mesons.

A hyperfragment and a proton with the energy higher than 60 MeV were emitted from the K^- star in 9 cases. Practically all these hypernuclei arise from multi-nucleon reactions. The fast protons predominantly were produced directly in two-nucleon reactions (or were due to the Λ^0-nucleon scattering?), while a smaller part of these protons might be due to the absorption of Σ^+ and Σ^0 hyperons produced in two-nucleon reactions (see ref. [19])).

In about 70 % of the cases, the K^- one-nucleon reactions produced directly or indirectly Λ^0 hyperons [20]). The hypernucleus formation probability, i.e. the number of hypernuclei per a produced Λ^0 particle, was found to be about 5.5 %. Kryptofragments were not taken into account in any calculations.

By assuming that the one-nucleon K^- capture at rest is a process taking place at the periphery of the nucleus and that therefore 50 % of directly produced Λ^0 particles do not pass through the nucleus, one obtains the percentage of the hypernuclei produced per a Λ^0 hyperon passing through nuclear matter to be about 7 %.

The following two estimates (obtained on the basis of very small event statistic) are also in accordance with the above values of the hypernucleus formation probability in K^- one-nuceon reactions:

1) π^- mesons produced in the reaction $K^- + n \rightarrow \Lambda^0 + \pi^-$ have the energy higher than 95 MeV in about 25 % of the cases in which a negative pion from this reaction was emitted. From the number of π^- mesons which has the energy higher than 95 MeV and which were emitted together with hyperfragments from K^- stars, one can roughly estimate that in about 5.5 % of the cases directly produced Λ^0 hyperons form hypernuclei. Further it is possible to estimate roughly that about 40 % of hypernuclei produced in K^- one-nucleon reactions arise from directly produced Λ^0 particles, while the remainder arise from indirectly produced Λ^0 hyperons via the Σ conversion (see also [17])).

2) π^+ mesons are produced in K^- interactions always together with the Σ^- hyperons. From π^+ mesons emitted together with hypernuclei, it was roughly estimated that in about 6 % of Σ^- absorptions the indirectly produced Λ^0 hyperons give rise to hypernuclei.

In a study of multi-nucleon captures in K^- interactions, Λ^0 hyperons were found to be directly produced in about 55 % of the multi-nucleon captures [19]. In ref. [19]) are given two-nucleon reaction rates and the Σ absorption probability, on the basis of which the hypernucleus formation probability by two-nucleon K^- reactions (per Λ^0 produced directly or indirectly) was estimated to be about 5 %. This is similar to the value obtained by the Berne group for K^- interactions in flight [18]).

By comparing the results obtained from K^- interactions at rest and in flight, it was confirmed that the Λ^0 trapping probability decreases as the energy increases [18]).

We also detected 4 possible hypernuclei produced in Σ^- captures at rest. The total number of Σ^- stars detected in the analysis of K^- interactions at rest[19]) is 34, which corresponds to the number of 88 Σ^- captures when one takes into account zero- and one-prong stars escaping the detection. This would correspond to a value of (4.5 ± 2.3) % for the probability of the hypernucleus formation by the Σ^- at rest.

Fry *et al.* [44]) found no hyperfragment in examining 115 Σ^- captures. Dascola *et al.* [45]) detected 5 hyperfragments in examining 415 Σ^- captures, which corresponds to the formation probability of $(1.2) \pm 0.5)$ %. These differences are probably due to the small statistic. It is evident, as Fry *et al.* already emphasized, that directly or indirectly produced Λ^0's from K^- captures have a higher probability of emerging in the form of a hyperfragment than do the Λ^0's produced by Σ^- captures.

Characteristics of parent K^- stars from which the hypernuclei are emitted, i.e. the prong number distribution and the number of events associated with the emission of fast protons from K^- stars, are given in ref. [19]) for the following different types of events: (π^+, HF), (π^-, HF), ($\pi^\pm$, HF) and (0π, HF).

The average number of prongs per star is 2.2 for all K^- stars and 2.4 for hyperfragment parent stars. (If $K\rho$'s are also taken into account, then the average number of prongs per star is 1.9 for all K^- stars.) About 20 % of the parent hyperfragment stars are associated with electrons and this percentage is approximately the same for K^- captures involving the emission of pions (the certain one-nucleon captures) and for K^- captures associated with no observed pions. These data do not point out that hypernuclei are preferentially produced either in light or in heavy nuclei.

We, too, confirmed the striking anisotropy of the distribution of the angle between the direction of the emission of the hyperfragment and the direction of flight of the fast proton from the parent star, found by Sacton [17]). We found the following forward-backward asymmetry for the protons with the energy higher than 30 MeV: $(F-B)/(F+B) = -\frac{5}{9}$ for hypernuclei produced in K^- interactions in flight and $-\frac{10}{16}$ for hypernuclei produced in K^- absorptions at rest.

As was already mentioned, of 17 hypernuclei produced in K^- interactions in flight, 11 were emitted in the forward hemisphere. The observed angular distribution of the hypernuclei relative to the direction of flight of K^- mesons is similar to that of stable heavy fragments [46]).

There are different hypotheses on the possible mechanism of the HF emission (see refs. [8, 46])). However, our event statistics is insufficient to obtain, from the observed energy, momentum and velocity distributions of the hypernuclei, a more detailed concept of the process by which the Λ^0 hyperon is bound to the fragment.

4. Summary

A study was made of the total of 60 possible hypernuclei detected during the search for double stars produced by 1104 K^- interactions at rest and 415 K^- interactions in flight in nuclear emulsions. General characteristics of the hypernuclei were considered and an analysis of the non-mesic and π^0 decay modes was made.

The yield of the hypernuclei was found to be about 4 % for K^- interactions both at rest and in flight. The forward to backward emission ratio of the hypernuclei with respect to the direction of flight of K^- mesons was estimated to be $11/6 = 1.8$.

3 of the analysed hypernuclei are compatible with the π^0 decay mode. Interpretable hypernuclei which decayed according to the non-mesic decay mode were found to consist of the following hypernucleides: ${}_{\Lambda}1H$, ${}_{\Lambda}5He$, ${}_{\Lambda}7Li$, ${}_{\Lambda}6Be$ and $12 \geqq {}_{\Lambda}B$. 5 further hypernuclei could be interpreted in terms of two or three different charges.

We found the overall non-π^- mesic to π^- mesic ratio to be 7.5 ± 5.6 for K^- interactions in flight, and 3.8 ± 1.4 for K^- absorptions at rest. We estimated the following non-mesic to π^- mesic ratio R as a function of charge of the hypernuclei: 0.4 for ${}_{\Lambda}H$, 1.2 for ${}_{\Lambda}He$, 6.6 for ${}_{\Lambda}Li$, 38 for ${}_{\Lambda}Be$ and 106 for $\geqq {}_{\Lambda}B$. The observed low values of R confirmed that the ratio p/s of the p and s channel amplitudes in the decay of Λ^0 cannot appreciably exceed unity.

The observed number of fast protons rising from decays of interpretable hypernuclei is appreciably lower than that to be expected from the mechanism of the one-nucleon stimulated decay.

It was estimated that the hypernuclei were produced with about the same probability in one- and multi-nucleon captures of K^- mesons. The hypernucleus formation probability was found to be about 5.5 % for one-nucleon K^- reactions, and about 5 % for two-nucleon K^- reactions. (The number of hypernuclei per Λ^0 hyperon passing through nuclear matter is for one-nucleon K^- capture about 7 %). By comparing the results obtained from K^- interactions at rest and in flight, it was confirmed that the Λ^0 trapping probability decreases as the energy increases.

This and the preceding work would not have been possible without the kind efforts of Drs. L. Jauneau, E. J. Lofgren and M. W. Teucher in arranging for the exposure at the Berkeley Bevatron. We are very grateful to Profs. F. G. Houtermans, A. Mercier and Ch. Peyrou for stimulating discussions. Our special thanks are due to Prof. W. Nef, Director of the Institute of Applied Mathematics, for his interest and helpful suggestions. We are indebted to Drs. Y. Eisenberg and M. Schneeberger, who took part in the initial state of this work. Our gratitude is due to Dr. B. Dayton for valuable discussions. We would like to express our gratitude to our scanning team for their efficient assistance, and particularly to Mrs. Ch. Plumettaz who also made some precise measurements. The financial support of the Swiss National Foundation is appreciated.

Appendix

THE BULL GAMMA AET PROGRAM FOR HYPERFRAGMENT ANALYSIS

Our analysis program is similar to that developed by Inman.

Because one cannot obtain reasonable energies in terms of ranges by employing the λ—τ relations [23]) for slow, multiply charged particles, the polynomials representing the best fit to the R—E relations (given by Demers and based on the Barkas and Papineau curves for each ion) were computed and fed into our machine. Since one of the criteria for the identification of a hyperfragment is an admissible Λ^0 binding energy, our computer calculated the proper binding energy errors. The latter were computed only for those combinations the binding energies of which were in a desirable restricted region.

1. *Input and steering.* In order to evaluate an event the machine reads the following information:

1) A card characterising the event with the prong number and a specification whether or not one is dealing with a decay accompanied by a charged pion. The card also gives the upper limit for the charge of the hyperfragment to be analyzed (up to 15) and an instruction imposing either a systematic printing-out of all combinations or an output of only those combinations the binding energies of which are within the desired limits given in advance.

2) Two cards for each prong containing the following data: the lower and upper limit ($Z_{\min}$, $Z_{\max}$) for the charge of the assumed isotopes (one can also single out a certain isotope), the range (R) with the corresponding experimental error (ΔR_0), and the azimuth (ϕ) and dip angle (θ) with corresponding experimental errors ($\Delta\phi$, $\Delta\theta$). Instead of the R and ΔR_0, the kinetic energy T and ΔT can be directly imposed.

The events involving up to 5 prongs can be taken into account.

2. *Computation* (see fig. 5). On the basis of the above data the machine computes within the imposed limits for each prong and for each assumed isotope the energy T, the momentum P with its components P_x, P_y, P_z and

the errors corresponding to the values mentioned. As soon as the data of individual prongs are evaluated and the results stored in the memory, the machine systematically combines all possible prong assignments. The computer calculates for each combination the momentum unbalance (P_t) and the energy balance by ascribing the former to 1) a neutron, 2) a π^0, if no charged pion is emitted,

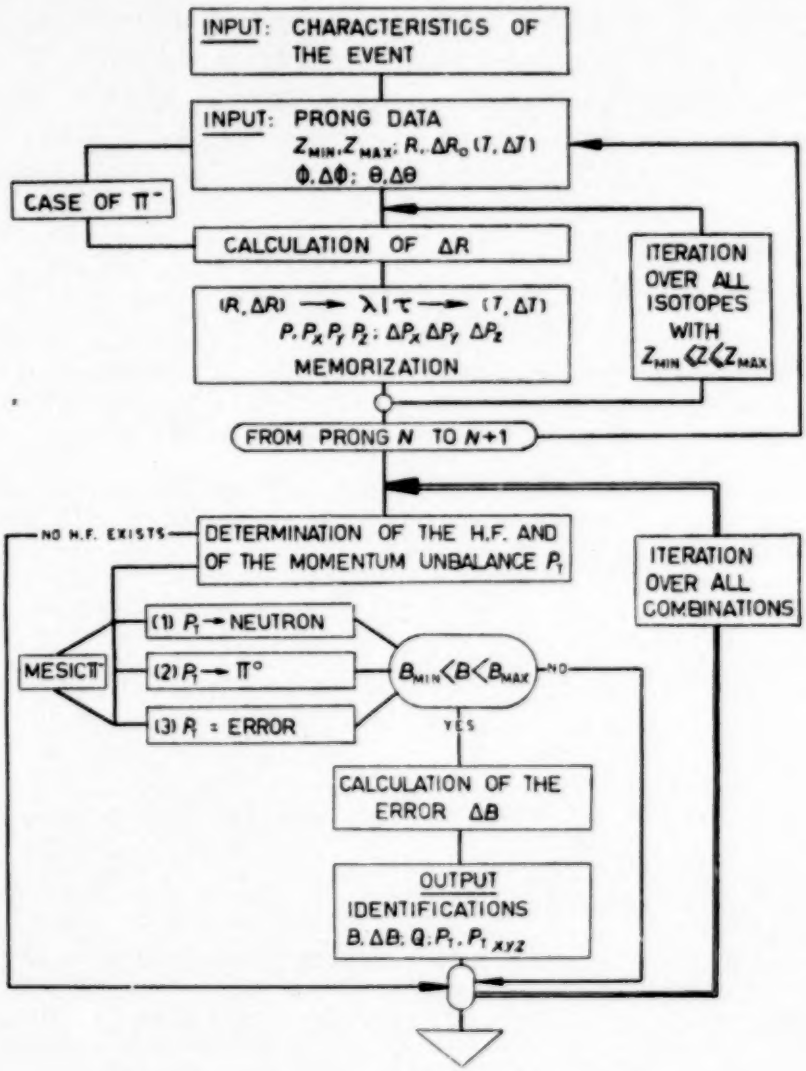
INPUT: CHARACTERISTICS OF THE EVENT
INPUT: PRONG DATA
Z_{MIN}, Z_{MAX}; R, ΔR_0 (T, ΔT)
$\Phi, \Delta\Phi$; $\Theta, \Delta\Theta$
CASE OF π^-
CALCULATION OF ΔR
ITERATION OVER ALL ISOTOPES WITH $Z_{MIN} \leq Z \leq Z_{MAX}$
(R, ΔR) → λ | τ → (T, ΔT)
P, P_x P_y P_z; ΔP_x ΔP_y ΔP_z
MEMORIZATION
FROM PRONG N TO N+1
NO H.F. EXISTS
DETERMINATION OF THE H.F. AND OF THE MOMENTUM UNBALANCE P_t
ITERATION OVER ALL COMBINATIONS
(1) P_t → NEUTRON
MESIC π^-
(2) P_t → π^0
(3) P_t = ERROR
$B_{MIN} < B < B_{MAX}$
NO
YES
CALCULATION OF THE ERROR ΔB
OUTPUT
IDENTIFICATIONS
B, ΔB, Q, P_t, $P_{t\,XYZ}$

Fig. 5. Flow-diagram of hyperfragment-analysis.

and 3) no neutral particle, if the momentum unbalance has the value lower than the imposed limit.

If the binding energy B is within the imposed limits in any of the above three cases, the machine also computes the corresponding error and prints out the combination.

3. *Output.* The following data are printed out: the assumed identities of each

prong and of the hyperfragment, the associated neutron particles, the binding energy B and its error ΔB, the total kinetic energy released Q, the momentum unbalance P_t with its components P_x, P_y, P_z, and the energy T_n of the neutral particle if the latter is present. If necessary, the intermediate results of the first stage can be printed out, too.

4. *Machine time.* A single run gives a complete survey of all possible identities of the event. Any computation which can be made outside the time-consuming combinations state is performed in the first stage, so that the time of the memorisation of intermediate results is economized as much as possible. Thus the computer takes about 20 sec for the evaluation of the prong data for an isotope, and an average of 3 sec for any combination with a certain neutral particle.

References

1) M. Danysz and J. Pniewski, Bulletin de l'Acad. polonaise **1** (1953) 42
2) A. Filipkowski, J. Gierula and P. Zielinski, Acta Phys. Polon. **16** (1957) 139
3) C. Franzinetti and G. Morpurgo, Suppl. Nuovo Cim. **6** (1957) 469
4) W. F. Fry, Ann. Rev. Nucl. Sci. **8** (1958) 105
5) J. Schneps, W. F. Fry and M. S. Swami, Phys. Rev. **106** (1957) 1062
6) R. Levi-Setti, W. E. Slater and V. L. Telegdi, Suppl. Nuovo Cim. **10** (1958) 68
7) W. E. Slater, Suppl. Nuovo Cim. **10** (1958) 1
8) E. M. Silverstein, Suppl. Nuovo Cim. **10** (1958) 41
9) R. Ammar, R. Levi-Setti, W. E. Slater, S. Limentani, P. E. Schlein and P. H. Steinberg, Nuovo Cim. **15** (1960) 181
10) R. G. Ammar, Nuovo Cim. **14** (1959) 1226
11) F. W. Inman, UCRL-3815, (1957) (Thesis)
12) S. Mora and I. Ortalli, Nuovo Cim. **12** (1959) 635
13) J. Sacton, Nuovo Cim. **15** (1960) 110
14) G. C. Deka, Nuovo Cim. **14** (1959) 1217
15) M. Baldo-Ceolin, C. Dilworth, W. F. Fry, W. D. B. Greening, H. Huzita, S. Limentani and A. E. Sichirollo, Nuovo Cim. **7** (1958) 328
16) P. E. Schlein, Thesis, Northwestern Univ. (1959)
P. E. Schlein, Phys. Rev. Letters **2** (1959) 220
17) J. Sacton, Contribution to the Kiev Conference 1959
18) Y. Eisenberg, W. Koch, E. Lohrmann, M. Nikolič, M. Schneeberger and H. Winzeler, Nuovo Cim. **9** (1958) 745
19) M. Nikolic, Y. Eisenberg, W. Koch, M. Schneeberger and H. Winzeler, Helv. Phys. Acta **3** (1960) 221
20) W. Koch, Y. Eisenberg, M. Nikolič, M. Schneeberger and H. Winzeler, Helv. Phys. Acta **3** (1960) 237
21) M. Nikolić, Nuclear Physics **21** (1960) 595
22) E. Lohrmann, M. Nikolič, M. Schneeberger, P. Waloshek and H. Winzeler, Nuovo Cim. **7** (1958) 163
23) W. H. Barkas, P. H. Barrett, P. C. Cüer, H. Heckman, F. M. Smith and H. K. Ticho, Nuovo Cim. **8** (1958) 185;
W. H. Barkas, Nuovo Cim. **8** (1958) 201
24) G. Alvial, A. Bonetti, C. Dilworth, M. Ladu, J. Morgan and G. Occhialini, Suppl. Nuovo Cim. **4** (1956) 244
25) G. Alvial, L. Grimaldi, J. Riquelme, E. Silva and S. Stantic, Nuovo Cim. **15** (1960) 25
26) R. G. Ammar, Suppl. Nuovo Cim. **15** (1960) 181

27) P. Demers, Ionographie (Presses universitaires de Montréal, 1958)
28) A. Papineau, Rapport C.E.A. Nr. **543** (1956)
29) W. H. Barkas and D. M. Young, UCRL-2579, (1954)
30) W. H. Barkas and A. H. Rosenfeld, UCRL-8030, (1958)
31) A. H. Wapstra, Physica **21** (1955) 367
32) M. Blau, Phys. Rev. **102** (1956) 495
33) M. Ruderman and R. Karplus, Phys. Rev. **102** (1956) 247
34) F. Cerulus, Nuovo Cim. **5** (1957) 1685
35) R. H. Dalitz, Phys. Rev. **112** (1958) 605
36) R. H. Dalitz, Rev. Mod. Phys. **31** (1959) 823;
R. H. Dalitz and L. Liu, Phys. Rev. **116** (1959) 1312
37) M. Gell-Mann and A. H. Rosenfeld, Ann. Rev. Nucl. Sci. **7** (1957) 407
38) S. B. Treiman, Proc. of the 1958 Ann. Intern. Conf. on High Energy Physics at CERN, edited by B. Ferretti (CERN Scientific Information Service, Geneva 1958), p. 276
49) W. B. Cheston and H. Primakoff, Phys. Rev. **92** (1953) 1537
30) T. K. Fowler, Phys. Rev. **102** (1956) 844
41) F. Ferrari and L. Fonda, Nuovo Cim. **7** (1958) 320
42) D. B. Lichtenberg and M. Ross, Phys. Rev. **103** (1956) 1131
43) N. Dallaporta and F. Ferrari, Nuovo Cim. **5** (1957) 111
44) W. F. Fry, I. Schneps, G. A. Snow, M. S. Swami and D. C. Wold, Phys. Rev. **107** (1957) 257
45) G. Dascola, C. Lamborizio, S. Mora and J. Ortalli, Nuovo Cim. **16** (1960) 241
46) O. Skjeggestad, Arch. Math. Naturv. B. **7** (1959)

7.C

Nuclear Physics **21** (1960) 624—630; © *North-Holland Publishing Co., Amsterdam*

Not to be reproduced by photoprint or microfilm without written permission from the publisher

RENORMALIZATION PROBLEM FOR VECTOR MESON THEORIES

A. KOMAR †

and

ABDUS SALAM

Imperial College of Science and Technology, London

Received 22 August 1960

Abstract: The renormalizability problem of the Yang-Mills theory of vector mesons with mass is considered. It is shown, that the divergences of such a theory are those of the electrodynamics of charged vector mesons. This general feature is illustrated by direct calculation of the lowest order divergent diagrams. It is concluded that renormalizability of this theory seems rather unlikely.

1. Introduction

It has been known for a long time [1]) that the theories of a massive neutral vector meson field U_μ interacting with spin zero and spin $\frac{1}{2}$ fields are renormalizable provided the meson current j_μ (defined as $(\Box-\mu^2)U_\mu$) is conserved. When this condition is satisfied such theories are simple extensions of quantum electro-dynamics. In recent papers [2]) by Salam and Kamefuchi, it has been shown that for renormalizability conservation of the current is not only sufficient but also necessary ††.

If there is more than one mutually interacting vector meson field, one may conjecture that for renormalizability the current of each field should be individually conserved. Such theories are not difficult to formulate. One example is the Yang-Mills [4]) theory of a triplet of mutually interacting (zero mass) fields U_μ^i. Yang and Mills have shown that this theory is indeed renormalizable.

In this note we consider Yang-Mills fields with mass (equal for all components of the triplet). Such inclusion of mass does not affect current conservation in analogy with the neutral case. However, very surprisingly, it appears that the renormalizability is lost.

2. S-matrix and Equivalence Theorem

The proof of renormalizability for the neutral vector case was based on the observation that by making a Struckelberg split of the field

† On leave of absence from Lebedev Physical Institute, Moscow, USSR.

†† This is contrary to the assertion made by S. Glashow [3]).

$$U_\mu = A_\mu + \frac{1}{\mu}\frac{\partial \Lambda}{\partial x_\mu},$$

where

$$\begin{aligned} i\langle T(U_\mu(x)U_\nu(y))\rangle_0 &= \left(\delta_{\mu\nu} - \frac{\partial_\mu\partial_\nu}{\mu^2}\right)\Delta_F(x-y), \\ i\langle T(A_\mu(x)A_\nu(y))\rangle_0 &= \delta_{\mu\nu}\Delta_F(x-y), \\ i\langle T(\Lambda(x)\Lambda(y))\rangle_0 &= \Delta_F(x-y). \end{aligned} \tag{1}$$

One can show, as a consequence of current conservation, that the Λ-field is completely uncoupled to other fields and can be omitted from further consideration. The propagator for the residual A_μ field is not so singular, as that for U_μ, and leads to the possibility of renormalization.

For the massive Yang-Mills triplet $U_\mu{}^i$ ($i = 1, 2, 3$) there are three Struckelberg Λ^i fields. The principal result of this note is only *one* of these Λ's is completely uncoupled with other fields so that the reduction in the divergence of S-matrix elements is rather slight. The Lagrangian for the theory is

$$\mathscr{L} = \mathscr{L}_f + \mathscr{L}_{\text{int}},$$

where

$$\mathscr{L}_f = -\tfrac{1}{4}\mathbf{f}_{\mu\nu}\mathbf{f}_{\mu\nu} - \tfrac{1}{2}\mu^2\mathbf{U}_\mu\mathbf{U}_\mu, \tag{2}$$

$$\mathscr{L}_{\text{int}} = -\tfrac{1}{2}e\mathbf{f}_{\mu\nu}(\mathbf{U}_\mu \wedge \mathbf{U}_\nu) - \tfrac{1}{4}e^2(\mathbf{U}_\mu \wedge \mathbf{U}_\nu)^2, \tag{3}$$

and

$$\mathbf{f}_{\mu\nu} = \frac{\partial \mathbf{U}_\nu}{\partial x_\mu} - \frac{\partial \mathbf{U}_\mu}{\partial x_\nu}.$$

The equation of motion is

$$\frac{\partial \mathbf{f}_{\mu\nu}}{\partial x_\mu} - \mu^2\mathbf{U}_\nu = -e\frac{\partial}{\partial x_\mu}(\mathbf{U}_\mu \wedge \mathbf{U}_\nu) - e[\mathbf{U}_\mu \wedge \{\mathbf{f}_{\mu\nu} + e(\mathbf{U}_\mu \wedge \mathbf{U}_\nu)\}]. \tag{4}$$

We define current as

$$\mathbf{j}_\mu = -e[\mathbf{U}_\mu \wedge \{\mathbf{f}_{\mu\nu} + e(\mathbf{U}_\mu \wedge \mathbf{U}_\nu)\}],$$

which differs from the full right hand side of the eq. (4) by the term $-e\partial(\mathbf{U}_\mu \wedge \mathbf{U}_\nu)/\partial x_\mu$ the divergence of which always vanishes. It is easily shown that, on account of (4), $\partial \mathbf{j}_\mu/\partial x_\mu = 0$. The S-matrix in this case is

$$S = T\exp\left(i\int \mathscr{L}_{\text{int}}(x)\mathrm{d}^4x\right), \tag{5}$$

where it is assumed that

$$\begin{aligned} i\langle T(U_\mu{}^i(x)U_\nu{}^k(y))\rangle_0 &= \delta_{ik}\left(\delta_{\mu\nu} - \frac{\partial_\mu\partial_\nu}{\mu^2}\right)\Delta_F(x-y), \\ i\langle T(f^i_{\mu\nu}(x)U_\lambda{}^k(y))\rangle_0 &= \delta_{ik}(\delta_{\nu\lambda}\partial_\mu - \delta_{\mu\lambda}\partial_\nu)\Delta_F(x-y), \\ i\langle T(f^i_{\mu\nu}(x)f^k_{\lambda\sigma}(y))\rangle_0 & \\ &= -\delta_{ik}(\delta_{\nu\sigma}\partial_\mu\partial_\lambda + \delta_{\mu\lambda}\partial_\nu\partial_\sigma - \delta_{\nu\lambda}\partial_\mu\partial_\sigma - \delta_{\mu\sigma}\partial_\nu\partial_\lambda)\Delta_F(x-y). \end{aligned} \tag{6}$$

A completely equivalent linearized formulation of the theory has been discussed recently by Glashow, Mayer and Kemmer [3, 5]) In this formulation additional independent variables $\mathbf{F}_{\mu\nu}$ are introduced. The Lagrangian is

$$\mathscr{L} = -\tfrac{1}{2}[\mathbf{F}_{\mu\nu}(\partial_\mu \mathbf{U}_\nu - \partial_\nu \mathbf{U}_\mu) - \tfrac{1}{2}\mathbf{F}_{\mu\nu}\mathbf{F}_{\mu\nu} + \mu^2 \mathbf{U}_\mu \mathbf{U}_\mu] - \tfrac{1}{2}e\mathbf{F}_{\mu\nu}(\mathbf{U}_\mu \wedge \mathbf{U}_\nu), \quad (7)$$

with equations of motion

$$\mathbf{F}_{\mu\nu} = \partial_\mu \mathbf{U}_\nu - \partial_\nu \mathbf{U}_\mu + e\mathbf{U}_\mu \wedge \mathbf{U}_\nu, \quad \frac{\partial \mathbf{F}_{\mu\nu}}{\partial x_\mu} - \mu^2 \mathbf{U}_\nu = -e\mathbf{U}_\mu \wedge \mathbf{F}_{\mu\nu}, \quad (8)$$

from which eq. (4) is easily derived.

The S-matrix is given by

$$S = T \exp\left(\tfrac{1}{2}ie \int \mathbf{F}_{\mu\nu}(\mathbf{U}_\mu \wedge \mathbf{U}_\nu)\mathrm{d}^4x\right), \quad (9)$$

where the operators are supposed to satisfy free field equations

$$\mathbf{F}_{\mu\nu} = \partial_\mu \mathbf{U}_\nu - \partial_\nu \mathbf{U}_\mu, \quad \frac{\partial \mathbf{F}_{\mu\nu}}{\partial x_\mu} - \mu^2 \mathbf{U}_\nu = 0. \quad (10)$$

The contractions of U_μ and $F_{\mu\nu}$ now are

$$\begin{aligned}
&i\langle T(U_\mu{}^i(x)U_\nu{}^k(y))\rangle_0 = \delta_{ik}\left(\delta_{\mu\nu} - \frac{\partial_\mu\partial_\nu}{\mu^2}\right)\Delta_{\mathrm{F}}(x-y),\\
&i\langle T(F^i_{\mu\nu}(x)U_\lambda{}^k(y))\rangle_0 = \delta_{ik}(\delta_{\nu\lambda}\partial_\mu - \delta_{\mu\lambda}\partial_\nu)\Delta_{\mathrm{F}}(x-y), \quad (11)\\
&i\langle T(F^i_{\mu\nu}(x)F^k_{\lambda\sigma}(y))\rangle_0\\
&\qquad = -\delta_{ik}[(\delta_{\nu\sigma}\partial_\mu\partial_\lambda + \delta_{\mu\lambda}\partial_\nu\partial_\sigma - \delta_{\nu\lambda}\partial_\mu\partial_\sigma - \delta_{\mu\sigma}\partial_\nu\partial_\lambda)\Delta_{\mathrm{F}}(x-y)\\
&+(\delta_{\mu\lambda}\delta_{\nu\sigma} - \delta_{\mu\sigma}\delta_{\nu\lambda})\delta(x-y)].
\end{aligned}$$

Notice the diference between $\langle T(F^i_{\mu\nu}(x)F^k_{\lambda\sigma}(y))\rangle_0$ and $\langle T(f^i_{\mu\nu}(x)f^k_{\lambda\sigma}(y))\rangle_0$. This change in the propagator essentially compensates for the absence of the 4th order term in the field in the interaction Hamiltonian. The two forms of the S-matrix (5) and (9) give identical results.

Following Salam and Ward [6]) we can rewrite the expression for interaction Hamiltonian $\frac{1}{2}e\mathbf{F}_{\mu\nu}(\mathbf{U}_\mu \wedge \mathbf{U}_\nu)$ in the new formalism as

$$H_{\mathrm{int}} = ieU_\mu{}^0(F^+_{\mu\nu}U_\nu{}^- - F^-_{\mu\nu}U_\nu{}^+) + \tfrac{1}{2}ieF^0_{\mu\nu}(U_\mu{}^-U_\nu{}^+ - U_\mu{}^+U_\nu{}^-). \quad (12)$$

Let us treat now $U_\mu{}^+$ and $U_\mu{}^-$ fields as source fields for $U_\mu{}^0$ and split $U_\mu{}^0$ in two parts,

$$U_\mu{}^0 = A_\mu{}^0 + \frac{1}{\mu}\frac{\partial \Lambda^0}{\partial x_\mu},$$

with the usual contractions (1) for A_μ^0 and Λ^0. Then the S-matrix (9) is

$$T\exp\left\{-i\int d^4x\left[-A_\mu^0 j_\mu^0-\frac{1}{\mu}\frac{\partial\Lambda^0}{\partial x_\mu}j_\mu^0+\tfrac{1}{2}ieF_{\mu\nu}^0(U_\mu^- U_\nu^+-U_\mu^+U_\nu^-)\right]\right\}, \quad (13)$$

where

$$j_\mu^0=-ie(F_{\mu\nu}^+U_\nu^- - F_{\mu\nu}^-U_\nu^+). \quad (14)$$

This may be rewritten as

$$S=T\left\{\sum_{n=0}^{\infty}\frac{(i)^n}{n!\mu^n}\int\!\!\int\ldots\int dx_1dx_2\ldots dx_n\left[\frac{\partial\Lambda^0}{\partial x_1^\mu}\frac{\partial\Lambda^0}{\partial x_2^\nu}\cdots\frac{\partial\Lambda^0}{\partial x_n^\rho}\right.\right.$$
$$\left.\left.\times(j_\mu^0(x_1)j_\nu^0(x_2)\ldots j_\rho^0(x_n))\right]\right\} \quad (15)$$
$$\cdot\exp\left[-i\int d^4x(-A_\mu^0 j_\mu^0+\tfrac{1}{2}ieF_{\mu\nu}^0(U_\mu^-U_\nu^+-U_\mu^+U_\nu^-))\right].$$

It can easily be shown that

$$\frac{\partial}{\partial x_\mu}T(j_\mu^0(x)A(x_1)B(x_2)\ldots C(x_n))$$
$$=T\left(\frac{\partial j_\mu^0}{\partial x_\mu}A(x_1)B(x_2)\ldots C(x_n)\right)-\mu\frac{\delta}{\delta\Lambda^0(x)}T(A'(x_1)B'(x_2)\ldots C'(x_n)). \quad (16)$$

Here $A(x_1)$, $B(x_2)$, ..., $C(x_n)$ are any of the operators $F_{\mu\nu}^\pm$, $U_\mu^\pm$ and

$$U_\mu^{\pm\prime}=\exp\left(\pm\frac{ie}{\mu}\Lambda^0(x)\right)U_\mu^\pm(x). \quad (17)$$

Notice now that $\partial j_\mu^0/\partial x_\mu=0$ as the consequence of the free equations for $U_\mu^\pm$ fields (eqs. (10)).

Following then very closely the arguments given in a previous paper [2]), we arrive at the expression for the S-matrix

$$S=T\left\{\sum_{n=0}^{\infty}\frac{(-i)^n}{n!}\int\!\!\int\ldots\int dx_1\ldots dx_n\left[\Lambda^0(x_1)\ldots\Lambda^0(x_n)\frac{\delta^n}{\delta\Lambda^0(x_1)\ldots\delta\Lambda^0(x_n)}\right]\right.$$
$$\left.\cdot\exp\left[-i\int d^4x(-A_\mu^0 j_\mu^{0\prime}+\tfrac{1}{2}ieF_{\mu\nu}^0(U_\mu^{-1}U_\nu^{+\prime}-U_\mu^{+\prime}U_\nu^{-1}))\right]\right].$$

Since $j_\mu^{0\prime}=j_\mu^0$ and

$$U_\mu^{-1}U_\mu^{+\prime}-U_\mu^{+\prime}U_\nu^{-\prime}=U_\mu^-U_\nu^+-U_\mu^+U_\nu^-$$

we are finally left with

$$S=T\{\exp\left[-i\int d^4x(-A_\mu j_\mu^0+\tfrac{1}{2}ieF_{\mu\nu}^0(U_\mu^-U_\nu^+-U_\mu^+U_\nu^-))\right]\}. \quad (18)$$

Thus for one of the fields (U_μ^0) we can remove its Λ-part. Ideally one would

now like to split both $U_\mu^{\pm}$ fields into their Struckelberg components and show that $A^{\pm}$ fields make no contribution to the matrix elements. This unfortunately is not true as the following second order examples bear out.

3. Lowest order Divergences

For all second order matrix-elements the effect of the result proved in section 2 will be to replace the propagator

$$i\langle T(U_\mu{}^i(x)U_\nu{}^k(y))\rangle_0 = \delta_{ik}\left(\delta_{\mu\nu}-\frac{\partial_\mu\partial_\nu}{\mu^2}\right)\Delta_F(x-y)$$

for *one* internal line by

$$i\langle T(A^i_{\mu\nu}(x)A_\nu{}^k(y))\rangle_0 = \delta_{ik}\delta_{\mu\nu}\Delta_F(x-y).$$

This means in momentum space, the reduction of the degree of divergence of a matrix-element by a factor of two. Thus a vacuum self energy graph would exhibit a 6th order divergence, a meson self-energy graph a quadratic divergence, a vertex part a quadratic divergence, and so on. Below we show that these expectations are justified and no further reduction of the order of divergence takes place. Essentially then the order of divergence of each graph in this theory is the same as that for the theory of charged vector mesons interacting with photons and the fact that charged meson currents themselves are conserved makes no difference to renormalizability.

It is necessary to emphasize that more than one counter term in the Lagrangian is needed in order to remove vertex part divergence. This is typical of the behaviour of the non-renormalizable theories where the number of counter terms itself is infinite.

4. Examples

4.1. VACUUM SELF-ENERGY GRAPH

The 2nd order matrix element corresponding to the graph is

$$P = \tfrac{3}{2}ie^2\frac{\delta(0)}{(2\pi)^4}\int\int \mathrm{d}^4q\,\mathrm{d}^4p\left(\frac{(pq)^2+11p^2q^2+6pq(p^2+q^2)}{\mu^2(q^2+\mu^2)}\right.$$
$$\left.+\frac{6p^2+12pq-3q^2}{q^2+\mu^2}+12\right)\frac{1}{(p^2+\mu^2)((p+q)^2+\mu^2)}. \tag{19}$$

The leading 8th order divergence vanishes in accordance with the theorem of section 2, but the 6th order divergence persists.

4.2. MESON SELF-ENERGY GRAPH

The corresponding matrix element is

$$M = -2e^2 \frac{\delta(p-p')}{2\omega_p} \int \frac{\mathrm{d}^4 q}{(q^2+\mu^2)((p-q)^2+\mu^2)} \Big\{ \delta_{\nu\sigma} \Big[3q^2 - 4pq + 3\mu^2 - \frac{1}{\mu^2}(2pq \cdot q^2 - 3q^2 p^2 + pq \cdot p^2 + \tfrac{1}{2} p^4) \Big] - q_\nu q_\sigma \Big(6 + \frac{2p^2}{\mu^2} + \frac{p^4}{2\mu^4} \Big) + q_\sigma p_\nu \Big(7 + \frac{2(q^2+pq)}{\mu^2} + \frac{p^2 \cdot pq}{\mu^4} \Big) - \frac{p_\nu p_\sigma}{\mu^2} \Big(3q^2 + \frac{(pq)^2}{2\mu^2} - pq - \tfrac{1}{2} p^2 \Big) \Big\} U_\nu(p) U_\sigma(p'). \tag{20}$$

The 4th order divergence is absent but the expression is still 2nd order divergent.

4.3. VERTEX-PART

The full expression for the matrix element is rather cumbersome and will not be quoted here. The leading (quadratic!) divergent terms are

$$\Gamma(\kappa_1, \kappa_2, \kappa_3) = \frac{-ie^3}{\mu^2} \frac{\delta(\kappa_1+\kappa_2+\kappa_3)}{(2\omega_{\kappa_1} 2\omega_{\kappa_2} \cdot 2\omega_{\kappa_3})^{\frac{1}{2}}} U_\mu{}^1(\kappa_1) U_\nu{}^2(\kappa_2) U_\rho{}^3(\kappa_3) \int \frac{\mathrm{d}^4 q}{q^2} \times \{ 2\delta_{\mu\rho}(\kappa_1-\kappa_3)_\nu - \tfrac{1}{4}\mu^2 [\kappa_3{}^2 (\delta_{\mu\nu}(\kappa_2-\kappa_1)_\rho - \delta_{\nu\rho}\kappa_\mu{}^2 + \delta_{\mu\rho}\kappa^2{}_\nu) + \kappa_\rho{}^3 (\kappa_\mu{}^2 \kappa_\nu{}^3 - \kappa_\nu{}^1 \kappa_\mu{}^3 - \delta_{\mu\nu}(\kappa_2\kappa_3 - \kappa_3\kappa_1))] \} + 1, 2, 3 \text{ cyclic permutated.} \tag{21}$$

This already implies that in order to cancel quadratic divergence one has to introduce in the Lagrangian besides the usual interaction term $\mathbf{F}_{\mu\nu}(\mathbf{U}_\mu \wedge \mathbf{U}_\nu)$ also the term of the form $(\Box\delta_{\mu\nu} - \partial_\mu \partial_\nu)\mathbf{U}_\mu(\mathbf{F}_{\nu\rho} \wedge \mathbf{U}_\rho)$. Generally Γ has the following structure

$$\Gamma \propto \Big[\Big(a_1 \frac{\kappa}{\mu^2} + a_2 \frac{\kappa\kappa\kappa}{\mu^4} \Big) \int \frac{\mathrm{d}^4 q}{q^2} + \Big(b_1 \kappa + b_2 \frac{\kappa\kappa\kappa}{\mu^2} + b_3 \frac{\kappa\kappa\kappa\kappa\kappa}{\mu^4} + b_4 \frac{\kappa\kappa\kappa\kappa\kappa\kappa\kappa}{\mu^6} \Big) \int \frac{\mathrm{d}^4 q}{q^4} \Big], \tag{22}$$

with logarithmically divergent terms also present. This makes the situation even more complicated. (In the above expression we only want to show symbolically the powers of momenta involved or correspondingly the number of derivatives in x-space).

It is indeed a surprising matter that Yang-Mills triplet of fields with and without mass behave so differently. Putting it in another way, we may say that the electrodynamics of charged vector mesons is renormalizable only if these have no bare mass.

We would like to thank Dr. S. Kamefuchi for stimulating discussions. One of the authors (A. K.) wishes to thank for the hospitality, extended to him during his stay at Imperial College.

References

1) P. T. Matthews, Phys. Rev. **76** (1949) 1254
2) A. Salam, Nuclear Physics **18** (1960) 681;
S. Kamefuchi, Nuclear Physics **18** (1960) 691
3) S. Glashow, Nuclear Physics **10** (1959) 107
4) C. N. Yang and R. L. Mills, Phys. Rev. **96** (1957) 191
5) M. E. Mayer, Preprint P. 212, Dubna 1958;
N. Kemmer, Helv. Phys. Acta (Pauli Memorial Volume, in the press)
6) A. Salam and J. C. Ward, Nuovo Cim. **11** (1959) 568

1.D.2:
2.H

Nuclear Physics **21** (1960) 631—651; © *North-Holland Publishing Co., Amsterdam*
Not to be reproduced by photoprint or microfilm without written permission from the publisher

COULOMB EXCITATION WITH 14—20 MeV α-PARTICLES: DOUBLE EXCITATIONS AND SYSTEMATICS OF VIBRATIONAL STATES IN THE RARE EARTH REGION

O. NATHAN and V. I. POPOV†

Institute for Theoretical Physics, University of Copenhagen, Denmark

Received 24 August 1960

Abstract: An exploratory investigation of nuclei in the rare earth region has been performed by means of the Coulomb excitation process, using 14–20 MeV α-particles as projectiles and studying the deexcitation γ-rays. Rotational double excitations were systematically observed in deformed, even nuclei and evidence for double E2–E2 excitations was also found in some non-rotational, even nuclei. In single excitation a number of γ-rays were seen which have not been reported previously in Coulomb excitations, and approximative values for the corresponding partial, reduced E2 transition probabilities $\varepsilon B(\mathrm{E2})$ have been determined. Tentative level schemes are proposed which will explain the observations, and the nature of the excited states is discussed on the basis of the measured $\varepsilon B(\mathrm{E2})$ values. In particular, it is pointed out that our results, together with other data, may indicate the presence of γ-vibrations in Ho^{165} and some other deformed nuclei with odd number of protons.

1. Introduction

The use of very energetic α-particles as projectiles in the Coulomb excitation process offers certain advantages over the more conventional type of Coulomb excitation experiments in which the bombarding energy is low compared to the Coulomb barrier: high lying nuclear states may become accessible to excitation, and certain higher order effects in the excitation process such as double excitations of rotational and vibrational states may be studied in detail. The limitation to the α-particle energy which can be used with advantage is, of course, determined by the fact that nuclear interactions start being important at energies close to the barrier, and in many cases the resulting background radiation may mask the radiations from Coulomb excitation processes. Additional background difficulties often arise from nuclear events, such as inelastic scattering, which take place in the inevitable target impurities carbon and oxygen.

One possible way to improve this situation is to observe the deexcitation γ-rays from the Coulomb process in coincidence with the scattered projectiles. Very successful results along this line have, for instance, been obtained in the heavy ion experiments performed at Berkeley [1]). For α-particle energies close to the barrier there still remains the problem of distinguishing the Coulomb

† On leave from The Lebedev Physical Institute, Moscow.

excitations from nuclear inelastic scatterings on the target nuclei. This distinction may be attempted by measuring the dependence of the γ-ray yield with the bombarding energy or by studying the angular distribution of the coincident γ-rays.

The purpose of this paper is to describe a series of Coulomb excitation experiments involving nuclei in the rare earth region, which have been carried out using an α–γ coincidence technique. The experiments were performed with the aim to give a survey, while a more detailed study of the properties of the excitation processes, such as angular distributions, has not been attempted. Some information was obtained on the yield as a function of the bombarding energy, but the practically available energy interval was rather small.

2. Experimental Procedure

The experiments were carried out with the 20 MeV external α-particle beam of the Copenhagen cyclotron. At a distance of 100 cm from the target the beam passed through a 1 mg/cm^2 mylar foil, and in the region between this foil and the target, the beam tube could be filled with He at a suitable pressure. In this way, the bombarding energy could be conveniently varied between 14 and 20 MeV. Observation of the scattered α-particles was accomplished in a standard backscattering geometry by means of an 0.12 mm thick, ring-shaped CsI crystal, 25 mm in outer diameter and provided with a 7 mm central hole. The incident beam passed through the hole before hitting the target, which was placed perpendicular to the beam at a distance of about 12 mm from the CsI crystal. In this way backwards scattered α-particles were detected in a rather large solid angle. The γ-rays were observed by means of a 38 mm$\times$38 mm NaI crystal which could be placed at either 0° or 115° with respect to the beam direction. The latter position was chosen for observation of low energy γ-quanta in order to avoid serious absorption of photons in the target. In those cases in which high energy γ-rays were involved, a 76 mm$\times$76 mm NaI crystal was used to improve the counting statistics and background conditions. Shielding of the detectors was not found necessary since most of the background radiation originated in the target itself. The electronics consisted of a conventional coincidence system and a 100-channel pulse height analyser for recording the coincident photon spectra. The electronic resolving time was 6×10^{-8} sec, which is less than the time interval between two successive bunches of the cyclotron beam. The number of random coincidences was, therefore, determined by the duty cycle of the accelerator. Empirically, we found that the counting rate of random coincidences could be estimated rather well from the single counting rates, if an effective resolving time of $2\tau \approx 3\times10^{-7}$ sec was used. This rather poor time resolution constituted the most serious limitation to the obtainable signal-to-noise ratio for most of the weaker γ-rays observed in coincidence.

Thick metal targets of each of the stable elements from $Z = 57$ to $Z = 75$ were investigated. Immediately before inserting in the vacuum the surface oxide layers were removed as far as possible by mechanical cleaning. In addition to the natural metal samples, we also studied some isotopically enriched targets belonging to the same region of the periodic table †. The majority of these consisted of approximately 5 mg/cm² oxide layers which were deposited by electrophoresis on 0.5 mm thick lead backings ††. For reasons of cost and availability the selection of enriched targets was far from complete, and in some cases we were therefore unable to assign γ-rays found with the metal targets to a definite nucleus. The quantitative estimates of electromagnetic transition probabilities, which will be discussed below, were based on measurements with the metal targets, since the thickness of the oxide targets could be only roughly estimated. Where more than one γ-ray was found to originate in the same nucleus the enriched targets could, however, be used for determination of relative γ-ray intensities. This was, for instance, very useful in the study of double excitations.

For each element the γ-ray region from about 100 keV and up to about 2 MeV was scanned for coincident events. For convenience, fixed bombarding energies of 14, 17 and 20 MeV were chosen throughout, and most of the measurements were done at 17 and 20 MeV. The accuracy to which the bombarding energy was known was limited to about 2 %, and no effort was made to determine its value more accurately.

The directly measured quantities were N_γ, the number of counts in a coincident γ-peak, and N_α, the number of counts in the α-counter which was biased to accept only pulses higher than two thirds of the maximum pulse height. The interesting nuclear quantity which one wants to extract from these numbers is the partial, reduced electromagnetic transition probability εB (defined in ref. [2])) which enters into the expression for the Coulomb excitation cross section. For the determination of this quantity from our data one has to make two important assumptions: 1) that the observed peak is due entirely to Coulomb excitation, and 2) that the multipole order of the transition is known. In our B value calculations we have, in fact, assumed that Coulomb excitation of the E2 type is responsible for almost all γ-rays observed with the 14 and 17 MeV α-particles. This point will be discussed further in section 3.

On the above assumptions it is possible to estimate $\varepsilon B(\mathrm{E2})$ from the measured number N_γ/N_α which is a measure of the number of Coulomb inelastic scattering events divided by the sum of elastic and inelastic Coulomb scatterings. Such calculations were performed for the thick metal targets only. Appropriate corrections were applied for random coincidences, for the effect of target thickness on the α- and γ-rays, and for the finite resolution of the α-counter.

† Supplied by Stable Isotopes Division, Oak Ridge National Laboratory.

†† We are indebted to Mrs. Helle Nordby for the preparation of numerous oxide targets.

The anisotropy in the angular distribution of the γ-rays was, however, neglected. In order to correct for target thickness, the excitation curves for the elastic and inelastic scattering processes, as well as the energy dependence of the α-particle stopping power, must be known. Since this procedure was applied only to cases where higher order excitation effects were estimated to be unimportant, we have used the well-known first order perturbation expressions given in ref. [2]) for the Coulomb excitation cross section. For the elastic cross section we have used the Rutherford expression. The stopping power of the target material was supposed to be proportional to $E^{-0.5}$. It is believed that $\varepsilon B(\mathrm{E2})$ values can be estimated in this way to within a factor of two. The validity of this estimate was supported by a comparison of our values with those from the literature in those cases where the transition probabilities had been determined previously.

Where higher order excitation effects were of importance we have used the "thin" targets for quantitative purposes and we have then taken only ratios of γ-ray intensities for comparison with the Coulomb excitation theory. Also in these cases γ-ray angular distribution effects have been neglected.

3. General Results

A general feature of the experiment was the observation of most of the γ-lines previously found by Coulomb excitation with lower energy projectiles in this region of the periodic table. Intensity measurements of some of these lines (especially the Nd, Sm and W lines in the region 300–1200 keV) were very useful in providing a partial check on the accuracy involved in the procedure described in section 2 for deriving $B(\mathrm{E2})$ values from thick target data. It was in general found that the $B(\mathrm{E2})$ values resulting from 14 and 17 MeV data were the same and that they agreed to within a factor of two with the literature, whereas the values obtained from the 20 MeV data for the lighter rare earths were up to four times the 14 and 17 MeV values. Thus, in all these cases the 14 and 17 MeV data seem to represent rather pure Coulomb excitation, whereas some kind of nuclear interaction apparently becomes important when the 20 MeV bombarding energy is applied for the lighter nuclei considered.

In addition to well-known lines we also observed a number of γ-rays which have not been seen earlier in Coulomb excitations. In some cases, the yields of these lines were measured at the three bombarding energies, and the same general trend was found as above: in going from 14 to 17 MeV, the calculated apparent $B(\mathrm{E2})$ values remained constant within the experimental uncertainties, and the 20 MeV data gave too high apparent $B(\mathrm{E2})$ values for the lighter rare earths. Guided by this experience we have assumed that all the new γ-rays observed at 14 and 17 MeV result from Coulomb excitation. Most of these we classify as single E2 excitations, others as double E2–E2 processes for reasons which will be discussed below. It should be pointed out, however,

that these assumptions could not be directly verified. In particular it should be noted that, when the spin and parity of the excited state in question are unknown, an experimental distinction between E1 and E2 excitation would require a much more detailed study of the excitation process than was attempted in the present survey work. Small contributions from nuclear effects at 17 MeV bombarding energy would, likewise, be very difficult to trace with our technique.

Some of the observed new lines have been attributed to double E2–E2 excitations. Evidence for such processes was particularly clear for the deformed, even nuclei where we systematically observed low energy γ-rays corresponding in energy to transitions between the $4+$ and $2+$ rotational states. Searches for transitions between higher members of the rotational bands were, however, unsuccessful. The $4+ \rightarrow 2+$ transitions were most prominent among the lighter, deformed, rare earths (see fig. 2), and on the basis of relative γ-ray intensities measured with enriched targets it was possible to some extent to verify that the yields were in agreement with the predictions of the theory [3]) for multiple Coulomb excitation. This point will be discussed more closely in the paragraph on Nd^{150}. Other nuclei which apparently exhibit double excitations are some even nuclei with neutron number 88. These nuclei do not have a rotational level structure, and both the first and the second excited states reached in Coulomb excitation are $2+$ states. The second $2+$ state † may be excited both directly from the ground state and by a double excitation through the first $2+$ state. Given the relative intensities of the three γ-transitions which connect the $0+$, $2+$ and $2+'$ states, one may estimate the relative amount of double excitation by comparsion with Coulomb excitation theory. This point will be discussed more closely in connection with Nd^{148} and Sm^{150}.

Most of the evidence on the new lines collected at 17 MeV bombarding energy is summarized in tables 1 and 2 and some representative coincident γ-ray spectra are shown in figs. 1—5. For reasons of completeness, tungsten is included in table 1 although Coulomb excitation of the states in question has been reported by several groups in the past. The first column of the tables indicates that particular target which was used for obtaining the quantitative data in the subsequent columns. Enriched targets are thus not listed in column one when they have been used merely for isotopic identification purposes. The γ-ray energies in column two are those measured in this experiment, while the energies used for constructing the level schemes of column five have been taken from the literature, when available. This procedure was adopted because many of our lines are weak coincident peaks measured with strong background radiation present and therefore are not too well suited for precise energy determinations. An exception to this energy convention is the first excited state of Nd^{148} where our energy is definitely outside the accepted

† In the following, all second $2+$ states will be denoted as $2+$ states.

TABLE 1

Summary of the main results for even nuclei obtained with 17 MeV bombarding energy. The description of the table is given in the text

Target	γ-ray energy (keV)	Assignment	$\varepsilon B(E2)$ $e^2\,10^{-48}\,cm^4$	Proposed level scheme	Ref.
Ce	1590±20	Ce^{140}	0.31	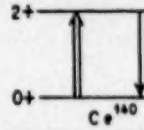	[4])
Ce	645±15	Ce^{142}	0.59	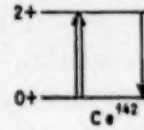	[5])
Nd	1570±20	Nd^{142}	0.34	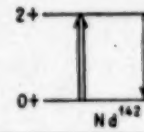	[4])
Nd	700±10	Nd^{144} (E.I.)	0.44	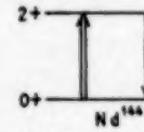	[4])
Nd^{148} (oxide)	460±10 600±15 ≈750 unre- ≈790 solved			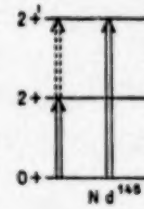	[4])
Nd^{148} (oxide)	320± 5 460±10 710±20 790±20		$\frac{B(2'\to 0)}{B(2'\to 2)}=0.04\pm0.02$ $\frac{B(2'\to 2)}{B(2\to 0)}=1.9\pm1.0$	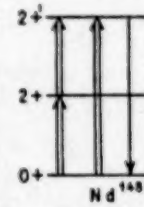	[4])
Nd^{150} (oxide)	135± 5 260± 5			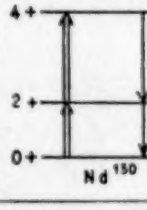	[4])
Sm^{150} (oxide)	340± 5 450±10 770±20		$\frac{B(2'\to 0)}{B(2'\to 2)}=0.05\pm0.02$ $\frac{B(2'\to 2)}{B(2\to 0)}=1.4\pm0.7$	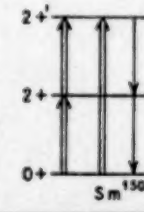	[4])

TABLE 1 (continued)

Target	γ-ray energy (keV)	Assignment	$\varepsilon B(E2)$ $e^2 10^{-48}$ cm^4	Proposed level scheme	Ref.
Gd	≈950	?		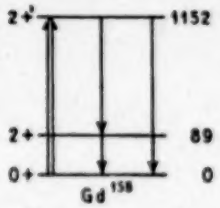	
	≈1050	$Gd^{156, 158}$	0.08		6)
	≈1160	$Gd^{156, 158}$	0.08	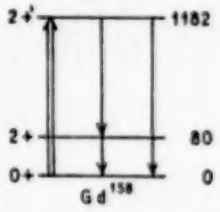	7)
Er	720±20	$Er^{166, 168}$	0.11	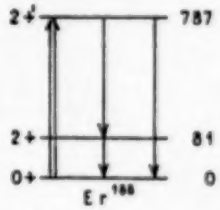	8)
	800±20	$Er^{166, 168}$	0.11	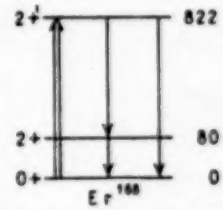	8)
W	1100—1200 (unresolved)	W^{182}	0.12	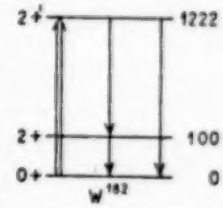	4)
W	780±15	W^{184}	0.06	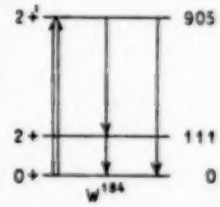	4)
	910±15	W^{184}	0.07		
W	615±10	W^{186}	0.05	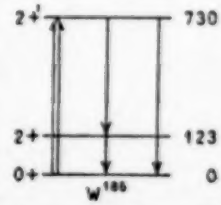	4)
	735±10	W^{186}	0.07		

TABBE 2

Summary of the main results for odd-mass nuclei obtained with 17 MeV bombarding energy. The description of the table is given in the text

Target	γ-ray energy (keV)	Assignment	$\varepsilon B(E2)$ $e^2\,10^{-48}$ cm^4	Proposed level scheme	Ref.
Sm	730±15	Sm^{147} (E.I.)	0.22	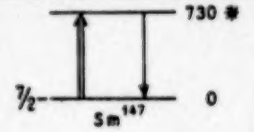	4)
Sm	650±20	Sm^{149} (E.I.)	0.21	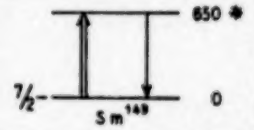	4)
Eu	510±15 570±20	Eu^{151} ?	0.09	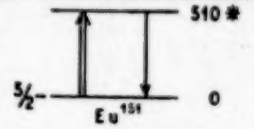	4)
Tb	200±10 360±15 560±20	Tb^{159}	0.010 0.013 0.019	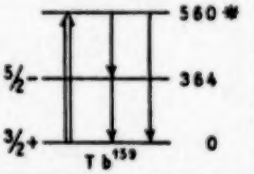	4, 9)
Ho	150±10 510±15 690±15	Ho^{165}	0.03 0.013 0.016	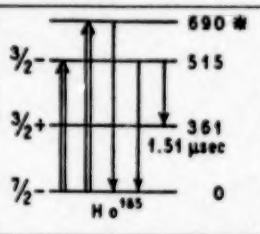	10, 11)
Tm	195±15 unresolved 220±15 unresolved 565±15	Tm^{169}	≈0.040 ≈0.040 0.010	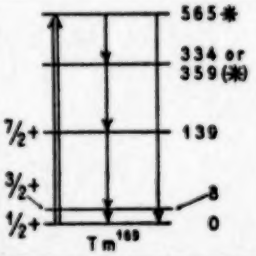	4, 20)
Re	645±15 750±25	Re^{185} (E.I.)	0.03 0.03	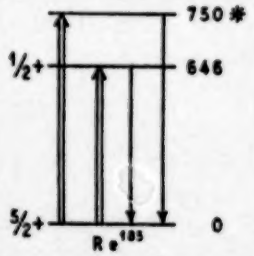	9)
Re	510±15 880±20	Re^{187} (E.I.)	0.04 0.05	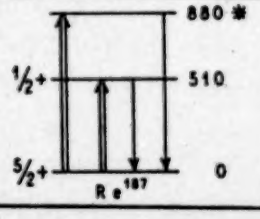	12)

one [4]). Column three gives isotopic assignments based partly on the literature, partly on our measurements with enriched isotopes. The latter type assignments are marked E.I. Column four contains our best values of $\varepsilon B(E2)$ for single excitations, and also some quantitative results concerning Nd^{148} and Sm^{150} which will be explained in section 4. Note that the calculated $B(E2)$ depends on the assumed excitation energy through the parameter ξ, defined in ref. [2]). A possible future change in some of the more uncertain level schemes proposed in this work may, therefore, affect the B values correspondingly. Column five, finally, contains possible level schemes that will explain the observations. New levels postulated on the basis of our data are marked with an asterisk. The references from which the other levels are taken are given in column six. Most of the schemes for the even nuclei (table 1) are rather unambiguous, since most of our γ-rays here could be identified with transitions between levels

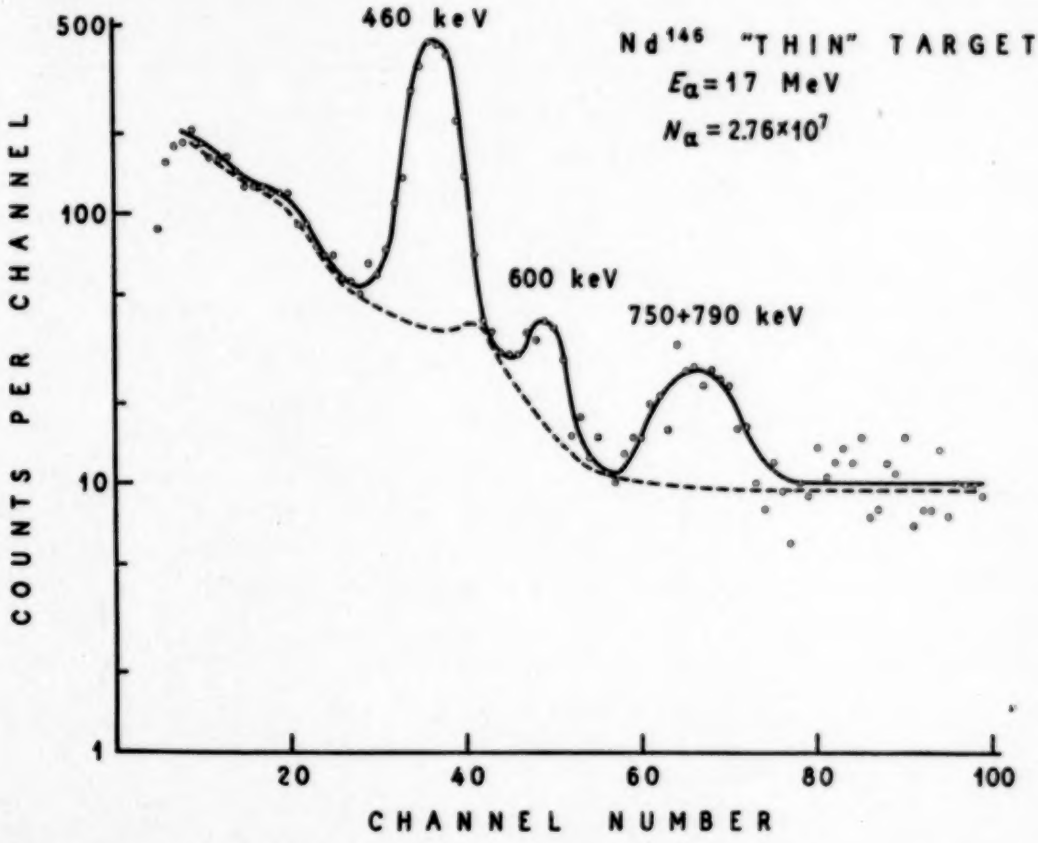

Fig. 1. Representative coincident γ-ray spectra are shown in figs. 1—5 (full curves). The spectra of figs. 1—4 were obtained with a 38 mm × 38 mm NaI crystal, and that of fig. 5 with a 76 mm × 76 mm crystal. The "thin" targets were approximately 5 mg/cm² oxide samples on lead backings. The thick targets were 0.5—2.0 mm thick metal pieces. N_α is the total number of counts in the biased α-counter. The counting rate in this counter was kept at approximately 2000 counts per sec. The dashed curves represent our estimate of the background due to random coincidences, which was evaluated from the single counting rates, using an effective resolving time of $2\tau \approx 3 \times 10^{-7}$ sec. This background estimation is, however, somewhat uncertain, since the resolving time depends on the cyclotron duty cycle which could not be kept rigorously constant during each run.

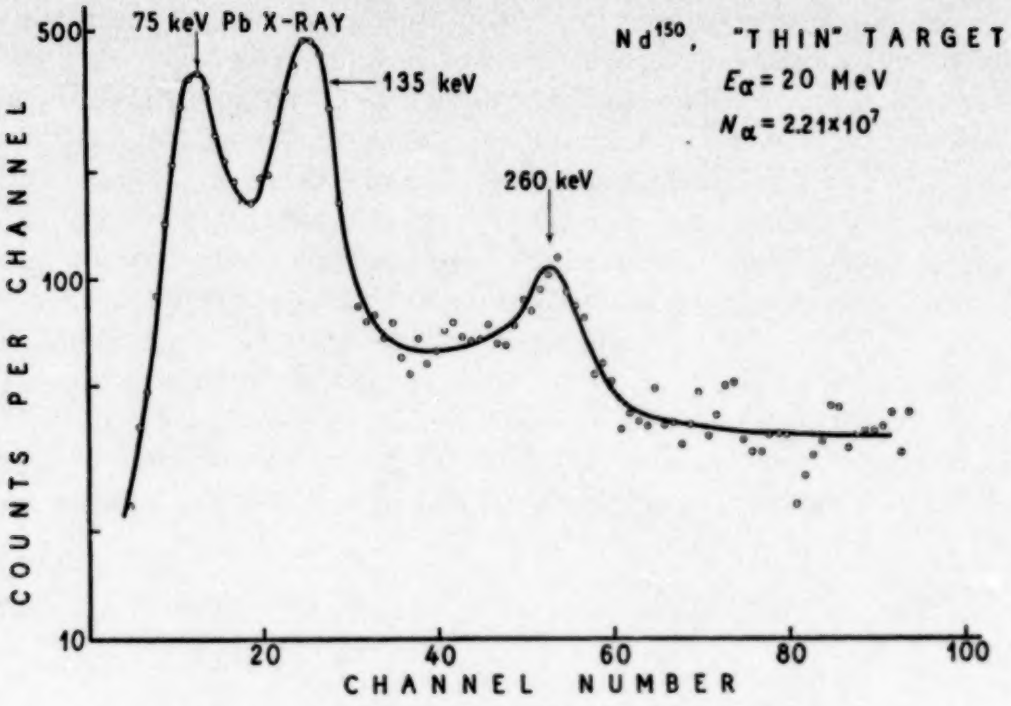

Fig. 2. See caption fig. 1.

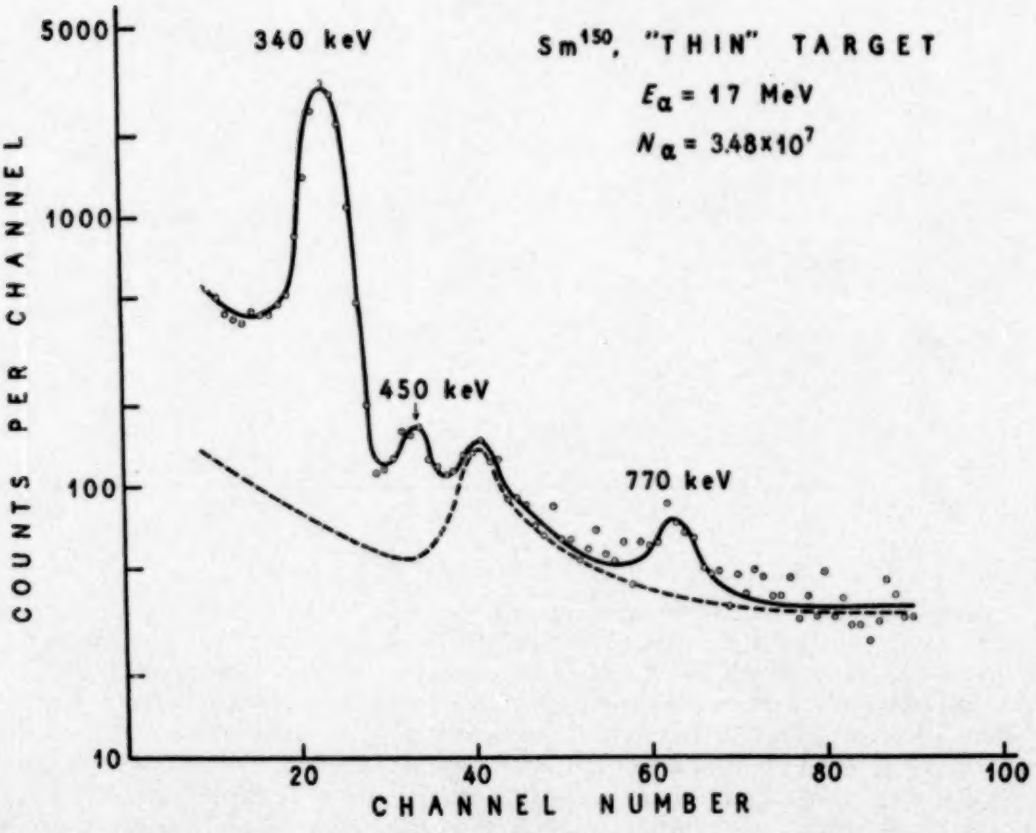

Fig. 3. See caption fig. 1.

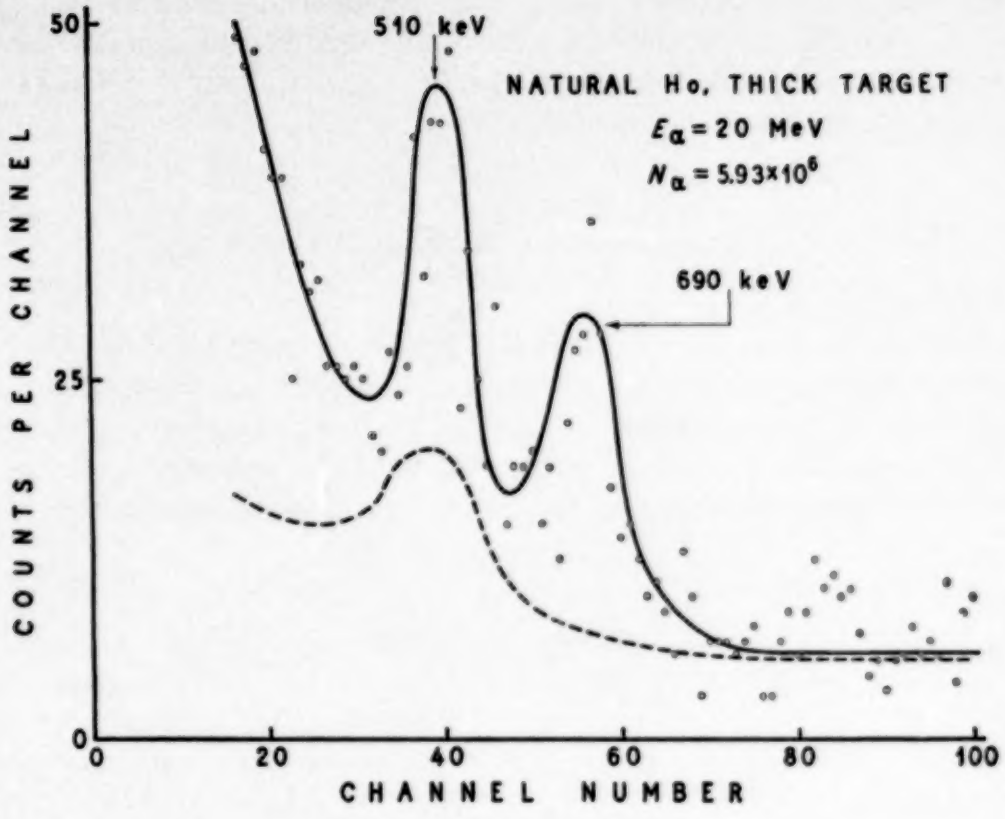

Fig. 4. See caption fig. 1.

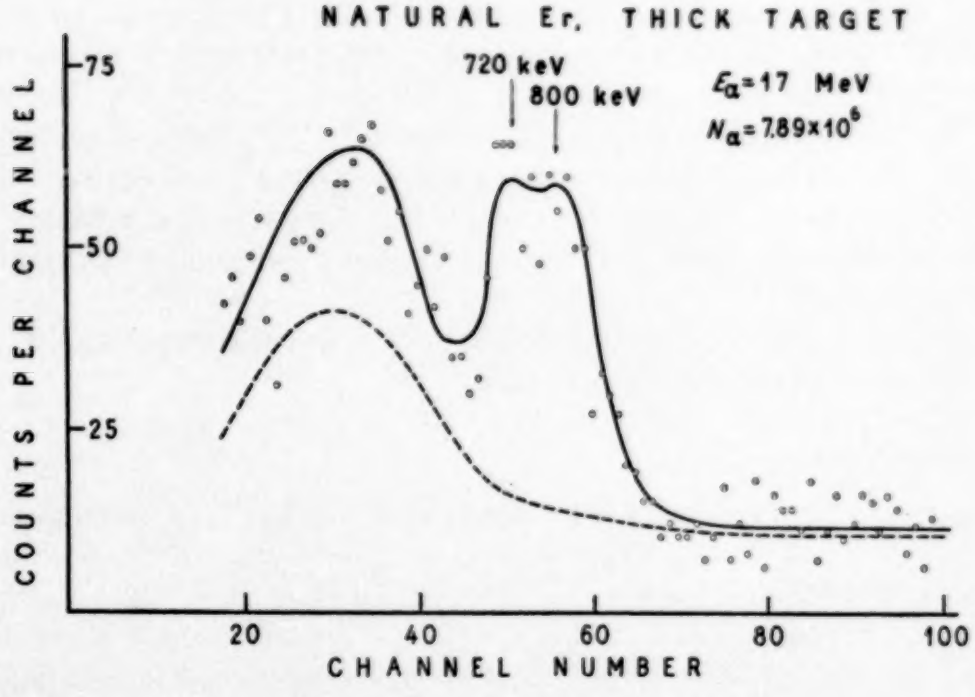

Fig. 5. See caption fig. 1.

already established from decay scheme work. For the odd-mass nuclei (table 2), however, several of the level schemes are of more speculative character, and it would be highly desirable to obtain further information on the postulated levels by means of more detailed experiments.

4. Comments on Individual Cases

4.1. LANTHANUM ($Z = 57$)

Several very weak and partly unresolved lines in the energy region 100—1300 keV were observed with the La metal target. These lines may possibly be interpreted as the result of Coulomb excitation of one or several high lying levels, which subsequently deexcite in γ-cascades, but more definite conclusions on La^{139} do not seem reasonable on the basis of the present data material.

4.2. CERIUM ($Z = 58$)

The lifetime of the 1.596 MeV level in Ce^{140} has recently been measured by Ofer and Schwarzschild [13]), using the resonance fluorescence technique. Their resulting $B(0 \rightarrow 2)$ value for excitation of the state is $0.36 \pm 0.04\ e^2\ 10^{-48}$ cm^4. Our result (0.31 in the same units) agrees with theirs within our experimental uncertainty.

Both this $B(E2)$ and that found for Ce^{142} are rather large compared to the single-particle estimate ($B(E2)_{s.p.} = 3 \times 10^{-5}\ A^{\frac{4}{3}}\ e^2\ 10^{-48}$ cm^4 $= 0.022\ e^2\ 10^{-48}$ cm^4 for Cerium) indicating that the first excited states have collective character. In the usual theoretical description of these nuclei [2]) the first $2+$ states are considered to be vibrational levels, corresponding to quadrupole vibrations about a spherical equilibrium shape. Recently, Kisslinger and Sorensen [14]) have made detailed calculations, including pairing correlation effects, on nuclei of this type having a single closed neutron or proton shell. Ce^{140} has a closed neutron shell of 82 neutrons, and for the first vibrational state Kisslinger and Sorensen find $B(E2) = 0.73$, about twice the experimental result. No similar calculation is available on Ce^{142}.

γ-rays which could correspond to the second excited state of Ce^{142} were searched for, but with negative result.

4.3. PRASEODYMIUM ($Z = 59$)

The situation in Pr^{141} seems to be much like that in La^{139}. Several unresolved high energy lines were observed in the region from 0.5 to 2.0 MeV, which might be the result of Coulomb excitation. The 142 keV transition known from the Ce^{141} decay appeared rather strongly in the spectrum at 20 MeV bombarding energy, but was quite weak at 17 MeV. No definite conclusions on Pr^{141} seem possible from our data alone.

4.4. NEODYMIUM ($Z = 60$)

This element has a large number of rather abundant stable isotopes. Evidence for Coulomb excitation was found in all the even isotopes, whereas no lines were found which could be attributed to Nd^{143} or Nd^{145}. The picture for Nd^{142} and Nd^{144} is analogous to Ce^{140} and Ce^{142}. Nd^{142} is a single closed shell nucleus and the theoretical prediction [14]) here is that the $B(E2)$ for excitation of the 2+ state should be 1.01 e^2 10^{-48} cm^4, thus being somewhat higher than for Ce^{140}. However, the experimental value does not change significantly in going from Ce^{140} to Nd^{142}, and we believe that the estimation of the relative magnitudes of the two $B(E2)$ values is rather accurate, since the experimental conditions were very similar in both cases. Evidence for the second excited state of Nd^{144} was looked for without success.

Four γ-rays were found with an enriched Nd^{146} target and two of these may be identified with already known levels, as shown in table 1. For the 600 and 790 keV γ-rays, however, the situation is not clear. The $\approx$ 790 keV γ-ray may possibly be identified with a transition from a 1.95 MeV level to the second excited state, which was observed in the Pr^{146} decay [15]). The reported 1.49 MeV transition from this level to the first excited state was, however, not seen in our experiment. A $\approx$ 590 keV line was observed in the Pr^{146} decay, and this photon might be identical with our 600 keV γ-ray. It is remarkable, however, that coincidence measurements on Pr^{146} failed to reveal the position of the 590 keV line in the scheme; this fact together with its appearance in a Coulomb excitation experiment may indicate the existence of a new level in Nd^{146} at this excitation energy.

From the systematics of nuclear levels in this region of the periodic table the 1.21 MeV state is possibly a 2+′ state. A 1.21 MeV cross-over transition to the ground state was looked for with negative result, and for this reason the amount of double excitation leading to the conjectured 2+′ state could not be determined (cf. Nd^{148}).

In Nd^{148} the situation is somewhat clearer. Three of the four γ-rays observed may be fitted into a consistent scheme, as shown in table 1. The cross-over character of the 790 keV γ-ray is supported by the fact that the intensity ratio $I_{\gamma,790}/I_{\gamma,460}$ was found to be the same at 20 and 17 MeV bombarding energy. The existence of a cross-over transition, together with the fact that we only consider E2 excitations, in turn requires a 2+′ assignment to the 780 keV state.

In such a case where all three γ-rays in a 0+, 2+, 2+′ scheme are observed it is possible, from our knowledge of the relative γ-ray intensities, to obtain an estimate of the ratios of the three $B(E2)$ values in question. The ratio

$$\frac{B(2' \to 0)}{B(2' \to 2)} \tag{1}$$

can immediately be calculated from the intensity ratio $I_\gamma(2' \to 0)/I_\gamma(2' \to 2)$,

assuming that the $2' \rightarrow 2$ transition is nearly pure E2. For Nd^{148} we find ratio (1) to be 0.04 ± 0.02, indicating the usual forbiddenness of the $2' \rightarrow 0$ transition in non-rotational nuclei.

The ratio

$$\frac{B(2' \rightarrow 2)}{B(2 \rightarrow 0)} \tag{2}$$

can be evaluated as follows. Using the formulas and the notation of Alder and Winther [3]), the ratio of the excitation probabilities of the $2+'$ and $2+$ states is approximately

$$\frac{P'_2}{P_2} \approx \frac{B(2' \rightarrow 2)}{B(2 \rightarrow 0)} \left(\frac{B(2' \rightarrow 0)}{B(2' \rightarrow 2)} + \frac{1}{14} \chi^2 \right), \tag{3}$$

where

$$\chi = 14.52 \frac{A_1^{\frac{1}{2}} [B(0 \rightarrow 2)]^{\frac{1}{2}}}{\left(1 + \frac{A_1}{A_2}\right)^2 Z_1 Z_2^2} E_{\text{bomb}}^{\frac{1}{2}}(\text{MeV}).$$

χ may be evaluated using our measured value for $B(0 \rightarrow 2)$, but we have chosen to use the value $0.7\ e^2\ 10^{-48}$ cm^4 quoted in the literature [2]). For a mean bombarding energy of 16.5 MeV, $Z_2 = 60$ and $A_2 = 148$ we thus find $\chi \approx 0.22$.

The first term in the brackets of (3) represents single excitation of the $2+'$ state, while the second represents double E2–E2 excitation through the $2+$ state. Using the above values of the ratio (1) and of χ, we find that double excitations in this case takes place in about 8 % of all excitations.

Eq. (3) is derived under the simplifying assumptions of 180° scattering and $\xi = 0$, where ξ is the well-known Coulomb excitation parameter which measures the suddenness of the collision. $\xi = 0$ represents the situation of a sudden impact. In the present case, we actually have a mean scattering angle of 150° and $\xi \approx 0.1$ for the $0 \rightarrow 2$ excitation. To derive the ratio (2) from eq. (3), we insert the value already found for the ratio (1) and the experimental value for P'_2/P_2 which is easily obtained from the relative γ-ray intensities. In doing this we introduce another uncertainty in the result, since we have neglected the γ-ray angular distribution. Consequently, eq. (3) will provide only a crude estimate of the desired ratio (2), and of the ratio between the double and single excitation probabilities. In the present case we find the ratio (2) to be 1.9 with an estimated uncertainty of ± 1.0. This result is in agreement with the theoretical expectation based on a vibrational description, which is $B(2' \rightarrow 2)/B(2 \rightarrow 0) = 2.0$. In view of the large experimental uncertainty, the excellent agreement must, however, be regarded as accidental.

With Nd^{150} (neutron number 90) we have entered the region of nuclei with well developed rotational level structures, where the second excited state is

usually a rotational 4+ state. This state has, however, not been observed previously in Nd^{150}. For the two well studied, even nuclei with 90 neutrons, Sm^{152} and Gd^{154}, the rotational energies deviate from the simple rotational formula, and the energy ratio E_{4+}/E_{2+} is ≈ 3.0 instead of 3.33. It thus seems very likely that the 260 keV γ-ray found in Nd^{150} can be identified with the $4+ \rightarrow 2+$ rotational transition. The mechanism for exciting the 4+ state is probably double E2–E2 excitation. We may test this hypothesis by comparing the observed γ-ray yields with the theory of Alder and Winther [3]).

For rotational excitations these authors introduce another parameter q which is connected with χ for the $0 \rightarrow 2$ transition in even nuclei through $q = \chi \sqrt{45/16}$. For a given q and a given scattering angle we find the probability P_n for exciting the n'th member of the rotational band directly from the tables of Alder and Winther. Experimentally, we observe the γ-ray from the first and second rotational states and, after suitable correction for internal conversion and for the feeding of the 2+ state by transitions from the 4+ state, one can obtain P_2/P_1 from the relative γ-ray intensities. Measurements were performed at all three bombarding energies and the results are summarized in table 3.

TABLE 3

Double excitation of the 4+ rotational level in Nd^{150}. The parameter q is defined in the text. Strictly, this q applies only to 180° scattering and for other deflection angles ϑ another quantity $q(\vartheta)$ should be used. We have evaluated $q(\vartheta)$ using a mean scattering angle of 150°. The correction is only small, since $q(150°)/q = 0.94$ [3]). q also depends on $B(0 \rightarrow 2)$. For this quantity we have used the value of the literature [2]) which is $2.3 \times e^2\,10^{-48}$ cm^4 rather than our own, less precise measurement. P_2/P_1 is the ratio of the probabilities for excitation of the 4+ and 2+ rotational levels, respectively. $(P_2/P_1)_{theor}$ is the theoretical value obtained from the work of Alder and Winther [3]). $(P_2/P_1)_{exp}$ shows the result of this experiment.

Bombarding energy MeV	Average $q(150°)$	$(P_2/P_1)_{theor}$	$(P_2/P_1)_{exp}$
20	0.78	0.040	0.23 ± 0.02
17	0.61	0.025	0.04 ± 0.01
14	0.44	0.013	0.01 ± 0.005

Keeping in mind that we have neglected the γ-ray angular distributions, the agreement must be regarded as satisfactory for the two lowest energies. For 20 MeV we find the remarkable result that the 4+ state is excited about six times more strongly relative to the 2+ state than expected from Coulomb excitation theory, indicating that other excitation mechanisms come into play for the rotational states at this energy. A similar situation was found in other even, deformed nuclei, where the double excitation process was studied in

detail. In the present survey we shall, therefore, not make any further quantitative remarks on the excitation of 4+ states.

4.5. SAMARIUM ($Z = 62$)

The two γ-transitions observed in Sm^{147} and Sm^{149} are interesting for their rather high $B(E2)$ values (about ten times the single-particle value). A possible interpretation is that the corresponding states represent quadrupole vibrations about a spherical equilibrium shape, analogous to the first excited 2+ states in the neighbouring even, non-rotational nuclei [2]). However, the experimental values of $B(E2)$ in these nuclei are 2—5 times larger than in Sm^{147} and Sm^{149}, and within the framework of a vibrational description one expects a sum rule to hold, according to which the sum of the $B(E2)$ values for all one-phonon vibrations in the odd nucleus should be equal to the $B(E2)$'s for the 2+ states in the neighbouring even nuclei [2]). If the sum rule holds, we must, therefore, conclude that we are missing some one-phonon transitions of appreciable total strength in the experimental spectra of the odd nuclei. Since altogether five one-phonon states are expected (with spins $\frac{11}{2}-, \ldots, \frac{3}{2}-$ in Sm^{147} and Sm^{149}), the remaining quadrupole strength may possibly be divided evenly between four states, in which case the transitions, indeed, might have escaped detection in the present investigation.

In Sm^{150} we find an analogous situation to Nd^{148}, except that here only the three γ-rays were observed which fit into the 0+, 2+, 2+′ scheme. Taking $B(0 \rightarrow 2)$ to be 1.30 e^2 10^{-48} cm^4 [16]), the parameter χ becomes ≈ 0.27 for Sm^{150} at 17 MeV bombarding energy. The results regarding B value ratios (table 1) are similar to those obtained for Nd^{148} and are also here consistent with a vibrational description. The amount of double excitation of the 2+′ state is found to be $\approx 10\,\%$ of all excitations of this state.

Sm^{152} has rotational energies close to Nd^{150}, and excitation of the known 367 keV, 4+ state was observed under conditions similar to Nd^{150}. The γ-rays from a Sm metal target were thoroughly investigated with the large NaI crystal in order to verify the observations of Sheline *et al.* [17]) regarding high lying states in Sm^{152}. In the energy region 0.8—1.2 MeV the spectrum showed a continuum of γ-rays above the background, but much better energy resolution would be required in order to interprete the situation.

4.6. EUROPIUM ($Z = 63$)

It is interesting to note that independent evidence for a level in Eu^{151} around 500 keV recently has been reported by Bernstein and Graetzer [18]). Their evidence is based on the observation in Coulomb excitation of 175 keV electron transition, whose yield curve indicated a level at about 500 keV. We have searched for γ-rays which might indicate a γ-cascade from such a level, but with negative result. Attempts with enriched isotopes to find a definite isotopic assignment for the weak 570 keV line were also unsuccessful.

As to the nature of the 510 keV level in Eu^{151} the same comments apply as to Sm^{147} and Sm^{149}.

4.7. GADOLINIUM ($Z = 64$)

Apart from double excitations of 4+ rotational states the only new feature found with Gd was the occurrence of unresolved groups of γ-rays at $\approx$ 950 keV, $\approx$ 1050 keV and $\approx$ 1160 keV, observed with a metallic target. We ascribe tentatively the two latter groups to the decays of the well-known [6, 7]) γ-vibrational states of Gd^{156} (abundance 20.5 %) and Gd^{158} (abundance 24.9 %). A significant contribution from Gd^{160} (abundance 21.9 %) may also be present, but cannot be evaluated since these high energy lines are too weak to be observed with the thin enriched targets, and no decay scheme data are available on Gd^{160}. Also we cannot resolve the contributions from Gd^{158} and Gd^{156} because of the small energy difference between the respective 2+′ levels. The $B(E2)$ values quoted in table 1 are, therefore, calculated on the assumption that only Gd^{156} and Gd^{158} contribute to the observed yield and that their $B(E2)$ are about equal. Note that double excitations of the 2+′ states play a negligible role in these cases. This is readily seen for Gd^{156} by inserting in eq. (3) the known values of $B(2' \to 0)/B(2' \to 2)$ and of $B(0 \to 2)$.

The resulting total $B(E2)$ values for excitation of the 2+′ states in Gd^{156} and Gd^{158} are $0.16 \pm 0.08\ e^2\ 10^{-48}$ cm^4. It is remarkable that recent calculations [19]) on this type of nuclei which include the effect of pairing correlations have given results close to this value, namely 0.10 for Gd^{156} and 0.11 for Gd^{158}.

4.8. TERBIUM ($Z = 65$)

The three new γ-rays observed with a Tb target have tentatively been put together in a level scheme for Tb^{159} (table 2) which includes the known 364 keV, $\frac{5}{2}-$ level. In the absence of more information one can only make speculations as to the nature of the 560 keV state. An interesting possibility is that it represents one of the two γ-vibrational modes associated with the ground state, in which case its spin would be $\frac{7}{2}+$, and the transition to the $\frac{5}{2}-$ state would then be E1. The $B(E2)$ value for excitation of the state is rather small compared to the corresponding values for the γ-vibrational states in the neighbouring even nuclei, but this is also the case for the 515 keV state of Ho^{165} where the γ-vibrational interpretation has a more solid experimental justification. More detailed experiments on Tb^{159} would be highly desirable to test the vibrational hypothesis.

4.9. DYSPROSIUM ($Z = 66$)

The only new lines observed with a metallic Dy target were low energy lines which could be attributed to 4+ rotational excitations and a broad, unresolved group at 700-850 keV. The isotopic assignment of these high energy γ-rays remains uncertain, since no enriched targets were available for their identifica-

tion, and not enough is known from decay scheme work about the levels of the stable, abundant Dy isotopes to explain their origin.

4.10. HOLMIUM ($Z = 67$)

We have identified our 510 keV line with the transition from the 515 keV state of Ho^{165} observed in the decay of Dy^{165m}. This decay has recently been studied in great detail by Cranston *et al.* [10]) and by Tornau [11]) and both groups have reached the conclusion that the 515 keV state must have $\frac{3}{2}-$ character. This spin assignment is of great interest because no low-lying, intrinsic $\frac{3}{2}-$ state is available in the Nilsson scheme [9]) for a $Z = 67$ nucleus. On the other hand, all the present experimental evidence on the 515 keV state is consistent with a γ-vibrational interpretation †. The theory predicts the existence of two such states, built upon the ground state, having in this case the characters $\frac{3}{2}-$ and $\frac{11}{2}-$. The $\frac{11}{2}-$ state might be the 690 keV state observed in our experiment, but with the present meager experimental data this remains only an interesting possibility. The experimental $B(E2)$ values for excitation of both of these states are rather small, about 8—10 times lower than the $B(E2)_{exc}$ for the γ-vibrational states observed in the Gd and Er isotopes. There are no quantitative, theoretical estimates available of the magnitudes of vibrational $B(E2)$ values in odd-mass deformed nuclei.

4.11. ERBIUM ($Z = 68$)

The experimental situation in Er resembles that in Gd. The 700—800 keV lines may be associated with the known γ-vibrational states of Er^{166} (abundance 33.4 %) and Er^{168} (abundance 27.1 %). Er^{170} (abundance 14.9 %) may also contribute, but, for lack of knowledge of its level structure, we have left it out of the calculations. Assuming that Er^{166} and Er^{168} have approximately equal $B(E2)$ values we find $B(0 \rightarrow 2') = 0.22 \pm 0.11\ e^2\ 10^{-48}\ cm^4$, which is consistent with the calculated values [19]) 0.12 for Er^{166} and 0.13 for Er^{168}.

4.12. THULIUM ($Z = 69$)

In order to fit the new γ-rays observed in Tm^{169} into a consistent scheme we are somewhat left with speculations. γ—γ coincidences or similar experiments would be desirable in the future to clear up the situation. We note that in one of the beta decay investigations of Tm^{169} [20]) a 336 keV level was postulated, decaying by a single γ-ray to the $\frac{7}{2}+$ rotational state. This level may be identical with the intermediate level tentatively postulated by us at either 334 or 359 keV. The position and the $B(E2)_{exc}$ found for the 565 keV level suggest an interpretation in terms of a γ-vibration in analogy to Ho^{165} and Tb^{159}, but more information is needed to test this hypothesis.

4.13. YTTERBIUM ($Z = 70$)

A broad peak $\approx$ 1.4 MeV indicates the excitation of one or more high lying states. Like for Dy, no isotopic identification seems possible at present.

† This interpretation was suggested already in 1959 by M. E. Bunker in a private discussion.

4.14. LUTETIUM ($Z = 71$)

Now new lines were observed with certainty.

4.15. HAFNIUM ($Z = 72$)

A metallic Hf target revealed a weak line at 1160 keV, but definite identification is hardly possible at the moment.

4.16. TANTALUM ($Z = 73$)

No new lines were observed.

4.17. TUNGSTEN ($Z = 74$)

All γ-rays observed in this experiment with a W target have been reported previously as a result of Coulomb excitation studies. However, the γ-vibrational levels in W^{182}, W^{184} and W^{186} provide an interesting check on our experimental accuracy and the corresponding partial B values are, therefore, included in table 1. The total $B(0 \rightarrow 2')$ values derived by summing the appropriate partial values are given in table 4 together with the values of Alkhazov *et al.* [21]).

TABLE 4

Coulomb excitation of the γ-vibrational levels in W^{182} W^{184}, W^{186}. The numbers are $B(E2)$ values corresponding to excitation of the $2+'$ states, measured in units of $e^2\,10^{-48}$ cm^4. The three columns give the experimental results of Alkhazov *et al.* [21]), our results, and the theoretical values calculated by Bès [19]). The two theoretical values for W^{186} correspond to two different values of the deformation parameter β. Experimental B values for W^{184} and W^{186} have also been reported by McGowan and Stelson [22]) and by Barlouthaud *et al.* [23]). Their results are close to those of Alkhazov *et al.*

Nucleus	Results of Alkhazov *et al.*	Our results	Calculated values
W^{182}	0.25	0.12	0.16
W^{184}	0.19	0.13	0.17
W^{186}	0.20	0.12	0.17 ($\beta = 0.20$) 0.37 ($\beta = 0.15$)

Alkhazov *et al.* estimated their overall error to be about 25 %, while our values are believed to be accurate to within a factor of two. Although there is agreement within the experimental uncertainties, our values are systematically somewhat lower than theirs. However, the relative constancy in the $B(E2)$ in going from W^{182} to W^{186} is common to both sets of measurements. The calculated values of Bès [19]) are also here in agreement with the experimental situation, being intermediate between the different sets of measurements.

4.18. RHENIUM ($Z = 75$)

The experimental situation in the two Re isotopes resembles that in Ho^{165}: a pair of levels in the energy region 500—900 keV was excited with $B(E2)$ values of the

order of the single particle estimate. Also here, the spin and parity of the lowest level are known from decay scheme work. However, the theoretical interpretation of this state is more ambiguous than was the case for Ho^{165}, since a low-lying, intrinsic $\frac{1}{2}+$ state is, indeed, available in the Nilsson scheme for a $Z = 75$ nucleus (see ref.[9])). On the other hand, it has been pointed out by Gallagher[12,24]) that an analysis of the Os^{185} and W^{187} decays indicates that there are difficulties in interpreting the $\frac{1}{2}+$ states as intrinsic levels, and that the γ-vibrational description may be more reasonable. Possibly, the higher lying states observed by us would then be the $\frac{9}{2}+$ vibrations.

Here, like in other similar cases, our results pose a question but they do not solve it. In particular one should keep in mind that among the excitations observed in the odd Z, deformed nuclei only the excitations leading to the $\frac{3}{2}-$ state of Ho^{165} and to the $\frac{1}{2}+$ states of Re^{185} and Re^{187} can be said to have an experimentally known multipole order. For the other excitations observed it is certainly not *a priori* precluded that we may be dealing with E1 excitations in some cases, a possibility which would change the theoretical interpretation completely.

For future experimental work in this field it would, therefore, seem important to study the Coulomb excitations of these nuclei more thoroughly than was attempted in this survey type investigation, in order to obtain a check on the multipolarities of the transitions and to determine the spins of the new levels. Other types of Coulomb excitation experiments than α–γ coincidences with a cyclotron beam may be more favourable for such purposes, since the sensitivity for coincidence detection of weak lines in our experiments was so strongly limited by the bunching of the cyclotron beam.

The authors wish to thank Professor Niels Bohr for the excellent working conditions at his institute and for the warm hospitality extended to one of us (V. I. P.). It is also a pleasure to thank Dr. N. O. Lassen and the personnel of the Copenhagen cyclotron whose generous collaboration made our experiments possible. We benefited also from suggestions made by Drs. S. Berko and F. S. Stephens in connection with this work. For many valuable discussions our thanks are due to Drs. Aage Bohr, Ben Mottelson, Kurt Alder and Aage Winther. We are indebted to Drs. D. Bès and C. Gallagher for placing their results at our disposal prior to publication.

References

1) Stephens, Diamond and Perlman, Phys. Rev. Letters **3** (1959) 435
2) Alder, Bohr, Huus, Mottelson and Winther, Revs. Mod. Phys. **28** (1956) 432
3) K. Alder and A. Winther, Mat. Fys. Medd. Dan. Vid. Selsk. **32**, No. 8 (1960)
4) Strominger, Hollander and Seaborg, Revs. Mod. Phys. **30** (1958) 585
5) H. Ryde and C. J. Herrlander, Ark. f. Fysik **13** (1958) 177
6) Gregers Hansen, Nielsen and Sheline, Nuclear Physics **12** (1959) 389

7) Knowles, Bartholomew and Campion, Bull. Am. Phys. Soc. **4** (1959) 246; J. W. Knowles, private communication
8) Jacob, Mihelich, Harmatz and Handley, Phys. Rev. **117** (1960) 1102
9) B. R. Mottelson and S. G. Nilsson, Mat. Fys. Skr. Dan. Vid. Selsk. **1**, No. 8 (1959)
10) Cranston, Bunker and Starner, Bull. Am. Phys. Soc. **5** (1960) 255
11) R. Tornau, Z. Physik **159** (1960) 101
12) Gallagher, Edwards and Manning, Nuclear Physics **19** (1960) 18
13) S. Ofer and A. Schwarzschild, Phys. Rev. **116** (1959) 725
14) L. S. Kisslinger and R. A. Sorensen, Mat. Fys. Medd. Dan. Vid. Selsk. **32**, No. 9 (1960)
15) Bernstein, Markowitz and Katcoff, Phys. Rev. **93** (1954) 1073
16) Elbek, Olesen and Skilbreid, Nuclear Physics **19** (1960) 523
17) Sheline, Nielsen and Sperduto, Nuclear Physics **16** (1960) 518
18) E. M. Bernstein and R. Graetzer, Bull. Am. Phys. Soc. **4** (1959) 426
19) D. Bès, private communication
20) S. A. E. Johansson, Phys. Rev. **100** (1955) 835
21) Alkhazov, Grimberg, Gusunskij and Erokhina, JETP **8** (1959) 926
22) F. K. McGowan and P. H. Stelson, Congrès International de Physique Nucléaire (Paris 1958) p. 765
23) Barlouthaud, Lévêque, Lehmann and Quidort, J. Phys. Radium **19** (1958) 60
24) C. Gallagher, private communication

2.A1:
2.L:3.A

Nuclear Physics **21** (1960) 652—675; © *North-Holland Publishing Co., Amsterdam*
Not to be reproduced by photoprint or microfilm without written permission from the publisher

ELASTIC SCATTERING AND RADIATIVE CAPTURE OF PROTONS BY C^{13}

D. F. HEBBARD † and J. L. VOGL

W. K. Kellogg Radiation Laboratory, California Institute of Technology, Pasadena, California ††

Received 15 August 1960

Abstract: Measurements of the elastic scattering of protons by C^{13} from 140 keV to 750 keV proton energy are reported. The radiative capture of protons by C^{13} has been investigated down to a proton energy of 130 keV, but no new levels are found that would influence the cross section at stellar energies. The only new level found has a resonance energy of 448.5 ± 0.5 keV. An upper limit is placed on the strength of radiative capture by any missed levels. Angular distribution measurements, combined with the results of $N^{14}(\alpha, \alpha')$ by other workers lead to an assignment $J^\pi = 2^-$ for the 448-keV resonance (7.966 MeV excitation). From the same target used for the $C^{13}(p, \gamma)$ measurements, the yield of $C^{12}(p, \gamma)$ radiation has been measured, and the cross sections of both reactions are extrapolated to stellar energies. The extrapolated cross section factor S_0 at 25 keV C.M. proton energy is 6.0 ± 0.8 keV-barn for the $C^{13}(p, \gamma)$ reaction, and is 1.33 ± 0.15 keV-barn for the $C^{12}(p, \gamma)$ reaction. The equilibrium ratio by number of C^{12}/C^{13} in the CNO-cycle is thus 4.1 ± 0.7 at a temperature of 15×10^6 °K.

1. Introduction

The reactions involving capture of protons by C^{13} and by C^{12} are of interest in astrophysics because both reactions form part of the CNO-cycle of energy generation. There have recently been some disagreements on the observed $C^{13} : C^{12}$ abundance ratio in stars [1, 2]), and this has prompted the present measurement of the ratio of the proton capture cross sections for C^{13} and C^{12} present in the same thin target. The capture cross sections at stellar energies can only be obtained by extrapolation, and this has already been done for the $C^{12}(p, \gamma)$ reaction [3, 4]). In the case of the $C^{13}(p, \gamma)$ reaction, the extrapolation depends on the assumed absence of levels in N^{14} at energies just above the proton threshold. The proton threshold occurs at an excitation energy of 7.549 MeV, at which energy, the known levels have an average spacing of a few hundred keV [5]). At a temperature of 15×10^6 °K, the effective stellar energy is 25 keV.

The energy levels of N^{14} have been investigated in this energy region by several workers. Seagrave [6]) has measured the excitation curve of the $C^{13}(p, \gamma)$ reaction from a proton bombarding energy of 400 keV to 2600 keV, while the

† Now at the Australian National University, Canberra, A.C.T., Australia.

†† Work supported in part by the joint program of the Office of Naval Research and the U. S. Atomic Energy Commission, and in part by the University of Melbourne.

nature of the gamma radiation at each of the five resonances found by Seagrave has been studied by Woodbury, Day, and Tollestrup [7]). Milne [8]) has studied the elastic scattering of protons from C^{13} in the energy region from 450 keV to 1600 keV, and has been able to assign spins and parities to the levels found by Seagrave. Christy [9]) has analyzed Milne's data for the 550-keV resonance, and concludes that better agreement with theory would be achieved if Milne's cross sections were reduced by approximately 10 %.

The energy levels of N^{14} have also been investigated by means of the reactions C^{13}(d, n), N^{14}(p, p′) and N^{14}(α, α′). Neutron groups from the deuteron bombardment of C^{13} have been detected by Benenson [10]) who found, in addition to the well-known level at 8.06 MeV, evidence for levels at 7.72 ± 0.04, 7.50 ± 0.04 MeV and 7.00 ± 0.04 MeV, as well as other levels of lower excitation. Gamma rays of energies 7.05 ± 0.04 and 7.30 ± 0.05 MeV from the C^{13}(d, n) reaction are attributed by Bent, Bonner and Sippel [11]) to levels in N^{14} at 7.02 and 7.40 MeV, after a Doppler correction is applied.

Inelastic proton scattering from N^{14} gives levels at 7.03 ± 0.02, 7.40 ± 0.02, and 7.60 ± 0.02 MeV. In this experiment of Burge and Prowse [12]), levels above 7.60 MeV were not observed because of the very short range of the resulting protons which were detected in nuclear emulsions.

Inelastic scattering of 21.5-MeV alpha particles has lead to the identification of a level by Miller *et al.* [13]) at an excitation energy of 7.94 ± 0.07 MeV. A level is also detected at 7.02 ± 0.08 MeV, but there are no alpha-particle groups corresponding to the levels reported between 7.4 and 7.8 MeV. The alpha-particle group to the 8.06-MeV level is also absent. It is presumed that the isobaric spin selection rule is operative in the case of the absent alpha-particle group to the 8.06-MeV level.

There is general agreement on the presence of a level in N^{14} at an excitation of 7.02 MeV. It is probable that the level identified by Benenson at 7.50 MeV is the same level as that identified by Bent *et al.* and by Burge and Prowse at 7.40 MeV and is a level below the proton threshold. Also, it is probable that the 7.72-MeV level of Benenson and the 7.60-MeV level of Burge and Prowse are the same level. Such a level, above the proton threshold, would not be observed by Bent *et al.* if the proton width or cascade gamma-ray widths were much larger than the ground state gamma-ray width.

The level below the proton threshold, probably at 7.40 MeV, can only contribute to the C^{13}(p, γ) reaction if the proton reduced width is large, in which case there is a non-resonant contribution to the cross section at higher proton energies. This non-resonant contribution will not be easily distinguishable from the other sources of the non-resonant capture cross section, and so will be automatically included in the cross section extrapolated from the measurable region to stellar energies.

The 7.60-MeV or 7.72-MeV level is particularly important from the point of

view of the stellar $C^{13}(p, \gamma)$ reaction rate. If the excitation energy of this level is sufficiently high to permit detection, the position and characteristics of this level may be studied directly by means of the $C^{13}(p, \gamma)$ reaction.

The present paper therefore reports absolute measurements of the $C^{13}(p, \gamma)$ cross section as a function of energy over the range from 450-keV to 130 keV proton energy (7.967 to 7.670 MeV excitation), in order to estimate the relative importance of the resonant and non-resonant contributions to the cross section. Simultaneously, limits have been placed on the widths of unobserved resonances in this reaction. From the same thin target, a measurement of the $C^{12}(p, \gamma)$ cross section has also been made, in order to determine the $C^{12}(p, \gamma)$ to $C^{13}(p, \gamma)$ cross section ratio as a function of energy.

A report is also made on the gamma-ray yields and angular distributions from a $C^{13}(p, \gamma)$ resonance at a proton energy of 448.5 keV, found during the course of this work. This resonance, at an excitation energy of 7.966 MeV, probably corresponds to the 7.94-MeV level found by Miller *et al.* The elastic scattering of protons by C^{13} has been investigated over the proton energy range from 750-keV to 140-keV. An improved fit to the theoretical cross section at the 550-keV elastic scattering anomaly is presented, and the 8.06-MeV energy level parameters so found have been used in the extrapolation of the low-energy tail of the 550-keV $C^{13}(p, \gamma)$ resonance to stellar energies.

2. Experimental Arrangements

2.1. ELASTIC SCATTERING

The targets used for the elastic scattering experiments were prepared from methyl iodide enriched to 66 % C^{13} supplied by the Eastman Kodak Company. This enriched methyl iodide was decomposed on red-hot tantalum target blanks that had previously been coated with a layer of natural carbon approximately 300 μg cm^{-2} thick. The layer of enriched carbon had a thickness of approximately 50 μg cm^{-2} (15 keV at $E_p = 600$ keV).

The University of Melbourne 1-MV electrostatic accelerator was used to bombard these targets. The proton beam was magnetically analyzed, and the scattered protons were detected in a double-focusing magnetic spectrometer stabilized by a fluxmeter. The spectrometer had an over-all momentum resolution of approximately 300, and a solid angle of acceptance such that $\Delta\theta \approx 0.7°$ and $\Delta\phi \approx 3°$ ($\Delta\Omega = 6.1 \times 10^{-4}$ sr). Bombardments were made with a fixed beam energy, and the proton momentum spectra were obtained by varying the spectrometer field. Fig. 1 shows a momentum spectrum of a target, bombarded by 420-keV protons. When a comparison is made between the maximum yield of protons elastically scattered from the C^{12} in a natural carbon target and in the C^{13}-enriched target, it is found that the percentage of C^{13} in the enriched targets is 66 ± 3 %, the error being based on the statistical error in the counts. This is in

good agreement with the supplier's value of 66 % which was used in the conversion of count rate to absolute cross section. The spectrometer constants entering into the conversion from count rate to cross section were determined by measuring the yield of protons scattered elastically from copper. It was assumed that the cross section for this reaction was the Rutherford cross section, and the stopping cross section used was that determined by Bader *et al.* [14]) for evaporated copper foils. The charge collection and the beam current integrator were conventional. The beam current integrator was calibrated with

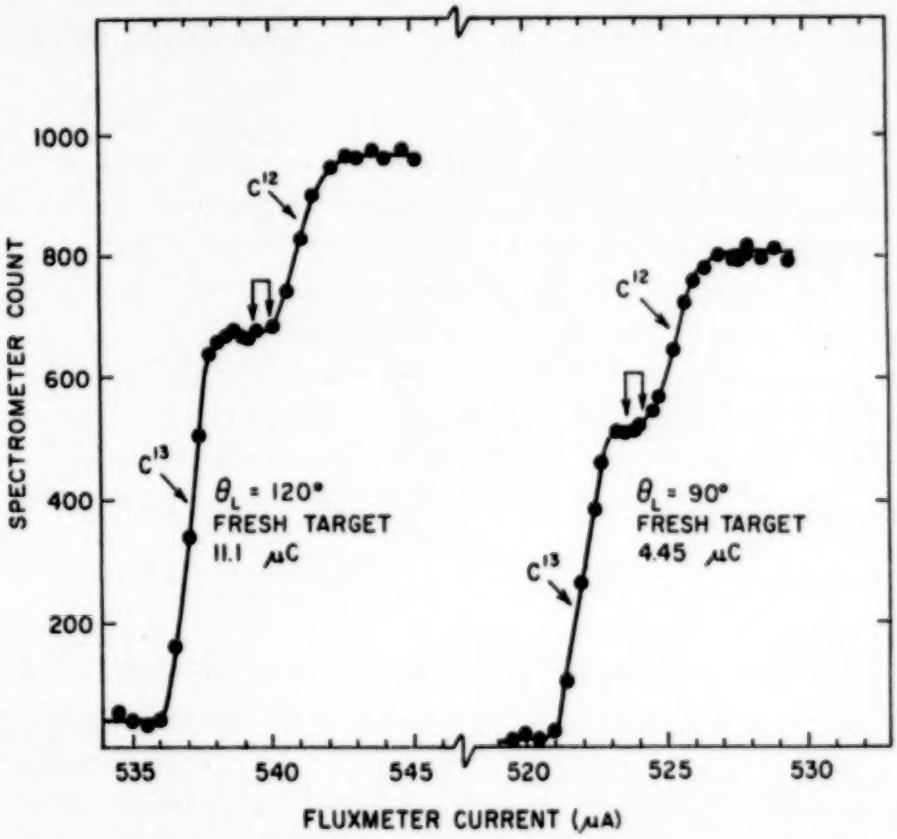

Fig. 1. The elastic scattering momentum spectra observed for 420-keV protons incident on a 66 % C^{13} target are shown. The vertical arrows indicate the interval in which counts were recorded for calculation of the C^{13} cross sections. At 90° the target is near the lower limit of its useful energy range, because of the loss of resolution caused by surface irregularities.

an accuracy of 0.4 %, under conditions similar to those of the experiment, and the calibration did not change detectably during the course of the experiment.

The yield of protons elastically scattered from C^{13} was measured as a function of proton energy at laboratory angles of 90° and 120°, which are close to the zeros of odd order Legendre polynomials and $P_2(\cos\theta)$ respectively. Each measurement consisted of three runs with slightly different magnetic field settings for the spectrometer in the flat region of the momentum spectrum between the rise due to C^{13} and the rise due to C^{12}. For the higher proton energies, targets lasted for approximately 500 μC bombardment before the three runs

gave significantly different counts. The procedure was then repeated for a fresh target. The background, generally of the order of 3 % of the count due to C^{13}, was due to iodine, present to the extent of 1 atom per 10^4 carbon atoms. This iodine background changes only very slowly with beam energy, and the surface contaminant oxygen peak does not overlap the portion of the momentum spectrum due to C^{13} during the useful life of the target, so that the background, determined for each new section of the target, was only measured occasionally as the beam energy was altered. The lower energy limit to the bombardments at the two angles was reached when the useful life of a target spot became as short as the bombardment time necessary to determine the yield of protons.

2.2. RADIATIVE CAPTURE

The target used for the radiative capture experiments was prepared from methyl iodide enriched to 61 % C^{13} supplied by the Eastman Kodak Company. The 0.5 -mm thick tantalum target blank was coated with a layer of approximately 20 μg cm^2 of enriched carbon, after cleaning and outgassing. It was found that the outgassing, conducted at a high temperature in a pyrex glass vessel had introduced a small amount of boron ($\approx 5\times 10^{-8}$g) into the tantalum backing, but this did not interfere with the $C^{13}(p, \gamma)$ measurements except at proton energies close to 180 keV on the front surface of the carbon (i.e. 163 keV near the surface of the tantalum backing). At this energy the 4.43-MeV gamma ray from the $B^{11}(p, \gamma)$ resonance obscured the contribution, to the $C^{13}(p, \gamma)$ cross section, of the cascade through the 3.95-MeV level in N^{14}.

The 600-keV electrostatic accelerator at the W. K. Kellogg Radiation Laboratory, California Institute of Technology, was the source of the proton beam, with electrostatic and magnetic analysis, for the gamma-ray measurements. The detector was a 10.2 cm $\times$ 10.2 cm NaI(Tl) crystal mounted on a Dumont 6364 photomultiplier, and the pulses were sorted in a 100-channel analyzer. For the yield measurements above 303-keV proton energy, the detector was at 90° to the proton beam at a distance of 3.8 cm from the target, held at 45° to the beam. Below 303-keV proton energy, the detector was at 0° with a distance of 1.9 cm. At the change-over energy of 303 keV, the change of count rate corresponded to that expected for an isotropic angular distribution.

For angular distribution measurements close to 448-keV proton energy, the target was held at 45° to the beam in a cylindrical glass target chamber with a 2 mm-wall thickness. The NaI crystal was able to rotate about a vertical axis through the target spot (approximately 4 mm horizontally and 8 mm vertically on the surface of the target) so that the front surface of the crystal was 8.25 cm from the target and target chamber axis. The cylindrical lead shielding of the NaI crystal did not extend past the front surface of the crystal. For this geometry, the smoothing factor[15]) for the $P_1(\cos\theta)$ coefficient of an angular distribution is 0.945. For the $P_2(\cos\theta)$ and $P_4(\cos\theta)$ coefficients of an angular distri-

bution, the smoothing factors are 0.840 and 0.536 respectively. The angular rotation of the NaI crystal was limited to the range from $+120°$ to $-120°$, and measurements were made at several angles within this range. The range of angles for which the target appears edge-on to the detector was not used because of the spectrum distortion at these angles.

It was necessary to apply a correction to the angular distributions for absorption in the target backing. In addition an estimate was made of the effect on the angular distributions of the spectrum distortion caused by the conversion of gamma rays in the target backing and subsequent electron detection. For the range of angles used, this effect was of little importance compared with the statistical errors in the counts.

3. Results and Discussion

3.1. ELASTIC SCATTERING

The cross sections for elastic scattering protons from C^{13}, plotted as a function of proton energy at laboratory angles of 90° and 120°, are shown in fig. 2.

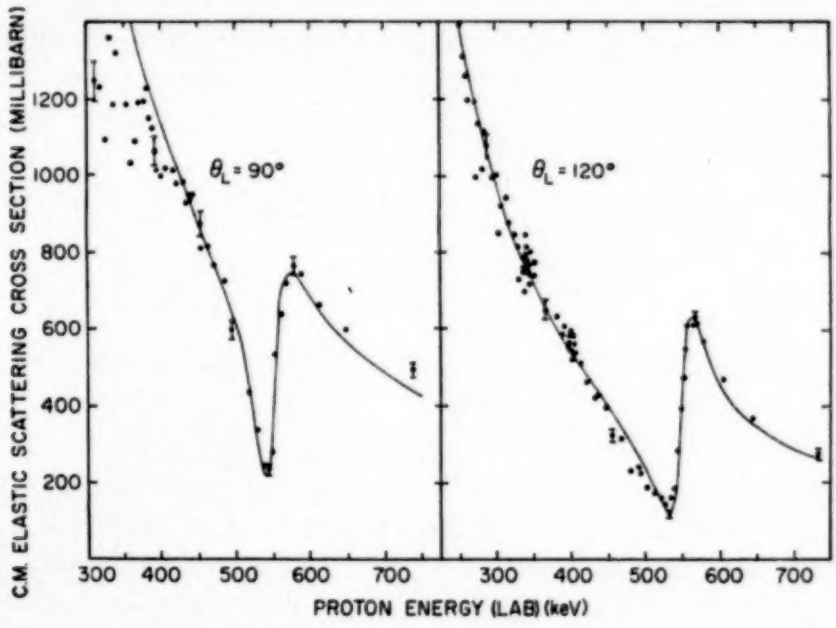

Fig. 2. Elastic scattering cross sections (C.M.) for protons on C^{13} are shown. The solid curves are computed for a single 1^- resonance at 550 keV proton energy, with the parameters given in the text. At 90°, below 400 keV proton energy, the deviation from the theoretical cross section is not believed to be real, but is caused by the increasing difficulty of separating the C^{12} and C^{13} momentum spectra satisfactorily. At 120°, the cross section follows the theoretical Rutherford curve down to an energy of 140 keV.

The curves passing through the experimental points are the theoretical curves for a 1^- resonance at a proton energy of 550 keV. The energy dependence of the proton width and the level shift have been taken into account explicitly. The

improvement in the fit away from the scattering anomaly is quite marked, when these energy dependences are introduced into the expression for the elastic scattering cross section. At the anomaly, the maximum and minimum cross sections are the same as those predicted when using constants for the resonance parameters. The cross sections at the two angles measured are about 10 % lower than the results of Milne, in the direction required [9]) by Christy's analysis.

At energies above the anomaly, there is a tendency for the experimental cross section to become larger than the theoretical curve, based only on the single level. This is presumably due to the inadequacy of the cross section formula used, since no allowance was made for any other levels. The parameters of the anomaly deduced from the theoretical fit were: Resonance energy $= 550 \pm 1$ keV, proton reduced width $\gamma_p^2 = 455$ keV, using a radius (for hard-sphere scattering and the determination of the level shift and the reduced width) of 4.72×10^{-13} cm.

The cross section below the anomaly has been investigated in average steps of 3.5 keV, and has been found to follow the Rutherford cross section closely down to an energy of 140 keV (after correction for the neutral scattered beam) at a scattering angle of 120°. At the 90° scattering angle, the experimental difficulty of separating the C^{13} and C^{12} steps in the momentum spectrum became acute below 400-keV proton energy, as shown by the spread of results, so that no useful measurements exist at 90° below 400 keV. However, the 120° curve limits the width of unobserved s or p-wave resonances at low energies to less than 500 eV.

3.2. RADIATIVE CAPTURE AT THE 448-keV RESONANCE

During the course of this work, a new resonance was found in the $C^{13}(p, \gamma)$ reaction at an excitation energy of 7.966 MeV in N^{14}. This resonance, at a proton energy of 448.5 ± 0.5 keV, has a total width less than 400 eV, as shown by the excitation function of fig. 3(a). This excitation curve shows the dependence on the proton energy of the count rate for the ground state gamma ray, when a target of 9 keV thickness is bombarded. The upper limit to the resonance width is sufficiently small to explain the absence of an easily detectable elastic scattering anomaly.

The curves of fig. 3(b) show the gamma-ray spectra at and below the 448-keV resonance. Apart from the changed yield, non-resonant spectra taken above and below the resonance are identical. The resonant yields of gamma rays to the ground state, 3.95-MeV state, and other states of N^{14} are given in table 1, together with the calculated widths $\omega\Gamma_p\Gamma_\gamma/\Gamma$. The majority of the pulses observed in the resonance spectrum of fig. 3(b) between channels 41 and 57 (4.5 to 6.2 MeV) can be attributed to the increased yield of ground-state gamma rays. However, there are some pulses in this energy range that cannot be attri-

buted to ground-state gamma rays. The majority of these extra pulses are caused by the simultaneous detection of two gamma rays. The gamma rays concerned are the high energy member and one or other of the low energy members of the cascade through the 3.95-MeV and the 2.31-MeV states. The peaks generated in the energy range from 4.5 to 6.2 MeV by this process account for approximately 80 % of the extra pulses, and obscure any weak radiation from the 7.97-MeV

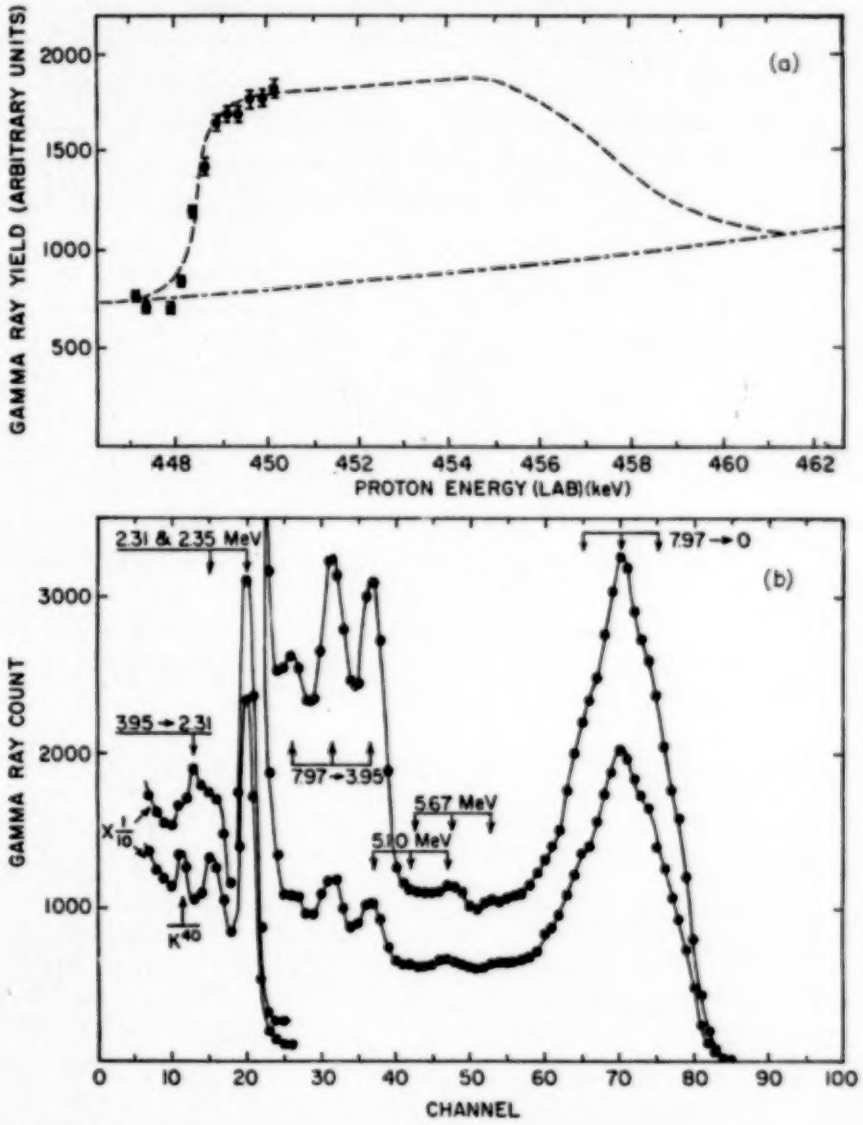

Fig. 3. (a). The excitation function for the narrow 448-keV resonance in $C^{13}(p, \gamma)$ for a target of 9-keV thickness is shown. All pulses above 3.5 MeV are recorded. The particular run used to determine an upper limit to the resonance width is plotted, and the dashed lines show a typical excitation function, taken to higher energies, and the underlying non-resonant radiation. (b). The gamma-ray spectra observed at and below the 448-keV resonance are shown. All the gamma rays marked (except for the K^{40} radiation and the 2.35-MeV gamma ray from $C^{13}(p, \gamma)$) are associated with transitions in N^{14}. The gamma rays marked at 5.10 and 5.67 MeV may be weakly resonant, but the peaks observed are explained in the text. The spectra displayed, taken 6 keV apart in energy, represent the yield integrated over a sphere, being the weighted sum of a number of spectra at different angles.

TABLE 1

Resonant gamma ray yields and widths

	Transition from the 7.97-MeV level to the		
	ground state	3.95-MeV state	other states [a])
Yield 10^{-12} γ/p (61 % C^{13})	9.7 $\pm$0.5	7.9 $\pm$0.5	$\leqq$ 0.5
$\frac{\omega\Gamma_p\Gamma_\gamma}{\Gamma}$(eV)	0.012	0.010	$\leqq$ 0.0005

[a]) The cascades to the 2.31-MeV state, 5.10-MeV state and 5.68-MeV state may all be weakly resonant at 448-keV proton energy. Only an upper limit to the strength of this cascade radiation can be given.

state to the 2.31-MeV state, from the 5.10-MeV state to the ground state, or from the 5.68-MeV state to the ground state. Thus table 1 can only give upper limits, based on an estimate of the error in the calculation of double pulses, to the strength of these other cascades.

The angular distributions of gamma rays to the ground state and 3.95-MeV state are shown in fig. 4. Table 2 gives the angular distribution coefficients. Because the 448-keV resonance is superposed on a background caused by the

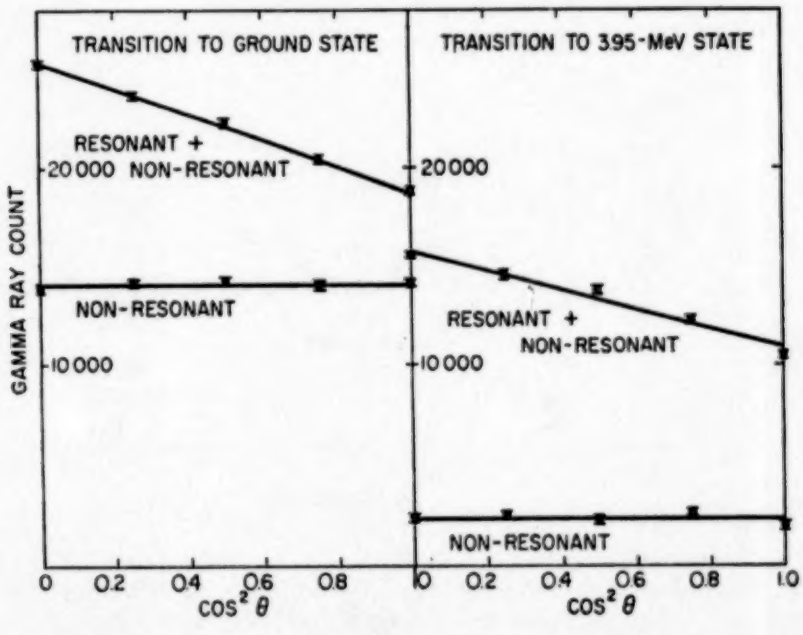

Fig. 4. The angular distributions of gamma rays from the 7.97-MeV level (and non-resonant radiation from this energy region) to the ground state and 3.95-MeV state are shown. The non-resonant distributions have been renormalized to correspond to the same proton energy as that for which the resonant + non-resonant radiation angular distributions are measured. An absorption correction has been made, but no correction has been made here for the finite solid angle of the detector. The least-squares fits to the experimental points are shown.

TABLE 2

Resonant gamma-ray angular distributions [a])

7.97-MeV level to	Angular distribution
ground state	$P_0-(0.570\pm0.020)P_2-(0.004\pm0.03)P_4$
3.95-MeV state [b])	$P_0-(0.33\ \pm0.03)P_2$

[a]) The non-resonant distributions from the close neighbourhood of the 448-keV resonance were found to be isotropic, within experimental errors. Neither for resonant nor for non-resonant radiations were any odd-order Legendre polynomial coefficients observed. The tabulated distributions have been corrected for the finite solid angle of the detector.

[b]) The angular distribution of gamma rays to the 3.95-MeV state was analyzed only for P_0 and P_2 terms. The subtractions necessary to eliminate the ground state radiation make the calculation of a $P_4(\cos\theta)$ term of doubtful value.

low-energy tail of the 550-keV resonance, the existence of possible odd-order Legendre polynomial interference terms was suspected. These were first shown to be absent, both at the resonance and below it, within the accuracy of the experimental measurements. Therefore the angular distributions were finally analyzed in terms of even-order Legendre polynomials up to $P_4(\cos\theta)$.

The magnitude of the radiative widths of table 1 indicates that the transitions to the 1^+ ground state and second excited state are dipole or quadrupole transitions. Therefore the possible values of the spin of the 7.97-MeV level are $J \leqq 3$. The fact that anisotropic radiation is observed shows that $J \neq 0$. Gamma-ray angular distributions have been calculated for the remaining spin assignments. For each angular distribution there are at least two unknown parameters. The amplitude ratio of quadrupole to dipole or octupole to quadrupole radiation is unknown, and another parameter is either the channel spin mixture or the complex ratio of amplitudes of the possible proton orbital angular momenta in the entrance channel, depending on the parity of the resonant state. For all values of the two parameters, the angular distributions, assuming $J = 3$ with either parity, are inconsistent with the experimental values, as the $P_2(\cos\theta)$ coefficient with $J = 3$ must always be positive.

The expressions for the angular distribution coefficients for the cases $J = 1$ and $J = 2$ are given in table 3. For $J = 2$ and positive parity, the minimum value of the $P_2(\cos\theta)$ coefficient is -0.515, and this is outside the experimental limits for the ground-state gamma-ray angular distribution. Four independent measurements of the ground-state gamma-ray angular distribution gave consistent values for the Legendre polynomial coefficients, each one differing from the extreme value allowed for $J^\pi = 2^+$ by two or three standard deviations. The effect of interference of a 2^+ state with the broad 1^- state at 8.06-MeV excitation will be to introduce odd-order Legendre polynomials only, and will not change the magnitude of the $P_2(\cos\theta)$ coefficient. Therefore it may be

TABLE 3
Theoretical angular distributions

Assumed J^π	Angular distribution to a 1^+ final state
1^+	$P_0+\frac{1}{2}P_2(1-\frac{3}{2}\alpha_1^2[(1+6\delta+\delta^2)/(1+\delta^2)]$
1^-	$P_0+\frac{1}{4}P_2[(D^2+2\sqrt{2}D\cos\phi)/(1+D^2)][(1+6\delta+\delta^2)/(1+\delta^2)]$
2^+ [a]	$P_0-\frac{7}{20}P_2[(1-\frac{2}{7}\sqrt{6}F\cos\xi+\frac{8}{7}F^2)/(1+F^2)]\times[(1-\delta/\sqrt{5}-\frac{5}{7}\delta^2)/(1+\delta^2)]$ $+\frac{8}{21}P_4[(F^2-2\sqrt{6}F\cos\xi)/(1+F^2)][\delta^2/(1+\delta^2)]$
2^- [b]	$P_0-\frac{1}{2}P_2(1-\frac{1}{2}\alpha_1^2)[(1-\delta/\sqrt{5}-\frac{5}{7}\delta^2)/(1+\delta^2)]+\frac{8}{7}P_4(1-\frac{5}{3}\alpha_1^2)[\delta^2/(1+\delta^2)]$ $\pm P_2(\sqrt{\frac{3}{2}})\alpha_1\left[\left(1-\sqrt{\frac{5}{18}}\delta\right)/(1+\delta^2)\right][\sigma_N/(\sigma_R-\sigma_N)]^{\frac{1}{2}}$

[a]) The amplitude ratio of f- to p-waves is F exp $(i\xi)$

[b]) This expression represents the average over a narrow resonance of the major terms for interfering 2^- and 1^- levels, with a subtraction of the terms referring to a pure 1^- intermediate state. This corresponds exactly with the experimental situation. The relative phase of the s and d-waves has been chosen as described in the text. This maximizes the fourth (i.e. the interference) term in the expression above for $J^\pi = 2^-$. The sign of the fourth term must be chosen negative to fit the ground-state gamma-ray angular distribution. The quantity σ_N refers to the non-resonant cross section in the neighbourhood of the resonance, while σ_R is the actual cross section at the peak of the resonance.

concluded that the 2^+ spin and parity assignment cannot explain the observed ground-state gamma-ray angular distribution. The remaining spin and parity assignments in table 3, each of which can reproduce the observed angular distributions will now be discussed in order of increasing likelihood.

(1) $J^\pi = 1^-$. In this case there are no interference terms due to the presence of the 8.06-MeV level. The ratio of the amplitude of d to s-wave formation of the 7.97-MeV level is $D\exp(i\phi)$, where D is a real number and the relative phase ϕ is the sum of the relative Coulomb phase shift at 448 keV (90.0°), the relative hard-sphere phase shift (−0.5° for a radius of 4.72×10^{-13} cm) and the phase shifts from neighbouring resonances. The latter resonant phase shifts are expected to be near 0° or 180°, the nearest resonance at 550 keV contributing an s-wave phase shift of 4°. Thus ϕ is expected to be quite close to $\pm90°$. This is in agreement with the elastic scattering data. The curves of fig. 5 with ϕ as a parameter show the relation between D and the magnetic quadrupole to electric dipole amplitude ratio δ that must be satisfied in order to reproduce the ground-state gamma-ray angular distribution. For $\phi = \pm90°$, the observed ground-state gamma-ray angular distribution cannot be achieved. If one starts at $\phi = +90°$, and gradually increases ϕ, then at $\phi = 133°$ a closed loop appears in the right-hand side of fig. 5 at the point representing equal quadrupole and dipole gamma-ray intensities and 36 % intensity of d-wave relative

to s-wave formation of the level. As ϕ is further increased, the closed loop expands to reach its maximum area at $\phi = 180°$, then shrinks to disappear again at $\phi = 227°$. The diagram is again blank for $\phi = 270°$ and a closed loop reappears in the left-hand side of fig. 5 at $\phi = -72°$. The point of appearance represents equal contributions of quadrupole and dipole intensities and an intensity of 14 % of s-wave relative to d-wave formation. As before, the closed loop expands, reaching its maximum extent for $\phi = 0°$ and disappearing again by the time ϕ reaches 72°. Since both D and δ are expected to be small, in order to minimize both, a relative phase $\phi = 180°$ (i.e., an error of 90° in calculating ϕ) is needed, and the minimum values of D and δ achieved are relatively large compared with our expectations (15 % by intensity each of d to s-wave formation and quadrupole to dipole decay).

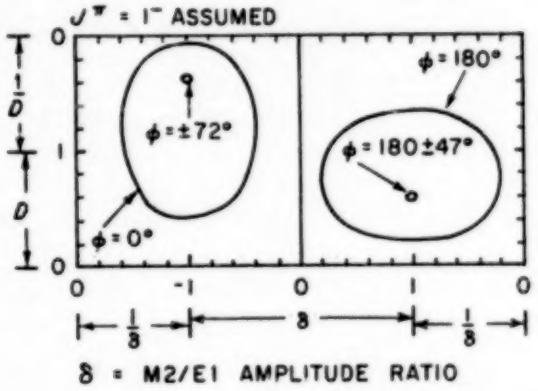

Fig. 5. The relation between δ (the M2/E1 amplitude ratio) and $D(De^{i\phi}$ is the d/s wave amplitude ratio) is shown, for the ground-state gamma ray from the 7.97-MeV level, assuming $J^\pi = 1^-$. The phase angle ϕ is a further parameter, causing the closed loops on the diagram to expand or contract within the limits indicated. For the expected phase angle $\phi \approx \pm 90°$, the diagram is blank, showing that the ground-state gamma-ray angular distribution cannot be achieved.

Another serious drawback to a 1^- assignment of the 7.97-MeV level is that a strong transition might be expected to the 2.31-MeV level and no such strong transition is found. The observed transitions to the ground state and 3.95-MeV level would be electric dipole, inhibited by the isobaric spin selection rule, but the transition to the 2.31-MeV state would be electric dipole with no such inhibition. One would have to rely on a small matrix element to explain the small radiative width to the 2.31-MeV state. This difficulty, combined with the large d to s-wave ratio, the unexpected relative phase, and the large magnetic quadrupole to electric dipole ratio required, serve to eliminate the possibility of the assignment 1^-.

(2) $J^\pi = 1^+$. A positive parity assignment of the 7.97-MeV level leads only to odd-order interference terms in the angular distribution caused by the presence of the broad 1^- state and these have been shown experimentally to be negligible. The relevant parameters for a 1^+ resonance are the fraction of formation by channel spin 1 ($0 \leqq \alpha_1^2 \leqq 1$) and the electric quadrupole to magnetic

dipole amplitude ratio δ. Since α_1^2 must be the same for both the ground state transition and the transition to the 3.95-MeV level, the difference in their angular distributions must be ascribed to different δ. The curves of fig. 6 show the relation between δ and α_1^2 for both 8-MeV and 4-MeV gamma-ray transitions. Provided $\alpha_1^2 \approx 1$ or 0, reasonable values of δ may be obtained for the two transitions, with $\alpha_1^2 \approx 1$ being preferred.

Warburton and Pinkston [16]) conclude that the $N^{14}(\alpha, \alpha')N^{14*}$ data implies that the 7.97-MeV level has $T = 0$ and is a single-particle excitation from the N^{14} ground state. To make such a positive parity state with a single-particle excitation requires that the excited nucleon either be kept in the 1 p shell or promoted to the $1f_{\frac{7}{2}}$ or $2p_{\frac{3}{2}}$ shell. The latter two configurations are expected to have a high excitation energy. A 1^+ level can be constructed with a promotion

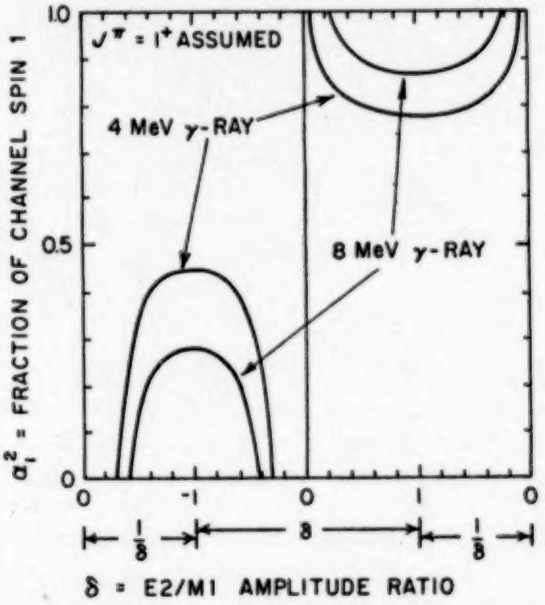

Fig. 6. Assuming a 1^+ level at 7.97 MeV, the gamma-ray angular distributions to the ground state and the 3.95-MeV state lead to the relation between α_1^2 and δ pictured above. Both transitions must have the same value of α_1^2, and as δ is expected to be small, values of α_1^2 close to 0 or 1 are preferred. From the point of view of angular distributions only, the assignment $J^\pi = 1^+$ cannot be ruled out, but difficulties in accounting for other experiments, as discussed in the text, eliminate this assignment.

to the $1f_{\frac{7}{2}}$ shell only by breaking up the C^{12} core, and leaving the two $p_{\frac{1}{2}}$ nucleons coupled to spin 1. The $2p_{\frac{3}{2}}$ shell is higher than the $1f_{\frac{7}{2}}$ shell, but construction of a 1^+ state does not require breaking up the C^{12} core. If the excited nucleon stays in the 1p shell, the difficulty arises of explaining why two M1 isobaric spin-forbidden transitions within the configuration are observed (to the ground and 3.95-MeV states) to be much stronger than an M1 isobaric spin-allowed transition within the configuration (to the 2.31-MeV state). In addition, the lowest unidentified 1^+ level of this configuration with zero isobaric spin is expected to be above 10 MeV excitation [16]).

(3) $J^\pi = 2^-$. For this spin and parity assignment of the 7.97-MeV state, the relevant parameters are the fraction of formation by channel spin 1 ($0 \leqq \alpha_1^2 \leqq 1$) and the magnetic quadrupole to electric dipole amplitude ratio δ (expected to be small). With no further parameters, the minimum value of the $P_2(\cos\theta)$ coefficient is -0.515, which is outside the range of experimental error for the ground state transition. However, interference of a 2^- resonance with the broad 1^- level at 8.06-MeV excitation can lead to changes in the $P_2(\cos\theta)$ angular distribution coefficients. Since the 8.06-MeV level is formed uniquely through channel spin 1, only the channel spin 1 contribution to the 2^- resonance will show interference. Of the eight interference terms actually occurring, only two have been calculated explicitly. The remaining six are expected to be extre-

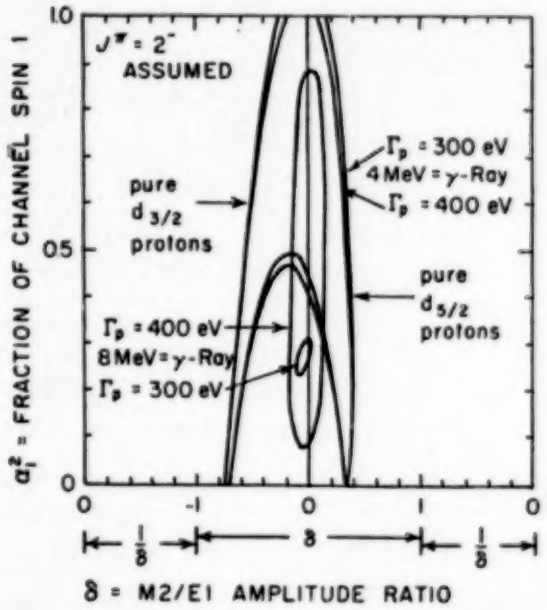

Fig. 7. The preferred assumption of $J^\pi = 2^-$ for the 7.97-MeV level leads to the relation between δ and α_1^2 shown above. Interference of the 2^- resonance with the 1^- background (required to explain the ground-state gamma-ray angular distribution) leads to the existence of a third parameter. This parameter is the width Γ_p of the 2^- resonance. The diagram contains information for two values of this parameter: one is the experimental upper limit to the width, and the second is the minimum width required by the ground-state gamma-ray angular distribution. Since the M2/E1 amplitude ratio is expected to be small and α_1^2 must be the same for both transitions, the only satisfactory portion of the diagram is close to $\alpha_1^2 = 0.4$, with $\Gamma_p \approx 350$ eV. The channel spin ratios for pure $d_{\frac{3}{2}}$ and pure $d_{\frac{5}{2}}$ incoming proton waves are indicated on the diagram.

mely small. The relative phases of resonant and background radiation (d to s-wave, $\phi = 90°$) are such that, when an average is taken over the resonance energy, the two terms expected to be most important are maximized, and four of the expected small terms average out to give a zero interference term. These four terms contain, as a factor, the amplitude ratio of d-wave to s-wave formation of the 8.06-MeV level, known to be small [17, 18]). The remaining two small terms contain, as a factor, the amplitude ratio of M2 to E1 transitions

for the strong E1 transition from the 8.06-MeV level. Therefore they are neglected. In order to reproduce the magnitude of the $P_2(\cos\theta)$ coefficient of the ground state transition, it is necessary that the difference of phase of the non-resonant s-wave background and the non-resonant part of the d-wave phase (d-waves are resonant) be close to 90°, as expected theoretically. A lower limit of 300 eV is also placed on the proton width of the resonance, in order to achieve a sufficiently large interference term. The experimentally determined upper limit to the width is 400 eV.

The curves of fig. 7 show the relation between α_1^2 and δ required to account for the 8-MeV and the 4-MeV gamma-ray angular distributions, with the resonance width as a third parameter. The value of δ is expected to be small for both radiations, and a satisfactory portion of the curves, from this point of view, is located near $\alpha_1^2 = 0.4$. On this analysis, the difference in the angular distributions of the 8-MeV and 4-MeV radiation is not caused by different δ but by the interference with the non-resonant background being of opposite sign (and of different magnitude) for the two radiations. The required total width of the resonance, $300\text{ eV} \leqq \Gamma \leqq 400\text{ eV}$, is just within the range of detection by present elastic scattering techniques, but preliminary attempts to detect the expected small elastic scattering anomaly have not yet been successful. Unfortunately, at backward angles where the resonance amplitude is large compared with the Rutherford amplitude of the scattered wave, the theoretical 2^- anomaly tends to disappear when averaged over a narrow resonance. The investigation of the energy range around 448-keV proton energy, shown in fig. 2, was not sufficiently intensive to disclose such a narrow anomaly.

A d-wave proton width of 350 eV at 448-keV proton energy corresponds to approximately 50 % of $3\hbar^2/2Ma^2$, and would imply that the configuration is mainly a C^{13} ground state core plus a d-wave proton. For this configuration, two 2^- states may be constructed. Warburton and Pinkston identify the 5.10-MeV level as one of these with a $(p_{\frac{1}{2}})^8 p_{\frac{1}{2}} d_{\frac{3}{2}}$ configuration, remarking that, between 7 and 11 MeV excitation, a 2^- level arises from coupling a $d_{\frac{3}{2}}$ nucleon to the C^{13} ground state. This configuration is consistent with the inelastic alpha particle scattering data, which implies a single particle excitation from the N^{14} ground state. The required channel spin ratio ($\alpha_1^2 = 0.4$) implies either pure $d_{\frac{3}{2}}$ incident protons or else $d_{\frac{3}{2}}$ protons with 4 % by intensity of $d_{\frac{5}{2}}$ protons.

Thus, no inconsistencies appear if a 2^- assignment is made to the 7.97-MeV level. It is felt that, although the assignments 1^- and 1^+ can reproduce the observed angular distributions, the difficulties to which these assignments lead eliminate them effectively from consideration, leaving a unique satisfactory assignment of 2^-.

3.3. RADIATIVE CAPTURE BELOW THE 448-keV RESONANCE

Using a target found to be 9.0 keV thick for 448-keV protons, the yield of

gamma rays from the $C^{13}(p, \gamma)$ reaction was measured at energy intervals of 8.25 keV down to 146 keV. The spectrum from the 10.2 cm NaI(Tl) detector was recorded in the 100-channel analyzer for each bombarding energy. After background subtraction, these spectra were used to obtain the yield of gamma-ray pulses (a) above 3.2 MeV and (b) above 5 MeV.

The conversion from the experimental yield curve to the experimental cross-section curve was accomplished by a method of successive approximations. An energy dependence of the cross section was assumed, and the assumed cross

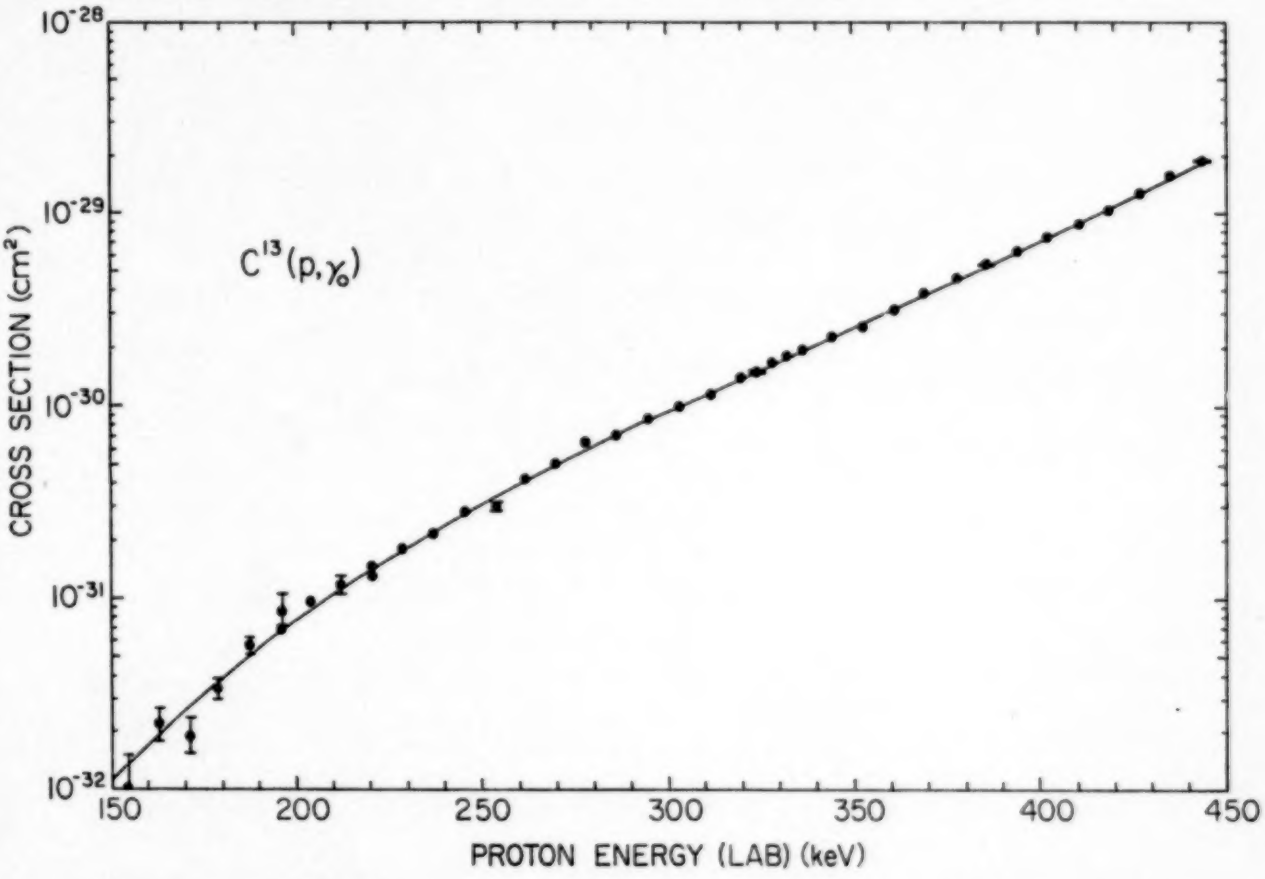

Fig. 8. The cross section for radiative capture of protons by C^{13}, with emission of the ground-state gamma ray, is shown. The target was 9.0 keV thick for 448-keV protons, and was enriched to 61 % C^{13}. Typical errors, due to counting statistics, are shown at intervals along the curve. The solid curve of this figure is derived from the solid curve in fig. 9 where an explanation will be found.

section was integrated over the known target thickness to produce a theoretical yield curve. This information gave a ratio of cross section to yield, based on the assumed cross section, that was used to convert the experimental yield curve to an approximated cross section. The approximated cross section obtained could then be used for further cycles leading to an improved approximation.

In practice, the first approximate cross section was assumed to be the tail of the 550-keV resonance. The calculation included such factors as the Thomas shift and the energy dependence of the proton and radiative widths, as well as

the energy dependence of the stopping cross section. The calculation was performed on the Datratron 205 computer at the California Institute of Technology. The parameters used for the calculation were the same as those used to fit the elastic scattering data, with the addition of a ground state radiative width of $\omega\Gamma_{\gamma_0} = 10.1$ eV. (This is equivalent, near the 550-keV resonance, to the simplified Breit-Wigner formula with $\omega\Gamma_\gamma = 9.2$ eV, of which 82 % is ground state radiative width.) This first approximation to the cross section was sufficiently close that, in the improved estimate of the cross section, the residual

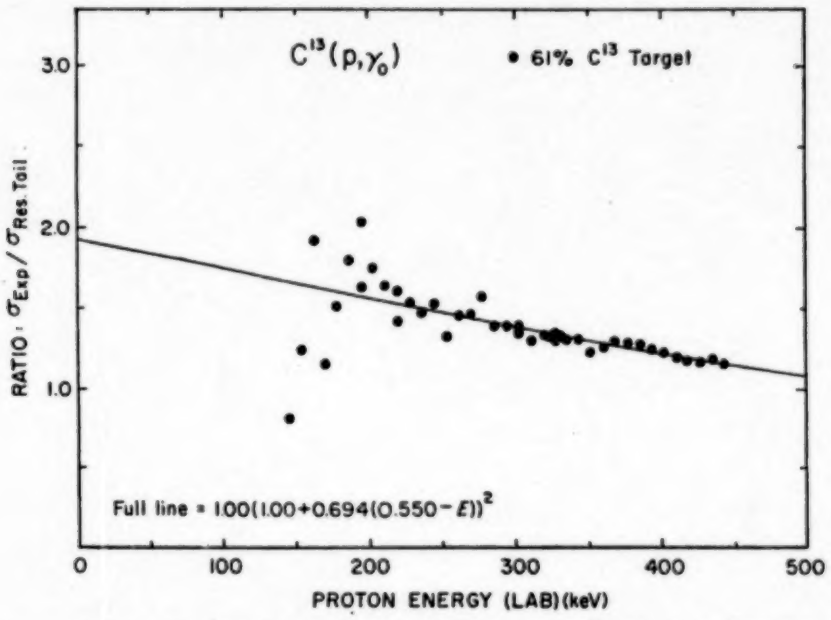

Fig. 9. The cross sections of fig. 8 have been divided by the computed tail of the 550-keV resonance, using the resonance parameters described in the text. The solid curve, with the equation given above (proton energy E in MeV), gives the expected form of the deviation from this computed tail, and is fitted to the experimental points. Although no errors are shown, the deviations of the points from the solid curve are consistent with the magnitude of the experimental errors at all energies.

error is less than 0.4 % at all energies. The ground-state gamma-ray cross section so obtained is shown as a function of proton energy in fig. 8.

The deviation of the experimental cross section from the 550-keV resonance tail is shown in fig. 9. This deviation can be caused by two processes. There is the possible interference of a non-resonant capture with the resonance capture (s-waves with channel spin 1) which has been treated by Thomas [3]) who includes a term $(1+A(E_{res}-E))^2$ multiplying the resonance tail. There are also non-interference terms contributing to the integrated cross section. These non-interference terms have been estimated by computing the tail of the 1250-keV $C^{13}(p,\gamma)$ resonance over the range of energies investigated experimentally. The ratio of the cross section contribution from the 1250-keV resonance to the contribution from the 550-keV resonance was found to be indistinguishable from a linear function of the energy over the whole energy

range. Since the tail of the 1250-keV resonance is dominated by the barrier penetration factor, it is expected that any other non-interfering non-resonant process, also dominated by the barrier penetration factor, will give a linear function of energy when compared with the 550-keV resonance tail. Furthermore, the coefficient A, in the extra term suggested by Thomas for the interference process, is of such a magnitude that the term $(1+A(E_{res}-E))^2$ is also a linear function in the energy range investigated experimentally. Therefore, the two processes causing deviation of the cross section from the computed tail of the 550-keV resonance cannot be distinguished experimentally. For this reason, the ratio of the experimental cross section to the theoretical tail of the 550-keV resonance has been fitted by a simple Thomas-type function of the energy, and this fit is shown in fig. 9. The extrapolation through the recent values of Hester[19]) is not very satisfactory, and this discrepancy remains unresolved. However, the extrapolation is in good agreement with the measurement by Woodbury and Fowler [20]) at 129 keV, assuming a 3-step cascade (see fig. 12). At a proton energy of 25 keV (C.M. system), the extrapolated value of the cross section factor $S(=\sigma E_{C.M.} \exp 2\pi\eta)$ is 6.0 ± 0.8 keV-barn. This value is to be compared with the previous extrapolation [4]) of 6.1 ± 2 keV-barn. This extrapolation takes into account all levels, above or below the proton threshold that have a large enough reduced width to affect the cross section in the energy range above 130 keV proton energy. Of course, a resonance may still be present in the critical energy range up to 100 keV to invalidate the extrapolation.

TABLE 4

Limit to unobserved narrow resonances

Proton energy (keV)	$\left(\frac{\omega\Gamma_p\Gamma_\gamma}{\Gamma}\right)_{max}$ (μeV)	$\Gamma_p = 1$ % of $3\hbar^2/2Ma^2$ (μeV)				
		$l=0$	1	2	3	4
450	85	1.3×10^{9}	2.0×10^{8}	8.0×10^{6}	1.3×10^{5}	1.1×10^{3}
400	50					
350	27	5.3×10^{8}	7.5×10^{7}	3.0×10^{6}	4.0×10^{4}	1.8×10^{2}
300	18					
250	6	8.0×10^{7}	1.0×10^{7}	3.0×10^{5}	4.0×10^{3}	1.5×10^{1}
200	4					
146	3	2.0×10^{6}	2.0×10^{5}	5.0×10^{3}	4.0×10^{1}	1.0×10^{-1}

An upper limit may be placed on the strength of radiation from any other resonances in the C^{13} (p, γ) reaction. No such resonances were observed in the energy range from 130 keV up to 448 keV (7.67—7.96 MeV excitation in N^{14}). This range of energies covers the level at 7.72 MeV reported by Benenson. In table 4, these upper limits are tabulated as a function of energy. For comparison, a proton width corresponding to 1 % of the Wigner limit is tabulated for various proton orbital angular momenta. It is clear that levels up to $J = 5$

would stand a very good chance of being detected, the limit being provided by the radiative width, rather than the proton width. Radiation up to octopole order could probably be detected, and there are states up to $J = 3$ below 7.5-MeV excitation that could participate in cascades to the ground state.

3.4. $C^{12}(p, \gamma)$ RADIATION

From the spectra obtained by bombardment of the 61 % C^{13}-enriched carbon target, the yield of gamma rays was determined for the $C^{12}(p, \gamma)$ reaction. The time-dependent background subtraction was known accurately, but the estimate of the subtraction necessary to eliminate the $C^{13}(p, \gamma)$ spectrum was considerably less accurate. The 2.31-MeV gamma ray intensity, coming from several different cascades, is not known with sufficient accuracy. Therefore, the $C^{12}(p, \gamma)$ yield from the C^{13}-enriched target has been used in the cross section determination only in the energy range from 448 keV down to 295 keV. At 295-keV proton energy, the beam-dependent background subtraction is considerably less than the $C^{12}(p, \gamma)$ yield, but the magnitudes are reversed within the next 50-keV lower proton energy. Below 295-keV proton energy, a carbon target of normal isotopic composition was used. The thickness of this target was not known as accurately as the thickness of the enriched target. Therefore, the yield from the natural carbon target has been used in the cross section determination only in the energy range from 380-keV down to 195-keV proton energy. In this energy range, calculation of the ratio of yield to cross section shows that the energy dependence of the cross section is not strongly influenced by the assumed target thickness. The cross sections in the energy range 195—380 keV were normalized so that, in the overlap with the range 295—448 keV, the two sets of data fitted together smoothly.

TABLE 5

Resonance parameters for $C^{12}(p, \gamma)$ [a])

Resonance energy (defined by $E_\lambda + \Delta_\lambda - E = 0$)	462 keV
Reduced proton width γ_p^2	1695 keV
Radiative width $\omega\Gamma_\gamma$	1.52 eV
Nuclear radius (for calculation of Δ_λ and $2\rho/(F_0^2+G_0^2)$)	4.64×10^{-13} cm

[a]) A single-level Breit-Wigner formula is used, with all energy dependences included. The energies quoted are in the laboratory system. These parameters lead to a peak cross section of 127 μb at an energy of 460.5 keV.

The conversion from yield to cross section was accomplished in the same manner as for the $C^{13}(p, \gamma)$ reaction. The resonance tail of the 462-keV $C^{12}(p, \gamma)$ resonance was calculated from the single-level Breit-Wigner formula, including all energy dependences. The parameters used are shown in table 5. The resonance energy and proton width are in agreement with the elastic scattering data of Milne [8]) and of Jackson and Galonsky [21]). The radiative width was chosen to

give a cross section of 127 μb at the peak of the $C^{12}(p, \gamma)$ resonance [22]). Calculations were also made with a resonance energy of 456 keV, as reported for the $C^{12}(p, \gamma)$ reaction by Hunt and Jones [23]) with widths of [23]) 39 keV and [24]) 35 keV. However, the shape of the yield curve below 448-keV proton energy agrees appreciably better with the curve calculated from the elastic scattering resonance parameters of table 5.

The conversion from yield to cross section was calculated on the assumption that the target, of 39 % C^{12}, was 9.0 keV thick for protons of 448 keV energy.

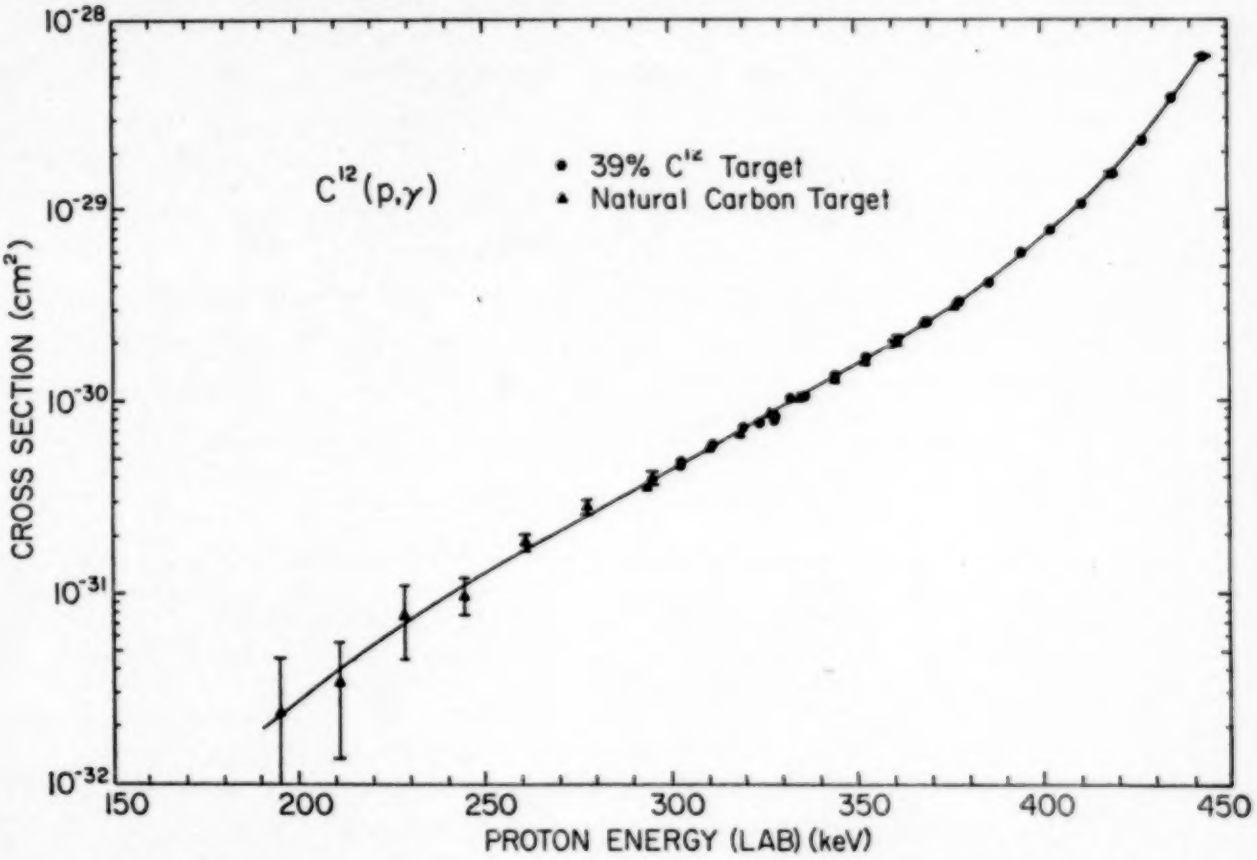

Fig. 10. The cross section for radiative capture of protons by C^{12} is shown. For the energy range from 295 keV to 444 keV, a target of 39 % C^{12} with a thickness of 9.0 keV for 448-keV protons was used. For the energy range from 195 keV to 378 keV, a natural carbon target, approximately 20 keV thick was used. The results from the latter target were normalized in the overlapping range to agree with the results from the target of known thickness, taken at higher energies. The experimental points have been corrected for the effect of the carbon contamination on the surface of the 39 % C^{12} target. Typical errors are shown at intervals in the energy range, and the origin of the solid curve is described in fig. 11.

This cross section was reduced by 10.7 %, because of a surface layer of carbon from the pump-oil contamination. This contaminant layer had a thickness of approximately 300 eV, but this was known only to an accuracy of ± 50 %, so the cross section was renormalized to make it agree with the calculated resonance cross section with a peak of 127 μb, as reported by Seagrave [22]). This

renormalization is consistent with the estimated contaminant layer. This corrected cross section is shown in fig. 10, and the ratio of the experimental cross section to the computed 462-keV resonance tail is shown in fig. 11. The deviation of the cross section from the computed resonance tail introduces negligible error into the conversion from yield to cross section.

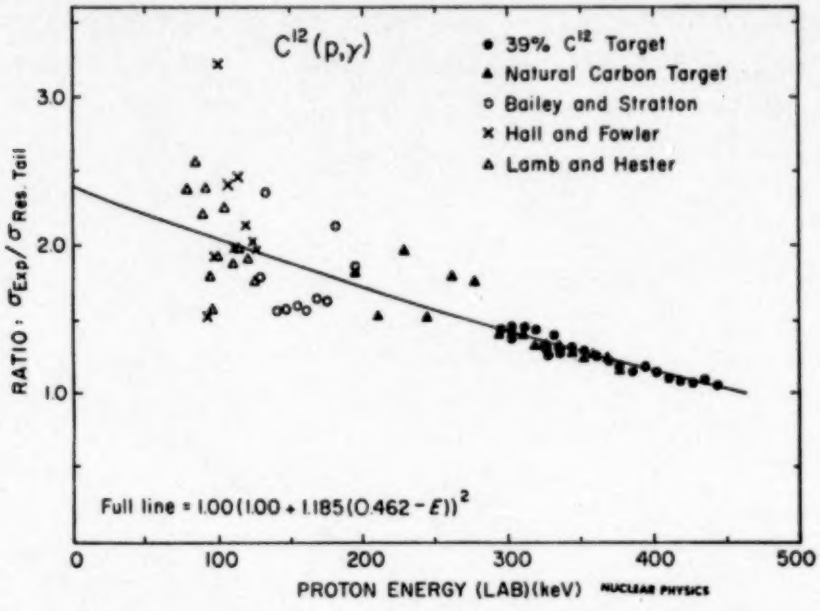

Fig. 11. The corrected experimental cross sections of fig. 10 are divided by the computed tail of the 462-keV $C^{12}(p, \gamma)$ resonance. (Resonance parameters in table 5.) The absolute cross sections reported by Bailey and Stratton, by Hall and Fowler, and by Lamb and Hester, have been treated similarly, and the results are also shown on this figure. The solid curve, with the equation above (proton energy E in MeV), giving the expected form of the deviation from the computed resonance tail, is the best fit to all the points. Although no errors are shown, the deviations from the solid curve of this figure are consistent with the experimental errors over the whole energy range.

In the same manner as for the $C^{13}(p, \gamma)$ cross section, the deviation of the $C^{12}(p, \gamma)$ cross section from the computed cross section is attributed [3]) mainly to a non-resonant contribution interfering with the resonance tail. The experimental points on fig. 11 have been fitted by a term of the form $(1+A(E_{res}-E))^2$, and the smooth curve of best fit also appears on fig. 11, passing satisfactorily through the lower energy cross section measurements of Bailey and Stratton [25]), of Hall and Fowler [26]), and of Lamb and Hester [27]), in the extrapolation to stellar energies. At a proton energy of 25 keV (C.M. system), the extrapolated value of S is 1.33 ± 0.15 keV-barn. This value should supersede the value 1.2 ± 0.2 keV-barn which has been used in recent astrophysical calculations [4, 28]).

3.5. CROSS SECTION RATIO

The ratio of the $C^{13}(p, \gamma)$ and the $C^{12}(p, \gamma)$ cross section factors, when extrapolated to stellar energies, is found to be 4.5 ± 0.8, a value not very different

from earlier reported values [4]). The individual values of the cross section factor S for the two reactions, from which the cross section ratio may be found at any energy, are plotted in fig. 12. The solid curves appearing in fig. 12 are derived

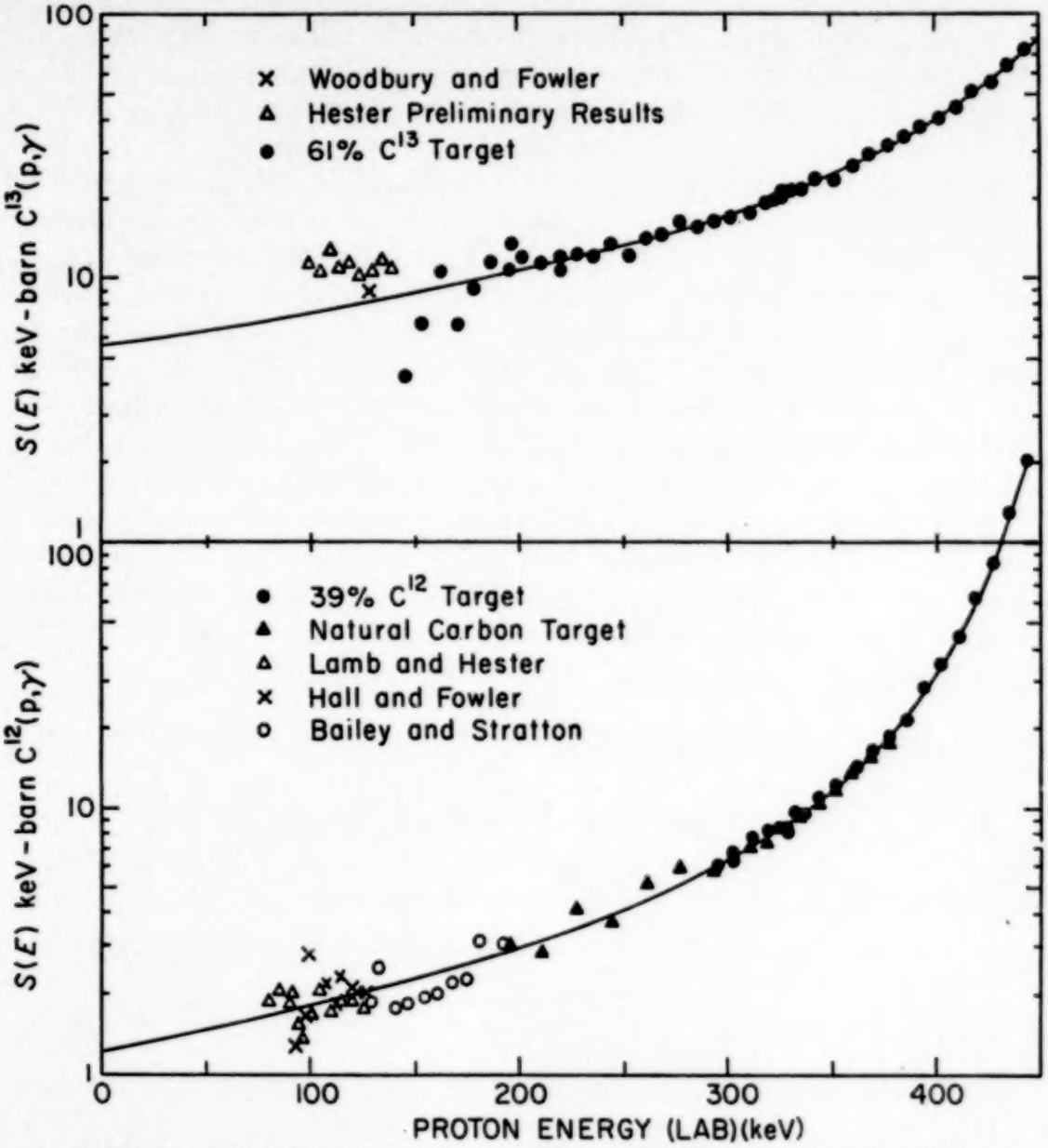

Fig. 12. The cross section factor is shown for the $C^{13}(p, \gamma)$ and $C^{12}(p, \gamma)$ reactions. The solid curves, derived from the solid curves of figs. 9 and 11, allow an extrapolation to stellar energies. For the $C^{13}(p, \gamma)$ reaction, the $C^{13}(p, \gamma_0)$ cross section factor has been corrected for the 18 % reported [5]) cascade radiation.

from the solid curves of figs. 9 and 11, fitting the deviations of the cross sections from the resonance tail. The uncertainty in the cross section ratio will not be very different from the uncertainties in the individual cross sections, since the major sources of error are not removed by taking the ratio. The major

sources of error are thought to lie in estimating the fraction of the gamma-ray spectrum used in measuring the yield of gamma rays, and in the estimate of the carbon contamination developed on the target surface, for which a correction was applied to the $C^{12}(p, \gamma)$ yield. Less important sources of error that are largely removed on taking the ratio are those involving charge integration, the crystal solid angle and tabulated gamma-ray efficiency.

McKellar and Climenhaga [1]) have made measurements on the $C^{12} : C^{13}$ abundance in some selected carbon-rich stars. The results of 4.7 : 1 or 5.8 : 1, depending on the technique employed for measurement, are consistent with the cross section ratio reported here. These selected carbon-rich stars are believed to be burning on the CNO-cycle, but is is not necessary to assume that the entire cycle is in equilibrium. Provided the formation and destruction of the C^{13} present occurs by means of the reactions $C^{12}(p,\gamma)N^{13}(\beta)C^{13}(p,\gamma)N^{14}$, the requirement of an equilibrium in the amount of C^{13} present is sufficient to require that the $C^{12} : C^{13}$ abundance ratios shoud be equal to the inverse ratio of their cross sections for proton capture provided that proper account is taken of C.M. effects. These effects cause the C^{13}/C^{12} cross section ratio to have the value 4.1 ± 0.7 for a temperature of 15×10^6 °K. The additional terms introduced into the reaction rate because of the energy variation of S are not, in general, important. For example, for $C^{12}(p, \gamma)$ at a temperature of 15×10^6 °K the extra multiplicative term [28]) $1 + (\frac{5}{6} kT/S_0)(dS_0/E)_{E_0}$ is equal to 1.004, and the term of the $C^{13}(p, \gamma)$ reaction is even closer to unity.

The authors wish to thank Professor R. F. Christy, Professor W. A. Fowler, and Professor T. Lauritsen for their valuable comments and discussions. The assistance of Professor Fowler at all stages of the work was particularly appreciated. One of us (D. F. H.) wishes to thank Professor D. N. F. Dunbar for his assistance and advice in many of the measurements.

References

1) J. L. Climenhaga,, Publ. Dom. Ap. Obs. **11**, no. 16 (1960)
2) A. A. Wyller, Astrophys. J. **125** (1957) 177, and Astrophysica Norvegica (1960), to be published
3) R. G. Thomas, Phys. Rev. **88** (1952) 1109
4) Burbidge *et al.*, Revs. Mod. Phys. **29** (1957) 547
5) F. Ajzenberg-Selove and T. Lauritsen, Nuclear Physics **11** (1959) 1
6) J. D. Seagrave, Phys. Rev. **85** (1952) 197
7) Woodbury, Day and Tollestrup, Phys. Rev. **92** (1953) 1199
8) E. A. Milne, Phys. Rev. **93** (1954) 762
9) R. F. Christy, Physica **22** (1956) 1009
10) R. E. Benenson, Phys. Rev. **90** (1953) 420
11) Bent, Bonner and Sippel, Phys. Rev. **98** (1955) 1237
12) E. J. Burge and D. J. Prowse, Phil. Mag. **1** (1956) 912
13) Miller *et al.*, Phys. Rev. **101** (1956) 740

14) Bader *et al.*, Phys. Rev. **103** (1956) 32
15) M. E. Rose, Phys. Rev. **91**. (1953) 610
16) E. K. Warburton and W. T. Pinkston, Phys. Rev, **118** (1960) 733
17) Warburton, Rose and Hatch. Phys, Rev, **114** (1959) 214
18) Broude *et al.*, Phil. Mag. **2** (1957) 1006
19) R. E. Hester, private communications to W. A. Fowler and D. F. Hebbard
20) E. J. Woodbury and W. A. Fowle, Phys. Rev. **85** (1952 51
21) H. L. Jackson and A. I. Galonsky, Phys. Rev. **89** (1953) 370
22) J. D. Seagrave, Ph. D. Thesis, California Institute of Technology
23) S. E. Hunt and W. M. Jones, Phys. Rev. **89** (1953) 1283
24) W. A. Fowler and C. C. Lauritsen, Phys. Rev. **76** (1949) 314
25) C. L. Bailey and W. R. Stratton, Phys. Rev. **77** (1950) 194
26) R. N. Hall and W. A. Fowler, Phys. Rev. **77** (1950) 197
27) W. A. S. Lamb and R. E. Hester, Phys. Rev. **107** (1957) 550
28) W. A. Fowler, Mém. Soc. R. Sc. Liège **16** (1960) 207

1.C

Nuclear Physics **21** (1961) 676—680; © *North-Holland Publishing Co., Amsterdam*

Not to be reproduced by photoprint or microfilm without written permission from the publisher

THE MOMENTUM DISTRIBUTION IN A DILUTE FERMI GAS AT ZERO TEMPERATURE

W. CZYŻ † and K. GOTTFRIED ††

Institute for Theoretical Physics, University of Copenhagen, Denmark

Received 2 September 1960

Abstract: The momentum distribution at zero temperature in a dilute Fermi gas with repulsive interactions is calculated to second order in the small parameter $p_F a$, the quantity p_F being the Fermi momentum, and a the free-space scattering length.

In the course of an investigation of inelastic electron scattering by complex nuclei we found it necessary to compute the momentum distribution $n(p)$ in a dilute Fermi gas [1]). This quantity tends to crop up rather frequently in theoretical discussions, and yet it has not, to our knowledge, appeared in the literature. We therefore present a brief account of our results in the hope that they may spare other workers a certain amount of tedious and unedifying computation.

We calculate $n(p)$ to second order in the "gaseousness" parameter $\zeta = p_F a/\pi$, where p_F is the Fermi momentum and a the conventional free-space scattering length ($a > 0$). In order to avoid a lengthy explanation of the details of the mathematical apparatus we employ, we retain intact the formulation of the dilute Fermi gas problem given by Galitski and Migdal [2, 3]), and make only a few unimportant changes in order to fit the present text to the main paper [1]) which will be published later.

As is well known (cf. e.g. ref. [2])), one can evaluate $n(p)$ from the one-particle Green's function $G(p, \varepsilon)$, viz.

$$n(p) = \frac{1}{2\pi i}\int_C G(p, \varepsilon)\mathrm{d}\varepsilon, \tag{1}$$

where the contour C consists of the real axis and a semicircle of infinite radius in the upper half plane. Now we exploit the Lehmann-Källén representation

$$G(p, \varepsilon) = \int_0^\infty \mathrm{d}E \left\{\frac{\rho_+(p, E)}{\varepsilon - E - \mu + i\alpha} + \frac{\rho_-(p, E)}{\varepsilon + E - \mu - i\alpha}\right\}, \qquad (\alpha \to 0), \tag{2}$$

μ being the chemical potential. We put (2) into (1) and get

$$n(p) = \int_0^\infty \mathrm{d}E\, \rho_-(p, E) = 1 - \int_0^\infty \mathrm{d}E\, \rho_+(p, E). \tag{3}$$

† Present address: Instytut Badan Jadrowych, Krakow, Bronowice, Poland.

†† Present address: Physics Department, Harvard University, Cambridge, Massachusetts.

The last member of (3) follows from the identity

$$\int_0^\infty dE[\rho_-(p, E)+\rho_+(p, E)] = 1, \tag{4}$$

which is implied by the equal-time commutation relations for a Fermi field.

On the other hand, we have

$$G^{-1}(p, \varepsilon) = G_0^{-1}(p, \varepsilon)- \Sigma (p, \varepsilon) = G_0^{-1}(p, \varepsilon)-R(p, \varepsilon)-iI(p, \varepsilon), \tag{5}$$

where $\Sigma(p, \varepsilon)$ is the self-energy, which we have split into its real and imaginary parts. According to (1) and (5),

$$\begin{aligned} \rho_+(p, E) &= -\frac{1}{\pi}\operatorname{Im} G(p, \mu+E) = -\frac{1}{\pi}\frac{I(p, \mu+E)}{(E_F+E-E_p^0-K)^2+I^2}, \\ \rho_-(p, E) &= \frac{1}{\pi}\operatorname{Im} G(p, \mu-E) = +\frac{1}{\pi}\frac{I(p, \mu-E)}{(E_F-E-E_p^0-K)^2+I^2}, \end{aligned} \tag{6}$$

where $E_p^0 = p^2/2m$, $E_F = p_F^2/2m$, $K = R-\mu+E_F$ and $E \geqq 0$.

In all these formulae we have not made any approximations. Now we shall discuss the second order approximation with respect to the parameter ζ. Ref. [3]) provides us with formulae for μ, R and I in this approximation, and one can easily see that K and I are second order quantities (the first order terms of R and μ cancel each other.) From (6) we see that $\rho_+(p, E)(\rho_-(p, E))$, as a function of E, has a sharp maximum when $p > p_F$ ($p < p_F$). To second order, (3) and (6) therefore lead to

$$\begin{aligned} n(p > p_F) &= \delta n_+(p) = -\frac{1}{\pi}\int_0^\infty dE\, \frac{I(p, E_F-E)}{(E+E_p^0-E_F)^2}, \\ n(p < p_F) &= 1+\delta n_-(p) = 1-\frac{1}{\pi}\int_0^\infty dE\, \frac{I(p, E_F+E)}{(E_F+E-E_p^0)^2}. \end{aligned} \tag{7}$$

The expression for $I(p, \varepsilon)$ given by Galitski [3]) is

$$\begin{aligned} I(p, \varepsilon) = \frac{a^2}{4\pi^3 m^2}\int d^3k d^3k_1 d^3k_2 [&\theta_+(k)\theta_-(k_1)\theta_-(k_2) \\ &-\theta_-(k)\theta_+(k_1)\theta_+(k_2)]\delta(E_{k_1}^0+E_{k_2}^0-E_k^0-\varepsilon)\delta(\mathbf{k}_1+\mathbf{k}_2-\mathbf{k}-\mathbf{p}), \end{aligned} \tag{8}$$

where

$$\theta_-(k) = \begin{cases} 1, & k < p_F \\ 0, & k > p_F \end{cases}, \quad \theta_+(k) = 1-\theta_-(k).$$

After some straightforward manipulations, we find that

$$\delta n_\mp(p) = \mp\frac{a^2}{4\pi^4 m^2}\int d^3k d^3\kappa\, \frac{\theta_\pm(k)\Lambda_\mp(\kappa)}{\left(\frac{1}{4m}P^2+\frac{1}{m}\kappa^2-E_k^0-E_p^0\right)^2}, \tag{9}$$

where $\mathbf{P}=\mathbf{k}+\mathbf{p}$, and

$$\Lambda_{\mp}(\kappa)=\theta_{\mp}(\tfrac{1}{2}\mathbf{P}+\kappa)\theta_{\mp}(\tfrac{1}{2}\mathbf{P}-\kappa).$$

Unfortunately one cannot perform all integrations in (9) analytically. We therefore give those formulae which we have found suitable for numerical integration:

$$\delta n_{-}(p)=\frac{2\zeta^2}{p}\Big\{\int_0^{\frac{1}{2}(1+p)}\mathrm{d}Q[F_0(Q)-QF_1(Q)]+\int_0^{\frac{1}{2}(1-p)}\mathrm{d}Q[QG_1(Q)-G_0(Q)]+\int_{\frac{1}{2}(1-p)}^{\frac{1}{2}(1+p)}\mathrm{d}Q[QH_1(Q)-H_0(Q)]\Big\}, \quad (10)$$

where p is measured in units of p_{F}, and

$$\begin{aligned}
F_0(Q)&=L[(1+Q)^2-(Q-p)^2]-L[(1-Q^2)-(p-Q)^2],\\
F_1(Q)&=2L(p+1)-2L(p-1-2Q),\\
G_0(Q)&=L[(Q+1)^2-(Q+p)^2]-L[(1-Q^2)-(p+Q)^2],\\
G_1(Q)&=2L(p+1+2Q)-2L(p-1),\\
H_0(Q)&=L[\tfrac{1}{2}(1+2Q)^2-\tfrac{1}{2}p^2]-L[\tfrac{1}{2}(1-p^2)],\\
H_1(Q)&=2L[\sqrt{\tfrac{1}{2}(p^2+1)-Q^2}+(1+Q)]-2L[\sqrt{\tfrac{1}{2}(p^2+1)-Q^2}-(1+Q)],
\end{aligned}$$

the function $L(x)$ being defined by $L(x)=x\ln|x|$. Similarly,

$$\delta n_{+}(p)=\frac{2\zeta^2}{p}\Big\{\int_0^{1}\mathrm{d}Q[J_0(Q)-QK_0(Q)]+\int_0^{\frac{1}{2}(p-1)}\mathrm{d}Q[J_1(Q)-QK_1(Q)]+\int_{\frac{1}{2}(p-1)}^{1}\mathrm{d}Q[J_2(Q)-QK_2(Q)],\Big\} \quad (11)$$

where

$$\begin{aligned}
J_0(Q)&=L[(p+Q)^2-(Q-1)^2]-L[(p+Q)^2+(Q^2-1)],\\
J_1(Q)&=L[(p-Q)^2+(Q^2-1)]-L[(p-Q)^2-(1-Q)^2],\\
J_2(Q)&=L[\tfrac{1}{2}(p^2-1)]-L[\tfrac{1}{2}(p^2-1)+2Q(1-Q)],\\
K_0(Q)&=2L(p+1)-2L(2Q+p-1),\\
K_1(Q)&=2L(p-1)-2L(p+1-2Q),\\
K_2(Q)&=2L[\sqrt{\tfrac{1}{2}(p^2+1)-Q^2}-(1-Q)]-2L[\sqrt{\tfrac{1}{2}(p^2+1)-Q^2}+(1-Q)].
\end{aligned}$$

The resulting values of $\delta n(p)$ are given in table 1. For $p=p_{\mathrm{F}}\pm 0$ the integrations can be carried out analytically, the result being

$$\delta n_{-}(p_{\mathrm{F}}-0)=-2\zeta^2(\tfrac{1}{3}+\ln 2), \quad \delta n_{+}(p_{\mathrm{F}}+0)=2\zeta^2(-\tfrac{1}{3}+\ln 2). \quad (12)$$

Thus $n(p)$ has a discontinuity of amount $(1-4\zeta^2 \ln 2)$ at the Fermi surface, which agrees with Galitski's result †. We might also mention that $\delta n(p)$ approaches p_F like $[(p/p_F)-1] \ln |(p/p_F)-1|$. This gives an infinite slope on the Fermi surface, which results in "rounding off" of $n(p)$ confined to a very small neighbourhood of p_F (not shown in fig. 1).

TABLE 1

Calculated values

p/p_F	0.2	0.6	0.8	1−0	1+0	1.1	1.2	1.5	2.0	3.0
$\lvert\delta n(p)\rvert/\zeta^2$	1.14	1.36	1.66	2.06	0.720	0.392	0.266	0.112	0.036	0.006

According to (11), $n(p)$ varies as p^{-4} when $(p/p_F) \to \infty$. The expressions given above are not, however, expected to be valid when $pa > 1$, since the detailed structure of the interparticle force, and not just the S-wave scattering length, comes into play for such large momenta. Therefore the p^{-4}-dependence should only be taken seriously when the inequalities $p \gg p_F$ and $pa < 1$ are satisfied simultaneously.

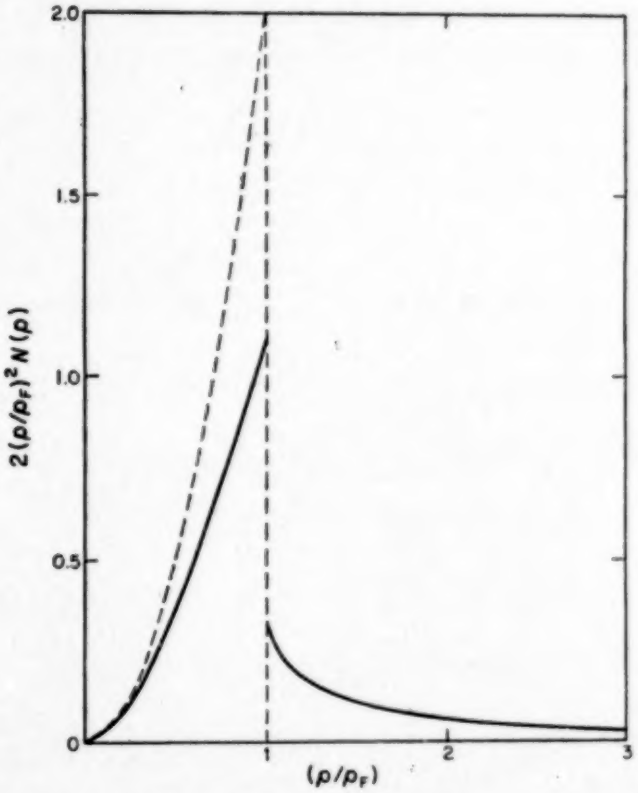

Fig. 1. The momentum distribution in an idealized dilute nucleon gas.

† Whether a discontinuity is also a property of the exact solution has been the subject of rather extensive but as yet inconclusive discussions. The interested reader is referred to ref. [4]).

All the above formulae and results apply to a system composed of one kind of spin $\frac{1}{2}$ particle, and $n(p)$ refers to the momentum distribution for those particles having one particular spin direction. In nuclear theory one is concerned with a system composed of two species of fermions (labelled by $\tau = \pm 1$) of equal concentration, and with the associated momentum distribution $N_\tau(p)$ for members of one species τ having a given spin direction. Again assuming a dilute system, and forces independent of spin and isospin variables, one easily finds $N_\tau(p) = 3n(p)$. As one is usually not interested in specifying the spin direction, we have plotted the more useful function $2(p/p_F)^3N(p)$ in fig. 1 for $p_F a = 0.6$. This is expected to give a good indication of the influence of the hard core ($a \approx 0.4 \times 10^{-13}$ cm) in the nucleon-nucleon interaction on the momentum distribution.

We wish to thank Professor Niels Bohr and Professor Aage Bohr for the generous support and hospitality of the Institut for Teoretisk Fysik, where most of this work was done.

References

1) W. Czyż and K. Gottfried, Bull. Am. Phys. Soc. **5** (1960) 30
2) V. M. Galitski and A. B. Migdal, JETP USSR **34** (1958) 139 (translation: Soviet Phys. JETP **7** (1958) 96)
3) V. M. Galitski, JETP USSR **34** (1958) 151 (translation: Soviet Phys. JETP **7** (1958) 104)
4) Proceedings of the conference on the many body problem, Utrecht, June 1960 (to be published in Physica)

8.C

Nuclear Physics **21** (1961) 681—685; ©*North-Holland Publishing Co., Amsterdam*

Not to be reproduced by photoprint or microfilm without written permission from the publisher

ON NEUTRAL SPIN-0 PARTICLES WITH IMAGINARY PARITY

RICHARD SPITZER

Purdue University, Lafayette, Indiana †

Received 22 September 1960

Abstract: Some consequences of the existence of a neutral spin-0 particle with imaginary parity are examined. The particle is subsequently identified with K^0 and it is shown that associated production is a consequence of a superselection law for parity. The parity of the K^0 is fixed by its electromagnetic interaction, which leads to certain results that differ from those predicted by strangeness. The theory accounts directly for the nonconservation of parity in non-neutrino decays of Λ, Σ's and K's.

According to the analysis of Wick, Wightman and Wigner [1]) the requirement of invariance of a theory under space inversion does not, in general, specify unambiguously the phase factors associated with the transformation of quantized fields under this symmetry operation. Nevertheless, in certain cases it is possible to assign these phase factors with less arbitrariness than in others. In particular, in a theory in which the only gauge groups are those connected with the conservation of charge and baryons, the intrinsic parity of a neutral spin-0 particle can be fixed to the extent of being imaginary.

The statement that the parity of a particle is necessarily imaginary is meaningful if there exists a transition between two states that necessarily implies such a parity ††). We shall subsequently return to this point, but now only remark that double space reflection for the corresponding field then produces a change of sign. Although this operation for a spin-0 field has generally been required to correspond to the identity transformation, apparently not all authors have realized that such a restriction constitutes an additional assumption regarding the physical nature of the theory upon which it is imposed.

As will now be shown, the production from a pion and a nucleon of a neutral spin-0 particle with imaginary parity, whose antiparticle must have opposite parity if the related fields are to have a simple transformation property under space reflection, can only occur in association with a baryon that is distinct from a nucleon.

Consider the production of a neutral spin-0 meson with imaginary parity M^0 and a baryon B:

$$\pi + N \rightarrow M^0 + B. \qquad (1)$$

† Work supported in part by the Air Force Office of Scientific Research. The Research was completed under the auspices of the U. S. Atomic Energy Commission while the author was a visitor at the Lawrence Radiation Laboratory (Livermore).

†† This point has been discussed in some detail by G. Feinberg and S. Weinberg [2]).

Given the charge structure of the pion and nucleon spectra, the particle B can be neutral or carry a negative, positive, or doubly positive charge. Multiply charged particles with hereafter be arbitrarily discounted. In the analysis use will be made of the relations between the intrinsic parities of pions and nucleons,

$$\eta(\pi^0) = -1, \quad \eta(\mathrm{p})\eta^*(\pi^+)\eta^*(\mathrm{n}) = -1, \tag{2}$$

and those of the M^0 and its antiparticle $\overline{M}^0$,

$$\eta(M^0) = \eta^*(\overline{M}^0) = -\eta^*(M^0) = -\eta(\overline{M}^0). \tag{3}$$

The parities of the particles in reaction (1) must then satisfy the relation

$$\eta^*(M^0)\eta^*(B)\eta(\pi)\eta(N) = \varepsilon, \tag{4}$$

where, depending on the space states involved, ε is $+1$ or -1. Using (2) we get

$$\eta(B^+) = \varepsilon_1\eta(M^0)\eta(\mathrm{p}), \quad \eta(B^0) = \varepsilon_2\eta(M^0)\eta(\mathrm{n}). \tag{5}$$

These equations state that the particles B are distinct from nucleons and so justify calling them by a different name. This much follows without restrictions on the form of the Hamiltonian and proves the statement made above about the nature of the baryon produced in association with the M^0.

Associated production of these particles is thus a consequence of a superselection rule in the following sense. A superselection principle is said to operate with respect to a quantity whose eigenvalues distinguish certain states of a system when it is in principle impossible to measure the relative phase of these states, i.e., when there exists no observable with nonvanishing matrix elements between these states. As orbital parities are necessarily real, a parity conserving interaction forbids transitions between states whose relative intrinsic parity is imaginary. The superselection principle that applies therefore — as long as parity is conserved — is that with respect to states belonging to eigenvalues of the parity operator that differ by the square root of minus one.

Similar considerations lead to the conclusion that the charged spin-0 particle produced from a pion and a nucleon in association with the B must differ from the charged pion by an imaginary parity.

The theory contains two features that are characteristic of the strong interactions of K mesons and hyperons: 1) a neutral spin-0 particle with a distinct antiparticle, and 2) associated production. The M^0 will now be identified with K^0 and B with Σ or Λ, i.e., we are in effect saying that the K^0 and $\overline{K}^0$ differ from each other and — aside from mass — from the π^0 *only* in their intrinsic parities †. There is one feature of the strong interactions of these particles,

† A connection between the selection rules that govern the strong interactions of these particles and parity was noted by A. Pais [3]), who, however, based his considerations on a theory with an additional gauge group (hypercharge), which led him to certain conclusions that differ fundamentally from mine. The generalization of the parity operator to $P^2 = -1$ for K mesons has previously

namely the absence of the reaction $\pi+N \to \bar{K}^0+\Sigma$ when $\pi+N \to K^0+\Sigma$ is allowed, which seems at first to contradict this conjecture and in order to account for which consistency with charge independence has to be invoked; however, this apparent distinction between K^0 and $\bar{K}^0$ clearly depends on the *given* spectrum of pions and nucleons.

In this connection it is relevant to remark on a conceptual point regarding charge independence. The fact that it is the K^+ rather than the $\bar{K}^-$ (or both) that is produced in association with the Σ is from our point of view considered on equal footing with the absence of a negatively charged nucleon in the sense that neither empirical fact is assumed to form a partial basis for the explanation of the other, but rather both are supposed to be consequences of the same physical principle, which accounts for the particle spectrum as well as providing an additional constraint on the allowed interactions. In other words, it is the author's contention that whereas the physical basis for the latter two empirical facts is not as yet understood, that for associated production is the previously discussed superselection law for parity.

A consequence of the preceding consideration is that Λ and Σ^0 differ from n only by an imaginary parity. Similarly Ξ^0 differs from Σ^0 and Λ only by an imaginary parity and therefore from n only by a real parity, i.e., Ξ^0 and n must have opposite parities. Hence the parity of Ξ^0 relative to $\Sigma^0(\Lambda)$ must be the same as the parity of $\Sigma^0(\Lambda)$ relative to n:

$$\begin{aligned} &\eta^*(K^0)\eta(n)\eta^*(\Sigma^0) = \eta^*(K^0)\eta(\Sigma^0)\eta^*(\Xi^0) = \varepsilon_3, \\ &\eta^*(K^0)\eta(n)\eta^*(\Lambda) = \eta^*(K^0)\eta(\Lambda)\eta^*(\Xi^0) = \varepsilon_4, \\ &\eta(\Xi^0) = -\eta(n). \end{aligned} \tag{6}$$

We stress that in deriving the above relations use has been made only of the initial hypothesis that K^0 and $\bar{K}^0$ differ only in their parities and that therefore particles that differ — aside from mass — only in the way in which they can be produced, must have different parities †. The last equation in (6) is therefore not subject to any convention such as , e.g., that the parities of n and p are the same.

The theory thus admits particles that differ from one another only in their intrinsic parities and allows electromagnetic decay of the heavier of such

---

been considered by F. Gursey [4]) and H. Katsumori [5]) also within the framework of the strangeness theory or a modification thereof. An important difference between their results and those of the author is the possibility in the latter case of comparing the parity of the K^0, or more precisely of two K^0's, with the vacuum. This will become evident when the mechanism for fixing this parity is discussed. According to A. M. Brodskii and D. D. Ivanenko [6]), spin-0 particles with imaginary parity have also been considered by M. Mirianashvili [7]).

† It has been assumed, however, that space inversion transforms Λ and Σ^0 into themselves rather than into each other. The particles K_1 and K_2, as usually defined, do in fact transform into each other under space inversion.

parity multiplets into a lighter one when their relative parity is real †. The Ξ^0 lifetime may therefore be shorter than those characteristic of decays induced by the weak interactions. Because the strong (charge independent and parity conserving) interactions available to particles with different parities depend on the particle spectrum, the differences in the masses within a multiplet are not small in the sense of being due to electromagnetic interactions only.

Proceeding analogously, we find that the theory can accommodate additional parity multiplets consistent with the given spectrum of pions and nucleons, whose parities are

$$\eta^*(\mathrm{K}^0)\eta(\Sigma^-)\eta^*(\Xi^-) = \eta^*(\mathrm{K}^0)\eta(\Xi^-)\eta^*(\Omega^-) = \varepsilon_5,$$
$$\eta(\Omega^-) = -\eta(\Sigma^-), \quad \eta(\Delta^+) = -\eta(\Sigma^+), \quad \eta(\theta^+) = -\eta(\pi^+), \quad \eta(\tau^0) = +1. \quad (7)$$

The Ω, Δ and θ would be produced in reactions such as $\pi^- + \mathrm{p} \to \Xi^- + \theta^+$, $\mathrm{K}^- + \mathrm{p} \to \Omega^- + \theta^+$ and $\mathrm{p} + \mathrm{p} \to \Sigma^+ + \Delta^+$.

As mentioned earlier, the use of an intrinsic parity as part of the definition of a particle rather than merely as a consistent parity assignment is meaningful only if the parity can be fixed unambiguously, which in the case under consideration depends essentially on the possibility of comparing the parity of two K^0's with that of the vacuum. Because experimental results indicate that strong interactions are not of a nature that would allow such a comparison, the parity of the K^0 has to be fixed by its electromagnetic interaction; thus, two K^0's (or two $\overline{\mathrm{K}}^0$'s) in a relative S state must decay electromagnetically like a pseudoscalar particle, whereas a K^0 and a $\overline{\mathrm{K}}^0$ in a relative S state would decay like a scalar particle ††. The former is forbidden in a theory with strangeness.

The selection rules that follow from the preceding considerations are therefore not identical to those that result from strangeness conservation. Indeed, associated production is a consequence of a multiplicative quantum number in the former case ‡, whereas in the latter it is due to an additive one. Other reactions that are forbidden in the Gell-Mann-Nishijima formalism but allowed in ours are a) $\mathrm{N} + \mathrm{N}' \to \mathrm{Y} + \mathrm{Y}' + \gamma$'s, b) K (or $\overline{\mathrm{K}}$) $+ \mathrm{N} \to \mathrm{Y} + \gamma$'s, and c) $\mathrm{N} + \overline{\Xi} \to \pi$'s $+ \gamma$'s, where N is a nucleon and Y is a Λ or Σ.

Finally, it can be readily verified that in the decays of Λ, Σ's and K's into nucleons and pions the parity operator cannot commute with the transition

† These particles represent a partial realization of the four kinds of spinors considered by C. N. Yang and J. Tiomno [8]). It is partial because the existence of baryons with all four parities in each of the three charge states is apparently inconsistent with charge independence. The two members of a parity multiplet that differ by a real parity are clearly different in nature from the parity doublets considered by T. D. Lee and C. N. Yang [9]).

†† The electromagnetic interaction of the K^0 has been discussed by G. Feinberg [10]). The interaction considered by Feinberg cannot, however, account for the decay in question.

‡ The possibility that the selection rules observed in the strong interactions of hyperons and K mesons are associated with a multiplicative quantum number has been considered by B. D'Espagnat and J. Prentki [11]) and by W. Heisenberg and W. Pauli [12]).

operator because the relative intrinsic parities — as defined by the strong and electromagnetic interactions — of the initial and final states are imaginary. Hence the occurrence in the decay interaction of either of the two terms that transform with opposite sign under reflection — and therefore decay into states of even and odd orbital parity — is a priori equally likely. Interference between states of opposite parity will therefore occur in general unless a pseudoscalar quantity cannot be formed for other reasons †. We therefore conclude that parity cannot be conserved in the decays in question. The theory thus provides a simple explanation for the simultaneous breakdown in such non-neutrino decays of the domains of validity of parity conservation and of the conservation law that characterizes the strong interactions of the relevant particles.

It may be of interest to note that the transition operator S for a decay such as $K \to 2\pi$, in which as a consequence of conservation of angular momentum the final state is an eigenstate of parity, has the transformation property $PSP^{-1} = \pm iS$ under space inversion.

Present experimental data are in agreement with the results of the theory if the weak decay of Ξ^0 can compete with its electromagnetic decay to the extent that the former can be observed ††.

The verification of the consequences of the theory that differ from those predicted by strangeness would, in the author's opinion, indicate that the questions of the spectrum of strongly interacting elementary particles and charge independence are intimately related to those of space inversion and parity conjugation.

† It is well known that in certain cases the observation in distinct decay modes of even and odd parity states represents the maximum evidence for nonconservation of parity. See, e.g., T. D. Lee and C. N. Yang [13]).

†† An event interpreted as the weak decay of Ξ^0 has been observed by L. W. Alvarez *et al.* [14]).

References

1) G. C. Wick, A. W. Wightman and E. P. Wigner, Phys. Rev. **88** (1952) 101
2) G. Feinberg and S. Weinberg, Nuovo Cim. **14** (1959) 571
3) A. Pais, Proc. Rochester Conf. High-Energy Phys., 1957 (Interscience Publishers, New York 1957) p. ix–36
4) F. Gursey, Phys. Rev. Letters **1** (1958) 98
5) H. Katsumori, Nuovo Cim. **11** (1959) 612
6) A. M. Brodskii and D. D. Ivanenko, JETP **36** (1959) 911, see ref. 12 therein
7) M. Mirianashvili, Phys. Inst. Georgian SSR, no. 4 (1958)
8) C. N. Yang and J. Tiomno, Phys. Rev. **79** (1950) 495
9) T. D. Lee and C. N. Yang, Phys. Rev. **102** (1956) 290
10) G. Feinberg, Phys. Rev. **109** (1958) 1381
11) B. D'Espagnat and J. Prentki, Phys. Rev. **102** (1956) 1684
12) W. Heisenberg and W. Pauli, preprint
13) T. D. Lee and C. N. Yang, Brookhaven National Laboratory Report, NBL 443 (T-91), p. 34
14) L. W. Alvarez, P. Eberhard, M. L. Good, W. Graziano, H. K. Ticho and S. G. Wojcicki, Phys. Rev. Letters **2** (1959) 215

1.B

Nuclear Physics **21** (1961) 686—687; © *North-Holland Publishing Co., Amsterdam*

Not to be reproduced by photoprint or microfilm without written permission from the publisher

n—p POLARIZATION AND LOW ENERGY p—p PHASE SHIFTS

R. J. N. PHILLIPS

Atomic Energy Research Establishment, Harwell, Berks.

Received 3 October 1960

Abstract: It is argued that n—p polarization at 90° c.m. depends only on $T = 1$ phase shifts to a fair approximation, over a range of low energies. Assuming charge independence, this helps to determine p—p phase shifts.

There are not enough data at present to determine p—p phase shifts directly at the lower energies [1, 2, 3]). For example, MacGregor [1]) exhibits four distinct families of solutions below 20 MeV: within each family, the phase shifts are only loosely fixed. The present note suggests that n—p polarization at 90° c.m. contains further useful information about the isobaric spin $T = 1$ phase shifts.

Consider the region in which S phase shifts are large (say $|\sin\delta| > 0.8$) and all others relatively small (say $|\sin\delta| < 0.2$); this appears [1–5]) to be 4 MeV $\leqq E_{\text{lab}} \leqq$ 20 MeV. Here the n—p cross section at 90° c.m. is dominated by S-wave scattering. Also the $^3S_1$—$^3D_1$ mixing parameter ε^1 (Blatt-Biedenharn notation, with Stapp sign convention [6])) appears to be rather small [4, 5]) and will be neglected for the present. Thus we write

$$\sigma(90°) \approx \frac{1}{4k^2}\{\sin^2\delta_0 + 3\sin^2\delta_0^1\}. \tag{1}$$

Here k is the relative momentum, δ_L and $\delta_L{}^J$ denote singlet and triplet phase shifts respectively, and we use units $\hbar = c = 1$. The leading corrections to (1) come from S—D and P—P terms, and from ε^1 (in second order).

The n—p polarized cross section at 90° c.m. is dominated by S—P interference. Ignoring $^3P_2$—$^3F_2$ mixing for the present, we have,

$$P(90°)\sigma(90°) \approx \frac{1}{4k^2}\{-2[\delta_0{}^1, \delta_1{}^0] - 3[\delta_0{}^1, \delta_1{}^1] + 5[\delta_0{}^1, \delta_1{}^2]\}, \tag{2}$$

where $[a, b]$ denotes $\sin a \sin b \sin(a—b)$.

$P(90°)$ will depend only on ^3P phase shifts if we make two more approximations:

(i) Replace $\sin(\delta_0{}^1 — \delta_1{}^J)$ by $\sin\delta_0{}^1$ in (2). We might expect this step to be worst at the upper energies; however, near 20 MeV $\delta_0{}^1$ is near 90°, and this approximation is quite good.

(ii) Replace δ_0 by δ_0^1 in (1). This appears rather crude; however, in the region of interest the error introduced is not more than 10 %.
Then we have, to an accuracy of perhaps 20 % at worst,

$$P(90°) \approx \tfrac{1}{4}\{-2 \sin \delta_1^0 - 3 \sin \delta_1^1 + 5 \sin \delta_1^2\}. \quad (3)$$

This approximation can be improved in several ways. F-waves and P—F mixing can be introduced and will appear as extra terms in (3). The approximation (ii) can be improved if the S phase shifts are known even roughly. For instance, at 20 MeV $\delta_0 \approx 50°$ [1]) and $\delta_0^1 \approx 90°$ (effective range theory); it is thus a better estimate to put $\sin^2\delta_0 \approx 0.6 \sin^2\delta_0^1$, giving a correction factor 1.1 in (3). Also in this way we can extend the region of interest down to zero energy. A rough estimate of ε^1 could be used too: in first order it would give a correction $(1+\varepsilon^1/\sqrt{2})$ to (2) and (3).

The Harwell time-of-flight experiments have given preliminary values for n—p polarization in the range 20—120 MeV [7]). The 20 MeV data are inconclusive, but the trend at neighbouring energies suggests the value

$$P(90°; 20 \text{ MeV}) = 0.035 \pm 0.015. \quad (4)$$

If we simply take the sign of $P(90°)$ as established, MacGregor's phase shift families II and IV at 19.8 MeV [1]) are eliminated (apart from a few extreme cases, which fit the p—p data poorly). It has been argued [1]) that families III and IV are inconsistent with nuclear potential models: if this is accepted, we are left with family I only.

If furthermore we take the estimate (4) at face value, and apply eq. (3) with the suggested correction factor 1.1, it places useful restrictions on the families I and III. Referring to MacGregor's table of examples, δ_2 is determined to within about 0.05° for given δ_0 (apart from the internal uncertainty of each solution), but a range of δ_0 is still possible.

Finally, we remark that if the splitting of the ^{3}P phase shifts is interpreted in terms of "effective" tensor and $\mathbf{L} \cdot \mathbf{S}$ potentials, through the Born approximation [5, 6]), $P(90°) \neq 0$ indicates a non-vanishing $\mathbf{L} \cdot \mathbf{S}$ effect in the region considered.

The author is grateful to the time-of-flight group at the Harwell cyclotron for communicating their preliminary n—p results.

References

1) M. H. MacGregor, Phys. Rev. **113** (1959) 1559
2) M. H. MacGregor, M. J. Moravcsik and H. P. Noyes, University of California, report UCRL-5582-T (1959)
3) J. Iwadare, University of Pennsylvania, preprint (to be published)
4) J. L. Gammel, R. S. Christian and R. M. Thaler, Phys. Rev. **105** (1957) 311
5) J. L. Gammel and R. M. Thaler, Phys. Rev. **107** (1957) 291, 1337
6) H. P. Stapp, T. Ypsilantis and N. Metropolis, Phys. Rev. **105** (1957) 302
7) P. H. Bowen, G. C. Cox, G. B. Huxtable, A. Langsford, J. P. Scanlon and J. J. Thresher, private communication

2.H

Nuclear Physics **21** (1960) 688—695; © *North-Holland Publishing Co., Amsterdam*

Not to be reproduced by photoprint or microfilm without written permission from the publisher

COULOMB EXCITATION OF Ge^{74} AND Ge^{76}

W. R. WISSEMAN and R. M. WILLIAMSON

Department of Physics, Duke University, Durham, N. C. †

Received 29 July 1960

Abstract: Deuterons and protons with energies from 3.5 to 4.0 MeV were used to excite the 598-keV level in Ge^{74} and the 564-keV level in Ge^{76}. The scattered particles were studied at angles from 75° to 150° with a magnetic analyzer by using photographic plate detection. The applicability of Coulomb excitation theory in this region of atomic number and incident energy was tested by measuring the energy dependence of the deuteron excitation cross sections for both nuclei, the angular distribution of inelastically scattered deuterons for Ge^{74} and the ratios of the deuteron to the proton excitation cross sections. These data indicate that Coulomb excitation theory may be applied for deuterons of less than 3.5 MeV and protons of less than 4.0 MeV. The values of the reduced transition probability, $B(E2)$, of Ge^{74} and Ge^{76} are 0.32 ± 0.03 and 0.29 ± 0.03, respectively. The $B(E2)$ value derived from 4.0-MeV deuteron data for Ge^{74} was 30 % higher than the above value. Part of this discrepancy may be due to departures from Rutherford scattering of the elastically scattered deuterons, as Rutherford scattering was assumed in deriving the inelastic cross sections.

1. Introduction

The Coulomb excitation process has been studied extensively both experimentally and theoretically, and the exctitation mechanism is well known [1–3]). The unified model of Bohr and Mottelson [4, 5]) has been successfully used to predict values of the intrinsic nuclear quantity, $B(E2)$, which is the reduced transition probability for electric quadrupole excitation. Three methods have been used to study Coulomb excitation and to obtain $B(E2)$. Measurements of the gamma rays and conversion electrons which result from excitation have been made for most nuclei. The results of these two methods are tabulated in the review article by Alder *et al.* [2]). The third method, which has been less widely used, involves measurement of the inelastically scattered projectiles. This method has been used primarily for rare earths and heavier elements [6–9a]). The Coulomb excitation cross section is determined in this method by comparing the number of inelastically scattered particles with the number elastically scattered and by assuming that the elastic scattering follows the Rutherford law. It is unnecessary to know the spectrometer solid angle, internal conversion coefficients, target thickness, and stopping power in order to obtain the excitation cross section and $B(E2)$. Knowledge of these quantities is necessary in order to obtain absolute cross sections by the other two methods. The main

† This work was supported by the U. S. Atomic Energy Commission.

disadvantages in this method are the necessity of assuming the Rutherford law for the elastically scattered particles, the problem of background reduction, the presence of elastic impurity peaks, and the very low yields from thin targets.

The object of the present experiment was to study the applicability of Coulomb excitation theory to the protons and deuterons of about 4-MeV energy, which were inelastically scattered by medium-weight nuclei. This energy is necessary in order to get reasonable yields of inelastically scattered particles from thin targets. Separated isotopes of Ge^{74} and Ge^{76} were chosen because studies of the gamma rays resulting from Coulomb excitation by alpha particles [10,11]) have shown that these isotopes have relatively high values of $B(E2)$. Measurements of the energy dependence of the deuteron excitation cross sections for both nuclei, the angular distribution of the inelastically scattered deuterons for Ge^{74}, and the ratios of the deuteron to the proton excitation yields were made in order to test the predictions of classical Coulomb excitation theory [2]).

These data may differ from the predictions of classical Coulomb excitation theory by amounts suggested by figure II.6 of ref. [2]), which shows the error made by using the classical instead of the quantum mechanical calculation for *total* cross sections. This error is between 3 and 7 % for the values of η_i (defined in ref. [2])) between 4 and 2.5 which apply to our experimental conditions. A very recent quantum mechanical calculation [11a]) of the differential cross section for Coulomb excitation indicates that the correction to the classical cross section at back angles is between 0 and 4 % ($4 > \eta_i > 2.5$) and that the form of the angular distribution at angles greater than 60° is within a few percent of the classical calculation.

The data reported here may also differ from Coulomb excitation theory because of the possibility of compound nucleus formation and direct inelastic scattering. The penetrabilities for 4 MeV protons and deuterons on germanium are about 4×10^{-3} and 4×10^{-4}, respectively. However, the possible effects of (p, n) competition and of direct inelastic scattering cannot be predicted.

The departures from Rutherford scattering for protons and deuterons on germanium have not been measured. However, work done at the University of Rochester [12,13]) on elements lighter than germanium indicates that 4 MeV protons should show little deviation from Rutherford scattering, and that 4 MeV deuteron scattering yields may fall 10 to 15 % below the Rutherford values at back angles. This would make experimental cross sections based on Rutherford scattering of deuterons too high.

2. Apparatus and Procedure

The Duke University 4-MeV Van de Graaff accelerator was used to provide bombarding particles which were magnetically deflected 17.5° for momentum

separation. The spread in the 4-MeV beam energy due to the width of the defining slits was about 10 keV. The 60° magnetic analyzer used to study the reaction products and the 25° to 155° pillbox target chamber have been described previously [14,15]). The target chamber contains a Faraday cup which is used for integration of the incident beam. The magnet chamber and the magnet entrance and exit tubes contain a set of 0.25 mm thick aluminium baffles which were added in order to reduce the background due to scattering within the magnet. These baffles are spaced approximately 7.6 cm apart along the path of the scattered particles, and they allow an acceptance solid angle of 0.0033 sr. The coupling section between the target chamber and the magnet also contains baffles which are located about 10 cm from the target.

Two detection methods can be used with the magnetic analyzer. The scintillation detector has been described previously. In this experiment it could be used only for preliminary measurements because of the low intensity of the Coulomb excitation groups. The magnet exit tube was modified so that the scintillation detector could be easily interchanged with the photographic plate chamber which was necessary for this work. The photographic plates were 5 cm × 30 cm glass plates which were coated with a 40 μm thick Ilford C2 emulsion. The plates were covered by 25 μm thick aluminium when protons were used as the projectiles in order to shorten the tracks; no cover was used when deuterons were the projectiles because of the higher stopping power for deuterons. The value for the dispersion of the magnetic analyzer previously reported [15]) has been modified slightly because of the more accurate photographic plate measurements. The new value is 1.06 ± 0.01 mm per 0.1 % momentum change perpendicular to the median ray. The focal plane makes an angle of 64.4° with the plane normal to the median ray. The energy spread across a 30 cm plate which lies along the focal plane is 24 % of the central energy.

The targets used in this experiment were evaporated under vacuum on formvar film. Since separated isotopes were used, a conical tantalum boat was used for directional evaporation, and it was surrounded by a glass box that was used to collect the isotope which did not strike the formvar. About 16 mg of the isotope were used to obtain targets 5—15 keV thick, and about 80 % of the isotope was recovered from the glass by scraping it with a razor blade.

The tracks on the photographic plates were counted by using a binocular microscope with a 5× eyepiece and a 43× objective. The diameter of the field of view was $\frac{1}{2}$ mm. In general, the plates were scanned by counting the tracks within the field of view along 4-cm strips which were perpendicular to the energy dispersion direction on the plate. A strip count was made every 2 mm along the plate except at the peaks. When the peaks of interest were located, the complete peak was counted.

The total amount of charge collected during each place run varied from 1000 to 2500 μC, and the beam currents were approximately 0.1 μA. In order to check

the energy and intensity of the elastic group, the target was examined before and after each run with the scintillation counter. A shutter was used to prevent the high intensity elastic group from hitting the plate continuously. The shutter was opened for a total of about 20 μC in 2.5 or 5 μC intervals regularly spaced throughout the run so that variations in current integration would average out.

The differential cross section for inelastic scattering was obtained by multiplying the calculated differential Rutherford cross section (for the centre-of-mass system incident energy and scattering angle) by the ratio of the area under the inelastic peak (minus background) to the area under the elastic peak. The small difference in the centre-of-mass corrections for the elastic and inelastic groups was neglected. The relative amount of charge collected in each case was taken into account along with the abundance of the isotope of interest. The background under the inelastic peaks was obtained from the average of the background in a number of strips on either side of the peak. The background consists primarily of scattered particles which arise from internal scattering of the strong elastic groups from the target element and from the carbon and oxygen in the target backing. Elastic peaks due to impurities may also contribute to the background if they are near the inelastic peaks. The use of baffles inside of the magnetic spectrometer and the use of a small acceptance solid angle decreased the background.

3. Results and Conclusions

An example of the photographic plate data which were obtained in this experiment is shown in fig. 1. This is a momentum spectrum for Ge^{74} (97.9 % abundant), and it was taken by using 3.8 MeV incident deuterons and a scattering angle of 140°. The elastic peak, which is labeled (0), was scaled down by a

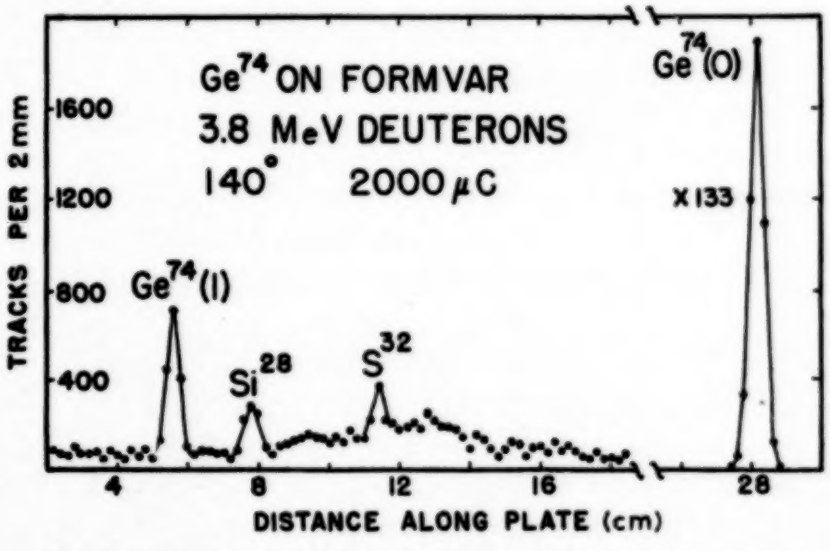

Fig. 1. Momentum spectrum of deuterons scattered from Ge^{74}.

factor of 133 by using the Rutherford shutter. The 598 keV excited state (1) is also shown along with Si^{28} and S^{32} impurity elastic peaks. These data show a Rutherford-peak to background ratio of about 3000 to 1; more recent data taken with extra baffles added close to the target show an improved ratio of about 5000 to 1.

An angular distribution of the inelastically scattered particles from the 598-keV level in Ge^{74} was taken with 3.8-MeV deuterons as the projectiles. Measurements were made at 75°, 105° and 140° in the laboratory system; the results of these measurements are shown in fig. 2 which is a plot of the differential cross section as a function of the angle in the centre-of-mass system. The

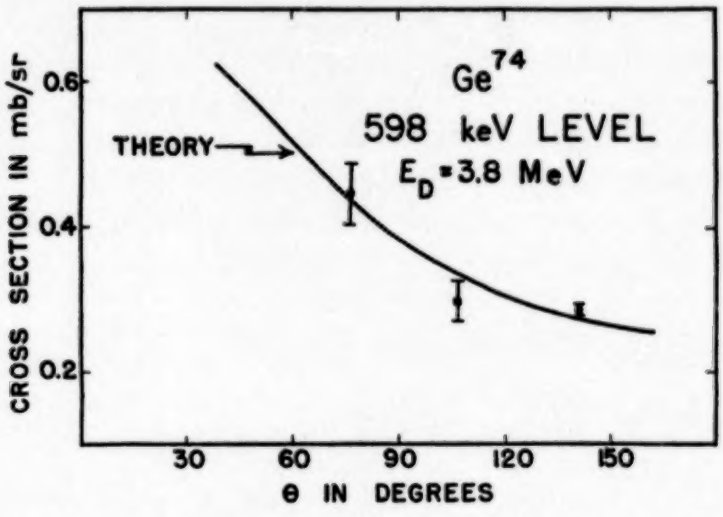

Fig. 2. Angular distribution of the inelastically scattered deuterons from Ge^{74}.

errors which are shown here and in the tables which follow are standard deviations, and they include both statistical errors and estimated experimental errors. The largest contribution is from stastistical errors which are usually about ± 10 %. Current integration and knowledge of isotopic abundances are reliable to about ± 1 %. An estimated error of $\pm 1°$ in the scattering angle causes errors in the differential cross section ranging from ± 1 % at large angles to ± 5 % at 75°. The effects of other possible experimental errors are thought to be negligible. The theoretical curve was normalized to the data for the best fit, and it is the Coulomb excitation differential cross section in barns/steradian:

$$\frac{\mathrm{d}\sigma_{\mathrm{E2}}}{\mathrm{d}\Omega} = c_{\mathrm{E2}}(E_{\mathrm{MeV}} - \Delta E'_{\mathrm{MeV}})\, B(\mathrm{E2})\, \frac{\mathrm{d}f_{\mathrm{E2}}(\theta, \xi, \eta_i)}{\mathrm{d}\Omega}.$$

$B(\mathrm{E2})$ has units of $e^2 \times 10^{-48}$ cm^4. All of the above quantities are defined in ref. [2]). The classical values of $\mathrm{d}f_{\mathrm{E2}}(\eta_i \to \infty)$ listed in table II.8 of ref.[2]) were used to calculate this curve. (ξ is 0.336 and η_i is 3.7 for these data.) One can conclude from these data that the relative differential cross section is within 5 to

10 % of agreement with classical theory. It seems evident that the effects on these data of possible competing reaction processes are negligible.

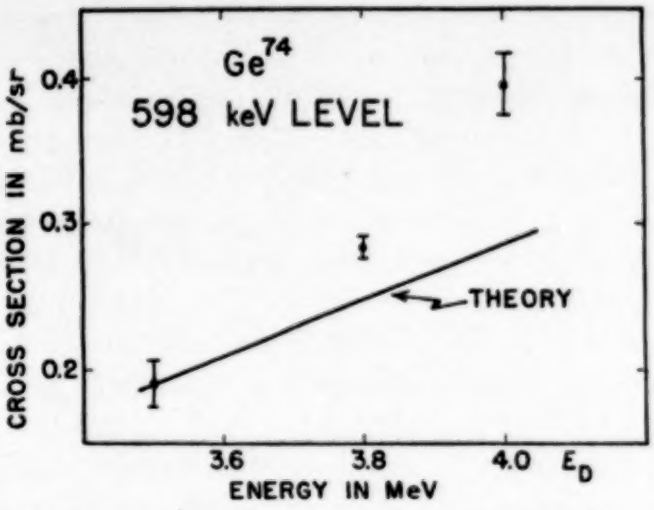

Fig. 3. Energy dependence of the cross section for the excitation of Ge^{74} with deuterons.

The energy dependence of the differential cross section for excitation of Ge^{74} is shown in fig. 3. These data were taken with incident deuterons with energies of 3.5, 3.8 and 4.0 MeV at angles of 150°, 140° and 135°, respectively. It was necessary to use slightly different angles in taking the data in order to avoid elastic impurity peaks. These data were normalized to 140° in order to test the energy dependence of the cross section. The theoretical curve was normalized to the data at 3.5 MeV since less deviation from theory was expected at this energy. The experimental points deviate appreciably from the theoretical curve with deviations of about 10 % at 3.8 MeV and 30 % at 4.0 MeV. As discussed in the introduction, 10 to 15 % of the deviation at 4.0 MeV could be explained by departures from Rutherford scattering. Since this conclusion is based on an

TABLE 1

Results for Ge^{74} and Ge^{76}

Nucleus and ΔE	E_{MeV} and projectile	θ_{lab}	$\frac{d\sigma_R}{d\sigma_{E2}}$	$\frac{d\sigma_{E2}}{d\Omega}$ (mb/sr)	$B(E2)$ ($e^2 \times 10^{-48}$ cm^4)
Ge^{74} 598±6 keV	3.5 d	150°	710	0.18	0.32±0.03
	3.8 d	140°	430	0.29	0.38±0.02
	3.8 d	105°	870	0.30	
	3.8 d	75°	1360	0.45	
	4.0 d	135°	300	0.41	0.43±0.03
	4.0 p	150°	590	0.31	0.32±0.04
Ge^{76} 564±6 keV	3.5 d	145°	710	0.19	0.31±0.03
	3.8 d	130°	480	0.30	0.34±0.03
	3.8 p	150?	700	0.15	0.28±0.04

extrapolation from elastic scattering data taken on lighter elements [12]), it is not a firm one. There is also the possibility of appreciable direct inelastic deuteron scattering at 4.0 MeV.

The results which have been obtained for Ge^{74} and Ge^{76} are shown in table 1. The experimentally determined ratios of the differential Rutherford cross section to the differential Coulomb excitation cross section include corrections for the relative percentage of the isotope of interest that is present in the target. The calculated values for the differential Coulomb excitation cross section and the values of $B(E2)$ include centre-of-mass corrections and the classical to quantum-mechanical correction for the total cross section shown in fig. II.6, ref. [2]).

The incident deuteron energy dependence seen in fig. 3 is also shown in table 1. However, it is most interesting that the $B(E2)$ values obtained with protons of 3.8- and 4.0-MeV energy are in good agreement with the 3.5-MeV deuteron data which should be least subject to the complications discussed in the introduction. We may therefore conclude that the effects of the competing proton reactions and the deviations of proton elastic scattering from Rutherford are both small. The best values for $B(E2)$ obtained in this experiment seem to be the proton values and the 3.5-MeV deuteron values.

TABLE 2

Comparison of results with gamma-ray measurements

	Nucleus	ΔE (keV)	$B(E2)$ ($e^2 \times 10^{-48}$ cm^4)
Duke University	Ge^{74}	598±6	0.32±0.03
	Ge^{76}	564±6	0.29±0.03
Temmer and Heydenburg [10])	Ge^{74}	593±6	0.25 ±0.04
	Ge^{76}	566±6	0.23 ±0.04
Stelson and McGowan [11])	Ge^{74}	600±6	0.317±0.008
	Ge^{76}	576±6	0.263±0.008

Table 2 shows a comparison of the results obtained here with the results of gamma-ray measurements of germanium excited by 7-MeV alpha particles [10]) and 3-MeV to 10-MeV alpha particles [11]). Both the energies of the excited states and the values of $B(E2)$ are in reasonable agreement with the gamma ray measurements. These data show that Ge^{74} has the higher $B(E2)$ value.

It is seen from our data that 3.5 MeV deuterons and 4.0 MeV protons may be used to obtain $B(E2)$ values of medium weight nuclei with at least 10 % accuracy. It is also seen that competing nuclear reactions and deviations from Rutherford scattering are just beginning to become important here. These factors make it difficult to study the accuracy of Coulomb excitation theory for the small values of η_i which apply to these data. Our data *suggest* that the

departures from classical theory are not larger than the predictions of quantum mechanical calculations. It is clear that further careful studies of elastic scattering angular distribution will be most helpful. The major advantage of using light, instead of heavy, projectiles for Coulomb excitation of medium weight nuclei would appear to be the improved ability to resolve closely spaced levels.

It is interesting that there is some indication that the (d, d') reaction proceeds partly by a process other than Coulomb excitation at 4.0 MeV, while the (p, p') reaction apparently does not show a second process even though the protons penetrate the Coulomb barrier much more easily than do the deuterons. The above effect could be due to a process in which only the neutron in the deuteron enters and leaves the target nucleus.

The authors would like to thank Dr. Otto Meier, Jr. and Mr. N. R. Fletcher for their help with the experimental work. We also wish to express our appreciation to Drs. H. W. Lewis, M. M. Duncan, and E. M. Bernstein for their helpful discussions of the results of this experiment.

References

1) N. P. Heydenburg and G. M. Temmer, Annual review of nuclear science (Annual Reviews Inc., Stanford, 1956) vol. 6, p. 77
2) Alder, Bohr, Huus, Mottelson and Winther, Revs. Mod. Phys. **28** (1956) 432
3) R. Huby, Reports on progress in physics, ed. by A. C. Strickland (The Physical Society, London, 1958) vol. 21, p. 59
4) A. Bohr, Mat. Fys. Medd. Dan. Vid. Selsk. **26**, No. 14 (1952)
5) A. Bohr and B. R. Mottelson, Mat. Fys. Medd. Dan. Vid. Selsk. **27**, No. 16 (1953)
6) B. Elbek and C. K. Bockelman, Phys. Rev. **105** (1957) 657
7) Elbek, Nielsen and Olesen, Phys. Rev. **108** (1957) 406
8) R. D. Sharp and W. W. Buechner, Phys. Rev. **109** (1958) 1698
9) Ramšak, Olesen and Elbek, Nuclear Physics **6** (1958) 451
9a) Bernstein and Skurnik, to be published
10) G. M. Temmer and N. P. Heydenburg, Phys. Rev. **104** (1956) 967
11) P. H. Stelson and F. K. McGowan, Annual progress report Oak Ridge National Laboratory, ORNL-2910 (1960) p. 12
11a) J. Bang, Mat. Fys. Medd. Dan. Vid. Selsk. **32**, No. 5 (1960) 1
12) I. Slaus and W. Parker Alford, Phys. Rev. **114** (1959) 1054
13) Charles A. Preskitt, Jr. and W. P. Alford, University of Rochester Report NYO-2172 (1958)
14) Otto Meier, Jr., Doctoral Dissertation Series (University Microfilms, Ann Arbor) no. 23 (1957) 618
15) Meier, Fletcher, Wisseman and Williamson, Rev. Sci. Instr. **29** (1958) 1004

6.C

Nuclear Physics **21** (1960) 696; © *North-Holland Publishing Co., Amsterdam*

Sign Convention for Particle Polarization

At the recent International Symposium on Polarization Phenomena of Nucleons held in Basle, the following convention was unanimously agreed upon regarding the sign of the polarization of particles taking part in any nuclear reaction:

If $\mathbf{k}_1$ represents the propagation vector of the incident particle and $\mathbf{k}_0$ the propagation vector of the outgoing particle, particles with spin pointing in the direction $\mathbf{k}_1 \times \mathbf{k}_0$ are to be considered as having positive polarization. This convention was first used by Wolfenstein. During the conference it was called the Basle convention.

10.D *Nuclear Physics* **21** (1960) 697—698; © *North-Holland Publishing Co., Amsterdam*

BOOK REVIEWS

J. SHARPE, B. Sc., A.M.I.E.E., *Nuclear Radiation Measurements* (Temple Press, London 1960. 71 p. 12s. 6d.)

This book in the series of monographs on nuclear-engineering subjects treats the methods of detecting nuclear radiation, dealing but little with problems more complicated than the mere counting of activities. It is mentioned that it is possible to measure the maximum energy of a beta spectrum by means of absorbers and to measure the gamma spectrum with a scintillation detector and a pulse-height analyzer. But the whole group of magnetic spectrometers is omitted although magnetic beta spectrometers are commercially available at a price comparable to that of a multi-channel pulse-height analyser.

Chapter two gives descriptions of the basic reactions of matter to nuclear radiation, all ending up with an ionization and a description of the movements of charged particles in matter.

Chapter three shows how these effects are used in general in detectors, and chapters four and five give a survey of ancillary equipment and the practical performance of the various kinds of detectors. These two chapters are so compressed in form that they are merely a list of definitions of the words, explained by means of a few figures — but a carefully worked-out list of references to all subjects mentioned in the text gives the reader an opportunity of going directly to the leading articles in the field.

It is my impression that this book fulfils its aim of giving a broad description of nuclear-radiation detection meant for persons who do not actually work in the field.

J. Thomas

M. DUQUESNE, R. GREGOIRE et M. LEFORT, *Travaux pratiques de physique nucléaire et de radiochimie*: Détection des rayonnements et méthodes d'étude de la structure nucléaire (Masson et Cie, Paris 1960. 324 pages. 39 N.F.)

This book gives detailed descriptions of 40 experimental exercises for students of nuclear physics and chemistry at the Faculté des Sciences de Paris. However, these are only the bones, on which is much flesh, so that the book gives a comprehensive account of some of the methods in experimental nuclear physics.

The introduction reviews the structure of the atom (11 pages), the structure of the nucleus (11 pages) and the interaction between different kinds of radiation and matter (21 pages).

Part I, "Méthodes de détection des rayonnements nucléaires", deals with the ionization chamber, the pulsed ionization chamber, the laws of statistics, the G.M. counter, the proportional counter, the scintillation counter, and nuclear emulsions. For example the ionization chamber: First the general principle is discussed and various types of chamber are mentioned. Then follows a description of an actual chamber, a quadrant electrometer and an arrangement for using the piezo-electricity of quartz in compensating the ionization current. Finally the procedure for measuring the intensity of a Po-source (Exercise I.1) is given in detail. Exercise I.2 consists in the measurement of a Bragg curve by means of another ion chamber. Exercise I.3 uses an "Electroscope Laborde" for measuring a radioactive period.

Part II, "Méthodes d'étude de la structure nucléaire", is similar in composition. Among the subjects treated are α, β and γ spectroscopy, coincidence methods, measurements of conversion coefficients, angular correlations, and excitation functions. Examples of exercises: IX.1: Measurement of a conversion coefficient by means of β—e^- coincidences. XI.1: Nuclear reactions by 12 MeV protons on copper. XII: The Szilard-Chalmers effect. XIII.2: The speed of isotopic exchange.

In Appendix I (24 pages) R. Devoret writes about biological effects of and protection against radiation.

The book is written in a way which will probably highly stimulate the interest of young students. It will also be useful for others interested in radiation measurements, for instance those using radioactive isotopes in industry and research. There are numerous illustrations. Although the language is mostly clear, there are many obscure passages. Besides, many misprints and small inaccuracies are found which may perplex the untrained reader. For instance, two symbols are sometimes used for the same thing almost simultaneously, and conversely it happens that a letter has two meanings in the same figure (τ in fig. 197). Rather often indices are erroneously interchanged. In the description of the method of delayed coincidences the wrong pulse is delayed. Dealing with the collective model, the text says $\mathbf{I} = \mathbf{R}+\mathbf{J}$, whereas the accompanying figure shows $\mathbf{J} = \mathbf{R}+\mathbf{I}$. Exercise X is Coulomb excitation (by means of α-particles) of Au^{198} (though Au^{197} is bombarded). And so on. In spite of this the book can be highly recommended.

N. O. Lassen

AUTHOR INDEX

ABDURAZAKOV, A., K. GROMOV, B. DALKHSUREN, B. DŽELEPOV, I. LEVENBERG, A. MURIN, YU. NORSEYEV, V. POKROVSKY, V. CHUMIN and I. YUTLANDOV, The decay chain $Yb^{164} \rightarrow Tm^{164} \rightarrow Er^{164}$ 164

ALBRIDGE, R. G. and J. M. HOLLANDER, The decay of neptunium-238 . 438

ALMQVIST, E., *see* KUEHNER

ARBMAN, E., S. BJØRNHOLM and O. B. NIELSEN, Levels in Th^{228} excited in the electron capture decay of Pa^{228}. 406

BARFIELD, W. D., *see* RABSON

BARUT, A. O. and K. H. RUEI, Extra solutions of the dispersion relations and resonance scattering. 300

BAUER, RUDOLF W., *see* DEUTSCH

BELL, R. E., *see* PEDERSON

BERNARD, D. L., *see* RABSON

BIEDENHARN, L. C., *see* PHILLIPS

BISWAS, S. N. and V. GUPTA, Effective range for K^+-nucleon interaction from dispersion relations 137

BJØRNHOLM, S., *see* ARBMAN

BODMER, A. R., Isotope shift calculations for non-uniform charge distributions. 347

BOLLINGER, L. M., *see* CARPENTER

BONNER, T. W., *see* RABSON

BROCKMAN, K. W., Jr., *see* OERS

BROMLEY, D. A., *see* KUEHNER

CARPENTER, R. T. and L. M. BOLLINGER, Parameters and gamma-ray spectra of neutron resonances in the isotopes of mercury 66

CERINEO, M., *see* CINDRO

CHUMIN, V., *see* ABDURAZAKOV

CINDRO, N., M. CERINEO and A. STRZALKOWSKI, Elastic scattering of 13 MeV deuterons on aluminium 38

COSTELLO, D. G., *see* DAHL

CZYŻ, W. and K. GOTTFRIED, The momentum distribution in a dilute Fermi gas at zero temperature 676

DAHL, P. F., D. G. COSTELLO and W. L. WALTERS, Aluminium (p, γ) resonances with H_1^+, H_2^+ and H_3^+ ions 106

DALKHSUREN, B., *see* ABDURAZAKOV

DECONNINCK, G. and A. MARTEGANI, Angular correlation in $C^{12}(n, n'\gamma)C^{12}$ at 14 MeV 33
DELOFF, A. and J. WRZECIONKO, Directional correlation of mesons in a cascade decay of baryons, resulting from a baryon-baryon reaction . . 237
DENNERY, P. and N. M. KROLL, On conservation of probability in the Lee model 276
DEUTSCH, M. and R. W. BAUER, Spins of the isomeric states of Hf^{178} and Hf^{180} 128
DOMOKOS, G. and A. SEBESTYÉN, Optical model analysis of negative pion-proton elastic scattering between 1.4 and 6.8 GeV 157
DŽELEPOV, B., *see* ABDURAZAKOW
EL BEDEWI, F. A. and M. A. EL WAHAB, Stripping analysis of the reaction $Na^{23}(d, p)Na^{24}$ 49
EL WAHAB, M. A., *see* EL BEDEWI
EVANS, L. E. and T. FULTON, Asymptotic conditions in quantum electrodynamics 492
FRIEDLÄNDER, E. M., Remarks on the energy distribution of mesons created in high-energy nuclear collisions 220
FULTON, T., *see* EVANS
GIRGIS, R. K., *see* RICCI
GIVENS, W. W., *see* RABSON
GOLDFARB, L. J. B. and R. C. JOHNSON, Selection rules and correlations for polarization in stripping and direct processes 462
GORGÉ, V., W. KOCH, W. LINDT, M. M. NIKOLIĆ, S. SUBOTIĆ-NIKOLIĆ and H. WINZELER, Hypernuclei produced by K^- interactions in nuclear emulsions. (II). General characteristics and non-mesic decays 599
GOTTFRIED, K., *see* CZYŻ
GRIFFY, T. A., *see* PHILLIPS
GROMOV, K., *see* ABDURAZAKOW
GUPTA, V., *see* BISWAS
HEBBARD, D. F. and J. L. VOGL, Elastic scattering and radiative capture of protons by C^{13} 652
HODGSON, P. E., Optical model analysis of the scattering of 96 MeV neutrons by nuclei 21
HODGSON, P. E., The elastic scattering of helium 3 by medium weight nuclei 28
HODGSON, P. E., *see* JOHANSSON
HOLLANDER, J. M., *see* ALBRIDGE
JANCOVICI, B., A model for the calculation of the optical potential in some finite nuclei 256
JEAN, M., Note sur l'interprétation collective des deux premiers niveaux $2+$ des noyaux pairs 142

JOHANSSON, A., G. TIBELL, K. PARKER and P. E. HODGSON, The elastic scattering of 160 MeV protons from lithium, aluminium, indium and gold 383
JOHNSON, R. C., *see* GOLDFARB
KOCH, W., *see* GORGÉ
KOMAR, A. and ABDUS SALAM, Renormalization problem for vector meson theories 624
KROLL, N. M., *see* DENNERY
KUEHNER, J. A., E. ALMQVIST and D. A. BROMLEY, Reaction mechanism studies on Si^{28}(d, p)Si^{29}. (II). Interference effects 555
KUMAR, KAILASH, Validity of the two-particle approximation in the many-body problem 99
LEVENBERG, I., *see* ABDURAZAKOV
LIESHOUT, R. VAN, *see* RICCI
LINDT, W., *see* GORGÉ
MAINSBRIDGE, B., The angular distributions of the gamma radiation from the Li^7(p, γ)Be^8 reaction from $E_p = 200$ keV to 1100 keV . . . 1
MANI, G. S., T. A. TOMBRELLO and D. A. A. S. N. RAO, Neutron cross sections in chlorine 344
MARCU, M. and M. SPÎRCHEZ, A Monte-Carlo calculation of the production spectrum of mesons in jets 526
MARTEGANI, A., *see* DECONNINCK
MORINAGA, H., *see* TAKAHASHI
MOSZKOWSKI, S. A., *see* SAWICKI
MOSZKOWSKI, S. A., *see* SOOD
MURIN, A., *see* ABDURAZAKOV
NARASIMHAIAH, H. and M. L. POOL, Radioactive decay of Tm^{167} 340
NATHAN, O. and V. I. POPOV, Coulomb excitation with 14—20 MeV α-particles: double excitations and systematics of vibrational states in the rare earth region 631
NEWTON, J. O., Resonances in the reactions Si^{28}+p 529
NIELSEN, O. B., *see* ARBMAN
NIKOLIĆ, M. M., Hypernuclei produced by K^- interactions in nuclear emulsions. (I). Mesic decays 595
NIKOLIĆ, M. M., *see* GORGÉ
NORSEYEV, YU., *see* ABDURAZAKOV
OERS, W. T. H. VAN, and K. W. BROCKMAN, Jr., Elastic scattering of 24.4 MeV deuterons by protons 189
PAPPAS, A. C. and G. RUDSTAM, An approach to the systematics of delayed neutron precursors 353
PARKER, K., *see* JOHANSSON
PEDERSON, E. C. B. and R. E. BELL, The half-life of the first excited

state of Tl^{203} 393
PHILLIPS, G. C., T. A. GRIFFY and L. C. BIEDENHARN, The significance of the generalized density of states function for nuclear spectra 327
PHILLIPS, G. C., *see* SPENCER
PHILLIPS, R. J. N., n—p polarization and low energy p—p phase shifts 686
POKROVSKY, V., *see* ABDURAZAKOV
POOL, M. L., *see* NARASIMHAIAH
POPOV, V. I., *see* NATHAN
RABSON, T. A., W. D. BARFIELD, D. L. BERNARD, T. W. BONNER and W. W. GIVENS, Gamma radiations from excited states of Ne^{20} . . . 43
RAO, D. A. A. S. N., *see* MANI
RICCI, R. A., R. K. GIRGIS and R. VAN LIESHOUT, Disintegration of ^{66}Ge 177
RIESS, F., *see* ROSE
RODBERG, L. S., The interaction radius in direct reactions 270
ROSE, H. J., F. RIESS and W. TROST, Ground state gamma transitions from states at 10.09 and 10.24 MeV in N^{14} and reinvestigation of the 9.17- and 10.43-MeV gamma ray distributions 367
RUDSTAM, G., *see* PAPPAS
RUEI, K. H., *see* BARUT
SALAM, ABDUS, *see* KOMAR
SALMON, G. L., The elastic scattering of 96 MeV neutrons by nuclei . . 15
SATCHLER, G. R., Spin-orbit coupling for spin-1 particles 116
SAWICKI, J. and S. A. MOSZKOWSKI, Imaginary part of the optical model potential in nuclear matter 456
SCHNEIDER, W., Contributions to the decay of Eu^{152} 55
SEBESTYÉN, A., *see* DOMOKOS
SENGUPTA, S., Coulomb energies of mirror nuclei 42
SERDOBOLSKY, V. I., Dispersion formulas in the theory of nuclear reactions 245
SHAPIRO, I. S., Weak interactions in the theory of elementary particles with finite space 474
SHELINE, R. K. and K. WILDERMUTH, Experimental evidence for cluster structures in light and medium weight nuclei 196
SINGH, B. P., Gamma-gamma angular correlations in Rh^{103} 450
SOLOMON, A. I., Mass differences in second order perturbation theory . 161
SOOD, P. C. and S. A. MOSZKOWSKI, Energy of a low density neutron gas 582
SPENCER, R. R., G. C. PHILLIPS and T. E. YOUNG, Energy levels of Be^9 and B^9 310
SPÎRCHEZ, M., *see* MARCU
SPITZER, RICHARD, On neutral spin-0 particles with imaginary parity 681
STRZALKOWSKI, A., *see* CINDRO
SUBOTIĆ-NIKOLIĆ, S., *see* GORGÉ

SWAN, P., An improved approximation for scattering problems (II) . . 233
TAKAHASHI, K. and H. MORINAGA, New nucleide actinium-231 133
THEIS, W. R., Relations for the electromagnetic self-masses of particles 170
THOULESS, D. J., Stability conditions and nuclear rotations in the Hartree-Fock theory 225
TIBELL, G., *see* JOHANSSON
TOMBRELLO, T. A., *see* MANI
TROST, W., *see* ROSE
VAN LIESHOUT, R., *see* RICCI
VAN OERS, W. T. H., *see* OERS
VERHAAR, B. J., A method for the elimination of spurious states in the nuclear harmonic oscillator shell model 508
VOGL, J. L., *see* HEBBARD
WALTERS, W. L., *see* DAHL
WEIDENMÜLLER, H. A., Shell model calculations for mass 12 nuclei, pertinent to a test of the conserved vector current theory 397
WILDERMUTH, K., *see* SHELINE
WILLIAMSON, R. M., *see* WISSEMAN
WINZELER, H., *see* GORGÉ
WISSEMAN, W. R. and R. M. WILLIAMSON, Coulomb excitation of Ge^{74} and Ge^{76} 688
WRZECIONKO, J., *see* DELOFF
YOUNG, T. E., *see* SPENCER
YUTLANDOV, I., *see* ABDURAZAKOV

SUBJECT INDEX

1. Nuclear Structure

1.A *General theory*

Stability conditions and nuclear rotations in the Hartree-Fock theory, D. J. Thouless 225

1.B *Two- and three-body problems*

An improved approximation for scattering problems (II), P. Swan 233
On neutral spin-0 particles with imaginary parity, Richard Spitzer 681

1.C *Many-particle systems*

Validity of the two-particle approximation in the many-body problem, Kailash Kumar 99
Imaginary part of the optical model potential in nuclear matter, J. Sawicki and S. A. Moszkowski 456
Energy of a low density neutron gas, P. C. Sood and S. A. Mcszkowski 582
The momentum distribution in a dilute Fermi gas at zero temperature W. Czyż and K. Gottfried 676

1.D *Nuclear models*

1.D.1 *Shell model*

Shell model calculations for mass 12 nuclei, pertinent to a test of the conserved vector current theory, H. A. Weidenmüller 397
A method for the elimination of spurious states in the nuclear harmonic oscillator shell model, B. J. Verhaar 508

1.D.2 *Collective model*

Note sur l'interprétation collective des deux premiers niveaux 2+ des noyaux pairs, M. Jean 142
Coulomb excitation with 14—20 MeV α-particles: Double excitations and systematics of vibrational states in the rare earth region, O. Nathan and V. I. Popov 631

1.D.3 *Other models*

Experimental evidence for cluster structures in light and medium weight nuclei, R. K. Sheline and K. Wildermuth 196
Energy levels of Be^9 and B^9, R. R.Spencer, G. C.Phillips and T. E. Young 310
The significance of the generalized density of states function for nuclear spectra, G. C. Phillips, T. A. Griffy and L. C. Biedenharn 327

1.E *Properties of nuclei*

1.E.2 *Binding energies; masses*

Coulomb energies of mirror nuclei, S. Sengupta 542

1.E.5 *Nuclear radii; matter distributions*

Isotope shift calculations for non-uniform charge distributions, A. R. Bodmer 347
Coulomb energies of mirror nuclei, S. Sengupta 542

2. Nuclear Reactions

2.A *General properties*

2.A.1 *Cross-sections, energy relations*

Neutron cross sections in chlorine, G. S. Mani, T. A. Tombrello and D.A.A.S.N. Rao 344
Elastic scattering and radiative capture of protons by C^{13}, D. F. Hebbard and J. L. Vogl. 652

2.B *Angular distributions, correlations; polarization*

The angular distributions of the gamma radiation from the $Li^7(p, \gamma)Be^8$ reaction from $E_p = 200$ keV to 1100 keV, E. Mainsbridge 1
The elastic scattering of 96 MeV neutrons by nuclei, G. L. Salmon 15
Angular correlation in $C^{13}(n, n'\gamma)C^{13}$ at 14 MeV, G. Deconninck and A. Martegani 33
Elastic scattering of 13 MeV deuterons on aluminium, N. Cindro, M. Cerineo and A. Strzalkowski 38
Spin-orbit coupling for spin-1 particles, G. R. Satchler 116
The elastic scattering of 160 MeV protons from lithium, aluminium, indium and gold, A. Johansson, G. Tibell, K. Parker and P. E. Hodgson 383
Selection rules and correlations for polarization in stripping and direct processes, L. J. B. Goldfarb and R. C. Johnson 462

2.C *Resonance reactions; R-matrix theory*

Parameters and gamma-ray spectra of neutron resonances in the isotopes of mercury, R. T. Carpenter and L. M. Bollinger 66
Aluminium (p, γ) resonances with H_1^+, H_2^+ and H_3^+ ions, P. F. Dahl, D. G. Costello and W. L. Walters 106
Dispersion formulas in the theory of nuclear reactions, V. I. Serdobolsky . . 245
Resonances in the reactions Si^{28}+p, J. O. Newton 529

2.E *Optical model*

Optical model analysis of the scattering of 96 MeV neutrons by nuclei, P. E. Hodgson 21
The elastic scattering of helium 3 by medium weight nuclei, P. E. Hodgson . . 28
Elastic scattering of 13 MeV deuterons on aluminium, N. Cindro, M. Cerineo and A. Strzalkowski 38
Spin-orbit coupling for spin-1 particles, G. R. Satchler 116
A model for the calculation of the optical potential in some finite nuclei, B. Jancovici 256
The elastic scattering of 160 MeV protons from lithium, aluminium, indium and gold, A. Johansson, G. Tibell, K. Parker and P. E. Hodgson 383
Imaginary part of the optical model potential in nuclear matter, J. Sawicki and S. A. Moszkowski 456

2.F *Direct interaction (other than stripping)*

The interaction radius in direct reactions, L. S. Rodberg 270
Selection rules and correlations for polarization in stripping and direct processes, L. J. B. Goldfarb and R. C. Johnson 462

2.G *Stripping and pick-up*

Stripping analysis of the reactions $Na^{23}(d, p)Na^{24}$, F. A. El Bedewi and M. A. El Wahab 49

Selection rules and correlations for polarization in stripping and direct processes, L. J. B. Goldfarb and R. C. Johnson 462
Reaction mechanism studies on Si^{28}(d, p)Si^{29}. (II). Interference effects, J. A. Kuehner, E. Almqvist and D. A. Bromley 555

2.H *Coulomb excitation*

Coulomb excitation with 14–20 MeV α-particles: Double excitations and systematics of vibrational states in the rare earth region, O. Nathan and V. I. Popov 631
Coulomb excitation of Ge^{74} and Ge^{76}, W. R. Wisseman and R. M. Williamson 688

2.J *Fission and spallation*

An approach to the systematics of delayed neutron precursors, A. C. Pappas and G. Rudstam 353

2.L *Scattering processes (except two-nucleon system and meson scattering)*

Elastic scattering of 24.4 MeV deuterons by protons, W. T. H. van Oers and K. W. Brockman, Jr. 189
Elastic scattering and radiative capture of protons by C^{13}, D. F. Hebbard and J. L. Vogl. 652

3. Electromagnetic Radiation

3.A *Gamma radiation*

Gamma radiations from excited states of Ne^{20}, T. A. Rabson, W. D. Barfield, D. L. Bernard, T. W. Bonner and W. W. Givens 43
Parameters and gamma-ray spectra of neutron resonances in the isotopes of mercury, R. T. Carpenter and L. M. Bollinger 66
Spins of the isomeric states of Hf^{178} and Hf^{180}, M. Deutsch and R. W. Bauer . 128
New nucleide actinium-231, K. Takahashi and H. Morinaga 133
Disintegration of ^{66}Ge, R. A. Ricci, R. K. Girgis and R. van Lieshout 177
Radioactive decay of Tm^{167}, H. Narasimhaiah and M. L. Pool 340
Ground state gamma transitions from states at 10.09 and 10.24 MeV in N^{14} and reinvestigation of the 9.17- and 10.43-MeV gamma ray distributions, H. J. Rose, F. Riess and W. Trost 367
The half-life of the first excited state of Tl^{203}, E. C. B. Pederson and R. E. Bell 393
Gamma-gamma angular correlations in Rh^{103}, B. P. Singh 450
Resonances in the reactions Si^{28}+p, J. O. Newton. 529
Elastic scattering and radiative capture of protons by C^{13}, D. F. Hebbard and J. L. Vogl. 652

3.B *Internal conversion*

Levels in Th^{228} excited in the electron capture decay of Pa^{228}, E. Arbman, S. Bjørnholm and O. B. Nielsen. 406
The decay of neptunium-238, R. G. Albridge and J. M. Hollander 438

4. Beta Decay; Parity

4.C *Evaluation of matrix elements*

Shell model calculations for mass 12 nuclei, pertinent to a test of the conserved vector current theory, H. A. Weidenmüller. 397

4.E *Analysis of data*

Contributions to the decay of Eu^{152}, W. Schneider 55
New nucleide actinium-231, K. Takahashi and H. Morinaga 133
The decay chain $Yb^{164} \rightarrow Tm^{164} \rightarrow Er^{164}$, A. Abdurazakov, K. Gromov, B. Dalkhsuren, B. Dželepov, I. Levenberg, A. Murin, Yu. Norseyev, V. Pokrovsky, V. Chumin and I. Yutlandov 164
Disintegration of ^{66}Ge, R. A. Ricci, R. K. Girgis and R. van Lieshout 177
The half-life of the first excited state of Tl^{203}, E. C. B. Pederson and R. E. Bell 393

6. Methods and Instruments

6.A *Experimental*

Aluminium (p, γ) resonances with H_1^+, H_2^+ and H_3^+ ions, P. F. Dahl, D. G. Costello and W. L. Walters 106

6.C *Constants, standards and units*

Sign convention for particle polarization 696

7. Quantum Field Theory

7.A *General*

On conservation of probability in the Lee model, Philippe Dennery and Norman M. Kroll 276
Extra solutions of the dispersion relations and resonance scattering, A. O. Barut and K. H. Ruei 300

7.B *Quantum electrodynamics*

Relations for the electromagnetic self-masses of particles, W. R. Theis . . . 170
Asymptotic conditions in quantum electrodynamics, L. E. Evans and T. Fulton 492

7.C π-meson field (*scattering and nuclear forces*)

Optical model analysis of negative pion-proton elastic scattering between 1.4 and 6.8 GeV, G. Domokos and A. Sebestyén 157
Renormalization problem for vector meson theories, A. Komar and Abdus Salam 624

8. Elementary Particles

8.A *Experimental*

Hypernuclei produced by K^- interactions in nuclear emulsions. (I). Mesic decays, M. M. Nikolić 595
Hypernuclei produced by K^- interactions in nuclear emulsions. (II). General characteristics and non-mesic decays, V. Gorgé, W. Koch, W. Lindt, M. M. Nikolić, S. Subotić-Nikolić and H. Winzeler 599

8.B *Theory; interactions, transformation properties*

Effective range for K^+-nucleon interaction from dispersion relations, S. N. Biswas and V. Gupta 137
Mass differences in second order perturbation theory, A. I. Solomon . . . 161
Directional correlation of mesons in a cascade decay of baryons resulting from a baryon-baryon reaction, A. Deloff and J. Wrzecionko 237

8.C *Fundamental theory of matter*

Weak interactions in the theory of elementary particles with finite space, I. S. Shapiro 474
n—p polarization and low energy p—p phase shifts, R. J. N. Phillips . . . 686

9. Cosmic Radiation

9.A *General*

Remarks on the energy distribution of mesons created in high-energy nuclear collisions, E. M. Friedländer 220
A Monte-Carlo calculation of the production spectrum of mesons in jets, M. Marcu and M. Spirchez 526

10. News Items

10.A *News items*

First annual report of O.E.E.C. "Dragon" high-temperature reactor project . 528

10.D *Book reviews*

J. SHARPE, Nuclear radiation measurements (J. Thomas) 697
M. DUQUESNE, R. GREGOIRE et M. LEFORT, Travaux pratiques de physique nucléaire et de radiochimie: Détection des rayonnements et méthodes d'étude de la structure nucléaire (N.O. Lassen) 697